12 11/92

Luk - H01769-35-P02447

AJR

35

American Journal of Roentgenology

July 1991

X-RAY ACCESSORIES

The Difference is Clear

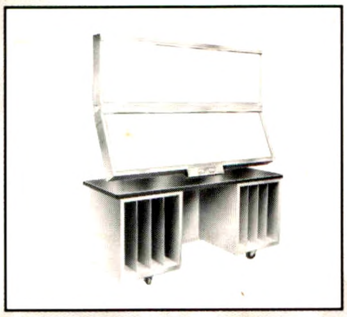

Tried, tested and trusted for over 40 years, S & S x-ray products deliver maximum proficiency and economy -- backed by quality, dependability and innovation.

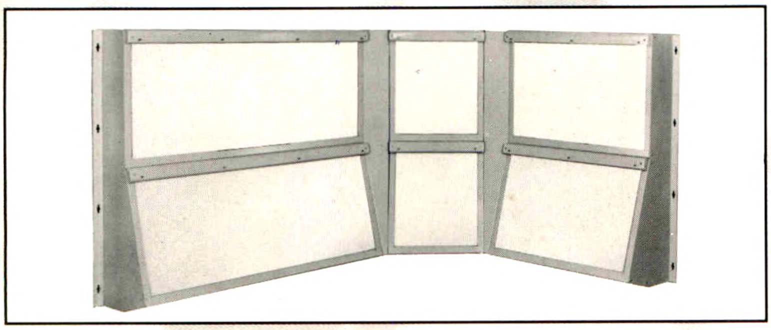

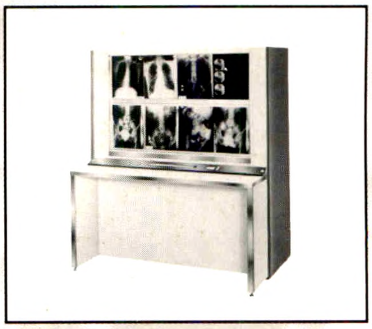

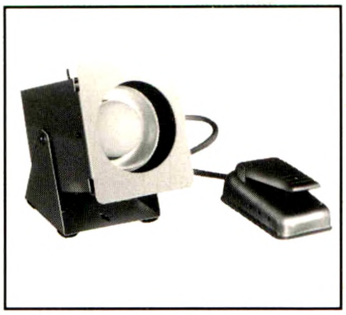

X-RAY Film Viewers ◆

X-RAY Protection ◆

X-RAY Files ◆

X-RAY Darkroom Equipment ◆

X-RAY Cabinets ◆

X-RAY Accessories ◆

For a FREE copy of our fully illustrated, 100+ page catalog, contact S & S directly or your local x-ray dealer.

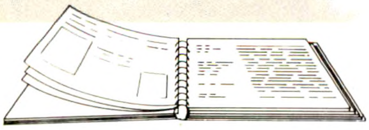

Phone: 718/649-8500
FAX: 718/257-0219
Toll Free: 800/347-XRAY

1101 Linwood Street
Brooklyn, N.Y. 11208

S&S X-RAY PRODUCTS
Factories in NY, NC, PA, TX

Official Journal of the American Roentgen Ray Society

AJR

American Journal of Roentgenology
Diagnostic Imaging and Related Sciences

Editor-In-Chief Robert N. Berk, *La Jolla, California*
University of California, San Diego
School of Medicine and Medical Center

Editor Emeritus Melvin M. Figley, *Seattle, Washington*

Associate Editor Karim Valji, *San Diego, California*

Consulting Editor Michael S. Huckman, *Chicago, Illinois*

Statistician Charles C. Berry, *San Diego, California*

P. 24471

Editorial Board

John R. Amberg
Ithamar Aviad
Mark E. Baker
Lawrence W. Bassett
Michael A. Bettmann
Felix S. Chew
N. Reed Dunnick
David K. Edwards
Ronald G. Evens
David S. Feigin
Sandra K. Fernbach
Richard H. Gold
William R. Hendee
John R. Hesselink
Charles B. Higgins
Melvyn T. Korobkin
Faye C. Laing
Thomas L. Lawson
Robert G. Levitt
Bruce L. McClennan
Richard P. Moser
Albert A. Moss
Jeffrey H. Newhouse
Donald L. Resnick
Stewart R. Reuter
Charles A. Rohrmann, Jr.
Peter M. Ronai
Sjef H. J. Ruijs
Stuart S. Sagel
David J. Sartoris
Stefan C. Schatzki
William P. Shuman
Edward A. Sickles
Barry A. Siegel
David D. Stark
Edward T. Stewart
Murali Sundaram
Eric vanSonnenberg
Robert K. Zeman

Editorial Staff: Margaret Levene, *managing editor*; Katie L. Spiller, Barbara Rose, Barbara L. Halliburton, and Janine Anderson, *manuscript editors*; Nancy Rydbeck, *office manager*; Sheri Smith, *administrative assistant*; Linda J. Waggoner, *administrative secretary*

AJR, AMERICAN JOURNAL OF ROENTGENOLOGY (ISSN 0361 803X) is the official journal of the American Roentgen Ray Society and is published monthly by Williams & Wilkins, 428 E. Preston St., Baltimore, MD 21202. Annual dues include $50 for journal subscription. Second-class postage paid at Baltimore, MD, and at additional mailing offices. Postmaster, send address changes (Form 3579) to AJR, 428 E. Preston St., Baltimore, MD 21202. Subscription rates $125 ($180 foreign); institutions $135 ($190 foreign); in training $25 ($80 foreign); single copy $18 ($22 foreign). The GST number for Canadian subscribers is 123394371. Airmail rates furnished on request. Indexed by *Current Contents* and *Index Medicus*. Copyright © 1991 by American Roentgen Ray Society.
0361-803X/90$3.00

O M M A L L

INCKRODT

The friendlier molecule and its pattern of protection

The toxic portion of the contrast agent molecule is the iodinated benzene ring. In modern contrast agents, the ring is sheltered by hydroxyl groups arranged around it. If the arrangement is less than optimal, it can leave "holes" in the structure.

The Optiray® molecular structure provides a superior pattern of protection from the benzene ring with six hydroxyl groups arranged symmetrically around it.[1] In addition, Optiray has no hydrophobic (lipid-soluble) methyl group as in iopamidol and iohexol molecules. These are the reasons why one investigator has called Optiray the "friendlier" contrast media molecule.[1]

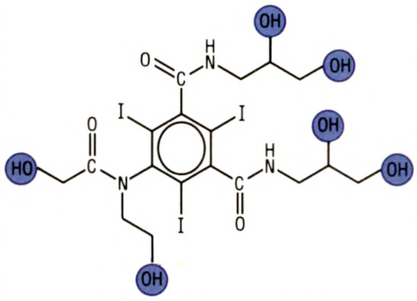

Balanced distribution of hydroxyl (OH) groups creates a pattern of protection around the toxic iodinated benzene ring.

With Optiray, you can expect a very low incidence of individual, drug-related adverse reactions.[2] Optiray also offers the safety, convenience, and cost-efficiency of the single-dose Ultraject® prefilled syringe. With all these advantages, shouldn't Optiray's friendlier molecule be your choice in a nonionic contrast agent? For more information, contact your Mallinckrodt Medical representative or call us toll free at (800) 325-3688.

All nonionic iodinated contrast media currently available inhibit blood coagulation, in vitro, less than ionic contrast media. Clotting has been reported when blood remains in contact with syringes containing nonionic contrast media. Therefore, meticulous intravascular administration technique is necessary to minimize thromboembolic events.

Please see adjacent brief summary of prescribing information.

References:

1. McClennan BL. Ionic and nonionic iodinated contrast media: evolution and strategies for use. *AJR.* 1990; 155:225-233.
2. Benamor M, Aten EM, McElvany KD, et al. Ioversol clinical safety summary. *Invest Radiol.* 1989;24 (suppl 1):S67-S72.

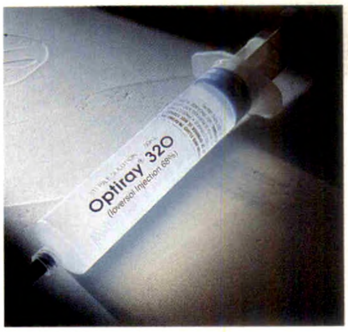

Nonionic

OPTIRAY®

(ioversol)

The friendlier molecule

OPTIRAY® 160 240 320
(Ioversol Injection)

DESCRIPTION: Each milliliter of OPTIRAY 160 (ioversol injection 34%) provides 339 mg of ioversol with 3.6 mg of tromethamine as a buffer and 0.2 mg of edetate calcium disodium as a stabilizer. OPTIRAY 160 provides 16% (160 mg/mL) organically bound iodine.

Each milliliter of OPTIRAY 240 (ioversol injection 51%) provides 509 mg of ioversol with 3.6 mg of tromethamine as a buffer and 0.2 mg of edetate calcium disodium as a stabilizer. OPTIRAY 240 provides 24% (240 mg/mL) organically bound iodine.

Each milliliter of OPTIRAY 320 (ioversol injection 68%) provides 678 mg of ioversol with 3.6 mg of tromethamine as a buffer and 0.2 mg of edetate calcium disodium as a stabilizer. OPTIRAY 320 provides 32% (320 mg/mL) organically bound iodine.

CONTRAINDICATIONS: None.

WARNINGS: Nonionic iodinated contrast media inhibit blood coagulation, in vitro, less than ionic contrast media. Clotting has been reported when blood remains in contact with syringes containing nonionic contrast media.

Serious, rarely fatal, thromboembolic events causing myocardial infarction and stroke have been reported during angiographic procedures with both ionic and nonionic contrast media. Therefore, meticulous intravascular administration technique is necessary, particularly during angiographic procedures, to minimize thromboembolic events. Numerous factors, including length of procedure, catheter and syringe material, underlying disease state and concomitant medications may contribute to the development of thromboembolic events. For these reasons, meticulous angiographic techniques are recommended including close attention to guidewire and catheter manipulation, use of manifold systems and/or three-way stopcocks, frequent catheter flushing with heparinized saline solutions and minimizing the length of the procedure. The use of plastic syringes in place of glass syringes has been reported to decrease but not eliminate the likelihood of in vitro clotting.

Serious or fatal reactions have been associated with the administration of iodine-containing radiopaque media. It is of utmost importance to be completely prepared to treat any contrast medium reaction.

As with any contrast medium, serious neurologic sequelae, including permanent paralysis, can occur following cerebral arteriography, selective spinal arteriography and arteriography of vessels supplying the spinal cord. A cause-effect relationship to the contrast medium has not been established since the patients' pre-existing condition and procedural technique are causative factors in themselves. The arterial injection of a contrast medium should never be made following the administration of vasopressors since they strongly potentiate neurologic effects.

Caution must be exercised in patients with severely impaired renal function, combined renal and hepatic disease, severe thyrotoxicosis, myelomatosis, or anuria, particularly when large doses are administered.

Intravascularly administered iodine-containing radiopaque media are potentially hazardous in patients with multiple myeloma or other paraproteinemia, particularly in those with therapeutically resistant anuria. Myeloma occurs most commonly in persons over age 40. Although neither the contrast agent nor dehydration has been proved separately to be the cause of anuria in myelomatous patients, it has been speculated that the combination of both may be causative. The risk in myelomatous patients is not a contraindication to the procedure; however, special precautions, including maintenance of normal hydration and close monitoring, are required. Partial dehydration in the preparation of these patients prior to injection is not recommended since this may predispose the patient to precipitation of the myeloma protein.

Administration of radiopaque materials to patients known or suspected of having pheochromocytoma should be performed with extreme caution. If, in the opinion of the physician, the possible benefits of such procedures outweigh the considered risks, the procedures may be performed; however, the amount of radiopaque medium injected should be kept to an absolute minimum. The blood pressure should be assessed throughout the procedure, and measures for treatment of a hypertensive crisis should be available.

Contrast media may promote sickling in individuals who are homozygous for sickle cell disease when administered intravascularly.

Reports of thyroid storm following the intravascular use of iodinated radiopaque agents in patients with hyperthyroidism or with an autonomously functioning thyroid nodule, suggest that this additional risk be evaluated in such patients before use of any contrast medium.

PRECAUTIONS: *General:* Diagnostic procedures which involve the use of iodinated intravascular contrast agents should be carried out under the direction of personnel skilled and experienced in the particular procedure to be performed. A fully equipped emergency cart, or equivalent supplies and equipment, and personnel competent in recognizing and treating adverse reactions of all types should always be available. Since severe delayed reactions have been known to occur, emergency facilities and competent personnel should be available for at least 30 to 60 minutes after administration.

Preparatory dehydration is dangerous and may contribute to acute renal failure in patients with advanced vascular disease, diabetic patients, and in susceptible non-diabetic patients (often elderly with pre-existing renal disease). *Patients should be well hydrated prior to and following the administration of OPTIRAY.*

The possibility of a reaction, including serious, life-threatening, fatal, anaphylactoid or cardiovascular reactions, should always be considered (See ADVERSE REACTIONS). Increased risk is associated with a history of previous reaction to a contrast medium, a known sensitivity to iodine and known allergies (i.e., bronchial asthma, hay fever and food allergies) or hypersensitivities.

The occurrence of severe idiosyncratic reactions has prompted the use of several pretesting methods. However, pretesting cannot be relied upon to predict severe reactions and may itself be hazardous to the patient. It is suggested that a thorough medical history with emphasis on allergy and hypersensitivity, prior to the injection of any contrast medium, may be more accurate than pretesting in predicting potential adverse reactions. A positive history of allergies or hypersensitivity does not arbitrarily contraindicate the use of a contrast agent when a diagnostic procedure is thought essential, but caution should be exercised. Premedication with antihistamines or corticosteroids to avoid or minimize possible allergic reactions in such patients should be considered. Reports indicate that such pretreatment does not prevent serious life-threatening reactions, but may reduce both their incidence and severity.

General anesthesia may be indicated in the performance of some procedures in selected patients; however, a higher incidence of adverse reactions has been reported in these patients, and may be attributable to the inability of the patient to identify untoward symptoms or to the hypotensive effect of anesthesia which can prolong the circulation time and increase the duration of exposure to the contrast agent.

In angiographic procedures, the possibility of dislodging plaques or damaging or perforating the vessel wall should be considered during catheter manipulations and contrast medium injection. Test injections to insure proper catheter placement are suggested.

Angiography should be avoided whenever possible in patients with homocystinuria because of the risk of inducing thrombosis and embolism.

Patients with congestive heart failure should be observed for several hours following the procedure to detect delayed hemodynamic disturbances which may be associated with a transitory increase in the circulating osmotic load.

Selective coronary arteriography should be performed only in selected patients and those in whom the expected benefits outweigh the procedural risk. The inherent risks of angiocardiography in patients with chronic pulmonary emphysema must be weighed against the necessity for performing this procedure.

Extreme caution during injection of a contrast medium is necessary to avoid extravasation. This is especially important in patients with severe arterial or venous disease.

Drug Interactions: Renal toxicity has been reported in a few patients with liver dysfunction who were given oral cholecystographic agents followed by intravascular contrast agents. Administration of any intravascular contrast agent should therefore be postponed in patients who have recently received a cholecystographic contrast agent.

Other drugs should not be mixed with ioversol injection.

Drug Laboratory Test Interactions: The results of PBI and radioactive iodine uptake studies, which depend on iodine estimation, will not accurately reflect thyroid function for up to 16 days following administration of iodinated contrast media. However, thyroid function tests not depending on iodine estimations, e.g., T3 resin uptake and total or free thyroxine (T4) assays are not affected.

Carcinogenesis, Mutagenesis, Impairment of Fertility: No long term animal studies have been performed to evaluate carcinogenic potential. However, animal studies suggest that this drug is not mutagenic and does not affect fertility.

Pregnancy Category B: No teratogenic effects attributable to ioversol have been observed in teratology studies performed in animals. There are, however, no adequate and well controlled studies in pregnant women. It is not known whether ioversol crosses the placental barrier or reaches fetal tissues. However, many injectable contrast agents cross the placental barrier in humans and appear to enter fetal tissue passively. Because animal teratology studies are not always predictive of human response, this drug should be used during pregnancy only if clearly needed. X-ray procedures involve a certain risk related to the exposure of the fetus.

Nursing Mothers: It is not known whether ioversol is excreted in human milk. However, many injectable contrast agents are excreted unchanged in human milk. Although it has not been established that serious adverse reactions occur in nursing infants, caution should be exercised when intravascular contrast media are administered to nursing women because of potential adverse reactions, and consideration should be given to temporarily discontinuing nursing.

Pediatric Use: Safety and effectiveness in children have not been established.

ADVERSE REACTIONS: Adverse reactions following the use of OPTIRAY formulations are usually mild to moderate, of short duration and resolve spontaneously (without treatment). However, serious, life-threatening and fatal reactions, mostly of cardiovascular origin, have been associated with the administration of iodine-containing contrast media.

Injections of contrast media are often associated with sensations of warmth and pain. In controlled double-blind clinical studies, significantly less warmth and pain were associated with the injection of OPTIRAY than with iothalamate meglumine, diatrizoate meglumine, and diatrizoate meglumine and diatrizoate sodium.

When OPTIRAY 320 is used for coronary arteriography and ventriculography in double-blind clinical trials, electrocardiographic and hemodynamic changes occur with less frequency and severity with ioversol injection than with diatrizoate meglumine and diatrizoate sodium.

Following coronary artery and left ventricular injection, electrocardiographic parameters were affected less with OPTIRAY (ioversol injection) than with diatrizoate meglumine and diatrizoate sodium injection. These parameters included the following: bradycardia, tachycardia, T-wave amplitude, ST depression and ST elevation.

OPTIRAY has also been shown to cause fewer changes in cardiac function and systemic blood pressure than conventional ionic media. These include cardiac output, left ventricular systolic and end-diastolic pressure, right ventricular systolic and pulmonary artery systolic pressures and decreases in systolic and diastolic blood pressures.

The following table of incidence of reactions is based upon clinical trials with OPTIRAY formulations in over 1100 patients. This listing includes all adverse reactions which were coincidental to the administration of ioversol regardless of their direct attributability to the drug or the procedure. Adverse reactions are listed by organ system and in decreasing order of occurrence. Significantly more severe reactions are listed before others in a system regardless of frequency.

Adverse Reactions

System	> 1%	≤ 1%
Cardiovascular	none	angina pectoris hypotension vascular spasm bradycardia conduction defect false aneurysm hypertension transient arrhythmia vascular trauma
Digestive	none	nausea vomiting
Nervous	none	cerebral infarct headache blurred vision vertigo lightheadedness vasovagal reaction disorientation dysphasia paresthesia visual hallucination
Respiratory	none	laryngeal edema nasal congestion sneezing coughing hypoxia
Skin	none	periorbital edema urticaria facial edema flush pruritus
Miscellaneous	none	extravasation shaking chills bad taste general pain

Regardless of the contrast medium employed, the overall incidence of serious adverse reaction is higher with coronary arteriography than with other procedures. Cardiac decompensation, serious arrhythmias, myocardial ischemia or myocardial infarction may occur during coronary arteriography and left ventriculography.

General Adverse Reactions to Contrast Media

The following adverse reactions are possible with any parenterally administered iodinated contrast medium. Severe life-threatening reactions and fatalities, mostly of cardiovascular origin, have occurred. Most deaths occur during injection or 5 to 10 minutes later; the main feature being cardiac arrest with cardiovascular disease as the main aggravating factor. Isolated reports of hypotensive collapse and shock are found in the literature. Based upon clinical literature, reported deaths from the administration of conventional iodinated contrast agents range from 6.6 per 1 million (0.00066 percent) to 1 in 10,000 patients (0.01 percent).

The reported incidence of adverse reactions to contrast media in patients with a history of allergy is twice that of the general population. Patients with a history of previous reactions to a contrast medium are three times more susceptible than other patients. However, sensitivity to contrast media does not appear to increase with repeated examinations.

Adverse reactions to injectable contrast media fall into two categories: chemotoxic reactions and idiosyncratic reactions.

Chemotoxic reactions result from the physicochemical properties of the contrast medium, the dose and the speed of injection. All hemodynamic disturbances and injuries to organs or vessels perfused by the contrast medium are included in this category.

Idiosyncratic reactions include all other reactions. They occur more frequently in patients 20 to 40 years old. Idiosyncratic reactions may or may not be dependent on the dose injected, the speed of injection, the mode of injection and the radiographic procedure. Idiosyncratic reactions are subdivided into minor, intermediate and severe. The minor reactions are self-limited and of short duration; the severe reactions are life-threatening and treatment is urgent and mandatory.

In addition to the adverse reactions reported for ioversol, the following additional adverse reactions have been reported with the use of other contrast agents and are possible with any water soluble, iodinated contrast agent.

Nervous: muscular spasm, convulsions, aphasia, syncope, paralysis, visual field losses which are usually transient but may be permanent, coma and death.

Cardiovascular: angioneurotic edema, peripheral edema, vasodilation, thrombosis and rarely thrombophlebitis, disseminated intravascular coagulation and shock.

Skin: maculopapular rash, erythema, conjunctival symptoms, ecchymosis and tissue necrosis.

Respiratory: choking, dyspnea, wheezing which may be an initial manifestation of more severe and infrequent reactions including asthmatic attack, laryngospasm and brochospasm, pulmonary edema, apnea and cyanosis. Rarely these allergic-type reactions can progress into anaphylaxis with loss of consciousness, coma, severe cardiovascular disturbances and death.

Miscellaneous: hyperthermia, temporary anuria or other nephropathy.

Other reactions may also occur with the use of any contrast agent as a consequence of the procedural hazard; these include hemorrhage or pseudoaneurysms at the puncture site, brachial plexus palsy following axillary artery injections, chest pain, myocardial infarction, and transient changes in hepatorenal chemistry tests. Arterial thrombosis, displacement of arterial plaques, venous thrombosis, dissection of the coronary vessels and transient sinus arrest are rare complications.

In cerebral arteriography, cardiovascular reactions that may occur with some frequency are bradycardia and either an increase or decrease in systemic blood pressure. Neurological reactions that may occur are: seizures, drowsiness, transient paresis, and mild disturbances in vision.

Central nervous system reactions with OPTIRAY in controlled clinical studies in cerebral arteriography that occurred with frequencies greater than 1% were: vertigo (4%) and blurred vision (3%).

In aortography, depending on the technique employed, the risks of this procedure also include the following: injury to the aorta and neighboring organs, pleural puncture, renal damage including infarction and acute tubular necrosis with oliguria and anuria, retroperitoneal hemorrhage from the translumbar approach and spinal cord injury and pathology associated with the syndrome of transverse myelitis. Under conditions of slowed aortic circulation there is an increased likelihood for aortography to cause muscle spasm. Occasional serious neurologic complications, including paraplegia, have also been reported in patients with aortoiliac obstruction, femoral artery obstruction, abdominal compression, hypotension, hypertension, spinal anesthesia, and injection of vasopressors to increase contrast. In these patients the concentration, volume, and number of repeat injections of the medium should be maintained at a minimum with appropriate intervals between injections. The position of the patient and catheter tip should be carefully monitored.

Entry of a large aortic dose into the renal artery may cause, even in the absence of symptoms, albuminuria, hematuria, and an elevated creatinine and urea nitrogen. Rapid and complete return of function usually follows.

Cardiovascular system reactions with OPTIRAY in controlled clinical studies in coronary arteriography with left ventriculography that occurred with frequencies greater than 1% were: angina (1.2%) and nausea (1.2%).

PRECAUTIONS FOR SPECIFIC PROCEDURES:

Cerebral Arteriography

Extreme caution is advised in patients with advanced arteriosclerosis, severe hypertension, cardiac decompensation, senility, recent cerebral thrombosis or embolism, and migraine.

Peripheral Arteriography

Pulsation should be present in the artery to be injected. In thromboangiitis obliterans, or ascending infection associated with severe ischemia, angiography should be performed with extreme caution, if at all.

Coronary Arteriography and Left Ventriculography

Mandatory prerequisites to the procedure are specialized personnel, ECG monitoring apparatus and adequate facilities for immediate resuscitation and cardioversion. Electrocardiograms and vital signs should be routinely monitored throughout the procedure.

Venography

Special care is required when venography is performed in patients with suspected thrombosis, phlebitis, severe ischemic disease, local infection or a totally obstructed venous system. In order to minimize extravasation during injection, fluoroscopy is recommended.

OVERDOSAGE: The adverse effects of overdosage are life-threatening and affect mainly the pulmonary and cardiovascular system. Treatment of an overdosage is directed toward the support of all vital functions, and prompt institution of symptomatic therapy.

Ioversol does not bind to plasma or serum protein and is therefore, dialyzable.

The intravenous LD_{50} values (gl/kg) for ioversol in animals were: 17 (mice), and 15 (rats).

DOSAGE AND ADMINISTRATION: Details on dosage are provided in the package insert. CONSULT FULL PACKAGE INSERT BEFORE USE.

MALLINCKRODT®

Changing the look of medicine.™

© 1991 Mallinckrodt Medical, Inc. 4/91 MI22377

It Is Now A Law*

Effective January 1, 1991, The U.S. Congress approved legislation affecting Medicare reimbursement for mammography screening.

What This Means To You:

Any supplier of mammography screening MUST have an equipment quality assurance program specific to mammography imaging! This program MUST cover all components of the x-ray system, from x-ray generator to the image developer!

A FREE Catalog Is Available For Your Use:

This FREE catalog contains ALL of the equipment you will need to comply with this new law plus ACR Accreditation for Quality Assurance! We will also send you a copy of this new law.

Call, Fax, or Write For Your FREE Copy:

Phone (516) 741-6360, FAX (516) 741-5414 or write Nuclear Associates, 100 Voice Rd., Carle Place, New York 11514
Ask for Catalog MMB-44.

NUCLEAR ASSOCIATES

VICTOREEN

Division of VICTOREEN, INC.
100 VOICE ROAD • P.O. BOX 349
CARLE PLACE, NY 11514-0349
(516) 741-6360 • FAX (516) 741-5414

**42CFR Part 494.64 "Condition for Coverage: Quality Assurance".*

AJR Business and Subscriber Information

The American Roentgen Ray Society

AJR, American Journal of Roentgenology, is published monthly to disseminate research on current developments in the radiologic sciences and commentary on topics related to radiology. It is published by the American Roentgen Ray Society, 1891 Preston White Dr., Reston, VA 22091; (703) 648-8992. Inquiries regarding society business, the annual ARRS meeting, and membership should be addressed to the Society at the above address.

Correspondence Concerning the *AJR*

Correspondence regarding display (not classified) advertising, subscriptions, address changes, reprints, and permission requests should be addressed to Williams & Wilkins, 428 E. Preston St., Baltimore, MD 21202; (301) 528-4000.

Correspondence regarding editorial matters and classified advertising should be addressed to Editorial Office, AJR, 2223 Avenida de la Playa, Ste. 103, La Jolla, CA 92037-3218; telephone (619) 459-2229; FAX (619) 459-8814. For information on manuscript submission, see Guidelines for Authors, pages A17–A19.

Subscriber Information

Subscription requests and inquiries should be sent to Williams & Wilkins, 428 E. Preston St., Baltimore, MD 21202. ARRS annual dues include $50 for journal subscription. Subscription rates are as follows: nonmembers, $125/year ($180 foreign); institutions, $135 ($190 foreign); nonmember in-training, $25 ($80 foreign). Single copies of the Journal may be purchased for $18 ($22 foreign). Airmail rates will be furnished on request. The GST number for Canadian subscribers is 123394371.

Call toll-free, 1-800-638-6423 (in Maryland call 1-800-638-4007), with subscription questions or problems. Please have the mailing label from your latest issue available when you call.

If a subscriber receives a damaged copy of the *AJR* or fails to receive an issue, the subscriber should notify Williams & Wilkins (428 E. Preston St., Baltimore, MD 21202) within 60 days of publication (90 days for foreign subscribers) and that issue will be replaced.

Change of address information should be sent to Williams & Wilkins, 428 E. Preston St., Baltimore, MD 21202. Allow 90 days for address changes.

Copyrights, Permissions, and Reprints

The American Roentgen Ray Society holds the copyright for all material published in the *AJR*. No part of this publication may be reproduced without permission from the ARRS. Requests for such permission should be addressed to Williams & Wilkins, 428 E. Preston St., Baltimore, MD 21202.

For reprints of a particular article, please contact the author designated in the footnotes for that article.

Indexes

The *AJR* provides volume and yearly indexes (subject and author) in the June and December issues each year. *AJR* articles are also indexed in *Current Contents*, *Index Medicus*, and the cumulative index published by *Radiology*.

AJR Guidelines for Authors

Address new and revised manuscripts, correspondence, and classified ads to the Editor:

AJR Editorial Office
2223 Avenida de la Playa, Suite 103
La Jolla, CA 92037-3218
Telephone: (619) 459-2229; FAX: (619) 459-8814

Inquiries regarding subscriptions, display advertising, reprints, or permission to republish *AJR* material should be addressed to the publisher:

The Williams & Wilkins Co.
428 E. Preston St.
Baltimore, MD 21202 Telephone: 1-800-638-6423

The *AJR* publishes original contributions to the advancement of medical diagnosis and treatment. Submitted manuscripts should not contain previously published material and should not be under consideration for publication elsewhere. Papers dealing with neuroradiology should be addressed to American Journal of Neuroradiology, Dept. of Diagnostic Radiology, 1653 W. Congress Pkwy., Chicago, Il 60612. At the discretion of the *AJR* Editor, *AJNR* articles that are of interest to the general reader may be republished in the *AJR*. Neuroradiologic papers sent to the *AJR* will be forwarded to the Editorial Office of the *AJNR*.

Manuscript decisions are based on peer review. Reviewers receive manuscripts without title pages to ensure an unbiased review. Statements made in the article, including changes made by the Editor or manuscript editor, are the responsibility of the author and not of the *AJR* or its publisher. Authors will be sent the edited manuscript, galley proof, and proofs of illustrations. If the corresponding author will be unavailable to review galleys, arrangements should be made for a coauthor or colleague to read and return the proof.

The following guidelines are based on instructions set forth in the **Uniform Requirements for Manuscripts Submitted to Biomedical Journals** (*Ann Intern Med* **1988;**108:258–265). Articles will be edited, however, to conform to the individual style of AJR.

General Guidelines for Major Papers

Abstract. Clearly state (in 200 words or less) the purpose, methods, results, and conclusions of the study. Include actual data.

Introduction. Briefly describe the purpose of the investigation and explain why it is important.

Methods. Describe the research plan, the materials (or subjects), and the methods used, in that order. Explain in detail how disease was confirmed and how subjectivity in observations was controlled.

Results. Present results in a clear, logical sequence. If tables are used, do not duplicate tabular data in text, but do describe important trends and points.

Discussion. Describe the limitations of the research plan, materials (or subjects), and methods, considering both the purpose and the outcome of the study. When results differ from those of previous investigators, explain the discrepancy.

AUTHOR'S CHECKLIST

For priority handling, complete the following checklist, sign the copyright form on the reverse side of this page, and include both with the manuscript.

________ Two copies of the manuscript (the original and a photocopy) and two complete sets of figures are submitted. One copy has been retained by the author.

________ If appropriate, *AJR* Guidelines for case reports, technical notes, pictorial essays, or letters to the Editor have been followed. (See page A19.)

________ The manuscript, including references, figure legends, and tables, is typed double-spaced on 8½ × 11 in. (21.6 × 27.9 cm) *nonerasable* paper. Right-hand margins are not justified.

________ All manuscript pages are numbered consecutively beginning with the abstract. Authors' names do not appear on the manuscript pages.

________ The manuscript is organized as follows: title page, blind title page (title only), abstract, introduction, methods, results, discussion, acknowledgments, references, tables, figure legends, and figures.

________ Informed consent has been obtained from patients who participated in clinical investigations. If experiments were performed on animals, authors complied with NIH guidelines for use of laboratory animals.

________ Use of unfamiliar acronyms and abbrevations is kept to a minimum. When abbreviations are used they are defined at first mention, followed by the abbreviation in parentheses.

________ Metric measurements are used throughout, or the metric equivalent is given in parentheses.

________ Names and locations (city and state only) of manufacturers are given for equipment and nongeneric drugs.

Title Page

________ The following information is given: title of article; names and complete addresses (including zip code) of all authors; current addresses of authors who have moved since study; acknowledgment of grant or other assistance. The corresponding author is clearly identified, and a current address, phone number, and FAX number are given.

________ A blind title page is included in each copy of the manuscript, giving only the title (without the authors' names) for use in the review process.

Abstract

________ An abstract of approximately 200 words concisely states the purpose, methods, and results of the study in one paragraph. Actual data are included. Conclusions are stated in a second, summary paragraph.

________ No abbreviations or reference citations are used

References

________ References (not to exceed 35) are typed double-spaced starting on a separate page and are **numbered consecutively in the order in which they appear in the text**.

________ All references are cited in the text and are enclosed in brackets and typed on line with the text (not superscript).

________ Unpublished data are not cited in the reference list, but are cited parenthetically in the text, for example, (Smith DJ, personal communication), (Smith DJ, unpublished data). This includes papers submitted, but not yet accepted, for publication.

________ Papers presented at a meeting are not cited in the reference list, but are cited parenthetically in the text (e.g., Smith DJ et al., presented at the annual meeting of the American Roentgen Ray Society, May 1990). After first mention, use (Smith DJ et al., ARRS meeting, May 1990).

________ Inclusive page numbers (e.g., 333–335) are given for all references.

________ Journal names are abbreviated according to *Index Medicus*.

________ Style and punctuation of references follow the format illustrated in the following examples (all authors are listed when six or fewer; when seven or more authors, the first three are listed, followed by "et al."):

Journal article

1. Long RS, Roe EW, Wu EU, et al. Membrane oxygenation: radiographic appearance. *AJR* **1986**;146:1257–1260

Book

2. Smith LW, Cohen AR. *Pathology of tumors*, 6th ed. Baltimore: Williams & Wilkins, **1977**:100–109

Chapter in a book

3. Breon AJ. Serum monitors of bone metastasis. In: Clark SA, ed. *Bone metastases*. Baltimore: Williams & Wilkins, **1983**:165–180

Tables

________ Each table is typed double-spaced on a separate page without vertical or horizontal rules; each has a short, descriptive title. Tables do not exceed two pages in length and contain at least four lines of data.

________ Tables are numbered in the order in which they are cited in the text.

________ Abbreviations are defined in an explanatory note below each table.

________ Tables are self-explanatory and do not duplicate data given in the text or figures.

________ All arithmetic (percentages, totals, differences) has been double checked for accuracy, and tabular data agree with data given in the text.

Figures and Legends

________ Two complete sets of original figures are submitted unmounted in labeled envelopes.

________ Figures are clean, unscratched, 5 × 7 in. (13 × 18 cm) glossy prints with **white borders.** A separate print is submitted for each figure *part*.

________ All figure parts relating to one patient have the same figure number.

________ Each figure is labeled on the back with the figure number and an arrow indicating "top." For black-and-white figures, labeling is done on a gummed label, which is then affixed to the back of the print. **Never** use labels on **color** figures, but write figure number on the back lightly in pencil. *Never* use ink on front or back of any figures.

________ Author's names are *not* written on the backs of figures.

________ Only removable (rub-on) arrows and letters are used on the figures. Symbols are uniform in size and style and are not broken or cracked.

________ Images are uniform in size and magnification.

________ Line drawings are done in black ink on a white background. They are professional in quality, and all use the same size type. (Only glossy prints are acceptable.)

________ Written permission has been obtained for use of all previously published illustrations (and copies of permission letters are included), and an appropriate credit line is given in the legends.

________ Legends are typed double-spaced, and figure numbers correspond with the order in which the figures are cited in the text.

Transfer of Copyright Agreement, Conflict of Interest Acknowledgment, Certification of Coauthors, and Exclusive Publication Statement

Complete copyright to the article entitled: ____

____

is hereby transferred to the American Roentgen Ray Society (for United States government employees to the extent transferable), effective if and when the article is accepted for publication in the *American Journal of Roentgenology*. In the case of the authors who are officers or employees of the United States government, the American Roentgen Ray Society recognizes that works prepared by officers or employees of the United States government as part of their official government duties are in the public domain.

Authors reserve all proprietary rights other than copyright, such as patent rights and the right to use all or part of this article in future works of their own. The authors retain the right of replication, subject only to crediting the original source of publication and receiving written permission from the publisher.

Authors guarantee that this manuscript contains no matter that is libelous or otherwise unlawful, invades individual privacy, or infringes any proprietary rights.

Authors understand that they will receive no royalty or other compensation from the American Roentgen Ray Society or the publisher.

Authors guarantee that the editor has been or will be informed of any proprietary or commercial interest or conflicts of interest the authors may have that relate directly or indirectly to the subject of this article.

All authors certify that they have made substantive and specific intellectual contributions to the article and assume public responsibility for its content.

Finally, the authors certify that none of the material in this manuscript has been published previously or is currently under consideration for publication elsewhere.

First author/date	Second author	Third author
Fourth author	Fifth author	Sixth author

This agreement must be signed by all authors in order for the manuscript to be published.

Case Reports

A case report is a brief description of a special case that provides a message that transcends the individual patient.

Format. There is no abstract. The introduction should be a short paragraph giving the general background and the specific interest of the case. No more than one case should be described in detail (similar ones can be mentioned briefly in the discussion). Emphasis should be on the radiologic aspects; clinical information must be limited to that necessary to provide a background for the radiology. The discussion should be succinct and should focus on the specific message and relevance of radiologic methods. A review of the literature is not appropriate.

Length. Maximum of five double-spaced, typewritten pages, including the references but not the title page or figure legends.

References. Maximum of eight.

Figures. Maximum of four, unless the text is shortened accordingly. Legends must not repeat the text.

Tables and Acknowledgments. Not appropriate in case reports.

Technical Notes

A technical note is a brief description of a specific technique or procedure, modification of a technique, or equipment of interest to radiologists.

Format. No abstract, headings, or subheadings are required. If headings are used, they should be a combination of "Case Report," "Materials and Methods," "Results," and "Discussion." A brief one-paragraph introduction should be included to give the general background. Discussion should be limited to the specific message, including the uses of the technique or equipment. Literature reviews and lengthy case reports are not appropriate.

Length. Maximum of five double-spaced, typewritten pages, including the references but not the title page or figure legends.

References. Maximum of eight.

Figures. Maximum of two, unless the text is shortened accordingly.

Tables and Acknowledgments. Not appropriate in technical notes.

Pictorial Essays

A pictorial essay is an article that conveys its message through illustrations and their legends. Unlike other *AJR* articles, which are based on original research, pictorial essays serve primarily as teaching tools, like exhibits at a scientific meeting. They are not encyclopedic book chapters. The abstract should be a short, introductory paragraph.

Length. Maximum of four double-spaced, typewritten pages, including the references but not the title page or figure legends.

References. Maximum of four.

Figures. Maximum of 30 figure *parts*. Number should be as few as necessary to convey the message of the paper.

Tables and Acknowledgments. Not appropriate in pictorial essays.

Letters to the Editor and Replies

Letters to the Editor and Replies should offer objective and constructive criticism of published articles. Letters may also discuss matters of general interest to radiologists. Do not end a letter with a hand-written signature.

Format. All letters should be typed double-spaced on nonletterhead paper, with no greeting or salutation. Name and affiliation should appear at the end of the letter. Titles for letters should be short and pertinent. The title for a reply is simply "Reply."

Length. Maximum of two double-spaced, typewritten pages, including references.

References. Maximum of four.

Figures. Maximum of two.

Tables and Acknowledgments. Not appropriate in Letters to the Editor and Replies.

Opinions, Commentaries, and Perspectives

Opinions, commentaries, and perspectives are special articles dealing with controversial topics or issues of special concern to radiologists.

Format. Include a title page but no abstract. Headings may be used to break up the text.

Length. Maximum of five double-spaced, typewritten pages.

References. Maximum of five.

Tables and Figures. Maximum of four.

Computer Page Articles

Articles published on the computer page deal with practical computer applications to radiology.

Format. Include a title page and an abstract.

Length. Maximum of eight double-spaced, typewritten pages.

References. Maximum of five.

Figures and Tables. Maximum of five. Computer printouts are not acceptable. Figures must be submitted as 5 × 7 in. glossy prints.

All submissions to the *AJR* must be accompanied by a completed copy of the Author's Checklist and the signed Copyright Agreement.

Increase your expertise in evaluating CNS lesions

AJNR
American Journal of Neuroradiology

Editor: **Michael S. Huckman, MD,** Rush-Presbyterian-St. Luke Medical Center

Outstanding clinical papers on every aspect of CNS imaging, including spinal diagnosis...informed coverage of head and neck radiology...clear, readable CTs, angiographs, MR imaging and ultrasound studies. These are the features you demand of a quality professional journal. You'll find them in every issue of **AJNR: American Journal of Neuroradiology.**

As you are called upon to perform and interpret more and more sophisticated diagnostic tests — from myelography to CT to newborn ultrasound studies — you need a comprehensive, reliable journal that can keep you abreast of all the latest developments. Each bimonthly issue of **AJNR** brings you timely, clinically pertinent information, as well as important clinical research presented with an eye toward immediate practical application.

Here's a brief sampling of the variety of articles you'll find in **AJNR:**

The Anatomic Basis of Vertebrogenic Pain and the Autonomic Syndrome Associated with Lumbar Disk Extrusion. *Jinkins JR, Whittemore AT, Bradley WG*

MR Imaging Determination of the Location of the Normal Conus Medullaris Throughout Childhood. *Wilson DA, Prince JR*

Closed Spinal Dysraphism: Analysis of Clinical, Radiological, and Surgical Findings in 104 Consecutive Patients. *Scatliff JH, Kendall BE, Kingsley DPE, Britton J, Grant DN, Hayward RD*

Alzheimer's Disease: Longitudinal CT Studies of Ventricular Change. *de Leon MJ, George AE, Reisberg B, et al*

Congenital Absence of the Cervical and Petrous Internal Carotid Artery with Intercavernous Anastomosis. *Quint DJ, Boulos RS, Spera TD*

Bimonthly
Personal $133/yr **Institutions** $160/yr
In-training $65/yr
(add $45.00 outside the US; in Canada, also add 7% GST.)

☎ ORDER FREE BY PHONE. Just call **1-800-638-6423** from anywhere in the US or Canada.

or clip and return coupon to:

Williams & Wilkins
P.O. Box 23291 Baltimore, Maryland 21203-9990

Subscribe to AJNR for 3 years and SAVE

Avoid future rate increases and ensure uninterrupted service by placing a multi-year subscription at current rates.

☐ 3 yrs ☐ 2 yrs ☐ 1 yr
☐ **Personal** $133 ☐ **Institutions** $160 ☐ **In-training*** $65
(add $45.00 outside the US; in Canada, also add 7% GST.)

☐ Also send me the **1991 Bound Volume** at $87.00 ($102.00 outside the US; in Canada, also add 7% GST). $2.00 discount for orders placed before October 31, 1991 and for prepaid orders. I understand that the bound volume is *in addition to* my regular subscription and is available only to subscribers. (To be shipped in early 1992. Bound volumes for years prior to 1991 are unavailable.) *All bound volume orders must be received by December 31, 1991.*

☐ Check enclosed (payable to Williams & Wilkins) ☐ Bill me
☐ VISA ☐ MasterCard ☐ American Express

Card # Exp.

Signature/P.O. #

Name

Address

City/State/Zip

MD residents, please add 5% sales tax. Subscription orders from outside the US must be prepaid in US dollars only. Rates valid through October 31, 1991.

**Residents, Fellows, Interns, and Students:* when applying for the in-training rate, available for 3 years, please specify name of institution and training status:

Please allow 8 weeks for order processing and delivery of your first issue. Surface mail delivery to countries outside the US may take up to 16 weeks. For surface air-lift (ISAL), add $38 in Europe and $49 in other areas of the world.

printed in USA

AJNR 52996

J1043S03

Review Article

Oriental Cholangiohepatitis: Pathologic, Clinical, and Radiologic Features

Jae Hoon Lim[1]

Oriental cholangiohepatitis, an endemic disease in Southeast Asia, is characterized by recurrent attacks of abdominal pain, fever, and jaundice. Pathologically, the intra- and extrahepatic ducts are dilated and contain soft, pigmented stone and pus. There is proliferation of bile ducts and infiltration of inflammatory cells along the periportal spaces and hepatic parenchyma. Localized intrahepatic segmental ductal stenosis may be present, especially in the lateral segment of the left lobe or posterior segment of the right hepatic lobe. The cause of the disease is not known, but associations with clonorchiasis, ascariasis, and nutritional deficiency have been suggested. Sonographic and CT findings include intra- or extrahepatic duct stones, dilatation of the extrahepatic duct with relatively mild or no dilatation of the intrahepatic ducts, localized dilatation of the lobar or segmental bile ducts, increased periportal echogenicity, segmental hepatic atrophy, and gallstones. Cholangiographic findings include bile duct stones; disproportionately severe dilatation of the extrahepatic ducts with mild or no dilatation of the intrahepatic ducts; and focal strictures, acute peripheral tapering, straightening, rigidity, decreased arborization, and an increased branching angle of the intrahepatic bile ducts.

Oriental cholangiohepatitis (OCH), also known as oriental cholangitis, recurrent pyogenic cholangitis, and intrahepatic pigmented stone disease, is characterized by recurrent attacks of fever, chills, abdominal pain, and jaundice [1–4]. Bile ducts are dilated or focally stenotic, harboring soft, pigmented stone or mud, and enteric bacteria can be cultured from the bile [1–3, 5]. The wall of the bile ducts is thickened by fibrosis and inflammatory cell infiltration. The disease is endemic to Southeast Asian countries [1–5], but sporadic cases have been reported in Europe [6] and South Africa [7]. The disease is now being encountered more often in western societies, especially in the United States and Canada, largely as a result of increased immigration from Asian countries [4, 5]. The purpose of this article is to review the sonographic, CT, and cholangiographic findings of OCH in light of the pathophysi-

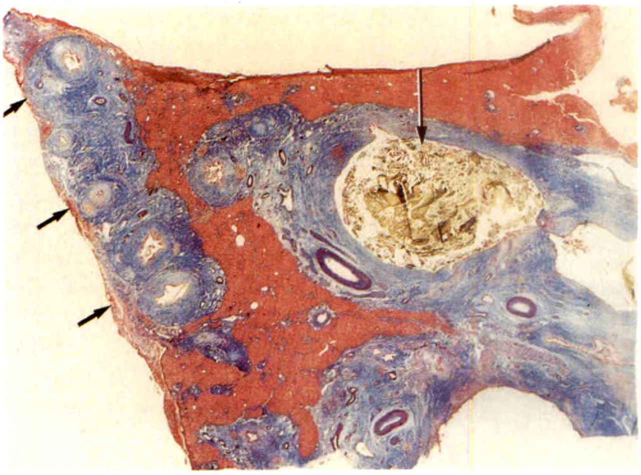

Fig. 1.—Microphotograph of resected liver specimen shows soft, pigmented stone (*long arrow*) in dilated medium-sized bile duct. Note also severe thickening of small bile ducts and periductal fibrosis (*short arrows*) obliterating lumen of bile ducts and encroaching on hepatic parenchyma. (Masson's trichrome stain, original magnification ×8)

Received December 26, 1990; accepted after revision February 14, 1991.

[1] Department of Diagnostic Radiology, Kyung Hee University Hospital, 1, Hoeki-dong, Dongdaemun-ku, Seoul 130-702, Korea. Address reprint requests to J. H. Lim.

***AJR* 157:1–8, July 1991** 0361–803X/91/1571–0001 © American Roentgen Ray Society

ology of the disease and to discuss the radiologist's role in the management of the disease.

Pathology

The primary pathologic changes are in the bile ducts. Histologically [1, 2, 8], there is proliferation of bile ducts, and inflammatory cells, mostly polymorphonuclear leukocytes, infiltrate from the portal tracts well into the hepatic parenchyma, accompanied by local hepatocellular necrosis. In more severe cases this inflammation undergoes suppuration. Fibrous tissue proliferates in the portal tracts, especially around the bile ducts (Figs. 1 and 2). The intrahepatic ducts frequently show dilatation and stricture and may contain pigmented stone (Fig. 1), pigmented mud, and debris and may shed epithelial cells, exudates, and sometimes frank pus. Liver changes are common and can be quite severe [2, 9]. The liver is usually enlarged and scarred, and capsular adhesions are evident. Occasionally, after multiple attacks, the liver becomes shrunken, especially the lateral segment of the left lobe. The papilla is usually hypertrophied [2], fibrosed, and rigid but patent, allowing passage of a large dilator without difficulty [9]. In some cases there is periampullary stricture due to fibrosis and passage of stone.

Dilatation of the extrahepatic ducts and large intrahepatic ducts such as the right and left hepatic ducts is observed in most patients (85–100%) [10, 11]. Dilatation of the intrahepatic biliary ducts tends to be disproportional, that is, central dilatation with rapid tapering toward the periphery [10]. The first and second divisions of the ducts are dilated, whereas the third and fourth divisions are not. The cause is not known, but periductal diffuse fibrosis may play a role (Fig. 2). This pattern of bile duct dilatation is quite different from the dilatation caused by obstruction. In obstruction, the intrahepatic bile ducts are dilated diffusely instead of rapidly tapering peripherally.

The dilatation of the extrahepatic duct generally is not related to the location of the stone [11]. Ducts both proximal and distal to the stone are dilated diffusely. Repeated passage of small pieces of stones through the sphincter of Oddi into the duodenum results in hypertrophy, ulceration, and stricture [2], and these changes may cause stenosis and proximal dilatation. However, localized stricture and resultant dilatation of the intrahepatic ducts are closely related to the location of stones. The left lateral segmental duct is affected earlier and more severely [2, 11, 12], followed by the posterior segmental duct of the right lobe [12]. This may be related to the more acute angulation of these ducts, resulting in less efficient drainage on this side of the biliary system [2, 12]. Stricture along the extrahepatic ducts is very unusual [2].

The bile duct stones encountered in western persons originate in the gallbladder and have the same chemical composition as gallstones [13]. On the other hand, the stones in patients with OCH originate in the bile ducts and are composed mostly of bile pigment with variable calcification. The stones are dark brown or black and vary in consistency from claylike, muddy material to concrete stones that are usually soft and friable [2, 3, 9]. There may be single or multiple stones. Multiple stones are scattered in the intra- or extrahepatic ducts or both. Occasionally the bile ducts are packed with stones.

Bile duct stones are present in about 75–80% of cases [2, 9]. In the remaining cases, the biliary tree is infected recurrently in the absence of stone. Gallstones are found frequently, and including the cases of previous cholecystectomy, gallstones are present in about 50–70% [10–12].

The reported prevalence of cholangiocarcinoma associated with OCH ranges from 2.4% to 5.0% [14, 15]. Chronic proliferative cholangitis in the presence of bile duct stones can undergo progressive changes to atypical epithelial hyperplasia, which may progress to cholangiocarcinoma [16]. To my knowledge there has been no report on an increased prevalence of hepatocellular carcinoma in patients with OCH.

Pathogenesis

Two theories have been advanced to explain the pathogenesis of OCH. Chronic infestation of the biliary tree with endemic parasites such as *Clonorchis sinensis* and *Ascaris lumbricoides* may induce ductal injury and strictures, leading to stone formation. Many patients with intrahepatic stone have evidence of clonorchiasis [1, 17, 18]. Evidence of infestation with *Ascaris* is observed in patients with OCH [7]. Microscopic sections of stones from extra- and intrahepatic bile ducts revealed evidence of *C. sinensis* (Fig. 3) and *A. lumbricoides* [1, 19]. As adult flukes or *Ascaris* eggs and desquamated epithelial cells block the intrahepatic ducts partially or completely, bile stasis is sure to follow [17]. Stagnation favors bacterial infection resulting in pyogenic cholangitis. When pyogenic infection occurs in the bile ducts, *C. sinensis* flukes are killed [17, 20]. Bile stasis and the presence of dead flukes and ova or their debris can form a nucleus (Fig. 3) for the formation of gallstones or bile duct stones [19], and this could instigate all the consequent pathologic processes, resulting in a cycle of repeated bouts of cholangitis and stone formation [3]. The formation of bilirubin stones may be attributed to bacterial deconjugation of bilirubin diglucuronoside

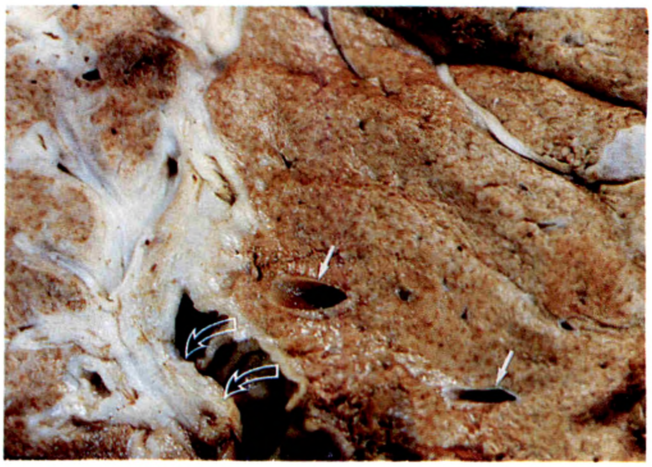

Fig. 2.—Cut surface of resected lateral segment of left hepatic lobe shows marked fibrous thickening of segmental bile duct (*open arrows*) and its tributaries. Hepatic veins (*solid arrows*).

with the formation of insoluble bilirubin during bouts of cholangitis [21].

Ong [2], however, found that patients with OCH had only a 5% higher rate of infestation with *C. sinensis* than did patients in general outpatient clinics. Large proportions of persons in endemic areas are infested with liver flukes without pyogenic cholangitis developing [8]. It was proposed that the primary cause was portal septicemia resulting from poor eating habits [2, 4]. Ong [2] believed infection reached the biliary tract from the portal vein: "The infection having reached the liver is excreted into the bile. Should there be obstruction by *C. sinensis*, tumor or stones, cholangitis would be the result." This theory was supported by animal experiments [8]. Bilirubinate stones may be formed in the liver as a result of an increase in deconjugation of bilirubin glucuronide by *Escherichia coli*, attributed to a net increase in β-glucuronidase activity. This arises when the intrahepatic environment is deficient in glucaric acid, a β-glucuronidase inhibitor that is lacking in a low-protein diet [22]. These two theories cannot explain the pathogenesis of OCH. Perhaps both factors play a role separately or synergistically.

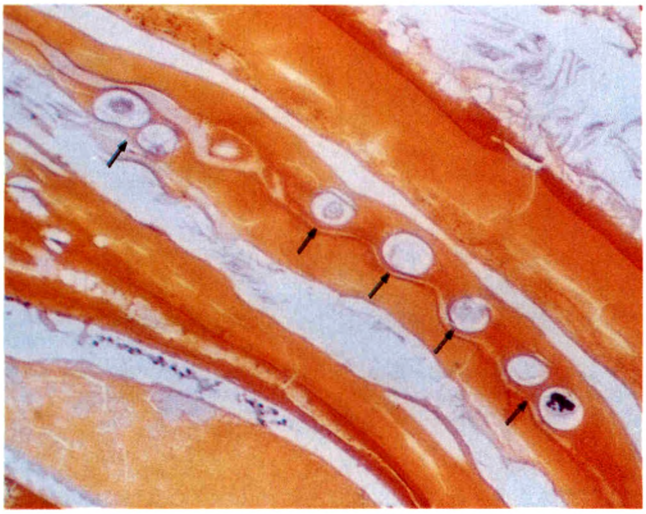

Fig. 3.—Microphotograph shows eggs of *Clonorchis sinensis* (*arrows*) embedded in pigmented stone. (H and E, original magnification ×100)

Clinical Manifestations

Men and women are affected almost equally [2, 9] and the highest number of cases occur in persons 20–40 years of age. There is a strong association with lower socioeconomic class. The symptoms are recurrent attacks and remissions of abdominal pain, nausea, vomiting often accompanied by fever, shaking chills, and jaundice. Visible jaundice is present in 77% of patients [2]. Physical examination reveals epigastric tenderness and rigidity and enlargement of the liver and gallbladder. Occasionally patients with severe disease such as sepsis present with shock and mental confusion.

Laboratory findings are leukocytosis, predominantly polymorphonuclear leukocytes; elevated levels of alkaline phosphatase; and excretion of urobilinogen in urine. Bile cultures yield *E. coli* or other enteric bacteria. The natural history of the disease is marked by recurrent attacks of cholangitis, usually once or twice a year [2, 9].

Many of the acute attacks respond to antibiotic treatment; many also require decompression of the biliary tree after control of the acute attack [2, 9], especially when there is a stone or stricture of bile ducts. OCH is a frequent reason for emergent surgery in the endemic areas. Recurrent disease is common postoperatively, especially when the operation does not include a drainage procedure [4, 23–25]. Even after surgery with drainage, stones and stricture return and the attacks of cholangitis recur sooner or later. In a study of 115 patients who had had surgery, 66 patients (57%) had residual intrahepatic stones [26]; biliary stricture caused the remnant stone in the majority of cases (81%).

Radiologic Findings

Radiologic assessment of the biliary tree is imperative if the correct preoperative evaluation is to be made regarding the need for and the type of surgery [4, 25]. Plain radiography is not helpful because the stones are rarely radiopaque [2, 6, 7, 12]. Oral cholecystography, IV cholangiography, and biliary scintigraphy are not useful [2, 27]: correct anatomic diagnosis cannot be made even if the biliary tract is visualized.

Fig. 4.—Sagittal sonogram shows dilatation of common bile duct containing three shadowing stones (*arrows*). Wall of common bile duct (D) is thick.

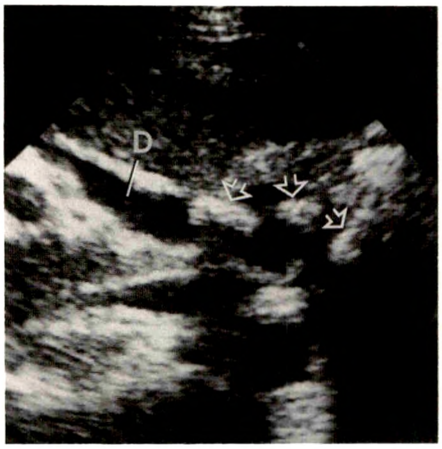

4

Fig. 5.—Transverse sonogram of liver shows a shadowing echogenic cast filling posterior segmental bile duct of right hepatic lobe (*arrows*).

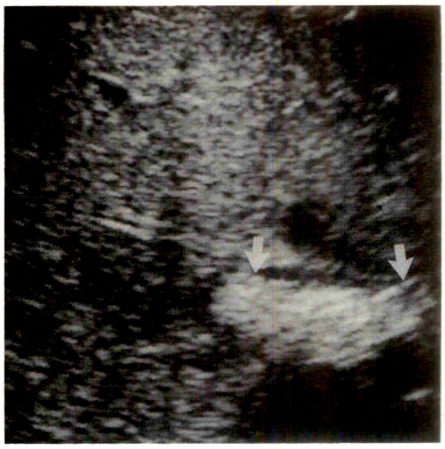

5

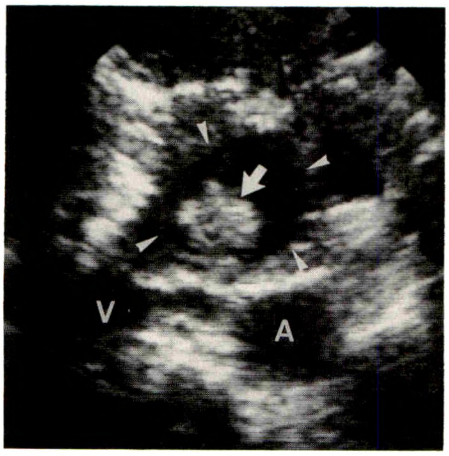

6

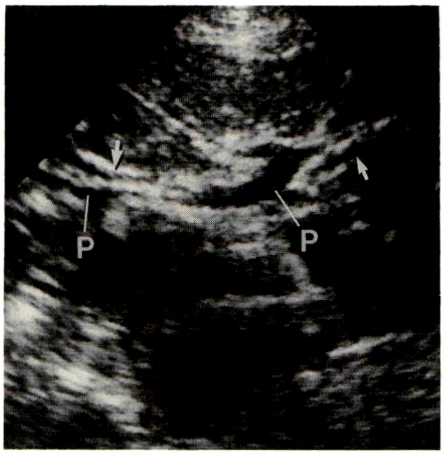

7

Fig. 6.—Transverse sonogram of common bile duct shows a round, nonshadowing stone (*arrow*). Proximal and distal portions of bile duct are dilated diffusely (*arrowheads*). A = abdominal aorta, V = inferior vena cava.

Fig. 7.—Transverse sonogram of left hepatic lobe shows thickening and increased echogenicity of walls of bile ducts (*arrows*) and umbilical portion of left portal vein (P).

Sonographic Findings

Sonography delineates bile duct dilatation in virtually all patients with OCH. The extrahepatic bile ducts are dilated in 85–100% of cases and the larger intrahepatic bile ducts are dilated in 66–79% of cases [10, 11]. Usually, the smaller intrahepatic bile ducts such as the tertiary or quaternary divisions proximal to the segmental bile ducts are dilated only slightly or not at all. In general, the dilatation of the extrahepatic duct is not related to the location of stone [11], although localized dilatation of the intrahepatic ducts is closely related to the location of stricture and stone lodgment, especially the lateral segmental ducts of the left hepatic lobe [11].

In a large proportion of patients with OCH (85–90%), a stone or stones can be detected with sonography [10, 11]. The stones may be in either the extrahepatic (Fig. 4) or intrahepatic (Fig. 5) ducts or both. In some cases, stones are only in the segmental bile ducts, such as the lateral segment of the left hepatic lobe or posterior segment of the right hepatic lobe (Fig. 5).

The stones may be more echogenic than the liver parenchyma and adjacent tissue or, less commonly, isoechoic. Some stones cast shadow and some do not, even in the same patient [10, 11]. In general, the intrahepatic stones are usually echogenic and shadowing (Fig. 5), whereas some extrahepatic stones (25%) do not cast shadow (Fig. 6). This may be due to the poor rate of detection of the intrahepatic stones, because hypoechoic intrahepatic stones without shadows can be missed on sonography.

The detectability of stones with sonography depends on the size, echogenicity, shadowing characteristics, and location of the stones [11, 28]. Biliary mud or isoechoic bile duct stones filling the biliary tree as a cast can be missed because sometimes they appear as soft-tissue masses and obscure visualization of intrahepatic ductal dilatation [10, 25, 29]. Biliary pneumatosis, as a result of prior choledochoenteric anastomoses or sphincter incompetency, obscures visualization of stone. A higher proportion of nonshadowing stones in the extrahepatic ducts can be detected compared with intrahepatic stones [10, 11]; this is because the duct is dilated, providing a larger space to enable the nonshadowing stone to be detected (Fig. 6).

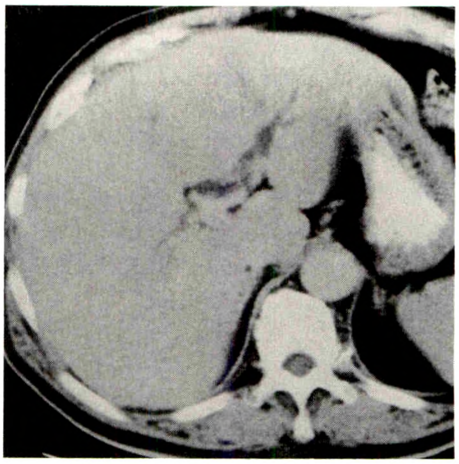

Fig. 8.—CT scan shows dilatation of central intrahepatic bile ducts around porta hepatis, with bile ducts tapering abruptly toward periphery.

Chau et al. [10] described prominent periportal echogenicity (Fig. 7) representing pericholangitis and periportal fibrous thickening in 30% of their cases. Gallstones are found frequently [10, 11]. Hepatic abscess or biloma complications in patients with OCH can be delineated on sonograms.

CT Findings

The optimal CT technique is enhanced scanning with a slice thickness of 5 mm and 2-mm interslice gap. Unenhanced scanning may be helpful in detecting stones. CT demonstrates the full extent of ductal dilatation [12]. Dilatation of the extrahepatic ducts is depicted clearly. Central, larger intrahepatic biliary dilatation; acute peripheral tapering; and nonvisualization toward the periphery of the liver give rise to the characteristic arrowhead appearance on contiguous sections (Fig. 8). There may be localized dilatation from obstruction by stricture (Fig. 9) or stone, such as that of lateral segmental ducts of the left hepatic lobe and posterior segmental ducts of the right hepatic lobe [12]. However, biliary strictures, which are usually short segments, are difficult to depict be-

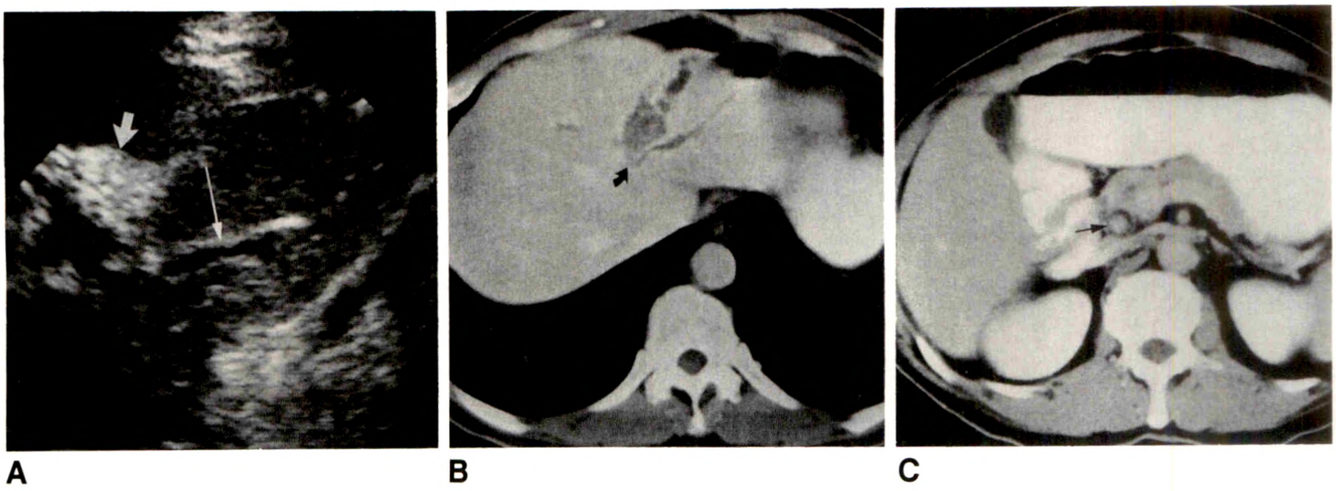

Fig. 9.—Multiple intrahepatic stones in lateral segment of left lobe and extrahepatic stone.

A, Transverse sonogram of epigastrium shows shadowing echogenic foci (*short arrow*). Note moderate dilatation of subsegmental bile duct with thick wall (*long arrow*).

B, CT scan of liver shows localized severe dilatation of lateral segmental bile duct of left hepatic lobe due to localized stricture (*arrow*). Multiple tiny high-density areas within dilated duct represent small stones that might have been overlooked on basis of CT alone. Wall of dilated bile ducts is enhanced.

C, CT scan at level of pancreatic head shows small, round, calcified stone (*arrow*) within dilated intrapancreatic common bile duct.

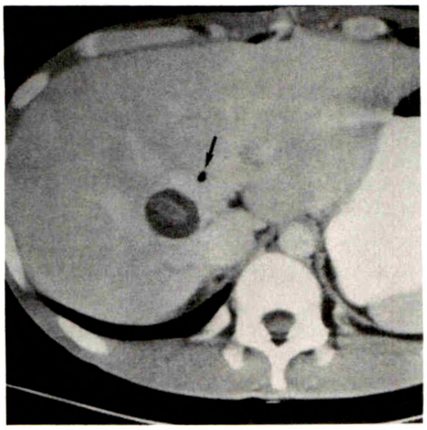

Fig. 10.—CT scan shows cystically dilated bile duct containing stone. Wall of dilated bile duct is enhanced. Biliary pneumatosis (*arrow*). The patient had had a cholecystectomy.

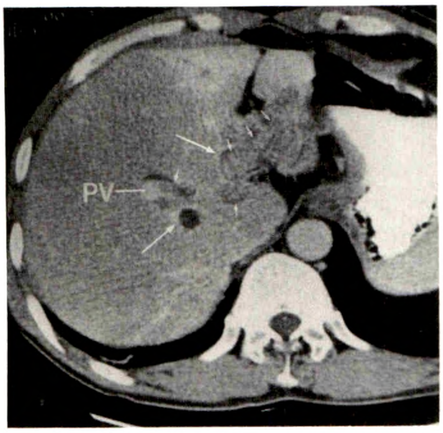

Fig. 11.—Enhanced CT scan shows homogeneous enhancement of left lobe of liver. Walls of bile ducts are enhanced (*long arrows*). Intrahepatic stones (*short arrows*) have same attenuation as liver. PV = right branch of portal vein.

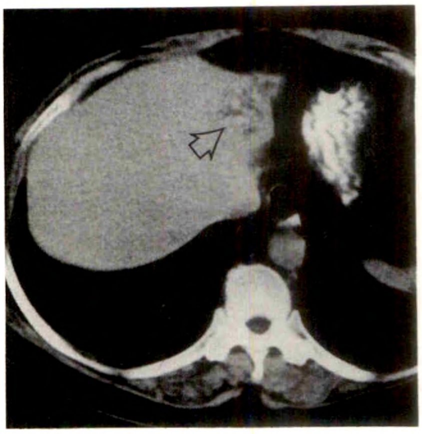

Fig. 12.—CT scan shows severe atrophy of lateral segment of left hepatic lobe harboring small calcific stones (*open arrow*).

cause of partial-volume averaging. Sometimes, dilatation may be fusiform or cystic (Fig. 10). The wall of the bile ducts may enhance on CT scans obtained with contrast material (Figs. 9 and 10), especially during an acute cholangitic episode [12].

The stones can be depicted with CT, but the detection rate (63–81%) is generally not as good as that of sonography [6, 30]. It has been stated that unlike cholesterol stones, which may be isodense with bile, pigmented stones are hyperdense on CT (Fig. 9C) because of their variable content of calcium salts, heavy metals, and other inorganic components [29, 30]. However, bile duct stones are sometimes not sufficiently hyperdense to be visualized on CT (Fig. 11). Often the stones are hypodense, and thus it is impossible to distinguish stones from bile or pus in the dilated duct [30]. Isodense stones that completely fill the ducts within the hepatic parenchyma (Fig. 11) could easily be missed on CT; in these patients, even the dilated bile ducts are difficult to recognize. Chan et al. [12] described both unenhanced and enhanced scans as desirable because stones are detected more easily on unenhanced scans, and enhanced CT scans are better in the detection of subtle intrahepatic biliary dilatation.

In addition to the ductal change and detection of stones, parenchymal loss and segmental atrophy (Fig. 12) can be correctly assessed with CT [12]. During the stage of acute exacerbation, persistent segmental or lobar parenchymal enhancement can be observed (Fig. 11), suggesting diffuse parenchymal inflammation or microabscess [12]. Frank hepatic abscess or biloma can be delineated.

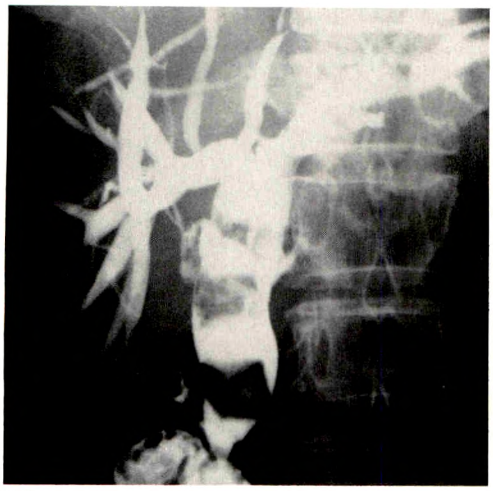

13

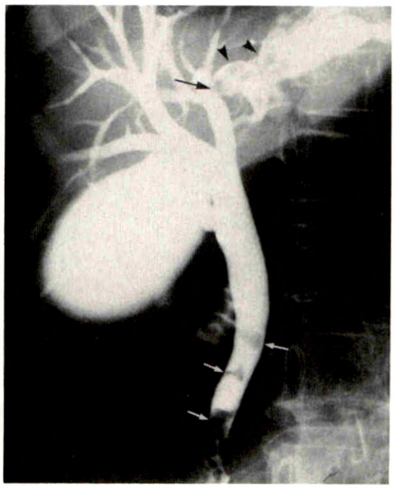

14

Fig. 13.—Endoscopic retrograde cholangiogram shows three stones with facets. Extrahepatic ducts are markedly dilated. Right and left hepatic ducts and their first divisions are moderately dilated but more peripheral ducts taper abruptly. Intrahepatic bile ducts show straightening and rigidity, right angle branching pattern, decrease in arborization, and acute peripheral tapering. (Reprinted from Lim et al. [11].)

Fig. 14.—Endoscopic retrograde cholangiogram shows mild dilatation of extra- and intrahepatic bile ducts with abrupt peripheral tapering, straightening, and increased angle of branching. Three small faceted stones are seen in common bile duct (*white arrows*). Lateral segmental bile duct of left hepatic lobe is diffusely dilated and harbors multiple filling defects of stones (*arrowheads*). Note mild stricture at junction (*black arrow*) of lateral segmental duct and left lobar ducts.

Cholangiographic Findings

Direct cholangiography, such as endoscopic retrograde cholangiography, percutaneous transhepatic cholangiography, operative cholangiography, and T-tube cholangiography, demonstrates the full spectrum of ductal changes and stones in patients with OCH (Fig. 13). Abnormal findings include disproportionately severe dilatation of the extrahepatic ducts with mild or no dilatation of the intrahepatic ducts and acute tapering, straightening, rigidity, increased or right-angle branching pattern, multiple focal strictures, and decrease in arborization [31–35]. These abnormalities are due to fibrosis and scarring of bile ducts [5]. Biliary duct dilatation is segmental or subsegmental [31] when there is stricture of intrahepatic bile ducts or obstruction by impacted stone (Fig. 14). Stricture of the extrahepatic bile ducts may occur, but this is unusual. Rarely, the segmental or subsegmental bile ducts dilate cystically because of persistent obstruction, resultant inflammation, and loss of the elasticity of the ducts.

Stones produce negative filling defects in the opacified bile ducts (Figs. 13 and 14). When the stones completely obstruct the orifice of the segmental or subsegmental bile ducts (missing duct sign), the stone cannot be detected (Fig. 15). Similarly, when there is a stricture at the segmental or subsegmental bile ducts, proximal bile ducts cannot be opacified, leading to an erroneous interpretation of no ductal stone or stricture [27]. A few patients (15–25%) have no stones, or stones pass spontaneously [2]; in these patients, the characteristic pattern of the biliary tree will lead to the correct diagnosis [35].

Differential Diagnosis

From the radiologic point of view, OCH is characterized by the presence of stone(s), dilatation of the extrahepatic ducts, large intrahepatic bile ducts with acute peripheral tapering, and thickening of the wall of bile ducts. Knowing these features, radiologic differentiation from other diseases of the bile ducts can be possible. In western patients, the differential diagnosis between gallstones passed into the extrahepatic duct and OCH is very difficult. The stone passed only into the extrahepatic duct from the gallbladder usually will result in dilatation mainly proximal to the stone [34], whereas in OCH the extrahepatic ducts both proximal and distal to the stone are dilated diffusely regardless of the level of the stone [33, 35].

Clonorchiasis, another prevalent infestational disease in the same endemic areas, causes diffuse dilatation of the intrahepatic bile ducts with no or minimal dilatation of the large bile ducts; these changes are easily recognizable on sonography [18], CT [36], and cholangiography [37, 38]. Periductal changes are encountered in both diseases, but are much more severe in clonorchiasis. Stones and flukes of *C. sinensis* can be differentiated easily.

In biliary obstruction by malignant tumors along the bile ducts, including cholangiocarcinoma and cancer of the pancreas or ampulla of Vater, the entire biliary tree proximal to the mass is dilated, including peripheral intrahepatic bile ducts, and an obstructing mass can be detected [1, 18, 38].

Sclerosing cholangitis may show bile duct dilatation and thickening of all of the bile ducts, but dilatation is focal and discontinuous, sometimes having a beaded appearance and serpiginous course [39].

Caroli disease is a developmental anomaly in which there is segmental saccular dilatation of the intrahepatic ducts. This results in stasis, cholangitis, liver abscess, and stone formation. The clinical picture is similar to that of OCH, but it occurs in a younger age group. Differentiation is possible by noting the dilated saccules in the intrahepatic bile ducts [40, 41].

Relative Roles of Imaging Tests

Sonographic evaluation of extrahepatic bile duct dilatation is easy, although duodenal gas sometimes hinders the visualization of the whole segment, especially the distal common bile duct. Most intra- and extrahepatic stones are recognized easily. However, those stones that do not cast an acoustic shadow are difficult to recognize unless corresponding ducts

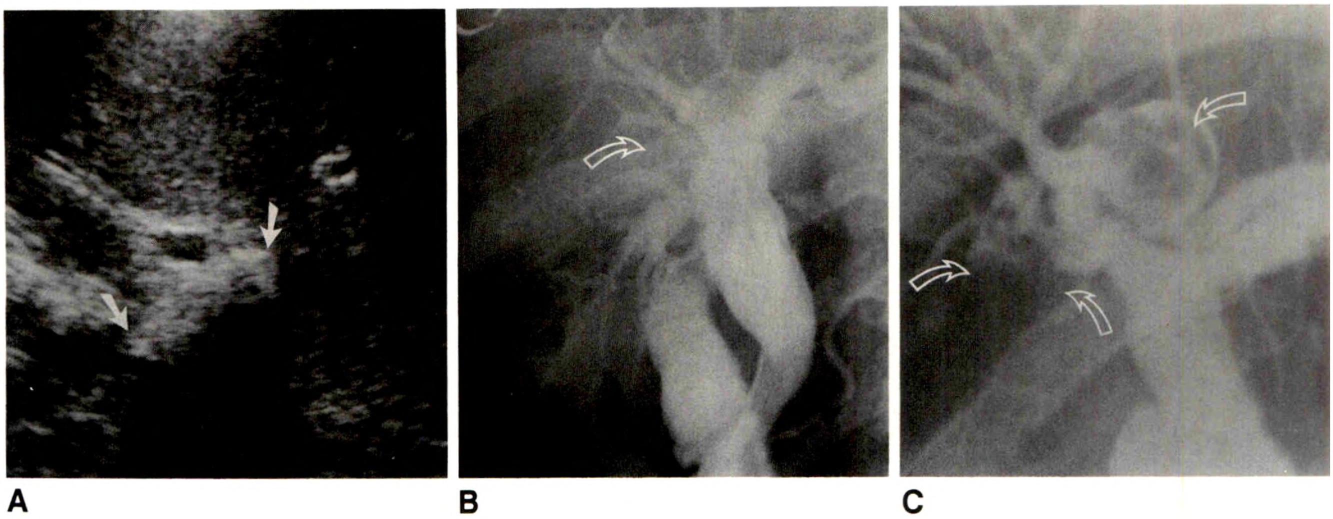

Fig. 15.—Remnant stone after surgical removal of some stones.

***A*, Sonogram of right hepatic lobe discloses a bandlike shadowing stone (*arrows*) filling posterior segmental bile duct.**

***B*, During surgery, several small pigmented stones were removed. Operative cholangiogram does not show any stone in biliary tree. Retrospective review suggests an area is devoid of bile ducts (missing duct sign, *arrow*) in lateral part of right hepatic lobe.**

***C*, T-tube cholangiogram discloses large stones packing markedly dilated posterior segmental duct of right hepatic lobe (*arrows*). Note hairpin turn o posterior segmental duct joining right hepatic duct.**

are markedly dilated [10, 11]. Bile duct stricture cannot be demonstrated easily. In the presence of biliary pneumatosis, bile ducts and stones are difficult to assess [25, 29].

CT demonstrates the full extent of ductal abnormality [12]. Biliary dilatation and isolated segmental or subsegmental biliary dilatation can be recognized easily. However, it is relatively insensitive in depicting stones. Pneumatosis, parenchymal enhancement, and segmental atrophy can be assessed by CT. However, biliary strictures, which usually are less than 1 cm long or are diaphragmlike, and ductal wall irregularities often are not diagnosed with CT [12].

Cholangiography is straightforward, as it directly delineates the biliary tree, including stones and strictures. However, sometimes it is difficult to visualize the whole biliary tree, especially when there is technical failure in the opacification of the whole biliary tree or obstruction due to ductal stricture or impaction of stones, leading to an erroneous normal interpretation.

Sonography should be the main technique used for screening and diagnosis in suspected OCH [10–12, 27, 29]. CT is not a screening procedure, but it is recommended when sectional imaging is mandatory but sonography is not confirmative or is equivocal, when space-occupying lesions complicate OCH, when hepatic resection is planned, and when imaging guidance is needed for complex drainage procedures or formation of safe access to an anastomotic loop of a bowel [12]. Direct cholangiography, although invasive, is mandatory as a “road map” in patients undergoing surgical intervention, because the exact location and number of stones and bile duct strictures must be assessed preoperatively [6]. Cholangiography is necessary for the detection of residual stones after surgery, assessment of biliary stricture and choledochoenteric fistulas, and preprocedural biliary intervention [25, 26].

Role of Interventional Radiology in the Management of Bile Duct Stones

Surgery used to remove stones after acute cholangitis i controlled [2, 9]. At surgery, an internal drainage procedur usually is essential [23–25]. In emergent cases with increase risk of surgical mortality, biliary decompression with a percutaneous catheter is the procedure of choice.

There are several nonsurgical means of treating bile duc stones and stricture. Flexible choledochoscopy and endoscopic papillotomy [42] have been used to remove postoperative residual stones. Recently, percutaneous removal o stones by basketing through a steerable catheter and balloo dilatation of stricture have been tried, and results were partially successful [25, 26, 43].

Extracorporeal shock-wave biliary lithotripsy is a recognized method for treating bile duct stones when other methods have failed; its success rate has been as high as 93 [44–46]. The technique may be useful as an adjunct t percutaneous radiologic technique. Nothing is perfect in th management of bile duct stones in OCH, as was noted b vanSonnenberg et al. [25]: “While surgical and radiologic techniques are jointly beneficial, the ultimate panacea for OC may be medical control of biliary lithogenic factors.”

ACKNOWLEDGMENTS

I thank my colleagues in our department for collection of cas material; Yong Koo Park, Department of Anatomic Pathology, Kyun Hee University Hospital, for preparation of specimens and microphotographs; and Sung Sook Won for secretarial assistance in manuscript preparation.

REFERENCES

1. Cook J, Hou PC, Ho HC, McFadzean AJS. Recurrent pyogenic cholangitis. *Br J Surg* **1954**;42:188-203
2. Ong GB. A study of recurrent pyogenic cholangitis. *Arch Surg* **1962**;84:199-225
3. Seel DJ, Park YK. Oriental infestational cholangitis. *Am J Surg* **1983**;146:188-203
4. Carmona RH, Crass RA, Lim RC, Trunkey DD. Oriental cholangitis. *Am J Surg* **1984**;148:117-124
5. Ho CS, Wesson DE. Recurrent pyogenic cholangitis in Chinese immigrants. *AJR* **1974**;122:368-374
6. Menu Y, Lorphelin J-M, Scherrer A, Grenier P, Nahum H. Sonographic and computed tomographic evaluation of intrahepatic calculi. *AJR* **1985**;145:579-583
7. Schulman A. Non-Western pattern of biliary stones and the role of ascariasis. *Radiology* **1987**;162:425-430
8. Chou ST, Chan CW. Recurrent pyogenic cholangitis: a necropsy study. *Pathology* **1980**;12:415-428
9. Kalser MH, Block MA. Cholangitis. In: Berk JE, ed. *Bockus gastroenterology*, 4th ed. Philadelphia: Saunders, **1985**:3721-3723
10. Chau EMT, Leong LY, Chan FL. Recurrent pyogenic cholangitis: ultrasound evaluation compared with endoscopic retrogade cholangiopancreatography. *Clin Radiol* **1987**;38:79-85
11. Lim JH, Ko YT, Lee DH, Hong KS. Oriental cholangiohepatitis: sonographic findings in 48 cases. *AJR* **1990**;155:511-514
12. Chan F-L, Man S-W, Leong LLY, Fan S-T. Evaluation of recurrent pyogenic cholangitis with CT: analysis of 50 patients. *Radiology* **1989**;170:165-169
13. Kalser MH, Schoenfield LJ, Marks JW, Tompkins RK. Cholelithiasis. In: Berk JE, ed. *Bockus gastroenterology*, 4th ed. Philadelphia: Saunders, **1985**:3619-3624
14. Koge A, Ichimiya H, Yamaguchi K, Miyazaki K, Nakayama F. Hepatolithiasis associated with cholangiocarcinoma. Possible etiologic significance. *Cancer* **1985**;55:2826-2829
15. Chen M-F, Jan Y-Y, Wang C-S, Jeng L-B B, Hwang T-L, Chen S-C. Intrahepatic stones associated with cholangiocarcinoma. *Am J Gastroenterol* **1989**;84:391-395
16. Nakanuma Y, Terada T, Tanaka Y, Ohta G. Are hepatolithiasis and cholangiocarcinoma aetiologically related? *Virchows Arch [A]* **1985**;406:48-58
17. Ho PC. The pathology of *Clonorchis sinensis* infestation of the liver. *J Pathol* **1955**;70:53-64
18. Lim JH, Ko YT, Lee DH, Kim SY. Clonorchiasis: sonographic findings in 59 proved cases. *AJR* **1989**;152:761-764
19. Teoh TB. A study of gallstones and included worms in recurrent pyogenic cholangitis. *J Pathol* **1963**;86:123-129
20. Rim HJ. The current pathobiology and chemotherapy of clonorchiasis. *Korean J Parasitol* **1986**;24[suppl]:7-20
21. Flavell DJ. Liver-fluke infection as an aetiological factor in bile duct carcinoma of man. *Trans R Soc Trop Med Hyg* **1981**;75:814-824
22. Matsushiro T, Suzuki N, Sato T, Mark T. Effect of diet on glucaric acid concentration in bile and the formation of calcium bilirubinate gallstones. *Gastroenterology* **1977**;72:630-633
23. Wen CC, Lee HC. Intrahepatic stones: a clinical study. *Ann Surg* **1972**;175:166-176
24. Chang TM, Passaro E. Intrahepatic stones: the Taiwan experience. *Am J Surg* **1983**;146:241-244
25. vanSonnenberg E, Casola G, Cubberley DA, et al. Oriental cholangiohepatitis: diagnostic imaging and interventional management. *AJR* **1986**;146:327-331
26. Park JH, Choi BI, Han MC, Sung KB, Choo IW, Kim C-W. Percutaneous removal of residual intrahepatic stones. *Radiology* **1987**;163:619-623
27. Ralls PW, Colletti PM, Quinn MF, Lapin SA, Morris UL, Halls J. Sonography in recurrent oriental pyogenic cholangitis. *AJR* **1981**;136:1010-1012
28. Lee JT, Yoo HS, Kim KW, Lee DY, Lee YH, Suh JH. The capability of realtime ultrasound in the detection of the biliary tract stones. *J Korean Soc Med Ultrasound* **1986**;5:33-40
29. Federle MP, Cello JP, Laing FC, Jeffrey RB. Recurrent pyogenic cholangitis in Asian immigrants. *Radiology* **1982**;143:151-156
30. Itai Y, Araki T, Furui S, Tasaka A, Atomi Y, Kuroda A. Computed tomography and ultrasound in the diagnosis of intrahepatic calculi. *Radiology* **1980**;136:399-405
31. Wastie ML, Cunningham IGE. Roentgenologic findings in recurrent pyogenic cholangitis. *AJR* **1973**;119:71-77
32. Lam SK, Wong KP, Chan PKW, Ngan H, Ong GB. Recurrent pyogenic cholangitis: a study by endoscopic retrograde cholangiography. *Gastroenterology* **1978**;74:1196-1203
33. Lim JH, Yoon YK, Kim SY, Min YI. Endoscopic retrograde cholangiographic findings in choledocholithiasis. *J Korean Radiol Soc* **1982**;18:116-124
34. Letourneau JH, Thompson WM. Intraoperative and postoperative cholangiography. *Semin Ultrasound* **1987**;8:126-133
35. Hong KS, Lim JH, Ko YT, Lee DH. Endoscopic retrograde cholangiography in recurrent pyogenic cholangitis. *J Korean Radiol Soc* **1990**;26:117-120
36. Choi BI, Kim HJ, Han MC, Do YS, Han MH, Lee SH. CT findings of clonorchiasis. *AJR* **1989**;152:281-284
37. Choi TK, Wong KP, Wong J. Cholangiographic appearance in clonorchiasis. *Br J Radiol* **1984**;57:681-684
38. Lim JH. Radiologic findings of clonorchiasis. *AJR* **1990**;155:1001-1008
39. Ferrucci JT, Adson MA, Mueller PR, Stanley RJ, Stewart ET. Advances in the radiology of jaundice: a symposium and review. *AJR* **1983**;141:1-20
40. Mittelstaedt CA, Volverg FM, Fischer GJ, McCartney WH. Caroli's disease: sonographic findings. *AJR* **1980**;134:585-587
41. Mujahed Z, Glenn F, Evans JA. Communicating cavernous ectasia of intrahepatic ducts (Caroli's disease). *AJR* **1971**;113:21-26
42. Vaira D, D'Anna L, Ainley C, et al. Endoscopic sphincterotomy in 1000 consecutive patients. *Lancet* **1989**;2:431-433
43. Kerlan RK Jr, Progany C, Goldberg HI, Ring EJ. Radiologic intervention in Oriental cholangiohepatitis. *AJR* **1985**;145:809-813
44. Lee SH, Fache JS, Burhenne HJ. The value of extracorporeal shock-wave lithotripsy in the management of bile duct stones. *AJR* **1990**;155:775-779
45. Moody FG, Amerson JR, Berci G, et al. Lithotripsy for bile duct stones. *Am J Surg* **1989**;158:241-247
46. Choi BI, Han JK, Park YH, Yoon YB, Han MC, Kim C-W. Piezoelectric lithotripsy combined with stone extraction in the management of retained intrahepatic stones. *Radiology* **1991**;178:105-108

Right and Left Ventricular Stroke Volume Measurements with Velocity-Encoded Cine MR Imaging: In Vitro and In Vivo Validation

Chisato Kondo[1]
Gary R. Caputo[1]
Richard Semelka[1]
Elyse Foster[2]
Ann Shimakawa[3]
Charles B. Higgins[1]

The accuracy of measurements of flow velocity determined by using cine MR phase velocity mapping—velocity-encoded cine (VEC) MR—was assessed by comparing VEC MR data with independent measurements in a flow phantom and in human subjects. Constant flow velocities generated in a phantom (range, 20–408 cm/sec) were determined correctly by VEC MR (r = .997, standard error of the estimate [SEE] = 7.9 cm/sec). Peak systolic velocities in the main pulmonary artery determined by VEC MR correlated well with the measurements obtained by using continuous-wave Doppler echocardiography (r = .91). Stroke volumes measured at the aorta by VEC MR and continuous-wave Doppler imaging also correlated well with each other (r = .80). VEC MR measurements of aortic and pulmonary flow provided left and right ventricular stroke volumes that correlated well with left ventricular stroke volumes determined by short-axis cine MR images (r = .98, SEE = 3.7 ml, and r = .95, SEE = 4.8 ml, respectively). Intra- and interobserver variabilities were small for both left and right ventricular stroke volumes as measured with VEC MR.

These results indicate that VEC MR accurately and reproducibly measures aortic and pulmonary flow velocities and volumes in the physiologic range of humans, and can be used to measure right and left ventricular stroke volumes under normal flow conditions.

***AJR* 157:9–16, July 1991**

Several methods [1–20] have been developed for measuring blood flow velocity with MR that should augment the application of MR for the evaluation of cardiovascular diseases. All MR flow techniques are classified into two major categories: time-of-flight techniques [2–4] and phase-modulation techniques [5–20]. In the phase-modulation techniques, phase velocity mapping [7–16] provides two-dimensional velocity maps of blood flow in a vascular cross section. Accordingly, the volume of blood flow is derived from the product of vascular cross-sectional area and flow velocity. The phase techniques also can be combined with gradient-echo cine imaging sequences and, consequently, provide velocity maps with high temporal resolution. This technique is called velocity-encoded cine (VEC) MR [9–13]. When it is used pulsatile flow can be segmented into many time frames throughout the cardiac cycle, and flow velocity at each frame is determined.

Stroke volume ejected from the left or right ventricle can be determined from time-integrated measurements of flow volume in the ascending aorta or pulmonary artery by using VEC MR. A noninvasive method for measuring biventricular stroke volume could be useful for monitoring global function of the two ventricles, measuring left-to-right shunts, and measuring regurgitant volume. The accuracy of flow measurement depends mainly on the following two factors: measurements of flow velocity and vascular cross-sectional area. Theoretically, the accuracy of velocity quantification with phase techniques may be influenced by the magnitude of velocity and higher-order derivatives of position, such as acceleration or jerk [7, 9]. Previous studies of phase-mapping methods have shown the accuracy of measuring constant flow velocity generated in a phantom [14–16]. However, the

Received November 2, 1990; accepted after revision January 25, 1991.

[1] Department of Radiology, University of California Medical Center, San Francisco, CA 94143. Address reprint requests to C. B. Higgins.

[2] Department of Cardiology, University of California Medical Center, San Francisco, CA 94143.

[3] General Electric Medical Systems, Milwaukee, WI 53201.

0361–803X/91/1571–0009
© American Roentgen Ray Society

ranges of velocities examined in these phantom studies were low compared with the velocity encountered in human physiologic states. Moreover, it has not been established if velocity of pulsatile flow can be measured accurately with phase techniques. The impact of flow turbulence, magnitude of velocity, and pulsatile flow pattern on the accuracy of velocity quantification with phase techniques has not been elucidated. Because this method may be useful for simultaneous measurement of stroke volumes in the right and left ventricles, it is necessary to define the accuracy of measurements of velocity and volume in humans and to determine that stroke volumes are equivalent for the two ventricles in normal subjects.

Accordingly, the current study was intended to validate VEC MR through the following studies: VEC MR measurements of constant flow velocities in phantoms, with velocities corresponding to the normal physiologic ranges existing in humans; comparison of pulsatile flow velocities in the main pulmonary artery and aorta determined in control subjects by using VEC MR and Doppler echocardiography; and flow volume in the aorta and pulmonary artery obtained in normal subjects by using VEC MR with measurements of volume determined by cine MR ventricular volume and with each other.

Materials, Subjects, and Methods

Sequences of Cine MR and VEC MR

An MR imager operating at 1.5 T (General Electric, Milwaukee, WI) was used for both in vitro and in vivo studies. For cine MR quantification of left ventricular volume, images were obtained in the cardiac short-axis plane, determined by double oblique angulation by using a flip angle of 30°, a TE of 5 msec, a TR of 20 msec, and a slice thickness of 10 mm, resulting in more than 16 time frames per cardiac cycle. The images were acquired by using a 128 × 256 matrix with a 32-cm field of view and displayed on a 256 × 256 matrix.

VEC MR was performed by using a flip angle of 30°, a TE of 13 msec, and a TR of 27 msec. Slice thickness, matrix size, field of view, and ECG gating were the same as for cine MR. Reconstruction of VEC data provides both a magnitude image (anatomic image) and a phase image (velocity mapping in the selected direction).

VEC MR was performed by using a bipolar gradient pulse to modulate the phase of proton spins [5, 6]. In order to eliminate the phase shifts introduced by field nonuniformities and chemical-shift phenomena, each acquisition consisted of two interleaved cine experiments (Fig. 1). The two experiments were performed under different flow-encoding gradients along the same direction. Velocity encoding could be selected by the operator in either the slice-select, phase-encoded, or frequency-encoded direction. Subtraction of phase data of one experiment from those of the other resulted in cancellation of all phase shifts except those due to flow along a velocity-encoded direction. The phase difference between the two experiments is proportional to the velocity of flow in the velocity-encoded direction:

$$\Delta \text{ Phase} = g \times M \times \text{velocity},$$

where g is a gyromagnetic ratio and M is the change in gradient moment in the two experiments. If the gradients of the two experiments are chosen so as to keep the phase shift less than 180° to avoid aliasing, the velocity component along the velocity-encoded direction can be determined directly from the phase difference and M. The *peak velocity*, which is the predicted highest velocity to be encoded, was selected by the operator before each acquisition over the range between +10 and −10 m/sec. If the actual maximum velocity exceeds the peak velocity selected by the operator, aliasing occurs, with resultant underestimation of the true maximum velocity. Of note, the current pulse sequences used mirror-image rephasing bipolar pulse gradients in the slice-select and read-out directions. These two sets of bipolar gradients were combined and formed three-lobed gradients (Fig. 1) [21]. These three-lobed gradients are effective in reducing signal loss caused by intravoxel spin-phase differences due to first-order derivatives of spin position [9, 22, 23].

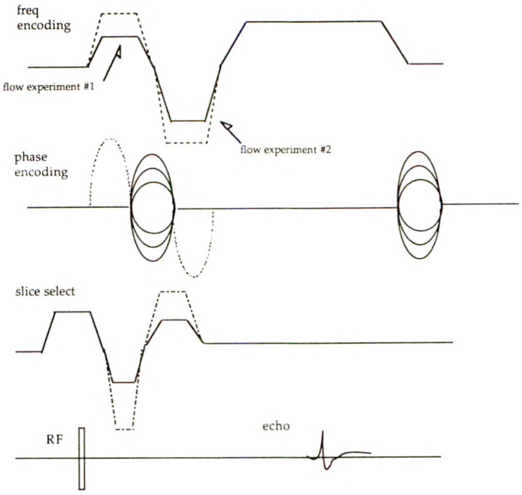

Fig. 1.—Pulse sequence diagram for velocity-encoded cine MR. Each acquisition consisted of two interleaved cine experiments. The two experiments were performed by using different flow-encoding gradients along same direction. *Broken lines* represent flow-encoding gradients. Note that only one gradient axis will vary its flow-encoding gradients during a scan. Rephasing gradients were used in slice-select and read-out directions. freq = frequency.

Flow Phantom Experiments

A flow phantom consisted of a tube 6 mm in internal diameter and water as the circulating fluid. Steady flow was generated by an electric pump in the velocity range of 20-408 cm/sec. Flow rates were measured repeatedly immediately before and after each experiment by timing the filling of a 1000- or 5000-ml cylinder. Cross sections of the flow phantom were imaged with flow encoding in the slice-select direction (Fig. 2). Circular regions of interest were used for measurements. The size of the region of interest was set close to the actual cross-sectional area of the tube. Mean flow velocities ranging from 20 to 408 cm/sec were chosen so as to cover the human physiologic range of the aortic or pulmonary flow velocity [24]. The directly determined velocities were compared with the velocities determined by VEC MR. The degree of flow turbulence for different velocities used in the phantom was determined by calculation of the Reynolds number: Reynolds number = rVd/m, where r and m are the density and kinetic viscosity of the fluid, respectively, and V (cm/sec) and d (cm) are the velocity of the flow and diameter of the tube, respectively. For water, $r = 1.0 \text{ g/cm}^3$ and $m = 0.01 \text{ g} \cdot \text{cm}^{-1} \cdot \text{sec}^{-1}$.

Subjects

After giving informed consent, 12 volunteers 21–56 years old with no history of cardiac disease were examined. These 12 subjects

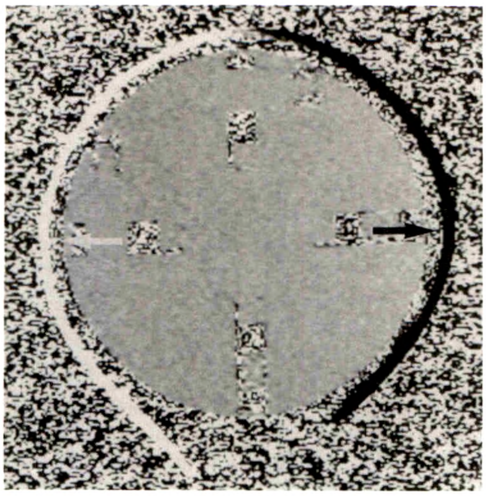

Fig. 2.—Coronal MR image of a flow phantom with a velocity-encoded phase reconstruction. Velocity was encoded along a frequency-encoded direction (vertical axis on image). Black signal indicates a flow direction from bottom to top on image; white one indicates flow in opposite direction. Transverse phase image of same phantom with velocity encoded along a slice-select direction was used for velocity measurements. *Arrows* indicate position of transverse slice.

underwent cine and VEC MR studies sequentially on the same day. Six of the 12 also underwent Doppler echocardiography within 2 weeks of the cine and VEC MR studies.

Left Ventricular Stroke Volume with Cine MR

After short-axis tomograms encompassing the entire left ventricle were obtained, end-diastolic and end-systolic time frames were defined as the largest and smallest areas of the blood pool, respectively, on each slice. Because the window and level settings can be critical for visual edge detection, the window width setting on the display was standardized to the difference of the signal intensities between the myocardium and blood pool. The level of the display was set as [(0.25 × window width) + myocardial signal intensity]. Left ventricular volumes were calculated by adding chamber cross-sectional areas multiplied by slice thickness. Left ventricular stroke volume was obtained as the difference between end-diastolic and end-systolic volumes.

Quantification of Left and Right Ventricular Stroke Volumes with VEC MR

Measurements of both aortic and pulmonary blood flow values were measured on two separate axial scans by using VEC MR. The slice level for aortic flow measurements was determined as the level of the center of the main pulmonary artery defined on oblique sagittal images. The direction of velocity encoding was selected along the slice-select gradient. The predicted peak velocity was set as 150 or 175 cm/sec. The ascending aorta was identified on each time-frame magnitude image, and its area was defined manually by using a circular region of interest (Fig. 3). The same region of interest was applied to the corresponding phase image, and the average pixel value in the region was measured. Because the pixel values on the phase image are directly proportional to flow velocity, the product of the cross-sectional area and average pixel value yielded the instantaneous flow volume for each frame. Stroke volume through the ascending aorta was obtained by summation of instantaneous flow volume for all frames throughout the cardiac cycle (Fig. 4).

Pulmonary flow was determined in a similar manner. The location of axial slices for measurements of pulmonary flow was determined to cross a reference point defined as 10–15 mm above the center of the pulmonary valve on oblique sagittal images. Thereafter, the line sectioning the pulmonary artery perpendicularly at the reference point was drawn, and then the direction of the pulmonary flow was defined as crossing the line perpendicularly. The angle θ between the flow direction and velocity-encoded direction was measured on the sagittal images. The area for measurements of velocity was defined manually on the axial velocity images, and the average velocity in the area was measured. In order to correct the effect of the angle θ, the value of the velocity measured on the axial images was divided by cos θ. The correction by cos θ of obliquely passing flow has been validated in previous phantom experiments in our laboratory.

Theoretically, the same region of interest used for measuring velocity can be used for measuring pulmonary cross-sectional area. Our preliminary studies, however, showed that the magnitude images at the level for measurements of velocity were not always suitable for this purpose because in some cases the edge of the main pulmonary artery was blurred as a result of oblique sectioning of the

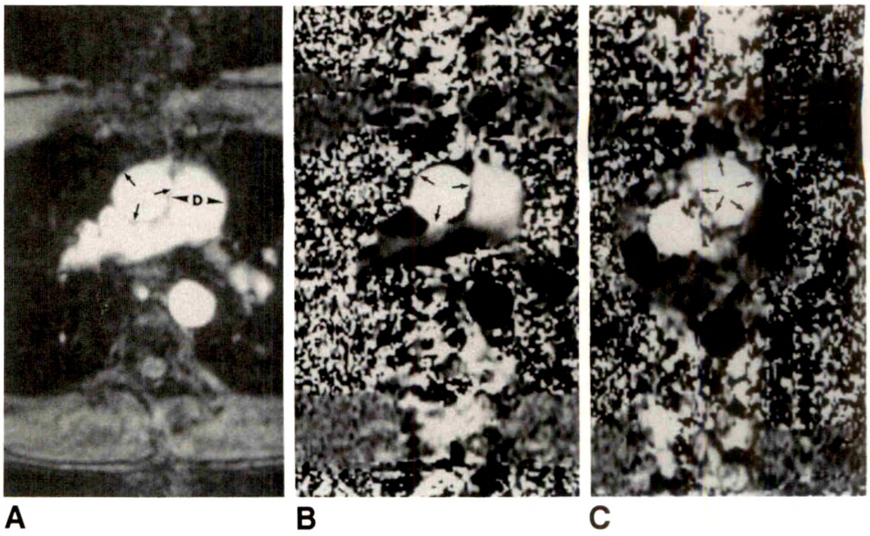

Fig. 3.—*A*, Ascending aorta (*arrows*) was identified on transverse magnitude images (anatomic images) at level that traversed center of main pulmonary artery, and its area was traced manually. In addition, diameter of main pulmonary artery (D) was measured to calculate cross-sectional area as $(D/2)^2 \times \pi$.

***B*, Same region of interest as in magnitude image was applied to corresponding phase image (velocity-encoded image in slice-select direction), and mean pixel value in region was measured. Each pixel has a value proportional to velocity of flow within it.**

***C*, Flow velocity in main pulmonary artery was measured separately at slice above pulmonary valve.**

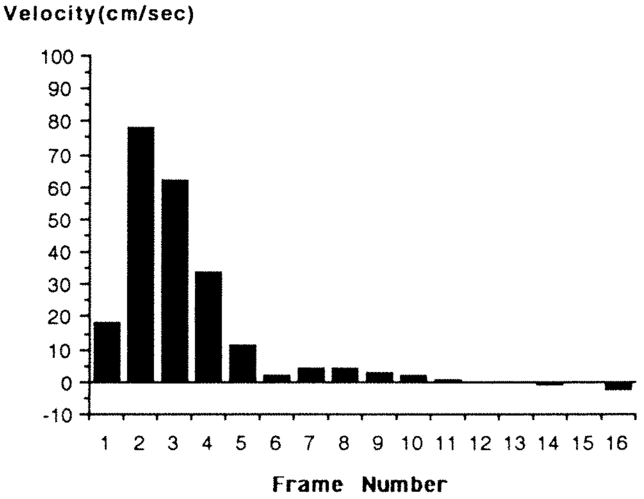

Fig. 4.—Graph shows representative profile of velocity of ascending aorta in a control subject. Cardiac cycle was divided into 16 frames. Product of cross-sectional area and mean velocity of aorta yielded instantaneous flow volume for each frame. Stroke volume was obtained by integration of instantaneous flow volumes for all frames. First frame was delayed 32 msec after R wave of ECG.

vessel and resultant partial-volume averaging and spatial misregistration [25], resulting in relatively high intra- and interobserver variabilities in measuring cross-sectional area. Therefore, we used the diameter of the main pulmonary artery at the same level that was used for the aorta, as the vascular edge was clear enough to be determined reproducibly in every case. The cross-sectional area of the vessel was calculated from the diameter of the main pulmonary artery (Fig. 3). In seven subjects in whom the edge of the main pulmonary artery was clear at both levels of the axial images, the capability of this alternative method was assessed. Pulmonary flow volume determined by the alternative method was not statistically different from that determined by the method using the same region of interest for velocity and cross-sectional area.

Doppler Echocardiography

Doppler echocardiography was performed in six subjects by using a commercially available instrument (Hewlett-Packard Sonos 1000, Andover, MA). Pulmonic flow signals were obtained from the parasternal short-axis view by using a 2.5-MHz duplex transducer with steerable continuous-wave Doppler capability. Aortic flow signals were obtained from the apical window by using a 1.9-MHz stand-alone transducer. Using the audio output and the spectral display, we described the ultrasound beam until the optimal signal was obtained. Ten cardiac cycles were recorded on videotape during suspended respiration at a sweep speed of 100 mm/sec for both aortic and pulmonic flows. The investigator who performed these studies did not know the results of VEC MR.

Measurements of Doppler recordings were performed off-line by using a computer-assisted and phantom-calibrated digitization system (Freeland Medical Systems, Indianapolis, IN). The peak velocities and flow velocity integrals for pulmonic and aortic flows were averaged from 10 cycles.

In order to determine stroke volume, a two-dimensionally directed M-mode echocardiogram was obtained through the leaflets of the aortic valve from the parasternal long-axis view. The maximum leaflet separation was measured in order to calculate stroke volume by using the method of Bouchard et al. [26] with the following formula: Stroke volume = $\pi \times (AVD^2/4) \times (FVI_{AoV})$, where AVD is the systolic leaflet separation on M mode measured in centimeters and FVI_{AoV} is the flow-velocity integral in centimeters.

Statistical Analysis

The paired *t* test was used for the comparison between the left ventricular stroke volumes determined by using VEC MR and volume measurements determined by using cine MR, for the comparison between the right and left ventricular stroke volumes determined by using VEC MR, and for the comparison between velocities determined by using Doppler echocardiography and VEC MR. Linear regression analysis was used to compare cine and VEC MR determinations of left ventricular stroke volumes, as well as the right and left ventricular stroke volumes determined with VEC MR. The slope of this regression equation was compared with the expected value of 1 with the Student's t test [27]. Inter- and intraobserver variabilities were assessed with linear regression analysis. In addition, the mean and standard deviation of paired differences (|measurement 1 − measurement 2|/mean of the two measurements) was used for the comparison between Doppler and VEC MR velocities and between measurements made by the two observers. A *p* value less than .05 was considered significant.

Results

Constant-Flow Phantom Studies

In constant-flow phantom studies, a straight-line correlation was produced between directly measured and velocities determined with VEC MR in the range of 20–408 cm/sec (Fig. 5). The standard error of the estimate (SEE) between these velocities was 7.9 cm/sec. The range of the Reynolds numbers corresponding to the velocities was 1340–24,480. The signal intensity of the flowing water on magnitude images was suppressed substantially at velocities higher than 288 cm/sec. However, phase signal still could be recognized on corresponding phase images, and the velocities were determined correctly up to 408 cm/sec.

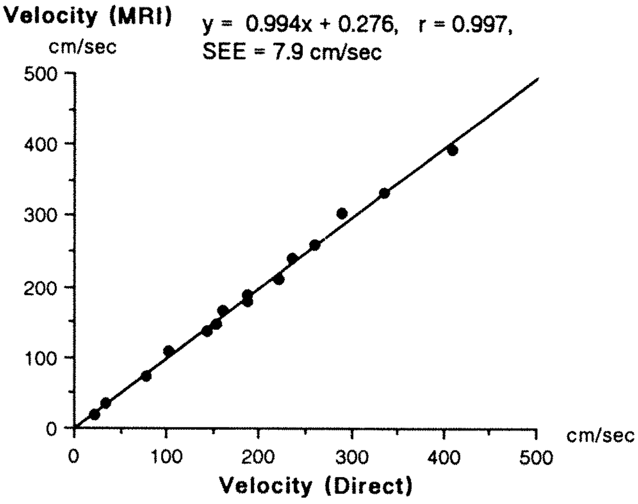

Fig. 5.—Graph shows correlation between flow velocity determined by using velocity-encoded cine MR and directly determined velocity for a constant flow phantom. SEE = standard error of the estimate.

Comparison with Doppler Measurements

Heart rates at the time of MR and Doppler examinations were not significantly different from each other (72 ± 10 vs 70 ± 11 beats/min). Maximum velocity in the main pulmonary artery at peak systole determined by VEC MR (97 ± 24 cm/sec [mean ± SD]; range, 82–145 cm/sec) was not significantly different from that obtained by using continuous-wave Doppler imaging (100 ± 26 cm/sec; range, 76–151 cm/sec). Linear regression analysis showed good correlation between results of VEC MR and Doppler echocardiography (r = .91). Peak aortic systolic velocity determined by using continuous-wave Doppler imaging was significantly higher than that determined in the ascending aorta by using VEC MR (125 ± 15 vs 98 ± 10 cm/sec). However, left ventricular stroke volumes measured by using continuous-wave Doppler imaging and VEC MR were not significantly different (70 ± 10 vs 70 ± 8 ml) and correlated well with each other (r = .80).

Right and Left Ventricular Stroke Volume and Cardiac Output

Mean left ventricular stroke volumes determined by using VEC and cine MR were 68 ± 14 and 69 ± 12 ml, respectively. Cardiac outputs determined by both methods were the same (4.4 ± 0.4 l/min). The left ventricular stroke volumes determined by VEC MR correlated well with the stroke volume measured from cine MR images (r = .98, SEE = 3.7 ml) (Fig. 6). The slope of the regression equation (1.13) was not significantly different from 1.

The average velocity in the cross section of the main pulmonary artery at peak systole was significantly lower than the maximum velocity in the same area (67 ± 12 vs 97 ± 24 cm/sec) as determined by VEC MR. Mean right ventricular stroke volume measured with VEC MR was 69 ± 13 ml, which was not significantly different from the left ventricular stroke volumes determined by using VEC MR. The stroke volumes of both sides of the heart determined by using VEC MR also correlated closely (r = .95, SEE = 4.8 ml) (Fig. 7).

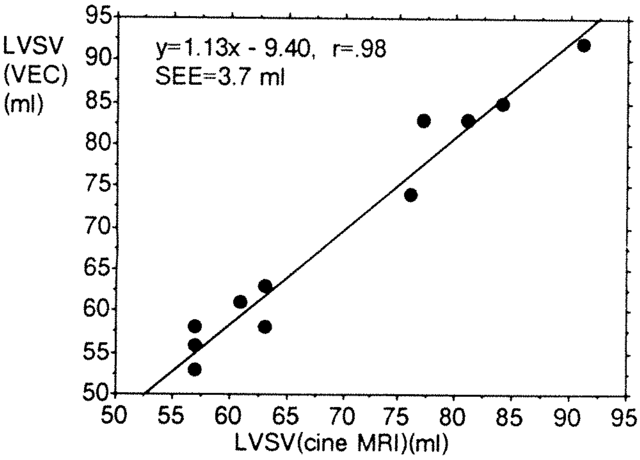

Fig. 6.—Graph shows correlation between left ventricular stroke volumes (LVSV) measured by using velocity-encoded cine MR (VEC) and those measured by using cine MR to determine difference of end-diastolic and end-systolic volumes. SEE = standard error of the estimate.

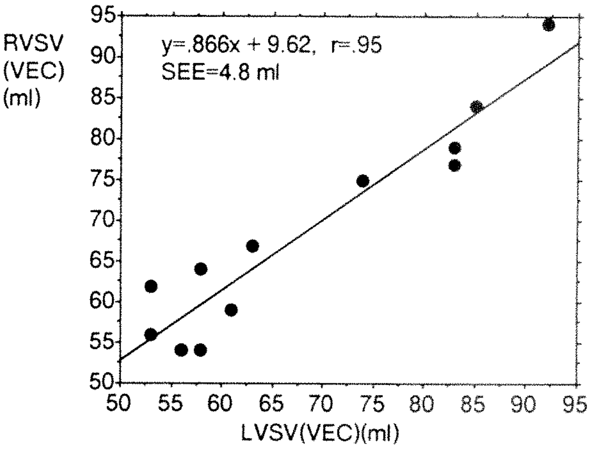

Fig. 7.—Graph shows correlation between right (RVSV) and left (LVSV) ventricular stroke volumes determined by using velocity-encoded cine MR (VEC).

The slope of the regression equation (0.87) was not significantly different from 1.

Inter- and Intraobserver Variability

Inter- and intraobserver variabilities were small for both left and right ventricular stroke volumes determined by using VEC MR (Figs. 8 and 9). Parameters indicating interobserver variability were as follows: r = .98, SEE = 3.9 ml for left ventricular stroke volumes and r = .92, SEE = 6.8 ml for right ventricular stroke volumes. Means and standard deviations of paired differences are shown in Table 1.

Discussion

This study showed the accuracy of VEC MR measurements of flow velocity of both in vitro constant and in vivo pulsatile flows. Right and left ventricular stroke volumes measured by using VEC MR had values similar to each other and were comparable to the left ventricular stroke volume determined by using cine MR volumetric analysis. It should be noted that VEC MR and other MR techniques for measuring blood flow do not measure blood flow changes on a beat-to-beat basis. The data for these flow measurements are acquired over 128–256 heartbeats and represent an average for this period. Blood flow can be presented in a phasic fashion for an average cardiac cycle by plotting flow for each of the multiple images corresponding to this cardiac cycle. Instantaneous measurement of beat-to-beat variations in cardiac output can be accomplished by Doppler echocardiography in humans and experimental use of hot wire anemometry and electromagnetic or Doppler flowmeters.

The constant flow velocities were measured accurately over a wide range (20–408 cm/sec). This range covers the peak velocity in the ascending aorta or main pulmonary artery encountered in normal subjects [24]. Previous studies with phase techniques examined the velocity up to only 100 cm/sec [14, 15, 23]. In a previous study the authors suggested

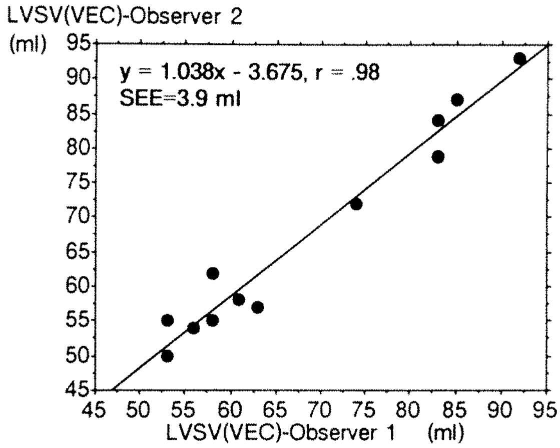

Fig. 8.—Graph shows correlation between measurements of left ventricular stroke volume (LVSV) obtained by observers 1 and 2. VEC = velocity-encoded cine MR, SEE = standard error of the estimate.

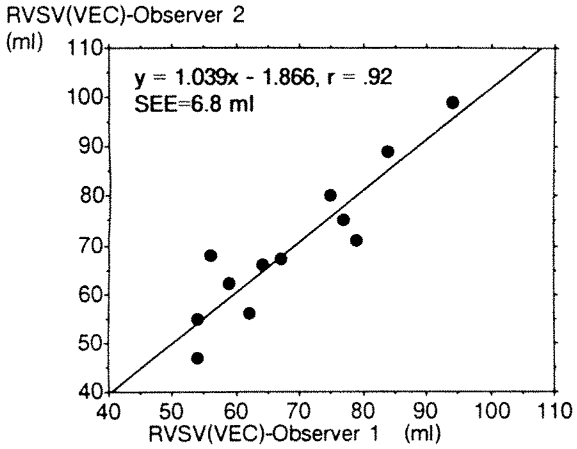

Fig. 9.—Graph shows correlation between measurements of right ventricular stroke volume (RVSV) obtained by observers 1 and 2. VEC = velocity-encoded cine MR, SEE = standard error of the estimate.

that measurements of velocity became unreliable at about 30 cm/sec owing to the onset of turbulence [14]. Another phase-modulation technique that used Fourier flow imaging methods measured flow velocity up to 90 cm/sec; however, higher velocity could not be quantified because of the signal loss caused by intravoxel dephasing [18]. For accurate MR measurements of high flow velocities, two phenomena may be important: signal loss due to high velocity itself and flow turbulence.

At high flow velocities, signal loss can be caused by velocity dispersion and concomitant phase dispersion within a voxel [9, 28]. The ability to measure flow by phase techniques depends on the presence of signal from flowing material. This factor is critical because it precluded flow measurements at high velocity (>90 cm/sec) in normal carotid arteries in previous studies [18]. In order to minimize signal loss, a rephasing gradient, which is a magnetic-field gradient designed to reduce phase-angle shift close to zero at the TE, is used [9]. These rephasing gradients are effective not only for compensation of intravoxel inhomogeneity of constant velocity but also for that of odd-order derivatives of position [9]. The sequences in our study used three-lobed rephasing gradients, and the signal was maintained at velocities up to 260 cm/sec. Signal on magnitude images at velocities higher than 288 cm/sec generated by the flow phantom was partially suppressed compared with signal on magnitude images at lower velocities. Interestingly, the velocity was determined correctly on phase images despite the partial loss of signal on the magnitude images. The results suggest that loss of signal on the magnitude image may not lead directly to errors in VEC MR measurements of velocity. Although even-order derivatives of position also produce phase dispersion and concomitant signal loss, this effect may be minimized by decreasing the TE. Therefore, our sequences might be improved by reducing the TE to minimize signal loss encountered at extremely high velocities.

In the present phantom study, Reynolds numbers ranged from 1340 to 24,480. For constant flow, transition from laminar to turbulent flow usually occurs when the Reynolds number is greater than 2500 [29]. Meier et al. [14] showed that flow quantification by using MR phase techniques was incorrect when the Reynolds number exceeded about 3000 in phantom experiments. They supposed that the inaccuracy was caused by turbulence. However, our results did not show such inaccuracy even at the highest flow with a very high Reynolds number (24,480). Our results were supported by a recent report [23] in which phase techniques could measure constant flow correctly with a Reynolds number near the critical value between laminar and turbulent flow. The reason for the discrepancy between our results and the results of Meier et al. may be related to differences of the sequences for velocity encoding. Our sequences used two alternating experiments with different gradient strengths for velocity encoding. Subtraction of the two experiments provides phase velocity data for velocity measurements in a specified direc-

TABLE 1: Inter- and Intraobserver Variability in Ventricular Stroke Volumes Determined by Using Velocity-Encoded Cine MR

Ventricular Stroke Volume Measured	Volume Measured (mean [in ml] ± SD)			Difference (mean % ± SD)	
	Observer 1 (1)	Observer 1 (2)	Observer 2	Intraobserver	Interobserver
Left	68 ± 14	68 ± 15	67 ± 15	2.9 ± 2.9	4.4 ± 2.5
Right	69 ± 13	71 ± 13	70 ± 15	4.6 ± 3.0	7.0 ± 5.6

Note.—Two measurements were made by observer 1. Mean difference ± SD = mean paired difference between measurements ± SD (paired difference in % = [measurement 1 − measurement 2]/mean of both measurements).

tion. In contrast, their sequences used the same gradients as those used for conventional two-dimensional Fourier transformation imaging for velocity encoding. The sequences have sensitivity to flow in both slice-select and read directions. Moreover, differently encoded phase velocity data sets were not subtracted. Therefore, their sequences are quite sensitive to flow problems both within and perpendicular to the imaging plane [15]. With turbulent flow, velocity components that are transverse to the main direction of flow occur. The flow in the direction of the imaging plane can add erroneous phase shift to the results [7]. Our results suggest that the sequences with three-lobed rephasing gradients and subtraction of double phase data may be effective in avoiding signal loss and minimizing the effect of turbulence. These options may be very important for the application of phase techniques to in vivo flow measurements.

Our study determined the accuracy of measurements of in vivo velocity obtained by using phase techniques. Peak systolic velocity in the main pulmonary artery determined by using VEC MR showed similar values when compared with those obtained by using continuous-wave Doppler echocardiography. In contrast, peak systolic velocity at the left ventricular outflow tract determined by using continuous-wave Doppler imaging was higher than that at the ascending aorta obtained by using VEC MR. The discrepancy between the values for velocities at the main pulmonary artery and aorta may be related to the selection of location for measurements of velocity. For the measurements of pulmonary flow, the Doppler ultrasound beam was through the pulmonary valve, and the location for VEC measurements was close to the pulmonary valve. However, for the aorta, the ultrasound beam was through the aortic valve. The maximum velocity measured by continuous-wave Doppler imaging across the aortic valve reflects the velocity at the narrowest point along the ultrasound beam [26]. This point most likely corresponds to the actual orifice of the aortic valve. Therefore, the locations of Doppler and VEC MR measurements may be apart by more than 5 cm; one was at the aortic valve orifice and the other was in the ascending aorta at the right pulmonary arterial level. Interestingly, despite the differences in aortic flow velocities, stroke volumes determined by the two methods were close to each other. Our results agree with the principles of mass conservation of flowing material [30].

The current result of the main pulmonary artery velocity suggests that the pulsatile flow profile has only a limited effect on the accuracy of VEC MR measurements of flow. The combination of the subtraction of differently encoded phase data sets and three-lobed rephasing gradients reduced to some extent the effect of acceleration [23]. Numeric analysis of the relation between spin phase and velocity and acceleration of flow has shown that the impact of the acceleration term on measurements of velocity can be estimated to produce less than 10% error under human physiologic conditions [14, 23]. Furthermore, detailed analysis of the relation [14] showed that the acceleration term may shift velocity profiles during systole less than 5 msec earlier if the acceleration term is taken into account. This effect has no influence on measurements of aortic flow volume [14]. Therefore, at least under physiologic conditions, the effect of acceleration may not be significant for in vivo flow and velocity measurements made by VEC MR.

We used a correction to compensate for the angle between the velocity-encoded direction and flow axes. Previous in vitro phantom studies in our laboratory showed that the effect of the obliquity (θ) between the flow and velocity-encoded directions could be corrected by using cos θ within the range of −40° to +40° (unpublished data). Because the angle θ between pulmonary flow and the velocity-encoded direction in the present study ranged from 25° to 38°, the correction was applied to the in vivo study. The current results suggest that the correction was also feasible for in vivo velocity quantification.

In regard to the angulation issue between flow and velocity-encoded directions, a previous study [15] using MR phase techniques showed that significant errors in quantification (>50%) were made if the obliquity was as little as 10° between the imaging plane and the flow direction. In that case, velocity was overestimated rather than underestimated on MR, and correction by cos θ seemed to be ineffective. The sequences, however, used single scans and did not use the subtraction of differently encoded phase data sets. Again, this method is quite sensitive to flow within as well as perpendicular to the imaging plane, resulting in intravoxel mixing of various phase shifts along both directions. Single-scan techniques require perfectly perpendicular sectioning of a vessel for correct quantification of flow [15], and this may preclude clinical use. In contrast, the technique in our study is sensitive only to the flow along a defined direction and seems to be more feasible for quantification of flow in vivo.

The correction of the effect of angulation by the cosine function, however, may not be effective for small vessels with high flow velocity. Such angulation may cause partial-volume averaging and spatial misregistration of velocity phase data on phase images [23], which may lead to substantial error. Therefore, perpendicular sectioning of the vessel may be more advisable for measurements of velocity in small vessels.

Aortic and pulmonary flow volumes were determined correctly by using VEC MR. Our results were consistent with those of a previous study [10] in which phase techniques were used. The flow volume determined by using VEC MR is derived from average velocity in the cross section of a vessel rather than the velocity at a given point in a vessel. Several methods for quantification of flow, such as Doppler echocardiography [30] and catheter-tip transducers [31], use the velocity at a single point instead of the velocity at every point in a vessel and, therefore, depend on an assumption of a flat velocity profile in a vascular cross section [31, 32]. In addition, these methods also need another assumption that the cross-sectional area of a vessel is constant throughout a cardiac cycle [31, 32]. Conversely, VEC MR provides pixel-based velocity mapping and measurements of cross-sectional areas of measurement at each instance and thus obviates such assumptions for quantification of flow volume. Interestingly, our study showed that maximum and average velocities in the cross section of the main pulmonary artery were substantially different. These findings suggest that even in a normal pulmonary artery, the velocity profile in the vascular cross section may not be perfectly flat. Dependency of velocity measurements on sampling site, which seems to be an inherent limitation of the method used in Doppler echocardiography, may lead to a substantial error in quantification of flow under pathologic conditions with highly inhomogeneous velocity profiles in a vascular cross section.

To date, the limitation of VEC MR has been related to the signal loss caused by severe dephasing within a voxel [11]. Although the rephasing gradient is effective for reducing the dephasing caused by nonuniform constant velocity in vascular cross section [9], severe dephasing still is produced by highly disordered flow or extremely fast flow, such as in the case of valvular stenosis or regurgitation. Even in control subjects, signal loss, which may be produced by eddy flow during systole, frequently was recognized during early systole behind the aortic cusps in the sinus of Valsalva. Therefore, the location of the slice for measurements of velocity should be selected carefully to avoid such signal loss. The signal loss caused by the intravoxel dephasing should be minimized by shortening the TE. Another option for MR measurements of flow is based on time-of-flight effects [2–4]. Although time-of-flight methods may be more resistant to intravoxel dephasing [4], they can provide information on the movement of a tracked bolus only. Two-dimensional velocity profiles in a vessel cannot be determined. Therefore, correct determination of velocity at every point in a vascular cross section would be difficult with time-of-flight methods. Although three-lobed rephasing gradients and subtraction of differently encoded phase data sets are effective for quantification of velocity, the tradeoff of these options is to decrease time resolution. The actual time resolution of the current sequences is 54 msec (twice the TR), which may not be short enough in patients with very short RR intervals. If TE is decreased, TR will be decreased, and, consequently, time resolution will be improved.

In summary, our study indicates that VEC MR is accurate for measuring aortic and pulmonary flow values in control subjects. This result was supported by the accuracy in quantification of in vitro constant and in vivo pulsatile flow velocities. Further technical development may be required for the application of this technique to measurement of extremely fast or disordered flow.

REFERENCES

1. Singer JR. Blood flow rates by nuclear magnetic resonance measurements. *Science* **1959**;130:1652–1653
2. Axel L, Shimakawa A, MacFall J. A time-of-flight method of measuring flow velocity by magnetic resonance imaging. *Magn Reson Imaging* **1986**;4:199–205
3. Matsuda T, Shimizu K, Sakurai T, et al. Measurement of aortic blood flow with MR imaging: comparative study with Doppler US. *Radiology* **1987**;162:857–861
4. Edelman RR, Mattle HP, Kleefield J, Silver MS. Quantification of blood flow with dynamic MR imaging and presaturation bolus tracking. *Radiology* **1989**;171:551–556
5. Moran PR. A flow zeugmatographic interface for NMR imaging in humans. *Magn Reson Imaging* **1982**;1:197–203
6. Moran PR, Moran R, Karstaedt K. Verification and evaluation of internal flow and motion. *Radiology* **1985**;154:433–441
7. Van Dijk P. Direct cardiac NMR imaging of heart wall and blood flow velocity. *J Comput Assist Tomogr* **1984**;8:429–436
8. Bryant DJ, Payne JA, Firmin DN, Longmore DB. Measurement of flow with NMR imaging using a gradient pulse difference technique. *J Comput Assist Tomogr* **1984**;8:588–593
9. Nayler GL, Firmin DN, Longmore DB. Blood flow imaging by cine magnetic resonance. *J Comput Assist Tomogr* **1986**;10:715–722
10. Firmin DN, Nayler GL, Klipstein RH, Underwood SR, Rees RSO, Longmore DB. In vivo validation of MR velocity imaging. *J Comput Assist Tomogr* **1987**;11:751–756
11. Underwood SR, Firmin DN, Klipstein RH, Rees RSO, Longmore DB. Magnetic resonance velocity mapping: clinical application of a new technique. *Br Heart J* **1987**;57:404–412
12. Klipstein RH, Firmin DN, Underwood SR, Rees RSO, Longmore DB. Blood flow patterns in the human aorta studied by magnetic resonance. *Br Heart J* **1987**;58:316–323
13. Borgen HG, Klipstein RH, Firmin DN, et al. Quantitation of antegrade and retrograde blood flow in the human aorta by magnetic resonance velocity mapping. *Am Heart J* **1989**;117:1214–1222
14. Meier D, Maier S, Bösiger P. Quantitative flow measurements on phantoms and on blood vessels with MR. *Magn Reson Med* **1988**;8:25–34
15. Pettigrew RI, Dannels W. Use of standard gradients with compound oblique angulation for optimal quantitative MR flow imaging in oblique vessels. *AJR* **1987**;148:405–409
16. Duerk JL, Pattany PM. In-plane flow velocity quantification along the phase encoding axis in MRI. *Magn Reson Imaging* **1988**;6:321–333
17. Feinberg DA, Crooks L, Sheldon P, Hoenninger J III, Watts J, Arakawa M. Magnetic resonance imaging of the velocity vector components of fluid flow. *Magn Reson Med* **1985**;2:555–566
18. Hennig J, Müri M, Brunner P, Friedburg H. Quantitative flow measurement with the fast Fourier flow technique. *Radiology* **1988**;166:237–240
19. Dumoulin CL, Hart HR. Magnetic resonance angiography. *Radiology* **1986**;161:717–720
20. Walker MF, Souza SP, Dumoulin CL. Quantitative flow measurement in phase contrast angiography. *J Comput Assist Tomogr* **1988**;12:304–313
21. Dumoulin CL. Flow imaging. In: Budinger TF, Margulis AR, eds. *Medical magnetic resonance: a primer—1988*. Berkeley: Society of Magnetic Resonance in Medicine, **1988**
22. Haacke EM, Lenz GW. Improving MR image quality in the presence of motion by using rephasing gradients. *AJR* **1987**;148:1251–1258
23. Firmin DN, Nayler GL, Kilner PJ, Longmore DB. The application of phase shifts in NMR for flow measurements. *Magn Reson Med* **1990**;14:230–241
24. Hatle L, Angelsen B. *Doppler ultrasound in cardiology: physical principles and clinical applications*, 2nd ed. Philadelphia: Lea & Febiger, **1985**:93
25. Axel L. Blood flow effects in magnetic resonance imaging. *AJR* **1984**;143:1157–1166
26. Bouchard A, Blumlein S, Schiller NB, et al. Measurement of left ventricular stroke volume using continuous wave Doppler echocardiography of the ascending aorta and M-mode echocardiography of the aortic valve. *J Am Coll Cardiol* **1987**;9:75–83
27. Zar JH. *Biostatistical anlaysis*, 2nd ed. Englewood Cliffs, NJ: Prentice-Hall, **1984**:271
28. Wehrli FW, Shimakawa A, MacFall JR, Axel L, Perman W. MR imaging of venous and arterial flow by a selective saturation-recovery spin echo (SSRSE) method. *J Comput Assist Tomogr* **1985**;9:537–545
29. Caro CG, Pedley TJ, Schroter RC, Seed WA. *The mechanics of the circulation.* Oxford, England: Oxford University Press, **1987**:57
30. Yoganathan AP, Cape EG, Sung H, Williams FP, Jimoh A. Review of hydrodynamic principles for the cardiologists: application to the study of blood flow and jets by imaging techniques. *J Am Coll Cardiol* **1988**;12:1344–1353
31. Mills CJ. A catheter tip electromagnetic velocity probe and its evaluation. *Cardiovasc Res* **1967**;1:263–273
32. Huntsman LL, Stewart DK, Barnes SR, Franklin SB, Colocousis JS, Hessel EA. Noninvasive Doppler determination of cardiac output in man. *Circulation* **1983**;67:593–602

Case Report

Traumatic Rupture of the Diaphragm Without Visceral Herniation: CT Diagnosis

Diane G. Holland[1,2] and Leslie E. Quint[1]

Controversy exists regarding the usefulness of CT in the diagnosis of traumatic rupture of the diaphragm [1-3]. No large studies concerning the accuracy of CT in this setting have been done, either in patients with or in those without visceral herniation. Two case reports in the literature show discontinuity of the left hemidiaphragm on CT with visceral herniation [4, 5]. We describe a case in which a posttraumatic left-sided diaphragmatic rent was shown on CT in the absence of visceral herniation.

Case Report

A 29-year-old man sustained a blow to the left side of the chest wall in a motor vehicle accident. Physical examination disclosed a lower left-sided flail chest. A portable supine chest radiograph showed left-sided basilar air-space disease and multiple left lateral rib fractures, with no definite pneumothorax.

A CT examination performed 4 hr after the accident showed a left-sided pneumothorax, bilateral pleural fluid collections, bibasilar atelectasis, and fractures of several lower left lateral ribs. Fat was present in the lower left hemithorax, immediately anterior to atelectatic lung (Fig. 1A) and lateral to the left hemidiaphragm (Fig. 1B). An abrupt discontinuity of the left hemidiaphragm was adjacent to the rib fractures; the two edges of the diaphragmatic rent were clearly outlined by adjacent fat (Fig. 1C). Traumatic rupture of the left hemidiaphragm was diagnosed.

Despite the patient's stable clinical status, the CT findings led to laparotomy 26 hr after the injury. The surgeon found a large tear of the posterolateral portion of the left hemidiaphragm. Portions of stomach, omentum, and spleen had herniated through the diaphragmatic rent. A search for additional intraabdominal injuries revealed only a hematoma of the gastrosplenic ligament. The abdominal contents were reduced, and the diaphragmatic rent was repaired without complication. The patient's postoperative recovery was unremarkable.

Discussion

Although chest radiography has a primary role in screening for diaphragmatic injury, it is often inconclusive [6]. Approximately 85% of patients with a ruptured hemidiaphragm have abnormal findings on chest radiographs, but only one third of these radiographs show pathognomonic evidence of a diaphragmatic tear, such as bowel loops or a nasogastric tube in the chest [2]. Other abnormalities suggestive but not diagnostic of diaphragmatic injury include an indistinct or elevated hemidiaphragm, hemothorax, pneumothorax, rib fractures, and pulmonary contusion [2, 6]. The nonspecificity of these findings contributes to the frequent initial misdiagnosis of diaphragmatic tears.

Current CT scanners, with fast scanning times and consequently little motion artifact, facilitate direct visualization of the diaphragm. In cross section, the intact left hemidiaphragm usually appears as a continuous, curvilinear structure of soft-tissue density outlined by lung superiorly and subdiaphragmatic fat inferiorly. The right hemidiaphragm is usually less well visualized, because it blends inferiorly with the liver, unless intervening fat or fluid is present [5]. Disruption of a

---

Received January 15, 1991; accepted after revision February 14, 1991.

[1] Department of Radiology, Box 0030, University of Michigan Hospitals, 1500 E. Medical Center Drive, Ann Arbor, MI 48109-0030. Address reprint requests to L. E. Quint.

[2] Present address: Department of Radiology, Henry Ford Hospital, Detroit, MI 48202.

AJR 157:17-18, July 1991 0361-803X/91/1571-0017 © American Roentgen Ray Society

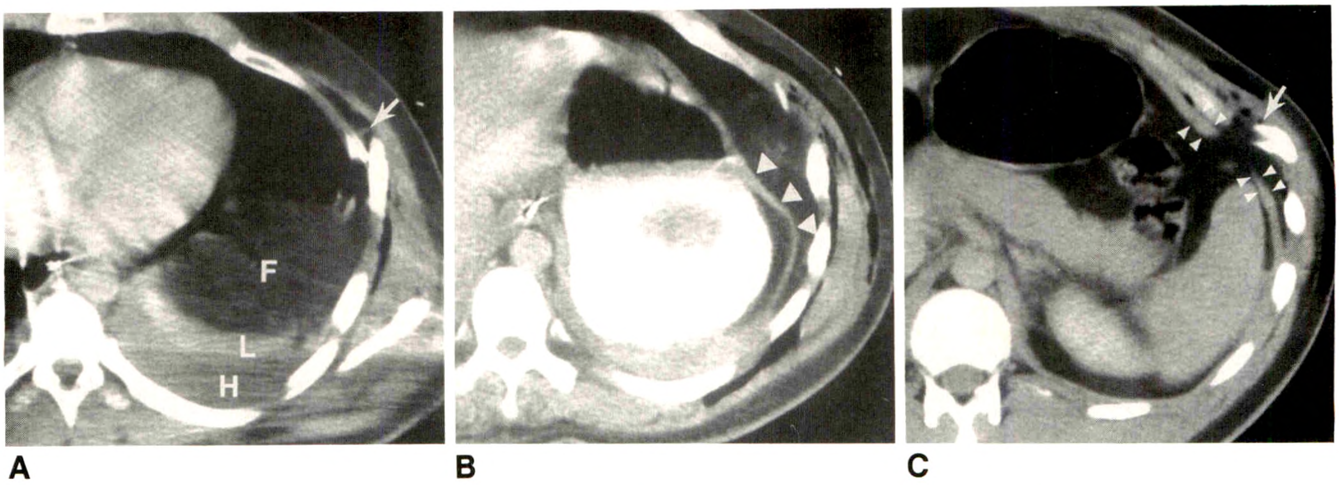

Fig. 1.—Contrast-enhanced CT (10-mm-thick contiguous sections, 2.0-sec scanning time) of left hemidiaphragmatic rupture.

***A*, Left rib fracture (*arrow*), air in left side of chest wall, and left-sided hemothorax (H) are visible. Fat (F) anterior to atelectatic lung (L) is consistent with herniated omentum.**

***B*, An intact portion of left hemidiaphragm (*arrowheads*) is visible, outlined on both sides by fatty tissue.**

***C*, Scan obtained farther caudad shows medial and lateral edges of left hemidiaphragmatic rent (*arrowheads*) immediately adjacent to a fractured rib (*arrow*).**

hemidiaphragm may appear as an abrupt discontinuity, with the edges of the tear outlined by fat and possibly by lung. In patients with suboptimal diaphragmatic visualization or equivocal findings of diaphragmatic rupture, thin sections (e.g., 3–5 mm) may be useful for better anatomic definition.

The accuracy of CT in diagnosing diaphragmatic rupture is controversial. In a retrospective review of 33 cases of blunt diaphragmatic injury, Voeller et al. [2] found CT to be an insensitive method of diagnosing diaphragmatic tears. However, only four patients were evaluated by CT, and the CT technique was not described or illustrated. In a study of 196 patients examined with CT for abdominal trauma, Kearney et al. [1] found CT to be 99% accurate for diagnosing diaphragmatic disruption; two of 196 patients had proved diaphragmatic rupture at laparotomy. Presence or absence of visceral herniation was not specified in either of these studies.

Case reports by Heiberg et al. [5] and Demos et al. [4] show CT examples of abrupt discontinuity of the medial portion of the hemidiaphragm. Both cases had associated abdominal visceral herniation. In our patient, the CT study showed both the medial and the lateral margins of the diaphragmatic rent. Although a small amount of omental tissue had herniated through the tear, no visceral herniation was seen during the CT examination. Visceral herniation probably was delayed, occurring during the 22-hr interval between the CT study and surgery.

Abdominal CT scanning in acute trauma can occasionally show diaphragmatic disruption before visceral herniation, leading to early surgical intervention and averting the potentially life-threatening complications of an undiagnosed herniation.

REFERENCES

1. Kearney PA, Vahey T, Burney RE, Glazer G. Computed tomography and diagnostic peritoneal lavage in blunt abdominal trauma. *Arch Surg* **1989**;124:344–347
2. Voeller GR, Reisser JR, Fabian TC, Kudsk K, Mangiante EC. Blunt diaphragm injuries. *Am Surg* **1990**;56:28–31
3. Toombs BD, Sandler CM, Lester RG. Computed tomography of chest trauma. *Radiology* **1981**;140:733–738
4. Demos TC, Solomon C, Posniak HV, Flisak MJ. Computed tomography in traumatic defects of the diaphragm. *Clin Imaging* **1989**;13:62–67
5. Heiberg E, Wolverson MK, Hurd RN, Jagannadharao B, Sundaram M. CT recognition of traumatic rupture of the diaphragm. *AJR* **1980**;135:369–372
6. Morgan AS, Flancbaum L, Esposito T, Coc EF. Blunt injury to the diaphragm: an analysis of 44 patients. *J Trauma* **1986**;26:565–568

Case Report

Delayed Appearance of Localized Pericardial Effusion After Cardiac Surgery

Hidetoshi Miyake,[1] Soji Iwanaga,[1] Koji Suzuki,[1] Michiko Shiga,[1] Hisayuki Aikawa,[1] Hiromu Mori,[1] and Osamu Shigemitsu[2]

A localized bulge of the heart border due to pericardial effusion is usually seen on chest radiographs within a month after cardiac surgery and resolves soon after [1–3]. However, the effusion may rarely occur a month or more after cardiac surgery [4, 5]. We report a case of apparent delayed onset of localized pericardial effusion after cardiac surgery, manifesting initially as a localized bulge of the cardiac contour on chest radiographs.

Case Report

A 55-year-old man had a mitral valve replaced because of mitral regurgitation. Chest radiographs obtained every 2 months after surgery showed a normal left border of the heart until 11 months after surgery, when a chest radiograph showed a bulge of the left border (Fig. 1A). The patient was asymptomatic, and laboratory data were normal. Echocardiography showed a pericardial effusion next to the left atrium and ventricle. CT revealed a localized pericardial effusion

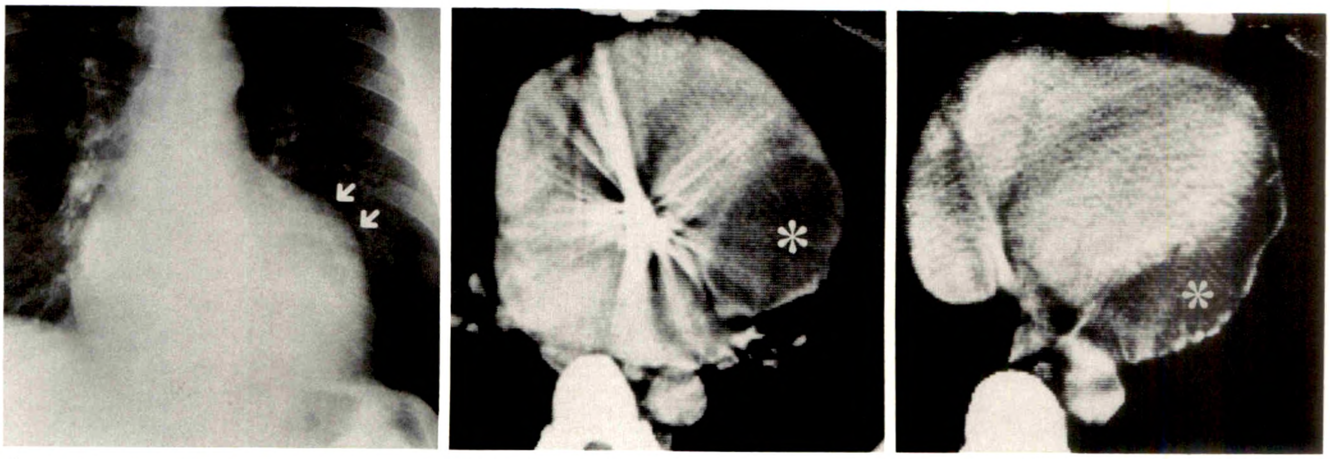

Fig. 1.—55-year-old man with localized pericardial effusion of delayed onset after cardiac surgery.
***A*, Chest radiograph obtained 11 months after mitral valve replacement shows a focal bulge (*arrows*) in left border of heart.**
***B* and *C*, Enhanced CT scans revealed a loculated unilateral pericardial effusion (*asterisk*) lateral to left atrium and posterolateral to left ventricle.**

---

[1] Department of Radiology, Medical College of Oita, 1-1, Idaigaoka, Hazama-machi, Oita-gun, Oita 879-56, Japan. Address reprint requests to H. Miyake.
[2] Department of Surgery, Medical College of Oita, 1-1, Idaigaoka, Hazama-machi, Oita-gun, Oita 879-56, Japan.

***AJR* 157:19–20, July 1991** 0361–803X/91/1571–0019 © American Roentgen Ray Society

lateral to the left atrium (Fig. 1B) and posterolateral to the left ventricle (Fig. 1C). Pericardial windows were created surgically, and 180 ml of serosanguineous pericardial fluid was evacuated. No organisms grew from the cultured fluid.

Discussion

Pericardial effusion is common after cardiac surgery. The effusion usually occurs immediately after surgery and reaches its largest size by the 10th day after surgery [1–3]. Delayed cardiac tamponade is an uncommon but well-described condition that occurs in 0.1–6.0% of patients [4, 5]. Delayed onset of pericardial effusion is unusual [4, 6].

Although the cause of delayed appearance of pericardial effusion after cardiac surgery is not clearly understood, previous studies suggested that the effusions are related to postoperative anticoagulation, perioperative bleeding into the pericardial space, postoperative irritation of the pericardium by intrapericardial blood and subsequent formation of a reaction effusion, postpericardiotomy syndrome, and infectious pericarditis [4–6]. The patient described here had no symptoms of postpericardiotomy syndrome, such as pericardial pain, friction rub, and low-grade fever. Schlesinger et al. [6] reported a patient with pericardial effusion that initially appeared 18 months after cardiac surgery. The effusion was presumed to have been due to viral pericarditis. In our case, traumatic (postoperative) pericarditis or viral pericarditis cannot be excluded.

Because of local stretching, weakness, or adhesions of the pericardium after cardiac surgery, an isolated pericardial effusion is seen as a focal bulge of the heart's border on chest radiographs. Besides loculated pericardial effusion, this bulge is seen in patients with giant atrium, ventricular aneurysm, and pleural or pericardial mass such as a fibroma or benign mesothelioma or pericardial cyst.

REFERENCES

1. Weitzman LB, Tinker WP, Kronzon I, Cohen ML, Glassman E, Spencer FC. The incidence and natural history of pericardial effusion after cardiac surgery: an echocardiographic study. *Circulation* **1984;**69:506–511
2. Ikaheimo MJ, Huikuri HV, Airaksinen J, et al. Pericardial effusion after cardiac surgery: incidence, relation to the type of surgery, antithrombotic therapy, and early coronary bypass graft patency. *Am Heart J* **1988;**116:97–102
3. Duvernoy O, Larsson SG, Persson K, Thuren J, Wikstrom G. Pericardial effusion and pericardial compartments after open heart surgery: an analysis by computed tomography and echocardiography. *Acta Radiol* **1990;**31: 41–46
4. Ofori-Krakye SK, Tyberg TI, Geha AS, Hammond GL, Cohen LS, Langou RL. Late cardiac tamponade after open heart surgery: incidence, role of anticoagulants in its pathogenesis and its relationship to the postpericardiotomy syndrome. *Circulation* **1981;**63:1323–1328
5. Merrill W, Donahoo JS, Brawley RK, Taylor D. Late cardiac tamponade: a potentially lethal complication of open-heart surgery. *J Thorac Cardiovasc Surg* **1976;**72:929–932
6. Schlesinger AE, Fernbach SK. Pericardial effusion presenting as an anterior mediastinal mass. *Pediatr Radiol* **1986;**16:65–66

P24471

The Prevalence of Carcinoma in Palpable vs Impalpable, Mammographically Detected Lesions

Lawrence W. Bassett[1,2]
Tsung-Han Liu[1]
Armando E. Giuliano[2,3]
Richard H. Gold[1,2]

Concern over excessive numbers of false-positive mammograms, leading to unnecessary investigations and surgical interventions, has been cited as a barrier to mammographic screening for breast cancer. We compared the biopsy results from palpable vs impalpable, mammographically detected lesions from one experienced breast surgeon's practice from July 1980 through July 1989. Overall, there were 372 biopsies in 346 women. Of 143 biopsies for palpable abnormalities, 48 (34%) yielded a primary malignant lesion. The length of the palpable cancers averaged 3.7 cm (median, 2.8 cm). Sixteen (33%) of the 48 biopsies were in patients who had positive axillary lymph nodes, and five (10%) were in patients who had distant metastases at the time of biopsy. Of 229 biopsies for impalpable, mammographically detected lesions, 72 (31%) yielded a primary breast carcinoma. Excluding 34 carcinomas that had only calcifications, the length of the mammographically detected tumors averaged 2.0 cm (median, 1.5 cm). Eleven (15%) of the 72 biopsies were in patients who had positive axillary nodes, and none were in patients who had distant metastases at the time of biopsy.

The positive predictive values (number of cancers detected divided by the number of biopsies recommended) were not significantly different when comparing biopsies indicated for palpable, clinically detected (34%) vs impalpable, mammographically detected (31%) abnormalities ($p = .669$). However, the mammographically detected cancers were smaller, more often noninvasive (32% vs 4%), less often associated with axillary metastases (15% vs 33%), and without distant metastases (0% vs 10%).

***AJR* 157:21–24, July 1991**

A positive predictive value (number of cancers detected divided by the number of biopsies recommended), also referred to as true-positive biopsy rate, as low as 10% has been considered reasonable in order to maximize the number of early cancers detected by screening mammography [1], and a wide range of true-positive biopsy rates have been reported in the literature [2–6]. However, concern over excessive numbers of false-positive mammograms leading to unnecessary investigations and surgical interventions has been cited as one of the barriers to breast cancer screening with mammography, causing referring physicians not to order it [7]. Therefore, a less aggressive approach to mammographic interpretation has been recommended recently, yielding a true-positive biopsy rate as high as 40% [6]. Radiologists have been encouraged to audit their own practices to determine their own true-positive and false-negative biopsy rates [8]. When investigating biopsy rates for a local population of patients, it is of interest to know the true-positive rate for biopsies of palpable breast lesions and for impalpable ones, and to understand how the palpable clinically detected lesions differ from those impalpable lesions detected solely with mammography. We undertook a retrospective study to compare the biopsy results in palpable vs impalpable, mammographically detected lesions from the practice of an experienced breast surgeon working with experienced mammographers.

Received June 15, 1990; accepted after revision January 14, 1991.

Presented at the annual meeting of the American Roentgen Ray Society, Washington, DC, May 1990.

[1] Iris Cantor Center for Breast Imaging, Department of Radiological Sciences, UCLA School of Medicine, Los Angeles, CA 90024. Address reprint requests to L. W. Bassett, Department of Radiological Sciences, CHS B2-125, UCLA Medical Center, Los Angeles, CA 90024-1721.

[2] Jonsson Comprehensive Cancer Center, UCLA School of Medicine, Los Angeles, CA 90024.

[3] Department of Surgery, UCLA School of Medicine, Los Angeles, CA 90024.

0361–803X/91/1571–0021
© American Roentgen Ray Society

Materials and Methods

We reviewed the results of 372 biopsies in 346 patients all operated on by a single surgeon who specializes in breast disease in a university referral practice setting, from July 1980 through July 1989. The ages of the patients at the time of biopsy were from 18 to 85 years, with a mean age of 54 years. Data abstracted from the medical records included clinical findings, mammographic interpretations, operative notes, and pathologic reports. All patients had mammograms before surgery. For the palpable lesions, mammograms had been used to exclude unexpected impalpable lesions, not to defer the biopsy of a suspicious palpable abnormality. The surgeon complied with all recommendations for biopsy prompted by abnormal mammograms and all requests for sonography of masses for differentiation between cysts and solid masses.

We defined positive predictive value as the percentage of women whose mammographic or clinical findings led to a biopsy that yielded a pathologic diagnosis of cancer (true positive/[true positive + false positive cases]) [9]. We compared the palpable with the impalpable lesions for positive predictive value, size of the cancer at the time of biopsy, status of the axillary lymph nodes, and presence or absence of distant metastases at the time of biopsy. The actual size (greatest dimension) of the masses was determined by examination of the excised specimen, or the size measured on mammograms when the size at pathologic examination had not been recorded, and on the basis of physical examination in four cases in which the palpable mass was not visible on mammograms and its size was not recorded at pathologic investigation. All impalpable lesions were removed by excisional biopsy after mammographically guided needle localization with direct needle placement or hookwire systems. We excluded women who had previous ipsilateral carcinoma from our study.

The histopathologic diagnoses of the carcinomas detected by physical examination or mammography were recorded. In order not to overestimate the effectiveness of mammography, lobular carcinoma in situ, thought to be a marker for breast cancer risk rather than a direct precursor of carcinoma [10], and sometimes referred to as lobular neoplasia [11], was recorded as a benign lesion.

Results

Of the 372 biopsies, 143 (38%) were done because of a palpable mass and 229 (62%) were performed for impalpable, mammographically detected abnormalities.

Palpable Lesions

The women with palpable lesions ranged in age from 18 to 85 years, with a mean age of 49 years. Of the 143 biopsies performed for palpable lesions, 48 yielded a primary breast carcinoma, for a positive predictive value of 34%. The age range for women with palpable carcinomas was 31 to 85 years, with a mean age of 58 years. Palpable carcinomas at the time of biopsy ranged from 1.0 cm to 13.0 cm (average, 3.7 cm; median, 2.8 cm) in greatest diameter. Sixteen (33%) of these patients with palpable carcinomas had positive axillary lymph nodes, and five (10%) had distant metastases at the time of biopsy. The histopathologic diagnoses of the palpable carcinomas included 38 invasive ductal carcinomas, five invasive lobular carcinomas, two invasive tubular carcinomas, two noninvasive ductal carcinomas (ductal carcinoma in situ), and one colloid carcinoma.

Impalpable Lesions

The age range of women with impalpable lesions was 32 to 84 years, with a mean age of 56 years. There were 229 biopsies of impalpable, mammographically detected lesions in 207 women. The majority (97%) of these impalpable lesions were found in asymptomatic women during screening mammography. Seventy-two of the 229 biopsies yielded a primary breast carcinoma, for a positive predictive value of 31%. The age range for the women with impalpable cancers was 32–84 years (median, 59 years). Excluding 34 carcinomas visualized only as calcifications, for which it was not possible to determine an accurate size in the absence of a tumor mass, the impalpable tumors ranged in size from 0.5 cm to 5.0 cm (average, 2.0 cm; median, 1.5 cm). Eleven (15%) of the patients with mammographically detected cancers had positive axillary lymph nodes, and none had evidence of distant metastases at the time of biopsy. The histopathologic diagnoses of the impalpable carcinomas included 39 invasive ductal carcinomas, 23 noninvasive ductal carcinomas (ductal carcinoma in situ), five colloid carcinomas, four invasive lobular carcinomas, and one invasive tubular carcinoma.

No significant difference was found in the yield of carcinomas detected for biopsies of palpable vs impalpable lesions ($p = .669$). However, a statistically significant ($p < .001$) greater percentage of cancers that were noninvasive or invasive but 1 cm or less in size with negative axillary lymph nodes were detected only by mammography. A statistically significant ($p = .02$) increase was found in the overall prevalence of axillary nodal involvement and distant metastases for the palpable cancers at the time of diagnosis compared with those that were impalpable and mammographically detected.

Tables 1 and 2 summarize the differences between the palpable and impalpable, mammographically detected carcinomas. Table 3 records the mammographic findings on the impalpable lesions. Lobular carcinoma in situ was found in one of the biopsies of palpable lesions and in five of the biopsies of impalpable, mammographically detected lesions.

Discussion

It was estimated that in the United States in 1990, 150,000 new cases of breast cancer would be diagnosed, and 44,000 women would die of the disease [12]. Studies in the United States and Europe have shown that the number of deaths from breast cancer can be decreased through the use of screening mammography [13, 14]. The National Cancer Institute (NCI), American Cancer Society, and many other professional medical organizations recommend that women have regular mammograms after the age of 40 [15]. Despite the fact that mammography can save lives, the Mammography Attitudes and Usage Study, conducted in February 1990 for the Jacobs Institute of Women's Health (an independent, nonprofit organization founded by the American College of Obstetricians and Gynecologists) with technical assistance from the NCI, reported that while almost two thirds of women had had at least one mammogram, less than one third of

TABLE 1: Comparison of Palpable and Impalpable Carcinomas in 372 Biopsies

	Palpable (%)	Impalpable (%)	p Values[a]
Number of cases[b]	143 (38)	229 (62)	—
Number of carcinomas[c]	48 (34)	72 (31)	.669
Average length (cm) of malignant masses ± SD	3.7 ± 3.0	2.0 ± 1.3	.239
Median length (cm) of malignant masses	2.8	1.5[d]	.183
Carcinomas with positive axillary nodes[e]	16 (33)	11 (15)	.020
Carcinomas with distant metastases[e]	5 (10)	0 (0)	—
Noninvasive cancers ≤1 cm with negative axillary nodes[e]	6 (13)	34 (47)	<.001
Invasive cancers ≤1 cm with negative axillary nodes[e]	4 (8)	11 (15)	.259

[a] <.05 is statistically significant. Dash means not calculated.
[b] Percentages are of total number of biopsies done (372).
[c] Percentages are of total number of palpable or impalpable lesions.
[d] Only 38 of the nonpalpable lesions had a measurable tumor mass; the other 34 were manifested only by calcifications. Therefore, the actual average size of impalpable cancers was much smaller than 2.0 cm.
[e] Percentages are of number of palpable or impalpable carcinomas.

TABLE 2: Histopathologic Diagnoses of Palpable vs Impalpable Carcinomas

Histopathologic Diagnosis	Palpable (%)	Impalpable (%)
Invasive ductal	38 (79)	39 (54)
Noninvasive ductal	2 (4)	23 (32)
Infiltrating lobular	5 (10)	4 (6)
Colloid	1 (2)	5 (7)
Tubular	2 (4)	1 (1)
Total	48	72

TABLE 3: Mammographic Findings of 229 Impalpable Lesions

Mammographic Finding	Benign (%)[a]	Malignant (%)[b]	Total (%)[c]
Calcifications only	109 (76)	34 (24)	143 (62)
Mass only	22 (52)	20 (48)	42 (18)
Mass with calcifications	3 (27)	8 (73)	11 (5)
Architectural distortion	3 (43)	4 (57)	7 (3)
Asymmetric density	3 (75)	1 (25)	4 (2)
Neodensity	17 (77)	5 (23)	22 (10)
Total	157	72	229

[a] Percentage of total with this mammographic feature that were benign.
[b] Percentage of total with this mammographic feature that were malignant.
[c] Percentage of total number of biopsies.

women aged 40 years or older were following mammography screening guidelines [16].

Noncompliance with mammography recommendations is a complex problem that relates to barriers perceived by both referring physicians and their patients [7]. Perceptions of excessive numbers of biopsies for benign abnormalities, so-called unnecessary or avoidable biopsies, discourage physicians from ordering screening mammograms and discourage women from obtaining them [7]. Excessive numbers of biopsies also increase the overall costs for breast cancer screening with mammography, reducing its cost-effectiveness [17–19]. Therefore, it is important to achieve a biopsy rate that yields the greatest number of cancers and the fewest negative biopsies. Experienced radiologists have reported cancer detection rates of 23–32% for biopsies prompted by mammography [4, 5, 20]. It has even been suggested that a rate as high as 40% can be achieved without a detrimental effect in terms of long-term survival [6]. It is important that radiologists audit the results of biopsies recommended in their own practice, not only to defend their practices but to improve their own effectiveness. An audit of mammography interpretation is an integral part of quality assurance programs for mammography and should be performed on a regular basis. The audit should include patients' demographic data, follow-up of positive cases, follow-up of a sample of negative cases, tabulation of tumor stage, and individual results for each of the radiologists interpreting mammograms [20, 21].

In our study, the positive predictive values for the detection of breast carcinoma were not significantly different for palpable lesions and for impalpable, mammographically detected lesions referred to our breast surgeon for evaluation. Thus, screening mammograms did not result in a larger percentage of negative or benign biopsies than did biopsy of dominant palpable masses. However, the lesions detected by mammography were more likely to be smaller and noninvasive and less likely to be associated with axillary metastases (Tables 1 and 2). At the time of biopsy, none of the cancers detected only by mammography had undergone distant metastasis.

Higher false-positive biopsy rates for both palpable and impalpable lesions have been published [22]. Because the surgeon and the radiologists in our study specialize in breast cancer detection and have many years of experience, the results are not representative of a typical practice. Over the years, efforts have been made by the surgeon and the radiologists to reduce the number of false-positive biopsies.

Several strategies have been used to reduce the number of avoidable biopsies due to false-positive screening mammograms. One strategy is to do a complete workup for abnormalities found on screening mammograms, including the appropriate use of magnification mammography and spot compression applied over a suspicious area [23–25]. Another strategy, the use of sonography for the evaluation of masses, eliminates the need for biopsies of most cysts [26]. Our surgeon used needle aspiration or sonography on palpable masses and sonography on mammographically detected masses so that no woman underwent open biopsy for a cyst. For lesions that show mammographic features with a high probability of benignity, such as masses smaller than 1 cm with sharp margins, and those that lack suspicious calcifications, we are more likely to recommend periodic follow-up, rather than biopsy. Although these maneuvers have resulted in a high predictive value when we recommend biopsy for impalpable masses, we have been less successful in reducing the number of biopsies for benign calcifications, whose mammographic features are often nonspecific (Table 3). We rarely recommend biopsy of an impalpable asymmetric density that shows neither microcalcifications nor architectural distortion [6, 8, 27]. In the future, mammographically guided fine-needle aspiration biopsy is likely to play an expanded role in further reducing the need for excisional biopsies of impalpable, mammographically detected abnormalities [28–30].

ACKNOWLEDGMENT

We thank Gil Fine, Department of Biostatistics, UCLA School of Public Health, for statistical assistance.

REFERENCES

1. Moskowitz M. Impact of a priori medical decisions on screening for breast cancer. *Radiology* **1989**;171:605-608
2. Rasmussen OS, Seerup A. Preoperative radiographically guided wire marking of nonpalpable breast lesions. *Acta Radiol* **1984**;25:13–16
3. Homer MJ. Localization of nonpalpable breast lesions: technical aspects and analysis of 80 cases. *AJR* **1983**;140:807–811
4. Gisvold JJ, Martin JK. Prebiopsy localization of nonpalpable breast lesions. *AJR* **1984**;143:477–481
5. Meyer JE, Kopans DB, Stomper PC, Lindfors KK. Occult breast abnormalities: percutaneous preoperative needle localization. *Radiology* **1984**;150:335-337
6. Hall FM, Storella JM, Silverstone DZ, Wyshak G. Nonpalpable breast lesions: recommendations for biopsy based on suspicion of carcinoma at mammography. *Radiology* **1988**;167:353-358
7. Howard J. Using mammography for cancer control: an unrealized potential. *CA* **1987**;33:33-48
8. Brenner RJ, Sickles EA. Acceptability of periodic follow-up as an alternative to biopsy for mammographically detected lesions interpreted as probably benign. *Radiology* **1989**;171:645-646
9. Schmidt RA, Metz CE. Please be specific (letter). *AJR* **1990**;154:1121–1122
10. Page DL, Anderson TJ, Rogers LW. Carcinoma in situ (CIS). In: Page DL, Anderson TJ, eds. *Diagnostic histopathology of the breast.* New York: Churchill Livingstone, **1987**:157–192
11. Haagensen CD, Lane N, Lattes R, Bodian C. Lobular neoplasia (so-called lobular carcinoma in situ) of the breast. *Cancer* **1978**;42:737–769
12. Silverberg E, Boring CC, Squires TS. Cancer statistics, 1990. *CA* **1990**;40:9–26
13. Shapiro S. Evidence on screening for breast cancer from a randomized trial, supplement. *Cancer* **1977**;39:2772–2782
14. Tabár L, Fagerberg CJG, Gad A, et al. Reduction in mortality from breast cancer after mass screening with mammography. Randomized trial from the Breast Cancer Screening Working Group of the Swedish National Board of Health and Welfare. *Lancet* **1985**;1:829–832
15. Breast cancer screening guidelines agreed on by AMA, other medically related organizations. *JAMA* **1989**;262:1155
16. Centers for Disease Control. Use of mammography—United States, 1990. *MMWR* **1990**;39:621–630
17. Moskowitz M. Costs of screening for breast cancer. *Radiol Clin North Am* **1987**;25:1031–1037
18. Cyrlak D. Induced costs of low-cost screening mammography. *Radiology* **1988**;168:661–663
19. Eddy DM, Hasselblad V, McGirney W, Hendee W. The value of mammography screening in women under age 50 years. *JAMA* **1988**;259:1512–1519
20. Sickles EA, Ominsky SH, Sollitto RA, Galvin HB, Monticciolo DL. Medical audit of a rapid-throughput mammography screening practice: methodology and results of 27,114 examinations. *Radiology* **1990**;175:323-327
21. Murphy WA, Destouet JM, Monsees BS. Professional quality assurance for mammography screening programs. *Radiology* **1990**;175:319–320
22. Spivey GH, Perry GW, Clark VA, Coulson AH, Coulson WF. Predicting the risk of cancer at the time of breast biopsy: variation in the benign to malignant ratio. *Am Surg* **1982**;48:326-332
23. Sickles EA. Further experience with microfocal spot magnification mammography in the assessment of clustered breast microcalcifications. *Radiology* **1980**;137:9–14
24. Berkowitz JE, Gatewood MB, Gayler BW. Equivocal mammographic findings: evaluation with spot compression. *Radiology* **1989**;171:369–371
25. Tabár L, Dean PB. *Teaching atlas of mammography*, 2nd ed. New York: Thieme-Stratton, **1985**
26. Bassett LW, Kimme-Smith C, Sutherland LK, Gold RH, Sarti D, King W III. Automated and hand-held breast US: effect on patient management. *Radiology* **1987**;165:103–108
27. Kopans DB, Swann CA, White G, et al. Asymmetric breast tissue. *Radiology* **1989**;171:639-643
28. Löfgren M, Andersson I, Bondeson L, Lindholm K. X-ray guided fine-needle aspiration for the cytologic diagnosis of nonpalpable breast lesions. *Cancer* **1988**;61:1032-1037
29. Dowlatshahi K, Gent HJ, Schmidt R, Jokich PM, Bibbo M, Sprenger E. Nonpalpable breast tumors: diagnosis with sterotaxic localization and fine-needle aspiration. *Radiology* **1989**;170:427–433
30. Ciatto S, Del Turco MR, Bravetti P. Nonpalpable breast lesions: stereotaxic fine-needle aspiration cytology. *Radiology* **1989**;173:57–59

Diagnostic Importance of the Radiographic Density of Noncalcified Breast Masses:

Analysis of 91 Lesions

Valerie P. Jackson[1]
Kris A. Dines[1,2]
Lawrence W. Bassett[3]
Richard H. Gold[3]
Handel E. Reynolds[1]

Radiographic density is considered an important feature in the evaluation of noncalcified breast masses, yet no studies assessing its value have been published. The radiographic densities of 91 biopsy-proved, nonfatty, noncalcified breast masses were evaluated by three mammographers. The density determinations made by each observer were compared with the histologic outcome for the 51 benign and 40 malignant lesions. With the kappa statistic, interobserver agreement was relatively poor (0.22 to 0.49), and intraobserver agreement for one expert mammographer was 0.50. When the majority opinion of the mammographers was used, sensitivity was 48%, specificity was 80%, and both positive and negative predictive values were 66%.

As a solitary feature in lesion analysis, mammographic density is difficult to assess and is of limited value for the prediction of the benign or malignant nature of noncalcified breast masses.

***AJR* 157:25-28, July 1991**

Radiographic density is considered an important feature in the evaluation of noncalcified breast masses. Masses that clearly contain fat are benign. It is widely believed that nonfatty, low-density radiopaque masses are usually benign, whereas most carcinomas are high-density lesions [1-4]. It is also generally assumed that density determination is relatively easy. However, no blinded studies evaluating the contribution of density to mammographic interpretation have been published. The purpose of this study was to evaluate observer agreement for the classification of radiographic density and to examine the value of such density determination in the prediction of the benign or malignant nature of noncalcified breast masses.

Materials and Methods

Mammograms from 91 consecutive biopsy-proved, nonfatty, noncalcified breast masses were selected from the files of a single hospital. The cases were thought to be representative of the range of mammographic abnormalities commonly seen in practice. All circumscribed masses were examined sonographically to exclude cysts. Therefore, all lesions in this selected series were solid. In addition, lesions documented to be stable on previous mammograms for at least 2 years were excluded from the study. The single original contact mammography film that best depicted the lesion was chosen for the study. There were 91 films, with one mass on each film. All mammograms were obtained with one of two dedicated mammography units, a Philips Mammodiagnost-UM (Philips Medical Systems, Shelton, CT) or a Thomson-CGR Senographe 500T (GE Medical Systems, Milwaukee, WI). All imaging was performed with a molybdenum anode, reciprocating grid, OM-1 film and Min-R screens (Eastman Kodak, Rochester, NY), 28 or 30 kVp, and the same dedicated 3-min film processor.

The films were randomized and sent for blind review to two highly experienced mammographers and a third radiologist with 2 months of mammography experience. Each observer was asked to evaluate independently whether the density of each mass was less than, equal to, or greater than normal radiographically dense structures on the mammogram, such as nonfatty parenchyma, ducts, and blood vessels [1]. One of the experienced mammographers

Received October 3, 1990; accepted after revision January 7, 1991.

[1] Department of Radiology, Indiana University School of Medicine, Wishard Memorial Hospital, 1001 W. 10th St., Indianapolis, IN 46202. Address reprint requests to V. P. Jackson.

[2] Department of Engineering and Technology, Indiana University Purdue University at Indianapolis, Indianapolis, IN 46202.

[3] Department of Radiological Sciences, Iris Cantor Center for Breast Imaging, UCLA School of Medicine, 18033 Le Conte Ave., Los Angeles, CA 90024.

0361-803X/91/1571-0025
© American Roentgen Ray Society

blindly reevaluated all of the cases 6 months after the first review to determine the intraobserver agreement. Inter- and intraobserver agreements were measured by using the kappa statistic [5]. Sensitivity and specificity of the density evaluation were calculated by comparing the evaluation with the pathologic diagnosis of the lesion [6]. For this, density scores of the masses were determined by using the consensus of at least two of the three observers.

Results

There were 51 benign and 40 malignant nonfatty, noncalcified masses, one mass in each film evaluated. Thirty-seven (41%) of the masses were smooth and circumscribed; 29 (32%) were circumscribed, but had one or more foci of indistinctness along their borders; and 25 (27%) were spiculated. Twenty-three (25%) of the masses were in fatty breasts, 12 (13%) were in radiographically dense breasts, and 56 (62%) were in mixed fatty/dense breasts. The masses ranged in size from 6 to 55 mm (mean, 19 mm; median, 16 mm). The mean size of the benign masses was 14.6 mm, and the mean size of the malignant tumors was 16.7 mm. By using Student's t test [7], we determined that this difference was not statistically significant ($p = .26$). All of the malignant tumors were invasive ductal carcinomas except for one papillary carcinoma and one colloid carcinoma.

When three categories of radiographic density (less than, equal to, or greater than density of normal parenchymal structures) were used, the agreement between the three observers was low. Observers 1 and 2, the expert mammographers, agreed only 51% of the time. We then grouped the densities into only two categories: (1) density less than or equal to and (2) density greater than the density of the normal parenchymal structures, as specified by Tabar and Dean [1]. As expected, the agreement improved. Observers 1 and 2 agreed in 78% of cases (kappa = 0.42), 1 and 3 agreed in 74% of cases (kappa = 0.49), and readers 2 and 3 agreed in 58% of cases (kappa = 0.22). By convention, a kappa statistic of 0.40–0.75 is considered to reflect good reproducibility, whereas a kappa of less than 0.40 is considered to reflect marginal or poor reproducibility [5].

The density recorded by each observer was compared with the pathologic findings, as shown in Table 1. Because of the lack of a gold standard for the subjective determination of radiographic density, the density specified by at least two of the three observers (using only two density categories) was also compared with the pathologic results (Table 2). The resulting sensitivity was 48% and specificity was 80%. For the subset of the 66 smooth or circumscribed masses, the sensitivity was 39% and specificity was 81%.

TABLE 1: Comparison of Pathologic Findings with Classification of Radiographic Density by Each Mammographer

Radiographic Density and Pathologic Result of Mass	Percentage of Lesions So Classified by Mammographer #		
	1	2	3
Low-density benign masses	80	96	55
High-density benign masses	20	4	45
Low-density malignant masses	50	70	33
High-density malignant masses	50	30	68

TABLE 2: Consensus Density Scores vs Pathologic Findings of Masses

Density	Pathologic Findings	
	Malignant	Benign
High	19	10
Low	21	41
Total	40	51

Note.—Sensitivity = 48%, specificity = 80%, positive predictive value = 66%, negative predictive value = 66%.

Discussion

Radiographic density is one of the features used in the evaluation of noncalcified masses seen on mammograms, and it is considered to be an important feature in the determination of their possible benign or malignant origin [1]. Although smooth, circumscribed masses that clearly contain fat are benign [1], no reports of blind studies that examined the actual contribution of the density of nonfatty, noncalcified masses to mammographic interpretation have been published. Density determination by the use of Hounsfield units has been done with CT of the breast [8–10]. Although those studies dealt primarily with contrast enhancement of malignant lesions, they showed little difference between the attenuation of normal, benign, and malignant processes in the absence of infused contrast material.

Sixty-six percent of the masses classified as high density by a majority of observers in this study were malignant (Fig. 1). Eighty percent of the benign masses were classified as low density (Fig. 2). Disturbingly, however, 52% of the malignant masses also were classified as low density or density equivalent to that of normal nonfatty parenchyma by at least two of the three observers (Fig. 3). Thus, in this study, low density could not have been used to exclude malignancy. It has been widely accepted that "rare" low-density carcinomas are usually papillary or colloid types [1]. In this study, all but two of the malignant tumors were infiltrating ductal carcinomas, and the single papillary and colloid carcinomas were classified as high density by a majority of observers (Fig. 4).

This study showed a marked lack of agreement in the determination of radiographic density. The kappa statistics for agreement were in the poor/marginal category or at the low end of the good reproducibility category. Although agreement, as might be expected, was poorer when comparing the results of the two expert mammographers with those of the less experienced mammographer, there was even a marked variation between the classifications of the two experts (who were at the same institution), and for one of the experts at different times (Fig. 5). This emphasizes the lack of standardization and agreement in the classification of radiographic density.

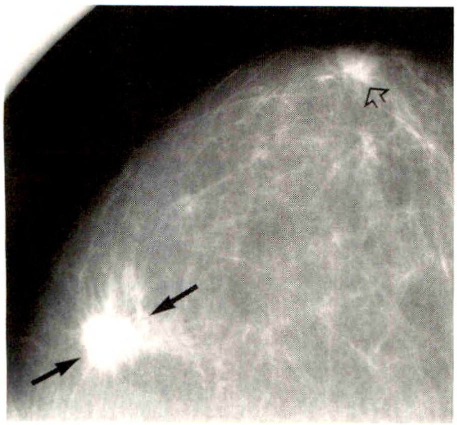

Fig. 1.—Craniocaudal mammogram of an invasive ductal carcinoma (*solid arrows*) classified as high density by all three observers. Normal parenchymal reference density in this case was nipple (*open arrow*).

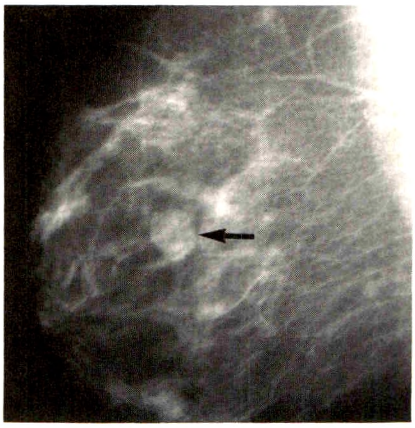

Fig. 2.—Oblique mammogram of a benign fibroadenoma (*arrow*) classified as low density by all observers.

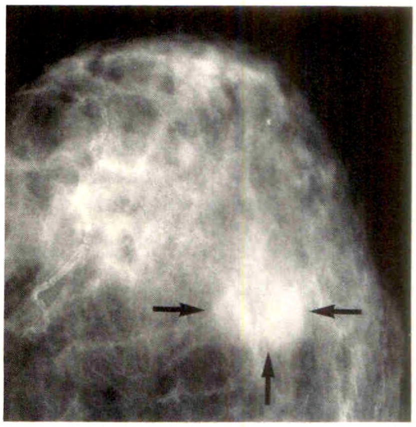

Fig. 3.—Craniocaudal mammogram of an infiltrating ductal carcinoma (*arrows*) classified as low density by all observers.

Fig. 4.—Craniocaudal mammogram of a colloid carcinoma (*arrows*) classified as high density by two of three observers.

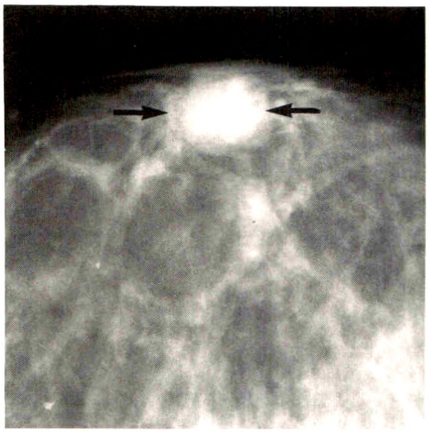

4

Fig. 5.—Craniocaudal mammogram of a benign fibroadenoma (*arrows*) classified as low density by one mammographer and high density by another. The third mammographer classified it as low density on the first reading and high density on the second. *Arrowhead* = nipple.

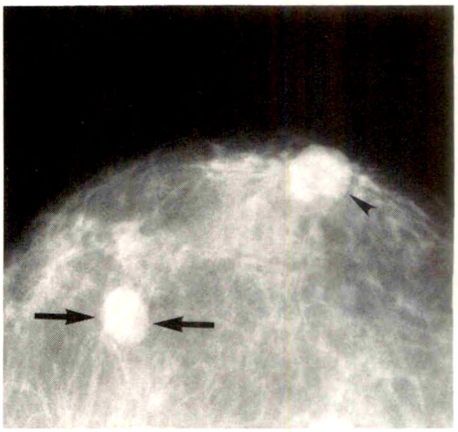

5

Had interobserver agreement been better, the positive and negative predictive values of 66% might appear to reflect a useful association between density and pathology. However, positive and negative predictive values are, in large part, related to the prevalence of the disease in the sample population [11]. In this series, the prevalence of breast carcinoma was 44%. If, for example, the prevalence of malignancy was increased to 70% (with the sensitivity and specificity remaining 48% and 80%, respectively), the positive predictive value would increase to 86%, whereas the negative predictive value would decrease to 40%. Conversely, if the prevalence of carcinoma was decreased to 20%, the resulting positive predictive value would be 38%, whereas the negative predictive value would increase to 87%. In clinical practice, the prevalence of breast cancer is very low, which would lead to an even lower positive predictive value.

Because all cases had surgical biopsy, some selection bias was unavoidable in this study. Cysts and mammographically stable masses were excluded. Using the standard maxim that low-density lesions tend to be benign, one would expect a preponderance of high-density lesions to be selected for biopsy. Such a selection bias would be expected to lead to a higher percentage of pathologically benign lesions in the high-density category. However, in this series, a higher percentage of the malignant lesions were classified as low or equivalent density than as high density.

It is difficult, if not impossible, for a mammographer to evaluate the density of a lesion independently of the other features, especially the border characteristics. Therefore, we also examined the subgroup of circumscribed masses to determine if density assessment was more or less accurate than for the entire group of masses. For the smooth and/or circumscribed masses, the sensitivity decreased slightly (39%) and the specificity remained the same (81%). The inter- and intraobserver agreements were unchanged. For the lesions with spiculated borders, the sensitivity of density improved to 55%, but at the expense of a drop in specificity to 67%.

Optimal radiographic contrast is necessary for density assessment. This involves the use of state-of-the-art mammography equipment with a molybdenum anode and reciprocating grid, vigorous compression, an appropriately low kilovoltage, a high-contrast film-screen combination, and the use of extended processing when feasible [12]. All of these factors were used for this study.

Because density is intuitively related to lesion size, optimally, the density of a mass should be compared with the density of an approximately equal volume of normal parenchyma [3]. This was done whenever possible. However, in some of the predominantly fatty breasts, it may have been difficult for the observers to find an area of similar size. This may have led them to base their determination of density on their ability or inability to see parenchymal structures through the masses or to estimate the relative density of parenchymal areas unequivalent in size to the masses. Indeed, this is what is done in clinical practice in such situations. However, further research is necessary to assess radiographic density as it is related to the size of a mass.

The analysis of a mass seen on mammography is a complex process involving assessment of its size, shape, border characteristics, and density. Little attention has been given to the exact role of each of these features in the analytic process. This study shows that density assessment is a difficult task, and the contribution of density to the mammographic analysis of nonfatty, noncalcified masses is less than had been previously thought.

ACKNOWLEDGMENTS

We thank Lorrie Kalasinski and Barry Katz for statistical advice and analysis for this study.

REFERENCES

1. Tabar L, Dean PB. *Teaching atlas of mammography*, 2nd ed. New York: Springer-Thieme, **1985**:18
2. Moskowitz M. Circumscribed lesions of the breast. In: Moskowitz M, ed. *Diagnostic categorical course in breast imaging*. Oak Brook, IL: Radiological Society of North America, **1986**:31–33
3. Andersson I. Mammography in clinical practice. *Med Radiogr Photogr* **1986**;62:1–41
4. Egan RL. Breast masses. In: *Breast imaging: diagnosis and morphology of breast diseases*. Philadelphia: Saunders, **1988**:324–343
5. Rosner B. Regression and correlation methods. In: *Fundamentals of biostatistics*. 2nd ed. Boston: Duxbury Press, **1986**:369–441
6. Rosner B. Probability. In: *Fundamentals of biostatistics*, 2nd ed. Boston: Duxbury Press, **1986**:42–66
7. Rosner B. Hypothesis testing: two-sample inference. In: *Fundamentals of biostatistics*, 2nd ed. Boston: Duxbury Press, **1986**:240–277
8. Chang CHJ, Sibala JL, Fritz SL, Dwyer SJ, Templeton AW. Specific value of computed tomographic breast scanner (CT/M) in diagnosis of breast diseases. *Radiology* **1979**;132:647–652
9. Gisvold JJ, Reese DF, Karsell PR. Computed tomographic mammography (CTM). *AJR* **1979**;133:1143–1149
10. Chang CHJ, Nesbit DE, Fisher DR, et al. Computed tomographic mammography using a conventional body scanner. *AJR* **1982**;138:553–558
11. Browner WS, Newman TB, Cummings SR. Designing a new study: III. Diagnostic tests. In: Hulley SB, Cummings SR, eds. *Designing clinical research*. Baltimore: Williams & Wilkins, **1988**:87–97
12. Sickles EA. Breast masses: mammographic evaluation. *Radiology* **1989**;173:297–303

Obstructive Dilatation of Extrahepatic Recipient and Donor Bile Ducts Complicating Orthotopic Liver Transplantation:
Imaging and Laboratory Findings

William J. Miller[1]
William L. Campbell[1]
Albert B. Zajko[1]
Antonio Pinna[2]
Giorgio Zetti[2]
Andrei C. Stieber[2]
Richard G. Foster[1]
James W. Lecky[1]
Kyung Y. Lee[3]

Biliary obstruction in liver transplants is most commonly due to stricture at the biliary anastomosis. The native common bile duct typically is normal. We retrospectively studied 28 patients with choledochocholedochostomy anastomoses who had marked native and donor extrahepatic bile duct dilatation associated with clinical evidence of biliary obstruction. Operative cholangiograms were compared with postoperative cholangiograms obtained a mean of 50 weeks (range, 2–246 weeks) later. Mean caliber of the native common bile duct increased from 7.5 ± 2.0 mm on operative cholangiograms to 14.8 ± 3.9 mm on postoperative cholangiograms ($p < .001$). Mean caliber of the donor common hepatic duct increased from 5.9 ± 1.3 mm on operative cholangiograms to 12.8 ± 3.8 mm on postoperative cholangiograms ($p < .001$). Dilatation of the cystic duct remnant was seen in 15 patients. All patients had surgical revision to choledochojejunostomy with improved results of liver function studies in most cases.

Diffuse dilatation of native and donor extrahepatic bile ducts may develop in liver transplant recipients. Typical features include native and donor extrahepatic ducts greater than 12 mm in diameter and a dilated cystic duct remnant on postoperative cholangiography in a patient with otherwise unexplained hepatic dysfunction.

***AJR* 157:29–32, July 1991**

Cholangiography is an important part of the postoperative evaluation of orthotopic liver transplant recipients, especially when complications of the biliary system are suspected [1, 2]. Cholangiography is performed to look for biliary stricture, obstruction, bile leak, and choledocholithiasis.

At our institution, the most common biliary surgery at the time of orthotopic liver transplantation is a choledochocholedochostomy, which consists of an anastomosis between donor and recipient extrahepatic bile ducts. A T-tube is placed to stent the anastomosis, permit monitoring of bile output, and provide access for follow-up cholangiography.

Anastomotic stricture is the most common cause of biliary obstruction after transplantation [1] and typically results in dilatation of the donor biliary duct. However, several patients have had laboratory evidence of biliary obstruction and dilatation of both native and donor biliary trees [3]. A number of these patients have been successfully treated for suspected obstruction at the ampulla of Vater by surgical revision of the biliary anastomosis to a choledochojejunostomy. We reviewed the radiologic findings and clinical laboratory data of diffuse extrahepatic bile duct dilatation associated with hepatic dysfunction after liver transplantation.

Materials and Methods

Between March 1980 and September 1990, approximately 1500 patients underwent primary orthotopic liver transplantation with choledochocholedochostomy biliary reconstructions. Twenty-eight patients with diffuse extrahepatic bile duct dilatation were identified in whom clinical and radiologic data could be retrieved. There were 15 females and 13 males with a mean age of 42 years (range, 11–64 years). All patients had undergone orthotopic

Received December 3, 1990; accepted after revision February 4, 1991.

Presented at the annual meeting of the American Roentgen Ray Society, Washington, DC, May 1990.

[1] Department of Radiology, University of Pittsburgh School of Medicine, Presbyterian University Hospital, DeSoto at O'Hara Sts., Pittsburgh, PA 15213. Address reprint requests to W. L. Campbell.

[2] Department of Surgery, University of Pittsburgh School of Medicine, Presbyterian University Hospital, DeSoto at O'Hara Sts., Pittsburgh, PA 15213.

[3] Department of Biostatistics, University of Pittsburgh, Pittsburgh, PA 15213.

0361–803X/91/1571–0029
© American Roentgen Ray Society

liver transplantation for the first time at our institution. All patients had end-to-end choledochocholedochostomy anastomoses, usually formed between the proximal donor common bile duct and either the native proximal common bile duct or distal common hepatic duct [4]. All exhibited clinical evidence of biliary obstruction and underwent subsequent biliary anastomotic revision to a Roux-en-Y choledochojejunostomy. Patients with anastomotic strictures and/or stones were excluded.

Cholangiograms were retrospectively reviewed to determine the sizes of the native extrahepatic duct, donor extrahepatic duct, and intrahepatic ducts. The caliber of the donor common hepatic duct was measured at the midpoint between the duct bifurcation and the biliary anastomosis; the caliber of the native common bile duct was measured at the midpoint between the anastomosis and the sphincter of Oddi. We attempted to use the least magnified films; no correction for radiographic magnification was made. Operative cholangiograms were compared with the last postoperative T-tube, percutaneous transhepatic, or endoscopic retrograde cholangiogram obtained before biliary anastomotic revision. The average time between operative cholangiography and the last cholangiogram before revision of the bile duct anastomosis was 50 weeks (range, 2–246 weeks). Biliary resting pressures were recorded in five patients through a 19-gauge butterfly needle inserted into the clamped T-tube. Pressure was recorded with a 50-cm manometer with the zero mark positioned at the midaxillary line. Normal pressure was considered to be less than 15 cm H_2O; 15–20 cm H_2O was borderline abnormal [5].

Serum levels of liver enzymes (aspartate aminotransferase [AST], alanine aminotransferase [ALT], γ-glutamyltransferase [GGT], alkaline phosphatase), serum bilirubin levels, and results of liver biopsies done at the time of the last cholangiogram and approximately 2 weeks after biliary anastomotic revision were compared.

Bile duct caliber was statistically analyzed with a paired t test and Wilcoxon signed-rank test (data of latter not shown). Results of liver profile studies were analyzed with a sign test of the median [6].

Results

Mean size of the donor common hepatic duct increased from 5.9 ± 1.3 mm to 12.8 ± 3.8 mm, an increase of 219% compared with operative cholangiograms ($p < .001$). Mean size of the native common bile duct at transplantation was 7.5 ± 2.0 mm in diameter and increased to 14.8 ± 3.9 mm on the last cholangiogram before surgery, an increase of 195% ($p < .001$). Maximal caliber of the extrahepatic bile duct before surgery ranged from 10 to 22 mm. Intrahepatic duct caliber exhibited little or no increase over time and/or with clinical evidence of obstruction (Fig. 1). Small-caliber (e.g., 8-French) T-tubes occasionally migrated distally in the dilated common bile ducts and rarely extended through the ampulla of Vater.

Serum levels of liver enzymes (AST, ALT, GGT, alkaline phosphatase) and bilirubin were elevated before anastomotic revision. Mean total serum bilirubin level was 3.4 mg/dl (58 μmol/l), range 0.7–10.8 mg/dl (12–184 μmol/l); mean GGT level was 464 U/l, range 18–2912 U/l; and mean alkaline phosphatase level was 274 U/l, range 52–1805 U/l. Twelve patients were jaundiced; none had abdominal pain. Liver enzyme and serum bilirubin levels decreased significantly approximately 2 weeks after surgery except for alkaline phosphatase levels, which did not decrease significantly. After revision, the mean total serum bilirubin level was 2.8 mg/dl (48 μmol/l), range 0.2–25.6 mg/dl (4–438 μmol/l); mean GGT level was 310 U/l, range 16–1605 U/l; and mean alkaline phosphatase level was 226 U/l, range 56–1178 U/l. Of 26 patients with complete liver function data before and after bile duct revision, the serum bilirubin level decreased in 19 and was unchanged in four, the GGT level decreased in 22, and the alkaline phosphatase level decreased in 17.

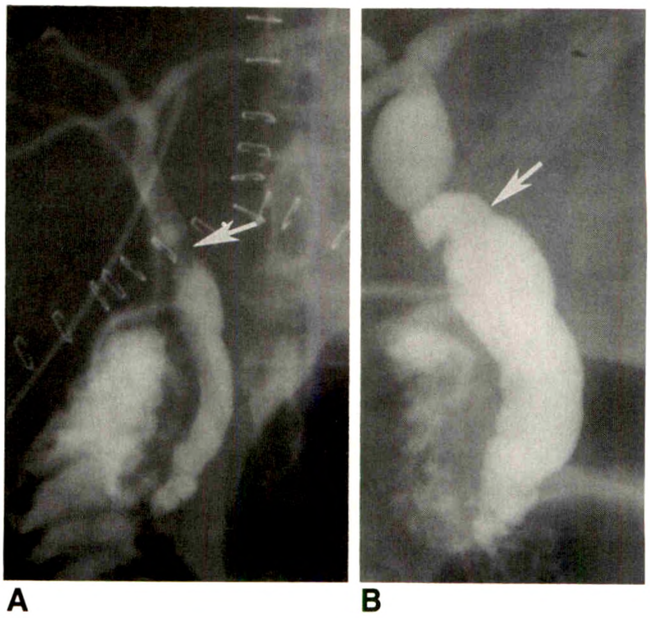

Fig. 1.—*A*, T-tube cholangiogram obtained 5 days after transplantation shows normal-caliber bile ducts. *Arrow* shows choledochocholedochostomy anastomosis.

***B*, T-tube cholangiogram obtained 1 month after transplantation reveals biliary dilatation, most marked in extrahepatic ducts. *Arrow* shows anastomosis. Patient was treated by revision to a choledochojejunostomy with a Roux-en-Y anastomosis.**

Liver biopsies were done before reconstructive biliary surgery in 25 patients; 12 showed cholestasis. Twelve patients had liver biopsies both before and after biliary revision to a Roux-en-Y anastomosis. Six of these patients showed resolution of cholestasis, and six showed findings of nonspecific inflammation or mild rejection that did not change after surgery.

Cystic duct remnants were shown in 18 patients and were dilated in 15. Dilatation was considered to be present if the lumen measured 5 mm or more in diameter and, if a cystic duct remnant was seen on operative cholangiography, increased in size by 3 mm or more.

Biliary resting pressures were measured via the T-tube in five of 28 patients; four measurements were normal (<15 cm H_2O) and one was borderline elevated.

No strictures or other anatomic causes for obstruction at the ampulla of Vater were identified in any of the cases.

Discussion

Diffuse dilatation of the native and donor bile ducts with clinical evidence of obstruction is an unusual complication of liver transplantation. Stieber et al. [3] were the first to report this finding and postulated the cause to be papillary dyskinesia due to devascularization or denervation of the ampulla of Vater during orthotopic liver transplantation.

Caliber of the extrahepatic bile duct remains stable over time in most orthotopic liver transplantation patients. Mild increases in extrahepatic duct size have been seen in some apparently uncomplicated orthotopic liver transplant recipients; that is, patients without clinical evidence of biliary obstruction. Transplantation patients with diffuse extrahepatic dilatation and hepatic dysfunction differ radiologically from transplantation patients without complications mainly by greater dilatation of the extrahepatic duct and cystic duct remnants. Intrahepatic duct dilatation is typically absent, but sporadic cases with borderline dilatation have been seen. This may reflect the tendency for the extrahepatic bile ducts to dilate earlier in obstruction than does the intrahepatic biliary tree.

Other possibly useful confirming tests for biliary obstruction were not available in most of the patients studied. Resting biliary pressures in five patients were not elevated, although the small number of examinations does not permit firm conclusions. Resting pressure measurements made during constant bile duct perfusion at several rates of perfusion might provide a more sensitive test for biliary obstruction in these patients [5]. Follow-up radiographs to detect delayed drainage of the bile ducts were obtained in two patients and showed abnormalities. Retention of contrast material in the common duct 45 min after administration was suggestive of obstruction [7]. Unpublished data from our own group indicate that the common duct in most orthotopic liver transplantation patients empties completely of contrast material within 15 min. Hepatobiliary scintigraphy was not performed in our patients. To date, no reliable endoscopic manometric data of the sphincter of Oddi are available in patients with ductal dilatation after transplantation.

Because diffuse extrahepatic dilatation may develop at any time after orthotopic liver transplantation (2–246 weeks, in our series) and may be associated with an insidious clinical and laboratory onset of liver dysfunction, diagnosis may be difficult. Some patients exhibited a slow but steady increase in bile duct caliber for several weeks after transplantation, which was associated with laboratory evidence of obstruction that prompted relatively early surgical intervention. Others showed little or no change in bile duct caliber for the immediate postoperative months and had their T-tubes removed. They returned months or years later with signs of obstruction and diffusely dilated ducts. Overall, bile duct dilatation was diagnosed in 10 of 28 patients within 3 months after transplantation, the period in which the T-tube normally remains in place and in which routine cholangiography facilitates diagnosis.

The decision to perform surgical reconstruction for diffuse bile duct dilatation must take into consideration the laboratory values, the radiologic findings, and the overall clinical status of the patient. Clearly, extrahepatic bile duct dilatation does not necessarily indicate current biliary obstruction, as in the case of a lax duct that may result from prior choledocholithiasis in nontransplantation patients [8]. Nevertheless, the acquired postoperative dilatation and the degree of caliber abnormality seen in our patients is highly suggestive of obstruction, perhaps of a low grade or intermittent nature. Thus, 26 of 28 patients had extrahepatic ducts that were 12 mm or more, one of the criteria used by Geenen et al. [9] for the diagnosis of dysfunction of the sphincter of Oddi. Although some transplantation patients without clinical evidence of obstruction have shown increases in extrahepatic duct size, the changes are typically milder than those seen in our study group. An investigation of extrahepatic bile duct caliber in uncomplicated liver transplants is currently underway.

The decision to operate on patients with extrahepatic bile duct dilatation is complicated by the not infrequent coexistence of multiple conditions such as rejection and infection that may cause abnormal results of liver function tests. More than one cause of hepatic dysfunction might explain why alkaline phosphatase values were not significantly decreased after reconstructive biliary surgery in our patients. Cholestasis on allograft liver biopsies may be associated with a number of conditions in addition to extrahepatic biliary obstruction. However, cholestasis of the type and degree seen in our patients is normally found in a minority of transplant biopsies. In the absence of a true gold standard test for biliary obstruction in patients with dilatation of the extrahepatic bile ducts, care and experience is required in selecting patients who will benefit from anastomotic revision.

Although the precise cause of diffuse extrahepatic ductal dilatation is not known, one possible mechanism is dysfunction of the sphincter of Oddi, perhaps due to operative interruption of inhibiting nerve fibers that normally accompany the common duct [10]. Other possible unproved causes include ischemia or opportunistic infection affecting the sphincter of Oddi. The possibility of increased duct laxity due to an unidentified factor in the posttransplantation environment cannot be entirely ruled out. None of our patients had an obvious cause of obstruction of the common bile duct, such as stricture, pancreatitis, tumor, or choledocholithiasis. None had clinical or laboratory evidence of significant biliary tract infection. Nevertheless, because opportunistic infections are common in liver allografts, the possible role of infection in diffuse duct dilatation cannot be excluded.

Despite the occurrence of diffuse obstructive dilatation of native and donor bile ducts in liver transplantation patients with choledochocholedochostomy reconstructions, the duct-to-duct anastomosis is still favored for adult patients by surgeons at our center. This preference is based on the low frequency of diffuse obstructive dilatation coupled with the advantages of having a T-tube in place for monitoring bile quantity and quality and for performing postoperative cholangiography.

In conclusion, marked diffuse biliary dilation affecting predominantly the recipient and donor extrahepatic bile ducts and associated with hepatic dysfunction may occur in liver transplants. The exact cause is unknown, but may be related to dysfunction of the sphincter of Oddi due to denervation. Surgical revision of the choledochocholedochostomy anastomosis to a choledochojejunostomy bypasses the sphincter of Oddi, and typically leads to clinical and laboratory improvement. Correct diagnosis depends on careful correlation of the cholangiographic findings, laboratory tests, biopsy results, and the overall clinical picture.

ACKNOWLEDGMENT

We thank Maggie Zdrodowski for assistance in manuscript preparation.

REFERENCES

1. Zajko AB, Campbell WL, Bron KM, et al. Cholangiography and interventional biliary radiology in adult liver transplantation. *AJR* **1985**;144:127–133
2. Lerut J, Gordon RD, Iwatsuki S, et al. Biliary tract complications in human orthotopic liver transplantation. *Transplantation* **1987**;43:47–51
3. Stieber AC, Ambrosino G, Kahn D, et al. An unusual complication of choledochocholedochostomy in orthotopic liver transplantation. *Transplant Proc* **1988**;20:619–621
4. Calne RY. In: Calne RY, ed. *Liver transplantation.* Philadelphia: Grune and Stratton, **1985:**169
5. vanSonnenberg E, Ferrucci JT, Neff CC, Mueller PR, Simeone JF, Wittenberg J. Biliary pressure: manometric and perfusion studies at percutaneous transhepatic cholangiography and percutaneous biliary drainage. *Radiology* **1983**;148:41–50
6. Steele R, Torrie J. *Principles and procedures of statistics.* New York: McGraw-Hill, **1960**
7. Belsito A, Marta JB, Cramer GG, Dickinson PB. Measurement of biliary tract size and drainage time. *Radiology* **1977**;122:65–69
8. Mueller PR, Ferrucci JT, Simeone JF, vanSonnenberg E, Hall DA, Wittenberg J. Observations on the distensibility of the common bile duct. *Radiology*, **1984**;142:467–472
9. Geenen JE, Hogan WJ, Dodds WJ, Toouli J, Venu RP. The efficacy of endoscopic sphincterotomy after cholecystectomy in patients with sphincter-of-Oddi dysfunction. *N Engl J Med* **1989**;310:82–87
10. Thune A, Jivegard L, Conradi N, Svanvik J. Cholecystectomy in the cat damages pericholedochal nerves and impairs reflex regulation of the sphincter of Oddi. *Acta Chir Scand Suppl* **1988**;154:191–194

Thin-Layer Chromatography to Monitor Cholesterol Gallstone Dissolution by Methyl *tert*-Butyl Ether

Horacio B. D'Agostino[1]
Eric vanSonnenberg[1, 2]
Claudio D. Schteingart[2]
Alan F. Hofmann[2]
Giovanna Casola[1]
John R. Mathieson[3]

We describe a simple and inexpensive method of monitoring methyl *tert*-butyl ether (MTBE) dissolution of cholesterol gallstones with thin-layer chromatography (TLC) in 10 patients. TLC is a routine semiquantitative laboratory method that can be used to measure the cholesterol concentration present in the MTBE and bile mixture aspirated through the cholecystostomy catheter during gallstone dissolution. TLC is practical in the clinical setting because it can be used to determine if gallstone dissolution is occurring and when MTBE lavage is no longer effective. TLC is performed in the laboratory with routine material and is completed in 15 min. Each TLC measurement costs about $1. The procedure provides objective and specific chemical information on effectiveness and progression of gallstone dissolution, apart from the radiologic and sonographic studies. In our study, TLC signaled effective dissolution in the initial phase of gallstone dissolution by detecting large amounts of cholesterol in the MTBE and bile mixture even *before* a visible change in size or shape of the stone became apparent by transcatheter cholecystography or by sonography (six of 10 patients). Conversely, lack of cholesterol on TLC after 1 hr or more of MTBE infusion indicates that the stones are pigmented or contain substantial calcium. This means that dissolution with MTBE will be ineffective and that solvent infusion should be terminated. In those cases in which dissolution is progressing well, when TLC shows decreasing amounts of cholesterol in the effluent, only residual fragments insoluble to MTBE remain or the stone is sequestered from MTBE; at this point, solvent infusion should be discontinued or the catheter must be repositioned.

Monitoring the rate of cholesterol dissolution by TLC provides important complementary information to cholecystography and sonography during gallstone treatment with MTBE.

***AJR* 157:33-36, July 1991**

Transcatheter contact dissolution with methyl *tert*-butyl ether (MTBE) is an effective method of dissolving cholesterol gallstones [1–4]. Currently, the procedure is considered investigational in the United States and is monitored by the Food and Drug Administration. At present, the only methods of determining the effectiveness and endpoint of gallstone dissolution with MTBE are catheter cholecystography and/or sonography. These imaging procedures offer a visible assessment of dissolution, but give no chemical information. Early leeching of cholesterol may not be shown by imaging, and residual stone fragments may not be shown by cholecystography because of limitations of fluoroscopic resolution, overlying bowel gas, or improper concentration of contrast material. Problems of sonographic monitoring include the coiled catheter that may obscure fragments and lack of gallbladder distension that precludes detection of residual fragments. Even if fragments are shown by cholecystography or by sonography, solubility or insolubility of the residual debris or fragments in MTBE cannot be predicted by these imaging methods.

We have complemented the two radiologic studies with adsorption thin-layer chromatography (TLC), a semiquantitative method that assesses the concentration

Received December 10, 1990; accepted after revision January 18, 1991.

This work was supported in part by NIH grants AM 21506 and 32130 and grant-in-aid from the Falk Foundation and Lithox Systems, Inc., Salem, MA.

[1] Department of Radiology, University of California, San Diego, La Jolla, CA 92093.

[2] Department of Medicine, Division of Gastroenterology, University of California, San Diego, La Jolla, CA 92093.

[3] Department of Radiology, St. Paul's Hospital, 1081 Burrard St., Vancouver, B. C. V6Z 1Y6, Canada.

0361-803X/91/1571-0033
© American Roentgen Ray Society

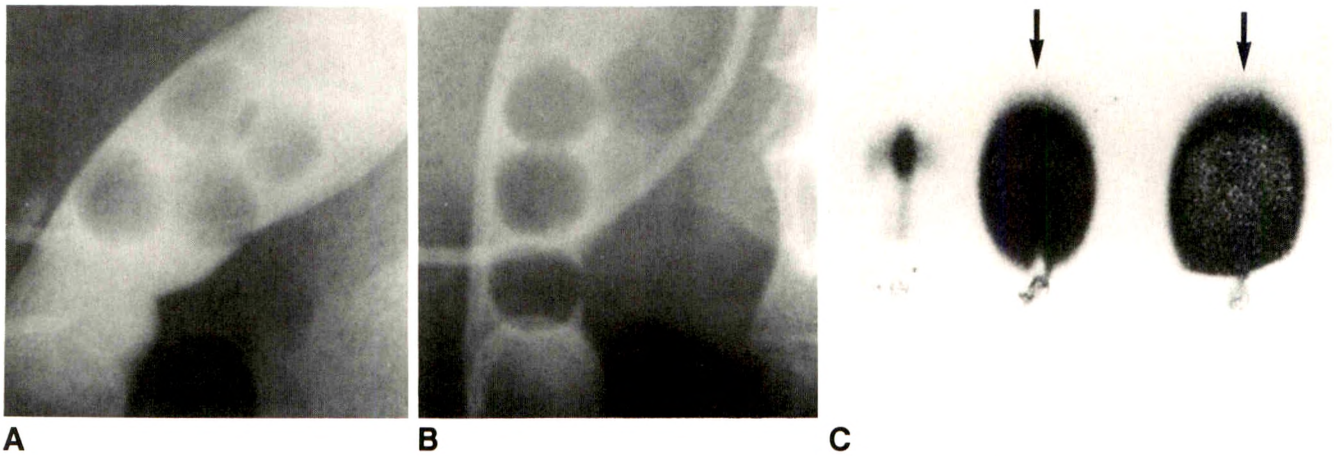

Fig. 1.—Thin-layer chromatography (TLC) shows effectiveness of dissolution, despite lack of visible change by cholecystography.
***A*, Cholecystogram before infusion of methyl *tert*-butyl ether (MTBE) in a 34-year-old woman with four 1.5-cm noncalcified gallstones.**
***B*, Cholecystogram 1 hr after MTBE infusion shows no significant change in size of stones.**
***C*, TLC after 1 hr of MTBE lavage reveals large concentration of cholesterol (*arrows*) in effluent MTBE. This indicates that dissolution is effective despite lack of a visible change on catheter cholecystogram. Faint spot at left indicates low cholesterol concentration in baseline bile sample.**

of cholesterol present in the MTBE that is aspirated through the cholecystostomy catheter. The technique yields information regarding the appropriateness of MTBE instillation and provides a method of monitoring the effectiveness of dissolution therapy. TLC also can document the presence of gallstones that are resistant to MTBE, thereby avoiding unnecessary solvent instillation.

Materials and Methods

TLC is performed on 5 × 7 cm aluminum-backed silica gel plates (DC-Alufollen, Klesselger 60, EM Science, Gibbstown, NJ). A 1-μl aliquot of the clear supernatant (MTBE phase) from the fluid aspirated during gallstone dissolution along with 1-μl samples of standard solutions of cholesterol in MTBE (0.2, 0.5, 1.0, 2.0, 5.0, and 10.0 g/l) are spotted 5 mm from the bottom of the plate at 5-mm intervals. The chromatogram is developed with chloroform-methanol 98:2 v:v in a glass TLC chamber until the solvent front travels approximately 6 cm from the bottom. The TLC plate is dried with a hair dryer, sprayed with a solution of phosphomolybdic acid in absolute ethanol (10 g/100 ml, Aldrich, Milwaukee, WI), and heated in an oven at 120–140°C for a few minutes until the spots develop a blue color (a laboratory hot plate also can be used). A semiquantitative estimation of the cholesterol concentration in the MTBE recovered from the patient is obtained by visual comparison of the diameter and intensity of the sample spot to the known cholesterol standards. The procedure takes no more than 15 min and should be done inside a fume hood, or at least in a well-ventilated area separate from the patient's suite. TLC is a routine laboratory procedure. A more detailed description of the TLC technique can be found in a standard reference manual [5]. The materials needed to perform each TLC measurement cost approximately $1. Results of TLC are examined in conjunction with oral cholecystograms and follow-up sonographic examinations to assess gallstone dissolution with MTBE.

The procedure has been used in nine women and one man, 27 to 70 years old, who were undergoing gallstone dissolution with MTBE. The patients had stones ranging from 5 to 45 mm in diameter, and the number of stones ranged from one to uncountable. Six patients had no calcification in their gallstones shown on plain films of the right upper quadrant and on CT scans; four patients had a few flecks of calcium or a calcified nidus shown on CT.

Percutaneous cholecystostomy and MTBE dissolution were performed in the standard fashion [1, 3]. A 7-French polyethylene locking gallbladder catheter (Medi-Tech, Watertown, MA) that is resistant to MTBE was used in all cases [4].

In order to obtain bile for the TLC, the gallbladder bile is drained completely through the percutaneous cholecystostomy catheter, then hepatic bile is aspirated for the sample. An aliquot of this hepatic bile is collected in a test tube. An equal volume of MTBE is added to the tube. The tube is shaken vigorously for 15 sec; the mixture is allowed to settle while the two layers separate into an upper layer (MTBE containing cholesterol) and a lower aqueous layer (bile). Baseline cholesterol concentration in the MTBE layer is measured by TLC. Aliquots of the supernatant layer from the MTBE lavage therapy are sampled at 1-hr intervals during the dissolution process. MTBE infusion is continued until TLC shows a return to baseline cholesterol levels.

Results

Baseline TLC from hepatic bile revealed visible cholesterol concentrations ranging from 0.1 to 0.2 g/l. With MTBE lavage therapy, TLC showed cholesterol concentrations from 5 to 10 g/l in the first hour of therapy in all patients except one. A comparison cholecystogram obtained after 1 hr showed appreciable reduction in the size of the stones in only three patients who had small stones initially; the remaining six patients, who had larger stones, showed no noticeable decrease in stone size by catheter cholecystography or by sonography, despite the large amount of cholesterol in the effluent on TLC (Fig. 1). The cholesterol concentration remained high throughout the procedure (2–12 hr) in nine patients while the size of the stones decreased slowly by

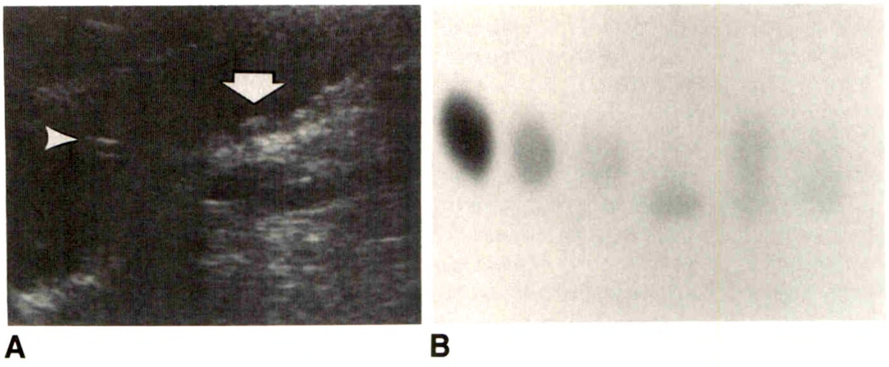

Fig. 2.—Use of thin-layer chromatography (TLC) to indicate methyl *tert*-butyl ether (MTBE) therapy should be terminated.

***A*, Sonogram obtained after 5 hr of MTBE dissolution shows residual stone fragments (*large arrow*); *arrowhead* points to percutaneous cholecystostomy catheter.**

***B*, TLC shows low cholesterol concentration similar to baseline in effluent, indicating that residual debris is insoluble in MTBE. From left to right, cholesterol concentrations are standard 1.0 g/l, 0.5 g/l, 0.2 g/l, baseline, and samples obtained 4 hr and 5 hr after MTBE dissolution.**

cholecystography. The cholesterol concentration shown by TLC decreased progressively in the samples of these patients as the remaining stone burden diminished with MTBE therapy.

When the gallbladder was shown free of stones by sonography and cholecystography, TLC showed absence of cholesterol in seven patients. Both imaging methods showed residual fragments remaining in the gallbladder in another patient, despite a low cholesterol level shown by TLC (Fig. 2); dissolution was discontinued in this patient because the debris was resistant to the solvent after 2 hr of MTBE lavage. The fragments were less than 3 mm in diameter. In the ninth patient, TLC showed low cholesterol levels, and a large (4 cm) stone was located in the neck of the gallbladder. The patient had pain with MTBE, and presumably the MTBE lavage did not reach the stone. The tenth patient had successful dissolution of innumerable gallstones with confirmatory TLC measurements of cholesterol. However, a solitary calculus remained impacted in the cystic duct, shown by cholecystography. TLC showed a low concentration of cholesterol because the solvent did not reach the impacted cystic duct stone. Subsequently, the tip of an end-hole catheter was juxtaposed to the stone; this permitted successful dissolution of the cystic duct stone and reestablishment of cystic duct patency.

Discussion

The initial effectiveness (or ineffectiveness) of gallstone dissolution with MTBE cannot be predicted accurately by current imaging studies. Because cholecystography and sonography reflect gross changes in size and shape, they are not sensitive to early leeching of cholesterol from gallstones. The primary value of TLC is to provide semiquantitative assessment of cholesterol dissolution that helps to monitor the dissolution of cholesterol gallstones by MTBE. Attempted dissolution of bilirubinate stones in which composition may not be appreciated by available imaging methods may lead to prolonged and inappropriate use of MTBE; TLC can avoid this problem as well.

As MTBE has potential deleterious side effects, unnecessary infusion should be avoided. Reported complications of MTBE include pain, sedation, renal failure, coma, and duodenitis [1, 3, 6]. Imaging studies may not necessarily reveal the exact or even the predominant composition of gallstones before MTBE infusion. For example, there is overlap in the appearance of cholesterol and bilirubinate stones by CT; both may appear isodense with bile. TLC is beneficial in the initial phases of attempted gallstone dissolution because it can detect and measure whether or not cholesterol is present. If cholesterol is present, dissolution should continue, and perhaps at a higher rate or volume. If cholesterol is not evident by TLC, MTBE should be discontinued.

Early in the dissolution process, it may be difficult to appreciate reduction in size of the stone radiologically (as occurred in six of our 10 patients) and, consequently, to know whether MTBE is effective. Lack of visible change may mean that the stone is insoluble to MTBE, that is, it is composed of calcium bilirubinate or calcium palmitate. However, cholesterol may be removed in large quantities by MTBE initially without any visible imaging correlation. Because the diameter of a stone decreases with the cubic root of the volume, a significant reduction in mass results in only a small decrease in diameter that may not be shown by cholecystography. An estimate of the total amount of cholesterol dissolved can be obtained at any time from the total volume of MTBE infused and the concentration of cholesterol measured; TLC provides this information in an ongoing fashion.

It is usually not feasible by gross examination of MTBE/bile effluent to determine whether or not cholesterol is being dissolved. The fluid aspirated from the percutaneous cholecystostomy catheter during solvent therapy is a mixture of bile and MTBE that often exceeds the volume of MTBE injected. If the aspirate is allowed to settle a few minutes in a glass syringe or metallic container, two definite layers form because of different densities and immiscibility of the components. The lower, turbid, yellow-green aqueous layer is mostly bile and contains minute debris and particles. The clear upper layer is composed of a solution of cholesterol in the solvent. The MTBE may be dried on a glass slide to reveal an opaque deposit of cholesterol, but this is not quantitative.

Residual insoluble fragments composed of material other than cholesterol may remain in the gallbladder after effective cholesterol dissolution. If these fragments are not cholesterol, it is futile to attempt to dissolve them. Continued use of MTBE under this circumstance may place the patient at unnecessary risk. If insoluble fragments remain after successful cholesterol dissolution, one can consider mechanical methods to extract the insoluble residue, such as flushing or tract dilatation with percutaneous removal of stones.

TLC appears promising from our early experience by virtue of adding useful information relatively easily and inexpensively. TLC is a helpful adjunct to sonography and cholecystography for monitoring gallstone dissolution with MTBE to avoid unnecessary use of the solvent. Gas chromatography is another potentially beneficial method for quantifying cholesterol gallstone dissolution that we are evaluating currently.

ACKNOWLEDGMENT

The authors thank Mary Heaivilin for her secretarial assistance in the preparation of this manuscript.

REFERENCES

1. Thistle JL, May GR, Bender CE, Williams HJ, et al. Dissolution of cholesterol gallbladder stones by methl-tert-butyl ether administered by percutaneous transhepatic catheter. *N Engl J Med* **1989**;320:633–639
2. Hellstern A, Leuschner M, Fischer H, et al. Percutaneous transhepatic lysis of gallstones by methyl-tert-butyl ether (MTBE). *Dtsch Med Wochenschr* **1988**;113:506–510
3. vanSonnenberg E, Casola G, Zakko SF, et al. Gallbladder and bile duct stones: percutaneous therapy with primary MTBE dissolution and mechanical methods. *Radiology* **1988**;169:505–509
4. vanSonnenberg E, D'Agostino HB, Casola G, Varney RR, Ainge GD. Interventional radiology in the gallbaldder: diagnosis, drainage, dissolution, and management of stones. *Radiology* **1990**;174:1–6
5. Stahl E. *Thin layer chromatography: a laboratory handbook*. New York: Springer-Verlag, **1969**
6. Ponchon T, Baroud J, Pujol B, Valette PJ, Perrot D. Renal failure during dissolution of gallstones by methyl-tert-butyl ether. *Lancet* **1988**;2: 276–277

American Roentgen Ray Society Residents' Award Papers, 1992

The ARRS announces competition for the 1992 President's Award and two Executive Council Awards for the best papers concerning the clinical application of the radiologic sciences.

Awards

The winner of the President's Award will receive a certificate and a $2000 prize. The winners of the two Executive Council Awards will each be given a certificate and a prize of $1000. The winners will be announced on March 16, 1992. Winning papers will be presented at the ARRS annual meeting at Marriott's Orlando World Center, Orlando, FL, May 10–15, 1992. Winning papers will be submitted for early publication in the *American Journal of Roentgenology*. All other papers will be returned to the authors.

Regulations

Eligibility is limited to residents or fellows in radiology who have not yet completed 4 years of approved training in a radiologic discipline. A letter from the resident's department chairman attesting to this status must accompany the manuscript. The resident must be the sole or senior author and be responsible for all or most of the project.

Submitted manuscripts must not exceed 5000 words and have no more than 10 illustrations. Four copies of the manuscript and illustrations are required. Submitted manuscripts should not contain previously presented or published material and should not be under consideration for publication elsewhere.

Deadline for submissions is February 14, 1992. Send papers to

Nancy O. Whitley, M.D.
Chairman, Committee on Education & Research
American Roentgen Ray Society
Department of Radiology
University of Maryland Medical Systems Hospital
22 S. Greene St.
Baltimore, MD 21201

Intraperitoneal Contrast Material Improves the CT Detection of Peritoneal Metastases

Robert A. Halvorsen, Jr.[1,2]
Cole Panushka[1]
Gerard J. Oakley[3]
Janis Gissel Letourneau[1]
Leon L. Adcock[3]

The preoperative detection of peritoneal metastases from gynecologic malignancies is difficult; in particular, CT often fails to detect peritoneal implants. This study was designed to determine if the administration of intraperitoneal iodinated contrast media would increase the CT detection of such peritoneal metastases. Prospectively, both standard and intraperitoneal contrast-enhanced CT studies of the abdomen and pelvis were performed in 16 patients with suspected gynecologic tumors. All patients then underwent operative staging, with the location and number of metastases documented. The intraperitoneal enhanced CT studies were more sensitive in the detection of peritoneal metastases than standard CT examinations. Whereas routine CT detected peritoneal metastases in seven (64%) of 11 patients with surgically proved implants, the intraperitoneal enhanced CT studies detected peritoneal metastases in all 11 patients. Depending on the specific intraperitoneal compartments involved, the sensitivity of intraperitoneal enhanced CT in the detection of peritoneal metastases was two- to fourfold greater than that of standard CT examinations.

Our results suggest that intraperitoneal enhanced CT is superior to standard CT in the detection of peritoneal metastases.

***AJR* 157:37–40, July 1991**

Standard CT of the abdomen is unreliable in the detection of peritoneal metastatic disease from gynecologic malignancy. Two recent studies report a sensitivity ranging from 8% to 63% [1, 2]. The aim of this study was to determine if the administration of intraperitoneal contrast material before CT scanning would increase the detectability of peritoneal metastases.

Subjects and Methods

Sixteen patients were included in a prospective study. The patients were referred from a gynecology-oncology clinic for preoperative CT evaluation because of pelvic masses detected on physical examination and strong clinical suggestion of a gynecologic malignancy. The patients were recruited consecutively; none were excluded. Before surgery, standard CT scans of the abdomen and pelvis were obtained followed by intraperitoneal contrast-enhanced CT scans. CT examinations were performed on Siemens DRH scanners with 5-sec exposures, a scan thickness of 8 mm, and a table incrementation of either 10 or 15 mm. Oral and IV contrast media were administered in all cases. IV contrast material was injected with a power injector at a flow rate of 2.5 ml/sec for the first half of the volume and 1 ml/sec for the remainder of the injection. The volume of IV contrast material varied from 100 to 150 ml. Intraperitoneal contrast enhancement was obtained by instilling 200 ml of diatrizoate meglumine (14% iodine) (Urovist, Berlex Laboratories, Cedar Knolls, NJ) into the peritoneal cavity through an 18-gauge percutaneously placed angiocatheter. The angiocatheter was placed approximately 3 cm below the umbilicus in patients with small amounts of ascites. In patients with a large amount of intraperitoneal fluid, the catheter was placed in the largest fluid collection based on the preceding CT examination, generally in the lower abdomen. The contrast material was followed by the instillation of saline (0–2 l). The amount of saline instilled

Received July 16, 1990; accepted after revision December 26, 1990

Presented at the annual meeting of the American Roentgen Ray Society, New Orleans, LA, May 1989.

[1] Department of Radiology, University of Minnesota, Minneapolis, MN 55455.

[2] Present address: Department of Radiology, San Francisco General Hospital, Room 1x55, 1001 Potrero Ave., San Francisco, CA 94110. Address reprint requests to R. A. Halvorsen, Jr.

[3] Department of Obstetrics and Gynecology, University of Minnesota, Minneapolis, MN 55455.

0361-803X/91/1571-0037

© American Roentgen Ray Society

TABLE 1: Routine CT (CT) and Intraperitoneal Enhanced CT (IPCT) vs Surgery in the Detection of Peritoneal Metastases

Peritoneal Compartment (No. of Cases/No. Surgically Detected)/ Study	True-Positive	True-Negative	False-Positive	False-Negative	% Sensitivity	% Specificity
R subhepatic & paracolic (16/11)						
CT	2	4	1	9	18	75
IPCT	9	5	0	2	82	100
L subphrenic (13/6)[a]						
CT	1	7	0	5	17	100
IPCT	4	6	1	2	66	86
Pelvis & bladder (16/10)						
CT	3	6	0	7	30	100
IPCT	6	4	2	4	60	66
R subphrenic (16/11)						
CT	2	4	1	9	18	80
IPCT	5	4	1	6	45	80
L paracolic (15/6)[b]						
CT	1	9	0	5	17	100
IPCT	2	6	3	4	33	66
Omentum (16/11)						
CT	10	4	1	1	91	80
IPCT	10	4	1	1	91	80
Mesentery (16/8)						
CT	0	7	1	8	0	87
IPCT	2	5	3	6	25	62

Note.—R = right; L = left.

[a] In three patients, no surgical information was available concerning the left subphrenic space.

[b] In one patient, no surgical information was available concerning the left paracolic gutter.

depended on the amount of ascites present and the patient's tolerance. Instillation of saline was terminated when the patient had pain or a feeling of excessive distension. At the beginning of the study, the contrast media and saline were administered by gravity, which was time-consuming and therefore required removal of the patient from the CT scanner. Later in the study the saline and contrast material were administered by hand injection. The hand injection technique was faster, allowing completion of both studies in one session without removal of the patient from the CT table. The contrast material was then distributed throughout the peritoneal cavity by having ambulatory patients walk or by turning the patient side to side if the patient was bedridden [3]. No attempt was made to drain the intraperitoneal contrast material following the examination.

Intraperitoneal enhanced CT and routine CT scans were interpreted separately by two radiologists without knowledge of surgical findings. Differences in interpretation were resolved in conference. The size and number of peritoneal metastases were determined on a compartment-to-compartment basis. The peritoneum was arbitrarily divided into right and left subphrenic compartments, paracolic gutters, mesentery, omentum, and pelvic peritoneal compartment. The subphrenic space was defined as the diaphragmatic surface of the liver and visceral peritoneal surface of the diaphragm. The right and left subphrenic spaces were separated by the falciform ligament. The peritoneal compartment was considered subphrenic if the CT scan showed the diaphragm. More caudad scans obtained below the diaphragm were considered paracolic gutter on the left and subhepatic/paracolic gutter on the right. The left subphrenic space was separated from the left paracolic gutter by the phrenicolic ligament. Soft-tissue masses were considered omental if located anterior to bowel and mesenteric if surrounded by loops of bowel. The peritoneal compartment was called pelvic if the innominate bone was visible on the CT scan. Nodular soft-tissue densities of any size were considered positive for peritoneal metastases. Plaquelike abnormalities were diagnosed as metastases only if they were longer than 1 cm. Both types of CT studies were evaluated for omental and mesenteric metastases, the size and number of pelvic masses, and direct pelvic side-wall extension.

Laparotomy and tumor debulking were performed within 1 week of all CT examinations. Surgical proof of the metastases consisted of detailed documentation of the size, number, and location of all peritoneal metastases.

Results

Explorative laparotomy confirmed gynecologic malignancy in 14 of the 16 patients (12 ovarian carcinomas, one fallopian tube carcinoma, one uterine carcinoma). Two patients had benign ovarian masses. Peritoneal metastases were present in 11 of the 14 patients with malignant lesions and varied in size from "pinpoint" to 6 cm in diameter. Standard CT, intraperitoneal enhanced CT, and surgical findings are compared in Table 1. Standard CT detected peritoneal metastases in seven of 11 patients with surgically proved implants. Intraperitoneal enhanced CT detected peritoneal metastases in all 11 patients (Figs. 1 and 2). Intraperitoneal enhanced CT correctly identified more peritoneal metastases than did routine CT in the subphrenic spaces, paracolic gutters, and pelvis (Fig. 3). Both intraperitoneal enhanced CT and routine CT detected 91% of omental metastases (Fig. 4). Intraperitoneal enhanced CT detected only 25% of mesenteric metastases, and standard CT detected mesenteric metastases in none of the eight patients in whom mesenteric tumors were found at surgery.

At surgery, all patients had pelvic masses that ranged from 3 to 16 cm in diameter. Standard CT detected pelvic masses

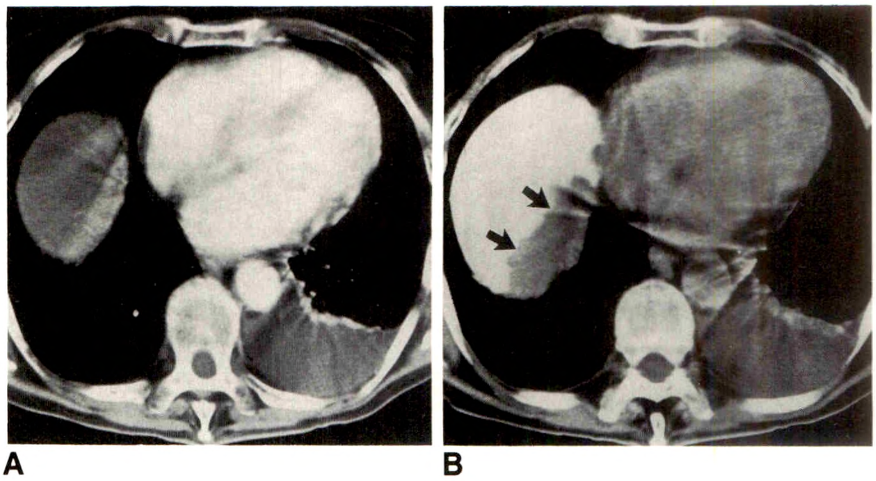

Fig. 1.—Right-sided subphrenic peritoneal metastasis detected on intraperitoneal enhanced CT scan but not routine CT scan.

A, Routine enhanced CT scan shows ascites in right upper quadrant and left-sided pleural effusion.

B, Intraperitoneal enhanced CT scan shows a large soft-tissue mass (*arrows*) in right subphrenic space.

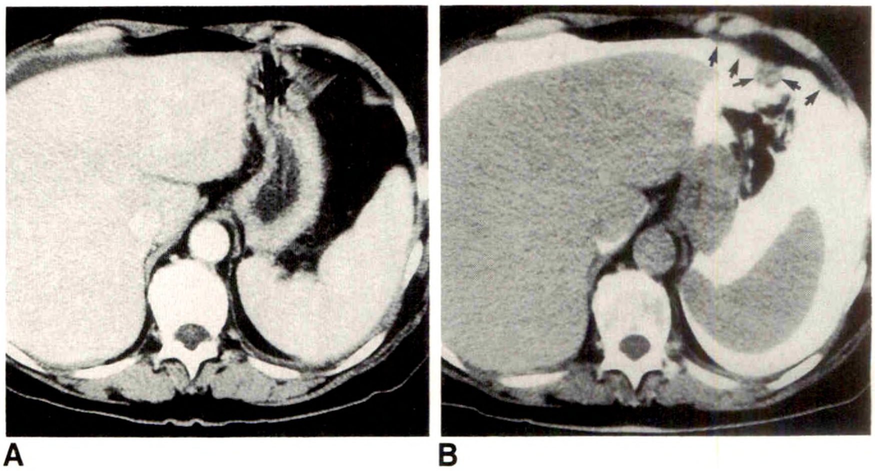

Fig. 2.—Left-sided subphrenic peritoneal metastasis detected on intraperitoneal enhanced CT scan but not routine CT scan.

A, CT scan at level of liver and spleen. Fluid is seen in gastric fundus.

B, Intraperitoneal enhanced CT scan shows multiple metastases (*arrows*) in subphrenic space.

in 12 out of 16 cases. The intraperitoneal enhanced CT studies detected an additional three pelvic masses. These three were cystic masses in patients with ascites in whom the pelvic mass was isodense relative to ascites and therefore undetectable on standard CT but easily visualized on intraperitoneal enhanced CT examinations (Fig. 5).

There were no complications from the intraperitoneal enhanced CT procedures.

Discussion

Previously, authors have suggested that the low sensitivity of CT in the detection of peritoneal implants is partially dependent on the location of the implant as well as the presence of ascites [2, 4]. When the amount of ascites present is insufficient to distend the peritoneal space, peritoneal implants may be indistinguishable from normal structures, such as unopacified loops of bowel. This lack of distension was the reason peritoneal implants were missed on the standard CT scans in our study (four of 11 cases). The intraperitoneal enhanced CT study offered the advantage of not only increasing the density difference between the implants and the surrounding ascites, but the saline infused in the intraperitoneal enhanced study increased the separation of intraperitoneal structures.

In all peritoneal compartments, intraperitoneal enhanced CT increased the sensitivity for the detection of peritoneal metastases two- to fourfold when compared with standard CT (Table 1, Fig. 5). In the right side of the abdomen, the specificity of intraperitoneal enhanced CT was the same or greater than that of standard CT. In the left side of the abdomen and pelvis, however, the specificity fell. This lower specificity was due in part to unopacified loops of bowel mistakenly thought to be peritoneal metastases. Other causes of error were encountered in patients with surgically categorized extensive omental disease and complex multilobular pelvic masses, when the intraperitoneal enhanced CT studies were interpreted as showing intraperitoneal metastases. This difference would appear to be of no clinical importance, and therefore the specificity may be underestimated.

Two patients had benign pelvic masses. In one woman with endometriosis, standard CT and intraperitoneal enhanced CT detected plaquelike lesions in the right subphrenic and subhepatic spaces, and these studies therefore were false-positive for detection of peritoneal tumor. In the other

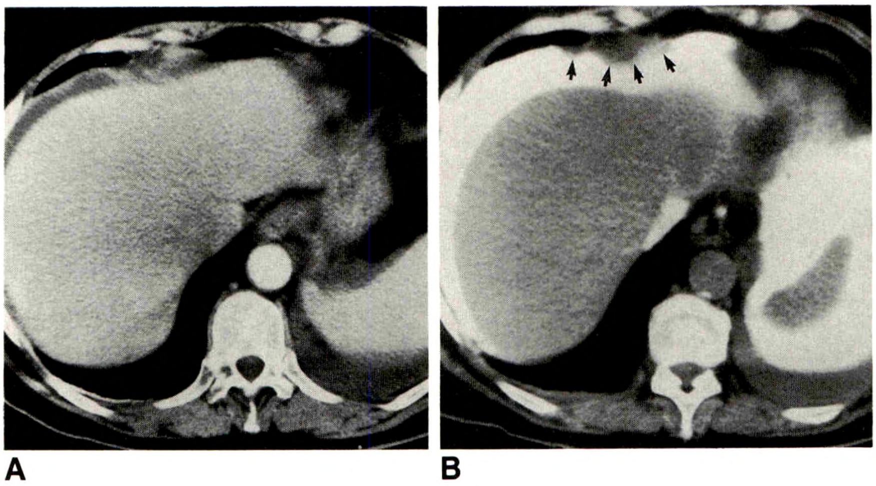

Fig. 3.—Right-sided subphrenic peritoneal metastases detected on intraperitoneal enhanced CT scan but not routine CT scan.

***A*, Routine CT scan shows ascites around liver and spleen.**

***B*, Intraperitoneal enhanced CT scan shows peritoneal metastases (*arrows*) in right subphrenic space.**

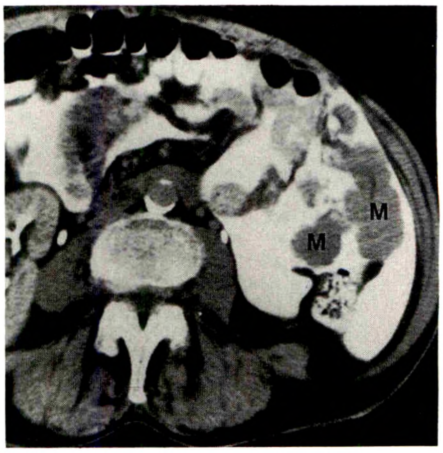

Fig. 4.—Intraperitoneal enhanced CT scan shows multiple omental metastases (M) in left paracolic gutter.

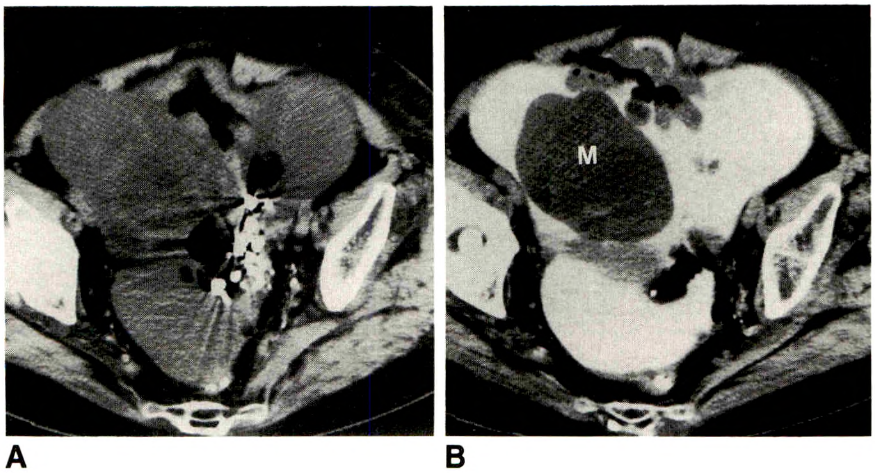

Fig. 5.—Cystic ovarian mass detected on intraperitoneal enhanced CT scan but not on routine CT scan.

***A*, Routine CT scan shows only ascites.**

***B*, Intraperitoneal enhanced CT scan distinguishes a large cystic pelvic mass (M) from ascites.**

woman with a benign pelvic mass, neither CT study detected peritoneal masses and none were seen at surgery.

The reliable detection of peritoneal metastases has important implications for women with ovarian cancer. In women in whom no clinical evidence of disease is found after surgery and chemotherapy, second-look surgery is proposed. In patients who undergo this operation, as many as 50% will have persistent disease found at surgery [5]. The results of standard CT examinations are too inaccurate to allow CT to replace second-look surgery. Brenner et al. [6] showed that CT detected less than 60% of metastases subsequently found at surgery. In our series, the sensitivity of conventional CT scanning was improved two- to fourfold with the administration of intraperitoneal contrast media. Intraperitoneal enhanced CT scans may be useful in sparing some patients a second-look surgical procedure.

REFERENCES

1. Silvermen PM, Osborne M, Dunnick NR, Bandy LC. CT prior to second-look operation in ovarian cancer. *AJR* **1988**;150:829–832
2. Buy JN, Moss AA, Ghossian MA, et al. Peritoneal implants from ovarian tumors: CT findings. *Radiology* **1988**;169:691–694
3. Dunnick RN, Jones RB, Doppman JL, Speyer J, Myers CE. Intraperitoneal contrast infusion for assessment of intraperitoneal fluid dynamics. *AJR* **1979**;133:221–223
4. Jeffrey RB. CT demonstration of peritoneal implants. *AJR* **1980**;135: 323–326
5. Barnhill DR, Hoskins WJ, Heller PB, Park RC. The second-look surgical reassessment for epithelial ovarian carcinoma. *Gynecol Oncol* **1984**;19:148–154
6. Brenner DE, Shaff MI, Jones HW, Grosh WW, Greco FA, Burnett LS. Abdominopelvic computed tomography: evaluation in patients undergoing second-look laparotomy for ovarian carcinoma. *Obstet Gynecol* **1985**;65:715–719

Afferent Loop Syndrome:

Sonographic Findings in Seven Cases

Dong Ho Lee[1]
Jae Hoon Lim
Young Tae Ko

We studied the sonographic findings in seven patients in whom afferent loop obstruction was first detected by sonography. All seven subsequently were proved at surgery to have afferent loop syndrome. The causes of the obstruction included internal hernia ($n = 3$), cancer recurrence ($n = 2$), marginal ulcer ($n = 1$), and development of cancer at the anastomosis site ($n = 1$). In all cases, the dilated afferent loop was seen on sonography as a tubular structure in the upper abdomen crossing transversely over the midline. The distal end of the afferent loop could be traced toward the anastomosis. The probable cause of the syndrome was predicted on the basis of sonography in two of three patients with cancer at the anastomosis.

Our experience suggests that afferent loop syndrome can be diagnosed sonographically on the basis of the detection, location, and shape of the dilated afferent loop.

***AJR* 157:41–43, July 1991**

Afferent loop syndrome (ALS) is an uncommon complication of subtotal gastrectomy with Billroth II gastrojejunostomy caused by obstruction of the duodenum and jejunum at any site proximal to the gastrojejunal anastomosis [1–4]. It may cause symptoms anytime from the first postoperative day to many years later [1]. Prompt recognition of the syndrome is important because perforation of the afferent loop may occur [5]. Because sonography may be the initial diagnostic procedure in patients with acute abdominal symptoms, the detection of the afferent loop obstruction on sonograms provides important diagnostic information. To date, only a few case reports describing the sonographic features have been reported [3, 6, 7]. We describe seven patients in whom the syndrome was first detected by sonography.

Subjects and Methods

Seven patients with afferent loop obstruction detected first by sonography between 1986 and 1989 were included in this study. There were four men and three women, ranging in age from 39 to 60 years. In all cases, the presence of ALS was confirmed at surgery. The reasons for the initial surgery were stomach cancer in three cases, gastric ulcer in two cases, and duodenal ulcer in two cases. The causes of ALS, established at surgery, included internal hernia (three patients), cancer recurrence (two patients), marginal ulcer (one patient), and development of cancer at the anastomosis site (one patient). The intervals between the initial operation and the second operation were 1–4 weeks in the three patients with internal hernia and 10 months to 16 years in the others. Plain abdominal radiographs and sonograms were obtained in all cases, upper gastrointestinal series in three cases, and CT scans in two cases.

Sonograms were obtained with a 3.5-MHz transducer on commercially available real-time scanners (Toshiba SSA-90A or SAL-55A, Tokyo). Both linear-array and sector transducers were used. The transducer was placed transversely and longitudinally on the midabdomen with the patient supine.

Received November 19, 1990; accepted after revision January 14, 1991.

[1] All authors: Department of Diagnostic Radiology, Kyung Hee University Hospital, 1, Hoeki-dong, Dongdaemun-ku, Seoul 130-702, Korea. Address reprint requests to D. H. Lee.

0361-803X/91/1571-0041
© American Roentgen Ray Society

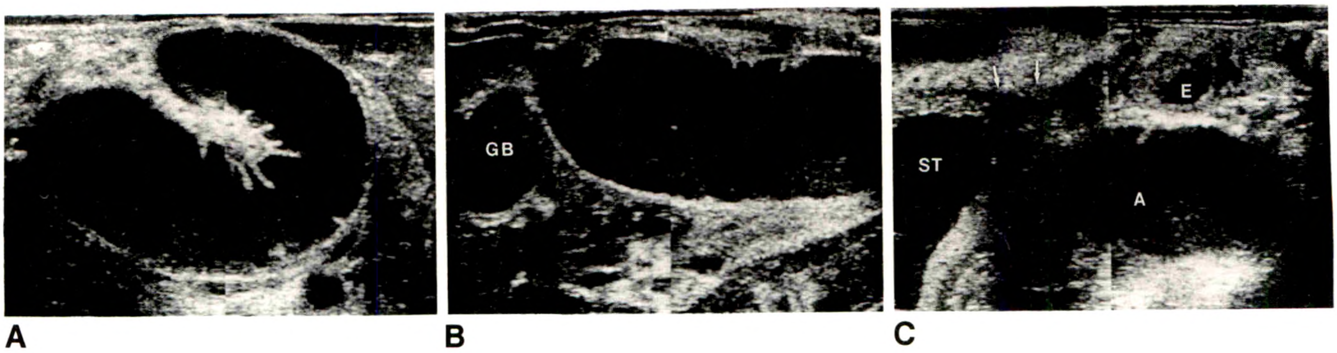

Fig. 1.—60-year-old man with afferent loop syndrome caused by internal hernia.

A, Longitudinal sonogram of midabdomen discloses a U-shaped and dilated duodenum.

B, Transverse sonogram of midabdomen discloses a dilated afferent loop crossing transversely over midline. GB = gallbladder.

C, On sonogram, distal end of dilated afferent loop can be traced toward anastomosis site of gastrojejunostomy (*arrows*). Efferent loop is not dilated, ST = remnant stomach, A = afferent loop, E = efferent loop.

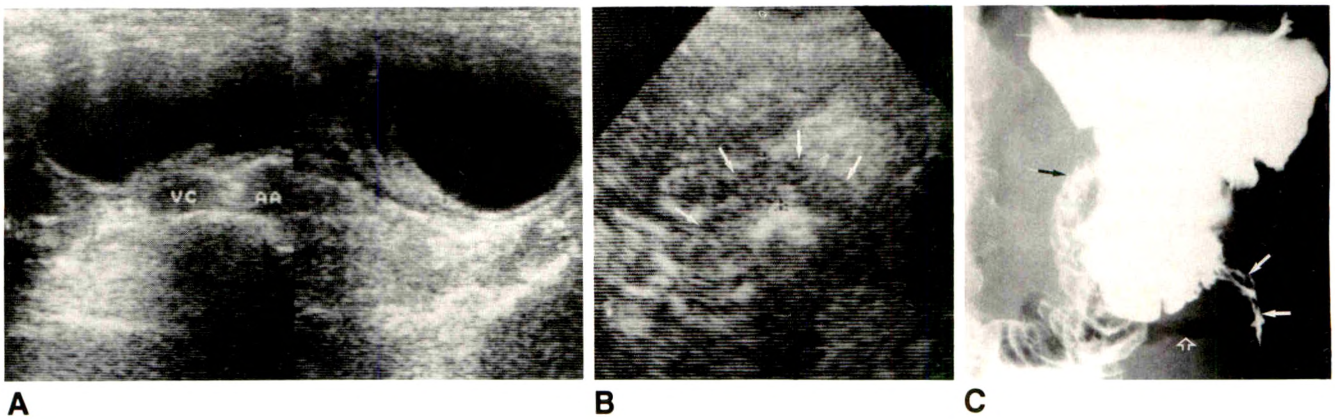

Fig. 2.—59-year-old woman with afferent loop syndrome caused by recurrent cancer.

A, Transverse sonogram of midabdomen shows markedly dilated afferent loop crossing transversely over midline with visible valvulae conniventes. VC = inferior vena cava, AA = abdominal aorta.

B, Longitudinal sonogram of left upper abdomen shows thickened wall of anastomosis (*arrows*).

C, Upper gastrointestinal series shows stenosis and luminal narrowing of afferent loop (*solid white arrows*) near anastomosis, dilated afferent loop with gas-fluid level (*open arrow*), and normal efferent loop (*black arrow*).

Results

In all seven patients, the dilated afferent loop was seen as a tubular or U-shaped structure in the upper abdomen crossing transversely over the midline (Figs. 1 and 2). The wall of the dilated afferent loop was not thickened. The diameter of a dilated loop varies from 38 to 60 mm (mean, 47 mm). The distal end of the afferent loop could be traced toward the anastomosis (Fig. 1). The causes of ALS were predicted on the basis of the sonograms in two of the three cancer patients; in these cases, the wall of the anastomosis was 10 mm thick, suggesting the presence of cancer (Fig. 2). In the third cancer patient, in whom afferent loop obstruction was due to tumor recurrence, the wall thickening at the anastomosis was not evident on sonography. Lymphadenopathy was seen at the porta hepatis in one of the three cancer patients.

In a retrospective review of the plain abdominal radiographs, the dilated afferent loop was detected in only one of the seven patients. A dilated afferent loop was shown on an upper gastrointestinal series in one of the three cases in which it was performed. The other two showed nonfilling of the afferent loop and normal efferent loop. CT showed the dilated afferent loop and recurrent cancer in the gastric remnant in both cases in which it was performed.

Discussion

Bilious vomiting due to afferent loop obstruction after gastroenterostomy was first reported by Wolfer in 1881. The mechanism of ALS was fully discussed by Wells and Welbourn in 1951 [3, 8–10]. The prevalence of ALS varies between 0.2% and 20.0% [8, 10]. The causes of ALS are internal hernia, kinking of the anastomosis, adhesive band, stomal stenosis, recurrent carcinoma or metastasis, and marginal ulcer [1, 3–5, 7–13]. Internal hernia is the most common cause of ALS [3, 8, 10]. Among 105 cases reported in the literature, the cause of ALS was internal hernia in 58 cases [8]. A long afferent loop may herniate through a gap between the anastomosis and the transverse colon [5]. Acute herniation is said to occur in 0.5 to 1.0% of patients who have undergone subtotal gastrectomy, and frequency is highest in the immediate postoperative period [12]. In 26 of the 51 cases of internal hernia reported by Dahlgren [10], the interval between the gastrectomy and the manifestation of acute ALS is 3 weeks or less. In our series, the interval between the first and second operations in three internal hernias was 1 week, 2 weeks, and 4 weeks, respectively.

In ALS, serum amylase level is often elevated owing to release of pancreatic enzymes into the peritoneal cavity and subsequent absorption by the lymphatics or bloodstream [3, 5, 10]. Therefore, the dilated afferent loop may be confused with pancreatic pseudocyst by its clinical features and imaging appearance [3, 6, 7, 11, 14].

The sonographic finding of ALS is a large and dilated bowel loop at midabdomen, lying anterior to the abdominal aorta, similar to that seen on CT [7, 13]. Its differentiation from a pancreatic pseudocyst may be difficult [6]. Feiss et al. [7] commented that a well-defined margin and good sound transmission were observed in pancreatic pseudocyst, but a poorly defined margin and poor sound transmission were seen in afferent loop obstruction. On the basis of a series of longitudinal and transverse scans, Berger [6] reported that the appearance of the wall echoes was not helpful in the differentiation of ALS from pancreatic pseudocyst, but the shape of the mass was most important. The differentiation of ALS from pancreatic pseudocyst may be possible by location of afferent loop behind the superior mesenteric artery and vein. In our seven patients, ALS was diagnosed by anatomic location and shape of the dilated afferent loop. The dilated afferent loop was seen as a tubular structure in the upper abdomen crossing transversely over the midline. One end of the afferent loop continued to the anastomosis and the other end to the biliary system. The cause of ALS can be detected in some cases by sonography, as in our two cases of cancer.

Kuwabara et al. [14] reported CT findings of the dilated afferent loop: a U-shaped cystic mass, the location of its caudal portion behind the superior mesenteric artery, and continuity of the mass with the biliary system. He emphasized that anterior displacement of the superior mesenteric artery by a mass was a useful CT finding to differentiate the dilated duodenum from a pancreatic pseudocyst, and this finding was also useful in sonography.

Abdominal radiographs may be useless because the afferent loop is fluid-filled and gasless owing to distal obstruction. In our series, only one case showed a gas-filled and dilated afferent loop. An upper gastrointestinal series may suggest the diagnosis of ALS because of nonfilling of the loop, but a firm diagnosis cannot be made because 20% of normal loops do not fill even in the best hands [1, 3, 4, 6, 13]. Delayed radiographs are essential to the diagnosis of partial obstruction of the afferent loop [2].

REFERENCES

1. Diba AA, Grossman ET, Dolan EP. Afferent loop syndrome: a different picture. *Am J Gastroenterol* **1976;**66:72–75
2. Burhenne HJ. The iatrogenic afferent-loop syndrome. *Radiology* **1968;**91:942–947
3. Brown CD, Kraus JW. Afferent loop syndrome revisited: new emphasis on ultrasound and computerized tomography. *South Med J* **1981;**74:599–601
4. Thomas JL, Cowan RJ, Maynard CD, Wu W. Radionuclide demonstration of small-bowel anatomy in the afferent-loop syndrome (case report). *J Nucl Med* **1977;**18:896–897
5. Hoffman WA, Spiro HM. Afferent loop problems. *Gastroenterology* **1961;**40:201–209
6. Berger LA. Chronic afferent loop obstruction diagnosed by ultrasound. *Br J Radiol* **1980;**53:810–812
7. Feiss JS, Raskin MM, Wolfe J, Plevy DJ, Luckman GS. A case of afferent loop obstruction secondary to recurrent carcinoma of the stomach with ultrasound and CT scan findings. *Am J Gastroenterol* **1977;**68:77–80
8. Mitty WF Jr, Grossi C, Nealon TF Jr. Chronic afferent loop syndrome. *Ann Surg* **1970;**172:996–1001
9. Jordan GL Jr. The afferent loop syndrome. *Surgery* **1955;**38:1027–1035
10. Dahlgren S. The afferent loop syndrome. *Acta Chir Scand Suppl* **1964;**327:7–149
11. Feiss JS, Plevy DJ, Luckman GS, Lenit OS Jr. A case of postgastrectomy afferent loop obstruction secondary to cancer of the stomach simulating pseudocyst of the pancreas. *Am J Dig Dis* **1975;**20:995–998
12. Beranbaum SL, Lawrence L, Schwartz S. Roentgen exploration of the afferent loop. *Radiology* **1968;**91:932–941
13. Gale ME, Gerzof SG, Kiser LC, et al. CT appearance of afferent loop obstruction. *AJR* **1982;**138:1085–1088
14. Kuwabara Y, Nishitani H, Numaguchi Y, Kamoi I, Matsuura K, Saito S. Afferent loop syndrome. *J Comput Assist Tomogr* **1980;**4:687–689

Splenic Hemangioma

David G. Disler[1] and Felix S. Chew

During staging of prostatic carcinoma in a 70-year-old man, a round, well-defined splenic mass was discovered on abdominal CT. The lesion had a peripheral zone of slightly decreased attenuation and an irregular central zone of greater attenuation (Fig. 1). The lesion was hyperintense on T2-weighted MR images. The abdomen was otherwise normal. The differential diagnosis included metastasis, primary benign or malignant neoplasm, lymphoma, and abscess. After splenectomy, the gross pathologic examination revealed a 4.5-cm nodule composed of whitish, focally hemorrhagic tissue. The final pathologic diagnosis was cavernous hemangioma.

A cavernous hemangioma is an unencapsulated mass of dilated, endothelially lined vascular channels filled with slowly flowing blood [1]. Typically 1–2 cm in diameter, a hemangioma can be much larger. Sonograms may show an inconsistent and nonspecific appearance of echogenicity and sharp margination, sometimes with cystic regions. Unenhanced CT shows a low-attenuation mass; with IV contrast infusion, the vascular channels slowly fill from the periphery inward. Larger lesions fill more slowly and may do so incompletely and inhomogeneously. Similarly, because of the slow blood flow, nuclear imaging with ^{99m}Tc-labeled RBCs shows slow accumulation of activity in the lesion followed by slow washout. Nuclear scans with ^{99m}Tc-labeled sulfur colloid show a photopenic defect because the radionuclide is accumulated only by the functional splenic tissue. T2-weighted MR images show bright signal similar to that of bile, CSF, or gastric fluid, because of long T2 relaxation times; this quality generally distinguishes hemangioma from solid neoplasms [2]. However, regions of liquefied necrosis in solid tumors will be bright on T2-weighted MR images also [2].

Most splenic hemangiomas are discovered incidentally, and their clinical importance generally lies in differentiating them from other conditions, particularly from metastases. Occasionally they may be associated with splenomegaly, abdominal pain, dyspnea, diarrhea, or constipation. Spontaneous rupture with hemorrhage is a risk with larger lesions [3]. No potential for malignancy exists. Hemangiomas are not treated unless they are symptomatic or very large, with increased risk of hemorrhage; treatment is splenectomy. Histologic examination is occasionally necessary for diagnosis. Although unusual, hemangioma is nonetheless the most common primary splenic neoplasm.

REFERENCES

1. Ros PR, Moser RP Jr, Dachman AH, Murari PJ, Olmsted WW. Hemangioma of the spleen: radiologic-pathologic correlation in ten cases. *Radiology* **1987**;162:73–77
2. Hahn PF, Weissleder R, Stark DD, Saini S, Elizondo G, Ferrucci JT. MR imaging of focal splenic tumors. *AJR* **1988**;150:823–827
3. Husni EA. The clinical course of splenic hemangioma. *Arch Surg* **1961**;83:681–688

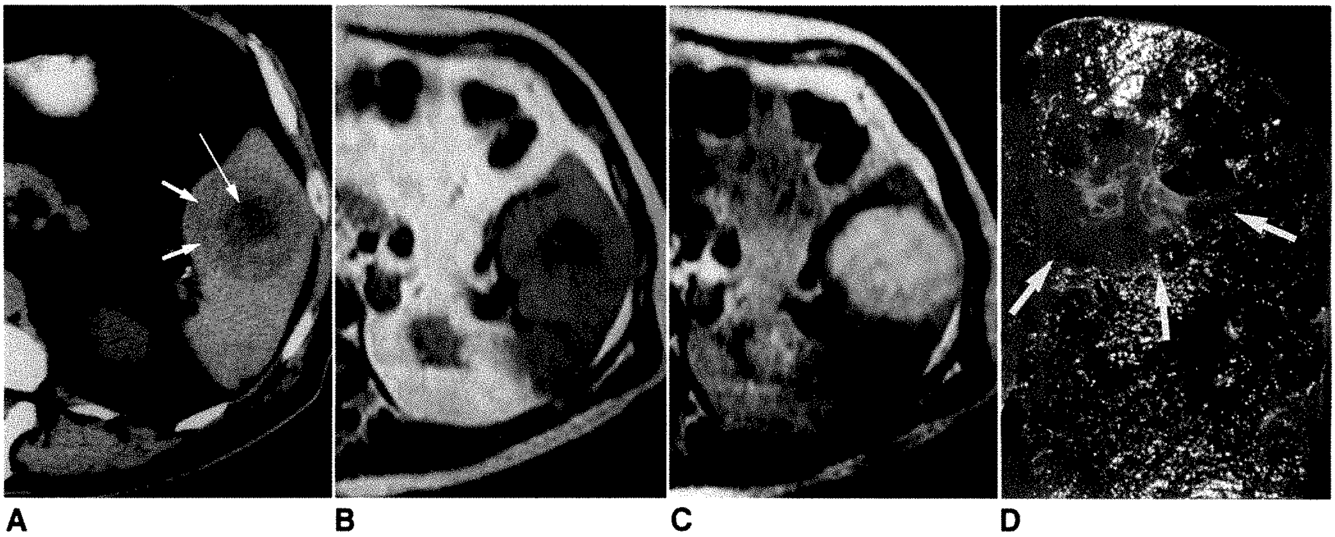

Fig. 1.—Splenic hemangioma.
***A*, Unenhanced CT scan shows a round splenic lesion with lower attenuation in center (*long arrow*) than in periphery (*short arrows*).**
***B*, Proton density-weighted MR image shows that center has low signal intensity but periphery is nearly isointense with spleen.**
***C*, Lesion becomes bright on T2-weighted MR image.**
***D*, Cut surface of gross specimen shows an unencapsulated hemorrhagic lesion (*arrows*) with central stellate scar.**

From the weekly radiologic-pathologic correlation conferences conducted by Jack Wittenberg. Pathology editor: Andrew E. Rosenberg. Radiology editors: William E. Palmer, Daniel P. Barboriak, Daniel I. Rosenthal, Felix S. Chew.

[1] Both authors: Department of Radiology, Massachusetts General Hospital and Harvard Medical School, 32 Fruit St., Boston, MA 02114. Address reprints requests to F. S. Chew.

***AJR* 157:44, July 1991** 0361-803X/91/1571-0044 © American Roentgen Ray Society

Case Report

Intramural and Intraperitoneal Hemorrhage Due to Duodenal Ulcer

D. Randall Radin[1]

Complications of peptic ulcer disease include hemorrhage into the bowel lumen, perforation into the peritoneal cavity, penetration into adjacent viscera, and gastric obstruction [1]. Intramural or intraperitoneal hematoma due to bleeding duodenal ulcer is rare. Two such cases are the subject of this report.

Case Reports

Case 1

A 47-year-old man with a long history of alcohol abuse and multiple episodes of pancreatitis complained of abdominal pain. Four weeks earlier an ulcer was diagnosed on upper gastrointestinal series performed at another hospital. The pain decreased after medical therapy but returned when the medication was stopped. The patient denied hematemesis and melena, but occult blood was detected in the stool. Laboratory values on admission included hematocrit of 45% and serum amylase level of 433 U/L. CT examination several hours after admission showed marked gastric distension, marked compression of the proximal portion of the duodenum by a large intramural hematoma, a small amount of blood in the right retroperitoneum, and evidence of chronic calcifying pancreatitis (Fig. 1A). Hematocrit on the next day was 31%. The patient improved gradually with medical treatment. Ten days later, upper gastrointestinal series showed a duodenal ulcer, narrowing of the descending duodenum, and a smooth-walled channel lateral and parallel to the descending duodenum, consistent with intramural dissection (Fig. 1B). Endoscopic examination showed a 2-cm ulcer with a central "diverticulum" in the duodenal bulb and partial obstruction of the lumen of the descending duodenum by a large submucosal mass with subepithelial hemorrhage. Biopsy specimens showed acute and chronic inflammation. Follow-up CT examination and upper gastrointestinal series showed resolution of the intramural duodenal hematoma.

Case 2

A 67-year-old man with a history of alcohol abuse was admitted with a 4-day history of abdominal pain and bilious emesis. He was febrile, dehydrated, and hypotensive. Laboratory evaluation showed anemia (hematocrit 29%) and leukocytosis. Serum amylase level was 499 U/L. Occult blood was present in the stool. CT examination showed a large hematoma inferior to the porta hepatis and lateral to the first portion of the duodenum (Fig. 2A). High-attenuation blood was seen in the lesser sac; blood of lower attenuation was present in the greater peritoneal sac. The pancreas was normal. Culture of nonclotting blood aspirated from the hematoma yielded *Enterobacter aerogenes*, *Citrobacter freundii*, and Group D enterococcus. One week later, contrast medium injected through a drainage catheter into the infected hematoma showed communication with a duodenal ulcer (Fig. 2B). Endoscopic biopsy showed nonspecific chronic inflammation. Arteriographic findings were normal. The patient was discharged after successful treatment by catheter drainage and antibiotic therapy. Results of follow-up CT examination 3 months later were normal.

Discussion

Duodenal ulcer is not often included on a list of causes of intramural hematoma or hemoperitoneum. Intramural duodenal hematoma is usually due to trauma, anticoagulant therapy, or bleeding diathesis. Less common causes include pancreatitis, collagen disease, ERCP, bowel biopsy, and endoscopic sclerosis of a bleeding ulcer [2, 3]. Intraperitoneal

---

Received January 10, 1991; accepted after revision February 12, 1991.

[1] Department of Radiology, University of Southern California School of Medicine, L.A. County–USC Medical Center, 1200 N. State St., Los Angeles, CA 90033-1084.

AJR 157:45–46, July 1991 0361–803X/91/1571–0045 © American Roentgen Ray Society

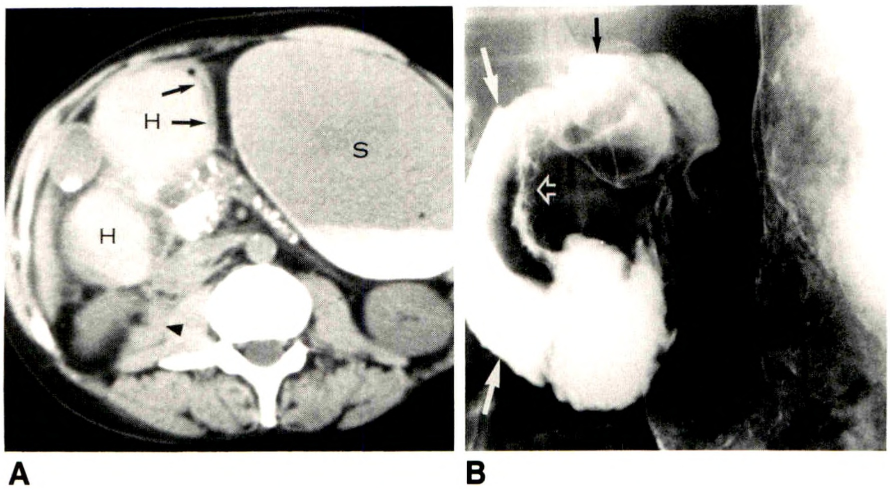

Fig. 1.—*A*, Unenhanced CT scan shows marked compression of duodenal lumen (*arrows*) by large intramural hematoma (H), distension of stomach (S), multiple pancreatic calcifications, and small amount of blood (*arrowhead*) in right retroperitoneum.

B, Spot radiograph shows duodenal ulcer (*black arrow*), narrowing of descending duodenum (*open arrow*), and intramural dissection of barium (*solid white arrows*).

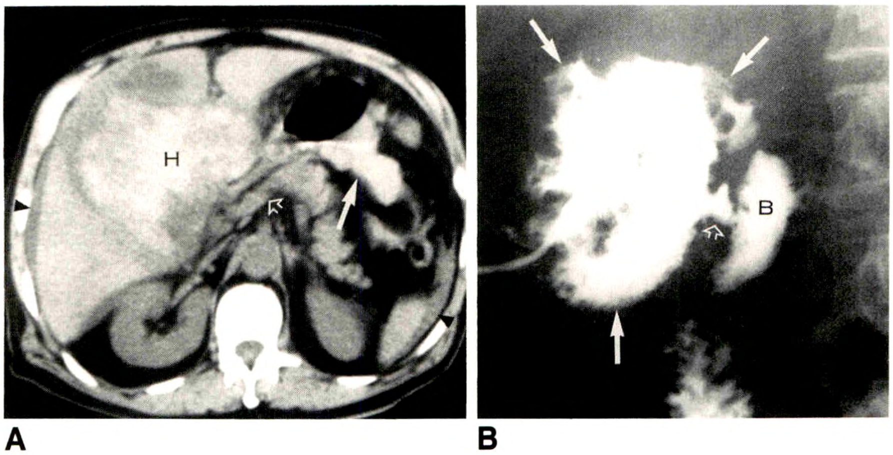

Fig. 2.—*A*, Unenhanced CT scan shows 12-cm hematoma (H) in right upper abdomen. Duodenum is seen between hematoma and pancreas (*open arrow*). Blood is present in lesser sac (*solid arrow*) and adjacent to liver and spleen (*arrowheads*).

B, Spot radiograph shows communication between infected hematoma (*solid arrows*) and duodenal bulb (B) via ulcer (*open arrow*).

hemorrhage can result from trauma; rupture of ovarian, hepatic, or small-bowel tumors; ectopic pregnancy; endometriosis; pancreatitis; cholecystitis; appendicitis; ruptured arteriosclerotic aneurysm or varices; and anticoagulant therapy [4].

In these two cases, the diagnosis of intramural or intraperitoneal hematoma was made by the demonstration of a high-attenuation fluid collection on unenhanced CT. However, in neither case was the source of hemorrhage apparent. Although trauma with either duodenal hematoma or hemorrhagic pancreatitis may occur in alcoholic patients, radiologic and endoscopic findings confirmed that duodenal ulcer was the cause in these two patients. In case 1, the extraluminal collection of barium lateral and parallel to the descending duodenum represented intramural dissection. It seems unlikely that an intramural duodenal hematoma due to blunt abdominal trauma would communicate with the bowel lumen via an eccentric ulcer. Although not, to my knowledge, previously reported in the duodenum, a similar radiologic appearance has been described as "double-barreled esophagus" in dissecting intramural esophageal hematoma [5]. In case 2, the preliminary CT diagnosis was hemorrhagic hepatic tumor. Diagnoses of pancreatitis with hemorrhagic pseudocyst or pseudoaneurysm were considered unlikely because the pancreas appeared normal and peripancreatic fat planes were intact. Duodenal ulcer was not suspected until the sinogram was performed. Arteriography failed to show a pseudoaneurysm or other vascular abnormality. In both cases, follow-up CT examination showed resolution of the hematoma.

Awareness of duodenal ulcer as a cause of intramural and intraperitoneal hemorrhage is important to enable diagnosis by upper gastrointestinal series or endoscopy, thus avoiding exploratory celiotomy, if hematoma is found in the region of the proximal duodenum in a patient without other known predisposing conditions. As illustrated by the two cases in this report, nonsurgical treatment may be sufficient.

REFERENCES

1. Pelot D, Hollander D. Complications of peptic ulcer disease. In: Berk JE, ed. *Bockus gastroenterology*, 4th ed. Philadelphia: Saunders, **1985**:1155–1185
2. Balthazar EJ, Hulnick D, Megibow AJ, Opulencia JF. Computed tomography of intramural intestinal hemorrhage and bowel ischemia. *J Comput Assist Tomogr* **1987**;11:67–72
3. Sadry F, Hauser H. Fetal pancreatitis secondary to iatrogenic intramural duodenal hematoma: a case report and review of the literature. *Gastrointest Radiol* **1990**;15:296–298
4. McCort JJ. Intraperitoneal and retroperitoneal hemorrhage. *Radiol Clin North Am* **1976**;14:391–405
5. Levine MS. Trauma. In: Levine MS, ed. *Radiology of the esophagus*. Philadelphia: Saunders, **1989**:209–227

Case Report

Aortoenteric Fistula Manifested as an Intramural Duodenal Hematoma

Michael A. Zeppa[1] and John V. Forrest

Aortoenteric fistula is an uncommon complication of aortic reconstructive surgery; however, it carries high rates of morbidity and mortality [1-3]. Communication of an aortic graft with the small bowel usually is associated with perigraft infection and almost always manifests as either gastrointestinal bleeding or sepsis [1, 3]. Clinical suspicion in the appropriate setting is necessary for making the correct diagnosis and allows prompt treatment. Intramural duodenal hematoma is a well-known entity with characteristic radiologic signs [4, 5]. Hematomas are self-limited, and most spontaneously resolve in 1-2 weeks with conservative treatment of nasogastric suction and IV fluids [4, 6]. A literature review revealed no previously reported association between duodenal hematoma and AEF. We describe a case of an aortoenteric fistula causing an intramural duodenal hematoma that manifested clinically as proximal obstruction of the small bowel.

Case Report

A 64-year-old man came to the emergency department because of the sudden onset of sharp, constant supraumbilical abdominal pain. The day before admission, he had had one episode of coffee-ground emesis followed by an episode of hematemesis. Eight years earlier, he had had an aortobifemoral bypass for occlusive disease. He was afebrile and nonorthostatic and had a soft, distended abdomen and mild epigastric tenderness. Stool was guaiac-negative. Hematocrit was 55.6, and leukocyte count was 19,100 cells/μl (19.1/l) with a normal differential.

Endoscopy showed moderate to severe diffuse esophagitis with possible bleeding and a large, pulsatile, submucosal mass in the third portion of the duodenum. CT with oral and IV contrast material was performed. A 7 × 4 cm, submucosal, sausage-shaped mass with inhomogeneous density filled the third portion of the duodenum (Fig. 1). A 3 × 3 cm, irregular, soft-tissue opacity without gas was present at the origin of the aortic graft. Duodenal hematoma due to aortoenteric fistula was diagnosed, but the diagnosis was not accepted by our clinicians and some other radiologists. During his initial hospital workup, the patient had a cerebral vascular accident that resulted in incomprehensible speech and right-sided paresis. Therefore, surgery was delayed, and he was treated with IV hydration, nasogastric suction, cimetidine, and prophylactic antibiotics.

Abdominal sonography confirmed a 7.4 × 4.6 cm complex mass overlying the midabdominal aorta. Findings on an aortogram and a superior mesenteric arteriogram were normal. MR showed findings similar to those on CT. Signal characteristics of the intramural duodenal mass were compatible with hematoma but did not show the characteristic high signal on T1-weighted images or the ring sign described by Hahn et al. [7].

Because of his evolving cerebral vascular accident, the patient was treated conservatively. He remained hemodynamically stable; nasogastric output was minimal and heme negative. CT repeated on hospital day 24 showed resolution of the duodenal mass. Endoscopy repeated the next day showed no duodenal mass but continued esophagitis. On hospital day 30, he complained of abdominal pain and tenderness, nausea, and lethargy. CT at that point showed new thickening of the wall of the third portion of duodenum with areas of increased density. Exploratory laparotomy on hospital day 33 revealed a paraprosthetic aortoenteric fistula with minimal pus. Culture of this area grew one colony of penicillinase-negative *Staphylococcus epidermidis*. The postoperative course was uneventful, and the patient was discharged 17 days after surgery with a Hickman catheter in place for long-term antibiotic treatment.

Received January 17, 1991; accepted after revision February 22, 1991.

[1] Both authors: Department of Radiology, University of California, San Diego, School of Medicine, La Jolla, CA 92093, and Department of Radiology (V-114), Veterans Affairs Medical Center, 3350 La Jolla Village Dr., San Diego, CA 92616. Address reprint requests to J. V. Forrest at Veterans Affairs Medical Center.

***AJR* 157:47-48, July 1991** 0361-803X/91/1571-0047 © American Roentgen Ray Society

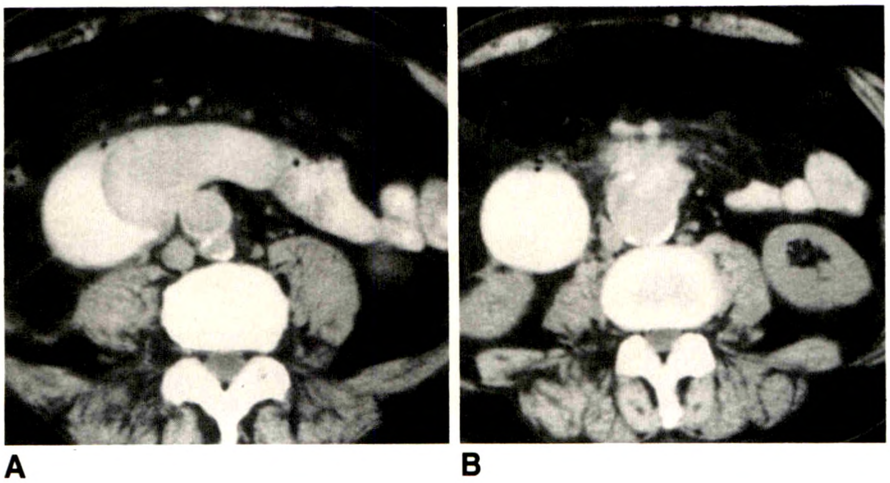

Fig. 1.—CT scans of aortoenteric fistula.

***A*, Image at level of transverse portion of duodenum shows a slightly inhomogeneous mass distending and obstructing bowel.**

***B*, Image 2 cm cephalad to *A* shows an irregular soft-tissue density around origin of aortic graft.**

Discussion

An aortoenteric fistula must be ruled out in any patient with a history of aortic reconstructive surgery who complains of gastrointestinal bleeding, sepsis, or abdominal pain. Patients classically have hematemesis, the so-called herald or sentinel bleeding, although hemorrhage can take the form of hematochezia, melena, or chronic guaiac-positive stools [1, 3]. The reported prevalence of aortoenteric fistula varies from 0.5% to 4.0%, with most of these patients also having a graft infection [1–3]. Development of an aortoenteric fistula is devastating, with a mortality rate of 30–75% [2, 3]. The most definitive diagnostic test for aortoenteric fistula is upper gastrointestinal endoscopy. The fistula most commonly is seen in the third or fourth portion of the duodenum [1, 3]. Findings of other upper gastrointestinal pathologic changes do not rule out an aortoenteric fistula.

Cross-sectional imaging allows assessment of the retroperitoneum and the perigraft space. Findings of graft infection include focal thickening of the bowel wall; collections of fluid, air, or soft tissue in the perigraft space; and loss of normal tissue planes around retroperitoneal structures [1, 2]. Extravasation of oral contrast material around the graft or perigraft air are virtually diagnostic of aortoenteric fistula or graft infection [3, 8].

Intramural duodenal hematoma is caused most commonly by blunt abdominal trauma when the abdominal muscles are relaxed. Rarer causes include anticoagulant therapy, bleeding disorders, ruptured aneurysm, and acute pancreatitis [6]. Most likely to occur in children, it often is due to abuse or handlebar accidents [4, 6, 7]. In adults, it often is seen with steering wheel injuries and in alcoholics [4]. Patients complain of pain and tenderness in the right upper quadrant, nausea, and vomiting.

Cross-sectional imaging also may be helpful in the diagnosis of intramural duodenal hematoma. The CT findings may include partial or complete duodenal obstruction, nodular filling defects projecting into the lumen, a submucosal mass, thickened wall or folds, and an inhomogeneous or initial high-density mass that decreases in size and density with time [4, 7].

On MR, the intramural duodenal hematoma may show a characteristic three-layered architecture. An outer capsule has very short T2 relaxation times, displaying low signal intensity on all sequences. A well-defined, concentric, bright ring inside the outer capsule has a high signal intensity on T1-weighted images. The core is often a central, low-intensity area thought to be a complex mixture of hemorrhagic solid and fluid components. These findings have been reported as the ring sign [7].

Our clinicians and some of our radiologists did not accept the original diagnosis of duodenal hematoma due to aortoenteric fistula. This led to the sonographic and MR studies and a delay in surgery. However, the findings on the CT scan done on hospital day 24 are most consistent with resolution of a hematoma. We hope that recognition of duodenal hematoma as a possible manifestation of aortoenteric fistula will allow others to avoid unnecessary further studies and proceed to prompt surgical repair.

REFERENCES

1. Goldstone J, Cunningham CC. Diagnosis, treatment and prevention of aortoenteric fistulas. *Acta Chir Scand Suppl* **1990**;555:165–172
2. Low RN, Wall SD, Jeffrey RB Jr, Sollitto RA, Reilly LM, Tierney LM Jr. Aortoenteric fistula and perigraft infection: evaluation with CT. *Radiology* **1990**;175:157–162
3. Wagner JR. Aortic graft-enteric fistula and paraprosthetic-enteric fistula: a review. *Mt Sinai J Med* **1989**;56:150–156
4. Hughes JJ, Brogdon BG. Computed tomography of duodenal hematoma. *J Comput Assist Tomogr* **1986**;10:231–236
5. Felson B, Levin EJ. Intramural hematoma of the duodenum: a diagnostic roentgen sign. *Radiology* **1954**;63:823–831
6. Vellacott KD. Intramural haematoma of the duodenum. *Br J Surg* **1980**;67:36–38
7. Hahn PF, Stark DD, Vici LG, Ferrucci JT Jr. Duodenal hematoma: the ring sign in MR imaging. *Radiology* **1986**;159:379–382
8. Olofsson PA, Auffermann W, Higgins CB, Rabahie GN, Tavares N, Stoney RJ. Diagnosis of prosthetic aortic graft infection by magnetic resonance imaging. *J Vasc Surg* **1988**;8:99–105.

Radiocontrast-Associated Renal Dysfunction: Incidence and Risk Factors

Everett Marc Lautin[1]
Neil Joshua Freeman[1,2]
Alan H. Schoenfeld[1]
Curtis W. Bakal[1]
Nogah Haramati[1,2]
Arnold C. Friedman[3]
Jeffrey L. Lautin[4]
Steven Braha[1]
Elisa G. Kadish[1]
Seymour Sprayregen[1]
Isaac Belizon[5]

Contrast-induced nephropathy is a potentially serious untoward reaction to radiologic contrast media. The incidence of this nephropathy and the predisposing conditions are not well established, possibly because of methodologic differences between studies. We evaluated the incidence of contrast-induced nephropathy after femoral arteriography in 394 patients by using multiple definitions (different increases in serum creatinine or blood urea nitrogen levels at various times). When an increase in the level of serum creatinine of greater than 0.3 mg/dl *and* greater than 20% on day 1, 2, or 3 *and* on day 5, 6, or 7 was used to define the disorder, the incidence in our group of patients was 10% for nonazotemic patients vs 30% for azotemic patients ($p < .001$); 2% for nondiabetic, nonazotemic patients vs 16% for diabetic, nonazotemic patients ($p = .003$); and 38% for patients who were both diabetic and azotemic vs 16% for diabetic, nonazotemic patients ($p = .022$). Baseline renal insufficiency and diabetes mellitus (especially when insulin dependent) were significant predisposing factors. The effects of dehydration and increased volume of contrast medium on the incidence of contrast-induced nephropathy were not clear; the age and sex of the patient were not important risk factors.

The incidence of contrast-induced nephropathy depends on the definition used. Although contrast-induced nephropathy may develop in any patient, diabetes, renal insufficiency, and, possibly, dehydration and dose of contrast medium are risk factors.

AJR **157:49–58, July 1991**

An acute and sometimes irreversible decrease in renal function is a well-documented complication of the use of radiologic contrast media [1–19]. The incidence of radiocontrast-associated renal dysfunction (RACARD) and any predisposing risk factors are, however, still open to question [20].

A significant rise in the level of serum creatinine (and occasionally blood urea nitrogen [BUN]) commonly has been used as an indicator of contrast-induced nephropathy [1–16]. Unfortunately, the definition of a significant change in creatinine level has varied widely in the literature [1, 20]. Baseline renal insufficiency has usually been defined as a precontrast level of serum creatinine (CrPre) above a threshold designated by the investigator. These baseline creatinine levels also have varied widely (Table 1) [2–15, 17].

We evaluated increases in serum creatinine level after femoral angiography in patients receiving either conventional high-osmolality contrast media (HOM), the newer lower-osmolality contrast media (LOM), or a combination of the two. Multiple criteria were used to evaluate the decrease in renal function after angiography and the baseline renal insufficiency before the procedure. Each criterion was evaluated statistically in an attempt to determine whether consistent trends could be detected and to determine which criteria are most appropriate. The significance of various reported possible risk factors, including elevated baseline levels of creatinine, diabetes (both insulin dependent and non–insulin dependent), volume of contrast medium administered, patient's state of hydration, and patient's age and sex were evaluated [1–7, 10, 11, 14, 21, 22].

Received March 14, 1989; accepted after revision November 30, 1990.

Presented at the annual meeting of the American Roentgen Ray Society, San Francisco, CA, May 1988.

[1] Department of Radiology, Montefiore Medical Center, 111 E. 210th St., Bronx, NY 10467. Address reprint requests to E. M. Lautin.

[2] Present address: Department of Radiology, Columbia College of Physicians and Surgeons, Columbia Presbyterian Medical Center, 630 W. 168th St., New York, NY 10032.

[3] Department of Radiology, Temple University Medical Center, Broad and Ontario Sts., Philadelphia, PA 19140.

[4] Department of Radiology, Columbia College of Physicians and Surgeons, 630 W. 168th St., New York, NY 10032. Present address: Department of Radiology, Mount Sinai Medical Center, One Gustave L. Levy Place, New York, NY 10029-6574.

[5] Department of Renal Medicine, Montefiore Medical Center, 111 E. 210th St., Bronx, NY 10467.

0361-803X/91/1571-0049
© American Roentgen Ray Society

TABLE 1: Definitions of Radiocontrast-Associated Renal Dysfunction (RACARD) and Elevation in Preangiography Creatinine Level Used in the Literature

Reference	Definition of Preexisting Renal Insufficiency (Serum Creatinine Level)	Definition of a Significant Increase in Serum Creatinine Level	Time for Increase (Days)	Type of Contrast Study	Incidence of RACARD (%)
[2]	Not given	≥25%	5	Excretory urography (prospective)	Prior azotemic patients only Nondiabetic 17/28 (61) Diabetic 11/12 (92)
[3]	≥1.5 mg/dl	>0.3 mg/dl and >20%	5	Renal angiography (retrospective)	All patients 45/266 (17) Prior nonazotemic 2/54 (4) Prior azotemic 43/212 (20)
[4]	>1.5 mg/dl	≥1.0 mg/dl	7	Excretory urography (retrospective)	All patients 18/377 (5) Nonazotemic, nondiabetic 1/169 (0.6) Nonazotemic, diabetic 0/19 (0)
[5]	≥1.6 mg/dl	≥2.0 mg/dl	2	All contrast studies (retrospective)	All nephrology consultations 18/12,000 (0.15)
[6]	≥1.8 mg/dl or BUN ≥ 30 mg/dl	BUN increase of 50% or 20 mg/dl or creatinine increase of >1.0 mg/dl	1	All angiography (prospective)	All patients: 500 ml/hr of normal saline given as prophylaxis 0/537 (0)
[7]	≥2.0 mg/dl	≥1.0 mg/dl	5	Excretory urography (retrospective)	Diabetics with elevated baseline creatinine level 22/29 (76)
[8]	≥1.5 mg/dl and BUN ≥ 30 mg/dl	≥1.0 mg/dl	3	Nonrenal angiography (prospective)	Prior nonazotemic, nondiabetic 1/199 (0.5) Prior nonazotemic, diabetic 1/95 (1) Prior azotemic, nondiabetic 1/10 (10) Prior azotemic, diabetic 3/13 (23)
[9]	≥1.5 mg/dl	≥0.5 mg/dl	2	All noncardiac angiography (prospective)	All patients 1/100 (1)
[10]	≥1.7 mg/dl	Two criteria: >50% and >1.4 mg/dl {>25% and >1.4 mg/dl}	2	All intravascular contrast studies (prospective)	Diabetic, nonazotemic 0/85 (0) {2/85 (2)} Diabetic, azotemic 3/34 (9) {3/34 (9)} Nondiabetic, azotemic 4/101 (4) {6/94 (6)}

Materials and Methods

We studied 394 patients who underwent femoral angiography at our institution in a period of less than 1 year. This group was chosen for its large proportion of elderly and/or diabetic patients, many of whom had underlying renal insufficiency and were presumably at increased risk for contrast-induced nephropathy [1]. Patients were studied consecutively by reviewing their charts and were excluded when records were unavailable. Historical data on each patient were obtained, and the patient's diabetic status, baseline BUN and serum creatinine levels, age, and sex were recorded. Diabetic status was determined from the patients' charts as either insulin dependent (the patient required the routine injection of insulin) or non-insulin dependent (only oral hypoglycemic agents were administered). The BUN/creatinine ratio, which correlates with the state of hydration, was used as an indicator of the status of the patient's fluid volume (the normal value is about 10; we used a ratio of >15 as the cutoff for dehydration) [23, 24].

HOM (sodium diatrizoate, Hypaque 60%, and sodium/meglumine diatrizoate, Hypaque 76%, Winthrop Pharmaceuticals, New York, NY) were used in 143 patients who were studied retrospectively. LOM (sodium/meglumine ioxaglate, Hexabrix, Mallinckrodt, Inc., St. Louis, MO, or iohexol, Omnipaque 300 or Omnipaque 350, Winthrop Pharmaceuticals) were given to 160 patients who were studied prospectively. A combination of LOM for power injections and HOM for hand test injections was used in 91 patients who were studied retrospectively. This group of patients underwent angiography before the inception of our study. LOM were used in order to decrease the pain associated with femoral angiography and because these patients had a poorer baseline medical status (i.e., congestive heart failure or a history of recent myocardial infarction), which was thought to place them at a higher risk for contrast-related complications. The total volume of contrast material administered (both power and hand injections) was recorded in the prospective study. Test volumes injected by hand were not recorded routinely and therefore could not be obtained for those patients studied retrospectively.

Serum creatinine values were recorded on the day of (and/or the day before) angiography (CrPre) and for 7 days after angiography (when available). Data availability in the prospective and the retrospective groups was as follows: Day 1: 83% and 90%; day 1, 2, or 3: 96% and 100%; day 5, 6, or 7: 64% and 29%, respectively. Surgery was performed on 180 (46%) of the 394 patients within 5 days of arteriography; almost all of these were for vascular repair of the lower extremity. Data beyond 7 days are not included in this study because they were difficult to obtain and are incomplete.

Patients received either unilateral femoral artery injections (47%), low-abdominal aortic injections (31%), or translumbar injections (8%); several patients had peripheral angioplasty (15%).

The incidence of contrast-induced nephropathy, as defined by multiple criteria, was determined for the groups of patients selected, and these incidences were compared; statistical analyses were performed using Fisher's exact probability test (two-tailed). Scatter plots of the maximal changes in the level of serum creatinine by day 7 were plotted against multiple parameters to evaluate correlation: CrPre, power-injected volume of contrast medium (bolus volume), BUN/creatinine ratio, and patient's age. Patients were excluded from a given analysis if relevant data were missing (e.g., appropriate creatinine and BUN values, diabetic status, age). However, a patient excluded from one analysis may have had sufficient data to be included in another analysis by different criteria. Hence, the total number of patients for each criterion varied depending on the parameters required.

We chose a serum creatinine value of greater than 1.5 mg/dl (CrPre) as the level for the definition of precontrast renal insufficiency. This roughly corresponds to the clinically significant level commonly used [3-5, 8, 9, 12] and to our laboratory's normal value. Use of upper limit of normal creatinine level below 1.5 mg/dl blurs the distinction between patients with normal and abnormal renal function because patients with normal function who have increased muscle mass often have serum creatinine values in the 1.2–1.5 mg/dl range. Selecting a higher value (in the 1.5–2.0 mg/dl range) excludes from the precontrast renal insufficiency group smaller patients who have significant renal insufficiency. (Preliminary analyses using >1.8 mg% as the definition of elevated CrPre level also were performed).

Additional analyses were conducted by using analysis of variance models on 381 patients (patients were excluded if they had no creatinine data on day 1 through day 3). We simultaneously evaluated the effects of CrPre levels (≤ 1.5 mg/dl vs >1.5 mg/dl), diabetic status (nondiabetic vs non–insulin-dependent diabetic vs insulin-dependent diabetic), dehydration (BUN/Cr ≤ 15.71 vs >15.71), volume of contrast medium (≤ 70 ml vs >70 ml), age of patient (≤ 70 years vs >70 years), and all two-way interactions between these variables on the maximal percentage of increase in serum creatinine level by day 3, while controlling for differences due to contrast medium. Preliminary analyses showed that neither the volume of contrast material, dehydration, nor any two-way interaction involving these two factors were a significant source of variation. Therefore, these factors were deleted from the final analysis of variance model. Paired comparisons were then conducted on the least squares means of those main effects and interactions that were found to be significant ($p < .05$). These statistical analyses were conducted by using the GLM (General Linear Models) procedure in the SAS (Statistical Analysis System) computer package.

Results

A large statistically significant increase was seen in the incidence of contrast-induced nephropathy for patients with preexisting renal insufficiency (Fig. 1). This was true for all five criteria (I–V) when a rise in creatinine level was used as the definition of contrast-induced nephropathy. The BUN criterion (VI) failed to show a difference. The results obtained (not shown) when elevated CrPre was considered greater than 1.8 mg/dl were similar. A scatter plot of CrPre vs maximal change in serum creatinine level after the administration of contrast material revealed a weak positive correlation (not shown, $r = .247$). The correlation was even lower when the data were subjected to a rank correlation or when the data were normalized.

Diabetics were at increased risk for contrast-induced nephropathy compared with nondiabetics (Fig. 2A). This was true for all six criteria and for all creatinine groups (except criterion IV, group L). Statistical significance was present in the combined group (A) by criteria I, II, and VI. When patients with normal CrPre (L) were considered, diabetics were at a statistically significant increased risk for contrast-induced nephropathy by criteria I and VI. When patients with elevated CrPre (G) were considered, diabetics were at a statistically significant increased risk for contrast-induced nephropathy by criterion II.

In addition, diabetics with preexisting renal insufficiency were at markedly greater risk for contrast-induced nephropathy than were diabetics who had normal renal function before the administration of contrast material. (Fig. 2A: the solid bar, diabetics, labeled G is markedly higher than the solid bar labeled L for all creatinine criteria. The p values are as follows: criteria I = .022, II = .002, III = .050, IV $<$ .001, V $<$ .001.) Also, nondiabetics with elevated CrPre were at considerably increased risk compared with nondiabetics with a normal CrPre. (Fig. 2A: the open bar, nondiabetics, labeled G is higher than the open bar labeled L for all creatinine criteria.

Key to Abbreviations Used in Figures

Criteria Definitions

I increase in creatinine level >0.3 mg/dl *and* $>20\%$ on day 1, or 2, or 3 *and* on day 5, or 6, or 7

II increase in creatinine level >0.3 mg/dl *and* $>20\%$ on day 1, or 2, or 3

III increase in creatinine level >0.3 mg/dl *and* $>20\%$ on day 1 or 2

IV increase in creatinine level ≥ 2.0 mg% on day 1 or 2

V increase in creatinine level ≥ 1.0 mg% on day 1

VI increase in blood urea nitrogen (BUN) level ≥ 20 mg% or $\geq 50\%$ on day 1

Abbreviations

A	all patients in the category
G	all patients in the category with CrPre >1.5 mg/dl
L	all patients in the category with CrPre ≤ 1.5 mg/dl
BUN	blood urea nitrogen
CrPre	creatinine level preangiography
HOM	high-osmolality media
LOM	lower-osmolality media
np/tn	number of patients who meet criteria/total number of patients in this group
RACARD	radiocontrast-associated renal dysfunction

Note

p values	calculated by using Fisher's exact probability test (2-tailed)

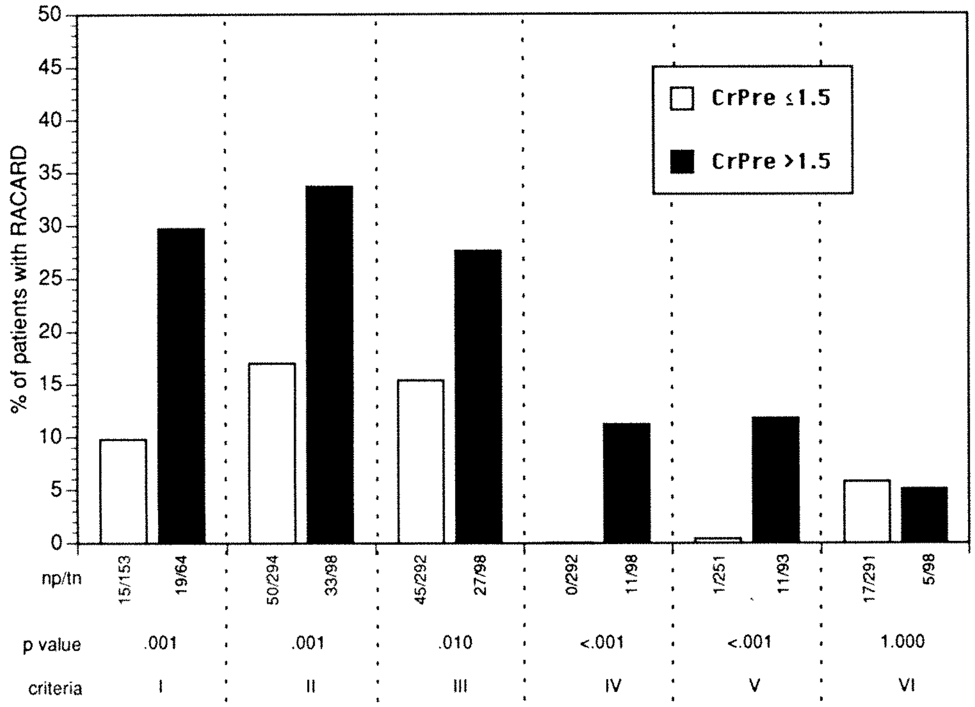

Fig. 1.—A comparison of incidence of RACARD in patients with normal and elevated CrPre when multiple criteria for RACARD are used. All patients are included regardless of type of contrast media administered. Note markedly higher and statistically significant risk of RACARD for patients with an elevated CrPre by all criteria except the poorly discriminatory BUN criterion (VI).

The *p* values are as follows: criteria I = .002, II = .146, III = .090, IV = .056, V = .017.)

Contrast-induced nephropathy occurred more often in insulin-dependent diabetics than in non–insulin-dependent diabetics (Fig. 2B) with criteria I–V; criterion VI, which used a rise in BUN, showed the opposite relationship between groups. Statistical significance was not present for any of the six criteria.

The additional analyses conducted by using an analysis of variance model showed significant differences in maximal percentage of increase in creatinine level (by day 3) on the basis of diabetic status, CrPre, and the two-way interactions of age by CrPre and diabetic status by CrPre (Table 2). Patients with an elevated CrPre had a significantly larger increase in creatinine levels than did patients who had a normal CrPre. Insulin-dependent diabetics had a significantly larger increase in creatinine level than did nondiabetics or non–insulin-dependent diabetics. There was no significant difference between the nondiabetic and non–insulin-dependent diabetic groups in the percentage of increase in creatinine levels. Insulin-dependent diabetics with an elevated CrPre had a significantly larger increase in creatinine than did insulin-dependent diabetics with a normal CrPre. The insulin-dependent diabetics with an elevated CrPre also had a significantly larger increase in serum creatinine level than did nondiabetics or non–insulin-dependent diabetics, regardless of the CrPre. Nondiabetics with an elevated CrPre had a significantly larger percentage of increase in creatinine level than did nondiabetics with a normal CrPre. Among non–insulin-dependent diabetics, no significant difference was seen in the percentage of increase in creatinine levels between the elevated and normal CrPre groups.

When evaluated with a scatter plot like that used by Miller et al. [22], the total volume of contrast medium administered during power injections (boluses) runs showed no relationship to the degree of increase in creatinine level (Fig. 3A). The possibility of a selection bias (a tendency for the angiographer to administer lower volumes of contrast medium to patients with higher CrPre) was refuted; a scatter plot of CrPre vs volume of contrast medium (not shown) showed no correlation. Those patients who had both the volumes of power- and hand-injected contrast medium recorded also showed no increase in contrast-induced nephropathy with increasing total volume of contrast material administered. We showed a direct correlation between total bolus volume and flush volume. Consequently, we think it reasonable to extrapolate a direct relationship between bolus volume and flush volume (and therefore total volume) in all 394 patients used in Figures 3A and 3B. Evaluation by using the analysis of variance model (with volume of contrast media injected as the independent variable) showed no significant influence of the dose of contrast material on the percentage of increase in creatinine level by day 3.

However, when the same volume data were analyzed for contrast-induced nephropathy by using multiple criteria, conflicting results were obtained (Fig. 3B). Patients who received more contrast material than the median volume were at increased risk for contrast-induced nephropathy by all criteria compared with those who received less; statistical significance was shown by using criteria II, III, and VI.

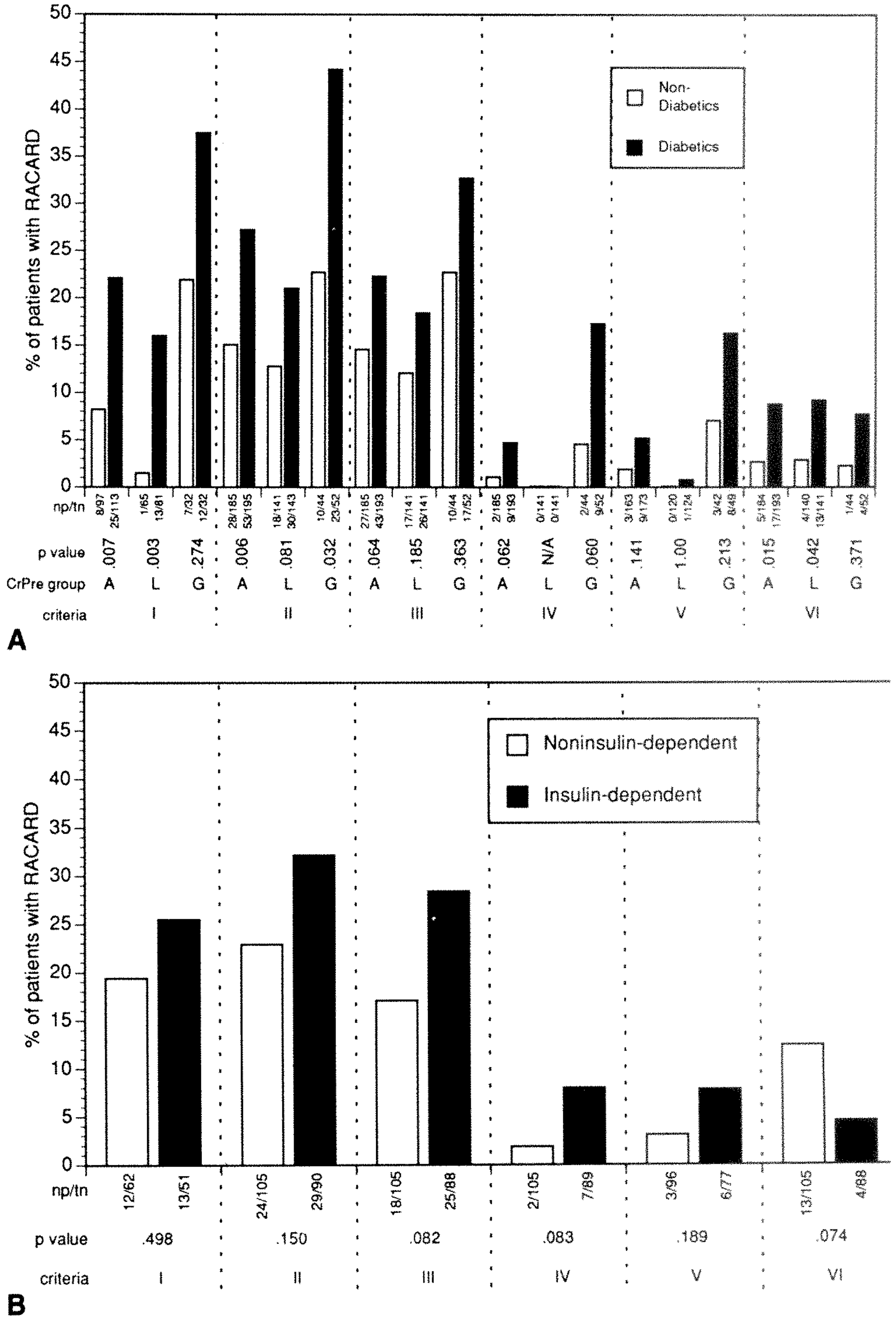

Fig. 2.—*A*, A comparison of incidence of RACARD for diabetics vs nondiabetics. This is shown for all patients regardless of CrPre (A), for patients with normal CrPre (L), and for patients with elevated CrPre (G). Six different criteria of RACARD are shown. Diabetics are at greater risk for RACARD for all CrPre groups and by all criteria. Note also that for each creatinine criterion, patients with an elevated CrPre (G) are at increased risk for RACARD vs normal CrPre (L) for both diabetics and nondiabetics.

B, A comparison of incidence of RACARD in patients with non-insulin-dependent diabetes vs insulin-dependent diabetes for all CrPre values.

Increasing age as an independent risk factor for contrast-induced nephropathy [5] is not supported by our data using the incidence of RACARD (Fig. 4) or by a scatter plot (plot not shown, $r = .00361$). No significant difference in the incidence of RACARD was present between men and women.

When a scatter plot (not shown, $r = .0618$) and the analysis of variance model (not shown) were used, the patient's state of hydration as measured by the BUN/creatinine ratio had no significant correlation with the maximal rise in creatinine level. When the incidence of RACARD was evaluated by criteria I–V (Fig. 5), no statistically significant difference is shown. However, criteria I–III, show a trend suggesting increased risk for the relatively hypovolemic patients. Criteria IV and V failed to demonstrate a difference. The BUN criterion VI showed

TABLE 2: Analysis of Variance of Maximal Percentage of Increase in Creatinine Level from Baseline by Day 3 After Angiography with Significant Main Effects and Interactions

Main Effects and Interactions	Least Squares Mean[a]
Type of diabetes	
None	17.72 a
Non–insulin-dependent	14.96 a
Insulin-dependent	40.62 b
Creatinine Level Preangiography (CrPre)	
>1.5 mg/dl	32.75 a
≤1.5 mg/dl	16.12 b
Age (years) × CrPre (mg/dl)	
≤70 × ≤1.5	13.28 a
≤70 × >1.5	41.06 b
>70 × ≤1.5	18.97 a
>70 × >1.5	24.43 ab
Diabetic Status × CrPre (mg/dl)	
Nondiabetic × ≤1.5	9.03 a
Nondiabetic × >1.5	26.41 b
Non–insulin-dependent × ≤1.5	18.93 ab
Non–insulin-dependent × >1.5	10.99 ab
Insulin-dependent × ≤1.5	20.41 ab
Insulin-dependent × >1.5	60.84 c

[a] Means within a main effect or interaction with the same letter (a, b, or c) are not significantly different from each other ($p = .05$).

the opposite relationship, possibly because the BUN was elevated disproportionately in the patients who had an increased preangiography BUN/creatinine ratio because of prerenal factors.

When groups of patients are compared, it is desirable to eliminate the state of hydration as a variable. The BUN/creatinine ratio was compared for nondiabetics vs diabetics and non–insulin-dependent vs insulin-dependent diabetics before and after angiography, and indeed, the fluid volume status was similar and did not appear to cause any bias in these groups.

Discussion

Regardless of the mechanism of renal injury (which is controversial [1, 5, 17]), the clinically significant nephrotoxic effects of radiologic contrast media are acknowledged universally. It has been estimated that 10% of cases of acute renal failure result from the administration of radiologic contrast media and that these agents are more commonly the cause of hospital-acquired renal insufficiency than are the aminoglycoside antibiotics [25].

Many conditions have been implicated as possible risk factors for contrast-induced nephropathy. Patients with preexisting renal insufficiency were considered to be at increased risk for this type of nephropathy from 1923 to 1963, contraindicating excretory urography in these patients during this time [1]. After the introduction of sodium diatrizoate in the late 1950s, excretory urography was reported to be safe in these patients [26]. Numerous reports of renal failure related to the use of radiologic contrast medium in diabetic and azotemic patients led to another reversal of opinion in the mid-1970s, with resultant reluctance to administer contrast material to such patients [1, 6]. The relationship of the osmolality of the contrast medium to the various postulated mechanisms of renal injury has not been established, and only recently have large clinical studies investigating the effect of low-osmolality contrast agents on contrast-induced nephropathy been published [27–29].

A variety of risk factors for contrast-induced nephropathy, in addition to preexisting renal disease, have been proposed, including diabetes mellitus, dehydration, multiple myeloma, large doses of contrast medium, peripheral vascular disease, hypertension, proteinuria, and age greater than 60 years [1].

The parameters used to identify contrast-induced nephropathy have included serial determinations of serum levels of creatinine and BUN [1–14, 16], measurement of urinary creatinine clearance [2], the identification of oliguria [15], measurement of urinary proteins such as β-hexosaminidase [30], and radiologic identification of a persistent nephrogram after exposure to contrast media [18, 31–33]. Because serum levels of creatinine may increase as early as 24 hr after exposure to contrast medium and tend to peak on the third to fifth day, measurement of serum creatinine level in the first 5 days after exposure to contrast material is the most practical method for identifying contrast-induced nephropathy [1, 14]. Changes in the fractional excretion of urinary electrolytes are not detectable in the absence of changes in the level of serum creatinine [14].

Table 1 summarizes several studies that examined renal function after the administration of radiologic contrast media. Note the wide variations in the definitions of preexisting renal insufficiency, the definition of significant change in serum creatinine level, and the time allowed for such change to occur. The reported incidences of radiocontrast-associated renal dysfunction (RACARD) vary widely, even when similar groups of patients are compared, which may be related to the definition of RACARD used.

In attempting to discriminate between the incidence of contrast-induced nephropathy in two groups of patients with different risk factors, the criteria chosen to define contrast-induced nephropathy, as well as the definition of preexisting renal insufficiency, may have significant impact. This makes it difficult to compare studies that use different definitions [1, 20]. Certain criteria (such as those used by Eisenberg et al. [6], by Byrd and Sherman [5] (Table 1), and our criteria numbers IV and V) are quite restrictive and more difficult to fulfill, possibly resulting in a falsely low incidence of contrast-induced nephropathy in some groups of patients, and thereby achieving little discriminating power (e.g., Fig. 2A, criteria IV and V, group L). For example, a rise in the serum level of creatinine of 1 mg/dl over 24 hr (criterion IV), may require a nearly complete cessation of glomerular filtration. A rise in BUN may be a poor discriminator because it is particularly subject to other variables, such as the state of hydration [24]. The lack of sensitivity and specificity of this latter criterion is seen in our criterion number VI (e.g., Figs. 1, 2B, and 5) and confirmed by examining another study [6]. In a recent article [10], contrast-induced nephropathy was defined initially as a rise in creatinine level of more than 50% and subsequently as a rise of more than 25%. Their latter criterion, although appearing less restrictive than their initial criterion, also required that the rise in creatinine level be "above 120 μmols per liter (1.4 mg/dl) on day 2." Consequently, a patient

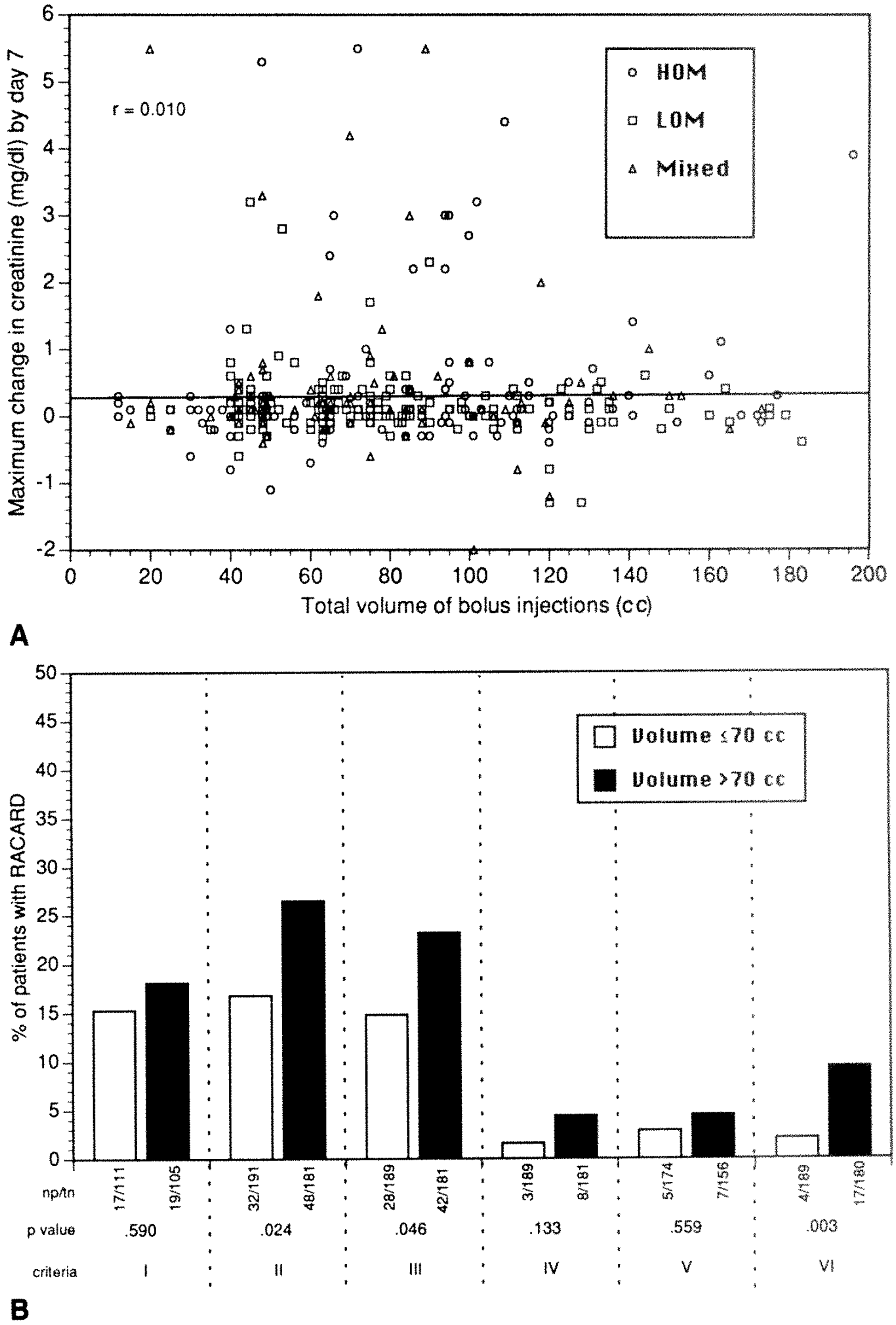

Fig. 3.—*A*, Scatter plot shows no correlation between total volume of contrast media administered and maximal change in creatinine level by day 7 in 394 patients. Similarly, no correlation exists between volume of contrast material and maximal change in creatinine level by day 3 (*not shown*).

B, A comparison of incidence of RACARD in patients receiving larger volumes of contrast media (>70 ml) vs those receiving smaller volumes of contrast media (≤70 ml) for all CrPre values when six different criteria for RACARD are used. An increase in incidence of RACARD in the >70 ml group is higher by all criteria. Statistical significance is shown by criteria II, III, and VI.

with a normal baseline creatinine level could have had a 100% rise in creatinine level (e.g., CrPre = 0.7, day 2 creatinine = 1.4 mg/dl) and presumably would not have been included in the group with a significant increase. After less restrictive, more sensitive discriminating criteria were applied to our data (criteria I–III), statistically significant differences between groups became apparent. Criteria II and III identify those patients for whom angiography has decreased glomerular filtration transiently by 10–20% or more [24]. Although in most cases renal function quickly recovers, such large fluctuations in renal physiology may reflect significant, and possibly irreversible, renal injury. Criterion I classifies as contrast-induced nephropathy only those patients whose initial rise in creatinine level persists into the fifth through seventh days

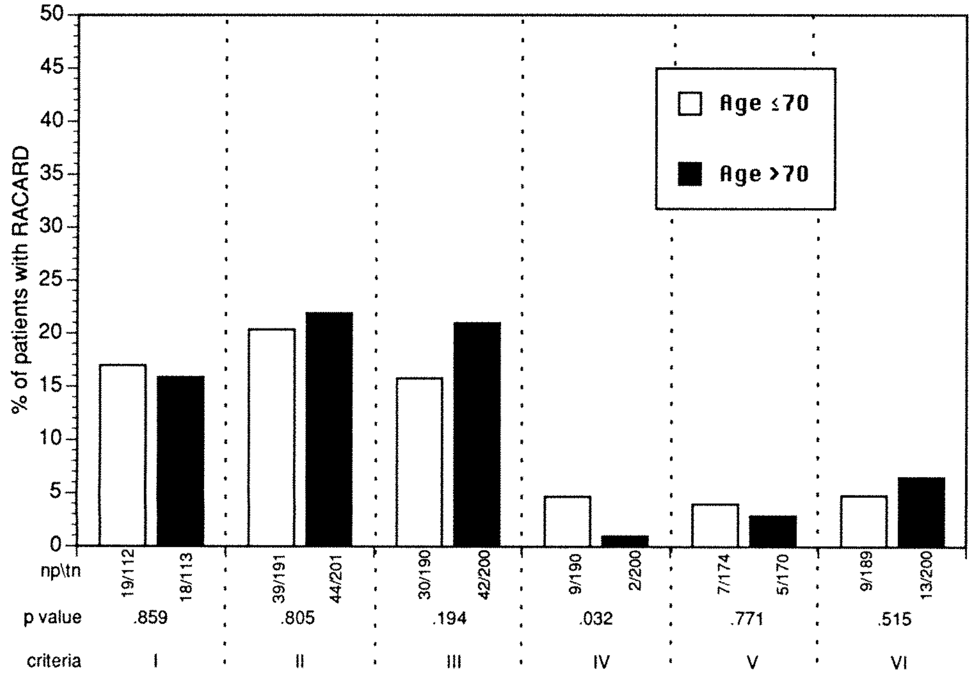

Fig. 4.—Comparison of incidence of RACARD in younger and older patients when six different criteria for RACARD are used. No consistent trend is seen by multiple criteria. Note, however, that if criterion IV only were used, one might think that a significant correlation exists.

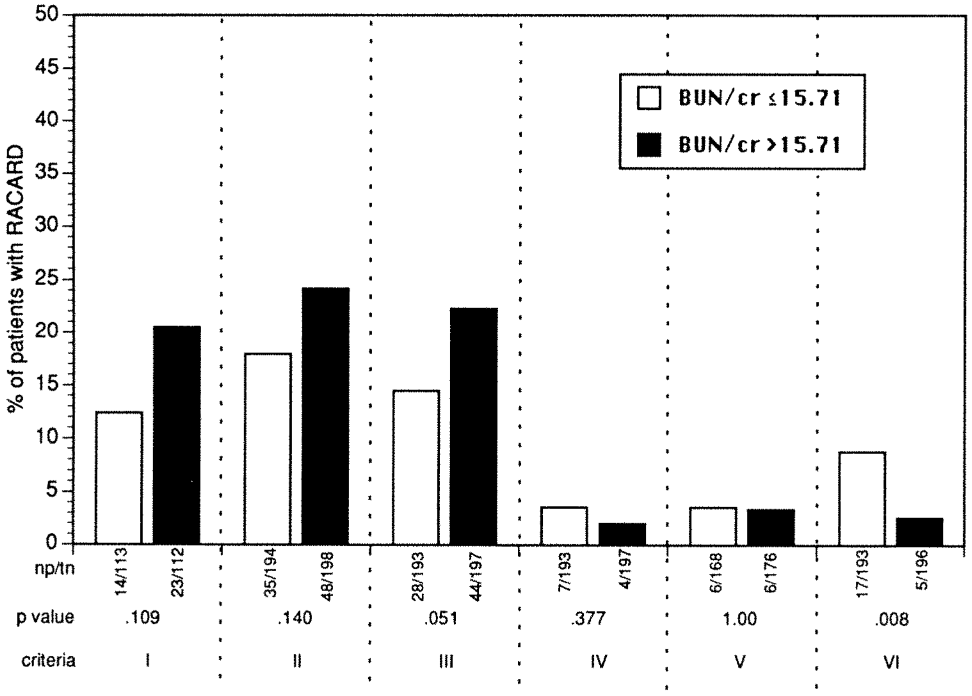

Fig. 5.—Comparison of incidence of RACARD when six criteria for RACARD are used and patients are divided into two groups, BUN/Cr ≤ 15.71 and BUN/Cr > 15.71 (15.71 is median value). Patients with higher BUN/Cr ratio show an increased risk for RACARD by criteria I, II, and III.

after angiography. With our data, this added restriction decreased the number of patients with sufficient data to be included in the group and therefore made it more difficult to attain statistical significance (e.g., Fig. 2A, criterion I, group G). Nevertheless, the trend is the same as with another less restrictive criterion, for which statistical significance is shown (Fig. 2A, criterion II, group G). Criterion I, by requiring a persistent elevation of creatinine level, probably reveals patients with more significant renal damage. Criteria II and III (more sensitive crirteria) have the virtue of eliminating the fewest patients on the basis of incomplete data in a clinical setting and are more sensitive for RACARD; however, these criteria will include some false-positives because of daily variation in serum levels of creatinine. Criteria I, IV, and V (more specific criteria for RACARD) require a persistent (I) and/or a substantial (IV and V) rise in serum creatinine level, showing patients with more significant renal damage. We conclude that all five creatinine criteria have merit and that they probably are used best in conjunction with each other.

All five creatinine criteria show a considerable, statistically significant increase in the incidence of RACARD in the group with an elevated CrPre (Fig. 1). The lack of a strong correlation between CrPre and maximal change in creatinine (r = .247) simply shows that the relationship is not linear.

Although the higher risk of contrast-induced nephropathy in patients with renal insufficiency and in patients with diabetes mellitus has been established [1, 17], the relationship of renal insufficiency and diabetes as separate and additive risk factors has been unclear. Earlier reports [4, 8] that used relatively stringent criteria (Table 1) found that diabetics with normal CrPre carried no more risk for contrast-induced nephropathy than did nondiabetics with normal CrPre. Our data, for which multiple criteria are used, may contradict this, showing that diabetics with normal CrPre are at greater risk for contrast-induced nephropathy than are nondiabetics with a normal CrPre (Fig. 2A). Two studies [3, 8] suggested that the likelihood of contrast-induced nephropathy is no greater for patients with diabetes and azotemia than for nondiabetic patients with azotemia. Our data show that azotemic patients with diabetes are at increased risk compared with both nondiabetics who have an elevated CrPre and diabetics who have a normal CrPre (Fig. 2A); this is supported by two other reports [2, 4]. We further showed that insulin-dependent diabetics are probably at higher risk than are non–insulin-dependent diabetics (Table 2). Moreover, we show that risk factors appear to be additive (Fig. 2A, Table 2), which is in agreement with Cochran et al. [3]: the highest risk is for insulin-dependent diabetics with elevated CrPre. It must be remembered that absence of risk factors does not preclude the development of contrast-induced nephropathy; by one definition its incidence was 13% in nondiabetic, nonazotemic patients after femoral angiography (Fig. 2A, criteria II, group L).

Some reports have suggested a positive relationship between the dose of contrast material and contrast-induced nephropathy [1, 10, 11, 34, 35], whereas other studies claim that increasing the dose does not increase the risk of contrast-induced nephropathy [1, 8, 14, 22]. Our results show that the method of interpreting data on the volume of contrast medium may make a difference. When scatter plots (Fig. 3A) are used, as used by Miller et al. [22], no effect of volume on the incidence of contrast-induced nephropathy is shown; this is also true for our analysis of variance model. However, when multiple criteria are used to determine if there is a correlation between the volume of contrast material administered and the incidence of contrast-induced nephropathy, an effect is shown (Fig. 3B).

Older retrospective studies and more recent prospective studies do not agree on the association of previous volume depletion with contrast-induced nephropathy [1]. When we used a scatter plot and the analysis of variance model, no correlation is present. Using the six criteria for RACARD, we showed only a nonstatistically significant trend that suggested a positive correlation between the BUN/creatinine ratio before angiography and the likelihood of contrast-induced nephropathy (Fig. 5). This lends some support to the contention that dehydration at the time of administration of contrast material is a risk factor for contrast-induced nephropathy.

Increasing age of the patient did not confer an increased risk of contrast-induced nephropathy in our study (Fig. 4), supporting the data of previous studies [2, 35]. We cannot evaluate peripheral vascular disease as an independent variable with our population of patients, nor can we compare intraarterial with IV injection.

In summary, the patients at increased risk for contrast-induced nephropathy are insulin-dependent diabetics (non–insulin-dependent diabetics do not seem to be at increased risk in our study group) and patients with underlying renal insufficiency. The effects of poor hydration and the volume of contrast medium administered are less clear but are possible risk factors; prudence and the requirements of the examination must determine the amount of contrast material used. The risk for contrast-induced nephropathy does not appear to be influenced by the patient's age or sex. Risk factors may be additive. The definition of contrast-induced nephropathy used has a significant effect on the incidence of the nephropathy. Using multiple criteria for contrast-induced nephropathy is somewhat cumbersome and inevitably does not always achieve statistical significance for all criteria; however, a closer estimation of the true risk of renal damage may be obtained. Those criteria in which statistical significance is not achieved usually show the same trend as the statistically significant criteria. Absence of risk factors does not preclude the development of contrast-induced nephropathy after femoral angiography; by one definition its incidence was 13% in nondiabetic nonazotemic patients (Fig. 2A).

ACKNOWLEDGMENTS

The authors thank Martin James and Deborah Babcock Buck of D. B. & P. Associates for their assistance with statistical analysis.

REFERENCES

1. Berkseth RO, Kjellstrand CM. Radiologic contrast induced nephropathy. *Med Clin North Am* **1984**;68:351–370
2. Shafi T, Chou S, Porush JG, Shapiro WB. Infusion intravenous pyelography and renal function effects in patients with chronic renal insufficiency. *Arch Intern Med* **1978**;138:1218–1221
3. Cochran ST, Wong WS, Roe DJ, Predicting angiography-induced acute renal function impairment: clinical risk model. *AJR* **1983**;141:1027–1033
4. Van Zee BE, Hoy WE, Talley TE, Jaenike JR. Renal injury associated with intravenous pyelography in nondiabetic and diabetic patients. *Ann Intern Med* **1978**;89:51–54
5. Byrd L, Sherman RL. Radiocontrast-induced acute renal failure: a clinical and pathophysiological review. *Medicine* **1979**;58:270–279
6. Eisenberg RL, Bank WO, Hedgock MW. Renal failure after major angiography can be avoided with hydration. *AJR* **1981**;136:859–861
7. Harkonen S, Kjellstrand CM. Exacerbation of diabetic renal failure following intravenous pyelography. *Am J Med* **1977**;63:939–946
8. D'Elia JA, Gleason RE, Alday M, et al. Nephrotoxicity from angiographic contrast material: a prospective study. *Am J Med* **1982**;72:719–725
9. Kumar S, Hull JD, Lathi S, et al. Low incidence of renal failure after angiography. *Arch Intern Med* **1981**;141:1268–1270
10. Parfrey PS, Griffiths SM, Barrett BJ, et al. Contrast material-induced renal failure in patients with diabetes mellitus, renal insufficiency, or both. *N Engl*

J Med **1989**;320:143–149

11. Martin-Paredero V, Dixon S, Baker D, et al. Risk of renal failure after major angiography. *Arch Surg* **1983**;118:1417–1420
12. Krumlovsky FA, Simon N, Santhanam S, Del Greco F, Roxe D, Pomarac MM. Acute renal failure: association with administration of radiographic contrast material. *JAMA* **1978**;239:125–127
13. Cramer BC, Parfrey PS, Hutchinson TA, et al. Renal function following infusion of radiologic contrast material: a prospective controlled study. *Arch Intern Med* **1985**;145:87–89
14. Hayman LA, Evans RA, Fahr LM, Hinck VC. Renal consequences of rapid high-dose contrast CT. *AJNR* **1980**;1:9–11
15. Teruel JL, Marcen R, Onaindia JM, Serrano A, Quereda C, Ortuno J. Renal function impairment caused by intravenous urography: a prospective study. *Arch Intern Med* **1981**;141:1271–1274
16. Mudge G. Nephrotoxicity of urographic radiocontrast drugs. *Kidney Int* **1980**;18:540–552
17. Misson RT, Cutler RE. Radiocontrast-induced renal failure. *West J Med* **1985**;142:657–664
18. Older RA, Miller JP, Jackson DC, Johnsrude IS, Thompson WM. Angiographically induced renal failure and its radiographic detection. *AJR* **1976**;126:1039–1045
19. Alexander RD, Berkes SL, Abuelo JG. Contrast media-induced oliguric renal failure. *Arch Intern Med* **1978**;138:381–384
20. Talner LB. Does hydration prevent contrast material injury? *AJR* **1981**;136:1021–1022
21. Davidson AJ, Becker J, Rothfield N, Unger G, Ploch DR. An evaluation of the effect of high-dose urography on previously impaired renal and hepatic function in man. *Radiology* **1970**;97:249–254
22. Miller DL, Chang R, Wells WT, Dowjat BA, Malinosky RM, Doppman JT. Intravascular contrast media: effect of dose on renal function. *Radiology* **1988**;167:607–611
23. Coe FL. Alterations in urinary function. In: Isselbacher KJ, Adams RD, Braunwald E, Petersdorf RG, Wilson JD, eds. *Harrison's principles of internal medicine*, 9th ed. New York: McGraw-Hill, **1980**:213–219
24. Kassirer JP, Gennari FJ. Laboratory evaluation of renal function. In: Earley LE, Gottschalk CW, eds. *Strauss and Welt's diseases of the kidney.* Boston: Little, Brown, **1979**:41–91
25. Hou S, Bushinsky DA, Wish JB, et al. Hospital-acquired renal insufficiency: a prospective study. *Am J Med* **1983**;74:243–248
26. Schwartz WB, Hurwit A, Ettinger A. Intravenous urography in the patient with renal insufficiency. *N Engl J Med* **1963**;269:277–283
27. Lautin EM, Freeman NJ, Schoenfeld AH, et al. Radiocontrast-associated renal dysfunction: a comparison of lower-osmolality and conventional high-osmolality contrast media. *AJR* **1991**;157:59–65
28. Schwab SJ, Hlatky MA, Pieper KS, et al. Contrast nephrotoxicity: a randomized controlled trial of a nonionic and an ionic radiographic contrast agent. *N Engl J Med* **1989**;320:149–153
29. Gomes AS, Lois JF, Baker JD, et al. Acute renal dysfunction in high-risk patients after angiography: comparison of ionic and nonionic contrast media. *Radiology* **1989**;170:65–68
30. Albrechtsson U, Hultberg B, Larusdottir H, Norgren L. Nephrotoxicity of ionic and non-ionic contrast media in aortofemoral angiography. *Acta Radiol* **1985**;26:615–618
31. Older RA. Contrast-induced renal failure: a radiological problem and a radiological diagnosis. *Radiology* **1979**;131:553–554
32. Older RA, Korobkin M, Cleeve DM, Schaaf R, Thompson W. Contrast-induced acute renal failure: persistent nephrogram as a clue to early detection. *AJR* **1980**;134:339–342
33. Berdon WE, Schwartz RH, Becker J, Baker DH. Tamm-Horsfall proteinuria: its relationship to prolonged nephrogram in infants and children and to renal failure following intravenous urography in adults with multiple myeloma. *Radiology* **1969**;92:714–722
34. Gruskin LB, Oetlikev OH, Wolfish NM, et al. Effects of angiography on renal function and histology in infants and piglets. *J Pediatr* **1970**;76:41–48
35. Weinrauch LA, Healy RW, Leland OS, et al. Coronary angiography and acute renal failure in diabetic azotemic nephropathy. *Ann Intern Med* **1977**;86:56–59

The reader's attention is directed to the commentary on this article, which appears on pages 66–68.

Radiocontrast-Associated Renal Dysfunction: A Comparison of Lower-Osmolality and Conventional High-Osmolality Contrast Media

Everett Marc Lautin[1]
Neil Joshua Freeman[1,2]
Alan H. Schoenfeld[1]
Curtis W. Bakal[1]
Nogah Haramiti[1,2]
Arnold C. Friedman[3]
Jeffrey L. Lautin[4]
Steven Braha[1]
Elisa G. Kadish[1]
Seymour Sprayregen[1]
Isaac Belizon[5]

Nephropathy is an established untoward event associated with intravascular administration of conventional high-osmolality contrast media (HOM). It has not been shown previously that lower-osmolality contrast media (LOM) are less nephrotoxic in a clinical setting. We evaluate the ability to replace HOM with LOM (in lower-extremity angiography) to reduce the incidence of nephropathy. We use multiple definitions for contrast-induced nephropathy (six different magnitudes of rise of serum levels of creatinine or blood urea nitrogen in various periods). The incidences of nephrotoxic effects with LOM vs HOM in patients with presumed risk factors, including preexisting renal insufficiency and diabetes, are evaluated also. When all patients are considered, the incidence of contrast-induced nephropathy for LOM vs HOM (defined as an increase in serum creatinine level >0.3 mg/dl *and* $>20\%$ on day 1, 2, or 3 *and* on day 5, 6, or 7, is 7% vs 26% ($p = .001$). When only patients with preangiography azotemia are considered, the incidence of contrast-induced nephropathy for LOM vs HOM is 10% vs 41% ($p = .017$); for diabetic patients, regardless of preangiography creatinine level, the incidence is 10% vs 31% ($p = .012$).

Although contrast-induced nephropathy may develop even in a patient with no risk factors who receives LOM, LOM is associated with a decreased incidence of this condition, to various degrees, depending on the presence of risk factors.

***AJR* 157:59-65, July 1991**

One of the alleged benefits of the new lower-osmolality contrast media (LOM) when compared with conventional high-osmolality contrast media (HOM), based on animal and in vitro studies, is a decrease in contrast-induced nephrotoxic effects [1-3]. Clinical studies comparing the nephrotoxic effects of LOM with those of HOM have suggested little or no difference [4-11]. The purpose of this study was to determine whether a switch to the more expensive [12, 13] LOM will decrease the incidence of radiocontrast-associated renal dysfunction (RACARD). Using multiple analyses, as in Lautin et al. [14], we compared the incidence of contrast-induced nephropathy in a group of patients who received HOM with the incidence in a group of patients who received LOM for femoral angiography.

The term "low osmolar" is a misnomer because these agents, although significantly lower in osmolality when compared with the conventional agents, are still hyperosmolar when compared with serum (e.g., HOM: diatrizoate meglumine 60% = 1400 mOsm/kg, diatrizoate 76% = 2016 mOsm/kg; LOM: iohexol 300 = 672 mOsm/kg, ioxaglate 320 = 600 mOsm/kg, iohexol 350 = 844 mOsm/kg; serum = 280 mOsm/kg) [12]. We, therefore, will use the term *lower*-osmolality contrast media.

Materials and Methods

Three hundred three patients undergoing femoral angiography were studied. This group was selected because it contained a large proportion of elderly and/or diabetic patients, many

Received March 14, 1989; accepted after revision November 30, 1990.

Presented at the annual meeting of the American Roentgen Ray Society, San Francisco, CA, May 1988.

[1] Department of Radiology, Montefiore Medical Center, 111 E. 210th St., Bronx, NY 10467. Address reprint requests to E. M. Lautin.

[2] Present address: Department of Radiology, Columbia College of Physicians and Surgeons, Columbia Presbyterian Medical Center, 630 W. 168th St., New York, NY 10032.

[3] Department of Radiology, Temple University Medical Center, Broad and Ontario Sts., Philadelphia, PA 19140.

[4] Department of Radiology, Columbia College of Physicians and Surgeons, 630 W. 168th St., New York, NY 10032. Present address: Department of Radiology, Mount Sinai Medical Center, One Gustave L. Levy Place, New York, NY 10029-6574.

[5] Department of Renal Medicine, Montefiore Medical Center, 111 E. 210th St., Bronx, NY 10467.

0361-803X/91/1571-0059
© American Roentgen Ray Society

of whom had underlying renal insufficiency and were presumably at increased risk for contrast-induced nephropathy [14].

One hundred forty-three patients received HOM (meglumine diatrizoate, Hypaque 60% and sodium/meglumine diatrizoate, Hypaque 76%, Winthrop Pharmaceuticals, New York, NY) and were studied retrospectively. Data for the HOM group were obtained by a retrospective review of consecutive patients' charts about 2 months before we started the prospective data collection on LOM patients. (Once we began using LOM for femoral angiography, we found that there was a marked reduction in pain and we could no longer justify the use of HOM. For this reason, HOM data had to be obtained retrospectively.) One hundred sixty consecutive patients received LOM (sodium/meglumine ioxaglate, Hexabrix, Mallinckrodt, Inc., St. Louis, MO, or iohexol, Omnipaque 300 or Omnipaque 350, Winthrop Pharmaceuticals); these patients were studied prospectively and were alternated between receiving ioxaglate alone and receiving iohexol alone. Clinical and baseline laboratory data for the LOM patients were obtained before the angiogram.

The demographics in the LOM and HOM groups were similar for percentage of diabetics, percentage of patients with preangiography azotemia, volume of contrast media injected, blood urea nitrogen/creatinine ratio (BUN/Cr), and sex and age distribution (Table 1). The number of patients who had surgery by day 5 after angiography is slightly greater for the LOM group. Serum creatinine values were recorded on the day of and/or the day before angiography (CrPre) and daily for 7 days after angiography (when available). Creatinine data availability for days 1 through 3 was slightly higher in the HOM group; for days 4 through 6, it was higher for the LOM group (Table 1).

All patients received either unilateral femoral artery injections or low-abdominal aortic injections. A smaller number of patients had translumbar injections or underwent peripheral femoral angioplasty. The distribution of the type of study performed is very similar in the LOM and HOM groups (Table 1).

The incidence of contrast-induced nephropathy, as defined by multiple criteria, was determined for the patient groups selected, and the incidences were compared (see abbreviation key for definitions of criteria) as in Lautin et al. [14]. Statistical analyses were performed using Fisher's exact probability test (two-tailed). Patients were excluded if the relevant data were missing. Blinded statistical analyses were performed through the research facilities of Mallinckrodt, Inc. (St. Louis, MO).

Additional investigation with an analysis of variance model was conducted on 290 patients to simultaneously examine the effects of CrPre level (≤ 1.5 mg/dl vs >1.5 mg/dl), the type of contrast medium used (LOM vs HOM), and the two-way interaction of these factors on the maximal percentage of increase in creatinine levels by day 3 after the procedure. Paired comparisons were then conducted on the least squares means of the main effects and interactions that were found to be significant ($p < .05$). These statistical analyses were conducted by using the GLM (General Linear Models) procedure in the SAS (Statistical Analysis System) computer package.

Results

There is a decrease in the incidence of contrast-induced nephropathy when LOM are used instead of HOM (Fig. 1). This is true for virtually all the criteria used and is statistically significant for many (Fig. 1: criteria I-A,L,G; II-A,G; III-A,G). This decrease in contrast-induced nephropathy with LOM is clearer in the setting of an elevated baseline creatinine level than with a normal baseline creatinine level (with a normal CrPre, statistical significance is only shown using criterion I; criteria II and III demonstrate the same trend, and no patient with a normal CrPre, from either the LOM or the HOM group, satisfies criteria IV or V). The analysis of variance model demonstrated that patients receiving HOM had a significantly larger percentage of increase in creatinine level than did patients receiving the LOM (least squares mean HOM = 32.55% vs LOM = 10.94%, $p < .05$).

In the HOM group, patients with an elevated CrPre are at considerably increased risk for contrast-induced nephropathy compared with those with a normal CrPre. (Fig. 1: the solid bar, HOM, labeled G is markedly higher than the solid bar labeled L for all creatinine criteria. The *p* values are as follows: criteria I = .068, II = .002, III = .005, IV $<$ .001, V $<$ .001). In the LOM group, the increase in contrast-induced nephropathy in elevated CrPre patients compared with the normal CrPre

Key to Abbreviations Used in Figures

Criteria Definitions

I	increase in creatinine level >0.3 mg/dl *and* $>20\%$ on day 1, or 2, or 3 *and* on day 5, or 6, or 7
II	increase in creatinine level >0.3 mg/dl *and* $>20\%$ on day 1, or 2, or 3
III	increase in creatinine level >0.3 mg/dl *and* $>20\%$ on day 1 or 2
IV	increase in creatinine level ≥ 2.0 mg% on day 1 or 2
V	increase in creatinine level ≥ 1.0 mg% on day 1
VI	increase in blood urea nitrogen (BUN) level ≥ 20 mg% or $\geq 50\%$ on day 1

Abbreviations

A	all patients in the category
G	all patients in the category with CrPre >1.5 mg/dl
L	all patients in the category with CrPre ≤ 1.5 mg/dl
BUN	blood urea nitrogen
CrPre	creatinine level preangiography
HOM	high-osmolality media
LOM	lower-osmolality media
np/tn	number of patients who meet criteria/total number of patients in this group
RACARD	radiocontrast-associated renal dysfunction

Note

p values	calculated by using Fisher's exact probability test (2-tailed)

TABLE 1: Comparison of Patients Receiving Lower-Osmolality Contrast Media (LOM) with Those Receiving High-Osmolality Contrast Media (HOM)

	LOM	HOM	*p* Value (LOM vs HOM)
No. of patients	160	143	
Men (%)	84 (53)	84 (59)	
Women (%)	76 (48)	59 (41)	
Age (years)			
Median	69	73	
Mean	67.2	71.8	
SD	14.4	10.6	
Percentage diabetic	49.7	50.6	.865[a]
Volume of contrast bolus (ml)	77.9	80.9	.501[b]
Blood urea nitrogen/creatinine (BUN/Cr)	16.6	16.4	.705[b]
Creatinine level preangiography			
Mean (mg/dl)	1.3	1.4	.135[b]
Percentage of patients >1.5 mg/dl	22.6	25.9	.512[b]
Percentage of patients ≤1.5 mg/dl	77.4	74.1	
Type of femoral angiogram			
Translumbar arteriogram (%)	14 (9)	10 (7)	
Bilateral femoral (%)	52 (33)	45 (32)	
Unilateral femoral (%)	77 (48)	56 (39)	
Angioplasty (%)	15 (9)	29 (20)	
Surgery performed by day 5 (%)	86 (54)	58 (41)	
Patients with data for creatinine (%)			
On day 1	133 (83)	128 (90)	
On days 1 or 2	147 (92)	140 (98)	
On days 1, 2, or 3	153 (96)	143 (100)	
On days 5, 6, or 7	102 (64)	41 (29)	

[a] Chi-square.

[b] Two-sample t test.

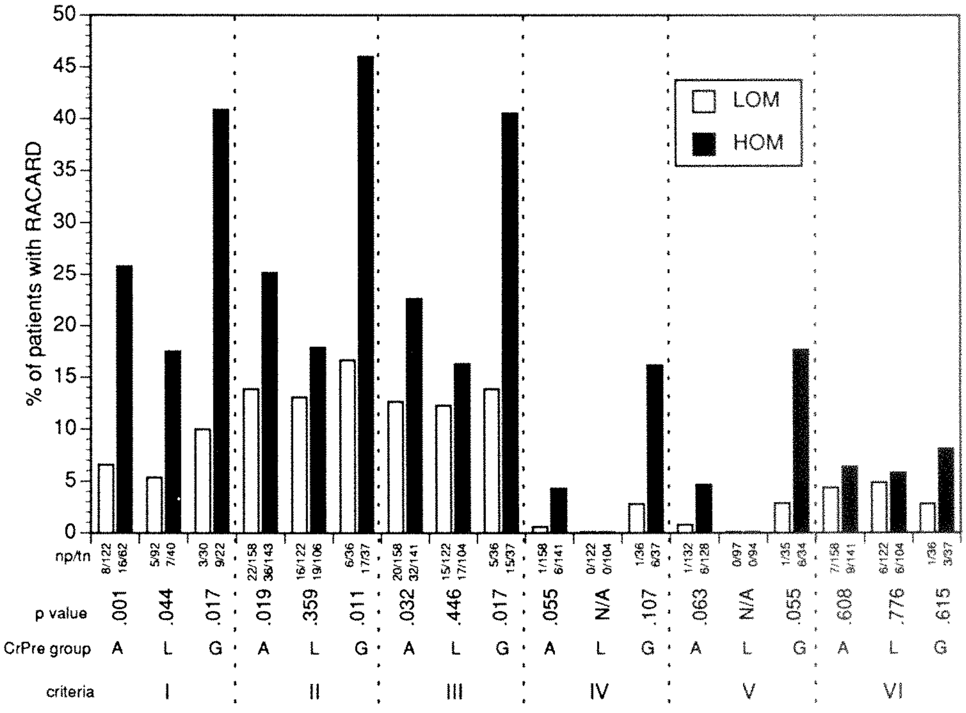

Fig. 1.—A comparison of the incidence of RACARD in all patients receiving LOM vs incidence in all patients receiving HOM using multiple criteria for RACARD. This comparison is made for all patients regardless of baseline renal function (A), for patients with normal baseline CrPre (L), and for patients with elevated baseline CrPre (G).

patients is small and not statistically significant. Similar results were obtained with the analysis of variance model. Specifically, patients with elevated CrPre who received HOM had a significantly larger percentage of increase in creatinine level than did HOM patients with a normal CrPre (50% vs 15%, $p < .05$); CrPre did not significantly influence the percentage of increase in creatinine among patients receiving LOM (12% vs 9%).

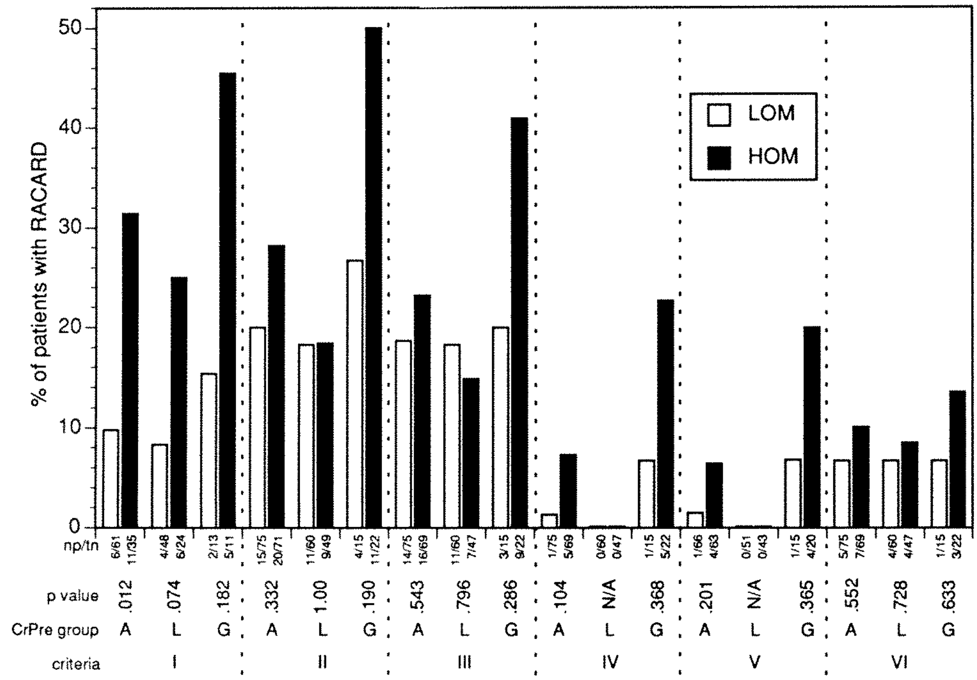

Fig. 2.—A comparison of incidence of RACARD in diabetic patients receiving LOM vs incidence in diabetic patients receiving HOM. As in Fig. 1, six different criteria are used and CrPre comparisons are made for each of the CrPre groups. Marked decrease in incidence of RACARD in LOM group is shown: in CrPre group G by most criteria and in CrPre group L only by criterion I.

In diabetic patients (Fig. 2), although LOM is seen to have a lower incidence of contrast-induced nephropathy compared with HOM in patients with elevated CrPre (>1.5 mg/dl) by all criteria, statistical significance is not demonstrated. In diabetics with normal CrPre (≤1.5 mg/dl), no statistically significant difference between HOM and LOM is shown. When both CrPre groups are combined, a decreased incidence of contrast-induced nephropathy with LOM is seen by all criteria but is statistically significant only with criterion I.

Diabetics with an elevated CrPre who receive HOM are at increased risk for contrast-induced nephropathy compared with those with a normal CrPre for all creatinine criteria (Fig. 2: the *p* values are as follows: criteria I = .263, II = .010, III = .030, IV = .002, V = .008). Comparison of diabetics receiving LOM, with elevated CrPre, to those with a normal CrPre, reveals only a small, not statistically significant, increase in contrast-induced nephropathy.

In nondiabetic patients, a decreased nephrotoxicity of LOM compared with HOM is demonstrated for elevated CrPre, normal CrPre, and the combined CrPre group; statistical significance is obtained for CrPre group A using criteria I, II, and III and CrPre group L using criteria II and III (Fig. 3). Nondiabetic patients with an elevated CrPre who receive HOM are at considerably increased percentage of risk for contrast-induced nephropathy compared with nondiabetics with a normal CrPre for all creatinine criteria (Fig. 3: the *p* values are as follows: criteria I = .128, II = .096, III = .096, IV = .217, V = .048). In patients receiving LOM, there is only a small, insignificant increase in the incidence of RACARD when comparing nondiabetics with an elevated CrPre to those with a normal CrPre.

There is no consistent demonstrable difference in the incidence of contrast-induced nephropathy between ioxaglate and iohexol in any group of patients (Fig. 4).

Discussion

The clinical advantages of LOM vs HOM proposed in the literature [15–23] create an ethical dilemma, that is, whether we are obligated to use this more expensive class of agent, and, if so, in which patients [13, 24, 25]. Of particular importance in peripheral angiography is the markedly decreased pain produced by LOM, which has been observed by us and by others [22, 23].

Experiments in dogs have shown LOM are significantly less nephrotoxic than HOM are [2, 4]. One study that used sensitive enzyme markers to measure nephrotoxicity in humans found less renal injury caused by iohexol than by meglumine metrizoate [9]. However, another study revealed no significant difference in renal injury comparing iopamidol, meglumine iothalamate, and meglumine diatrizoate [26]. Measuring changes in serum creatinine level, no difference in nephrotoxic effects between LOM and HOM used for angiography has been shown by several investigators [5–8]. However, these groups monitored the serum levels of creatinine for up to only 24 hr (with the exception of 20 patients followed up for 48 hr) after angiography. In a recent large prospective series [4], no relationship existed between dose of contrast medium and changes in levels of serum creatinine or BUN for either iopamidol or meglumine diatrizoate. Another recent large prospective series [11] showed a lower but not statistically significant difference in the incidence of nephrotoxic effects produced by LOM vs HOM; the protective effect of vigorous IV hydration may have decreased the incidence of nephrotoxic effects in both groups, thereby diminishing the difference between LOM and HOM.

We believe that our retrospective HOM and prospective LOM groups are comparable. The referring vascular surgeons, staff angiographers, indications for arteriography, de-

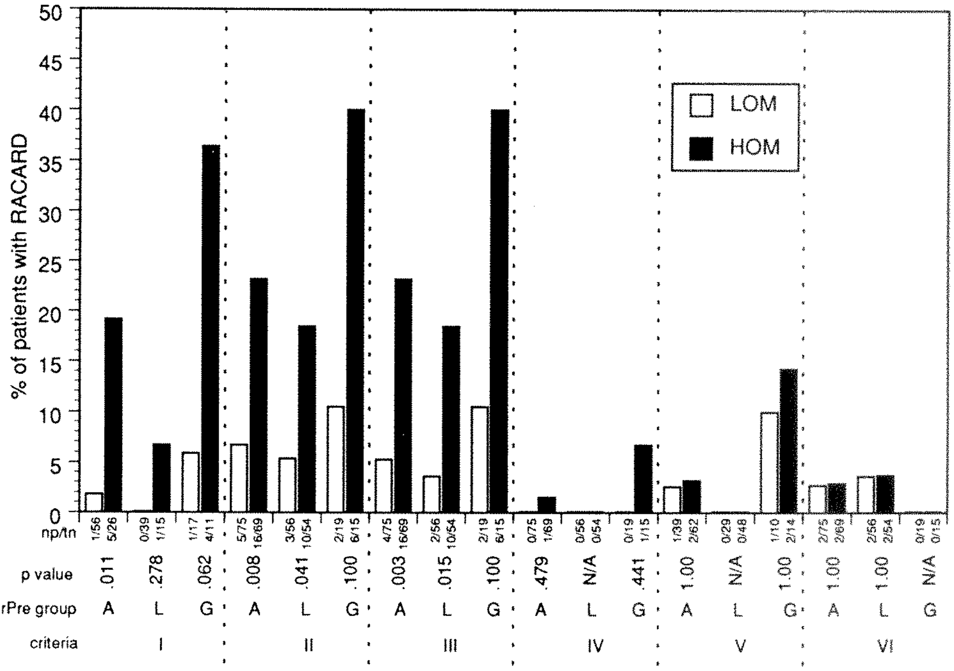

Fig. 3.—A comparison of incidence of RACARD in nondiabetic patients receiving LOM vs incidence in nondiabetic patients receiving HOM. Marked benefit of LOM in decreasing incidence of RACARD is clear using criteria I–III.

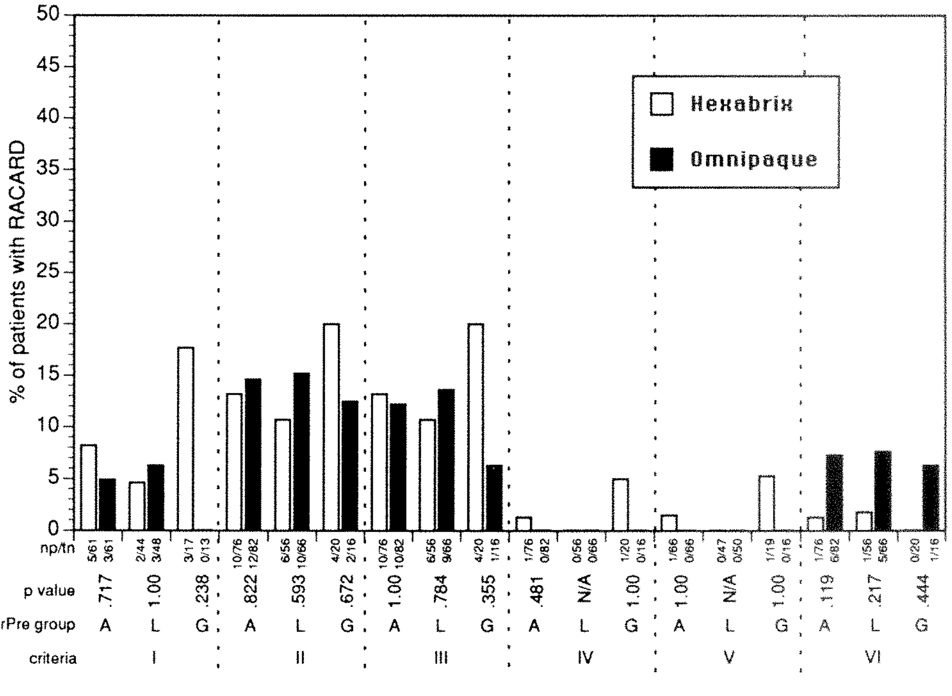

Fig. 4.—Two different lower-osmolality contrast media are compared: ioxaglate (Hexabrix) and iohexol (Omnipaque). No consistent difference between these two agents is shown.

mographic characteristics, and angiographic techniques were the same. Availability of creatinine data (Table 1) was similar in both LOM and HOM groups for days 1–3. Creatinine data were available for more patients in the LOM group on days 5–7, but this only affects the number of patients evaluated by criterion I, with fewer patients able to be evaluated in the HOM group. The state of hydration before angiography was similar in both groups (Table 1). The surgical housestaff who cared for these patients were unaware of our study, so that no alterations in care occurred before or after angiography for the LOM group. Although we were not able to obtain reliable data on administration of nephrotoxic antibiotics, the number of patients receiving aminoglycosides on the vascular surgery service is small, and there is no reason to believe there should be a significant difference in this regard between these two sizeable groups of patients. Although patients in the HOM group underwent angioplasty at a somewhat higher rate, no significant difference was seen between the two groups in the average amount of contrast medium administered (Table 1). Furthermore, the amount of contrast medium administered may have only a minimal effect on contrast-induced nephropathy [4, 14]. Thus, it is likely that the observed differential effect on renal function of HOM vs LOM is a result of the type of contrast agent rather than a function of differences in selection of patients or angiographic technique.

The effect of choosing various criteria on the incidence of contrast-induced nephropathy may be dramatic, causing lack of sensitivity and poor discrimination between groups. For example, the marked diminution in the incidence of contrast-induced nephropathy in the LOM group (vs the HOM group) is demonstrated for all CrPre groups using criterion I, and for CrPre groups A and G using criteria II and III (Fig. 1). However, if the group of patients with normal CrPre (L) is evaluated with the more restrictive criteria IV or V, the results show that contrast-induced nephropathy did not develop in any patient from either contrast group (LOM or HOM); therefore, no difference between these groups can possibly be discerned. The lack of discrimination between the two contrast groups using the BUN criterion as the definition of RACARD (criterion VI) may be due to the dependence of BUN on extrarenal factors. The impact of using differing definitions for RACARD on the detected incidence of contrast-induced nephropathy is discussed in detail by Lautin et al. [14] and mentioned in an editorial by Talner [27].

Using multiple criteria for RACARD, we have demonstrated a considerable statistically significant decrease in the incidence of contrast-induced nephropathy in patients receiving LOM vs HOM (Fig. 1, groups A and G, criteria I-III; criteria IV and V showed the same trend). This finding was supported by using an analysis of variance model. The decreased risk with LOM vs HOM is not clearly shown when the CrPre is normal. Elevated CrPre as a risk factor for contrast-induced nephropathy has been discussed in the literature [28-36], and in Lautin et al. [14]; we found this to be true for HOM but not for LOM (Fig. 1 and the analysis of variance model). In diabetic patients, the incidence of contrast-induced nephropathy with LOM is less than with HOM but statistical significance is only shown by using criteria I for all CrPre levels (Fig. 2, group A). In nondiabetic patients, a decrease in contrast-induced nephropathy is seen with LOM vs HOM in all CrPre groups (Fig. 3: groups A, L, G, by criteria I-III). For both diabetic and nondiabetic patients (Figs. 2 and 3), it is seen that elevated CrPre is a risk factor for contrast-induced nephropathy when HOM is used and only a minimal risk factor when LOM is used.

LOM are associated with a lower incidence of postcontrast acute decrease in renal function compared with HOM; this difference is considerable in some groups. The choice between the two LOM, iohexol and sodium/meglumine ioxaglate, should not be influenced by the possibility of contrast-induced nephropathy. The effect of LOM in reducing—but not eliminating—the possibility of contrast-induced nephropathy is clearer in high-risk patients (those with elevated CrPre). Therefore, the use of LOM in these patients seems justified by our results despite its increased cost. The use of LOM in all patients, including those who have no known risk factors for contrast-induced nephropathy, is less clear.

ACKNOWLEDGMENTS

The authors thank Martin James and Deborah Babcock Buck of D. B. & P. Associates for their assistance with statistical analysis.

REFERENCES

1. McClennan BL. Low osmolality contrast media: premises and promises. *Radiology* **1987**;162:1-8
2. Tornquist C, Almen T, Golman K, Holtas S. Proteinuria following nephroangiography: comparison between ionic monomeric, monoacidic dimeric and non-ionic contrast media in the dog. *Acta Radiol Suppl* **1980**;362:49-52
3. Lund G, Einzig S, Rysavy J, et al. Effect of prostaglandin inhibition on the renal vascular response to ionic and non-ionic contrast media in the dog. *Acta Radiol* **1984**;25:407-410
4. Miller DL, Chang R, Wells WT, Dowjat BA, Malinosky RM, Doppman JT. Intravascular contrast media: effect of dose on renal function. *Radiology* **1988**;167:607-611
5. Smith HJ, Levorstad K, Berg KJ, Rootwelt K, Sveen K. High dose urography in patients with renal failure: a double blind investigation of iohexol and metrizoate. *Acta Radiol* **1985**;26:213-220
6. Barth KH, Mertens MA. A double-blind comparative study of Hexabrix and Renografin-76 in aortography and visceral arteriography. *Invest Radiol* **1984**;19:S323-S325
7. Bettman MA, Higgins CB. Comparison of an ionic with a nonionic contrast agent for cardiac angiography: results of a multicenter trial. *Invest Radiol* **1985**;20:S70-S74
8. Wolf GL. Adult peripheral angiography: results from four North American randomized clinical trials of ionic media versus iohexol. *Invest Radiol* **1985**;20:S108-S111
9. Albrechtsson U, Hultberg B, Larusdottir H, Norgren L. Nephrotoxicity of ionic and non-ionic contrast media in aorto-femoral angiography. *Acta Radiol* **1985**;26:615-618
10. Schwab SJ, Hlatky MA, Pieper KS, et al. Contrast nephrotoxicity: a randomized controlled trail of a nonionic and an ionic radiographic contrast agent. *N Engl J Med* **1989**;320:149-153
11. Gomes AS, Lois JF, Baker JD, et al. Acute renal dysfunction in high-risk patients after angiography: comparison of ionic and nonionic contrast media. *Radiology* **1989**;170:65-68
12. White RJ, Halden WJ. Liquid gold: low-osmolality contrast media. *Radiology* **1986**;159:559-560
13. Jacobson JD, Rosenquist CJ. The introduction of low-osmolar contrast agents in radiology: medical, economic and public policy issues. *JAMA* **1988**;260:1586-1592
14. Lautin EM, Freeman NJ, Schoenfeld AH, et al. Radiocontrast-associated renal dysfunction: incidence and risk factors. *AJR* **1991**;157:49-58
15. Grainger RG. A clinical trial of a new osmolality contrast medium sodium and meglumine ioxaglate (Hexabrix) compared with meglumine iothalamate (Conray) for carotid arteriography. *Br J Radiol* **1979**;52:781-786
16. Grainger RG. Osmolality of intravascular radiologic contrast media. *Br J Radiol* **1980**;53:739-746
17. Lasser EC, Berry CC, Talner LB, et al. Pretreatment with corticosteroids to alleviate reactions to intravenous contrast material. *N Engl J Med* **1987**;317:845-849
18. Reagan K, Bettman MA, Finkelstein BA, Ganz P, Grassi CJ. Double-blind study of a new nonionic contrast agent for cardiac angiography. *Radiology* **1988**;167:409-413
19. Jacobsson BF, Jorulf H, Kalantar MS, Narasimham DL. Nonionic versus ionic contrast media in intravenous urography: clinical trial in 1,000 consecutive patients. *Radiology* **1988**;167:601-605
20. Spataro RF, Katzberg RW, Fischer HW, McMannis MJ. High-dose clinical urography with the low-osmolality contrast agent Hexabrix: comparison

with a conventional contrast agent. *Radiology* **1987**;162:9–14

21. Swanson DP, Thrall JH, Shetty PC. Evaluation of intravascular low-osmolality contrast agents. *Clin Pharm* **1986**;5:877–891
22. Kolbenstvedt A. Iohexol in lower extremity, renal and visceral angiography: survey and present state. *Acta Radiol Suppl* **1983**;366:153–156
23. Sacks BA, Ellison HP, Bartek S, Vine HS, Palstrant A. A comparison of Hexabrix and Renografin 60 in peripheral arteriography. *AJR* **1983**;140:975–977
24. Wolf GL. Safer, more expensive iodinated contrast agents: how do we decide? *Radiology* **1986**;159:557–558
25. Fischer HW. Cost vs safety: the use of low-osmolar contrast media. *JAMA* **1988**;260:1614
26. Gale ME, Robbins AH, Hamburger RJ, Widrich WC. Renal toxicity of contrast agents: iopamidol, iothalamate and diatrizoate. *AJR* **1984**;142:333-335
27. Talner LB. Does hydration prevent contrast material injury? *AJR* **1981**;136:1021–1022
28. Byrd L, Sherman RL. Radiocontrast-induced acute renal failure: a clinical and pathophysiological review. *Medicine* **1979**;58:270–279
29. Cochran ST, Wong WS, Roe DJ. Predicting angiography-induced acute renal function impairment: clinical risk model. *AJR* **1983**;141:1027–1033
30. Harkonen S, Kjellstrand CM. Exacerbation of diabetic renal failure following intravenous pyelography. *Am J Med* **1977**;63:939–946
31. Shafi T, Chou S, Porush JG, Shapiro WB. Infusion intravenous pyelography and renal function effects in patients with chronic renal insufficiency. *Arch Intern Med* **1978**;138:1218–1221
32. Van Zee BE, Hoy WE, Talley TE, Jaenike JR. Renal injury associated with intravenous pyelography in nondiabetic and diabetic patients. *Ann Intern Med* **1978**;89:51–54
33. Berkseth RO, Kjellstrand CM. Radiologic contrast-induced nephropathy. *Med Clin North Am* **1984**;68:351-370
34. Cramer BC, Parfrey PS, Hutchinson TA, et al. Renal function following infusion of radiologic contrast material: a prospective controlled study. *Arch Intern Med* **1985**;145:87-89
35. Martin-Paredero V, Dixon S, Baker D, et al. Risk of renal failure after major angiography. *Arch Surg* **1983**;118:1417–1420
36. Misson RT, Cutler RE. Radiocontrast-induced renal failure. *West J Med* **1985**;142:657-664

The reader's attention is directed to the commentary on this article, which appears on the following pages.

Commentary

The Evaluation of Contrast-Related Renal Failure

Michael A. Bettmann[1]

One of the most widely acknowledged adverse effects of administration of contrast agents is renal failure. Unlike life-threatening anaphylactoid reactions, which have multiple causes and target organs, contrast-induced renal failure on the face of it appears relatively straightforward. It is widely accepted that contrast administration may induce renal failure in patients without or worsen it in patients with preexistent azotemia. Many risk factors for renal failure have been proposed, and numerous clinical and experimental studies have addressed this topic, including two papers in this issue of the *AJR*. Despite this interest, however, many unanswered questions exist surrounding contrast-induced renal failure. These relate to four major areas: the definition and incidence of contrast-related renal failure, the role of risk factors or comorbid events, the cause of acute renal failure, and, finally, the design of studies intended to study this topic. There is currently much interest in all of these because of the debate concerning the use of high-vs low-osmolality contrast agents.

Clinical studies of contrast-related renal failure have shown wide variations in the prevalence of this process [1–8]. This in part relates to the various definitions used for what constitutes renal failure. It also relates to the difficulty of accurately establishing both a baseline and alterations in renal function. In theory, an optimal approach would involve serial measurements of creatinine clearance, beginning with a steady-state baseline level before contrast administration and reliable continual evaluations for at least 48 hr after the contrast agent has been given. In fact, this kind of approach is very difficult. Alternatively, sequential measurements of serum creatinine levels may reasonably reflect alterations in renal function, as long as a stable baseline level is established first, multiple values are obtained subsequent to the incident event, and changes are carefully interpreted. As has been noted [3], isolated measurements of serum creatinine levels may change substantially because of spontaneous or laboratory variation. Additionally, alterations in serum creatinine levels are thought to be logarithmically related to alterations in glomerular filtration rate [9]. That is, a rise in the serum creatinine level from 0.7 mg/dl (50 μmol/l) to 1.4 mg/dl (110 μmol/l) probably reflects a drop of 50% in the glomerular filtration rate, but would lead to little clinical concern. A rise from 1.5 mg/dl (110 μmol/l) to 3.0 mg/dl (220 μmol/l) would similarly indicate a halving of the glomerular filtration rate and would raise great concern. Both should be reconfirmed and considered carefully. If serum creatinine level is used as an indicator, the results are dependent, first, on laboratory reliability and reproducibility and, second, on when, how often, and at what intervals measurements are obtained. Alternative methods of measuring renal function have been suggested, including measurement of clearance of contrast media [10, 11]. These are attractive because of their simplicity and evident accuracy, but further clinical confirmation is necessary before they can be reliably used in clinical investigations.

In attempting to define the prevalence of contrast-related renal failure, then, it is not surprising that no single reliable number exists. This follows from the lack of a single reliable definition and method of investigation. Similarly, any answers arrived at will vary with the risk factors present. That is, there are many known causes of chronic and acute renal failure, including diabetes mellitus, long-standing hypertension, pronounced hypotension, and various medications. In many of the patients who are receiving contrast media, other possible causes of renal failure are also present. To isolate the effect of contrast agents, then, becomes a difficult logistic problem

---

This article is a commentary on the preceding articles by E. M. Lautin.

[1] Department of Radiology, Boston University School of Medicine, University Hospital, 88 E. Newton St., Boston, MA 02118. Address reprint requests to M. A. Bettmann.

AJR 157:66–68, July 1991 0361–803X/91/1571–0066 © American Roentgen Ray Society

and a complex statistical one. This may account for the fairly wide variation in the literature regarding the relative importance of specific risk factors [1-5, 11, 12]. For example, diabetes is frequently cited as a risk factor for contrast-related renal failure. Lautin et al. [1] conclude that diabetes is a risk factor but, on examination of their data, most categories and definitions do not statistically confirm this. Similarly, some studies suggest that dehydration, or more precisely, intravascular volume depletion, is a major risk factor [3]. Using a less rigorous definition, perhaps in part mandated by the retrospective nature of the study, Lautin et al. [1] did not find this to be true. Although the focus of studies in the radiology literature has been on contrast agents per se, conflicting results suggest that they may not be an independent risk factor [3-5]. The lack of definition of the importance of comorbid events with contrast administration suggests not only that no clear answer currently exists, but also that the role of risk factors is complex. The additive effect of any single factor may well be quite small [3]. This must be kept in mind in attempting to define, or even find, differences between high- and low-osmolality contrast agents.

Determining the cause of contrast-related renal failure presents additional problems. The major question that must be addressed is, is there a single cause? It is obvious that the kidney is a complex organ, and that it may fail because of pathologic processes in various areas. That is, there is no single type of renal failure [13]. Investigations have shown that contrast agents have various effects on the kidney. The hemodynamic effects are well delineated [14, 15]. They consist of an initial brief rise in renal blood flow followed by a prolonged fall with a gradual return to baseline. Histologically, an effect described as "osmotic nephrosis" also has been described [16], with vacuolization in the glomerular tubules. The pathologic importance of this finding is unclear. Additionally, proteinuria has been described after contrast administration in both humans and animal models and attempts have been made to assess contrast effects by analyzing for proteins from specific locations [17, 18]. To date, no single clear explanation for contrast-related renal failure has emerged, almost certainly because there is no single cause [13]. The effect of administering contrast agents is likely to be additive to underlying renal damage, whether the latter is clinically evident or not. Because of the relative inaccuracy of isolated measurements of serum creatinine level, due to laboratory variability, fluctuating baseline, and alterations with age, it is unlikely that definitive answers about nephrotoxic effects of contrast material in normal subjects can be found without accurate, continual measurements of either glomerular filtration rate or multiple parameters of renal function. The complex interaction between contrast agents, underlying renal damage at various sites and of varying severity, and the presence of other putative risk factors, such as congestive heart failure, intercurrent surgery, or aminoglycosides, helps to explain why it is difficult to elucidate the effects of contrast agents in any patients.

Added to this complex picture is the ongoing debate concerning the relative effects of high- vs low-osmolality contrast agents. Animal data unequivocally show that low-osmolality contrast agents have fewer effects on the kidney in an experimental setting than do high-osmolality contrast agents [17, 18]. Clinically, however, no substantial randomized trials have been able to show a difference [4, 5, 8, 12, 19]. It must be kept in mind that the studies published to date have not focused on high-risk patients, such as those with underlying renal failure. Conversely, it is also important to recognize that these studies have for the most part been sponsored by companies that, quite appropriately, have a vested interest in the outcome. The lack of a clear clinical difference between these two classes of agents raises several interesting possibilities. First, it is possible that the effect of contrast agents in causing renal failure is so dependent on other factors, including underlying renal function and specific site of renal disease, that the studies to date have simply not been sensitive enough to the various risk factors to show a clinical difference that is actually present. On the other hand, the results of experimental studies notwithstanding, a clinical difference between high- and low-osmolality contrast agents may not exist with regard to renal failure. Finally, a real difference *may* exist, as suggested by the experimental studies and by nonsignificant trends in the clinical studies. This may be so minor, however, that the clinical relevance or importance of this difference is minimal or nil. Given the effort that has been expended in trying to show a difference, and the lack of a demonstrable difference in effect to date, this latter explanation, if not increasingly likely, is at least increasingly possible.

The papers by Lautin et al. [1, 2] conclude that the risk of contrast-related renal failure is absolutely increased in patients with underlying renal dysfunction, that this risk is increased in diabetics, that these differences cannot be explained by age or hydration, and that a significant difference exists between high- and low-osmolality contrast agents, favoring the latter, both overall and in certain groups of patients undergoing arteriography. These conclusions disagree with those of several published studies [3-6], although they agree with others. As noted, these disparities can probably be explained in part by the complex nature of renal disease and the interaction of various risk factors or comorbid events. The disparities also, however, raise questions concerning the determinants and parameters of a well-designed, valid clinical investigation [20-22]. The classic investigation is a prospective randomized double blind trial, for reasons that are largely obvious. Such trials are designed to eliminate both observer and selection bias. Additionally, unknown factors that may affect the outcome can be assumed to be balanced equally between the groups, to the extent that any known biasing factors are considered in the study design. In designing a retrospective analysis, it is even more important, for the sake of accuracy and validity, to attempt to balance risk factors as closely as possible between the groups being compared. In the best case, this is accomplished by a case control analysis, in which precollected data are carefully analyzed to match patients with to patients without a specific event or process, for multiple risk factors. Again, this type of analysis requires laborious, time-consuming data collection and evaluation.

Additional types of clinical investigations can be undertaken, and to a large extent the usefulness and reliability of the results depend directly on the common sense used in the design of the trial and the analysis of the data. Perhaps one good example of this is the ISIS-II trial [23], which showed, as other studies have, that thrombolytic therapy decreased morbidity and mortality rates in acute myocardial infarctions. In examinations of patients with acute myocardial infarctions randomized to streptokinase, aspirin, both, or placebo, the mortality rate was reduced with all three treatments. In a subgroup analysis, designed to assess not only risk factors but also statistical validity, the investigators were able to demonstrate that patients with a birth sign of Gemini or Libra had an increased mortality rate when treated with aspirin than did patients born under other signs. This was taken to prove not a lack of benefits among those born under these two signs, but rather to indicate that statistical aberrations can occur even in very large studies. It is likely that had these investigators used different definitions, they could have proved to a statistically significant level that various other factors were either important or unimportant. This is brought to mind by the various definitions used throughout the literature for contrast-related renal failure, and particularly by the various definitions used in the articles by Lautin et al. [1, 2]. It may be valid to use various definitions, but only if they are used consistently throughout and only if they can be validated in a well-defined group. It is also important to remember that statistics are not generally considered a democratic discipline. The generally accepted definition of a statistically significant comparison is one that is likely to occur purely by chance five or fewer times out of 100. If this definition is not used, appropriate reasons must be given. It follows that a trend, that is, a difference that has a probability value of greater than .05, is accepted as a trend, not as supportive of a true difference. One of the difficulties with the Lautin et al. papers is that one definition is not used throughout. Rather, definitions that achieve statistical significance are used to draw a conclusion, and those that do not are either used to suggest a supportive trend or are ignored. For example, whereas diabetes per se is a statistically significant risk factor by two of five criteria, diabetes among nonazotemics and among azotemics are each significant by only one of five criteria, a different one for each.

Similarly, the authors conclude that age is not a risk factor, but examination of their data suggests that patients under 70 are at increased risk of an early increase in serum creatinine levels. Along the same lines, questions must be raised about the validity of using age as a binary variable, rather than a continuous one. The same holds true for the use of an arbitrary definition of azotemia as a serum creatinine level greater than 1.5 mg/dl (110 μmol/l). Regarding risk factors, the effect of intercurrent surgery and nephrotoxic medications must be carefully assessed, not assumed to be equivalent or unimportant.

The papers by Lautin et al. represent extensive and intelligent work. These comments are by no means intended to denigrate the work, but rather to highlight the complexity of the topic. Because of this complexity, as many factors as are feasible must be taken into account, and consistent quantitative methods must be used throughout. Some of the points raised may help to explain differences between the papers presented in this issue and other published studies [4, 5, 8, 13].

Contrast-related renal failure remains a perplexing and incompletely defined problem. Neither its incidence, cause, or prognosis is yet well understood. Risk factors clearly exist—the primary factor is probably underlying renal failure—but the importance of these risk factors almost certainly varies with the type and severity of underlying disease. It is likely that a small difference exists between high- and low-osmolality contrast media in regard to nephrotoxicity in clinical situations. It is unlikely, however, that this difference is marked or that it is important in all patients. To understand contrast-related renal failure better, carefully designed studies that use validated and accurate definitions, carefully matched patient groups, and carefully applied, consistent statistical techniques are necessary.

REFERENCES

1. Lautin EM, Freeman NJ, Schoenfeld AH, et al. Radiocontrast-associated renal dysfunction: incidence and risk factors. *AJR* **1991**;157:49–58
2. Lautin EM, Freeman NJ, Schoenfeld AH, et al. Radiocontrast-associated renal dysfunction: a comparison of lower-osmolality and conventional high-osmolality contrast media. *AJR* **1991**;157:59–65
3. Shusterman N, Strom BL, Murray TG, Morrison G, West SL, Maislin G. Risk factors and outcome of hospital acquired acute renal failure. *Am J Med* **1987**;83:65–71
4. Schwab SJ, Hlatky MA, Pieper KS, Davidson CJ, Morris KG, Shelton TN, Bashore TM. Contrast nephrotoxicity: a randomized controlled trial of a nonionic and an ionic radiographic contrast agent. *N Engl J Med* **1989**;320:149–153
5. Parfrey PS, Griffith SM, Barrett BJ, et al. Contrast material-induced renal failure in patients with diabetes mellitus, renal insufficiency or both. *N Engl J Med* **1989**;320:143–149
6. Older RA, Miller JP, Jackson DC, Johnsrude IS, Thompson WM. Angiographically induced renal failure and its radiographic detection. *AJR* **1976**;126:1039–1045
7. Eisenberg RL, Bank WO, Hedgcock MW. Renal failure after major angiography. *Am J Med* **1980**;68:43–46
8. Gomes AS, Lois JF, Baher JD, et al. Acute renal dysfunction in high-risk patients after angiography: comparison of ionic and nonionic contrast media. *Radiology* **1989**;170:65–68
9. Brezis M, Epstein FH. A closer look at radiocontrast-induced nephropathy. *N Engl J Med* **1989**;320:179–181
10. Boijsen M, Granerus G, Jacobsson L, Bjornfeld L, Aurell M, Tyler U. Glomerular filtration rate estimated after multiple injections of contrast medium during angiography. *Acta Radiol* **1988**;29:669–674
11. Efersoe H, Rosenkilde P, Groth S, Jensen LI, Golman K. Measurement of renal function with iohexol: a comparison of iohexol, ^{99m}Tc-DTPA and ^{51}Cr-EDTA clearance. *Invest Radiol* **1990**;25:778–782
12. Moore RD, Smith CR, Lipsky JJ, Mellits EP, Lietman PS. Risk factors for nephrotoxicity in patients with aminoglycosides. *Ann Intern Med* **1984**;100:352–357
13. Miller DL, Chang R, Wells WT, Dowjat BA, Malinosky RM, Doppmen JL. Intravascular contrast media: effect of dose on renal function. *Radiology* **1988**;167:607–611
14. Hietala SO, Almen T. Patient risk factors of importance in nephrotoxicity of contrast media. In: Enge I, Edgren J, eds, *Patient safety and adverse events in contrast media examinations*. Amsterdam: Excerpta Medica, **1989**:121–130
15. Forrest JB, Howards SS, Gillenwater JY. Osmotic effects of intravenous contrast agents on renal function. *J Urol* **1981**;125:147–150
16. Tornquist C, Almen T, Golman K, Holtas S. Renal function following nephroangiography with metrizoate and iohexol: effects on renal blood flow, glomerular permeability and filtration rate and diuresis in dogs. *Acta Radiol* **1985**;26:483–489
17. Moreau J-F, Droz D, Jungers P, Kleinknecht P, Hinglais N, Michel J-R. Osmotic nephrosis induced by water-soluble tri-iodinated contrast media in man. *Radiology* **1975**;115:329–336
18. Thomsen HS, Dorph S, Mygird T, et al. Intravenous injection of ioxilan, iohexol and diatrizoate: effects on urine profiles in the rat. *Acta Radiol* **1988**;29:131–136
19. Gale EM, Robbins AH, Hamburger RJ, Widrich WC. Renal toxicity of contrast agents: iopamidol, iothalamate, and diatrizoate. *AJR* **1984**;142:333–335
20. Fuchs VR, Garber AM. The new technology assessment. *N Engl J Med* **1990**;323:673–677
21. Laupacis A, Sackett DL, Roberts RS. An assessment of clinically useful measures of the consequences of treatment. *N Engl J Med* **1988**;318:1728–1733
22. Linton AL, Naylor CD. Organized medicine and the assessment of technology: lessons fron Ontario. *N Engl J Med* **1990**;323:1463–1467
23. ISIS-2 (Second international study of Infarct Survival) Collaborator Group. Randomized trial of intravenous streptokinase, oral aspirin, both, or neither among 17,187 cases of suspected acute myocardial infarction:ISIS-2. *Lancet* **1988**;350–359

Ureteral Pseudodiverticula:
Frequent Association with Uroepithelial Malignancy

Neil F. Wasserman[1]
Gang Zhang[2]
Irene P. Posalaky[3]
Pratap K. Reddy[2]

Ureteral pseudodiverticula are tiny outpouchings usually seen as incidental findings on retrograde urography during routine work-up for common urinary tract disorders. We report 37 patients with ureteral pseudodiverticula, of whom 17 (46%) had associated uroepithelial malignancy. Ureteral pseudodiverticula were diagnosed in all patients on excretory or retrograde urography as an incidental finding during evaluation for a variety of urologic symptoms and signs. All patients were assessed with urinalysis, urine culture, cystoscopy, and when indicated, ureteroscopy. Diagnosis of transitional cell carcinoma was made by surgery or endoscopic biopsy in 16 patients and squamous cell carcinoma in one. In nine patients with radiographs showing ureteral pseudodiverticula and a urinary tract filling defect (usually in the bladder), 78% of the cases were proved malignant. In six patients with ureteral pseudodiverticula and a stricture in the ureter or renal collecting system, 67% of the cases were proved malignant. Of the patients with tumor, 53% had a single ureteral pseudodiverticulum. In two cases, the pseudodiverticula antedated the diagnosis of malignancy by 2 and 4 years, respectively.

Our experience suggests that the association between ureteral pseudodiverticula and uroepithelial malignancy may be more common than previously assumed, approaching 50%. Even a single ureteral pseudodiverticulum should be regarded as a serious marker for potential malignancy, antedating cancer by 2–10 years, and such patients should be closely followed up. The coexistence of ureteral pseudodiverticula and a stricture or filling defect in the urinary tract is highly suggestive that a tumor is present.

***AJR* 157:69–72, July 1991**

Ureteral pseudodiverticula (UPD) are bilateral outpouchings of the ureter less than 5 mm in diameter often identified as incidental findings on retrograde urography and occasionally on excretory urography. Fewer than 80 cases have been reported in the literature since the initial description of four cases in 1957, in which an association with chronic urinary tract infection was postulated [1]. Microscopic evidence of chronic inflammatory changes in the ureter was later well documented [2–4]. UPD are neither pulsion diverticula, as they do not penetrate the muscular wall of the ureter, nor are they true diverticula containing all layers of the ureteral wall [3, 4]. An association between UPD and uroepithelial neoplasm has been suggested [3–5].

In this report, we review 37 new cases of UPD and emphasize that the association with uroepithelial malignancy is more common than it is thought to be and that a single ureteral diverticulum occurs more frequently and is of greater significance than previously suspected.

Materials and Methods

This study included 37 patients (mean age, 69 years; range, 39–91 years) who were found to have UPD on excretory or retrograde urography while being evaluated for hematuria (21 cases), urinary tract infections (six), flank pain (four), routine renal stone follow-up (two),

Received November 9, 1990; accepted after revision January 9, 1991.

[1] Department of Radiology (114), Department of Veterans Affairs Medical Center, One Veterans Dr., Minneapolis, MN 55417. Address reprint requests to N. F. Wasserman.

[2] Department of Urology, Department of Veterans Affairs Medical Center, One Veterans Dr., Minneapolis, MN 55417.

[3] Department of Pathology, Department of Veterans Affairs Medical Center, One Veterans Dr., Minneapolis, MN 55417.

0361-803X/91/1571-0069
© American Roentgen Ray Society

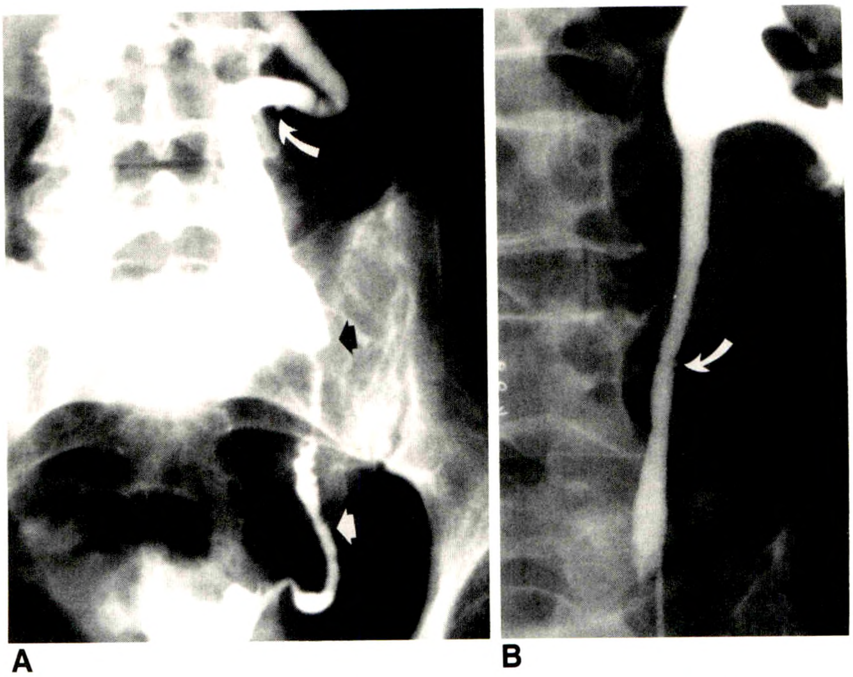

Fig. 1.—*A* and *B*, 73-year-old man with hematuria. Retrograde urograms obtained on same day show a single ureteral pseudodiverticulum (*curved arrows*) in association with squamous cell carcinoma of distal ureter (between *short arrows*). Transitional cell carcinoma of bladder developed later.

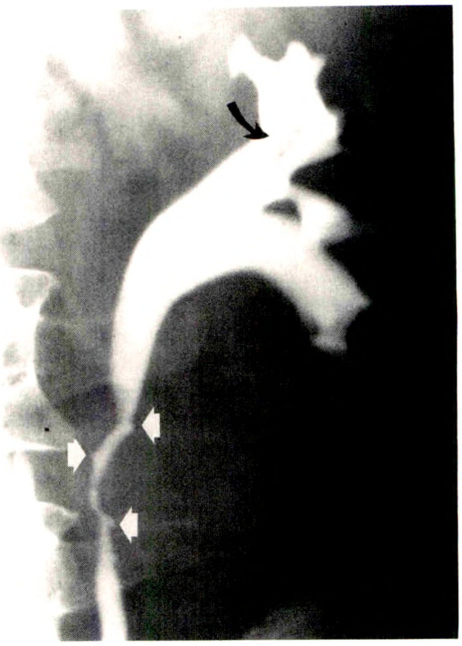

Fig. 2.—74-year-old man with hematuria. Retrograde urogram shows ureteral pseudodiverticula (*white arrows*) and associated filling defect in left upper calix (*black arrow*). Histologic examination of surgical specimen showed filling defect was transitional cell carcinoma.

azotemia (one), and follow-up for transitional carcinoma of the bladder (one), prostatic carcinoma (one), or benign prostatic hyperplasia (one). There were 36 men and one woman. Thirty-five were male veterans of American wars. Radiographs were analyzed by a radiologist for multiplicity and bilaterality of UPD and for stenotic foci and/or radiolucent filling defects in the renal collecting system, ureter, or bladder that were suggestive of malignancy. Urine cytology was done in all patients, along with routine urinalysis and culture. All patients had cystoscopic examination, and those with abnormalities in the renal collecting system or ureter had those areas examined endoscopically. Biopsy was performed when indicated. Diagnosis of malignancy was made on the basis of histologic examination of samples obtained either by endoscopic biopsy or surgery. Patients with malignancy in the renal collecting system underwent nephroureterectomy. Those with ureteral tumor had segmental resections, and patients with cancer of the bladder were either treated locally or by radical cystectomy and diversion.

Results

Twenty uroepithelial malignant tumors were seen in 17 (46%) of 37 consecutive patients with UPD. Nineteen were transitional cell carcinoma and one was squamous cell carcinoma. Thirteen tumors (65%) involved the bladder, five (25%) involved the calices or renal pelvis, and two were ureteral (10%). One of the ureteral tumors was squamous cell carcinoma (Fig. 1). Three patients (18%) had metachronous tumors. One had a bladder tumor followed by renal pelvic tumor, and two patients had ureteral tumors (one transitional cell and one squamous cell) followed by transitional tumor of the bladder and renal pelvis, respectively. Excretory urograms were not available in all patients with UPD, but the outpouchings were diagnosed in all cases with retrograde pyeloureterography. Wasserman et al. [6] previously reported detecting UPD in more than 50% of cases by using excretory urography.

One patient had synchronous carcinoma of the renal pelvis and bladder. One had carcinoma of the ureter followed 1 year later by carcinoma of the ipsilateral renal pelvis. Another had squamous cell carcinoma of the ureter followed 8 months later by transitional carcinoma of the bladder. An additional patient without uroepithelial malignancy was found to have renal cell carcinoma. UPD were synchronous with presentation of uroepithelial malignancy in 10 (59%) of 17 cases, but in four cases (23%) the temporal relationship was unknown. The UPD antedated by 2 and 3 years, respectively, the appearance of malignancy in two patients (12%). One patient continues to have positive cytologic findings in the absence of proved tumor or infection. Findings on urine cytology in the other 20 patients remain negative.

The association of UPD with a radiolucent filling defect in the urinary tract on urography (Figs. 2 and 3) was seen in nine subjects; the defect was proved to be tumor in seven (78%) of the nine. In patients with tumor, filling defects were equally divided between the renal collecting system (calices and pelves) and bladder. The urographic association of UPD with a stricture (Fig. 4) was seen in six patients and occurred in the presence of tumor in four (67%): in the ureter in one, the renal pelvis in one, and the bladder in two. The other tumors were bladder transitional carcinoma that was not identifiable on urography but was proved on cystoscopic biopsy. Of the 17 patients with uroepithelial malignancy, nine

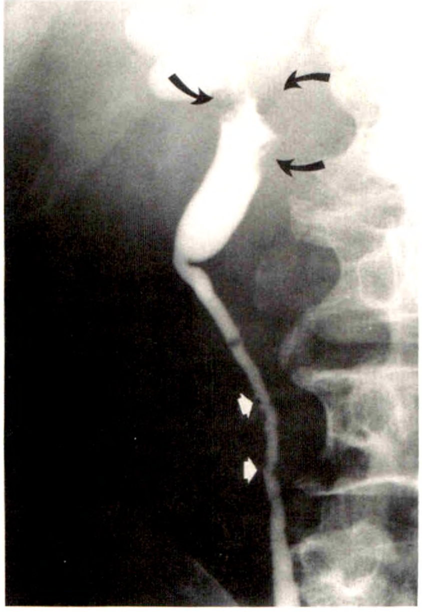

Fig. 3.—63-year-old man with hematuria. Retrograde urogram shows association of ureteral pseudodiverticula (*white arrows*) with multiple coarse irregular filling defects in right renal pelvis (*black arrows*) causing obstructive caliectasis. Histologic examination of surgical specimen showed filling defects were transitional cell carcinoma.

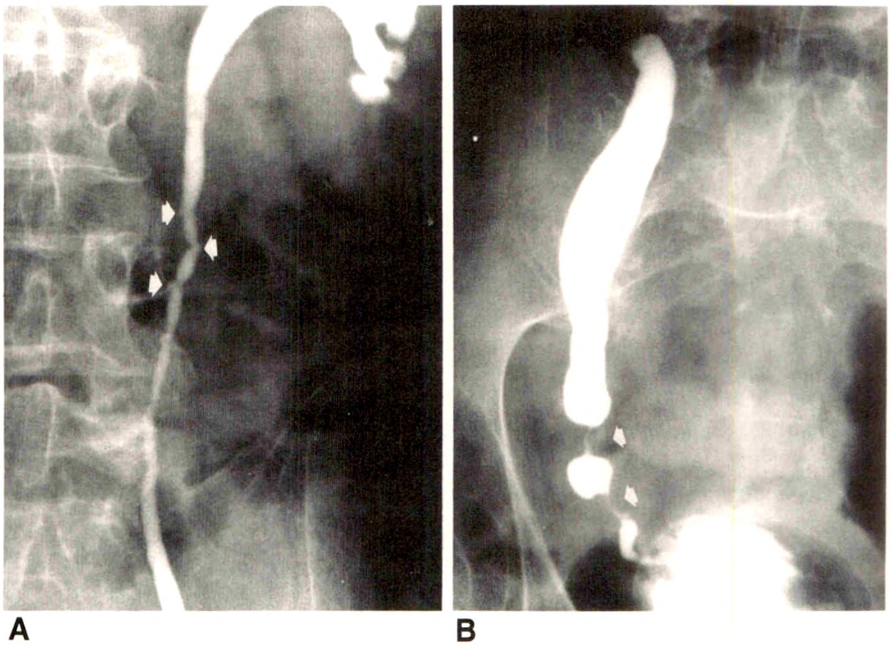

Fig. 4.—71-year-old man with chronic urinary tract infection.

A, Left retrograde urogram shows ureteral pseudodiverticula (*arrows*). Upper ureteral filling defects are air bubbles.

B, Right retrograde urogram shows ureteral strictures (*arrows*), which were found on histologic examination to be transitional cell carcinoma.

(53%) showed only a single unilateral ureteral pseudodiverticulum. However, the status of the contralateral ureter was unknown in two cases; thus, solitary unilateral ureteral pseudodiverticula may be associated with tumor in as few as 41%. In the 20 patients with ultimately proved benign disease in conjunction with UPD, an additional two patients with strictures and two with filling defects were seen.

The ureters were included in the surgical resections of tumors of the renal collecting system or ureter in seven patients. Histologic examination of surgical specimens did not usually include a careful search for UPD, but in the one case (Fig. 1) in which the ureter was carefully sectioned in the area of UPD, microscopic ureteritis glandularis and ureteritis cystica were noted without adjacent tumor.

Discussion

Multiple small diverticula of the ureters were first described in 1957 by Holly and Sumcad [1], who postulated that they were caused by chronic urinary tract infection. They were the first to apply the term *pseudodiverticula* to these lesions, although they had no direct pathologic evidence of such changes in the ureter. Cochran et al. [3] were the first to show the pathologic changes in ureters of five patients with these tiny diverticula, showing them to be outpouchings of proliferated hyperplastic transitional epithelium into the loose subepithelial connective tissue with associated chronic inflammatory changes. They noted that the diverticula neither protruded through the muscularis propria nor included all layers of the ureteral wall. Wasserman et al. [4] described the pathologic changes in a postmortem study of 200 ureters in subjects without history of urinary tract disorders and found an incidental occurrence rate of 11% for UPD. The findings were described as epithelial hyperplasia with proliferation into the subepithelial connective tissue forming epithelial crypts leading to outpouchings characteristic of UPD. In these cases, the UPD were invariably associated with microscopic ureteritis cystica and glandularis, but no ureteral evidence of uroepithelial malignancy, cellular atypia, or metaplasia was seen [4].

The relationship between chronic proliferative epithelial changes in the urinary tract and primary tumor is well established and has been reproduced experimentally [7]. The association of uroepithelial malignancy with UPD has been reported to be 26% in the largest series [6]. Cochran et al. [3] reported transitional cell carcinoma in seven of their 10 patients, but they cautioned that this may reflect a sampling bias. A recent small series demonstrated pathologic or clinical evidence of tumor in three of six patients [5]. The cumulative reported world experience has shown an approximate 25% association [6]. The occurrence of uroepithelial malignancy in 46% of patients with UPD in this series is much higher than the cumulative reported world experience has suggested. This may reflect our own sampling bias (male veterans), with a high degree of alcohol and tobacco abuse or exposure to some other unidentified toxin. Notwithstanding, until more data accumulate from other population samples, a strong suspicion for coexisting uroepithelial malignancy must be exercised when even a single unilateral UPD is identified.

This series adds two additional cases to the literature that show the development of tumor 2 and 3 years after the documentation of UPD. To our knowledge, only one similar case was previously reported, in which the latency period between identification of UPD and development of tumor was 10 years [8]. Messing et al. [9] also hypothesize that "there is a long pre-clinical phase of urological cancers." These cases are important because they support the theory that chronic proliferative epithelial changes in the urinary tract may sometimes be premalignant and that UPD represent a clinical marker for epithelium that is predisposed to malignant transformation.

With this in mind, it seems prudent to monitor carefully any patient with known UPD even in the absence of urinary tract malignancy on baseline examination. Periodic urinalysis alone for microscopic hematuria has been disappointing as a screening tool in normal populations because of the intermittency of bleeding from uroepithelial tumors [10]. However, repetitive home screening with a recently developed hematuria dipstick may prove more effective because of its sensitivity, convenience, and cost-effectiveness [9, 10]. We recommend semiannual urine cytology in addition to urinalysis even though the value of urine cytology in the follow-up of UPD has yet to be proved [6]. The results of this study combined with a previous series [6] suggest that more than 70% of the tumors will be found in the bladder. Accordingly, we recommend annual cystoscopy. Evaluation of the upper urinary tract and ureters may be reserved for patients with positive symptoms or signs suggesting malignancy.

Conclusions

The association of UPD with uroepithelial malignancy is higher than previously thought, perhaps approaching 50%. The presence of UPD in patients with radiolucent filling defects or urinary tract strictures indicates malignancy in up to 71%. UPD represent a clinical marker for the future development of uroepithelial carcinoma, antedating cancer by 2–10 years. Although the malignant lesion is usually transitional cell carcinoma in the bladder, the first case of UPD associated with squamous cell carcinoma is reported. No correlation was found between the number of UPD and the likelihood of associated malignancy. Thus, a single well-documented ureteral pseudodiverticulum must be taken as a serious sign of potential synchronous or metachronous malignancy.

REFERENCES

1. Holly LE, Sumcad B. Diverticular ureteral changes: a report of four cases. *AJR* **1957**;78:1053–1060
2. Lester PD, Kyaw MM. Ureteral diverticulosis. *Radiology* **1973**;106:77–80
3. Cochran ST, Waisman J, Barbaric ZL. Radiographic and microscopic findings in multiple ureteral diverticula. Radiology **1980**;137:631–636
4. Wasserman NF, Posalaky IP, Dykoski R. The pathology of ureteral pseudodiverticulosis. *Invest Radiol* **1988**;23:592–598
5. Parker MD, Rebsamen S, Clark RL. Multiple ureteral diverticula: a possible radiographically demonstrable risk factor in development of transitional cell carcinoma. *Urol Radiol* **1989**;11:45–48
6. Wasserman NF, LaPointe S, Posalaky IP. Ureteral pseudodiverticulosis. *Radiology* **1985**;155:561–566
7. Hicks RM, Chowaniec J. Experimental induction, histology and ultrastructure of hyperplasia and neoplasia of the urinary bladder epithelium. *Int Rev Exp Pathol* **1978**;18:199–280
8. Kenney PJ, Wasserman NF. Ureteral pseudodiverticulosis associated with carcinoma of the renal pelvis: report of a case. *Urol Radiol* **1987**;9:161–163
9. Messing EM, Young TB, Hunt VB, Emoto SE, Wehbie JM. The significance of asymptomatic microhematuria in men age 50 and older: findings of a homescreening study using urinary dipsticks. *J Urol* **1987**;137:919–922
10. Messing EM, Young TB, Hunt VB, Wehbie JM, Rust P. Urinary tract cancers found by homescreening with hematuria dipsticks in healthy men over 50 years of age. *Cancer* **1989**;64:2361–2367

Sonography of the Cervix During the Third Trimester of Pregnancy:

Value of the Transperineal Approach

Barbara S. Hertzberg[1]
James D. Bowie
Therese M. Weber
Barbara A. Carroll
Mark A. Kliewer
Sheryl G. Jordan

Transabdominal sonography reliably depicts the cervix during the first and second trimesters of pregnancy, but cervical visualization becomes increasingly difficult as the third trimester progresses. To evaluate the possibility of using a perineal approach to bypass the fetus and image the cervix during the third trimester, we used transperineal sonography to image the cervix of 158 third-trimester patients in whom transabdominal visualization was inadequate. The internal os and upper cervix were successfully visualized on transperineal sonograms in all 158 patients, but the region of the external os was obscured by rectal gas in 22 (14%) cases. In some patients in whom the external portion of the cervix was obscured by bowel gas, the problem could be overcome by scanning with the patient in the lateral decubitus position or by rotating the patient.

Transperineal sonography is an effective technique for imaging the cervix during the third trimester of pregnancy, allowing cervical visualization in most patients in whom transabdominal sonography of this area is unsuccessful.

***AJR* 157:73–76, July 1991**

Visualization of the maternal cervix is an important component of the obstetric sonographic examination, aiding in the detection and management of placenta previa, preterm labor, and cervical incompetence [1–9]. Transabdominal sonography reliably depicts the cervix in most patients during the first and second trimesters, but cervical visualization becomes increasingly difficult as the third trimester progresses, predominantly because of attenuation of sound by the presenting part of the fetus [10, 11]. A variety of techniques, including external fetal manipulation, overdistension of the maternal urinary bladder, and Trendelenburg positioning, have been used to elevate the presenting part of the fetus from the pelvis and facilitate visualization of the cervix [1, 10–12]. However, such maneuvers can be uncomfortable for the patient, distort the appearance of the cervix, and are frequently unsuccessful late in the third trimester [2, 10]. Given the problems inherent in evaluating the third-trimester cervix by transabdominal sonography, we undertook this study to evaluate the feasibility of using a transperineal approach for imaging the cervix.

Subjects and Methods

Between November 1989 and April 1990, we prospectively evaluated the use of transperineal sonography to visualize the cervix of 158 third-trimester patients in whom transabdominal attempts to image the cervix were unsuccessful. Transabdominal sonography was performed with a 3.5-MHz, electronically focused, phased-array sector transducer (Acuson 128, Mountain View, CA), with the patient's bladder empty. Graded pressure was applied to the maternal pelvis with the transducer in an attempt to elevate the presenting part of the fetus away from the cervix before transabdominal visualization of the cervix was considered unsuccessful.

After completion of the transabdominal portion of the examination, a protective covering (Hefty Baggie, Mobile Chemical Co., Pittsford, NY) was applied to the transducer head,

Received October 12, 1990; accepted after revision January 8, 1991.

[1] All authors: Department of Radiology, Box 3808, Duke University Medical Center, Durham, NC 27710. Address reprint requests to B S. Hertzberg.

0361–803X/91/1571-0073
© American Roentgen Ray Society

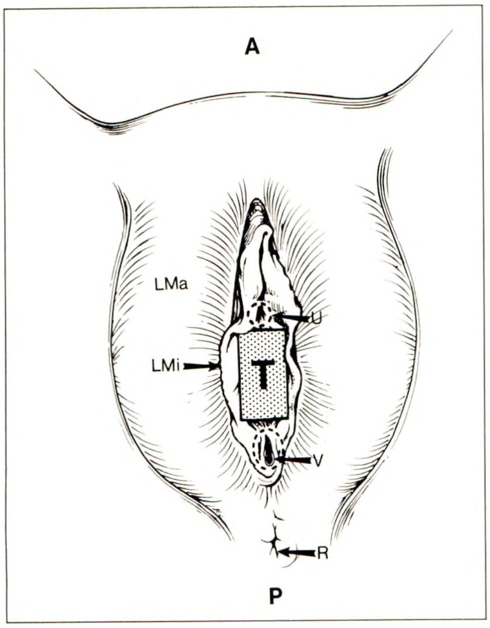

Fig. 1.—Schematic diagram of perineum shows location of transducer (T) during transperineal sonography. Transducer is applied directly over labia minora (LMi) in a sagittal plane just posterior to urethra (U). Transducer location and angle are adjusted under sonographic control to optimize visualization of cervix. A = anterior, LMa = labia majora, V = vaginal orifice, R = rectal orifice, P = posterior.

secured with a rubber band, and covered with sterile sonographic gel or KY Jelly (Johnson & Johnson, New Brunswick, NJ). Scans were performed by sonographers, sonologists, sonographic fellows, and senior radiology residents who received instruction on performing the technique and observed transperineal studies performed by others before attempting transperineal sonography. A female chaperone was present in the room during all transperineal scanning done by men. The technique and indications for transperineal scanning were explained to the patient, and examination was begun with the patient supine, with the thighs abducted sufficiently to allow placement and lateral angulation of the transducer. The transducer was positioned on the perineum in a sagittal orientation between the labia majora, usually applied directly over the labia minora, but occasionally placed between the labia minora (Fig. 1). The center of the transducer was located posterior to the urethra and anterior to the vagina. Under sonographic guidance, mild pressure was applied to the perineum with the transducer, and the location and angle of the transducer were altered slightly in order to optimize visualization of the cervix. In most cases the transperineal component of the study was completed in less than 5 min. Hard copy images of the cervix were obtained and reviewed to determine if cervical visualization was improved compared with the transabdominal study. Cervical visualization was considered improved when a significant portion of the cervix, not seen transabdominally, was identified transperineally. Additionally, a record was kept of whether the entire length of the cervix was imaged by transperineal sonography and of any problems encountered with cervical visualization.

After completing the initial series of 158 patients, we continued to incorporate transperineal views of the cervix in our routine obstetric sonographic study whenever transabdominal images were inadequate. In 11 patients scanned after the initial series, transperineal images were attempted with the patients in both the right and left lateral decubitus positions because transperineal scans obtained with the patient supine were suboptimal owing to shadowing of the external portion of the cervix by rectal gas. We kept a record of whether these additional positions improved transperineal visualization of the cervix.

Results

Compared with transabdominal sonography, the transperineal approach resulted in improved visualization of the cervix in all 158 patients scanned. On transperineal sonograms, the cervix contained a central echogenic stripe, which was frequently surrounded by a hypoechoic region in the expected position of the endocervical canal, similar to the pattern seen by transabdominal scanning (Fig. 2) [10]. The entire length of the cervix was seen in 136 (86%) of the 158 patients scanned transperineally. In the remaining 22 patients, the internal os and upper portion of the cervix were successfully visualized, but the external os and caudal portion of the cervix were not seen because of shadowing from gas in the adjacent rectum (Fig. 3).

Results in the 11 patients who underwent transperineal scanning in the right and left lateral decubitus positions because the external portion of the cervix was not visualized on transperineal sonograms obtained with them supine were

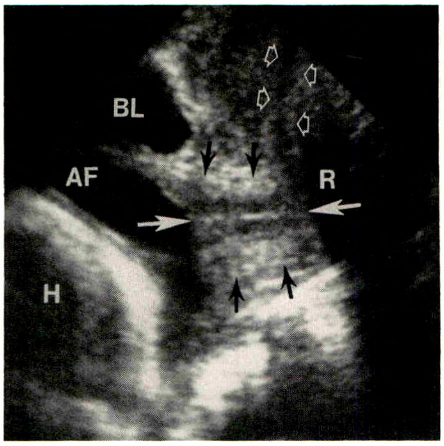

2

Fig. 2.—Transperineal sonogram of third-trimester cervix (*black arrows*) reveals endocervical canal (*solid white arrows*) in a horizontal plane, approximately perpendicular to ultrasound beam. Region of canal is depicted as a central echogenic stripe surrounded by a hypoechoic region, similar to pattern seen during transabdominal sonography. Vagina is oriented in a nearly vertical plane. BL = maternal urinary bladder, AF = amniotic fluid, R = rectal gas, H = fetal head, *open arrows* = vagina.

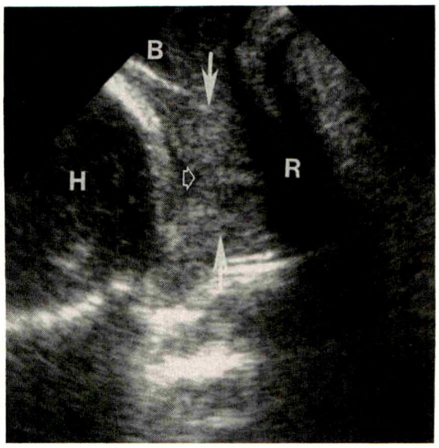

3

Fig. 3.—Internal os (*open arrow*) and upper portion of cervix (*solid arrows*) are visualized by transperineal sonography, but shadowing from rectal gas (R) obscures area of external os. B = maternal urinary bladder, H = fetal head.

Fig. 4.—*A*, Transperineal sonogram with patient supine fails to show external portion of cervix because of shadowing by rectal gas (R).

B, Transperineal sonogram of same patient in left lateral decubitus position successfully reveals entire cervix. Rotating patient into a decubitus position caused bowel gas to shift into a more favorable location, facilitating cervical visualization.

B = maternal urinary bladder, H = fetal head, *open arrow* = internal os, *curved arrow* = external os, *solid arrows* = cervix.

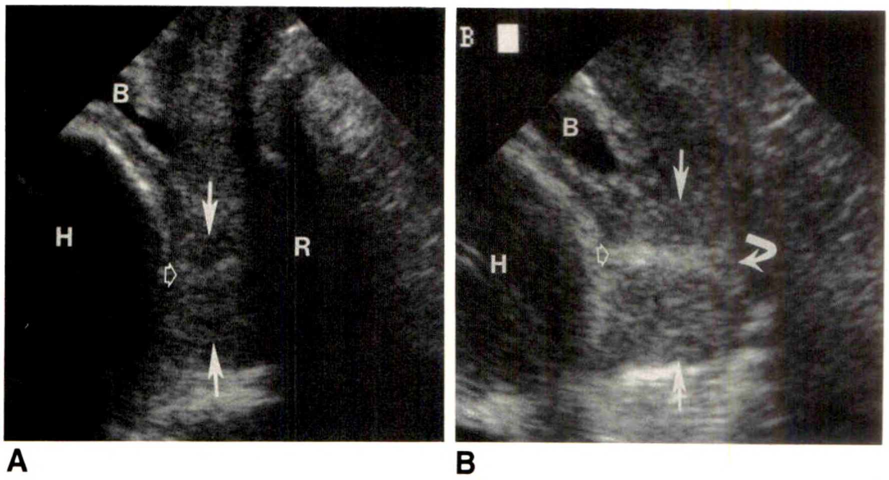

cervical visualization optimized by left lateral decubitus position in five patients, visualization optimized by right lateral decubitus position in two patients, and no improvement with decubitus views in three patients (Fig. 4A and 4B). In one additional case, the external portion of the cervix could not be seen during the initial attempt with the patient supine, and there was no improvement with right and left lateral decubitus views, but the entire cervix was successfully imaged after the patient was rotated back from the right lateral decubitus position to supine.

One other problem encountered during initial scans of three of the patients imaged early in the study involved mistaking the urethra for the cervix and the urinary bladder for amniotic fluid. In all three cases, this difficulty was overcome by increasing the field of view, and with the increasing transperineal imaging experience gained as the study progressed, this interpretative error did not recur.

All patients tolerated the transperineal scanning procedure well, without significant physical discomfort, and the procedure was uniformly accepted by our population of patients. We are not aware of any complications attributed to use of the transperineal technique. To date, formal follow-up documenting the absence of complications up to the time of delivery is available on 116 patients who delivered at our institution.

Discussion

The importance of attempting to visualize the cervix during obstetric sonography is well established [1–12]. Sonographic depiction of the cervix is of particular value in the diagnosis and management of placenta previa, preterm labor, and cervical incompetence, as well as in examining patients with ruptured membranes in whom repeated digital examinations may be undesirable because of the risk of infection. In the case of placenta previa, direct visualization of the cervix is necessary to establish the relationship between the lower edge of the placenta and the internal cervical os [1, 2, 10–12]. Similarly, sonographic changes may be the first indicators of impending cervical failure in patients with preterm labor or cervical incompetence, because early changes occur at the level of the internal os, which is inaccessible by routine vaginal examination [4–6, 8].

Our study reveals that use of transperineal sonography dramatically increases the chances of cervical visualization during the third trimester. After instruction was given regarding the anatomic orientations displayed during transperineal sonography, the technique was readily learned by radiologists and technicians with various levels of sonographic expertise and added a minimum of time to the sonographic examination. The internal os and upper cervix were successfully shown by transperineal sonography in all 158 patients in whom transabdominal visualization was inadequate. Although the region of the external os was not imaged in 22 (14%) patients because of shadowing from adjacent rectal gas, we expect that in many patients visualization of the internal os and upper cervix will be sufficient to evaluate for placenta previa or cervical shortening. However, for those patients in whom demonstration of the entire length of the cervix is desirable because cervical shortening is suspected after initial views, scanning with the patient in the decubitus position or supine after being rotated can be used in an attempt to shift gas away from the external portion of the cervix.

Because of the different transducer positions used during transabdominal and transperineal sonography, the cervix is displayed in different orientations with the two techniques. With transabdominal sonography, the long axis of the cervix is oriented in an approximately vertical plane, whereas with transperineal sonography, the vagina is depicted in a vertical plane with the cervix horizontal, its long axis approximately perpendicular to the ultrasound beam (Figs. 5A and 5B) [10].

Endovaginal sonography offers an alternative approach for visualizing the cervix and lower uterine segment when transabdominal views are inadequate [13–15]. The use of endovaginal sonography has been shown to improve the chances of cervical visualization, but this technique is not always successful in imaging the cervix and has the disadvantages of requiring a specialized transducer and vaginal penetration, neither of which are necessary to perform the transperineal technique.

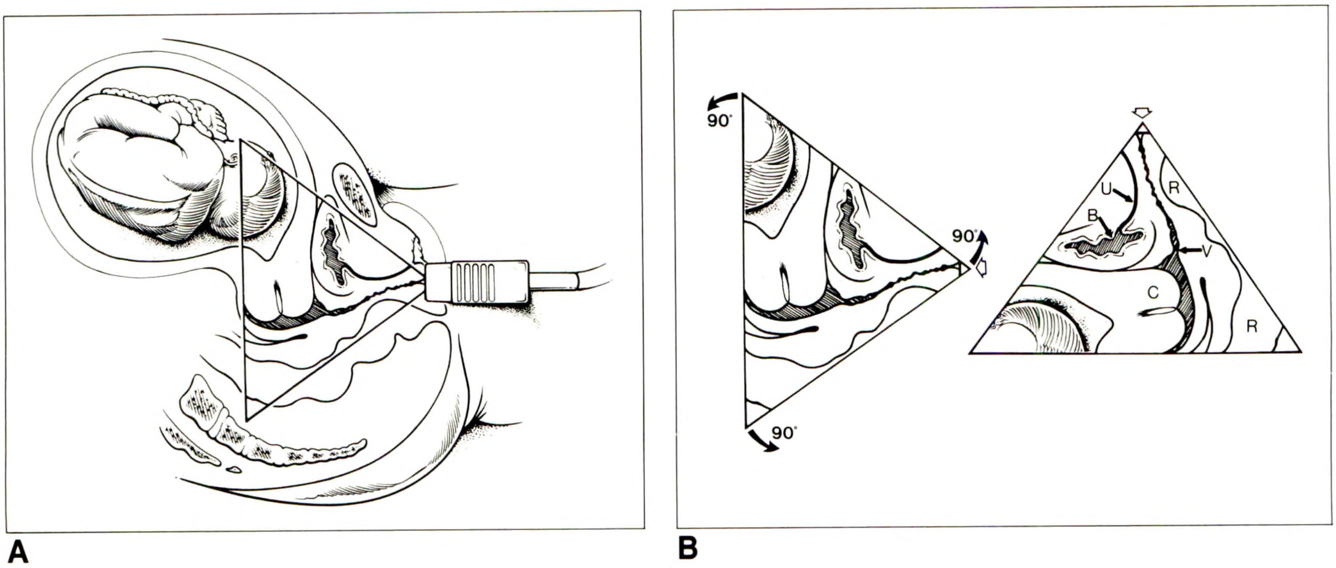

Fig. 5.—*A*, Sagittal illustration of gravid uterus in a supine patient with transducer positioned on perineum reveals typical scanning plane obtained during transperineal sonography.

***B*, Before display, scanning plane depicted in *A* is rotated 90° counterclockwise. As a result, portion of image closest to transducer (*open arrow*) is displayed at top of image in traditional fashion. Long axis of cervix is displayed in an approximately horizontal orientation with vagina oriented in a vertical plane. U = urethra, R = rectum, B = bladder, V = vagina, C = cervix.**

Variations on the transperineal sonographic technique described here (use of stand-off pads, linear transducers, etc.) have been used to assess female stress urinary incontinence, vaginal atresia, and umbilical cord presentation and to image the gravid cervix, but to date the potential of using transperineal sonography in the pregnant patient has not received widespread recognition [16–22]. The current study demonstrates that transperineal sonography is a safe, simple to perform, effective method of imaging the cervix in the third trimester of pregnancy, and we now routinely incorporate transperineal views of the cervix in our obstetric sonographic studies when transabdominal visualization is inadequate. Further investigations are under way to assess the accuracy of transperineal sonography in specific clinical situations, such as the evaluation for placenta previa and cervical incompetence.

REFERENCES

1. Townsend RR, Laing FC, Nyberg DA, Jeffrey RB, Wing VW. Technical factors responsible for "placental migration": sonographic assessment. *Radiology* **1986**;160:105–108
2. Artis AA, Bowie JD, Rosenberg ER, Rauch RF. The fallacy of placental migration: effect of sonographic techniques. *AJR* **1985**;144:79–81
3. Main DM, Hadley CB. The role of ultrasound in the management of preterm labor. *Clin Obstet Gynecol* **1988**;31:53–60
4. Michaels WH, Montgomery C, Karo J, Temple J, Arger J, Olson J. Ultrasound differentiation of the competent from the incompetent cervix: prevention of preterm delivery. *Am J Obstet Gynecol* **1986**;154:537–546
5. Ayers JWT, DeGrood RM, Compton AA, Barclay M, Ansbacher R. Sonographic evaluation of cervical length in pregnancy: diagnosis and management of preterm cervical effacement in patients at risk for premature delivery. *Obstet Gynecol* **1988**;71:939–944
6. Podobnik M, Bulic M, Smiljanic N, Bistricki J. Ultrasonography in the detection of cervical incompetency. *J Clin Ultrasound* **1988**;13:383–391
7. Ludmir J. Sonographic detection of cervical incompetence. *Clin Obstet Gynecol* **1988**;31:101–109
8. Bartolucci L, Hill WC, Katz M, Gill PJ, Kitzmiller JL. Ultrasonography in preterm labor. *Am J Obstet Gynecol* **1984**;149:52–56
9. Brook I, Feingold M, Schwartz A, Zakut H. Ultrasonography in the diagnosis of cervical incompetence in pregnancy: a new diagnostic approach. *Br J Obstet Gynaecol* **1981**;88:640–643
10. Bowie JD, Andreotti RF, Rosenberg ER. Sonographic appearance of the uterine cervix in pregnancy: the vertical cervix. *AJR* **1983**;140:737–740
11. Jeffrey RB, Laing FC. Sonography of the low-lying placenta: value of Trendelenburg and traction scans. *AJR* **1981**;137:547–549
12. Lee TG, Knochel JQ, Melendez MG, Henderson SC. Fetal elevation: a new technique for placental localization in the diagnosis of previa. *J Clin Ultrasound* **1981**;9:467–471
13. Brown JE, Thieme GA, Shah DM, Fleischer AC, Boehm FH. Transabdominal and transvaginal endosonography: evaluation of the cervix and lower uterine segment in pregnancy. Am J Obstet Gynecol **1986**;155:721–726
14. Farine D, Fox HE, Jakobson S, Trimor-Tritsch IE. Is it really a placenta previa? *Europ J Obstet Gynecol Reprod Biol* **1989**;31:103–108
15. Farine D, Fox HE, Trimor-Tritsch. Vaginal ultrasound for ruling out placenta previa (case report). *Br J Obstet Gynaecol* **1989**;96:117–119
16. Kohorn EI, Scioscia AL, Jeanty P, Hobbins JC. Ultrasound cystourethrography by perineal scanning for the assessment of female stress urinary incontinence. *Obstet Gynecol* **1986**;68:269–272
17. Kolbl H, Bernaschek G, Wolf G. A comparative study of perineal ultrasound scanning and urethrocystography in patients with genuine stress incontinence. *Arch Gynecol Obstet* **1988**;244:39–45
18. Scanlan KA, Pozniak MA, Fagerholm M, Shapiro S. Value of transperineal sonography in the assessment of vaginal atresia. *AJR* **1990**;154:545–548
19. Graham D, Nelson MW. Combined perineal-abdominal sonography in the evaluation of vaginal atresia. *J Clin Ultrasound* **1986**;14:735–738
20. Sakamoto H, Takagi K, Masaoka N, et al. Clinical application of the perineal scan: prepartum screening for cord presentation. Am J Obstet Gynecol **1986**;155:1041–1043
21. Mahony BS, Nyberg DA, Luthy DA, Hirsch JH, Hickok DE, Petty CN. Translabial ultrasound of the third trimester uterine cervix: correlation with digital examination. *J Ultrasound Med* **1990**;9:717–723
22. Jeanty P, d'Alton M, Romero R, Hobbins JC. Perineal scanning. *Am J Perinatol* **1986**;3:289–295

Organic vs Functional Obstruction of the Fallopian Tubes:
Differentiation with Prostaglandin Antagonist- and β_2-Agonist-Mediated Hysterosalpingography and Selective Ostial Salpingography

Erich K. Lang[1]

In order to determine the prevalence and cause of functional vs organic obstruction of the fallopian tubes, hysterosalpingography was repeated after pharmacologic manipulation with a prostaglandin antagonist (aspirin) and/or a β_2-agonist (terbutaline) in 100 patients in whom the fallopian tubes did not fill with contrast medium on the initial hysterosalpingogram. Selective ostial salpingography was performed in those in whom the fallopian tubes did not fill on the second hysterosalpingogram. Patients referred from three infertility clinics were included in the study if they could be rescheduled for a second hysterosalpingogram after at least 1 week of preparation with aspirin. Hysterosalpingograms obtained after administration of aspirin showed normal filling in 21 of 100 patients with initially obstructed tubes; the tubes filled in four more patients after administration of terbutaline. Selective ostial salpingography opacified the tubes in another 36 patients in whom the tubes had so far failed to fill. On the basis of the radiographic appearance and sometimes laparoscopic observation, initial nonfilling was attributed to spasm and debris in 49 patients, submucosal fibroids in six, synechiae in three, salpingitis isthmica nodosa in two, and septated uterus in one.

Hysterosalpingography, after pharmacologic manipulation with aspirin and/or selective ostial salpingography, revealed false-positive and functional tube obstructions in 61 of 100 patients. Moreover, the radiologic appearance improved categorization of organic obstructions.

***AJR* 157:77–80, July 1991**

Tubal occlusion (organic obstruction) is a common cause of female infertility that, depending on its location and underlying cause, calls for vastly different surgical procedures. In cases of functional obstruction of the fallopian tubes, surgical intervention is not necessary and contraindicated. The difference between organic obstruction (occlusion) and functional obstruction was emphasized as early as 1954 [1]. However, nonfilling of the tubes during conventional hysterosalpingography has proved to be an unreliable criterion for differentiating these conditions. DeCherney [2] and Sulak et al. [3] found amorphous material in the lumen to be the cause of obstruction in the proximal tubes in as many as half of the patients in whom tubes did not opacify on hysterosalpingograms. Spasm was another cause of nonfilling. In order to plan effective therapy, organic and functional obstruction must be distinguished preoperatively. Moreover, contemplated surgical correction mandates categorization of the disease afflicting both the proximal and distal tubes. Although laparoscopy provides some information, opacification of diseased segments of both proximal and distal tubes with contrast medium will greatly enhance understanding of underlying disease.

Subjects and Methods

The study group comprised 100 women 23–42 years old who were evaluated for infertility at three different infertility clinics. In all patients, the fallopian tubes had failed to fill with

Received November 1, 1990; accepted after revision January 23, 1991.

[1] Department of Radiology, Charity Hospital of Louisiana at New Orleans, and Louisiana State University Medical Center, 1542 Tulane Ave., New Orleans, LA 70112-2822. Address reprint requests to E. K. Lang.

0361–803X/91/1571–0077
© American Roentgen Ray Society

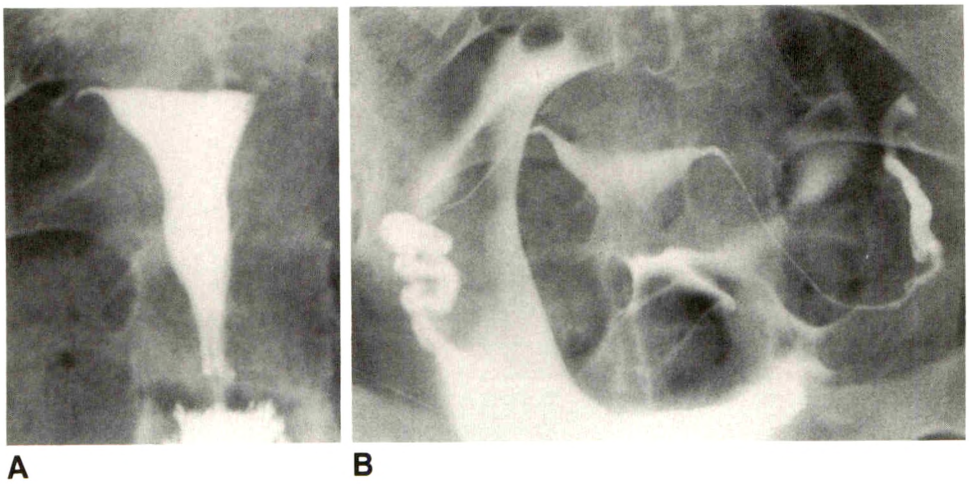

Fig. 1.—Ability of aspirin, a prostaglandin antagonist, to relieve spasm of interstitial segment of tubes. This 36-year-old woman was referred for hysterosalpingography to evaluate longstanding infertility.

***A*, Hysterosalpingogram shows satisfactory filling of uterine cavity, including uterine cornua, but fails to show opacification of either tube.**

***B*, After administration of aspirin, 325 mg orally for 6 days, hysterosalpingogram shows filling of both fallopian tubes and spillage into peritoneal cavity.**

contrast medium on hysterosalpingography. Each had an endocrine profile assaying estradiol, follicle-stimulating hormone, luteinizing hormone, prolactin, and dehydroepiandrosterone levels. The initial hysterosalpingogram, showing obstruction of the tubes, was obtained during the follicular phase of the menstrual cycle.

A second hysterosalpingogram was obtained after oral administration of 325 mg of aspirin per day for at least 1 week and a prophylactic antibiotic, doxycycline hyclate (Warner Chilcott Laboratories, Morris Plains, NJ), 100 mg twice daily for 2 days. The latter was given in anticipation of selective ostial salpingography being performed immediately after the second hysterosalpingogram in patients with persistent nonfilling of the fallopian tubes. If selective salpingography was performed, the antibiotic was continued for another 3 days.

In 20 patients in whom the fallopian tubes did not opacify on the second hysterosalpingogram, terbutaline (0.25 mg) was administered intramuscularly, and in another five of these patients, glucagon was given IV, and a third hysterosalpingogram was obtained at the same sitting.

Routine hysterosalpingograms were obtained with a balloon catheter. The balloon was placed at the cephalic end of the endocervical canal and inflated to block leakage from the cervical canal into the vagina. Conray-60 (Mallinckrodt, St. Louis, MO), in variable amounts of 6–15 ml, was then infused. The phases of filling were recorded on both spot and 105-mm films.

Customarily, patients were premedicated with 25 mg of meperidine (Winthrop, New York, NY) intramuscularly. Those patients who reported discomfort received an additional 25 μg of fentanyl (Elkins-Sinn, Cherry Hill, NJ) IV.

For selective ostial salpingography, a 9-French Teflon sheath (Cook Urological, Spencer, IN) was introduced into the lower uterine segment. A tenaculum was attached to the cervix for control and, if necessary, to rotate the uterus slightly. Thereafter, a curved 5.5-French torque-control polyethylene catheter and J guidewire (0.035-in. [0.89 mm]; Cook, Inc., Bloomington, IN) were advanced under fluoroscopic control into the uterine cornu. Seating of the 5.5-French catheter was further improved by advancing a 0.014-in. (0.36-mm) soft-nosed platinum-tipped guidewire (Target Therapeutics, Santa Monica, CA) 1 cm into the interstitial segment of the tube and then wedging the 5.5-French catheter into position. Once the 5.5-French catheter was seated, a selective salpingogram was obtained by injecting 1.5–2 ml of Conray-60 contrast medium. Radiographs were obtained at this time to demonstrate both the proximal and distal segments of the tubes and spillage into the peritoneal cavity.

Results

Of 100 women with obstruction of both fallopian tubes on the initial hysterosalpingogram, one or both tubes proved to be patent in 21 patients on the hysterosalpingogram obtained after premedication with aspirin for at least 1 week (Fig. 1). A third hysterosalpingogram was obtained in 20 women after administration of terbutaline (0.25 mg intramuscularly), and in four of these one or both tubes filled. In another five women, IV glucagon was given and a third hysterosalpingogram was obtained; none of these had evidence of tube filling. These 25 patients had been randomly selected from the group of 79 patients in whom the fallopian tubes had not filled with contrast medium on the second hysterosalpingogram.

Selective ostial salpingograms were obtained in the 75 patients whose tubes thus far had failed to opacify. Unilateral (four) or bilateral (32) filling of the tubes was achieved in 36 of these 75 patients (Fig. 2). In 39 patients, the tubes could not be opacified on selective ostial salpingograms.

In 14 of the 61 patients in whom the tubes were ultimately opacified, distal disease was demonstrated. On the basis of the radiographic appearance, cause for initial nonfilling of the tubes was attributed to submucosal fibroids in six, uterine synechiae in three, an unrecognized septation of the uterus in one, and salpingitis isthmica nodosa in two. The precise cause could not be established on the basis of radiographic or other criteria in the remaining 49 patients, but spasm or debris was considered likely (Fig. 3).

Sixteen patients became pregnant in a follow-up period of 6–18 months. Twelve pregnancies occurred in the 61 patients who were ultimately proved to have patent tubes. The four others occurred in patients in whom a proximal obstruction had been successfully corrected by transcervical bougie dilatation. In addition, laser-assisted fimbriolysis and fimbrioplasty for adhesions were performed in one of these patients,

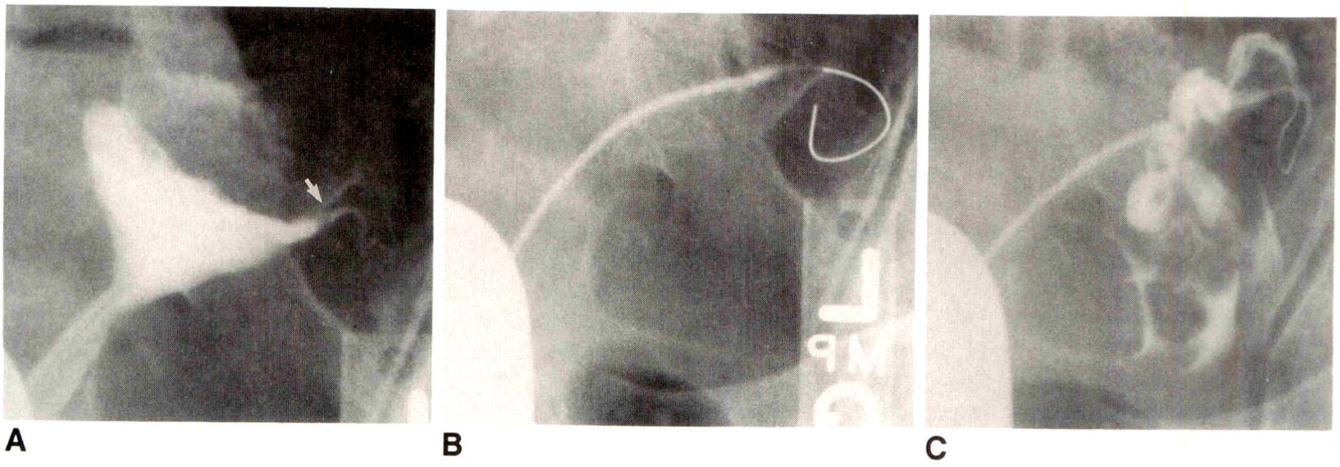

Fig. 2.—Value of ostial salpingography in showing normal tubes despite persistent nonfilling caused by spasm or blockage by refluxed debris. This 37-year-old woman was referred for hysterosalpingography to evaluate long-standing infertility.

A, Hysterosalpingogram obtained after administration of a prostaglandin antagonist shows that tubes still fail to opacify. The 90° angle formed between interstitial and isthmic segments (*arrow*) is indicative of spasm.

B, 0.015-in. Target guidewire with flexible platinum tip has been advanced from a precurved 5.5-French catheter through interstitial and isthmic segments of left fallopian tube.

C, Subsequent ostial salpingogram shows filling of left tube. Initial nonfilling may have been caused by spasm or blockage by refluxed desquamated debris from uterine cavity.

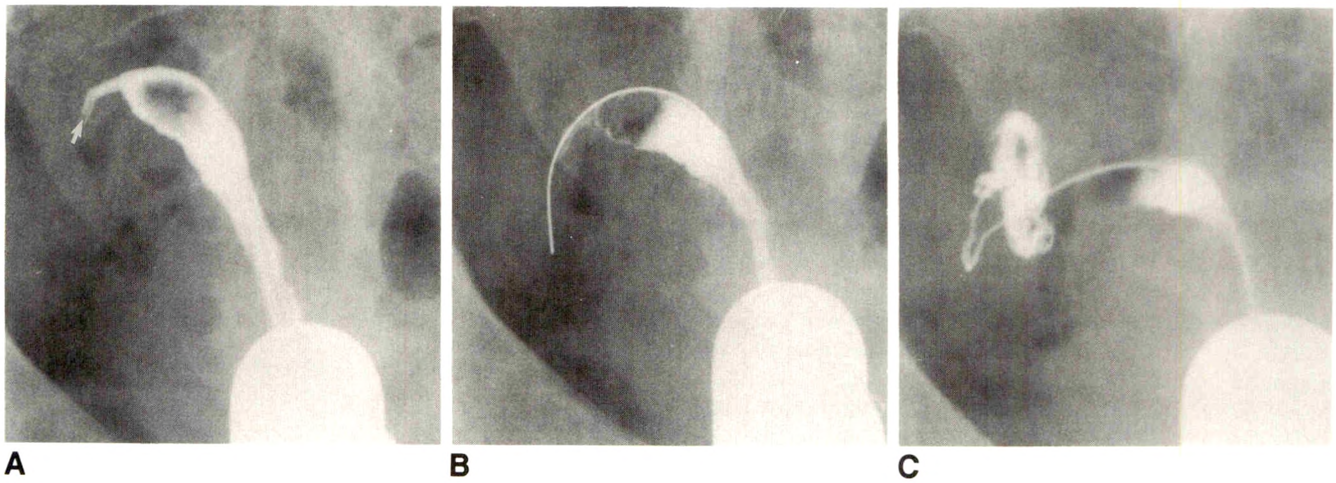

Fig. 3.—Value of selective salpingography in revealing tubal occlusion by debris. This 29-year-old woman with known unicornuate uterus was referred for selective ostial salpingography to assess tubal patency.

A, Ostial salpingogram shows a mantle of contrast medium in interstitial segment of tube. Central filling defect is probably due to inspissated debris (*arrow*).

B, 0.015-in. Target guidewire has been advanced from unicornuate uterus through interstitial segment into isthmic segment of tube.

C, Subsequent selective salpingogram through tapered 2-French catheter introduced into isthmic segment of tube shows a normal and patent tube.

and a hydrosalpinx was diagnosed only after recanalization of the proximal tube.

Discussion

Nonfilling of the tubes can result from either functional or organic obstruction [1]. Obstruction implies a time-limited (functional) process, occlusion implies a permanent (organic) one [1]. Obstruction can occur attendant to inspissated amorphous material in the proximal segment of the tubes or spasm of, particularly, the interstitial segment. DeCherney [2] suggested that nonfilling may be attributable to tubal obstruction in one half of patients and to tubal occlusion in the other half [2]. Amorphous material was identified as the cause for such obstruction in two of six patients on histologic examination of resected segments of fallopian tubes [3].

Tubal function is controlled by three intrinsic systems: the estrogen-progesterone system, the adrenergic-noradrenergic system, and prostaglandins [4].

Estrogen stimulates and progesterone inhibits oviductal muscular activity [5]. Adrenergic nerves are involved in isthmic motility changes; estrogen potentiates activation of the α-adrenergic receptors and progesterone that of β-adrenergic receptors. Stimulation of α-adrenergic receptors reduces transisthmic flow, whereas β-adrenergic receptors stimulate and increase transisthmic flow. β_2-agonists such as terbutaline cause isthmic relaxation and increase transisthmic flow [5].

Although the contractile response to prostaglandin varies depending on the stage of the menstrual cycle and hormone levels, prostaglandins E_1 and E_2 clearly inhibit and prostaglandin $F_{2\alpha}$ stimulates fallopian tube contractions [6–9].

The uterotubal junction shows predominant β-innervation of the innermost longitudinal and abutting circular muscle layers, whereas α-adrenergic receptors predominate in the outer longitudinal (spiral) layer [10]. Receptor stimulation during the phase of estrogen dominance of the outer layers of the uterotubal junction can thus cause spasm (Fig. 2A). In addition to oviductal contractility, prostaglandins E_1 and E_2 also tend to stimulate ciliary activity.

Anatomically, the oviduct can be divided into four distinct parts, interstitial (100-μm diameter), isthmic (500-μm diameter), ampullary (1 cm), and infundibular (larger than 1 cm). The isthmic segment features a thick muscular wall and dense adrenergic innervation, making it a physiologic sphincter [4]. Ciliated cells increase dramatically from the interstitial to the infundibular segments [4].

Nonfilling of the fallopian tubes on an initial hysterosalpingogram can be caused by functional or organic obstruction (occlusion). Functional obstruction in turn can be caused by muscular spasm of the interstitial segment, the uterotubal junction, or isthmic segment; by amorphous debris in the tubes; or, most likely, by a combination thereof. The sine curve of the interstitial segment of the tube further encourages a fluid lock at the uterotubal junction (Fig. 3A).

Prostaglandin antagonists and particularly β_2-agonists (terbutaline) cause isthmic relaxation and relax existing spasm. Straightening of the angle formed by the interstitial and isthmic segments of the fallopian tubes, as observed in some of our patients, supports this supposition (Fig. 2A). Moreover, in some instances, performing the second hysterosalpingogram in the progesterone-dominated phase of the menstrual cycle, when relaxation of the uterotubal junction segment is physiologically occurring, may further facilitate tubal filling. With increased relaxation of the outer longitudinal muscle layers and resultant straightening of the sine curve formed by the interstitial and isthmic segments, the mechanical flush effect of the hysterosalpingogram or the even greater flush effect of the selective ostial salpingogram may then clear the tube of debris and demonstrate an entirely normal and patent tube [2, 3, 11]. These factors explain the initial nonfilling of the tubes on hysterosalpingography and the subsequent demonstration of normal tubes in 21% of patients after administration of aspirin, a prostaglandin antagonist, and in perhaps another 20% of patients after administration of a β_2-agonist (terbutaline), and an additional 36% by selective salpingography (Figs. 2B and 2C).

In about 10% of the patients, uterine causes, such as submucosal fibroids, synechiae, intramucosal endometriosis, or even misdiagnosis of a bicornuate uterus may be responsible for the initial nonfilling. Synechiae and submucosal fibroids as well as intramucosal endometriosis can cause mechanical or ball-valve obstruction at the ostium. Rarely (2% of patients), salpingitis isthmica nodosa may cause stenosis that fosters obstruction by amorphous material flushed from the uterus during the desquamation phase into the tubes.

Selective ostial salpingography before and after transcervical recanalization of the proximal tubes by bougie or, rarely, balloon dilatation has improved demonstration and categorization of obstructive disease of the tubes (Fig. 3B). Not only can obstructive disease of the proximal tube be categorized and classified, but after recanalization, assessment of the status of the distal tube is possible (Fig. 3C). Because obstruction of the distal tube is a definitive indication for surgical intervention, fimbrioplasty, or laser-assisted fimbriolysis, this added diagnostic information should improve the ability to restore tubal function [12, 13]. Likewise, improved visualization and categorization of disease of the proximal tubes should identify those lesions that mandate such microsurgical interventions as tubocornual or ampullary-isthmic anastomosis for extensive perisalpingitis [13–16].

Although this study offers no information as to the prevalence of tubal patency when a second hysterosalpingogram is obtained without the benefit of a prostaglandin antagonist or after the use of a placebo, the patency rate should not exceed that of tubes in the pharmacologically manipulated group, unless the study is performed during the progesterone phase and thus benefits from increased transisthmic flow.

The routine use of aspirin before hysterosalpingography and in cases of nonfilling, selective ostial salpingography at the same sitting, might be considered for resolving the problem in one session, optimizing diagnostic yield, and reducing radiation dose. The risk attendant to drug therapy with aspirin is considered inconsequential. The minor risk of infection introduced during ostial selective salpingography could be minimized by administration of IV antibiotics at the time of the procedure.

REFERENCES

1. Rubin IC. Uterotubal insufflation: value in the treatment of tubal obstruction to ovular migration. *Fertil Steril* **1954**;5:311–324
2. DeCherney AH. Anything you can do I can do better—or differently. *Fertil Steril* **1987**;48:374–376
3. Sulak PJ, Letterie G, Coddington C, Hayslip C, Woodward J, Klein TA. Histology of proximal tubal obstruction. *Fertil Steril* **1987**;48::437–440
4. Hershlag A, Diamond MP, DeCherney AH. Tubal physiology: an appraisal. *Gynecol Surg* **1989**;5:3–25
5. Lindblom B, Hamburger L, Ljung B. Contractile patterns of isolated oviductal smooth muscle under different hormonal conditions. *Fertil Steril* **1980**;33:283–287
6. Strom CH, Dahlstrom A, Lindblom B, Ahlman H. Effects of intraluminal administration of adrenoceptor agonists on transisthmic flow in the rabbit oviduct. *Biol Reprod* **1983**;29:295–300
7. Sandberg FA, Ingelman-Sundberg A, Ryden G. The effect of prostaglandin E_1 on the human uterus and the fallopian tubes in vitro. *Acta Obstet Gynecol Scand* **1963**;42:269–278
8. Spilman GH, Harper MJK. Comparison of the effects of adrenergic drugs and prostaglandins on rabbit oviduct motility. *Biol Reprod* **1974**;10: 549–654
9. Elder MG, Myatt L, Chandhun G. The role of prostaglandins in the spontaneous motility of the fallopian tube. *Fertil Steril* **1977**;28:86–90
10. Wilhelmsson L, Lindblom B. Adrenergic responses of the various smooth muscle layers at the human uterotubal junction. *Fertil Steril* **1980**;33: 280–282
11. Sweeny WJ. The interstitial portion of the uterine tube: its gross anatomy, course and length. *Obstet Gynecol* **1962**;19:3–8
12. Sulak PJ, Letterie J, Hayslip C, Coddington CC, Klein TA. Hysteroscopic cannulation and lavage in the treatment of proximal tubal occlusion. *Fertil Steril* **1987**;48:493–494
13. Bateman DG, Nunley WC Jr, Kitchin JD III. Surgical management of distal tubal obstruction—are we making progress? *Fertil Steril* **1987**;48: 523–542
14. McComb P. The determinants of successful surgery for proximal tubal disease. *Fertil Steril* **1986**;46:1002–1004
15. Creasy JL, Clark RL, Cuttino JT, Groff TR. Salpingitis isthmica nodosa: radiologic and clinical correlates. *Radiology* **1985**;154:597–600
16. Lang EK, Dunaway HE Jr, Roniger WE. Selective ostial salpingography and transvaginal catheter dilatation in the diagnosis and treatment of fallopian tube obstruction. *AJR* **1990**;154:735–740

MR Examination of the Knee:

Interpretation with Multiscreen Digital Workstation vs Hardcopy Format

Jeffrey J. Brown[1]
Steven C. Malchow
William G. Totty
Anthony J. Wilson
Joseph K. T. Lee
Michael W. Vannier
R. Gilbert Jost

A multiscreen imaging workstation was compared with conventional hardcopy format for diagnostic interpretation of MR images of the knee. MR examinations from 30 patients were interpreted by two observers using film displayed both on a standard film panel alternator and an eight-screen digital workstation. Arthroscopic examination of these patients disclosed 30 meniscal tears and five anterior cruciate ligament tears in 28 patients. Two patients had normal arthroscopic examinations. The MR examinations were evaluated with a five-point confidence rating scale. Results were correlated with arthroscopic findings, and receiver-operating-characteristic curves were generated from these data. No significant difference was found between the areas under the receiver-operating-characteristic curves for film and digital display. The time required for image interpretation was greater when using the digital workstation than when using the film by a factor of approximately 2.7.

Our data indicate that a multiscreen digital workstation can be used for interpreting MR examinations of the knee without impairment of diagnostic performance, but with increased time required for image interpretation when compared with radiographic film and a film panel alternator.

***AJR* 157:81–85, July 1991**

The use of a picture archiving and communication system (PACS) for display of MR images has several inherent advantages over conventional radiographic film. These include the capability for on-line monitoring of current cases, more efficient image storage via connection to an electronic archive, and manipulation of various image parameters such as window and level settings. The implementation of PACS is also expected to reduce costs associated with the use of film [1]. However, the effects on diagnostic performance of replacing film with a digital workstation have not been determined.

The effective interpretation of MR examinations requires that multiple cross-sectional images be displayed simultaneously, allowing the viewer to make spatial associations and scan rapidly through the image set [2, 3]. Therefore, an eight-screen imaging workstation was developed with the video display arranged in a similar configuration to a standard film panel alternator (Siemens PACS Diagnostic Reporting Console DRC/80, Siemens Gammasonics, Inc., Hoffman Estates, IL). We hypothesized that the quality of interpretation of MR examinations of the knee viewed on the multiscreen PACS would be comparable with the interpretation quality when using film. This study was undertaken to test this hypothesis.

Materials and Methods

Patients and Arthroscopy

The study population consisted of 30 patients who had undergone both MR imaging and arthroscopic examination of the knee. This group included eight women and 22 men ranging from 17 to 72 years old (mean, 38 years).

Received November 20, 1990; accepted after revision January 9, 1991.

[1] All authors: Mallinckrodt Institute of Radiology, Washington University School of Medicine, 510 S. Kingshighway Blvd., St. Louis, MO 63110. Address reprint requests to J. J. Brown.

0361-803X/91/1571-0081

© American Roentgen Ray Society

Arthroscopy was performed by four different orthopedic surgeons. Thirty knees were examined arthroscopically (one per patient). Two of the knees were normal; the remaining knees had evidence of tears involving one or both menisci and/or the anterior cruciate ligament. A total of 60 menisci (two per patient) were evaluated, including medial and lateral menisci, of which 30 were normal and 30 abnormal. Thirty anterior cruciate ligaments were evaluated, of which 25 were normal and five were abnormal.

MR Imaging Technique

Imaging was performed with a 1.5-T superconducting magnet (Magnetom; Siemens Medical Systems, Iselin, NJ). The knees were imaged in a dedicated knee coil with a 20-cm aperture. The imaging protocol included a coronal T1-weighted spin echo (SE) pulse sequence with a repetition time (TR) of 600 msec and an echo delay time (TE) of 17 msec (SE 600/17), and a double-echo sagittal sequence with SE 2500/25, 90. Contiguous slices 5-mm thick were acquired with one data acquisition in all imaging planes. The coronal images were acquired with a 128 × 512 matrix and displayed at 128 × 256; sagittal images were acquired at 256 × 512 with a display matrix of 256 × 256. The field of view was 16 cm, yielding an in-plane resolution of 1.250 mm × 0.625 mm for coronal images and 0.625 mm × 0.625 mm for sagittal images. All patients were examined supine with the knee in approximately 10–15° of external rotation to aid visualization of the anterior cruciate ligament in the sagittal plane [4].

Equipment

For the film interpretation sessions, T1-weighted (SE 600/17) coronal and T2-weighted (SE 2500/90) sagittal images were printed on 14 × 17 in. (36 × 43 cm) film with a 15-on-1 format. The proton-density-weighted (SE 2500/25) sagittal images were enlarged by using a six-on-one format with 14 × 17 in. film. Windowing for the T1- and T2-weighted images was chosen to allow visualization of bone marrow, cartilage, muscle, and subcutaneous fat. Higher contrast settings were chosen for the proton-density-weighted images for optimal visualization of the menisci and articular cartilage. The studies were printed on Kodak Ektascan SO-497 Laser film (Rochester, NY) by using a 4096 × 5120 matrix laser film printer (Kodak Ektascan Laser Printer, Model 100). The films were arranged on a 50-panel alternator. Two panels were viewed simultaneously, allowing a maximum of eight films to be displayed. All of the images for each MR examination fit on the two film panels, thereby allowing simultaneous visual access to the entire examination without the need to change the film-panel position.

The PACS consisted of eight 1024 × 1280 pixel monitors with a Microvax II host computer (Digital Equipment Corporation, Maynard, MA) and two parallel transfer disks, each with 474 megabytes of storage space. The observers interacted with the workstation via a keyboard and a mouse (track-ball controller). The mouse was used for image manipulation functions, including reordering of images, image magnification, and manipulation of window and level settings. The video monitors used in the PACS viewing console were 19-in. (48 cm) diagonal, high-performance white phosphor monochrome monitors. The CRTs were mounted with the longer dimension oriented vertically ("portrait" mode) with a 90° angle of deflection. The supported video rate was 60 Hz interlaced (120-Hz fields). Screen luminance was 30 foot Lamberts at screen center. The host computer was a DEC 630 QE dual chassis Microvax II equipped with 9 megabytes of RAM, two Fujitsu M2344K 690 megabyte Winchester disk drives (Fujitsu America, San Jose, CA), and a TK50 cartridge tape drive. The image disk system (IDS) was a high-speed image storage system capable of transferring image data at sustained rates of up to 8 megabytes/sec. The system consisted of a Storage Concepts Concept 21 parallel transfer disk (PTD) processor (Siemens Gammasonics, Inc.) and two 474-megabyte Fujitsu M2350A PTD drives.

All MR examinations were preloaded onto the parallel transfer disk subsystem linked to the workstation. Cases were selected from a displayed list by using the interactive mouse and menu screen prompts. The examinations were initially displayed on the video monitors with 16 images per monitor. The reviewers then selected key images for magnification during the image interpretation sessions. The image magnification function doubled the image dimensions, resulting in a fourfold increase in image area.

Study Design

The MR examinations were reviewed by two radiologists with substantial experience in musculoskeletal MR imaging. Interpretation of MR findings was limited to three anatomic structures for which arthroscopic correlation was readily available: the medial and lateral menisci and the anterior cruciate ligament. The order of the MR studies was randomized on the basis of a computer-generated random number list. The 50 MR examinations were then divided into two equal groups. During the first set of image interpretation sessions, each observer evaluated 25 MR examinations on the digital display and the remaining 25 examinations on film. After each group of cases was interpreted by both observers, the MR examinations were reinterpreted by each observer by using the opposite format. Therefore, all of the examinations were interpreted twice by each observer, once on film and once on digital display. Each session consisted of one observer interpreting five or 10 cases using one format. The next group of five or 10 cases was then reviewed by the same person using the other format so that image interpretation sessions alternated between film and PACS for each observer. For each case, 4–6 weeks elapsed between the initial interpretation with one format and the subsequent interpretation with the opposite format to minimize the likelihood of observer recognition of a specific case or finding.

Clinical history, arthroscopic results, and all patients' identification information were withheld during image interpretation sessions. The observers were informed that normal cases were intermixed with abnormal cases but were unaware of the percentage of normal cases. MR studies were reviewed by using a five-point confidence rating scale to facilitate receiver-operating-characteristic (ROC) analysis. The observers were asked to rate the likelihood of the presence of tears of the menisci and anterior cruciate ligament. The responses were categorized as follows: 1 = definitely normal, 2 = probably normal, 3 = possibly abnormal, 4 = probably abnormal, and 5 = definitely abnormal. Examples of MR images of the medial meniscus from categories 1 and 5 of the confidence rating scale are shown in Figure 1.

The image interpretation sessions were recorded with a color video camera (Newvicon Omnipro, Panasonic Consumer Electronics Division, Secaucus, NJ) to allow calculation of the time elapsed during the interpretation of each case.

After completion of the image interpretation sessions, the findings on MR examinations were compared with arthroscopic findings, which served as the gold standard.

Statistical Methods

ROC curves were generated by correlating the presence of meniscal and anterior cruciate ligament tears with the observers' confi-

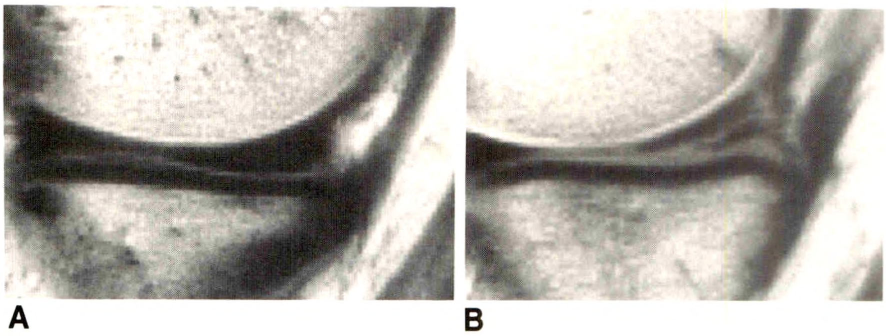

Fig. 1.—Sagittal proton density-weighted (SE 2500/25) MR images of medial menisci from two categories in confidence rating scale.

A, Category 1 (definitely normal): MR image shows smoothly tapering anterior and posterior horns of medial meniscus without evidence of abnormal intrameniscal signal. Arthroscopy showed no evidence of a meniscal tear.

B, Category 5 (definitely abnormal): MR image shows a linear area of increased signal intensity that extends to the inferior articular surface of posterior horn of medial meniscus. Arthroscopy revealed a tear in posterior horn of medial meniscus.

dence ratings. The curves were fit to the confidence levels by means of maximum likelihood estimation [5, 6]. Diagnostic performance was evaluated by calculating A_z, which represents the area under a binormal ROC curve when it is plotted in the unit square [7, 8]. The statistical significance of apparent differences between ROC curves was determined by applying a "two-tailed" univariate z-score test [9] to the reader-specific A_z values.

The two-sample Wilcoxon test for equality of ranks was used to compare distributions of the elapsed time for image interpretation [10].

Results

The ROC curves comparing film and PACS are shown in Figure 2. The areas under the ROC curves were slightly greater for PACS (0.907 ± 0.027 SD, reviewer 1; 0.932 ± 0.027 SD, reviewer 2) than for film (0.893 ± 0.027 SD, reviewer 1; 0.880 ± 0.034 SD, reviewer 2) for both reviewers. The difference between PACS and film A_z values for observer 1 was not significant ($p = .47$). For observer 2, the difference approached but did not achieve statistical significance ($p = .08$).

There was a marked difference in the amount of time required for interpretation of MR images when comparing film and digital formats. Both observers required significantly more time for image analysis with PACS (3.0 ± 1.1 min SD, reviewer 1; 4.7 ± 1.5 min SD, reviewer 2) than with film (1.1 ± 0.5 min SD, reviewer 1; 1.7 ± 0.6 min SD, reviewer 2) ($p < .001$). The average time per case was greater on PACS than on film by a factor of approximately 2.7.

Discussion

We have addressed the effects on diagnostic performance of using a multiscreen digital workstation vs film for detecting meniscal and anterior cruciate ligament tears on MR examinations of the knee. Analysis of the data revealed no signifi-

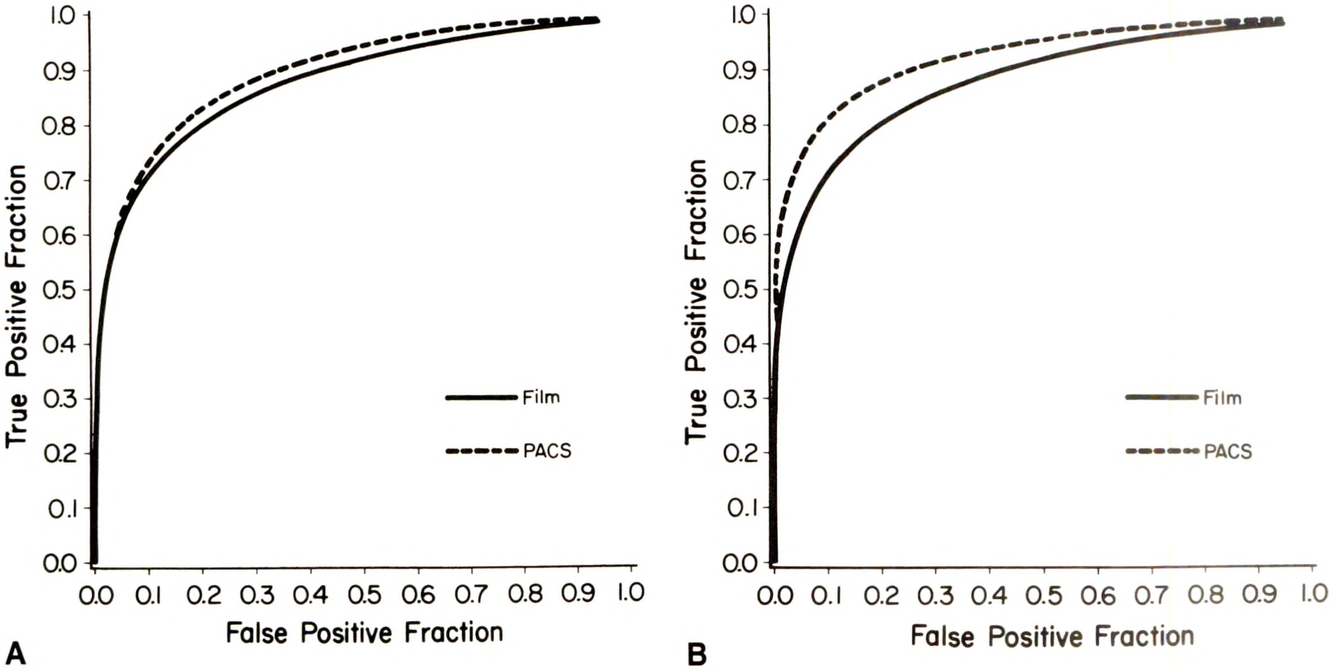

Fig. 2.—*A*, Receiver-operating-characteristic (ROC) curves for diagnosis of meniscal and anterior cruciate ligament tears, film vs picture archiving and communication system (PACS), for observer 1. Areas under curves are not significantly different ($p = .47$).

B, ROC curves, observer 2. Areas under curves are not significantly different ($p = .08$).

cant difference ($p > .05$) between the areas under the individual ROC curves for each observer. However, a dramatic increase was seen in the time required for image interpretation with the digital workstation.

The increase in image interpretation time with PACS is attributable to several factors. Both observers had limited experience with the digital workstation before this study; their experience with film was far greater and this presumably contributed to their faster interpretations with the conventional format. The imaging workstation also offered several functions that most likely contributed significantly to the prolonged image interpretation time, including image magnification, image reordering, and interactive windowing. The observers frequently selected key images from different locations on the digital display and moved them to one of the lower middle monitors for review. This would be done, for example, to evaluate the menisci on sagittal and coronal images, or the anterior cruciate ligament on T1- and T2-weighted images. In addition, the digital images invariably required some adjustment of window and level settings, whereas the images on film had been photographed at optimal settings by the MR technologist. A more recent version of the software for the digital workstation allows window and level settings to be preset at optimal settings for different pulse sequences and examinations. It is hoped that this will significantly shorten the image interpretation time in the future. The diagnostic performance of PACS vs hardcopy format will have to be reassessed once this and other changes are implemented because the present results are valid only under the conditions described above.

Observer-performance testing with ROC analysis is an accepted format for evaluating the efficacy of digital display methods [11-15]. However, several important caveats should be considered when applying data derived from carefully controlled observer-performance tests to routine radiologic practice. Each observer in the present study was aware that his performance was being carefully evaluated and compared with that of the other observer. In addition, the viewing conditions (e.g., ambient light, freedom from interruptions) were controlled to a greater extent than in routine clinical practice. These factors may have had an influence on diagnostic performance, although the extent of this influence is difficult to ascertain. At any rate, the effect on image interpretation is presumably similar with film and PACS.

Although most of the clinical PACS research to date has focused on chest radiographs [11-20] and other projectional radiographic examinations [21-25], MR imaging may be a more logical starting place for PACS implementation. MR images are acquired in digital format and can be transferred to digital workstations without alteration, whereas the conversion of standard radiographs (i.e., analog images) to digital format entails a potential for loss of information and degradation of image quality. In addition, the spatial resolution requirements for MR images are significantly less stringent than for most projectional studies, a factor of major importance with regard to design costs, transmission-speed requirements, and data archiving [26].

In this study, the use of a multiscreen digital workstation resulted in lengthening the time of interpretation of MR examinations without a significant improvement in observer performance. These results do not support the replacement of film with PACS for interpreting MR examinations. However, the results should be considered in the context of the greater scope of the potential impact of PACS implementation. PACS has many inherent advantages in the areas of archiving, display, and transmission of images and information. For these reasons, it has been widely predicted that digital workstations will eventually replace most radiographic film [1]. In order for this to occur, it must be shown that diagnostic performance will not be impaired by the conversion from film to PACS. The present results suggest that, from the standpoint of diagnostic accuracy, the multiscreen PACS may serve as a practical alternative to radiographic film displayed on a conventional film panel alternator for the detection of meniscal and anterior cruciate ligament tears on MR examinations of the knee. The implications of these findings concerning the general application of PACS to MR imaging are promising but require further testing in the clinical arena.

ACKNOWLEDGMENTS

We thank Bradley Wilson for statistical analysis, Roberta Yoffie for videotape analysis, Charles Hildebolt and Gary Roesel for critical review, and Sheila Doerhoff for preparation of the manuscript.

REFERENCES

1. Arenson RL, Chakraborty DP, Seshadri SB, Kundel HL. The digital imaging workstation. *Radiology* **1990**;176:303-315
2. Rogers DC, Johnston RE, Brenton B, Staab EV, Thompson B, Perry JR. Predicting PACS console requirements from radiologists' reading habits. *SPIE PACS III* **1985**;536:88-96
3. Kasaday LR. Human factor considerations in PACS design. *SPIE Med XIV PACS IV* **1986**;626:581-592
4. Reicher MA, Rauschning W, Gold RH, Bassett LW, Lufkin RB, Glen W Jr. High-resolution magnetic resonance imaging of the knee joint: normal anatomy. *AJR* **1985**;145:895-902
5. Metz CE. ROC methodology in radiologic imaging. *Invest Radiol* **1986**;21:720-733
6. Dorfman DD, Alf E. Maximum likelihood estimation of parameters of signal detection theory and determination of confidence intervals: rating method data. *J Math Psych* **1969**;6:487-496
7. Swets JA. ROC analysis applied to the evaluation of medical imaging techniques. *Invest Radiol* **1979**;14:109-121
8. Hanley JA, McNeil BJ. The meaning and use of the area under a receiver operating characteristic (ROC) curve. *Radiology* **1982**;143:29-36
9. Metz CE, Wang P, Kronman HB. A new approach for testing the significance of differences between ROC curves measured from correlated data. In: DeConinck F, ed. *Information processing in medical imaging.* The Hague: Martinus Nijhoff, **1984**:432-445
10. Marascuilo LA, McSweeney M. *Non-parametric and distribution-free methods for the social sciences.* Monterey, CA: Brooks/Cole, **1977**
11. MacMahon H, Vyborny CJ, Metz CE, Doi K, Sabett V, Solomon S. Digital radiography of subtle pulmonary abnormalities: an ROC study of the effect of pixel size on observer performance. *Radiology* **1986**;158:21-26
12. Chakraborty DP, Breatnach ES, Yester MV, Soto B, Barnes GT, Fraser R. Digital and conventional chest imaging: a modified ROC study of observer performance using simulated nodules. *Radiology* **1986**;158:35-39
13. Lams PM, Cocklin ML. Spatial resolution requirements for digital chest

radiographs: an ROC study of observer performance in selected cases. *Radiology* **1986**;158:11-19

14. Goodman LR, Foley WD, Wilson CR, Rimm AA, Lawson TL. Digital and conventional chest images: observer performance with film digital radiography system. *Radiology* **1986**;158:27-33
15. Hayrapetian A, Aberle DR, Huang HK, et al. Comparison of 2048-line digital display formats and conventional radiographs: an ROC study. *AJR* **1989**;152:1113-1118
16. Foley WD, Wilson CR, Keyes GS, et al. The effect of varying spatial resolution on the detectability of diffuse pulmonary nodules. *Radiology* **1981**;141:25-31
17. Huebener K-H. Scanned projection radiography of the chest versus standard film radiography: a comparison of 250 cases. *Radiology* **1983**;148:363-368
18. Niklason LT, Hickey NM, Chakraborty DP, et al. Simulated pulmonary nodules: detection with dual energy digital versus conventional radiography. *Radiology* **1986**;160:589-593
19. Barnes GT, Sabbagh EA, Chakraborty DP, et al. A comparison of dual-energy digital radiography and screen-film imaging in the detection of subtle interstitial pulmonary disease. *Invest Radiol* **1989**;24:585-591
20. Ishigaki T, Sakuran S, Ikeda M, Itoh Y, Suzuki M, Shunsuke I. Clinical evaluation of irreversible image compression: analysis of chest imaging with computed radiography. *Radiology* **1990**;175:739-743
21. Chan H, Vyborny CJ, MacMahon H, Metz CE, Doi K, Sickles EA. Digital mammography ROC studies of the effects of pixel size and unsharp-mask filtering on the detection of subtle microcalcifications. *Invest Radiol* **1987**;22:581-589
22. Oestmann JW, Kopane D, Hall DA, McCarthy KA, Rubens JR, Greene R. A comparison of digitized storage phosphors and conventional mammography in the detection of malignant microcalcifications. *Invest Radiol* **1988**;23:725-728
23. Kastan DJ, Ackerman LV, Feczko PJ. Digital gastrointestinal imaging: the effect of pixel size on detection of subtle mucosal abnormalities. *Radiology* **1987**;167:854-856
24. Fajardo LL, Hillman BJ, Hunter TB, Claypool HR, Westerman BR, Mockbee B. Excretory urography using computed radiography. *Radiology* **1987**;162:345-351
25. Murphey MD. Digital skeletal radiography: spatial resolution requirements for detection of subperiosteal resorption. *AJR* **1989**;152:541-546
26. Seeley GW, Fisher HD, Stempski MO, Borgstrom M, Jelland J, Capp MP. Total digital radiology department: spatial resolution requirements. *AJR* **1987**;148:421-426

Radiology Outreach Foundation

The Radiology Outreach Foundation (ROF) is a nonprofit corporation whose goal is to help disadvantaged countries improve their health care by providing radiology equipment, books, consultation, education, and training to their practitioners. This assistance is on an application basis that is independent of political, ethnic, or religious orientation of the grantee. It depends on the need of the people and the ability of the ROF to meet that need. The ROF is approved by the U.S. Internal Revenue Service as a tax-exempt organization. It is endorsed by the following radiologic societies: American Association of Women Radiologists, American College of Radiology, American Roentgen Ray Society, Association of University Radiologists, Radiological Society of North America, Society of Chairmen of Academic Radiology Departments, Society for Pediatric Radiology, European Society of Pediatric Radiology.

All donations to the ROF are tax deductible. Persons who would like to contribute financially to the ROF, would be interested in being a visiting professor, would like to send books or journals to any of the institutions supported by the ROF, or would like further information about the ROF should write to Charles A. Gooding, M.D., President, Radiology Outreach Foundation, 3415 Sacramento St., San Francisco, CA 94118 USA.

Appointment of New Associate Editor

Robert N. Berk[1]

Saskia von Waldenburg Hilton

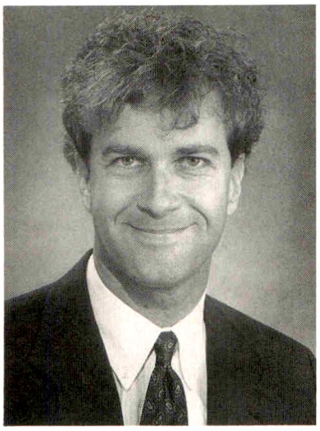

Karim Valji

Beginning with this issue, Saskia von Waldenburg Hilton will step down as associate editor of the Journal. She will be replaced by Karim Valji. The *AJR* is grateful to Dr. Hilton for her dedicated service as editor during the past 6 years. The Journal has benefited from her astute ability to make appropriate editorial decisions, her insistence on high standards, and her willingness to personally help authors with their manuscripts. She has been especially generous in spending many hours steering new authors through the peer-review process and the task of writing revisions.

Karim Valji is a member of the radiology faculty at the University of California, San Diego (UCSD), School of Medicine. A graduate of Harvard College and Harvard Medical School, Dr. Valji joined the UCSD faculty after completing his residency in radiology at UCSD. His perspicacity, enthusiasm, talents as an author and reviewer, and extraordinary competence are certain to stand him in good stead in his new role as associate editor. We look forward to working with him in the editorial office.

---

[1] Editor-in-Chief, *American Journal of Roentgenology*, 2223 Avenida de la Playa, Ste. 103, La Jolla, CA 92037-3218.

***AJR* 157:86, July 1991** 0361-803X/91/1571-0086 © American Roentgen Ray Society

Effect of Radiation Therapy on Thoracic and Lumbar Bone Marrow: Evaluation with MR Imaging

David F. Yankelevitz[1]
Claudia I. Henschke
Pamela H. Knapp
Lourdes Nisce
Yun Yi
Patrick Cahill

Bone marrow suppression is often the limiting factor in the use of radiation therapy. In order to determine if MR imaging can be used to quantify bone marrow changes, we performed a serial prospective study of patients with lung cancer (six cases) and lymphoma (six cases). Quantitative and qualitative assessments of T1-weighted sagittal images, 750/33 (TR/TE), obtained at 0.6 T before, during, and after radiotherapy showed increased signal intensity in the radiated portions of the spine. These changes appeared as early as 2 weeks after the beginning of radiation, continued to increase until a maximum value was attained, and then persisted during the follow-up period of 2 years. A significantly higher ($p < .04$) ratio of pretreatment to maximum posttreatment signal intensity was seen in patients with lymphoma than in those with lung cancer, and pretreatment values in patients with lymphoma were significantly lower ($p < .01$). The lower pretreatment values found in the patients with lymphoma may have been due to the smaller amount of yellow marrow in these patients, who were significantly younger (33 vs 62 years). The higher ratio of pre- and posttreatment signal intensity may have been related to the larger amount of hematopoietic marrow available to undergo fatty replacement. The persistence of elevated signal intensity for as long as 2 years after radiation suggests an endpoint in the process of marrow conversion, but not reversal in the form of regeneration of hematopoietic bone marrow.

Quantitative MR evaluation of bone marrow may be of considerable value as a noninvasive means of monitoring the effects of radiotherapy.

***AJR* 157:87–92, July 1991**

The pathology of radiation effect on bone marrow has been well documented by needle aspiration or microscopic/macroscopic examination of autopsy specimens [1–6]. Gross anatomic and histologic specimens have shown that irradiated bone marrow becomes hypocellular, with destruction of fine vasculature followed by fatty marrow replacement of the normal hematopoietic marrow [5]. This is detected as increased signal intensity on MR images owing to the decreased T1 relaxation time of the increased fatty marrow content and is well documented histologically [7]. The destruction of sinusoidal circulation precludes migration of hematopoietic cells from distant nonirradiated sites. This is the limiting factor in toxicity of radiotherapy, because it is unlikely that any remaining reticulum cells would have stem cell activity sufficient to promote regeneration [2].

To date, investigations of MR imaging of radiation-induced marrow changes have been retrospective studies, and usually the patients were imaged only once [8, 9]. We performed a prospective MR study in a series of patients with lung cancer and lymphoma who were treated with radiotherapy and had not had treatment before. Our goal was to determine the time at which signal intensity changes in the bone marrow first become evident and whether they persist or change on subsequent scans. To document the qualitative changes seen on MR images and to more accurately assess these changes over time, we also developed a method for standardizing the quantitative evaluation of signal intensity.

Received October 5, 1990; accepted after revision January 28, 1991.

[1] All authors: Department of Radiology, The New York Hospital-Cornell University Medical College, New York, NY 10021. Address reprint requests to C. I. Henschke.

0361-803X/91/1571-0087
© American Roentgen Ray Society

Subjects and Methods

Twelve consecutive patients, six with newly diagnosed lymphoma and six with newly diagnosed lung cancer, underwent MR imaging at specified times in the course of radiation treatment (part of the New York State Demonstration Project on the Efficacy of MRI). The average ages of the five women and seven men were 62 years in those with lung cancer and 33 years in those with lymphoma. None of the patients had undergone previous irradiation or chemotherapy, nor were they receiving concomitant chemotherapy at the time of the investigations.

Patients with lung cancer underwent a standard treatment protocol of 4140 cGy to the mediastinum (T1–T9, 200 cGy/day, 5 treatments/week) and an additional 1980 cGy to the mass itself, which did not include the spine. Patients with lymphoma underwent a standard treatment protocol of 3600 cGy to the mantle area (T1–T9) and 3600 cGy to the paraaortic area (T10–L4). The doses were administered as 200 cGy/day, 5 days per week, and alternated between the two regions every 2 weeks; an additional boost of 500 cGy was delivered to the supraclavicular region at the completion of the course.

MR images (0.6 T) were obtained before therapy; every 2 weeks during therapy; and 2, 3, 6, and 12 months after the completion of therapy. T1-weighted sagittal images, 750/33 TR/TE), were examined for changes in the signal intensity of vertebral bodies relative to that of subcutaneous fat during and after treatment.

In order to quantify the signal intensity of each of the vertebral bodies, corrections are needed to adjust for variations in tip angles, RF coil response, patient loading in the coil, and patient motion and blood flow. A calibration phantom was developed consisting of a long rectangular tube (2.5 × 2.5 × 40 cm) filled with polyunsaturated oil

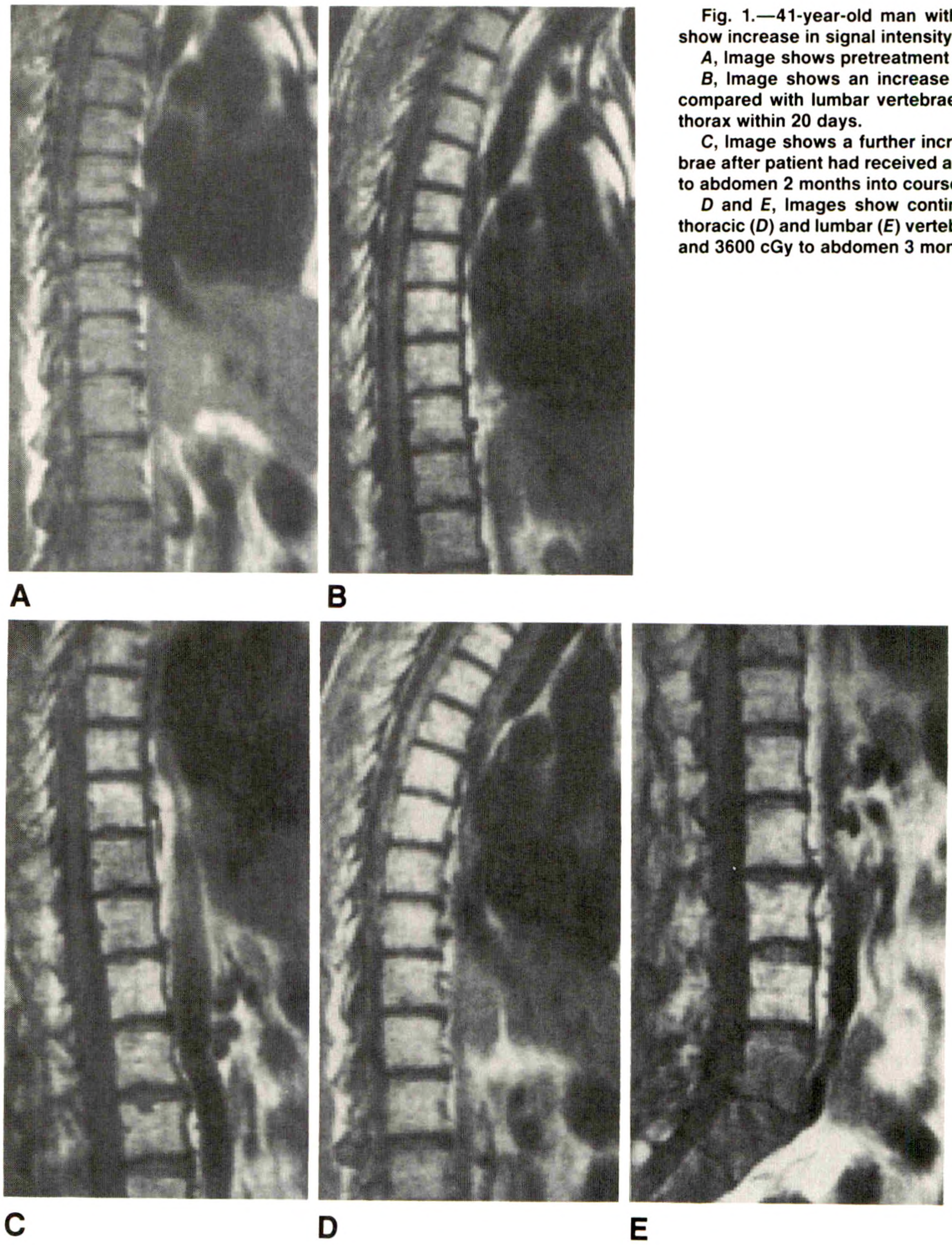

Fig. 1.—41-year-old man with Hodgkin lymphoma. Serial MR images show increase in signal intensity with treatment.

***A*, Image shows pretreatment signal intensity of vertebrae.**

***B*, Image shows an increase in signal intensity of thoracic vertebrae compared with lumbar vertebrae after patient had received 1600 cGy to thorax within 20 days.**

***C*, Image shows a further increase in signal intensity of thoracic vertebrae after patient had received a total of 3600 cGy to thorax and 1600 cGy to abdomen 2 months into course of radiation therapy.**

***D* and *E*, Images show continued increase in signal intensity in both thoracic (*D*) and lumbar (*E*) vertebrae after total dose of 4000 cGy to thorax and 3600 cGy to abdomen 3 months after start of radiation therapy.**

(Crisco, Procter & Gamble, Cincinnati, OH) that was positioned underneath the patient.

In order to determine the appropriate corrections, MR body coil response curves were generated for the spatial variations of the RF coil and changes in the tip angles by using a calibration phantom filled with a solution containing 50% glycol in water. Also, volunteers were imaged at various pulse TRs in order to develop the additional corrections created by the eddy currents within the patient. Finally, a net correction response curve weighted for the RF response of the body coil, for fat signal changes (tip angle variations), and for the response of volunteers was determined for each of the 256 columns of a sagittal image for a given slice thickness and TR/TE. This correction matrix was applied for all columns and rows of each sagittal image containing vertebral bodies. The signal intensity value for each vertebral body was defined as the ratio of the corrected MR intensity for that vertebral body to the subcutaneous fat.

To summarize the signal intensity changes of the irradiated spine for a particular patient at any one time, we calculated the average pretreatment signal intensity value of the irradiated vertebrae as well as the average maximum posttreatment value. To assess the relative increase in the signal intensity over the pretreatment values, we calculated the ratio of the average maximum posttreatment value attained for that patient to his or her average pretreatment value. The general linear model (one-way analysis of variance with covariates) was used to analyze the relationship between these summary signal intensity values for the irradiated spine by type of tumor and the covariates age and complete blood cell count (WBCs, hemoglobin, hematocrit, and platelets) before and after radiation treatment.

Results

Scans of both lung cancer and lymphoma patients showed increased signal intensity of vertebral bodies in the region of irradiation. The earliest changes were noted 2 weeks after beginning radiation therapy (after receiving 1600 cGy). The signal intensity continued to increase on subsequent scans during the treatment period. In patients with lymphoma, who received sequential radiation to two anatomic regions, it was observed that the newly irradiated marrow in the abdominal regions increased in signal intensity just as the marrow in the thorax had increased in signal intensity after irradiation of that region (Fig. 1). In some cases only one half of the vertebral body was involved (Fig. 2). In patients with lung cancer, the areas of irradiation were sharply delineated by MR (Fig. 3).

In all patients the signal intensity of irradiated marrow continued to increase rapidly for the first 6 weeks and then more slowly toward a maximum value. Thereafter, the signal intensity remained unchanged through the last follow-up scans obtained, which took place 1 year later in 10 patients and 2 years later in two patients who were available for follow-up.

The nonirradiated marrow showed no change in signal intensity, either during radiation treatment or well afterward, even when maximal increases in intensity were observed in irradiated regions. Quantitatively, these changes in signal

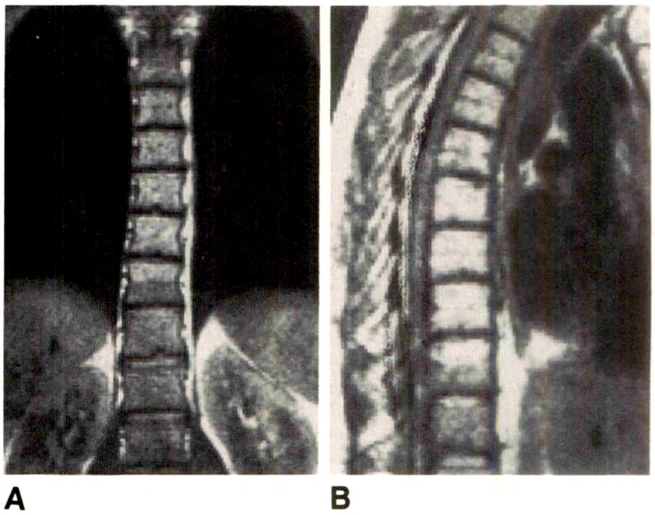

Fig. 2.—27-year-old man with Hodgkin lymphoma.
_A_ and _B_, Coronal (_A_) and sagittal (_B_) MR images show increased signal intensity of thoracic vertebrae. This area is so clearly delineated that increased signal intensity can be seen in half of a vertebral body that was included in the port.

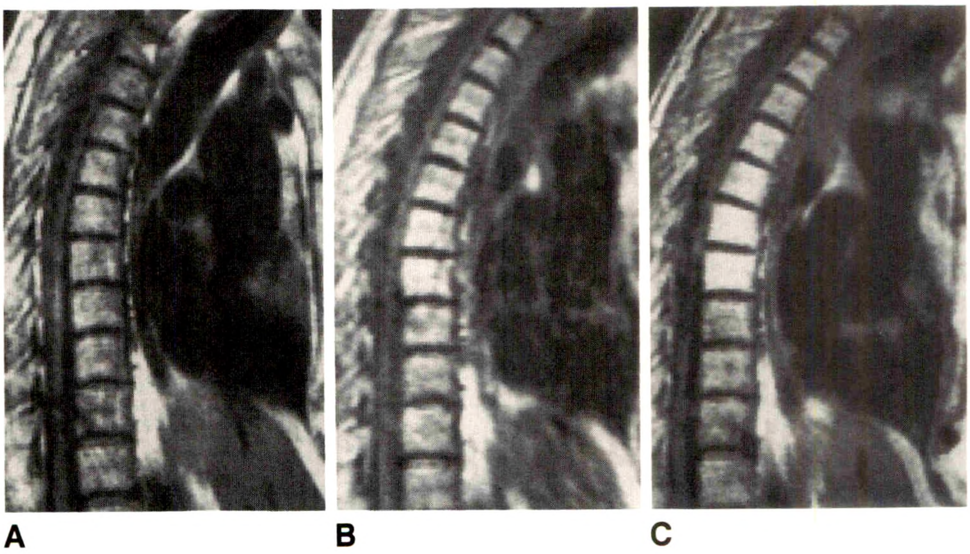

Fig. 3.—71-year-old man with adenocarcinoma of upper lobe of left lung.
_A_, Pretreatment sagittal MR image shows pretreatment signal intensity of vertebrae.
_B_, Sagittal MR image after 1 month of radiation therapy (3060 cGy) shows slightly increased signal intensity in T2–T8 region.
_C_, Sagittal MR image 2 months after completion of treatment shows markedly increased signal intensity of irradiated vertebrae (T2–T8).

intensity values for individual patients could be depicted for each vertebral body (Figs 4 and 5). The average pretreatment and maximum posttreatment values attained by each patient were determined (Figs. 6 and 7).

The average pretreatment value for the vertebral bodies from C7 to L5 for all patients combined was 53 (standard error of 2.0). In patients with lung cancer, the average pretreatment value was 57, which was significantly higher ($p <$ .01) than the average pretreatment value of 48 for patients with lymphoma. The maximum posttreatment value increased in both groups, but was no longer significantly different ($p <$ .08): 95 for the patients with lung cancer and 87 for the patients with lymphoma. The ratio of the maximum posttreatment to pretreatment value was significantly different ($p <$ .04) for the two tumor groups, 1.67 for lung cancer and 1.80 for lymphoma. Although age was a significant factor in accounting for the difference in pretreatment ($p <$ .02) and maximum posttreatment ($p <$ .03) values, it could not account for the significant difference in the ratio of the maximum posttreatment to pretreatment values ($p <$ .18).

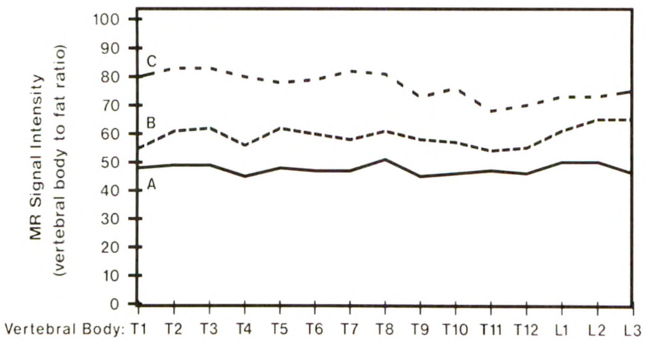

Fig. 4.—Quantitative values for MR signal intensity of spine (lymphoma patient shown in Fig. 1).
***Line A*, Before treatment.**
***Line B*, After receiving 3600 cGy to thorax and 1600 cGy to abdomen.**
***Line C*, After completion of therapy.**

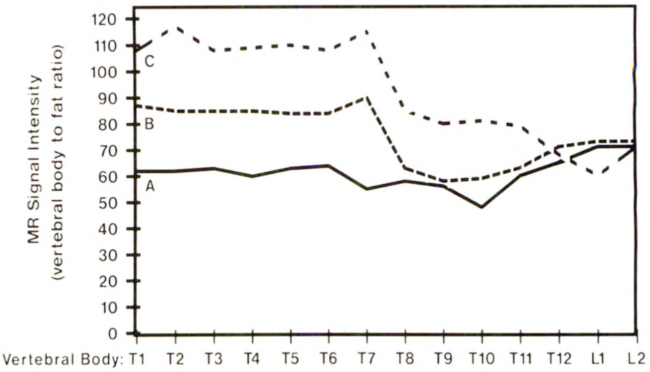

Fig. 5.—Quantitative values for MR signal intensity of spine (lung cancer patient in Fig. 3).
***Line A*, Before treatment.**
***Line B*, After receiving 4020 cGy to thoracic spine.**
***Line C*, 9 months after start of radiation therapy.**

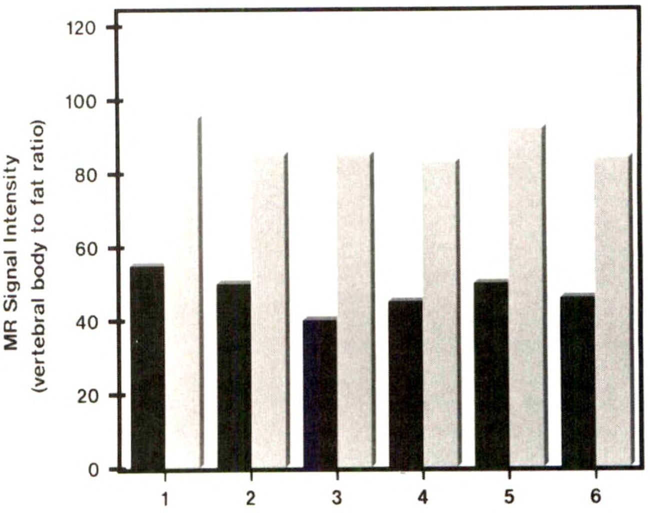

Fig. 6.—Average pretreatment (*black columns*) and maximum posttreatment (*gray columns*) signal-intensity values for patients with lymphoma.

Discussion

MR is known to be an accurate technique for imaging both vertebral bodies and disk spaces [10–13], with T1-weighted images superior in revealing abnormalities of the spine [11, 13]. It has been shown that the increased signal intensity of bone marrow seen on MR is due to fatty replacement of the normal hematopoietic marrow [7, 14], which is a histologically documented effect of irradiation [5]. T1 and T2 relaxation times in vertebral bodies appear to reflect the relative amounts of trabecular bone, red (hematopoietic) marrow, and yellow (fatty) marrow. The normal adult distribution of red and yellow marrow [15, 16] can be altered by the presence of marrow-infiltrating diseases [17] and treatment, particularly therapeutic irradiation, which causes a well-documented sequence of bone marrow changes [5].

The use of calibration phantoms allowed us to standardize signal intensity values and perform accurate quantitative assessments of signal intensities in all patients. It also provided consistency during serial examinations in the documentation of quantitative increases in signal intensity, which were also observed qualitatively. The average signal intensity value for the vertebral bodies before therapy was 53. This result may reflect the fact that hematopoietic and fatty marrow are approximately equal in the vertebral body. Numeric signal intensity values were consistent with the observed visual assessment of the progression, showing an initially rapid increase after irradiation, followed by a more gradual increase to a maximum value, and thereafter remaining elevated for as long as the patients were followed up. The average maximum posttreatment value of all 12 patients increased 1.7 times over the baseline pretreatment values. In all patients, the regions of increased signal intensity in vertebral bodies corresponded closely to areas defined by port films.

Lymphoma and lung cancer populations responded similarly to irradiation, and we found that anatomic site or sequence of regions irradiated had no bearing on the resulting

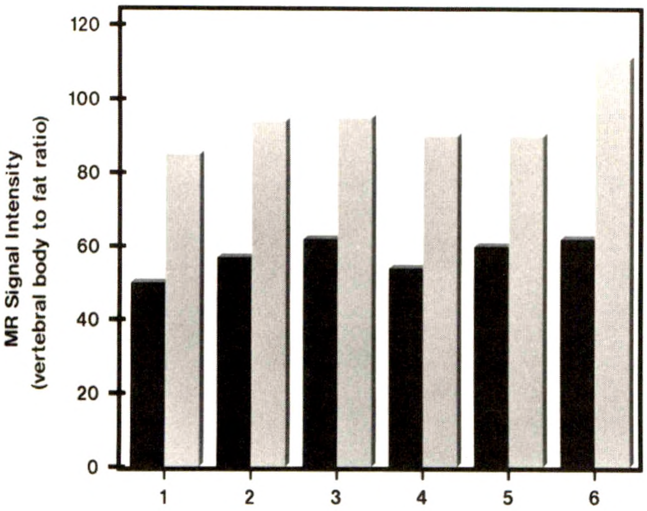

Fig. 7.—Average pretreatment (*black columns*) and maximum posttreatment (*gray columns*) signal-intensity values for patients with lung cancer.

increase in signal intensity. The patients with lymphoma received two courses of radiation alternating between the thorax and abdomen. Both sites showed similar time courses and magnitudes of increase in marrow signal intensity whether the patient received radiation only to the thorax (as in patients with lung cancer) or alternately to the thorax and abdomen (as in patients with lymphoma). The increased signal intensity of the thoracic spine persisted throughout irradiation of the lumbar spine, which subsequently increased in signal intensity also.

Statistical analysis of signal intensity changes revealed a significant difference ($p < .01$) between patients with lung cancer and lymphoma with respect to the pretreatment values (57 vs 48). Furthermore, age was found to be a significant factor ($p < .02$) in this difference because the patients with lymphoma were much younger (33 vs 62 years). The lower pretreatment values of the lymphoma group can be explained in terms of what we already know about fatty replacement. Because the patients with lymphoma were younger, they had proportionately less fatty marrow to begin with than did the older patients with lung cancer, in whom fatty replacement had already progressed further as part of the normal aging process. The maximum posttreatment value attained was higher, although not significantly ($p < .08$), in the patients with lung cancer. Assuming that the endpoint of total fatty replacement sets a limit for increase in signal intensity, we can posit that the older patients with lung cancer were already further along on a continuum of fatty change when they began their radiation treatment, or that the difference was due to their slightly higher total dose to the thoracic spine (540 cGy).

The significantly higher ($p < .04$) maximum posttreatment to pretreatment ratio obtained in patients with lymphoma (1.8 vs 1.6) can be attributed to their lower baseline values, resulting in a higher proportion of hematopoietic marrow undergoing fatty replacement after irradiation. Alternatively, this higher ratio in the patients with lymphoma may be due to irradiation of both the thoracic and lumbar spine, thus limiting the possibility of repopulation from the lumbar bone marrow. The latter possibility would, however, be suggested only if the signal intensity of the thoracic bone marrow in the patients with lung cancer had decreased during the follow-up period.

The persistence of high signal intensity as long as 2 years after completion of therapy gives no evidence that marrow regeneration has taken place. The process of regeneration has been defined as the reconstitution of fine vasculature and sinusoids, with eventual repopulation by hematopoietic cells [2]. If regeneration had taken place, we would have expected to see an eventual decrease in signal intensity after 1 year, when regeneration becomes evident histologically [2, 4]. Such regeneration has been consistently demonstrated 1 year after doses of 4000 cGy of local [1–4] and total nodal [4] irradiation. Alternatively, reconversion of yellow to red marrow may occur in distal nonirradiated sites when the usual adult volume of functioning red marrow is reduced by disease or radiation damage. The persistence of heightened signal intensity suggests either that significant regeneration and reconversion did not occur in our subjects or that increases in hematopoietic marrow volume did not cause a measurable change in MR signal intensity [18]. As there was no significant depression of peripheral blood cell counts during or after the course of radiation therapy, reconversion may have occurred at peripheral sites that were not scanned in order to maintain the required blood cell volume. However, other researchers have found peripheral blood counts to be a poor index of bone marrow function [5, 8], so we cannot be certain that compensatory hematopoiesis was in fact occurring anywhere in response to radiation changes in the vertebrae. In fact, there may not have been a sufficient stimulus for marrow regeneration or reconversion because the patients received fractionated radiation to limited regions of the axial bone marrow [4].

In summary, our prospective study documented increased signal intensity in bone marrow of patients with lung cancer or lymphoma as early as 2 weeks after initiation of radiation therapy. Because we obtained serial MR scans that were evaluated quantitatively through the use of calibration phantoms, we were able to document the course of increasing signal intensity over time. In comparing patients with lung cancer and lymphoma, we found that the pretreatment and maximum posttreatment values were probably dependent on the proportion of yellow marrow present before treatment. The significantly higher maximum posttreatment to pretreatment ratio in patients with lymphoma may be related to the relatively higher proportion of hematopoietic marrow undergoing fatty replacement, or to their treatment with irradiation of both the thoracic and lumbar spine. The persistence of elevated signal intensity for as long as 2 years suggests an endpoint in the process of marrow conversion, but not reversal in the form of regeneration or reconversion. This, however, cannot be decided with certainty, as there must be sufficient underlying stimuli, as well as sufficient sensitivity in the quantitative assessment of the MR images. Both of these issues are important topics for future study, which may define an important clinical role for MR as a noninvasive means of monitoring the volume of functional bone marrow. Finally, the underlying marrow changes causing the increased signal intensity on MR may be a combination of several biochemical and histologic processes, which should also be elucidated further.

REFERENCES

1. Knopse WH, Rayudu VMS, Cardello M, Friedman AM, Fordham EW. Bone marrow scanning with ^{52}iron (^{52}Fe): regeneration and extension of marrow after ablative doses of radiotherapy. *Cancer* **1976;**37:1432–1442
2. Knopse WH, Blom J, Crosby WH. Regeneration of locally irradiated bone marrow. I. Dose dependent, long-term changes in the rat, with particular emphasis upon vascular and stromal reaction. *Blood* **1966;**28:398–415
3. Sykes MP, Chu FH, Wilkerson WG. Local bone-marrow changes secondary to therapeutic irradiation. *Radiology* **1960;**75:919–924
4. Sacks S, Edmund L, Goris ML, Glatstein E, Gilbert E, Kaplan HS. Bone marrow regeneration following large field radiation: influence of volume, age, dose, and time. *Cancer* **1978;**42-1057–1065
5. Rubin P, Casarett GW. *Clinical radiation pathology*, vol. II. Philadelphia: Saunders, **1968**:557–608
6. Patt HM, Maloney MA. Bone marrow regeneration after local injury: a review. *Exp Hematol* **1975;**3:135–148
7. Hajek PC, Baker LL, Goobar JE, et al. Focal fat deposition in axial bone marrow: MR characteristics. *Radiology* **1987;**162:245–249
8. Ramsay RG, Zacharias CE. MR imaging of the spine after radiation therapy: easily recognizable effects. *AJR* **1985;**144:1131–1135
9. Remedios PA, Colletti PM, Raval JK, et al. Magnetic resonance imaging of bone after radiation. *Magn Reson Imaging* **1988;**6:301–304
10. Han JS, Kaufman B, El Y, et al. NMR imaging of the spine. *AJR* **1983;**141:137–145
11. Moffit B, Reicher M, Lufkin R, Bentson J. Comparison of T1 and T2 weighted images of the lumbar spine. *Comput Med Imaging Graph* **1988;**12:271–276
12. Jenkins JPR, Hickey DS, Zhu XP, Machin M, Isherwood I. MR imaging of the intervertebral disc: a quantitative study. *Br J Radiol* **1985;**58:705–709
13. Jenkins JPR, Stehling M, Sivewright G, Hickey DS, Hillier VF, Isherwood I. Quantitative magnetic resonance imaging of vertebral bodies: a T1 and T2 study. *Magn Reson Imaging* **1989;**7:17–23
14. Rosethal DI, Hayes CW, Rosen B, Mayo-Smith W, Goodsitt MM. Fatty replacement of spinal bone marrow due to radiation: demonstration by dual energy quantitative CT and MR imaging. *J Comput Assist Tomogr* **1989;**13:463–465
15. Moore SG, Dawson KL. Red and yellow marrow in the femur: age-related changes in appearance at MR imaging. *Radiology* **1990;**175:219–223
16. Dooms GC, Fisher MR, Hricak H, Richardson M, Crooks LE, Genant HK. Bone marrow imaging: magnetic resonance studies related to age and sex. *Radiology* **1985;**155:429–432
17. Krikun ME. Red-yellow marrow conversion: its effect on the location of some solitary bone lesions. *Skeletal Radiol* **1985;**14:10–19
18. Vogler JB, Murphy WA. Bone marrow imaging. *Radiology* **1988;**168:679–693

Pictorial Essay

Normal and Degenerated Intervertebral Disk: In Vivo and In Vitro MR Imaging with Histopathologic Correlation

Mark L. Schiebler,[1] Nicolas Grenier,[2] Michael Fallon,[3] Vicki Camerino,[4] Michael Zlatkin,[5] and Herbert Y. Kressel[6]

The components of the intervertebral disk serve two purposes. The hydrophilic matrix is contained by circumferential rings of fibrocartilage (outer anulus) and Sharpey's fibers. The gellike hydrophilic matrix acts as a cushion between the vertebral body endplates by providing an even distribution of axial and rotational compressive forces. The construction and integrity of the intervertebral disk are assessed well by MR. The purpose of this pictorial essay is to show the in vitro and in vivo MR appearances of the normal and degenerated disk, and to correlate these MR changes with their respective histopathologic findings.

Normal Disk Microarchitecture

Sharpey's fibers and the rings of the outer anulus are demonstrated well with high-resolution MR. This is because the collagen fibrils are extremely well organized and have an almost infinite T1 and a very short T2. This causes them to have a low signal intensity on short TR/short TE (e.g., 600/20), long TR/short TE (e.g., 2500/40), and long TR/long TE (e.g., 2500/80) spin-echo (SE) images (Fig. 1).

The central disk is composed of wispy fibrocartilage from the inner anulus and the gelatinous matrix of the nucleus pulposus. These two regions of the disk are inseparable on SE imaging. The loose collagen fibrils of the inner anulus are too small to be seen. The hydrated gel of the nucleus pulposus has the same signal intensity on long TR/TE pulse sequences as the inner anulus does, even though the nucleus pulposus has the physical consistency of gelatin (Fig. 1).

The intranuclear cleft should be seen in normal adult disks [1]. The intranuclear cleft is composed of a fibrous transformation of the previously gellike matrix.

Microarchitecture of Early Disk Degeneration

Disk degeneration may occur without a loss in disk height or signal intensity on long TR/long TE SE images. The first evidence of this is infolding of the fibers of the outer anulus (Figs. 2 and 3). Infolding is occasionally accompanied by the formation of an anterior region of low signal intensity, which we have arbitrarily named the central dot (Figs. 2 and 3). We have found the central dot to correlate with compression of the apex of the infolding fibers of the outer anulus (Fig. 2). Myxoid degeneration of the fibers of the outer anulus may occur without any other changes. This degeneration is analogous to the degeneration that occurs within the fibrocartilage of the menisci in the knee. Within the intervertebral disk, myxoid degeneration can be seen as alternating areas of

---

Received October 19, 1990; accepted after revision January 4, 1991.

[1] Department of Radiology, University of North Carolina, Chapel Hill, NC 27599-7510. Address reprint requests to M. L. Schiebler.
[2] Department of Radiology, Hopital Pellegrin, Place de Amelie Rabat-Leon, 33000 Bordeaux, France.
[3] Department of Pathology, Thomas Jefferson University Hospital, Philadelphia, PA 19104.
[4] Rye Radiology Group, Rye Ridge Plaza, Ryebrook, NY 10573.
[5] Department of Radiology, Memorial Hospital, Hollywood, FL 33021.
[6] Department of Radiology, Hospital of the University of Pennsylvania, Philadelphia, PA 19104.

AJR **157:93–97, July 1991** 0361–803X/91/1571–0093 © American Roentgen Ray Society

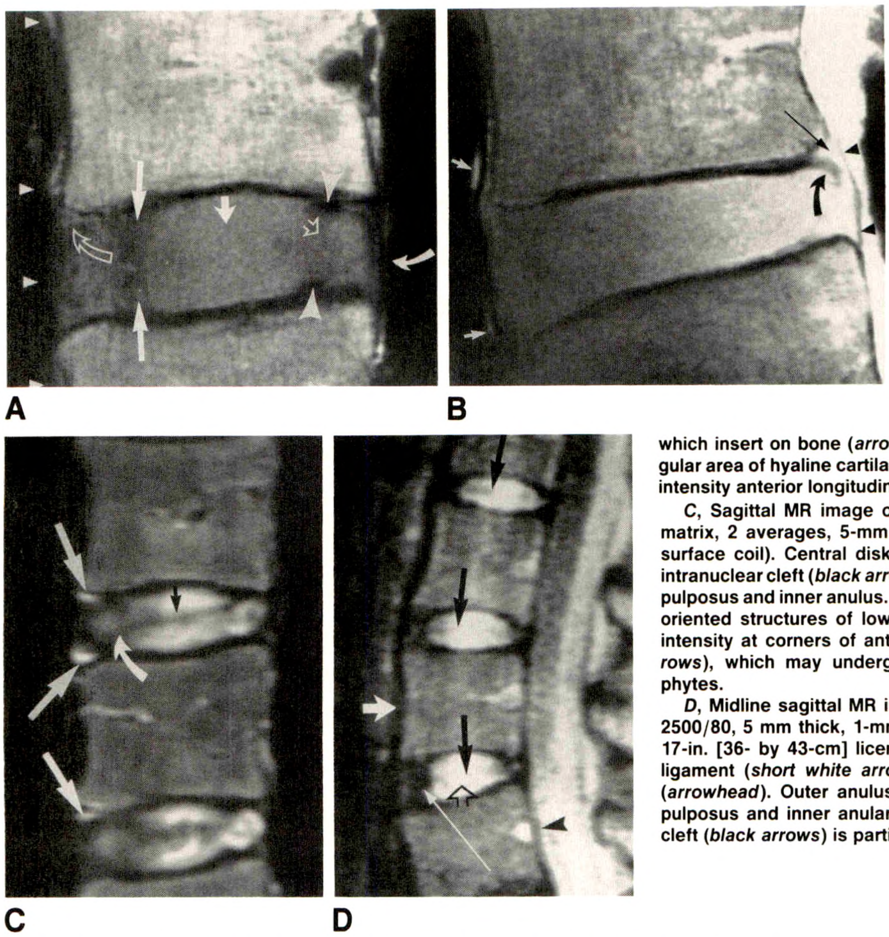

Fig. 1.—Normal disk microarchitecture.

A, Sagittal MR image (SE 600/20, 256 × 256 matrix, 3 mm thick, 0.6-mm slice skip, 8-cm field of view, 4 averages, 5-in. [13-cm] receive-only surface coil) shows anterior longitudinal ligament (*small arrowheads*); central fibers of anterior outer anulus (*long straight arrows*); inner anulus and nucleus pulposus (*short solid arrow*), which are inseparable on MR; calcification of posterior aspect of hyaline cartilage endplate (*large arrowheads*) at insertion of vertical fibers of posteromedial outer anulus (*open arrow*); and Sharpey's fibers (*solid curved arrow*). Thin rim of hyaline cartilage endplate is barely observable anteriorly (*open curved arrow*).

B, Sagittal MR image of L5–S1 specimen disk (same imaging parameters as *A*) shows relationship between convex posterior margin of outer anular fibers (*curved arrow*), which insert on hyaline cartilage endplate, and Sharpey's fibers, which insert on bone (*arrowheads*). Between these two structures is a triangular area of hyaline cartilage endplate (*straight black arrow*). Note low-signal-intensity anterior longitudinal ligament (*white arrows*).

C, Sagittal MR image of L3–L5 specimen disks (SE 2500/80, 128 × 256 matrix, 2 averages, 5-mm slice skip, 16-cm field of view, 5-in. receive-only surface coil). Central disk (L3–L4) shows low signal intensity of horizontal intranuclear cleft (*black arrow*) surrounded by higher signal intensity of nucleus pulposus and inner anulus. Fibers of anterior outer anulus are seen as vertically oriented structures of low signal intensity (*curved arrow*). Note high signal intensity at corners of anterior hyaline cartilage endplate (*straight white arrows*), which may undergo endochondral ossification and become osteophytes.

D, Midline sagittal MR image of lumbar spine in a 35-year-old patient (SE 2500/80, 5 mm thick, 1-mm slice skip, 2 averages, 128 × 256 matrix, 14- by 17-in. [36- by 43-cm] license-plate surface coil) shows anterior longitudinal ligament (*short white arrow*) and posterior longitudinal ligament and dura (*arrowhead*). Outer anulus (*long white arrow*) is thicker anteriorly. Nucleus pulposus and inner anular fibers are inseparable (*open arrow*). Intranuclear cleft (*black arrows*) is partially seen as an area of central low signal intensity.

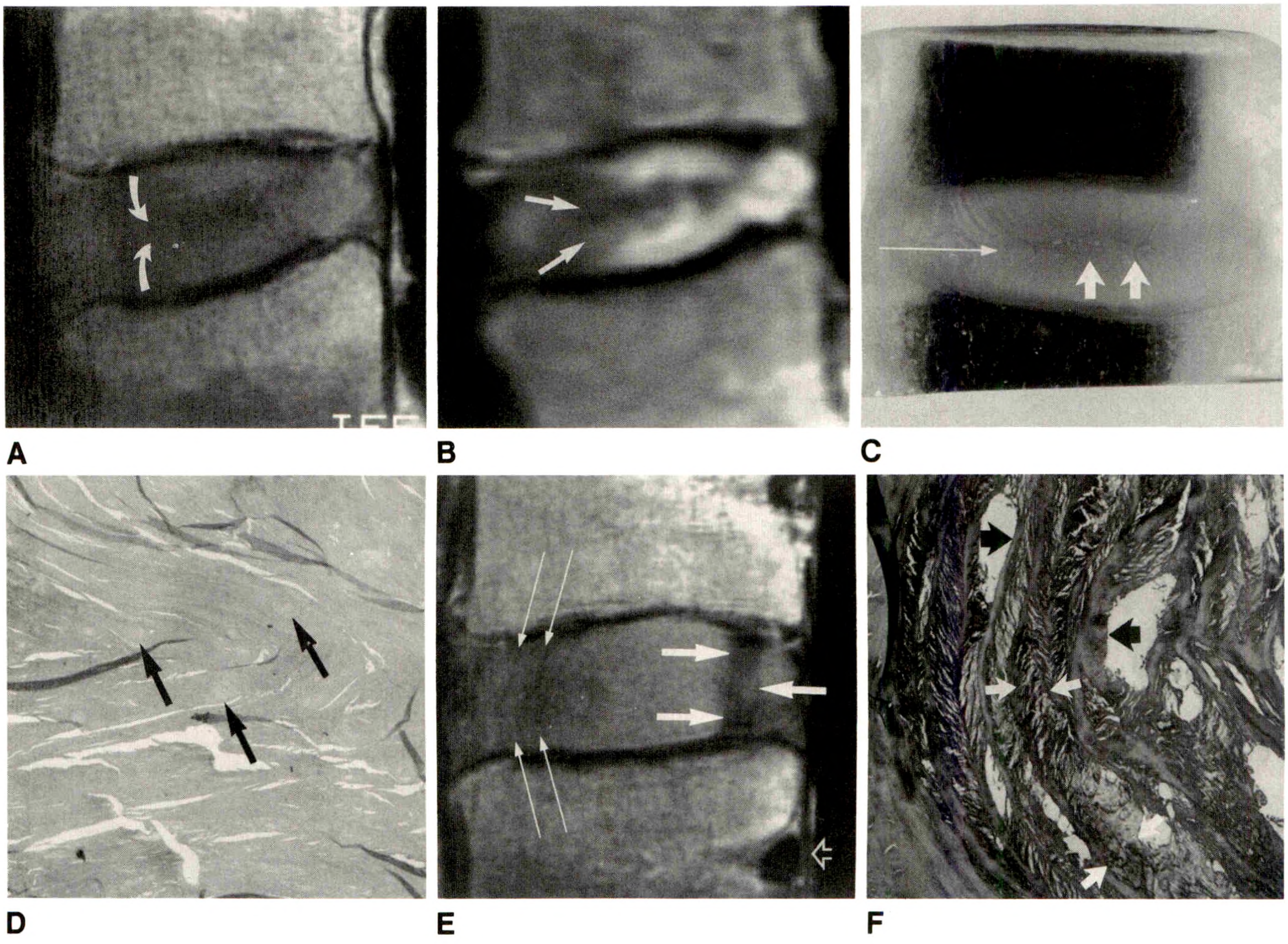

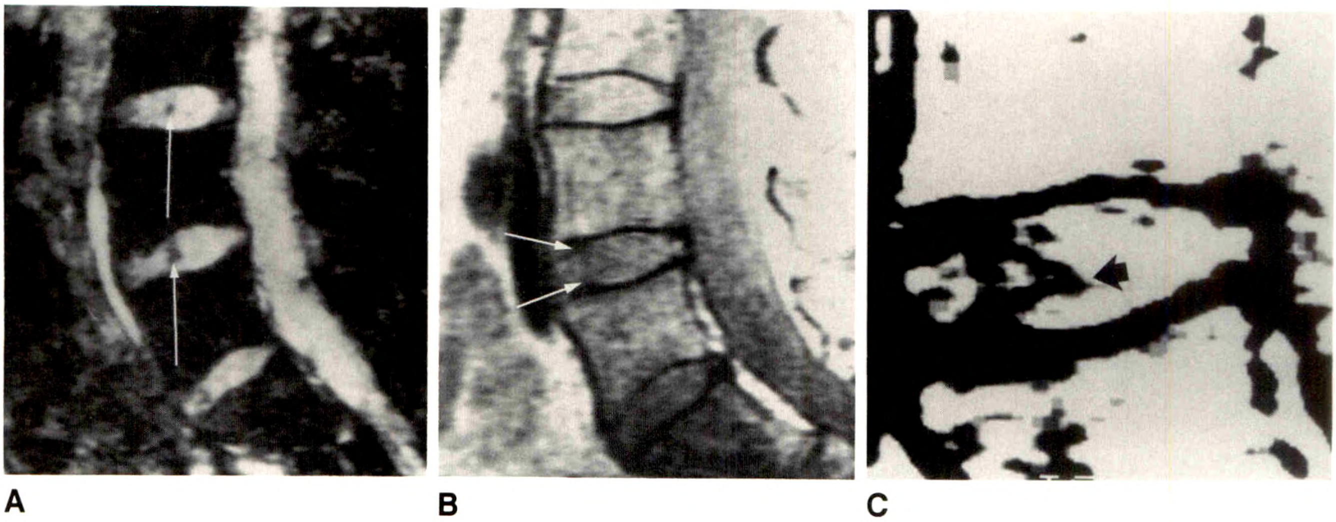

Fig. 3.—Early disk degeneration in vivo in a 40-year-old patient.

A, Sagittal MR image (gradient echo 400/25, <25°, 5 mm thick, 1-mm slice skip, 2 averages, 14- by 17-in. [36- by 43-cm] license-plate surface coil) shows central dots in anterior aspects of disks (*arrows*).

B, Sagittal MR image (SE 600/20, 5 mm thick, 1-mm slice skip, 2 averages, 128 × 256 matrix, license-plate receive-only coil) shows infolding of anterior aspect of outer anular fibers at L4–L5 level (*arrows*).

C, Magnified sagittal MR image with a very narrow window width shows involuting fibers (*arrow*).

increased signal intensity between the low signal intensity fibers of the outer anulus (Fig. 2).

Microarchitecture of Late Disk Degeneration

Separation between the hyaline cartilage endplate and the inner anulus and nucleus pulposus occurs in disks that show both a loss of height and signal intensity on long TR/long TE SE images (Fig. 4). These areas are true fibrin-lined clefts that may contain either nitrogen gas or water (Fig. 4).

Microarchitecture of Intradiskal Herniation

Many disk herniations probably start as intradiskal tears of the fibers of the outer anulus from internal herniation of the central hydrated proteoglycan matrix of the nucleus pulposus [2]. These intradiskal tears can be seen on high-resolution MR as regions of discontinuity of outer anular fibers. The tract of the dissecting bolus of nucleus pulposus may be seen even on long TR/long TE SE images (Fig. 5).

Microarchitecture of a Retained Disk Herniation

The dissecting bolus of a hydrated proteoglycan matrix may tear through Sharpey's fibers and come to rest immediately anterior to the posterior longitudinal ligament [3, 4]. It then may undergo desiccation (Fig. 6).

Conclusions

High-resolution MR imaging of the disk can provide a highly accurate picture of the disk's microarchitecture prior to histologic sectioning. Findings of early disk degeneration can be seen in vivo before either the loss of disk height or loss of central disk signal intensity has occurred on long TR/long TE images.

◄ **Fig. 2.**—Early disk degeneration in specimen disk.

A, Sagittal MR image (SE 600/20, 256 × 256 matrix, 3 mm thick, 0.6-mm slice skip, 4 averages, 8-cm field of view, 5-in. [13-cm] receive-only surface coil) shows infolding of fibers of outer anulus toward shrinking nucleus pulposus and inner anulus. This occurs circumferentially and primarily involves more central fibers (*arrows*) of outer anulus.

B, Sagittal MR image (SE 2500/40, 256 × 128 matrix, 5 mm thick, 2 averages, 16-cm field of view, 5-in. receive-only surface coil) of same disk shows simple infolding (*arrows*) and intranuclear cleft.

C, Photograph of sagittal tissue block from disk shows infolding fibers of anterior outer anulus (*long arrow*). Region of intranuclear cleft is seen as a darker area in center of disk (*short arrows*).

D, Photomicrograph (original magnification × 40) of apex of collapsed collection of anterior outer fibers. This central coalescence of fibers may cause MR finding of a central dot. These fibers assume a horizontal V configuration. Air spaces between stained fibers are section artifacts. Note presence of scattered metaplastic cartilage cells (*arrows*).

E, Sagittal MR image (SE 600/20, 256 × 256 matrix, 3 mm thick, 0.6-mm slice skip, 4 averages, 8-cm field of view) shows myxoid degeneration of fibers of outer anulus. Alternating regions of higher-signal-intensity material (myxoid degeneration) are between low-signal-intensity collagen fibers of outer anulus (*long solid arrows*). Note vertical bar of fibers in central posterior outer anulus (*short solid arrows*). Posterior longitudinal ligament is seen (*open arrow*) covering basivertebral vein, which is filled with air.

F, Histopathologic section shows collagen fibers of outer anulus (*black arrows*), which are separated by myxoid material (*white arrows*). (H and E, original magnification ×40).

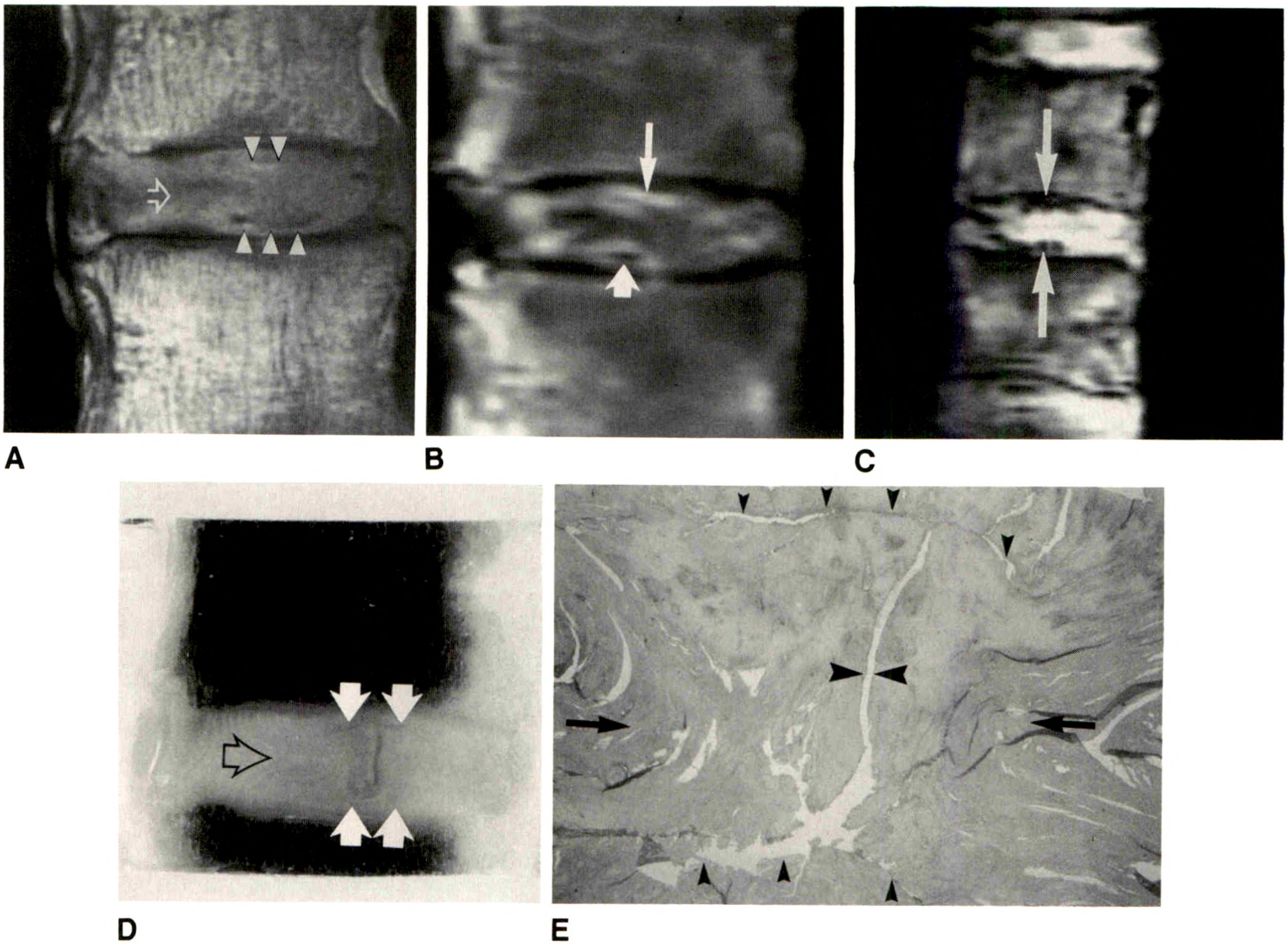

Fig. 4.—Disk degeneration with separation between nucleus pulposus and hyaline cartilage endplate in specimen disk.

A, Sagittal MR image (SE 600/20, 256 × 256 matrix, 3 mm thick, 4 averages, 8-cm field of view, 5-in. [13-cm] receive-only surface coil) shows infolding (*arrow*) and separation of nucleus pulposus and inner anulus from hyaline cartilage endplate (*arrowheads*).

B, Sagittal MR image (SE 2500/80, 258 × 256 matrix, 5 mm thick, 2 averages, 16-cm field of view, 5-in. receive-only surface coil) shows that site of separation superiorly has a linear area of high signal intensity (*long arrow*), probably due to fluid, whereas inferior site is hypointense (*short arrow*) due to gas.

C, Sagittal MR image (gradient-recalled acquisition in the steady state 22.75/12.5, 30° flip angle, 256 × 128 matrix, 24-cm field of view, 5 mm thick, 2 averages) shows multiple oval areas of signal void (*arrows*) representing pockets of gas at sites of separation.

D, Photograph of tissue block shows I-beam shape of sites of separation (*solid arrows*) and infolding of outer anular fibers (*open arrow*).

E, Photomicrograph from macrosection staining shows fibrin-lined clefts of separation within shrinking nucleus pulposus. Clefts have joined through a central vertical fibrin-lined cleft forming an I-beam shape (*arrowheads*). This vertical cleft was not seen on MR. Note infolding of fibers of outer anulus (*arrows*). (H and E, original magnification ×40)

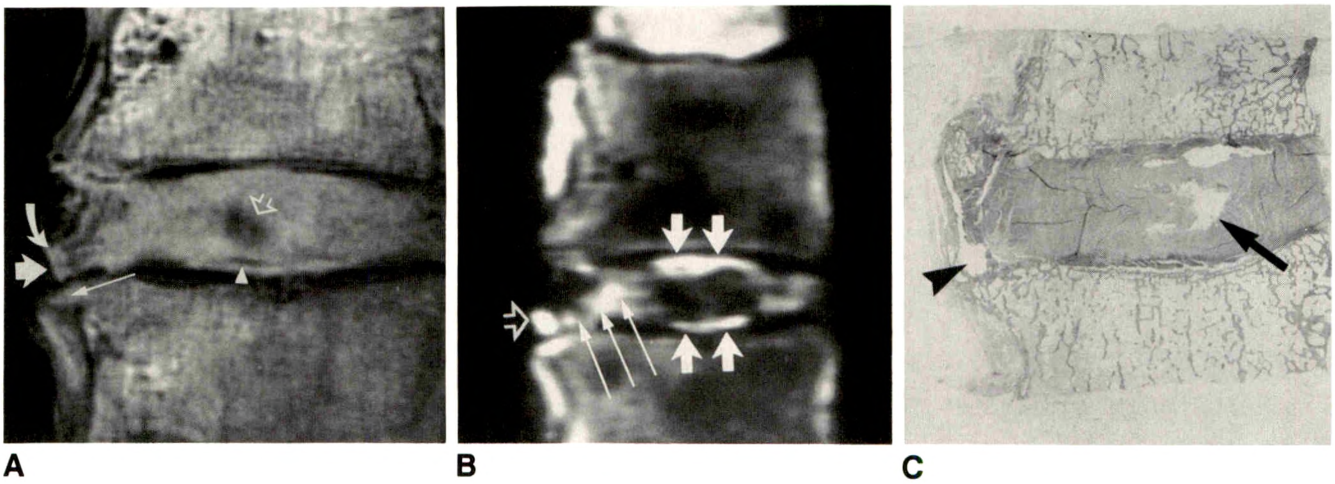

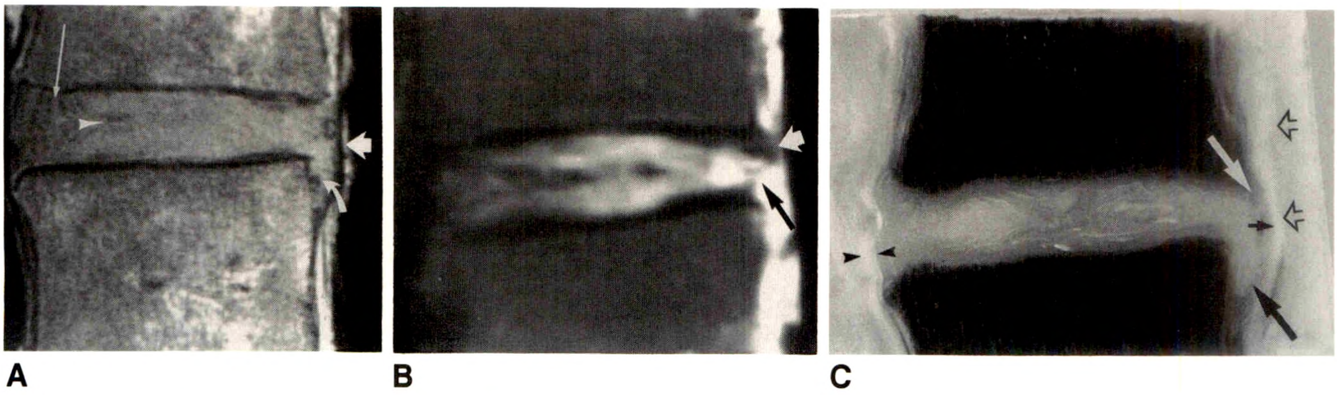

Fig. 6.—Herniation retained by posterior longitudinal ligament in specimen disk.

***A*, Sagittal MR image (SE 600/20, 0.6-mm slice skip, 256 × 256 matrix, 3 mm thick, 4 averages, 8-cm field of view) shows a posterior herniation (extruded disk) retained by posterior longitudinal ligament (*short straight arrow*). Note site of avulsion of Sharpey's fibers (*curved arrow*) and infolding of anterior outer anular fibers (*arrowhead*) with intervening region of myxoid degeneration (*long straight arrow*).**

***B*, Sagittal T2-weighted MR image (SE 2500/80, 5 mm thick, 1-mm slice skip, 128 × 256 matrix, 16-cm field of view, 2 averages, 5-in. [13-cm] receive-only surface coil) shows same posterior herniation (*black arrow*). Collection of posterior anular fibers and Sharpey's fibers posteriorly (*white arrow*) together have the appearance of a hanging cherry.**

***C*, Photograph of tissue block shows retained posterior herniation (*long solid black arrow*) and white posterior longitudinal ligament (*short solid black arrows*). Anterior longitudinal ligament also can be seen as a white structure (*arrowheads*). Coalescence of fibers of posterior outer anulus and Sharpey's fibers seen in *B* is seen immediately posterior to posterior inferior vertebral endplate (*white arrow*).**

ACKNOWLEDGMENT

This paper is dedicated to Michael D. Fallon, who died in the fall season of 1990. We grieve his early departure from this earth.

REFERENCES

1. Aguila LA, Piraino DW, Modic MT. The intranuclear cleft of the intervertebral disk: magnetic resonance imaging. *Radiology* **1985**;155:155–158
2. Yu S, Sether LA, Ho PSP, Wagner M, Haughton VM. Tears of the anulus fibrosus: correlation between MR and histopathologic findings in cadavers. *AJNR* **1988**;9:367–370
3. Grenier N, Greselle JF, Vital JM, et al. Normal and disrupted lumbar longitudinal ligaments: correlative MR and anatomic study. *Radiology* **1989**;171:197–205
4. Masaryk TJ, Ross JS, Modic MT, Boumphrey F, Bohlman H, Wilber G. High-resolution MR imaging of sequestered lumbar intervertebral disks. *AJR* **1988**;150:1155–1162

◄ Fig. 5.—Intradiskal herniation in a specimen disk.

***A*, Sagittal MR image (SE 600/20, 256 × 256 matrix, 4 averages, 3 mm thick, 1-mm slice skip, 8-cm field of view, 5-in. [13-cm] surface coil) shows intradiskal herniation (dissection of nucleus pulposus material through fibers of outer anulus but not past Sharpey's fibers), separation of nucleus pulposus from hyaline cartilage endplate (*arrowhead*), and anterior avulsion of anterior fibers of outer anulus (*curved arrow*). Fused portions of Sharpey's fibers and anterior longitudinal ligament are intact (*short solid arrow*). Note inferior osteophyte, which contains fatty marrow (*long solid arrow*). Also seen is infolding with a central dot (*open arrow*).**

***B*, Sagittal MR image (SE 2500/80, 128 × 256 matrix, 2 averages, 5 mm thick, 16-cm field of view, 5-in. surface receive-only coil) shows linear area of high signal intensity in separation sites (*short solid arrows*) and low signal intensity of remaining inner anulus. Herniated nucleus pulposus has dissected through barrier of outer anulus leaving a tract of high signal intensity (*long solid arrows*) and lies at anterior inferior corner of disk endplate (*open arrow*).**

***C*, Photograph of histopathologic section shows that fixation process has removed most of nucleus pulposus from center of disk (*arrow*) and from its anterior site of herniation (*arrowhead*). At ×100, however (*not shown*), this anterior herniation site did show evidence for extruded nuclear material.**

Book Review

Tissue Characterization in MR Imaging. Clinical and Technical Approaches. Edited by H. Peter Higer and Gernot Bielke. New York: Springer-Verlag, 340 pp., 1990. $149

This text is a formalized collection of papers presented at a European workshop held in 1989. The contents are divided into two general sections: (1) methods and techniques and (2) clinical results. Methods and techniques contains a number of discussions of relaxation parameters (14 presentations on estimation approaches, fundamental limitations, and comparative analyses of measurement techniques). A section on signal mechanisms and influences contains four good papers on types of MR contrast agents, and the section on pattern recognition contains nine papers on feature analysis of MR images. The general section on clinical results contains discussions of the musculoskeletal system, body, breasts, head and brain, and miscellaneous organ systems.

It appears that the goal of the proceedings was to identify the information (exclusive of flow, perfusion, or spectrascopic analysis) that can be gleaned from the MR signal and used to improve diagnosis. The general (although unwritten) message is that by itself the morphologic information of MR images does not tell the whole story.

Unfortunately, although the appeal of the usefulness of MR parameters (T1, T2, spin density) has increased with the introduction of contrast agents and other paramagnetic species (either administered or injected), the use of these parameters does not appear to have added value to the nonmorphologic data.

One presentation, "Comparison of Algorithms for the Decomposition of Multiexponential Relaxation Processes Using SUNRISE," by Staemmler et al. shows nicely the ability of analytical techniques to separate multicompartmental relaxation processes. The authors constructed a phantom with two separate tanks that were imaged concurrently. The two tanks contained materials that had different T2 times. The analytic techniques used readily separated the values of the "unknown" T1 and T2 phantom materials. Thus, the authors conclude that the limitation in performing tissue characterization is not faulty mathematical analysis. Most likely, it is the complexity of the tissue under study. In other words, identifying the relaxation processes of a tumor is not altogether different from trying to answer the question, "What is the density of a Chevrolet?"

One of the shortcomings of the text is the lack of an invited presentation on acceptably normal T1 and T2 values for commonly encountered tissues. T1 and T2 values can be measured in a variety of ways; however, it would be nice in a text such as this to have a paper specifying *nominally* accurate relaxation values within the realm of clinically specified pulse sequences and magnet field sizes. Another shortcoming is the substantial limitations in the discussion of the relaxation parameter T1; only two presentations address this parameter.

When the dependence on signal intensity and flow (motion) is considered, it does not appear reasonable to exclude discussions of the effects of motion on accuracy of T1 and T2 data. This is a well-known phenomenon; however, it is not addressed in this text.

The clinical result section has little new information. The exception is a discussion on trace paramagnetic metal contents in the gastrointestinal tract and bone marrow by Ranade et al., which demonstrates the surprisingly large variety of paramagnetic species that can affect any measured relaxation time.

In summary, it is not clear to me what specific audience would be interested in this collection of papers. Obviously, research is continuing in the analysis of MR signals with respect to tissue characterization in the hope of identifying pathologic-specific relaxation rates. Although the limited number of color plates in the text contribute little to the understanding of the concepts presented by the authors, they probably added dearly to the cost of the book.

It is difficult to recommend that this text be purchased for general radiologic library usage, and the cost of the book ($149) is not insignificant. More appropriately, it should be located in a research laboratory. However, persons in this active field of research may use a collection of refereed articles in lieu of this text.

William Pavlicek
Mayo Clinic
Rochester, MN 55905

Overall Body Fat and Regional Fat Distribution in Young Women:

Quantification with MR Imaging

Elizabeth L. Gerard[1]
Rachel C. Snow[2]
David N. Kennedy[1]
Rose E. Frisch[3]
Alexander R. Guimaraes[1]
Robert L. Barbieri[4,5]
A. Gregory Sorensen[1]
Thomas K. Egglin[1]
Bruce R. Rosen[1]

Overall body fat and its distribution in different regions are important predispositions to known aberrations in lipid and glucose metabolism. The accuracy of MR imaging in estimating overall body fatness and regional fat distribution at individual landmarks was determined by comparing it with well-accepted measures by deuterium-oxide (D_2O) dilution and bioimpedance analysis. Fourteen normal young women (athletes and control subjects) were studied. A total of 308 axial, T1-weighted, spin-echo MR images over a specific region in the trunk (21–24 scans per subject) were obtained. Morphometric computer image analysis was performed to determine the subcutaneous, internal, and total fat volumes in each image. The data were analyzed in two ways: data from all slices were summed to assess overall body fatness, and six anatomic landmarks were chosen for regional comparisons. MR-determined estimates of overall body fatness strongly correlated with total body fat measures by D_2O dilution in both total fat ($r = .91$) and subcutaneous fat ($r = .92$) determinations. Athletes in both the low- and high-intensity training phases had significantly lower values of MR-determined total body fatness than did control subjects. Parallel to total body fatness, athletes had significantly lower MR-determined ratios of total fat/total volume in four of six individual landmarks compared with control subjects.

Our experience suggests that MR is an accurate method to quantify overall body fatness, when compared with D_2O dilution and bioimpedance analysis. MR could also discriminate regional components of subcutaneous and internal body fat at individual landmarks.

***AJR* 157:99–104, July 1991**

The quantity and regional distribution of body fat have important physiological implications. Numerous methods are used to estimate the overall fatness of the body, with errors obtained from these methods ranging from 3% to 15% [1]. In addition, these methods are limited by their inability to delineate regional fat differences of subcutaneous and internal fat depots. CT has demonstrated good spatial resolution in measuring regional adipose tissue distributions [1–11]; however, the radiation exposure incurred by CT precludes widespread use of this technique. Better computer image analysis and the noninvasiveness of MR imaging make it potentially an ideal tool with which to quantify subcutaneous and internal fat stores over large regions of the body [12]. Validation of this possibility against well-established standards is necessary.

The purpose of this investigation was to obtain spin-echo MR images in a group of young women athletes and control subjects in order to (1) document errors of reproducibility of MR body fat quantification by using repeated measurements in subjects; (2) validate MR-determined estimates of relative fatness by comparison with measurements from deuterium-oxide (D_2O) dilution and estimates from bioimpedance analysis (BIA); and (3) investigate the feasibility of MR for quantifying regional fat distributions of subcutaneous and internal fat stores.

Received October 15, 1990; accepted after revision January 25, 1991.

This work was supported in part by public health grant numbers RO1-HD23536 and RO1-CA40303.

[1] Department of Radiology, Massachusetts General Hospital, NMR Imaging Center, 13th St., Bldg. 149E, Charlestown, MA 02129. Address reprint requests to B. R. Rosen.

[2] Department of Population Sciences, Harvard School of Public Health, 665 Huntington Ave., Boston, MA 02115.

[3] Center for Population Studies, 9 Bow St., Cambridge, MA 02138.

[4] Department of Obstetrics and Gynecology, Brigham and Women's Hospital, 75 Francis St., Boston, MA 02115.

[5] Present address: Department of Obstetrics and Gynecology, Health Science Center, T-9, Rm. 0-20, SUNY at Stony Brook, Stony Brook, NY 11794.

0361-803X/91/1571-0099
© American Roentgen Ray Society

Subjects and Methods

As part of a larger study of estrogen metabolism in women who exercise, five oarswomen athletes and four nonathletic control subjects were studied. A total of 14 MR images were obtained. The five female athletes, of mean age (± SEM) 25.4 ± 1.1 yr and mean height 170.7 ± 2.8 cm, were studied during a phase of low-intensity training (mean weight, 65.5 ± 1.8 kg) and 4 months later, during a phase of high-intensity training (mean weight, 62.8 ± 2.0 kg). The four female control subjects were of mean age 21.8 ± 1.2 yr, mean height 162.7 ± 5.8 cm, and mean weight 60.8 ± 3.9 kg. Informed consent was obtained from all subjects.

MR imaging was performed on a 0.6 Clinical Imager (Teslacon, Technicare). T1-weighted spin-echo pulse sequences were chosen to enhance fat image contrast. Axial T1-weighted (400/20 [TR/TE], four excitations, 20-mm slice thickness, 25% gap) spin-echo MR images were obtained over a specific volume delineated by upper and lower internal landmarks (from the level of the fifth thoracic vertebral body, T5, to the initial cleavage of the legs), comprising 21–24 axial images per subject.

In order to measure structure and form, morphometric analysis of the subcutaneous and internal fat for each image was performed on a Sun (Model 4/260) computer, with semiautomated image segmentation software previously described [13, 14]. On the basis of an image signal intensity selected by the investigator, intensity contours create a continuous outline that approximates the border location (segmentation). In this study, in order to determine the subcutaneous fat borders, an intensity contour was created for the innermost and outermost extents of the subcutaneous fat region. The RF homogeneity was adequate for clearly distinguishing fat from the surrounding tissues. The subcutaneous fat area was then determined by subtracting the area of the inner border from the total area in each slice. These measurements were made by the same operator for all patients.

Owing to the greater complexity of internal fat distribution, the intensity contour value selection for internal fat was facilitated by the use of an image intensity histogram (number of pixels for each intensity value), determined from the region within the inner border of the subcutaneous fat. Different tissue types were represented as transition points in the image intensity distribution. Intensity contours from the transition points were evaluated by a single operator to determine the best representation of the internal fat outlined. The area contained within the internal fat region was obtained by integration of the histogram for intensity values greater than the selected contour value. This process was applied for each image individually to account for possible inter- and intrapatient variation in signal intensities. Figure 1 shows the results of segmentation of both the subcutaneous and the internal fat at landmark L4 in an athlete and a control subject.

Each pixel area, once determined, can be converted to volume by multiplication of the pixel dimensions and the effective slice thickness [13]. The effective slice thickness is determined by the actual slice thickness plus the gap thickness (half of each gap, above and below). Volumes determined in this manner implicitly assume that each slice provides an average measure of border location within the slice and a linear interpolation between slices. The accuracy of our planar measurement of area, and our subsequent determination of volume, was validated previously [14]. Our system has a gradient linearity of better than 1% in each linear direction over a 25-cm sphere. This implies a less than 3% variation in voxel volume over this region.

The reproducibility of fat morphometric determinations was measured in vivo in four subjects. Two determinations per subject in six anatomic landmarks on the same image were performed for the subcutaneous and internal fat measures. An average coefficient of variation was determined for both subcutaneous and internal fat measures.

The volumetric measures determined in each axial slice were the following: total volume, subcutaneous fat volume, and internal fat volume. Total fat was calculated from the addition of subcutaneous fat and internal fat in each slice. The following ratios were then determined: total fat to total volume (TF/TV%), subcutaneous fat to total volume (SF/TV%), and internal fat to total volume (IF/TV%). In addition, the relative proportion of subcutaneous fat to total fat was determined (SF/TF%). The corresponding ratio of internal fat to total fat was thus equal to 100 − (SF/TF%).

The data from each subject were analyzed in two ways. For the first analysis, six specific anatomic slices were chosen for regional comparisons. For the second analysis, data from all slices were summed over the total volume to determine total body fat indices. The six individual anatomic landmarks chosen for each subject for regional comparisons of TF/TV% and SF/TF% corresponded to the vertebral bodies of thoracic five (T5), lumbar one (L1), lumbar four (L4), sacral one (S1), sacral four (S4), and femoral fat at the initial cleavage of the legs (FF).

An index of overall relative fatness was determined in each subject by summing all individual slices, from the upper landmark to the lower landmark, to obtain a total fat/total volume ratio ($TF/TV\%_{total}$). The respective subcutaneous ($SF/TV\%_{total}$) and internal fat ($IF/TV\%_{total}$) components were similarly summed over this volume. To measure the relative proportions of subcutaneous fat to overall body fat, we also determined the subcutaneous fat/total fat ratio over this volume ($SF/TF\%_{total}$).

Within 7 days of the MR study, subjects underwent D_2O dilution and BIA to quantify total body water (TBW), a measure of lean body mass. In order to estimate relative fatness, fractional water (TBW/body wt%) values, which are inversely proportional to the percentage of body fat [15], were determined. D_2O was determined by measuring the concentration of excess deuterium atoms in plasma water 3 hr after the oral administration of 50 g of 99.8 atom% (Sigma Chemical Co., St. Louis, MO). D_2O concentration was measured by infrared

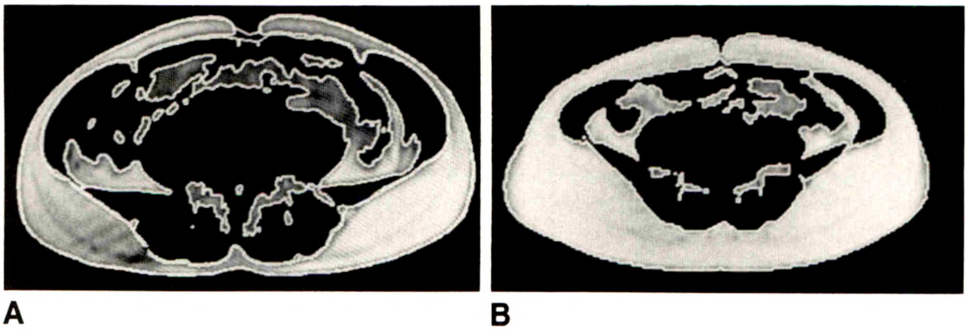

Fig. 1.—*A* and *B*, Axial scans at level of L4 in an athlete (*A*) and a control subject (*B*) show intensity contour outlines of subcutaneous and internal fat.

spectrophotometry (Foxboro Co., South Norwalk, CT); TBW was calculated by the isotope dilution principle [15, 16] (coefficient of variation of D_2O measurements was 4.0%). Total body resistivity (ohms) was measured by BIA with a four-terminal impedance analyzer (RJL Systems, Detroit, MI) for each subject after an overnight fast. The analyzer determined the voltage drop of an excitation current of 800-μA alternating current at 50 kHz from the wrist to the ankle. TBW was estimated from ohms, height, weight, and age by using different equations for oarswomen (Snow RC, unpublished data) and control subjects [17].

Statistical analysis was done with the Stat-view 512+ software (BrainPower Inc, Calabasas, CA) [18]. Repeated measurements of the five athletic females conducted at two different phases of the training year were included in the regression analyses of TBW/wt% on MR values as independent observations. Statistical support for the treatment of these repeated measurements as independent observations was obtained as follows. We used a repeated-measurements analysis of variance (ANOVA) model (BMDP3V) [19] and found the subject error component to be zero, signifying that the intrasubject variability was greater than or equal to the intersubject variability. As further support for the independence of the repeated measures among athletes, the (observed-predicted) residuals for phase I and phase II measures on individual athletes were not correlated ($r = -.15$, $p = .81$). In addition, simple linear regressions of D_2O-determined TBW/body wt% on MR-determined total fat at individual landmarks were performed. To determine if differences in these individual correlations were statistically significant, we did a single-factor ANOVA, and multiple pairwise comparisons were done with the Student-Newman-Kuels test [20].

Results

Errors of Reproducibility

Reproducibility of the morphometric measures was achieved by two determinations of both the subcutaneous and internal fat for each subject at six landmarks in four subjects, using the same image. The average coefficient of variation was 3% for subcutaneous fat measures and 9% for internal fat measures. Reproducibility of the image acquisition was not determined.

MR Findings Compared with Measures of Total Body Water

To validate the application of MR imaging in estimating overall relative fatness, we compared the MR findings with the D_2O dilution measurements of fractional water (TBW/body wt%), an index inversely proportional to body fat, as previously described (Fig. 2). Significant correlations were seen between the D_2O dilution TBW/body wt% values and the MR-determined indices of $\text{TF/TV\%}_{\text{total}}$ ($r = .91$, $p < .0001$), as well as the corresponding subcutaneous fat component, $\text{SQ/TV\%}_{\text{total}}$ ($r = .92$, $p < .0001$). The corresponding internal fat measures of $\text{IF/TV\%}_{\text{total}}$ also correlated with D_2O dilution TBW/body wt% ($r = .72$, $p < .004$). MR findings were then compared with BIA, an indirect measure of fractional body water: significant correlations were seen between the BIA-

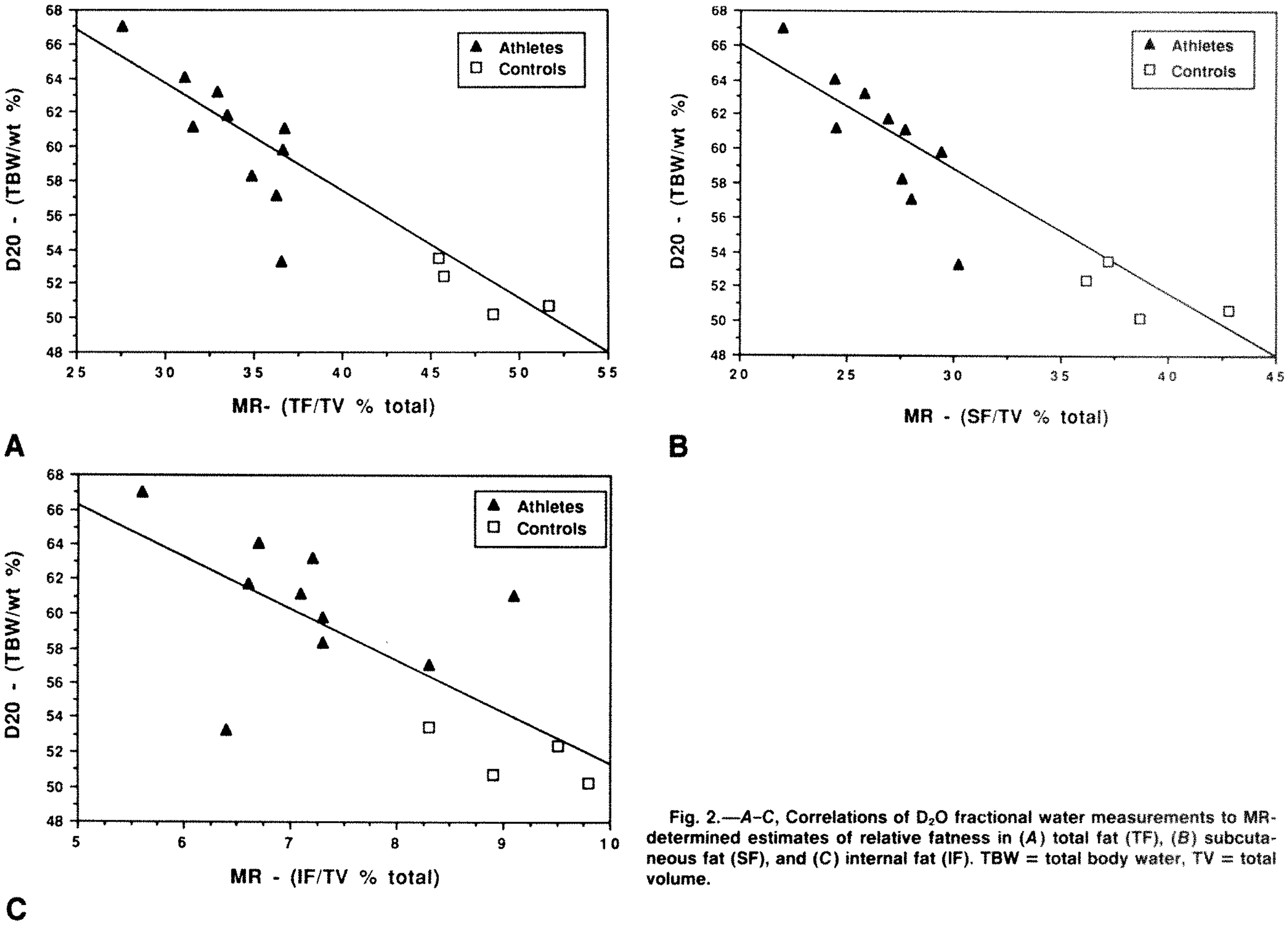

Fig. 2.—*A–C*, Correlations of D_2O fractional water measurements to MR-determined estimates of relative fatness in (*A*) total fat (TF), (*B*) subcutaneous fat (SF), and (*C*) internal fat (IF). TBW = total body water, TV = total volume.

determined TBW/body wt% and the MR-determined TF/TV%$_{total}$ ($r = .92$, $p < .0001$).

In the endocrine literature, it is of interest to observe whether one landmark correlates highly with indices of overall body fatness. To determine which individual landmarks were correlated with the D_2O dilution measurements, we performed simple linear regressions of D_2O-determined TBW/body wt% on MR-determined TF/TV% at each landmark. In decreasing order, the correlations of the individual landmark TF/TV% with D_2O dilution values were FF ($r = .91$, $p < .0001$), S1 ($r = .87$, $p < .0001$), L1 ($r = .80$, $p < .0006$), L4 ($r = .78$, $p < .001$), T5 ($r = .64$, $p < .02$), and S4 ($r = .57$, $p < .05$). Although the use of individual landmarks appeared to correlate well with D_2O dilution measurements, the small sample size precluded definition of statistically significant intergroup differences at individual landmarks.

MR Fat Values Across Subject Groups

Values of TF/TV%$_{total}$ (mean ± SEM) were significantly lower in athletes during low-intensity training phase I (35 ± 0.8%) and high-intensity training phase II (33 ± 1.7%), as compared with control subjects (48 ± 1.5%). Similarly, values of SQ/TV%$_{total}$ were significantly lower in athletes during phase I (28 ± 0.7%) and phase II (26 ± 1.3%), as compared with control subjects (39 ± 1.5%; Table 1).

Interestingly, when comparing the summed subcutaneous fat to the total fat over all scans (SQ/TF%$_{total}$), significant differences were not seen between athletes in either phase as compared with control subjects. All group means were approximately 80%.

Regional Fat Differences

Differences were seen in the total fat to total volume (TF/TV%) at individual landmarks (Fig. 3A). In both athletes and control subjects, the highest values of TF/TV% were seen at the level of the femoral fat at the initial cleavage of the legs. The lowest values were seen at the level of L1.

Similar to the summed total fat to total volume over all scans (TF/TV%$_{total}$), regional differences in TF/TV% measures between athletes at both training intervals were significantly less ($p < .01$) at all landmarks except two (S1 and S4), as compared with control subjects (Fig. 3A). Similar to the summed subcutaneous fat to total fat over all scans (SF/TF%$_{total}$), values of SF/TF% at individual landmarks were, in general, not significantly different between subject groups (Fig. 3B).

TABLE 1: Mean (SEM) Body Fat Values in Athletes and Control Subjects

Body Fat	Athletes I	Athletes II	Control Subjects
TF/TV%$_{total}$	35 (0.8) $p < .0001$	33 (1.7) $p < .0003$	48 (1.5)
SF/TV%$_{total}$	28 (0.7) $p < .0002$	26 (1.3) $p < .0003$	39 (1.5)
IF/TV%$_{total}$	7 (0.5) $p < .0002$	7 (0.4) $p < .008$	9 (0.3)
SF/TV%$_{total}$	79 (1.2) $p < .26$	79 (0.6) $p < .05$	81 (0.8)
IF/TF%$_{total}$	21 (1.2) $p < .26$	21 (1.4) $p < .05$	19 (0.8)

Note.—TF = total fat, TV = total volume, SF = subcutaneous fat, IF = internal fat.

Discussion

In this investigation of the ability of MR imaging to quantify body fat in young women over a specific volume of the trunk, there were three major findings. (1) MR imaging provided a reproducible means of measuring total and regional body fat, with subcutaneous stores measured with higher reproducibility than internal fat stores. MR determinations of relative body fatness were strongly correlated with total body fat as measured by D_2O dilution methods. (2) Regional differences in fat measures at specific landmarks were determined. The landmark with the highest total fat/total volume was the femoral fat at the initial cleavage of the legs. (3) Athletes and nonathletes did not differ significantly in either the ratio of subcutaneous fat to total fat at individual landmarks or over the entire volume.

Total Body Fat Measures

Total body fat as a percentage of body weight is associated with changes in estrogen metabolism and ovarian function in women. Low relative fatness is associated with increased estrogen 2-hydroxylase oxidation in some women [21], and also with anovulation [22]. Skinfold measures are one of the more commonly used measures; however, much evidence exists that they do not necessarily correlate with total body fatness [23]. D_2O dilution provides one of the best estimates of overall relative leanness, with fractional body water inversely correlated with the percentage of body fat. BIA provides an indirect measurement of total body water and is easily applied in the field. In this investigation, MR-determined total fat and subcutaneous fat measurements were strongly correlated with both D_2O dilution measurements and BIA measures. The similar, strong correlations of total fat measures and subcutaneous fat measurements to D_2O dilution measurements is not surprising, because subcutaneous fat accounted for 80% of the total fat. In a study of eight women, Sjostrom et al. [4] found comparable correlations of body fat determined by CT and tritium dilution methods ($r = .93$). General use of CT, however, is limited by the radiation exposure [4]. Staten et al. [12] showed that the body fat determined by MR imaging in six patients at three specific landmarks was highly correlated with the body fat determined by hydrostatic weighing. Our study extended these results by correlating MR findings with more accurate measures, such as D_2O dilution, and by imaging over a larger body volume.

Regional Body Fat Measures

The literature increasingly supports the importance of quantifying regional differences in body fat distribution, as well as delineating subcutaneous and internal fat depots. Obesity is well established as a risk factor in coronary heart disease among men, and recent literature supports this association among women [24]. Furthermore, it is known to be the regional distribution of body fat that determines risk [25–29]. The preponderance of body fat deposition above the umbilicus (android obesity) is more positively associated with diabetes, gout, hyperlipidemia, hypertension, and atheroscler-

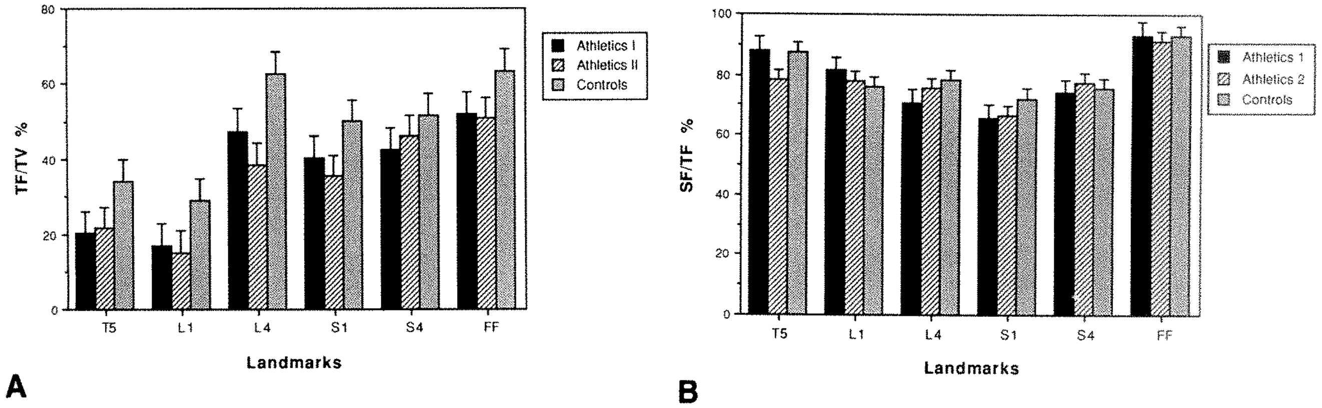

Fig. 3.—*A* and *B*, Regional fat differences between subject groups at individual landmarks (mean with standard error bars) in (*A*) total fat/total volume (TF/TV%) and (*B*) subcutaneous fat/total fat (SF/TF%).

sis than its preponderance in the lower abdomen and femoral region (gynoid obesity) [25]. Thus, upper-body fat distribution in android obesity is a better predictor of cardiovascular disease than is the overall degree of obesity in both men [28] and women [29]. Conventional methods of total body fat quantification cannot discriminate regional deposition of fat. The regional distribution of subcutaneous and internal fat stores have been shown in CT studies; however, limited regions of the body were studied [2–11], and regional values could not be validated. In this investigation, after documenting the validity of use of MR imaging to quantify overall body fatness, we explored the ability of MR imaging to noninvasively quantify regional differences in total body fat deposition and to delineate between subcutaneous and internal fat stores at specific landmarks. Like CT, these regional differences in body fat cannot be validated by conventional measures; however, our results at regional landmarks were consistent with overall body fatness.

Regional differences in the total fat measurements at individual landmarks paralleled the trends seen in overall measurements of total fat: athletes in general had significantly lower values than did control subjects. In our study, the landmark with the highest ratio of total fat to total volume was the femoral fat at the initial cleavage of the legs (FF). In a report of body fat determinations by CT in eight men, Borkan et al. [7] demonstrated that the highest percentage of body fat to total area was at L4; however, the scans were limited to the abdomen. Our results in young women contrast with the findings of Borkan et al. in men, supporting the differences in fat distribution between men and women. In addition, our study shows that the single landmark having the highest correlation with D_2O dilution measurements was the femoral fat region ($r = .91$); however, caution must be used because of the small sample size. In a report measuring body fat in eight females by using CT, Kvist et al. [1] determined that body fat measured at L4 showed a higher correlation than any other single scan with the CT-determined total fat volume, comprising 22 scans. In Kvist's study, however, the body fat at individual landmarks was not correlated with such independent measurements as D_2O dilution. Further study with additional subjects is needed to determine more definitively if one scan, or selective scans, could be used as an accurate index of body fatness.

Recent literature has demonstrated interesting differences in regional variations in subcutaneous fat and internal fat stores relative to the total fat in specific diseases. Internal fat stores were increased at the level of the umbilicus in patients with Cushing disease [2, 3], whereas the subcutaneous stores were reduced in patients with anorexia compared with control subjects [3]. In this investigation, we studied young, healthy women who differed in their degree of fitness. Neither total nor regional ratios of subcutaneous fat to total fat differed significantly between athletes and control subjects. This implies that the decreased total fat observed in the athletic women as compared with control subjects was a result of decreases in equal proportions of subcutaneous and internal fat stores.

Improvements in this method should be directed toward the measurement of the internal fat. Like CT, internal fat measures with MR imaging are hampered by the degree of partial volume effects. Improvements in the internal fat measures can thus be made by using thinner slices. Unlike CT, MR imaging is more sensitive to bowel and respiratory motion. These can be reduced either by increasing the number of signal averages or by using rapid scanning techniques. Other factors, such as B1 and gradient inhomogeneities, will also lead both to geometric and signal-intensity variations across the image plane. Proper gradient and RF tuning should minimize these errors. In this study, the reproducibility of our internal fat measure was found to be 9%. It is important to note that the internal fat encompassed approximately 20% of the total fat; thus, this error had a small effect on the total body fat determination. Although the reproducibility of our image acquisition technique could not be determined given the design of our study, our results are comparable with those reported by another MR study of body fat determination, which cited the reproducibility of both image acquisition and morphometric analysis to be less than 10% for internal fat and less than 5% for subcutaneous fat [12].

Summary

This study demonstrates that MR imaging is accurate for the noninvasive measurement of body fat in a population of young women. After finding strong correlations between MR imaging and D_2O dilution measurements of overall body fatness, MR was used to determine regional fat differences. Unlike conventional measures that are limited to measuring total body fatness, MR imaging can specifically measure regional fat differences in subcutaneous and internal fat stores without ionizing radiation. From a clinical point of view, the regional distribution of fat is more predictive of cardiovascular disease and other metabolic complications of obesity than is overall fatness [25-29]. Thus, the ability of MR imaging to quantify regional fat distribution noninvasively gives it the potential to screen for predisposition to these diseases. Although this method was studied in a population of normal young women, the extension of this method in a more diverse population should be possible.

Other areas of research in body fat demonstrate correlations between morphology, hormonal sensitivity, and metabolic behavior of adipocytes from different regions, as well as the metabolic complications of obesity [26, 27, 30-33]. For example, studies of fat cells from different regions reveal that subcutaneous abdominal fat cells are larger and have higher rates of lipolysis in android obese women than in gynoid obese women, potentially explaining observed metabolic aberrations [27]. Future applications of MR in lipid physiology may be the use of MR-localized spectroscopy to determine the heterogeneity of the metabolic behavior of body fat in different regions in vivo. Combined with detailed regional morphometric analysis, these techniques should allow the use of MR technology to address fundamental issues of lipid physiology in humans.

ACKNOWLEDGMENTS

We thank Holly F. Brink and Jo Anne Fordham for their assistance in preparation of this manuscript. Technical assistance was provided by Bernice E. Hoppel and James M. Vevea.

REFERENCES

1. Kvist H, Sjostrom L, Tylen U. Adipose tissue volume determination in women by computed tomography: technical considerations. *Int J Obes* **1986**;10:53-67
2. Enzi G, Gasparo M, Biondetti P, Fiore D, Semisa M, Zurlo F. Subcutaneous and visceral fat distribution according to sex, age, and overweight, evaluated by computed tomography. *Am J Clin Nutr* **1986**;44:739-746
3. Mayo-Smith W, Hayes CW, Biller BMK, Klibanski A, Rosenthal H, Rosenthal D. Body fat distribution measured with CT: correlations in healthy subjects, patients with anorexia nervosa, and patients with Cushing syndrome. *Radiology* **1989**;170:515-518
4. Sjostrom L, Kvist H, Cederblad A, Tylen U. Determination of total adipose tissue and body fat in women by computed tomography, 40K, and tritium. *Am J Physiol* **1986**;250:E736-E745
5. Ashwell M, Cole TJ, Dixon AK. Obesity: new insight into the anthropometric classification of fat distribution shown by computed tomography. *Br Med J* **1985**;290:1692-1694
6. Dixon AK. Abdominal fat assessed by computed tomography: sex difference in distribution. *Clin Radiol* **1983**;14:189-191
7. Borkan GA, Gerzof SG, Robbins AH, Hults KE, Silbert CK, Silbert JE. Assessment of abdominal fat content by computed tomography. *Am J Clin Nutr* **1982**;36:172-177
8. Grauer WO, Moss AA, Cann CE, Goldberg HI. Quantification of body fat distribution in the abdomen using computed tomography. *Am J Clin Nutr* **1984**;39:631-637
9. Borkan GA, Hultz DE, Gerzof SF, Robbins AH, Silbert CK. Age changes in body composition revealed by computed tomography. *J Gerontol* **1983**;38:673-677
10. Sparrow D, Borkan GA, Gerzof SG, Wisniewski C, Silbert CK. Relationship of fat distribution to glucose tolerance: results of computed tomography in male participants of the normative aging study. *Diabetes* **1986**;35:411-415
11. Seidell JC, Oostenlee A, Thijssen MAO, et al. Assessment of intrabdominal and subcutaneous abdominal fat: relation between anthropometry and computed tomography. *Am J Clin Nutr* **1987**;45:7-13
12. Staten MA, Totty WG, Kohrt WM. Measurement of fat distribution by magnetic resonance imaging. *Invest Radiol* **1989**;24:345-349
13. Kennedy DN, Filipek PA, Caviness VS. Anatomic segmentation and volumetric calculations in nuclear magnetic resonance imaging. *IEEE Trans Med Imaging* **1989**;8:1-7
14. Filepek PA, Kennedy DN, Caviness VS, Rossnick SL, Spraggins TA, Starewicz PM. Magnetic resonance imaging-based brain morphometry: development and application to normal subjects. *Ann Neurol* **1989**;25:61-67
15. Schloerb PR, Friis-Hansen BJ, Edelman IS, Solomon AK, Moore FD. The measurement of total body water in the human subject by deuterium oxide dilution, with a consideration of the dynamics of deuterium distribution. *J Clin Invest* **1950**;29:1296-1310
16. Lukaski HC, Johnson PE. A simple, inexpensive method of determining total body water using a tracer dose of D20 and infrared absorption of biological fluids. *Am J Clin Nutr* **1985**;41:363-370
17. Van Loan M, Mayclin P. Bioelectrical impedance analysis: is it a reliable estimator of lean body mass and total body water? *Hum Biol* **1987**;59:299-309
18. Feldman D, Gagnon J, Hofmann R, Simpson J. *Statview 512+ interactive statistics and graphics package, version 1.1.* Calabasas, CA: Brainpower, **1986**:89-102
19. Winer, BJ. *Statistical principles in experimental design*, 2nd ed. New York: McGraw-Hill, **1971**
20. Zar JH. *Biostatistical analysis*. Englewood Cliffs, NJ: Prentice-Hall, **1984**:162-166, 190-191
21. Snow RC, Barbieri RL, Frisch RE. Estrogen 2-hydroxylase oxidation and menstrual function among elite oarswomen. *J Clin Endocrinol Metab* **1989**;69:369-376
22. Frisch R. Fatness, menarche, and female fertility. *Perspect Biol Med* **1985**;28:611-615
23. Cohn SH, Ellis KJ, Vartsky D, et al. Comparison of methods of estimating body fat in normal subjects and cancer patients. *Am J Clin Nutr* **1981**;34:2839-2847
24. Manson JE, Colditz GA, Stampfer MJ, et al. A prospective study of obesity and risk of coronary heart disease in women. *N Engl J Med* **1990**;322:882-889
25. Vague J. The degree of masculine differentiation of obesities: a factor determining predisposition to diabetes, atherosclerosis, gout, and uric calculous disease. *Am J Clin Nutr* **1956**;4:20-34
26. Krotkiewski M, Bjorntorp P, Sjostrom L, Smith U. Impact of obesity on metabolism in men and women: importance of regional adipose tissues distribution. *J Clin Invest* **1983**;72:1150-1162
27. Kissebah AH, Vydelingum N, Murray R, et al. Relation of body fat distribution to metabolic complications of obesity. *J Clin Endocrinol Metab* **1982**;54:254-260
28. Larsson B, Svardsudd K, Welin L, Wilhelmsen L, Bjorntorp P, Tibblin G. Abdominal adipose tissue distribution, obesity, and risk of cardiovascular disease and death: 13 year follow up of participants in the study of men born in 1913. *Br Med J* **1984**;288:1401-1404
29. Lapidus L, Bengtsson C, Larsson B, Pennert K, Rybo E, Sjostrom L. Distribution of adipose tissue and risk of cardiovascular disease and death: a 12 year follow up of participants in the population study of women in Gothenburg, Sweden. *Br Med J* **1984**;289:1257-1261
30. Evans DJ, Hoffman RG, Kalkoff RK, Kissebah AH. Relationship of body fat tomography to insulin sensitivity and metabolic profiles in premenopausal women. *Metabolism* **1984**;33:68-75
31. Bolinder J, Kager L, Ostman J, Arner P. Differences at the receptor and postreceptor levels between human omental and subcutaneous adipose tissue in the action of insulin on lipolysis. *Diabetes* **1983**;32:117-123
32. Ostman J, Arner P, Engfeldt P, Kager L. Regional differences in the control of lipolysis in human adipose tissue. *Metabolism* **1979**;28:1198-1205
33. Evans DJ, Hoffman RG, Kalkhoff RK, Kissebah AH. Relationship of androgenic activity to body fat topography, fat cell morphology, and metabolic aberrations in premenopausal women. *J Clin Endocrinol Metab* **1983**;57:304-310

Unidirectional Joint Communications in Wrist Arthrography: An Evaluation of 250 Cases

Anthony J. Wilson[1]
Louis A. Gilula
F. A. Mann

Although arthrographically demonstrable communications between various compartments of the wrist occur in older persons without symptoms, similar communications in younger persons may indicate clinically significant posttraumatic ligament tears and other pathologic processes. However, detection of communications varies depending on the arthrographic technique used. It has been claimed that if triple-compartment arthrography is not used in all patients, clinically significant unidirectional ligament tears may be overlooked. We determined the frequency and distribution of unidirectional intercompartmental communications, using a modification of techniques described in the literature. Separate injections of contrast material were made in sequence into the midcarpal, distal radioulnar, and radiocarpal joints of 250 consecutive patients. We found 38 unidirectional communications (17 lunotriquetral, nine scapholunate, three radial capsular, one ulnar capsular, six combined sites, and two indeterminate sites) between the midcarpal and radiocarpal joints. Nine unidirectional communications between the radiocarpal and distal radioulnar joints were found.

Comparison of these results with the frequency and direction of unidirectional communications reported by others suggests that demonstration of communications depends on specific technical factors, such as which joint is injected first, the amount of contrast material used, and the delay between injections. This dependence on technical factors raises questions about the value of routine three-compartment wrist arthrography.

***AJR* 157:105-109, July 1991**

The primary functions of wrist arthrography are to assess directly the integrity of intrasynovial intercarpal ligaments and the triangular fibrocartilage complex and to assess indirectly the status of intracapsular extrasynovial ligaments. At least three reports [1-3] have suggested that it is necessary to inject the midcarpal joint (MCJ), radiocarpal joint (RCJ), and distal radioulnar joint (DRUJ) separately to be certain that all abnormal communications are identified. The contention of these investigators has been that failure to inject all three joints may cause numerous ligament injuries to be overlooked. As ligament injuries can result in significant wrist instability, documentation of these injuries is important for surgical management.

Because the duplication of specific results depends on exact replication of examination technique [4], we were concerned that reported results may not apply to our patients. We therefore studied the frequency and distribution of interjoint communications using our own modification of triple-joint wrist arthrography, in which the midcarpal joint is injected first.

Materials and Methods

A retrospective study of 250 consecutive three-compartment wrist arthrograms was done. The patients had been referred for evaluation of wrist pain or instability between July 1987 and November 1989. Of these 250 patients, 119 were female and 131 male, ranging in age

Received September 27, 1990; accepted after revision January 7, 1991.

Presented at the annual meeting of the American Roentgen Ray Society, Washington, DC, May 1990.

[1] All authors: Mallinckrodt Institute of Radiology, Washington University School of Medicine, 510 S. Kingshighway Blvd., St. Louis, MO 63110. Address reprint requests to A. J. Wilson.

0361-803X/91/1571-0105

© American Roentgen Ray Society

from 12 to 74 years, with a mean age of 26 years and a median age of 30 years.

After obtaining plain radiographs of the symptomatic wrist, a bilateral instability series was performed under fluoroscopic guidance. This series included posteroanterior views in neutral, radial deviation, and ulnar deviation; oblique views; anteroposterior closed-fist views in neutral, radial deviation, and ulnar deviation; lateral views in neutral, radial deviation, ulnar deviation, palmar flexion, and dorsiflexion; off-lateral pisotriquetral views; lateral volar and dorsal stress views; and posteroanterior radial and ulnar stress views.

After the instability series, three-compartment arthrography of the symptomatic wrist was performed. The injection sequence was MCJ, DRUJ, RCJ. In those patients in whom a communication with the RCJ was not demonstrated by MCJ injection, DRUJ injection was performed immediately. In those patients with filling of the RCJ from the MCJ injection, the DRUJ injection was delayed for at least 30 min. Finally, the RCJ was injected approximately 1 hr after the DRUJ injection. Each joint was gradually but fully distended with Conray-43 (Mallinckrodt, Inc., St Louis, MO) until the patient had mild discomfort, with fluoroscopic visualization throughout the injection and frequent spot filming. The actual volume of contrast agent used varied considerably from less than 1 ml in the DRUJ of some patients to more than 5 ml in the MCJ of others. In a few cases, the contrast agent was diluted slightly with lidocaine. The exact site of needle puncture varied and was not recorded. In each case a 23- or 25-gauge needle was inserted into the joint as far from the site of the patient's major symptoms as possible.

After each joint was filled with contrast material, the wrist was observed under fluoroscopy through a range of motion, and spot films were obtained in neutral position, ulnar deviation, radial deviation (in both prone and supine projections), and in neutral position in the lateral projection. After DRUJ injection, multiple oblique views of the triangular fibrocartilage were obtained under fluoroscopic control. After each injection and fluoroscopic sequence, standard four-view radiographs (posteroanterior, ulnar deviation, lateral, and oblique views) were obtained with an overhead X-ray tube.

The sites, frequency, and direction of all intercompartmental communications were recorded. The arthrograms were obtained and reported under the direction of six different musculoskeletal radiologists, with many of the injections made by residents. All cases were reviewed by one of the authors, and the findings recorded represent a consensus between the radiologist in charge of the case and one of the authors. Sites of communication between the RCJ and MCJ were classified as either scapholunate, lunotriquetral, radial capsular, or ulnar capsular. The last two classifications (radial capsular and ulnar capsular) refer to all peripheral communications between the MCJ and RCJ on the radial and ulnar sides of the joint, respectively, and include defects in the scaphotrapezial, triquetrohamate, or pisotriquetrohamate attachments. All communications between the RCJ and DRUJ were recorded as defects of the triangular fibrocartilage.

Results

Seventy-six patients (30%) had a total of 123 communications between the MCJ and RCJ (Table 1), and 174 patients (70%) had no evidence of communication between these two joints. Of the 76 patients with communication between MCJ and RCJ, 38 (50%) had communications that were unidirectional (Tables 1 and 2). In 35 (92%) of the 38 patients with unidirectional communications, the contrast agent flowed from MCJ to RCJ (Fig. 1). In two (5%) of the 38 patients, contrast agent flowed from RCJ to MCJ via capsular defects, one ulnar and one radial. In one (3%) of the 38 patients, a tiny amount of contrast medium was found in the MCJ after RCJ injection, when no communication had been shown by MCJ injection. In this patient, the site of the defect through which

TABLE 1: Number (%) of Patients Studied for Midcarpal to Radiocarpal Joint Communications

Age (years)	Patients with Communications		Site of Communication				Total Patients
	Total	One Way	LT	SL	UC	RC	
0–20	1 (5)	1 (5)	1 (5)	0 (0)	0 (0)	1 (5)	19
21–30	23 (23)	14 (14)	14 (14)	13 (13)	4 (4)	4 (4)	100
31–40	25 (34)	12 (16)	19 (26)	14 (19)	4 (5)	4 (5)	74
41–50	16 (42)	7 (18)	15 (39)	6 (16)	2 (5)	3 (8)	38
51–60	6 (50)	3 (25)	4 (33)	4 (33)	1 (8)	0 (0)	12
61–70	4 (80)	1 (20)	4 (80)	3 (60)	1 (20)	1 (20)	5
>70	1 (50)	0 (0)	0 (0)	1 (50)	0 (0)	0 (0)	2
Total	76 (30)	38 (15)	57 (23)	41 (16)	12 (5)	13 (5)	250

Note.—LT = lunotriquetral, SL = scapholunate, UC = ulnar capsular, RC = radial capsular.

TABLE 2: Direction of Unidirectional Communications Between the Radiocarpal and Midcarpal Joints

Direction	Site of Communication								Total
	LT	SL	RC	UC	LT and SL	LT and RC	RC and UC	Unknown	
RCJ to MCJ	0	0	1	1	0	0	0	1	3
MCJ to RCJ	17	9	2	0	4	1	1	1	35
Total	17	9	3	1	4	1	1	2	38

Note.—LT = lunotriquetral, SL = scapholunate, RC = radial capsular, UC = ulnar capsular, RCJ = radiocarpal joint, MCJ = midcarpal joint.

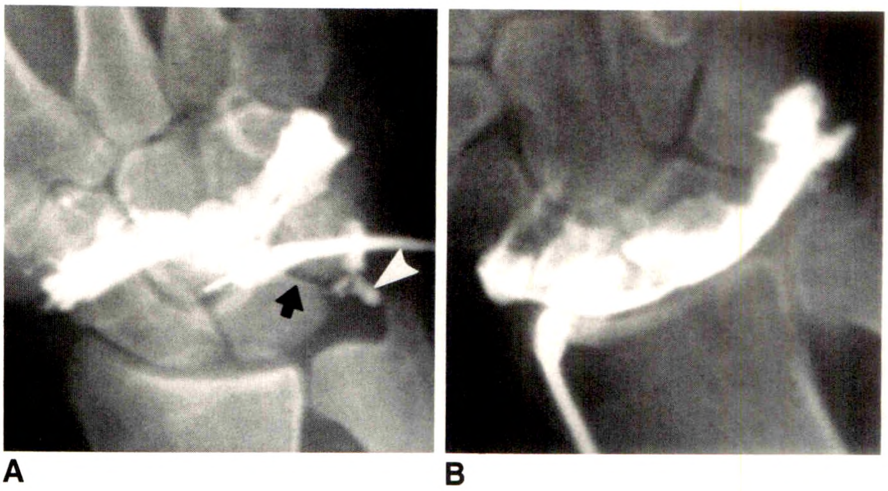

Fig. 1.—47-year-old woman with unidirectional tear of lunotriquetral ligament.

_A_, Midcarpal joint arthrogram shows contrast medium flowing from midcarpal joint to radiocarpal joint (_arrowhead_), between lunate bone and triquetral bone (_arrow_).

_B_, Arthrogram after radiocarpal joint injection does not show communication.

the contrast agent had flowed could not be found. No scapholunate or lunotriquetral defects that allowed unidirectional flow of contrast agent from RCJ to MCJ were shown.

Of the 35 patients with unidirectional communications allowing flow from MCJ to RCJ, 17 (49%) had isolated lunotriquetral defects, nine (26%) had isolated scapholunate defects, and two (6%) had isolated radial capsular defects. In one (3%) of these 35 patients, the site of contrast agent flow could not be determined. In the remaining six (17%) of the 35, more than one defect was shown. Four of these six had both scapholunate and lunotriquetral defects, one had radial capsular and lunotriquetral defects, and one had radial capsular and ulnar capsular defects. No isolated ulnar capsular defects were found in these 35 patients.

In 49 patients, communications were shown between the DRUJ and RCJ via defects in the triangular fibrocartilage (Table 3). Of these 49 communications, nine (18%) were unidirectional (Fig. 2). Seven of the nine unidirectional triangular fibrocartilage defects allowed contrast agent to flow from RCJ to DRUJ and two allowed flow from DRUJ to RCJ.

In 11 patients, all three compartments were filled by a single injection of contrast agent. This three-compartment communication (carpus communis) was not always demonstrated by all three injections. In fact, only two of these 11 patients had three compartments filled by all three injections. In four patients, both the RCJ and MCJ injections filled all three compartments, in three patients only the MCJ injection filled all compartments, and in two patients only the RCJ injection filled all three compartments.

Fifty capsular defects were recorded in 45 patients; 25 patients had defects on the radial side of the carpus, and 25 had defects on the ulnar side. Twenty of these 45 patients had complete capsular defects, which allowed contrast material to flow from one joint to another, and 25 had incomplete defects. Of the 20 patients with complete defects, seven had flow of contrast agent in one direction only. Five of these seven unidirectional defects were in the radial capsule, and two were in the ulnar capsule.

Although the overall prevalence of communications between the RCJ and MCJ increased with age, unidirectional communications did not correlate with age (Table 1). Similarly there was no correlation between patients' age and unidirectional communications between the DRUJ and the RCJ (Table 3).

Discussion

Ligament and/or cartilage defects, which allow contrast material to flow from one compartment to another, have been shown to occur in asymptomatic wrists [5]. However, it is generally accepted that the presence of such defects in

TABLE 3: Number (%) of Patients Studied for Radiocarpal to Distal Radioulnar Joint Communications

Age (years)	Patients with Communications			Total Patients
	Two Way	One Way	Total	
0–20	4 (21)	1 (5)	5 (26)	19
21–30	13 (13)	3 (3)	16 (16)	100
31–40	17 (23)	3 (4)	20 (27)	74
41–50	5 (13)	1 (3)	6 (16)	38
51–60	0 (0)	1 (8)	1 (8)	12
61–70	1 (20)	0 (0)	1 (20)	5
>70	0 (0)	0 (0)	0 (0)	2
Total	40 (16)	9 (4)	49 (20)	250

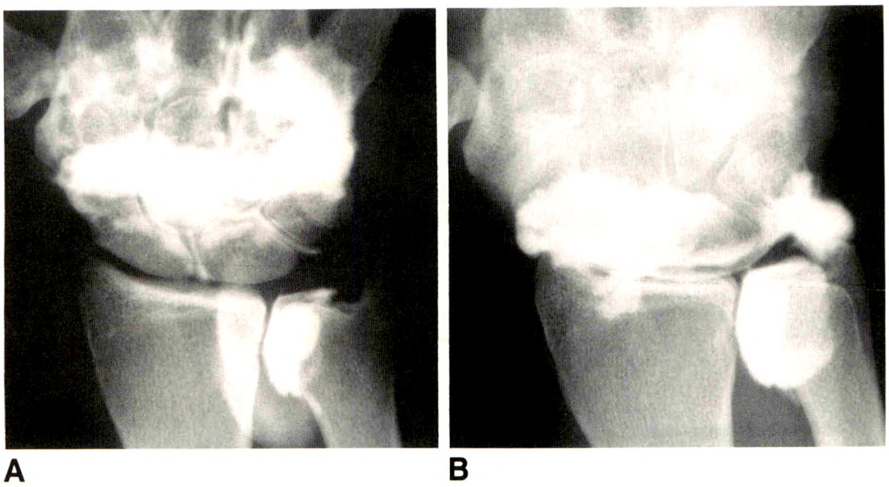

Fig. 2.—23-year-old man with unidirectional triangular fibrocartilage tear.

A, Distal radioulnar joint arthrogram does not show any communication between distal radioulnar joint and radiocarpal joint.

B, Arthrogram after radiocarpal joint injection reveals a communication between two joints, confirming a tear in triangular fibrocartilage.

symptomatic wrists documents the presence of torn ligaments [1–3, 5–12]. Therefore, arthrography is used to assess ligament tears and plan reparative surgery. Previous reports of unidirectional communications [1–3] have suggested that significant ligament defects may be overlooked if all three wrist compartments are not injected routinely during arthrography.

The results of our study show that three-compartment wrist arthrography consistently shows unidirectional intercompartmental communications. However, the frequency, distribution, and direction of contrast agent flow in our cases (Tables 1–3) are different from those of other authors [1–3, 5–11, 13, 14]. This variation could be due to differences in populations of patients, differences in examination technique and interpretation, or a combination of these two.

We cannot rule out differences in the patients and the interpretive criteria as important variables, because these are incompletely described in available reports. Technical differences between reported studies include: needle size, technique and site of needle placement, type and volume of contrast agent used, differing methods of recording the examination, time between injections, and interpretive criteria. Much of this information is not clearly stated by most authors, but some aspects can be evaluated. Those authors [1–3, 5–9, 11, 13] who reported needle size used 23- or 25-gauge needles, similar to our technique. Needle placement, when reported [1–3, 5–8, 11, 13], generally differed from our approach. Concentration of contrast agents has varied from 30% to 60% in those studies in which this information was supplied [1–3, 6–9, 11, 13, 14]. Some investigators [2, 8, 9] used digital subtraction techniques, which have been claimed to be more sensitive [8, 9] than the conventional radiographs that we used. Not all investigators fully distend the joint as we do [1, 3]. Many inject the RCJ first [1–3, 11], whereas we injected the MCJ first.

It is significant that the majority of ligament defects with unidirectional flow detected in our patients allowed flow in the same direction, from MCJ to RCJ. This appears to corroborate the findings of other investigators [1, 3, 13]. However, flow in the opposite direction was shown by one investigator who injected the RCJ first [11]. In that study and in our own, the joints were fully distended and contrast agent flowed away from the first site of injection. Those investigators [1–3] who have shown unidirectional defects with contrast agent flowing in either direction do not indicate that they distended the joint fully. This incomplete distension of a compartment may result in failure to demonstrate all defects. Another possible reason for the variation between reported results is difference in time between injections.

The strengths of our study are that it involved a large number of patients in whom three-compartment arthrography was performed, with the midcarpal joint injected first. The arthrograms show the full range of locations of interjoint communications with few (two in 38) indeterminate sites of unidirectional communication. Although the examinations were performed by several different radiologists, the technique and interpretive criteria were standardized and constant. On the other hand, weaknesses include a lack of surgical findings to correlate with the radiologic findings and failure to study individual technical variables directly.

Our results indicate that three-compartment wrist arthrography can show unidirectional ligament tears. However, when correlated with prior studies, our results suggest that visualization of unicompartmental communications is at least partially related to technique. Small intercompartmental communications may be overlooked if the joint compartments are not fully distended with contrast agent and the wrist is not exercised. Failure to show intercompartmental communications between joints until after exercise has been reported [12]. We have shown intrinsic unidirectional ligament defects (i.e., scapholunate and lunotriquetral) after the first injection only. We have shown extrinsic unidirectional defects (i.e., radial capsular and ulnar capsular) infrequently (seven occurrences in 250 cases), and these do not often allow flow toward the first joint injected (two occurrences). Unidirectional defects of the triangular fibrocartilage also were uncommon in our series (nine occurrences in 250 cases), but the majority of these (seven of nine) flowed toward the joint first injected (DRUJ). Although these triangular fibrocartilage defects may indeed represent the "flap-valve" tears suggested by others

[2], our data do not support the existence of flap-valve tears of the scapholunate or lunotriquetral ligaments.

We conclude that although unidirectional communications between the wrist joints can be shown reliably by three-joint arthrography, the direction of these communications is as likely to be a function of examination technique as one of the patient's abnormality. Without further studies on the effect of different technical parameters, each center is encouraged to develop and validate a standardized technique with its own group of patients.

We do not believe that it is necessary to inject all three joint compartments in all patients. If the purpose of an arthrogram is to detect defects in the scapholunate and lunotriquetral ligaments, our results suggest that MCJ injection alone should be used. If complete tears of the triangular fibrocartilage are the only concern, the majority will be shown by RCJ injection only (in our series two of 49 tears would have been missed in 250 patients). However, in order to show all defects arthrographically in all patients, all three wrist-joint compartments must be fully distended with contrast agent.

REFERENCES

1. Levinsohn EM, Palmer AK, Coren AB, Zinberg EM. Wrist arthrography: the value of the 3-compartment injection technique. *Skeletal Radiol* **1987**;16:534–544
2. Quinn SF, Pittman CC, Belsole R, Greene T, Rayhack J. Digital subtraction wrist arthrography: evaluation of the multiple-compartment technique. *AJR* **1988**;151:1173–1174
3. Zinberg EM, Palmer AK, Coren AB, Levinsohn EM. The triple-injection wrist arthrogram. *J Hand Surg* **1988**;13A:803–809
4. Miller RE. Editorial. The areae gastricae: epilogue. *AJR* **1979**;132:1023–1024
5. Herbert TJ, Faithfull RG, McCann DJ, Ireland J. Bilateral arthrography of the wrist. *J Hand Surg* **1990**;15B:233–235
6. Levinsohn EM, Palmer AK. Arthrography of the traumatized wrist: correlation with radiography and the carpal instability series. *Radiology* **1983**;146:647–651
7. Palmer AK, Levinsohn EM, Kuzma GR. Arthrography of the wrist. *J Hand Surg* **1983**;8A:15–23
8. Resnick D, Andre M, Kerr R, Pineda C, Querra J, Atkinson D. Digital arthrography of the wrist: a radiographic-pathologic correlation. *AJR* **1984**;142:1187–1190
9. Manaster BJ. Digital wrist arthrography: precision in determining the site of radiocarpal-midcarpal communication. *AJR* **1986**;147:563–566
10. Braunstein EM, Vydareny KH, Louis DS, Hanvein FM. Cost effectiveness of wrist fluoroscopy and arthrography in the evaluation of obscure wrist pain. *Orthopedics* **1986**;9:1504–1510
11. Manaster BJ. The clinical efficacy of triple injection wrist arthrography. *Radiology* **1991**;178:267–270
12. Gilula LA, Totty WG, Weeks PM. Wrist arthrography. *Radiology* **1983**;146:555–556
13. Tirman RM, Weber ER, Synder LL, Koonce TW. Midcarpal wrist arthrography for detection of tears of the scapholunate and lunotriquetral ligaments. *AJR* **1985**;144:107–108
14. Trentham DE, Hamm RL, Masi AT. Wrist arthrography: review and comparison of normals, rheumatoid arthritis, and gouty patients. *Semin Arthritis Rheum* **1975**;5:105–120

Blue Medicine

Stefan C. Schatzki[1]

George Catlin's paintings were the first in-depth pictorial record of the American Plains Indians. His works record a part of America's heritage that was lost later, during the westward migration of American settlers.

Catlin was born in Wilkes Barre, PA, on July 26, 1796. He lived on a farm as a youth and first became interested in American Indians as a child, perhaps influenced by the story of his mother's capture by Indians during the Wyoming Massacre of 1778. At the age of 21, Catlin went to Connecticut to study law. After working as a lawyer for a few years in rural Pennsylvania, he moved in 1823 to Philadelphia, where he "commenced the art of painting." Without any formal training and with a great deal of determination and self-assurance—which would serve him well on his later adventures in the West—Catlin began a career as a painter. He was successful quickly and by 1824 was elected to the Pennsylvania Academy of Fine Arts and soon had orders for portraits from many prominent Americans. After a delegation of American Indians stopped in Philadelphia, Catlin became dedicated to commemorating "the history and customs of such a people" and indicated that "nothing shall prevent me from visiting their country and of becoming their historian."

Unable to travel immediately, Catlin first painted the Iroquois of New York. By 1830, he was ready to go west. During the next 6 years, Catlin traveled throughout the West, painting many Indian tribes, from the Blackfoot and Crow of North Dakota to the Comanches and Cherokees of Oklahoma. During these years, Catlin made many trips into the wilderness west of the Mississippi to catalog the Indians and their customs. Working without any formal training, Catlin was not an accomplished landscape painter. Despite these limitations, his many paintings done during these years represent the primary pictorial record of the customs of these tribes. His hundreds of portraits of American Indians from more than 50 tribes remain an important part of American history.

In 1835, while at Fort Snelling, near what is today St. Paul, MN, Catlin painted a portrait of Blue Medicine, a Sioux medicine man. Catlin recognized that the medicine men were conjurers as well as healers and depicted Blue Medicine with the artifacts of his trade, including a medicine or mystery drum, rattle, and looking glass. This striking portrait is of one of several medicine men of the Sioux, Blackfoot, Mandan, and Iowa tribes that were painted by Catlin, some of which depicted the medicine man performing his mysterious profession.

Having completed his visits to the western tribes, in 1837 Catlin began the second part of his unusual career. For the next 35 years, Catlin was a showman, presenting the remarkable heritage of the American Indians to the people of America and Europe. The years of Catlin's "Indian Gallery" performances will be discussed with another portrait in a future article in this series.

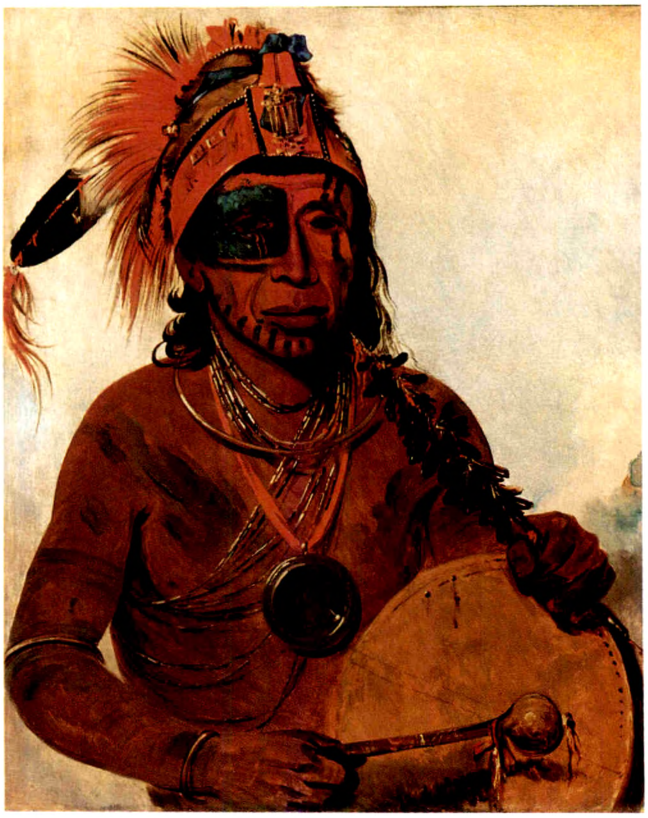

George Catlin (1796–1872). *Blue Medicine, A Medicine Man of the Ting-ta-to-ah Band,* 1835. Oil on canvas, 29 × 24 in. National Museum of American Art, Smithsonian Institution, Washington, DC; gift of Mrs. Joseph Harrison, Jr.

George Catlin's paintings remain an important part of America's heritage and a vital link to the American Indian culture.

---

[1] Department of Radiology, Mount Auburn Hospital, 330 Mount Auburn St., Cambridge, MA 02238.

***AJR* 157:110, July 1991** 0361–803X/91/1571–0110 © American Roentgen Ray Society

Safety-Belt Injuries in Children with Lap-Belt Ecchymosis: CT Findings in 61 Patients

Carlos J. Sivit[1]
George A. Taylor
Kurt D. Newman[2,3]
Dorothy I. Bulas[1]
Catherine S. Gotschall[2]
Cynthia J. Wright[2]
Martin R. Eichelberger[2,3]

We have noted a complex of common injuries in children wearing lap-styled safety belts during vehicular accidents. Sixty-one children who were restrained passengers in motor vehicle crashes had linear ecchymosis across the abdomen and had CT for abdominal trauma. Thirteen children (21%) had a lumbar spine injury, and 14 children (23%) injured a hollow viscus (bowel, 12; bladder, two); five children (8%) had both spine and hollow viscus injuries. Abnormal findings on abdominal CT were recognized retrospectively in three of 13 children with lumbar spinal injury. Lateral radiographs of the spine showed lumbar spinal injury in all cases. Free intraperitoneal air was noted in only three (25%) of 12 children with bowel injury. In eight of those children, CT showed large, unexplained collections of peritoneal fluid.

The presence of lap-belt ecchymosis should prompt a careful search for spine, bowel, and bladder injury. Recognition of the limitations of CT diagnosis of these injuries is important to reduce errors in interpretation.

***AJR* 157:111–114, July 1991**

We have observed an increasing frequency of injury in children with linear abdominal or flank ecchymosis caused by a lap safety belt. These injuries, which primarily involve the lumbar spine and hollow viscera, are difficult to identify on CT scans. As a result, this study was undertaken to delineate further the pattern of injury in this population and to identify associated pitfalls in their CT diagnosis.

Materials and Methods

Between January 1983 and December 1990, 965 children who sustained blunt trauma and who were suspected clinically of having injury to intraabdominal organs had abdominal CT at our institution. Two-hundred seventy of these children were passengers in motor vehicle crashes; of these, 61 (23%) were secured by an adult lap safety belt that had caused linear abdominal or flank ecchymosis. This was designated as *lap-belt ecchymosis* (Fig. 1). These 61 children form the basis for this report.

Additional indications for CT in these children included abdominal tenderness (49), distension (19), absent bowel sounds (17), hematuria (16), neurologic obtundation (14), low hematocrit (nine), or vomiting (nine).

Demographic data, indications for CT, and radiologic findings were recorded during the initial examination. Additionally, all of the scans were reviewed retrospectively by one of the authors. The CT findings listed are based on the retrospective evaluation. Clinical records were reviewed retrospectively to determine the type of treatment (operative or nonoperative) and clinical outcome. CT criteria included solid-organ injury, free peritoneal fluid, pneumoperitoneum, mesenteric hematoma, pelvic or lumbar spine fracture or dislocation, and lower thoracic injury.

CT was performed on a GE 9800 CT scanner (GE Medical Systems, Milwaukee, WI) with 1-cm-thick sections obtained at 1-cm intervals through the abdomen and pelvis. Three milliliters per kilogram (maximal dose, 120 ml) of 43% iodinated contrast material (iothalamate meglumine [Conray 43]; Mallinckrodt, St. Louis, MO) was administered by means of rapid IV bolus injection.

Received October 9, 1990; accepted after revision February 12, 1991.

[1] Departments of Diagnostic Imaging and Radiology and Pediatrics, Children's National Medical Center, 111 Michigan Ave., N.W., Washington, DC, 20010 and The George Washington University School of Medicine and Health Sciences, Washington, DC 20037. Address reprint requests to C. J. Sivit.

[2] Department of Surgery, Children's National Medical Center, 111 Michigan Ave., N.W., Washington, DC 20010.

[3] The George Washington University School of Medicine and Health Sciences, Washington, DC 20037.

0361-803X/91/1571-0111
© American Roentgen Ray Society

Results

Thirty-nine (64%) of 61 injured children with lap-belt ecchymosis had abdominal, pelvic, or lumbar spine injuries (age range, 2–17 years; mean age, 7 years). Twenty-two (36%) of these children had an injury of the lumbar spine or a hollow viscus (age range, 2 to 16 years; mean age, 8 years). Injuries of both the lumbar spine and a hollow viscus were noted in five of the children. Seventeen of 22 children with injury of the lumbar spine or a hollow viscus were secured by lap belts only; five were secured by three-point restraints (lap belt and shoulder harness).

Lumbar Spinal Injury

Thirteen children with lap-belt ecchymosis had the following injuries to the lumbar spine between L1 and L4: compression fracture only (five), subluxation or distraction and fracture (five), and distraction only (three). The spinal cord was injured in three children. The initial abdominal CT study showed the injury to the spine in only three children (23%; Fig. 2). A lateral scout radiograph of the lumbar spine, obtained with the child on the CT gantry, was added to the trauma CT protocol during the study (Fig. 3). This radiograph has shown the abnormality in nine (90%) of 10 subsequent cases.

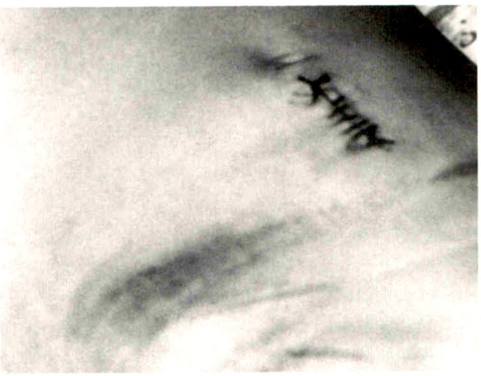

Fig. 1.—Linear lap-belt ecchymosis across lower abdomen of a child. Sutures are seen below umbilicus.

Hollow Viscus Injury

Twelve children with lap-belt ecchymosis had bowel or mesenteric injury. These included six partial bowel tears, three complete transections, and one contusion; two children developed subsequent strictures. Both strictures were identified on follow-up upper gastrointestinal series between 2 and 3 weeks after the injury and were confirmed at surgery. The injury locations were as follows: jejunum (seven), duodenum (three), ileum and cecum (one), and sigmoid colon (one). Four mesenteric contusions or lacerations also were noted.

Free intraperitoneal air was noted in only three (25%) of the examinations. Large peritoneal fluid collections were noted in 11 children (92%) with bowel injuries (Fig. 4). In eight of these children, peritoneal fluid was noted in the absence of solid viscus injury or pelvic fracture.

CT examination was repeated with oral contrast medium within 24 hr in five of the 12 children with bowel injury (two with partial tears, two with subsequent strictures, one with complete transection. This second examination did not provide any additional information in any case.

Two children had intraperitoneal bladder rupture. Both cases were identified by the first CT study. Extravasation of IV contrast material was present throughout the peritoneal cavity in both cases (Fig. 5).

Additional Injuries

Seventeen children (28%) with lap-belt ecchymosis had a solid-organ injury. These included 13 hepatic, eight splenic, two pancreatic, and one renal injury. Three children (5%) had pelvic fractures, two had fractures of an iliac wing, and two had fractures of the pubic rami. Six children (10%) had lower thoracic cavity abnormalities noted on the abdominal CT scan;

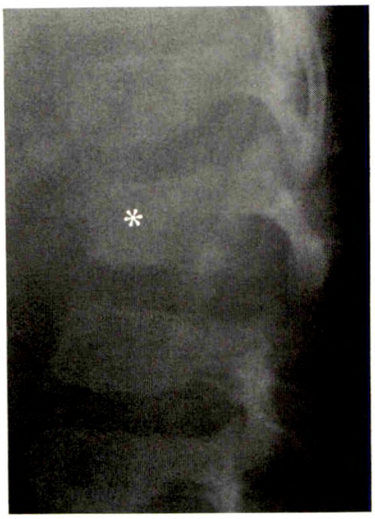

2

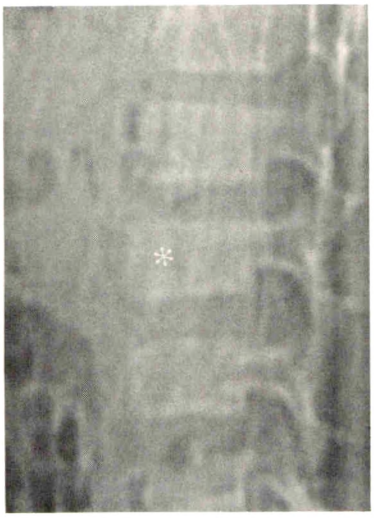

3

Fig. 2.—Lateral radiograph of lumbar spine shows distraction of L2–L3 facets and anterior loss of height (compression fracture) of L2 vertebral body (*asterisk* marks L2). CT scans through L2–L3 region showed no abnormalities.

Fig. 3.—Lateral radiograph of lumbar spine obtained on CT gantry shows distraction of L3–L4 facet joints (*asterisk* marks L3).

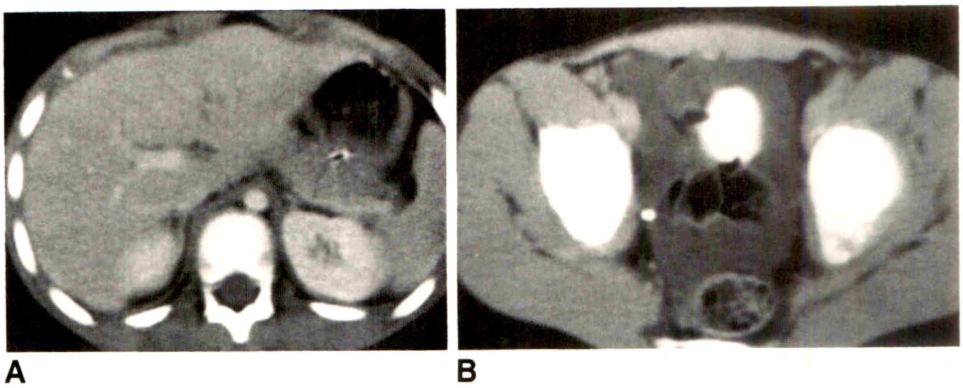

Fig. 4.—*A* and *B*, Partial jejunal tear with unexplained peritoneal fluid. CT scan through upper abdomen (*A*) shows no solid organ injury, whereas CT scan through pelvis (*B*) shows a moderate amount of fluid.

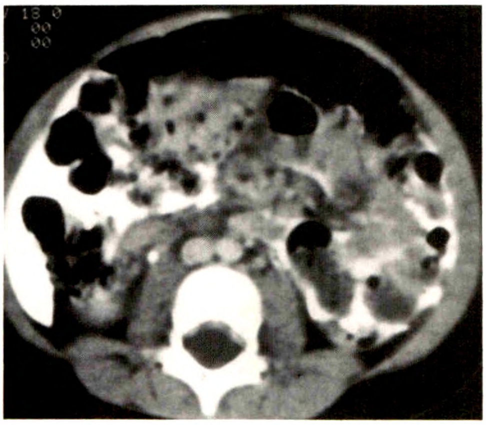

Fig. 5.—Intraperitoneal bladder rupture. CT scan shows intraperitoneal contrast material. Bladder perforation was noted during surgery.

these included five pulmonary contusions, one pneumothorax, and one pneumomediastinum. All of these injuries were identified on the initial CT scan.

Discussion

Although fatalities have been reduced through the use of safety belts [1–3], certain types of injuries have increased. Lap-belt restraints, in particular, have been associated with a specific complex of hollow viscus and lumbar spinal injuries [4–15]. This injury complex originally was described by Garrett and Braunstein [4] in 1962 and labeled the *seat belt syndrome*. The hallmark of the syndrome is abdominal wall or flank ecchymosis suggesting the pattern of a lap belt. The mechanism of injury is sudden flexion of the upper body on a fulcrum formed by the lap belt, which causes sudden compression of the abdominal viscera and lumbar spine [16].

The risk of injury is increased in children for several reasons. First, lap-belt restraints were designed for adults. They are meant to be worn over the anterosuperior iliac spines of the pelvis, which in adults provide strong anchor points [14]. Because children have relatively underdeveloped iliac spines and their sitting posture is often slouched rather than upright, lap belts tend to ride cephalad over the midabdomen [9]. The only anchor becomes the relatively weak abdominal wall musculature. As the child moves forward beneath an improperly placed lap belt, sudden flexion occurs at approximately the level of the umbilicus [14]. Second, children have a higher center of gravity because of an increased head-to-body ratio [9], resulting in an increased force of flexion across the fixed lap belt.

The three-point shoulder harness was developed in an attempt to prevent the complex of injuries associated with wearing lap belts alone. Many three-point restraints are worn incorrectly [17], and their use has not eliminated lap-belt complex injuries entirely. Twenty-three percent of children (5/22) in our study group with hollow viscus or lumbar spinal injuries were secured by adult-type three-point restraints.

Lap-belt ecchymosis was a high-risk indicator of intraabdominal injury in our population, with abdominal injury present in 64% (39/61) of children. This compared with a 28% (249/904) rate of injury in all other children with blunt trauma studied by CT. Additionally, although children with lap-belt ecchymosis represented only 6% (61/965) of the total examined with CT after blunt trauma, they accounted for 68% (27/40) of all hollow viscus and lumbar spinal injuries seen in this population.

The recognition of the associated complex of injuries is important because of the difficulty in CT diagnosis. Findings of intestinal trauma may be subtle and nonspecific on CT [18–21]. The presence of pneumoperitoneum is neither sensitive nor specific for the diagnosis of bowel injury [19, 20, 22, 23]. Review of these cases indicates that unexplained peritoneal fluid is a useful indicator of bowel injury. We have observed that peritoneal fluid or blood is rarely seen after blunt trauma as an isolated finding. We have identified peritoneal fluid in the absence of a solid viscus injury, pelvic fracture, or hypoperfusion complex [24] in only 17 of 965 children studied by CT after blunt trauma (unpublished data). Ten of these (59%) had a bowel injury (two of these bowel injuries occurred in patients not involved in motor vehicle crashes).

The CT diagnosis of bowel injury remains a difficult one, however, when there is a coexisting solid organ injury or pelvic fracture to account for the peritoneal fluid, as occurred in three of our cases. Additionally, in one case no CT abnormalities were noted.

We do not routinely administer oral contrast material for CT examination of the abdomen after blunt trauma. In five of these children, however, CT examination was repeated after the administration of oral contrast medium. The presence and location of focal bowel perforation could not be shown in any case.

Findings of lumbar spinal injury also may be difficult to identify on CT scans of the abdomen. This is due to the limitations of CT in detecting horizontal fractures and facet distractions [25]. Only 23% of lumbar spinal injures in our series were noted on the abdominal CT scan. All 13 of the injuries were seen on lateral radiographs of the spine. In our early cases, the radiographs were not obtained for several days because a spinal injury was not clinically suspected. Since we added a lateral radiograph of the abdomen to the CT evaluation, we have identified prospectively nine of 10 lumbar spinal injuries. We now obtain a cross-table lateral view of the lumbar spine also in all of these patients.

The lateral scout radiograph, which is obtained with the child in the CT gantry, is not meant to replace radiographs of the lumbar spine, which allow visualization of the spine in greater detail. In a recent case, the lateral scout radiograph revealed no injury, whereas a subsequent standard cross-table lateral view of the abdomen revealed distraction of the L3-L4 facets.

Rupture of the urinary bladder is an uncommon injury that is usually associated in adults with pelvic fracture [26-29]. The type of extravasation (intraperitoneal vs extraperitoneal) depends on the location of the tear and its relationship to the peritoneal reflection [26]. The diagnosis can usually be made on the basis of cystographic findings [26, 27]. Neither of the children with bladder rupture had associated pelvic fractures. Both injuries were identified on CT scan.

Solid organ injuries were slightly more common in this group of children than in the general blunt-trauma population studied with CT, although the differences were not statistically significant. Hepatic, splenic, renal, or pancreatic injuries were noted in 28% (17/61) of children with lap-belt ecchymosis compared with 21% (190/904, $p = .2$) in all other children studied with CT after blunt trauma. It is unclear whether these injuries were related to the seat belt itself or were due to the patient's striking other objects after the crash.

In conclusion, the presence of lap-belt ecchymosis should prompt a careful search for lumbar spine and hollow viscus injuries. Recognition of the limitations of CT diagnosis of these injuries is important to help reduce errors in interpretation.

REFERENCES

1. Denis R, Allard M, Atlas H, Farkouth E. Changing trends with abdominal injury in seatbelt wearers. *J Trauma* **1983**;23:1007-1008
2. Petrucelli E. Seat belt laws: the New York experience—preliminary data and some observations. *J Trauma* **1987**;27:706-710
3. Reath DB, Kirby J, Lynch M, Maull K. Injury and cost comparison of restrained and unrestrained motor vehicle crash victims. *J Trauma* **1989**;29:1173-1177
4. Garrett JW, Braunstein PW. The seat belt syndrome. *J Trauma* **1962**;2:220-238
5. Huelke DF, Kaufer H. Vertebral column injuries and seatbelts. *J Trauma* **1975**;15:304-318
6. Smith WS, Kaufer H. Patterns and mechanisms of lumbar spine injuries associated with lap seat belts. *J Bone Joint Surg [Am]* **1969**;51-A:239-254
7. LeGay DA, Petrie DP, Alexander DI. Flexion-distraction injuries of the lumbar spine and associated abdominal trauma. *J Trauma* **1990**;30:436-444
8. Reid AB, Letts RM, Black GB. Pediatric chance fractures: association with intra-abdominal injuries and seat belt use. *J Trauma* **1990**;30:384-391
9. Argan PF, Dunkle DE, Winn DG. Injuries to a sample of seatbelted children evaluated in a hospital emergency room. *J Trauma* **1987**;27:58-64
10. Holt BW. Spines and seat belts: mechanisms of spinal injury in motor vehicle crashes. *Med J Austral* **1976**;2:411-413
11. Taylor GA, Eggli KD. Lap-belt injuries of the lumbar spine in children: a pitfall in CT diagnosis. *AJR* **1988**;150:1355-1358
12. Newman KD, Bowman LM, Eichelberger MR, et al. The lap belt complex in children. *J Trauma* **1990**;30:1133-1138
13. Williams JS, Kirkpatrick JR. The nature of seat belt injuries. *J Trauma* **1971**;11:207-212
14. Miller MA. The biochemical response of the lower abdomen to belt restraint loading. *J Trauma* **1990**;29:1571-1584
15. Appleby JP, Nagy AG. Abdominal injuries associated with the use of seatbelts. *Am J Surg* **1989**;157:457-458
16. Gumley G, Taylor TK, Ryan MD. Distraction fractures of the lumbar spine. *J Bone Joint Surg [Br]* **1982**;64-B:520-525
17. Soto TB. Effects of seat belts and injuries resulting from improper use. *J Trauma* **1987**;27:754-758
18. Sherck JP, Oakes DD. Intestinal injuries missed by computed tomography. *J Trauma* **1990**;30:1-7
19. Bulas DI, Taylor GA, Eichelberger MR. The value of CT in detecting bowel perforation in children after blunt abdominal trauma. *AJR* **1989**;153:561-564
20. Cobb LM, Vinocur CD, Wagner CW, Weintraub WH. Intestinal perforation due to blunt trauma in children in an era of increased nonoperative management. *J Trauma* **1986**;26:461-463
21 Dickinson SJ, Shaw A, Santulli TV. Rupture of the gastrointestinal tract in children by blunt trauma. *Surg Gynecol Obstet* **1970**;131:655-657
22. Rizzo MJ, Federle MP, Griffiths BG. Bowel and mesenteric injury following blunt trauma: evaluation with CT. *Radiology* **1989**;173:143-148
23. Winek TG, Mosely HS, Grout F, Luallin D. Pneumoperitoneum and its association with ruptured abdominal viscus. *Arch Surg* **1988**;123:709-712
24. Taylor GA, Fallat ME, Eichelberger MR. Hypovolemic shock in children: abdominal CT manifestations. *Radiology* **1987**;165:643-646
25. Cacayorin ED, Kieffer SA. Applications and limitations of computed tomography of the spine. *Radiol Clin North Am* **1982**;20:185-200
26. Sandler CM, Hall JT, Rodriguez MB, Corriere JN. Bladder injury in blunt pelvic trauma. *Radiology* **1986**;158:633-638
27. Flancbaum L, Morgan AS, Fleisher M, Cox EF. Blunt bladder trauma: manifestation of severe injury. *Urology* **1988**;31:220-222
28. Corriere JN, Sandler CM. Mechanisms of injury, patterns of extravasation and management of extraperitoneal bladder rupture due to blunt trauma. *J Urol* **1988**;139:43-44
29. Cass AS, Luxenberg M. Features of 164 bladder ruptures. *J Urol* **1987**;138:743-745

Urinary Tract Calculi That Form on Surgical Staples: A Characteristic Radiologic Appearance

Barbara C. Dangman[1]
Robert L. Lebowitz

An autostapler is frequently used when bowel is interposed in the urinary tract during reconstructive urologic surgery in children. Usually the metallic staples are buried beneath the intestinal mucosa. However, if a portion of a staple is unintentionally left exposed or becomes exposed through migration and is then bathed by urine, it can become the nidus for formation of a calculus. The radiologic studies of 30 patients having surgery of this type in our hospital from 1980 to 1990 were reviewed prospectively, and stones were found to have developed on staples in eight patients. None of the patients had metabolic abnormalities. The stones were easily visible on plain radiographs because they were calcified. They formed in the lumen of the bladder or the bowel segment on the exposed portion of the staple. Thus, the staple was eccentric in the calculus and not central, as is usually the case with a stone forming on a foreign body.

This experience suggests that stones forming on surgical staples during reconstructive urologic surgery have a characteristic radiologic appearance that may aid in their identification.

AJR **157:115–117, July 1991**

Patients who have undergone continent urinary diversion or urinary tract "undiversion" often have bowel interposed in the urinary tract [1–10]. When the ileocecal valve is reinforced, or the bowel modified to serve as either an antireflux or continence mechanism, an autostapler is frequently used. If a portion of the staple becomes exposed to urine, it may serve as a nidus for formation of a stone. This type of stone has a characteristic radiologic appearance that has not been described before.

Materials and Methods

Between 1980 and 1990, approximately 30 patients at the Children's Hospital had metallic surgical staples used for urinary tract reconstruction. All of these patients had follow-up radiologic studies. Those found to have stones forming on staples were the basis for this study. Their radiographs and medical records were reviewed.

Results

Eight patients who had calculi forming on surgical staples were seen. Seven ranged in age from 4½ to 23 years, and one was 41 years old, when their stones were discovered. Their diagnoses included bladder exstrophy in two patients, meningomyelocele in two, isolated epispadias in one, cloacal exstrophy in one, neurogenic bladder of uncertain cause in one, and vaginal rhabdomyosarcoma in one. The most recent surgical procedures that had been performed with staples included continent ileocecal diversion, bladder augmentation with sigmoid colon, creation of a nonrefluxing jejunocecal conduit, urinary tract undiversion with ileoce-

Received October 24, 1990; accepted after revision January 23, 1991.

[1] Both authors: Department of Radiology, Children's Hospital, 300 Longwood Ave., Boston, MA 02115. Address reprint requests to R. L. Lebowitz.

0361-803X/91/1571-0115
© American Roentgen Ray Society

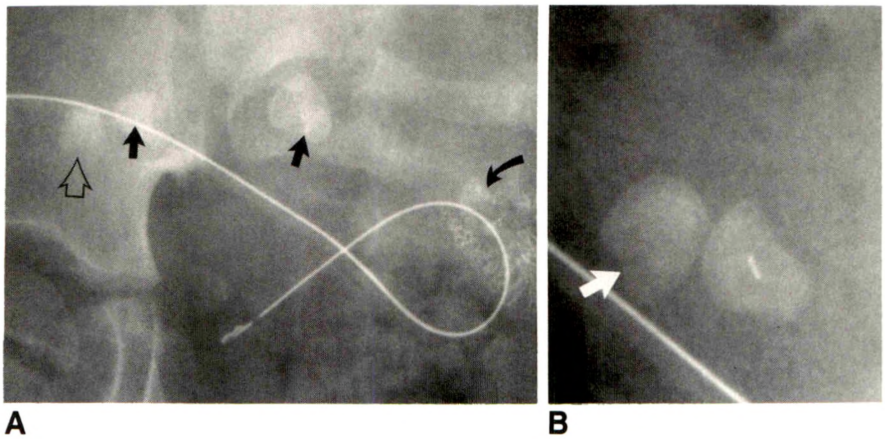

Fig. 1.—4½-year-old boy with bladder exstrophy, 15 months after continent ileocecal diversion. A routine follow-up sonogram showed stones in conduit.

A, Abdominal radiograph reveals three large stones, two with eccentric staples (*solid straight arrows*), free within lumen of conduit. No staple is present in the third stone (*open arrow*). A smaller stone is still eccentrically attached to one of staples at suture line (*curved arrow*). Stones were removed surgically and conduit was revised.

B, Close-up of two lateral stones seen in *A* shows that one has broken free from its staple, but notch where staple was attached is evident (*arrow*). Other stone appears to have a central staple, but staple is characteristically eccentric in another projection.

2

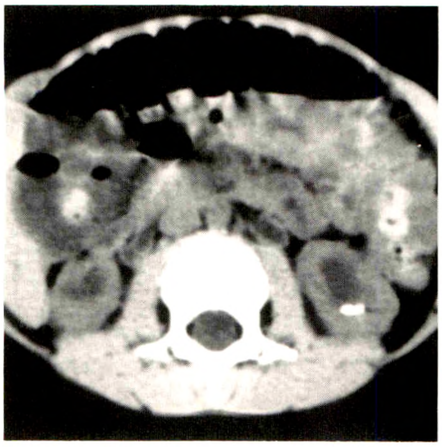

3

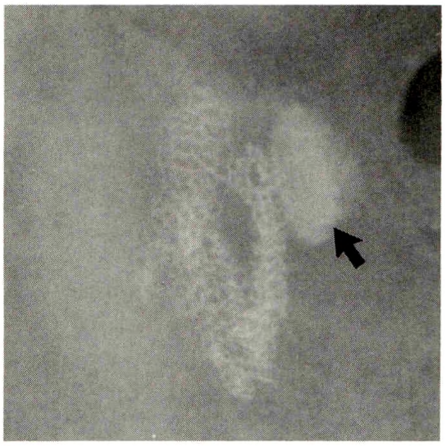

Fig. 2.—8-year-old boy with bladder exstrophy, 3½ years after Mitrofanoff procedure [12]. Sonography performed because of urinary tract infections showed multiple stones in cecal pouch. Abdominal radiograph showed multiple small calculi forming eccentrically on surgical staples. CT scan shows that a free calculus had refluxed into left kidney. Stones were removed surgically.

Fig. 3.—41-year-old woman, after multiple surgical continence procedures because of neurogenic dysfunction of bladder of uncertain cause. Most recent procedure was augmentation of colonic loop with jejunum and formation of Kock continent nipple 2½ years previously. She presented because of spontaneous passage of a stone. Abdominal radiograph reveals a large calculus that has formed eccentrically on surgical staples (*arrow*). Most of this was removed endoscopically. Remainder was fragmented with extracorporeal shock-wave lithotripsy.

cal interposition, and augmentation of a colonic conduit with construction of a Kock continent nipple [11]. In seven of the patients, a GIA (gastrointestinal anastomosis) autosuture device (United States Surgical Corporation, Norwalk, CT) was used with stainless steel staples. The eighth patient had surgery at another institution, and the type of staple used was not known. The interval from the surgery until the appearance of stones ranged from 15 months to 6 years. Although not all of these stones were subjected to pathologic/metabolic analysis, the composition of those that were analyzed included magnesium ammonium phosphate hexahydrate (struvite), calcium phosphate (apatite), and ammonium urate. Two of the patients had a history of urinary tract infections around the time of the formation of stones. Only one of the patients had serum calcium and phosphorus levels measured, and these were normal. No metabolic abnormalities were seen in any of the patients.

In each of the patients, one or more opaque stones were seen, each with the same characteristic appearance. Each had formed eccentrically around an embedded surgical staple (Figs. 1–4). The exposed edge of the staple had served as the nidus for the formation of the stone, accounting for the eccentric position of the staple. Some of the stones, with or without their embedded staples, had broken free from the mucosa and dropped into the lumen of the conduit or bladder (Fig. 1), and in one case such a stone had refluxed into the kidney (Fig. 2).

Discussion

Foreign material in the urinary tract that is exposed to urine frequently serves as the nidus for formation of calculi. Surgical staples are no exception, and stones forming on such staples are well known to urologists [1–10, 13]. The staples may be either stainless steel or tantalum [2, 5, 10, 13]. The composition of the stones varies, but is most often struvite, apatite, or magnesium ammonium phosphate [1–3, 6, 7, 13]. The average time until development of the first stone has been reported to be approximately 14 months after the surgery during which the staples were used [5]. Surgical procedures that use staples and result in stones have included a variety of large- and small-bowel conduits and end-to-end anastomosis of renal transplants to native ureter [13]. Hendren and

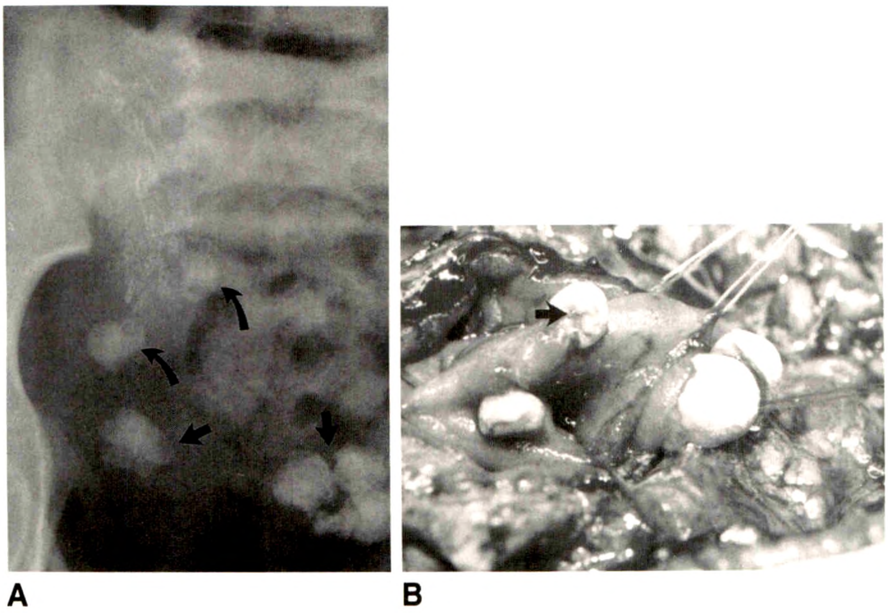

Fig. 4.—8½-year-old girl with complete epispadias, after urinary tract diversion and, most recently, undiversion with augmentation of bladder with ileocecal conduit and reinforcement of ileocecal valve with staples.

A, Abdominal radiograph shows that several stones are free in lumen, each with an eccentric staple (*straight arrows*). Two others are still attached to mucosa (*curved arrows*).

B, Surgical photograph when bladder was open shows stones attached to mucosa and projecting into lumen. *Arrow* points to eccentric staple of one of these.

Hendren [14] noted that stone formation on surgical staples used for an antireflux nipple was a relatively common complication among patients who had bladder augmentation. The majority of the reported patients have passed the stones spontaneously through a stoma [1–3, 5, 7, 10], although others have required surgical removal of the stones [6, 9–10, 13]. Some have had extracorporeal shock-wave lithotripsy [4]. One patient had impaction of a refluxed stone in the ureter [10]. Virtually all of the reported cases have been in older adolescents and adults.

Although previous descriptions have characterized the staple as being centrally located within the stone, in fact the characteristic appearance is that of a stone formed eccentrically around the staple. This is related to the pathophysiology of the stone's formation. When the staples are placed during surgery, they are buried beneath the mucosa and are not exposed to urine. However, with time, part of the staple may migrate through the mucosal surface, and the portion that becomes exposed to urine can then serve as a nidus for formation of a stone. If the stone enlarges, or the staple migrates further, the staple may pull free from the bowel wall, and the stone with the staple attached will fall into the lumen of the conduit or bladder (Fig. 1). Occasionally the stone may fall into the lumen and leave the staple behind (Fig. 1B). In the majority of cases, such intraluminal stones have passed spontaneously without difficulty or have been removed endoscopically. However, in one reported case [10] and in one patient reported here, a stone refluxed into the ureter.

It is important for every radiologist who deals with such patients to learn to recognize these calculi, because they are a local problem that is easily managed and are not a sign of some more ominous problem with stasis or metabolic derangement.

ACKNOWLEDGMENTS

Paulette Fontaine and Elaine Donnelly typed the manuscript, Arnold H. Colodny provided Figure 4B, and Donald Sucher took the photographs.

REFERENCES

1. Assadnia A, Lee CN, Petre JH, Lyons RC. Two cases of stone formation in ileal conduits after using staple gun for closure of proximal end of isolated loop. *J Urol* **1972**;108:553
2. Bergman SM, Sears HF, Javadpour N. Complication with mechanical stapling device in creation of ileoconduit. *Urology* **1978**;12:71–73
3. Bisson J, Vinson RK, Leadbetter GW. Urolithiasis from stapler anastomosis. *Am J Surg* **1979**;137:280–282
4. Boyd SD, Everett RW, Schiff WM, Fugelso PD. Treatment of unusual Kock pouch urinary calculi with extracorporeal shock wave lithotripsy. *J Urol* **1987**;139:805–806
5. Brenner M, Johnson DE. Ileal conduit calculi from stapler anastomosis: a long term complication? *Urology* **1985**;26:537–540
6. Cohn MS, Breslin TG, Coulombe RD. An intussuscepted ileal ureter bladder nipple. *J Urol* **1985**;133:849–850
7. Heney NM, Dretler SP, Hensle TW, Kerr WS. Autosuturing device in intestinal urinary conduits. *Urology* **1978**;12:650–653
8. Karamcheti A. O'Donnell WF, Hakala TR, Schwentker FN, Steichen FM. Autosuture ileal conduit construction: experience in 110 cases. *J Urol* **1978**;120:545–548
9. Ward HC. Surgical staples in bladder calculi after caecocystoplasty. *Br J Urol* **1987**;60:375
10. Webster GD, Henry HH, Tomlin EM. Calculus formation and ureteral obstruction after ileal conduit construction using autosuture stapling device. *Urology* **1987**;30:571–573
11. Ralls PW, Barakos JA, Skinner DG, et al. Imaging of the Kock continent ileal urinary reservoir. *Radiology* **1986**;161:477–483
12. Weingarten JL, Cromie WJ. The Mitrofanoff principle: an alternative form of continent urinary diversion. *J Urol* **1988**;140:1529–1531
13. Motayne GG, Jindal SL, Irvine AH, Abele RP. Calculus formation in renal transplant patients. *J Urol* **1984**;132:448–449
14. Hendren WH, Hendren RB. Bladder augmentation: experience with 129 children and young adults. *J Urol* **1990**;144:445–453

Come to the American Roentgen Ray Society

92nd

ANNUAL MEETING

Orlando, FL

Marriott's Orlando World Center
May 10–15, 1992

Scientific Program (200 papers)
Instructional Courses (60 hours)
Categorical Course on Neuroradiology
The Caldwell Lecture
Award Papers
Scientific Exhibits
Social, Golf, and Tennis Programs
Guest Programs

Normal Splenic Size in Infants and Children: Sonographic Measurements

Henrietta Kotlus Rosenberg[1]
Richard I. Markowitz[1]
Heidi Kolberg[1,2]
Chanhi Park[1,3]
Anne Hubbard[1]
Richard D. Bellah[1]

The purpose of this study was to establish guidelines for normal splenic size at different ages by using a simple and reproducible sonographic method. Two hundred thirty patients, from neonate to 20-year-old, had sonography because of abdominal and/or pelvic problems unrelated to the spleen. Findings on sonograms of the liver and kidneys were normal in all cases. Splenic size was measured by obtaining a coronal view that included the hilum, while the patient was breathing quietly. The greatest longitudinal distance between the dome of the spleen and the tip (splenic length) was measured and correlated with age, height, and weight. The following guidelines are proposed for the upper limit of normal splenic length based on this simple, easy to use, one-measurement technique: splenic length no greater than 6.0 cm at 3 months, 6.5 cm at 6 months, and 7.0 cm at 12 months, 8.0 cm at 2 years, 9.0 cm at 4 years, 9.5 cm at 6 years, 10.0 cm at 8 years, 11.0 cm at 10 years, 11.5 cm at 12 years, 12.0 cm at 15 years or older for girls, and 13.0 cm at 15 years or older for boys. Twenty-two patients with known abnormalities of the spleen were randomly selected and their splenic lengths compared with the proposed guidelines; in each case, the length of the spleen exceeded the upper limit of normal for that age.

Normal values of a single measurement of the greatest longitudinal diameter of the spleen, from the dome to the tip measured at the hilum in the coronal plane, were obtained in patients from newborn to 20 years old.

***AJR*157:119-121, July 1991**

Evaluation of splenic size by percussion and palpation is notoriously inaccurate. Radiologic methods and scintigraphy, although dependable, require radiation exposure [1, 2]. The calculation of splenic volume in children by using sonographic measurements can be cumbersome and time-consuming and therefore impractical for routine clinical use [3]. Our purpose was to establish the normal range of splenic size in a population of children, from full-term neonate to 20-year-old, to develop a practical, reliable sonographic approach for measurement, and to establish guidelines for normal splenic size in children.

Materials and Methods

We prospectively studied 230 nonconsecutive patients, including 89 boys and 141 girls. Of these, 58 were infants from full-term neonate to 12 months old. Among the 172 children between 1 and 20 years old, 58 were boys and 114 were girls. The patients selected for the study were being evaluated sonographically for abdominal and/or pelvic problems unrelated to the spleen, most often because of urinary tract infection or abdominal pain. They had no history of disease related to the liver or spleen and no gastrointestinal, hematologic, oncologic, or traumatic conditions. Their liver and both kidneys had to be normal in size, position, and echotexture to qualify for inclusion in the study. Splenic length was measured sonographically during quiet breathing with the patient supine or in a slightly right lateral decubitus position. In the first 90 patients, we measured four different parameters. On the transverse coronal image, a measurement of the width of the spleen was made at the hilum, followed by a depth measurement taken at a point bisecting the line indicating the width. The width of the spleen

Received August 23, 1990; accepted after revision January 28, 1991.

Presented at the annual meeting of the Society for Pediatric Radiology, Cincinnati, OH, April 1990.

[1] Department of Radiology, Division of Ultrasound, The Children's Hospital of Philadelphia, 34th St. and Civic Center Blvd., Philadelphia, PA 19104. Address reprint requests to H. K. Rosenberg.

[2] Present address: The Graduate Hospital, One Graduate Plaza, Philadelphia, PA 19146.

[3] Present address: Holy Cross Hospital, 1500 Forrest Glen Rd., Silver Springs, MD 20910.

0361-803X/91/1571-0119
© American Roentgen Ray Society

was also measured at the hilum on a longitudinal coronal image and the maximal splenic length, determined optically, was made in a plane where the hilum was visualized (Fig. 1). As it became obvious that the only reliable, reproducible measurement was the one made in the longitudinal coronal plane, we obtained only this measurement in the last 140 patients. The data were plotted as a function of age in months, sex, height, and weight. We ascertained that the height and weight of our patients followed normal growth curves.

In addition, we obtained coronal measurements of the spleen in 22 randomly selected patients (14 boys, eight girls) with clinically apparent and explainable splenomegaly. Eleven children were less than 10 years old and 11 were more than 10 years old. Seven patients had chronic hemolytic anemia, five had portal hypertension, four had a viral infection, three had leukemia/lymphoma, and three had miscellaneous reasons for splenomegaly. We compared the maximal coronal measurement of each enlarged spleen with the upper limit of normal seen in the same age group in our normal population.

Results

A roughly logarithmic correlation between splenic length and age (r = .7) was found for the total group of 230 infants and children (Fig. 2). Likewise, good correlation was found between splenic length and patient's height (r = .73) and weight (r = .78). No statistically significant difference was seen between boys and girls except in teenagers more than 15 years old, where males had slightly longer spleens than females, generally correlating with their larger size overall (Table 1). The data were grouped by age, and calculations of the median splenic length and the 10th and 90th percentile were made for each group (Table 2). These results are shown graphically in Figure 3. A suggested upper limit of normal was derived by using the next highest whole integer above the 90th percentile figure. Note that exceptions were made for three groups in which a half integer higher was thought to be more appropriate. Different guidelines for boys and girls were suggested for the 15- to 20-year-old group.

In all the children with clinically obvious splenomegaly, the splenic length exceeded the suggested upper limit of normal (Fig. 4). In each patient more than 1 year old, the splenic length exceeded the suggested guideline by at least 2 cm.

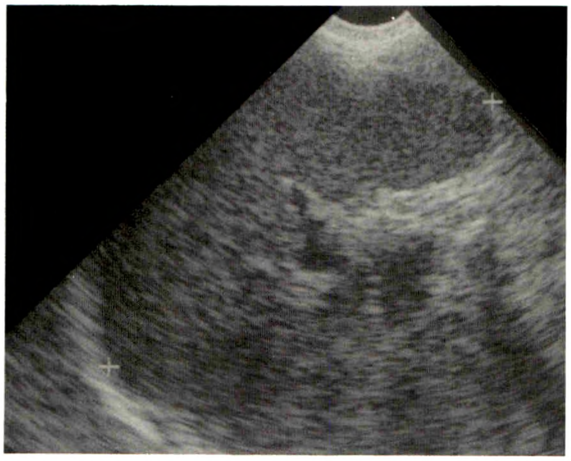

Fig. 1.—Coronal sonogram of spleen. Maximal splenic length, determined optically, is measured in longitudinal coronal plane, with splenic hilum visualized.

Discussion

Sonography provides a simple, practical, reliable means for obtaining splenic length measurements in infants and children. Our technique, however, does not allow volume measurements as other authors' techniques have, but instead serves as a guide for selecting those patients who require more quantitative estimations of splenic size.

Several groups have determined normal splenic volume and weight [4–6]. DeLand used data from 440 autopsy specimens in adults and found that splenic weight is related to the age and sex of the patient [7]. He noted that splenic weight decreases from 20 to 29 years of age and above 60 years, but is relatively constant from 30 to 59 years. He also observed that splenic weight is lower in women than in men for all ages.

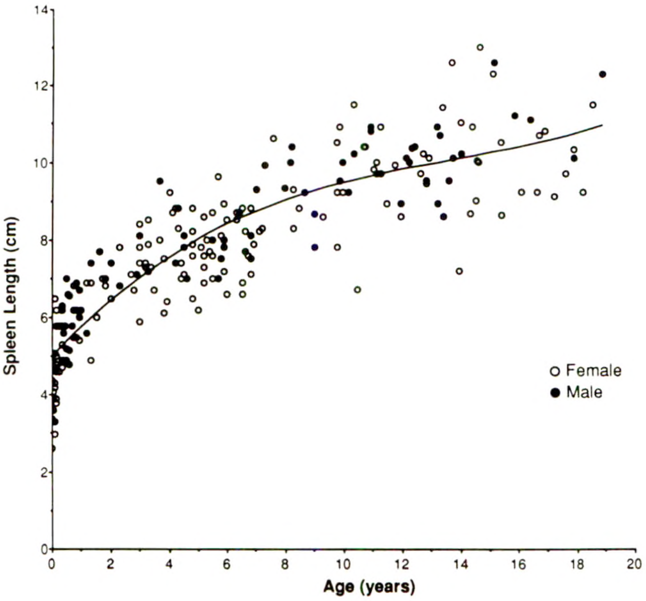

Fig. 2.—Length of spleen (cm) plotted against age (years) shows a roughly logarithmic correlation (r = .7) for total group of 230 normal infants and children.

TABLE 1: Median Splenic Length in 230 Male and Female Infants and Children

Age	Male (n = 89)	Female (n = 141)	p[a]
0–3 months	4.6 (n = 7)	4.4 (n = 21)	NS[b]
3–6 months	5.6 (n = 11)	5.0 (n = 2)	NS
6–12 months	6.2 (n = 13)	5.9 (n = 4)	NS
1–2 years	7.4 (n = 5)	6.8 (n = 7)	NS
2–4 years	7.3 (n = 6)	7.5 (n = 18)	NS
4–6 years	7.8 (n = 10)	7.8 (n = 29)	NS
6–8 years	8.7 (n = 7)	8.2 (n = 14)	NS
8–10 years	9.5 (n = 7)	9.2 (n = 9)	NS
10–12 years	9.7 (n = 7)	10.0 (n = 10)	NS
12–15 years	10.1 (n = 11)	10.0 (n = 15)	NS
15–20 years	11.2 (n = 5)	10.0 (n = 12)	<.05

[a] p values calculated with the Mann-Whitney U-test.

[b] NS = No statistically significant difference between males and females.

TABLE 2: Age and Splenic Length in 230 Infants and Children

Age (Number)	Length of Spleen (cm)			
	10th %ile	Median	90th %ile	Suggested Upper Limit
0–3 months ($n = 28$)	3.3	4.5	5.8	6.0
3–6 months ($n = 13$)	4.9	5.3	6.4	6.5
6–12 months ($n = 17$)	5.2	6.2	6.8	7.0
1–2 years ($n = 12$)	5.4	6.9	7.5	8.0
2–4 years ($n = 24$)	6.4	7.4	8.6	9.0
4–6 years ($n = 39$)	6.9	7.8	8.8	9.5
6–8 years ($n = 21$)	7.0	8.2	9.6	10.0
8–10 years ($n = 16$)	7.9	9.2	10.5	11.0
10–12 years ($n = 17$)	8.6	9.9	10.9	11.5
12–15 years ($n = 26$)	8.7	10.1	11.4	12.0
15–20 years ($n = 17$)				
Female	9.0	10.0	11.7	12.0
Male	10.1	11.2	12.6	13.0

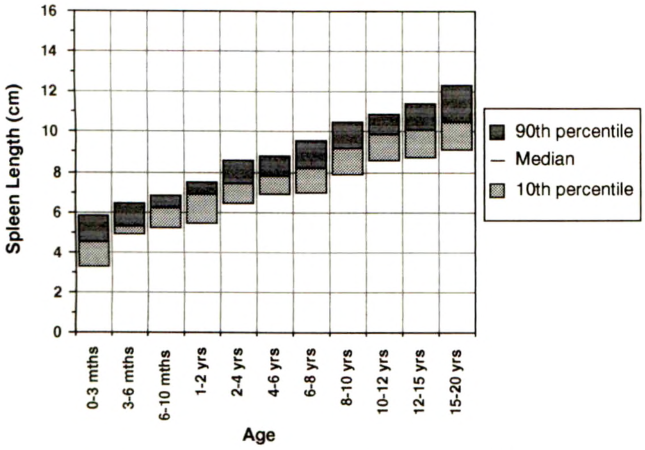

Fig. 3.—Median length of spleen, 10th percentile, and 90th percentile plotted against various age groups (full-term neonate to 20-year-old) in our normal population of 230 infants and children.

Other measurements of splenic volume, in adults, have been described by using rectilinear scintigraphic scans after injection of ^{113m}In-labeled heat-damaged RBCs [1] and sonography [8–10]. Niederau et al. [9] found, using sonographic measurements in adults, that splenic size decreases with age and that splenic diameters correlate poorly with physical data.

To our knowledge, only two papers that describe imaging techniques for determination of splenic size in children have been published. Markisz et al. [2] used sulfur colloid scintigraphy to measure splenic volume (using the equation for a prolate spheroid) in 116 patients and found linear correlation with age or weight to be poor, but obtained improved correlation when considering splenic volume as a linear function of either age or weight. Dittrich et al. [3] established a nomogram for determining splenic size sonographically on the basis of data collected from 194 healthy children of all ages, using a volume formula for an ellipsoid.

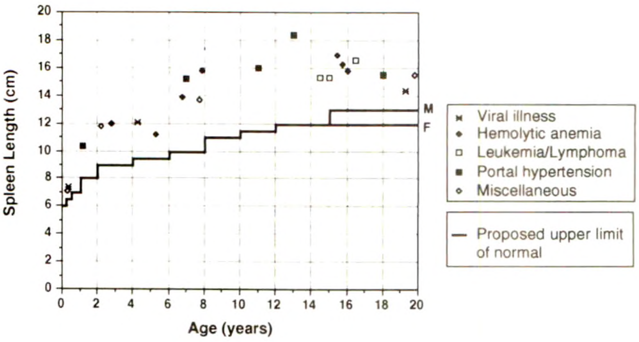

Fig. 4.—Length of spleen in 22 cases of splenomegaly compared with upper limits of normal in our normal population shows that length of spleen in all cases of splenomegaly exceeded suggested upper limit of normal for same age group.

We found these techniques far too cumbersome and time-consuming for practical everyday use and suggest the following upper-limit guidelines for sonographically assessing splenic length in infants and children with our one-step coronal measurement: 0–3 months, 6.0 cm; 3–6 months, 6.5 cm; 6–12 months, 7.0 cm; 1–2 years, 8.0 cm; 2–4 years, 9.0 cm; 4–6 years, 9.5 cm; 6–8 years, 10.0 cm; 8–10 years, 11.0 cm; 10–12 years, 11.5 cm; 12–15 years, 12.0 cm; female 15–20 years, 12.0 cm; and males 15–20 years, 13.0 cm.

ACKNOWLEDGMENTS

We thank Peter N. Burns for help with the statistical analysis. We also thank Henry Rosenberg and Kenneth E. Fellows for reviewing the manuscript; sonographers Margaret Muller, Charlene Fessler, Sivan Pillai, and Carole Barletta for technical assistance; and Janet L. Birkmann and Nisha Merchant for secretarial assistance.

REFERENCES

1. Zhang B, Lewis SM. Use of radionuclide scanning to estimate size of spleen in vivo. *J Clin Pathol* **1987**;40:508–511
2. Markisz JA, Treves ST, Davis RT. Normal hepatic and splenic size in children scintigraphic determination. *Pediatr Radiol* **1987**;17:273–276
3. Dittrich M, Milde S, Dinkel E, Baumann W, Weitzel D. Sonographic biometry of liver and spleen size in childhood. *Pediatr Radiol* **1983**;13:206–211
4. McCormick WF, Kashgarian M. The weight of the adult human spleen. *Am J Clin Pathol* **1965**;43:332–333
5. Boyd E. Normal variability in weight of the adult human liver and spleen. *Arch Pathol Lab Med* **1933**;16:350–372
6. Meyer WW, Peter B, Solth K. Die organgliwichte in den hoheren Alterss-trufen (70-92 Jahre) in ihrer Beziehung zum Alter und Korsergewicht. *Virchows Arch [A]* **1963**;37:17–32
7. DeLand FH. Normal spleen size. *Radiology* **1970**;97:589–592
8. Koga T, Morikawa Y. Ultrasonographic determination of the splenic size and its clinical usefulness in various liver diseases. *Radiology* **1975**;115:157–161
9. Niederau C, Sonnenberg A, Muller JE, Erckenbrecht JF, Scholten T, Fritsch WP. Sonographic measurements of the normal liver, spleen, pancreas and portal vein. *Radiology* **1983**;149:537–540
10. Pietri H, Buscaini M. Determination of a splenic volumetric index by ultrasonic scanning. *J Ultrasound Med* **1984**;3:19–23

Book Review

Magnetic Resonance Imaging of the Pediatric Brain. An Anatomical Atlas. By G. Salamon, C. Raynaud, J. Regis, and C. Rumeau. New York: Raven, 350 pp., 1990. $105

This MR atlas of the pediatric brain is organized into nine chapters that show sequential changes in anatomic appearance and, to a lesser degree, in myelination of the pediatric brain with maturation. The authors chose an axial plane parallel to the canthotragal line as the plane for all the MR studies, with correlations to line drawings of the brain viewed laterally (external and internal projections) and axially. All images are T1 weighted. Corresponding anatomically labeled line drawings illustrate supratentorial structures of normal infants at 1- to 4-month intervals to the age of 18 months and then at 1- to 3-year intervals to the age of 16 years. The authors emphasize that anatomic localizations correlated with anatomy based on an atlas of the adult brain fail to account for growth in the craniofacial structures, potentially resulting in errors in localization of intracranial structures in the child.

The introductory chapter describes the methods used for localization of various gyri and sulci based on two- or three-dimensional line drawings. Sagittal MR images are presented sequentially by age with corresponding line drawings, although unfortunately the line drawings reverse in left-right orientation inconsistently from page to page. The introductory chapter concludes with detailed illustrations of phylogenetic brainstem development in a variety of species; the atlas subsequently omits anatomy of the brainstem and cerebellum.

Subsequent chapters include a level-by-level demonstration of supratentorial gyral and sulcal development by age, with correlative line drawings of supratentorial anatomy. The pulse sequences used for the MR images are not described; however, visually these and the window and level of the MR images vary from image to image, making it difficult to assess sequential myelination. For example, the intensity of subcortical white matter on the illustration of the newborn is markedly hypointense compared with the other images of infants less than 3 months old. Although the importance of a constant scan angle in ensuring correct anatomic localization is stressed, several of the images of infants were obtained at an unspecified "alternate" angle.

In summary, this atlas illustrates the anatomic development of supretentorial sulcal and gyral structures with maturation in children. This is helpful for correct gyral and sulcal identification and for correlation with other imaging techniques. The omission of posterior fossa anatomic structures, T2-weighted images, and multiplanar MR images limits the usefulness of this text as a generally applicable atlas for radiologists who perform and interpret MR examinations of the brains of infants and children.

Patricia C. Davis
Emory University School of Medicine
Atlanta, GA 30322

MR Imaging of the Brain in Patients with Diabetes Insipidus

Robert Tien[1,2]
John Kucharczyk
Walter Kucharczyk

Diabetes insipidus is a clinical syndrome characterized by the excretion of copious volumes of dilute urine combined with persistent intake of abnormally large quantities of fluid. There are two general forms of the disease, central (vasopressin deficient) and nephrogenic (vasopressin resistant). Diabetes insipidus of central origin most often results from lesions in the hypothalamic-neurohypophyseal axis. Twenty-six cases of central diabetes insipidus were evaluated with the use of high-field-strength MR imaging. A wide variety of precipitating conditions were found, including Langerhans cell histiocytosis, neoplasia, trauma, and infection. A thickened pituitary infundibulum was seen in most patients, and an absence of high intensity signal in the posterior pituitary lobe on T1-weighted images was seen in every case. Analysis of stalk morphology; associated brain findings; and correlation with the patient's age, sex, history, and radiographs of other body parts improved diagnostic specificity.

When combined with clinical information, MR imaging is able to provide a specific diagnosis in almost all cases of central diabetes insipidus.

***AJNR* 12:533-542, May/June 1991; *AJR* 157:123-132, July 1991**

Diabetes insipidus (DI) is a disorder characterized by abnormally large volumes (>30 ml/kg per day) of dilute urine (<250 mosmol/l) and persistent thirst [1]. Probably the most common causative defect is inadequate secretion of antidiuretic hormone (ADH), a disorder variously termed neurogenic, central, or hypothalamic DI. DI can also result from renal insensitivity to the antidiuretic effects of ADH (nephrogenic DI). Patients with central DI who fail to ingest adequate volumes of water (hypodipsia) are at risk for developing life-threatening hypernatremia, and constant care may be required to ensure fluid-electrolyte balance [2]. Symptomatic polydipsia and polyuria can also result from inappropriately excessive fluid intake in the absence of any underlying defect in ADH biosynthesis or release (psychogenic polydipsia), although this cause is very rare [2].

Earlier studies [3] suggested that idiopathic central DI accounted for approximately 50% of all cases. More recent work suggests, however, that head injury and surgery in the sellar area are responsible for a higher percentage of cases. In a study of 119 patients with long-standing (>6 months) central DI, Moses [1] reported that 50% developed DI after head injury or surgery on the pituitary or hypothalamus, whereas 25% had idiopathic central DI. In 8% of the patients, DI developed from cancer metastases to the hypothalamus, 6% of the cases resulted from malignant brain tumors, 6% were related to nontraumatic encephalomalacia, and 3% were related to Langerhans cell histiocytosis [4]. The hereditary forms of central DI are extremely rare, accounting for about 1% of all cases [5]. Other rare causes include thrombotic thrombocytopenic purpura [6], pituitary apoplexy [7], postpartum pituitary necrosis [8, 9], Wegener granulomatosis [10], and systemic blastomycosis [11]. Infiltration of the hypothalamus by amyloid or sarcoidosis has also been reported [2]. Imaging studies (CT or MR) of the hypothalamic-pituitary

Received September 5, 1990; revision requested November 20, 1990; revision received December 12, 1990; accepted December 21, 1990.

[1] All authors: Department of Radiology, Neuroradiology Section, University of California, San Francisco, CA 94143.

[2] Present address: Department of Radiology, University of California, San Diego, 225 Dickinson St., San Diego, CA 92103. Address reprint requests to R. Tien.

0361-803X/91/1571-0123
© American Roentgen Ray Society

TABLE 1: Clinical and MR Findings in Patients with Diabetes Insipidus (DI)

Cause of DI/Case No.	Age (yr)	Sex	Type of DI; Signs/Symptoms	MR Findings in Hypothalamus/Pituitary	MR Enhancement	Pathologic Documentation/Further Pathologic Findings
Langerhans cell histiocytosis						
1	29	F	Acute	Symmetric, thickened stalk; no hyperintensity in post pituitary on T1	Homogeneously enhanced thickened stalk	Stalk biopsy
2	14	F	Acute	Symmetric, thickened stalk; no hyperintensity in post pituitary on T1	Enhanced studies not performed	Mastoid biopsy
3	1	F	Acute	Symmetric, thickened stalk; no hyperintensity in post pituitary on T1	Homogeneously enhanced thickened stalk	Skin biopsy
4	57	F	Acute	Symmetric, thickened stalk; no hyperintensity in post pituitary on T1	Homogeneously enhanced thickened stalk and hypothalamic nodule	Stalk biopsy
5	32	F	Acute	Symmetric, thickened stalk; no hyperintensity in post pituitary on T1	Enhanced studies not performed	Lung biopsy
6	28	F	Acute	Symmetric, thickened stalk; no hyperintensity in post pituitary on T1	Enhanced studies not performed	Lung biopsy
Germinoma						
7	19	M	Acute; Parinaud syndrome	No hyperintensity in post pituitary on T1; thickened upper stalk	Enhancement of hypothalamus and R trigonal subependymal nodule; heterogeneously enhanced pineal mass	Pineal biopsy
8	19	M	Acute; Parinaud syndrome	No hyperintensity in post pituitary on T1; thickened upper stalk	Enhanced studies not performed	Pineal biopsy
9	12	M	Acute; Parinaud syndrome	No hyperintensity in post pituitary on T1; thickened upper stalk	Enhanced studies not performed	Pineal biopsy
10	13	M	Chronic	No hyperintensity in post pituitary on T1; thickened upper stalk	Enhancement of hypothalamus and optic chiasm	Hypothalamic mixed germ cell tumor
Craniopharyngioma						
11	10	M	Acute	Hypothalamic mass; no hyperintensity in post pituitary on T1	Enhanced cystic mass occupying third ventricle	-
12	8	F	Acute; headache	Hypothalamic mass; no hyperintensity in post pituitary on T1	Enhanced studies not performed	-
Hypothalamic glioma						
13	12	M	Acute; visual field defect	Hypothalamic mass; no hyperintensity in post pituitary on T1	Enhanced studies not performed	-
Tuberculosis						
14	17	F	Acute transient; seizures	Symmetric, thickened stalk; no hyperintensity in post pituitary on T1	Abnormal enhancement in basal cisterns	-
Sarcoidosis						
15	24	M	Chronic	Symmetric, thickened stalk; no hyperintensity in post pituitary on T1	Enhanced studies not performed	-
Metastasis						
16	57	M	Transient; visual defect	Sellar/suprasellar mass; no hyperintensity in post pituitary on T1	Inhomogeneously enhancing mass	Oat cell lung carcinoma
17	69	M	Transient; visual defect	Sellar/suprasellar mass; no hyperintensity in post pituitary on T1	Inhomogeneously enhancing mass	Adenocarcinoma
Sellar surgery						
18	42	F	Transient	Postop sellar change; marked structural distortion with high signal due to methemoglobin in sella	Enhanced studies not performed	-
19	37	M	Transient	Postop sellar change; marked structural distortion with high signal due to methemoglobin in sella	Enhanced studies not performed	-
20	47	M	Transient; fever	Postop sellar change; marked structural distortion with high signal due to methemoglobin in sella	Multiloculated enhancing pituitary mass	Pituitary mass

Table 1 continues

TABLE 1—*Continued*

Cause of DI/Case No.	Age (yr)	Sex	Type of DI; Signs/Symptoms	MR Findings in Hypothalamus/ Pituitary	MR Enhancement	Pathologic Documentation/ Further Pathologic Findings
Transection stalk after trauma						
21	17	F	Transient; amenorrhea	Transection of stalk; aberrantly placed hyperintensity in median eminence of post pituitary after resolution of DI	Enhanced studies not performed	–
22	14	M	Transient	Transection of stalk; no hyperintensity in post pituitary on T1	Enhanced studies not performed	–
Erdheim-Chester disease						
23	39	M	Chronic	No hyperintensity in post pituitary on T1; thickened upper stalk	Homogeneously enhanced thickened median eminence	–
Unknown						
24	25	F	Acute	Symmetric, thickened stalk; no hyperintensity in post pituitary on T1	Enhanced studies not performed	–
25	29	F	Acute	Symmetric, thickened stalk; no hyperintensity in post pituitary on T1	Homogeneously enhanced thickened stalk	–
26	52	M	Chronic	Empty sella; downward displaced chiasm; no hyperintensity in post pituitary on T1	Enhanced studies not performed	–

Note.—post = posterior; T1 = T1-weighted images; R = right; postop = postoperative.

region are important in the diagnosis of DI. MR imaging is particularly useful in documenting the presence or absence of a structural lesion, as opposed to assigning a diagnosis of idiopathic DI for which only symptomatic therapy is prescribed.

We report our MR imaging findings in 26 patients with clinically proved DI.

Materials and Methods

We retrospectively studied the MR findings in 26 patients (14 males and 12 females 1–69 years old; mean, 27.7 years of age) seen during the period 1986–1990 with clinical evidence of DI. Clinical histories were correlated with imaging findings. All patients were imaged on a 1.5-T General Electric system. Eleven patients were scanned before and after IV administration of gadopentetate dimeglumine. Surgical specimens were obtained from the hypothalamic-pituitary area or other affected body sites in 19 patients.

The MR technique consisted of unenhanced T1-weighted spin-echo (SE) scans, 600/20/4 (TR/TE/excitations), through the sella in sagittal and coronal planes with 3-mm slices and a 0.5-mm interslice gap. Enhanced studies were obtained in the same planes. Images were reconstructed with two-dimensional Fourier transform on a 256 × 256 image matrix. Axial T2-weighted images (2000/40,80/2) of the whole brain were obtained also in most patients. Additional axial T1-weighted images (600/20/4) of the brain were obtained in 11 patients after contrast administration.

Unenhanced and enhanced images were reviewed by two neuroradiologists. The size, shape, and signal intensity of the pituitary stalk, hypothalamus, and pituitary gland and any associated abnormalities were evaluated. MR findings were correlated with clinical history and surgical pathology.

Results

Results of MR examinations, correlated with the clinical symptoms and signs, associated imaging findings, and surgical pathology, are summarized in Table 1.

Langerhans Cell Histiocytosis

Six female patients 1–57 years old with acute onset and persistent DI were found to have uniformly thickened pituitary stalks 3–4 mm wide in the coronal plane and 3–17 mm wide in the sagittal plane (Fig. 1) (stalks in normal controls were less than 2.8 mm in both planes). One patient had a destructive mastoid lesion. Another had clinical Letterer-Siwe disease (with skin rash and hepatosplenomegaly). Two patients had honeycomb-like interstitial lung disease and the other two had thickened pituitary stalks alone. In none of the patients was high signal intensity seen in the posterior lobe. Enhanced MR was performed in three patients. In two there was normal enhancement of the stalk (cases 1 and 3); in the third (case 4), an enhancing nodule in the hypothalamus proved to be Langerhans cell histiocytosis.

Germ Cell Tumor

Abnormally enlarged upper pituitary stalks were seen in four patients 12–19 years old with acute onset and persistent DI. Coexisting lobulated pineal masses were present in three patients. Abnormal contrast enhancement of the subependymal lining in the anterior recess of the third ventricle from CSF metastasis was seen in one patient (Fig. 2). In another patient, an isolated hypothalamic mass showed enhancement (Fig. 3).

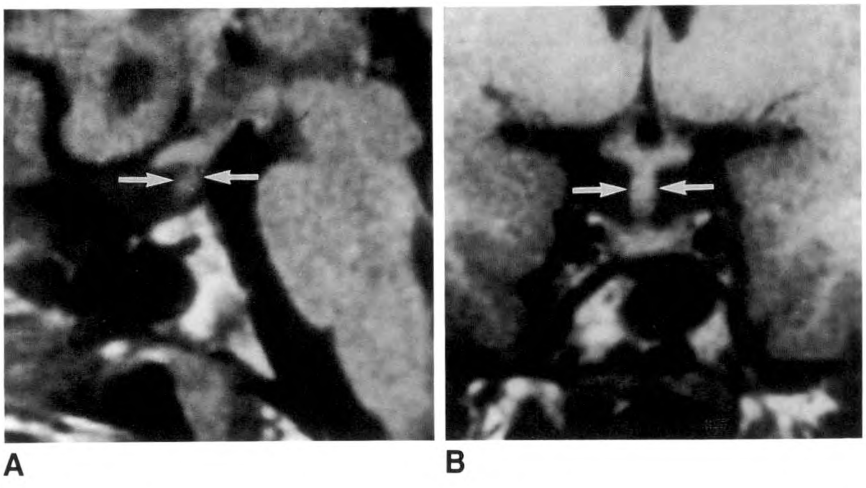

Fig. 1.—Case 5: Uniformly thickened pituitary infundibulum from Langerhans cell histiocytosis.

***A* and *B*, Sagittal (*A*) and coronal (*B*) T1-weighted images (600/20) reveal uniformly thickened (4 mm) pituitary infundibulum (*arrows*). No posterior pituitary hyperintensity was observed.**

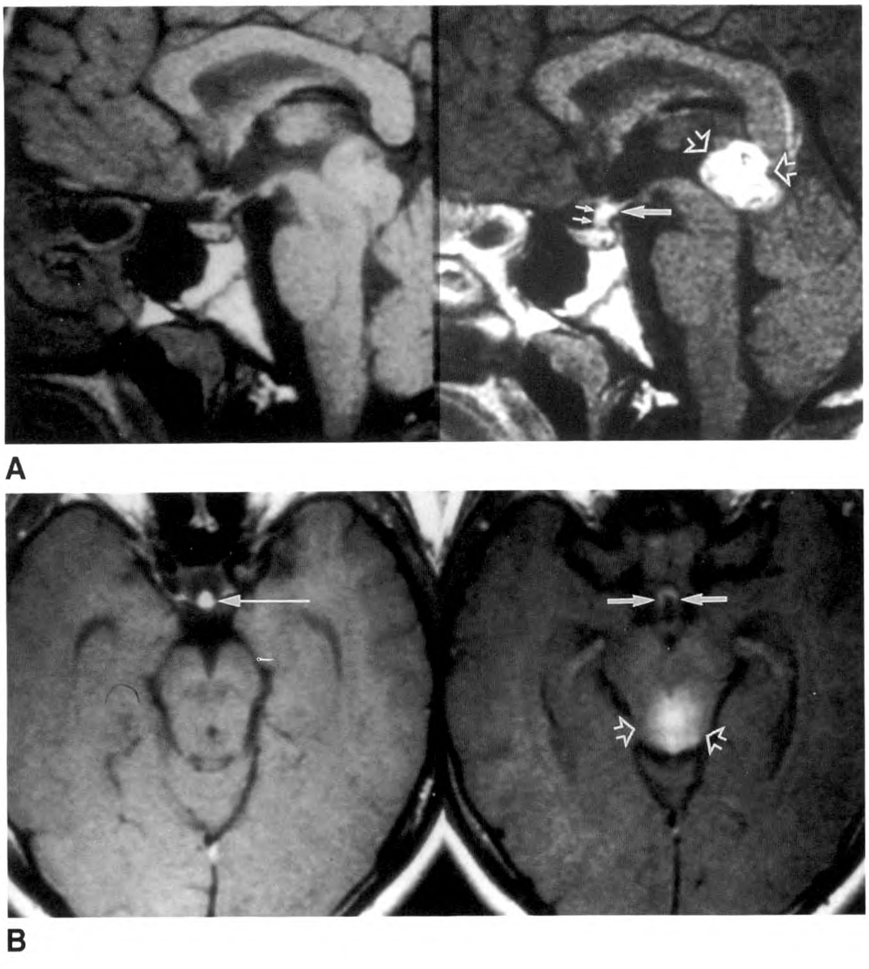

Fig. 2.—Case 7: Hypothalamic metastasis from pineal germinoma.

***A*, Sagittal SE 600/20 images before (left) and after (right) infusion of gadopentetate dimeglumine show heterogeneous enhancement of pineal mass (*open arrows*) and enhancing nodule in median eminence (*long solid arrow*). Pituitary infundibulum is asymmetrically thickened (*short solid arrows*).**

***B*, Axial SE 600/20 images after infusion of gadopentetate dimeglumine reveal enhancing pineal tumor (*open arrows*) as well as subependymal metastasis in anterior recess of third ventricle (*short solid arrows*) and thickened pituitary infundibulum (*long solid arrow*).**

Craniopharyngioma

Craniopharyngiomas were found in two patients (10-year-old boy and 8-year-old girl) with acute onset and persistent DI. In one patient (case 12), a large, rather homogeneous sellar and suprasellar mass was seen that obliterated the anterior third ventricle. Another patient (case 11) with a history of craniopharyngioma was admitted because of sudden onset of DI. After enhancement, MR revealed enhancing sellar and suprasellar masses with a large multicystic lesion that filled the posterior third ventricle, representing the recurrent craniopharyngioma.

Hypothalamic Glioma

A 12-year-old boy (case 13) with acute onset of DI and a visual field defect was evaluated by MR. A 3-cm hypothalamic

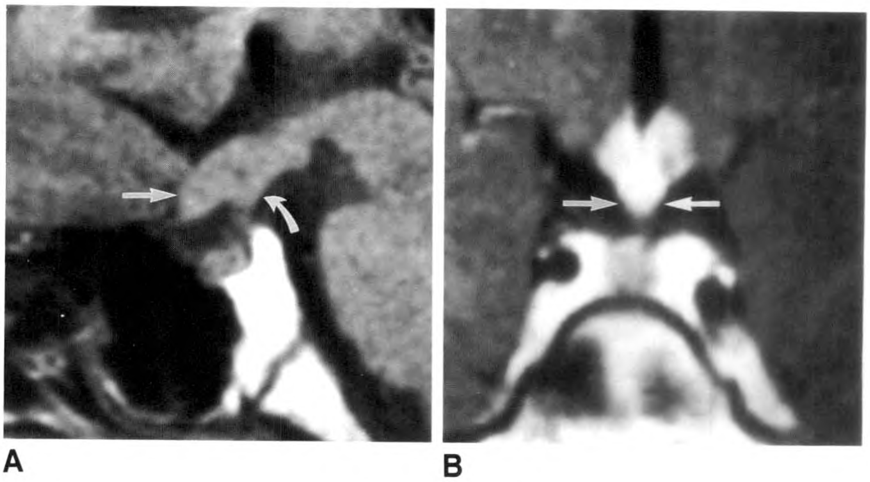

Fig. 3.—Case 10: Hypothalamic mixed germ cell tumor.

A, Sagittal SE 600/20 image reveals hypothalamic mass involving optic chiasm (*straight arrow*) and median eminence (*curved arrow*). Pituitary infundibulum is asymmetrically thickened.

B, Coronal SE 600/20 image after infusion of gadopentetate dimeglumine shows strong but slightly heterogeneous enhancement of hypothalamic mass with involvement of median eminence (*arrows*).

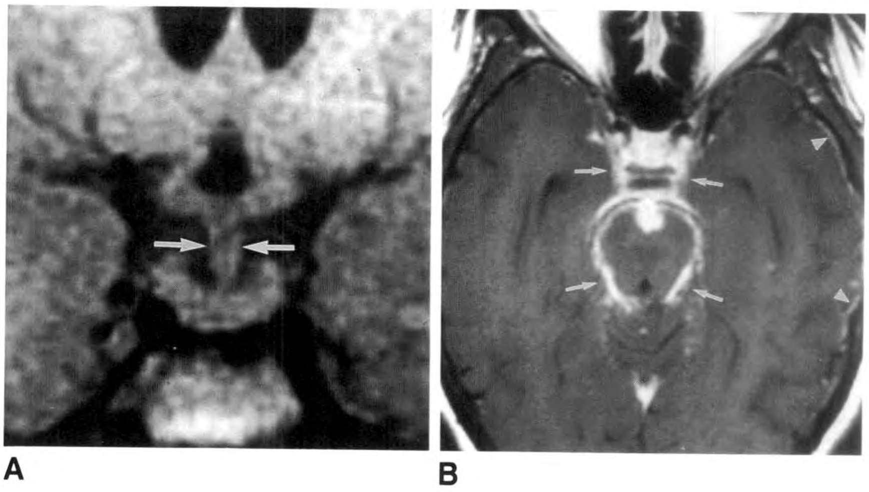

Fig. 4.—Case 14: Uniformly thickened stalk from tuberculosis.

A, Coronal SE 600/20 image reveals uniformly thickened (4 mm) pituitary infundibulum (*arrows*).

B, Axial SE 600/20 image after infusion of gadopentetate dimeglumine shows abnormal enhancement of suprasellar and circummesencephalic cisterns (*arrows*) as well as of leptomeninges (*arrowheads*).

lesion was detected. It was isointense on T1-weighted images and hyperintense on T2-weighted images. There was some mass effect on the chiasm.

Tuberculosis and Sarcoidosis

The patient with tuberculosis was a 17-year-old girl admitted with seizures and acute onset of DI. MR showed a uniformly thickened stalk (Fig. 4A). After administration of contrast material, there was diffuse enhancement in the basal cisterns (Fig. 4B). A spinal epidural abscess was noted also. CSF revealed tuberculosis bacilli. After antituberculous treatment, the DI resolved. The other patient (a 24-year-old man) was known to have a history of pulmonary sarcoidosis with chronic DI. MR revealed a uniformly thickened stalk, presumably representing neurosarcoidosis.

Metastases

Two patients (a 57-year-old man and a 69-year-old man) with transient DI and visual defects were evaluated. MR showed destructive, inhomogeneously enhancing sellar and suprasellar masses in both cases (Fig. 5). Systemic examinations revealed the primary carcinomas.

Postoperative Sella

Transsphenoidal hypophysectomy for pituitary adenoma had been performed recently in three patients (cases 18–20). Transient DI was noted in each case. T1-weighted MR images within 2 weeks after surgery in cases 18 and 19 showed an area of signal hyperintensity in the pituitary fossa with associated mass effect. This most likely represented methemoglobin accumulation in the surgical bed, a fairly typical feature of the early postoperative sella (Fig. 6). No treatment was given in case 18 or 19. In case 20, a patient with severe headache and fever, enhanced MR images revealed a multiloculated enhancing sellar mass (Fig. 7); pituitary abscess was suspected. DI disappeared after drainage.

Post-Traumatic Transection of the Stalk

Two patients (cases 21 and 22) had been injured in car accidents and had a history of transient DI. One patient (case 21) also had amenorrhea. In case 21, MR performed 2 years after the accident showed a transected stalk with bright signal at the proximal stalk stump. In this patient, DI had resolved completely by the time of MR imaging (Fig. 8). In the other patient (case 22), MR performed 3 months after the car accident showed a ruptured anterior third ventricle and a

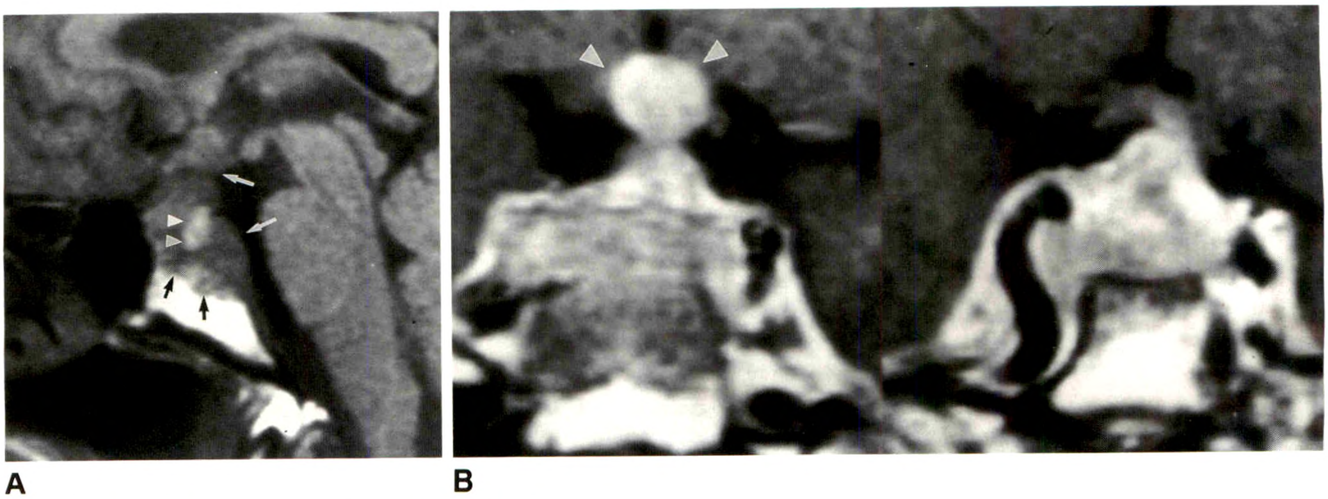

Fig. 5.—Case 16: Sellar and suprasellar mass from lung cancer.

A, Sagittal SE 600/20 MR image reveals an inhomogeneous sellar mass with suprasellar extension (*white arrows*). Irregular border of pituitary floor (*black arrows*) is attributable to tumor invasion. Central high signal intensity (*arrowheads*) most likely represents methemoglobin from intratumoral hemorrhage.

B, Coronal SE 600/20 contiguous MR images after infusion of gadopentetate dimeglumine show inhomogeneous enhancement of this sellar and suprasellar mass. Hypothalamus is involved (*arrowheads*).

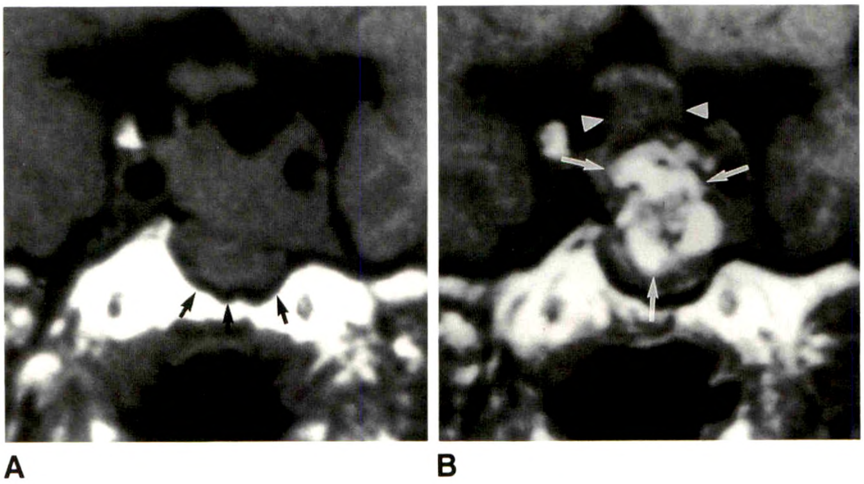

Fig. 6.—Case 18: Pre- and postoperative sella.

A, Preoperative coronal SE 600/20 MR image shows irregularly shaped pituitary macroadenoma with depression of floor of sella (*arrows*).

B, Postoperative coronal SE 600/20 MR image 2 weeks after surgery. Large hyperintense area in sella with associated mass effect (*arrows*) probably represents methemoglobin accumulation in surgical bed. Tumor or residual gland appears to have been displaced into suprasellar region (*arrowheads*).

completely transected stalk. The bright spot was not identified at any location. The patient continued to have DI for several months after the MR study.

Erdheim-Chester Syndrome

A 39-year-old man had an 8-year history of bone pain and DI. Enhanced MR showed a thickened enhancing upper pituitary stalk (Fig. 9A); the bone scan showed symmetric diffuse osteoblastic changes in peripheral long bones (Fig. 9B). Bone biopsy showed changes typical of Erdheim-Chester disease.

Unknown Etiology

Two young women 25 and 29 years old (cases 24 and 25, respectively) had acute onset and persisting DI. MR showed a uniformly thickened stalk in each case. No other abnormalities were noted. In several respects the MR findings were similar to those in case 1, a patient in whom Langerhans cell histiocytosis was diagnosed by biopsy. Since no biopsy data were obtained, these two patients were categorized as unknown. In another patient (case 26), a 52-year-old man with chronic DI, an empty sella and a downwardly displaced chiasm were seen on MR.

In summary, a total of 10 cases of uniformly thickened pituitary infundibulum were seen in six patients with Langerhans cell histiocytosis, one patient with tuberculosis, one patient with sarcoidosis, and two patients with DI of unknown origin. A thickened upper stalk was seen in the four patients with germ cell tumor and the one patient with Erdheim-Chester syndrome. In the remaining patients, the integrity of the infundibulum was either directly compromised by the tumor itself, distorted by surgery, or transected as a result of

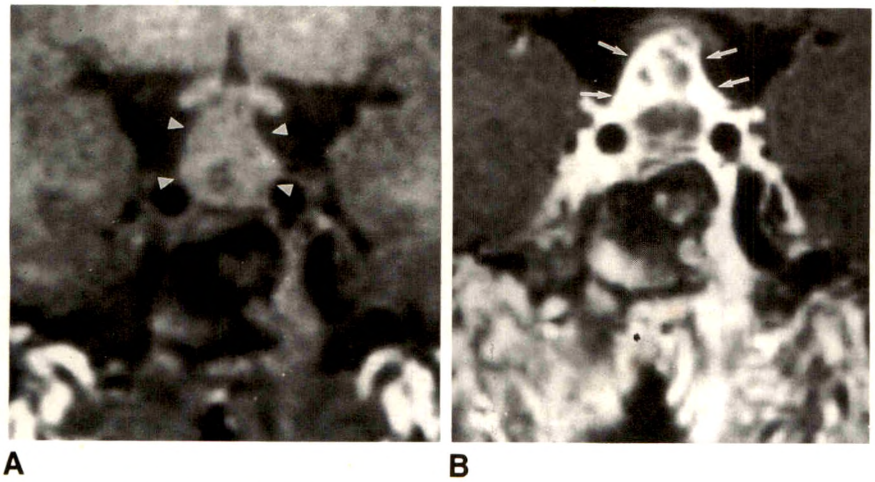

Fig. 7.—Case 20: Postoperative pituitary abscess.

A, Coronal SE 600/20 MR image shows inhomogeneous pituitary mass with suprasellar extension (*arrowheads*).

B, Coronal SE 600/20 MR image after infusion of gadopentetate dimeglumine shows abnormal multiloculated enhancement pattern of this mass (*arrows*).

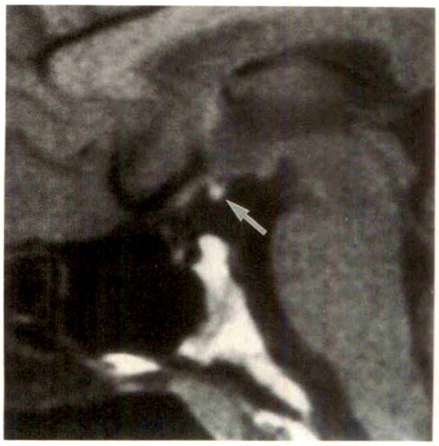

Fig. 8.—Case 21: Transection of pituitary infundibulum resulting from car accident accompanied by transient diabetes insipidus. Sagittal SE 600/20 MR image shows transected pituitary infundibulum and hypoplastic pituitary gland. High-signal focus at median eminence (*arrow*) represents the same material noted in normal high-signal posterior pituitary. Diabetes insipidus had resolved completely by the time this image was obtained.

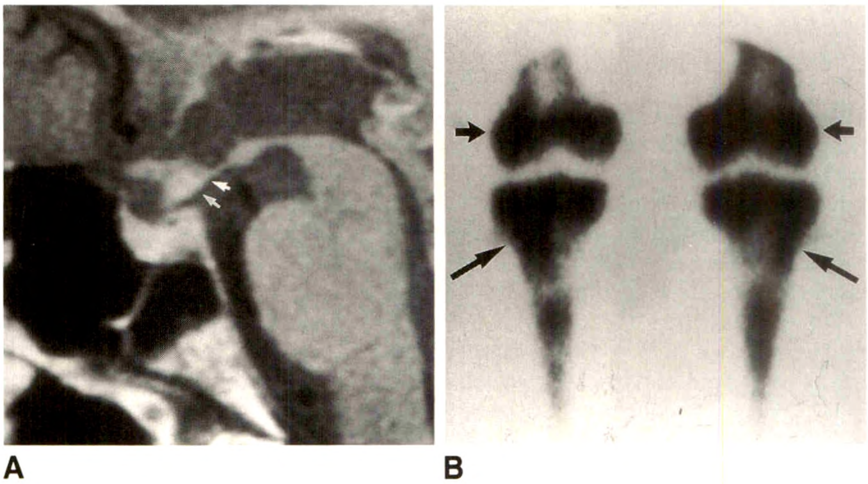

Fig. 9.—Case 23: Erdheim-Chester disease.

A, Sagittal SE 600/20 MR image after infusion of gadopentetate dimeglumine shows enhancement in a thickened median eminence (*arrows*) of pituitary infundibulum.

B, ^{99m}Tc bone scan reveals increased osteoblastic activity bilaterally in femur (*short arrows*) and tibia (*long arrows*).

mechanical trauma in the region; thus, identification of an isolated thickened infundibulum was not possible.

The normally hyperintense posterior pituitary region was not observed in 22 patients. In three postoperative cases, postsurgical changes made identification of the posterior lobe signal intensity impossible to establish. In another patient with a history of transient DI, an aberrant bright spot was observed at the median eminence after resolution of DI.

Discussion

In the vast majority of cases, the diagnosis of DI is made on clinical grounds. The role of imaging is to determine the cause of DI, and the available data indicate that MR is currently the best imaging technique for this purpose. MR images clearly demonstrate hypothalamic-pituitary morphology and can detect subtle abnormalities in the region of the sella. A diagnosis of idiopathic DI should be considered only after appropriate MR imaging has been completed and the presence of structural lesions excluded.

Approximately two thirds of patients with central DI have infiltrative lesions involving the hypothalamic-neurohypophyseal axis [1]. Langerhans cell histiocytosis was the single leading cause of DI in the present study, accounting for 23% of cases. All patients with this etiology were females with DI of acute onset that persisted despite treatment. A review of 180 patients with multifocal eosinophilic granulomas indicated that 56% had DI, 25% had skin manifestations, 15% had pulmonary infiltrates, and 15% had otitis media [12]. This suggests that imaging studies of the lungs, temporal bones, or even the peripheral long bones may be useful diagnostic adjuncts in patients with Langerhans cell histiocytosis (cases 2, 3, 5, and 6). At the same time, it is also noteworthy if a thickened stalk is the only presentation of Langerhans cell histiocytosis (such as in case 1). In two other patients (both females), MR findings were similar. Although these cases (cases 24 and 25) were categorized as DI of unknown origin based on the patients' ages, histories, and imaging results, Langerhans cell histiocytosis may have been responsible for the DI in these cases also. As well, some patients with thickened stalks noted on CT, who were listed as having idiopathic DI [1], may also represent cases of Langerhans cell histiocytosis.

Germ cell tumor was found in the next largest group of patients with DI and was the most common intracranial tumor associated with central DI in children, in agreement with prior reports [13]. All of our patients were teenage boys. Three had a pineal mass with CSF metastasis and Parinaud syndrome (paralysis of upward gaze). MR clearly demonstrated a thickened upper pituitary stalk and lobulated pineal mass. Enhanced MR revealed enhancing CSF metastases (case 7) and suprasellar hypothalamic enhancing mixed germ cell tumor (case 10). In a previous study, dysgerminoma was found to be the most common intracranial tumor associated with neurogenic DI in children, with craniopharyngioma the second most common [13]. DI has been reported in 40% of children with Langerhans cell histiocytosis [13].

DI associated with infiltrative inflammatory processes such as tuberculosis or sarcoidosis is also well established [14]. MR revealed a uniformly thickened stalk resembling that in Langerhans cell histiocytosis, which has been reported by other investigators also [14]. However, the chest radiographs provided crucial evidence for the diagnosis. Transient DI was noted in a patient with tuberculosis meningitis, as evidenced by contrast-enhanced MR. Transient DI has been reported previously in patients with meningitis [15, 16].

The prevalence of metastases within the pituitary gland ranges from 1.8–12% in different series. Most common are metastases from the breast, followed by carcinoma of the gastrointestinal system. About 20% of these metastases are diagnosed clinically with DI as the main presenting symptom [17]. DI of a transient nature may represent metastases to the posterior lobe of the pituitary without significant encroachment on the supraoptic and paraventricular nuclei of the hypothalamus. In the present study, MR revealed the destructive nature of such lesions. Therefore, in older individuals in particular, metastases merit some consideration in the diagnosis.

An association between transient DI and the postoperative sella is not uncommon. It appears to represent selective damage to the posterior lobe without concurrent damage to the hypothalamic neurosecretory nuclei. DI is often associated with persistent anterior lobe dysfunction from surgical damage. The presence of transient DI with fever, headache, visual disturbances, and anterior lobe dysfunction in a patient who recently underwent sellar surgery strongly suggests pituitary abscess [18]. A loculated ring-enhancing sellar mass on MR with clinical symptomatology of DI is diagnostic.

Posttraumatic transection of the stalk with DI has been described in previous MR studies [19]. In most cases the DI develops within a few days after stalk section and is transient, but in one third of the patients it remains as a chronic complication without concurrent dysfunction of the anterior lobe [20]. Differential diagnosis from congenital pituitary dwarfism is based on the clinical history. It has been reported that dwarfs have a hypoplastic stalk and anterior pituitary lobe [21].

An interesting etiologic combination was seen in the patient with Erdheim-Chester disease and central DI. Erdheim-Chester disease is a rare entity, typically represented by symmetric osteoblastic changes in peripheral long bones with lipid-laden histiocytes and giant cells in bones and visceral organs [22, 23]. One case of Erdheim-Chester disease involving the brain parenchyma was described [24] in which enhancement on MR persisted 7 days after administration of contrast material. However, involvement of the hypothalamus with associated DI has not been reported previously, which is somewhat surprising given the highly infiltrative nature of this disease. Of some interest also is the MR finding in the patient in our study in whom enhancement was no longer seen 1 day after contrast administration. The explanation for this observation is not known.

Another patient had chronic DI and an empty sella with herniation of the optic chiasm. Hypopituitarism, with or without visual field defects secondary to herniation of the suprasellar visual system and third ventricle into the empty sella, has been reported previously [25]. However, the cause of DI in our particular patient remains unknown.

The median age of onset of idiopathic DI in a previous study [1] was 16 years, and the majority of patients (63%) were male. Most of these patients had evidence of anterior pituitary dysfunction, and some had thickened infundibular stalks on CT. Growth hormone deficiency is the most common accompanying anterior pituitary deficit, but inadequate secretion of thyroid-stimulating hormone (TSH) and adrenocorticotropic hormone (ACTH) is also seen [13]. Patients with idiopathic central DI have been shown in pathologic studies to have a striking depletion of Nissl granules and fewer neurons in the supraoptic and paraventricular nuclei of the hypothalamus [5]. Some patients with idiopathic DI have circulating antibodies to vasopressin neurosecretory cells [1], which suggests a possible immunologic basis for the disease. Idiopathic DI is almost always permanent [1]. About 30% of all cases of DI in children are classified as idiopathic [13]. Familial DI is clinically similar to idiopathic DI, but is very rare [5, 13]. Both autosomal-dominant and sex-linked modes of inheritance have been postulated [26].

In children, neurogenic DI affects both sexes equally, and may begin at any age from a few months to adolescence. Polyuria is unusual in neonates, who usually present with chronic dehydration, unexplained fever, vomiting, and constipation, often leading to serious long-term neurologic deficits [13]. In adolescents, polyuria is the main symptom and often has a dramatic onset. Growth hormone deficiency is the most common accompanying anterior pituitary deficiency in children with neurogenic DI, but deficiency of TSH and ACTH secretion may occur also. Inadequate ACTH synthesis and release may require special attention in patients with DI because it can camouflage the underlying polyuria of DI [13]. Another frequent cause of childhood central DI is a hypothalamic tumor, such as a craniopharyngioma or a hypothalamic glioma [4, 27]. In the present study, MR was able to clearly demarcate the diencephalic mass in different planes (cases 11–13).

In all the patients with DI, the high-intensity signal normally seen in the posterior lobe on T1-weighted MR images was not observed, in agreement with previous reports [28, 29]. In normal subjects, the frequency of the bright signal has varied from 90–100% [28, 29] to as low as 63% [30]. An age-related decline in the rate of detection of the bright signal of approximately 1% per year between 7 months and 85 years of age has also been reported [30]. The source of the hyperintense MR signal in the normal neurohypophysis has been the subject of recent controversy [28–33]. A recent study [33] investigated the effect of two chemical components of the posterior lobe, phospholipids and vasopressin, on the observed MR signal. It was found that a solution containing phospholipid vesicles has T1 and T2 characteristics analogous to those of the neurohypophysis, and that this solution exhibits a single peak that is chemically shifted with respect to water. Vasopressin had no effect on the signal, either in solution or in the vesicles. These data suggest that phospholipids act as a relaxation enhancer of water protons, and that the MR characteristics of the phospholipid vesicles are consistent with the observed MR properties of the neurohypophysis.

The absence of the hyperintensity that is normally seen in the posterior lobe of the pituitary gland is not in itself diagnostically significant, as this bright signal is occasionally absent in some normal subjects [31]. However, we believe that the presence of a bright signal is inconsistent with the diagnosis of DI. We have encountered one case (described below) in which the finding of normal bright signal in the posterior lobe in a patient thought to have DI led to an alternative diagnosis.

We saw one woman who developed DI and preeclampsia late in the third trimester of pregnancy. MR imaging of the hypothalamic-pituitary area was performed 1 month postpartum to exclude a structural lesion. The scan was remarkable in that it was entirely normal, including the presence of hyperintensity in the posterior lobe. We believe that this finding was inconsistent with the diagnosis of vasopressin deficiency. Subsequent testing documented the presence of vasopressinase in her serum. Serum vasopressinase is an enzyme that occasionally appears late in pregnancy [34, 35]. It results in the inactivation of circulating vasopressin and leads to polyuria/polydipsia syndrome, which is indistinguishable from DI [34-36]. This relatively rare diagnosis can be established by incubating pharmacologic preparations of vasopressin with the test patient's serum and demonstrating rapid inactivation of the hormone [34, 35].

In conclusion, central DI can result from a wide variety of diseases. The most common causes of DI appear to be Langerhans cell histiocytosis, germinoma, craniopharyngioma, hypothalamic glioma, granulomatous inflammation, surgery, and trauma. MR is currently the imaging method of choice in the evaluation of dysfunction of the hypothalamic-neurohypophyseal secretory system. MR imaging, particularly when coupled with clinical information, allows a specific diagnosis in almost all cases of central DI.

REFERENCES

1. Moses AM. Clinical and laboratory observations in the adult with diabetes insipidus and related syndromes. *Front Horm Res* **1985**;13:156–175
2. Robertson GL. Posterior pituitary. In: Felig P, Baxter J, Broadhus AE, Frohman LA, eds. *Endocrinology and metabolism*, 2nd ed. New York: McGraw-Hill, **1987**:339–386
3. Blotner H. Primary or idiopathic diabetes insipidus, a system disease. *Metabolism* **1958**;7:191
4. Tien RD, Newton TH, McDermott MW, Dillon WP, Kucharczyk JK. Thickened pituitary stalk on MR features in patients with diabetes insipidus and Langerhans cell histiocytosis. *AJNR* **1990**;11:703–708
5. Braverman L, Mancini J, McGoldrick D. Hereditary idiopathic diabetes insipidus. A case report with autopsy findings. *Ann Intern Med* **1965**;63:503–508
6. Van Slyck E, Jurgensen J, Cargill J. Diabetes insipidus complicating thrombotic thrombocytopenic purpura. *JAMA* **1969**;209:768–770
7. Veldhius J, Hammond J. Endocrine function after spontaneous infarction of the human pituitary: report, review and reappraisal. *Endocr Rev* **1980**;1:100–107
8. Schwartz A, Leddy A. Recognition of diabetes insipidus in postpartum hypopituitarism. *Obstet Gynecol* **1982**;59:394–398
9. Baylis PH, Milles JJ, London DR, Butt WR. Postpartum cranial diabetes insipidus. *Br J Med* **1980**;1:20
10. Haynes B, Fauci A. Diabetes insipidus associated with Wegener's granulomatosis successfully treated with cyclophosphamide. *N Engl J Med* **1978**;299:764
11. Kelly P. Systemic blastomycosis with associated diabetes insipidus. *Ann Intern Med* **1982**;96:66–67
12. Avioli LV, Lastersohn JT, Lopresti JM. Histiocytosis-X (Schüller-Christian disease): clinico-pathological survey: review of ten patients and the results of prednisone therapy. *Medicine* **1963**;42:115–147
13. Czernichow P, Pomarede B, Brauner B, Rappaport R. Neurogenic diabetes insipidus in children. *Front Horm Res* **1985**;13:190–209
14. Lewis R, Wilson J, Smith FW. Diabetes insipidus secondary to intracranial sarcoidosis confirmed by low-field magnetic resonance imaging. *Magn Reson Med* **1987**;5:466–470
15. Lam A, Sibbald WJ, Boone J, et al. Transient diabetes insipidus as a complication of *Hemophilus* meningitis. *Pediatrics* **1978**;61:785
16. Pai KG, Rubin HM, Wedemeyer PP, et al. Hypothalamic-pituitary dysfunction following group beta hemolytic streptococcal meningitis in a neonate. *J Pediatr* **1987**;88:289
17. Szuwrit V, Koonig HJ, Bennefeld H, Weritz C, Kleinhans G. Clinical aspects of typophyseal metastasis (German). *Onkologie* **1988**;11:66–69
18. Dominique JN, Wilson CB. Pituitary abscesses. Report of seven cases and review of the literature. *J Neurosurg* **1977**;46:601–608
19. Halimi P, Sigal R, Doyon D, et al. Post-traumatic diabetes insipidus: MR demonstration of pituitary stalk rupture. *J Comput Assist Tomogr* **1988**;12:135–137
20. Paxson CL Jr, Brown DR. Post-traumatic anterior hypopituitarism. *Pediatrics* **1976**;57:893
21. Kelly WM, Kucharczyk W, Kucharczyk J, et al. Posterior pituitary ectopia: an MR feature of pituitary dwarfism. *AJNR* **1988**;9:453–460
22. Chester W. Uber lipoidgranulomatoses. *Virchows Arch [A]* **1930**;279:561–602
23. Jaffe HL. Lipid (cholesterol) granulomatosis. In: Jaffe HL, ed. *Metabolic, degenerative, and inflammatory diseases of bones and joints*. Philadelphia: Lea & Febiger, **1972**:535–541
24. Tien RD, Brasch RC, Jackson DE, Dillon WP. Cerebral Erdheim-Chester disease: persistent enhancement with Gd-DTPA on MR images. *Radiology* **1989**;172:791–792
25. Kaufman B, Tomsak RL, Kaufman BA, et al. Herniation of the suprasellar visual system and third ventricle into empty sella: morphologic and clinical considerations. *AJNR* **1989**;10:65–76
26. Forssman H. On hereditary diabetes insipidus. With special reference to a

sex-linked form. *J Intern Med Suppl* **1945**;159:1

27. Thomas WC. Diabetes insipidus. *J Clin Endocrinol Metab* **1957**;17:565
28. Columbo N, Berry I, Kucharczyk J, et al. Posterior pituitary gland: appearance on MR images in normal and pathologic states. *Radiology* **1987**;165:481–485
29. Fujisawa I, Nishimura K, Asato R, et al. Posterior lobe of the pituitary in diabetes insipidus: MR findings. *J Comput Assist Tomogr* **1987**;11:221–225
30. Brooks BS, El Gammal T, Allison JD, Hoffman WH. Frequency and variation of the posterior pituitary bright signal on MR images. *AJNR* **1989**;10:943–948
31. Fujisawa I, Kikuchi K, Nishimura K, et al. Transection of the pituitary stalk: development of an ectopic posterior lobe assessed with MR imaging. *Radiology* **1985**;165:487–489
32. Kucharczyk J, Kucharczyk W, Berry I, et al. Histochemical characterization and functional significance of the hyperintense signal on MR images of the posterior pituitary. *AJNR* **1988**;9:1079–1083
33. Kucharczyk W, Lenkinski RE, Kucharczyk J, Henkelman RM. The effect of phospholipid vesicles on the NMR relaxation of water: an explanation for the appearance of the neurohypophysis? *AJNR* **1990**;11:683–700
34. Shah SV, Thakus V. Vasopressinase and diabetes insipidus of pregnancy. *Ann Intern Med* **1988**;109:435
35. Durr JA, Hoggard JG, Hunt JM, Schrier RW. Diabetes insipidus in pregnancy associated with abnormally high circulating vasopressinase activity. *N Engl J Med* **1987**;316:1070–1074
36. Krege J, Katz VL, Bowes WA. Transient diabetes insipidus of pregnancy. *Obstet Gynecol Surv* **1989**;44:789–795

MR Imaging of Intracerebral Blood: Diversity in the Temporal Pattern at 0.5 and 1.0 T

Amer Zyed[1]
L. Anne Hayman[2]
R. Nick Bryan[3]

MR scans were obtained at 0.5 and 1.0 T in 40 patients with 46 intracerebral hematomas categorized as hyperacute (0–2 days), acute (3–7 days), subacute (8–14 days), and chronic (15 days to 6 years). In a retrospective review, the signal intensity of the lesions was compared with that of normal white matter of the brain on spin-density, T1-, and T2-weighted spin-echo and T1-weighted gradient-echo sequences. The classic appearance and evolution of hematomas described in the literature at 1.5 T were not found in a significant number of the cases reviewed. In the hyperacute group, only five of eight hematomas had signal intensities that were hypointense relative to brain on T2-weighted images. Two of eight hyperacute hematomas were hyperintense relative to brain on the T1-weighted spin-echo images. However, T1-weighted gradient-echo images reliably demonstrated a hypointense signal in some portion of the hematoma in 45 of 46 cases.

We conclude that while there is no constant temporal pattern on spin-echo or gradient-echo sequences, there are signal-intensity changes suggestive of hemorrhage in nearly all hematomas imaged at 0.5 and 1.0 T. Although the inconsistency may be frustrating from a diagnostic standpoint, this variability may reveal important individual differences in hematomas and the brain that surrounds them, and thus be clinically significant. Before these data can be mechanistically analyzed, the reason for contrast on MR scans of hematoma must be better understood.

***AJNR* 12:469–474, May/June 1991; *AJR* 157:133–138, July 1991**

MR of intracranial hematomas should be clinically useful because of the sensitivity of MR to many physical and chemical changes that accompany hemorrhage. Current concepts of the appearance of intracerebral hemorrhage are based on empirical clinical observations, theoretical explanations predicated on prior MR data, and very limited in vitro analysis of human blood clot and components. Currently, the most popular mechanistic explanation for the appearance of intracerebral hemorrhage is that of Gomori et al. [1], which emphasizes the importance of the paramagnetic hemoglobin phenomenon at 1.5 T. However, this hypothesis, which depends on magnetic field strength, does not explain certain obvious clinical observations, such as low-signal lesions on T2-weighted spin-echo (SE) images obtained with lower field strengths [2, 3], nonspecific bright T2-weighted SE images of very early (<48 hr) hematomas at any field strength, and the occasional high signal intensity on T1-weighted SE images of very early hemorrhage [3]. In this report, we review the clinical appearance of intracerebral hemorrhage at field strengths of 0.5 and 1.0 T. In a companion article [4], we propose a theory to explain the MR patterns of cerebral hemorrhage at these field strengths by focusing on factors that influence T1 and T2 relaxation and thereby determine MR image contrast in clinical hematomas examined by SE and gradient-echo (GE) images at field strengths below 1.5 T.

Received March 7, 1989; revision requested May 1, 1989; final revision received November 26, 1990; accepted November 26, 1990.

This work was supported in part by grant NS 19056-06.

[1] Department of Radiology, Al-Azhar University, Cairo, Egypt.

[2] Department of Radiology, Baylor College of Medicine, 1 Baylor Plaza, Houston, TX 77030.

[3] Department of Radiology and Radiological Science, The Johns Hopkins University School of Medicine, The Johns Hopkins Hospital, 600 N. Wolfe St., Baltimore, MD 21205. Address reprint requests to R. N. Bryan.

0361-803X/91/1571-0133
© American Roentgen Ray Society

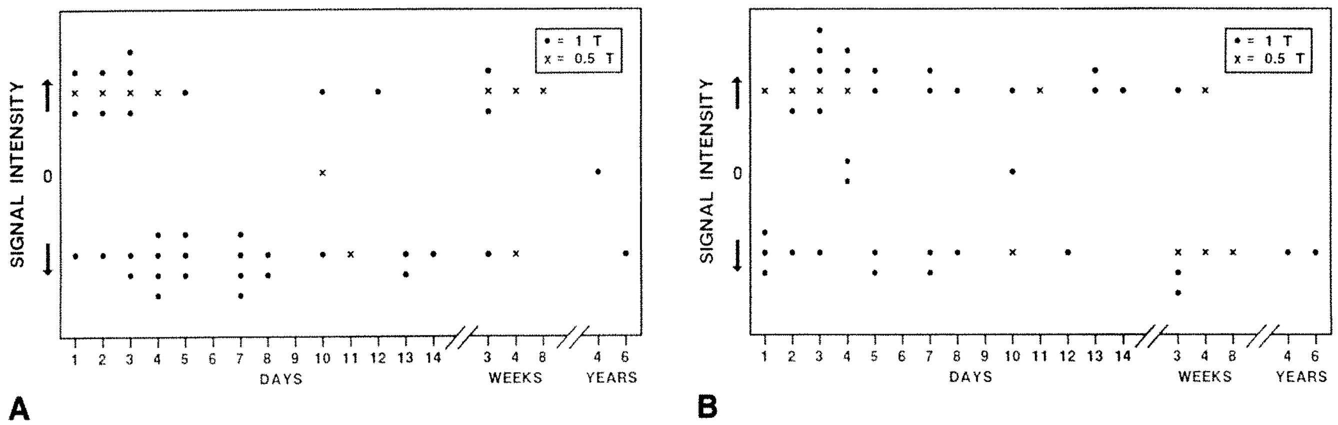

Fig. 1.—*A* and *B*, Signal intensities of the center (*A*) and rim (*B*) of hematomas vs age of hemorrhage on spin-density-weighted SE images obtained at 0.5 and 1 T.

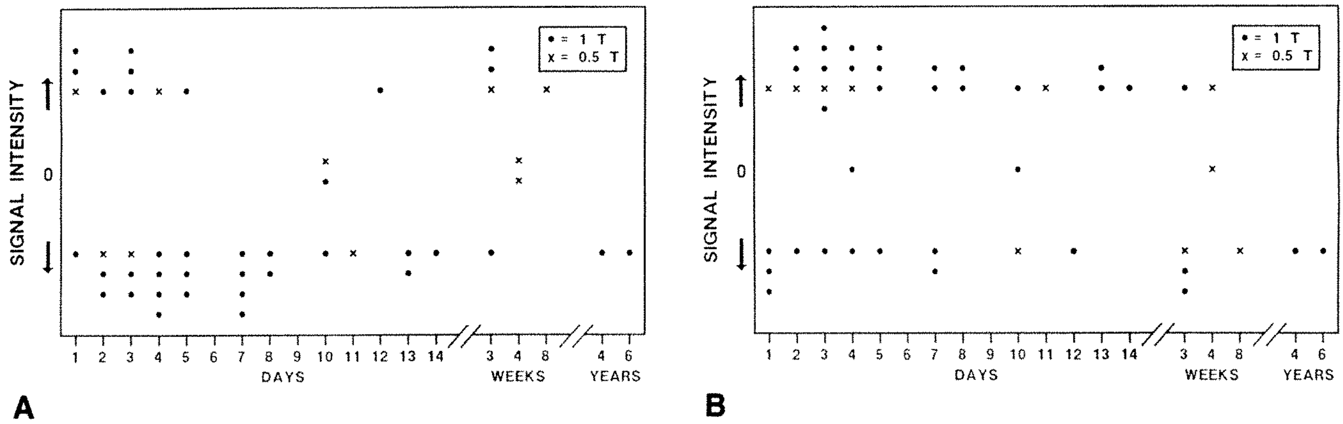

Fig. 2.—*A* and *B*, Signal intensities of the center (*A*) and rim (*B*) of hematomas vs age of hemorrhage on T2-weighted SE images obtained at 0.5 and 1 T.

Materials and Methods

All MR examinations performed from May 1986 to April 1988 were retrospectively reviewed for evidence of cerebral hemorrhage. This included MR studies in patients referred for known or suspected intracranial hemorrhage, as well as MR studies suggesting the presence of a hematoma in patients referred for other indications. From the initial 107 patients reviewed, 40 patients were chosen for inclusion because there was convincing evidence of cerebral hemorrhage and the time of hemorrhage was well documented. When hematomas were multiple (two cases), they were evaluated separately because they often had different MR appearances. Serial studies (four cases) were also evaluated individually. Thus, the total number of hematomas (46) exceeded the number of patients (40). Twelve hematomas were confirmed surgically and pathologically, 20 hematomas were diagnosed and staged by clinical findings and CT examinations, while eight hematomas were documented by clinical findings and MR characteristics only.

Thirty-six hematomas were scanned on a 1.0-T superconducting unit (Siemens, Iselin, NJ) and 10 hematomas on a 0.5-T superconducting unit (Siemens). The following pulse sequences were used in all patients: spin-density-weighted SE, >3000/<35 (TR/TE); T2-weighted SE, >3000/>88; T1-weighted SE, <500/<35; and T1-weighted GE, <500/17/90° (TR/TE/flip angle). Images were obtained with 1–4 excitations and a 256 × 256 acquisition matrix. Images were 5–10 mm thick.

Each image type was independently evaluated by two neuroradiologists as to the signal intensity (SI) relative to the white matter of the brain. Since the SI pattern of a hematoma was not uniform, the hematoma was roughly separated into two compartments: center and rim (which presumably represents the outer part of the hematoma). The hematomas were arbitrarily divided by age into four stages. Eight hematomas were hyperacute (0–2 days old), 19 were acute (3–7 days old), 10 were subacute (8–14 days old), and nine were chronic (more than 14 days old).

Results

Rapid, dynamic, and even reversible changes in intensity patterns were observed that varied greatly with age of hemorrhage and pulse sequence. The SIs of hematoma regions are graphed as a function of the age of hemorrhage in Figures 1–4.

The hyperacute stage (0–2 days) was characterized by variable appearances rather than a consistent pattern. Hematomas examined with double-echo scans (spin-density- and T2-weighted SE) were noted to be predominantly hyper-

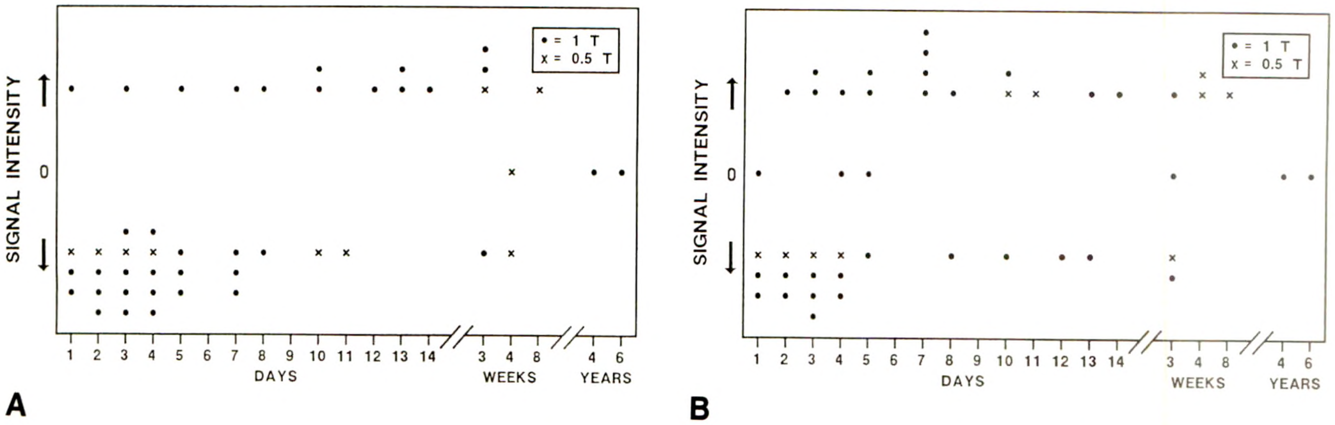

Fig. 3.—*A* and *B*, Signal intensities of the center (*A*) and rim (*B*) of hematomas vs age of hemorrhage on T1-weighted SE images obtained at 0.5 and 1 T.

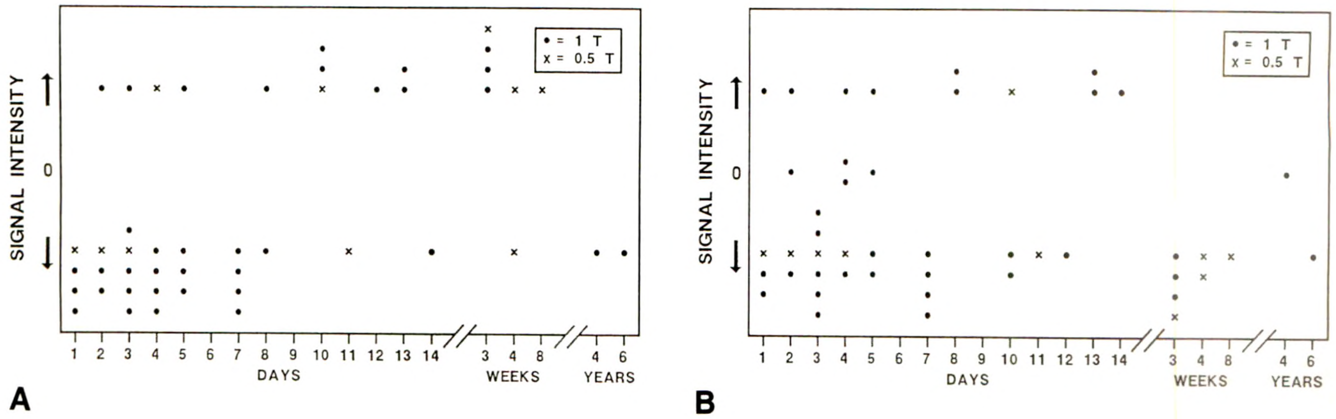

Fig. 4.—*A* and *B*, Signal intensities of the center (*A*) and rim (*B*) of hematomas vs age of hemorrhage on T1-weighted GE images obtained at 0.5 and 1 T.

intense peripherally with foci of varying degrees of hypointensity scattered within the hematoma, particularly on the second-echo image. In three of eight cases, hypointensity on T2-weighted SE images was not sufficient to allow a definite diagnosis of hemorrhage. This nondiagnostic appearance occurred at both 1.0 T (two cases) and 0.5 T (one case). On T1-weighted SE images, most lesions were slightly hypointense, but two had hyperintense regions. On T1-weighted GE images, hematomas typically had a central hypointensity with variable hyperintensity about the rim. However, only minimal evidence of hypointensity was seen on T1-weighted GE images in one case (Fig. 5).

The acute (3–7 days) hematomas were typified by low SI centrally on spin-density- and T2-weighted SE and T1-weighted GE pulse sequences. The rim most frequently had increased SI on spin-density- and T2-weighted SE images but low SI on T1-weighted GE images.

The central portion of subacute lesions (8–14 days) most often had decreased SI on spin-density- and T2-weighted SE and T1-weighted GE scans. In all cases (10 of 10), there was increased SI on T1-weighted SE sequences, either centrally or at the rim.

Chronic lesions (>14 days) also varied in appearance, but the most common pattern was of central increased SI on spin-density-, T2-, and T1-weighted SE and T1-weighted GE images with decreased signal in the rim on spin-density- and T2-weighted SE and T1-weighted GE scans. Smaller or older hematomas had smaller or no central regions of bright signal. Such lesions were seen only as areas of decreased SI on T2-weighted SE, and particularly on T1-weighted GE images (Fig. 6).

In addition to analyzing hematoma SI by arbitrary location in the hemorrhage (i.e., center and rim), we also evaluated the SI of hemorrhage independent of location in the hematoma. Table 1 summarizes SI patterns as a function of age of hemorrhage, independent of lesion region. Thirty-seven hematomas (80%) had low SI somewhere within the lesion on T2-weighted SE images. This was seen with comparable frequency in hemorrhages of all ages. Twenty-eight hematomas (61%) had increased SI on T1-weighted SE images; this was seen most frequently in subacute hemorrhages. Forty-five hematomas had low SI on T1-weighted GE images. Only one hematoma, a 22-hr-old hemorrhage imaged at 1.0 T, lacked this relatively distinctive SI. There were no known

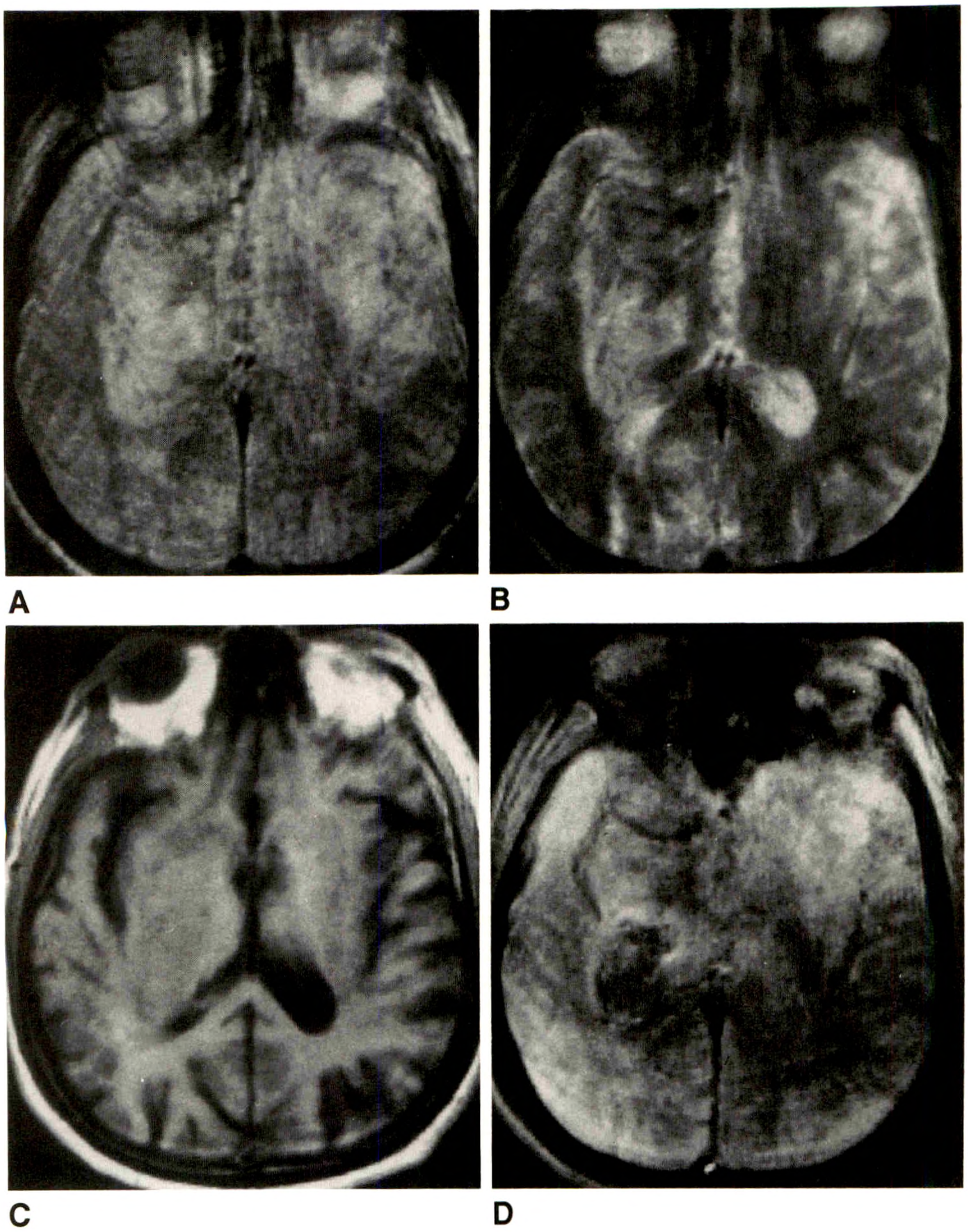

Fig. 5.—22-hr-old right thalamic hematoma.

***A–D*, Despite patient motion, MR appearance on spin-density-weighted SE (*A*), T2-weighted SE (*B*), T1-weighted SE (*C*), and T1-weighted GE (*D*) MR images at 1 T is relatively nonspecific, except for iso- to slightly hypointense signal on GE image.**

blood or clotting abnormalities to account for this anomalous appearance.

Discussion

The empirical observations of this study document the variable MR appearance of intracerebral hemorrhage on SE and GE images at 0.5 and 1.0 T. This finding is consistent with the more current literature. For instance, Gomori et al. [1] reported decreased central SI on T2-weighted SE images of acute hemorrhage, while our results and those of Zimmerman et al. [3] show some acute hematomas to have hyperintense central SI. Likewise, Gomori et al. [1] indicated that acute hematomas have isointense to low SI centrally on T1-weighted images, while our results and those of Zimmerman et al. [3] show some hematomas with hyperintense SI.

Some authors have suggested that variations in the MR appearance of hematomas can be attributed to differences in field strength, pulse sequences, or other technical factors. For instance, Gomori et al. [5] suggested that acute hematomas have central low SI on T2-weighted SE images at "high" field strengths (1.5 T), but not necessarily at lower field strengths. Zimmerman et al. [3] have reported such appearances at 0.5 T, and Sapponen et al. [2] and Bydder et al. [6] have seen similar low SI at 0.17 and 0.15 T, respectively. The variable pattern of hematomas on SE scans was recently confirmed at 0.5 and even 1.5 T by Seidenwurm et al. [7].

Our study also documents the variable, but sensitive, MR appearance of hemorrhage on GE images. Gradient echoes

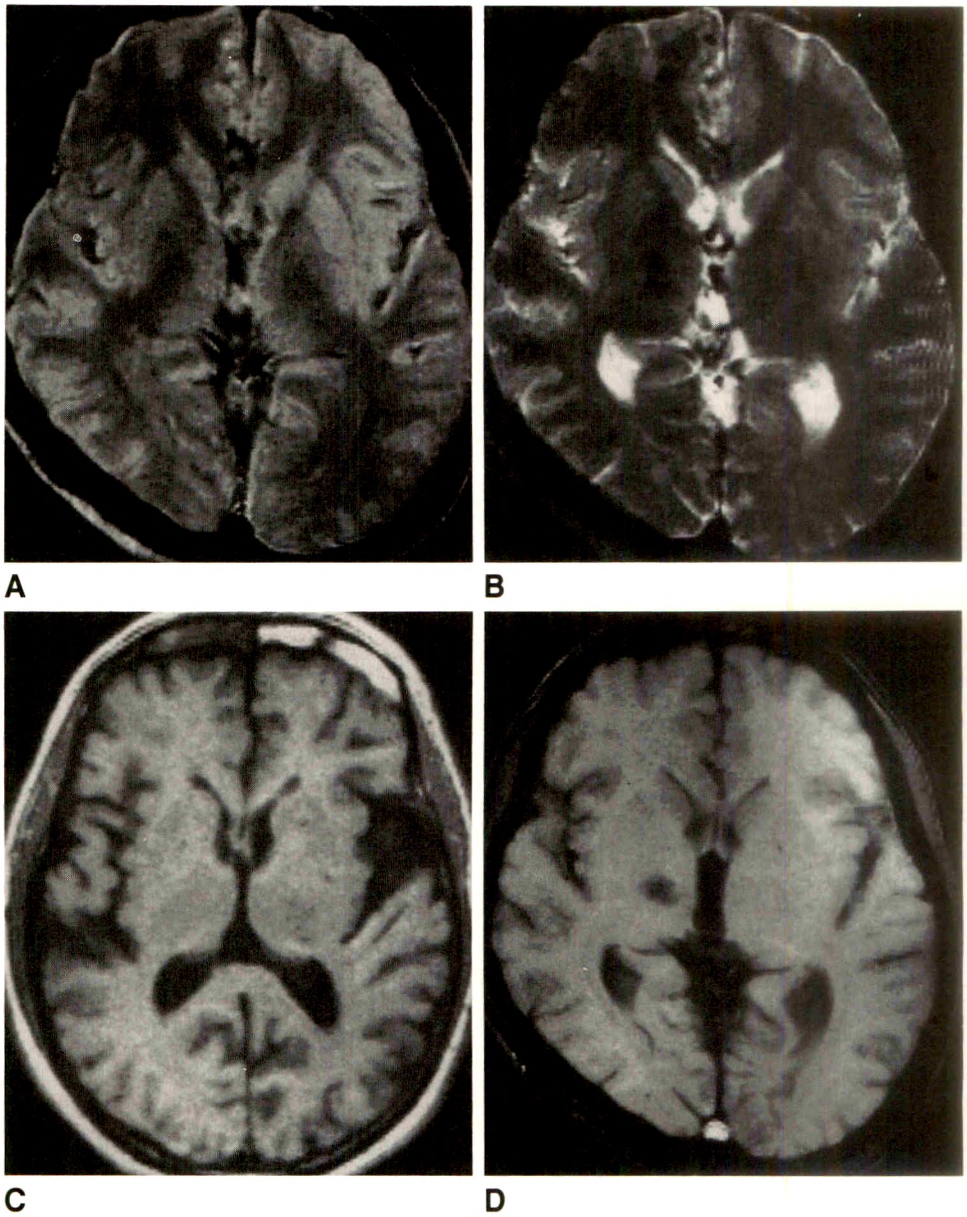

Fig. 6.—6-year-old right thalamic hematoma.
***A–D*, Spin-density-weighted SE (*A*), T2-weighted SE (*B*), T1-weighted SE (*C*), and T1-weighted GE (*D*) MR images at 1.0 T. T1-weighted GE image is most sensitive in detecting old hemorrhage.**

TABLE 1: Signal-Intensity Changes Suggestive of Hemorrhage

Age of Hematoma	Total No. of Hematomas	No. That Decreased on T2-Weighted Spin Echo	No. That Increased on T1-Weighted Spin Echo	No. That Decreased on T1-Weighted Gradient Echo
Hyperacute	8	5	2	7
Acute	19	16	10	19
Subacute	10	9	10	10
Chronic	9	7	6	9
Total	46	37	28	45

should be intrinsically more sensitive than spin echoes to magnetic susceptibility effects [7, 8]. However, there are many possible GE pulse sequences with an infinite variety of TRs, TEs, and flip angles. This study used a T1-weighted sequence with a 90° flip angle and TR and TE approximating those of the T1-weighted SE sequence. Although this GE sequence is not clinically popular, it was found to be very sensitive to magnetic susceptibility effects, and, importantly, it differs by a single variable from the T1-weighted SE image. Thus, the SI difference between tissues with stationary spins is due primarily to the magnetic susceptibility hetereogeneity of local tissue.

The more popular GE gradient-recalled acquisition in the steady state (GRASS) sequences, which use a shorter TR and lower flip angle, are difficult to evaluate in terms of magnetic susceptibility influence because the relative spin-density, T1, and T2 contrast properties differ from those of the SE sequences. The GRASS type of GE sequence is not more sensitive in the detection of the magnetic susceptibility effects of hemorrhage than the T1-weighted GE sequence used in this study. This opinion is based on our experience with in vitro blood clots and a limited number of clinical hematomas imaged with both types of GE sequences and on the comparability of these clinical results (decreased SI in 45 of 46 hematomas) with those of others using GRASS sequences [1, 3, 7, 8]. However, both types of GE sequences are very reliable in detecting hematomas of any age.

T1-weighted GE scans showed mixed SI patterns with regions of hyperintensity simulating those noted on T1-weighted SE and/or regions of hypointensity simulating those noted on T2-weighted SE. This reflects the sensitivity of T1-weighted GE to both T1 and T2* effects. Hypointensity with this pulse sequence was also noted at the periphery of acute and subacute hematomas, immediately around the hematoma. This may represent a boundary zone between two areas of differing magnetic susceptibility (hemorrhage vs normal brain). This appearance may mimic the appearance of hemosiderin in chronic hemorrhage [8].

While our results and the literature show a variable appearance of intracerebral hemorrhage, a general pattern is found in over two thirds of cases. Initially, there is low SI on T1-weighted GE scans, and shortly thereafter on T2-weighted SE. This appearance is followed by and mixed with areas of increased SI on T1-weighted SE. While this pattern is vague as to region and age of a hematoma, it is relatively specific in terms of determining evidence of hemorrhage. Thus, this general pattern is very sensitive for the detection of hemorrhage, which is usually the critical clinical issue.

In summary, there was no consistent temporal or regional SI pattern for intracerebral hematomas examined by a set of MR sequences (spin-density-, T1-, and T2-weighted SE and T1-weighted GE). However, there was a general pattern that effectively defined the presence of hemorrhage. We hypothesize that the appearance of a hematoma on MR is an indirect measure of individual factors present in the hematoma and the surrounding brain. Thus, the diverse appearances of hematomas on MR may hold important diagnostic information about the surrounding brain. For this information to be more meaningful, the biological basis of the individually variable MR signals must be understood.

ACKNOWLEDGMENTS

We thank Michael Mawad, Barry Horowitz, Randy Blackwell, and Marlin Sandlin at The Methodist Hospital for clinical help and Marge Eddy for help in manuscript preparation.

REFERENCES

1. Gomori JM, Grossman RI, Goldberg HI, Zimmerman RA, Bilaniuk LT. Intracranial hematomas: imaging by high-field MR. *Radiology* **1985**; 157:87–93
2. Sipponen JT, Sepponen RE, Tanttu JK, Sivula A. Intracranial hematomas studied by MRI at 0.17 and 0.02 T. *J Comput Assist Tomogr* **1985**;9: 698–704
3. Zimmerman RD, Heier LA, Snow RB, Liu DPC, Kelly AB, Deck MDF. Acute intracranial hemorrhage: intensity changes on sequential MR scans at 0.5 T. *AJNR* **1988**;9:47–57
4. Hayman LA, Taber KH, Ford JJ, Bryan RN. Mechanisms of MR signal alteration by acute intracerebral blood: old concepts and new theories. *AJNR* (in press)
5. Gomori JM, Grossman RI, Yu-Ip C, Asakura T. NMR relaxation times of blood: dependence on field strength, oxidation state, and cell integrity. *J Comput Assist Tomogr* **1987**;11:684–690
6. Bydder GM, Pennock JM, Porteous R, Dubowitz LMS, Gadian DG, Young IR. MRI of intracerebral hematoma at low field (0.15T) using T2 dependent partial saturation sequences. *Neuroradiology* **1988**;30:367–371
7. Seidenwurm D, Meng T-K, Kowalski H, Weinreb JC, Kricheff II. Intracranial hemorrhagic lesions: evaluation with spin-echo and gradient-refocused MR imaging at 0.5 and 1.5T. *Radiology* **1989**;172:189–194
8. Edelman RR, Johnson K, Buxton R, et al. MR of hemorrhage: a new approach. *AJNR* **1986**;7:751–756

Dural Sinus Occlusion: Evaluation with Phase-Sensitive Gradient-Echo MR Imaging

Jay S. Tsuruda[1]
Ann Shimakawa[2]
Norbert J. Pelc[3]
David Saloner[4]

The purpose of this study was to evaluate the usefulness of limited-flip-angle, phase-sensitive velocity imaging with gradient-recalled-echo (VIGRE) MR when combined with spin-echo MR in the diagnosis of dural sinus thrombosis. The VIGRE sequence consists of a rapid single-slice acquisition, 50/15/2 (TR/TE/excitations), and 30° flip angle. At each slice position, a total of four images were reconstructed; these consisted of one magnitude image and three images sensitive to proton motion in each orthogonal direction. The flow direction and flow velocity (cm/sec) were obtained from each of the phase images, and results were correlated with data obtained from a phantom experiment. In normal controls, dural sinus velocities ranged from a mean of 9.9 to 14.4 cm/sec for the transverse and superior sagittal sinuses, respectively. Three patients with proved dural sinus occlusion were studied with spin-echo images at 1.5 T. Three-dimensional time-of-flight MR angiography was also performed in one patient. The presence of dural sinus occlusion was determined by the lack of flow void on the spin-echo images, the absence of phase shift on the VIGRE study, and the presence of retrograde flow on the phase image in the sinus proximal to the occluded segment. Time-of-flight angiography overestimated the extent of the thrombosis caused by spin saturation. Follow-up VIGRE studies detected the formation of collateral flow in one patient and recanalization with the establishment of normal antegrade sinus flow in the other.

We conclude that phase-sensitive MR imaging is helpful in establishing the diagnosis and extent of dural sinus occlusion. Because of the short acquitition time, selected images can be obtained whenever the flow within the dural sinus is in question on a routine spin-echo study. Retrograde sinus flow appears to be a sensitive indicator of distal sinus occlusion or high-grade obstruction

***AJNR* 12:481–488, May/June 1991; *AJR* 157:139–146, July 1991**

Dural venous sinus thrombosis has been associated with several pathologic conditions [1]. Its clinical diagnosis may be difficult because of the wide variety of nonspecific findings [2]. Early recognition of this condition may be necessary in order to institute prompt therapy [3]. In the past, cerebral angiography or venography was required to establish this diagnosis. Less invasive techniques such as CT may indicate the presence of dural sinus occlusion with the findings of the cord and delta signs, congested deep subcortical veins, or increased tentorial or gyral enhancement [4, 5]. These CT signs may be subtle and easily overlooked. In one clinical series on septic lateral sinus thrombosis, the majority of CT examinations were completely normal [6].

MR imaging has become the method of choice in the noninvasive diagnosis of dural sinus thrombosis and may be positive when the CT findings are nondiagnostic [5]. Sinus thrombosis may be suggested on the basis of spin-echo (SE) or gradient-echo MR imaging alone [4, 5, 7–9]; however, unequivocal distinction between venous stasis and physiologic slow flow may be difficult [10]. The interpretation of high-intensity signal as flow-related enhancement, and thus as sinus patency, may be incorrect in the presence of methemoglobin within thrombus, or with gadopentetate dimeglumine enhancement.

Received August 27, 1990; revision requested November 13, 1990; final revision received December 27, 1990; accepted December 27, 1990.

[1] Department of Radiology, Division of Diagnostic and Interventional Neuroradiology, Box 0628, University of California, San Francisco, 505 Parnassus Ave., San Francisco, CA 94143-0628. Address reprint requests to J. S. Tsuruda.

[2] General Electric Medical Systems, Milwaukee, WI 53188.

[3] Department of Radiology, Stanford University, Stanford, CA 94305.

[4] Department of Radiology, San Francisco Veterans Administration Medical Center, and University of California, San Francisco, San Francisco, CA 94143-0628.

0361-803X/91/1571-0139
© American Roentgen Ray Society

Because of these potential pitfalls, the use of phase-shift imaging with SE techniques [10–15], which yields direct measurements of blood velocity as well as flow direction, may contribute additional MR specificity. More recently, preliminary experience with rapid phase-sensitive, limited-flip-angle gradient-recalled-echo pulse sequences has been described as a method for evaluating portal hypertension, discriminating arterial from venous flow as well as clot from slow flow, and quantifying blood flow within the carotid arteries [16, 17]. Our experience with the use of this method in proved cases of dural sinus occlusion is described.

Materials, Subjects, and Methods

A velocity-sensitive technique based on phase contrast and gradient-recalled echoes, VIGRE (velocity imaging with gradient-recalled echoes, General Electric Medical Systems), was initially tested with a flow phantom. The theory behind phase-shift velocity imaging and methods of image reconstruction using this technique are described in greater detail elsewhere [17]. Briefly, in the most basic mode, VIGRE requires two separate gradient schemes resulting in two views that are acquired for each phase-encoding increment. The first view is a flow-compensated sequence that results in zero phase shift for both stationary spins and spins moving with constant velocity during TE. This first view is the equivalent of a conventional GRASS study, and the data can be used to reconstruct a magnitude image (Fig. 1A). The second view is a flow-encoded sequence that uses a slightly altered gradient waveform such that the constant-velocity spins accumulate a phase shift related to that component of the flow vector that lies along the flow-encoding gradient axis. Again, the stationary spins do not accumulate any phase shifts. The TR and TE are kept constant for both views. From the data acquired with both views, a single-phase image is constructed such that the degree of phase shift is directly related to the flow velocity at each voxel (Fig. 1B). The flow sensitivity for this single-phase image is limited to the vector component parallel to the flow-encoded gradient, which can be selected to lie along any one of the three orthogonal directions. Stationary voxels in the phase image correspond to the special case of zero velocity and appear as intermediate (gray) intensity, representing 1024-magnitude units. Spatial resolution of the phase-reconstructed image is similar to that of a standard MR image.

In our clinical examples, the basic VIGRE acquisition described above is modified such that the flow-compensated and flow-encoded view is repeated three times in an interleaved fashion during each phase-encoding increment as a single data set. The purpose for this more complex set is to acquire flow information along all three orthogonal directions corresponding to the frequency, phase, and slice-select axes. As a result, the imaging time is increased by a factor of three. The rationale for obtaining separate velocity measurements in all three axes during a single imaging session is to ensure that velocities in vessels that are obliquely oriented to the plane of section can be analyzed. The sequences are interleaved to minimize motion between flow encodings. The resulting data are then combined to produce four separate images: a conventional-magnitude or GRASS image, a flow image in which pixel intensity is related to the flow velocity along the frequency-encoding direction, a flow image in which pixel intensity is related to the flow velocity in the phase-encoded direction, and a flow image in which pixel intensity is related to flow velocity along the slice-select direction. The imaging parameters include 35/15/2 (TR/TE/excitations), 30° flip angle, 4-mm slice thickness, 24-cm field of view (FOV), and 192 × 256 matrix. Two excitations are performed in order to improve the signal-to-noise ratio. Because of the short TR, data acquisition for a complete single slice study is 55 sec. Multiple single-slice images can also be prescribed depending on the area of coverage required.

Phase-sensitive techniques are sensitive to aliasing artifact if the actual velocity within the vessel is greater than the expected velocity range. This artifact results in a misrepresentation of flow such that the flow direction and actual velocity are displayed incorrectly. To avoid this problem, one can specify a peak velocity that controls the flow-encoding gradient lobes. In the flow-encoded experiment, the gradient lobes are designed so that a spin moving at the specified peak velocity accumulates a phase shift of +pi. A spin moving in the opposite direction at the specified peak velocity would accumulate a phase shift of −pi. This peak velocity specifies the maximum velocity that can be resolved without aliasing. On the basis of preliminary work (Mattle H, et al. Presented at the annual meeting of the Radiological Society of North America, November 1989), the peak velocity for our patients was set at 50 cm/sec for the analysis of dural sinus velocity. Because the sign of the phase shift is recorded, flow directionality is displayed by either relative hypointensity or hyperintensity with respect to the background stationary spins set at 1024-intensity units, which is midscale on the phase-reconstructed image. The magnitude of the difference between the intensity of the moving

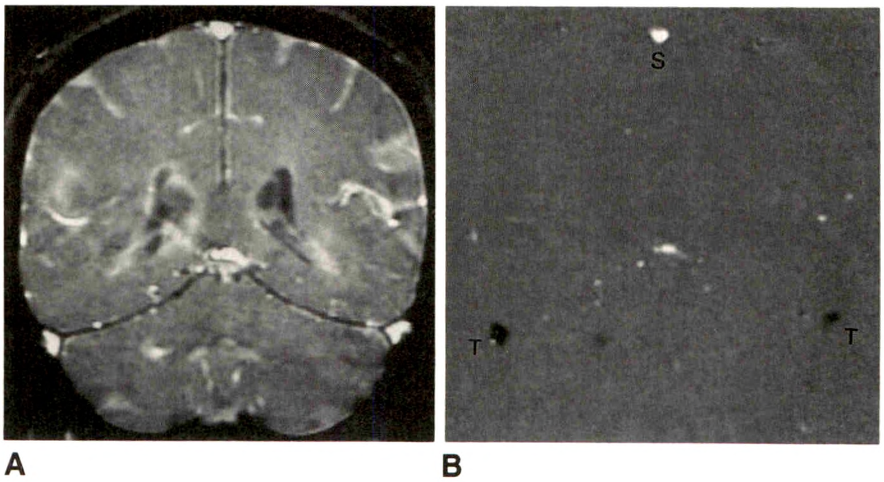

Fig. 1.—Example of VIGRE images of a normal volunteer with acquisition parameters as described in the text.

***A,* Conventional-magnitude or GRASS image through posterior aspect of cranium in coronal plane. Hyperintensity within superior sagittal and transverse sinuses is due in part to flow-related enhancement.**

***B,* Phase-reconstructed image with flow-sensitive axis oriented in slice-select (anteroposterior) direction. Blood moving anteriorly is depicted as a region of hypointensity, such as in transverse sinuses (T), whereas blood moving posteriorly, such as in superior sagittal sinus (S), is hyperintense relative to background stationary spins, which are of intermediate intensity.**

and stationary spins will allow a direct calculation of the velocity within the dural sinus.

VIGRE Calibration and Normal Controls

An in vitro phantom was constructed with two parallel Plexiglas tubes with 3- and 7-mm inner diameters placed in a water bath filled with tap water. Tap water circulated through the two tubes by means of a nonpulsatile gravity-fed device with mean and peak velocities calculated from a timed collection in a graduated cylinder. Actual velocities ranged from 2.3 to 122 cm/sec. An assumption was made that laminar flow was present in the phantom. Appropriate adjustments in the peak velocity settings were made for the in vitro VIGRE studies. VIGRE imaging was performed with the long axis of the tube oriented perpendicular to the imaging plane. A mean velocity was calculated from the phase image by specifying a region of interest across the entire cross section of the tube and measuring the mean voxel intensity. A peak velocity was also obtained by measuring the central voxel with the greatest deviation from 1024.

Direct coronal images were obtained perpendicular to the superior and transverse sinuses in normal volunteers ($n = 5$; mean age, 30). On the phase image, a region of interest was drawn to include the entire cross section of the dural sinus, and a mean intensity and velocity were obtained.

Studies in Patients

Over a 6-month period, we had the opportunity to use the VIGRE technique with a 1.5-T imager (General Electric Signa Performance Plus, Milwaukee, WI) to examine three inpatients proved to have dural sinus occlusion. All patients were initially imaged with a multislice T1-weighted sagittal sequence, SE 600/20/2, with 5-mm-thick slices, a 1-mm interslice gap, a 22-cm FOV, and a 192 × 256 matrix. This was followed by a multislice, multiecho T2-weighted sequence, 2800/30,80/1, with 5-mm-thick slices, a 2.5-mm interslice gap, a 20-cm FOV, and a 192 × 256 matrix. Gradient-moment nulling (Flow Compensation, General Electric Medical Systems) was used on the long TR images. Additional coronal and axial T1-weighted images were obtained in selected cases for further anatomic detail.

After completion of the SE acquisitions, the major dural sinuses were viewed on the monitor for the possible use of VIGRE images. The criteria for their use in these patients included atypical flow features in the dural sinus, such as the lack of flow void; the presence of subacute thrombus; replacement or compression of the dural sinus; the lack of normal rephasing with the application of gradient-moment nulling; and poor visualization of the dural sinus. A midline sagittal plane for the VIGRE study was selected to evaluate the entire course of the superior sagittal sinus, straight sinus, and torcular Herophili. The coronal plane through the posterior fossa was selected to evaluate the transverse and superior sagittal sinuses. An axial VIGRE image was used to evaluate the distal superior sagittal sinus, torcular Herophili, jugular bulb, and occasionally the transverse sinus if this vessel was parallel to the axial plane of section. Usually, one to four single-slice VIGRE images were obtained during a total acquisition time ranging from 55 sec to 3:40 min.

One patient was also studied with time-of-flight MR angiography [18]. This sequence consisted of a flow-compensated, three-dimensional, spoiled gradient-echo sequence (50/7/1/15° flip angle) consisting of 64 0.9-mm-thick partitions, a 23-cm FOV, and a 256 × 256 matrix. IV gadopentetate dimeglumine was not administered. The partitions were oriented in the axial plane. Selective maximum-intensity-projection reconstructions were performed through the dural sinuses.

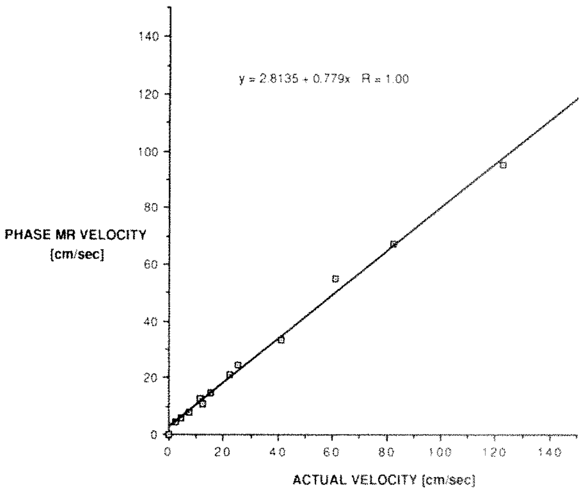

Fig. 2.—In vitro comparison between actual and observed flow velocities with VIGRE sequence. Because of velocity range tested, peak velocity was set higher than velocity range used in clinical imaging.

Results

Phantom Experiments and Normal Controls

The MR velocity data obtained from the phantom experiment was compared with the actual flow velocities (Fig. 2). A nearly linear relationship was noted between actual and measured velocities. In the normal controls, the calculated mean velocity was 14.4 cm/sec (range, 10.6–17.5 cm/sec) in the superior sagittal sinus and 9.9 cm/sec (range, 2.7–14.2 cm/sec) in the transverse sinus. The greater range of velocities in the transverse sinuses was due to developmental asymmetry in one patient. In all normal controls, anterior to posterior flow was demonstrated in the superior sagittal sinus and posterior to anterior flow in the transverse sinus.

Studies in Patients

The clinical information and imaging findings in the three patients are summarized in Table 1. Representative SE and VIGRE images from the three patients are depicted in Figures 3–5.

Discussion

MR imaging has become the noninvasive method of choice in the evaluation of dural sinus occlusion. Characteristically, direct visualization of thrombus within the sinus and loss of normal flow void on SE imaging have been reported in clinical examples [1, 5, 8, 9, 19, 20]. Initially, acute thrombosis may appear as a region of isointensity relative to normal brain parenchyma on T1-weighted images (Fig. 4B), becoming progressively hyperintense corresponding to the formation of methemoglobin (Fig. 3E) [20]. In acute thrombosis, the use of T2-weighted images alone may be potentially misleading since magnetic susceptibility effects, accentuated when im-

TABLE 1: Summary of Patients with Dural Sinus Occlusions Studied by Velocity Imaging with Gradient-Recalled Echoes (VIGRE)

Variable	Case 1	Case 2	Case 3
Age (years)	79	2	40
Sex	F	M	F
History	New onset of seizures and left-sided weakness 7 days after partial resection of posterior fossa meningioma	Ear pain, poor appetite, increased irritability with fevers and retroauricular swelling	"Pounding" sensations in the back of the head with findings of papilledema
Pathogenesis	Postoperative complication	Epidural abscess with septic thrombosis	Meningioma
Occluded sinus	Superior sagittal	Left sigmoid and transverse	Left sigmoid and transverse
Method of confirmation	Clinical course and imaging findings	Surgical	Surgical
Spin-echo findings at site of sinus obstruction	Loss of normal flow void and acute hemorrhagic venous infarcts	Loss of normal flow void and dilated venous collaterals	Loss of normal flow void and flow-related enhancement on MR angiogram
VIGRE findings			
Loss of phase shift	Yes	Yes	Yes
Retrograde flow	Yes	Yes	Yes
Therapy	Hypervolemic therapy	Debridement and antibiotics	Meningioma resection
Outcome	Slow improvement of hemiparesis	Reestablishment of normal antegrade flow in sinus	Improved

aging at high field strengths, can produce hypointense signal mimicking flow void [20, 21]. The absence of flow void on SE imaging may not necessarily represent thrombosis, since the lack of flow void may be confused with flow-related enhancement or rephasing of spins caused by even-echo rephasing and/or gradient-moment nulling [5, 15]. As a result, the suspected area should be evaluated in multiple planes with both long and short TR SE techniques [1].

The potential pitfalls of SE imaging can be partially overcome by the use of enhancement with gadopentetate dimeglumine, which may show nonenhancing thrombus within enhancing dural sinus as well as improved delineation of venous collaterals [1]. One should also be aware that contrast enhancement in the presence of slow-flow states may lead to some pitfalls in interpretation (Boyko O. Presented at the annual meeting of the Radiological Society of North America, November 1990). RF presaturation pulses [22] also may aid in identifying flow voids without the presence of flow-related enhancement, which on occasion may mimic thrombus. More recently, single-slice gradient-recalled-echo MR has proved to be valuable in the assessment of sinus patency [7]. Reliance on gradient-echo techniques alone may be misleading, since hyperintense thrombus may mimic flow [23, 24]. In addition, the presence of paradoxical enhancement is not a quantitative measurement of flow, and the minimum flow rate required to yield hyperintensity on either SE or gradient-echo images needs further clinical evaluation [7, 10].

Phase-contrast MR angiography has been anecdotally shown to be helpful in detecting dural sinus occlusion [25]. However, the authors in this report did not specify the velocity sensitivity with their technique. In addition, their study did not supply any information about flow directionality. In one of our cases, three-dimensional time-of-flight MR angiography confirmed sinus occlusion by a meningioma. However, the MR angiography results were somewhat misleading in that the proximal left transverse sinus appeared to be completely occluded. This contradicted the finding on both the VIGRE and conventional angiographic studies, which showed a patent proximal transverse sinus and retrograde filling toward the contralateral side. This misleading finding on MR angiography is due to the saturation of spins in this dural sinus secondary to the relatively long dwell time within the imaging volume. A similar saturation effect was noted in the right lateral sinus distal to partial obstruction by an arachnoid granulation, in which faint flow-related enhancement of the right sigmoid sinus and jugular bulb was noted on MR angiography (Fig. 5B). The VIGRE study (Fig. 5D), however, showed high flow velocities in this saturated region. The use of IV gadopentetate dimeglumine may improve MR time-of-flight venoangiography (Okumura R, et al. Paper presented at the annual meeting of the Radiological Society of North America, November 1990), and if it had been used in this patient, the dural sinuses with poor flow-related enhancement would have been visualized better. However, we elected not to use gadopentetate dimeglumine because of the concern that the densely enhancing portions of a meningioma within the occluded sinus may simulate flow-related enhancement on time-of-flight angiography, especially when the results are viewed with the use of a maximum-intensity-projection reconstruction algorithm [26].

A strong argument could be made that the parameters we used for our time-of-flight MR angiography are sensitive only for fast flow in arteries and major dural sinuses. In our experience, the major dural sinuses in normal subjects are adequately visualized with these parameters. This sequence, however, is very sensitive to reduced flow states, and therefore is a sensitive indicator of altered flow patterns such as in this patient. Multislice two-dimensional time-of-flight MR angiography is more immune to saturation effects. Unfortunately, this sequence was not available to us when this patient (case 3) was studied. However, the VIGRE technique does produce a single-slice two-dimensional magnitude image that can be used to evaluate the presence of flow-related enhancement.

MR velocity imaging based on phase shift is a well-known process in which a relationship is established between the

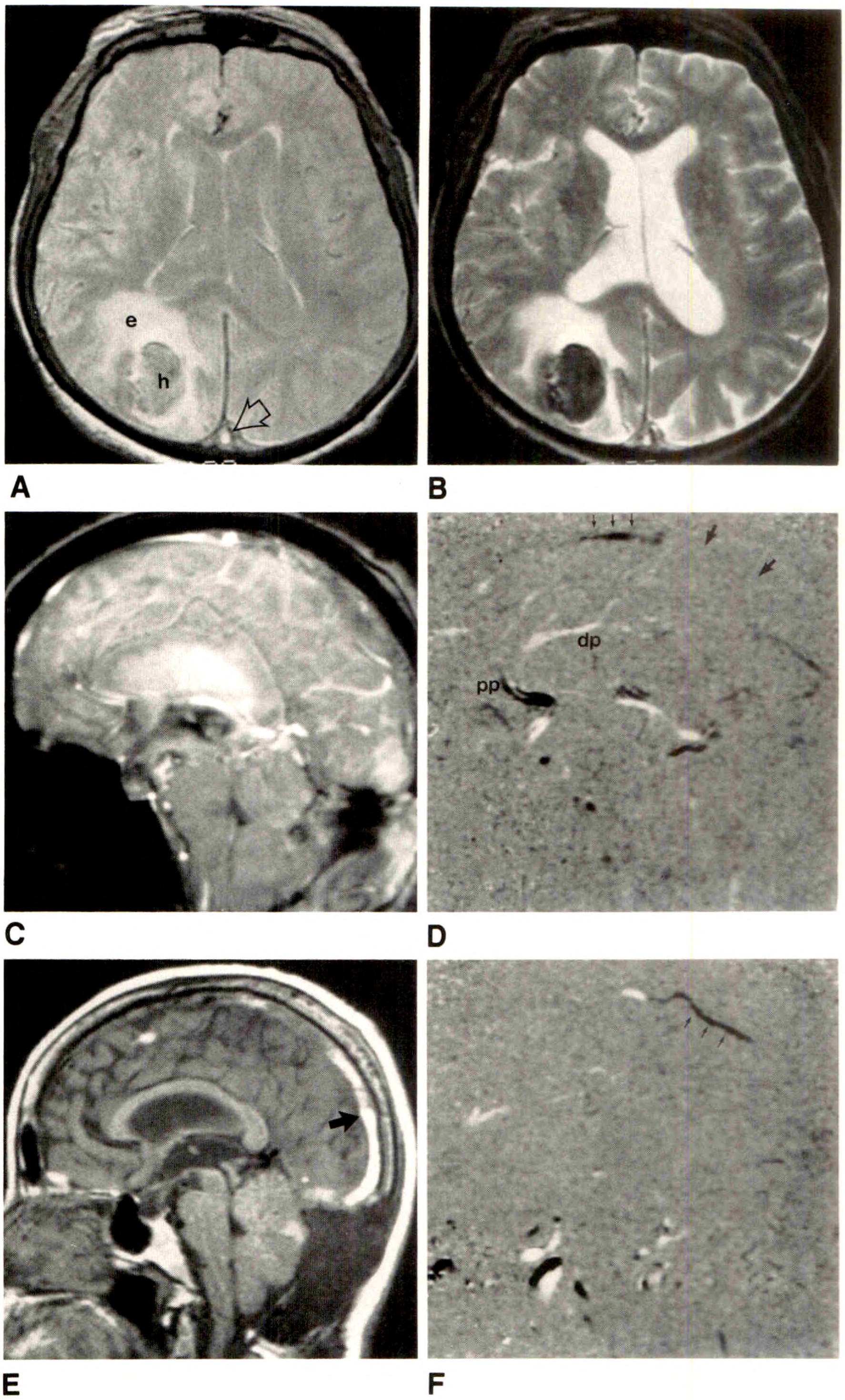

Fig. 3.—Case 1: Postoperative superior sagittal sinus occlusion.

***A* and *B*, SE 2800/30 (*A*) and SE 2800/80 (*B*) images. Loss of normal flow void (*arrow*) within posterior aspect of sinus represents either occlusion or slow flow with rephasing due to presence of gradient-moment nulling. Portions of acute hemorrhagic infarct (*h*) with T2 shortening, surrounding edema (e), and mass effect are noted.**

***C* and *D*, Conventional (*C*) and midline VIGRE image with flow-sensitive axis in anteroposterior direction (*D*). VIGRE image shows lack of expected high signal within distal aspect of sinus on magnitude image and corresponding absent flow on phase reconstruction (*large arrows*). Proximal aspect of sinus is patent (*small arrows*); however, retrograde or anterior flow is seen owing to its hypointensity. For reference, note that anterior flow direction of normal proximal pericallosal (pp) arteries is similarly represented by hypointensity, whereas posterior flow direction of normal distal pericallosal arteries (dp) is represented by hyperintensity.**

***E*, Follow-up SE 600/20 sagittal midline section shows evolution of subacute thrombus with corresponding hyperintensity (*arrow*) within sinus.**

***F*, Follow-up VIGRE phase image obtained at a parasagittal location depicts a developing venous collateral (*arrows*) with flow directed anteriorly (flow-sensitive axis in anteroposterior direction). Focus of high signal intensity is noted directly anterior to collateral vessel, which represents another cortical vein sectioned obliquely that has a velocity vector directed posteriorly just before it enters proximal superior sagittal sinus.**

relative phase of the transverse magnetization and the flow velocity in the direction of the magnetic field gradient [11–13]. One method of extracting this information is to introduce bipolar (dephasing and rephasing) gradient pulses during an imaging sequence [10]. If the protons are stationary, there is no net change in phase. If there is net motion of protons, there will not be complete rephasing resulting in a net phase shift proportional to velocity. If the applied field gradient is known, a direct velocity measurement can be estimated [14].

The VIGRE technique used in this study is based on these principles [17]. Because of the use of a short TR and gradient-recalled echoes, data acquisition is reasonably fast and can be added to a normal imaging sequence if the SE study is equivocal, as was described in the Materials, Subjects, and Methods section. In our clinical examples, only a limited number of VIGRE images were required to evaluate the sinus in question without appreciably increasing the imaging time. Flow-sensitive images can be obtained in an interleaved fash-

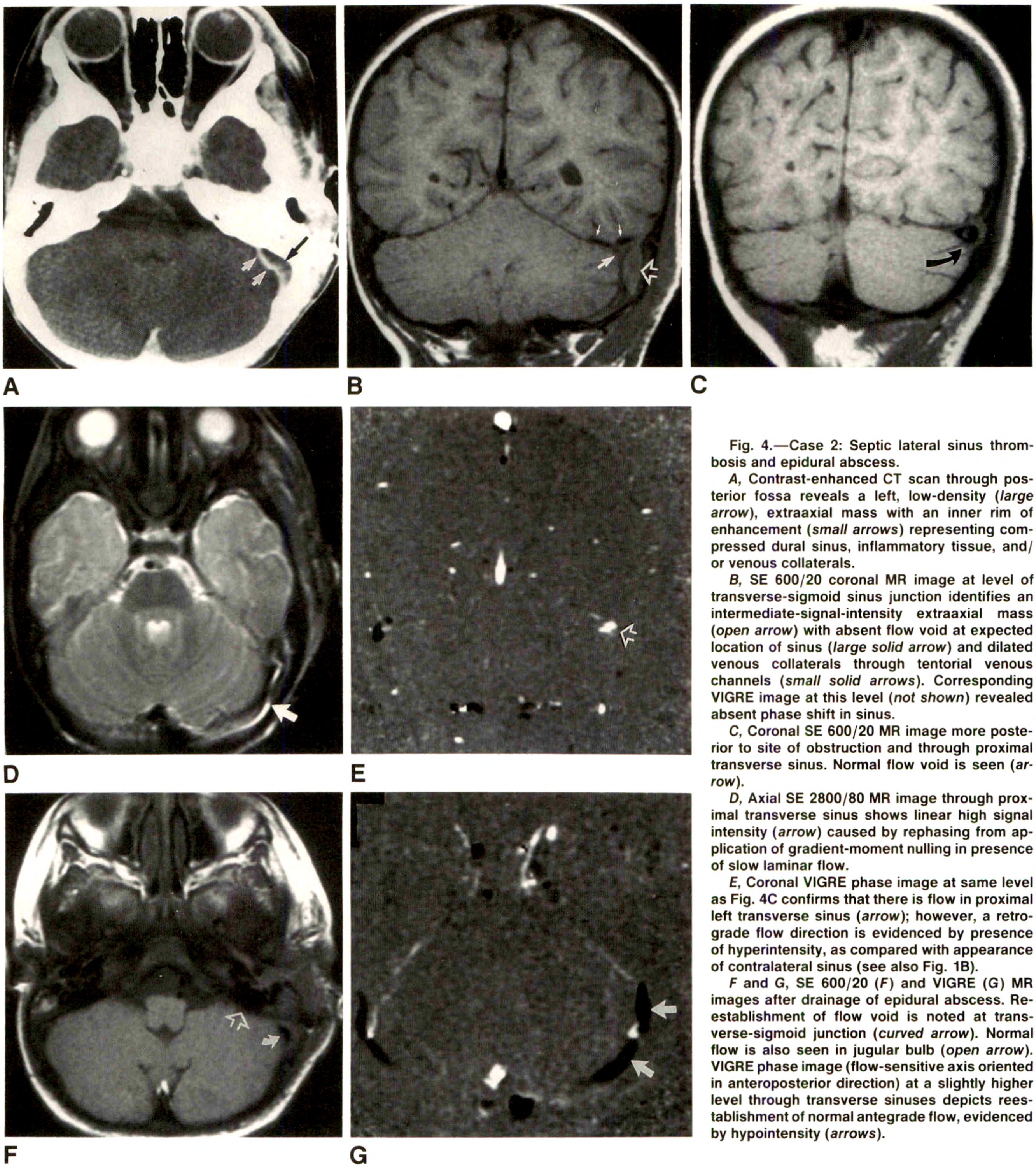

Fig. 4.—Case 2: Septic lateral sinus thrombosis and epidural abscess.

A, Contrast-enhanced CT scan through posterior fossa reveals a left, low-density (*large arrow*), extraaxial mass with an inner rim of enhancement (*small arrows*) representing compressed dural sinus, inflammatory tissue, and/or venous collaterals.

B, SE 600/20 coronal MR image at level of transverse-sigmoid sinus junction identifies an intermediate-signal-intensity extraaxial mass (*open arrow*) with absent flow void at expected location of sinus (*large solid arrow*) and dilated venous collaterals through tentorial venous channels (*small solid arrows*). Corresponding VIGRE image at this level (*not shown*) revealed absent phase shift in sinus.

C, Coronal SE 600/20 MR image more posterior to site of obstruction and through proximal transverse sinus. Normal flow void is seen (*arrow*).

D, Axial SE 2800/80 MR image through proximal transverse sinus shows linear high signal intensity (*arrow*) caused by rephasing from application of gradient-moment nulling in presence of slow laminar flow.

E, Coronal VIGRE phase image at same level as Fig. 4C confirms that there is flow in proximal left transverse sinus (*arrow*); however, a retrograde flow direction is evidenced by presence of hyperintensity, as compared with appearance of contralateral sinus (see also Fig. 1B).

F and *G*, SE 600/20 (*F*) and VIGRE (*G*) MR images after drainage of epidural abscess. Reestablishment of flow void is noted at transverse-sigmoid junction (*curved arrow*). Normal flow is also seen in jugular bulb (*open arrow*). VIGRE phase image (flow-sensitive axis oriented in anteroposterior direction) at a slightly higher level through transverse sinuses depicts reestablishment of normal antegrade flow, evidenced by hypointensity (*arrows*).

ion along all three orthogonal imaging planes, which we found helpful in analyzing obliquely oriented vessels. If necessary, velocity analysis in these obliquely oriented vessels can be performed by vector addition [12]. Overall, the VIGRE images allowed high contrast and conspicuity in identifying flowing spins on the clinical studies.

The phantom study showed reasonable correspondence between measured and actual velocities in the useful diagnostic range for dural sinuses. The known limitations of VIGRE, including gradient imperfections, eddy currents, sensitivity as a function of the peak velocity settings, resolution, and the distribution of velocities within the imaging voxel, may account for the slight discrepancies between the actual vs measured velocities [17]. Similar calibration curves using phase mapping have been shown by other investigators [16]. The results obtained in the normal controls are interesting in

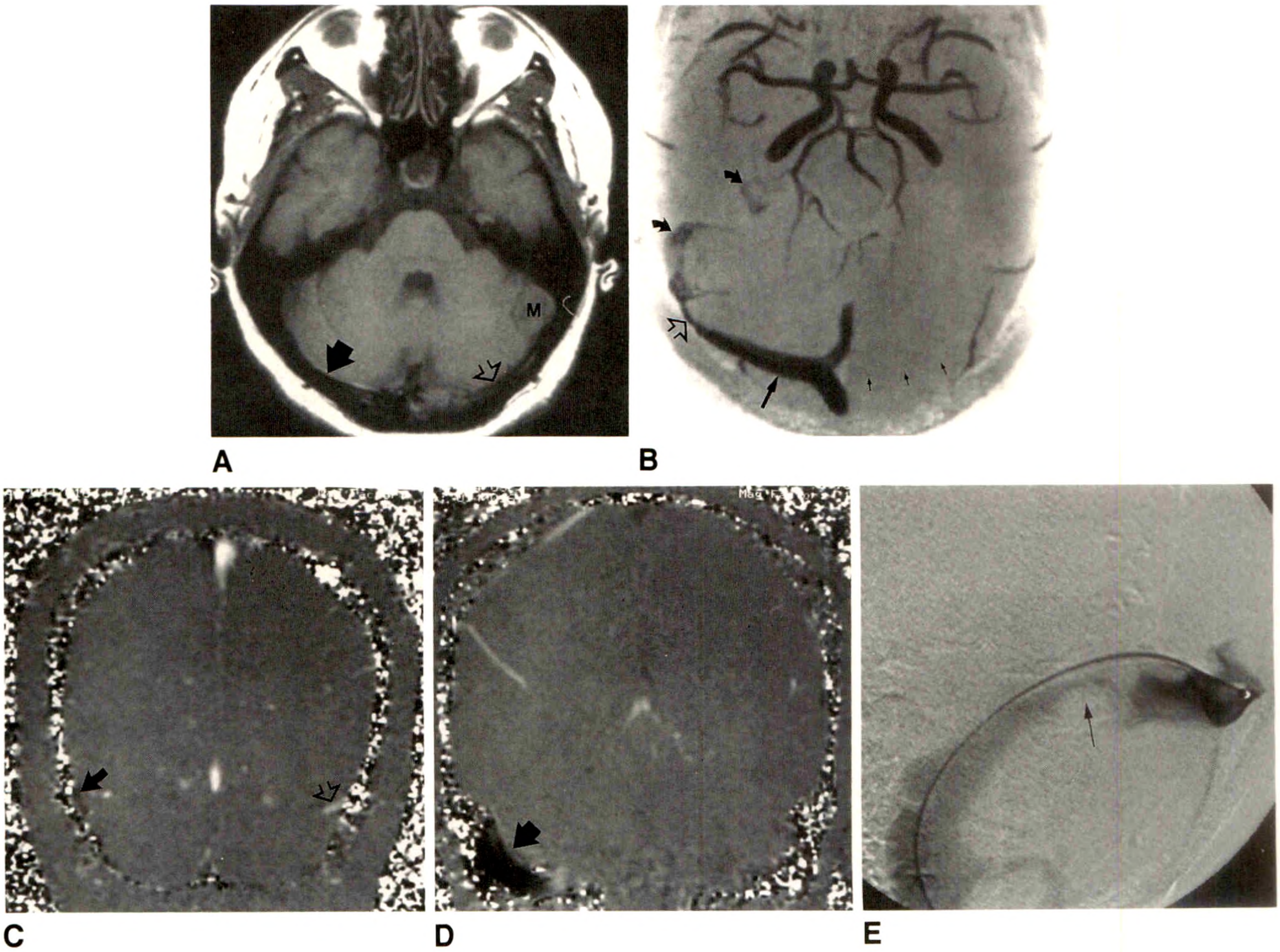

Fig. 5.—Case 3: Left posterior fossa meningioma with sinus occlusion.

A, Axial SE 600/20 MR image shows isointense mass (M) involving left transverse-sigmoid sinus junction. There is definite flow void in right transverse sinus (*solid arrow*) and possible flow void in left proximal transverse sinus (*open arrow*).

B, MR angiogram, from an axially oriented maximum-intensity projection, shows complete absence of left transverse sinus (*small straight solid arrows*). Unexpected findings are noted on right. A patent right proximal transverse sinus (*large straight solid arrow*) is seen, along with marked narrowing (*open arrow*) and incomplete flow-related enhancement distally in sigmoid sinus and jugular bulb (*curved arrows*).

C, Coronal VIGRE study through mid transverse sinuses shows retrograde flow (hyperintense signal) in left transverse sinus (*open arrow*) proximal to occlusion and faint antegrade flow (hypointense signal) at level of right transverse sinus stricture (*solid arrow*).

D, Coronal VIGRE image at level of sigmoid sinus, with flow-encoding axis in superoinferior direction, depicts normal inferior flow (hypointense signal) on right (*arrow*). A similar finding is expected normally on left; however, in this case there is proximal obstruction by tumor. Venous phase from a posterior fossa arteriogram (*not shown*) revealed identical flow patterns in dural sinuses.

E, Lateral projection, retrograde right transverse sinus venogram, confirms a segmental narrowing and filling defect (*arrow*) seen initially on MR angiography and presumably caused by arachnoid granulation. Pressure measurement across this stricture indicated a moderate gradient of 10 mm Hg. It was postulated that complete occlusion of left transverse sinus by a meningioma as well as partial obstruction on the right resulted in venous hypertension leading to the finding of papilledema.

that a range of velocities can be seen within the sinuses, particularly in cases of developmental asymmetry. Because of this range, any single measurement of the absolute velocity of a dural sinus in a given patient may be difficult to interpret. Measurement of the actual flow through the sinuses has been proposed as an estimate of cerebral perfusion (Mattle et al. RSNA, November 1989). More work in this area needs to be performed.

In our series, the presence of dural sinus occlusion was determined on the basis of several imaging criteria. First, in all instances the normal flow void was not seen on the SE images. Second, both the magnitude and phase-reconstruction VIGRE images demonstrated diminished or absent flow at the point of obstruction owing to the lack of flow-related enhancement or phase shift, respectively. Third, if patency is seen in the proximal segment of the distally obstructed sinus, retrograde flow was noted. This latter finding makes physiologic sense, since normal blood flow is expected to be shunted to other collaterals in the case of distal obstruction. With further clinical experience, this retrograde sign may prove to be quite specific in the diagnosis of sinus occlusion or high-grade obstruction.

Several assumptions are required for VIGRE imaging to be applicable in dural sinus thrombosis. First, the absence of phase shift alone is insufficient evidence for complete occlusion since its sensitivity to very slow states (less than 1 cm/

sec) has not been tested by us or others [17]. The finding of proximal retrograde flow, therefore, is used as an indirect indicator of a hemodynamically significant lesion due to either high-grade stenosis or obstruction. Second, an assumption was made that dural sinus velocity is nonpulsatile, and therefore a gated acquisition was not obtained. We based this assumption on other experimental results with a bolus-tagging technique, which demonstrated no evidence of significant pulsatile motion due to the lack of dispersion of the bolus boundaries (unpublished results) when imaging the superior sagittal sinus. Even if significant pulsations exist within the sinus, VIGRE velocity measurements remain reasonably accurate [17]. Third, the retrograde flow seen in the proximal sinus represents true reversal of flow and not an aliasing artifact. This flow reversal was proved angiographically in one patient. If an aliasing artifact were present in the other two patients, the flow velocities would have been uniformly greater than the peak velocity of 50 cm/sec. It would be difficult to explain this on a physiological basis. Also, in our experience, an aliasing artifact is usually depicted as nonuniform and variable signal intensity within the vessel. This was not the case in the sinuses demonstrating retrograde flow.

Overall, owing to its quantitative nature, phase imaging adds improved diagnostic confidence in the diagnosis of dural sinus occlusion, since the potential pitfalls encountered in trying to distinguish between the loss of flow void due to physiological MR phenomena and/or slow flow from actual occlusion can be reduced. An improvement in study specificity leading to an earlier diagnosis may affect patient management, such as with the institution of heparin or urokinase therapy [3] or prompt surgical treatment including mastoidectomy, exposure of the sinus, or incision and drainage in the case of septic lateral sinus thrombosis [27].

In summary, phase-sensitive limited-flip-angle gradient-recalled imaging is an accurate and useful adjunct to SE MR imaging and three-dimensional time-of-flight MR angiography in the noninvasive diagnosis of dural sinus thrombosis, confirming the development of collateral flow, and determining the results of therapy. Retrograde flow in the proximal sinus caused by distal obstruction can be readily detected and appears to be a specific indicator of sinus occlusion or significant obstruction to antegrade flow. Further work needs to be performed to determine the sensitivity of VIGRE imaging in states of very slow flow. Quantitative phase imaging allows insight into the pathophysiological changes of venoocclusive disease and shows promise in the further evaluation of normal and abnormal flow conditions of both intracranial arteries and veins.

ACKNOWLEDGMENTS

We thank Robert K. Jackler, Mark L. Rosenblum, and Charles B. Wilson for providing the cases used for this study and Petra Schmalbrock for providing the MR angiography software.

REFERENCES

1. Harris T, Smith R, Koch K. Gadolinium-DTPA enhanced MR imaging of septic dural sinus thrombosis. *J Comput Assist Tomogr* **1989**;13:682-684
2. Bousser M, Chiras J, Bories J, Castaigne P. Cerebral venous thrombosis—a review of 38 cases. *Stroke* **1985**;16:199-213
3. Di Rocco C, Iannelli A, Leone G, Moschini M, Valori V. Heparin-urokinase treatment in aseptic dural sinus thrombosis. *Arch Neurol* **1981**;38: 431-435
4. Anderson S, Shah C, Murtagh F. Congested deep subcortical veins as a sign of dural venous thrombosis: MR and CT correlations. *J Comput Assist Tomogr* **1987**;11:1059-1061
5. Hulcelle P, Dooms G, Mathurin P, Cornelis G. MRI assessment of unsuspected dural sinus thrombosis. *Neuroradiology* **1989**;31:217-221
6. Samuel J, Fernandes C. Lateral sinus thrombosis (a review of 45 cases). *J Laryngol Otol* **1987**;101:1227-1229
7. Daniels D, Czervionke L, Hendrix L, et al. Gradient recalled echo MR imaging of superior sagittal sinus occlusion. *Neuroradiology* **1989**;31: 134-136
8. Baram T, Butler I, Nelson MJ, McArdle C. Transverse sinus thrombosis in newborns: clinical and magnetic resonance imaging findings. *Ann Neurol* **1988**;24:792-794
9. Savino P, Grossman R, Schatz N, Sergott R, Bosley T. High-field magnetic resonance imaging in the diagnosis of cavernous sinus thrombosis. *Arch Neurol* **1986**;43:1081-1082
10. Ridgway J, Smith M. A technique for velocity imaging using magnetic resonance imaging. *Br J Radiol* **1986**;59:603-607
11. Wedeen V, Rosen B, Chesler D, Brady T. MR velocity imaging by phase display. *J Comput Assist Tomogr* **1985**;9:530-536
12. Feinberg D, Crooks L, Sheldon P, Hoenninger J, Watts J, Arakawa M. Magnetic resonance imaging of the velocity vector components of fluid flow. *Magn Reson Med* **1985**;2:555-566
13. Axel L. Blood flow effects in magnetic resonance imaging. *AJR* **1984**;143:1157-1166
14. Altobelli S, Caprihan A, Davis J, Fukushima E. Rapid average-flow velocity measurement by MR. *Magn Reson Med* **1986**;3:317-320
15. Tavares N, Auffermann W, Brown J, Gilbert T, Sommerhoff C, Higgins C. Detection of thrombus by using phase-image MR scans: ROC curve analysis. *AJR* **1989**;153:173-178
16. Bendel P, Buonocore E, Bockisch A, Besozzi M. Blood flow in the carotid arteries: quantification by using phase-sensitive MR imaging. *AJR* **1989**;152:1307-1310
17. Spritzer C, Pelc N, Lee J, Evans A, Sostman H, Riederer S. Rapid MR imaging of blood flow with a phase-sensitive, limited-flip-angle, gradient recalled pulse sequence: preliminary experience. *Radiology* **1990**;176:255-262
18. Schmalbrock P, Yuan C, Chakeres D, Kohli J, Pelc N. Volume MR angiography: methods to achieve very short echo times. *Radiology* **1990**;175:861-865
19. Bauer W, Einhaupl K, Heywang S, Vogl T, Seiderer M, Clados D. MR of venous sinus thrombosis: a case report. *AJNR* **1987**;8:713-715
20. Macchi P, Grossman R, Gomori J, Goldberg H, Zimmerman R, Bilaniuk L. High field MR imaging of cerebral venous thrombosis. *J Comput Assist Tomogr* **1986**;10:10-15
21. McMurdo S, Brant-Zawadzki M, Bradley W, Chang G, Berg B. Dural sinus thrombosis: study using intermediate field strength MR imaging. *Radiology* **1986**;161:83-86
22. Edelman R, Wentz K, Mattle H, et al. Intracerebral arteriovenous malformations: evaluation with selective MR angiography and venography. *Radiology* **1989**;173:831-837
23. Tsuruda J, Halbach V, Higashida R, Mark A, Hieshima G, Norman D. MR evaluation of large intracranial aneurysms using cine low flip angle gradient-refocused imaging. *AJNR* **1988**;9:415-424
24. Yousem D, Balakrishnan J, Debrun G, Bryan R. Hyperintense thrombus on GRASS MR images: potential pitfall in flow evaluation. *AJNR* **1990**;11:51-58
25. Rippe D, Boyko O, Spritzer C, Meisler W, Dumoulin C, Souza S. Demonstration of dural sinus occlusion by the use of MR angiography. *AJNR* **1990**;11:199-201
26. Anderson C, Saloner D, Tsuruda J, Shapeero L, Lee R. Pictorial essay. Artifacts in maximum-intensity-projection display of MR angiograms. *AJR* **1990**;154:623-630
27. Teichgraeber J, Per-Lee J, Turner JJ. Lateral sinus thrombosis: a modern perspective. *Laryngoscope* **1982**;92:744-751

Pictorial Essay

Differential Diagnosis of Head and Neck Lesions Based on Their Space of Origin. 1. The Suprahyoid Part of the Neck

H. Ric Harnsberger[1] and Anne G. Osborn

This pictorial essay reviews the spaces of the suprahyoid portion of the head and neck, focusing on the normal spatial anatomy as defined by the deep cervical fascia, the appearance of a generic mass in each of the spaces defined, and the unique differential diagnoses involved in each individual space.

The cylindrical soft-tissue core of the extracranial portion of the head and neck, excluding the more anterior parts of the orbit, sinonasal region, and oral cavity, can be subdivided at the hyoid bone into two distinct regions: the suprahyoid and infrahyoid portions. The three layers of deep cervical fascia that cleave this area of the body into functional spaces converge on the hyoid bone, dividing the neck into these two parts (Fig. 1) [1, 2]. The suprahyoid area encompasses the deep spaces between the skull base and hyoid bone, and the infrahyoid portion lies inferiorly between the hyoid bone and the clavicles.

In the suprahyoid area, the three layers of deep cervical fascia delineate the individual spaces of the deep part of the face (Figs. 1–4). As the contents of these spaces are some-

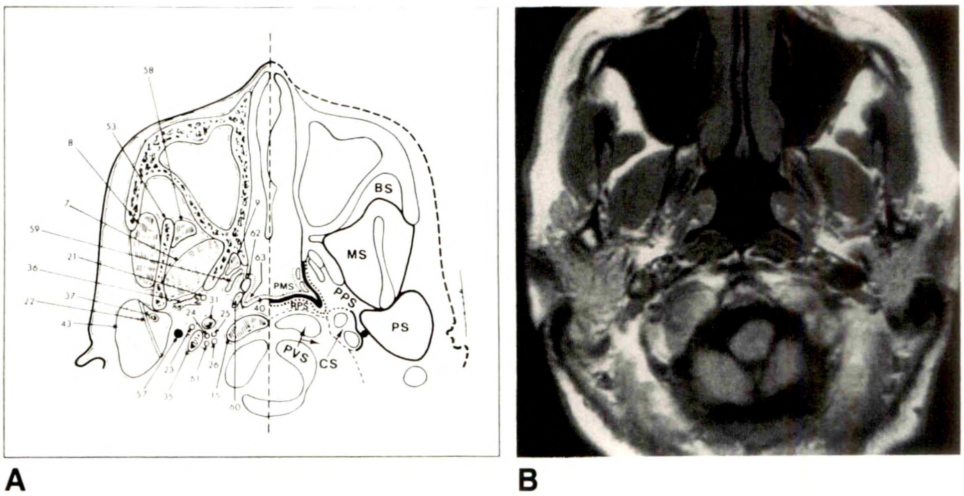

Fig. 1.—*A* and *B*, Axial drawing (*A*) and corresponding MR image (*B*) of normal anatomy of mid nasopharynx. Left side of drawing shows critical normal anatomy of region. Right side shows three layers of deep cervical fascia and spaces they define. See key on page 148. (Reprinted with permission from Harnsberger [2].)

Received October 15, 1990; accepted after revision December 17, 1990.

[1] Both authors: Department of Radiology, University of Utah Medical Center, 50 N. Medical Dr., Salt Lake City, UT 84132. Address reprint requests to H. R. Harnsberger.

AJR **157:147–154, July 1991** 0361–803X/91/1571–0147 © American Roentgen Ray Society

Key to Abbreviations and Symbols Used in Figures

1	buccinator muscle
5	hyoglossus muscle
6	intrinsic muscles of tongue
7	lateral pterygoid muscle
8	masseter muscle
9	medial pterygoid muscle
10	mylohyoid muscle
11	palatoglossus muscle (anterior tonsillar pillar)
12	palatopharyngeus muscle (posterior tonsillar pillar)
13	paraspinal muscles
14	platysma muscle
15	prevertebral muscles
16	sternocleidomastoid muscle
17	styloglossus muscle
18	superior pharyngeal constrictor muscle
19	trapezius muscle
20	inferior alveolar nerve (branch of V_3)
21	lingual nerve (branch of V_3)
22	facial nerve (VII)
23	glossopharyngeal nerve (IX)
24	vagus nerve (X)
25	hypoglossal nerve (XII)
26	sympathetic plexus
30	external carotid artery
31	internal carotid artery
32	internal maxillary artery
33	lingual artery
34	facial vein
35	jugular vein
36	pharyngeal venous plexus
37	retromandibular vein
40	adenoids
41	faucial tonsil
43	parotid gland
45	submandibular gland
46	submandibular gland duct
48	cartilaginous eustachian tube
49	soft palate
50	uvula
51	hyoid bone
53	ramus of the mandible
54	mandibular canal
57	styloid process
58	temporalis muscle
59	tensor veli palatini muscle
60	levator veli palatini muscle
61	spinal accessory nerve
62	torus tubarius
63	lateral pharyngeal recess (fossa of Rosenmüller)
a	artery
BS	buccal space
CS	carotid space
DS	danger space
m	muscle
MS	masticator space
n	node
PCS	posterior cervical space
PMS	pharyngeal mucosal space
PPS	parapharyngeal space
PS	parotid space
PVS	prevertebral space
RPS	retropharyngeal space
SLS	sublingual space
SMS	submandibular space
TS	temporal space (suprazygomatic masticator space)
v	vein
━━━	heavy black line outlines pharyngobasilar fascia
———	medium black line outlines superficial layer of deep cervical fascia
....	dotted line outlines middle layer of deep cervical fascia
-------	broken line outlines deep layer of deep cervical fascia

what unique, differential diagnostic possibilities can be suggested when a lesion is identified within a given space (Table 1). A simple method of assigning a suprahyoid lesion to a specific space of origin is accomplished by establishing the center of the lesion and assessing its displacement of the parapharyngeal space fat (Figs. 5–8) [2, 4]. This method is particularly effective in lesions involving the four spaces surrounding the parapharyngeal space: the pharyngeal mucosal (Fig. 5), masticator (Fig. 6), parotid (Fig. 7), and carotid (Fig. 8) spaces.

Lesions involving the two midline spaces, the retropharyngeal and prevertebral spaces, are best evaluated by noting the relationship of the lesion to the prevertebral muscles. A retropharyngeal space lesion displaces the prevertebral muscles posteriorly (Fig. 9), whereas a prevertebral space lesion displaces the muscles anteriorly (Fig. 10) [4].

The parapharyngeal space is an area of fatty areolar tissue with complex fascial margins that lies in a central location in the deep face (Figs. 1–3). It extends from the skull base to the hyoid bone, containing only fat, branches of the trigeminal nerve, and the pterygoid venous plexus. In order to definitely ascribe a lesion as primary to the parapharyngeal space, fat must be identified surrounding the whole circumference of the lesion [5].

The pharyngeal mucosal space is medial to the parapharyngeal space. It is delimited by the middle layer of deep cervical fascia (Fig. 5). Its major contents include the mucosa, lymphoid tissues of Waldeyer ring, minor salivary glands, cartilaginous eustachian tube, superior and middle constrictor muscles, pharyngobasilar fascia, and levator palatini muscles. A mass in the pharyngeal mucosal space is centered medial to the parapharyngeal space, displacing it laterally (Fig. 5A) [2, 4].

Anterior to the parapharyngeal space is the masticator

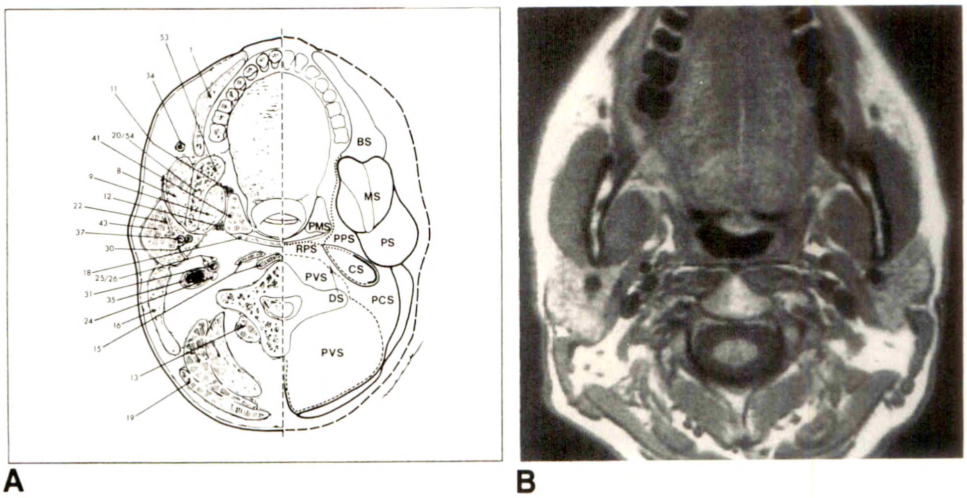

Fig. 2.—*A* and *B*, Axial drawing (*A*) and corresponding MR image (*B*) of normal anatomy of mid oropharynx. Critical contents of spaces are on left; three layers of deep cervical fascia are on right. See key on page 148. (Reprinted with permission from Harnsberger [2].)

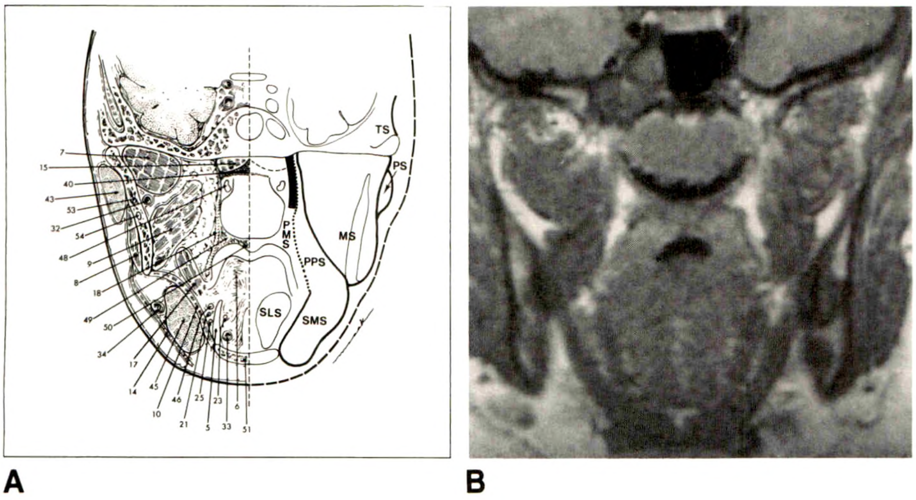

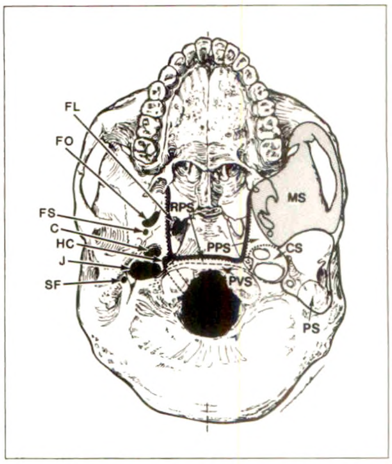

Fig. 3.—*A* and *B*, Coronal drawing (*A*) with corresponding MR image (*B*) of normal anatomy of spaces of suprahyoid part of neck. Note craniocaudal extent of these spaces, especially parapharyngeal and masticator spaces. Critical contents of spaces on left; three layers of deep cervical fascia on right. See key on page 148. (Reprinted with permission from Harnsberger [2].)

Fig. 4.—Axial drawing of skull base shows relationship of spaces of suprahyoid part of neck to skull base apertures. Foramen ovale (FO), through which passes mandibular division of trigeminal nerve, empties into masticator space, whereas stylomastoid foramen (SF) transmits facial nerve directly into parotid space. Carotid space receives cranial nerves IX–XI from jugular foramen (J) and cranial nerve XII from hypoglossal canal (HC). FL = foramen lacerum, FS = foramen spinosum, C = carotid canal. See key on page 148. (Reprinted with permission from Osborn et al. [3].)

space. The superficial layer of deep cervical fascia splits to envelop this space. It has a suprazygomatic component (Fig. 3A) and extends inferiorly to the inferior margin of the mandible. Principal components include the muscles of mastication, ramus and posterior body of the mandible, masticator and inferior alveolar nerves, and inferior alveolar vein and artery. A mass is said to originate from the masticator space when its center is anterior to the parapharyngeal space, displacing the fat from anterior to posterior (Fig. 6A). Masticator space malignancy may spread perineurally along the mandibular division of the trigeminal nerve into the middle cranial fossa (Fig. 6C).

Lateral to the parapharyngeal space is the parotid space. It too is circumscribed by the superficial layer of deep cervical fascia (Fig. 7A). The superior margin of the parotid space abuts the external auditory canal, whereas the parotid tail often extends inferiorly below the inferior mandibular margin. Important contents include the parotid gland, intraparotid facial nerve, retromandibular vein, external carotid artery, and lymph nodes. A mass is described as originating in the parotid space when it is centered within the parotid gland lateral to the parapharyngeal space and displaces the parapharyngeal fat from lateral to medial. Associated widening of the stylomandibular notch (Fig. 7A) is usually seen. Parotid space

TABLE 1: Differential Diagnosis of Deep Facial Lesions Based on Their Space of Origin

Space/Type of Abnormality	Possible Diagnosis
Parapharyngeal	
Pseudomass	Asymmetric pterygoid venous plexus
Congenital	Second branchial cleft cyst, atypical
Inflammatory	Infection spreading from adjacent spaces
Benign tumor	Pleomorphic adenoma of salivary gland rest; lipoma; nerve sheath tumors
Malignancy	Malignant tumor of salivary gland rest; direct spread of tumor from adjacent spaces
Pharyngeal mucosal	
Pseudomass	Asymmetric fossa of Rosenmüller; mucosal inflammation (pharyngitis or radiation)
Inflammatory	Tonsil hypertrophy, tonsillitis, abscess; postinflammatory calcification or retention cyst
Benign tumor	Benign mixed tumor of minor salivary gland origin
Malignancy	Squamous cell carcinoma; non-Hodgkin lymphoma; minor salivary gland malignancy; metastases
Miscellaneous	Thornwaldt cyst
Masticator	
Pseudomass	Benign masseteric hypertrophy; accessory parotid gland; denervation atrophy (mandibular division V)
Congenital	Hemangioma/lymphangioma
Inflammatory	Odontogenic abscess, mandibular osteomyelitis
Benign tumor	Leiomyoma; nerve sheath tumor
Malignancy	Sarcoma (soft tissue, chondrosarcoma, osteosarcoma); malignant schwannoma; non-Hodgkin lymphoma; mandibular metastases; squamous cell carcinoma from oropharynx
Parotid	
Congenital	First branchial cleft cyst; hemangioma/lymphangioma
Inflammatory	Abscess/cellulitis/reactive adenopathy; benign lymphoepithelial cysts (AIDS); autoimmune/Sjögren syndrome
Benign tumor	Benign mixed tumor (pleomorphic adenoma); Warthin tumor; lipoma
Malignancy	Mucoepidermoid carcinoma; adenoid cystic carcinoma; non-Hodgkin lymphoma; malignant mixed tumor; other: acinar cell carcinoma, adenocarcinoma, squamous cell carcinoma
Metastases	Skin squamous cell carcinoma or melanoma; breast or lung carcinoma; nodal non-Hodgkin lymphoma
Carotid	
Pseudomass	Ectatic common or internal carotid artery; asymmetric internal jugular vein
Inflammatory	Carotid space cellulitis or abscess
Vascular	Jugular vein thrombosis or thrombophlebitis; internal carotid artery mural thrombus, aneurysm; internal carotid artery dissection
Benign tumor	Paraganglioma; nerve sheath tumor (schwannoma, neurofibroma)
Malignancy	Squamous cell carcinoma nodal metastasis; direct invasion by primary squamous cell carcinoma; non-Hodgkin lymphoma; metastases
Retropharyngeal	
Pseudomass	Tortuous carotid artery; edema secondary to deep venous obstruction
Congenital	Hemangioma
Inflammatory	Reactive adenopathy/cellulitis/abscess
Benign tumor	Lipoma
Malignancy	Nodal metastases from squamous cell carcinoma, melanoma, thyroid carcinoma, non-Hodgkin lymphoma; direct invasion from primary squamous cell carcinoma
Prevertebral	
Pseudomass	Vertebral body osteophyte/anterior disk herniation
Vascular	Vertebral artery aneurysm, pseudoaneurysm, ectasia
Inflammatory	Vertebral body osteomyelitis
Benign tumor	Chordoma; schwannoma, neurofibroma (brachial plexus); vertebral body benign bony tumors
Malignancy	Vertebral body/epidural metastasis; non-Hodgkin lymphoma; vertebral body primary malignant tumor

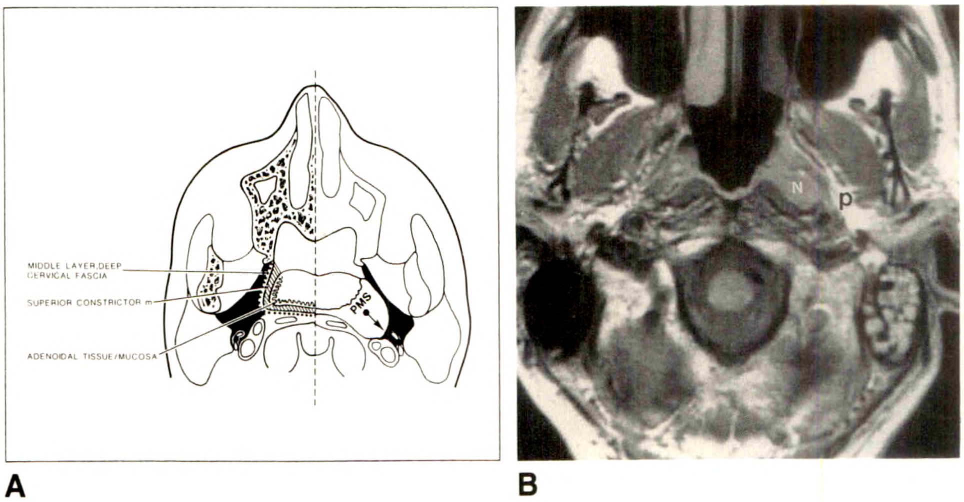

Fig. 5.—*A*, Axial drawing through low nasopharynx shows contents and fascial boundaries of pharyngeal mucosal space (PMS) on left and pharyngeal mucosal space mass on right. Middle layer of deep cervical fascia (*dotted line*) encompasses posterolateral margin of superior constrictor muscle, defining pharyngeal mucosal space. Center of pharyngeal mucosal space mass (*black dot*) is medial to laterally displaced parapharyngeal space (*black area*), invading parapharyngeal space from medial to lateral. m = muscle. (Reprinted with permission from Harnsberger [4].)

B, Axial density-weighted MR image in patient with early nasopharyngeal carcinoma (N) in lateral pharyngeal recess of nasopharyngeal mucosal space. p = parapharyngeal space.

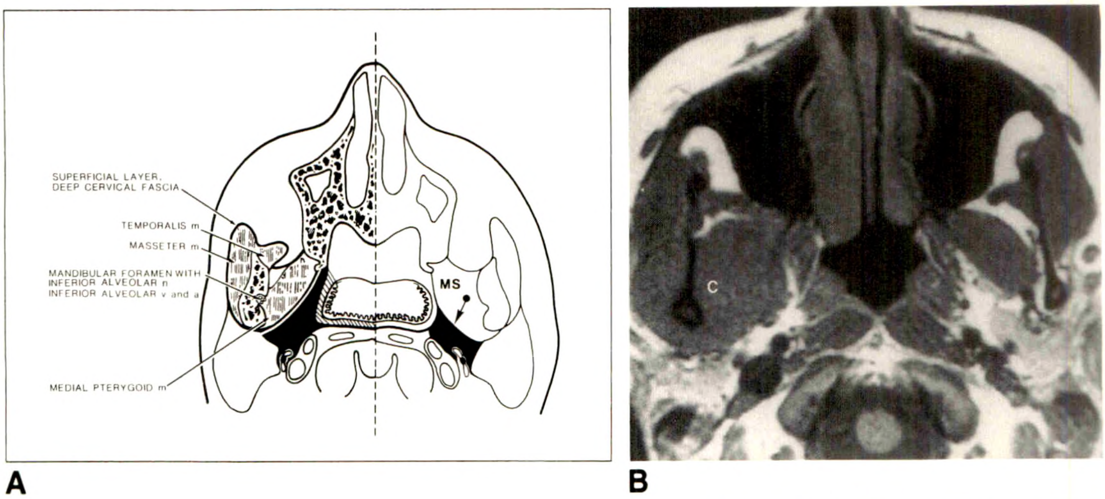
SUPERFICIAL LAYER, DEEP CERVICAL FASCIA
TEMPORALIS m
MASSETER m
MANDIBULAR FORAMEN WITH INFERIOR ALVEOLAR n INFERIOR ALVEOLAR v and a
MEDIAL PTERYGOID m
MS
A
C
B

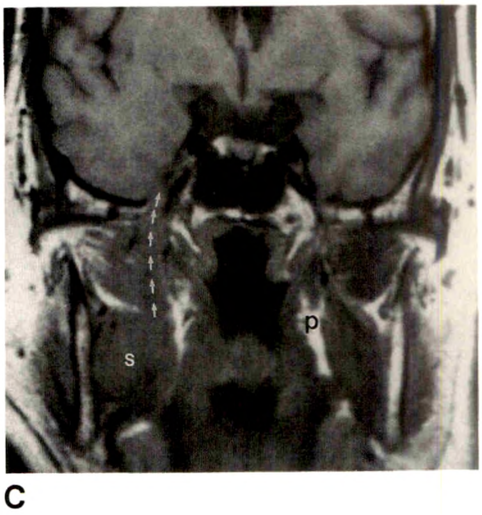

Fig. 6.—*A*, Axial drawing through low nasopharynx shows contents and fascial boundaries of masticator space on left and appearance of masticator space mass (MS) on right. Superficial layer of deep cervical fascia surrounds muscles of mastication and mandible, defining masticator space. Center of masticator space mass (*black dot*) is anterior to posteriorly displaced parapharyngeal space (*black area*), invading parapharyngeal space from anterior to posterior. See key on page 148. (Reprinted with permission from Harnsberger [4].)

B, Axial T1-weighted unenhanced MR image of masticator space chondrosarcoma (C). Tumor involves muscles of mastication and mandible.

C, Coronal MR image of masticator space malignant schwannoma (S) with perineural tumor spread along mandibular division of trigeminal nerve (*arrows*) to skull base and through foramen ovale. p = parapharyngeal space.

malignancy may follow the facial nerve into the temporal bone (Fig. 7C).

Posterior to the parapharyngeal space is the carotid space. All three layers of deep cervical fascia contribute to the carotid sheath that circumscribes this space (Fig. 8A). This space extends from the skull base to the aortic arch. Its suprahyoid contents include the internal carotid artery, jugular vein, cranial nerves IX–XII, and deep cervical lymph node chain. A

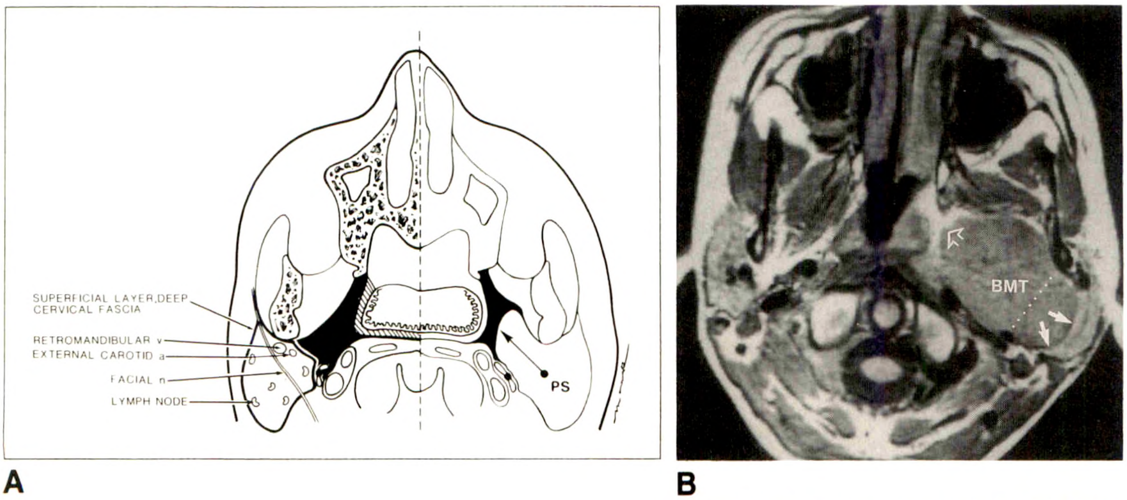

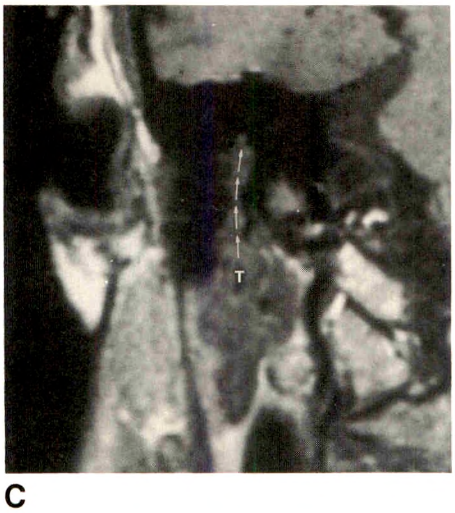

Fig. 7.—*A*, Axial drawing through low nasopharynx shows contents and fascial boundaries of parotid space on left and appearance of a parotid space mass (PS) on right. Superficial layer of deep cervical fascia surrounds parotid gland and its contents, defining parotid space. Center of mass (*black dot*) is lateral to medially displaced parapharyngeal space (*black area*), invading parapharyngeal space from lateral to medial. See key on page 148. (Reprinted with permission from Harnsberger [4].)

B, T1-weighted axial MR image in a patient with a large benign mixed tumor (BMT) of parotid space that widens stylomandibular notch (*dotted line*) and impinges on fatty parapharyngeal space from lateral to medial (*open arrow*). Note lack of identifiable fat plane between remaining normal parotid gland and mass (*solid arrows*).

C, Mucoepidermoid carcinoma of parotid space with perineural tumor following mastoid segment of facial nerve. Coronal T1-weighted MR image shows an intraparotid tumor (T) with a long "tail" extending to posterior genu of facial nerve canal within adjacent temporal bone along mastoid segment of facial nerve (*arrows*).

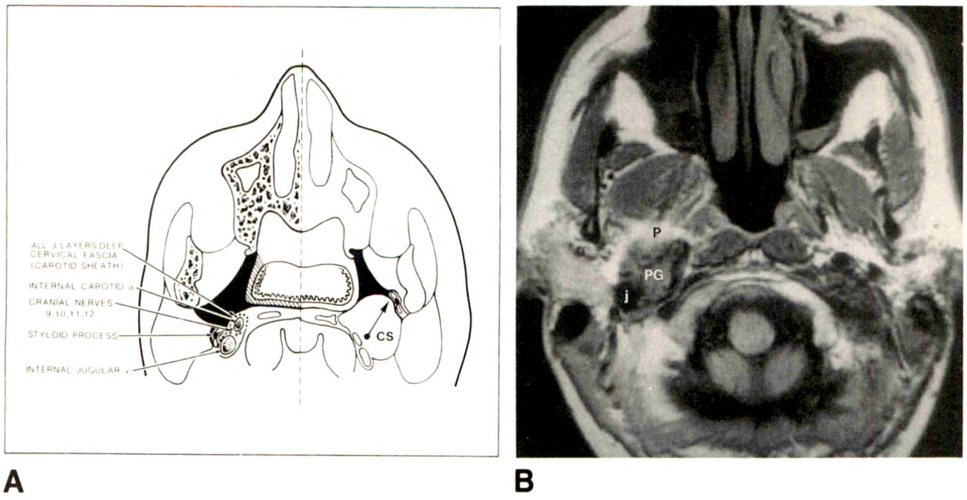
ALL 3 LAYERS DEEP CERVICAL FASCIA (CAROTID SHEATH)
INTERNAL CAROTID a
CRANIAL NERVES 9,10,11,12
STYLOID PROCESS
INTERNAL JUGULAR v
CS
A
P
PG
j
B

Fig. 8.—*A*, Axial drawing through low nasopharynx shows contents and fascial boundaries of carotid space on left and appearance of a carotid space mass (CS) on right. All three layers of deep cervical fascia contribute to carotid sheath, which circumscribes carotid artery, jugular vein, and associated cranial nerve and lymph nodes, defining carotid space. Center of mass (*black dot*) is posterior to anteriorly displaced parapharyngeal space (*black area*), invading it from posterior to anterior. a = artery, v = vein. (Reprinted with permission from Harnsberger [4].)

B, Glomus vagale paraganglioma of nasopharyngeal carotid space. Axial T1-weighted MR image of a right carotid space paraganglioma (PG) shows anterior displacement of parapharyngeal space fat (P). Plethora of serpiginous vascular flow voids within tumor signals its vascular nature and probable histology. Right internal carotid artery is thrombosed. j = internal jugular vein.

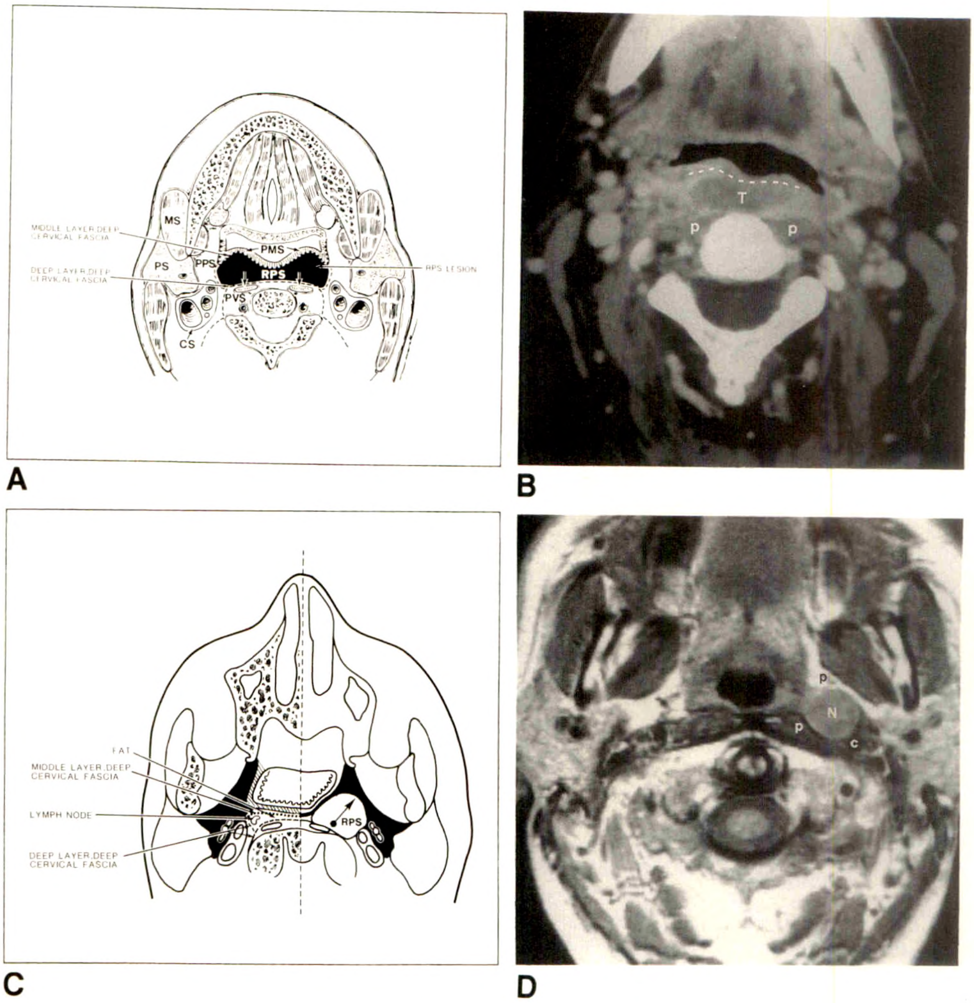
MS
MIDDLE LAYER,DEEP CERVICAL FASCIA
PMS
PS
PPS
RPS
RPS LESION
DEEP LAYER,DEEP CERVICAL FASCIA
PVS
CS
A
T
p
p
B
FAT
MIDDLE LAYER,DEEP CERVICAL FASCIA
LYMPH NODE
RPS
DEEP LAYER,DEEP CERVICAL FASCIA
C
p
N
p
c
D

Fig. 9.—*A*, Axial drawing of extranodal mass lesion of retropharyngeal space (RPS) at level of oropharynx causing posterior displacement of prevertebral muscles (*arrows*) within prevertebral space proper (PVS) and anterior displacement of pharyngeal mucosal space (PMS). Note somewhat "bow tie" shape of retropharyngeal space mass. See key on page 148. (Reprinted with permission from Harnsberger [4].)

B, Squamous cell carcinoma of posterior wall of oropharynx invading adjacent retropharyngeal space. Enhanced axial CT scan shows tumor (T) within oropharyngeal retropharyngeal space. Pharyngeal mucosal space (*broken line*) is displaced anteriorly, whereas prevertebral muscles (p) are flattened along their anterior surface.

C, Axial drawing through low nasopharynx shows appearance of nodal mass lesion of retropharyngeal space (RPS), which has its center (*black dot*) posteromedial to parapharyngeal space (*black area*) and displaces it anterolaterally (compare with Fig. 8A). Carotid space masses can be confused with lateral retropharyngeal space lesions unless there is awareness of their unique characteristics. Key differential feature is direction of displacement of carotid space contents, especially carotid artery. In lateral retropharyngeal space masses, internal carotid artery is displaced laterally. (Reprinted with permission from Harnsberger [4].)

D, Malignant squamous cell carcinoma node within lateral nodal chain of retropharyngeal space. Density-weighted MR image through low nasopharynx reveals a lateral retropharyngeal space malignant node (N) that displaces internal carotid artery (c) posterolaterally, parapharyngeal space fat (*black* p) anterolaterally, and prevertebral muscle (*white* p) posteriorly.

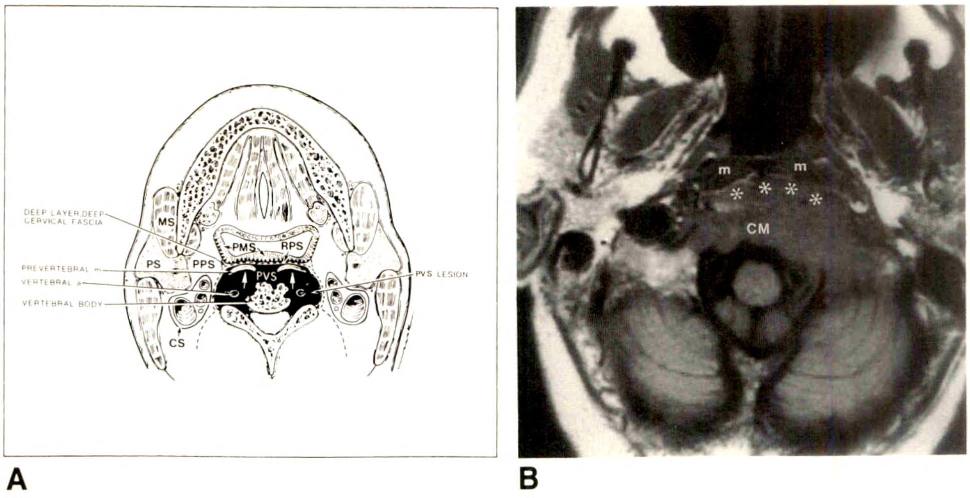

Fig. 10.—*A*, Axial drawing at level of low oropharynx shows a mass lesion originating within prevertebral space (PVS) proper with anterior displacement of prevertebral muscles (*arrows*), retropharyngeal space (RPS), and pharyngeal mucosal space (PMS). As is commonly the case in infection and malignancy of the prevertebral space, vertebral body is partially destroyed by lesion. See key on page 148. (Reprinted with permission from Harnsberger [4].

B, Colonic metastasis to lower clivus with extension into adjacent prevertebral space. Axial T1-weighted MR image shows clival colonic metastatic deposit (CM) extending into adjacent prevertebral space (*asterisks*). Prevertebral muscles (m) are displaced anteriorly.

mass lesion is primary to the carotid space when it is centered posterior to the parapharyngeal space and displaces it anteriorly (Fig. 8B).

The retropharyngeal space is a posterior midline space that has the middle layer of deep cervical fascia as its anterior margin and the deep layer of deep cervical fascia as its posterior and lateral margins (Fig. 9A). It extends from the skull base to the level of the T3 vertebral body. The suprahyoid retropharyngeal space contains only lymph nodes and fat. When disease affects the retropharyngeal space diffusely, the prevertebral muscles are seen to be displaced posteriorly (Fig. 9B). When the mass occurs in the laterally placed nodes, it will impinge on the parapharyngeal space posteromedially (Figs. 9C and 9D).

The prevertebral space proper is defined by the deep layer of deep cervical fascia as it passes superficial to the prevertebral muscles to attach to the cervical transverse processes (Fig. 10A). This space contains the prevertebral muscles; the vertebral body, artery, and vein; and the spinal cord. A lesion originates from the prevertebral space proper when it displaces the prevertebral muscles anteriorly (Fig. 10B).

REFERENCES

1. Grodlinsky M, Holyoke E. The fascia and fascial spaces of the head and neck and adjacent regions. *Am J Anat* **1938**;63:367–407
2. Harnsberger HR. CT and MRI of masses of the deep face. *Curr Probl Diagn Radiol* **1987**;16:147–173
3. Osborn AG, Harnsberger HR, Smoker WRK. Base of skull imaging. *Semin Ultrasound CT MR* **1986**;7:91–106
4. Harnsberger HR. *Handbooks in radiology. Head and neck radiology volume.* St. Louis: Mosby–Year Book Medical, **1990**
5. Som PM, Sacher M, Stollman AL, Biller HF, Lawson W. Common tumors of the parapharyngeal space: refined imaging diagnosis. *Radiology* **1988**:169:81–85

Pictorial Essay

Differential Diagnosis of Head and Neck Lesions Based on Their Space of Origin. 2. The Infrahyoid Portion of the Neck

Wendy R. K. Smoker[1,2] and H. Ric Harnsberger[1]

The infrahyoid portion of the neck can be considered as a series of contiguous fascial planes and intervening spaces that lend themselves well to axial imaging. These spaces can serve as a basis on which to formulate differential diagnoses for diseases in this region. This pictorial essay describes the fascia and fascial spaces of the infrahyoid portion of the neck. The contents of each space, the common abnormalities affecting the space, and the characteristic displacements produced by disease in each space are reviewed.

Anatomy

The two major fascial layers of the infrahyoid neck are the superficial and deep cervical fasciae. The more important deep cervical fascia comprises three distinct layers, the superficial, middle, and deep layers, and cleaves the infrahyoid portion of the neck into a number of fascial spaces [1].

Completely surrounding the neck, the superficial layer of deep cervical fascia lies deep to the skin and superficial cervical fascia, extending from the skull base to the clavicles and scapulae. It splits to enclose a number of muscles and contributes to formation of the carotid sheath (Fig. 1). The space external to the superficial layer of deep cervical fascia is the superficial space.

Extending from the hyoid bone anteriorly, the middle layer of the deep cervical fascia envelops the anterior infrahyoid strap muscles and merges with the superficial layer. A portion of the middle layer splits to enclose the contents of the visceral space (Fig. 2). Posteriorly, the middle layer extends from the skull base to the upper mediastinum, forming the anterior wall of the retropharyngeal space and contributing to formation of the carotid sheath.

The deep layer of the deep cervical fascia encircles the paraspinous and prevertebral muscles and associated struc-

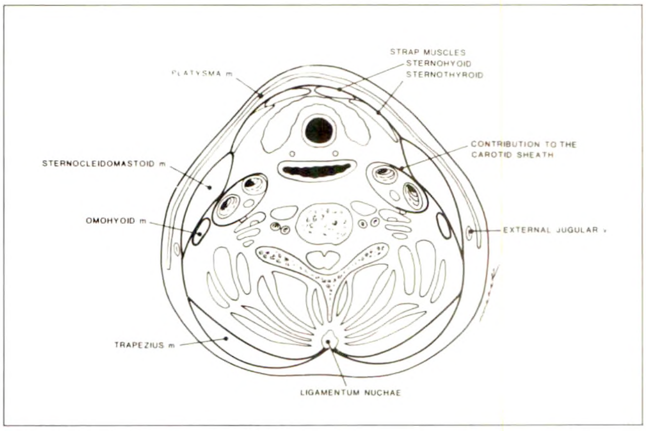

Fig. 1.—Axial line diagram illustrates superficial layer of deep cervical fascia (*bold lines*). This fascia splits to enclose sternocleidomastoid and trapezius muscles, forms a sling around inferior belly of omohyoid muscle (anchoring it to clavicle), and contributes to formation of carotid sheath. External jugular veins lie external to, or embedded within, this fascial layer. Superficial space, external to deepest fibers of superficial layer, contains platysma, sternocleidomastoid, inferior omohyoid, and trapezius muscles and external jugular veins. m = muscle, v = vein.

Received October 15, 1990; accepted after revision January 4, 1991.

[1] Department of Radiology, University of Utah, 50 North Medical Dr., Salt Lake City, UT 84132.

[2] Present address: Department of Radiology, Medical College of Virginia, Box 615, MCV Station, Richmond, VA 23298. Address reprint requests to W. R. K. Smoker.

***AJR* 157:155–159, July 1991** 0361–803X/91/1571–0155 © American Roentgen Ray Society

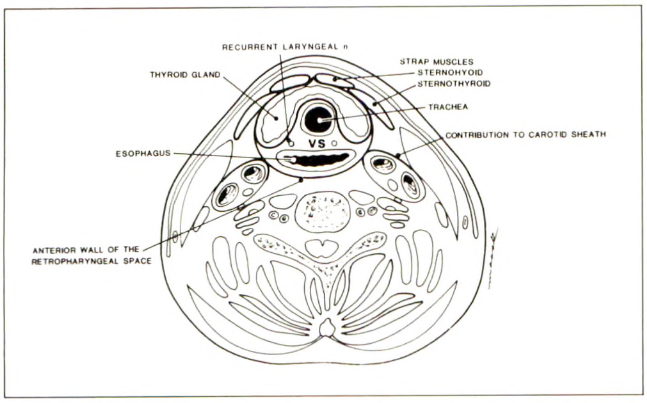

Fig. 2.—Axial line diagram illustrates middle layer of deep cervical fascia (*bold lines*). This layer envelops anterior strap muscles and fuses with superficial layer anteriorly. Main portion of middle layer forms a fascial sheath around contents of visceral space (vs). A capsule for thyroid gland is formed by a splitting of middle layer. Posteriorly, middle layer forms anterior wall of retropharyngeal space, contributes to formation of carotid sheath, and merges with superficial layer covering deep surface of sternocleidomastoid muscle. n = nerve.

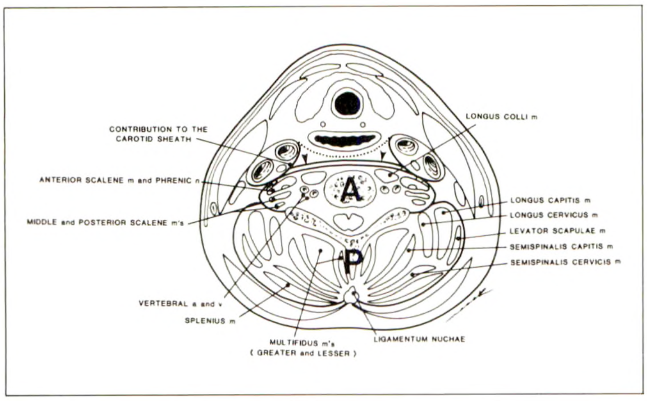

Fig. 3.—Axial line diagram illustrates deep layer of deep cervical fascia (*bold lines*). Anterior aspect of deep layer splits into alar (anterior) and prevertebral (posterior) portions, forming danger space. Alar portion (*arrowheads*) forms lateral and posterior walls of retropharyngeal space and contributes to formation of carotid sheath. (Anterior wall of retropharyngeal space is formed by middle layer of deep cervical fascia [*dotted line*]). Attaching to transverse processes, the major prevertebral portion subdivides prevertebral space into anterior prevertebral space proper (A) and posterior paraspinal portion of prevertebral space (P). m = muscle, n = nerve, a = artery, v = vein.

tures (Fig. 3). Attaching to the transverse processes, the deep layer subdivides the prevertebral space into the prevertebral space proper and the paraspinal portion of the prevertebral space. Anteriorly the deep layer splits into two portions. The more anterior alar portion, forming the posterior and lateral walls of the retropharyngeal space and contributing to carotid sheath formation, extends from the skull base to the diaphragm. The more posterior prevertebral portion extends from the skull base to the coccyx. The space created by the anterior splitting of the deep layer is called the danger space (Figs. 4 and 5) [1, 2].

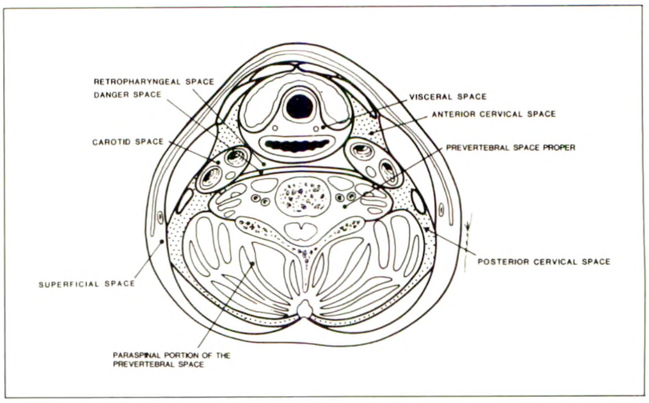

Fig. 4.—Axial line diagram shows spaces of infrahyoid portion of neck. Note how anterior and posterior cervical spaces (*stippled area*) lie among other deep spaces of neck.

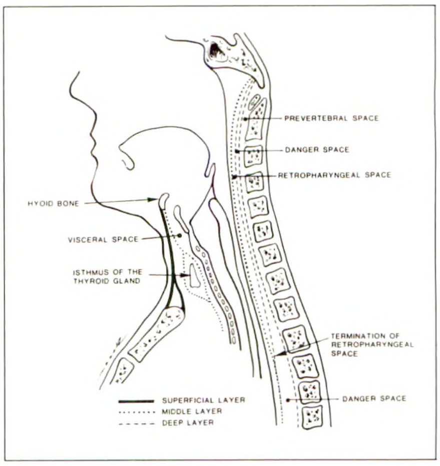

Fig. 5.—Midsagittal line diagram shows fascial layers and spaces of infrahyoid portion of neck. Note that termination of retropharyngeal space is caused by fusion of middle layer and alar portion of deep layer of deep cervical fascia in upper thoracic region. However, infections within retropharyngeal space may transgress thin alar fascia and continue inferiorly via danger space, below termination of retropharyngeal space.

Spaces of the Infrahyoid Portion of the Neck

The carotid spaces are circumscribed by the carotid sheaths, composed of all three layers of deep cervical fascia. The carotid spaces contain the internal jugular veins, common or internal carotid arteries, and vagus nerves. The sympathetic plexus is embedded in the medial sheath walls. Numerous lymph nodes of the deep cervical chain are also enmeshed within the sheaths. Typical displacements of surrounding structures produced by a carotid space mass are illustrated in Figure 6. Diseases common to the carotid space include carotid body paragangliomas (Fig. 7), neurogenic tumors, internal jugular vein thrombophlebitis (Fig. 8), vascular pseudotumors (asymmetric internal jugular vein, ectatic carotid artery), and isolated nodal disease (inflammatory or neoplastic).

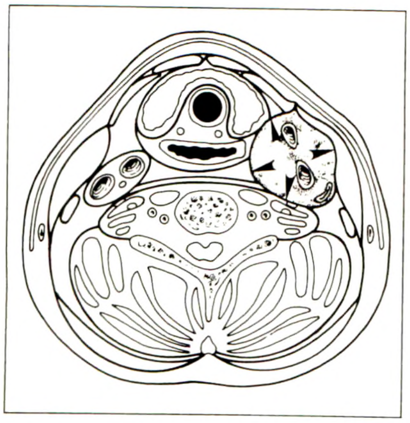

Fig. 6.—Mass in carotid space. Axial line diagram illustrates typical displacements of surrounding spaces (*arrowheads*).

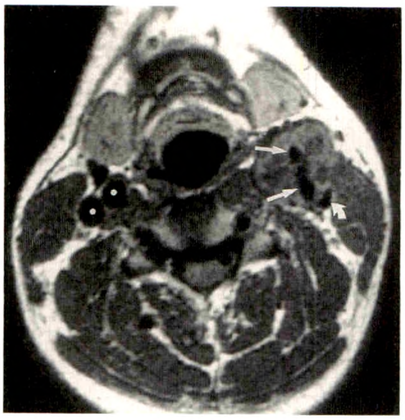

Fig. 7.—Paraganglioma in carotid space. Axial MR image, 750/25 (TR/TE), reveals normal flow voids that localize normal right carotid space vessels (*dots*). Splaying of proximal left internal and external carotid arteries (*straight arrows*) plus compression and posterior displacement of left internal jugular vein (*curved arrow*) localizes lesion to left carotid space.

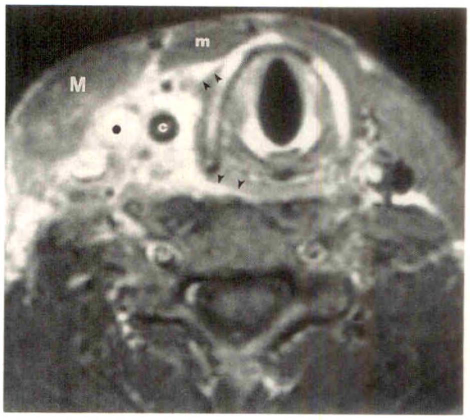

Fig. 8.—Thrombosis and thrombophlebitis of jugular vein in carotid space. Axial T1-weighted MR image, 1000/20 (TR/TE), enhanced with gadopentetate dimeglumine shows thrombosis of right internal jugular vein (*dot*) and marked inflammatory changes in right carotid space. Right sternocleidomastoid muscle (M) and anterior strap muscles (m) are enlarged. Right anterior cervical and retropharyngeal spaces (*arrowheads*) also are enhanced. c = common carotid artery.

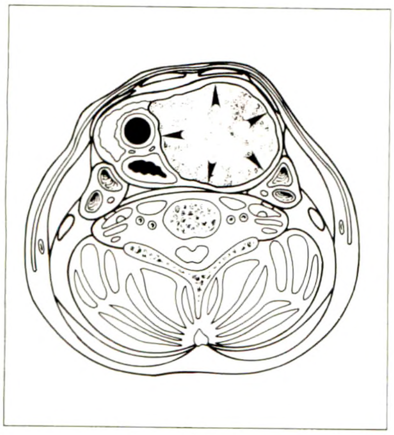

Fig. 9.—Mass in visceral space. Axial line diagram depicts characteristic displacements of surrounding spaces (*arrowheads*).

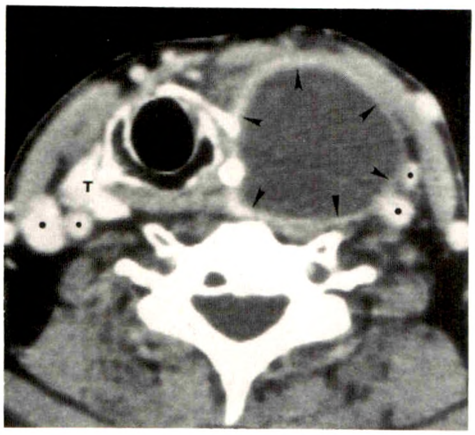

Fig. 10.—Colloid cyst in visceral space. Enhanced CT scan shows large cyst involving left lobe of thyroid; displacement of other visceral space structures to right, across midline; and lateral displacement of carotid space vessels bilaterally (*dots*), left greater than right. Although right lobe of thyroid gland (T) is well visualized, left lobe is represented by thin rim of enhancing tissue (*arrowheads*) around cyst.

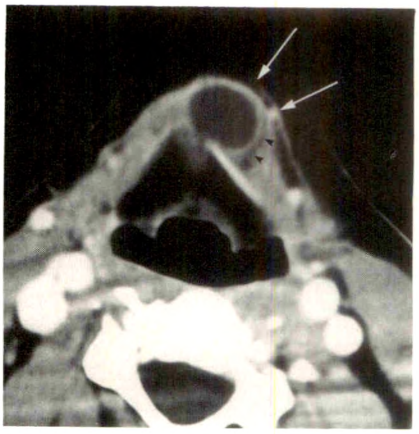

Fig. 11.—Thyroglossal duct cyst in visceral space. Enhanced CT scan localizes lesion to superficial aspect of visceral space by showing that, in addition to lying deep to platysma muscle (*arrows*), lesion also lies deep to, and is embedded within, anterior strap muscles. A faint fat plane is visible between cyst and displaced strap muscles (*arrowheads*).

The visceral space is delimited by the middle layer of deep cervical fascia (Fig. 2). The visceral space contains the thyroid and parathyroid glands, trachea, esophagus, paraesophageal nodes, and recurrent laryngeal nerves. A diagram of the typical displacements of surrounding spaces produced by a visceral space mass is presented in Figure 9. Thyroid gland disease (cysts [Fig. 10], carcinomas, adenomas, multinodular goiters) predominates in this space, with parathyroid and esophageal disease being much less common. As most thyroglossal duct cysts are embedded in the anterior strap muscles (which are enclosed by the middle layer of deep cervical fascia), they are also considered to lie within the visceral space (Fig. 11).

Although separately defined fascial spaces, the retropharyngeal and danger spaces are considered together, because, within the infrahyoid portion of the neck, disease affecting these spaces cannot be differentiated radiologically. From a clinical standpoint, the danger space is important because, terminating at the level of the diaphragm, it represents a pathway by which retropharyngeal space infections may con-

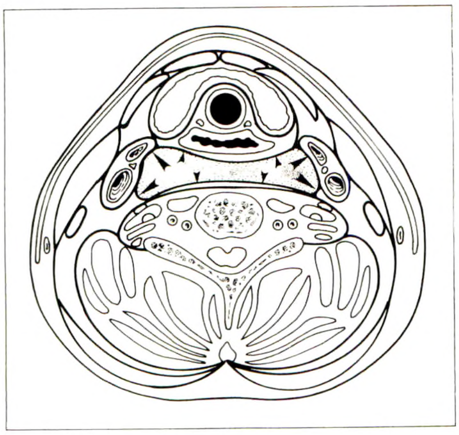

12

Fig. 12.—Mass in retropharyngeal space. Axial line diagram shows characteristic displacements of surrounding spaces (*arrowheads*).

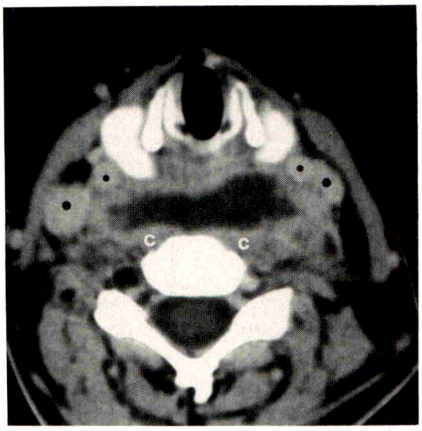

13

Fig. 13.—Abscess in retropharyngeal space. Enhanced CT scan shows visceral space and prevertebral space proper widely separated by abscess. Longus colli muscles (c) are compressed posteriorly and vessels in carotid spaces are displaced bilaterally (*dots*). This lesion cannot be localized to retropharyngeal vs danger spaces on the basis of CT scan.

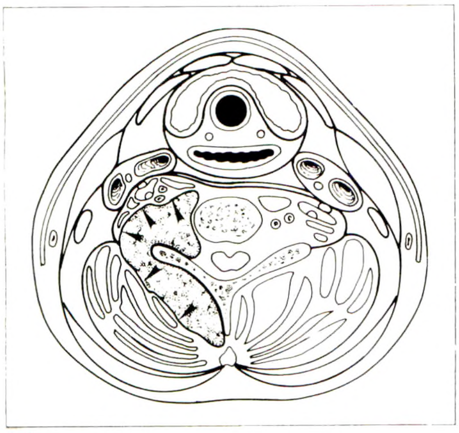

14

Fig. 14.—Mass in prevertebral space. Axial line diagram illustrates typical displacements of surrounding spaces produced by a lesion involving both prevertebral space proper and paraspinal portion of prevertebral space (*arrowheads*).

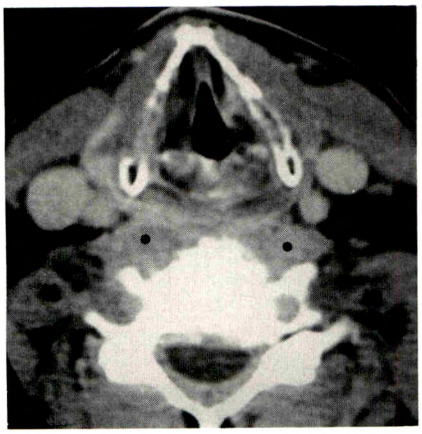

15

Fig. 15.—Abscess in prevertebral space. Enhanced CT scan shows abscess involving prevertebral space proper after interbody cervical fusion. Abnormality can be compartmentalized by observing abnormal enhancement and enlargement of longus colli muscles bilaterally (*dots*). (Bone windows [*not shown*] also revealed vertebral body destruction.) Although perceived separation between visceral space and vertebral body might suggest mass in retropharyngeal space, configuration of this lesion is not characteristic for disease of retropharyngeal space, and longus colli muscles are not compressed posteriorly, as was seen in Fig. 13.

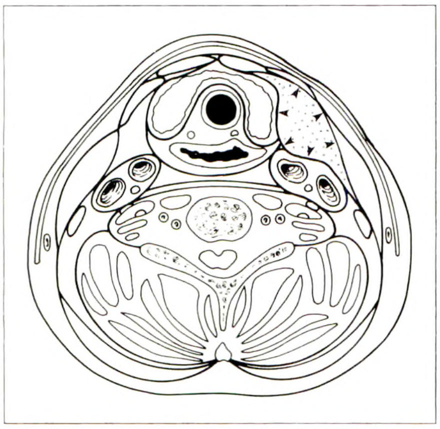

16

Fig. 16.—Mass in anterior cervical space. Axial line diagram depicts typical surrounding fascial space displacements (*arrowheads*).

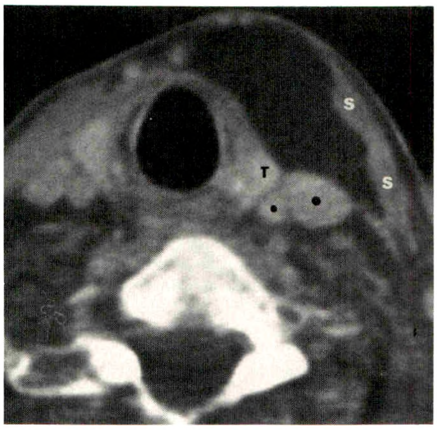

17

Fig. 17.—Lipoma in anterior cervical space. Enhanced CT scan shows marked compression and displacement of left sternocleidomastoid muscle (s), posteromedial displacement of carotid space vessels (*dots*), and slight compression of left lobe of thyroid gland (T).

tinue inferiorly in the posterior mediastinum (Fig. 5) [3]. These spaces contain only fat in the infrahyoid portion of the neck, and disease in them presents a somewhat characteristic bow-tie appearance (Fig. 12) [4]. These spaces are most often involved by infection (Fig. 13), hematoma, extranodal metastatic disease, lipomas, or edema associated with internal jugular vein thrombosis or lymphatic obstruction [4].

The prevertebral space is delimited by the deep layer of deep cervical fascia (Fig. 3). It contains the prevertebral, paraspinal, and scalene muscles; vertebral artery and vein; vertebral body; and spinal cord. A line diagram of the characteristic displacements of surrounding spaces produced by a lesion involving both the prevertebral space proper and the paraspinal portion of the prevertebral space is presented in Figure 14. The prevertebral space proper can be involved by infection (osteomyelitis/diskitis) (Fig. 15), chordomas, pseudomeningoceles associated with brachial plexus avulsions, and a variety of pseudotumors (anterior herniated disks,

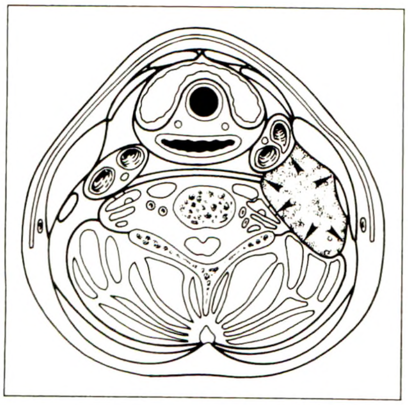

Fig. 18.—Mass in posterior cervical space. Axial line diagram illustrates characteristic displacements of surrounding spaces (*arrowheads*).

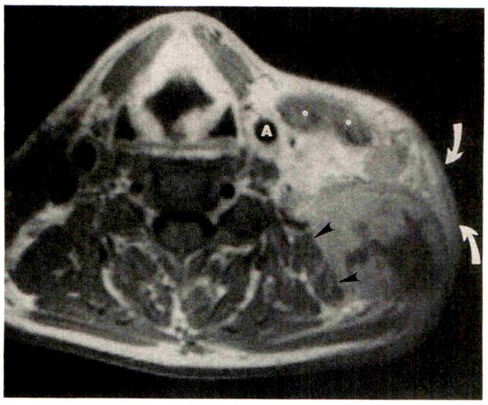

Fig. 19.—Malignant node in posterior cervical space. Axial T1-weighted MR image, 600/20 (TR/TE), enhanced with gadopentetate dimeglumine, reveals nodal disease of the spinal accessory chain of the left posterior cervical space in a patient with Hodgkin lymphoma. Note marked deformity of external neck contour (*arrows*), flattening of muscles in paraspinal portion of prevertebral space (*arrowheads*), anterior displacement of sternocleidomastoid muscle (*dots*), and anteromedial displacement of left carotid artery (A).

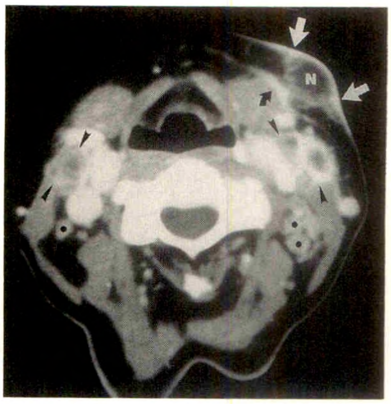

Fig. 20.—Multispatial tularemia. Enhanced CT scan shows a large suppurative node in external aspect of superficial space (N) with thickening and enhancement of overlying skin (*white arrows*) and underlying platysma muscle (*black arrow*). Suppurative adenopathy is also present bilaterally in deep cervical chain nodes of carotid spaces (*arrowheads*), and smaller, reactive-appearing nodes are present in spinal accessory nodes of posterior cervical spaces (*dots*).

vertebral osteophytes, longus colli tendon calcification). The paraspinal portion of the prevertebral space can be involved by a variety of primary bone tumors (osteoblastoma, chordoma, aneurysmal bone cysts) and by the pseudotumor appearance of levator scapulae muscle hypertrophy accompanying injury to the spinal accessory nerve. Lymphomas, metastatic disease, and neurogenic tumors may involve either compartment.

The anterior and posterior cervical spaces are situated among the other spaces of the infrahyoid portion of the neck, with complex fascial boundaries involving all three layers of deep cervical fascia (Fig. 5). Because they are primarily fat filled, these spaces typically provide symmetric imaging landmarks on axial imaging. Isolated disease of the anterior cervical space produces characteristic displacements of surrounding fascial spaces (Fig. 16) and is limited to lipomas (Fig. 17) and more inferiorly located second branchial cleft cysts. Disease isolated to the posterior cervical space is much more common and easily localized by displacement of surrounding fascial spaces (Fig. 18). Cystic hygromas/lymphangiomas, lipomas, liposarcomas, and third branchial cleft cysts occur within this space. Because it contains the spinal accessory lymph node chain, the posterior cervical space is also commonly affected by both inflammatory and malignant nodal disease (Fig. 19).

Although often isolated to a single space, disease of the infrahyoid part of the neck may involve many spaces simultaneously. This is especially common with nodal disease involving the major node-bearing spaces (deep cervical chain of the carotid space and spinal accessory chain of the posterior cervical space). Discrete involvement of these nodes presents a pattern of multispatial disease and is most often seen with lymphoma, infection (Fig. 20), and nodal metastatic disease (especially squamous cell carcinoma metastases).

Knowledge of the fascial planes and spaces, their contents, the characteristic displacements of surrounding spaces produced by disease isolated to each space, and the common abnormalities affecting each space allows an organized approach to the evaluation of infrahyoid neck disease.

REFERENCES

1. Grodinsky M, Holyoke EA. The fasciae and fascial spaces of the head, neck and adjacent regions. *Am J Anat* **1938**;63:367–408
2. Stiernberg CM. Deep-neck space infections: diagnosis and management. *Arch Otolaryngol Head Neck Surg* **1986**;112:1274–1279
3. Levit GW. Cervical fascia and deep neck infections. *Laryngoscope* **1970**;80:409–435
4. Davis WL, Harnsberger HR, Smoker WRK, Watanabe AS. The radiologic evaluation of the normal and diseased retropharyngeal space. *Radiology* **1990**;174:59–64

News

Robert H. Ackerman, 1991–1992 Distinguished Scientist, Armed Forces Institute of Pathology

James L. Buck[1]

Robert H. Ackerman will serve as the Distinguished Scientist in the Department of Radiologic Pathology, Armed Forces Institute of Pathology (AFIP), for the academic year July 1, 1991, through June 30, 1992.

Dr. Ackerman currently is an associate professor of radiology at Harvard Medical School and a radiologist and neurologist at Massachusetts General Hospital, where he also is director of the neurovascular laboratory. He is certified by the American Board of Radiology (diagnostic radiology) and the American Board of Psychiatry and Neurology (neurology).

His major research interests have been in stroke disease, especially in the application of radiologic tools to better identify and treat patients who are stroke-prone or who have just had a stroke. He helped pioneer the development of noninvasive techniques for the diagnosis of carotid disease and the use of positron emission tomography in the study of ischemic stroke and has been program director of the Interdepartmental Stroke Center, Massachusetts General Hospital, funded by the National Institutes of Health. His bibliography includes nearly 100 scientific publications on neurovascular disease. He is on the editorial boards of the *American Journal of Neuroradiology*, *Stroke*, and the *Archives of Neurology*.

Dr. Ackerman received his B.A. degree from Brown University in 1957 and his M.D. degree from the University of Rochester in 1964. He interned at the Mary Imogene Bassett Hospital in Cooperstown, NY, and completed his residencies in neurology (1970) and radiology (1975) at the Massachusetts General Hospital. In 1970–1971, he was a Dalton Scholar at the Neurological Institute Queen Square, London, England, where he studied techniques used to measure cerebral blood flow.

The Distinguished Scientist program in the Department of Radiologic Pathology was established in 1985 through the efforts of the director of the AFIP, the American Registry of Pathology, and the four major radiologic societies represented on the Conjoint Committee on Radiology at the AFIP. The current members of this committee include Mark M. Mishkin, chairman, American College of Radiology; Ernest J. Ferris, Radiological Society of North America; John E. Madewell, American Roentgen Ray Society; and Thomas S. Harle, Association of University Radiologists. Otha Linton, associate executive director of the American College of Radiology, is the liaison between the committee and the AFIP. The Department of Radiologic Pathology is grateful for the continued generous support of these individuals and organizations.

The Distinguished Scientist program at the AFIP has been a huge success. The previous Distinguished Scientists have made and continue to make important contributions to the research and educational programs at the AFIP. No doubt, Dr. Ackerman will continue this fine tradition.

The opinions and assertions contained herein are the private views of the author and are not to be construed as official or as reflecting the views of the Department of Navy or the Department of Defense.

[1] Department of Radiologic Pathology, Armed Forces Institute of Pathology, Washington, DC 20306-6000.

***AJR* 157:160, July 1991** 0361–803X/91/1571–0160

Radiologic Evaluation of the Normal and Diseased Posterior Cervical Space

Geoffrey D. Parker[1]
H. Ric Harnsberger

The posterior cervical space seen on cross-sectional imaging of the neck constitutes most of the posterior triangle seen on clinical examination. Although triangular anatomy relates best to the surface perspective of the clinician, a spatial approach to anatomy works better for the radiologist viewing axial images. The posterior cervical space is defined as the area in the posterolateral portion of the neck from the skull base to the clavicles deep to the sternomastoid and trapezius muscles but superficial to the prevertebral space. Its principal contents are fat, the spinal accessory nerve, and lymph nodes. We analyzed CT and MR images and clinical records of 63 patients known or suspected to have disease of the posterior cervical space to determine the imaging features that mark a lesion as originating in the posterior cervical space and the spectrum of diseases that arise there. Of the 63 patients in the study, four had clinical pseudomasses, nine had congenital lesions, 10 had inflammatory disease, six had benign tumors, and 34 had malignant tumors. A typical mass lesion of the posterior cervical space was centered within the fat of the space, between the deep and superficial layers of the deep cervical fascia. Characteristic displacements caused by a mass in the posterior cervical space included anteromedial displacement of the carotid space and posteromedial displacement of the prevertebral space.

Our study shows that the differential diagnosis of lesions of the posterior cervical space reflects the normal contents of the space, and that diagnosis can thereby be predicted from knowledge of the normal anatomy and contents of the space.

***AJR* 157:161–165, July 1991**

The posterior cervical space (PCS) constitutes a major portion of the posterior triangle of the neck, a term that has long been used by anatomists and clinicians when referring to the posterior and lateral aspects of the neck [1]. The posterior triangle continues to be a useful term for describing the location of a mass in the posterolateral aspect of the neck between the posterior margin of the sternomastoid muscle and the anterior margin of the trapezius muscle during palpation. However, as it is primarily a two-dimensional, longitudinal concept, it is difficult to apply accurately during interpretation of cross-sectional images (CT or MR), particularly in the axial plane.

The term *posterior cervical space* was originally introduced when neck infections in the posterior triangle of the neck were described (Fig. 1) [2]. Recent authors have applied this term to the space seen on CT and MR posteromedial to the sternomastoid muscle from the skull base to the clavicles [3, 4].

We performed a retrospective review of patients with lesions in the PCS in order to identify the specific features on CT or MR images that indicate that a lesion has originated in the PCS. The study was also undertaken to identify the spectrum of diseases occurring in the PCS.

Materials and Methods

Clinical and radiologic records of 63 patients with known or suspected abnormalities in the PCS who underwent imaging between 1981 and 1990 were analyzed. These records were

Received November 21, 1990; accepted after revision January 15, 1991.

Presented at the annual meeting of the American Society of Head & Neck Radiology, New Orleans, LA, May 1990.

[1] Both authors: Department of Radiology, University of Utah School of Medicine, 50 N. Medical Dr., Salt Lake City, UT 84132. Address reprint requests to H. R. Harnsberger.

0361-803X/91/1571-0161
© American Roentgen Ray Society

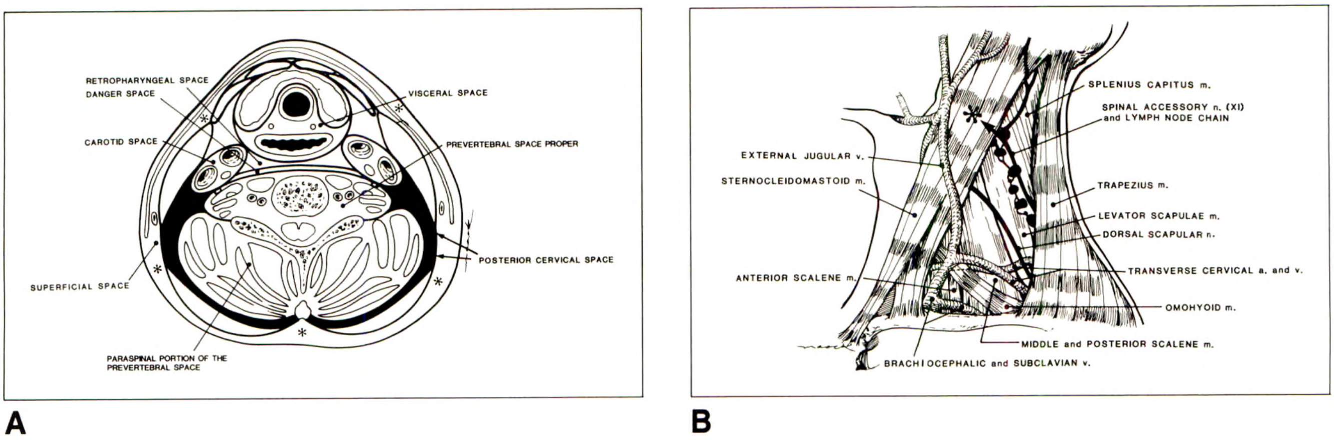

Fig. 1.—*A*, Axial drawing through infrahyoid neck at level of thyroid gland shows posterior cervical space (*black area*) and bordering spaces. Superficial space (*asterisks*).

***B*, Lateral drawing of posterior cervical space shows normal contents of space and structures of its floor. Spinal accessory lymph node chain angles anteromedially toward apex of deep cervical nodal chain (*arrow*), ending at jugulodigastric node (*asterisk*) beneath sternomastoid muscle. V = vein, m = muscle, n = nerve, a = artery.**

reviewed to determine the age and sex of the patients and the diagnoses, which were established pathologically in all cases except when CT findings (e.g., typical density in a lipoma) were diagnostic. Of the 63 study patients, 40 were male and 23 were female, ranging from 6 months to 77 years. All imaging studies were reviewed by two radiologists to identify characteristic imaging features of a mass in the PCS.

Of the 63 patients, 60 underwent CT scanning; in 54 of the 60, bolus-drip IV contrast enhancement was used. CT scanning was performed on a Siemens Somatom 2 (Siemens, Iselin, NJ) or a GE 9800 (General Electric Medical Systems, Milwaukee, WI) scanner. Contiguous 4- or 5-mm axial images were obtained in all cases.

MR imaging was performed with a GE Signa scanner in eight patients. Axial short and long TR images were obtained in all patients. Five of these patients also underwent CT scanning. Three patients had MR imaging enhanced with gadopentetate dimeglumine; all three had unenhanced short TR MR sequences also.

Results

Review of the mass lesions in the study group revealed a typical appearance of a mass lesion of the PCS (Fig. 2). Features that were thought to identify a mass as primary to the PCS included a lesion centered within the fat of the PCS or, if larger than the PCS, displacing the carotid space anteromedially and the prevertebral space posteromedially. When the mass was smaller and within the infrahyoid portion of the PCS, a fat plane was usually present between the mass and the carotid space.

Four patients had pseudomasses, defined as a mass lesion suspected clinically with no tumor revealed on radiologic examination (Fig. 3). Nine patients had congenital lesions, of which four were in the cystic hygroma/lymphangioma spectrum (Fig. 4A) and four were PCS branchial cleft cysts (Fig. 4B). One patient had a PCS hemangioma.

Ten patients had inflammatory disease related to the spinal accessory lymph node chain. Three of these patients had simple reactive lymphadenopathy (Fig. 5A), and an additional three patients had suppurative adenopathy. In four patients the inflammatory process had extended through the capsule of the involved lymph node to form a true PCS abscess (Fig. 5B).

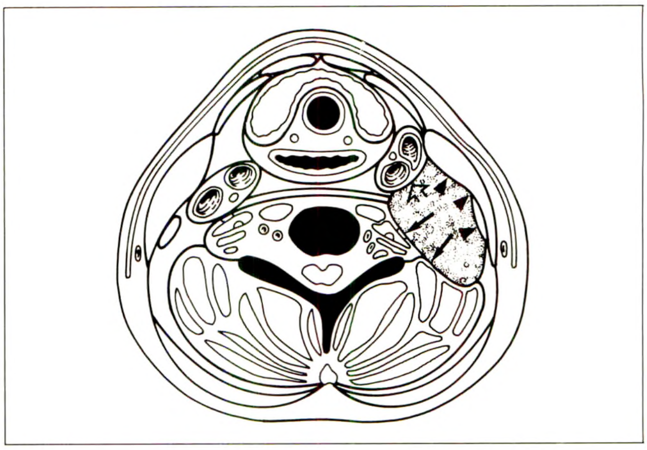

Fig. 2.—Axial drawing shows typical appearance of mass in posterior cervical space. Carotid space is displaced anteromedially (*open arrow*), sternomastoid muscle is displaced anterolaterally (*arrowheads*), and musculature of prevertebral space is displaced posteromedially (*solid arrows*).

Six patients had benign neoplasms. The most common of these, lipoma (Fig. 6A), was present in three patients. Thirty-four patients had malignant neoplasia. Primary malignant neoplasms of the PCS were rare. Single examples of a liposarcoma (Fig. 6B) and a synovial sarcoma were seen. Thirty-two patients had malignant lymphadenopathy; metastatic squamous cell carcinoma was seen in 16 of these (Fig. 7). Nine patients had non-Hodgkin lymphoma (Fig. 8A). Three patients had metastatic papillary carcinoma of the thyroid (Fig. 9) and two patients had Hodgkin lymphoma (Fig. 8B).

Discussion

The PCS is a three-dimensional space largely corresponding to the posterior triangle of the neck. As spatial terminology permits more accurate description of the position of a mass

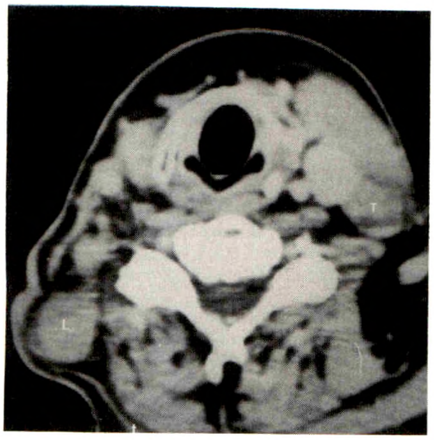

Fig. 3.—Pseudomass in posterior cervical space (PCS). Axial enhanced CT scan shows a hypertrophied right levator scapulae muscle (L) with atrophy of right trapezius muscle (t) and absence of right sternomastoid muscle owing to previous radical neck dissection for undifferentiated parotid carcinoma. Hypertrophied muscle produced a clinical PCS pseudomass, which led to clinical concern for recurrent PCS tumor. Clinically unsuspected nodal recurrent tumor is seen also in contralateral carotid space (T).

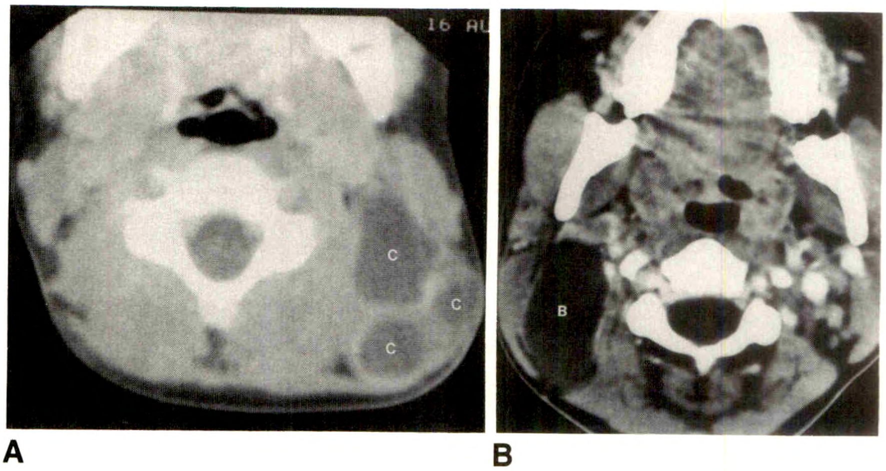

Fig. 4.—Congenital lesions in posterior cervical space (PCS).

A, Cystic hygroma. Axial enhanced CT scan in a 6-month-old boy shows a multilobulated PCS mass with fluid-density contents and smooth enhancing margins typical of a cystic hygroma. In this case, density of fluid in cysts (c) is increased owing to superimposed infection.

B, Branchial cleft cyst. Axial enhanced CT scan shows a right-sided unilocular fluid-density mass (B) in PCS. Most second branchial cleft cysts are found anteromedial to carotid space. Location of this cyst suggests a third branchial cleft cyst.

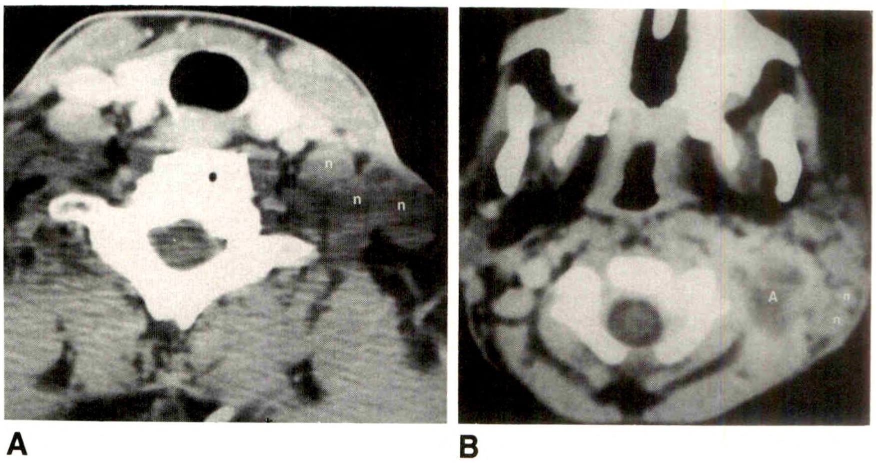

Fig. 5.—Inflammatory lymphadenopathy and complications.

A, Axial enhanced CT scan shows reactive lymphadenopathy (n) in posterior cervical space (PCS). Concern over possibility of low-grade lymphoma led to surgical biopsy. No infectious cause was identified.

B, Abscess in PCS. Axial enhanced CT scan in a 6-month-old boy with fever and a mass on left side of neck. Poorly defined fluid collection (A) in PCS with surrounding enhancement is due to spread of inflammatory process beyond capsule of node. Multiple small reactive nodes (n) are also present in PCS adjacent to abscess.

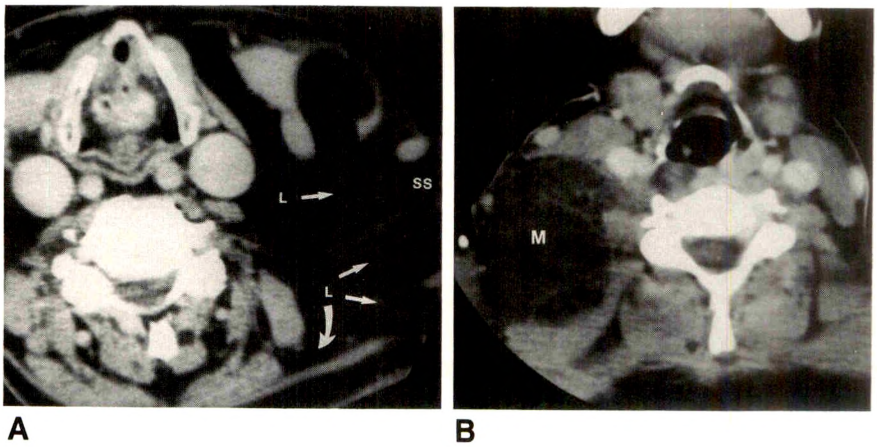

Fig. 6.—Neoplasms in primary posterior cervical space (PCS).

A, Axial enhanced CT scan shows a lipoma (L) with its center in PCS. Lipoma extends laterally into superficial space (SS).

B, Axial enhanced CT scan shows a liposarcoma (M) in PCS.

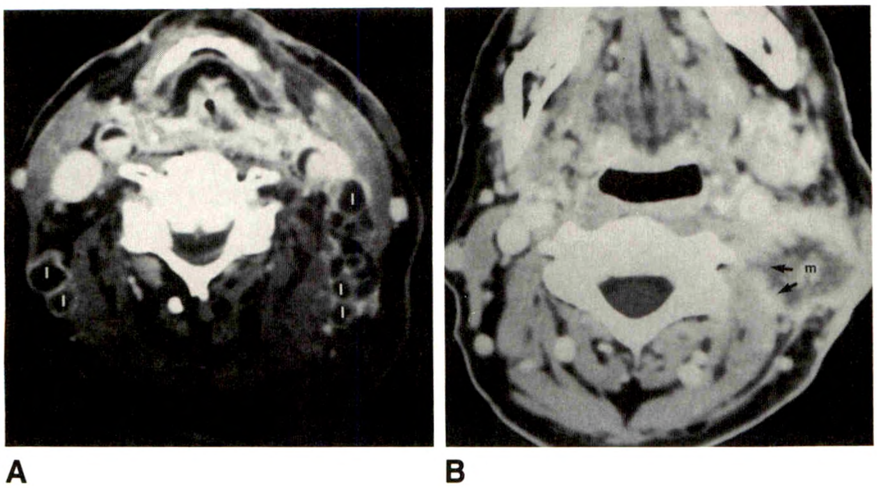

Fig. 7.—Malignant squamous cell carcinoma lymphadenopathy.

A, Intranodal metastases. Axial enhanced CT scan shows multiple ring-enhancing lymph nodes (l) in posterior cervical space (PCS) with necrotic centers due to metastatic deposits from laryngeal squamous cell carcinoma.

B, Extranodal metastatic spread. Axial enhanced CT scan shows a large necrotic extranodal metastatic deposit in PCS (m) and early extension through prevertebral fascia into paraspinal portion of prevertebral space (*arrows*). Recognition of this spread beyond PCS mandates more extensive resection than was clinically planned and underscores importance of fascial boundaries and spatial localization in assessment of extent of disease.

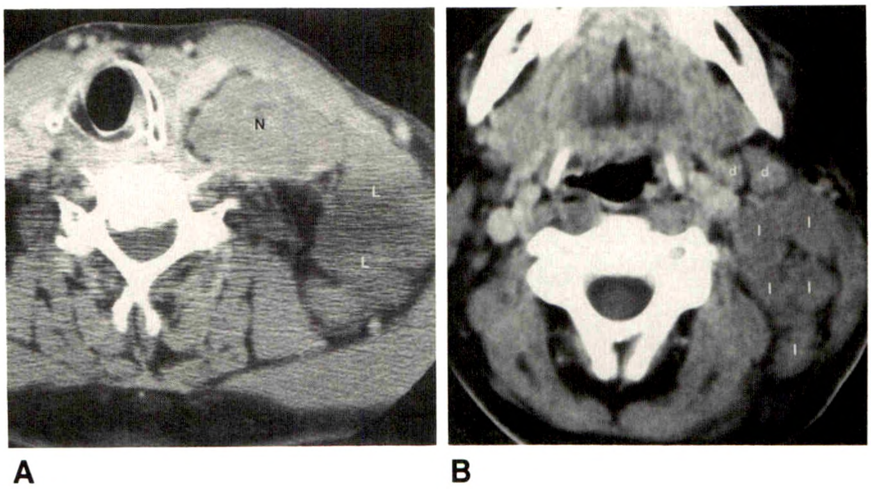

Fig. 8.—Lymphoma.

A, Non-Hodgkin lymphoma. Axial CT scan shows large deposits of extranodal non-Hodgkin lymphoma (L) in left posterior cervical space. No central necrosis is evident; involvement of internal jugular nodal chain within carotid space is present (N).

B, Hodgkin lymphoma. Axial enhanced CT scan shows early spinal accessory nodal Hodgkin lymphoma (l). More anterior internal jugular nodal disease (d) is present also.

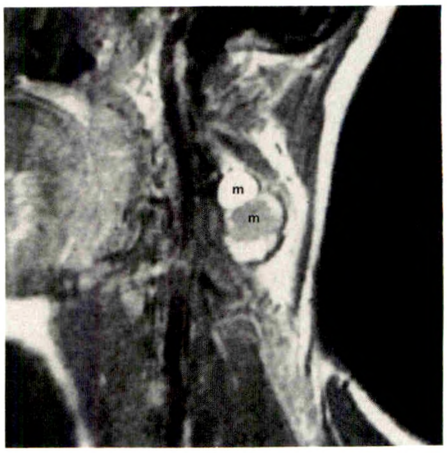

9

Fig. 9.—Hemorrhagic metastatic nodal papillary carcinoma of thyroid. Oblique sagittal T1-weighted MR image, 857/30 (TR/TE), shows a mixed-intensity mass (m) of the posterior cervical space with areas of isointensity and hyperintensity consistent with methemoglobin. When hemorrhage is associated with a nodal deposit in infrahyoid neck, thyroid origins should be suspected.

on cross-sectional imaging studies than does two-dimensional triangle terminology, the term PCS is a more useful concept to the imager than the term posterior triangle. Because a PCS lesion has a limited differential diagnosis, localization of a mass to this space allows construction of a more focused or limited differential diagnosis than would be possible with triangle localization. Spatial localization of a lesion also permits more accurate surgical treatment of inflammatory disease [2] and malignant tumors (Fig. 7B).

The PCS is found in the posterolateral aspect of the neck (Fig. 1A), extending from the skull base to the clavicle (Fig. 1B). The space is bounded on its deep margin by the deep layer of deep cervical fascia, which separates the PCS from the anterior prevertebral space proper and the more posterior paraspinal prevertebral space (Fig. 1A). Superficially, the PCS is bounded by the superficial layer of deep cervical fascia, which splits to enclose the sternomastoid and trapezius muscles [4]. Anteromedially, the PCS is separated from the carotid space by the carotid sheath. Seen from the side, the PCS has the appearance of a posteriorly tilted triangle (Fig. 1B).

The main contents of the PCS are the spinal accessory lymph node chain, the spinal accessory nerve, and fat [5, 6]. As the contents of the PCS are limited, the differential diagnosis of diseases affecting the PCS is also limited. The principal abnormality occurring in this space arises from involvement of the spinal accessory lymph node chain. Notable exceptions to this pattern of PCS nodal involvement include lesions arising from the fat of the PCS (lipoma and liposarcoma) and congenital lesions (cystic hygroma and branchial cleft cysts) [7].

The most common disease of the PCS is metastatic squamous cell carcinoma. Spinal accessory chain lymphadenopathy within the PCS is a classic manifestation of an occult nasopharyngeal mucosal space malignancy [8, 9]. Nevertheless, in our series lymphadenopathy in the PCS occurred more often as a result of lesions elsewhere in the pharyngeal mucosal space and the larynx, owing to their greater overall frequency.

Lymphoma, both Hodgkin and non-Hodgkin types, was represented frequently in our series. The disease typically occurred intranodally within the PCS, although extranodal, extralymphatic deposits were seen also [10]. Lymphomatous deposits typically showed no evidence of necrosis unless previously treated or of high grade.

Metastatic lymphadenopathy tended to be seen in other lymph node chains in the adjacent neck in the majority of cases, especially in patients with both non-Hodgkin and Hodgkin lymphoma and metastatic squamous cell carcinoma. In one patient with metastatic adenocarcinoma of the lung, PCS lymphadenopathy was confined to the immediate supraclavicular region. In such patients with predominantly low PCS lymphadenopathy, the primary tumor should be sought in the thyroid, thorax, or abdomen [4, 9].

Inflammatory lymphadenopathy also is common in the PCS. Inflammatory processes begin with enlargement of a lymph node and may progress if virulent or untreated to suppuration within the lymph node. If the process continues to go untreated, spread through the capsule of the lymph node is seen, forming an abscess in the PCS. Suppurative lymphadenopathy tends to occur with unusual pathogens. Those identified in our study were tularemia, atypical mycobacteria, and cat scratch fever.

Congenital lesions are seen not infrequently in the PCS. Most commonly these are multiseptated lesions in the cystic hygroma/lymphangioma spectrum [11, 12]. The branchial cleft cysts seen in this study were atypical in that they were centered in the PCS, not the submandibular space where the second branchial cleft cysts are found [7]. Although difficult to prove, it is tempting to speculate that these PCS branchial cleft cysts are actually third branchial cleft cysts.

Benign tumors of the PCS are rare. Lipoma is seen most often. Neurofibromas and hemangiomas also can be found in this space. These lesions also are derived from the tissues normally found in the PCS.

Three kinds of pseudomasses were identified in the PCS. The term pseudomass is used when there is a clinically palpable lesion of the posterior triangle and CT or MR identifies it as a nonsurgical abnormality outside of the PCS. Cervical ribs and prominent cervical transverse processes are the common bony pseudomasses. Another clinical pseudomass is found in levator scapulae hypertrophy commonly seen after radical neck dissection with sacrifice of the spinal accessory nerve. The hypertrophied levator scapulae muscle can cause concern for tumor recurrence in the posterior triangle of the neck [4].

REFERENCES

1. Last RJ. *Anatomy: regional and applied*, 6th ed. New York: Churchill-Livingstone, **1978**:363–366
2. Nyberg DA, Jeffrey RB, Brant-Zawadzki M, Federle M, Dillon W. Computed tomography of cervical infections. *J Comput Assist Tomogr* **1985**;9:288–296
3. Davis WL, Harnsberger HR, Smoker WRK, Watanabe AS. Retropharyngeal space: evaluation of normal anatomy and diseases with CT and MR imaging. *Radiology* **1990**;174:59–64
4. Harnsberger HR. *Handbooks in radiology: head and neck imaging*. Chicago: Year Book Medical, **1990**:138–187
5. Basmajian JV, ed. *Grant's method of anatomy*, 10th ed. Baltimore: Williams & Wilkins, **1980**:426–432
6. Rouviere M. Lymphatic system of the head and neck. In: Tobias MJ, trans. *Anatomy of the human lymphatic system*. Ann Arbor, MI: Edwards Brothers, **1938**;24–25
7. Harnsberger HR, Mancuso AA, Muraki AS, et al. Branchial cleft anomalies and their mimics: computed tomographic evaluation. *Radiology* **1984**;152:739–748
8. Becker W, Nauman HH, Platz CR. Neck (Including the thyroid). In: Buckingham RA, ed. *Ear, nose and throat diseases*. New York: Thieme, **1989**:472–523
9. Som PM. Lymph nodes of the neck. *Radiology* **1987**;165:593–600
10. Harnsberger HR, Bragg DG, Osborn AG, et al. Non-Hodgkin lymphoma of the head and neck: CT evaluation of nodal and extranodal sites. *AJR* **1987**;149:785–791
11. Silverman PM, Korobkin M, Moore AV. CT diagnosis of cystic hygroma of the neck. *J Comput Assist Tomogr* **1983**;7:519–520
12. Karmody CS, Fortson JK, Calcaterra VE. Lymphangiomas of the head and neck in adults. *Otolaryngol Head Neck Surg* **1982**;90:283–288

Book Review

Atlas of Interventional Radiology. By Constantin Cope, Dana R. Burke, and Steven G. Meranze. Philadelphia: Lippincott, 325 pp., 1990. $89.50

To most of us who enjoy tinkering with catheters and conjuring ways to simplify procedures, Constantin Cope is the master. He manages to see complex problems as a series of simple steps and finds ways to modify his instruments to accomplish those steps. He devised many of the procedures in common use today and continues to apply interventional techniques to new organs and new diseases. Heretofore, his innovations have reached the medical community piecemeal in journals, at meetings, or in catheter company brochures. At last comes a book that shows the reader not just a series of clever wrinkles and intricate maneuvers but an overview of Dr. Cope's way of doing interventional radiology.

It is a wonderfully satisfying book. Dr. Cope writes with a casual, commonsense directness and makes clear the why at the same time that he explains the how. Sentences are short and concise; jargon is kept to a minimum; explanations are patient and complete. Burke and Meranze, the coauthors, have contributed five of the book's 13 chapters. Although their chapters contain more standard techniques and fewer innovations, they nonetheless provide solid, accurate, and clear descriptions of problems and of the means for solutions.

The book is organized into five sections, each with several chapters. The first section addresses general issues, informed consent, quality control, room design and equipment, and personnel. Although it is brief, useful insights are offered, including a floor plan of a properly equipped interventional suite. The second section, the book's best, describes techniques used in the vascular system. It discusses everything from choice of arterial puncture needles, through solutions to common and uncommon catheter manipulative problems, to methods for performing embolectomy and atherectomy and placing stents. Sections 3–5 shift gears from a presentation of techniques to discussions of clinical problems. Section 3 covers arterial bleeding, balloon angioplasty, atherectomy, and thrombolysis. Section 4 covers biopsy and aspiration procedures. Section 5 covers drainage procedures. These sections address rationale, preparation of the patient, indications, and contraindications and have detailed discussions of the procedures and of how the procedures can be tailored to fit the problems of specific organs. Brief surveys of the literature cite results and complications. Radiographs from illustrative patients are included.

The book consists of 350 pages and 1000 illustrations. About half of the illustrations are color sketches. The book obviously was designed to make the illustrations preeminent. Wherever compromises were necessary, they were made to favor visual clarity. The sketches are more detailed and therefore more useful than line drawings. Color is used thoughtfully to distinguish contiguous tissues from instruments. The effect is to make complex three-dimensional maneuvers quickly comprehensible. The illustrations are large and never are crowded on the page. They are always close to the descriptive text, usually on the same page, even when this requires that large sections of pages remain blank. Even the print is large and favors quick and easy reading.

Although the book claims not to be a reference text, it is. Every interventional procedure that uses imaging is described for every organ system except the heart and the CNS, from preoperative orders to follow-up. The reader will find useful insights on every page, many not previously published, all interesting, some brilliant. It should be near the top of the reading lists of residents and fellows and should be in the reference libraries of all interventionalists.

Morton G. Glickman
Yale University School of Medicine
New Haven, CT 06510

Stenoses of Vascular Anastomoses After Hepatic Transplantation: Treatment with Balloon Angioplasty

Nigel Raby[1]
J. Karani[1]
S. Thomas[1]
J. O'Grady[2]
Roger Williams[2]

Vascular complications after liver transplantation include occlusion or stenosis at the sites of anastomosis in the hepatic artery, portal vein, and vena cava. From our experience with more than 600 liver transplants, vascular stenoses have been identified in 10 patients and treated by balloon angioplasty in nine. Three patients with hepatic artery stenosis and deteriorating graft function were treated by balloon angioplasty with a coaxial technique. A specially designed catheter facilitated a successful femoral artery approach. Portal vein stenoses in three patients resulted in portal hypertension. These were treated by balloon dilatation via transhepatic catheterization of the portal vein. Stenoses of the suprahepatic caval anastomosis were dilated in three patients with severe lower limb edema. Technical success was achieved in all three cases of hepatic artery stenosis with improvement in graft function. Recurrent stenoses in two patients were successfully treated with repeated dilatations. Portal hypertension resolved in two of three patients after portal venoplasty. Dilatation of a caval stenosis resulted in the resolution of leg edema in all three cases. Repeated dilatation was required in one case. No reduction in the portal venous pressure gradient occurred after venoplasty in one case, and an ultimately fatal caval thrombosis developed in one patient with caval stenosis before venoplasty could be performed.

Our experience suggests that balloon angioplasty of arterial and venous stenoses complicating hepatic transplantation carries little risk and is a useful procedure for the treatment of these problems.

***AJR* 157:167–171, July 1991**

During orthotopic liver transplantation, four vascular anastomoses are fashioned. The donor hepatic artery and portal vein are anastomosed to the recipient vessels. The intrahepatic portion of the inferior vena cava requires two anastomoses of donor to recipient cava: one at the level of the diaphragm (the suprahepatic cava) and one below the liver above the level of the renal vessels (the infrahepatic cava). Stenosis or occlusion of any of these anastomoses may occur postoperatively. In this report, we describe nine cases in which anastomotic stenoses were treated by percutaneous angioplasty with improvement in graft function or relief of other significant complications. Another patient with caval stenosis who developed fatal caval thrombosis proximal to a suprahepatic stenosis is also described.

Materials and Methods

The 10 cases included in the study were culled from our experience with more than 600 liver transplants. Posttransplantation angiography was done to assess arterial patency in cases of graft failure and suspected chronic rejection in which liver biopsy had failed to identify a specific cause and in patients with biliary strictures or hepatic abscesses. Hepatic angiography, arterioportography, and inferior venacavography were all performed via a transfemoral approach, with images obtained on conventional film and with digital subtraction imaging. Arterial stenosis was defined as a solitary short narrowing of the hepatic artery at the site of anastomosis just distal to the origin of the gastroduodenal artery. Narrowing of

Received October 29, 1990; accepted after revision January 11, 1991.

[1] Department of Radiology, Kings College Hospital, Denmark Hill, London SE5 9RS, England.

[2] Liver Unit, Kings College Hospital, Denmark Hill, London SE5 9RS, England.

0361-803X/91/1571-0167
©American Roentgen Ray Society

more than 70% of the transverse diameter was considered to be significant. Hepatic artery angioplasty was done with a coaxial balloon and a Thomas catheter (Schneider, London, U.K.), specifically designed for this purpose. This is a 7-French catheter that is introduced into the femoral artery with a sheath. The sidewinder configuration is formed at the aortic bifurcation because the catheter is too short to allow formation in the aortic arch. Once formed, the catheter can be used selectively to catheterize the common hepatic artery, thus allowing delivery of the balloon catheter coaxially at the site of stenosis (Fig. 1). A satisfactory result after angioplasty was defined as reduction of the narrowing to no more than 30% of the arterial transverse diameter.

Portal vein studies were indicated when evidence of raised portal venous pressure, manifested as variceal bleeding or splenomegaly, was detected clinically and sonographically. Further investigation consisted of measurement of hepatic wedge pressure and splenic pulp pressure. Hepatic wedge pressures were obtained by using cobra or sidewinder catheters with balloon occlusion of the hepatic vein. Splenic pulp pressures were measured after direct splenic puncture with a 23-gauge needle. A difference of 5 mm Hg between these two measurements was taken as evidence of a significant pressure gradient across the stenosis that warranted venoplasty. A pressure gradient across the stenosis was confirmed during transhepatic balloon venoplasty. Portal venoplasty has been described in detail elsewhere [1]. The portal vein was punctured via an intercostal transhepatic route and catheterized with a fine-needle introducer. A 5-French sheath was inserted over a guidewire into the donor portal vein. A 5-mm precurved balloon catheter was passed coaxially across the stenosis and inflated. In one case, two balloons were used (Fig. 2) to obtain the necessary effective diameter in a large portal vein. The pressure gradient across the stenosis was measured before and after inflation. A gradient across the stenosis of more than 5 mm Hg was considered abnormal, and reduction of the gradient to below this level after venoplasty was considered to indicate technical success.

Patients were examined by venacavography because of bilateral lower limb edema. Pressure studies across the anastomoses in the inferior vena cava were obtained with a single end-hole catheter. Caval venoplasty was achieved via a right femoral vein approach. The stenosis was traversed with a guidewire, and a conventional balloon angioplasty catheter was inflated across the stenosis. The pressure gradient was measured before and after the procedure. A gradient of 10 mm Hg was considered to be abnormal, and reduction of the gradient to less than this was considered to indicate success. All procedures were done with the patients taking prophylactic antibiotics.

Results

Anastomotic stenoses of the hepatic artery were successfully dilated in three adult patients. These stenoses occurred

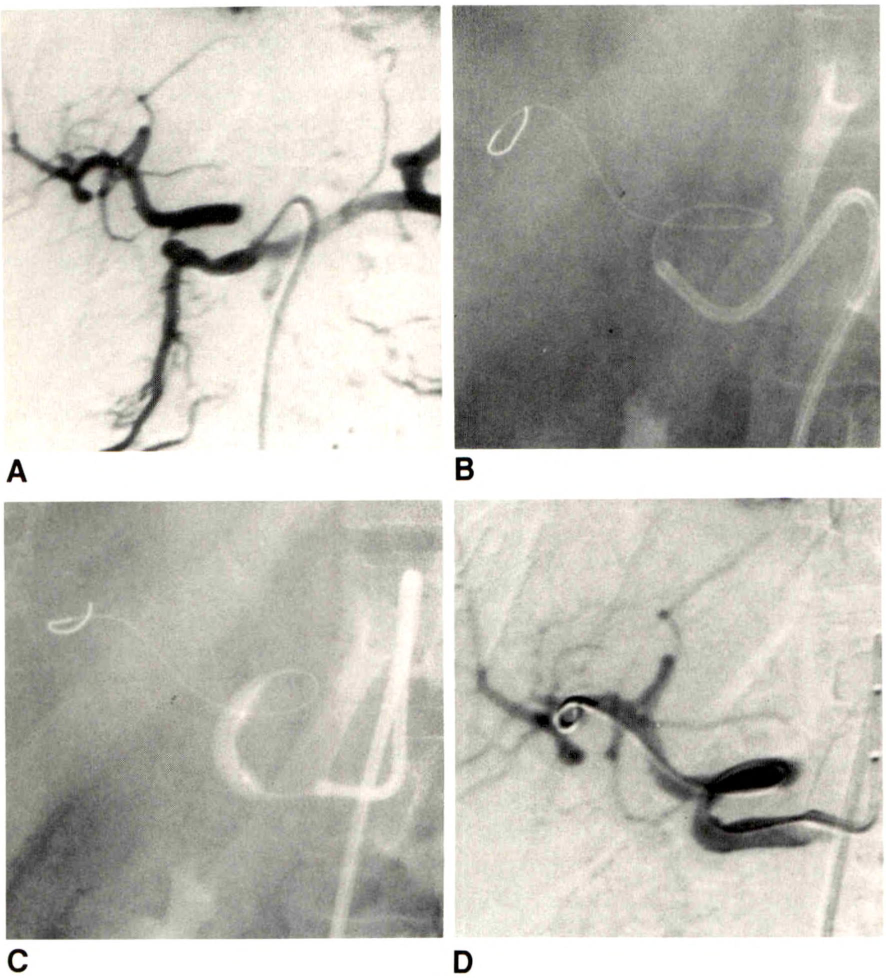

Fig. 1.—Hepatic angiograms of 36-year-old man with deteriorating liver function.

***A*, Anastomosis has 90% stenosis just distal to origin of gastroduodenal artery.**

***B*, Thomas guide catheter in common hepatic artery. A fine guidewire has been passed across stenosis.**

***C*, Balloon catheter passed coaxially through Thomas catheter and inflated across stenosis.**

***D*, After angioplasty, severity of anastomotic narrowing is markedly reduced to 30%.**

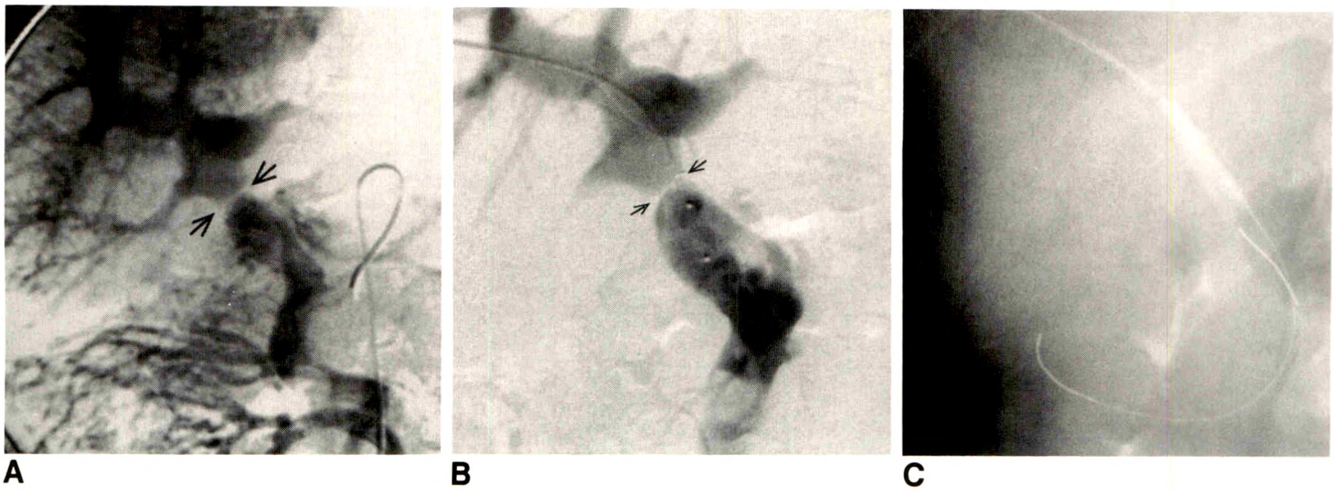

Fig. 2.—Angiograms of 6-year-old boy with anemia and splenomegaly.
***A*, Aortoportogram shows anastomotic narrowing of portal vein (*arrows*).**
***B*, Transhepatic portal vein puncture confirms anastomotic stenosis (*arrows*) and allows direct measurement of pressure gradient.**
***C*, Two balloons inflated across stenosis. Pressure gradient measured when catheter was withdrawn across stenosis confirmed reduction of gradient.**

at 10 days, 2 months, and 8 months after transplantation. All patients had abnormal liver function as evidenced by elevated levels of bilirubin and liver enzymes. These showed marked improvement after angioplasty. Repeated arteriography showed no evidence of stricture recurrence at 6 months in one patient who underwent a second transplantation shortly afterward because of vanishing bile duct syndrome. One patient reexamined on two occasions because of deterioration in liver function showed restenosis at 6 and 9 months after the initial procedure. On each occasion, the degree of stenosis, although still abnormal, was progressively less. Results of liver function tests became normal after each angioplasty. This patient remains well, with normal liver function 9 months after the last angioplasty. The third patient had an intrahepatic abscess and strictures of the common hepatic duct. These were managed by endoscopic placement of an 8-French biliary stent and percutaneous drainage of the abscess. Repeated arteriography at 4 and 8 months after angioplasty showed restenosis on each occasion, but these were also progressively less severe and were successfully redilated. Twelve months after initial presentation, the liver parenchyma and biliary tree are normal on sonographic examination, and the patient is well, with normal findings on liver function tests.

Portal vein stenosis was diagnosed in three patients (two children aged 2 and 4 and one adult) 2, 4, and 5 years after transplantation, respectively. Gradients across the stenoses of 24 and 12 mm Hg in the children were reduced to 2 mm Hg after venoplasty. Both have reduction in splenomegaly on sonographic examination, and no evidence of variceal bleeding has been seen in 1 year of follow-up. The adult patient had a stenotic gradient of 14 mm Hg, which did not alter after venoplasty. Spleen size has not altered, however, and the patient has not had any episodes of variceal bleeding.

Four cases of suprahepatic caval stenosis were encountered at 8 and 15 months in two cases and at 2.0 and 4.5 years in the other two cases. In one case, caval thrombosis occurred 1 week after demonstration of the stenosis, and pressure studies were not obtained. In this case, despite intracaval streptokinase (Hoechst, Hounslow, U.K.) and subsequent surgical thrombectomy, the patient died as a result of recurrent caval thrombosis. The presence of a significant pressure gradient was confirmed in the three remaining cases. In one of these, venacavography showed reversed flow down the inferior vena cava, mimicking a caval thrombosis (Fig. 3). Superior venacavography from the arm showed a suprahepatic caval stenosis with reversed flow in the inferior vena cava, with the hepatic and renal veins decompressing retrogradely into the inferior vena cava and hemiazygous collaterals. After dilatation of the stenosis, flow within the inferior vena cava was in a normal direction and the pressure gradient was reduced from 24 to 6 mm Hg. Leg edema resolved after the procedure but recurred 9 months later. Recurrent stenosis confirmed by venacavography was treated by another balloon dilatation with a similar good result, which has been maintained for a year. The other two patients remain free of symptoms 10 and 14 months after treatment.

Discussion

Vascular complications of liver transplantation that can be corrected by nonsurgical methods are rare. The 10 cases described in this paper represent our experience with more than 600 transplantations.

Hepatic artery occlusion in the immediate posttransplantation period requires urgent surgical intervention, usually retransplantation. In some patients, slowly progressive graft ischemia occurs, usually due to arterial thrombosis. In a few instances, however, ischemia is due to an anastomotic stenosis. The usual reason for examining these patients is the development of abnormal liver function; sonography is the primary method of examination. If biliary obstruction is ex-

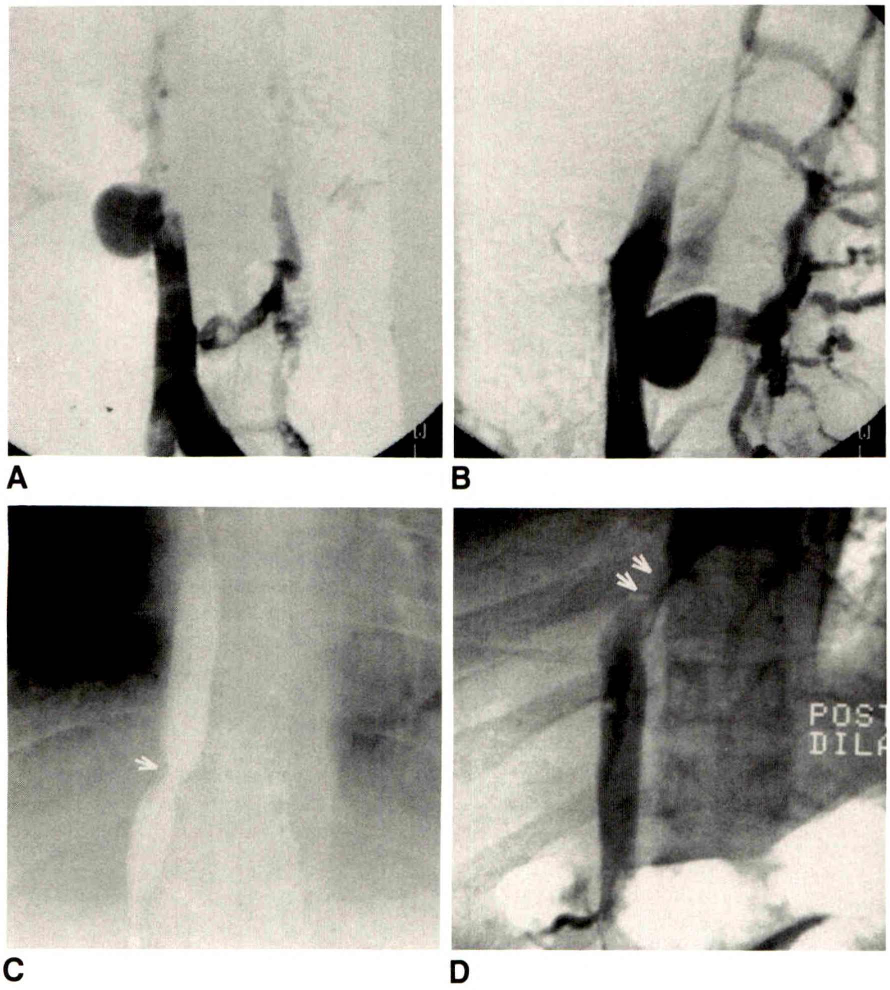

Fig. 3.—Angiograms of 25-year-old woman with edema in both legs.

A and *B*, Anteroposterior (*A*) and lateral (*B*) views of inferior venacavogram show nonfilling of intrahepatic cava, mimicking thrombosis. A superior caval injection showed a suprahepatic caval anastomotic stenosis with retrograde flow in inferior vena cava and hemiazygous collaterals.

C, Balloon dilatation of caval stenosis. Note "waisting" of balloon (*arrow*) at site of stenosis.

D, Postangioplasty appearance. Some residual stenosis persists (*arrows*), but pressure gradient is gone, and normal direction of flow reestablished.

cluded, a liver biopsy is performed and if the diagnosis is not clear cut, assessment of graft vascularization is indicated. Doppler sonography often can exclude occlusion of the hepatic artery and may suggest the presence of an arterial stenosis, but angiographic evidence is required for confirmation in such cases [2]. Additionally, the detection by sonography of focal areas of altered reflectivity within the hepatic parenchyma strongly suggests graft ischemia [2]. Attempts at treatment without ensuring that the graft is adequately vascularized are generally unsuccessful.

Ischemia also is regarded as a factor in the development of bile duct strictures [3], although the association is not as strong as with parenchymal abnormalities. One of our patients with arterial stenosis had both focal liver lesions and biliary stricturing in keeping with the above observations. Stenosis of the hepatic artery is uncommon, although occlusion is encountered more frequently [4].

Only four previous cases of percutaneous hepatic artery angioplasty have been described [4–6]. In two of these cases, a transfemoral approach failed and a brachial artery had to be used. This problem was overcome in our series by the use of a guide catheter specially developed for angioplasty of renal and hepatic transplants. The Thomas catheter allows selective catheterization of the common hepatic artery and the subsequent passage of an angioplasty balloon through the guide catheter and across the stenosis. Although long-term experience is limited, it appears that, as with arterial stenoses encountered in the transplanted kidney, restenosis after angioplasty is highly probable. However, as in renal transplantation patients, repeated angioplasty of the stenosis may be beneficial [7] and ultimately may result in satisfactory long-term patency, as has occurred in two patients described here.

To our knowledge, the use of percutaneous venoplasty of the portal vein after liver transplantation has not been described previously. According to Wozney et al. [4], significant portal vein stenosis is an uncommon complication after transplantation. Our experience agrees with that of Wozney et al., who noted that this complication usually occurs several years after transplantation and most often in children. Increasing spleen size and the development of varices with subsequent gastrointestinal hemorrhage and anemia are signs of this complication. Narrowing of the site of the portal vein anastomosis is seen commonly on real-time sonography [8], and Doppler studies often show turbulent flow at the anastomosis, but such abnormalities do not appear to be of functional significance. When patients are being considered for portal vein angioplasty, it is essential to confirm with pressure studies that the stenosis is hemodynamically significant by showing a pressure gradient across the stenosis. After a patent but narrowed portal vein is demonstrated, hepatic wedge pressure and direct splenic pulp pressure measurements enable patients with a significant gradient to be selected without traversing the graft parenchyma. Once a pressure gradient has been identified, it can be confirmed during transhepatic portal vein puncture.

Stenosis of the suprahepatic caval anastomosis also is rare. Graft function is not impaired unless hepatic venous outflow is severely compromised; thus, caval stenosis manifests as lower limb edema. The diagnosis can be suggested by sonography, but angiographic confirmation with evidence of a significant pressure gradient must be obtained. Percutaneous dilatation is relatively straightforward, and in the three cases in which this was achieved, the symptoms have resolved. Repeated dilatation at 9 months was successful in one patient, and all three patients have had long-term relief of symptoms. The finding of a significant stenosis should be dealt with urgently, because in one patient a delay of 1 week after the initial diagnosis of stenosis resulted in the development of caval thrombosis proximal to the stenosis. The occurrence of acute caval thrombosis carries a very poor prognosis, with both thrombolytic therapy and surgery failing to prevent death in this case. The association of thrombus proximal to caval stenoses has been noted before [9]. In his series, Cardella et al. [9] noted several cases of caval thrombosis that extended into the hepatic veins. We have not encountered this complication. Figure 3 shows how abnormal flow in the inferior vena cava proximal to a stenosis may lead to nonopacification of blood in the inferior vena cava, thus leading to an erroneous diagnosis of thrombus formation. Venacavography from above and below the stenosis may be required to define the situation accurately. If a flow artifact is not recognized as such, thrombolytic therapy may be instituted needlessly. Other than the first case in this series, which has been previously reported [10], we are aware of only one other balloon dilatation of the suprahepatic caval anastomosis [11]. Rose et al. [12] reported the dilatation of an infrahepatic caval stenosis, but we have not seen any examples of this complication.

With the improving survival rate of patients after liver transplantation, the number of patients with late complications of vascular anastomoses is likely to increase. The addition of successful nonsurgical measures to deal with these complications is therefore welcome. Long-term follow-up is, however, required to define fully the role of these techniques. Short-term technical success is achievable in most cases. The techniques described are safe, and the only significant complication has been sepsis after portal vein angioplasty. No serious sequelae occurred.

REFERENCES

1. Olliff S, Pain J, Karani J, Mowat AP, Williams R. Percutaneous transhepatic dilatation of late portal vein stenosis following orthotopic liver transplantation. *Intervent Radiol* (in press)
2. Segel M, Zajko A, Delbert A, Bron K, Skolnick M, Starzl T. Hepatic artery thrombosis after liver transplantation. *AJR* **1986**;146:137–141
3. Zajko A, Campbell W, Logsdon G, et al. Cholangiographic findings in hepatic artery occlusion after liver transplantation. *AJR* **1987**;149:485–489
4. Wozney P, Zajko AB, Bron KM, Point S, Starzl TE. Vascular complications after liver transplantation. *Radiology* **1986**;147:657–663
5. Abad J, Hidalgo EG, Cantarero JM, et al. Hepatic artery anastomotic stenosis after transplantation: treatment with percutaneous transluminal angioplasty. *Radiology* **1989**;171:661–662
6. Zajko AB, Bron KM, Starzl TE, et al. Angiography of liver transplantation patients. *Radiology* **1985**;157:305–311
7. Raynaud A, Bedrossian J, Remy P. Brisset J-M, Angel C-Y, Gaux J-C. Percutaneous transluminal angioplasty of renal transplant arterial stenoses. *AJR* **1986**;146:853–857
8. Raby N, Meire H, Forbes A, Williams R. The role of ultrasound scanning in management after liver transplantation. *Clin Radiol* **1988**:39:507–510
9. Cardella JF, Castañeda-Zúñiga WF, Hunter D, Young A, Amplatz K. Angiographic and interventional radiologic considerations in liver transplantation. *AJR* **1986**;146:143–153
10. Reading NG, O'Grady JG, Williams R, Nunnerly H. Balloon dilatation of an anastomotic stenosis of the inferior vena cava. *Intervent Radiol* **1987**;2:81–82
11. Cardella JF. Evaluation and treatment of vascular problems after liver transplantation. *Semin Intervent Radiol* **1986**;3:131–138
12. Rose BS, Van Aman EM, Simon DC, et al. Transluminal balloon angioplasty of infrahepatic caval anastomotic stenosis following liver transplantation (case report). *Cardiovasc Intervent Radiol* **1988**;11:79–81

Book Review

Atlas of Normal and Variant Angiographic Anatomy. By Saadoon Kadir. Philadelphia: Saunders, 544 pp., 1991. $95

This book is divided into five sections and 18 chapters. Sections 1 and 2 on the arterial and venous systems, respectively, of the trunk and extremities have five chapters each. Section 3 on arterial and venous anatomy of the reproductive organs has two chapters. Section 4 on arterial and venous systems of the viscera has four chapters. Section 5 on arterial and venous anatomy of the head and Section 6 on the lymphatic system have one chapter each.

Chapters 1 and 2 are short. The illustrations in chapter 2 are of fair quality. However, diagrams are included to help in the interpretation of the angiograms. Only one arteriogram depicts the arterial supply to the esophagus (usually not shown by arteriography). More diagrams might be helpful.

Chapter 3 lists variants of the arterial supply to the upper extremities but does not provide references for percentages. The term *upper arm* is incorrect; it should be *arm.* Chapter 4 has too few abdominal aortograms. Instead of hemorrhoidal arteries, it should say rectal arteries. The chapter also has too little text on the abdominal aorta and the lower extremities (as compared with the upper extremities). In chapter 5, Figure 5-16 incorrectly shows "a low origin of the posterior tibial artery." I think that the posterior tibial artery is occluded proximally and reconstituted from collateral vessels. Figures 5-18 and 5-19 show "hypoplasia of the anterior and posterior tibial arteries." This is questionable. Spasm is possible.

Chapters 6–9 are short and sparingly illustrated. In chapter 10, the angiograms of the pulmonary veins are of fair to poor quality. Chapters 11 and 12 are adequate. The quality of the penile angiograms is excellent.

Chapter 13 is long (67 pages), reflecting the special interest of the author. It provides tables of percentages of normal variants but does not give references. Figure 13-1 (a copy from other articles) does not include acknowledgments. Figure 13-38 does not seem to represent the arch of Buhler as suggested. There is controversy concerning the arch of Riolan. Figure 13-41 shows an anastomosis between the left colic artery (branch of the inferior mesenteric artery) and the middle colic artery (branch of the superior mesenteric artery), not the arch of Riolan as suggested. A more detailed description would be interesting.

Chapter 14 provides few illustrations of hepatic veins. Chapter 15 gives a good diagram of the renal arterial and venous circulation. Chapter 16 is complete (25 pages). Unfortunately, it is of limited practical interest since the advent of CT. Chapter 17 briefly covers neurovascular anatomy. Only half of a page deals with venous anatomy. This probably is enough, as neurovascular anatomy usually is covered in neuroradiology textbooks. Chapter 18 has diagrams of lymphatic vessels and nodes of the upper extremities, chest, head, and neck but no lymphangiograms, reflecting the inexperience of the authors.

The book has a mixture of conventional arteriograms, photographic subtraction arteriograms, and digital subtraction arteriograms. Many of the illustrations are reprinted from Dr. Kadir's well-known textbook: *Diagnostic Angiography.* The text has been kept at a minimum according to the goals of the contributors: to write an atlas of angiographic anatomy. The quality of the illustrations is fair to good. The angiograms are of different sizes throughout the atlas. Some are large enough to show details. Others, however, are too small for this purpose. The book has several clear diagrams that clarify the anatomy. Most of the material in this text can be found in several published textbooks of angiography.

This basic atlas will be of benefit to radiology residents, general radiologists who do vascular and interventional radiology part-time, fellows in cardiovascular and interventional radiology, and average vascular radiologists. It will not be of major impact for the expert vascular radiologist. Other possible users of this book are vascular and general surgeons and clinicians who deal with vascular diseases. The price is reasonable for an atlas of this type with numerous illustrations. I would have preferred an atlas with a larger format, illustrations of the same size, and groups of illustrations immediately following the respective text in each chapter, rather than having the entire text at the beginning of the chapter followed by all the corresponding illustrations.

Jaime Tisnado
Medical College of Virginia
Richmond, VA 23298-0615

Randomized Double-Blind Trial of Midazolam/Placebo and Midazolam/Fentanyl for Sedation and Analgesia in Lower-Extremity Angiography

Andrew H. Cragg[1]
Tony P. Smith
Kevin S. Berbaum
Nobuo Nakagawa

Safety and efficacy of two drug regimens used for sedation and analgesia during lower-extremity angiography were studied. Midazolam (loading dose 14.5 μg/kg; maintenance dose, 7.2 μg/kg) with or without fentanyl (loading dose, 0.725 μg/kg; maintenance dose, 0.362 μg/kg) was administered in a blind fashion as an IV bolus to 50 patients. Hemodynamic responses were monitored, and a standardized questionnaire was given to the patient before, immediately after, and 8–24 hr after the procedure. Physicians also were asked questions after the procedure. Heart rate and oxygen saturation were not significantly different before and 2 min after administration or between groups. A small but significant decrease in blood pressure occurred 2 min after the loading dose was given in both groups. Both drug regimens had statistically significant anxiolytic effects; however, anxiolytic effects were superior in the midazolam/fentanyl group ($p < .02$). Patients rated the overall effectiveness of anesthesia with midazolam/fentanyl as superior ($p < .02$). Analysis of physicians' judgments of the effectiveness of sedation and analgesia showed a statistically significant advantage for the midazolam/fentanyl group ($p < .01$).

We conclude that midazolam/fentanyl appears to be as safe as and more efficacious than midazolam alone for sedation and analgesia during lower-extremity angiography.

AJR **157:173–176, July 1991**

As the complexity and length of angiographic procedures have increased, the need for more effective sedation and analgesia has arisen. In many institutions, premedication of patients has been replaced by IV sedation and analgesia during interventional procedures. The use of more potent sedation and analgesia in the angiography suite has been made possible, in part, by improvements in monitoring of patients and newer agents.

The use of the narcotic analgesic fentanyl in combination with the sedative diazepam has been described for patients having interventional procedures [1]. Fentanyl is used widely as an agent for induction of anesthesia [2], but its use by radiologists is more recent. Currently, many practitioners prefer midazolam to diazepam for conscious sedation, partly because of its more rapid onset of action and improved amnestic effects [3–5].

No randomized trial to determine the safety and efficacy of midazolam and fentanyl in a radiologic setting has been reported. We report the results of a randomized, double-blind trial of midazolam alone and midazolam/fentanyl for conscious sedation and analgesia during lower-extremity angiography.

Patients and Methods

All patients undergoing diagnostic lower-extremity angiography at The University of Iowa Hospitals and Clinics between October 1988 and March 1989 were offered entry into the study. The study was approved by our institutional review board, and admission of patients was based on informed consent.

Received November 19, 1990; accepted after revision January 15, 1991.

[1] All authors: The University of Iowa College of Medicine, Department of Radiology, Iowa City, IA 52242. Address reprint requests to A. H. Cragg, The University of Iowa Hospitals and Clinics, Iowa City, IA 52242.

0361–803X/91/1571–0173
© American Roentgen Ray Society

Exclusion criteria included (1) age less than 18 years or more than 75 years; (2) known hypersensitivity to midazolam or fentanyl; (3) documented history of liver disease, which would alter drug clearance; (4) administration of other sedative or analgesic drugs less than 2 hr before the procedure; and (5) performance of an interventional procedure (e.g., angioplasty) at the same sitting. Patients less than 18 years old were excluded in part because our human use committee requires special consent for study of minors. Minors represent a small fraction of our lower-extremity angiography patients. Also, in elderly patients we are very cautious in our use of sedative agents, particularly benzodiazepines, because they are metabolized more slowly, they produce greater cardiorespiratory depression than in younger patients, and we have found that they can cause paradoxical agitation [6]. We therefore excluded patients older than 75 years from this study. Patients undergoing interventional procedures at the same sitting were excluded because these procedures are frequently lengthy, which would confound our data analysis. Thrombolysis procedures, for example, which are generally protracted and done at multiple sittings do not lend themselves well to this type of study.

The study had 23 men and 27 women (30–75 years old; mean, 60 years). Two patients were excluded from the analysis because of incomplete data. One additional patient in the midazolam/fentanyl group was too sleepy to answer questions immediately after the procedure.

Before the angiographic procedure, patients were asked to rate their level of anxiety. Patients were shown the questionnaire and asked to choose a word that matched their feelings. The choices were 1 = relaxed, 2 = tense, 3 = nervous, and 4 = terrified. This question was asked again immediately after the procedure, along with a series of questions relating to the patient's level of satisfaction with the sedation and analgesia he or she received. Additional questions were asked 8–24 hr after the procedure. The physician involved in the procedure asked the patient questions and also responded to questions about the patient's level of cooperation and the effectiveness of sedation and analgesia during the procedure. Eight physicians (staff and residents) completed at least one questionnaire.

Drug Regimens

Patients were randomized to receive one of two drug regimens. For randomization, a card containing the drug regimen was drawn from a shuffled deck. Regimen A consisted of 14.5 μg/kg (1.0 mg/70 kg) midazolam (Versed, Roche Laboratories, Nutley, NJ) and normal saline administered IV as a slow bolus infusion (30–60 sec) for induction. Additional maintenance doses could be given at 50% of the loading dose (i.e., 7.25 μg/kg of midazolam). The interval between doses was at least 2.5 min.

Regimen B consisted of 14.5 μg/kg of midazolam and 0.71 μg/kg (50 μg/70 kg) of fentanyl (Sublimaze, Janssen Pharmaceutical, Piscataway, NJ) administered IV as a slow infusion. Additional doses could be given at 50% of the induction dose. The bolus time and minimum interval between doses was the same as in Regimen A.

Drugs were prepared by a nurse not involved in the procedure. The drugs were administered by a second nurse at the request of the physician performing the case. Neither the administering nurse, the physician, nor the patient was aware of which drug regimen was used. Both drugs were prepared in precise concentrations so that an induction dose (dose of midazolam/placebo or midazolam/fentanyl) equaled 0.030 ml/kg and a maintenance dose equaled 0.015 ml/kg.

All patients received a loading dose before administration of local anesthesia. The sedative end point was determined by slurring of speech and the presence of ptosis (Verrill sign), at which point the procedure was begun.

Patients were monitored continuously during the procedure. The ECG, noninvasive measurement of blood pressure, and noninvasive measurement of arterial oxygen saturation were monitored continuously and recorded intermittently (immediately before and 2 min after each dose) during the procedure. Routine supplemental oxygen via nasal cannula was administered to all patients at a rate of 3 l/min.

Angiographic Protocol

Our protocol for lower-extremity angiography consists of three separate aortic injections of diluted contrast material (30 ml each) and digital filming over the infrarenal aorta and pelvis. A unilateral leg angiogram then is performed by using a translating table and film screen. A bolus of 60 ml of low-osmolality contrast material (Hexabrix, Mallinckrodt, St. Louis, MO) is injected in the external iliac artery during serial filming. We routinely obtain unilateral lower-extremity angiograms because we have shown that they are superior to the conventional aortic flush technique [7]. This protocol was followed for all patients in the study. The large bolus of contrast medium that we use produces studies of excellent quality, but considerable pain is associated with its injection even with the new low-osmolality agents.

Results

Procedural Data

The procedure time was equivalent between groups (43.2 min for midazolam alone vs 42.6 min for midazolam/fentanyl). The trend was toward fewer maintenance doses in the midazolam/fentanyl group (4.8 vs 3.5), which did not achieve statistical significance. The average dose per patient in the midazolam group was 4.6 ± 4.1 mg of midazolam; the average dose in the midazolam/fentanyl group was 2.9 ± 1.3 mg of midazolam and 132.5 ± 45.2 μg of fentanyl.

Hemodynamic Data

The hemodynamic data are shown in Table 1. Each of the parameters presented in the table was analyzed by using a two-way analysis of variance with a within-subject factor for predosing and postdosing and a between-subject factor for drug regimens. Heart rate and oxygen saturation were not significantly different before and 2 min after dosing or between groups. A small but significant decrease in blood pressure occurred 2 min after the loading dose in both groups (systolic, $p < .06$; diastolic $p < .04$). No hemodynamic changes related to the contrast injection occurred, even though the contrast dose (60 ml) in a single leg was equivalent to what many angiographers use for both legs.

Questionnaire Data

Ratings of anxiety levels before and immediately after the procedure (questions 1 and 2) were converted to numeric scores: relaxed = 1, tense = 2, nervous = 3, and terrified = 4. These data were analyzed by using a two-way analysis of variance with a within-subject factor for preprocedure and postprocedure and a between-subject factor for drug regimen. A statistically significant main effect for preprocedure

TABLE 1: Hemodynamic Data for Patients Given Midazolam Alone or with Fentanyl Before Lower-Extremity Angiography

Parameter	Midazolam/ Placebo ($n = 24$)	Midazolam/ Fentanyl ($n = 24$)
Heart rate (beats/min)		
Predosing	82 ± 16	88 ± 17
Postdosing	81 ± 14	87 ± 17
Systolic blood pressure (mm Hg)		
Predosing	162 ± 26	159 ± 32
Postdosing	136 ± 26	149 ± 33
Diastolic blood pressure		
Predosing	94 ± 14	92 ± 4
Postdosing	90 ± 13	89 ± 16
O_2 saturation (%)		
Predosing	96 ± 3	96 ± 5
Postdosing	96 ± 2	95 ± 6

Note.—Values are expressed as mean ± standard deviation. Postdosing = 2 min after loading dose.

and postprocedure was anxiolytic effects for both drug regimens ($p = .0001$). A statistically significant interaction of preprocedure and postprocedure by drug ($p = .0134$) suggested a greater anxiolytic effect with fentanyl (2.43 mean rating reduced to 1.26) than without (1.80 mean rating reduced to 1.50). This effect may however be attributable to a statistical fluke in which twice as many patients in the midazolam-only group described themselves as relaxed before the procedure. This difference is reflected by a lower initial anxiety score in the midazolam-only group (1.80 vs 2.43). More than half the patients in each group described themselves as tense, nervous, or terrified before the procedure. Immediately after the procedure, 84% described themselves as relaxed during the procedure.

Regarding the "overall rating of the anesthesia received" without and with fentanyl, ratings were scored as follows: excellent = 5, good = 4, fair = 3, somewhat unpleasant = 2, and extremely unpleasant = 1. These data were analyzed by using a two-group t test. Without fentanyl, the overall rating of anesthesia was significantly poorer ($t[46] = 2.48, p < .02$).

The remainder of the questionnaire's data was analyzed by using chi-square contingency tables. Regarding amnesia, approximately 50% of patients in both groups had no recollection of the administration of local anesthesia or of the injection of the contrast material for the lower-extremity angiogram. Similarly, most patients described the amount of pain during the procedure as minimal or moderate, characterized the procedure as pleasant or tolerable, and rated the overall quality of anesthesia as excellent or good. No other significant differences between groups occurred.

Postprocedure complaints of nausea, vomiting, headache, and dizziness were similar between groups. More patients in the midazolam/fentanyl group complained of prolonged drowsiness (seven vs one).

Physicians' responses to the questionnaire indicated a perception of significantly greater cooperation by patients in the midazolam/fentanyl group ($p < .01$). In addition, physician ratings for effectiveness of sedation ($p < .0005$) strongly favored the midazolam/fentanyl combination. Physicians also found patients in the midazolam/fentanyl group to be more somnolent during the procedure ($p < .008$).

Complications

One patient in the midazolam/fentanyl group had exacerbation of congestive heart failure during preparation for the angiogram. The left ventricular ejection fraction at the time of the angiogram was 20%. The patient had received a total of 1.4 mg of midazolam and 68 μg of fentanyl. She was treated in the interventional suite and transferred to the medical intensive care unit, where she made an uneventful recovery.

Discussion

In a retrospective review of 100 miscellaneous interventional radiology cases, Miller and Wall [1] recently reported that fentanyl, in combination with diazepam, is safe and efficacious for conscious sedation and analgesia. Our study confirms that fentanyl, in combination with the anxiolytic agent midazolam, provides both safe and effective sedation and analgesia for short procedures.

Our findings are supported by similar studies in the anesthesia and surgery literature that have examined the safety and efficacy of midazolam alone or in combination with fentanyl for both sedation and general anesthesia. Persson et al. [8] administered midazolam and fentanyl at doses 40–100 times greater than those used in our study to produce total IV anesthesia in patients undergoing abdominal hysterectomies. Although patients required assisted ventilation, they remained hemodynamically stable even at these high doses. In this study, fentanyl decreased the requirement for midazolam to produce the same level of sedation.

In another study, Ochs et al. [9] compared midazolam or diazepam alone or in combination with fentanyl in patients undergoing outpatient tooth extractions. At doses similar to those in our study, they noted slightly prolonged recovery time, as measured by standardized psychomotor tests, when midazolam was used alone. They did not report complications or degree of amnesia with each regimen.

Magni et al. [3] compared the effectiveness of midazolam and diazepam for sedation in upper gastrointestinal endoscopy. They found midazolam to produce superior amnesia. With both drugs, recovery was incomplete 2 hr after the procedure.

In many centers, IV sedation and analgesia during an interventional radiologic procedure has replaced premedication. Many think it provides a more predictable response. We believe that the judicious use of IV anxiolytic and narcotic agents by radiologists has enhanced the practice of interventional radiology for both the patient and physician.

The pharmacology and uses of midazolam were reviewed recently in an excellent article by Reves and colleagues [6]. Midazolam is similar to diazepam in many respects. It is approximately 1.5–2.0 times as potent as diazepam. The drug appears to exert its effect by increasing a glycine inhibitory neurotransmitter, possibly in the mammillary body. The mechanism by which midazolam produces amnesia is unknown. At doses commonly used for sedation (0.1 mg/kg), midazolam has little cardiovascular or respiratory effect; however, in larger doses (0.15 mg/kg), the drug reduces blood pressure and produces respiratory depression. Respiratory depression is not reversed by naloxone. Fluazenil (RO-15-1788), marketed by Roche Laboratories in Europe as Anexate, is a benzodiazepine antagonist. The drug has undergone clinical trials in the United States but is not expected to be approved by the Food and Drug Administration until at least 1992 (Roche Laboratories, personal communication). Midazolam is metabolized by microsomal oxidation in the liver and excreted in the urine. The half life in healthy patients is 1–4 hr although it may be significantly longer in elderly patients or those with liver failure. Because the drug is inactivated in the liver, renal insufficiency has little effect on its clearance and its duration of action. Compared with diazepam, midazolam appears to produce more rapid onset of sedation and better amnesia. Recovery times are similar.

The pharmacology of fentanyl pertinent to the interventional radiologist has been nicely summarized in a recent article by Miller and Wall [1]. Fentanyl is a potent synthetic opioid with a more rapid onset and shorter duration of action than both morphine and meperidine. The drug is metabolized in the liver and excreted in the urine. A typical IV dose is 50–100 μg. Fentanyl has little cardiovascular effect at sedative doses, but produces respiratory depression and in high doses can block spontaneous respiration. Decreased oxygen saturation is a somewhat delayed but useful indicator of fentanyl-induced respiratory depression. For this reason, we recommend that pulse oximetry always be used when administering IV sedation and analgesia. Naloxone, administered IV in 0.1- to 0.2-mg increments titrated to effect, is an effective antagonist to fentanyl overdose.

We found the hemodynamic responses to both of our drug regimens to be predictable and stable. These findings are similar to those of other studies, which have noted stable cardiovascular responses to both midazolam and fentanyl [2, 10]. We noted a small decrease in blood pressure with both drug regimens, which has been reported by others, particularly with the midazolam/fentanyl combination [11].

Both midazolam and fentanyl have been shown to produce respiratory depression via different mechanisms [2, 12]. In a study by Tucker et al. [13], patients receiving the midazolam/fentanyl combination had significant decreases in P_{O_2} and arterial oxygen saturation. In our study, oxygen saturation was not decreased in either group. A major difference between the studies is that our loading doses were significantly smaller. In addition, we routinely administered supplemental oxygen via a nasal cannula during the procedure.

Because fentanyl has a rapid onset and a short duration of action, it has been promoted as an effective agent for procedures of short duration. Ochs et al. [9] have suggested that fentanyl can lower the requirement for midazolam and therefore shorten recovery time. Our study suggests that less midazolam is required to achieve the same level of sedation when used in combination with fentanyl. We noted a trend toward fewer maintenance doses in the midazolam/fentanyl group; however, we found no evidence of shortened recovery time with midazolam/fentanyl. To the contrary, seven of eight patients who complained of prolonged drowsiness were in the midazolam/fentanyl group. This finding could make the use of the midazolam/fentanyl combination less appealing in outpatient situations in which rapid recovery is important. In our patients who experienced prolonged drowsiness, complete recovery required several hours.

Several important points should be made about patients' and physicians' acceptance of the two drug regimens tested. First, although patients reported greater reduction in anxiety with midazolam/fentanyl, no difference was seen in other effects such as amnesia and pain control between the two groups. Second, physicians thought midazolam/fentanyl was superior in terms of improved cooperation by patients and overall effectiveness of sedation and analgesia. We attribute this difference to several effects. Midazolam has excellent amnestic effects, and it appears that most patients who had pain did not recall it. Physicians, however, reported better cooperation with midazolam/fentanyl probably because these patients had better pain control during the procedure and thus were less agitated during potentially painful stimuli. Most interventional radiologists will agree that improved cooperation by patients and diminished agitation are extremely desirable effects of any sedative regimen. In this respect, midazolam/fentanyl is clearly superior to midazolam alone.

In conclusion, our study shows that the combination of midazolam and fentanyl appears to be as safe as and more efficacious than midazolam alone for sedation and analgesia during lower-extremity angiography. The use of these agents in combination facilitates the performance of high-quality diagnostic angiography. Our experience has demonstrated their usefulness in interventional procedures as well.

REFERENCES

1. Miller DL, Wall RT. Fentanyl and diazepam for analgesia and sedation during radiologic special procedures. *Radiology* **1987**;162:195–198
2. Grell FL, Koons RA, Denson JS. Fentanyl in anesthesia: a report of 500 cases. *Anesth Analg* **1970**;49:523–532
3. Magni VC, Frost RA, Leung JWC, Cotton PB. A randomized comparison of midazolam and diazepam for sedation in upper gastrointestinal endoscopy. *Br J Anaesth* **1983**;55:1095–1101
4. Ayre-Smith G. Fentanyl and midazolam: an alternative to diazepam (letter). *Radiology* **1987**;164:285
5. Redmond PL, Kumpe DA. Fentanyl and diazepam for analgesia and sedation during radiologic special procedures (letter). *Radiology* **1987**;164:284
6. Reves JG, Fragen RJ, Vinik HR, Greenblatt DJ. Midazolam: pharmacology and uses. *Anesthesiology* **1985**;62:310–324
7. Smith TP, Cragg AH, Berbaum KS, Ryals TJ, Sato Y. Techniques for lower-limb angiography: a comparative study. *Radiology* **1990**;174:951
8. Persson MP, Nilsson A, Hartvig P. Relation of sedation and amnesia to plasma concentrations of midazolam in surgical patients. *Clin Pharmacol Ther* **1988**;43:324-331
9. Ochs MW, Tucker MR, White RP Jr, Anderson JA. Recovery following sedation with midazolam or diazepam alone or in combination with fentanyl for outpatient surgery. *Anesth Prog* **1986**;33:230–234
10. Stanley TH, Webster LR. Anesthetic requirements and cardiovascular effects of fentanyl-oxygen and fentanyl-diazepam-oxygen anesthesia in man. *Anesth Analg* **1978**;57:411–416
11. Skarvan K, Schwinn W. Hamodynamische Interaktion zwischen Midazolam und Alfentanil bei Koronarkranken. *Anaesthesist* **1986**;35:17–23
12. Forster A, Gardaz JP, Suter PM, Gemperle M. Respiratory depression by midazolam and diazepam. *Anesthesiology* **1980**;53:494–497
13. Tucker MR, Ochs MW, White RP Jr. Arterial blood gas levels after midazolam or diazepam administered with or without fentanyl as an intravenous sedative for outpatient surgical procedures. *J Oral Maxillofac Surg* **1986**;44:688–692

Case Report

Spontaneous Fracture of a Vena-Tech Inferior Vena Caval Filter

Mark H. Awh,[1] Frank C. Taylor, and Chien-Tai Lu

Percutaneous placement of filters in the inferior vena cava (IVC) has become increasingly common for the prevention of pulmonary embolism. Among these devices is the Vena-Tech filter (Vena-Tech Corp., Evanston, IL). The filter is inserted percutaneously through a 12-French (outer diameter) sheath from either a jugular or femoral vein approach. In a multicenter European trial, the filter was reported to be 98% effective in the prevention of pulmonary embolism while maintaining caval patency of 92% [1]. Reported complications associated with the use of the Vena-Tech filter have included tilting, migration, and incomplete opening of the filter [1]. We report a unique case of spontaneous fracture of a Vena-Tech filter.

Case Report

A 51-year-old man who had had orthotopic liver transplantation for hepatocellular carcinoma complained of increasing back pain, shortness of breath, and pleuritic chest pain. A CT scan showed osteomyelitis of the spine at T8–T9 with an inflammatory mass. A thrombus also was seen in the IVC. An inferior venacavogram obtained via the right femoral vein confirmed the presence of a large thrombus above the renal veins at the level of the anastomosis of the donor to native IVC. A Vena-Tech filter was placed via the right internal jugular approach. The filter was placed above the thrombus in the suprarenal IVC without incident. A radiograph obtained immediately showed the filter in proper alignment and at the desired level. Anticoagulant therapy was started and the patient was treated with antibiotics.

A radiograph obtained 10 months after filter placement revealed a fracture at the apex of the filter (Fig. 1). The filter was divided along its longitudinal axis into equal halves. The three limbs of each half remained joined to their respective apices. Each half was angled somewhat relative to the other. The filter had not migrated cephalad or caudad.

At follow-up, the patient was asymptomatic and had experienced no clinical symptoms of pulmonary embolism since filter placement. A duplex sonogram of the IVC showed normal flow within the IVC and no evidence of residual thrombus.

The patient was seen again 16 months after placement of the filter and consented to a second inferior venacavogram. The venacavogram showed no residual thrombus within the cava and no further change in the position of the filter. Again, the patient had not had any suggesting pulmonary embolism in the interim. Anticoagulant therapy is being continued.

Discussion

With the recent introduction of a variety of new IVC filters, interest in the placement of these devices has increased. The stainless steel Greenfield filter is generally accepted as the standard to which other IVC filters are compared. Potential complications with the use of the Greenfield filter have been well documented and include hematoma and thrombosis at the insertion site, migration and tilting of the filter, caval thrombosis, and caval perforation [2–4]. Intraoperative disruption of a filter has been described [5], and spontaneous fracture after otherwise uneventful percutaneous placement also has been reported [4, 6]. To our knowledge, fracture of the Vena-Tech filter has not been reported before. We describe several mechanisms that may explain this complication.

The diameter of the IVC is known to be affected by respiration and cardiac pulsations. The stabilizing side rails of the

---

Received January 25, 1991; accepted after revision February 19, 1991.

[1] All authors: Department of Radiology, Box 429, University of Chicago, 5841 S. Maryland Ave., Chicago, IL 60637. Address reprint requests to F. C. Taylor.

AJR 157:177–178, July 1991 0361–803X/91/1571–0177 © American Roentgen Ray Society

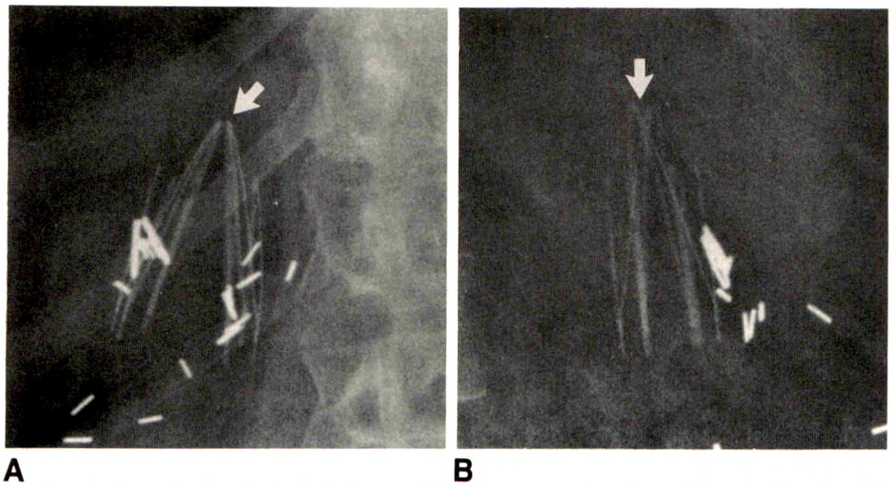

Fig. 1.—Radiographs show fracture of filter cone and separation of filter.

***A*, Anteroposterior projection shows a 2-mm transverse separation of apices (*arrow*).**

***B*, Lateral radiograph shows a 4-mm anteroposterior separation of apices (*arrow*).**

filter, which are welded to the limbs of the filter cone, remain parallel to the caval wall and should be virtually unaffected by any changes in IVC diameter. The conical portion of the filter, however, is subjected to repeated, although minute, changes in its apical angle in response to changes in caval diameter. The filter apex is therefore most vulnerable to metal fatigue, and it was at this point that the fracture occurred. Changes in caval diameter due to the force of transmitted cardiac pulsations should be proportional to the distance from the heart. We expect that the suprarenal position of the filter would increase the likelihood of a metal fatigue fracture.

In cases of spontaneous fracture of the Greenfield filter, migration of the broken fragments has been associated with penetration into extracaval structures, including the aorta, the psoas muscle, and vertebral bodies [7]. The design of the Vena-Tech stabilizing side rails, which run parallel to the caval wall, makes their perforation unlikely. In the porcine model, IVC filter components have been shown to become incorporated into the caval media with reendothelialization of the lumen in 1 month [8]. Assuming that the development of sufficient metal fatigue to cause a fracture of this type requires more time than the incorporation of the filter's side rails into the caval wall, it is unlikely that migration of all or part of the filter would occur.

In this case, with the small separation of the filter apices, the filter might still protect the patient against a large embolus, but clot trapping efficiency is obviously decreased. Placement of a second filter is a reasonable alternative in such a case. In this instance, the patient was far beyond the high-risk postoperative period when the fracture was discovered, and it was therefore recommended that anticoagulation therapy simply be continued.

REFERENCES

1. Ricco JB, Crochet D, Sebilotte P, et al. Percutaneous transvenous caval interruption with the "LGM" filter: early results of a multicenter trial. *Ann Vasc Surg* **1988**;3:242–247
2. Dorfman GS, Cronan JJ, Paolella LP, et al. Iatrogenic changes at the venostomy site after percutaneous placement of the Greenfield filter. *Radiology* **1989**;173:159–162
3. Goff JM, Puyan FA, Rice JC, Kerstein MD. Problems in placement of the Greenfield inferior vena cava filter. *Am Surg* **1988**;54:544–547
4. Kim D, Porter DH, Siegel JB, Simon M. Perforation of the inferior vena cava with aortic and vertebral penetration by a suprarenal Greenfield filter. *Radiology* **1989**;172:721–723
5. Alexander JJ, Gewertz BL, Zarins CK. Intraoperative disruption of a Greenfield vena cava filter. *J Cardiovasc Surg* **1989**;30:130–133
6. Lang W, Schweiger H, Fietkau R, Hofman-Preiss K. Spontaneous disruption of two Greenfield vena caval filters. *Radiology* **1990**;174:445–446
7. Messmer JM, Greenfield LJ. Greenfield caval filters: long term radiographic follow-up study. *Radiology* **1985**;156:613–618
8. Teitelbaum GP, McGurrin M, Davies BL, et al. Insertion and recovery of a new retrievable vena caval filter. *Invest Radiol* **1988**;23:527–533

Technical Note

Preoperative CT-Guided Percutaneous Localization of Small Masses with a Kopans Needle

Ira J. Finch[1]

Percutaneous preoperative localization of breast tumors with a hookwire has become a standard radiologic practice [1, 2]. We describe the use of a standard spring hookwire needle, placed precisely under CT guidance, for the preoperative localization of two masses not in the breast. Both were sufficiently small that they would otherwise have been difficult to find at surgery.

Case Reports

Case 1

A 35-year-old man with known melanoma had a recently enlarged right axillary lymph node measuring 2.1 × 1.0 × 1.2 cm on a routine follow-up chest CT examination. As the patient had previously undergone a lymph node dissection in this region, the surgeon was concerned that finding and excising this single node might be difficult. The patient was positioned supine in the CT scanner with his right arm elevated and his right hand tucked under his head to simulate positioning in the operating room. IV contrast material was administered by drip infusion via a vein in the patient's right hand. The abnormal lymph node was identified on axial 10-mm contiguous slices. The patient's skin was marked at the level of the abnormal lymph node with hatch marks drawn with barium (Esophotrast; Armour Pharmaceutical, Kankakee, IL), and the patient was rescanned at this level. After the most direct vertical entry site had been accurately marked on the patient's skin, he was prepared and draped and the skin was anesthetized with 1% xylocaine. A 5-cm, 21-gauge Kopans needle (Cook, Inc., Bloomington, IN) was introduced into the lesion. The needle tip was positioned within the lymph node, and proper placement was verified by CT. The needle was exchanged for the J-wire by using standard technique, and accurate placement was again verified by CT (Fig. 1). The patient was immediately transferred to the operating room, where the surgeon dissected along the course of the needle. The lymph node was excised with the J-wire, yielding a diagnosis of metastatic melanoma.

Case 2

A 43-year-old woman with a right C8 radiculopathy had an MR image that showed an enhancing soft-tissue mass measuring 2.4 × 2.0 × 2.0 cm, thought to be a neurofibroma of the brachial plexus (Fig. 2A). At surgery, the brachial plexus was dissected in the region of interest, but no mass was found. The incision was closed and the patient was transferred while under anesthesia to the CT suite for localization of the lesion. IV contrast material was administered. Scans showed the mass approximately 15 mm inferior to the surgical site. By using a technique similar to that used in case 1, a Kopans needle was placed in the lesion, avoiding the lung, and exchanged for the J-wire. Again, proper positioning was verified by CT (Fig. 2B). The patient was immediately returned to the operating room, where the incision was reopened. The surgeon dissected along the course of the needle and successfully removed a neurofibroma of the inferior cord of the brachial plexus.

Discussion

These cases illustrate a safe and efficient method of preoperative localization for small lesions that may be difficult to find operatively. The localization is as well tolerated as percutaneous needle aspiration and was performed in approxi-

---

Received December 19, 1990; accepted after revision February 14, 1991.

[1] Department of Radiology, Interventional Radiology Section, Santa Clara Valley Medical Center, 751 S. Bascom Ave., San Jose, CA 95128. Address reprint requests to I. J. Finch.

AJR 157:179–180, July 1991 0361-803X/91/1571-0179 © American Roentgen Ray Society

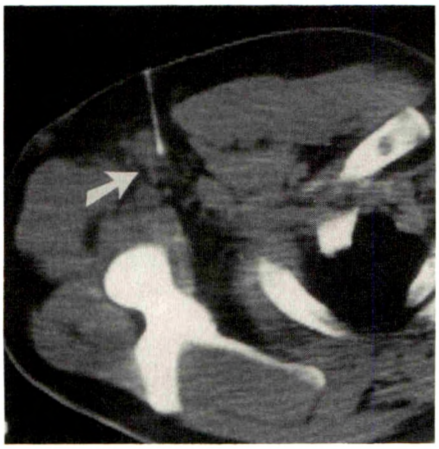

Fig. 1.—Case 1. Metastatic melanoma. Contrast-enhanced CT scan shows J-wire in right axillary lymph node (*arrow*).

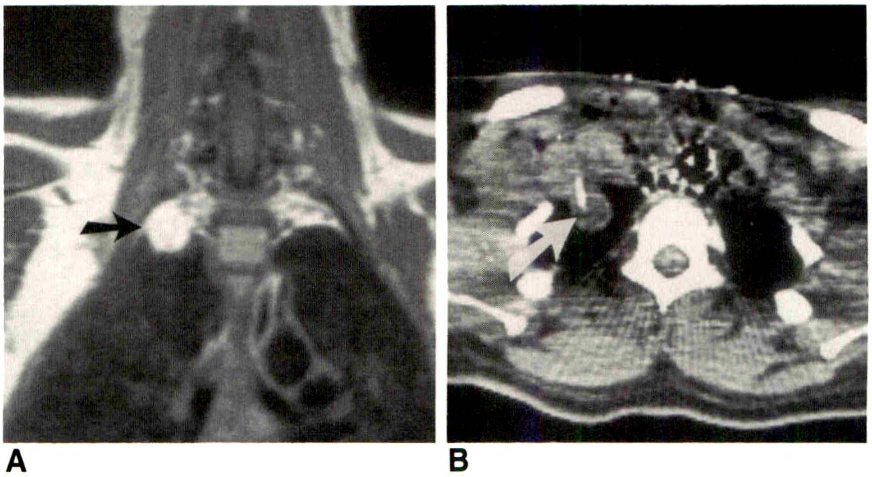

Fig. 2.—Case 2. Neurofibroma.

A, Coronal MR image (800/30) after injection of gadopentetate dimeglumine shows a high-signal mass (*arrow*) at apex of right lung.

B, Contrast-enhanced axial CT scan shows tip of J-wire in mass (*arrow*). Esophotrast (Armour Pharmaceutical, Kaukakee, IL) hatch-marks used for localization are apparent on skin anteriorly. Note subcutaneous air from surgery.

mately half an hour in each case. The technique is particularly useful in situations in which normal anatomic relationships are distorted or complex and the surgical exposure is limited. The Kopans needle provides stable localization, and wire migration is less likely than it is in the breast, where fatty tissue provides less support for the hookwire.

The CT scan should be made with the patient in the same position as will be used during surgery to simplify following the course of the wire during surgery. As with breast needle localizations, a needle wire system of adequate length must be chosen to avoid losing the end of the wire under the skin with movement. This technique could also be adapted to sonographic localization, because sonography accurately shows the position of needles for biopsies. MR localization also would be possible, with a nonferromagnetic needle-wire system [3]. A nonferromagnetic corkscrew wire made of nitinol is available (Cook, Inc., Bloomington, IN) that can be passed through a 20-gauge needle of the same composition and appropriate length (Biggs D, Cook, Inc., personal communication).

REFERENCES

1. Hall FM, Frank HA. Preoperative localization of non-palpable breast lesions. *AJR* **1979**;132:101–105
2. Kopans DB, Meyer JE. Versatile spring hookwire breast lesion localizer. *AJR* **1982**;138:586–587
3. Lufkin R, Teresi L, Hanafee W. New needle for MR-guided aspiration cytology of the head and neck (technical note). *AJR* **1987**;149:380–382

Pictorial Essay

Artifacts in Computed Radiography

Steven L. Solomon,[1] R. Gilbert Jost, Harvey S. Glazer, Stuart S. Sagel, Dixie J. Anderson, and Paul L. Molina

Storage-phosphor digital radiographic systems are becoming widely used in a variety of diagnostic procedures. The equipment is reliable and produces images of consistently high quality. However, the images may contain artifacts directly related to the digital techniques used, to the phosphor imaging plate, or to radiography in general. This article illustrates many of the artifacts encountered that are specific to computed radiography, some of which can simulate pathologic lesions. Their causes and remedies are discussed briefly.

Computed radiographic systems that use photostimulable storage phosphors have been introduced into radiology departments throughout the world over the past 5 years in increasing numbers. More than 50 systems are in operation in the United States and approximately 500 systems have been installed in Japan (Armstrong D, Fuji Medical Systems U.S.A., personal communication). Many articles have described the potential benefits of computed radiography and its clinical usefulness in chest, pediatric, genitourinary, gastrointestinal, vascular, and neuroradiology imaging [1–6]. A Philips Computed Radiography 901 system (Philips Medical Systems, Shelton, CT) has been in operation at our institute for more than 3 years and is used for nearly all the inpatient mobile ("portable") chest and abdominal radiographs [4]. The device has been reliable and image quality has been excellent, but on occasion, puzzling artifacts have been encountered, some of which have the potential to mimic true disease. Artifacts that are not unique to computed radiography (fogging, double exposure, foreign bodies) can be modified in severity or appearance by computed radiographic systems.

"Light-Bulb" Effect

The lower, outer portions of a film occasionally appear darkened relative to the remainder of the image (Fig. 1). This artifactual darkening, referred to as the light-bulb effect by Fuji Medical Systems, is caused by back-scattered radiation entering the photostimulable phosphor imaging plate from the patient's bed. This artifact is seen most frequently when the exposure is increased for obese patients or when the X-ray beam has not been collimated to the region of interest. The wide dynamic range and high sensitivity of the imaging plate makes computed radiography more susceptible to this artifact than conventional film-screen portable examinations. With chest radiography, the artifact could be misconstrued as representing a pneumothorax or pneumoperitoneum in a supine patient; in addition, it can alter the contrast and brightness of the affected portions of the image, potentially obscuring abnormalities. Reducing backscatter by lowering the kilovoltage or by more precise collimation will limit the prevalence and impact of this artifact. A lead backing applied to the cassette has been proposed as a possible solution (Armstrong D, personal communication).

Fogging

The wide dynamic range and high sensitivity of the imaging plate used in computed radiography results in a greater susceptibility to fogging (Fig. 2). Because the imaging plates have such a high sensitivity, extra precautions should be taken so that they are not exposed to extraneous radiation.

Received October 15, 1990; accepted after revision December 17, 1990.

[1] All authors: Edward Mallinckrodt Institute of Radiology, Washington University School of Medicine, 510 S. Kingshighway Blvd., St. Louis, MO 63110. Address reprint requests to S. L. Solomon.

AJR 157:181–185, July 1991 0361-803X/91/157-0181 © American Roentgen Ray Society

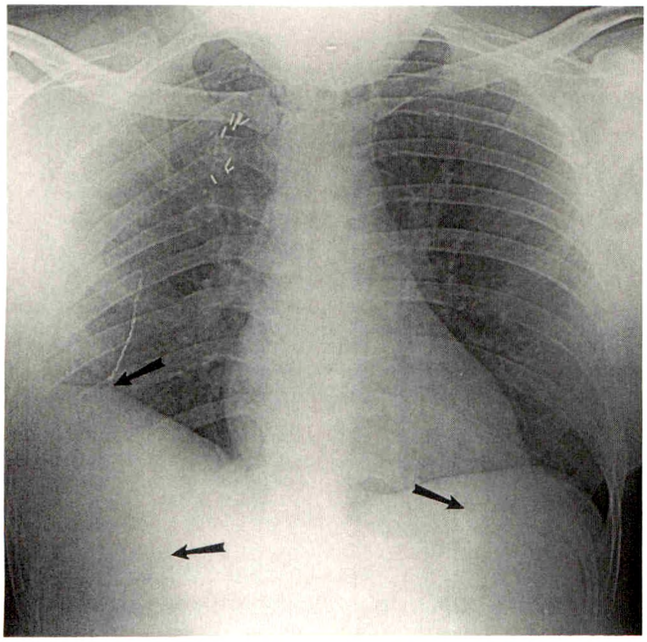

Fig. 1.—Light-bulb effect. Lower, outer portions of this computed radiograph (*arrows*) are darkened because of back-scattered radiation from patient's bed. Wide dynamic range and high sensitivity of photostimulable phosphor imaging plate make computed radiographs much more susceptible to this artifact than conventional portable film-screen radiographs.

Double Exposure

With conventional film-screen techniques, most double exposures result in a darkened, unreadable image. The wide dynamic range of the imaging plate used in computed radiography allows an image similar in density to a single exposure to result from most inadvertent double exposures (Fig. 3). If the relative exposure of both examinations is comparable, they will be equally well seen on the output image and the nature of the problem should be readily apparent. If one exposure is significantly less than the other, the artifact may be subtle and simulate abnormalities. A related and visually indistinguishable situation can occur if a latent image on the imaging plate has not been completely erased. Computed radiographic systems are capable of erasing an imaging plate that has received up to five times the normal exposure. If an exposure greater than this has occurred, the imaging plate is transported to a special unerased plate tray after it has been read. If this imaging plate is inadvertently used for another examination, a double-exposure artifact may result. Incompletely erased imaging plates should be carefully erased in the "imaging plate erasure mode."

Quantum Mottle

The wide dynamic range of the imaging plate can create an image when underexposure or overexposure would result in an unreadable image with conventional film-screen methods. In the case of marked underexposure, the image will appear grainy owing to quantum mottle (Fig. 4). Such images, which can be readily identified by noting a high sensitivity number in the parameter display area, must be interpreted with caution, as subtle findings may not be apparent because of the reduced signal-to-noise ratio.

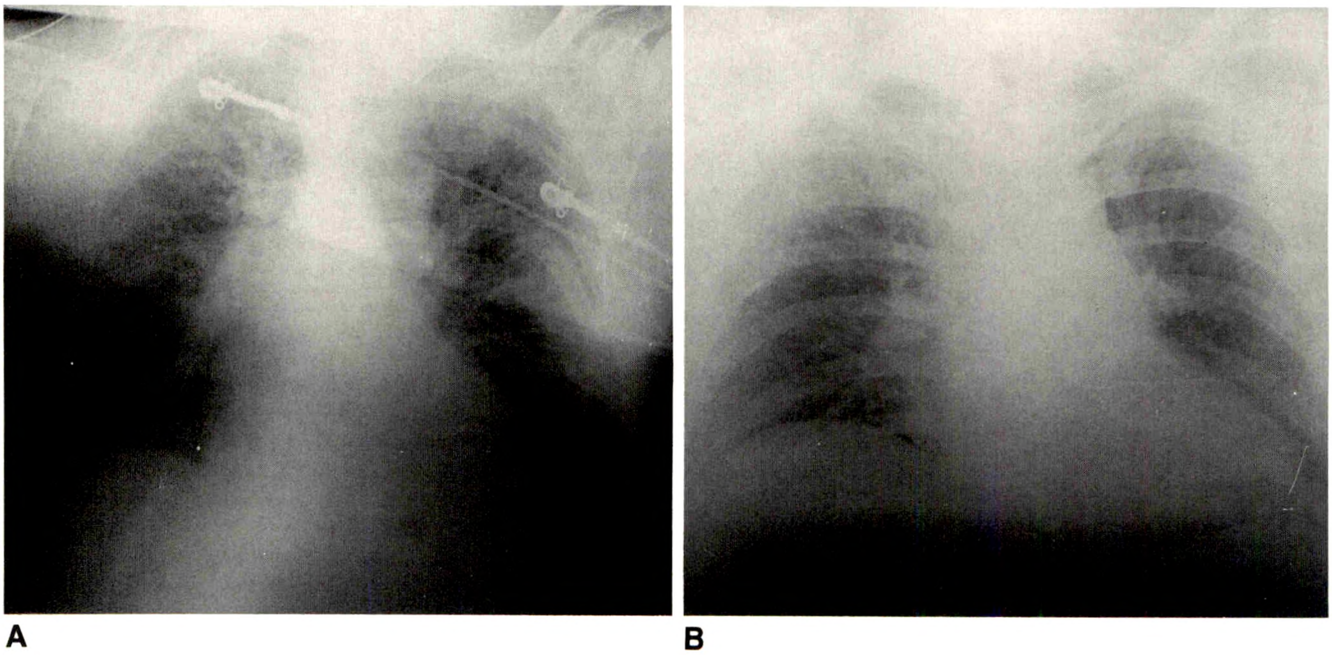

Fig. 2.—Fogging artifacts on a computed radiograph.

A, Lower half of image is darkened by exposure to extraneous radiation. High sensitivity of imaging plates requires that extra precautions be taken to prevent inadvertent radiation exposure.

B, Fogging in lower portion of image is caused by radium implants placed in pelvis to treat cervical cancer. We have not seen this artifact to the same degree with conventional film-screen techniques.

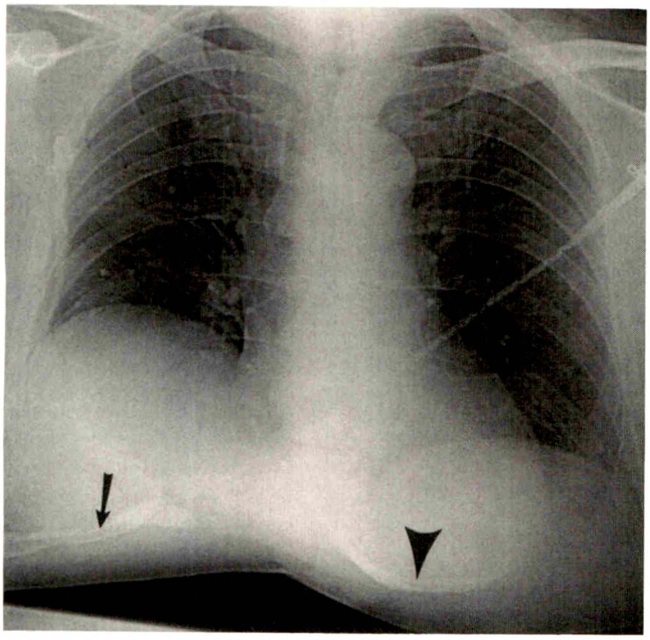

Fig. 3.—Double exposures on computed radiograph. Horizontally oriented abdominal examination is seen overlying dominant chest study. Portions of right ribs (*arrow*) and right iliac crest (*arrowhead*) are apparent.

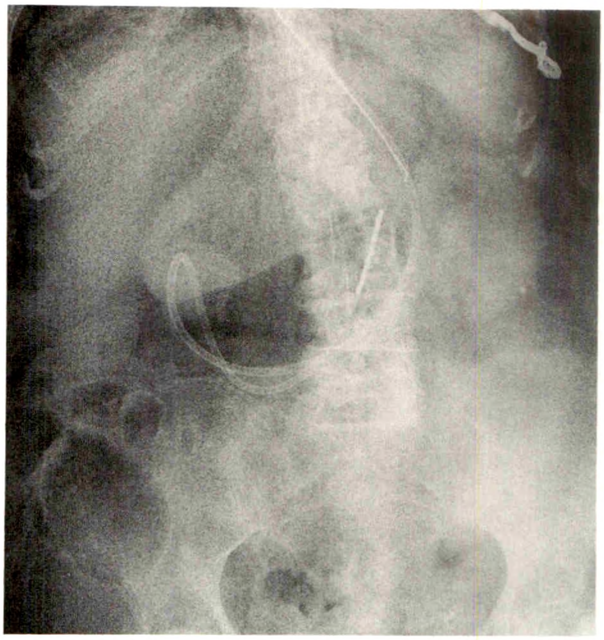

Fig. 4.—Quantum mottle on computed radiograph. Marked underexposure of this abdominal examination results in an interpretable, albeit grainy and suboptimal, image because of wide dynamic range of imaging plate.

Simulated Diaphragmatic Calcification

The unsharp masking edge-enhancement algorithm used in the edge-enhanced computed radiographic image can result in artifactual black and white bands at the interface of structures with markedly disparate densities. This can result in the appearance of diaphragmatic calcification (Fig. 5). The erroneous diagnosis of asbestos exposure could result. This artifact is always much less apparent on the non–edge-enhanced image, an important differential point. Comparison with prior radiographs, if available, or a follow-up conventional radiograph is helpful in ambiguous cases. If this artifact is problematic, the spatial frequency processing parameters can be modified to lessen the effect.

Alterations in Image Contrast and Density

A contrast resolution of 10 bits per pixel (1024 shades of gray) was chosen in the design of the currently used computed radiographic systems. The imaging plate, on the other hand, has a dynamic range exceeding 10^4. The image information contained on the imaging plate must be mapped onto these relatively few shades of gray. As part of this mapping process, the imaging plate is scanned twice. The first scan is obtained with a high-speed low-intensity laser, and histogram analysis is performed on the light emission from portions of the image. The portions of the image examined are determined by the algorithm chosen for the image. The result of this analysis determines the density and contrast parameters used in the final reading of the imaging plate and creation of the output image.

The algorithms designed for each body part make certain assumptions about the expected useful density range contained in the image. If the expected density range is exceeded, information can be lost (Fig. 6). For example, the chest algorithm does not guarantee the preservation of image information from the skin. Fortunately, most losses of information will occur outside of the regions of interest for the examination. If an algorithm for the wrong body part is chosen, the density and contrast settings will not be optimal for the body part imaged (Fig. 7).

The "auto" modes use the entire image for histogram analysis as opposed to the "semiauto" modes, which only perform histogram analysis on selected portions of the image data. The shape of collimation is critically important in the auto modes on computed radiographic devices that use first-generation software. If a collimation border is more than 3° from parallel to the edge of the imaging plate, the area of collimation will not be recognized as such and will be included in the subsequent determination of image density and contrast. This can result in marked image darkening in the region of interest (Fig. 8).

Foreign Bodies

As with conventional film-screen systems, foreign bodies, such as dust, can adhere to the imaging plate and result in artifacts simulating calcifications. Spillage of a liquid on the imaging plate prior to its processing by the computed radiographic device is shown in Figure 9. The repetitive nature of the artifact is due to the rollers used in the plate transport mechanism. Newer computed radiographic systems use belts to transport the plates and therefore would not propagate the artifact.

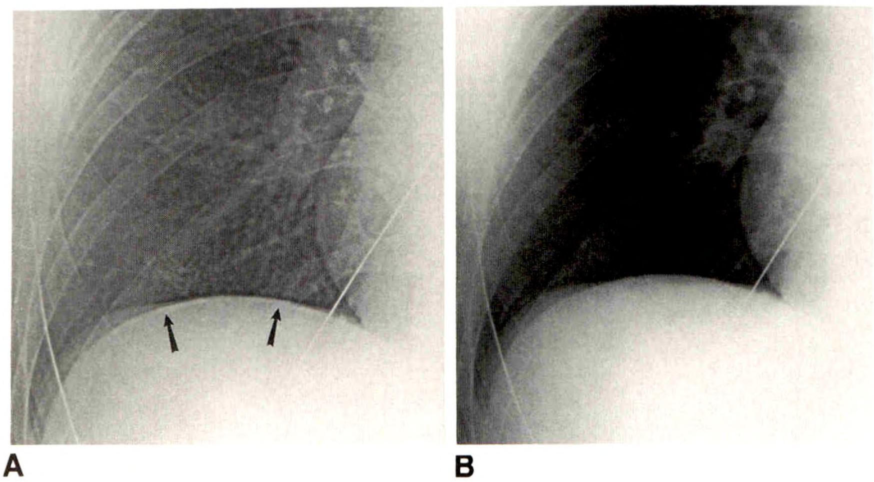

Fig. 5.—Simulated diaphragmatic calcification on computed radiograph.
A and *B*, Edge-enhanced image (*A*) shows apparent calcification (*arrows*) of right hemidiaphragm that is not seen on unenhanced image (*B*), an important differential point. This artifact almost always involves right hemidiaphragm, probably because of heart and pericardial fat overlying left hemidiaphragm, which reduce abrupt changes in tissue density at this site. A similar artifact is also seen frequently at edges of both breasts.

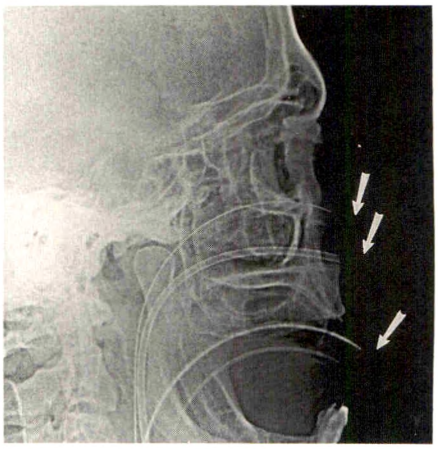

Fig. 6.—Loss of information on computed radiograph. External portions of nasogastric, feeding, and endotracheal tubes are not visualized (*arrows*) because expected useful density range for a skull examination has been exceeded at these sites.

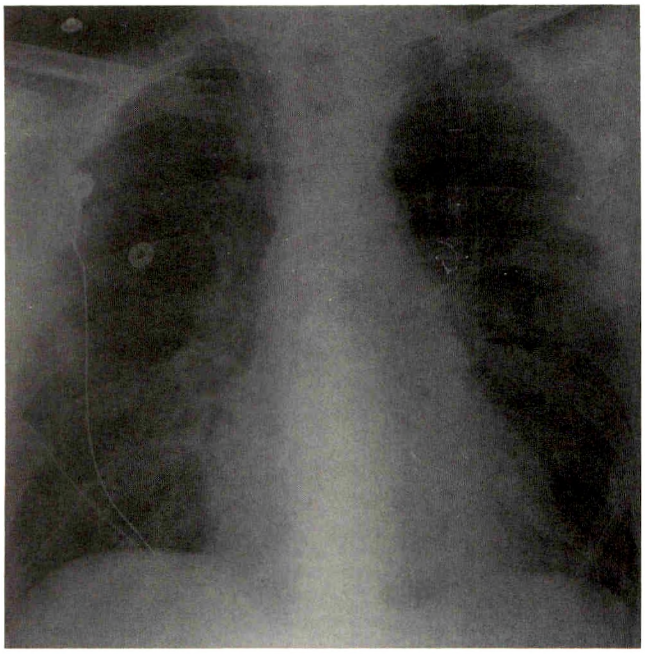

Fig. 7.—Altered contrast parameters on computed radiograph. This chest image was inadvertently printed with an algorithm designed for mandible. Result is a darkened image with suboptimal contrast.

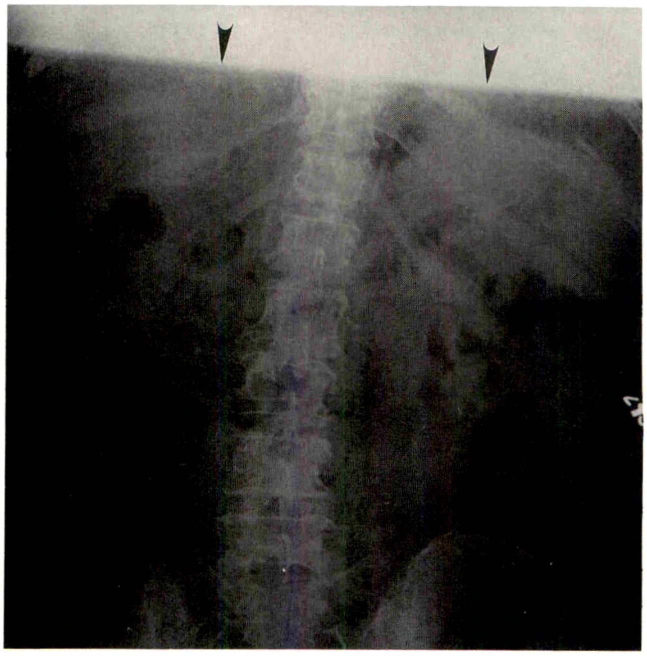

Fig. 8.—Poor collimation on computed radiograph. First generation of computed radiographic software relies on collimation margins (*arrowheads*) being less than 3° from parallel to edge of imaging plate when "auto" modes are used. If this angle is exceeded, as has occurred in this image, area of collimation will not be recognized as such, and display algorithm will include this area in its determination of image density and contrast. Result will be overall darkening of region of interest.

Equipment Malfunction

The normal computed radiographic output consists of two images, one processed to resemble a normal film-screen radiograph and one processed with a degree of edge enhancement and widened latitude. On occasion, images have been observed in which the edge enhancement has been augmented dramatically (Fig. 10). This is probably the result of an alteration of the image processing parameters stored in memory due to noise from the electrical power supply (Hishinuma K, Fuji Medical Systems Japan, Inc., personal communication). This artifact has been seen only on edge-enhanced images, a potential clue to its presence in more subtle cases. The problem should be corrected by turning off and restarting the computed radiographic device. The power sup-

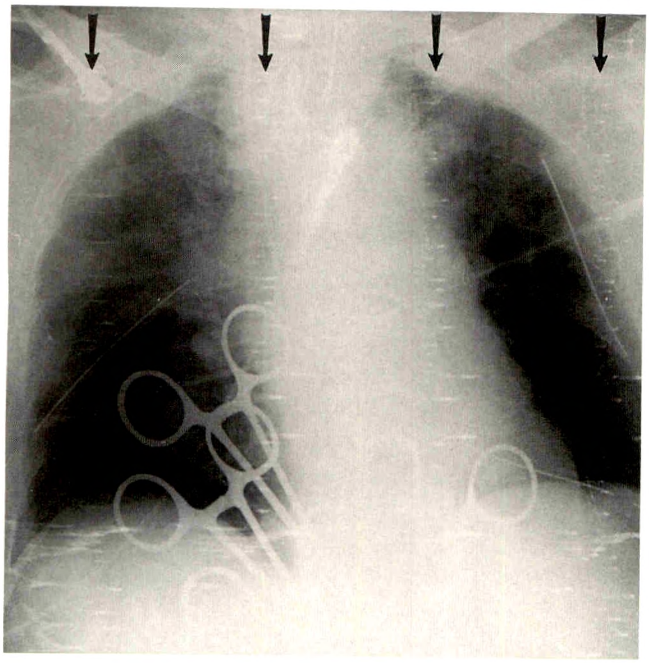

Fig. 9.—Foreign substances on a computed radiograph. A liquid, possibly blood, was spilled on imaging plate during this intraoperative examination. Owing to rollers used in early computed radiographic equipment, this manifests as an artifact (*arrows*) seen all across image at constant intervals.

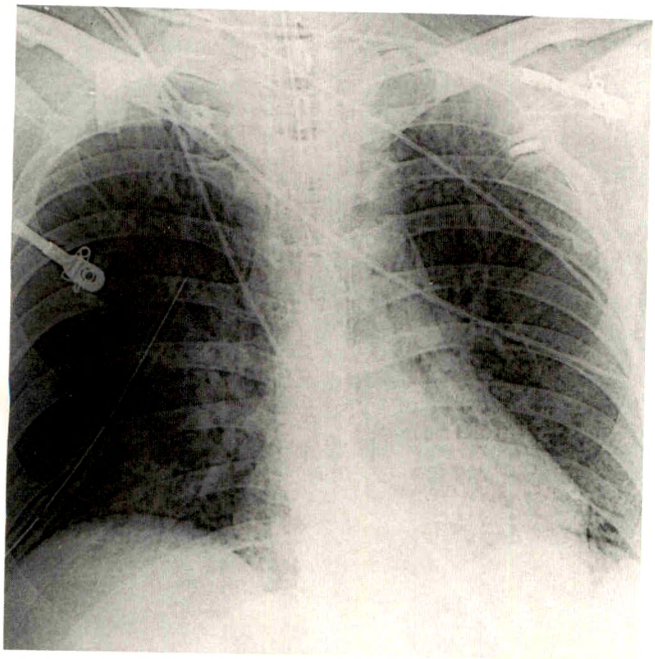

Fig. 10.—Abnormal edge enhancement. Edge-enhancement image processing parameters have been altered on this computed radiograph, resulting in dramatic augmentation of edge enhancement. This artifact probably is due to noise from electrical power supply and should be corrected by turning off and restarting computed radiographic device.

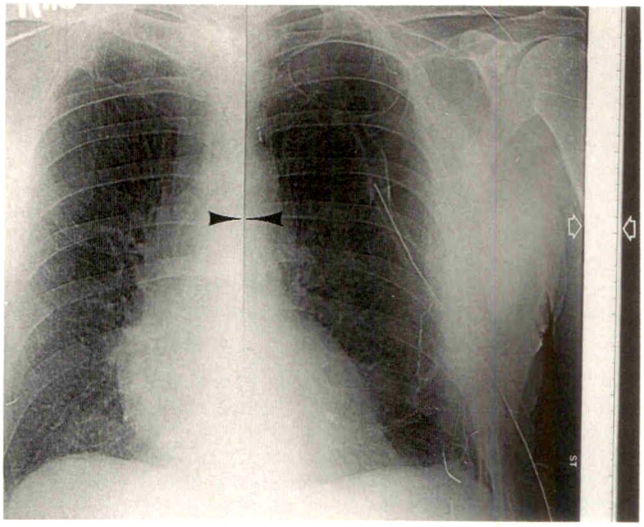

Fig. 11.—Zipper artifact. Information from central portion of this computed radiograph (*arrowheads*) is missing, with apparent absence of a portion of vertebral bodies. Amount of information lost is reflected by width of a white vertical band at right side of image (*arrows*). This artifact is caused by temporary interruption of image-plate reading while plate continues to be transported through reading device. Cause is probably a sudden drop in power supply voltage.

ply noise and variance may need to be checked if the problem is recurrent.

Rarely, images are seen in which multiple vertical scan lines are missing with apparent narrowing of the affected portion of the image (Fig. 11), referred to by us as the "zipper" artifact. The exact amount of missing information is reflected by the width of a lucent vertical band at the right side of the image. This artifact results when the reading process is temporarily discontinued while the imaging plate continues to move through the reading device. The cause is probably a sudden drop in the power supply voltage (Hishinuma K, personal communication).

REFERENCES

1. Fajardo LL, Hillman BJ, Hunter TB, Claypool HR, Westerman BR, Mockbee B. Excretory urography using computed radiography. *Radiology* **1987**;162:345–351
2. Kangarloo H, Boechat MI, Barbaric Z, et al. Two-year clinical experience with a computed radiography system. *AJR* **1988**;151:605–608
3. Kogutt MS, Jones JP, Perkins DD. Low-dose digital computed radiography in pediatric chest imaging. *AJR* **1988**;151:775–779
4. Sagel SS, Jost RG, Glazer HS, et al. Digital mobile radiography. *J Thorac Imaging* **1990**;5(1):36–48
5. Tateno Y, Iinuma T, Takano M, eds. *Computed radiography*. Tokyo: Springer-Verlag, **1987**
6. Yang PJ, Seeley GW, Carmody RF, Seeger JF, Yoshino MT, Mockbee B. Conventional vs computed radiography: evaluation of myelography. *AJNR* **1988**;9:165–168

Books Received

Receipt of books is acknowledged as a courtesy to the sender. Books considered of sufficient interest are reviewed as space permits. If the book has been reviewed in the *AJR*, the date of its review is given in parentheses.

Quantitative Imaging. Neuroreceptors, Neurotransmitters, and Enzymes. Edited by J. James Frost and Henry N. Wagner, Jr. New York: Raven, 199 pp., 1990. $98 (4/91)

Clinical Profiles of Diffuse Interstitial Pulmonary Disease. By Richard A. DeRemee. Mount Kisco, NY: Futura, 203 pp., 1990. $43 (4/91)

The Year Book of Diagnostic Radiology, 1990. Edited by David G. Bragg. Chicago: Year Book Medical, 569 pp., 1990. $54.95 (4/91)

The Radiologic Clinics of North America. Imaging the Lymphomas. Guest editor: Herman I. Libshitz. Philadelphia: Saunders, July 1990;28(4):669–903. $25; by subscription, 6 issues annually for $93 (4/91)

The Abdominal Plain Film. By Stephen R. Baker. Norwalk, CT: Appleton & Lange, 422 pp., 1990. $95 (4/91)

Nuclear Medicine Annual 1990. Edited by Leonard M. Freeman. New York: Raven, 256 pp., 1990. $98 (4/91)

Radiation Protection. A Guide for Scientists and Physicians, 3rd ed. By Jacob Shapiro. Cambridge, MA: Harvard University Press, 494 pp., 1990. $35 (4/91)

Trauma Radiology. Edited by James J. McCort. New York: Churchill Livingstone, 483 pp., 1990. $110 (4/91)

Cancer Imaging with Radiolabeled Antibodies. (Vol. 46 in the series Cancer Treatment and Research.) Edited by David M. Goldenberg. Boston: Kluwer, 467 pp., 1990. $160 (4/91)

MRI. Musculoskeletal System. By Javier Beltran. New York: Gower Medical (distributed by Lippincott, Philadelphia), 250 pp., 1990. $79.50 (4/91)

MRI. Central Nervous System. Edited by Walter Kucharczyk. New York: Gower Medical (distributed by Lippincott, Philadelphia), 288 pp., 1990. $79.50 (4/91)

Control of Radon in Houses. Recommendations of the National Council on Radiation Protection and Measurements. (NCRP Report No. 103.) Bethesda: National Council on Radiation Protection and Measurements, 90 pp., 1989. $15 (5/91)

Orthopedic Radiology. A Practical Approach. By Adam Greenspan. Philadelphia: Lippincott, 640 pp., 1988. $225 (5/91)

Cardiovascular Applications of Doppler Ultrasound. Edited by Abdul-Majeed Salmasi and Andrew N. Nicolaides. New York: Churchill Livingstone, 368 pp., 1989. $150 (5/91)

MRI of MS and White Matter Disease. By Murray A. Solomon. (Tape 1 in series 2 of Murray Solomon's Magnetic Resonance Video Review.) Burlingame, CA: Murray Solomon's MRVR, (408) 374-8897 1990. Single tape, $125; series of 6 tapes, $545 (5/91)

RSNA Today, Vol. 4, No. 3. Oak Brook, IL: The Radiological Society of North America. 1990. $55; by subscription, 6 issues annually at $185 for RSNA members and $225 for nonmembers (VHS videotape) (5/91)

Trauma of the Spine. CT and MRI. By B. Wimmer, E. Hofmann, and A. Jacob. New York: Springer-Verlag, 90 pp., 1990. $89.50 (5/91)

Maxillofacial Imaging. By Angelo M. Delbalso. Philadelphia: Saunders, 815 pp., 1990. $125 (5/91)

Wolf-Heidegger's Atlas of Human Anatomy, 4th ed. Edited by Hans Frick, Benno Kummer, and Reinhard Putz. New York: Karger, 600 pp., 1990. $100 (5/91)

MRI of the Brain Stem. By Murray A. Solomon. (Tape 2 in series 2 of Murray Solomon's Magnetic Resonance Video Review.) Burlingame, CA: Murray Solomon's MRVR, (408) 374-8897, 1990. Single tape, $125; series of 6 tapes, $545 (5/91)

Practical Echocardiography and Doppler. By Mark J. Monaghan. New York: Wiley & Sons, 176 pp., 1990. $69.50 (5/91)

Fuchs's Principles of Radiographic Exposure, Processing and Quality Control, 4th ed. By Quinn B. Carroll. Springfield, IL: Thomas, 380 pp., 1990. $39.75 (5/91)

Duplex Scanning in Vascular Disorders. By D. Eugene Strandness, Jr. New York: Raven, 256 pp., 1990. $85 (5/91)

Pocket Atlas of Normal CT Anatomy of the Head and Brain. By Anton N. Hasso and Miyuki Shakudo. New York: Raven, 85 pp., 1990. $14.95, softcover (6/91)

Angiocardiography in Congenital Heart Malformations. By Benigno Soto and Albert D. Pacifico. Mount Kisco, NY: Futura, 669 pp., 1990. $175 (6/91)

Computed Tomography, Anatomy, and Morphometry of the Lower Extremity. By H.-M. Hoogewoud, G. Rager, and H.-B. Burch. New York: Springer-Verlag, 124 pp. and floppy disk, 1990. $163.50 (6/91)

Radiology of the Eye and Orbit. Edited by Thomas H. Newton and Larissa T. Bilaniuk. (Vol. 4 in the series Modern Neuroradiology.) New York: Raven, 320 pp., 1990. $115 (6/91)

Congenital Heart Disease. Echocardiography and Magnetic Resonance Imaging. By Charles B. Higgins, Norman H. Silverman, Barbara A. Kersting-Sommerhoff, and Klaus Schmidt. New York: Raven, 405 pp., 1990. $135 (6/91)

Modern Dermatologic Radiation Therapy. By Herbert Goldschmidt and Renato G. Panizzon. New York: Springer-Verlag, 165 pp., 1991. $69

Academic Laboratory Chemical Hazards Guidebook. By William J. Mahn. New York: Van Nostrand Reinhold, 342 pp., 1991. $79.95

Cancer Pain Relief and Palliative Care. By a WHO Expert Committee. Geneva: World Health Organization, 75 pp., 1990. $7.20

The Relative Biological Effectiveness of Radiations of Different Quality. Recommendations of the National Council on Radiation Protection and Measurements. (NCRP Report No. 104.) Bethesda: National Council on Radiation Protection and Measurements, 218 pp., 1990. $18

Mediastinal Surgery. Edited by Thomas W. Shields. Philadelphia: Lea & Febiger, 400 pp., 1991. $85

Surgery of Skull Base Tumors. Edited by C. Gary Jackson. New York: Churchill Livingstone, 291 pp., 1991. $95

Summary Report on the Evaluation of Short-term Tests for Carcinogens. Collaborative Study on In Vivo Tests. By World Health Organization. Albany, NY: WHO, 96 pp., 1990. $10.40

Meeting News

The Society of Gastrointestinal Radiologists: 20th Annual Meeting, February 1991

Elizabeth Whalen[1]

The 20th annual meeting of The Society of Gastrointestinal Radiologists (SGR) was held February 18–21, 1991, at the La Costa Resort and Spa, Carlsbad, CA. Among the activities offered at the meeting were 36 presentations of scientific papers, 21 workshops, five panel discussions, a categorical course on gastrointestinal oncoradiology, poster sessions, clinical vignettes, and an unknown-film contest between East Coast and West Coast teams of society members. The Walter B. Cannon lecture is always a highlight of this annual meeting; this year, David Eddy (Duke University, Durham, NC) spoke on the role of the barium enema in screening for colorectal cancer.

Three prizes for excellence were awarded. Deborah Day and Becky Carpenter (University of Minnesota Hospital, Minneapolis) won an award for their poster presentation, "Abdominal Complications in Pediatric Bone Marrow Patients." The Roscoe Miller award for the best scientific paper was presented to James A. Nelson (University of Washington, Seattle) for his presentation of "Percutaneous Portacaval Shunt," which is described in the section on gastrointestinal bleeding complications. Randall Radin was the winner of the Memorial Award, which recognizes the best presentation by a first presenter at an SGR meeting; Dr. Radin (University of Southern California, Los Angeles) presented a study of CT findings that may distinguish *Mycobacterium tuberculosis* from *Mycobacterium avium-intracellulare* in patients with AIDS, which is described in the section on gastrointestinal imaging in AIDS.

AJR page limitations do not allow complete coverage of the entire program. However, the next few pages contain summaries of presentations in seven major subject areas of gastrointestinal radiology: liver imaging, pancreatic imaging, gallbladder imaging, colorectal imaging, gastrointestinal imaging in AIDS, gastrointestinal bleeding, and contrast materials.

Liver Imaging

In a study of 15 patients with hepatic metastases from colonic carcinoma, William F. Bennett and colleagues (The Ohio State University Hospitals, Columbus) found that three-dimensional (3-D) MR imaging can be helpful to surgeons who resect the metastases. Studies have shown that total removal of the hepatic tumor improves 5-year survival rate, but despite the improvement of preoperative and intraoperative techniques, no imaging technique has yet been able to identify every small lesion. These researchers obtained preoperative T2-weighted MR images in these patients; they then generated a 3-D image of the liver parenchyma that showed portal veins, hepatic veins, the inferior vena cava, hemangiomas, and metastases. Also, they photographed certain projections with wedged sections and discussed these with the surgeon before surgery. After surgery, the surgeons rated these preoperative 3-D MR images as not useful at all; somewhat useful (e.g., helped in overall perception of surgical

---

[1] Contributing editor, *American Journal of Roentgenology*, Ste. 103, 2223 Avenida de la Playa, La Jolla, CA 92037.

Editor's note.—"Meeting News" articles report the highlights of important national radiology meetings. The intent is to provide Journal readers with succinct, substantive, and accurate reviews of topics of current interest, written in a readable fashion and published promptly after the meeting.

The articles will not undergo the peer review usually required of *AJR* publications, nor will they offer a critique of the information provided. The sole purpose of the series is to apprise *AJR* readers of topics of current concern in an interesting and timely fashion.

AJR 157:187–193, July 1991 0361–803X/91/1571–0187 © American Roentgen Ray Society

needs); or very useful (e.g., altered course of surgery). In seven patients, resections were performed (three wedge resections, three trisegmentectomies, and one right lobectomy); in five, no resections were performed because of extrahepatic disease seen on preoperative imaging; in two, no resections were performed because of extensive hepatic metastases (<1 cm in size) that were not seen on MR images; and in one, cysts were confirmed. The 3-D MR images were rated as very useful in 10 of 15 cases, rated as not useful in two cases, and not assessed in three cases because of incomplete resection due to problems found early in surgery. The usefulness of the 3-D MR images was specified as follows: convinced surgeon that the lesion was resectable (four patients); led the surgeon to search for specific lesions that had not been detected before (four); provided a map for confirming cysts (one); showed well the spatial relationship of the large cystic tumors to the liver (one); and directed the surgeon to the area of maximum involvement (one).

Ruedi F. Thoeni and colleagues (University of California, San Francisco) compared the results of conventional T2-weighted spin-echo MR imaging of the abdomen with the results of the same MR sequence plus fat saturation. In 50 patients with 140 liver lesions (all proved by surgery or biopsy), fat-saturation imaging allowed detection of significantly more lesions than did conventional MR imaging (sensitivities of 99% and 82%, respectively). Conspicuity of the lesion and image quality were each rated on a scale of 1 to 4 (nondiagnostic to excellent, or definite abnormality): for lesion conspicuity, the mean conspicuity rating for fat-saturation images was 3.6 (compared with 2.7 for conventional images); the mean image-quality rating for fat-saturation images was 2.8 (compared with 2.5 for conventional images). In addition, fat-saturation imaging was also superior to conventional imaging in the assessment of vascular structures. Dr. Thoeni noted that he is now regularly using fat-saturation techniques for MR imaging of the liver; surprisingly, however, only one of the participants in the audience indicated that fat saturation was being used in his department for MR liver imaging. This study indicates that fat-saturation MR imaging results in significantly improved liver lesion detection rate, lesion conspicuity, and image quality.

A retrospective study of CT arterial portography (CT-AP) of liver lesions was presented by Maria Fernandez (Emory University Hospital, Atlanta, GA). Of 50 patients studied, 36 had metastatic lesions from primary colonic cancer, three had hepatomas, and 11 had other liver lesions. CT-AP scans were reviewed to determine the prevalence and location of hepatic pseudolesions, low-density areas seen on CT-AP, but not confirmed at surgery, delayed hepatic CT, follow-up CT, and/or MR imaging. Sixteen pseudolesions were found in 14 patients; they varied in size (1.0–3.2 cm) and in shape (band, wedge, oval, or round). Of the 16 pseudolesions, 11 (69%) were adjacent to a densely enhancing vessel. Of these 11, seven were noted in the medial segment of the left hepatic lobe, immediately anterior to the porta hepatis. Pseudolesions not related to a densely enhancing vessel were noted as follows: two were located at the junction of hepatic segments; one was an irregular left lobe; one was a peripheral wedge defect in the left lobe; and one was a caudate lobe defect. From the results of this study, Dr. Fernandez concluded that certain pseudolesions may be seen on CT-AP, the cause of these pseudolesions is not always clear (they may be artifacts or unusual perfusion defects), and awareness of pseudolesions and their most common locations is important for improving the interpretation of CT-AP images.

Pancreatic Imaging

Studies of the pancreas included research on MR imaging of islet cell carcinomas (rare, relatively slow-growing pancreatic malignant tumors) and on CT of the superior mesenteric artery (SMA) root in pancreatitis and pancreatic carcinoma.

Blake A. Carlson (Mayo Clinic, Rochester, MN) discussed a study of MR imaging of 33 patients with islet cell carcinomas and metastases, which require treatment options different from those of pancreatic ductal carcinoma. Of 27 primary tumors, 21 (78%) were detected on MR images; 18 of these tumors were functioning, and nine were nonfunctioning. The smallest tumor found was 3.5 cm, and the average sizes for functioning and nonfunctioning tumors were 6.1 and 9.8 cm, respectively. On T1-weighted images of 20 of the primary tumors, the tumor signal intensity was less than or equal to the signal intensity of the normal pancreas in all cases. On T2-weighted images, the signal intensity of the tumor was greater than or equal to fat in 18 (86%) of 21 tumors and mixed in three (14%). MR imaging permitted detection of 85% of hepatic metastases and 55% of extrahepatic metastases. The results of MR imaging correlated well with those of CT in patients who underwent both types of examination. MR imaging shows promise as a sensitive method of detecting both primary and metastatic islet cell carcinoma; it may be particularly helpful in the follow-up of patients with this disease.

In a retrospective study of 173 patients with either proved pancreatitis (103) or proved pancreatic ductal adenocarcinoma (70), Scott J. Schulte and colleagues (University of Washington Medical Center, Seattle) sought to determine whether irregularity, thickening, and encasement of the SMA root is specific for neoplasm. By autopsy, biopsy, or ERCP, pancreatic carcinoma was diagnosed in 70 patients, acute pancreatitis in 56, chronic pancreatitis in 24, and pancreatic abscess in 23. IV contrast material was administered in 162 patients; no contrast material was used in the other 11 patients. When the images were evaluated, everything on the image was masked except for the SMA root, and the readers were blinded to the final diagnoses; a consensus was obtained in every case. The following four abnormalities in the SMA roots of these patients were found on the CT scans: streaky infiltration (found in 27 cases of acute pancreatitis, in four cases of chronic pancreatitis, in 12 cases of pancreatic abscess, and in 25 cases of pancreatic carcinoma); periarterial lymph nodes (found in 14 cases of acute pancreatitis, in three cases of chronic pancreatitis, in six cases of pancreatic abscess, and in 11 cases of pancreatic carcinoma); focal mass (found in 10 cases of acute pancreatitis, in two cases of chronic pancreatitis, in four cases of pancreatic abscess, and in 24 cases of pancreatic carcinoma); and encasing mass (not found in acute pancreatitis, but found in one case of chronic pancreatitis, in four cases of pancreatic abscess, and in 14 cases of pancreatic carcinoma). Obliteration of fat in the presence of a mass has been considered specific to carcinoma; however, in this study, obliteration of fat with a focal mass was seen in seven cases of acute pancreatitis and in one pancreatic abscess (as well as in 18 cases of pancreatic carcinoma); also, this finding was seen with encasing masses in one case of chronic pancreatitis and in three pancreatic abscesses (as well as in all 14 encasing masses in pancreatic carcinoma). Three of the four abnormal CT findings in the SMA root occurred in all four diagnostic categories in this study, indicating that SMA root abnormalities are not specific for pancreatic neoplasm.

Gallbladder Imaging

Included in the presentations and discussions of gallbladder imaging were the following: nonsurgical treatment of gallstones, prediction of gallstone composition, the reproducibility of gallbladder contraction on sonographic studies, and the prevalence of asymptomatic gallstones in the general population.

Michael Zeppa (University of California, San Diego, Medical Center, San Diego) presented the results of 49 patients who had undergone nonsurgical treatment of gallstones; all patients were treated with methyl *tert*-butyl ether (MTBE) and/or percutaneous stone removal. Initial results had shown that stones were eliminated in 24 patients, symptoms improved in 47 patients, and residual debris or stones were found immediately after treatment in 23 patients. Follow-up data were obtained in 59% of these patients and included clinical results (79% asymptomatic, 10% improved, and 10% symptomatic) and sonographic findings (38% no recurrence, 13% sludge and debris present, 50% stones present, 6% thickened gallbladder wall, and no dilated ducts). Dr. Zeppa concluded that gallstone dissolution with MTBE was safe and effective; he reported high patient satisfaction and low frequency of changes in gallbladder function (based on oral cholestography studies) with posttreatment symptoms similar to those after cholecystectomy.

To incorporate CT into the morphoradiologic analysis of gallstones, James A. Brink (Mallinckrodt Institute of Radiology, St. Louis, MO) and coworkers studied the gallstones from 120 cholecystectomy patients. They reviewed the data for size, number, and shape of each generation of stones, as well as for the degree and pattern of calcification as determined by specimen radiography and CT. Of the gallstones studied, 64% were cholesterol stones, 18% were mixed (50–80% cholesterol), and 18% were pigment; 51% of the stones were radiolucent and 49% were opaque. Recent, single, cholesterol stones were seen as spherical, floating stones with a jagged contour; these are the stones most suited to nonsurgical treatment. A high content of insoluble calcium bilirubinate (which will make chemical dissolution difficult) is indicated by an atypical faceted appearance. Ellipsoid floating stones with a transverse diameter of less than 16 mm are probably well suited to nonsurgical techniques; if such stones are larger than 2 cm in diameter, their content of insoluble calcium bilirubinate is probably too high for chemical dissolution. Using both CT and morphoradiographic features, these researchers correctly distinguished cholesterol stones, mixed-composition stones, and pigment stones in 83% of cases; they were able to differentiate cholesterol from noncholesterol stones in 86% of cases and pigment from nonpigment stones in 98% of cases.

A study presented by Jennifer J. Donald (Vancouver General Hospital, Vancouver, B.C.) investigated the sonographic evaluation of the reproducibility of gallbladder contraction. The purpose of the study was to identify variations in gallbladder contraction and indicate the reliability of a single sonographic study to evaluate this contraction. Thirty healthy volunteers took part in the study; none had a history of biliary disease, gastric surgery, or diabetes mellitus–and none had asymptomatic gallstones. After an overnight fast (8–12 hr), each subject underwent a sonographic examination, which yielded a fasting gallbladder volume (FGBV) based on the ellipsoid method. Residual gallbladder volume (RGBV) was obtained sonographically after each subject had ingested a standard fatty meal stimulus. These measurements were taken on three separate occasions for each volunteer; and the percentage gallbladder contraction was calculated by the following calculation: $[(\text{FGBV} - \text{RGBV})/(\text{FGBV})] \times 100\%$. A significant negative correlation was found between RGBV and the percentage of gallbladder contraction ($r = -.7136$), and the ranges of values for all data sets were large (FGBV, 1.9–45.5 ml; RGBV, 0.1–21.0 ml; percentage of gallbladder contraction, −10% to 99%—the negative percentage reflects one subject whose gallbladder appeared larger after the fatty meal). Of all subjects, 93% showed a variation in percentage of gallbladder volume that was greater than 10%; 60% showed a variation larger than 20%; and 20% showed a variation larger than 40%. In regard to the use of 20% gallbladder contraction as a criterion for nonsurgical therapy of gallstones, only two of the total 90 examinations (three each for 30 healthy subjects) would have failed to meet this criterion—but even those two subjects showed gallbladder contraction greater than 20% when the examination was repeated. These researchers conclude that a single sonographic evaluation of gallbladder volume is *not* reproducible and is potentially misleading and that the 20% gallbladder contraction cutoff point is a reliable criterion for suitability of treatment with biliary lithotripsy or oral chemolithiasis.

In another study, the prevalence of asymptomatic gallstones in the general population was explored. Kenneth D. Hopper (Penn State University, Hershey, PA) described his study of the data from 2041 patients, all of whom underwent real-time sonography of the gallbladder and biliary system on which the gallbladder was visualized (none had symptomatic gallstones or previous gallbladder or biliary symptoms). Among the 287 men studied, age was the most important variable and the only statistically significant risk factor for gallstones ($p < .01$): of men less than 25 years old, none had asymptomatic gallstones; of those between 25 and 40 years old, 2% had gallstones; and of those over 40 years old, 14% had gallstones. In the women studied, age, obesity, and parity were all significant risk factors for developing gallstones. Only 3% of the women under 20 years old had asymptomatic gallstones; between 20 and 30 years old, the percentage rose to 4%; between 30 and 40 years old to 5%; and in women 40 years old or older, 11% had asymptomatic gallstones. However, obesity is the most important risk factor for women. As age increases, the risk of gallstones in obese women increases: for 20-year-old women, for every additional grade of body mass index (BMI), the risk of gallstones increases 1%; at age 45, each additional BMI class increases the risk 2%; and at age 70, the risk is increased by 3% with each additional BMI class. Finally, with each successful pregnancy, a woman's chance for developing asymptomatic gallstones increases from 3% after the first pregnancy to 17% after six or more pregnancies. No significant difference in risk for gallstones was found between men and women who are more than 40 years old.

Colorectal Imaging

The studies concerning imaging of the colon were on the following topics: preoperative MR imaging to evaluate radiation therapy for rectal carcinoma, positron-emission tomography (PET) for use in diagnosing metastatic and recurrent colonic cancer, and colonic ischemia as a complication of immunotherapy.

Eduard E. de Lange and colleagues (University of Virginia Health Sciences Center, Charlottesville) studied the use of MR imaging in the preoperative evaluation of the effectiveness of radiotherapy in 11 patients with primary rectal carcinoma. All patients underwent MR imaging before the start of radiotherapy; radiotherapy was administered for 4–6 weeks; and 5–6 weeks after the completion of radiotherapy, new MR images were obtained for each patient. These preoperative MR images were used to estimate change in tumor volume and tumor stage. Tumor volume decreased an average of 50% with radiation treatment (mean preoperative volume, 37.6 cm^3; mean postoperative volume, 19.8 cm^3). MR staging indicated that, after radiation treatment, one tumor had "downstaged" (improved), one had progressed (worsened), and nine showed no change. No significant differences were found between pretreatment and posttreatment signal intensity ratios (tumor compared with fat). Dr. de Lange concluded that MR imaging may be helpful in monitoring tumor size, but that further studies are needed to determine whether MR imaging can help monitor staging and other changes.

Because barium enema studies are 98% accurate for detection of recurrence of colonic cancer, CT has been relegated to the role of helping to localize the tumor for biopsy. CT reliability even for this function is not perfect; nonspecific and benign liver defects sometimes cause false-positive findings, and postsurgical changes can appear to represent recurrent disease. Edward Buonocore and coworkers (University of Tennessee Medical Center, Knoxville) have begun research based on a new concept: perhaps recurrence of colonic cancer can be detected by metabolic changes that are found by ^{18}FDG-PET. Follow-up in eight patients with recurrent colorectal tumor showed local recurrence in four patients (three on the suture line and one in the peritoneum) and distant recurrence in the liver in four patients. On PET scans with perfusion (^{13}N-ammonia) and metabolic (^{18}F-glucose) agents, these researchers identified metabolically active tissue related to active extracolonic neoplasms; moreover, the PET results influenced the medical care in these patients. Dr. Buonocore listed the disadvantages of PET as follows: slow (long scanning time), limited spatial resolution (4–7 mm), nonspecific, nonanatomic, and expensive. As PET scanners begin to be mass produced and less expensive, these disadvantages may be balanced by the advantages of the important supplementary information provided by metabolic imaging (which may aid in tumor grading and follow-up of therapeutic course) and the fact that PET information is not affected by anatomic changes (e.g., reactive fibrosis or necrosis).

A study of the gastrointestinal complications of immunotherapy in 141 consecutive cancer patients was presented by Ellen L. Wolf (Albert Einstein-Montefiore Cancer Center, Bronx, NY). Dr. Wolf and her colleagues investigated the complications after treatment with various protocols, including different combinations of interleukin-2 (IL-2), lymphokine-activated killer cells (LAK cells), and interferon-a (IFN-a). Most patients receiving this treatment were those who had advanced renal cell carcinoma and melanoma. Previously known complications of IFN treatment include fatigue, anorexia, fever, and diarrhea; IL-2 has been shown to cause hypotension, oliguria, fluid overload, and nausea and vomiting. In this study, the complication of colonic ischemia occurred in 14% of the patients treated with IFN-a/IL-2 and LAK cells but in none of the 111 treated with IL-2 and LAK cells. Other observed complications of IL-2/LAK-cell therapy included perforated ulcer, rupture of a liver metastasis, and exacerbation of Crohn disease. Dr. Wolf concluded that colonic ischemia is an unusual complication of IL-2 immunotherapy, but the risk is increased by adding interferon to the protocol, and that the patients at risk for developing this complication are those with severe diarrhea.

Gastrointestinal Imaging in AIDS

Randall Radin (USC School of Medicine, Los Angeles, CA), this year's winner of the Memorial Award for a first-time SGR presenter, discussed his study of use of CT findings to distinguish *Mycobacterium tuberculosis* (MTB) from *Mycobacterium avium-intracellulare* (MAI) in patients with AIDS. This distinction is important because MTB can usually be treated successfully with standard antimycobacterial therapy, whereas MAI in patients with AIDS is usually treated with experimental drugs with limited success. If CT can help distinguish the two, appropriate therapy can be started while waiting 4–6 weeks for the mycobacterial culture results. Dr. Radin studied abdominal CT scans of 27 AIDS patients with proved MTB and 44 AIDS patients with proved MAI (identity of infection was proved by lymph node biopsy, bone marrow biopsy, and/or blood culture results). An interesting finding in the study was that, in 85% of the patients with MTB, MTB infection was the only AIDS-defining illness, whereas 82% of the patients with MAI had another previous or concurrent AIDS-defining illness. CT findings included mild hepatomegaly and mild splenomegaly in both MTB and MAI patients; however, marked hepatomegaly and marked splenomegaly were found only in MAI patients. Furthermore, 44% of the patients with MTB—but only 14% of the MAI patients—had focal lesions in the solid viscera. No significant differences were found in CT results concerning adrenal abnormalities (none in both), ascites (about 5% in both), of gastrointestinal tract abnormalities (15% for MTB vs 18% for MAI, but the types of abnormalities did differ). Significant differences were found in CT appearance of nodes: solid nodes only, 7% of MTB patients and 86% of MAI patients; necrotic nodes, 93% of MTB patients and 14% of MAI patients. Recognition of the CT differences between MTB and MAI infections in patients with AIDS may allow physicians to start necessary treatment at an earlier stage than was possible previously.

A study about cryptosporidial cholangitis in patients with AIDS was presented by Hind S. Teixidor (The New York Hospital-Cornell University Medical College, New York). Cryptosporidiosis is a disease caused by a protozoan parasite that occurs with increased frequency in patients with AIDS (in 6% of all AIDS patients and in 21% of AIDS patients who have diarrhea). In this study, 13 AIDS patients with biliary cryptosporidiosis were studied; the cryptosporidiosis was confirmed only by autopsy in six patients, only by surgery in two, and by both surgery and autopsy in one (the diagnosis was presumptive—based on abnormal imaging findings—in the remaining four patients). This represents the largest series of biliary cryptosporidiosis patients studied to date. Imaging studies performed included CT (eight patients), sonography (seven), cholangiography (six), and repeated comparable studies (seven); results of these studies were retrospectively evaluated and correlated with histopathologic findings. The following cholangiographic findings appear to be specific to biliary cryptosporidiosis: attenuation of intrahepatic bile duct (IHBD; eight patients, including two with beading and stricturing of the primary IHBD); dilatation of the extrahepatic bile duct (EHBD; six patients, none with EHBD stricturing); irregularity of the bile duct (four); and papillary stenosis (three). Other imaging findings suggestive of biliary cryptosporidiosis included thickening of the gallbladder wall with no calculi (CT, five; sonography, two); pericholecystic fluid (CT, three); thickening of the wall of the common bile duct (sonography, three); dilatation of the IHBD (CT, seven; sonography, two); and dilatation of the EHBD (CT, seven; sonography, five).

Gastrointestinal Bleeding

The report presented by James A. Nelson (University of Washington, Seattle) won the Roscoe Miller Award for the best scientific paper of this year's SGR meeting. Dr. Nelson discussed the development of an interventional approach to acute portacaval shunting. These researchers sought an acute interventional technique to help treat variceal bleeding complications of portal hypertension. The 24,000 deaths/year due to bleeding varices and an even greater number of nonfatal bleeding problems are a major drain on United States blood banks. With the increasing use of liver transplants, a nonsurgical shunt would be a useful temporizing measure for potential recipients in whom variceal bleeding develops, because surgical shunting makes transplantation technically more difficult. Using the Seldinger technique, Dr. Nelson and his colleagues placed matching catheters into the portal and femoral veins of four domestic swine. Acute portal hypertension was produced effectively by intraportal injection of Ivalon into the portal system. The two catheters were then connected via a Biomedicus vortex pump primed with heparinized saline, and the hypertensive portal system was pumped into the normotensive systemic circulation. The shunt was established successfully in all animals, and a logarithmic change in portal pressure was noted in response to linear changes in shunt flow. In this model, pump flows of 150–200 ml/min reduced portal pressure to baseline or lower, with prompt return to higher or control pressures when pump flow was reduced or discontinued. Shunt function could be confirmed angiographically, and the pump speed varied to preserve hepatic portal perfusion. This type of portacaval shunting may serve as primary emergent therapy, as an adjunct to other more definitive interventions, or even as a temporizing measure or new method for intraportal therapy (e.g., thrombolysis) in transplantation candidates with variceal bleeding.

Another paper presented on gastrointestinal bleeding indicated that negative angiographic results after massive upper gastrointestinal bleeding are not a sufficient reason for physicians' complacency in these patients. Elvira Lang (VA Medical Center, Palo Alto, CA) discussed a study of 12 patients; inclusion criteria were massive arterial upper gastrointestinal bleeding (>3 units of packed RBCs); arteriography of celiac artery, superior mesenteric vein, and left gastric artery; and clinical diagnosis of gastric bleeding. These patients required 6–20 units of packed RBCs (mean, 11 units); conservative treatment was used in five patients, and prophylactic embolization was performed in seven. Of the five patients treated conservatively, one had exsanguination from an overlooked 6-cm midesophageal ulcer; two had massive recurrent hemorrhage, one case of which was fatal. One patient with embolization had exsanguination. In these types of cases, a major question is whether physicians can rely on the results of endoscopy performed during the acute phase of bleeding. In four of six acute-phase endoscopies in this study, visibility was markedly impaired and one fatal ulcer was missed; in one, the diagnosis of a Mallory-Weiss tear led to treatment of that problem, but the patient died from a undiagnosed bleeding pyloric ulcer 9 days later; and in one case, the acute-phase endoscopy results were correct. Dr. Lang emphasized that, in accepting negative angiography as a sign of successful treatment in these patients, physicians risk overlooking significant lesions in noninjected territories; these patients run a high risk of ongoing or recurrent hemorrhage. She strongly recommended continued and aggressive workup of such patients (regardless of angiographic results) and suggested that a multicenter trial might be able to evaluate the benefits of prophylactic embolization of the left gastric artery in patients with massive upper gastrointestinal bleeding.

Contrast Materials

Gadopentetate Dimeglumine

Maureen White (Evanston Hospital, Evanston, IL) presented a study of 40 patients with hepatic tumors (including metastatic disease, hemangioma, and hepatocellular carcinoma) who underwent MR imaging with and without the use of gadopentetate dimeglumine. The MR protocol included use of axial, 10-mm slices, 256 × 128 matrix, respiratory compensation, cardiac gating, and presaturation pulses. After the precontrast images were obtained, gadopentetate dimeglumine was injected at 0.1 mmol/kg body weight. Patterns seen with contrast enhancement included 70% heterogeneous enhancement (43% mixed, 23% peripheral, and 4% central), 23% uniform enhancement, and 7% isointense enhancement. Blinded reviewers evaluated the MR images for the number and size of lesions; the reviews were done in correlation with other studies, and a lesion was considered confirmed if it was seen on two or more studies. The highest detection rate for lesions was found with the precontrast T2-weighted spin-echo imaging (87%); the second highest detection rate occurred when the reviewers evaluated postcontrast gradient-recalled echo images (80%). With gadopentetate dimeglumine-enhanced MR imaging, various patterns on lesion contrast were found, and some contrast reactions occurred. Dr. White and coworkers concluded that use of gadopentetate dimeglumine did not significantly improve conspicuity of liver lesions on MR images and suggested that dynamic imaging with gadopentetate dimeglumine may produce better results.

Barium

Presenting the paper that received the 1990 SGR Research Award, Pablo Ros (University of Florida, Gainesville) discussed the evaluation of barium as a gastrointestinal negative contrast agent for MR imaging in normal subjects. The advantages of barium are its safety, acceptance by patients, low cost, and availability; these researchers specifically assessed the usefulness of barium as an oral or rectal MR contrast agent, as well as patients' tolerance of side effects of barium used with MR imaging. The 10 subjects underwent MR imaging before and after administration of 60% weight/weight barium sulfate (600–900 cm^3 orally or 400 cm^3 rectally). For evaluation of the images, precontrast and postcontrast images were separated and randomized, and three independent readers assessed image quality on a rating scale of 1 to 5; the parameters evaluated included bowel marking for six segments and anatomic delineation for 12 anatomic structures. After the administration of barium, the mean score of bowel delineation on MR images improved (percent change) as follows: 79%, coronal T1-weighted images; 67%, axial T1-weighted images; 52%, axial T2-weighted images; and 55%, proton-density-weighted images. In terms of anatomic structures, the rectum and distal bowel were the structures whose delineation was most improved on T1-weighted axial images; the uterus and vagina were the structures whose delineation was most improved on T2-weighted images; the pelvic side walls and seminal vesicles were the structures whose delineation was most improved on proton-density-weighted images. Only one structure, the vagina, was seen less well after contrast administration than before (on coronal T1-weighted images). In summary, with barium as a contrast agent, a significant improvement was seen in the quality of gastrointestinal MR images ($p < .01$); better bowel opacification was seen; and a trend of improvement was seen on all pulse sequences, with the most improvement seen on axial T1-weighted images. No image degradation or artifacts occurred in any case. The only side effects in patients were nausea (four cases), cramps (three), and constipation (two); these are similar to the side effects that occur when barium is used as a radiologic contrast medium, and they all resolved without medication. Ros noted that all the subjects in this study were normal volunteers, and he and his colleagues are now pursuing the important question of whether the use of barium as a negative contrast agent is clinically useful.

On the basis of their observation of a variety of coating artifacts with barium (including one that mimicked a villous tumor), Abraham H. Dachman and colleagues (Uniformed Services University, Bethesda, MD) conducted a study to demonstrate coating-related double-contrast artifacts and to study the mechanism of this type of flow-related artifact. They reviewed clinical material and performed experiments on dog colon, pig colon, and balloons to mimic a human colon. In the experiments, after the colon model was flushed with saline, 100 cm^3 of liquid barium was introduced; the colon models were rotated 15 times in the course of imaging. The six balloon experiments showed interdigitating artifacts related to luminal flow and polypoid artifacts related to surface flow. In the three animal studies, luminal-flow artifacts were seen (including interdigitating and foreign-matter artifacts). The results indicated that, even with good coating, coating artifacts can occur with the flow of viscous barium. The types of coating artifacts observed included those related to bare areas, luminal flow, surface flow, and nodular patterns. The anterior surface of the stomach is the most likely place to find a bare area on the wall, and contact time and changing the position of the patient may help avoid these artifacts. Luminal-flow artifacts include pseudo-intraluminal diverticulum and irregular ("villous") structures. To summarize the findings of this study, Dr. Dachman noted the variable appearance of coating artifacts, the importance of recognizing such artifacts and not confusing them with lesions, and the further study required for the nodular-pattern artifacts and complete factor analysis.

The role of latex sensitivity in adverse reactions to barium enema (administered using a latex tip) was discussed by Peter J. Feczko (William Beaumont, Royal Oak, MI). The study focused on 194 patients who had a nonfatal reaction to barium enema and 13 whose reaction was fatal. In the group that had nonfatal reactions, the time between administration of the enema and the onset of the reaction was less than 2 min in 38 patients, 3–5 min in 47, 5–15 min in 63, and more than 15 min in 35 (including three in which the time to reaction was more than 1 hr). The most common nonfatal reactions were urticaria/rash/itch (80 patients), facial edema (64), difficulty breathing (52), dizziness/faintness (35), and nausea/"sick" feeling (34). Less common reactions included warmth/burning sensation (20 patients), anxiety (18), sneezing (11), a "funny feeling" (11), and seizures (eight). In this group, 37 patients revealed either before or after the procedure that they were allergic to latex, and only one patient had had a previous reaction to barium. In the group of patients with fatal reactions to barium enema, all enemas appeared to have been administered with a latex-tipped device. Five patients had autopsies, and no cardiovascular disease was found in this group. Data from 13 of these patients shows that the onset of fatal reactions was less than 2 min in seven patients, 3–5 min in four patients, and more than 5 min in two patients. The allergic reaction to latex is probably due to a protein molecule and has been reported in all kinds of devices from different manufacturers. Although one cannot say conclusively that latex reaction was the cause of all these deaths, Dr. Feczko believes that it probably was the cause in the great majority of them and that changing materials used in barium enema tips should resolve some of the negative side effects and prevent many of the deaths occurring after that procedure.

Come to the
American Roentgen
Ray Society
92nd
ANNUAL MEETING
Orlando, FL
Marriott's Orlando World Center
May 10–15, 1992

Scientific Program (200 papers)
Instructional Courses (60 hours)
Categorical Course on Neuroradiology
The Caldwell Lecture
Award Papers
Scientific Exhibits
Social, Golf, and Tennis Programs
Guest Programs

Forthcoming Articles

REVIEW ARTICLES

The biliary tract: imaging for the 90s. *Burrell MI, Zeman RK, Simeone JF, et al.*

Laparoscopic cholecystectomy: evolution, early results, and impact on nonsurgical gallstone therapies. *Brandon JC, Velez MA, Teplick SK, et al.*

Commentary. A surgeon's perspective on laparoscopic cholecystectomy. *Easter*

Characterization of tumor hypoxia by ^{31}P MR spectroscopy. *Steen RG*

PULMONARY RADIOLOGY

Broncholithiasis: CT features in 15 patients. *Conces DJ Jr, Tarver RD, Vix VA*

Case report. Noncardiogenic pulmonary edema resulting from the intravascular administration of contrast material. *Bouachour G, Varache N, Szapiro N, L'Hoste P, Harry P, Alquier P*

BREAST RADIOLOGY

Lobular carcinoma in situ of the breast: clinical, pathologic, and mammographic features. *Beute BJ, Kalisher L, Hutter RVP*

Gadopentetate dimeglumine–enhanced chemical-shift MR imaging of the breast. *Rubens D, Totterman S, Chacko AK, et al.*

Pictorial essay. Lipid cysts of the breast: classic and atypical appearances. *Evers K, Troupin RH*

GASTROINTESTINAL RADIOLOGY

Abdominal desmoids: CT findings in 25 patients. *Einstein DM, Tagliabue JR, Desai RK*

Bile duct diverticula and webs: nonspecific cholangiographic features of primary sclerosing cholangitis. *Gulliver DJ, Baker ME, Putnam W, Baillie J, Rice R, Cotton PB*

Biliary lithotripsy: correlation between pretreatment gallbladder contractility and the success of treatment. *Donald JJ, Fache JS, Burhenne HJ*

Technical note. The management of occluded metallic self-expandable biliary endoprostheses. *Jackson JE, Roddie ME, Chetty N, Benjamin IS, Adam A*

Diagnosis of portal vein thrombosis: value of color Doppler imaging. *Tessler FN, Gehring BJ, Gomes AS, et al.*

MR imaging of the portal venous system: value of gradient-echo imaging as an adjunct to spin-echo MR. *Silverman PM, Patt RH, Garra BS, et al.*

Diagnosis and staging of hepatocellular carcinoma: comparison of CT and sonography in 36 patients with liver transplants. *Miller WJ, Federle MP, Campbell WL*

Case report. Acute torsion of a wandering spleen: diagnosis by CT and duplex Doppler and color flow sonography. *Nemcek AA Jr, Miller FH, Fitzgerald SW*

Gastric carcinoma in patients with Crohn disease: report of four cases. *Glick SN*

Case report. Diffuse stenosis of the ileum after ureteroileal interposition: radiologic-pathologic correlation in two cases. *Tung GA, Papanicolaou N, Zukerberg LR, Yoder IC*

Case report. Giant thoracic osteophyte causing esophageal food impaction. *Underberg-Davis S, Levine MS*

GENITOURINARY RADIOLOGY

Retroperitoneal fibrosis: a review. *Amis ES Jr*

Color Doppler sonography in the evaluation of erectile dysfunction: patterns of temporal response to papaverine. *Fitzgerald SW, Erickson SJ, Foley WD, Lipchik EO, Lawson TL*

Abnormalities of the seminal tract causing infertility: diagnosis with endorectal sonography. *Abbitt PL, Watson L, Howards S*

MUSCULOSKELETAL RADIOLOGY

Early avascular necrosis: MR and histologic examination in a dog model. *Brody AS, Strong M, Babikian G, Sweet DE, Seidel FG, Kuhn JP*

Preoperative evaluation of osteosarcoma: value of gadopentetate dimeglumine–enhanced MR imaging. *Seeger LL, Widoff BE, Bassett LW, Rosen G, Eckardt JJ*

Soft-tissue sarcoma: MR vs sonography for detection of local recurrence after surgery. *Choi H, Varma DGK, Fornage BD, Kim EE, Johnston DA*

Improved bone radiography with scan equalization radiography. *Wandtke JC, Plewes DB*

Pictorial essay. Imaging bacterial osteomyelitis: from plain film to MR imaging. *Gold RH, Hawkins RA, Katz RD*

PEDIATRIC RADIOLOGY

A comparison of synthetic and human surfactants in the treatment of respiratory distress syndrome: radiographic findings. *Levine D, Edwards DK III, Merritt TA*

Pictorial essay. CT on the pancreas in children. *Herman TE, Siegel MJ*

Case report. Esophageal histoplasmosis in a child with immunodeficiency. *Tu RK, Peters ME, Gourley GR, Hong R*

Case report. Renal tubular dysgenesis. *Luisiri A, Salinas-Madrigal L, Noguchi A, Graviss ER, Silberstein MJ*

NEURORADIOLOGY

MR imaging of the brain in patients with migraine headaches. *Osborn RE, Alder DC, Mitchell CS*

High-intensity signals within the posterior pituitary fossa: a study with fat-suppression MR techniques. *Mark LP, Haughton VM, Hendrix LE, et al.*

The role of contrast-enhanced MR imaging in the diagnosis of neurocysticercosis. *Chang KH, Lee JH, Han MH, Han MC*

Imaging of the basal cerebral arteries and measurements of blood velocity in adults by using transcranial real-time color-flow Doppler sonography. *Tsuchiya T, Yasaka M, Yamaguchi T, Kimura K, Omae T*

Carotid duplex sonography: bisferious pulse contour in patients with aortic valvular disease. *Kallman CE, Gosink BB, Gardner DJ*

RESIDENT EDUCATION

Perspective. Radiologic physics instruction for diagnostic radiologists: a survey of residency programs. *Committee on Training of Radiologists, American Association of Physicists in Medicine*

Letters

A Report on Radiology at Muhimbili Medical Center, Dar es Salaam, Tanzania

In December 1990, we were sent by our chairman, Carl Ravin, to assess Muhimbili Medical Centre (MMC) in Dar es Salaam, Tanzania, including the technical and equipment needs of their department, to determine whether our department could develop an outreach relationship with this facility.

As might be expected of any developing country, the medical needs in Tanzania are almost overwhelming. The health care system is organized rationally into a hierarchy of progressively larger institutions, the largest of which are the four referral hospitals. With approximately 1300 beds, MMC is the largest medical center in Tanzania, serving as both the referral hospital for the region around Dar es Salaam and the tertiary hospital for the country. In addition to a large inpatient population, it has an active trauma center and an outpatient facility.

The entire country has only seven radiologists (five at MMC and two at another referral hospital). As a result, only two of the four-referral hospitals and none of the 25 regional hospitals have radiologists. Of the five radiologists at MMC, three are Tanzanians. They are well trained (two in Australia, and one has just completed a neuroradiology fellowship in Switzerland). All could leave Tanzania and practice elsewhere, but they choose to stay in their own country.

The radiology department at MMC participates in the training of technologists and medical students, but its greatest commitment of time involves clinical radiology. According to the official count, 60,000 examinations are performed each year; 90% are on outpatients, and 40% are chest radiographs. Interestingly, only about 5% of the films are "officially" interpreted by the radiologists. All the films are screened by a radiologist, but a report is dictated only when requested by the referring physician. Obviously, the amount of work that each radiologist can do is a limiting factor.

The equipment and working environment at MMC would make any modern radiologist cringe. A significant problem in the entire country is the absence of stable voltage. This makes working with electronic equipment difficult and adds to the stress on that equipment. The radiographic rooms have no air conditioning. The main hospital has one RF unit with a table that does not tilt and equipment for spot films and fluoroscopy that often is broken. The hospital has an old chest unit (cassette type) and two basic radiographic units for extremity work. For high technology, it has a small linear-array sonographic unit that produces substandard images because of the variations in voltage.

To give an example of the working conditions, we witnessed a thoracic myelogram performed on a table that did not tilt, and without spot film capabilities and fluoroscopy. The patient was a 10-year-old with Burkitt lymphoma who had a neurologic block in the thoracic region. The radiologist punctured the cisterna magna and injected contrast material (nonionic, water soluble). The patient then was elevated with pillows. After a few minutes, plain anteroposterior and lateral films of the thoracic region were obtained without knowledge of the level of blockage. Despite these difficulties, it was determined that the tumor was in the midthoracic region.

In addition to these difficult working conditions, the intellectual resources of the medical center are also inadequate. Neither the MMC library nor the radiology department has any recent journals or textbooks. The most current issues of *AJR* and *Radiology* are from 1983.

Why do these conditions exist? Unfortunately, as with many countries, Tanzania has an acute lack of hard currency. With few items to export and broad-based needs, it has little money for health care. What little money it has for this area of service is spent wisely for immunization programs and other basic needs. As a result, almost no funds are available for radiology.

Obviously, the needs are great, and we left Tanzania with a strong sense that those of us who have many resources should reach out and give to those who have fewer. What should we do? First, with Dr. Berk's help, *AJR* will be sent complimentary to the department at MMC to help them keep up with the rapidly changing field of radiology. We also will be sending them a subscription to *Radiology* as a gesture from our department. Even though they will be unable to apply much of what they read, current journals will alleviate their sense of isolation from the world. Their most important pressing need is radiographic equipment—and not just expensive, large units. None of the wards have simple view boxes. The cassettes are outdated and lead to excessive techniques (these are hard on the old equipment and result in excessive doses of radiation to the patient). Accessory items such as bright lights and lead markers are also in short supply. Last, important basic radiographic equipment is needed to upgrade the rapidly deteriorating units currently in place.

In closing, we encourage the readers of *AJR* to assess their own resources to determine if radiographic equipment, especially older analog units, could be donated to MMC to upgrade the center's department. This would include even small items such as cassettes, view boxes, and lead markers. Those interested in donating can contact Mark Baker (919-681-2711, ext. 5238) at Duke University. By working together, we should be able to help raise the level of health care at MMC and in Tanzania.

Mark E. Baker
Frederick R. Porter
Duke University Medical Center
Durham, NC 27710

On Teaching Radiology in Developing Countries

I have just returned from Kathmandu, Nepal, where I was a visiting professor in the Department of Radiology, Tyruban University, College of Medicine, for 3 weeks. From 9 a.m. to noon each day, I critiqued the five postgraduate students' (residents') handwritten reports of current cases in small group discussions. Dr. Budathoki, departmental chair, and Dr. Shrestha, senior lecturer, participated enthusiastically, occasionally saying, "We just don't see that in Nepal." For example, Paget disease never is seen.

In the afternoons, I either gave prepared lectures or led small group discussions on subjects of the residents' choice. Although the lectures were for the residents, they were attended by all the staff members, radiologists from other hospitals, many academic physicians from other departments, and the technologists.

Last January and February, I was a visiting professor in the Department of Radiology at the University of Nairobi in Kenya for 8 weeks. This was a much larger academic department, with 16 registrars (residents), seven "teaching radiologists," and 12 "government radiologists." Kenyatta National Hospital is a 1600-bed government teaching hospital.

My mornings were spent doing arteriography and trying to get an ancient dedicated mammography machine to work properly. Afternoons were spent with the residents in small group discussions. Lectures were given in the evenings, with attendance by all the radiologists of Nairobi as a result of Chairperson Dr. J. K. Kitonyi's promotion.

In both these locations, I was in the only academic department in the nation. The equipment was minimal and old. Obtaining repairs was difficult. Nuclear imaging and CT were not available. Nairobi did not have sonography because their sonographic machine was broken. No radiation therapy was available anywhere in Nepal.

Despite inadequate equipment, the radiology practiced in these academic departments was first rate. The radiologists were vibrant, enthusiastic, and well trained. They were widely read on current literature. The residents were highly motivated. The strongest impression I have of both departments is the tremendous hunger for knowledge and for information of "how it is done" in Western developed countries. I never have considered myself a good formal lecturer, but it was easy when every member of the audience was hanging onto every word.

Working in a country is quite different from being a tourist. My wife and I were accepted as residents in the country and learned much about politics, culture, and religion. Although we stayed only 3 weeks in Nepal, a 2- to 3-month stay is desirable for good mutual understanding.

These visiting professorships were arranged and supported by the Radiology Outreach Foundation as a part of their goal of providing support to academic radiology departments of developing countries. It is a wonderful experience. I hope that other radiologists will volunteer for this deeply satisfying task.

Willard J. Howland
Canton, OH 44708

Catheters for Barium Enemas

Dr. Gelfand's excellent article [1], "Barium Enemas, Latex Balloons, and Anaphylactic Reactions," in the January issue of the *AJR* nicely summarizes the subject. However, there is a mandatory correction.

Bardex catheters, Model 658 (C. R. Bard, Murray Hill, NJ), have been recalled. Model 659 is still available. Each catheter costs approximately $23, and they should not be resterilized. Although I agree with Dr. Gelfand that resterilization of these catheters is a reasonable procedure, the U. S. Food and Drug Administration disagrees, and it is illegal to reuse these devices.

Also, balloon catheters for barium enemas are available from other manufacturers, such as MMI, Inc., Southfield, MI.

Murray L. Janower
Saint Vincent Hospital, Inc.
Worcester, MA 01604

REFERENCE

1. Gelfand DW. Barium enemas, latex balloons, and anaphylactic reactions. *AJR* **1991**;156:1-2

Reply

Dr. Janower is correct in stating that the manufacturer of Bardex rectal catheters (C. R. Bard, Murray Hill, NJ) recommends that the catheters not be reused. However, it is not illegal to reuse such a device. The unfavorable aspect of reuse lies in any potential liability should reuse result in cross infection due to improper sterilization.

Since I submitted the article on latex allergy [1], my colleagues and I have been using a similar rectal balloon catheter made by Akron Catheter and distributed by Picker International, both of Mayfield, OH. This catheter is designed and recommended for reuse.

The aforementioned catheters are made of latex rubber, as are those made by MMI, Inc., noted by Dr. Janower, and thus they carry the risk of latex allergy. A more definitive solution is the silicon balloon–equipped enema tip recently developed by E-Z-EM, Inc., of Westbury, NY, which should be available by the time this letter and reply are published.

David W. Gelfand
Bowman Gray School of Medicine
Winston-Salem, NC 27103

REFERENCE

1. Gelfand DW. Barium enemas, latex balloons, and anaphylactic reactions. *AJR* **1991**;156:1-2

Barium Enema Retention Catheters

A recent commentary by Dr. Gelfand [1] stated that C. R. Bard, Inc., makes a nondisposable Bardex rubber catheter that can be "repeatedly cleaned, sterilized, and reused" for the purposes of performing a barium enema. Although we appreciate Dr. Gelfand's praise and recommendation of our product, we would like to advise your readers that C. R. Bard manufactures no latex catheters that are intended for reuse or resterilization. Further, using a urinary catheter to perform a barium enema is outside the catheter's indications, and such practices are not endorsed by our company. Bard does, however, manufacture two catheters specifically for use in performing a barium enema: the Weber and the Virden rectal catheters (catalog numbers 658 and 659, respectively; Davol, Inc., 100 Sockanossett Crossroad, P. O. Box 8500, Cranston, RI 02920; 401-463-7000). Both are double-lumen rubber catheters with latex balloons designed to assist in the administration and retention of a barium enema. They are supplied nonsterile and must be sterilized before use. Neither is intended for reuse or resterilization.

I hope that knowledge of the availability of these products and reinforcement of the warnings against their reuse or resterilization will be helpful your readers.

Frank M. Krakowski
C. R. Bard, Inc.
Murray Hill, NJ 07974

REFERENCE

1. Gelfand DW. Barium enemas, latex balloons, and anaphylactic reactions. *AJR* **1991**;156:1–2

Barium Enemas in Older Patients

I read with interest the commentary by David Gelfand, "Barium Enemas, Latex Balloons, and Anaphylactic Reactions" [1], in the January 1991 issue of *AJR*. As he suggests, the proscription against using latex balloons makes it difficult to perform barium enemas on older patients who have poor rectal tone. He recommends taping the patient's buttocks to help retain the enema.

I offer an additional alternative. I have found that a 26-French Foley catheter with a 30-ml silicone rubber balloon (Travenol Laboratories, Inc., Deer Field, IL) is useful in older patients. By using a 5 in 1 Sims Connector (Seamless Hospital Products Co., WallingFord, CT), the Foley catheter can be attached directly to the tubing of the enema bag.

Dimitri Merine
The Johns Hopkins Hospital
Baltimore, MD 21205

REFERENCE

1. Gelfand DW. Barium enemas, latex balloons, and anaphylactic reactions. *AJR* **1991**;156:1–2

Inadvertent Vaginal Filling During a Barium Enema

While reading the letter "Detection of Inadvertent Vaginal Filling During Cystography" from Merchant et al. [1] in the February 1991 issue of *AJR*, I was reminded of one of my most startling moments as a resident. I was doing a repeat barium enema on an attractive, well-coiffed, elderly lady, the reason for which I can no longer remember. While I was seriously studying what appeared to be a very unusual cutoff of the barium column, the patient calmly stated, "Doctor, the last time they did this through the rectum." I nearly fainted! I laugh aloud every time I think of this incident, still astounded by the woman's incredible poise in already compromised circumstances. She is my definition of an unflappable lady!

Sandra B. McCann
Hughston Sports Medicine Hospital
Columbus, GA 31995-3499

REFERENCE

1. Merchant S, Patel V, Morparia H, Someshwar R. Detection of inadvertent vaginal filling during cystography (letter). *AJR* **1991**;156:406–407

Unusual Cause of Obstructive Jaundice

We report a case of obstructive jaundice after cholecystectomy that was due to a foreign body (silk suture) in the common duct.

A 60-year-old woman was admitted with jaundice 3.5 months after she had had cholecystectomy and sphincterotomy. CT showed a dilated biliary tree, and the results of blood chemistry tests were consistent with obstructive jaundice. An ERCP showed a dilated biliary tree and a 1 × 4 cm elongated filling defect in the common duct (Fig. 1). At laparotomy for exploration of the common duct, a free fragment of silk surgical suture was found covered with grumous material.

Stone formation around unusual foreign bodies has been reported; the most common foreign body is silk surgical suture. Ahlberg [1] reported nine cases of stone forming around silk suture and estimated that this complication occurs in 0.6% of all cholecystectomies. He suggested that resorbable suture material be used to ligate the cystic duct. However, nonresorbable suture material or metallic clips continue to be used, presumably because resorbable suture material might allow the cystic duct to open before healing can occur. When the rapidity with which stone formation occurred in this case (3.5 months) is considered, this complication might be possible even with resorbable suture.

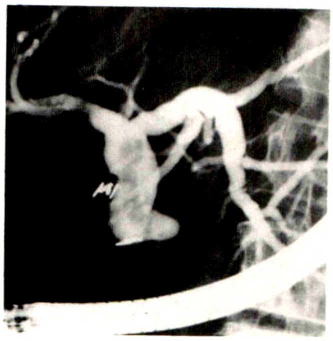

Fig. 1.—ERCP shows elongated filling defect occupying most of common bile duct, with dilated biliary system.

Donald Stallard
Murali Sundaram
St. Louis University, Medical Center
St. Louis, MO 63110-0250

REFERENCE

1. Ahlberg A. Silk ligature as a cause of choledocholithiasis after cholecystectomy. *Acta Chir Scand* **1959**;118:22–24

Dissecting Intramural Hematoma of the Esophagus in Boerhaave Syndrome: CT Findings

A 42-year-old alcoholic man was admitted because of tightness in the chest and substernal pain of acute onset. These symptoms had developed suddenly the day before after he drank alcohol and then vomited. Chest radiograph showed bilateral superior mediastinal and paraspinal widening. Contrast-enhanced CT scan showed a low-attenuation (45 H) lesion encircling the gas-filled esophageal lumen through the entire course of the esophagus (Fig. 1). This abnormality also was found in the gastric fundus and body along the side of the lesser curvature. A high-attenuation rim of uniform thickness, presumed to be the muscular layer of the esophagus, was noted in the outer aspect of the abnormality. Esophagography with 37% Gastrografin (meglumine diatrizoate) showed marked narrowing of the entire esophageal lumen and no extravasation of contrast medium. The diagnosis was extensive intramural hematoma accompanying esophageal perforation. Because the patient was stable, we decided to use conservative treatment. On the patient's fifth day in the hospital, shock suddenly developed. A CT scan showed a high-attenuation hematoma in the distal esophagus, extensive hematoma in the mediastinum, contrast medium from the previous esophagogram in the pleural space, and fluid in the lesser and greater peritoneal sac. At surgery, a deep and extensive laceration in the posterior wall of the gastric cardia and fundus extending to the distal esophagus, empyema, and mediastinal hematoma and abscess were found.

Dallemand et al. [1] reported two cases of intramural hematoma of the esophagus and suggested that the combination of a dissecting intramural hematoma and a perforation of the esophagus is rare. On esophagography, a long, smooth filling defect in the mid and lower esophagus, usually on the posterior wall, is characteristic of intramural hematoma. An esophageal hematoma also may dissect the

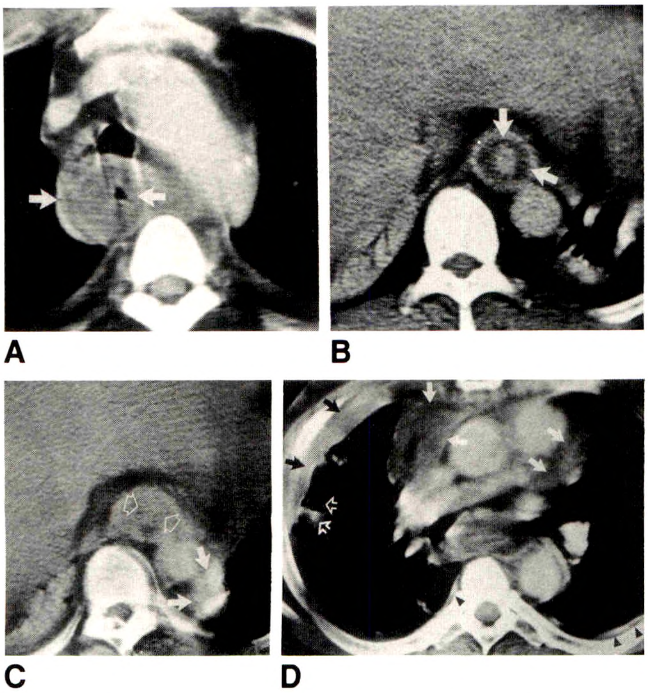

Fig. 1.—Boerhaave syndrome with esophageal intramural hematoma.

***A* and *B*, CT scans obtained at admission. Scan at level of aortic arch (*A*) shows low-attenuation hematoma (*arrows*) encircling gas-filled esophageal lumen and small bilateral pleural effusions. Scan at level of distal esophagus *B* shows low-attenuation lesion surrounding true lumen of esophagus and higher attenuation rim (*arrows*), presumed muscle layer of esophagus, in outer area of hematoma.**

***C* and *D*, CT scans obtained 5 days after admission. Scan (*C*) at same level as *B* shows high-attenuation intramural hematoma (*open arrows*), contrast medium (*solid arrows*) from previous esophagogram in pleural space, and fluid in peritoneal space. Scan at subcarinal level (*D*) shows mediastinal (*white solid arrows*) and pleural (*black arrows*) abscess or hematoma, esophageal hematoma, contrast medium (*arrowheads*) in pleural space, and infrafissural empyema (*white open arrows*) with air-fluid level in right major fissure.**

esophageal wall in a fashion similar to that of an aortic dissection; the result is an esophagus with a double lumen and extensive intramural hematoma, as in our case. In cases of dissecting hematoma, esophagography usually shows a double-barreled esophagus in which contrast medium can be seen in both the true lumen and the false lumen. In some patients, the hematoma does not communicate with the lumen and does not fill with contrast medium [2]. Spontaneous closure of esophageal rupture in Boerhaave syndrome has been reported [3]. In our case, the initial esophagogram showed no extravasation of contrast material, but subsequent CT scans showed contrast material in the pleural space.

Kyung Soo Lee
Il Young Kim
Pyo Nyun Kim
and colleagues
Soonchunhyang University Hospital
Chunan, 330-100, Korea

REFERENCES

1. Dallemand S, Amorosa JK, Morris DW, Iyer S. Intramural hematoma of the esophagus. *Gastrointest Radiol* **1983**;8:7–9
2. Shay SS, Berendson RA, Johnson LF. Esophageal hematoma: four new cases, a review, and proposed etiology. *Dig Dis Sci* **1981**;26:1019–1024
3. Maglinte DDT, Edwards MC. Spontaneous closure of esophageal tear in Boerhaave's syndrome. *Gastrointest Radiol* **1979**;4:223–225

Trilateral Retinoblastoma

A 5-month-old male neonate had bilateral leukocoria and inability to follow a light source. White reflex was present in both eyes. CT showed calcified masses in both retinas (Fig. 1A). Both optic nerves were normal, and no tumor spread was evident. Cranial CT showed a large enhancing mass with well-defined margins in the region of the pineal gland (Fig. 1B). The posterior third ventricle was obliterated, and the anterior third ventricle and lateral ventricles were mildly dilated. The right eyeball was enucleated, and histologic examination confirmed the diagnosis of retinoblastoma. The patient received radiotherapy and chemotherapy. A repeat CT scan done after 2 months showed a reduction in the size of the left eye and pineal masses. The patient's parents refused enucleation of the left eye, and he was discharged.

Multicentric retinoblastomas are known to be associated with a number of extra- and intracranial tumors [1]. Of these, pineal neoplasms are of special interest because they have been shown to be histologically identical to retinoblastomas [2]. Other pineal neoplasms such as pineoblastomas are rare in children, and the pineal gland of lower animals is known to have photoreceptor cells that are functionally and morphologically similar to retinal photoreceptors. On the basis of these findings, it has been suggested that the pineal neoplasm in cases of multicentric retinoblastomas is a true retinoblastoma, and the syndrome is termed trilateral retinoblastoma [3]. Eleven cases of this rare condition have been reported so far [4]. Simultaneous detection of intracranial and orbital neoplasms and the early onset were unique features in our case. Also, CT findings were not recorded in any of the cases reported earlier. CT allows simultaneous examination of the orbital contents and intracranial region, and pineal neoplasms thus can be detected well before they become symptomatic. In the earlier cases, the pineal neoplasm may have been present initially but remained undetected until it became symptomatic. The occasional occurrence of trilateral retinoblastomas makes it imperative that CT examination of retinoblastomas include a routine intracranial scan so that any pineal neoplasms present are not missed.

Mandira Mukherjee
Rajesh Gothi
Shyam S. Doda
Sudershan K. Aggarwal
Diwan Chand Satpal Aggarwal Imaging Research Centre
New Delhi-110001, India

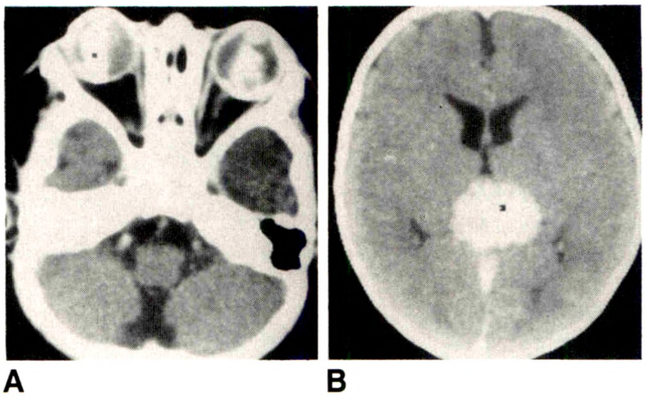

Fig. 1.—Trilateral retinoblastoma.

***A*, Axial CT scan through orbits shows bilateral retinoblastoma. Optic nerves are not involved.**

***B*, CT scan obtained after administration of contrast material shows a large enhancing pineal mass.**

REFERENCES

1. Jakobiec FA, Tso MD, Zimmerman LE, Davis P. Retinoblastoma and intracranial malignancy. *Cancer* **1977**;39:2048–2058
2. Bader JL, Meadows AT, Zimmerman LE, et al. Bilateral retinoblastoma with ectopic intracranial retinoblastoma: trilateral retinoblastoma. *Cancer Genet Cytogenet* **1982**;5:203–213
3. Bader JL, Miller RW, Meadows AT, Zimmerman LE, Champion LAA, Voute PA. Trilateral retinoblastoma. *Lancet* **1980**;2:582–583
4. Zimmerman LE, Burns RP, Wankun G, Tully R, Esterly JA. Trilateral retinoblastoma: ectopic intracranial retinoblastoma associated with bilateral retinoblastoma. *J Paediatr Ophthalmol Strabismus* **1982**;19:320–325

Percutaneous Retrieval of Tandem Right Atrial Greenfield Filters

Migration of Greenfield inferior vena caval filters is a complication reported in 7–9% of cases [1]. Several techniques have been devised to remove a migrated filter percutaneously. We recently had an unusual situation in which two Greenfield filters had migrated inadvertently to the patient's right atrium.

A 67-year-old man was treated for pulmonary embolism, which recurred despite adequate anticoagulation at another institution. Via a jugular cut-down approach, a vascular surgeon released two Greenfield filters, which migrated to the patient's right atrium (Fig. 1). Three days later, the patient was transferred to our institution for further management of his extensive pulmonary embolism and migrated filters. Because of his tenuous clinical status, we decided to use percutaneous retrieval rather than surgical removal. Both filters were removed readily by using the technique described by Tsai et al. [2].

Shortly after the procedure, the patient died. An autopsy showed that the cause of death was massive subacute and chronic pulmonary embolism. Careful examination of the right side of the heart showed only a 1-mm nick of a chorda tendineae cordis. No other significant injury to the endocardium or myocardium was found.

To the best of our knowledge, only four cases of percutaneous retrieval of intracardiac migrated Greenfield filters have been reported in the English literature, and no cases of two simultaneously migrated filters [3, 4]. In limited animal studies, Greenfield and Crute [5] showed that misplaced filters could be retrieved and removed up to 7 days after insertion without significant risk of injury to the heart. This case illustrates that migrated Greenfield filters can be retrieved percutaneously from the right atrium without significant injury to the endocardium despite the relative vigorous instrumentation required to capture and remove them.

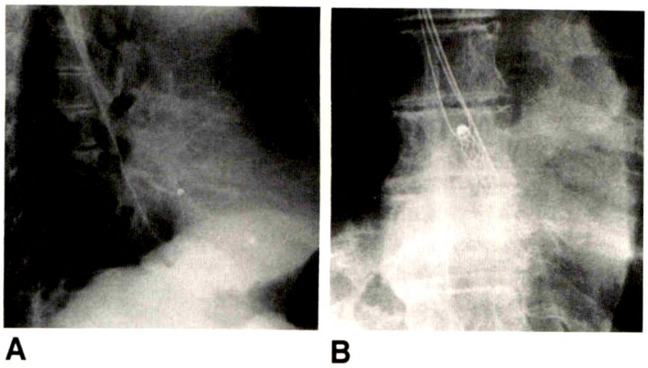

Fig. 1.—Percutaneous removal of intracardiac Greenfield filters.
***A,* Lateral chest radiograph shows vertically and horizontally oriented Greenfield filters in right atrium.**
***B,* Frontal chest radiograph obtained after retrieval of one filter shows capture and removal of the second filter.**

Michael A. Braun
Mark B. Collins
Mohammed Sarrafizadeh
Allan R. Koslow
Albany Medical Center Hospital
Albany, NY 12208

REFERENCES

1. Greenfield LJ, Peyton R, Crute S, Barnes R. Greenfield vena caval filter experience: later results in 156 patients. *Arch Surg* **1981**;116:599–606
2. Tsai FY, Myers TV, Ashraf A, Shah DC. Aberrant placement of a Kimray-Greenfield filter in the right atrium: percutaneous retrieval. *Radiology* **1988**;167:423–424
3. Yakes WF. Percutaneous retrieval of Kimray-Greenfield filter from right atrium and placement in inferior vena cava. *Radiology* **1988**;169:849–851
4. Deutsch LS. Percutaneous removal of intracardiac Greenfield vena caval filter. *AJR* **1988**:151:677–679
5. Greenfield LJ, Crute SL. Retrieval of the Greenfield vena caval filter. *Surgery* **1980**;11:719–722

Ipsilateral Antegrade Femoral Arteriography

The catheter described for conversion of retrograde to antegrade catheterization of the femoral artery [1] also has been used for ipsilateral antegrade femoral arteriography in 45 patients. We have used this technique in patients who require unilateral arteriograms of the lower extremity when visualization of the aortic bifurcation and iliac arteries is not needed.

The catheter has a double curve and is triangular (Cook Inc., Bloomington, IN). The common femoral artery is catheterized by using the Seldinger technique. The tip of the catheter is inserted into a visceral or renal artery, and by means of a pushing and rotational motion of the catheter at the groin, the triangular shape of the catheter is reformed. The catheter then is brought down into the common and external iliac artery with its tip facing the lateral wall. The catheter is placed in the middle of the external iliac artery for the angiogram (Fig. 1). Twenty milliliters of a medium-density contrast material is injected at 5 ml/sec. Diagnostic studies are obtained in all cases.

The advantage of this technique is the smaller volume of contrast material used in diagnostic studies. The entire bolus of contrast material injected is used to opacify the vessels in the lower extremity.

Yashwant D. Patel
Albert Einstein College of Medicine
Bronx, NY 10461

REFERENCE

1. Patel YD. Catheter for conversion of retrograde to antegrade femoral artery catheterization. *AJR* **1990**;154:179–180

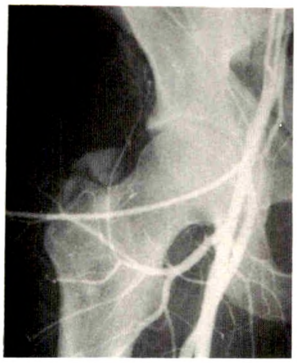

Fig. 1.—Angiogram shows catheter in external iliac artery for antegrade femoral arteriography.

Nomenclature of Veins in the Lower Extremity

Recently, some of our referring clinicians have been misled by the diagnosis of thrombus in the "superficial femoral vein," thinking that the clot did not predispose to pulmonary embolism because it was in a superficial vein. This prompted us to review the nomenclature of the veins in the lower extremity.

According to anatomy texts [1, 2], the deep veins of the leg are the *popliteal vein* from the junction of the *anterior and posterior tibial veins* to the adductor canal, the *femoral vein* from the adductor canal to the inguinal ligament, and the *profunda femoris vein* draining the thigh muscles and joining the femoral vein just below the inguinal ligament. These are named for the accompanying arteries. The superficial veins of the thigh are somewhat variable but include the *great (long) saphenous vein*, the *medial and lateral cutaneous veins*, the *superficial epigastric vein*, the *superficial circumflex iliac vein*, and the *external pudendal vein*. They lie in the subcutaneous fat, superficial to the muscles.

Many radiologists refer to the deep veins of the thigh as (1) the *superficial femoral vein* from the adductor canal to its junction with the profunda femoris vein and (2) the *common femoral vein* from the junction to the inguinal ligament [3–5]. Unfortunately, the term *superficial femoral vein* is a misnomer, as this vessel is a deep vein. As significant pulmonary embolism is thought to arise only from the deep veins, a physician whose anatomic knowledge is rusty may be confused by the diagnosis of thrombosis in a "superficial" vein. Therefore, we have returned to standard anatomic nomenclature for these veins in the interests of better communication with our clinicians and of anatomic precision.

Eric L. Bressler
Suburban Radiologic Consultants, Ltd.
Riverside Medical Center
Minneapolis, MN 55454

REFERENCES

1. Hollinshead WH. *Textbook of anatomy.* New York: Harper & Row, **1962**:441
2. Gray H. *Anatomy, descriptive and surgical.* New York: Bounty Books, **1977**:6163.
3. Abrams HL, ed. *Abrams angiography: vascular and interventional radiology*, 3rd ed. Boston: Little, Brown, **1983**:1879–1881
4. Foley WD, Middleton WD, Lawson TL, et al. Color Doppler ultrasound imaging of lower extremity venous disease. *AJR* **1989**;152:371–376
5. Vogel P, Laing FC, Jeffrey RB Jr, Wing VW. Deep venous thrombosis of the lower extremity: US evaluation. *Radiology* **1987**;163:747–751

Carotid Sonography Contralateral to Severe Stenosis

Beckett et al. [1] describe a series of 23 patients in whom they used carotid duplex sonography to examine the artery contralateral to an artery that had significant stenosis or occlusion. The authors conclude that an increase in blood-flow velocity in the internal carotid artery on the side opposite an artery with a tight stenosis or occlusion is a common source of error.

This conclusion is opposite that drawn by Robinson et al. [2]. In that study, my colleagues and I found only a weak correlation between the peak systolic velocity (PSV) in the ipsilateral nonstenotic vessel compared with the area of stenosis in the contralateral vessel ($r^2 = .036$, $p = .21$). This included 19 vessels with a contralateral stenosis of >90% reduction in area or occlusion (Fig. 1 from Robinson [2]). We think these discrepant conclusions can be explained as follows.

First, the diagnostic duplex sonographic criteria for stenosis used by Beckett et al. may be too liberal. They used criteria published by Bluth et al. [3] but relied entirely on peak systolic velocity ratio (SVR). Bluth et al. [3] also describe criteria that include PSV, peak end-diastolic velocity (PEDV), diastolic velocity ratio, and spectral broadening. Of the nine cases with a stenosis overestimated on Doppler sonography, two were attributed to tortuosity of the vessel and inability to see the vessel well. Of the remaining seven, only four fulfill the criterion of Bluth et al. of SVR >1.8, and only three fulfill the criterion of PEDV >40 cm/sec for the diagnosis of a stenosis >60% in diameter. If our criteria [2] had been applied, only four of the seven patients would have reached the threshold criterion of SVR >2.0, and none would have reached the threshold criterion of PEDV >50 cm/sec for a >70% area (45% in diameter) of stenosis. When the two criteria are in disagreement, a third criterion, such as PSV, may be helpful. These data are not provided by Beckett et al. for their patients, but examination of their Figure 2 shows a PSV estimated as about 110 cm/sec by comparison with the displayed PEDV of 36 cm/sec. This meets neither threshold (Bluth et al. or Robinson et al.) for a stenosis >60% in diameter. Therefore, we think that few, if any, of the patients presented had duplex examinations that overestimated the degree of stenosis found at angiography.

Second, for PSV <130 cm/sec, PSV may be more accurate than SVR in excluding significant stenosis. In the series of 205 vessels that we examined [2], no vessels had an area of stenosis >70% (45% diameter) if the PSV was <130 cm/sec. This included 17 vessels with SVR >1.8 and seven vessels with SVR >2. For this reason, information about PSV in the series of Beckett et al. would be useful.

Third, the diameter of stenosis determined on the basis of angiography may not be accurate. As stated by Bluth et al., asymmetric stenoses are assessed most reliably by determining the percentage of the area that is stenotic. The criteria of Bluth et al. are based on the diameter of stenosis as measured from the narrowest section of the vessel, which was the measurement also used by Beckett et al. The criteria of Robinson et al. are based on calculations that determine the area of stenosis by using measurements of the reduction in diameter in two planes. If the patients presented had asymmetric stenoses, the criteria of Robinson et al. would be preferable.

For these reasons, we disagree with the conclusion of Beckett et al. that use of duplex sonography to determine the degree of stenosis in the carotid artery contralateral to a severely stenotic or occluded internal carotid artery is more prone to error than is use of duplex sonography in general.

David Sacks
Reading Hospital
West Reading, PA 19603

REFERENCES

1. Beckett WW Jr, Davis PC, Hoffman JC Jr. Duplex Doppler sonography of the carotid artery: false-positive results in an artery contralateral to an artery with marked stenosis. *AJNR* **1990**;11:1049–1053, *AJR* **1990**; 155:1091–1095
2. Robinson ML, Sacks D, Perlmutter GS, Marinelli DL. Diagnostic criteria for carotid duplex sonography. *AJR* **1988**;151:1045–1049
3. Bluth EI, Stavros AT, Marich KW, Wetzner SM, Aufrichtig D, Baker JD. Carotid duplex sonography: a multicenter recommendation for standardized imaging and Doppler criteria. *RadioGraphics* **1988**;8:487–506

Reply

We appreciate Dr. Sacks's interest in our work on duplex sonography [1], and we would like to address the points that he has questioned.

Our criteria for grading stenoses are adapted from those of Zweibel and Dreisbach (refresher course presented at the annual meeting of the Radiological Society of North American, December 1986), as shown in Table 1 of our paper [1]. Although these criteria rely heavily on systolic velocity ratio (SVR), they also include real-time imaging and peak end-diastolic velocity (PEDV). The criteria of Bluth et al. [2] and Robinson et al. [3] had not been published when we did our study (January 1987 to May 1988). Our results might have been slightly different if we had used different duplex sonographic quantifications for our criteria. We chose to use diameter rather than area for angiographic and duplex sonographic measurements of stenosis so that our measurements would correlate better with many previous studies, which have achieved accurate duplex sonographic quantification of stenosis by using measurements of diameter.

Our criteria for overestimation were that a vessel be miscategorized on the basis of duplex sonographic criteria; that is, the stenosis would be more severe according to duplex sonographic measurements than shown angiographically. We did not suggest that the degree of overestimation necessarily placed that vessel in a hemodynamically significant category. Several of the vessels for which stenosis was overestimated on the basis of duplex sonographic data would not be hemodynamically significant by any criteria. The patient shown in Figure 2 of our paper (peak systolic velocity [PSV], 112; SVR, 2.0; and PEDV, 36 cm/sec) meets criteria for both the 40–59% and the 60–79% categories of Bluth et al. Thus, these criteria, like all grading systems, are guidelines that must be applied in real life to patients who may not fall into a clearly defined category.

We do not use degree of spectral broadening for grading stenosis. Spectral broadening is neither a necessary nor a sufficient criterion for quantification of stenosis. It is a common occurrence in the absence of stenosis and is associated with vessel branching, tortuosity, changes in vessel diameter (i.e., carotid bulb), and so forth [4].

Our criteria as adapted from Zweibel and Dreisbach stress SVR rather than PSV. We think this is necessary because many of our patients with hypertension or aortic valve disease have elevated PSV throughout the common and internal carotid arteries. In this setting, we think that an arbitrary threshold value for the PSV of the internal carotid artery has less significance than the ratio of internal carotid to common carotid velocity. We are not aware of data suggesting that measurements of PSV are superior to measurements of SVR for quantification of stenosis. Robinson et al. found that PSV, SVR, and PEDV were "equivalent predictors of significant disease"; PSV was preferred in that study because of the "ease of measurement" [4]. Previously reported studies [3, 5] have used multiple parameters for quantification of stenosis; SVR was equally, if not more, reliable than PSV for this purpose.

Patricia C. Davis
William W. Beckett, Jr.
James C. Hoffman, Jr.
Emory University School of Medicine
Atlanta, GA 30322

REFERENCES

1. Beckett WW Jr, Davis PC, Hoffman JC Jr. Duplex Doppler sonography of the carotid artery: false-positive results in an artery contralateral to an artery with marked stenosis. *AJNR* **1990**;11:1049–1053, *AJR* **1990**;155:1091–1095
2. Bluth EI, Stavros AT, Marich KW, Wetzner SM, Aufrichtig D, Baker JD. Carotid duplex sonography: a multicenter recommendation for standardized imaging and Doppler criteria. *RadioGraphics* **1988**;8:487–506
3. Robinson ML, Sacks D, Perlmutter GS, Marinelli DL. Diagnostic criteria for carotid duplex sonography. *AJR* **1988**;151:1045–1049
4. Powis RL. Doppler spectral broadening in normal blood flow and disease. *Am Rev Diagn* **1983**;1:3–8
5. Garth KE, Carroll BA, Sommer FG, Oppenheimer DA. Duplex ultrasound scanning of the carotid arteries with velocity spectrum analysis. *Radiology* **1983**;147:823–827

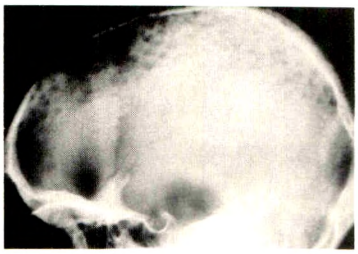

Fig. 1.—Radiograph shows multiple osteolytic defects in skull extending from frontal area to posterior parietal region in a bandlike fashion.

Multiple Osteolytic Skull Defects: Significance of a Band Pattern

Multiple osteolytic defects in the skull are a well-established radiologic entity. Iatrogenic causes for the appearance of such lesions rarely have been described. We report one more iatrogenic cause.

During a routine reporting session, we saw a lateral radiograph of the skull that showed multiple small osteolytic defects. The defects were well defined, strikingly equal in size, and fairly evenly spaced. Another odd feature was their bandlike distribution from the frontal to the posterior parietal region (Fig. 1). This bandlike pattern along with the equal size and even spacing suggested an iatrogenic cause, which was confirmed. Details are as follows.

A 19-year-old woman had a gross avulsion injury of the scalp as a result of having her long hair entangled in a weaving machine. The scalp was avulsed from the frontal area up to the posterior parietal region. Skull radiographs at admission were normal. After a period of primary treatment, which was complicated by wound infection, the plastic surgeons decided to enhance the chances of the wound's healing by drilling the outer table of the skull. Multiple small holes were drilled in the outer table, extending from the frontal region to the posterior parietal region. These were the osteolytic skull defects noted on the radiograph we saw.

Trephining of the skull was performed by the Incas of Peru before 1500 A.D. [1]. Spontaneous healing apparently occurred in many cases of infection that complicated this ancient practice. Multiple surgical holes also have been made on one side of the cranium for the treatment of epilepsy or for benign intracranial hypertension (pseudotumor cerebri) [1]. A regular array of discrete round holes was fashioned in Turkey in an effort to promote vascularization and growth of skin grafts [1]. In our case, holes were drilled in the outer table to promote the growth of granulation tissue from the diploë so that grafting could be attempted later.

Vimal H. Patel
Suleman Merchant
Abbas Mistry
and colleagues
King Edward Memorial Hospital
Parel, Bombay 400 012, India

REFERENCE

1. Hodges FJ III. Pathology of the skull. In: Taveras JM, ed. *Radiology: diagnosis, imaging, intervention*, vol. 3. *Neuroradiology and radiology of the head and neck.* Philadelphia: Lippincott, **1986**:1–21

Letters are published at the discretion of the Editor and are subject to editing.

Letters to the Editor must not be more than two *double-spaced*, typewritten pages. One or two figures may be included. Abbreviations should not be used. See Author Guidelines, page A5.

Material being submitted or published elsewhere should not be duplicated in letters, and authors of letters must disclose financial associations or other possible conflicts of interest.

Letters concerning a paper published in the *AJR* will be sent to the authors of the paper for a reply to be published in the same issue. Opinions expressed in the Letters to the Editor do not necessarily reflect the opinions of the Editor.

Review of Current Literature

Initials and addresses of corresponding authors are provided in parentheses for each article so that the reader can obtain reprints directly. Abstracts are printed verbatim from each journal.

The New England Journal of Medicine

Twelve-year comparison of a Bjork-Shiley mechanical heart valve with porcine bioprostheses. Bloomfield P, Wheatley DJ, Prescott RJ, Miller HC (HCM, Dept. of Cardiology, Royal Infirmary, Edinburgh EH3 9YW, Scotland). *N Engl J Med* 324(9):573-579, Feb. 1991

Background. Patients undergoing heart-valve replacement may receive a mechanical prosthesis, necessitating lifelong anticoagulant treatment, or a porcine bioprosthesis, which involves no absolute need for anticoagulants.

Methods. We carried out a randomized, prospective trial to compare the durability of the Bjork-Shiley mechanical prosthesis (spherical tilting-disk model) and the incidence of valve-related complications with those variables in the Hancock and the Carpentier-Edwards porcine prostheses. The mitral valve was replaced in 261 patients, the aortic valve in 211, and both in 61; the survivors have been followed up for a mean of 12 years.

Results. We found a trend toward improved actuarial survival after 12 years with the Bjork-Shiley prosthesis, but this trend was not statistically significant (group with Bjork-Shiley valve vs. group with porcine valve [mean ± SE], 51.5 ± 3.2 vs. 44.4 ± 3.2 percent; $P = 0.08$). There was no significant difference in the actuarial incidence of reoperation after 5 years, but after 12 years significantly more patients with a porcine prosthesis had undergone reoperation (8.5 ± 2.0 vs. 37.1 ± 4.1 percent, $P < 0.001$). An analysis combining death and reoperation as end points for an actuarial assessment of survival with the original prosthesis intact confirmed that the patients with Bjork-Shiley prostheses had improved survival (48.6 ± 3.2 vs. 30.0 ± 3.0 percent after 12 years, $P < 0.001$). Bleeding requiring hospitalization or blood transfusion was significantly more frequent in the patients with Bjork-Shiley prostheses (18.6 ± 3.2 vs. 7.1 ± 2.3 percent after 12 years, $P < 0.01$). There was no significant difference after 12 years in the actuarial occurrence of embolism (Bjork-Shiley vs. porcine, 21.1 ± 3.1 vs. 26.4 ± 3.5 percent) or endocarditis (3.7 ± 1.4 vs. 4.6 ± 1.6 percent).

Conclusions. Survival with an intact valve is better among patients with the Bjork-Shiley spherical tilting-disk prosthesis than among patients with porcine bioprostheses, but use of the Bjork-Shiley valve carries an attendant increased risk of bleeding associated with the need for anticoagulant treatment.

Chest

Treatment of end-stage chronic obstructive pulmonary disease with double lung transplantation. Emery RW, Graif JL, Hale K, et al. (RWE, 920 E. 28th St., Minneapolis, MN 55407). *Chest* 99(3):533-537, March 1991

Six patients with end-stage emphysema (age 44 ± 2 years) underwent double lung transplantation (Tx) from June 1988 through May 1990. All suffered from severe inanition and required oxygen therapy. The ischemic time was 193 ± 28 minutes. Post-Tx immune suppression was OKT3 (14 days), cyclosporine (trough levels of 150 ± 25 ng/ml), azathioprine to keep WBC at 3,000 to 5,000/cu mm (1 to 3.0 mg/kg/day) and following OKT3, a tapering prednisone regimen. Two rejection episodes that occurred in two patients on post-Tx day 5 and 10 were treated with bolus doses of methylprednisolone. The mean hospital stay was 32 ± 7 days (range, 20 to 69 days). Four patients required treatment of cytomegalovirus (CMV) infection: gastritis (+donor, +recipient) in one and CMV pneumonia in two (+donor, −recipient). A fourth (+donor, −recipient) had right-sided Candida empyema six weeks post-Tx, developed CMV and staphylococcal sepsis, and died 64 days post-Tx. One patient required pyloroplasty eight weeks post-Tx and one patient underwent tracheal suture line repair at eight weeks. During a follow-up of 81 patients months (range, 8 to 24 months), one patient had developed Epstein-Barr viral (EBV) induced lymphoproliferative disease in the lung and one patient had developed EBV lymphoma. Three patients are at work, one is continuing rehabilitation, and one is at home. Double lung Tx offers a definitive benefit to patients with emphysema; however, a prolonged postoperative course can be expected. Viral infections remain serious but treatable problems.

Gastroenterology

Adenovirus colitis in the acquired immunodeficiency syndrome. Janoff EN, Orenstein JM, Manischewitz JF, Smith PD (ENJ, Infectious Disease Section, Dept. of Medicine, Veterans Affairs Medical Center, University of Minnesota School of Medicine, Minneapolis, MN). *Gastroenterology* 100:976-979, 1991

Adenovirus was identified in colonic tissue by transmission electron microscopy or culture in 5 of 67 (7.4%) homosexual men seropositive for human immunodeficiency virus (51 with the acquired immunodeficiency syndrome) with diarrhea. Colonoscopy showed the mucosa to be normal in 3 cases and mildly inflamed in 2. Light microscopy showed foci of mucosal necrosis that contained chronic inflammatory cells and degenerating and necrotic epithelial cells with amphophilic nuclear inclusions. By transmission electron microscopy, hexagonal viral particles characteristic of adenovirus were identified within the inclusions. Only 1 patient was concomitantly infected by a second potential enteric pathogen. It was concluded that adenovirus, an uncommon enteric pathogen in immunocompetent adults, causes intestinal pathology and may be associated with diarrheal illness in persons with the acquired immunodeficiency syndrome.

Reprinted with permission by the American Gastroenterological Association.

Adenocarcinomas of the colon and rectum in persons under 40 years old: a population-based study. Griffin PM, Liff JM, Greenberg RS, Clark WS (PMG, Enteric Diseases Branch, Division of Bacterial and Mycotic Diseases, Center for Infectious Diseases, Centers for Disease Control, Public Health Service, U.S. Dept. of Health and Human Services, Atlanta, GA). *Gastroenterology* 100:1033–1040, 1991

Data collected by nine population-based tumor registries participating in the Surveillance, Epidemiology, and End Results Program of the National Cancer Institute were analyzed to characterize the epidemiology of noncarcinoid adenocarcinomas of the colon and rectum in young adults. Tumors diagnosed in persons under 40 years old between 1973 and 1984 (n = 1736) were compared with those in persons 40 years and older (n = 106,760). This first large U.S. population-based study of colorectal adenocarcinomas in the young shows a higher incidence in blacks than whites and later detection in black males. It also shows a higher proportion of tumors of mucinous and signet ring histological type than in older age groups. Among the younger group, the average annual age-adjusted incidence rate was 34% higher in black males than in white males (12.6 vs. 9.4 per million persons) and 46% higher in black females than in white females (13.0 vs. 8.9 per million persons). The proportion of tumors that were right-sided varied by age: 0–29 years, 30%; 30–39 years, 26%; 40–49 years, 22%; 50–59 years, 21%; 60–69 years, 24%; 70–79 years, 30%; and 80+ years, 35%. Males under age 40 were less likely to present with localized disease (whites, 27%; blacks, 21%) than were those aged 40 and older (whites, 39%; blacks, 36%). The proportion of tumors classified as mucinous decreased with age, from 28% among those aged 0–19 years to 5% among those 40 years and older. A similar trend was observed for signet ring tumors. Although this latter type accounted for 10% of large-bowel tumors among subjects aged 0–19 years, this proportion decreased with age to 0.2% in those 40 years and older.

Reprinted with permission of the American Gastroenterological Association.

Quantitative cholescintigraphy in the assessment of choledochoduodenal bile flow. Cicala M, Scopinaro F, Corazziari E, et al. (MC, Cattedra di Gastroenterologia I, Clinica Medica II, Universitá La Sapienza, Rome, Italy). *Gastroenterology* 100:1106–1113, 1991

Quantitative cholescintigraphy has been proposed as a noninvasive method to assess function of the sphincter of Oddi in cholecystectomized subjects. The present study evaluated several quantitative cholescintigraphic variables to assess their time-related variability as well as their capability to detect delay of choledochoduodenal bile flow. Cholescintigraphy with 2,6-diethylphenylcarbahoylmethyl diacetic acid ^{99m}Tc was performed in 24 cholecystectomized patients with recurrent biliarylike pain, laboratory evidence of bile stasis, normal hepatocelluar function tests, and no evidence of choledocholithiasis. The study was also performed in 26 asymptomatic cholecystectomized subjects and repeated at 2-week intervals during identical experimental conditions in 10 of them. Of the following quantitative cholescintigraphic variables investigated, (a) hepatic T peak, (b) 50% hepatic retention (T peak, ½), (c) percent hepatic retention at 30 minutes, (d) percent hepatic retention at 40 minutes, (e) vein–hepatic hilum transit time, (f) vein–duodenum transit time, and (g) hepatic hilum–duodenum transit time, only the hepatic hilum–duodenum transit time showed a statistically significant correlation between the duplicate studies. Only vein-duodenum transit time and hepatic hilum–duodenum transit time discriminated the symptomatic from the asymptomatic patients; of the two variables, however, hepatic hilum–duodenum transit time showed less intrasubject variability and no overlap between the two groups of patients. Hepatic hilum–duodenum transit time showed a positive linear correlation with the maximum diameter of the choledochus. It is concluded that in cholecystectomized patients, the hepatic hilum–duodenum transit time appears to detect a delay of bile flow into the intestine better than any other cholescintigraphic variable. However, in patients with a dilated common bile duct, this variable cannot discriminate bile flow delay due to increased choledochal capacity and/or obstruction of the sphincter of Oddi.

Reprinted with permission by the American Gastroenterological Association.

Digestive Diseases and Sciences

Biliary pain in postcholecystectomy patients without biliary obstruction: a prospective radionuclide study. Grimon G, Buffet C, André L, Etienne JP, Desgrez A (GG, Hopital de Bicetre, 94700 Le Kremlin-Bicetre, France). *Dig Dis Sci* 36(3):317–320, March 1991

Biliary pain without obvious biliary obstruction is common in postcholecystectomy patients. We studied 20 symptomatic patients with episodes of biliary-type pain after cholecystectomy (all having undergone endoscopic retrograde cholangiography), and in 18 asymptomatic postcholecystectomy controls. We performed quantitative hepatobiliary radionuclide analysis with dimethyl-imidodiacetic acid. From a series of 90 dynamic images at 1-min intervals using a gamma camera coupled to a computer, time–activity curves were produced in regions of interest in the liver, intrahepatic biliary tree, common duct, and heart, from which quantitative biliary excretion indexes were obtained. The results demonstrate a biliary kinetic dysfunction in patients with postcholecystectomy pain without morphological abnormalities.

The Journal of Bone and Joint Surgery

Total hip replacement with cemented, uncemented, and hybrid prostheses: a comparison of clinical and radiographic results at two and four years. Wixson RL, Stulberg SD, Mehlhoff M (RLW, 233 E. Erie St., Chicago, IL 60611). *J Bone Joint Surg [Am]* 73-A(2):257–270, Feb. 1991

One hundred and thirty-one patients who had 144 cemented or uncemented hip prostheses were followed prospectively for two to four years. A cemented or a hybrid prosthesis (consisting of a cemented femoral component and an uncemented acetabular component) was used in men older than seventy years, in women older than sixty years, and in younger patients in whom adequate initial fixation could not be obtained without cement. Uncemented, porous-surfaced implants were used in all other patients.

The over-all clinical results were similar for the three groups. For the fifty-two hips that had a cemented prosthesis, the mean total Harris hip rating was 91 points and the score for pain, 42 points; for the twenty-seven hips that had a hybrid prosthesis, 90 and 43 points; and for the sixty-five hips that had an implant allowing ingrowth of bone in both the acetabulum and the femur, 95 and 43 points.

Two prosthetic stems that were designed to allow ingrowth of bone had aseptic loosening; one was revised. Pain in the thigh, usually slight and not disabling, occurred at one year in 24 per cent of the patients in whom a femoral component allowing ingrowth had been used; the prevalence of pain then declined. The incidences of migration of the components and of radiolucent lines were greater in the acetabula that had a cemented component than in those that had a cup allowing ingrowth of bone.

Clinical Orthopaedics and Related Research

A clinical perspective on common forms of acquired heterotopic ossification. Garland DE (DEG, Rancho Los Amigos Medical Center, 7601 E. Imperial Hwy., Downey, CA 90242). *Clin Orthop* 263:13–29, Feb. 1991

The clinical courses of heterotopic ossification (HO) as a consequence of trauma and central nervous system insults have many similarities as well as dissimilarities. Detection is commonly noted at two months. The incidence of clinically significant HO is 10%–20%. Approximately 10% of the HO is massive and causes severe restriction in joint motion or ankylosis. The most common sign and symptom are decreased range of motion and pain. The locations are the proximal limbs and joints. Sites of HO about a joint may vary according to the etiology of the HO. Roentgenographic evolution of HO occurs during a six-month period in the majority of patients. Treatment modalities include diphosphonates, indomethacin, radiation, range of motion exercises, and surgical excision. Surgical timing differs according to etiology; traumatic HO may be resected at six months; spinal cord injury HO is excised at one year; and traumatic brain injury HO is removed at 1.5 years. A small number of patients have progression of HO with medicinal treatment and recurrence after resection. The patients seem recalcitrant to present treatment methods regardless of the HO etiology.

Congenital anomalies of the cervical spine. Hensinger RN (RNH, Section of Orthopaedic Surgery, 1500 E. Medical Center Dr., 2912 TC/0328, Ann Arbor, MI 48109). *Clin Orthop* 264:16–38, March 1991

Congenital anomalies of the cervical spine are uncommon. The majority of afflicted individuals are asymptomatic or have only mild restriction of neck motion. If symptoms develop, they are usually due to cervical instability or degenerative osteoarthrosis. Recent information indicates that patients with upper cervical anomalies such as atlantooccipital fusion, anomalies of the odontoid, or the transverse atlantal ligament have a great propensity to develop early instability and neurologic problems secondary to minor traumatic events. If symptoms occur in the lower cervical spine, it is usually in adult life and due to degenerative arthritis in the hypermobile articulations adjacent to the area of synostosis. The relatively good prognosis of cervical lesions is overshadowed by the "hidden" or unrecognized associated anomalies. There is a high incidence of significant scoliosis. Sprengel's deformity, renal anomalies, deafness, and neurologic malformations. Early recognition and treatment of these problems may be of substantial benefit, sparing the patient further deformity or serious illness.

The Journal of Urology

Spontaneous perinephric hemorrhage: imaging and management. Zagoria RJ, Dyer RB, Assimos DG, Scharling ES, Quinn SF (RJZ, Dept. of Radiology, Bowman Gray School of Medicine, Winston-Salem, NC 27103). *J Urol* 145:468–471, March 1991

We report on 10 patients with spontaneous perinephric hemorrhage associated with underlying disease, including renal cell carcinoma (5), angiomyolipoma (2), malignant melanoma (1), periarteritis nodosa (1) and severe portal hypertension (1). The etiology could not be identified with computerized tomography (CT) in 5 cases (50%), including 2 renal cell carcinomas, 1 angiomyolipoma, 1 periarteritis nodosa and 1 portal hypertension. Arteriography demonstrated underlying lesions in 4 of these 5 cases (80%) including the case of vasculitis. CT combined with magnetic resonance imaging is accurate for the diagnosis of spontaneous perinephric hemorrhage but the underlying pathological condition is often undetectable in the acute phase due to the perinephric blood. CT should be the first study performed if this diagnosis is suspected. Arteriography is recommended if a renal mass is not detected. If a mass is not identified with these 2 imaging studies and the patient is clinically stable, followup thin slice CT should be performed.

Gastrointestinal Radiology

Duodenitis: a reliable radiologic diagnosis? Levine MS, Turner D, Ekberg O, Rubesin SE, Katzka DA (MSL, Dept. of Radiology, Hospital of the University of Pennsylvania, 3400 Spruce St., Philadelphia, PA 19104). *Gastrointest Radiol* 16:99–103, 1991

The authors performed a retrospective study of 50 patients with endoscopically diagnosed duodenitis who had undergone double-contrast upper gastrointestinal (GI) examinations. Duodenitis was diagnosed on the original radiographic reports in six of 37 patients (16%) with mild-to-moderate duodenitis, five of 13 patients (38%) with severe duodenitis, and 11 of 50 patients (22%) with all grades of duodenitis on endoscopy. Subsequent analysis of the films revealed one or more radiologic signs of duodenitis (including folds more than 4 mm in thickness, mucosal nodularity, bulbar deformity, and erosions) in 18 of 37 patients (49%) with mild-to-moderate duodenitis, eight of 13 patients (62%) with severe duodenitis, and 26 of 50 patients (52%) with all grades of duodenitis on endoscopy. In a separate part of the study, the authors identified another 20 patients with radiographically diagnosed duodenitis who had undergone endoscopic examinations. Nine of those 20 patients (45%) had duodenitis on endoscopy. Subsequent analysis of the films revealed one or more signs of duodenitis in 17 patients from this group. Nine of the latter patients (53%) had duodenitis on endoscopy. Using established radiologic criteria for duodenitis, our rate of false-positive and false-negative radiologic diagnoses still was about 50%. Thus, the double-contrast upper GI examination is a relatively unreliable technique for diagnosing duodenitis.

Hyperplasia of Brunner glands: the spectrum of its radiographic manifestations. Merine D, Jones B, Ghahremani GG, Hamilton SR, Bayless TM (BJ, Dept. of Radiology, The Johns Hopkins Hospital, 600 N. Wolfe St., Baltimore, MD 21205). *Gastrointest Radiol* 16:104–108, 1991

Radiographic features of the duodenal mucosa were analyzed in a series of 26 patients in whom the diagnosis of Brunner gland hyperplasis (BGH) had been established by endoscopic biopsies. The observed mucosal patterns could be classified into five categories: (1) focal BGH causing a solitary submucosal adenoma or a cluster of sessile polyps in the otherwise smooth duodenal bulb surface (five cases); (2) diffuse BGH manifested by a myriad of small and uniform mucosal elevations (six cases); (3) multifocal BGH producing large and well-demarcated polygonal masses (six cases); (4) BGH with concomitant acute and/or chronic duodenitis showing marked thickening and nodularity of duodenal folds (four cases); or (5) BGH with predominant erosive duodenitis, leading to ulcerations (five cases). These radiographic findings showed a good correlation with the endoscopic and histopathologic manifestations of BGH and the frequently coexistent duodenitis.

Primary gallbladder carcinoma: imaging findings in 50 patients with pathologic correlation. Franquet T, Montes M, Ruiz de Azua Y, Jimenez FJ, Cozcolluela R (TF, Dept of Radiology, Hospital "Virgen del Camino," c/Irunlarrea s/n, Pamplona 31008, Spain). *Gastrointest Radiol* 16:143–148, 1991

Different diagnostic imaging modalities [contrast cholangiography, ultrasonography, and computed tomography (CT)] in a large group of patients with proven gallbladder carcinoma are reviewed. Noninvasive cross-sectional imaging methods strongly correlated with the different gross pathologic types of gallbladder carcinoma. The most common observed type was a mass replacing the gallbladder (39%). Other types observed either by sonography and/or CT were a focal/diffuse gallbladder wall thickening and the presence of an intraluminal polypoid mass. Despite the improvement in several imaging modalities, most of the preoperatively diagnosed gallbladder carcinomas were in advanced stage (84%). A combined approach using noninvasive diagnostic methods and percutaneous aspirative biopsies may reduce the number of explorative laparotomies in the final diagnosis of gallbladder carcinoma.

Journal of Ultrasound in Medicine

Effect of measurement errors on sonographic evaluation of ventriculomegaly. Heiserman J, Filly RA, Goldstein RB (RAF, Dept. of Radiology, M/S 0628, University of California School of Medicine, San Francisco, CA 94143). *J Ultrasound Med* 10:121–124, March 1991

Ventriculomegaly is a sensitive indicator of maldevelopment of the fetal brain and spinal cord. The fetal ventricular atrium is an optimal portion of lateral ventricular system to measure in order to judge ventriculomegaly. We tested the susceptibility of this measurement to inaccuracies created by errors in cursor placement or improper selection of the plane of section for measurement in 52 normal fetuses. This measurement was shown to be reasonably insensitive to errors in cursor placement along the axis of the ventricular system. However, choice of an off-axis image plane of section, an angled measurement, or improper choice of ventricular boundary leads to a relatively large number of false-positive test results (approximately 10%). None of the simulated errors in atrial measurements underestimates the size of the ventricle, and thus, they are unlikely to result in a diminution of test sensitivity.

Reprinted with permission by the American Institute of Ultrasound in Medicine.

News

Nuclear Medicine Update

The Dept. of Radiology, Division of Nuclear Medicine, Emory University School of Medicine, will present Nuclear Medicine Update, July 7–11, at Lake Lanier Islands Hotel and Golf Club, Lake Lanier Islands, GA. The course is designed for radiologists, nuclear medicine physicians, and technologists. It will review several areas of clinical nuclear medicine and present information on recent developments in each area. Topics will include infection, bone, renal, cardiac, brain, hepatobiliary, endocrine, and lung imaging, with emphasis on single-photon emission CT. Course codirectors: Naomi P. Alazraki, Ernest V. Garcia, and Andrew Taylor, Jr. Category 1 credit: 17 hr. Fee: $500. Information: Continuing Medical Education, Emory University School of Medicine, 1440 Clifton Rd., N.E., 111-A WHSCAB, Atlanta, GA 30322; telephone: (404) 727-5695; fax: (404) 727-5667.

Summer Imaging and Interventional Techniques IX

The Dept. of Radiology, Emory University School of Medicine, will present Summer Imaging and Interventional Techniques IX, Aug. 5–9, at Amelia Island Plantation, Amelia Island, FL. State-of-the-art imaging techniques, including MR, CT, Doppler sonography, scintigraphy, and interventional techniques, will be demonstrated. The techniques will be presented in an organ-oriented format to aid in specific problem solving. The discussions will include correlation among the various techniques so the clinician will have a better understanding of which techniques to use in specific situations. Course directors: Bruce R. Baumgartner and Maria del Pilar Fernandez. Guest faculty: A. D. Elster, I. Laufer, T. G. McLoud, and M. D. Rifkin. Category 1 credit: 20.5 hr. Fee: physicians, $550; residents in training (letter required), $250. Information: Continuing Medical Education, Emory University School of Medicine, 1440 Clifton Rd., N.E., 111-A WHSCAB, Atlanta, GA 30322; telephone: (404) 727-5695; fax: (404) 727-5667.

Registry Preparation Courses for Sonographers

Several registry preparation courses for sonographers will be offered in August, September, and October. Abdominal Ultrasound Review will be given Aug. 22–23 at the Ritz-Carlton Pentagon City Hotel, Washington, DC. Instructor: Kenneth J. W. Taylor. Fee: $220. OB/GYN Ultrasound Review will be offered Aug. 24 at the Ritz-Carlton Pentagon City and Sept. 22 at the Doubletree Marine Beach Hotel, Los Angeles. Instructors will be Kenneth J. W. Taylor and Dale R. Cyr, respectively. Fee: $125. Ultrasound and Doppler Physics will be given Aug. 25–26 at the Ritz-Carlton Pentagon City, Washington, DC; Sept. 7–8 at the Radisson Suite Hotel O'Hare Airport, Chicago; Sept. 20–21 at the Doubletree Marina Beach, Los Angeles; and Oct. 5–6 at the Hyatt Regency Dallas at Reunion Hotel, Dallas. Instructor: Frederick W. Kremkau. Fee: $250. Vascular Technology will be presented Aug. 27–28 at the Ritz-Carlton Pentagon City, Washington, DC. Instructor: Cynthia B. Burnham. Fee: $250. Information: Office of Postgraduate and Continuing Medical Education, Yale University School of Medicine, 333 Cedar St., P. O. Box 3333, New Haven, CT 06510; (203) 785-4578.

Physics of Diagnostic Radiology, Nuclear Medicine, and Radiation Biology

The Dept. of Radiology and the Office of Continuing Medical Education, University of California, Davis School of Medicine, are offering Physics of Diagnostic Radiology, Nuclear Medicine, and Radiation Biology, Sept. 5–8, at the University of California, Davis. The course is intended to be a review for residents in diagnostic radiology and nuclear medicine. Course directors: Jerrold T. Bushberg and J. Anthony Seibert. Category 1 credit: 25 hr. Fee: $395. Information: Office of Continuing Medical Education, University of California, Davis School of Medicine, 2701 Stockton Blvd., Sacramento, CA 95817; (916) 734-5390.

International Imaging Course

The 4th International Imaging Course: Neuroradiology and Paediatric Radiology will be held Sept. 30–Oct. 5 at the Regal Riverside Hotel, Hong Kong. Course organizers: L. Kreel, C. Metreweli, and T. L. Lawson. Category 1 credit: 35 hr. Information: Miss Rebecca Tsui, Dept. of Radiology, Prince of Wales Hospital, Shatin, Hong Kong; telephone: (852) 6363213; fax: (852) 6360012.

Magnetic Resonance Imaging 1991: Back to the Future

The Dept. of Radiology, University of Cincinnati College of Medicine, will present Magnetic Resonance Imaging 1991: Back to the Future, Oct. 2–5, at the Westin Hotel Fountain Square, Cincinnati. Course directors: George S. Bisset III, Robert R. Lukin, and Jonathan S. Moulton. Guest faculty: R. A. Clark, B. Drayer, C. A. Helms, and D. Resnick. Category 1 credit: 20 hr. Information: Lynne K. Tiras, CMP, Conference Coordinator, International Meeting Managers, Inc., 4550 Post Oak Pl., Ste. 248, Houston, TX 77037; telephone: (713) 965-0566; fax: (713) 960-0488.

Breast Cancer Diagnosis: State-of-the-Art

Breast Cancer Diagnosis: State-of-the-Art will be presented Oct. 7-8 at NYU Medical Center, New York City. The focus of the conference will be a comprehensive review of the mammographic detection of small cancers and their further evaluation with interventional methods. Emphasis will be on improving the detection of early breast lesions. Registrants will have the opportunity to enhance their diagnostic skills by participating in film review screening sessions with the faculty and by attending workshops on the practical aspects of interventional techniques. Category 1 credit: 14 hr. Fee: $275. Information: NYU Medical Center, Post-Graduate Medical School, 550 First Ave., New York, NY 10016; (212) 263-5295.

Practical Training in Interventional Radiology

Training courses will be held at the Radiology Experimental Research Center, University Hospital, Lund, Sweden, Oct. 7-11 and Nov. 4-8. Participants will be trained in performing a variety of interventional procedures, such as superselective arterial catheterization, embolization, vascular stenting, placement of filters, percutaneous transhepatic cholangiography, percutaneous pyelostomy, percutaneous cholecystostomy, and retrieval of foreign bodies from the vascular system. All procedures will be done on anesthetized pigs. The number of participants will be limited to five in each course. Program directors: Oct. 7-11, Anders Lunderquist and Sydney Wallace; Nov. 4-8, Anders Lunderquist and Josef Rösch. Information: Anders Lunderquist, M.D., Dept. of Radiology, University Hospital, S-221 85 Lund, Sweden; fax: (46) 116956; or Eva Jönsson, telephone: (46) 173001.

MRI: Clinical State of the Art 1991

MRI: Clinical State of the Art 1991 will be presented at the NYU Medical Center, New York City, Oct. 9-12. The course will provide a practical, clinically oriented review and analysis of the state of the art of MR imaging and an introduction to some of the promising new developments in MR. The emphasis will be on anatomy, applications, techniques, and interpretation. Areas to be covered include brain, spine, bones and joints, cardiovascular system, and body. Category 1 credit: 25.5 hr. Fee: $500. Information: NYU Medical Center, Post-Graduate Medical School, 550 First Ave., New York, NY 10016; (212) 263-5295.

Interventional Radiology Course

The Dept. of Radiology, University of California, San Diego School of Medicine, will present the 11th annual Interventional Radiology Course, Nov. 1-3, at the Hotel Del Coronado, Coronado (San Diego), CA. Program director: Eric vanSonnenberg. Fee: physicians, $375; residents, fellows, and technologists, $300. Information: Dawne Ryals, Ryals and Associates, P. O. Box 1925, Roswell, GA 30077-1925; telephone: (404) 641-9773; fax: (404) 552-9859.

Seminar on Bone and Joint Diseases

Maricopa Medical Center, Phoenix, AZ, is sponsoring the 20th annual seminar, Bone and Joint Diseases, Nov. 15-17, at Marriott's Camelback Inn, Scottsdale, AZ. Program director: Alex Newman. Category 1 credit: 24 hr. Fee: 3 days, $480; 2 days, $320. Information: Alex Newman, M.D., Dept. of Radiology, Maricopa Medical Center, P. O. Box 5099, Phoenix, AZ 85010; (602) 267-5361.

Asian Oceanian Congress of Radiology

The Indian Radiological and Imaging Association will host the 6th Asian Oceanian Congress of Radiology (AOCR) Dec. 14-18 in New Delhi. The theme of the congress will be Optimisation in Radiological Services in Third World Countries. The scientific sessions will include state-of-the-art lectures, symposia, film reading sessions, daily continuing medical education programs, and proffered papers. President: K. R. Chaudhari. Secretary General: Sudarshan K. Aggarwal. Category 1 credit: 13.5 hr. Information: Dr. Sudarshan K. Aggarwal, Secretary General 6th ACOR, c/o Dr. Diwan Chand Aggarwal Imaging Research Centre, 10-B, Kasturba Gandhi Marg, New Delhi-110 001, India; telephone: 3713302; fax: 3713308.

The American Board of Radiology Examinations

Written examinations for the American Board of Radiology (ABR) are scheduled for Oct. 3-4, 1991; Oct. 1-2, 1922; and Oct. 14-15, 1993. Oral examinations will be held at the Executive West Hotel in Louisville, KY, June 3-7, 1991; June 1-5, 1992; and May 31-June 4, 1993. The ABR will accept applications for admission to the examinations after July 1, but not later than Sept. 30, *in the year preceding* the year in which the examination is to be taken. For application forms and further information: Office of the Secretary, The American Board of Radiology, 300 Park, Ste. 440, Birmingham, MI 48009.

Meeting and Course Review

For the reader's convenience, a summary of upcoming meetings and courses is provided. Detailed listings are given in the *AJR* issue given in parentheses.

Visiting Fellowships in Interventional Radiology, times arranged, Baltimore (Oct 1990)
Swallowing Center Preceptorship, times arranged, Baltimore (Jan)
Imaging Fellowship, times arranged, Miami Beach, FL (Jan)
Preceptorships in Ultrasound at Johns Hopkins, time arranged, Baltimore (June)
Workshop on New Devices for Cardiac and Peripheral Vascular Laboratories, July 1-3, Lake Buena Vista, FL (June)
Leeds Gastroenterology Course for Radiologists, July 1-5, Leeds, England (Dec 1990)
International Congress of Radiation Research, July 7-12, Toronto (May 1990)
Neuroradiology in the Rockies, July 7-12, Snowmass at Aspen, CO (Feb)
Mackinac Island Imaging Conference, July 8-11, Mackinac Island, MI (May)
Physics and Instrumentation, July 8-12, Philadelphia (June)
Mammography and the Search for Breast Cancer, July 12-13, Rochester, NY (April)
Alaska 91—Cruise the Inland Passage—Magnetic Resonance Imaging at Sea, July 14-21 (April)
Advances in Gastroenterology, July 15-19, Coronado (San Diego), CA (March)
Cross Sectional Anatomy, July 15-19, Philadelphia (June)
Radiology for the Non-Radiologist, July 18-21, Coronado (San Diego), CA (March)
Evaluation & Treatment of the Injured Athlete, July 22-26, Chatham (Cape Cod), MA (May)
Obstetrics & Gynecology Ultrasound, July 22-26, Philadelphia (June)

Issues in Musculoskeletal Imaging and Magnetic Resonance Imaging, July 22–27, Laguna Niguel, CA (March)
Imaging on Lake Coeur d'Alene, July 25–27, Coeur d'Alene, ID (June)
Abdominal Ultrasound, July 29–Aug. 1, Philadelphia (June)
Contemporary Diagnostic Imaging, July 29–Aug. 2, Aspen, CO (April)
Pittsburgh Breast Imaging Seminar, Aug. 1–4, Pittsburgh (May)
Prostate Ultrasound, Aug. 2, Philadelphia (June)
Napa Valley Imaging Update, Aug. 4–8, Napa, CA (June)
MR Imaging Fellowships at LAC/USC Imaging Science Center, Aug. 5–9, Sept. 16–20, Oct. 7–11, and Nov. 4–8, Los Angeles (Feb)
Body Imaging, Aug. 5–9, Santa Fe, NM (April)
Symposium on Diagnostic Imaging, Aug. 12–15, Newport, RI (June)
Imaging of the Head, Spine, and Musculoskeletal System, Aug. 12–16, Whistler, B.C. (April)
Radiology for Clinicians, Aug. 12–16, Coronado (San Diego), CA (April)
Society of Computed Body Tomography Summer Practicum, Aug. 18–22, Keystone, CO (April)
Diagnostic Imaging Update, Aug. 26–30, Vancouver, B.C. (April)
Radiation, Physics, and Biology, Aug. 26–30, New York City (May)
World Congress in Ultrasound, Sept. 1–6, Copenhagen (Sept 1990)
Pacific Northwest Diagnostic Ultrasound Symposium, Sept. 6–8, Seattle (June)
International Workshop on Hypertrophic Osteoarthropathy, Sept. 8–11, Dubrovnik, Yugoslavia (Jan)
European Society of Gastrointestinal Radiologists Annual Meeting, Sept. 8–11, Oxford, England (March)
Sonography Update Conference and Exhibit, Sept. 11–13, Coronado (San Diego), CA (May)
Mallinckrodt Institute's 60th Anniversary Celebration, Sept. 12–14, St. Louis (May)
Transrectal Ultrasound in the Diagnosis and Management of Prostate Cancer, Sept. 13–14, Chicago (May)
Diagnostic Ultrasound in Gynecology and Obstetrics and Abdomen, Sept. 13–15, Baltimore (June)
Sonography Registry Review, Sept. 14–15, Coronado (San Diego), CA (May)
European Congress of Radiology 1991, Sept. 15–20, Vienna, Austria (Oct 1990)
Mammographic Interpretation: A Practical Approach, Sept. 23–26 and Oct. 28–31, Boston (March)
Applied Ultrasound: Accent on Doppler, Sept. 23–26, Laguna Niguel, CA (May)
Diagnosis of Musculoskeletal Disorders, Sept. 25–28, Coronado (San Diego), CA (May)
Diagnostic Uses of Radiolabeled Monoclonal Antibodies, Sept. 26–27, Washington, DC (June)
Annual International Body Imaging Congress, Oct. 5–12, Maui, HI (June)
Neuroradiology Update: Emphasis on MRI, Oct. 7–11, Hilton Head, SC (June)
Western Neuroradiological Society Annual Meeting, Oct. 17–20, Laguna Niguel, CA (June)
Progress in Magnetic Resonance Imaging, Oct. 24–25, Cologne, Germany (June)
Neuroradiologic and Musculoskeletal Seminars, Oct. 24–27, Orlando, FL (June)
Advanced Imaging of the Musculoskeletal System, Oct. 26–27, Coronado (San Diego), CA (June)
San Diego Postgraduate Radiology Course, Oct. 28–Nov. 1, Coronado (San Diego), CA (June)
Diagnosis and Treatment of Bone and Soft-Tissue Tumors, Nov. 21–23, Sacramento, CA (May)
International Symposium on Recent Advances in Diagnostic Imaging and Radiation Oncology, March 24–27, 1992, Kathmandu, Nepal (June)

AJR carries announcements of courses, symposia, and meetings of interest to its readers if received a minimum of 5 months before the event. There is no charge; receipt of items by the *AJR* Editorial Office is not acknowledged. Submit items for publication typed double-spaced. Provide title, date, location, brief description, sponsor, course directors, fees, category I credit, and address and telephone number for additional information. Faculty from the host institution will not be listed. Guest faculty names will appear **only** if initials are provided. Mail news items to *AJR* Editorial Office, 2223 Avenida de la Playa, Suite 103, La Jolla, CA 92037-3218.

American Roentgen Ray Society 92nd Annual Meeting
May 10–15, 1992, Orlando, FL
Marriott's Orlando World Center

Registration and Hotel Reservations

Forms for advance registration and hotel reservations will be in the February and March 1992 issues of the *AJR*.

Scientific Program

Abstracts of papers to be considered for the program must be submitted by November 1, 1991. Forms on which to submit abstracts are in this issue of the *AJR*. The ARRS Program Committee will select papers and notify authors in early January. The *AJR* has first rights to all papers accepted for presentation at the ARRS meeting. Mail original and five copies to

ARRS President-Elect
c/o Paul R. Fullager
American Roentgen Ray Society
1891 Preston White Dr.
Reston, VA 22091

Scientific Exhibits

Proposals for scientific exhibits must reach the Chairman of Exhibits by November 1, 1991. Forms, which may be photocopied, are in this issue of the *AJR*. Send completed form to

N. Reed Dunnick, M.D.
c/o Paul Fullager
American Roentgen Ray Society
1891 Preston White Drive
Reston, VA 22091
Telephone (703) 648-8992

Refresher Course Program

A summary of the refresher courses will appear in the *AJR* in February along with advance registration forms. Early registration is an advantage in ensuring preferred courses in this popular program.

Local Program

A program of sightseeing, shopping, and entertainment will be developed by the Local Arrangements Chairman. Information and advance registration forms will be in the February issue of the *AJR*.

Residents' Award Papers

The society offers several cash awards for the best scientific papers prepared by residents in radiology. The President's Award has a $2000 prize. There are two Executive Council awards of $1000 each. All are presented at the annual meeting. Papers should be submitted by February 15, 1992, for consideration in this competition. Send entries to

Nancy O. Whitley, M.D.
Dept. of Radiology
University of Maryland Medical Systems Hospital
22 S. Greene St.
Baltimore, MD 21201

Deadlines

Abstracts of papers: November 1, 1991
Scientific exhibit proposals: November 1, 1991
Residents' Award papers: February 14, 1992

Call for Papers

American Roentgen Ray Society 1992 Annual Meeting: May 10–15, 1992, Orlando, FL

ADDRESS OF PRESENTING AUTHOR

Department

Institution

Street

City, State__________ Zip

Phone: __________

Type title, authors, and abstract in the space provided below. (Instructions are on reverse side of this page. Abstract should not exceed 300 words.)

Select one category: ______Angio/Interventional ______Breast ______Chest ______CT ______Gastrointestinal Tract ______Genitourinary Tract ______MR ______Neuroradiology ______Skeletal ______Sonography

Projection Requirements: ______35 mm, single or double (circle one) ______16 mm silent film ______½''VHS ______¾''

Has this been presented elsewhere? ______yes ______no. If yes, please describe on reverse side of this page.

Instructions for Scientific Abstracts

1. Type the information single-spaced. Underline the name of the presenting author. Append as a last line of the abstract any research grant support, if applicable (e.g., Supported by USPHS Grant HE-80144). If the abstract is accepted, it will not be proofread; it will appear exactly as typed. Use the following format:

   MR IMAGING OF THE SPINE AND NECK
   F. S. Lau, M.D., A. N. Kirk, M.D., and R. A. Beck, Ph.D.
   University of California, Bakersfield, Bakersfield, CA 92338

2. Abstracts should include four paragraphs devoted sequentially to the following topics: (1) object or purpose of the study, (2) materials, methods, and procedures, (3) results, (4) significance of the results and conclusions. The text should not exceed 300 words. Specific data are essential. The abstract should be a succinct summary of work done rather than a promissory note.
3. The Program Committee will grade each abstract and determine acceptance. Further information will be forwarded to those whose abstracts are accepted for presentation.

Deadline for submission of abstract is November 1, 1991. Mail abstract and four copies to

ARRS President-Elect
c/o Paul R. Fullagar
American Roentgen Ray Society
1891 Preston White Dr.
Reston, VA 22091

Call for Scientific Exhibits

American Roentgen Ray Society
1992 Annual Meeting:
May 10–15, 1992, Orlando, FL

FOR COMMITTEE USE ONLY

Date Received______ Application No. ______
Subject______ Score______
Rejected______ Accepted______
Assigned______ Space No. ______

Principal Exhibitor's Mailing Address

Name______ Institution______

Department______ Street Address______ City______

State______ Zip Code______ Telephone: office ( ) home ( )

Names of Exhibitors (List principal exhibitor first and telephone number of each person.)

Last	First	Middle	Telephone	Degree (one only)	Member ARRS?

Title of Exhibit______

Type abstract single-spaced in the space provided below. (See instructions on the reverse side of this page.)

Instructions for Abstract

The abstract should be a brief paragraph that states the purpose, principal information, and conclusions of the exhibit. Promissory statements are not acceptable. Type single-spaced in the space provided on the reverse side. Brevity is desirable but not at the expense of specific information. **The abstract will appear in the program book as submitted.** Please use typewriter and complete the application form on both sides. List space requirements.

What Type of Exhibit Is Proposed? (Check one and fill in all appropriate blanks.)

______**Free-standing.** This is a self-contained display created in total by the exhibitor. It may be a fold-open unit, a unit shipped in cases and assembled on site, or a tabletop unit. Linear feet required ______.

______**Poster Board (backboard panels).** Backboard panels are 4 × 8 ft. (1.2 × 2.5 m). Number of panels required ______. If two panels are needed, there will be a ¼-in. frame separating the panels, thus requiring a separation in the presentation.

______**Viewbox.** Mounted materials (radiographs and other transparencies) for display on the society's illuminators. Each illuminator is 39.5 × 59.5 in. (100 × 151 cm). Number of illuminators required ______. Materials should not be glass mounted.

Please Indicate Most Appropriate Category.

______Bone ______Cardiovascular ______Chest ______Gastrointestinal ______Genitourinary ______Breast ______Medical physics
______Neuroradiology ______Nuclear medicine ______Pediatric ______Radiation oncology ______Sonography

Exhibits will be chosen on the basis of the quality of the abstract and space available. Poster board and computer-based exhibits are encouraged, as they do not require a viewbox.

Signature of Principal Exhibitor______________________________

Exhibitors will receive instructions for exhibit preparation.

Applications must be received no later than November 1, 1991. Mail original and five copes to

N. Reed Dunnick, M.D.
c/o Paul R. Fullagar
American Roentgen Ray Society
1891 Preston White Dr.
Reston, VA 22091

Telephone: (703) 648-8992

American Roentgen Ray Society:
Officers, Committees, and Membership Information

Officers

President: John A. Kirkpatrick, Jr.
President-elect: A. Everette James, Jr.
1st Vice-president: Andrew K. Poznanski
2nd Vice-president: George R. Leopold
Secretary: Joseph T. Ferrucci, Jr.
Treasurer: Beverly P. Wood

Executive Council: R. N. Berk, M. P. Capp, W. J. Casarella, N. R. Dunnick, R. G. Evens, J. T. Ferrucci, Jr., A. E. James, Jr., J. A. Kirkpatrick, Jr., A. M. Landry, Jr., G. R. Leopold, J. E. Madewell, T. C. McLoud, A. A. Moss, A. K. Poznanski, R. J. Stanley, J. H. Thrall, K. H. Vydareny, N. O. Whitley, B. P. Wood, R. J. Alfidi, chairman

Committees

Editorial Policy: R. N. Berk, E. Buonocore, Melvin M. Figley, M. S. Huckman, C. R. B. Merritt, A. G. Osborn K. Valji, C. A. Rohrmann, Jr., W. J. Casarella, chairman

Education and Research: R. R. Hattery, C. B. Higgins, B. J. Hillman, R. J. Stanley, W. M. Thompson, N. O. Whitley, chairman

Finance and Budget: R. K. Gedgaudas-McClees, A. A. Moss, J. R. Thornbury, K. H. Vydareny, J. H. Thrall, chairman

Nominating: R. G. Evens, P. J. Fritzsche, A. A. Moss chairman

Publications: E. Buonocore, C. R. B. Merritt, A. G. Osborn, C. A. Rohrmann, Jr., W. J. Casarella, chairman

Membership: J. E. Madewell, T. C. McLoud, A. A. Moss, K. H. Vydareny, chairman

Representatives to Other Organizations

American Board of Radiology: W. J. Casarella, J. A. Kirkpatrick, Jr., L. F. Rogers

American College of Radiology: R. A. Gagliardi, J. E. Madewell, B. L. McClennan, R. J. Stanley

American Medical Association: S. F. Ochsner, delegate; K. L. Krabbenhoft, alternate; K. L. Kidd, CPT Advisory Committee

American National Standards Institute: M. E. Haskin

National Council on Radiation Protection and Measurements: F. D. Miraldi, E. L. Saenger

Armed Forces Institute of Pathology: J. E. Madewell

Meeting Arrangements

Annual Meetings: May 10–15, 1992, Marriott's World Center, Orlando, FL; April 25–30, 1993, Marriott San Francisco, San Franciso, CA

Annual Meeting Committee: J. K. Crowe, N. R. Dunnick, R. R. Lukin, N. H. Messinger, R. J. Stanley, R. D. Steele, Jr., A. M. Landry, Jr., chairman

Instructional Courses: Bruce L. McClennan, associate chairman; R. J. Stanley, chairman

Scientific Program: P. H. Arger, T. B. Hunter, D. Kushner, T. C. McLoud, L. B. Talner, J. H. Thrall, A. E. James, Jr. chairman

Scientific Exhibits: J. R. Haaga, D. S. Hartman, R. G. Ramsey, N. R. Dunnick, chairman

ARRS Membership

An application form is printed in this issue of the Journal. For consideration at the 1992 ARRS meeting, send completed forms before February 1, 1992, to American Roentgen Ray Society, 1891 Preston White Dr., Reston, VA 22091. Active members are graduates of an approved medical or osteopathic school or hold an advanced degree in an allied science. They must practice radiology or work in an associated science in the United States or Canada and be certified by the American Board of Radiology, American Osteopathic Board of Radiology, or Royal College of Physicians of Canada or otherwise adequately document training and credentials. Corresponding members are foreign radiologists or scientists who are active in radiology or an allied science. Members-in-training are residents or fellows in radiology or postgraduate students in an allied science. Additional application forms can be obtained from the ARRS offices in Reston, VA.

Business Office

Paul Fullagar, Executive Director, American Roentgen Ray Society, 1891 Preston White Dr., Reston, VA 22091; (703) 648-8992.

Information and Application for Membership in the American Roentgen Ray Society

General Information

The American Roentgen Ray Society, founded in 1900, has been a forum for progress in radiology since shortly after the discovery of X-rays. From its beginning and continuing to today, the ARRS has been guided by dedication to the goal of the advancement of medicine through the science of radiology and its allied sciences.

The goal of the ARRS is maintained through an annual scientific and educational meeting, and through publication of the *American Journal of Roentgenology*.

The annual meeting consists of instructional courses, scientific sessions, a symposium, scientific exhibits, and commercial exhibits. A special categorical course is also offered. Category I CME credits are available on an hour-for-hour basis.

The monthly *American Journal of Roentgenology* is a highly respected peer review journal with a worldwide subscription base. For over 75 years the *AJR* has been accepted as one of the best specialty journals available in the world, and this reputation grows each month.

A recently developed quarterly ARRS newsletter keeps members informed of events and general Society news.

Application Instructions

Candidates for Active Membership

1. An Active member must be a graduate of an approved medical school or hold an advanced degree in one of the physical, chemical or biological sciences and be certified by the American Board of Radiology, the American Osteopathic Board of Radiology, the Royal College of Physicians of Canada, or document training and credentials that are adequate to qualify for membership. Active members shall actively practice radiology or one of its branches in the United States or Canada. Such members are eligible to participate in all activities of the Society, including membership on committees, and have full voting privileges.
2. Application must be on an official form, signed by the applicant and at least two members of the American Roentgen Ray Society, active or emeritus, in good standing, who endorse the applicant.
3. Application fee is $50 (payable when billed for dues).
4. Annual dues are $150, payable on January 1 of each year following the initial year. First year dues will be invoiced following candidate election at the annual meeting. Of this amount, $50 is for a 1-year subscription to the *American Journal of Roentgenology*, beginning with the July issue following election to membership.
5. Application must be received by February 1 for action during the current year's meeting.

Candidates for In-Training Membership

1. In-training members must be serving in a radiology residency program approved by the Radiology Residency Review Committee, the American Osteopathic Board of Radiology, or the Royal College of Physicians of Canada, or in an approved post-residency fellowship, or be a postgraduate student in an allied science. Training status must be verified by the program director. In-training members have special consideration in fees and subscription rates to the Society journal. Such members cannot hold Society offices or vote.
2. Application must be on an official form and signed by the applicant and by the applicant's training or residency program director.
3. In-training status is limited to a maximum of five years starting with the entrance date into the radiology residency. In the last year, each in-training member will receive an application for active membership from the Society. Those who do not apply for transfer to active membership shall be dropped from membership at the end of the fifth year, but can later apply as a new member through the process outlined for active status.
4. There is no application fee. Annual dues are $25. Membership includes a subscription to the *American Journal of Roentgenology* and admission to the annual meeting without payment of the registration fee.
5. Membership applications will be acted on when received.

Corresponding Membership

A corresponding member must meet the qualifications of active membership, but reside and practice in a foreign country. Corresponding members shall pay dues and fees, but shall not have the privileges of voting nor of holding elective office.

All Applicants

1. **Do not remit application fee or dues until requested.**
2. **Send completed forms to: American Roentgen Ray Society**
   1891 Preston White Drive
   Reston, Virginia 22091

For ARRS
Office Use
Date Rec'd ______
I.D.# ______

AMERICAN ROENTGEN RAY SOCIETY
APPLICATION FOR MEMBERSHIP

Date: ______

Category of Membership: (Check One)
☐ Active
☐ Corresponding
☐ In-Training

Name (Please Print) ______ First Initial Last
Degree(s) ______
Mailing Address ______ Street/Box
Date of Birth ______
______ City/State/Country Zip Code
Telephone ( ) ______

A. Education: (List name of institution, years attended, and degree and type received.)

Undergraduate: ______

Graduate (Medical School, Graduate School, etc.): ______

Postgraduate (Internship, Residency, Fellowship, etc.): ______

B. Licensure:

Licensed to practice ______ (Type) in ______ (State, Province, etc.) since ______

C. Appointments/Memberships: (In-Training applicants: skip to Section F on reverse.)

Present Appointments: Academic ______

Hospitals ______

Memberships in Scientific Societies: ______

Offices or Committee Assignments: ______

Government Service (Military or Civilian) ______ (Position) (Years)

Continued on Reverse Side

D. Credentials: (To be completed by Active and Corresponding applicants only.)

I hereby certify that I was issued a certificate of qualification in ______________________ (Specialty)

in ____________ (Year) by the ______________________ (Name of Qualifying Board)

Other Credentials: ______________________

Signature: ______________________

E. References: (To be completed by Active and Corresponding applicants only.)

We, active or emeritus members in good standing of the American Roentgen Ray Society, and acquainted with the applicant, do recommend him/her for membership in the Society. (Two references are required.)

Name (Please Print)	1. ____________	2. ____________
Address	____________	____________
	____________	____________
Signatures:	____________	____________

F. IN-TRAINING APPLICANTS MUST COMPLETE THIS SECTION

Credentials:

I certify that I am serving as a Resident/Fellow in ______________________ (Specialty)

at ______________________ (Name of Institution). Date program began (begins): ______________;

date program to end: ______________. I understand that in-training membership is limited to a maximum of 5 years.

Applicant Signature: ______________________

Verification: (Program Director or Department Chairman *only*)

I certify that the applicant is in training at the institution named and qualifies for enrollment as a member-in-training of the American Roentgen Ray Society.

Name (Please Print) ______________________

Address: ______________________

____

Signature ______________________

Send completed form to:

American Roentgen Ray Society
1891 Preston White Drive
Reston, Virginia 22091

Classified Advertisements

Positions Available

THE DEPT. OF RADIOLOGY AT TRIPLER ARMY MEDICAL CENTER, HONOLULU, HI, is recruiting academic radiologists for several divisions of the dept. including ultrasound, chest radiology, skeletal, neuroradiology, general diagnostic radiology, MRI, interventional radiology, and mammography. Our dept. offers a fully accredited residency program with 21 residents and 16 attending full-time staff. Numerous consultants from across the country lecture on a continuing and regular basis. The hospital is a modern, tertiary-care center serving Hawaii and the entire Pacific Basin. A strong residency program, diverse and interesting patient population, excellent equipment, and tropical lifestyle are positive aspects of the practice. Academic credentials and/or experience are necessary. Recently graduated fellows are encouraged to apply. Board certification is mandatory. Candidates should be particularly interested in patient care, teaching, and research. Salary and benefits are competitive and generous. Tripler is an EO/EEO employer. Please contact Dr. Mark F. Hansen, Col., MC, Chief, Dept. of Radiology, TAMC, HI 96859-5000; (808) 433-6393. 7–6a

BC/BE RADIOLOGIST—Group practice in New Orleans, LA, has a great opportunity leading to partnership. Looking for a radiologist with imaging background or interest in special procedures. Imaging center with 1.5-T GE Advantage System. Excellent hospitals and working conditions. Send CV to B.B.N. & H., 440 General Meyer Ave., Ste. 211, New Orleans, LA 70131; (504) 368-5074. 7–10ap

THE PORTLAND DEPT. OF VETERANS AFFAIRS MEDICAL CENTER, a 490-bed teaching hospital affiliated with Oregon Health Sciences University, is seeking a staff radiologist with interest in body imaging and general radiology. Located in Portland's West Hills adjacent to the university, this new, well-equipped facility has a commanding view of the Cascade Range, with its ski resorts, white-water rafting, mountaineering, and other outdoor opportunities. There are 2 state-of-the-art CT scanners, 2 Acuson ultrasound units with color flow, a GE 1.5-T MRI scanner, and 2 digital angiographic suites. All staff hold university appointments. An interest in teaching is essential and research is encouraged, but not required. Portland is a small city that offers everything from rodeo to opera and is surrounded by the natural beauty of the Pacific Northwest. It offers a comfortable backdrop for career development and family life. Contact Dr. Ruza Antonovic or Dr. Mary Burry, Radiology Dept., Portland VA Medical Center; (503) 220-8262, ext. 6510. Equal opportunity employer. 7a

LOCUM TENENS—Earn top pay. Don't work for an agency. Work for yourself. For details, send name and address to Dr. Monroe, 7035 Hwy. 6 South, Ste. R 175, Houston, TX 77083; (713) 341-9703. 7–8ap

OPENING FOR BE/BC DIAGNOSTIC RADIOLOGIST to join a 6-person group in Missoula, a university city of 45,000 located in mountainous western Montana. Looking for a general radiologist with proficiency in MRI, ultrasound, CT, angiography, etc. Administrative skills preferable. Our group of 6 full-time radiologists covers both of Missoula's hospitals (210 and 130 beds). Progressive medical environment with 200 physicians. One yr to full partner income and 2 yr to partnership. Competitive salary. Abundant nearby recreational opportunities include skiing, fishing, backpacking, and hunting. Send CV to Missoula Radiology, Inc., P.O. Box 2039, Missoula, MT 59806. 7–11ap

THE DEPT. OF RADIOLOGY AT THE UNIVERSITY OF MASSACHUSETTS MEDICAL CENTER in Worcester is seeking a BC/BE general radiologist with a major interest in chest and musculoskeletal radiology. A strong interest in teaching and collaborative clinical research is desired. Rank and salary are commensurate with experience. The medical center is a 370-bed university hospital and medical school located approximately 40 mi. west of Boston. The dept. consists of 22 staff, 13 residents, and 2–4 fellows and does approximately 130,000 exams/yr. The dept. is well-equipped with 2 GE 9800 Quick CT scanners as well as 2 GE 1.5-T MRI scanners in a stand-alone facility and a 2.0-T small-bore unit for animal research. The hospital is a major trauma center and is serviced by 2 Life Flight helicopters. For further information, contact Edward H. Smith, M.D., Professor and Chair, Dept. of Radiology, University of Massachusetts Medical Center, 55 Lake Ave., N., Worcester, MA 01655; (508) 856-3252. UMMC is an equal opportunity/affirmative action employer. 7xa

OREGON—Opportunity for BC/BE radiologist to join 7 BC radiologists in growing practice in the Portland metropolitan area. Training/expertise in all aspects of radiology including MRI is required. The practice includes 2 suburban hospitals, an outpatient clinic, and a new multimodality outpatient imaging clinic. Competitive compensation with generous fringe package and partnership in 2 yr. Send letter and CV to Jon C. Sewell, M.D., P.O. Box 227, Oregon City, OR 97045; (503) 655-1439. 7–8ap

PEDIATRIC RADIOLOGIST—The Division of Pediatric Radiology, Oregon Health Sciences University, Portland, OR, invites applications for a faculty position available on or about July 1, 1991. Completion of approved fellowship in pediatric radiology and ABR certification required. Send CV to William Weidner, M.D., Diagnostic Radiology, UHN-72, Oregon Health Sciences University, Portland, OR 97201-3098; (503) 494-4498. Equal opportunity, affirmative action employer. 7–9a

ACADEMIC BONE RADIOLOGIST—The Ohio State University is looking for a successor to direct the active musculoskeletal section which supports the orthopedics dept. with strong sports medicine, rehabilitation medicine, and prosthetic/reconstruction divisions. Salary negotiable. Start on or before July 1, 1991. Inquire to Charles F. Mueller, M.D., Chief of Diagnostic Radiology, Ohio State University Hospitals, Dept. of Radiology, Columbus, OH 43210; (614) 293-8315, or fax (614) 298-8322. 7a

CROSS-SECTIONAL IMAGING/MRI/CT/ULTRASOUND—Diagnostic Radiology, Oregon Health Sciences University, Portland, OR, is recruiting a board-certified radiologist for its Body Imaging Section. Academic rank and salary depend on candidate's experience and achievements. Send CV and reference letters to William Weidner, M.D., Chairman, Diagnostic Radiology, UHN 72, Oregon Health Sciences University, Portland, OR 97201-3098. OHSU is an equal opportunity, affirmative action employer. 7–8a

THE DIVISION OF NUCLEAR MEDICINE, Oregon Health Sciences University, Portland, OR, invites applications for a faculty position available immediately either part-time in nuclear medicine or full-time divided between nuclear medicine and another division of diagnostic radiology. Board certification in nuclear medicine is required. Send CV and references to William Weidner, M.D., Chairman, Diagnostic Radiology, UHN 72, Oregon Health Sciences University, Portland, OR 97201-3098. OHSU is an affirmative action, equal opportunity employer. 7–8a

IMMEDIATE OPENING IN KANSAS CITY, MO—Group of young, well-trained radiologists seek to fill a recently vacated position. General radiologist or subspecialty training acceptable. Experience or training in angiography and interventional work desirable, but not required. Excellent salary, vacation, and other benefits leading to early partnership in rapidly growing practice. Reply to George F. Drasin, M.D., 4949 Rockhill Rd., Kansas City, MO 64110. 7ap

MRI/ABDOMINAL IMAGING NEW YORK/NEW JERSEY METROPOLITAN AREA—Board-certified/eligible radiologist needed for a position beginning July 1, 1991. Must have fellowship training in MRI and training in CT, ultrasound, and GI studies. Private practice with 400-bed hospital and outpatient imaging center located in northern New Jersey, near New York City. Send inquiries to James A. Heimann, M.D., Dept. of Radiology, Clara Maass Medical Center, 1 Franklin Ave., Belleville, NJ 07109. 7–12ap

NORTHERN CALIFORNIA, IMMEDIATE OPENING—Large, diagnostic group seeks BC/BE radiologist to join diversified practice (4 hospitals and 7 offices) on full partnership basis. All modalities available. Send CV or call Andrew Koo, M.D., P.O. Box 9525, San Jose, CA 95157; (408) 244-2100. 7–9ap

TRAUMA RADIOLOGIST—The State University of New York Health Science Center at Brooklyn seeks to add a board-certified/eligible radiologist to join the Division of Traumatology at Kings County Hospital Center, a 1300-bed tertiary facility and Level I Trauma Center with an international reputation in trauma services. The radiologist is an integral member of the trauma service of the Dept. of Surgery. Opportunities to join ongoing clinical investigations of the use of radiography, CT, angiography/interventional radiology, and ultrasound in the trauma patient are available. Academic rank and salary are commensurate with experience. CV should be addressed to Salvatore J. A. Sclafani, M.D., Dept. of Radiology, Kings County Hospital Center, 451 Clarkson Ave., Brooklyn, NY 11203. An EO/AA employer. 7–9ap

CARDIOVASCULAR AND INTERVENTIONAL RADIOLOGIST—The State University of New York Health Science Center at Brooklyn seeks a board-certified/eligible radiologist with fellowship training in interventional radiology for a faculty position. The institution is a 1700-bed facility, including the Kings County and the State University hospitals. The medical center performs approximately 2000 diagnostic and interventional procedures, including angioplasty, embolization, caval filters, gastrointestinal, genitourinary, and pulmonary interventions. When ongoing renovations are complete, there will be 5 new vascular digital rooms. Research time and facilities are available. Rank and salary are commensurate with qualifications. CV should be addressed to Salvatore J. A. Sclafani, M.D., Kings County Hospital Center, Dept. of Radiology, 451 Clarkson Ave., Brooklyn, NY 11203; (718) 245-4447. An EO/AA employer. 7–9ap

NORTHERN CALIFORNIA—The Permanente Medical Group, Inc., is seeking a BC radiologist with multimodality interests and fellowship training in MR to join a 12-person group serving a 337-bed, acute-care hospital and 2 outpatient clinics. Teaching opportunities are available with residents of subspecialty services on rotation from Stanford University Hospital as well as our own medical residents. We have sited a GE 1.5-T MRI system. Competitive salary and excellent benefits. Send CV to Bruce Baker, M.D., Chief, Dept. of Radiology, Kaiser Permanente Medical Center, 900 Kiely Blvd., Santa Clara, CA 95051; (408) 236-4444. EOE. 7–8a

INDIANAPOLIS, IN—Practice opportunity for a radiologist to serve as medical director of a new, freestanding, privately owned, imaging center with CT and high-field MR. Facility will be managed by and affiliated with the Center for Diagnostic Imaging in Minneapolis, MN. MR experience mandatory. Subspecialty experience in MR desirable. Board certification and ability to obtain licensure in Indiana required. Please send inquiries with CV to Cooper R. Gundry, M.D., Center for Diagnostic Imaging, 5775 Wayzata Blvd., Ste. 190, Minneapolis, MN 55416. All inquiries entirely confidential. No telephone calls please. 7–9ap

RADIOLOGIST—Second radiologist needed for a 54-physician, multispecialty clinic located in western Montana. Experience or formal training in mammography a must; general radiologic procedures excluding CT and MRI. Offered salary and benefits generous. Send CV to Administrator, Western Montana Clinic, P.O. Box 7609, Missoula, MT 59807. 7ap

THIRD STAFF RADIOLOGIST sought at the VA Medical Center, Fayetteville, NC. Must have current license in any of the 50 states and be BC/BE in radiology. Well-equipped dept. is 3 yr old with new CT suite (Picker) to open in May. Latest Acuson ultrasound model is planned as well. Hospital has 180 active beds with general medicine, surgery, and psychiatry population. Presently no angio, and night call is minimal. Quiet lifestyle and easy access to mountains, beaches, and big cities. Contact Ms. Johnson, Personnel Service, (919) 822-7056, or write VAMC, Personnel Service, Fayetteville, NC 28301. EOE/M/F. 7a

LARGE, GROWING RADIOLOGY PRACTICE IN CENTRAL NEW JERSEY and adjacent Pennsylvania region seeks diagnostic radiologist with expertise in 1 or more of the following: CT/ultrasound, angio/interventional, or nuclear medicine. Send resume to E. Tarasov, M.D., 838 W. State St., Trenton, NJ 08618. 7–9a

RADIOLOGIST wanted with diagnostic and interventional radiology experience including CT, sonography, mammography, angiography, interventional, nuclear radiology, and plain film interpretation and fluoroscopy. M.D. degree, certification in diagnostic and nuclear radiology by the American Board of Radiology, and 5 yr postcertification experience required. $100,000/yr, 50 hr/wk. Interested parties should send resumes in duplicate to New York State Job Service, 68 W. Huron St., Buffalo, NY 14202, Attn. P. Oldenburg (Order No. 0702560). 7ap

IMMEDIATE OPENING FOR A BC/BE DIAGNOSTIC RADIOLOGIST—Join 1 other as a full-time partner under fee-for-service billing. Ideal family community located in western Pennsylvania, approximately 60 mi. north of Pittsburgh. This is an acute-care hospital with 180 beds doing approximately 30,000–35,000 exams/yr. Need experience in general radiology, some angiography and interventional procedures, ultrasound, CT, MRI (mobile), and mammography services. Applicant should respond as soon as possible with letter of interest and current CV to Wan Jo Kim, M.D., Director of Radiology, St. Francis Hospital of New Castle, 1000 S. Mercer St., New Castle, PA 16101; (412) 656-6011/6116 (before 5 p.m.), (412) 656-0752 (after 5 p.m.). 7–9ap

DIAGNOSTIC RADIOLOGIST, LONG ISLAND, NY—Board-certified radiologist with expertise in MRI needed to join a 5-member group starting in July 1991. Fellowship training in MRI or neuroradiology is desirable. Must be willing to do most aspects of diagnostic radiology. This well-established practice includes a 325-bed community hospital, a private diagnostic radiology office, and a 1-yr-old MRI facility with a high-field-strength magnet. Generous salary leading to full partnership. Contact Ira Langer, M.D., 250 Hospital Rd., Patchogue, NY 11772; (516) 475-1030. 7–8ap

VETERANS AFFAIRS MEDICAL CENTER, WASHINGTON, DC, a major, tertiary hospital affiliated with George Washington University Medical School, Georgetown University Medical School, and Howard University Medical School, is seeking a qualified neuroradiologist to fill an immediate opening. Qualifications include board certification in radiology with fellowship training in neuroradiology. Send cover letter and CV to Chief of Staff (11), Dept. of Veterans Affairs, 50 Irving St., N.W., Washington, DC 20422. EOE. 7a

DIAGNOSTIC RADIOLOGIST, FLORIDA—Staff radiologist is being sought by the University of Florida Health Science Center/Jacksonville for a full-time faculty position. Special interest, expertise, or fellowship training in CT, ultrasound, MR, interventional, or nuclear radiology is preferable. Florida license required. Salary and fringe benefits are excellent. An academic appointment will be at the instructor/assistant professor/associate professor/professor academic rank depending on training, background, and experience. Application recruiting deadline is Sept. 1, 1991. Send CV and references to Chairman, Search Committee, Dept. of Radiology, University Medical Center, 655 W. Eighth St., Jacksonville, FL 32209. AA/EOE. 7–8a

MAMMOGRAPHY STAFF POSITION—The Dept. of Radiology of the Ochsner Clinic is seeking a radiologist to head a rapidly growing Section of Mammography. Currently over 15,000 mammograms and 500 localization procedures are performed annually. Equipment includes 4 ACR-accredited mammographic units and stereotactic localization equipment. A major expansion in space for the mammography section will be completed in mid-1992, providing capability for approximately 30,000 procedures/yr. The mammography section provides imaging services for a multidisciplinary breast center with a high degree of clinical and research interaction with surgical, medical, and pathology services. The radiology dept. is active in teaching and clinical research, with a staff of 22 residents and fellows. Candidates for this position should have fellowship training or a strong background in mammography and be interested in teaching and clinical research as well as patient care. Compensation and benefits are highly competitive. For additional information, contact Christopher R. B. Merritt, M.D., Chairman, Dept. of Radiology, Ochsner Clinic, 1514 Jefferson Highway, New Orleans, LA 70121; (504) 838-3495. 7–9a

ULTRASOUND STAFF POSITION—The Dept. of Radiology of the Ochsner Clinic is seeking an additional radiologist to meet growing clinical needs in the Section of Ultrasonography. The ultrasound section of the dept. currently performs over 12,000 procedures/yr, including a full range of abdominal, OB/GYN, vascular, small parts, operative, interventional, and pediatric studies. State-of-the-art imaging, duplex color Doppler, and intraoperative equipment is available. A major expansion in space for the ultrasound section will be completed in mid-1992. The dept. is active in teaching and clinical research, with a staff of 22 residents and fellows. Candidates for this position should have fellowship training or a strong background in ultrasonography and be interested in teaching and clinical research as well as patient care. Compensation and benefits are highly competitive. For additional information, contact Christopher R. B. Merritt, M.D., Chairman, Dept. of Radiology, Ochsner Clinic, 1514 Jefferson Highway, New Orleans, LA 70121; (504) 838-3495. 7–9a

RADIOLOGIST—BC/BE radiologist needed to join 2-person practice covering 2 hospitals in the central mountains of Colorado. Ample free time and excellent outdoor recreational opportunities. Contact E. J. Loeffel, M.D., P.O. Box 415, Buena Vista, CO 81211; (719) 539-3782. 7–9ap

UCSD SCHOOL OF MEDICINE—The Dept. of Radiology is seeking a neuroradiologist to participate in clinical, teaching, and research programs. Qualifications required are board-eligibility/certification, California medical license, and a 2-yr fellowship in neuroradiology including MR imaging. Title series is assistant/associate professor (in-residence or clinical series — not currently a tenure-track position); level is based on years' experience, and salary is commensurate with rank and step of appointment based on the established salary schedule of the UCSD School of Medicine Faculty Compensation Plan. The University of California, San Diego, is an equal opportunity/affirmative action employer. All CVs received before Aug. 31, 1991, or thereafter until position is filled, will be assured full consideration. Send to John Hesselink, M.D., Professor of Radiology, Dept. of Radiology, UCSD Medical Center, 225 Dickinson St., San Diego, CA 92103. 7a

CHIEF, NEURORADIOLOGY—A large, southern California radiology practice offers this prestigious opportunity. Various imaging modalities are used, including significant MRI volume. Candidates must be board-certified and possess the experience a position of this nature warrants. Please send CV in confidence to Physician Recruitment, 14755 Ventura Blvd., Ste. 1-850, Sherman Oaks, CA 91403, Attn. Chief Operating Officer. 7ap

UCSD SCHOOL OF MEDICINE—The Dept. of Radiology is seeking a cardiovascular radiologist to participate in clinical, teaching, and research programs. Qualifications required are board-eligibility/certification, California medical license, and a 1-yr fellowship in cardiovascular radiology or vascular/interventional radiology. Title series is assistant/associate professor (in-residence or clinical series); level is based on years' experience, and salary is commensurate with rank and step of appointment based on the established salary schedule of the UCSD School of Medicine Faculty Compensation Plan. The University of California, San Diego, is an equal opportunity/affirmative action employer. All CVs received before Sept. 1, 1991, or thereafter until position is filled, will be assured full consideration. Send to Joseph J. Bookstein, M.D., Professor of Radiology, Dept. of Radiology, UCSD Medical Center, 225 Dickinson St., San Diego, CA 92103-1990. 7a

THE DEPT. OF RADIOLOGY AT THE UNIVERSITY OF MASSACHUSETTS MEDICAL CENTER in Worcester is seeking a BC/BE radiologist with a major interest in abdominal radiology with fellowship experience desirable. A strong interest in teaching and collaborative clinical research is desired. Rank and salary are commensurate with experience. The medical center is a 370-bed university hospital and medical school located approximately 40 mi. west of Boston. The dept. consists of 22 staff, 13 residents, and 2–4 fellows and does approximately 130,000 exams/yr. The dept. is well-equipped with 2 GE 9800 HiLite CT scanners, 2 GE 1.5-T MRI scanners in a standalone facility, a 2.0-T small-bore unit for animal research, several state-of-the-art ultrasound scanners, color Doppler, transrectal ultrasound, etc. The hospital is a major trauma center and is serviced by 2 Life Flight helicopters. For further information, contact Edward H. Smith, M.D., Professor and Chair, Dept. of Radiology, University of Massachusetts Medical Center, 55 Lake Ave. N., Worcester, MA 01655; (508) 856-3252. UMMC is an equal opportunity/affirmative action employer. 7xa

IMMEDIATE OPENING IN PALM SPRINGS, CA Radiologist with MRI expertise/specialization needed to join 10-person group in community hospital/office practice. Contact Marvin J. Friedenberg, M.D., Dept. of Radiology, Desert Hospital, 1150 N. Indian, Palm Springs, CA 92262. 7xap

DIAGNOSTIC RADIOLOGIST POSITIONS AVAILABLE IN THE SOUTHEASTERN UNITED STATES—Starting salary $200,000 at most locations. Paid vacation, malpractice, and CME. Must be board-eligible or certified. Submit CV to C. G. Dudley, M.D., Benning Radiology, Inc., 7 Stonewood Ct., Columbus, GA 31904; (800) 829-4613. Women and minorities are encouraged to apply. 7ap

IMMEDIATE OPENING IN PALM SPRINGS, CA Radiologist with mammography expertise/specialization needed to join 10-person group in community hospital/office practice. Contact Marvin J. Friedenberg, M.D., Dept. of Radiology, Desert Hospital, 1150 N. Indian, Palm Springs, CA 92262. 7xap

THERAPEUTIC RADIOLOGIST/RADIATION ONCOLOGIST—The VA Medical Center, Dayton, OH, is actively recruiting a second radiation oncologist to staff our new and expanding radiation therapy unit. Our equipment includes a dual-energy linear accelerator with multiple electron beam capability. Patient care services will include brachytherapy. Our medical center is a full-service, 1454-bed facility affiliated with Wright State University School of Medicine with a new, acute-care facility due to be completed by fall 1991. We offer an excellent salary program, flexible benefit package, and relocation expenses. Dayton is an expanding community located in southwestern Ohio 1½ hr from Columbus and 1 hr from Cincinnati. Contact Judy Williams (05), VA Medical Center, 4100 W. Third St., Dayton, OH 45428; (513) 268-6511, ext. 2509. An equal opportunity employer. 7a

RADIOLOGIST/ANGIOGRAPHER—There is an opportunity to join a progressive group of 11 board-certified radiologists practicing at the Lehigh Valley Hospital Center, a 500-bed, university-affiliated hospital. The position requires angiographic/interventional skills and an interest in general radiology including CT and ultrasound. The radiology dept. has state-of-the-art equipment including 2 angiographic suites, 3 CT scanners, color flow Doppler, and MRI. The hospital is an acute-care facility and a state-designated Level 1 Trauma Center, located 1 hr from Philadelphia and 1½ hr from New York. The radiology dept. offers a postresidency fellowship program that includes training in angiography. The position offers a competitive salary and benefit package that leads to full partnership. For further information, contact Robert Kricun, M.D., Dept. of Radiology, Lehigh Valley Hospital Center, P.O. Box 689, Allentown, PA 18105; (215) 776-8088. 6–8ap

SUPERB PARTNERSHIP POSITION IN LAS VEGAS, NV—Rapidly expanding, 7-member group practice covering 2 full-service imaging centers and a small hospital has an immediate opening. We are looking for an additional board-certified radiologist with an uncommon dedication to excellence in patient care. Our outpatient facilities include 2 MR, 2 CT, angio with a 4-bed recovery area, 5 ultrasound, 5 mammography, 2 SPECT, plus R & F. This is an excellent opportunity for a partnership position with a well-respected group in a growing community. Please send CV to Dr. Mark Winkler, SDMI, 2950 S. Maryland Pkwy., Las Vegas, NV 89109. 5–10a

BC/BE BREAST IMAGING RADIOLOGIST needed part/full-time to join 2 member group for outpatient women's diagnostic center. Mammography and OB/GYN sonography expertise required. Flexible hr/no call. Ideal for radiologist with family responsibilities or semiretired. Immediate availability. Contact Frankie Weier, Director, Women's Center for Radiology, 615 E. Princeton St., Ste. 101, Orlando, FL 32803; (407) 894-2466. 6–7ap

LOCUM TENENS, 1 YR—I will be taking a yr of sabbatical and need a BC/BE radiologist to cover my hospital practice in a northern California summer and winter recreational area. Practice includes routine radiography, CT, ultrasound, mammography, and nuclear medicine. Please reply to Box M32, *AJR* (see address this section). 6–7ap

RADIOLOGIST/NUCLEAR MEDICINE—A 25-person radiology group in central New Jersey seeks a board-certified radiologist with additional nuclear medicine boards or ABR special competency to share responsibilities in nuclear medicine and some general radiology. Cardiac, nuclear, and SPECT experience required. Practice includes 2 450-bed hospitals, 3 offices, a radiology residency, and medical student teaching. Send CV to Richard Feinstein, M.D., c/o Kathy McGrath, Radiology Group of New Brunswick, 230 Old Bridge Tpk., South River, NJ 08882. 6–7a

PHYSICIAN/RADIOLOGIST—Full-time opening for board-certified radiologist in a desirable southern New Jersey shore location. This is an active, challenging, expanding hospital- and office-based practice. Must have training in CT, ultrasound, and MRI. Send CV to RABC, P.O. Box 729, Mt. Holly, NJ 08060. 6–8ap

DIAGNOSTIC RADIOLOGIST—Position for a board-certified radiologist to provide sole coverage for a 27-bed hospital in a southeast Idaho community of 20,000. Immediate potential for a $220,000 practice while still having time to enjoy geographical amenities. Contract available. Please call or write Randall G. Holom, 1224 8th St., Rupert, ID 83350; (208) 436-0481. 6–8a

ANGIOGRAPHY/INTERVENTIONAL RADIOLOGIST needed to join the staff at William Beaumont Hospital, a modern, major, tertiary-care, teaching medical center in southeastern Michigan with residency and fellowship programs in diagnostic radiology. The dept. is expanding its state-of-the-art facilities to accommodate increasing demands on patient care. Fellowship in angiography/interventional radiology is required. Past experience in academic institutions is desirable. Area offers 1 of the best educational and recreational facilities. Excellent compensation. Write to Jalil Farah, M.D., Chairman, Diagnostic Radiology, William Beaumont Hospital, 3601 W. 13 Mile Rd., Royal Oak, MI 48073. 6–8ap

CHEST RADIOLOGIST, CLEVELAND CLINIC FOUNDATION—The Cleveland Clinic Foundation has an opening for a staff position in the Section of Thoracic Imaging. The foundation is a 1000-bed hospital with a large outpatient population and an international referral base. Successful applicants will be involved in all diagnostic modalities, including CT, MRI, and interventional procedures. A strong interest in teaching, research, and patient care is required. Applicants should be board-certified, fellowship-trained, or have equivalent experience. Excellent salary and benefit package. Send CV to Moulay A. Meziane, M.D., Head, Section of Thoracic Imaging, Cleveland Clinic Foundation, One Clinic Center Dr., Cleveland, OH 44195-5021. The Cleveland Clinic Foundation is an equal opportunity employer. 5–10ap

NEURORADIOLOGIST—Join the current staff of 2 neuroradiologists at William Beaumont Hospital, a modern, tertiary-care medical center in southeastern Michigan with residency and fellowship programs in diagnostic radiology. The dept. is expanding its state-of-the-art facilities to accommodate increasing demands on patient care. Area offers 1 of the best educational and recreational facilities. Excellent compensation. Write to Jalil Farah, M.D., Chairman, Diagnostic Radiology, William Beaumont Hospital, 3601 W. 13 Mile Rd., Royal Oak, MI 48073. 5–7a

NUCLEAR MEDICINE—The UCLA Dept. of Radiological Sciences is seeking a board-certified radiologist in nuclear medicine and/or radiology at the assistant professor level with extensive experience in positron emission tomography and related imaging methods. Added experience in imaging processing and mathematical modeling is desirable. Send application, CV, and names and addresses of 3 references or inquiries to Hooshang Kangarloo, M.D., Chairman, Dept. of Radiological Sciences, UCLA Medical Center, Los Angeles, CA 90024-1721. An EO/AA employer. 5–7a

DIAGNOSTIC RADIOLOGIST / PARTNERSHIP POTENTIAL—Well-established, multioffice practice offers an outstanding opportunity for growth to a BC/BE radiologist. Procedures include standard radiography and fluoroscopy, mammography, nuclear medicine, and ultrasound. IVF-associated procedures are a key specialty. Large referral base. Physician has 25+ yr experience and needs to share the burden of a still-expanding practice. Collateral earnings potential by reading for other medical groups with imaging capability. We are located in the Boston area near major roadways; you can live in any of Boston's beautiful suburbs. First-class equipment and excellent technologists will support your efforts. Please send your current CV and a cover letter to Box L21, *AJR* (see address this section). 5–7a

DIAGNOSTIC RADIOLOGIST, EL PASO, TX—BE/BC radiologist with special competence in body imaging sought to join busy hospital radiology practice at a community medical center with a total of 330 beds. Modern imaging dept. with 1.5-T GE MR, CT, nuclear medicine with SPECT, ultrasound, angiography with DSA, mammography, and diagnostic radiography. Excellent salary, vacation, and benefits leading to early partnership. Send inquiries with CV to Roy K. Poth, M.D., 1625 Medical Center Dr., El Paso, TX 79902. 5–8ap

IMMEDIATE OPENING—BC diagnostic radiologist, imaging fellowship preferred, with experience in general radiology and expertise in interventional procedures and angiography, sought to join a group of 4 active, university-trained radiologists. Modern, 220-bed hospital in south suburb of Chicago with active ER and outpatient services. State-of-the-art equipment includes MRI, CT, ultrasound, nuclear medicine, and mammography. Attractive and competitive benefits package leading to early partnership. Contact John M. Nayden, M.D., South Suburban Hospital, 17800 S. Kedzie Ave., Hazel Crest, IL 60429; (708) 799-8010, ext. 3276. 5–7ap

LOCUMS NATIONWIDE—BC or BE diagnostic radiologists needed for nationwide locums. Opportunities range from 1 wk to several mo. Exceptional compensation and all travel expenses. Call Professional Temporary Services, Inc., 790 Cardinal Rd., P.O. Box 2702, New Bern, NC 28561; (800) 872-4534. 5–8a

THE UNIVERSITY OF MASSACHUSETTS MEDICAL CENTER, a tertiary-care hospital situated 40 mi. from Boston, is seeking a third pediatric radiologist. The pediatric dept. services central and eastern Massachusetts as well as southern New Hampshire and northern Connecticut. All medical and surgical pediatric subspecialties are represented and a broad range of pediatric pathology is encountered. Pediatric radiologists have the primary responsibility in ultrasound, CT, MRI, and interventional procedures in general radiologic exams. Competitive salaries and generous benefits are provided. For further information, contact Paul K. Kleinman, M.D., Dept. of Radiology, University of Massachusetts Medical Center, 55 Lake Ave., N., Worcester, MA 01655; (508) 856-3124, fax (508) 856-4669. 7xa

DIAGNOSTIC RADIOLOGIST with skills in CT, MR, interventional, ultrasound, and nuclear medicine needed to join group of 8 board-certified radiologists. Growing practice in eastern Washington at a 228-bed hospital, a new multimodality imaging center, and 2 private offices. Potential for long-term practice is excellent. Top-notch school system, including 3 first-rate universities. Excellent hunting, fishing, boating, and skiing. Contact L. E. Crecelius, M.D., N. 5901 Lidgerwood, Ste. 18B, Spokane, WA 99207; (509) 482-2385. 5-10ap

MAMMOGRAPHY, UNIVERSITY OF PENNSYLVANIA, HALF- OR FULL-TIME POSITION—Exceptional opportunity in academic mammography within a high-volume, rapidly expanding, breast imaging section. Ongoing screening and problem-solving mammography, breast ultrasound, and collaborative projects. Academic rank and salary commensurate with credentials. Resident and student teaching responsibilities along with negotiable participation in bone and chest outpatient radiology. Position available immediately. Applicant must be ABR-certified and able to obtain license in Pennsylvania. U of P is an affirmative action, equal opportunity employer, and specifically encourages applications from women and minorities. Send letter and CV to Rosalind H. Troupin, M.D., Dept. of Radiology, H.U.P., 3400 Spruce St., Philadelphia, PA 19104. 5-7ap

BC/BE RADIOLOGIST—Full-time staff radiologist sought for active, tertiary-care medical center. Duties include interpreting general diagnostic films (excluding mammography), performing radiologic procedures and fluoroscopy, and supervising and training residents with affiliated medical center. Additional subspecialty skills or training in ultrasound/CT, and/or angiography and interventional procedures are beneficial. Candidate should be qualified to hold a faculty position with Yale University School of Medicine, and must be a U.S. citizen or qualify as a permanent resident of the United States. CV and letters of reference should be sent to Caroline Taylor, M.D., Chief, Radiology, Dept. of Veterans Affairs Medical Center, West Haven, CT 06516. The DVA Medical Center and Yale University are equal opportunity/affirmative action employers. Applications from women and minority group members are encouraged. Application deadline is Aug. 1, 1991. 5-7a

DIRECTOR OF NEURORADIOLOGY—Position available for Director of Neuroradiology in 700-bed, university-affiliated teaching hospital with fully approved residency program. Modern equipment includes digital subtraction angiography, 2 CT, and 1 MRI. Staff of 12 full-time radiologists. Excellent salary and fringe package. Send CV to David Bryk, M.D., Maimonides Radiology Associates, P.C., 4802 Tenth Ave., Brooklyn, NY 11219. 5-7ap

DIAGNOSTIC RADIOLOGIST—Immediate opening leading to partnership in expanding, 4-member, hospital-based practice near Boston. Seeking recently trained BC/BE radiologist with skills and experience in general radiology, ultrasound, mammography, CT, and angio/interventional. Interested persons should contact Steven Sitzman, M.D., The Malden Hospital, One Hospital Rd., Malden, MA 02148; (617) 322-7560. 5-7ap

BC/BE RADIOLOGIST, SOUTHEASTERN MICHIGAN—Seven radiologists covering a 350-bed community hospital with a new women's center seek a radiologist with a fellowship in ultrasound and special interest in OB ultrasound. Practice involves all aspects of imaging modalities including MRI. Competitive compensation package leading to partnership. Send inquiries and a CV with references to Bhaskar U. Shenai, M.D., Professional X-Ray Center, 67 Cass Ave., Mt. Clemens, MI 48043. 5-7ap

PRACTICE OPPORTUNITY IN FAST-GROWING LAS VEGAS, NV—Expanding, 6-member radiology group is seeking 2 additional BE/BC radiologists for July 1991 and Jan. 1992. We currently serve 2 hospitals with an outpatient imaging center to open in Jan. 1992. Outstanding salary and benefits package leading to full partnership in 2 yr. Send CV or contact Marc Pomerantz, M.D., Head of Search Committee, 1925 Spode Ave., Henderson, NV 89014; (702) 388-4640. 5-9ap

IMAGING RADIOLOGIST—Join the current staff of 5 imaging radiologists (MR/CT/ultrasound) at William Beaumont Hospital, a modern, tertiary-care medical center in southeastern Michigan with residency and fellowship programs in diagnostic radiology. The dept. is expanding its state-of-the-art facilities to accommodate increasing demands on patient care. Area offers 1 of the best educational and recreational facilities. Excellent compensation. Write to Jalil Farah, M.D., Chairman, Diagnostic Radiology, William Beaumont Hospital, 3601 W. 13 Mile Rd., Royal Oak, MI 48073. 5-7a

DIAGNOSTIC RADIOLOGIST, IMMEDIATE OPENING—Ten-person radiology group seeks a diagnostic radiologist with fellowship training, including body MRI/body imaging, to join a busy, hospital-based practice located in rapidly growing north Dallas. GE 1.5-T magnet, Toshiba midfield magnet, 2 GE 9800 scanners, Acuson 128 with color flow Doppler, and new special procedures suite with DSA. Please send CV to Box K54, *AJR* (see address this section). 7xa

UTMB, GALVESTON, TX—The Dept. of Radiology of the University of Texas Medical Branch in Galveston has openings for persons trained and experienced in ultrasonography and mammography. The opportunity for academic advancement is great and benefits are generous. Salaries are competitive and living conditions are desirable. Interested persons should contact Melvyn H. Schreiber, M.D., Chairman, Dept. of Radiology, UTMB, Galveston, TX 77550; (409) 761-1823. UTMB is an equal opportunity M/F/H/V affirmative action employer. UTMB hires only individuals authorized to work in the United States. 4-9a

RADIOLOGIST—Immediate opening for a qualified, board-certified/eligible radiologist to work in an outpatient imaging center located 40 mi. north of El Paso, TX. Must have knowledge of general radiology and experience with ultrasound, CT, and nuclear medicine. Interested doctors should send CV to Sun View Imaging Services, P.O. Box 8624, Las Cruces, NM 88006. 6-7ap

DALLAS, TX—A 12-member, subspecialty group seeks a board-certified, general radiologist for an immediate opening. Fellowship training preferred, but will consider qualified individual with special expertise. CT/ultrasound, MRI, nuclear medicine, or angiography background particularly helpful. All imaging modalities available (state-of-the-art CT, angio, ultrasound, R & F, SPECT nuclear medicine, and MRI center). Salary and bonuses are excellent. Health and malpractice paid. No buy-in to partnership. Send CV to H. Stuart Peake, M.D., P.O. Box 814129, Dallas, TX 75381; (214) 888-7055. 4-9ap

IMMEDIATE OPENING FOR BC/BE GENERAL RADIOLOGIST with experience in interventional and vascular radiology. Join a group of 4 radiologists in a 160-bed hospital located in Allentown, PA, about 60 mi. northwest of Philadelphia. The daily practice includes all aspects of general radiology, CT, ultrasound, and nuclear medicine. Please call or send CV to Asad Shohadai, M.D., Allentown Osteopathic Medical Center, 1736 Hamilton St., Allentown, PA 18104; (215) 770-8700. 7xa

RADIOLOGIST, CAPITOL DISTRICT, NEW YORK STATE—Well-established, hospital-based group practice in upstate New York seeks a board-certified, general diagnostic radiologist with special competence and interest in nuclear medicine and MRI. Angiography and interventional experience will be helpful. This will be an additional opening to a 5-person group currently performing all aspects of radiology. Salary first yr leading to full partnership. Please send CV to John J. Gorman, M.D., Dept. of Medical Imaging, St. Clare's Hospital, 600 McClellan St., Schenectady, NY 12304; (518) 382-2310. 4-7ap

DIAGNOSTIC RADIOLOGIST needed in Conway Hospital, a community hospital located 10 mi. west of the resort/seaside community of Myrtle Beach, SC. The dept. performs 44,000 exams/yr including CT, MRI, nuclear medicine, ultrasound, mammography, and special procedures. All exams are done on state-of-the-art equipment. Our 3-person group offers a very strong financial package with all benefits including 17-wk vacation. Lovely, rapidly growing resort area includes 60 mi. of sandy beaches, 70 golf courses, and beautiful seaside homes. Contact Gary Rike, M.D., P.O. Box 917, Conway, SC 29526; (803) 347-7277. 6-8ap

BOSTON, IMMEDIATE OPENING—Radiologist wanted to join busy, well-established, private-practice group with 4 outpatient facilities. Expertise in ultrasound and mammography. No evening or weekend call. Excellent life-style, partnership opportunity. Send letter and CV to Box E49, *AJR* (see address this section). 6-11ap

NEURORADIOLOGIST, BIG SKY COUNTRY—Group of 5 radiologists seek a BC, fellowship-trained colleague. Hospital and busy clinical practice. Must be a capable, general diagnostic radiologist. One yr to partnership. Send letter/CV to Bruce Pinkerton, M.D., Dept. of Diagnostic Radiology, Deaconess Medical Center. P.O. Box 2547, Billings, MT 59103. 2-7ap

DUKE UNIVERSITY MEDICAL CENTER/STAFF RADIOLOGISTS—Duke University Medical Center is seeking qualified candidates for staff positions in the Dept. of Diagnostic Radiology. A limited number of staff positions currently are available in the following sections: general diagnostic, pediatric, chest, vascular/interventional, and musculoskeletal radiology. We offer an excellent salary and benefits package. The radiology dept. is state-of-the-art in diagnostic imaging with diverse resources available for clinical, teaching, and academic pursuits. Staff members have guaranteed academic time and research support. Interested board-certified radiologists with appropriate experience should phone Robert Vandemark, M.D. at (919) 681-2711 ext. 5233, for additional information. Letters of inquiry should be sent to Carl E. Ravin, M.D., Dept. of Radiology, Box 3808, Duke University Medical Center, Erwin Rd., Durham, NC 27710. AA/EOE. 2-7a

SAN ANTONIO, TX—Group covering multiple hospitals and clinics seeks radiologists with imaging and angiography skills. Send CV to Search Committee, M & S X-Ray Associates, P.O. Box 15920, San Antonio, TX 78212-9510. 3-8ap

SEATTLE COLLEAGUE WANTED—Growing radiology group seeks new member. Full-service radiology dept. (50,000 procedures/yr) offers diagnostic, nuclear medicine, ultrasound (including vascular-Doppler), interventional, CT, and MRI. Outpatient imaging dept. (building permits pending) scheduled to open late 1991 that will include high-field GE Signa MR with MRA. Extremely favorable track for partnership. For further information regarding this opening, please contact Mr. Richard G. Wedig, Highline Community Hospital, 16251 Sylvester Rd., S.W., Seattle, WA 98166; (206) 248-4561. 7-8ap

COME TO CALIFORNIA WITH A LICENSE FROM ANY STATE—Loma Linda VA Hospital has a vacancy for a board-certified radiologist. A current license from any state is acceptable. Loma Linda is located 70 mi. east of Los Angeles near beaches, mountain ski resorts, and southland theme parks. This is a 500-bed, full-service hospital with a comprehensive diagnostic facility including ultrasound, CT, and MRI integrated with the Loma Linda University Medical Center residency training program. Opportunities exist to pursue clinical or academic interests. For additional information, contact Peter Dure-Smith, M.D., Chief, Radiology (114), Jerry L. Pettis Memorial Veterans Hospital, 11201 Benton St., Loma Linda, CA 92357; (714) 422-3069, fax (714) 422-4106. Equal opportunity employer. 3–8ap

TEN-PERSON RADIOLOGY GROUP located in Corpus Christi is seeking a new associate to start July 1990 or as late as July 1991. Must be board-certified or eligible. Will perform all diagnostic studies, including interventional, CT, MRI, nuclear medicine, and ultrasound. Please send CV to Search Committee, P.O. Box 5608, Corpus Christi, TX 78465-5608. 7xa

DIAGNOSTIC RADIOLOGIST—BC/BE radiologist wanted to join expanding practice of 12 radiologists in northeastern Pennsylvania. Practice includes 3 hospitals (720 beds) and free-standing MRI. Candidate must have experience in angiography and interventional radiology, and be willing to cover other areas of diagnostic imaging. Contact Paul M. Leiman, M.D., Dept. of Radiology, Moses Taylor Hospital, 700 Quincy Ave., Scranton, PA 18501; (717) 963-2601. 6–7ap

Positions Desired

MUSCULOSKELETAL RADIOLOGIST, fellowship-trained at a major university program with over 10 yr experience in all imaging techniques, including CT and MR, seeks a full-time position in an academic or private musculoskeletal radiology practice. Currently an active clinical faculty member at 2 university programs and chief of a bone section in a radiology residency program at a large teaching/county facility (1 of the hospitals covered by our large, private-practice group). Current duties include a significant amount of general radiology. Priorities include high-quality practice of radiology, state-of-the-art equipment, and congenial working environment. Western U.S. preferred, but not mandatory. Enthusiastic, healthy, ABR-certified, mid-40s, and looking for a change. Excellent references. Reply to Box N42, *AJR* (see address this section). 7–9bp

JULY 1991 RADIOLOGY RESIDENCY POSITION SOUGHT—Radiology resident completing second yr June 1991 seeks to transfer into the third yr of an academic university program. Also interested in programs offering 1 yr of research with faculty member(s) before beginning third yr. Plan a career in academic radiology. Have training in all modalities. Research experience in diagnostic imaging. Excellent references. Reply to Box L27, *AJR* (see address this section). 7bp

Fellowships and Residencies

VASCULAR/INTERVENTIONAL RADIOLOGY FELLOWSHIP—The Western Pennsylvania Hospital has an unexpected opening in a 1-yr fellowship program beginning July 1992. The program includes extensive experience in invasive and noninvasive vascular diagnosis and all aspects of vascular and nonvascular interventions. Interventional procedures include angioplasty, atherectomy, vascular and biliary stenting, thrombolysis, embolization, biliary, GU and GI interventions. Contact Gordon K. McLean, M.D., Director of Vascular and Interventional Radiology, The Western Pennsylvania Hospital, 4800 Friendship Ave., Pittsburgh, PA 15224; (412) 578-1787. 7c

FELLOWSHIP POSITIONS—The Dept. of Radiology and Radiological Sciences of Vanderbilt University School of Medicine is offering fellowship positions for 1992–1993 in angiography, musculoskeletal radiology, neuroradiology (2), and pediatrics. Research opportunities are available and encouraged. Candidates must be board-certified or qualified in diagnostic radiology and able to obtain a Tennessee medical license. Address inquiries and CV to Martin P. Sandler, M.D., Director, Fellowship Programs, Dept. of Radiology and Radiological Sciences, Vanderbilt University, Nashville, TN 37232-2675. An equal opportunity/affirmative action employer. 7–9cp

CARDIOVASCULAR-INTERVENTIONAL RADIOLOGY FELLOWSHIP—Unexpected opening available July 1, 1991, for a 1-yr fellowship program at a 750-bed teaching hospital. Extensive clinical experience involving all aspects of cardiovascular imaging, interventional vascular and nonvascular procedures, and availability for clinical or animal research. Send CV and inquiries to Oscar H. Gutierrez, M.D., Dept. of Radiology, Box 648, University of Rochester, Rochester, NY 14642-8648. An equal opportunity employer (M/F). 5–8c

CARDIOVASCULAR AND INTERVENTIONAL RADIOLOGY—The Harvard Medical School and Brigham and Women's Hospital, Dept. of Radiology, is offering a 2-yr fellowship starting July 1, 1992, in cardiovascular and interventional radiology including peripheral and coronary angiography, cardiac catheterization, digital vascular imaging, all types of interventional procedures, noninvasive vascular techniques, and cardiovascular MRI. Research time available for participation in original or ongoing clinical and/or laboratory projects. Please send CV to B. Leonard Holman, M.D., Chairman, Dept. of Radiology, Brigham and Women's Hospital, 75 Francis St., Boston, MA 02115. Brigham and Women's Hospital/Harvard Medical School is an affirmative action/equal opportunity educator and employer. 3–8c

FELLOWSHIP IN CROSS-SECTIONAL IMAGING The Dept. of Radiology, Dartmouth-Hitchcock Medical Center, has an opening for July 1992 for a 1-yr fellowship in MRI/CT/ultrasound. Training includes experience in all aspects of MRI, including neuro and body, CT, and ultrasound, including obstetric and vascular imaging. Imaging-guided biopsies and drainage procedures will be an integral part of the program. The Medical Center has a completely new 420-bed, tertiary-care hospital with state-of-the-art imaging equipment opening in the fall of 1991. Protected research time will be available for the fellow. There is ample opportunity for clinical radiologic research as well as technology assessment and outcome analysis in collaboration with Dartmouth Medical School Center for Evaluative Sciences. For further information, contact Robert D. Harris, M.D., Dept. of Radiology, Dartmouth-Hitchcock Medical Center, Hanover, NH 03756; (603) 646-5686. 7xc

FELLOWSHIPS AT THOMAS JEFFERSON UNIVERSITY HOSPITAL—The Dept. of Radiology at Thomas Jefferson University Hospital in Philadelphia offers the following fellowship programs each yr. Ultrasound/CT/MRI — Jefferson's ultrasound division is 1 of the largest in the world and performs all currently available exams including obstetric, vascular, lithotripsy, invasive, and endoluminal. We also operate 4 GE 1.5-T MRI units and 3 CT scanners. Contact Barry Goldberg, M.D., regarding this program. Cardiovascular/interventional — this division is housed in a new suite containing Philips angio units with DSA and performs the full range of vascular and nonvascular interventional procedures. Contact Geoffrey Gardiner, Jr., M.D. Neuro/ENT radiology — very active clinical services supply a wealth of material to this division, which is housed in a neurosciences imaging center containing all imaging modalities. Contact Carlos Gonzalez, M.D. Breast Imaging — Jefferson's new breast imaging center performs approximately 85 studies/day including ultrasound and needle localizations. Contact Stephen Feig, M.D. Chest — includes biopsies and CT. Contact Robert Steiner, M.D. MRI — a dedicated body MRI program including excellent research opportunities in addition to a large clinical case load. Contact Matthew Rifkin, M.D. Ultrasound — a dedicated ultrasound program. Contact Barry Goldberg, M.D. Musculoskeletal — includes MRI of the musculoskeletal system. Contact David Karasick, M.D. All program directors listed above can be contacted at the Dept. of Radiology, Thomas Jefferson University Hospital, Philadelphia, PA 19107. Jefferson is an equal opportunity/affirmative action employer. 7xc

MUSCULOSKELETAL RADIOLOGY FELLOWSHIP—Applications are now being accepted for a musculoskeletal fellow position for 1992 at the Cleveland Clinic Foundation (CCF). CCF is a 1000-bed, tertiary-care, teaching medical center with a large radiology residency program. Local, national, and international patients provide an interesting and varied mix of bone pathology. Training includes all aspects of musculoskeletal radiology including MR, CT, arthrography, biopsy, bone densitometry, and a large plain film experience. Fellowship includes patient care, teaching, and research. There is a close working relationship with the orthopedic, rheumatology, and endocrinology depts. There are presently 4 musculoskeletal staff in the section. For further information, please contact Bradford J. Richmond, M.D., Head, Section of Musculoskeletal Radiology, Desk A-21, 9500 Euclid Ave., Cleveland, OH 44195; (216) 444-3931. 5–10c

DUKE UNIVERSITY MEDICAL CENTER FELLOWSHIP POSITIONS — Duke University Medical Center is seeking qualified candidates for fellowship positions in the Dept. of Diagnostic Radiology. Currently there are positions available in the following areas: chest, musculoskeletal, and vascular/interventional radiology, ultrasound, advanced diagnostic imaging, MRI, neuroradiology, abdominal imaging, mammography, and research fellowships. The radiology dept. is state-of-the-art in diagnostic imaging with diverse resources available for clinical, teaching, and academic pursuits. Fellowship training is generally organized by organ systems, although experience can be individualized to accommodate special interests. Salary and benefits are competitive and academic time is guaranteed. For additional information, please phone Richard Leder, M.D. at (919) 681-2711 ext. 5310. Applications are due Feb. 1 of the preceding yr and can be obtained by writing to N. Reed Dunnick, M.D., Dept. of Radiology, Duke University Medical Center, Erwin Rd., Box 3808, Durham, NC 27710. AA/EOE. 2–7c

FELLOWSHIPS IN PEDIATRIC RADIOLOGY AND PEDIATRIC NEURORADIOLOGY—The Dept. of Radiology, Children's Hospital Medical Center, Cincinnati, OH, offers 1- or 2-yr fellowships in pediatric radiology beginning July 1, 1993. A 1-yr pediatric neuroradiology fellowship program is also offered and may be taken separately or combined with 1 yr of adult neuroradiology fellowship at the University of Cincinnati Medical Center. Children's Hospital Medical Center (CHMC) is a 355-bed institution. The dept. performs over 105,000 radiologic exams annually in the largest children's hospital and ambulatory practice in the U.S. The dept. has 14 full-time faculty pediatric radiologists, 6 fellows, and many resident trainees. Five pediatric radiology and 1 pediatric neuroradiology fellowship positions are available annually. Training includes all aspects of pediatric imaging: neonatal radiology, neuroimaging, musculoskeletal radiology, cardiovascular and thoracic imaging, abdominal imaging, oncologic imaging, ultrasonography, nuclear medicine, CT, MRI, and vascular/interventional procedures. The dept. has an active clinical service with state-of-the-art equipment as follows: digital fluoroscopy; Acuson, AI, and ATL ultrasound units with Doppler and color flow Doppler capabilities; planar SPECT gamma cameras; GE 9800 Quick CT scanner; 1.5-T GE MRI with spectroscopy; and cardiac catheterization/angiographic suite with digital vascular imaging. The fellowship provides a broad clinical experience in pediatric radiology as well as numerous opportunities to participate in both clinical and basic research. Candidates must be board-certified or board-qualified in diagnostic radiology and must be able to obtain an Ohio medical license. Salary and fringe benefits are highly competitive. Applications are due before Jan. 1992, with interviews scheduled during the fall and winter of 1991–1992. There are numerous career opportunities in pediatric radiology in academic and private practice settings. To receive more information about the fellowships at CHMC or careers in pediatric radiology, please contact Donald R. Kirks, M.D., Director, Dept. of Radiology, Children's Hospital Medical Center, Cincinnati, OH 45229-2899; (513) 559-8058. Children's Hospital Medical Center and the University of Cincinnati College of Medicine are affirmative action/equal opportunity employers. 5–4cp

IMAGING FELLOWSHIP—A 1-yr fellowship in ultrasound, MRI, and body CT is available July 1, 1992–June 30, 1993, at a 576-bed teaching hospital. The Dept. of Radiology performs more than 140,000 exams with state-of-the-art equipment. The ultrasound section is responsible for all aspects of sonography including OB-GYN, pediatric, abdominal, and small parts. Extensive training in color flow imaging, duplex Doppler, transvaginal, transrectal techniques, and sonographically guided procedures. Two GE MRI scanners and 2 GE 9800 Quick CT units provide high-volume caseloads in these areas. Opportunities are available for participation in imaging research. For further information, please contact Marcela Bohm-Velez, M.D., Imaging Fellowship Director, West Penn Hospital, 4800 Friendship Ave., Pittsburgh, PA 15224. 5–10c

FELLOWSHIP IN ULTRASOUND/CT/ANGIO/INTERVENTIONAL—A 1-yr fellowship program available beginning July 1992 at Lehigh Valley Hospital Center in Allentown, PA. LVHC is a 492-bed, acute-care, university-affiliated hospital. The fellowship program offers training in CT (head and body), ultrasound, angiography (neuro and visceral), and interventional radiography. MRI experience is also available. For further information, contact Robert Kricun, M.D., Dept. of Radiology, Lehigh Valley Hospital Center, P.O. Box 689, Allentown, PA 18105. 2–7c

IMMEDIATE OPENING, FELLOWSHIP IN PEDIATRIC RADIOLOGY—Position available for fellowship in pediatric radiology, 1- or 2-yr, beginning July 1, 1992, or July 1, 1993. Full training with abundant hands-on experience with all imaging modalities. Supported by strong Dept. of Pediatrics with a good mixture of patient material. Excellent teaching on a 1-to-1 basis and ample opportunity for pursuing academic interests. Apply to Leonard E. Swischuk, M.D., Dept. of Radiology, The University of Texas Medical Branch, Child Health Center, C-65, Galveston, TX 77550; (409) 761-2096. UTMB is an equal opportunity M/F/H/V affirmative action employer. UTMB hires only persons authorized to work in the United States. 5–7c

FELLOWSHIP IN CALIFORNIA, JULY 1991—Interventional, cross-sectional imaging (MRI, CT, ultrasound) at a large trauma center. Send CV to Dr. Levan, Dept. of Radiology, St. Mary Medical Center, 1050 Linden Ave., Long Beach, CA 90813 or call (213) 491-9900 for information. 5–7cp

Tutorials/Courses

MAUI, HAWAII 1991—16th Annual Body Imaging Congress, October 5–12, 1991. CME I, Grand Hyatt Wailea. Medical Seminars International, Inc., 18981 Ventura Blvd., Ste. 303, Tarzana, CA 91356; (818) 774-9077, fax (818) 774-0244. 6–9d

AJR Classified Advertisements Information

Box Responses and Address for Ad Placement

Write Box ______, *AJR*, 2223 Avenida de la Playa, Suite 103, La Jolla, CA 92037-3218; Telephone: (619) 459-2229; FAX: (619) 459-8814.

How to Place an Ad

AJR accepts classified advertising for Positions Available, Positions Desired, Fellowships and Residencies, and Tutorials/Courses. Ads are accepted by mail or FAX.

Rates: $6.00/line with a $30 minimum charge. Box service is $10 additional for each month the ad appears. There are discounts for multiple insertions: 10% for 2–3 insertions; 20% for 4 or more. To estimate lines, count all words and divide by 7.

Billing: Ads *must* be prepaid, or advertisers will be billed after the ad appears *providing* a purchase order number is submitted with the advertising copy. Terms are net 30 days.

Deadlines: 6 weeks prior to issue date. For specific deadlines, telephone the *AJR* editorial office.

Estimating Ad Charges

Line charge: divide total words by 7 and multiply by $6.00 ..... $ ________
Multiple insertions? If so, multiply by number .... × ________
Subtotal .... $ ________
Discount applies to two or more insertions. Subtract 10% if ad appears 2–3 months; 20% if 4 months or more ...... − ________
Subtotal .... $ ________
Box response requested? If so, multiply number of months by $10.00 .... + ________
Approximate advertising charge .... $ ________

The Osler Institute
Radiology Review Course
September 26-October 1, 1991 – Chicago
May, 1992 – Louisville

OBJECTIVES

- Improve basic knowledge and clinical skills in radiology
- Assist residents and fellows to study efficiently
- Prepare recent graduates to meet their next milestones
- Provide practicing radiologists with a review and update

METHODS

- HOME STUDY MATERIALS consisting of written questions with assignments and answers with explanations
- SEMINAR with projection slides and syllabus
- PRACTICE EXERCISES with oral and written parts

*"The faculty was outstanding. The most pleasant thing was learning a tremendous amount, not only from world-famous authorities but from people who are relatively unknown as well."**

Radiologic Physics
Radiation and Radiology
X-rays and Imaging
Fluoroscopy
Tomography
Computed Tomography
Ultrasonography
MRI
Quality Assurance

Chest
Infiltrates and Cavities
Nodules and Masses
Mediastinum

Cardiovascular
Heart and Aorta
Coronary Arteries
Peripheral Arteries
Echocardiography

Nuclear Radiology
Decay and Detectors
Statistics & Instrumentation
Radiopharmaceuticals
Quality Control & Licensure
Endocrine Scans and Rx
GI, GU, Bone, and Brain
Liver, Spleen, and Lung
Ga, In, and Heart

Gastrointestinal
Esophagus and Stomach
Small Bowel and Colon
Liver and Gallbladder
Pancreas and Spleen

Genitourinary
Kidney and Ureter
Bladder and Pelvis
Abdominal Ultrasound
Ob. and Pelvic Ultrasound

Bone and Joints
Tumors and Trauma
Metabolic and Endocrine
Infection
Dysplasia
Articular Disorders

Mammography

Neuro., Head and Neck
Skull and Contents
Spine, Disc and Cord
Temporal and Facial Bones
Sinuses, Larynx and Neck

Pediatric
Pediatric Chest
Cardiovascular System
Gastrointestinal Tract
Genitourinary Tract
Bones and Joints
Central Nervous System

FACULTY

Behrooz Azar-Kia, M.D.
Loyola Univ. of Chicago

Michael Blend, Ph.D.,D.O.
Univ. of Illinois at Chicago

Richard Cooper, M.D.
Loyola Univ. of Chicago

Harry Griffiths, M.D.
University of Minnesota

Fernando Gutierrez, M.D.
Washington University

Donald Jacobson, M.S.
Med. College of Wisconsin

Stephen Karesh, Ph.D.
Loyola Univ. of Chicago

Gary Loy, M.D.
University of Chicago

Mahmood Mafee, M.D.
Univ. of Illinois at Chicago

Geno Sebes, M.D.
University of Tennessee

Robert Seevers, Ph.D.
Michael Reese Chicago

Marilyn Siegel, M.D.
Washington University

Andrew Taylor, M.D.
Med. College of Wisconsin

Aruna Vade, M.D.
Loyola Univ. of Chicago

William Wehunt, M.D.
George Washington Univ.

Limited Enrollment: RADIOLOGY REVIEW REGISTRATION

Name______________________________

Address ______________________________

City/State/Zip ______________________________

Phone______________________________

Mail today to:

1094 Dawn Lane, Dept. 107
P.O. Box 2218
Terre Haute, IN 47802

For: ☐ Sept. 26-Oct. 1, 1991 – Chicago
☐ May, 1992 – Louisville
☐ Check enclosed for $_______
☐ Please send **FREE SAMPLE**

*"Accommodations were comfortable...."**

COURSES AND LOCATION: These courses are designed, scheduled and located to serve the needs of radiology residents and recent graduates. Home study questions are sent upon registration. The courses include both lectures and question sessions — faculty and students both questioning and answering in practice for what will follow. The early fall courses are more theoretical and the spring courses are more clinical. Your best value is to repeat the seminar for half price. The September course will be at the Hilton Inn, Lisle, Illinois.

*"...and those little extras...."**

LOWEST AIR FARES: Please call toll-free 1-800-548-8185 for special group fares.

*"...the most education for the money."**

FEES AND COURSE HOURS:

• **Physician or Resident:**	**Phy.**	**Res.**	**hrs.**
• Sept. 26: Radiology Physics	$135	$ 90	10
• Sept. 27 -Oct. 1: Clin. Rad.	$660	$440	50
• Sept. 26 -Oct. 1: Full Course	$750	$500	60
Repeating within 2 years:	$375	$375	60
• Mock oral exams:	$ 70	$ 70	1/2
• Private mock orals:	$100	$100	1/2

- **Add 10% within 10 days of the course.**
- Attendees not in course hotel add $20/day.
- $50.00 will reserve your position.
- Most home study material will be mailed after half of the registration fee is received.

*"...home study material was extremely helpful."**

REFUNDS: Subject to a $50 fee, refunds will be made up until the seminar begins.

- Cancellation after mailing home study material requires retention of half the fee.

INFORMATION:

Joseph H. Selliken, Jr., M.D.
The Osler Institute
1094 Dawn Lane, P.O. Box 2218
Terre Haute, IN 47802
(800) 356-7537 or **(812) 299-5658**

* *Comments by past Osler participants*

Volume 157 **American Journal of Roentgenology** July 1991

REVIEW ARTICLE

1 **Oriental cholangiohepatitis: pathologic, clinical, and radiologic features.** *Lim JH*

CARDIOPULMONARY RADIOLOGY

9 **Right and left ventricular stroke volume measurements with velocity-encoded cine MR imaging: in vitro and in vivo validation.** *Kondo C, Caputo GR, Semelka R, Foster E, Shimakawa A, Higgins CB*

17 **Case report. Traumatic rupture of the diaphragm without visceral herniation: CT diagnosis.** *Holland DG, Quint LE*

19 **Case report. Delayed appearance of localized pericardial effusion after cardiac surgery.** *Miyake H, Iwanaga S, Suzuki K, et al.*

BREAST RADIOLOGY

21 **The prevalence of carcinoma in palpable vs impalpable, mammographically detected lesions.** *Bassett LW, Liu T-H, Giuliano AE, Gold RH*

25 **Diagnostic importance of the radiographic density of noncalcified breast masses: analysis of 91 lesions.** *Jackson VP, Dines KA, Bassett LW, Gold RH, Reynolds HE*

GASTROINTESTINAL RADIOLOGY

29 **Obstructive dilatation of extrahepatic recipient and donor bile ducts complicating orthotopic liver transplantation: imaging and laboratory findings.** *Miller WJ, Campbell WL, Zajko AB, et al.*

33 **Thin-layer chromatography to monitor cholesterol gallstone dissolution by methyl *tert*-butyl ether.** *D'Agostino HB, vanSonnenberg E, Schteingart CD, Hofmann AF, Casola G, Mathieson JR*

37 **Intraperitoneal contrast material improves the CT detection of peritoneal metastases.** *Halvorsen RA Jr, Panushka C, Oakley GJ, Letourneau JG, Adcock LL*

41 **Afferent loop syndrome: sonographic findings in seven cases.** *Lee DH, Lim JH, Ko YT*

45 **Case report. Intramural and intraperitoneal hemorrhage due to duodenal ulcer.** *Radin DR*

47 **Case report. Aortoenteric fistula manifested as an intramural duodenal hematoma.** *Zeppa MA, Forrest JV*

GENITOURINARY RADIOLOGY

49 **Radiocontrast-associated renal dysfunction: incidence and risk factors.** *Lautin EM, Freeman NJ, Schoenfeld AH, et al.*

59 **Radiocontrast-associated renal dysfunction: a comparison of lower-osmolality and conventional high-osmolality contrast media.** *Lautin EM, Freeman NJ, Schoenfeld AH, et al.*

66 **Commentary. The evaluation of contrast-related renal failure.** *Bettmann MA*

69 **Ureteral pseudodiverticula: frequent association with uroepithelial malignancy.** *Wasserman NF, Zhang G, Posalaky IP, Reddy PK*

73 **Sonography of the cervix during the third trimester of pregnancy: value of the transperineal approach.** *Hertzberg BS, Bowie JD, Weber TM, Carroll BA, Kliewer MA, Jordan SG*

77 **Organic vs functional obstruction of the fallopian tubes: differentiation with prostaglandin antagonist- and β_2-agonist–mediated hysterosalpingography and selective ostial salpingography.** *Lang EK*

MUSCULOSKELETAL RADIOLOGY

81 **MR examination of the knee: interpretation with multiscreen digital workstation vs hardcopy format.** *Brown JJ, Malchow S, Totty WG, et al.*

87 **Effect of radiation therapy on thoracic and lumbar bone marrow: evaluation with MR imaging.** *Yankelevitz DF, Henschke CI, Knapp PH, Nisce L, Yi Y, Cahill P*

93 **Pictorial essay. Normal and degenerated intervertebral disk: in vivo and in vitro MR imaging with histopathologic correlation.** *Schiebler ML, Grenier N, Fallon M, Camerino V, Zlatkin M, Kressel HY*

99 **Overall body fat and regional fat distribution in young women: quantification with MR imaging.** *Gerard EL, Snow RC, Kennedy DN, et al.*

105 **Unidirectional joint communications in wrist arthrography: an evaluation of 250 cases.** *Wilson AJ, Gilula LA, Mann FA*

PEDIATRIC RADIOLOGY

111 **Safety-belt injuries in children with lap-belt ecchymosis: CT findings in 61 patients.** *Sivit CJ, Taylor GA, Newman KD, et al.*

115 **Urinary tract calculi that form on surgical staples: a characteristic radiologic appearance.** *Dangman BC, Lebowitz RL*

119 **Normal splenic size in infants and children: sonographic measurements.** *Rosenberg HK, Markowitz RI, Kolberg H, Park C, Hubbard A, Bellah RD*

NEURORADIOLOGY

123 **MR imaging of the brain in patients with diabetes insipidus.** *Tien R, Kucharczyk J, Kucharczyk W*

133 **MR imaging of intracerebral blood: diversity in the temporal pattern at 0.5 and 1.0 T.** *Zyed A, Hayman LA, Bryan RN*

139 **Dural sinus occlusion: evaluation with phase-sensitive gradient-echo MR imaging.** *Tsuruda JS, Shimakawa A, Pelc NJ, Saloner D*

147 **Pictorial essay. Differential diagnosis of head and neck lesions based on their space of origin. 1. The suprahyoid part of the neck.** *Harnsberger HR, Osborn AG*

155 **Pictorial essay. Differential diagnosis of head and neck lesions based on their space of origin. 2. The infrahyoid portion of the neck.** *Smoker WRK, Harnsberger HR*

161 **Radiologic evaluation of the normal and diseased posterior cervical space.** *Parker GD, Harnsberger HR*

VASCULAR AND INTERVENTIONAL RADIOLOGY

167 **Stenoses of vascular anastomoses after hepatic transplantation: treatment with balloon angioplasty.** *Raby N, Karani J, Thomas S, O'Grady J, Williams R*

173 **Randomized double-blind trial of midazolam/placebo and midazolam/fentanyl for sedation and analgesia in lower-extremity angiography.** *Cragg AH, Smith TP, Berbaum KS, Nakagawa N*

177 **Case report. Spontaneous fracture of a Vena-Tech inferior vena caval filter.** *Awh MH, Taylor FC, Lu C-T*

179 **Technical note. Preoperative CT-guided percutaneous localization of small masses with a Kopans needle.** *Finch IJ*

DIGITAL IMAGING

181 **Pictorial essay. Artifacts in computed radiography.** *Solomon SL, Jost RG, Glazer HS, Sagel SS, Anderson DJ, Molina PL*

MEETING NEWS

187 **The Society of Gastrointestinal Radiologists: 20th annual meeting, February 1991.** *Whalen E*

OTHER CONTENT

Book reviews 98, 122, 166, 172

36 **ARRS 1992 resident award papers information**

44 **Radiologic-pathologic conference**

110 **Medicine in American art**

160 **R. H. Ackerman, AFIP Distinguished Scientist.** *Buck JL*

186 **Books received**

194 **Forthcoming articles**

195 **Letters**

202 **Review of current literature**

205 **News**

208 **ARRS 1992 meeting announcement**

213 **American Roentgen Ray Society information**

214 **ARRS membership information and application**

217 **Classified advertisements**

A6 ***AJR* business and subscriber information**

A17 **Guidelines for authors**

1992 ARRS Meeting: May 10–15, Orlando, FL

V Cm

12 11/92

AJR

American
Journal of
Roentgenology

August 1991

At last! Lavage with 'La Taste'!

NuLYTELY®

PEG 3350, Sodium Chloride, Sodium Bicarbonate
and Potassium Chloride for Oral Solution

A double-blinded multicenter study[1] comparing NuLYTELY® and GoLYTELY® demonstrates:

Preference. Patients prefer the taste of NuLYTELY 3 to 1.[1]

Manufactured for Braintree Laboratories, Inc., Braintree, MA 02184
by Lyne Laboratories, Inc., Stoughton, MA 02072.

Reference: 1. Gastrointest Endosc 1990; 36: 285-289

Braintree LABORATORIES · INC

© 1991 BRAINTREE LABORATORIES, INC. TRE-1080

Official Journal of the American Roentgen Ray Society

AJR

American Journal of Roentgenology
Diagnostic Imaging and Related Sciences

Editor-In-Chief Robert N. Berk, *La Jolla, California*
University of California, San Diego
School of Medicine and Medical Center

Editor Emeritus Melvin M. Figley, *Seattle, Washington*

Associate Editor Saskia von Waldenburg Hilton, *San Diego, California*

Consulting Editor Michael S. Huckman, *Chicago, Illinois*

Statistician Charles C. Berry, *San Diego, California*

Editorial Board

John R. Amberg
Ithamar Aviad
Mark E. Baker
Lawrence W. Bassett
Michael A. Bettman
Felix S. Chew
N. Reed Dunnick
David K. Edwards
Ronald G. Evens
David S. Feigin
Sandra K. Fernbach
Richard H. Gold
William R. Hendee
John R. Hesselink
Charles B. Higgins
Melvyn T. Korobkin
Faye C. Laing
Thomas L. Lawson
Robert G. Levitt
Bruce L. McClennan
Richard P. Moser
Albert A. Moss
Jeffrey H. Newhouse
Donald L. Resnick
Stewart R. Reuter
Charles A. Rohrmann, Jr.
Peter M. Ronai
Sjef H. J. Ruijs
Stuart S. Sagel
David J. Sartoris
Stefan C. Schatzki
William P. Shuman
Edward A. Sickles
Barry A. Siegel
David D. Stark
Edward T. Stewart
Murali Sundaram
Eric vanSonnenberg
Robert K. Zeman

Editorial Staff: Margaret Levene, *managing editor*; Katie L. Spiller, Barbara Rose, Barbara L. Halliburton, and Janine Anderson, *manuscript editors*; Nancy Rydbeck, *office manager*; Sheri Smith, *administrative assistant*; Linda J. Waggoner, *administrative secretary*

AJR, AMERICAN JOURNAL OF ROENTGENOLOGY (ISSN 0361 803X) is the official journal of the American Roentgen Ray Society and is published monthly by Williams & Wilkins, 428 E. Preston St., Baltimore, MD 21202. Annual dues include $50 for journal subscription. Second-class postage paid at Baltimore, MD, and at additional mailing offices. Postmaster, send address changes (Form 3579) to AJR, 428 E. Preston St., Baltimore, MD 21202. Subscription rates $125 ($180 foreign); institutions $135 ($190 foreign); in training $25 ($80 foreign); single copy $18 ($22 foreign). The GST number for Canadian subscribers is 123394371. Airmail rates furnished on request. Indexed by *Current Contents* and *Index Medicus*. Copyright © 1991 by American Roentgen Ray Society.

0361-803X/90$3.00

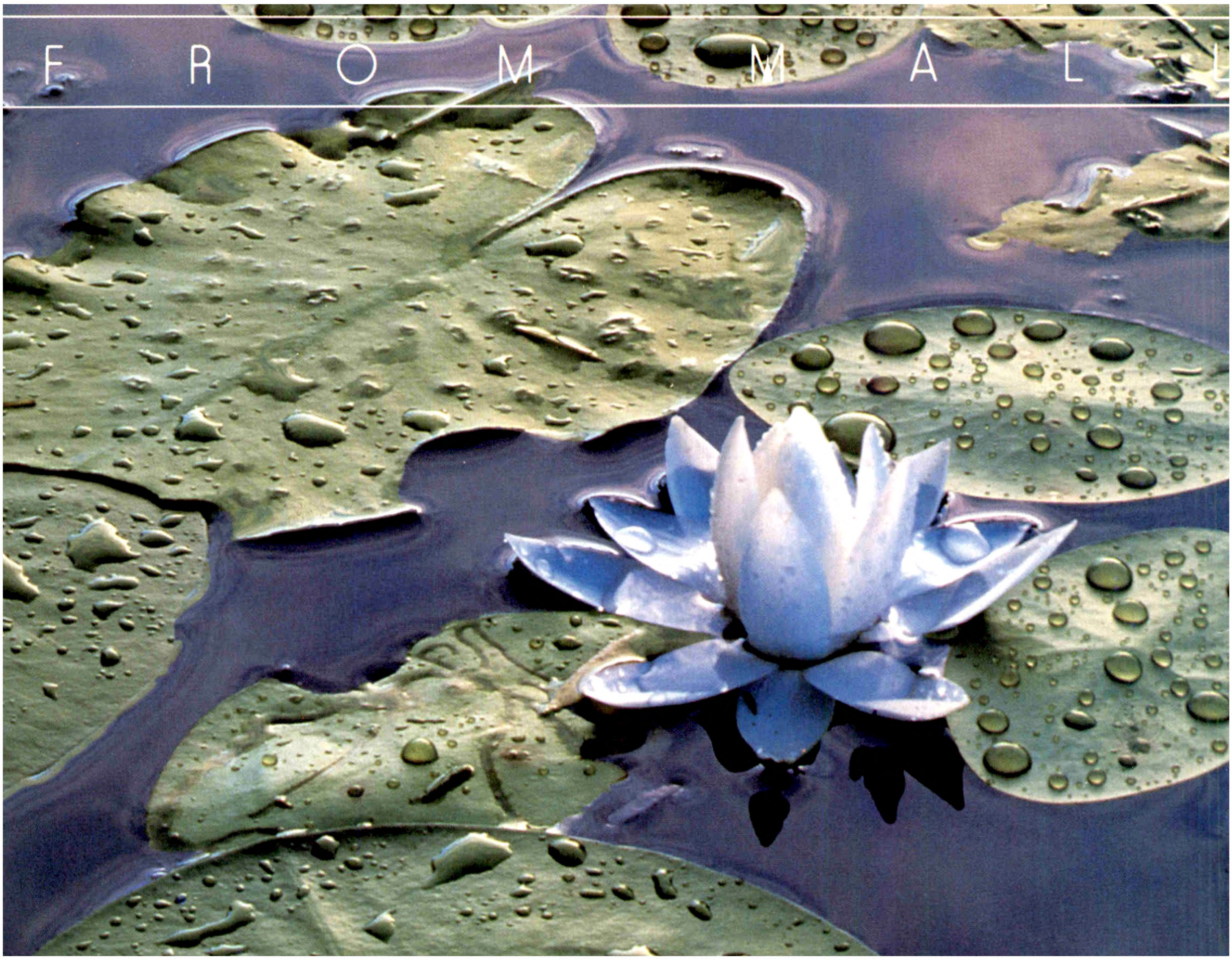
FROM MAL

INCKRODT

A water-loving medium. And the advantages it brings.

It has been suggested that water-loving contrast agents are less toxic than lipid-loving compounds.[1,2]

Hydrophilic agents attract water when injected into the bloodstream and the body perceives them as "friendlier" molecules[1]; they are less likely to cross the blood-brain barrier or to diffuse across the lipid bilayers of neural cell membranes.[2]

One measure of hydrophilicity is the octanol:water partition coefficient. By this standard, Optiray is the most hydrophilic of the nonionic media.

The ordering of LD_{50} values is consistent with the ordering of octanol:water partition coefficients. The most hydrophilic agent, Optiray, demonstrates the least intracisternal toxicity.

Relative Toxicity and Hydrophilicity of Nonionics[3]*

Contrast Agents	LD_{50} Values† (mg I/kg)	Partition Coefficients§ (Octanol:Water)
Optiray	>1,200	4
Iohexol	977	8
Iopamidol	800	19

*Caution must be used to avoid drawing clinical conclusions based solely upon nonclinical data.
†Comparative acute intracisternal toxicity in rats.
§$\times 10^{-4}$.

(Higher LD_{50} value indicates less toxicity; lower partition coefficient indicates greater hydrophilicity.)

With Optiray, you can expect a very low incidence of individual, drug-related adverse reactions.[4] Optiray also offers the safety, convenience, and cost efficiency of the single-dose Ultraject® prefilled syringe. For more information, contact your Mallinckrodt Medical representative or call us toll free at (800) 325-3688.

All nonionic iodinated contrast media currently available inhibit blood coagulation, in vitro, less than ionic contrast media. Clotting has been reported when blood remains in contact with syringes containing nonionic contrast media. Therefore, meticulous intravascular administration technique is necessary to minimize thromboembolic events.

References:
1. McClennan BL. Ionic and nonionic iodinated contrast media: evolution and strategies for use. *AJR*. 1990; 155: 225-233.
2. Hilal SK, et al. Development and evaluation of a new water-soluble iodinated myelographic contrast medium with markedly reduced convulsive effects. *Radiology*. 1978; 126:417-422.
3. Ralston WH, Robbins MS, Coveney J, Blair M. Acute and subacute toxicity studies of ioversol in experimental animals. *Invest Radiol*. 1989;24 (suppl 1):S2-S9.
4. Benamor M, Aten EM, McElvany KD, et al. Ioversol clinical safety summary. *Invest Radiol*. 1989;24 (suppl 1):S67-S72.

Nonionic

OPTIRAY®

(ioversol)

The friendlier molecule

Please see adjacent page for brief summary of prescribing information.

OPTIRAY® 160 240 320
(Ioversol Injection)

DESCRIPTION: Each milliliter of OPTIRAY 160 (ioversol injection 34%) provides 339 mg of ioversol with 3.6 mg of tromethamine as a buffer and 0.2 mg of edetate calcium disodium as a stabilizer. OPTIRAY 160 provides 16% (160 mg/mL) organically bound iodine.

Each milliliter of OPTIRAY 240 (ioversol injection 51%) provides 509 mg of ioversol with 3.6 mg of tromethamine as a buffer and 0.2 mg of edetate calcium disodium as a stabilizer. OPTIRAY 240 provides 24% (240 mg/mL) organically bound iodine.

Each milliliter of OPTIRAY 320 (ioversol injection 68%) provides 678 mg of ioversol with 3.6 mg of tromethamine as a buffer and 0.2 mg of edetate calcium disodium as a stabilizer. OPTIRAY 320 provides 32% (320 mg/mL) organically bound iodine.

CONTRAINDICATIONS: None.

WARNINGS: Nonionic iodinated contrast media inhibit blood coagulation, in vitro, less than ionic contrast media. Clotting has been reported when blood remains in contact with syringes containing nonionic contrast media.

Serious, rarely fatal, thromboembolic events causing myocardial infarction and stroke have been reported during angiographic procedures with both ionic and nonionic contrast media. Therefore, meticulous intravascular administration technique is necessary, particularly during angiographic procedures, to minimize thromboembolic events. Numerous factors, including length of procedure, catheter and syringe material, underlying disease state and concomitant medications may contribute to the development of thromboembolic events. For these reasons, meticulous angiographic techniques are recommended including close attention to guidewire and catheter manipulation, use of manifold systems and/or three-way stopcocks, frequent catheter flushing with heparinized saline solutions and minimizing the length of the procedure. The use of plastic syringes in place of glass syringes has been reported to decrease but not eliminate the likelihood of in vitro clotting.

Serious or fatal reactions have been associated with the administration of iodine-containing radiopaque media. It is of utmost importance to be completely prepared to treat any contrast medium reaction.

As with any contrast medium, serious neurologic sequelae, including permanent paralysis, can occur following cerebral arteriography, selective spinal arteriography and arteriography of vessels supplying the spinal cord. A cause-effect relationship to the contrast medium has not been established since the patients' pre-existing condition and procedural technique are causative factors in themselves. The arterial injection of a contrast medium should never be made following the administration of vasopressors since they strongly potentiate neurologic effects.

Caution must be exercised in patients with severely impaired renal function, combined renal and hepatic disease, severe thyrotoxicosis, myelomatosis, or anuria, particularly when large doses are administered.

Intravascularly administered iodine-containing radiopaque media are potentially hazardous in patients with multiple myeloma or other paraproteinemia, particularly in those with therapeutically resistant anuria. Myeloma occurs most commonly in persons over age 40. Although neither the contrast agent nor dehydration has been proved separately to be the cause of anuria in myelomatous patients, it has been speculated that the combination of both may be causative. The risk in myelomatous patients is not a contraindication to the procedure; however, special precautions, including maintenance of normal hydration and close monitoring, are required. Partial dehydration in the preparation of these patients prior to injection is not recommended since this may predispose the patient to precipitation of the myeloma protein.

Administration of radiopaque materials to patients known or suspected of having pheochromocytoma should be performed with extreme caution. If, in the opinion of the physician, the possible benefits of such procedures outweigh the considered risks, the procedures may be performed; however, the amount of radiopaque medium injected should be kept to an absolute minimum. The blood pressure should be assessed throughout the procedure, and measures for treatment of a hypertensive crisis should be available.

Contrast media may promote sickling in individuals who are homozygous for sickle cell disease when administered intravascularly.

Reports of thyroid storm following the intravascular use of iodinated radiopaque agents in patients with hyperthyroidism or with an autonomously functioning thyroid nodule, suggest that this additional risk be evaluated in such patients before use of any contrast medium.

PRECAUTIONS: *General:* Diagnostic procedures which involve the use of iodinated intravascular contrast agents should be carried out under the direction of personnel skilled and experienced in the particular procedure to be performed. A fully equipped emergency cart, or equivalent supplies and equipment, and personnel competent in recognizing and treating adverse reactions of all types should always be available. Since severe delayed reactions have been known to occur, emergency facilities and competent personnel should be available for at least 30 to 60 minutes after administration.

Preparatory dehydration is dangerous and may contribute to acute renal failure in patients with advanced vascular disease, diabetic patients, and in susceptible non-diabetic patients (often elderly with pre-existing renal disease). *Patients should be well hydrated prior to and following the administration of OPTIRAY.*

The possibility of a reaction, including serious, life-threatening, fatal, anaphylactoid or cardiovascular reactions, should always be considered (See ADVERSE REACTIONS). Increased risk is associated with a history of previous reaction to a contrast medium, a known sensitivity to iodine and known allergies (i.e., bronchial asthma, hay fever and food allergies) or hypersensitivities.

The occurrence of severe idiosyncratic reactions has prompted the use of several pretesting methods. However, pretesting cannot be relied upon to predict severe reactions and may itself be hazardous to the patient. It is suggested that a thorough medical history with emphasis on allergy and hypersensitivity, prior to the injection of any contrast medium, may be more accurate than pretesting in predicting potential adverse reactions. A positive history of allergies or hypersensitivity does not arbitrarily contraindicate the use of a contrast agent when a diagnostic procedure is thought essential, but caution should be exercised. Premedication with antihistamines or corticosteroids to avoid or minimize possible allergic reactions in such patients should be considered. Reports indicate that such pretreatment does not prevent serious life-threatening reactions, but may reduce both their incidence and severity.

General anesthesia may be indicated in the performance of some procedures in selected patients; however, a higher incidence of adverse reactions has been reported in these patients, and may be attributable to the inability of the patient to identify untoward symptoms or to the hypotensive effect of anesthesia which can prolong the circulation time and increase the duration of exposure to the contrast agent.

In angiographic procedures, the possibility of dislodging plaques or damaging or perforating the vessel wall should be considered during catheter manipulations and contrast medium injection. Test injections to insure proper catheter placement are suggested.

Angiography should be avoided whenever possible in patients with homocystinuria because of the risk of inducing thrombosis and embolism.

Patients with congestive heart failure should be observed for several hours following the procedure to detect delayed hemodynamic disturbances which may be associated with a transitory increase in the circulating osmotic load.

Selective coronary arteriography should be performed only in selected patients and those in whom the expected benefits outweigh the procedural risk. The inherent risks of angiocardiography in patients with chronic pulmonary emphysema must be weighed against the necessity for performing this procedure.

Extreme caution during injection of a contrast medium is necessary to avoid extravasation. This is especially important in patients with severe arterial or venous disease.

Drug Interactions: Renal toxicity has been reported in a few patients with liver dysfunction who were given oral cholecystographic agents followed by intravascular contrast agents. Administration of any intravascular contrast agent should therefore be postponed in patients who have recently received a cholecystographic contrast agent.

Other drugs should not be mixed with ioversol injection.

Drug Laboratory Test Interactions: The results of PBI and radioactive iodine uptake studies, which depend on iodine estimation, will not accurately reflect thyroid function for up to 16 days following administration of iodinated contrast media. However, thyroid function tests not depending on iodine estimations, e.g., T3 resin uptake and total or free thyroxine (T4) assays are not affected.

Carcinogenesis, Mutagenesis, Impairment of Fertility: No long term animal studies have been performed to evaluate carcinogenic potential. However, animal studies suggest that this drug is not mutagenic and does not affect fertility.

Pregnancy Category B: No teratogenic effects attributable to ioversol have been observed in teratology studies performed in animals. There are, however, no adequate and well controlled studies in pregnant women. It is not known whether ioversol crosses the placental barrier or reaches fetal tissues. However, many injectable contrast agents cross the placental barrier in humans and appear to enter fetal tissue passively. Because animal teratology studies are not always predictive of human response, this drug should be used during pregnancy only if clearly needed. X-ray procedures involve a certain risk related to the exposure of the fetus.

Nursing Mothers: It is not known whether ioversol is excreted in human milk. However, many injectable contrast agents are excreted unchanged in human milk. Although it has not been established that serious adverse reactions occur in nursing infants, caution should be exercised when intravascular contrast media are administered to nursing women because of potential adverse reactions, and consideration should be given to temporarily discontinuing nursing.

Pediatric Use: Safety and effectiveness in children have not been established.

ADVERSE REACTIONS: Adverse reactions following the use of OPTIRAY formulations are usually mild to moderate, of short duration and resolve spontaneously (without treatment). However, serious, life-threatening and fatal reactions, mostly of cardiovascular origin, have been associated with the administration of iodine-containing contrast media.

Injections of contrast media are often associated with sensations of warmth and pain. In controlled double-blind clinical studies, significantly less warmth and pain were associated with the injection of OPTIRAY than with iothalamate meglumine, diatrizoate meglumine, and diatrizoate meglumine and diatrizoate sodium.

When OPTIRAY 320 is used for coronary arteriography and ventriculography in double-blind clinical trials, electrocardiographic and hemodynamic changes occur with less frequency and severity with ioversol injection than with diatrizoate meglumine and diatrizoate sodium.

Following coronary artery and left ventricular injection, electrocardiographic parameters were affected less with OPTIRAY (ioversol injection) than with diatrizoate meglumine and diatrizoate sodium injection. These parameters included the following: bradycardia, tachycardia, T-wave amplitude, ST depression and ST elevation.

OPTIRAY has also been shown to cause fewer changes in cardiac function and systemic blood pressure than conventional ionic media. These include cardiac output, left ventricular systolic and end-diastolic pressure, right ventricular systolic and pulmonary artery systolic pressures and decreases in systolic and diastolic blood pressures.

The following table of incidence of reactions is based upon clinical trials with OPTIRAY formulations in over 1100 patients. This listing includes all adverse reactions which were coincidental to the administration of ioversol regardless of their direct attributability to the drug or the procedure. Adverse reactions are listed by organ system and in decreasing order of occurrence. Significantly more severe reactions are listed before others in a system regardless of frequency.

Adverse Reactions

System	> 1%	≤ 1%
Cardiovascular	none	angina pectoris hypotension vascular spasm bradycardia conduction defect false aneurysm hypertension transient arrhythmia vascular trauma
Digestive	none	nausea vomiting
Nervous	none	cerebral infarct headache blurred vision vertigo lightheadedness vasovagal reaction disorientation dysphasia paresthesia visual hallucination
Respiratory	none	laryngeal edema nasal congestion sneezing coughing hypoxia
Skin	none	periorbital edema urticaria facial edema flush pruritus
Miscellaneous	none	extravasation shaking chills bad taste general pain

Regardless of the contrast medium employed, the overall incidence of serious adverse reaction is higher with coronary arteriography than with other procedures. Cardiac decompensation, serious arrhythmias, myocardial ischemia or myocardial infarction may occur during coronary arteriography and left ventriculography.

General Adverse Reactions to Contrast Media

The following adverse reactions are possible with any parenterally administered iodinated contrast medium. Severe life-threatening reactions and fatalities, mostly of cardiovascular origin, have occurred. Most deaths occur during injection or 5 to 10 minutes later; the main feature being cardiac arrest with cardiovascular disease as the main aggravating factor. Isolated reports of hypotensive collapse and shock are found in the literature. Based upon clinical literature, reported deaths from the administration of conventional iodinated contrast agents range from 6.6 per 1 million (0.00066 percent) to 1 in 10,000 patients (0.01 percent).

The reported incidence of adverse reactions to contrast media in patients with a history of allergy is twice that of the general population. Patients with a history of previous reactions to a contrast medium are three times more susceptible than other patients. However, sensitivity to contrast media does not appear to increase with repeated examinations.

Adverse reactions to injectable contrast media fall into two categories: chemotoxic reactions and idiosyncratic reactions.

Chemotoxic reactions result from the physicochemical properties of the contrast medium, the dose and the speed of injection. All hemodynamic disturbances and injuries to organs or vessels perfused by the contrast medium are included in this category.

Idiosyncratic reactions include all other reactions. They occur more frequently in patients 20 to 40 years old. Idiosyncratic reactions may or may not be dependent on the dose injected, the speed of injection, the mode of injection and the radiographic procedure. Idiosyncratic reactions are subdivided into minor, intermediate and severe. The minor reactions are self-limited and of short duration; the severe reactions are life-threatening and treatment is urgent and mandatory.

In addition to the adverse reactions reported for ioversol, the following additional adverse reactions have been reported with the use of other contrast agents and are possible with any water soluble, iodinated contrast agent.

Nervous: muscular spasm, convulsions, aphasia, syncope, paralysis, visual field losses which are usually transient but may be permanent, coma and death.

Cardiovascular: angioneurotic edema, peripheral edema, vasodilation, thrombosis and rarely thrombophlebitis, disseminated intravascular coagulation and shock.

Skin: maculopapular rash, erythema, conjunctival symptoms, ecchymosis and tissue necrosis.

Respiratory: choking, dyspnea, wheezing which may be an initial manifestation of more severe and infrequent reactions including asthmatic attack, laryngospasm and brochospasm, pulmonary edema, apnea and cyanosis. Rarely these allergic-type reactions can progress into anaphylaxis with loss of consciousness, coma, severe cardiovascular disturbances and death.

Miscellaneous: hyperthermia, temporary anuria or other nephropathy.

Other reactions may also occur with the use of any contrast agent as a consequence of the procedural hazard; these include hemorrhage or pseudoaneurysms at the puncture site, brachial plexus palsy following axillary artery injections, chest pain, myocardial infarction, and transient changes in hepatorenal chemistry tests. Arterial thrombosis, displacement of arterial plaques, venous thrombosis, dissection of the coronary vessels and transient sinus arrest are rare complications.

In cerebral arteriography, cardiovascular reactions that may occur with some frequency are bradycardia and either an increase or decrease in systemic blood pressure. Neurological reactions that may occur are: seizures, drowsiness, transient paresis, and mild disturbances in vision.

Central nervous system reactions with OPTIRAY in controlled clinical studies in cerebral arteriography that occurred with frequencies greater than 1% were: vertigo (4%) and blurred vision (3%).

In aortography, depending on the technique employed, the risks of this procedure also include the following: injury to the aorta and neighboring organs, pleural puncture, renal damage including infarction and acute tubular necrosis with oliguria and anuria, retroperitoneal hemorrhage from the translumbar approach and spinal cord injury and pathology associated with the syndrome of transverse myelitis. Under conditions of slowed aortic circulation there is an increased likelihood for aortography to cause muscle spasm. Occasional serious neurologic complications, including paraplegia, have also been reported in patients with aortoiliac obstruction, femoral artery obstruction, abdominal compression, hypotension, hypertension, spinal anesthesia, and injection of vasopressors to increase contrast. In these patients the concentration, volume, and number of repeat injections of the medium should be maintained at a minimum with appropriate intervals between injections. The position of the patient and catheter tip should be carefully monitored.

Entry of a large aortic dose into the renal artery may cause, even in the absence of symptoms, albuminuria, hematuria, and an elevated creatinine and urea nitrogen. Rapid and complete return of function usually follows.

Cardiovascular system reactions with OPTIRAY in controlled clinical studies in coronary arteriography with left ventriculography that occurred with frequencies greater than 1% were: angina (1.2%) and nausea (1.2%).

PRECAUTIONS FOR SPECIFIC PROCEDURES:

Cerebral Arteriography

Extreme caution is advised in patients with advanced arteriosclerosis, severe hypertension, cardiac decompensation, senility, recent cerebral thrombosis or embolism, and migraine.

Peripheral Arteriography

Pulsation should be present in the artery to be injected. In thromboangiitis obliterans, or ascending infection associated with severe ischemia, angiography should be performed with extreme caution, if at all.

Coronary Arteriography and Left Ventriculography

Mandatory prerequisites to the procedure are specialized personnel, ECG monitoring apparatus and adequate facilities for immediate resuscitation and cardioversion. Electrocardiograms and vital signs should be routinely monitored throughout the procedure.

Venography

Special care is required when venography is performed in patients with suspected thrombosis, phlebitis, severe ischemic disease, local infection or a totally obstructed venous system. In order to minimize extravasation during injection, fluoroscopy is recommended.

OVERDOSAGE: The adverse effects of overdosage are life-threatening and affect mainly the pulmonary and cardiovascular system. Treatment of an overdosage is directed toward the support of all vital functions, and prompt institution of symptomatic therapy.

Ioversol does not bind to plasma or serum protein and is therefore, dialyzable.

The intravenous LD_{50} values (gl/kg) for ioversol in animals were: 17 (mice), and 15 (rats).

DOSAGE AND ADMINISTRATION: Details on dosage are provided in the package insert. CONSULT FULL PACKAGE INSERT BEFORE USE.

MALLINCKRODT®

Changing the look of medicine.™

© 1991 Mallinckrodt Medical, Inc. 4/91 MI22376

X-RAY ACCESSORIES

The Difference is Clear

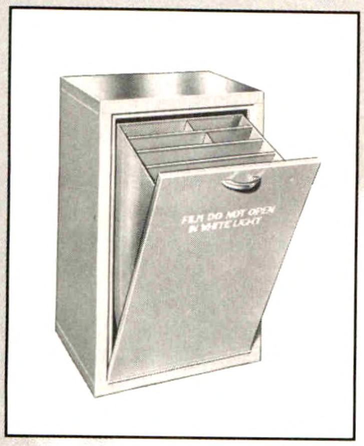

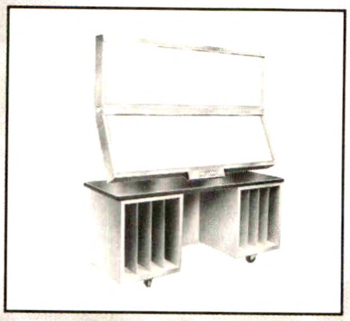

Tried, tested and trusted for over 40 years, S & S x-ray products deliver maximum proficiency and economy -- backed by quality, dependability and innovation.

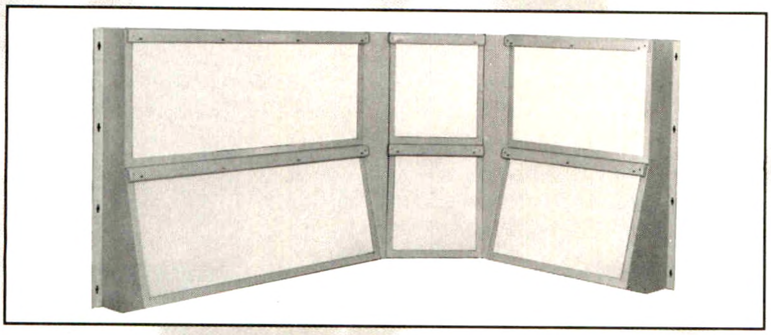

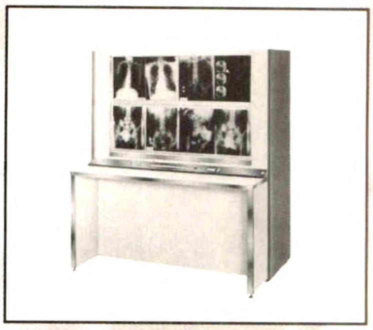

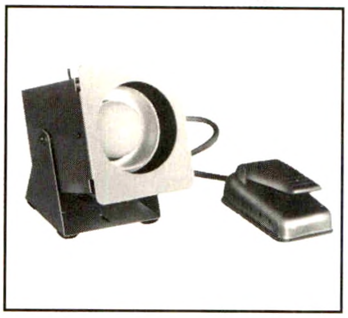

- **X-RAY** Film Viewers ◆
- **X-RAY** Protection ◆
- **X-RAY** Files ◆
- **X-RAY** Darkroom Equipment ◆
- **X-RAY** Cabinets ◆
- **X-RAY** Accessories ◆

For a FREE copy of our fully illustrated, 100+ page catalog, contact S & S directly or your local x-ray dealer.

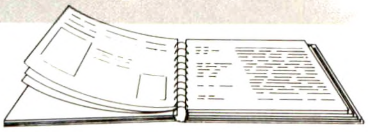

1101 Linwood Street
Brooklyn, N.Y. 11208

Phone: 718/649-8500
FAX: 718/257-0219
Toll Free: 800/347-XRAY

S&S X-RAY PRODUCTS
Factories in NY, NC, PA, TX

AJR Business and Subscriber Information

The American Roentgen Ray Society

AJR, American Journal of Roentgenology, is published monthly to disseminate research on current developments in the radiologic sciences and commentary on topics related to radiology. It is published by the American Roentgen Ray Society, 1891 Preston White Dr., Reston, VA 22091; (703) 648-8992. Inquiries regarding society business, the annual ARRS meeting, and membership should be addressed to the Society at the above address.

Correspondence Concerning the *AJR*

Correspondence regarding display (not classified) advertising, subscriptions, address changes, reprints, and permission requests should be addressed to Williams & Wilkins, 428 E. Preston St., Baltimore, MD 21202; (301) 528-4000.

Correspondence regarding editorial matters and classified advertising should be addressed to Editorial Office, AJR, 2223 Avenida de la Playa, Ste. 103, La Jolla, CA 92037-3218; telephone (619) 459-2229; FAX (619) 459-8814. For information on manuscript submission, see Guidelines for Authors, pages A13–A15.

Subscriber Information

Subscription requests and inquiries should be sent to Williams & Wilkins, 428 E. Preston St., Baltimore, MD 21202. ARRS annual dues include $50 for journal subscription. Subscription rates are as follows: nonmembers, $125/year ($180 foreign); institutions, $135 ($190 foreign); nonmember in-training, $25 ($80 foreign). Single copies of the Journal may be purchased for $18 ($22 foreign). Airmail rates will be furnished on request. The GST number for Canadian subscribers is 123394371.

Call toll-free, 1-800-638-6423 (in Maryland call 1-800-638-4007), with subscription questions or problems. Please have the mailing label from your latest issue available when you call.

If a subscriber receives a damaged copy of the *AJR* or fails to receive an issue, the subscriber should notify Williams & Wilkins (428 E. Preston St., Baltimore, MD 21202) within 60 days of publication (90 days for foreign subscribers) and that issue will be replaced.

Change of address information should be sent to Williams & Wilkins, 428 E. Preston St., Baltimore, MD 21202. Allow 90 days for address changes.

Copyrights, Permissions, and Reprints

The American Roentgen Ray Society holds the copyright for all material published in the *AJR*. No part of this publication may be reproduced without permission from the ARRS. Requests for such permission should be addressed to Williams & Wilkins, 428 E. Preston St., Baltimore, MD 21202.

For reprints of a particular article, please contact the author designated in the footnotes for that article.

Indexes

The *AJR* provides volume and yearly indexes (subject and author) in the June and December issues each year. *AJR* articles are also indexed in *Current Contents*, *Index Medicus*, and the cumulative index published by *Radiology*.

AJR Guidelines for Authors

Address new and revised manuscripts, correspondence, and classified ads to the Editor:

AJR Editorial Office
2223 Avenida de la Playa, Suite 103
La Jolla, CA 92037-3218
Telephone: (619) 459-2229; FAX: (619) 459-8814

Inquiries regarding subscriptions, display advertising, reprints, or permission to republish *AJR* material should be addressed to the publisher:

The Williams & Wilkins Co.
428 E. Preston St.
Baltimore, MD 21202 Telephone: 1-800-638-6423

The *AJR* publishes original contributions to the advancement of medical diagnosis and treatment. Submitted manuscripts should not contain previously published material and should not be under consideration for publication elsewhere. Papers dealing with neuroradiology should be addressed to: American Journal of Neuroradiology, Dept. of Diagnostic Radiology, 1653 W. Congress Pkwy., Chicago, Il 60612. At the discretion of the *AJR* Editor, *AJNR* articles that are of interest to the general reader may be republished in the *AJR*. Neuroradiologic papers sent to the *AJR* will be forwarded to the Editorial Office of the *AJNR*.

Manuscript decisions are based on peer review. Reviewers receive manuscripts without title pages to ensure an unbiased review. Statements made in the article, including changes made by the Editor or manuscript editor, are the responsibility of the author and not of the *AJR* or its publisher. Authors will be sent the edited manuscript, galley proof, and proofs of illustrations. If the corresponding author will be unavailable to review galleys, arrangements should be made for a coauthor or colleague to read and return the proof.

The following guidelines are based on instructions set forth in the **Uniform Requirements for Manuscripts Submitted to Biomedical Journals** (*Ann Intern Med* **1988**;108:258–265). Articles will be edited, however, to conform to the individual style of AJR.

General Guidelines for Major Papers

Abstract. Clearly state (in 200 words or less) the purpose, methods, results, and conclusions of the study. Include actual data.

Introduction. Briefly describe the purpose of the investigation and explain why it is important.

Methods. Describe the research plan, the materials (or subjects), and the methods used, in that order. Explain in detail how disease was confirmed and how subjectivity in observations was controlled.

Results. Present results in a clear, logical sequence. If tables are used, do not duplicate tabular data in text, but do describe important trends and points.

Discussion. Describe the limitations of the research plan, materials (or subjects), and methods, considering both the purpose and the outcome of the study. When results differ from those of previous investigators, explain the discrepancy.

AUTHOR'S CHECKLIST

For priority handling, complete the following checklist, sign the copyright form on the reverse side of this page, and include both with the manuscript.

________ Two copies of the manuscript (the original and a photocopy) and two complete sets of figures are submitted. One copy has been retained by the author.

________ If appropriate, *AJR* Guidelines for case reports, technical notes, pictorial essays, or letters to the Editor have been followed. (See page A19.)

________ The manuscript, including references, figure legends, and tables, is typed double-spaced on 8½ × 11 in. (21.6 × 27.9 cm) *nonerasable* paper. Right-hand margins are not justified.

________ All manuscript pages are numbered consecutively beginning with the abstract. Authors' names do not appear on the manuscript pages.

________ The manuscript is organized as follows: title page, blind title page (title only), abstract, introduction, methods, results, discussion, acknowledgments, references, tables, figure legends, and figures.

________ Informed consent has been obtained from patients who participated in clinical investigations. If experiments were performed on animals, authors complied with NIH guidelines for use of laboratory animals.

________ Use of unfamiliar acronyms and abbrevations is kept to a minimum. When abbreviations are used they are defined at first mention, followed by the abbreviation in parentheses.

________ Metric measurements are used throughout, or the metric equivalent is given in parentheses.

________ Names and locations (city and state only) of manufacturers are given for equipment and nongeneric drugs.

Title Page

________ The following information is given: title of article; names and complete addresses (including zip code) of all authors; current addresses of authors who have moved since study; acknowledgment of grant or other assistance. The corresponding author is clearly identified, and a current address, phone number, and FAX number are given.

________ A blind title page is included in each copy of the manuscript, giving only the title (without the authors' names) for use in the review process.

Abstract

________ An abstract of approximately 200 words concisely states the purpose, methods, and results of the study in one paragraph. Actual data are included. Conclusions are stated in a second, summary paragraph.

________ No abbreviations or reference citations are used.

References

________ References (not to exceed 35) are typed double-spaced starting on a separate page and are **numbered consecutively in the order in which they appear in the text.**

________ All references are cited in the text and are enclosed in brackets and typed on line with the text (not superscript).

________ Unpublished data are not cited in the reference list, but are cited parenthetically in the text, for example, (Smith DJ, personal communication), (Smith DJ, unpublished data). This includes papers submitted, but not yet accepted, for publication.

________ Papers presented at a meeting are not cited in the reference list, but are cited parenthetically in the text (e.g., Smith DJ et al., presented at the annual meeting of the American Roentgen Ray Society, May 1990). After first mention, use (Smith DJ et al., ARRS meeting, May 1990).

________ Inclusive page numbers (e.g., 333–335) are given for all references.

________ Journal names are abbreviated according to *Index Medicus*.

________ Style and punctuation of references follow the format illustrated in the following examples (all authors are listed when six or fewer; when seven or more authors, the first three are listed, followed by "et al."):

Journal article

1. Long RS, Roe EW, Wu EU, et al. Membrane oxygenation: radiographic appearance. *AJR* **1986**;146:1257–1260

Book

2. Smith LW, Cohen AR. *Pathology of tumors*, 6th ed. Baltimore: Williams & Wilkins, **1977**:100–109

Chapter in a book

3. Breon AJ. Serum monitors of bone metastasis. In: Clark SA, ed. *Bone metastases*. Baltimore: Williams & Wilkins, **1983**:165–180

Tables

________ Each table is typed double-spaced on a separate page without vertical or horizontal rules; each has a short, descriptive title. Tables do not exceed two pages in length and contain at least four lines of data.

________ Tables are numbered in the order in which they are cited in the text.

________ Abbreviations are defined in an explanatory note below each table.

________ Tables are self-explanatory and do not duplicate data given in the text or figures.

________ All arithmetic (percentages, totals, differences) has been double checked for accuracy, and tabular data agree with data given in the text.

Figures and Legends

________ Two complete sets of original figures are submitted unmounted in labeled envelopes.

________ Figures are clean, unscratched, 5 × 7 in. (13 × 18 cm) glossy prints with **white borders.** A separate print is submitted for each figure *part*.

________ All figure parts relating to one patient have the same figure number.

________ Each figure is labeled on the back with the figure number and an arrow indicating "top." For black-and-white figures, labeling is done on a gummed label, which is then affixed to the back of the print. **Never** use labels on **color** figures, but write figure number on the back lightly in pencil. *Never* use ink on front or back of any figures.

________ Author's names are *not* written on the backs of figures.

________ Only removable (rub-on) arrows and letters are used on the figures. Symbols are uniform in size and style and are not broken or cracked.

________ Images are uniform in size and magnification.

________ Line drawings are done in black ink on a white background. They are professional in quality, and all use the same size type. (Only glossy prints are acceptable.)

________ Written permission has been obtained for use of all previously published illustrations (and copies of permission letters are included), and an appropriate credit line is given in the legends.

________ Legends are typed double-spaced, and figure numbers correspond with the order in which the figures are cited in the text.

Transfer of Copyright Agreement, Conflict of Interest Acknowledgment, Certification of Coauthors, and Exclusive Publication Statement

Complete copyright to the article entitled: ____

____

is hereby transferred to the American Roentgen Ray Society (for United States government employees to the extent transferable), effective if and when the article is accepted for publication in the *American Journal of Roentgenology*. In the case of the authors who are officers or employees of the United States government, the American Roentgen Ray Society recognizes that works prepared by officers or employees of the United States government as part of their official government duties are in the public domain.

Authors reserve all proprietary rights other than copyright, such as patent rights and the right to use all or part of this article in future works of their own. The authors retain the right of replication, subject only to crediting the original source of publication and receiving written permission from the publisher.

Authors guarantee that this manuscript contains no matter that is libelous or otherwise unlawful, invades individual privacy, or infringes any proprietary rights.

Authors understand that they will receive no royalty or other compensation from the American Roentgen Ray Society or the publisher.

Authors guarantee that the editor has been or will be informed of any proprietary or commercial interest or conflicts of interest the authors may have that relate directly or indirectly to the subject of this article.

All authors certify that they have made substantive and specific intellectual contributions to the article and assume public responsibility for its content.

Finally, the authors certify that none of the material in this manuscript has been published previously or is currently under consideration for publication elsewhere.

------------------------------	------------------------------	------------------------------
First author/date	Second author	Third author
------------------------------	------------------------------	------------------------------
Fourth author	Fifth author	Sixth author

This agreement must be signed by all authors in order for the manuscript to be published.

Case Reports

A case report is a brief description of a special case that provides a message that transcends the individual patient.

Format. There is no abstract. The introduction should be a short paragraph giving the general background and the specific interest of the case. No more than one case should be described in detail (similar ones can be mentioned briefly in the discussion). Emphasis should be on the radiologic aspects; clinical information must be limited to that necessary to provide a background for the radiology. The discussion should be succinct and should focus on the specific message and relevance of radiologic methods. A review of the literature is not appropriate.

Length. Maximum of five double-spaced, typewritten pages, including the references but not the title page or figure legends.

References. Maximum of eight.

Figures. Maximum of four, unless the text is shortened accordingly. Legends must not repeat the text.

Tables and Acknowledgments. Not appropriate in case reports.

Technical Notes

A technical note is a brief description of a specific technique or procedure, modification of a technique, or equipment of interest to radiologists.

Format. No abstract, headings, or subheadings are required. If headings are used, they should be a combination of "Case Report," "Materials and Methods," "Results," and "Discussion." A brief one-paragraph introduction should be included to give the general background. Discussion should be limited to the specific message, including the uses of the technique or equipment. Literature reviews and lengthy case reports are not appropriate.

Length. Maximum of five double-spaced, typewritten pages, including the references but not the title page or figure legends.

References. Maximum of eight.

Figures. Maximum of two, unless the text is shortened accordingly.

Tables and Acknowledgments. Not appropriate in technical notes.

Pictorial Essays

A pictorial essay is an article that conveys its message through illustrations and their legends. Unlike other *AJR* articles, which are based on original research, pictorial essays serve primarily as teaching tools, like exhibits at a scientific meeting. They are not encyclopedic book chapters. The abstract should be a short, introductory paragraph.

Length. Maximum of four double-spaced, typewritten pages, including the references but not the title page or figure legends.

References. Maximum of four.

Figures. Maximum of 30 figure *parts*. Number should be as few as necessary to convey the message of the paper.

Tables and Acknowledgments. Not appropriate in pictorial essays.

Letters to the Editor and Replies

Letters to the Editor and Replies should offer objective and constructive criticism of published articles. Letters may also discuss matters of general interest to radiologists. Do not end a letter with a hand-written signature.

Format. All letters should be typed double-spaced on nonletterhead paper, with no greeting or salutation. Name and affiliation should appear at the end of the letter. Titles for letters should be short and pertinent. The title for a reply is simply "Reply."

Length. Maximum of two double-spaced, typewritten pages, including references.

References. Maximum of four.

Figures. Maximum of two.

Tables and Acknowledgments. Not appropriate in Letters to the Editor and Replies.

Opinions, Commentaries, and Perspectives

Opinions, commentaries, and perspectives are special articles dealing with controversial topics or issues of special concern to radiologists.

Format. Include a title page but no abstract. Headings may be used to break up the text.

Length. Maximum of five double-spaced, typewritten pages.

References. Maximum of five.

Tables and Figures. Maximum of four.

Computer Page Articles

Articles published on the computer page deal with practical computer applications to radiology.

Format. Include a title page and an abstract.

Length. Maximum of eight double-spaced, typewritten pages.

References. Maximum of five.

Figures and Tables. Maximum of five. Computer printouts are not acceptable. Figures must be submitted as 5 × 7 in. glossy prints.

All submissions to the *AJR* must be accompanied by a completed copy of the Author's Checklist and the signed Copyright Agreement.

FROM MALL

The Comfortable Choice for Angiography

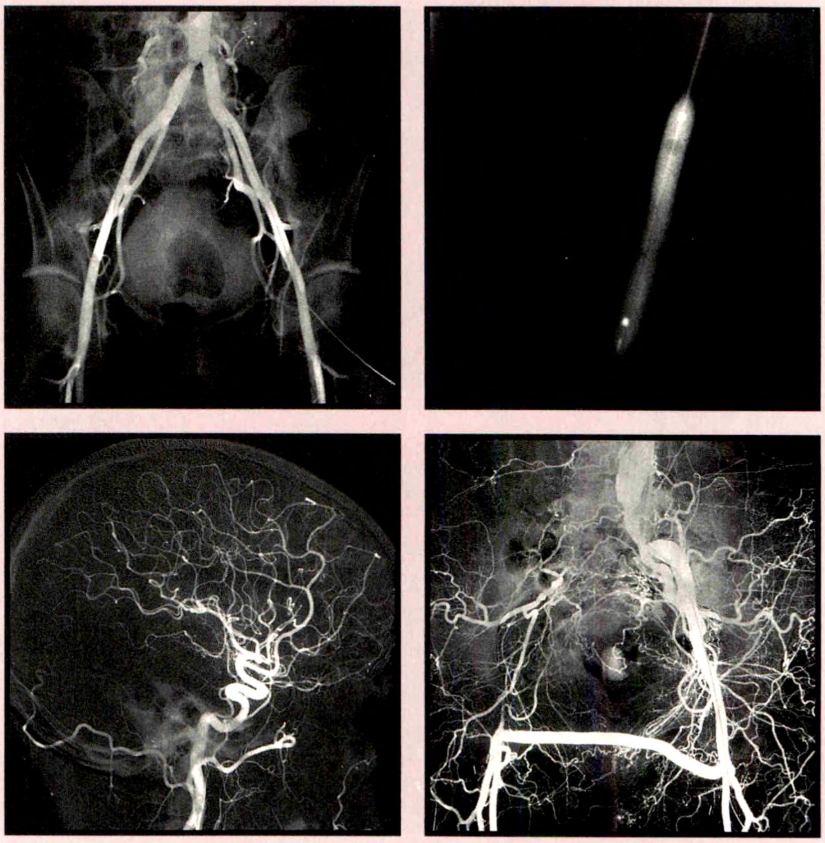

Review Article

The Biliary Tract: Imaging for the 1990s

Morton I. Burrell,[1] Robert K. Zeman,[2] Joseph F. Simeone,[3] Abraham H. Dachman,[4] John P. McGahan,[5]
Eric vanSonnenberg,[6] David S. Zimmon,[7] William Torres,[8] and Igor Laufer[9]

This paper is the result of a panel of experts convened at the annual meeting of the Society of Gastrointestinal Radiologists in Hawaii, January 14–19, 1990, to discuss the current status of diagnostic radiology of the biliary tract and biliary intervention. The focus of discussion was to update and touch on the highlights of each area rather than to provide a comprehensive review.

Hepatobiliary Anatomy

Refinements in imaging of the biliary tract have increased understanding of biliary anatomy and heightened awareness of common pitfalls [1]. The intrahepatic bile ducts branch in a predictable manner, following the distribution of the hepatic segments. The bile ducts that drain the medial and lateral segments of the left lobe are relatively anterior to the right lobar ducts. When cholangiography is performed, contrast material tends to flow into dependent portions of the biliary tree. When the patient is prone, as for most ERCPs, the intrahepatic ducts in the left lobe preferentially fill with contrast material, whereas the intrahepatic ducts in the right lobe often remain unopacified. Failure initially to fill the ducts on the right side should not be construed as evidence of segmental obstruction.

As the right and left hepatic ducts join to form the common hepatic duct, they arch anteriorly over the portal vein. The common hepatic duct, portal vein, and hepatic artery all lie within the hepatoduodenal ligament (Fig. 1). Although the normal intrahepatic bile ducts are not seen on CT, the common hepatic duct can readily be distinguished from the adjacent contrast-enhanced blood vessels. An oblique sonogram, made perpendicular to the right costal margin, is the standard view for visualizing the common hepatic duct. The diameter of the normal common hepatic duct should not be more than 6.0 mm. In elderly patients, more liberal criteria are used [2].

Because the correct identification of ductal dilatation is important, several common pitfalls should be avoided on imaging studies. On sonography, distinguishing blood vessels from dilated bile ducts may be difficult. Dilated bile ducts can usually be followed to the porta hepatis, where they converge to form the common hepatic duct. The portal vein branches are parallel to the bile ducts and also are in the central portion of each of the hepatic segments. The portal vein branches diverge from the main portal vein, which can be traced directly into the splenoportal confluence. Tubular channels can be identified by tracing them into the porta hepatis. If uncertainty remains, Doppler or color flow sonography is useful to distinguish between blood vessels and dilated bile ducts.

Received November 7, 1990; accepted after revision March 28, 1991.

[1] Department of Radiology, Yale University School of Medicine, 333 Cedar St., New Haven, CT 06510. Address reprint requests to M. I. Burrell.
[2] Department of Radiology, Georgetown University Hospital, 3800 Reservoir Rd., N.W., Washington, DC 20007-2197.
[3] Department of Radiology, Harvard Medical School, Massachusetts General Hospital, Fruit St., Boston, MA 02114.
[4] Department of Radiology/Nuclear Medicine, Uniformed Services University of Health Services, 4301 Jones Bridge Rd., Baltimore, MD 20814.
[5] Department of Diagnostic Radiology, University of California, Davis, Medical Center, 2516 Stockton Blvd., TICON II, Sacramento, CA 95817.
[6] Department of Radiology, University of California, San Diego, Medical Center, 225 Dickinson St., San Diego, CA 92103-1990.
[7] Department of Medicine, New York University School of Medicine, 36 7th Ave., New York, NY 10011.
[8] Department of Radiology, Emory University School of Medicine, Emory University Hospital, 1365 Clifton Rd., N.E., Atlanta, GA 30322.
[9] Department of Radiology, Hospital of the University of Pennsylvania, 3400 Spruce St., Philadelphia, PA 19104.

AJR 157:223-233, August 1991 0361-803X/91/1572-0223 © American Roentgen Ray Society

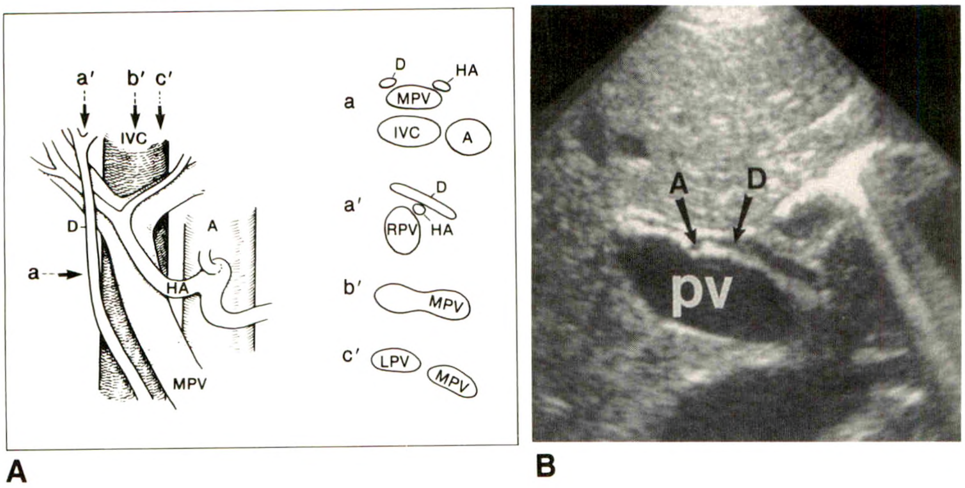

Fig. 1.—Structures of hepatoduodenal ligament.

***A*, Drawing shows common hepatic duct (D) lies anterior to hepatic artery (HA) and right portal vein (RPV). Cross-sectional appearance (a, a′–c′) of these structures is easily predicted. MPV = main portal vein, IVC = inferior vena cava, A = aorta, LPV = left portal vein.**

***B*, Oblique sonogram corresponding to section a′ shows common hepatic duct (D) and hepatic artery (A) anterior to portal vein bifurcation (pv).**

(Modified from Zeman and Burrell [1].)

On CT, contrast-enhanced scans should be used to identify dilated bile ducts. High levels of circulating contrast material in the blood vessels will eliminate confusion between vascular and biliary structures. In patients with portal vein thrombosis or Budd-Chiari syndrome, thrombus within unenhanced blood vessels may mimic ductal dilatation. In these cases, the patchy enhancement of the liver parenchyma on dynamic CT often will provide a clue to the diagnosis.

Gallbladder Disease

Acute Cholecystitis

Imaging of acute cholecystitis changed markedly in the late 1970s and early 1980s as a result of improvements in sonography and cholescintigraphy. The two techniques have comparable sensitivities and specificities when performed by experienced radiologists [3]. Regardless of which radionuclide is used, the hallmark of acute cholecystitis on cholescintigraphy is obstruction of the cystic duct, resulting in nonvisualization of the gallbladder. In patients with biliary stasis associated with hyperalimentation or fasting, the gallbladder may be slow to fill with radionuclide. Before the use of morphine, it often was necessary to obtain delayed views up to 4 hr or more after the injection of radionuclide in order to determine if nonvisualization of the gallbladder was related to poor uptake in the distended gallbladder or to obstruction of the cystic duct due to acute cholecystitis.

The sonographic diagnosis of acute cholecystitis requires the presence of three findings. Because at least 90% of patients with acute cholecystitis have cholelithiasis, sonographic evidence of gallstones in the gallbladder is usually present. A sonolucent band caused by edema within the gallbladder wall is often present also. When this sonolucency is focal or striated, acute inflammation can be diagnosed with relative specificity [4] (Fig. 2). This appearance can be seen on CT also. The third finding is the sonographic Murphy sign: palpation of the inflamed gallbladder with the transducer causes pain. The value of this sign is controversial.

The most common complications of acute cholecystitis are gangrenous cholecystitis, emphysematous cholecystitis, perforation of the gallbladder, and Mirrizzi syndrome. Gangrenous cholecystitis implies the presence of severe inflammation and broad areas of necrosis of the gallbladder wall. Secondary perforation may occur. Sonographic findings include thickening of the gallbladder wall, with multiple sonolucent layers. On cholescintigraphy, a rim of increased uptake of radionuclide within the liver adjacent to the inflamed (and nonvisualized) gallbladder has been reported.

Emphysematous cholecystitis is the result of a gas-producing infection of the gallbladder. About one third of patients have *Clostridium perfringens* in their bile. On sonography, echoes that do not move with gravity are present within the gallbladder. Gallstones may or may not be present because some cases are related to ischemia. Gas within the wall or lumen of the gallbladder is readily detected on CT.

Perforation of the gallbladder is a life-threatening sequela of acute cholecystitis. When it occurs, biloma, pericholecystic abscess, or bile peritonitis may result. Sonography and CT show fluid next to the gallbladder [5]. Cholescintigraphy may show extravasation if the cystic duct is incompletely obstructed.

Mirrizzi syndrome occurs when a stone erodes from the inflamed cystic duct into the common hepatic or common bile duct, leading to an inflammatory mass that obstructs the bile duct. It is often difficult to diagnose the syndrome on the basis of imaging studies; however, visualization of a stone straddling the junction of the cystic duct and the common hepatic duct and associated severe inflammation of the gallbladder wall and biliary obstruction suggest the diagnosis. Failure to recognize this condition has resulted in inadvertent ligation of the common bile duct during surgery.

Thickening of the Gallbladder Wall

In a patient who has been fasting for at least 8 hr, the minimum period recommended for gallbladder evaluation, the normal thickness of the gallbladder wall in the axial plane on sonography is 3 mm [6]. The thickness of the wall of a normal gallbladder examined 30 min to 2 hr after the patient has eaten a meal is greater than 3 mm.

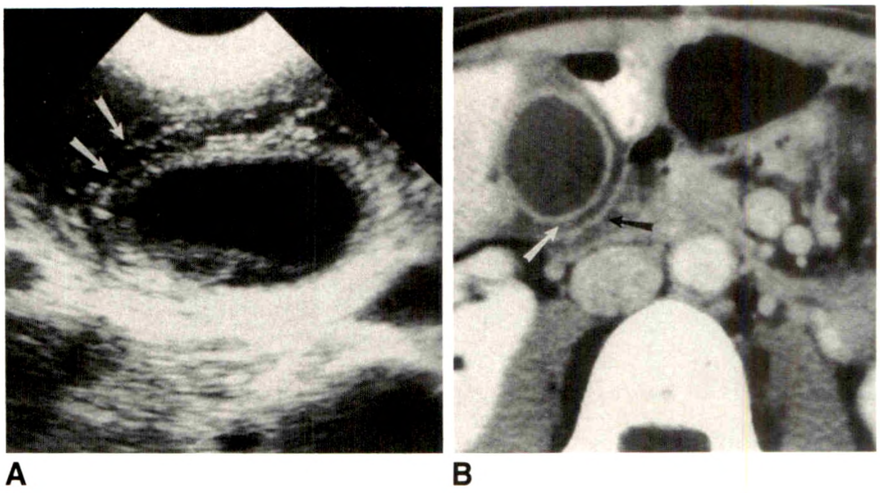

Fig. 2.—Acute cholecystitis.
***A*, Sonogram shows multiple sonolucent bands (*arrows*) suggestive of acute edema. This so-called striated appearance is relatively specific for inflammation.**
***B*, CT scan shows comparable findings with edema present as multiple low-attenuation bands (*arrows*).**
(Modified from Zeman and Burrell [1].)

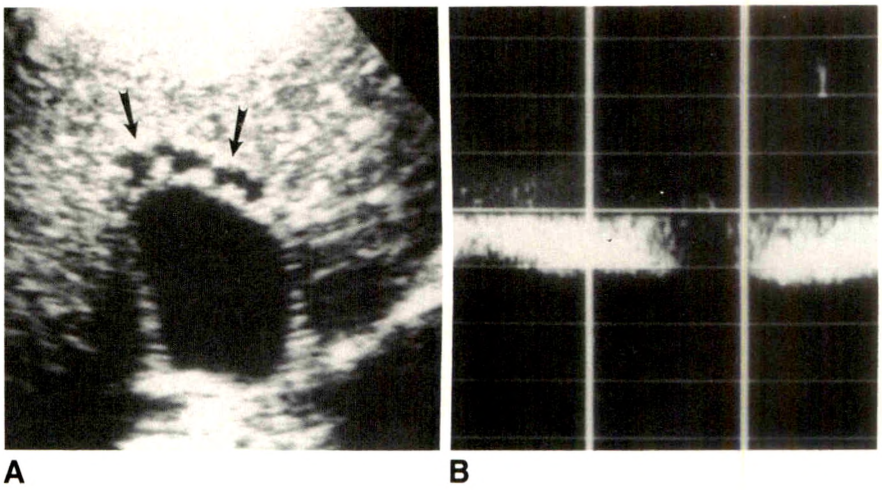

Fig. 3.—Gallbladder wall varices.
***A*, Transverse sonogram shows intramural sonolucency (*arrows*) of gallbladder wall. Lucencies have a varicoid appearance. (Reprinted with permission from West et al. [9].)**
***B*, Doppler tracing shows a typical venous pattern.**

In chronic cholecystitis, thickening of the gallbladder wall occurs in association with a contracted gallbladder. In the diagnosis of chronic cholecystitis, the finding of thickening of the gallbladder wall is by itself, of limited usefulness, and it becomes important only when seen in association with stones, when it is, of course, redundant. Other causes of focal or diffuse thickening of the gallbladder wall are adenomyosis and carcinoma. Carcinoma of the gallbladder causes thickening of the wall; however, an early, usually incidentally detected gallbladder carcinoma most often will appear as a focal mass.

Hepatitis may cause thickening of the gallbladder wall [7]. In about half the patients, increased thickness of the gallbladder wall is accompanied by reduced gallbladder volume and decreased flow of bile from the liver. As the patient's hepatitis improves, the gallbladder wall progressively returns to normal.

Portal venous hypertension also may cause thickening of the gallbladder wall because of venous congestion [8]. At times, the veins in the gallbladder wall may actually be recognized on conventional (Fig. 3) or color flow Doppler sonography. In patients with ascites, thickening of the gallbladder wall may indicate the ascites is due to portal hypertension rather than to metastatic disease [10]. In the former, the thickening of the wall is related to venous distension; in the latter, the wall should be unaffected.

AIDS also causes thickening of the gallbladder wall. Histologic examination of the gallbladder shows no specific pathologic changes. The exact cause of the thickening is unknown, although it may be related to hepatic dysfunction.

The most controversial cause of thickening of the gallbladder wall is hypoalbuminemia. Some authors [11] suggest that thickness greater than 3 mm occurs in 60% of patients with hypoalbuminemia.

Biliary Obstruction

General Principles of Diagnosis

The three phases of biliary obstruction have been referred to as the functional phase, the anatomic phase, and the icteric phase [1, 12].

In the initial or functional phase, seen after ligation of the common bile duct in a cholecystectomized dog, liver enzyme levels, including alkaline phosphatase, 5-nucleotidase, and aspartate aminotransferase (AST), begin to rise along with the bilirubin level but remain in the normal range. Although

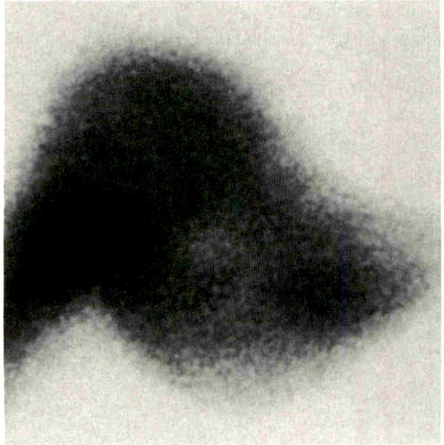
4

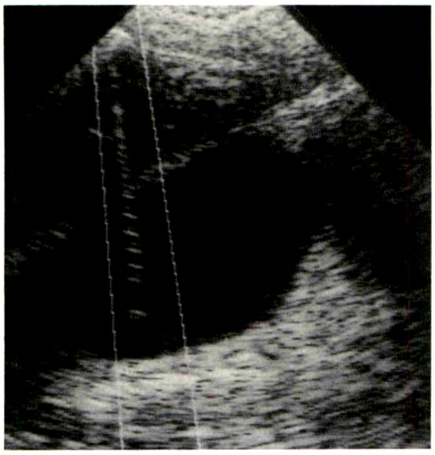
5

Fig. 4.—Complete obstruction of common bile duct with normal-sized ducts. Scintigram obtained 4 hr after injection of ^{99m}Tc-iminodiacetic acid shows good hepatic uptake of radionuclide and no evidence of excretion, suggesting complete obstruction. Study was carried out to 24 hr, and no excretion was seen. Sonography showed a normal-sized duct, and ERCP showed a small, nonobstructing-looking stone, floating freely in a normal-sized duct.

Fig. 5.—Under sonographic guidance, cholecystostomy catheter is placed transhepatically via trocar method into gallbladder. (Reprinted with permission from McGahan [27].)

we do not often image patients this early in the sequence of biliary obstruction, it has been shown that ^{99m}Tc-iminodiacetic acid (IDA) scintigraphy is highly sensitive and likely to show abnormal biliary drainage at the earliest phases of such obstruction [13]. If patients are serendipitously examined in this preclinical phase of obstruction, the more sensitive functional examinations (cholescintigraphy, Fig. 4) will have abnormal results before the tests that show anatomic changes will (sonography).

As obstruction progresses, biliary dilatation can be detected. This dilatation precedes the onset of jaundice [1] and involves the extrahepatic ducts before the intrahepatic ducts. Disparate dilatation [14] occurs when extrahepatic ductal dilatation occurs in the absence of intrahepatic ductal dilatation. This may be the result of tamponade of the intrahepatic ducts by hepatic parenchyma and of Laplace's law (the pressure or bursting force of a sphere or cylinder is proportional to its diameter), and thus the maximal effect is seen in the larger extrahepatic ducts.

In the third or icteric phase of biliary obstruction, patients are grossly icteric, and the level of bilirubin is greatly elevated. The anatomic findings are those of diffuse biliary dilatation. These findings occur more rapidly when cholecystectomy has been performed previously.

Partial obstruction does not always lead to total obstruction, and so the sequence of functional, anatomic, and icteric phases is not always seen. Calculi in the common bile duct can impact and disimpact within the duct and can result in little change or rapid alteration of the diameter of the duct. In cases in which dilatation is not present, scintigraphy may be useful [15].

In confusing or borderline cases, functional evaluation of the biliary tract with cholescintigraphy or sonography after cholecystokinin stimulation often is helpful. Cholecystokinin stimulates bile flow, and if true obstruction is present, the common bile duct will dilate transiently; in normal patients, the size of the duct will decrease or remain the same.

"Biliary obstruction" should not be used interchangeably with "biliary dilatation." Obstruction can be present without dilatation early in the course of disease or in cases in which the obstruction is intermittent. This is the case in many patients with stones and in some patients with stenosis of the sphincter of Oddi.

Likewise, dilatation can exist without obstruction. This is seen in patients who have had enlarged ducts and have had surgical decompression or bypass. The duct remains dilated despite normal excretory dynamics. Perhaps a loss of elasticity or autonomic tone of the biliary system occurs, but regardless of the reason, the bile ducts may not return to their normal size [16]. Evaluating biliary drainage with cholescintigraphy may be prudent in this group of patients. Establishing the diagnosis of recurrent obstruction may require cholangiography in some postoperative patients.

Yet another situation in which the clinical significance of ductal dilatation must be interpreted carefully is the patient who has had a cholecystectomy. In patients who have had cholecystectomy, the bile ducts maintain their normal caliber. Early studies had suggested that the ducts dilated in response to cholecystectomy. Subsequent longitudinal studies of large groups of patients undergoing sonography before and after cholecystectomy revealed no evidence that this occurs.

Radiology/Pathology of Selected Causes

In the neonate, pathologic jaundice is evaluated by sonography and ^{99m}Tc-IDA scintigraphy to detect masses and determine biliary patency. Biliary atresia, which requires early diagnosis and surgical therapy, may mimic neonatal hepatitis histologically. Differentiation is made on the basis of findings on Tc-IDA scintigraphy, which, in biliary atresia, shows good hepatic uptake and absent bowel activity if the patient is premedicated with phenobarbital. A misdiagnosis of neonatal hepatitis may be made if premedication is inadequate or the patient has cystic fibrosis or diarrhea.

Choledochal cyst is one of a number of hepatobiliary malformations, not necessarily related (polycystic liver disease, congenital hepatic fibrosis, and Caroli disease), that can be seen in an older child or adult. Communication between the cyst and the biliary tree is ascertained by using Tc-IDA scintigraphy or sonography or by MR demonstration of contents identical to bile. When a high-grade obstruction is present, Tc-IDA may enter the cyst slowly or not at all. In Caroli disease, pathologic studies show a polypoid wall protrusion containing a central portal vein and hepatic artery, suggesting a developmental abnormality. This correlates with enhancing central dots within the dilated bile ducts on CT as distinguished from nonenhancing opacities representing small stones [17].

In adults, sclerosing cholangitis, AIDS-associated cholangitis, oriental cholangiohepatitis, cholangiocarcinoma, and rare biliary tumors should be considered among the primary biliary processes that may cause obstructive jaundice in addition to gallbladder carcinoma extending into the common bile duct.

Once causes of secondary cholangitis are excluded, primary sclerosing cholangitis is considered when obstructive symptoms develop insidiously. In more than 50% of cases, the patient has a history of universal, moderate to severe ulcerative colitis. Our understanding of the histopathologic changes is based on analysis of the intrahepatic ducts from hepatectomy specimens in patients undergoing liver transplantation [18]. We can extrapolate these data to the extrahepatic ducts. Cholangiectasis associated with fibrous crests and formation of diverticula, combined with fibrous cholangitis, ultimately obliterate the ducts. This correlates with the nodularity, beadlike strictures, and narrow-necked diverticula seen on cholangiography, with correlative findings on sonography and CT. In the differentiation of primary sclerosing cholangitis from multifocal/diffuse cholangiocarcinoma, the presence of diverticula, fine shaggy nodules, or enhancing intraluminal nodules on high-resolution CT; sequential rather than synchronous obstruction; and a relative lack of dilatation proximal to a high-grade stricture favor primary sclerosing cholangitis. Involvement of the gallbladder (15%), cystic duct (18%), and pancreatic duct (8%) often is overlooked in this disease.

The clue to AIDS-associated cholangitis is the presence of papillary stenosis (i.e., a common bile duct >1 cm in diameter, a stricture that may be as short as several millimeters, and a delay in drainage of contrast material from the duct) alone or in association with findings similar to those of primary sclerosing cholangitis [19]. Sonography is better than CT for showing wall thickening in the gallbladder and bile ducts, and pericholecystic fluid also may be present. Associated pathologic findings include ulcers of the common duct, inflammatory changes in the duodenum, portal fibrosis, and evidence of infection with cytomegalovirus, *Cryptosporidium*, or *Mycobacterium avium-intracellularae* [20].

The pathophysiology of oriental cholangitis is uncertain; stones, cholangitis, parasites, and dietetic factors are implicated. The combination of stones in focally dilated ducts and strictures results in recurrent pain, fever, and jaundice. Cholangiography is useful in defining the obstruction, finding residual stones, and, postoperatively, evaluating the anastomoses. It should be done gently to avoid iatrogenic sepsis, bile peritonitis, or hepatic hemorrhage. Sonography or CT is used to assess development of an apparent mass, which often represents an abscess or biloma or, rarely, an associated carcinoma [21]. When the disease is focal, a low-density stone seen on CT could be misconstrued as a tumor with focal biliary dilatation. On sonography, casts filling the duct could obscure the dilatation, and sludge could be mistaken for an intraductal tumor. When segmental obstruction is complicated by focal pyogenic hepatitis, segmental liver enhancement may be seen.

Patients with a slow-growing extrahepatic or central cholangiocarcinoma may have jaundice; 84% of cases involve the bifurcation and/or common duct. Among the predisposing factors are chronic ulcerative colitis, primary sclerosing cholangitis, and choledochal cyst. The pattern of growth may be infiltrative, nodular, or papillary, and the associated desmoplasia accounts for the frequent false-negative results of needle biopsy. The main role of the radiologist is to determine the proximal extent of the tumor and judge its resectability. Most of the tumors are infiltrative with little bulk, and only thickening of the wall and abrupt obstruction are seen. Cross-sectional imaging studies are useful to search for metastases and adenopathy. The overall 5-year survival rate is 5%, but patients with papillary tumors in the distal duct have 5-year survival rates up to 25%. Transplantation results have been discouraging.

Biliary Intervention

Emergent Percutaneous Cholecystostomy

Emergent percutaneous cholecystostomy is useful in treatment of patients with acute cholecystitis or biliary sepsis. Successful percutaneous cholecystostomy was reported just 10 years ago [22]. Since then, the technique has been perfected, with development of catheter systems especially designed for placement into the gallbladder [23, 24]. The indications for emergent percutaneous cholecystostomy are still evolving, but clearly the most common are treatment of patients with acute cholecystitis or patients with obstruction of the common bile duct and cholangitis [25, 26].

The technique is relatively simple. The catheter can be placed into the gallbladder by using either a trocar method or guidewire exchange technique. Sonography often is used to guide emergent percutaneous cholecystostomy done via the transhepatic route (Fig. 5). The catheter should have some sort of securing device to prevent its dislodgement [23, 24].

Percutaneous cholecystostomy is an effective alternative to surgical cholecystostomy for decompressing the acutely inflamed gallbladder (Fig. 6). In high-risk patients, percutaneous cholecystostomy can be a temporizing maneuver to allow the patient to stabilize before definitive cholecystostomy.

Percutaneous cholecystostomy has several advantages: (1) In a large series, it has fewer complications than does surgical cholecystostomy. (2) It is extremely expedient; insertion of the catheter takes only a few minutes. (3) If sonography is used to guide placement of the catheter, the procedure can be done at the patient's bedside (this may be extremely important in desperately ill, hospitalized patients). (4) Finally,

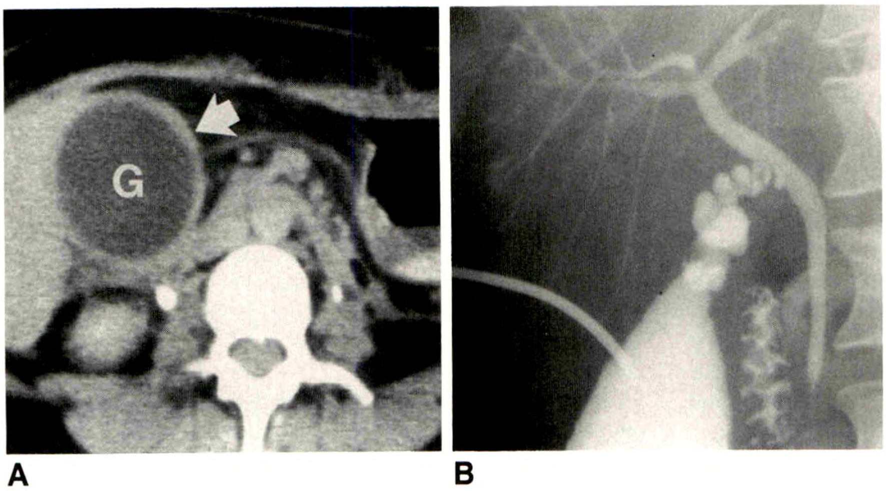

Fig. 6.—Cholecystostomy used to treat acute cholecystitis with obstruction of cystic duct.

***A*, CT scan of upper abdomen shows an enlarged gallbladder (G) with a thickened wall (*arrow*).**

***B*, Cholangiogram obtained 4 days after *A*, after insertion of cholecystostomy catheter, shows cystic duct and common bile duct are patent.**

percutaneous cholecystostomy is a definitive treatment in some patients with acute acalculous cholecystitis; thus cholecystostomy can be avoided [25].

Emergent percutaneous cholecystostomy also is useful for decompressing the biliary system in highly selected patients with obstruction of the common bile duct and cholangitis. The procedure can be helpful for providing "quick" access to the biliary system for temporary decompression before more definitive treatment [26].

In summary, emergent percutaneous cholecystostomy is useful for treating patients with acute cholecystitis or those with cholangitis associated with obstruction of the common bile duct.

Percutaneous Contact Dissolution of Gallstones and Mechanical Extraction

Despite leaving an intact gallbladder, removal of gallbladder stones appears to decrease gallbladder-related symptoms [28]. Numerous options exist for eliminating gallstones through a percutaneous tract, including contact dissolution [28, 29], mechanical extraction of the stone, and gallstone fragmentation and removal [30]. All of these percutaneous methods have been effective in a high percentage of cases because of proper selection of patients. Advantages of these techniques are no need for general anesthesia, rapid recovery time, no major scar, and cost-savings (at least in the short run). Gallbladder-sparing procedures have the disadvantage of leaving behind a diseased gallbladder in which gallstones could recur and gallbladder carcinoma could develop.

Contact dissolution is most applicable for patients with symptomatic gallstones, who have a gallbladder that is reasonably distensible with no or minimal calcium in the stone(s) [28, 29]. Although calculi in the cystic duct are more difficult to treat, their presence does not exclude contact dissolution. Mechanical methods of gallstone extraction can be used even if the stones are heavily calcified.

The main agent for contact dissolution of cholesterol gallstones is methyl *tert*-butyl ether (MTBE). MTBE is a powerful, low-viscosity solvent that is used in its anhydrous state. Although it has a noxious odor and is potentially flammable, its effects on the gallbladder mucosa are relatively minimal histologically. Another anticholesterol agent is monooctanoin; the high viscosity of this agent has precluded its use in the gallbladder. A new agent, ethyl proprionate, is being tested in the laboratory; it has many of the advantageous qualities of MTBE, but fewer of the adverse properties. Calcium-dissolving agents, including EDTA and acetylcysteine compounds, have shown some effectiveness but are not in major clinical use.

The gallbladder is catheterized initially through a 5- to 7-French tube. The preferred method for placement of the catheter is via a transhepatic tract, traversing the bare area of the gallbladder; this route simplifies insertion of the catheter and may prevent leakage of bile. Locking catheters help to avoid dislodgment [31].

MTBE is delivered by hand lavage or by pressure- or volume-driven pumps. Dissolution usually is accomplished within 2–10 hr, depending on the size, number, position, and degree of calcification of the stones. Contact dissolution is labor intensive, and the instillation and retrieval of MTBE must be monitored carefully. When used in proper amounts and evacuated thoroughly, MTBE is safe. The solvent should not be allowed to spill into the common bile duct; it could be absorbed from the duodenum and injure the intestinal mucosa.

The only reported major complication from MTBE itself was due to loss of a large amount of the agent from the gallbladder; this patient had hemolysis with renal failure and became semicomatose. In properly selected patients, MTBE has been effective in dissolving gallstones in 85–96% of patients [28, 29].

Gallstone fragmentation can be accomplished by a variety of methods, each with advantages and disadvantages. Mechanical fragmentation with stone baskets certainly is cheapest, whereas intracorporeal electrohydraulic lithotripsy (EHL) is most powerful [30]. Ultrasonic contact lithotripsy has the advantage of simultaneous fragmentation and extraction, but it can be done only through a rigid scope. Laser fragmentation is safest with respect to damage to the mucosa and wall, but it is not as powerful as other contact methods. The laser is the most costly instrument. These devices are used through cholecystoscopy alone or in combination with fluoroscopic guidance. Another method of stone fragmentation is use of a rotating blade placed percutaneously into the gallbladder. This procedure sucks up stones in a vortex and then fragments the stones relatively rapidly. Patients with acute cholecystitis or obstruction of the cystic duct are excluded from this procedure. Results of this procedure are too preliminary to permit meaningful evaluation.

Anesthesia for percutaneous procedures depends on the size of the tract and whether the procedure is performed in one step or is delayed. In general, the larger the tract and the more expeditious the procedure, the greater the need for anesthesia. Thus, for a one-session percutaneous cholecystolithotomy through a 26-French (or greater) tract, general anesthesia is used; on the other hand, for contact dissolution with MTBE through a 7-French catheter, only local anesthesia and IV sedation and analgesia are necessary.

Recurrence of gallstones after these percutaneous procedures should be expected in up to 50% of patients, in accord with data from oral dissolution studies. Generally accepted rates of recurrence are 10% per year for 5 years and a leveling off after 5 years. Recurrence is more common in patients with many stones, as opposed to one or few stones.

Methods of gallbladder ablation are being evaluated in the laboratory and in clinical studies [32]. In order to ablate the gallbladder, the bile ducts must be sequestered from the gallbladder to ensure that stricture of the common bile duct does not result from the sclerosis. Methods to isolate the gallbladder via cystic duct exclusion include mechanical clipping, RF cautery, detachable coils, and glue. Gallbladder sclerosants include alcohol, sodium salts, and heated contrast material. The combination of RF coagulation and alcohol with sodium tetradecyl sulfate sclerosis has been effective in animals and has had limited success in its first clinical trial [32].

Further experience and refinements are necessary to decide the role for each of these percutaneous techniques in eliminating gallstones. Undoubtedly the patient who is at high risk for surgery should benefit most from these alternative techniques.

The Biliary Tree: Endoscopic Intervention

Endoscopic intervention, performed in conjunction with upper gastrointestinal endoscopy with retrograde cholangiopancreatography, includes such techniques as sphincterotomy and forceps biopsy of intraductal mucosal lesions within the biliary or pancreatic ducts or of submucosal lesions after incision (sphincterotomy) [33]. Additional maneuvers such as insertion of a stent or drain are similar to those performed percutaneously but do not violate the pleural or peritoneal cavities. This reduces risk and eliminates pain but is particularly important because tract seeding from biopsy or leakage of bile during placement of a stent has been shown to disseminate cholangiocarcinoma and pancreatic cancer and prejudice surgical resection in the 20% of patients who are considered candidates for surgery [34].

Indications for endoscopic therapy have expanded because of its low-risk and noninvasive character, particularly in older patients. Endoscopic sphincterotomy (1) gives a permanent choledochoduodenostomy, (2) prevents recurrence of gallstone pancreatitis, (3) defunctionalizes the gallbladder, (4) allows submucosal biopsy of distal biliary tumors, and (5) ensures repeated biliary access. Obstructive cholangitis with pancreatitis and gallstone pancreatitis require emergent endoscopic therapy, which has reduced the morbidity and mortality rates of these entities substantially when compared with the rates for traditional surgical management [35]. Choledocholithiasis is managed without cholecystectomy because only 10% of high-risk patients who had jaundice or cholangitis required cholecystectomy after prolonged follow-up. Currently, cholecystitis in these patients would be treated with surgical resection under local anesthesia or percutaneous cholecystostomy. The mortality rate for endoscopic sphincterotomy (0.5%) is equal to that for cholecystectomy (0.5%) and less than that for exploration of the common bile duct (1.5%) in low-risk patients, with a vast reduction in pain, convalescence, and hospitalization. The use of preoperative ERCP with selective endoscopic sphincterotomy combined with gallbladder removal during surgery or, preferentially, during laparoscopy if necessary, yields the best results [36]. This advantage is increased when the patient is at greater risk because of the limited stress of uncomplicated endoscopic procedures.

The endoscopic therapy of pancreatitis and its complications, including pseudocyst, duct stenosis, and precipitating causes such as anomalous biliary-pancreatic junction, sphincter dysfunction, and microcholedocholithiasis, has similar benefits that are not discussed here (Figs. 7 and 8).

Malignant biliary obstructions can be treated palliatively by using endostents (plastic or self-expanding metal), sphincterotomy, and brachytherapy. Tumor ablation by injection of alcohol or by laser controls bleeding or mass lesions. This broad range of treatments emphasizes the need for diagnostic precision and careful consideration of therapeutic options.

When successful cannulation of the duct is not possible, the endoscopist may request percutaneous assistance. Combined percutaneous and endoscopic procedures are valuable in overcoming mechanical problems such as a large mass or an impassable stenosis. In most instances, a percutaneously passed 480-cm guidewire is grasped in the duodenum by the endoscopist and withdrawn out of the mouth. The endoscope then is passed over the wire, and sphincterotomy or stent placement is performed. Alternatively, the stent may be passed directly over the wire without use of the endoscope. The latter technique allows insertion of large (14-French) stents, but no evidence exists that these larger devices are more effective, and they may be difficult to exchange because of their bulk and stiffness. The immediate withdrawal of the percutaneous wire and brief use of only 5-French catheters without drainage may limit the bile leakage, tract seeding, and pain that complicate percutaneous transhepatic insertion of a stent.

The prudent endoscopist limits efforts when complications are likely or defers to a percutaneous or surgical technique when indicated. Not infrequently, a diagnostic study reveals

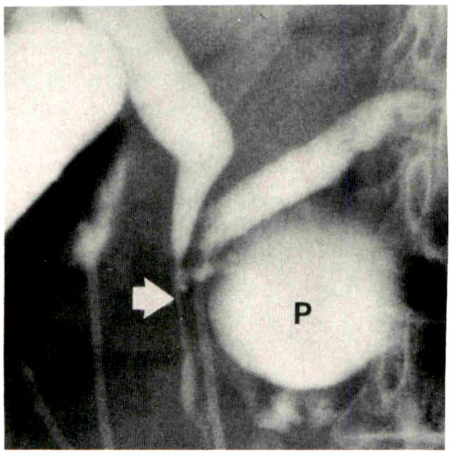

7

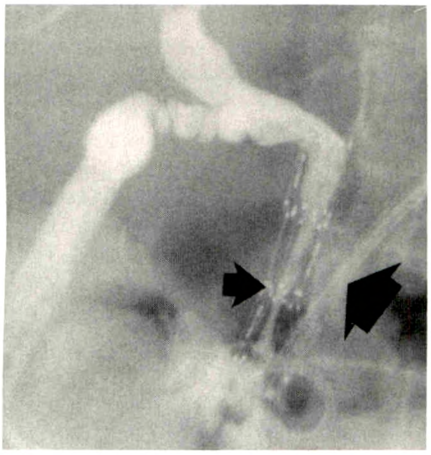

8

Fig. 7.—Endoscopic drainage of pseudocyst. ERCP of 47-year-old woman referred for treatment of two pancreatic pseudocysts and a bile duct stenosis arising after an episode of gallstone pancreatitis shows a caudal 3-cm pseudocyst (P) arising from an uncinate duct compressing and obstructing both pancreatic and bile ducts (*arrow*). A 6-French nasal pancreatic drainage tube was placed in pancreatic duct, decompressing both duct and pseudocyst. Residual choledocholiths were removed with a choledochoscope via cholecystostomy.

Fig. 8.—Pancreatic and biliary endoscopic stents. After an endoscopic sphincterotomy to separate biliary and pancreatic ducts, a 4.5 cm × 8 mm Z stent (self-expanding) was placed in common bile duct (*small arrow*). Three pancreatic endostents were placed in pancreatic duct to dilate stenosis and ensure pancreatic drainage (*large arrow*). Pseudocysts resolved completely with internal pancreatic drainage. With gallbladder and biliary tree well decompressed, cholecystostomy tube was removed. After 6 months, pancreatic stents were removed.

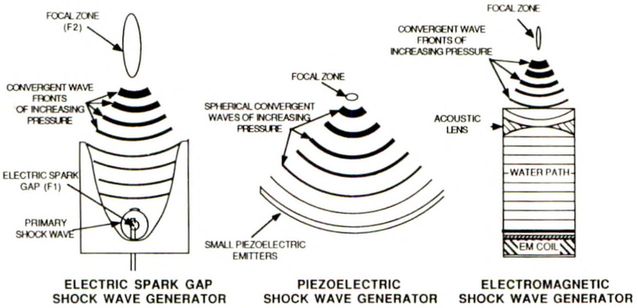
FOCAL ZONE (F2)
CONVERGENT WAVE FRONTS OF INCREASING PRESSURE
ELECTRIC SPARK GAP (F1)
PRIMARY SHOCK WAVE
FOCAL ZONE
SPHERICAL CONVERGENT WAVES OF INCREASING PRESSURE
SMALL PIEZOELECTRIC EMITTERS
FOCAL ZONE
CONVERGENT WAVE FRONTS OF INCREASING PRESSURE
ACOUSTIC LENS
WATER PATH
EM COIL
ELECTRIC SPARK GAP SHOCK WAVE GENERATOR
PIEZOELECTRIC SHOCK WAVE GENERATOR
ELECTROMAGNETIC SHOCK WAVE GENERATOR

Fig. 9.—Drawing shows three types of shock-wave generators that are commercially available.

incurable disease with few therapeutic options. This prognostic information is particularly important in patients for whom only painless palliation is desired. Endoscopic intervention provides these options.

Biliary Lithotripsy

Technical Considerations

Since its first use to treat kidney stones, lithotripsy has been clinically investigated for treatment of gallstones in more than 2000 patients in the United States. The technology has evolved from the early spark-gap "bathtub" machines to devices with more sophisticated power sources that can be focused and targeted better. Shock waves are an acoustic phenomenon. Their frequency is similar to that produced by diagnostic ultrasound transducers. Their waveform, however, differs substantially; it has a high-pressure, positive-amplitude component and a low-pressure negative-amplitude or rarefactive component. Peak positive pressures ranging from 300 to 1200 bar (atmospheres) and negative pressures of −10 to −50 bar have been reported [37, 38].

There are three means of generating shock waves. Spark-gap, electromagnetic, and piezoelectric sources are all commercially available (Fig. 9). When current is applied to an underwater spark-plug gap, a localized steam cloud is created, which expands at supersonic speed. As the expansion of this plasma state exceeds the ability of the conducting medium (water), a shock-wave front is formed. This front is focused by using a metal ellipse and is brought to bear in what has been called the F2 focal zone. In the case of a spark-gap device, the electrical discharge actually produces a shock wave before focusing.

Electromagnetic and piezoelectric devices produce high-power sound waves that become shockwaves only after focusing [39]. Electromagnetic power sources use a slab coil adjacent to a metallic membrane. When a voltage is applied to the slab coil, it transiently magnetizes the metal membrane, causing sudden displacement. This displacement generates a high-powered sound wave similar to the mechanism of sound generation by a loudspeaker. The sound waves are focused by an acoustic lens to create a shock wave. Piezoelectric lithotriptors produce shock waves by spatially and temporally focusing converging sound waves. The sound waves are produced by applying an electric current to a piezoelectric crystal similar to that found in diagnostic sonographic devices. The summation of these individual sound waves produces a high-powered shock wave.

As the technology became refined, the water bath was enclosed by a plastic membrane that could be coupled to the patient. Biplane fluoroscopic guidance was used to treat radiopaque kidney stones. Most vendors added in-line (in the plane of the shock-wave focal zone) ultrasound transducers for gallstone targeting. In-line ultrasound probes are subject to the deleterious effects of shock waves, and a variety of schemes for protecting these probes have evolved. Most commonly this consists of metal shielding or retraction of the probe into a safe position behind the shock-wave focal zone. Because of sound attenuation at the water bath–patient interface and suboptimal placement of the transducer's focal zone, producing high-quality images for targeting requires considerable radiologic skill.

Stone fragmentation results from the positive and negative pressure components of shock waves. Shock-wave compressive force is imparted to a stone because of its impedance differences from the surrounding tissues or fluids. The compressive force probably is transmitted internally within the stone and is variably attenuated and reflected. This compressive force appears to open up internal fissures along the radially oriented cholesterol plates within gallstones. Although fissures and crevices may cross the band of pigment within gallstones, these appear more disruptive of shock-wave propagation than is cholesterol [40].

The negative pressure associated with shock waves gives rise to cavitation effects. These cavitation effects occur primarily in the bile or tissue surrounding a gallstone [41]. As these biological substances are exposed to negative pressures, microbubbles are formed. These microbubbles bombard the surface of a gallstone and cause surface erosion. Cavitation effects also are thought to occur in solid tissues and may be responsible for hepatocellular injury during gallstone lithotripsy. Currently, this injury does not appear to be clinically significant.

Clinical Overview

After the success of renal extracorporeal shock-wave lithotripsy (ESWL), physicians began investigating the use of ESWL on gallstones. In 1988, promising biliary ESWL results in 175 patients were published by Sackmann et al. [42]; in this study fragments had disappeared completely in 30% of patients within 2 months of ESWL, in 48% at 2–4 months, in 63% at 4–8 months, in 78% at 8–12 months, and in 91% at 12–18 months. The dissolution rate was highest (95%) for single radiolucent stones, 20 mm or smaller in diameter.

The study by Sackmann et al. has become the gold standard to which all others are compared. All patients in their study received a combination of chemolytic agents, chenodeoxycholic acid and ursodeoxycholic acid. Additionally, a modified renal water-bath unit (Dornier HM3) was used and general anesthesia was required.

In trials in the United States and Europe, patients accepted for lithotripsy must be symptomatic and have (1) radiolucent gallstones that can be detected by sonography and (2) a functioning gallbladder as determined by oral cholecystography or sonography. General exclusion criteria include relevant defective coagulation, pregnancy, stones in the common bile duct, and pigmented stones. Patients who have aneurysm or hepatic cysts or hemangioma or have lung tissue in the shock-wave path are excluded also.

Two main factors make the comparison of data difficult: (1) the lack of uniformity in presenting data and (2) the technical differences between the three different techniques for generating shock waves: piezoelectric, electromagnetic, and electrohydraulic. To augment the initial ESWL procedure, investigators may use adjuvant oral chemolysis, perform retreatments, or both. Most protocols in the United States include use of ursodeoxycholic acid for oral chemolysis along with ESWL. However, some investigators [43] have had good gallstone clearance rates when using ESWL without oral chemolysis.

Methods of presenting biliary ESWL results vary, but, in general, one can look at the stone populations, fragmentation rates, retreatment percentages, and stone-free rates in the various studies. As far as stone populations are concerned, most current protocols restrict the number and size of the gallstones or have a limit based on gallstone volume or total diameter [42–46].

Initial rates of fragmentation range from 76% to 99%, with satisfactory fragmentation (i.e., fragments ≤5 mm) seen in 22–78% [45]. Several factors affect fragmentation of gallstones, including the volume, number, size, and composition of the stones. When corrected for volume, single gallstones are fragmented more easily into pieces 5 mm or less in diameter (the initial target size) than are multiple gallstones. More shock-wave energy is needed to achieve the same results in patients with multiple stones than in patients with single stones. With this in mind, the aim of many investigators is to pulverize gallstones into 2- to 3-mm fragments. In theory, this would clear fragments faster and eliminate or at least decrease the need for adjuvant oral chemolysis.

Piezoelectric lithotriptors have the highest retreatment rates, and electrohydraulic machines have the lowest [45]. The treatment strategy for piezoelectric technology involves several sessions; theoretically, this can be done either by using small amounts or without the use of IV sedation or analgesia. Economic considerations, physicians' time, and patients' compliance will determine the ultimate acceptance of the multiple treatment strategy.

A wide range of stone-free rates have been reported. The results vary from 20% to 63% 6 months after treatment and from 22% to 83% 12 months after treatment [42–46]. The clearance rates in patients with calcified or partially calcified gallstones are not as satisfactory; partially calcified or densely calcified stones can be fragmented, but the stone-free rate is significantly lower than that for radiolucent stones [42, 44].

Stone clearance, in part, appears to be directly related to the size of the gallstone fragments after lithotripsy [42] and the amount of energy used in the fragmentation process; patients with fragments 2 mm or smaller in diameter after lithotripsy have a higher rate of stone clearance than do patients with larger fragments (i.e., ≥5 mm).

The reported biliary ESWL studies [43–46] have, in general, stone-free rates lower than those seen in the study by Sackmann et al. [42]. The group at the Grosshadern Klinikum [44] and other European investigators who used more shock-wave energy (i.e., increased number of shock waves at a higher kilovoltage) have a better fragmentation rate and increased stone clearance at 6 months than do groups that use treatment parameters similar to those used in the United States. We think that if increased shock-wave energy were used, the efficacy of biliary ESWL in the United States would be similar to that in Germany. This procedure is still in its infancy when compared with other long-established methods of gallstone therapy. As our knowledge of the procedure grows, the efficacy of the procedure will most likely increase.

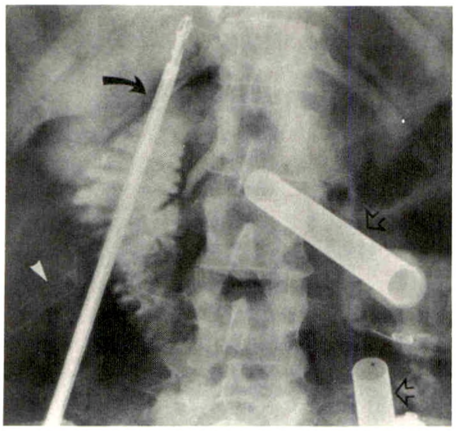

Fig. 10.—Cholangiogram from laparoscopic cholecystectomy shows upper and lower central trocars (through which laparoscope passes) centrally (*open arrows*), a smaller trocar in flank (*arrowhead*), and a forceps (*curved arrow*) through site of a second trocar in flank. Common bile duct and gallbladder are opacified. (Courtesy of C. Elton Cahow.)

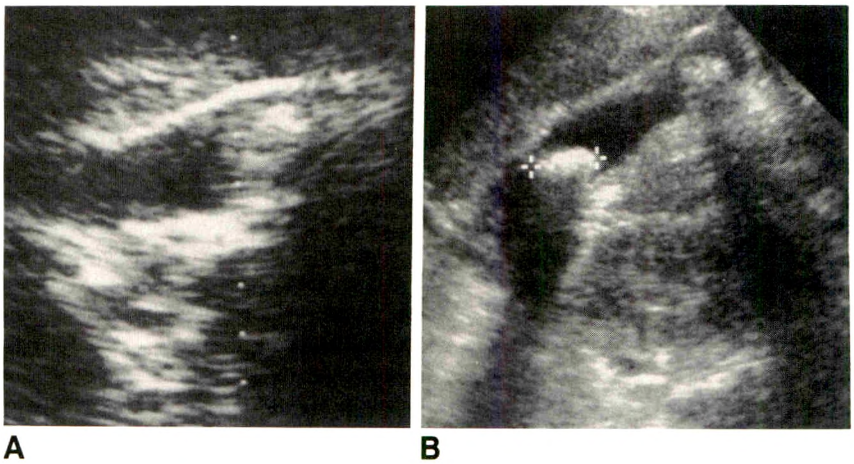

Fig. 11.—Hidden-fragment phenomenon.

A, Sonogram obtained during lithotripsy shows cloud of dust due to fragments. Discrete large fragments cannot be identified.

B, Sonogram obtained 1 day after *A* shows two large fragments that could not be identified during lithotripsy.

Evolving Issues

Before considering some of the unsettled issues in the area of biliary lithotripsy, it is important to consider the facts that appear to be well established. The current generation of biliary lithotriptors is clearly capable of fragmenting the vast majority of gallstones [47]. Further, it is clear that if the size of the fragments can be reduced to less than 3 mm, a high proportion of these patients (>70%) will become fragment-free within 6–12 months. Furthermore, it has become clear that biliary lithotripsy is a remarkably safe procedure with essentially no adverse effects from the shock waves themselves [48]. The only significant complications occur as a result of passage of fragments through the cystic and common bile ducts. The most serious and frequent of these complications appears to be acute pancreatitis.

Laparoscopic cholecystectomy.—At this time, the major turmoil in lithotripsy research has been caused by the development of the laparoscopic cholecystectomy [49], with its promise of same-day, definitive treatment without the need for hospitalization, abdominal scarring, or bile salts (Fig. 10). This technique is being adopted aggressively by surgeons worldwide, even though virtually no scientific publications are available on its efficacy and short- or long-term complications. These surgeons have raised the question of whether lithotripsy will be useful, now that laparoscopic cholecystectomy is available. This question remains unanswered, and the answer will depend on the success rate and complication rate of the new surgical procedure as its use becomes widespread. It is quite possible, if not likely, that a group of gallstone patients will remain who will choose noninvasive lithotripsy as the best treatment.

Optimization of lithotripsy treatment regimens.—Clinical studies to date have adopted somewhat arbitrarily their treatments regimens. The optimization of treatment involves some obvious considerations such as energy deposited within the stones. In general, this is related to the product of the number of shock waves and their energy. However, a number of other less-obvious factors have not been adequately explored. These include the accuracy of targeting [50], the frequency of retreatment, and the direction of shock-wave entry. It is by no means clear that the results reported so far have used similar treatment regimens.

Importance of imaging.—The importance of sonographic imaging has not been appreciated adequately with regard to its role in the performance and follow-up of lithotripsy. It is becoming clear that the cloud of dust caused by swirling fragments during treatment obscures larger fragments, giving a false impression of successful treatment (Fig. 11). Sonography the next day shows the larger fragments after the dust has settled (Fig. 10B). Furthermore, it has been shown that the evaluation of the size and the number of fragments after lithotripsy is complicated by the tendency of smaller fragments to clump and simulate large fragments. This has led to the suggestion that the patient be rolled over in an attempt to disperse the fragments so that number and size of stones can be measured more accurately [51].

Role of bile salts.—Most studies have concluded that bile salts are necessary for optimal clearance of gallstone fragments. Certainly, in the Dornier National Biliary Lithotripsy Study, this was the conclusion. However, closer analysis of those results suggests that when fragments were reduced to 3 mm or smaller, little difference was seen between the placebo group and the bile-salt group. This raises the possibility that bile salts may not be necessary in those patients who have very small fragments, particularly if they have good gallbladder contraction. Certainly, additional work is required in this area, because the omission of bile salt therapy would reduce substantially the overall cost of these treatments.

Stone recurrence.—As expected, it seems that stones will recur in patients who have become stone-free, at a rate of approximately 10% per decade up to a maximum of approximately 50% [42]. The original hope was that these recurrences would be easily treated with oral bile salts. Unfortunately, this appears not to be the case. Certainly, much work must be done to develop strategies for preventing recurrence of stones or an effective means of early treatment of recurrence.

During the next few years, the role of laparoscopic cholecystectomy and its safety will need to be assessed as its use becomes more common. Basic research in lithotripsy should be aimed at determining the optimal treatment strategy not only with regard to energy levels but also fractionation, targeting, and characteristics of the shock wave. A more precise role for oral bile salts must be determined. Are they needed in every case or only in selected cases? The recurrence rate of gallstones remains an important problem, and, in particular, the treatment of recurrent stones must receive further consideration.

REFERENCES

1. Zeman RK, Burrell MI. *Gallbladder and bile duct imaging: clinical radiologic approach.* New York: Churchill-Livingstone, **1987**:1–46, 385–469
2. Wu CC, Ho YM, Chen CY. Effect of aging on common bile duct diameter: a real time ultrasonographic study. *JCU* **1984**;12:473–478
3. Zeman RK, Burrell MI, Cahow CE, Caride V. Diagnostic utility of cholescintigraphy and ultrasonography in acute cholecystitis. *AJR* **1981**;141: 446–451
4. Cohan RH, Mahony BS, Bowie JD, Cooper C, Baker ME, Illescas FF. Striated intramural gallbladder lucencies on US studies: predictors of acute cholecystitis. *Radiology* **1987**;164:31–35
5. Siskind B, Hawkins M, Zeman RK, Burrell MI. Perforation of the gallbladder: radiologic-pathologic correlation. *J Clin Gastroenterol* **1987**;9:670–678
6. Wegener M, Borsch G, Schneider J, et al. Gallbladder wall thickness: a prospective study. *JCU* **1978**;15:307–312
7. Giorgio A, Francica G, Amoroso P, et al. Morphologic and motility changes of the gallbladder in response to acute liver injury: a prospective real time sonographic study in 255 patients with acute viral hepatitis. *J Ultrasound Med* **1989**;8:499–506
8. Saigh J, Williams S, Cawley K, et al. Varices: cause of focal gallbladder wall thickening. *J Ultrasound Med* **1985**;4:371–378
9. West MS, Garra BS, Horii SC, et al. Gallbladder varices: imaging findings in patients with portal hypertension. *Radiology* **1991**;179:179–182
10. Bonmati-Marti L, Andre JC, Aguade C. Sonographic relationship between gallbladder wall thickness and etiology of ascites. *JCU* **1989**;17:497–501
11. Kaftori JK, Pery M, Green J, Gaitini D. Thickness of the gallbladder wall in patients with hypoalbumenemia. *AJR* **1987**;148:1117–1118
12. Zeman RK, Burrell MI, Gold JA, Russo R Jr. The intrahepatic and extrahepatic bile ducts in surgical jaundice: radiological evaluation and therapeutic implications. *CRC Crit Rev Diagn Imaging* **1984**;21:1–36
13. Zeman RK, Lee C, Jaffe MH, Burrell MI. Hepatobiliary scintigraphy and sonography in early biliary obstruction. *Radiology* **1984**;153:793–798
14. Zeman RK, Dorfman GS, Burrell MI, et al. Disparate dilatation of the intrahepatic and extrahepatic bile ducts in surgical jaundice. *Radiology* **1981**;138:129–136
15. Darweesh RMA, Dodds WJ, Hogan WJ, et al. Efficacy of quantitative hepatobiliary scintigraphy and fatty meal sonography for evaluating patients with suspected partial common duct obstruction. *Gastroenterology* **1988**;94:779–786
16. Zeman RK, Burrell MI, Dobbins J, Jaffe MH, Choyke PL. Post-cholecystectomy syndrome: evaluation using biliary scintigraphy and endoscopic retrograde cholangiopancreatography. *Radiology* **1985**;156:787–792
17. Chol BI, Yeon KM, Kim SH, Han MC. Caroli disease: central dot sign in CT. *Radiology* **1990**;174:161–163
18. Ludwig J, MacCarthy RL, LaRusso NF, Krom RAF, Wiesner RH. Intrahepatic cholangiectases and large-duct obliteration in primary sclerosing cholangitis. *Hepatology* **1986**;6:560–568
19. Dolmatch BL, Laing FC, Federlie MP, Brooke JR, Cello J. AIDS-related cholangitis: radiographic findings in nine patients. *Radiology* **1987**;163:313–316
20. Cello JP. Acquired immunodeficiency syndrome cholangiopathy: spectrum of disease. *Am J Med* **1989**;86:539–546
21. Chan FL, Man SW, Leong LLY, Fan ST. Evaluation of recurrent pyogenic cholangitis with CT: analysis of 50 patients. *Radiology* **1989**;170:165–169
22. Elyaderani M, Gabriele OF. Percutaneous cholecystostomy and cholangiography in patients with obstructive jaundice. *Radiology* **1979**;130: 601–602
23. Hawkins IF Jr. Percutaneous cholecystostomy. *Semin Intervent Radiol* **1985**;2:97–103
24. McGahan JP. A new catheter design for percutaneous cholecystostomy. *Radiology* **1988**;166:49–52
25. McGahan JP, Lindfors KK. Percutaneous cholecystostomy: an alternative to surgical cholecystostomy for acute cholecystitis? *Radiology* **1989**;173:481–485
26. vanSonnenberg E, D'Agostino HB, Casola G, Varney RR, Taggart SC, May S. Obstructive jaundice: percutaneous cholecystostomy for decompression in selected patients. *Radiology* **1990**;176:15–18
27. McGahan JP. Gallbladder. In: *Interventional ultrasound.* Baltimore: Williams and Wilkins, **1990**:159–170
28. Thistle JL, May GR, Bender CE, et al. Dissolution of cholesterol gallbladder stones by methyl tert-butyl ether administered by percutaneous transhepatic catheter. *N Engl J Med* **1989**;320:633–639
29. vanSonnenberg E, Casola G, Zakko SF, et al. Gallbladder and bile duct stones: percutaneous therapy with primary MTBE dissolution and mechanical methods. *Radiology* **1988**;169:505–509
30. Picus D, Weyman PJ, Marx MV. Role of percutaneous intracorporeal electrohydraulic lithotripsy in the treatment of biliary tract calculi. *Radiology* **1989**;170:989–993
31. vanSonnenberg E, D'Agostino HB, Casola G, Varney RR, Ainge GD. Interventional radiology in the gallbladder: diagnosis, drainage, dissolution, and management of stones. *Radiology* **1990**;174:1–6
32. Becker CD, Fache JS, Malone DE, Stoller JL, Burhenne HJ. Ablation of the cystic duct and gallbladder: clinical observations. *Radiology* **1990**;167:687–690
33. Zimmon DS. Gastrointestinal endoscopy in the diagnosis and management of hepatobiliary disease, 6th ed. In: Schiff L, Schiff ER, eds. *Diseases of the liver.* Philadelphia: Lippincott, **1987**:311–340
34. Chapman WC, Sharp KW, Weaver F, Sawyers JL. Tumors seeding from percutaneous biliary catheters. *Ann Surg* **1989**;205:708–715
35. Neoptolemos JP, Carr-Locke DL, London NJ, Bailey IA, James D, Fossard DP. Controlled trial of endoscopic retrograde cholangiopancreatography and endoscopic sphincterotomy versus conservative treatment for acute pancreatitis due to gallstones. *Lancet* **1988**;2:979–983
36. Heinerman PM, Boeckl O, Pimpl W. Selective ERCP and preoperative stone removal in bile duct surgery. *Ann Surg* **1989**;209:267–272
37. Davros WJ, Garra BS, Zeman RK. Gallstone lithotripsy relevant physical principals and technical issues. *Radiology* **1991**;178:397–408
38. Reichenberger H. Lithotripter systems. *Proc IEEE* **1988**;76:1236–1246
39. Wilbert DM, Reichenberger H, Noske E, Ridemiler H, Allen P, Hohenfellner R. New generation shock wave lithotripsy. *J Urol* **1987**;138:563–565
40. Zeman RK, Marchand T, Davros WJ, et al. Gallstone fragmentation during biliary lithotripsy: effect of stone composition and structure. *AJR* **1991**;156:493–499
41. Zeman RK, Davros WJ, Garra BS, Horii SC. Cavitation effects during lithotripsy: I. results of in-vitro experiments. *Radiology* **1990**;177:157–161
42. Sackmann M, Delius M, Sauerbruch T, et al. Shock-wave lithotripsy of gallbladder stones: the first 175 patients. *N Engl J Med* **1988**;318: 393–397
43. Fache JS, Rawat B, Burhenne HJ. Extracorporeal cholecystolithotripsy without oral chemolitholysis. *Radiology* **1990**;177:719–721
44. Schoenfield LJ, Berci G, Carnovale R, et al. The effect of ursodiol on the efficacy and safety of extracorporeal shock wave lithotripsy of gallstones: the Dornier National Biliary Lithotripsy Study. *N Engl J Med* **1990**;323:1239–1274
45. Barkun ANG, Ponchon T. Extracorporeal biliary lithotripsy: review of experimental studies and a clinical update. *Ann Intern Med* **1990**;112: 126–137
46. Ell CH, Kerzel W, Heyder N, et al. Piezoelectric lithotripsy of gallstones. *Lancet* **1987**;2:1149–1150
47. Burhenne HJ, Becker CD, Malone DE, Rawat B, Fache JS. Biliary lithotripsy: early observations in 106 patients. *Radiology* **1989**;171:363–367
48. Paumgartner G. Shock-wave lithotripsy of gallstones. *AJR* **1989**;153: 235–242
49. Reddick EJ, Olsen DO. Laparoscopic laser cholecystectomy. *Surg Endosc* **1989**;3:131–133
50. Steinberg HV, Torres WE, Nelson RC. Gallbladder lithotripsy. *Radiology* **1989**;172:7–11
51. Khouri MR, Goldszmidt JB, Laufer I, et al. Intact stones or fragments? Potential pitfalls in imaging patients after biliary ESWL. *Radiology* **1990**;177:147–151

AJR
AMERICAN JOURNAL OF ROENTGENOLOGY

MELVIN M. FIGLEY FELLOWSHIPS IN RADIOLOGY JOURNALISM
1992

The American Roentgen Ray Society announces two one-month fellowships in radiology journalism in the La Jolla editorial office of the AJR. Board-certified radiologists with special academic promise are invited to apply.

PURPOSE	The purpose of the fellowship is (1) to stimulate bright young radiologists to continue with an academic career, to accelerate their progress, and to stimulate their interest in good radiology journalism and (2) to improve the quality of radiology journals by teaching the fundamentals of medical journalism to academicians, training manuscript reviewers and future editors, and providing core teachers of medical journalism in radiology departments around the country.
CURRICULUM	The fellows will be taught the fundamentals of medical writing, manuscript preparation, peer review, manuscript editing, the ethics of scientific journalism, and journal publication and printing in personal tutorials given by the AJR editors and editorial staff through hands-on experience in the editorial office. They will visit Williams & Wilkins in Baltimore to observe the publication and printing process.
STIPEND	The successful candidates will each be awarded $10,000, which includes the cost of travel to La Jolla and Baltimore, living expenses for the month, and an honorarium.
APPLICATIONS	Candidates should apply in writing to Robert N. Berk, M.D., Editor-in-Chief, AJR Editorial Office, 2223 Avenida de la Playa, Suite 103, La Jolla, CA 92037. The letter must include a curriculum vitae and a description of the candidate's goals during the fellowship. Letters of recommendation from his or her department chairman and one other senior person are required. Deadline for receipt of applications is Nov. 1, 1991. The successful candidates will be notified Dec. 2, 1991.

Review Article

Laparoscopic Cholecystectomy: Evolution, Early Results, and Impact on Nonsurgical Gallstone Therapies

Jeffrey C. Brandon,[1] Miguel A. Velez,[2] Steven K. Teplick,[3] Peter R. Mueller,[4] David W. Rattner,[5]
J. Ralph Broadwater, Jr.,[6] Nicholas P. Lang,[6] and John F. Eidt[6]

Laparoscopic cholecystectomy, a surgical technique first performed in France, has gained widespread acceptance among surgeons in the United States. The abdominal cavity is inflated by carbon dioxide, a video monitor is inserted via a laparoscope placed periumbilically, and the gallbladder is freed and removed from the liver bed by using small subcostal ports for access and dissection. Intraoperative cholangiography is routinely performed, but uncertainty exists about how best to manage choledocholithiasis. Compared with traditional cholecystectomy, initial reports describing laparoscopic cholecystectomy cite shorter recovery times because no large incisions are made, thus potentially reducing the cost and morbidity of cholecystectomy. A survey of 614 early cases supports these claims, with a reported complication rate of 1.5% and quick resumption of normal activities by patients. Because of its promise for reduced morbidity, laparoscopic cholecystectomy is challenging open cholecystectomy as the therapeutic gold standard for symptomatic cholelithiasis.

Thus, the standard to which the nonsurgical gallstone therapies, such as lithotripsy and contact dissolution, will be compared may shift to laparoscopic cholecystectomy. As the laparoscopic complications are similar to those of traditional cholecystectomy, such as abscesses and bile leaks, their percutaneous treatment should not change.

Continuing advances in nonsurgical methods of treating gallstones have expanded the options available for treating patients with symptomatic cholelithiasis. Oral bile acid therapy, biliary lithotripsy, contact gallstone dissolution, and fragmentation by a variety of devices all have varying degrees of success. However, many of the methods are still in their infancy; few studies have been completed that clearly define their roles. At present, traditional cholecystectomy remains the gold standard, both because it virtually eliminates gallstone recurrence and because of its documented safety. Surgeons, borrowing from the extensive gynecologic experience with the laparoscope, have recently developed a laparoscopic method of removing the gallbladder that incorporates many of the advantages of percutaneous techniques into the traditional surgical approach. In this report, we describe the technical evolution and current status of laparoscopic cholecystectomy and discuss its possible implications on both imaging and the nonsurgical methods of gallstone therapy.

Historical Perspective

Laparoscopic cholecystectomy was first performed in 1987 in Lyon, France, by Mouret. In 1988, Dubois et al. [1] reported using this technique on 36 patients. In 1989, Saye and McKernan successfully completed the first laparoscopic cho-

---

Received January 4, 1991; accepted after revision February 15, 1991.

[1] Department of Radiological Sciences, University of California Irvine, 101 City Drive, Rte. 140, Orange, CA 92668. Address reprint requests to J. C. Brandon.
[2] Department of Surgery, University of California Irvine, 101 City Drive, Orange, CA 92668.
[3] Department of Radiology, University of Arkansas Medical Sciences, 4301 W. Markham, Little Rock, AR 72205-7199.
[4] Department of Radiology, Massachusetts General Hospital, Boston, MA 02114.
[5] Department of Surgery, Massachusetts General Hospital, Boston, MA 02114.
[6] Department of Surgery, University of Arkansas Medical Sciences, 4301 W. Markham, Little Rock, AR 72205.

AJR 157:235-239, August 1991 0361-803X/91/1572-0235 © American Roentgen Ray Society

lecystectomy in the United States, and, in the same year, Reddick et al. [2, 3] described their initial series of 25 patients in whom laser laparoscopic techniques were used to remove the gallbladder. These and subsequent series, including one report of more than 300 cases, support the initial reports of decreased morbidity and reduced time of hospitalization with laparoscopic as opposed to traditional cholecystectomy [2, 4–7].

Selection and Preparation of Patients

When laparoscopic cholecystectomy was first performed, only patients who were good surgical risks, with nonacute disease and no prior abdominal surgeries, were selected for the procedure [1, 2, 8]. However, as experience was gained, the pool of patients expanded to encompass those who were otherwise candidates for conventional cholecystectomy, and some surgeons included patients who had acute disease [7, 9]. Current absolute contraindications are peritonitis, which could be aggravated by the laparoscopic technique, and pregnancy, because of reduced intraperitoneal space and possible untoward fetal effects due to the maternal hypercapnia caused by CO_2 insufflation of the abdomen [1, 2, 7, 8]. Relative contraindications are extensive adhesions from prior upper abdominal surgery, which hinder insufflation of the peritoneal cavity, and extreme obesity, because the instruments used may not be long enough to reach the gallbladder bed [3, 4]. Choledocholithiasis also has been considered a relative contraindication to the procedure because of the difficulty of laparoscopically removing stones in the common bile duct [3, 5]. However, newly developed instruments are useful for exploration of and stone retrieval from the common bile duct. Preoperative ERCP is not routinely performed but can be used to remove stones in the common bile duct before laparoscopic cholecystectomy.

Operative Technique

While under general endotracheal anesthesia, the patient's abdominal cavity is insufflated to a pressure of 12–14 mm Hg (1.6–1.9 kPa) with 3-4 l of CO_2 through a 1-cm periumbilical incision. A laparoscope connected to a video monitor is then introduced through this incision to assist in accurate placement of three additional 5-mm to 10-mm subcostal cannulas evenly spaced from the midline to the right anterior axillary line. With the help of an assistant, subsequent manipulations are performed entirely through these four ports, with videoscopic guidance provided by the laparoscope. Blunt dissection is used to isolate the cystic duct and cystic artery. The cystic artery is double clipped and divided. Many surgeons then routinely perform cholangiography by clipping the cystic duct proximal to its junction with the common bile duct and inserting a small catheter into the cystic duct through a small distal incision. When the anatomy is clearly defined after cholangiography, the cystic duct is then double clipped and ligated, and the gallbladder is dissected free from the liver bed by using either electrocautery or a laser for cutting and hemostasis. Should the gallbladder be inadvertently perforated, the area is closed with either a clip or suture, and any spilled contents are irrigated and suctioned and/or retrieved through one of the ports.

Once the gallbladder is dissected free from the liver, the laparoscope is usually switched to another port, and the gallbladder is pulled through the umbilical site, neck first, with a forceps. Stones too large to squeeze through this site are crushed and retrieved through the gallbladder neck as it is being pulled out of the abdomen. Occasionally, it is necessary to widen the incision to facilitate delivery of the gallbladder. Drains can be placed through the subcostal ports, but are infrequently used. The CO_2 is subsequently expelled through the ports by opening the cannulas, and the skin incisions are then closed with subcuticular absorbable sutures and sterile adhesive tape. Only in the umbilical site is an absorbable fascial suture placed to prevent subsequent herniation.

Postoperative Care

Nasogastric tubes and Foley catheters are used if a lengthy procedure is anticipated, but their routine use may not be necessary. Clear liquid feedings are begun the afternoon or evening after the procedure. Postoperatively, mild nausea, pain in the right shoulder, and abdominal cramping are not unusual, but typically subside quickly. Initially, patients were hospitalized overnight for observation, but many are now being discharged on the same day as the procedure was done [2, 6]. Most patients who remain hospitalized do so because of persistent abdominal or shoulder pain that is usually well controlled with mildly narcotic analgesic agents.

Results

No randomized, prospective study comparing the morbidity and mortality rates of laparoscopic vs open cholecystectomy has been reported. However, the Society of American Gastrointestinal Endoscopic Surgeons is coordinating a prospective, international, multicenter data collection effort enlisting the results of at least 2000 consecutive patients (Saltzman B, personal communication). Until these results are released, the efficacy of laparoscopic cholecystectomy can only be inferred from retrospective studies currently in print or in press. Nevertheless, laparoscopic cholecystectomy has been successful in almost all reports. In five large series (Table 1), 4% of patients had open cholecystectomy after laparoscopic attempts; two thirds of these conversions were done because hemorrhage or an extensively inflamed or gangrenous gallbladder was encountered. Most of these conversions occurred early in the surgeons' experience. Only nine complications (1.5%) occurred in 614 patients; these included pain requiring readmission, umbilical cellulitis, or perihepatic fluid collections (managed nonsurgically), and one death (a postoperative myocardial infarction in an 80-year-old man). This

TABLE 1: Rates of Conversion from Laparoscopic to Open Cholecystectomy

Reported Series	No. of Patients	No. of conversions (%)
Daly[a]	250	12 (5)
Corbitt [6]	200	6 (3)
Dubois et al. [1]	39	4 (10)
Velez et al. [5]	100	4 (4)
Reddick and Olsen [7][b]	25	0 (0)
Total	614	26 (4)

Note.—Laparoscopic cholecystectomy converted to an open cholecystectomy for control of hemorrhage, or on encountering impacted calculi in common bile duct, dense adhesions, or acutely inflamed, gangrenous gallbladders.

[a] Daly CJ, poster presented at the American College of Surgeons 76th Clinical Congress, October 1990.

[b] Conversion data not published on subsequent patients in that study.

complication rate is biased by the criteria used to select patients, because four of the five investigators initially enrolled patients without acute cholecystitis who were good surgical candidates without prior abdominal surgery or evidence of choledocholithiasis. With experience, these groups have expanded selection of patients to include virtually all patients who were otherwise candidates for the open procedure.

Reddick et al., in a prospective nonrandomized study on 25 nonacute patients without prior upper abdominal surgery, compared laparoscopic cholecystectomy with the muscle-sparing "mini-cholecystectomy." He found a reduction in both the postoperative hospital stay (1.96 days vs 2.80 days) and ability to return to work (6.5 days vs 34 days) for those undergoing laparoscopic cholecystectomy [3]. Although no mention was made of cost, fewer hospitalization days and a more rapid return to work should have a beneficial economic impact.

Reddick and Olsen [7], in their first 125 patients, also showed that a learning curve exists for surgeons performing laparoscopic cholecystectomy. The first 25 patients required 2 days of hospitalization and returned to work in 7 days, on average, whereas patients 100–125 had significantly reduced times of hospitalization and recuperation (1 day and 4 days, respectively). In a separate study, Zucker et al. (presented at the annual meeting of the Society for Surgery of the Alimentary Tract, May 1989) described a higher prevalence of bile duct injuries during the surgeons' learning phase. These results parallel ours and those reported in other large series (Daly CJ, poster presented at the American College of Surgeons 76th Clinical Congress, October 1990).

The most recent retrospective report, describing more than five decades of experience with open cholecystectomy performed at one institution on over 10,000 patients, cites an overall mortality rate of 0.6% [10]. The mortality rate rose to 1.2% for patients with acute disease and to 4.5% for patients more than 65 years old. Other large series cite a major morbidity rate of about 5%, most commonly caused by cardiovascular or pulmonary disease, and less often by sepsis or surgically related incidents in the wound or subhepatic regions [11–14]. Higher risks prevail in the elderly. Although the figures vary, depending on the source, this type of data will serve as the standard with which laparoscopic cholecystectomy can be compared.

Because laparoscopic cholecystectomy is a minimally invasive procedure performed percutaneously, it has many of the advantages familiar to radiologists experienced in biliary intervention. The absence of any significant muscle-splitting incision, the reduced hospitalization time, and the early resumption of nearly normal activity have both cosmetic and economic appeal when compared with open cholecystectomy. Laparoscopic patients typically resume normal work activities within 1 week of surgery rather than the 5–6 weeks or more necessary for mini-cholecystectomy or traditional cholecystectomy [7, 15].

A certain degree of morbidity is associated with laparoscopy itself. Every 3 years, the American Association of Gynecological Laparoscopists surveys its members to report their experience with diagnostic and operative laparoscopy [16, 17]. Despite the deficiencies of this type of survey, its results provide useful insights into this procedure. In the 3 years before August 15, 1989, 41,160 diagnostic laparoscopies were reported, of which 94% were performed with the patient under general anesthesia. Complications requiring conversion to laparotomy occurred in 0.31%, with two deaths [16]. In 36,928 operative laparoscopies for the management of endometrial implants, ovarian cysts, or adhesions; for uterosacral nerve ablation; for myomectomy; or for the treatment of ectopic pregnancy, hydrosalpinx, or pelvic abscess; complications developed in 1.25% of cases (excluding persistent elevations of beta human chorionic gonadotropin levels for those with ectopic pregnancies) [17]. More than half of these were extended hospitalizations or readmissions, with a 0.42% rate of conversion to laparotomy for hemorrhage or injuries to the bowel or urinary system, which often occur when the abdominal cavity is initially pierced. Two deaths were reported. Comparable outcomes have been reported by other clinicians performing invasive laparoscopy [18–22]. The preliminary laparoscopic cholecystectomy results show a higher rate of conversion to laparotomy than is seen in the gynecological literature, but most of those procedures that were converted were done early in the surgeons' series and probably would not have had to be converted if the surgeon had been more experienced. The 1.5% complication rate described here parallels the rate in the gynecological reports, but may rise as more elderly patients, patients with acute disease or patients with disease of the common bile duct, are treated.

Training

Currently, no specific credentialing criteria are required for physicians performing laparoscopic cholecystectomy. In general, it is considered an extension of currently available techniques. However, laparoscopy and laser surgical techniques are infrequently taught in most general surgical training programs in the United States. In order to fill this void, courses were created offering 1 day of classroom instruction and 1 or 2 days of hands-on experience with live pigs. Ideally, graduate surgeons are then proctored by an experienced laparoscopist for subsequent cases, the number being set according to local hospital standards. If lasers are used, surgeons must conform to rules established by the laser committee of the participating institution because of the additional expertise required to operate these instruments safely. Guidelines for physicians performing laparoscopic cholecystectomy have been outlined in the following statement by the American College of Surgeons [23]:

> For optimal quality patient care, laparoscopic cholecystectomy should be performed by surgeons who are qualified to perform open cholecystectomy. Only such surgeons possess the skills to perform biliary tract surgical procedures; such surgeons are able to determine the best method of cholecystectomy; and only such surgeons can treat complications consequent to laparoscopic cholecystectomy.

Choledocholithiasis

Uncertainty exists about how to treat patients who have stones in the common bile duct. Preoperative endoscopic sphincterotomy with stone extraction is recommended by some surgeons. Other treatment options that have been proposed are laparoscopic or open exploration of the common bile duct, postoperative endoscopic or percutaneous management with contact dissolution, basket extraction, extracorporeal lithotripsy, or placement of a T tube or similar drainage catheter with subsequent percutaneous management. Several flexible ureteroscopes and choledochoscopes and balloon catheters are currently available or under development to assist the surgeon who encounters stones in the common bile duct. Selecting a strategy will depend heavily on the expertise available locally.

Impact on Nonsurgical Techniques and Imaging

The recent development of several nonsurgical approaches for the treatment of cholelithiasis has made it increasingly difficult to choose the most appropriate method for each patient. Concern for diminished morbidity is compounded by growing interest in outcome analysis in terms of cost and relief of symptoms. Moreover, informed consent requires that patients have knowledge of all current therapeutic options and their relative success rates and morbidity, thus influencing the decision-making process. To propose a strategy encompassing these factors is beyond the scope of this paper and would be premature because most of these questions remain unanswered. However, if laparoscopic cholecystectomy largely replaces open cholecystectomy, it seems reasonable that the standard with which the nonsurgical techniques will be compared will merely shift to laparoscopic cholecystectomy.

One way to assess the merits of all the methods of managing gallstone disease is to evaluate their comparative effectiveness. The newest oral bile acid, ursodeoxycholic acid, is successful in dissolving about 40% of radiolucent gallstones less than 2 cm in diameter in 1 year, on average, with better results for floating stones [24–26]. For extracorporeal lithotripsy, success varies from about 35% after 6 months in the largest American experience for patients with a single radiolucent stone less than 2 mm in diameter who are concomitantly undergoing oral ursodeoxycholic bile acid therapy, to about 70% for similar stones as reported by Sauerbruch et al. [27], who used a different lithotriptor and combined chenodeoxycholic and ursodeoxycholic oral bile acid therapy [27–29]. However, only 10–15% of patients with symptomatic gallstones have such a stone burden. Percutaneous catheterization and methyl *tert*-butyl ether (MTBE) instillation dissolves any number of cholesterol stones and large fragments in 95% of cases, with complete clearing of all debris in 48% in 6–35 months [30]. Percutaneous cholecystolithotomy can remove all stones of any type and number in 90% of patients [31]. But any kind of catheterization requires initial hospitalization, and all nonsurgical methods must address the problem of stone recurrence, because the gallbladder remains in place.

The future of radiologic management of gallstones depends on improvement of the efficacy of gallstone clearance, such as that provided by lithotripsy, coupled with a reproducible and safe technique of cystic duct occlusion and gallbladder ablation. The studies by Becker et al. [32] on gallbladder ablation may give some direction for the future of techniques that eliminate gallstones, but prolonged catheterization is still required. Only by perfecting a method to ablate the gallbladder in a single session without subsequent catheterization would percutaneous gallbladder procedures approach the low hospitalization and convalescent times of laparoscopic cholecystectomy.

As with open cholecystectomy, patients having laparoscopic cholecystectomy will show free air during intraoperative cholangiography and on postoperative films. Its persistence, however, may herald intestinal injury. Anecdotal reports have surfaced that describe burns to abdominal viscera from either electrical arcing caused by improper grounding of the patient to electrocautery devices or by misguided laser pulses. Some of the surgical cholangiographic catheters being developed have anchoring balloons, which can mimic ductal stones when inflated. Because the gallbladder is dissected in much the same manner during laparoscopic cholecystectomy as it is when the open approach is used, percutaneous intervention for subsequent complications such as abscess or bile leakage should not change.

Conclusions

Laparoscopic cholecystectomy is an operative technique that removes the gallbladder without a muscle-splitting incision and requires minimal hospitalization and convalescence. Oral bile acid therapy, extracorporeal lithotripsy, and contact dissolution with MTBE and/or percutaneous basket extraction all suffer from the problem of stone recurrence but can be performed without general anesthesia. Unlike open cholecystectomy, the preliminary data suggest that morbidity and mortality rates are lower in patients undergoing laparoscopic cholecystectomy and that this procedure may replace traditional cholecystectomy as the gold standard with which the other gallstone therapies are compared.

REFERENCES

1. Dubois F, Icard P, Berthelot G, Levard H. Coelioscopic cholecystectomy: preliminary report of 36 cases. *Ann Surg* **1990**;211:60–62
2. Reddick EJ, Olsen DO, Daniel TF, et al. Laparoscopic laser cholecystectomy. *Laser Med Surg News* **1989**;7:38–40
3. Reddick EJ, Olsen DO. Laparoscopic laser cholecystectomy. *Surg Endosc* **1989**;3:131–133
4. Velez MA, Roys G, Ryan JJ. Laparoscopic cholecystectomy. *Contemp Surg* **1991**;38:21–25
5. Velez MA, Klein SR. Laparoscopic biliary surgery. In: White RA, Klein SR, eds. *Endoscopic general and vascular surgery*. St. Louis: Mosby-Year Book Medical, **1991**:97–116
6. Corbitt JD. Laparoscopic cholecystectomy: laser vs. electrocautery. *Endosc Surg* (in press)
7. Reddick EJ, Olsen DO. Reddick laparoscopic cholecystectomy. KTP/532 Clinical Update, No. 31. San Jose, CA: Laserscope, **1990**
8. Rubio PA, Rowe G, Freste JR. Endoscopic laser cholecystectomy. *Houston Med* **1989**;5:124–126
9. Cooperman AM. Laparoscopic cholecystectomy for severe acute, embedded, and gangrenous cholecystitis. *J Laparoendosc Surg* **1990**;1:37–40
10. McSherry CK. Cholecystectomy: the gold standard. *Am J Surg* **1989**;158:174–178
11. Glenn F, McSherry CK, Dineen P. Morbidity of surgical treatment for nonmalignant biliary tract disease. *Surg Gynecol Obstet* **1968**;126:15–26
12. Gallbladder Survey Committee, Ohio Chapter American College of Surgeons. 28,621 cholecystectomies in Ohio. *Am J Surg* **1970**;119:714–717
13. Pickleman J, Gonzalez RP. The improving results of cholecystectomy. *Arch Surg* **1986**;121:930–934
14. Meyer KA, Capos NJ, Mittlepunkt AI. Personal experiences with 1,261 cases of acute and chronic cholecystitis and cholelithiasis. *Surgery* **1967**;61:661–668
15. Rothschild JG, Holbrook RF, Reinhold RB. Gallstone lithotripsy vs cholecystectomy: preliminary cost-benefit analysis. *Arch Surg* **1990**;125:710–714
16. Hulka JF, Peterson HB, Phillips JM. American Association of Gynecologic Laparoscopists' 1988 membership survey on laparoscopic sterilization. *J Reprod Med* **1990**;35:584–586
17. Peterson HB, Hulka JF, Phillips JM. American Association of Gynecologic Laparoscopists' 1988 membership survey on operative laparoscopy. *J Reprod Med* **1990**;35:587–589
18. Huggins GR, Sandheimer SJ. Complications of female sterilization: immediate and delayed. *Fertil Steril* **1984**;14:337–353
19. DeStefano F, Greenspan JR, Dicker RC, Peterson HB, Strauss LT, Rubin GL. Complications of interval laparoscopic tubal sterilization. *Obstet Gynecol* **1983**;61:153–158
20. Gunnanan RG, Courey NG, Lippes J. Complication of laparoscopic tubal sterilization. *Obstet Gynecol* **1980**;55:501–506
21. Thompson BH, Wheelers CR. Gastrointestinal complications of laparoscopy sterilization. *Obstet Gynecol* **1973**;41:669–676
22. Baggish MS, Lee WK, Miro SJ, Dacko L, Cohen G. Complications of laparoscopic sterilization. *Obstet Gynecol* **1979**;54:54–59
23. Tompkins RK. Laparoscopic cholecystectomy: threat or opportunity? *Arch Surg* **1990**;125:1245
24. Roda E, Taroni F, Festi D. Gallstone disease: a clinical lesson from epidemiology. *J Litho Stone Dis* **1990**;2:279–288
25. Roda E, Bazzoli F, Morselli Labate AM, et al. Ursodeoxycholic acid vs chenodeoxycholic acid as cholesterol gallstone dissolving agents: a comparative randomized study. *Hepatology* **1982**;2:804–810
26. Fromm H, Roat JW, Gonzales V. Comparative efficacy and side effects of ursodeoxycholic acid in dissolving gallstones: a double-blind controlled study. *Gastroenterology* **1983**;85:1257–1264
27. Sauerbruch T. Gallstone lithotripsy by extracorporeal shock waves. *Am J Surg* **1989**;158:188–191
28. Schoenfield LJ, Berci G, Carnovale RL, et al. The effect of ursodiol on the efficacy and safety of extracorporeal shock-wave lithotripsy of gallstones. *N Engl J Med* **1990**;323:1239–1273
29. Sackmann M, Delius M, Sauerbruch T, et al. Shockwave lithotripsy of gallbladder stones: the first 175 patients. *N Engl J Med* **1988**;318:393–397
30. Thistle JL, May GR, Bender CE, et al. Dissolution of cholesterol gallstones using methyl tert-butyl ether administered by percutaneous transhepatic catheter. *N Engl J Med* **1989**;320:633–639
31. Cope C, Burke DR, Meranze SG. Percutaneous extraction of gallstones in 20 patients. *Radiology* **1990**;176:19–24
32. Becker CD, Fache JS, Malone DE, Stoller JL, Burhenne HJ. Ablation of the cystic duct and gallbladder: clinical observations. *Radiology* **1990**;176:687–690

The reader's attention is directed to the commentary on this article, which appears on the following pages.

Come to the
American Roentgen Ray Society
92nd
ANNUAL MEETING

Orlando, FL

Marriott's Orlando World Center
May 10–15, 1992

Scientific Program (200 papers)
Instructional Courses (60 hours)
Categorical Course on Neuroradiology
The Caldwell Lecture
Award Papers
Scientific Exhibits
Social, Golf, and Tennis Programs
Guest Programs

Commentary

A Surgeon's Perspective on Laparoscopic Cholecystectomy

David W. Easter[1]

The "laparoscopic cholecystectomy revolution" continues to gain momentum. The pace of its nearly complete acceptance by the medical and lay publics alike has been truly astounding. It is only natural that after the initial flood of enthusiasm crests, one attempts to view this new modification of an old operation in its proper perspective. This is the motivation and objective of the preceding article by Brandon et al. [1].

The authors have certainly chosen a timely subject, and they have done well to give us their views with the scant data available. Their first objective, to describe the history and evolution of laparoscopic cholecystectomy, warrants some expansion and clarifications.

French surgeons were the first to perform successful laparoscopic removal of the gallbladder, as stated by Brandon et al. This method evolved from the truly pioneering work of Kurt Semm and his group in obstetrics and gynecology. The application of these methods of exposure, retraction, dissection, ligature, and resection of pelvic tissues to biliary disease was a natural, if delayed, sharing of technologies between specialists. Furthermore, the diagnostic value of laparoscopic assessment of biliary disease antedated therapeutic biliary laparoscopy by at least 60 years [2]. Few surgeons recognized this valuable tool before the wildfire of laparoscopic cholecystectomy. But, as early as 1988, surgeons were practicing methods of laparoscopic gallbladder cannulation, extraction of stones, and mucosal ablation techniques [3]—clear forerunners of the current methods.

The data available to date are certainly favorable to this new procedure when compared with the gold standard of open cholecystectomy. However, one must remember that the experiences reported to date are not only those of enthusiasts in the field of "minimal access surgery," but those of very skilled surgeons who have, through natural selection if you will, been in the vanguard of this dramatic revolution. It can be expected that when undertaken by the leagues of enthusiastic but less-experienced general surgeons, inferior results will occur. This projection will await the reports of prospective trials, such as those being conducted by the Society of American Gastrointestinal Endoscopic Surgeons (Los Angeles, CA), and possibly randomized prospective studies. But, unbiased randomization of patients into treatment groups with such different outcomes (at least in terms of postoperative comfort and recovery) may not be possible.

With most surgical procedures, there are often as many variations as there are surgeons. Many surgeons would differ with some of the techniques reported by Brandon et al. A few of my preferences follow.

Operative cholangiography should be *routine* for both open and laparoscopic cholecystectomy. There are many reasons for this view, including the possibility of finding incidental stones in the common bile duct. The most important reason, however, is to identify the structures to be ligated and divided before irreparable damage is caused. Cholangiography is a critical adjunct to visual inspection, especially for the beginner in laparoscopic techniques, in which perspectives are dra-

---

This article is a commentary on the preceding article by Brandon et al.

[1] Department of Surgery, Division of Surgical Oncology, University of California, San Diego, Medical Center (H-891B), 225 Dickinson St., San Diego, CA 92103-9981. Address reprint requests to D. W. Easter.

AJR 157:241-242, August 1991 0361-803X/91/1572-0241 © American Roentgen Ray Society

matically altered. Furthermore, cholangiography gives the best chance of recognizing injuries when they occur. Early recognition of such complications is crucial to their successful management.

Routine laparoscopic cholangiography also is critical if surgeons are to become sufficiently skilled to perform cholangiography when required by the clinical situation. Furthermore, these skills are the natural first step toward laparoscopic exploration of the common bile duct—a procedure already being practiced by some experienced surgeons.

There are many options for dealing with stones in the common bile duct. My preference for known or suspected choledocholithiasis (such as the unusual case detected by sonography), is to clear the stones endoscopically on the day before planned laparoscopic cholecystectomy. The patient who recovers quickly (as expected) from an episode of gallstone pancreatitis does not require preoperative endoscopic cholangiography.

If tiny stones are found during operative cholangiography, an attempt is made to wash the "gravel" through the sphincter of Oddi with saline irrigation through the cystic duct catheter. A second set of films will often show clearance of the common bile duct. If the common bile duct is of normal caliber and residual stones are trivial in size, I recommend completing the cholecystectomy and endoscopically clearing the duct in the first few days after surgery. Finally, if stones are substantial in number or size, or if the bile duct is enlarged, "open" exploration of the common bile duct is warranted. As we gain further experience with laparoscopic methods, options for dealing with this particular problem will certainly increase.

The use of laser energy for dissection and hemostasis by the inexperienced laparoscopic surgeon adds unnecessary hazards. We have recently had 10 referrals to our hospital for surgical reconstruction of laparoscopic injuries to the common bile duct and hepatic ducts. Nine of these injuries were clearly associated with laser dissection. The tenth was questionably so. We think that laser dissection should be evaluated on its own merit separately from laparoscopic techniques, and moreover should not be performed by surgeons inexperienced in laparoscopy [4] (Moossa AR, Easter DW, unpublished data). This caution should lower the chance of bile duct injury during the learning curve with this new technique.

The beginning laparoscopist should be proctored by one who already has training and significant experience with both laparoscopy and open cholecystectomy. Experience has no equal when a difficult or unexpected situation is encountered in the operating room.

Finally, special emphasis should be placed on informed consent. Every patient must understand the very real possibility of conversion to an open procedure. Conversion to open cholecystectomy should not be viewed as a failure of the laparoscopic methods, but rather as an intraoperative decision meant to minimize risk to the patient.

In the past 10 years, the medical community has witnessed significant advances in the alternatives for dealing with biliary calculi. With experience, we will learn which options are best for which patients. I eagerly await the objective comparison of laparoscopic cholecystectomy with conventional cholecystectomy and the alternative treatment methods available.

REFERENCES

1. Brandon JC, Velez MA, Teplick SK, et al. Laparoscopic cholecystectomy: evolution, early results, and impact on nonsurgical gallstone therapies. *AJR* **1991**;157:235–239
2. Kalk, H. Erfahrungen mit der laparoscopie (Zugleich mit Beschreibung eines neuen Instrumentes.) *Z Klin Med* **1929**;111:303–348
3. Cuschieri A, Abd el Ghany AA, Holley MP. Successful chemical cholecystectomy: a laparoscopic guided technique. *Gut* **1989**;30:1786–1794
4. Easter DW, Moossa AR. Laser and laparoscopic cholecystectomy—a hazardous union? *Arch Surg* **1991**;126:423

Review Article

Characterization of Tumor Hypoxia by ^{31}P MR Spectroscopy

R. Grant Steen[1]

Tumor hypoxia is of considerable importance to the oncologist in selecting and optimizing cancer therapy, because hypoxia can determine the effectiveness of various therapies. The relationship between tumor hypoxia and tumor bioenergetics, assessed by ^{31}P MR spectroscopy, is examined to determine whether ^{31}P MR spectroscopy can be clinically useful to measure or characterize tumor hypoxia.

Work with experimental tumors has suggested that several different types of hypoxia may exist and that ^{31}P MR spectroscopy cannot be used to characterize all types. Metabolic hypoxia is the level of hypoxia that results in mitochondrial impairment in cells, and it is associated with declining cellular bioenergetic status, which can be measured by enzymatic assay of adenosine triphosphate (ATP). Because ^{31}P MR spectroscopy is sensitive to levels of ATP, it is potentially sensitive to metabolic hypoxia in vivo and may provide a rapid and noninvasive technique for characterizing metabolic hypoxia in tumors. Radiobiologic hypoxia is the level of hypoxia that results in attenuated cell death due to radiation, because radiotoxicity is directly related to tissue levels of oxygen. Radiobiologic hypoxia of tumors thus has more impact on choice of therapy, yet the relationship between metabolic hypoxia and radiobiologic hypoxia remains to be elucidated.

An analysis of published data suggests that ^{31}P MR spectroscopy is directly sensitive to metabolic hypoxia in tumors, but it is only indirectly sensitive to radiobiologic hypoxia in tumors. Therefore, ^{31}P MR spectroscopy may be unable to quantify the cell fraction of a tumor that has radiobiologic hypoxia. However, preliminary data suggest that MR spectroscopy may prove useful for determining the effectiveness of therapeutic interventions designed to manipulate radiobiologic hypoxia in tumors or for monitoring the kinetics of tumor reoxygenation after treatment.

Knowledge of the extent of hypoxia within a tumor could be of substantial clinical importance to the oncologist in selecting and optimizing cancer therapy. Hypoxic cells within a tumor are more resistant to radiotherapy because radiotoxicity is directly related to levels of oxygen in tissue [1]. Hypoxic cells are also more likely to be resistant to many forms of chemotherapy because most drugs have poor access to hypoxic cells [2]. Recent evidence further suggests that tumor hypoxia can modulate synthesis of certain oxygen-regulated proteins [3], depress the activity of mitochondrial enzymes involved in energy production [4], enhance the frequency of methotrexate resistance by inducing gene amplification [5], and enhance metastatic potential of murine tumor cells [6]. A rapid and accurate method of assessing tumor hypoxia could permit a more rational choice of therapy and may allow monitoring or prediction of tumor response to treatment.

MR spectroscopy can provide in vivo information about a number of biologically important isotopes, such as hydrogen-1, carbon-13, sodium-23, nitrogen-15, and phosphorus-31 [7]. ^{31}P is a 100% naturally abundant isotope present in measurable concentration in only a few metabolites, but these

---

Received February 11, 1991; accepted after revision March 25, 1991.

This work was supported in part by a Biomedical Research Support Grant (RR-05432) and an American Cancer Society Institutional Grant (IN-26-31).

[1] Departments of Radiology (RC-05) and Bioengineering, University of Washington School of Medicine, Seattle, WA 98195. Address reprint requests to R.G. Steen.

AJR 157:243-248, August 1991 0361-803X/91/1572-0243 © American Roentgen Ray Society

metabolites are the critical bioenergetic intermediates in all living tissues. Tumor response to therapy has been monitored by ^{31}P MR spectroscopy and, in a range of experimental and human tumors in vivo, tumor response to therapy shows one of two qualitatively different patterns [7]. Some treatments, notably hyperthermia and photodynamic therapy, produce a tumor with little or no high-energy phosphate and a large amount of inorganic phosphate. This has been hypothesized to result from severe tumor ischemia. Conversely, response to chemotherapy or irradiation often appears to involve the reversal of trends seen in untreated tumor progression, leading to apparent increases in levels of high-energy phosphates. The mechanism behind tumor activation is unknown, but the activation may result from reversal of the ischemic conditions that often prevail within a tumor [7].

In the sections to follow, we review the relationship between tumor bioenergetics, assessed by ^{31}P MR spectroscopy, and tumor hypoxia. This review will necessarily emphasize experimental animal tumors for several reasons, the most important of which is that no correlations have been made between MR spectra and the extent of tumor hypoxia in humans. However, a number of other reasons exist for emphasizing experimental tumor research: heterogeneity within experimental tumors is often less than within the larger, more invasive human tumors; protocols of treatment and examination are often inadequately described in MR spectroscopic studies of human tumors; and, although a range of types of human tumors have been studied by ^{31}P MR spectroscopy, many types have been examined only once [7]. Reference will be made to studies of tumor bioenergetics in humans whenever possible.

Oxygenation and Hypoxia in Tumors

Hypoxia can be broadly defined as oxygen-limited mitochondrial energy flux [8]. Mitochondrial oxidative phosphorylation is thought to be the major cellular source of ATP even in rapidly growing tumors [9]. Although oxygen delivery to mitochondria in tumor cells can be compromised by poor perfusion [10], oxygen consumption by tumor cells is low enough that oxygen need not become limiting to mitochondrial respiration. The oxygen consumption rate of various human malignant tissues tends to be lower than that of corresponding normal tissues and is considerably lower than that of organs such as kidney, liver, brain, heart, and working skeletal muscle [10]. The oxygen consumption rate in tumor cells may be reduced because tumor mitochondria frequently differ functionally from normal mitochondria, and because the number of mitochondria per tumor cell may be reduced as much as 80% relative to control cells [9].

We will define metabolic hypoxia as the partial pressure of oxygen (Po_2) below which mitochondrial function is impaired. This can occur in human neuroblastoma cells in vitro at oxygen tensions of about 3–6 mm Hg [11]. Radiobiologic hypoxia is the Po_2 at which relative radiosensitivity is attenuated. Although partial radioresistance begins at oxygen tensions as high as 10 mm Hg, complete radiobiologic hypoxia results at partial pressures of oxygen less than 1 mm Hg [1]. The Po_2 value at which cellular radiation sensitivity is midway between fully oxygenated and anoxic is approximately 3–4 mm Hg [12]. Because complete radiobiologic hypoxia occurs at a lower oxygen tension than metabolic hypoxia does, we anticipate that any tumor that exhibits a radiobiologic hypoxic cell fraction (HCF) will have a metabolic HCF also.

It should be noted that if radiobiologic hypoxia and metabolic hypoxia are distinct from one another, then a difference may also exist in how these types of hypoxia are affected by tumor reoxygenation. Tumor reoxygenation is generally expected to affect only the radiobiologic HCF and to result in those cells becoming more sensitive to radiation [13]. However, radiobiologically hypoxic cells that undergo reoxygenation could still be suffering metabolic hypoxia. Although this would be of little consequence to a radiobiologist interested only in hypoxic radioprotection, it is of potential importance in understanding tumor biology. Furthermore, metabolically hypoxic cells can undergo reoxygenation, to become fully oxic cells, without necessarily having an effect on radioresistance of the tumor. This suggests that metabolic reoxygenation can be an event distinct from radiobiologic reoxygenation.

Characterization of Tumor Metabolic Hypoxia by ^{31}P MR Spectroscopy

Mitochondrial impairment in cells at low oxygen tension in vitro is associated with declining cellular bioenergetic status as measured by enzymatic assay of ATP [14]. Because MR spectroscopy is sensitive to levels of ATP in vivo, it should be capable of detecting cellular metabolic hypoxia in vivo.

The hypothesis that tumor bioenergetics are sensitive to metabolic hypoxia was first suggested by tumor ligation experiments, in which tumor perfusion is prevented by clamping off the blood supply to the tumor. ^{31}P MR spectra derived from ligated tumors show characteristic decreases in high-energy phosphates such as phosphocreatine (PCr) and ATP, and increases in inorganic phosphate (P_i) [15, 16]. However, tumor ligation stops blood flow and produces ischemia rather than merely hypoxia, so the decline in high-energy phosphates in ligated tumors could result from the absence of metabolic substrates, such as glucose, or from accumulation of metabolic waste products such as lactate.

Further support for the hypothesis that tumor bioenergetics are sensitive to metabolic hypoxia has come from experiments in which tumor spectra were acquired during ventilation of the host animal with different gas mixtures [17]. A murine fibrosarcoma (FSaII) showed a relative increase in PCr and ATP after 20 min of hyperoxia (1.0 atmosphere O_2), and a depression of these metabolites after 20 min of hypoxia (0.1 atmosphere O_2). Resumption of air breathing caused a near normalization of metabolite levels [17]. A rat rhabdomyosarcoma (BA1112) showed increases in tumor Po_2 and in the spectroscopic ratio of PCr/P_i, when the host animal was ventilated with 100% O_2. These changes were further enhanced when the animal was given a transfusion of a perfluorochemical that increased the oxygen-carrying capacity of the blood [18].

In general, MR spectroscopy appears to be sensitive to the level of tumor oxygenation in vivo. Two murine tumors (RIF-1, KHT) and two human ovarian carcinoma xenografts (MLS, OW1) showed a correlation between tumor bioenergetics and vascular oxygen availability [19]. Analysis of intracapillary hemoglobin saturation in the tumor showed a positive correlation between vessel hemoglobin saturation and tissue ATP, measured enzymatically. A positive correlation also was found between the total amount of ATP measured by MR spectroscopy and tissue ATP measured enzymatically, and a negative correlation was found between total P_i and tissue ATP. Bioenergetic status of these tumors was therefore dependent on oxygen supply to the tumor tissue [19]. Correlations also were found between tumor oxygenation and MR spectral parameters in a murine fibrosarcoma (FSall), suggesting that the bioenergetic status of this tumor also is sensitive to oxygen limitation [12].

During untreated growth of most tumors, the levels of energy-rich phosphorus compounds observed by ^{31}P MR spectroscopy decline relative to other spectral resonances, while the resonance due to P_i increases [7]. These changes may be associated with an acidic shift in pH of tumor tissue [20]. Because such changes resemble those observed in normal tissues made ischemic (Fig. 1), it was proposed that growing tumors suffer increasing hypoxia as the tumor outgrows its blood supply [15]. Recent data show that mean tumor Po_2, measured by polarography, declines during growth of murine fibrosarcoma (FSall) and that tumor Po_2 is closely correlated with levels of high-energy phosphates visible on MR spectroscopy [12].

The relationships among bioenergetics, vascular oxygenation, and hypoxia during tumor growth have been elucidated by using several tumor lines [21]. In three different tumor models (KHT, RIF-1, and MLS), decreasing tumor bioenergetic status is correlated with increasing volume growth, whereas in a fourth tumor (OW1), no change occurred in PCr, ATP, or P_i with growth. Similarly, vascular oxygenation decreased with growth in volume in several tumors (KHT, RIF-1, and MLS) but was independent of tumor volume in another (OW1). Linear correlations were found between bioenergetic status and hemoglobin saturation in individual tumors, except for OW1. These observations indicate a direct relationship between MR spectral parameters and tumor oxygenation. However, this relationship was not identical for each of the different tumor lines, implying that bioenergetic status of the tumor also is affected by intrinsic properties of tumor cells, such as the rate of cellular respiration and the ability of cells to survive under hypoxic conditions [21].

As tumor bioenergetic status declines with tumor volume, tumor perfusion also declines, suggesting that ^{31}P MR spectroscopy is indirectly sensitive to tumor perfusion. In a rat gliosarcoma (9L), tumor growth is associated with a decline in the PCr and ATP resonances [22], concurrent with a decline in tumor perfusion measured by xenon-133 washout [23]. In a murine fibrosarcoma (RIF-1), an inverse correlation was found between the well-perfused fraction of the tumor, measured by ^{15}O washout, and the ratio P_i/ATP [24]. The ratio of ATP to P_i was found to be correlated directly with blood flow within a limited range; below this range the ATP resonance was undetectable, whereas above this range the ratio was variable but greater than 1.0 [25].

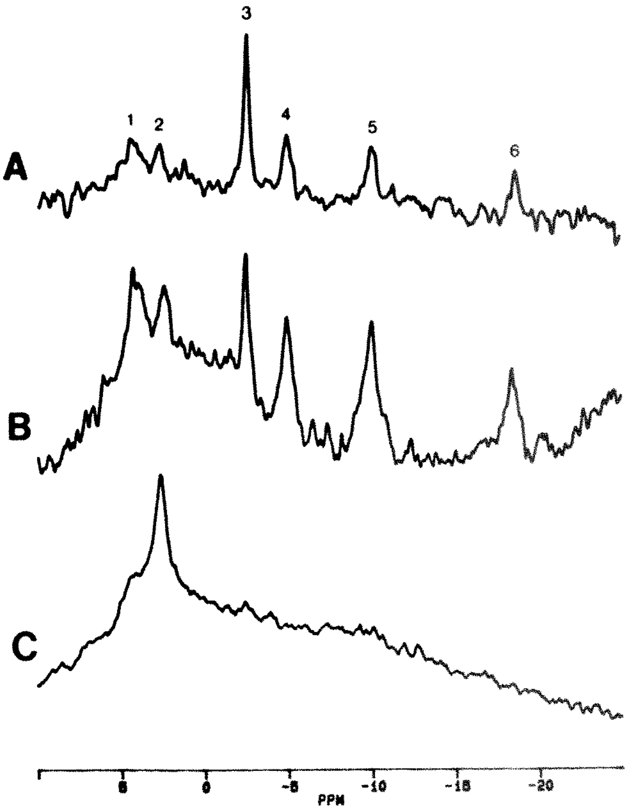

Fig. 1.—In vivo ^{31}P MR spectra obtained from brain of adult Fischer 344 rats at 8.5 T, by using a 5-mm surface coil applied directly to brain surface after craniectomy. Spectra were acquired at 145.8 MHz with a 3-sec relaxation delay and 1000 scans.

A, Normal rat brain. Resonance identifications as follows: (1) phosphomonoesters (PME), (2) inorganic phosphate (P_i), (3) phosphocreatine (PCr), (4) β-phosphate of nucleoside diphosphate (NDP) and γ-phosphate of nucleoside triphosphate (NTP), (5) α-phosphate of NDP and NTP, (6) β-phosphate of NTP. The ratio PCr/P_i is greater than or equal to 5, suggesting this spectrum was derived from aerobic tissue.

B, Intracranially implanted 9L gliosarcoma. Signal was detected exclusively from tumor, not from surrounding brain, because of small size of coil. This plot is somewhat misleading because ATP peaks look larger in *B* than in *A*. This is because, in both *A* and *B*, highest peak (PCr) was scaled to same height for the sake of clarity. Because PCr declines in a tumor, *B* was plotted with a different vertical scale than *A*, and this exaggerated vertical scale leads to an artifactual apparent increase in the ATP peaks in *B*. Ratio PCr/P_i is less than or equal to 1, suggesting hypoxic tissue. Note also that PME peak is strikingly larger in tumor tissue.

C, Ischemic rat brain. Rat shown in *A* was sacrificed with pentobarbital, and a spectrum was collected within 30 min of death. The ratio PCr/P_i is essentially equal to zero, suggesting ischemic tissue.

Manipulation of tumor perfusion with vasoactive agents such as hydralazine [25–27] or flunarizine [27] demonstrates that agents that decrease blood flow produce a decrease in high-energy phosphates measured by MR spectroscopy, whereas agents that increase blood flow produce the opposite effect. Spectra obtained from a murine fibrosarcoma (RIF-1) when the host animal was under pentobarbital anesthesia showed a decline in high-energy phosphates, compared with tumor spectra obtained under anesthesia with ketamine plus acepromazine (KA) [28]. In vivo near-infrared spectroscopy demonstrated that the total oxyhemoglobin level in the tumor was reduced by more than 20% after pentobarbital ($p < .01$), but was not significantly affected by KA [28]. In a murine fibrosarcoma (RIF-1) treated with human interleukin (IL)-1α injection, MR spectroscopy showed an increase in P_i/ATP and a decrease in PCr/P_i within a few hours of treatment [29]. Blood flow in the tumor, estimated by rubidium-86 uptake, decreased within 30 min of treatment, with minimum perfusion detected at 4 hr and recovery between 6 and 12 hr after IL-1α treatment. The time course of bioenergetic changes in RIF-1 parallels the reduction and subsequent recovery of blood flow in the tumor, suggesting that the tumor's bioenergetic status is determined by vascular perfusion [29].

Metabolic activation, a relative increase in high-energy phosphates, is observed in many tumors after therapy, but the physiological mechanism of this phenomenon is poorly understood [7] (Fig. 2). To test the hypothesis that metabolic activation is associated with a decrease in metabolic hypoxia in tumors, we measured blood flow and oxygenation in a rat gliosarcoma (9L) concurrently with analysis by MR spectroscopy [23]. Treated tumors showed a significant increase in high-energy phosphates with respect to control tumors ($p <$ .01), and both tumor oxygenation and tumor perfusion were significantly higher after carmustine (BCNU) treatment. If polarographic measurements of Po_2 in the range of 0–5 mm Hg approximate the fraction of cells experiencing metabolic hypoxia, then control tumors were roughly 23% hypoxic, whereas treated tumors were only about 2% hypoxic [23].

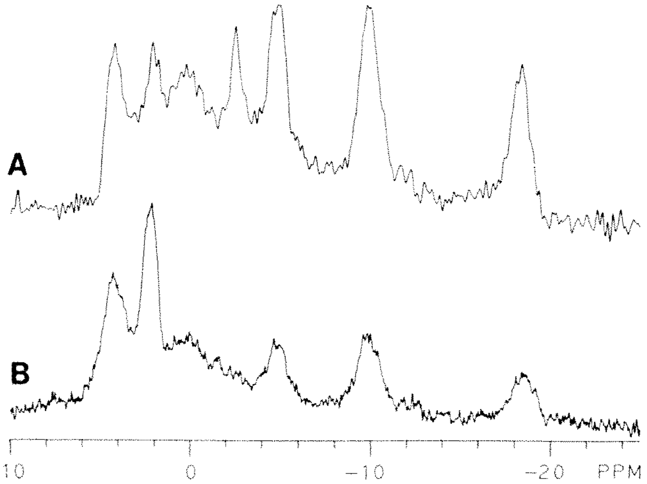

Fig. 2.—In vivo ^{31}P MR spectra from 36B-10 glial tumor subcutaneously implanted in flank of adult Fischer 344 rats. Spectra were obtained at 2 T, by using a 3.5-cm solenoidal coil and by surrounding tumor with a Faraday shield to isolate tumor from body wall. Spectra were acquired at 34.6 MHz with a 3-sec delay and 200 scans.

***A*, Tumor treated with carmustine (BCNU, 40 mg/kg). Resonance identifications as in Fig. 1. Ratio PCr/P_i is greater than or equal to 0.5.**

***B*, Age-matched untreated control tumor. Ratio PCr/P_i is essentially equal to zero.**

Metabolic activation of tumors after therapy may generally be associated with a decrease in metabolic hypoxia. Phosphorus spectra obtained from a murine fibrosarcoma (RIF-1) show an increase in high-energy phosphates and an alkaline shift in pH after tumor irradiation [30, 31]. The increase in PCr/P_i and ATP/P_i was correlated with an increase in blood perfusion in the tumor as measured by infusion of [^{14}C]iodoantipyrine [30]. It was concluded that improvement in tumor perfusion resulted in an increase in oxidative phosphorylation in the tumor, and that MR spectroscopic changes indirectly reflect changes in tumor perfusion [30]. Therefore, metabolic activation may actually be the result of reoxygenation of those tumor cells suffering metabolic hypoxia.

Perhaps the strongest evidence that ^{31}P MR spectroscopy is sensitive to tumor metabolic hypoxia has come from in vitro studies of tumor cell spheroids [32, 33]. A range of spheroid sizes was studied, up to sizes at which 40% of the spheroid volume was necrotic [33]. In well-perfused spheroids, no correlation was found between the extent of necrosis and the ratio ATP/P_i. This was because chronic hypoxia of spheroid cells resulted in cell death, loss of high-energy metabolites, and loss of cellular P_i. Thus necrotic tumor areas were not visible by MR spectroscopy because they contained neither P_i nor high-energy phosphates [33].

If spheroids were acutely deprived of oxygen, a depression of cellular high-energy phosphates resulted, and cells were visible by MR spectroscopy as low-energy cells [33]. Acutely hypoxic spheroid spectra showed elevated levels of P_i, low ATP, low or absent PCr, and an acidic pH, so that they were similar in appearance to spectra from tumors in vivo. Prolonged reduction of perfusion resulted in death of the inner region of cells and expansion of the necrotic core during a 12-hr period [33]. After those cells in the core of the spheroid died, the relative proportion of high-energy phosphates increased, so that spectra of chronically hypoxic spheroids were indistinguishable from spectra of well-perfused spheroids [33]. Depression of high-energy metabolites in tumors in vivo may thus be seen in tumors having a high proportion of low-energy but still viable cells, suggesting that ^{31}P MR spectroscopy is directly sensitive to acutely hypoxic cells in vivo. However, the relationships between acute hypoxia and metabolic or radiobiologic hypoxia are unclear.

Tumor hypoxia can result in lactate production through glycolysis, with a resulting acidification of tumor pH. As ^{31}P MR spectroscopy can measure tissue pH in vivo, this could provide another means of characterizing tumor hypoxia. Tumor pH can be estimated from the chemical shift of the P_i peak with respect to a peak such as PCr, whose chemical shift is not pH dependent. However, this estimate can suffer from a number of potential sources of error, as ionic strength, metal ion binding, and temperature all influence the chemical shift of P_i [34]. As P_i may be associated predominantly with transiently hypoxic cells [33], the estimated pH may be weighted for these cells. In general, tumor pH undergoes little change after treatment in many tumors [7, 35] and can be poorly correlated with perfusion [25], suggesting that the inherent buffering capacity of tumor cells also may be important in determining tumor pH.

Tumor pH has been estimated by MR spectroscopy in a range of human neoplasms [36]. In most tumors, pH was either normal or slightly alkaline before treatment. During fractionated radiotherapy, pH tended to become more alkaline even in unresponsive tumors, so pH was uninformative about treatment response. It was concluded that human tumors are generally well oxygenated, with only a small fraction of chronically hypoxic cells [36]. However, because pH measurement is fraught with potential sources or error, these findings must be corroborated. The conclusion that human tumors are well oxygenated conflicts with reports that, in human squamous cell carcinoma, tumor Po_2 is variable and often low and can be predictive of radioresponse [37].

A significant linear relationship has been found between pretreatment tumor pH, measured by MR spectroscopy, and posttreatment tumor necrosis in a group of patients with soft-tissue sarcomas [38]. Changes in diagnostic CT scans and MR images did not predict tumor necrosis after treatment. In fact, tumor pH was the only pretherapy predictor of ultimate tumor necrosis, although changes in PCr/P_i and ATP/P_i during therapy also predicted subsequent tumor necrosis. Alterations in phosphorus metabolites occurred without any change in tumor volume in seven of eight patients [38].

Characterization of Radiobiologic Hypoxia in Tumors by ^{31}P MR Spectroscopy

Although a relationship should exist between metabolic hypoxia and radiobiologic hypoxia, it is by no means clear how close that relationship is in tumors. However, recent evidence suggests that ^{31}P MR spectroscopy may be sensitive to tumor hypoxia even in the range of radiobiologic hypoxia. Correlations have been noted between poor tumor oxygenation (the proportion of Po_2 readings at 0–2.5 mm Hg) and tumor volume, and between the radiobiologic HCF and tumor volume [12]. As MR spectral parameters also are correlated with tumor volume, this indirectly suggests that both HCF and tumor oxygenation are correlated with MR spectral parameters [12].

Manipulation of the radiobiologic HCF of a tumor can alter MR spectral parameters. Anesthetizing mice with pentobarbital produced transient depression of high-energy phosphates in a murine fibrosarcoma (RIF-1) [28]. Tumors were significantly more radioprotected when irradiation was done with pentobarbital anesthesia than when irradiation was done with an anesthetic protocol that did not produce MR spectral changes. This indicates that changes in radiobiologic hypoxia of tumors can be accompanied by detectable differences in MR spectroscopic parameters [28]. Another study that suggests that ^{31}P MR spectroscopy may be sensitive to radiobiologic hypoxia in tumors used a rat rhabdomyosarcoma (BA1112), which normally has a radiobiologic HCF of 18% [18]. Tumor HCF decreased to 6.60% when the host animal was ventilated with carbogen or 100% O_2, and HCF underwent a further reduction to 0.34% when the host animal was given a transfusion of a perfluorocarbon, which increased the oxygen-carrying capacity of the blood. MR spectroscopic measurements showed concurrent increases in PCr/P_i and ATP/P_i, indicating that MR spectroscopy can detect changes in tumor oxygenation that have an effect on tumor radiobiologic HCF [18].

Tumor bioenergetics, characterized by MR spectroscopy, were correlated with the radiobiologic HCF in each of three tumor lines (KHT, RIF-1, MLS), but not in a fourth (OW1) [21, 39]. In these three tumor lines, the bioenergetic status of the tumor declined sharply as the hypoxic fraction increased: for a murine fibrosarcoma (RIF-1), the total quantity of high-energy phosphates was reduced more than fourfold as the radiobiologic HCF went from 0.9% to 1.7% [21]. In the one tumor line in which HCF did not vary with tumor size (OW1), bioenergetic status did not vary with tumor size either [39]. However, despite the correlation between bioenergetic status and HCF in three of four cell lines, no correlation was seen between MR spectroscopy and HCF across cell lines [39].

Further evidence suggesting that ^{31}P MR spectroscopy cannot quantitatively measure radiobiologic hypoxia across tumor lines has been obtained recently. Small murine mammary carcinomas (MCa) implanted in the hind foot dorsum of a mouse have a radiobiologic HCF of 67%, whereas small murine fibrosarcomas (FSaII) in the same location have a radiobiologic HCF of 11%, as measured by the tumor control dose (TCD_{50}) technique [40]. Despite this very large difference in HCF, MR spectral parameters showed no consistent differences between these tumors in bioenergetic status. This indicates that parameters of energy status are not accurate predictors of radiobiologic hypoxia between tumor types [40]. These results can be partially explained if chronically hypoxic regions of tumors contain neither P_i nor high-energy phosphates, because they would be invisible by MR spectroscopy [33].

Conclusion

This analysis suggests that ^{31}P MR spectroscopy is directly sensitive to metabolic hypoxia in tumors, but is only indirectly sensitive to radiobiologic hypoxia in tumors. As the relationship between metabolic and radiobiologic hypoxia is likely to remain obscure for an individual patient's tumor, ^{31}P MR spectroscopy may be of little clinical usefulness in accurately quantifying the radiobiologic HCF of a tumor. But if further work confirms that MR spectroscopy is sensitive to the relative radiobiologic HCF within a given tumor, MR spectroscopic data could become useful in assessing changes in radiobiologic HCF induced by treatment of tumors. The ability of MR spectroscopy to give a qualitative indication of changes in tumor hypoxia in vivo may enable clinicians to monitor the kinetics of tumor oxygenation after therapy in order to achieve maximal tumor radiotoxicity. This is a first step toward individualizing therapy for the cancer patient.

ACKNOWLEDGMENTS

I am grateful to J. Freyer, S. Dager, W. O'Loughlin, and two anonymous reviewers for helpful comments on the manuscript.

REFERENCES

1. Hall EJ, Cox JD. Physical and biologic basis of radiation therapy. In: Moss WT, Cox DJ, eds. *Radiation oncology: rationale, technique, results,* 6th ed. St. Louis: Mosby, **1989**:1-57
2. Teicher BA, Holden SA, Al-Achi A, Herman TS. Classification of antineoplastic treatments by their differential toxicity toward putative oxygenated and hypoxic tumor subpopulations in vivo in the FSallC murine fibrosarcoma. *Cancer Res* **1990**;50:3339-3344
3. Wilson RE, Sutherland RM. Enhanced synthesis of specific proteins, RNA, and DNA caused by hypoxia and reoxygenation. *Int J Radiat Oncol Biol Phys* **1989**;16:957-961
4. Murphy BJ, Robin ED, Tapper DP, Wong RJ, Clayton DA. Hypoxic coordinate regulation of mitochondrial enzymes in mammalian cells. *Science* **1984**;223:707-709
5. Rice GC, Hoy C, Schimke RT. Transient hypoxia enhances the frequency of dihydrofolate reductase gene amplification in Chinese hamster ovary cells. *Proc Natl Acad Sci USA* **1986**;83:5978-5982
6. Young SD, Marshall RS, Hill RP. Hypoxia induces DNA overreplication and enhances metastatic potential of murine tumor cells. *Proc Natl Acad Sci USA* **1988**;85:9533-9537
7. Steen RG. Response of solid tumors to chemotherapy monitored by in vivo ^{31}P nuclear magnetic resonance spectroscopy: a review. *Cancer Res* **1989**;49:4075-4085
8. Connett RJ, Honig CR, Gayeski TEJ, Brooks GA. Defining hypoxia: a systems view of VO_2, glycolysis, energetics, and intracellular pO_2. *J Appl Physiol* **1990**;68:833-842
9. Pedersen PL. Tumor mitochondria and the bioenergetics of cancer cells. *Prog Exp Tumor Res* **1978**;22:190-274
10. Vaupel P, Kallinowski F, Okunieff P. Blood flow, oxygen and nutrient supply, and metabolic microenvironment of human tumors: a review. *Cancer Res* **1989**;49:6449-6465
11. Robiolio M, Rumsey WL, Wilson DF. Oxygen diffusion and mitochondrial respiration in neuroblastoma cells. *Am J Physiol* **1989**;256:C1207-C1213
12. Vaupel P, Okunieff P, Kallinowski F, Neuringer LJ. Correlations between 31-P NMR spectroscopy and tissue O_2 tension measurements in a murine fibrosarcoma. *Radiat Res* **1989**;120:477-493
13. Kallman RF. Reoxygenation and repopulation in irradiated tumors. *Front Radiat Ther Oncol* **1988**;22:30-49
14. Anundi I, de Groot H. Hypoxic liver cell death: critical pO_2 and dependence of viability on glycolysis. *Am J Physiol* **1989**;257:G58-G64
15. Evanochko WT, Ng TC, Lilly MB, et al. In vivo ^{31}P NMR study of the metabolism of murine mammary 16/C adenocarcinoma and its response to chemotherapy, X-radiation, and hyperthermia. *Proc Natl Acad Sci USA* **1983**;80:334-338
16. Lilly MB, Katholi CR, Ng TC. Direct relationship between high-energy phosphate content and blood flow in thermally treated murine tumors. *J Natl Cancer Inst* **1985**;75:885-889
17. Okunieff PG, McFarland E, Rummeny E, et al. Effects of oxygen on the metabolism of murine tumors using in vivo phosphorus-31 NMR. *Am J Clin Oncol* **1987**;10:475-482
18. Sostman HD, Rockwell S, Sylvia AL, et al. Evaluation of BA1112 rhabdomyosarcoma oxygenation with microelectrodes, optical spectrophotometry, radiosensitivity, and magnetic resonance spectroscopy. *Mag Reson Med* **1991** (in press)
19. Mueller-Klieser W, Schaefer C, Walenta S, Rofstad EK, Fenton BM, Sutherland RM. Assessment of tumor energy and oxygenation status by bioluminescence, nuclear magnetic resonance spectroscopy, and cryospectrophotometry. *Cancer Res* **1990**;50:1681-1685
20. Li S-J, Wehrle JP, Rajan SS, Steen RG, Glickson JD, Hilton J. Response of radiation-induced fibrosarcoma-1 in mice to cyclophosphamide monitored by in vivo ^{31}P nuclear magnetic resonance spectroscopy. *Cancer Res* **1988**;48:4736-4742
21. Rofstad EK, DeMuth P, Fenton BM, Sutherland RM. ^{31}P nuclear magnetic resonance spectroscopy studies of tumor energy metabolism and its relationship to intracapillary oxyhemoglobin saturation status and tumor hypoxia. *Cancer Res* **1988**;48:5440-5446
22. Steen RG, Tamargo RJ, McGovern KA, et al. In vivo ^{31}P nuclear magnetic resonance spectroscopy of subcutaneous 9L gliosarcoma: effects of tumor growth and treatment with 1,3-bis(2-chloroethyl)-1-nitrosourea on tumor bioenergetics and histology. *Cancer Res* **1988**;48:676-681
23. Steen RG, Graham MM. ^{31}P magnetic resonance spectroscopy is sensitive to tumor hypoxia: perfusion and oxygenation of rat 9L gliosarcoma after treatment with BCNU. *NMR Biomed* **1991** (in press)
24. Evelhoch JL, Sapareto SA, Nussbaum GH, Ackerman JJH. Correlations between 31-P NMR spectroscopy and 15-O perfusion measurements in the RIF-1 murine tumor in vivo. *Radiat Res* **1986**;106:122-131
25. Bhujwalla ZM, Tozer GM, Field SB, Proctor E, Busza A, Williams SR. The combined measurement of blood flow and metabolism in RIF-1 tumours in vivo: a study using H_2 flow and ^{31}P NMR spectroscopy. *NMR Biomed* **1990**;3:178-183
26. Okunieff PG, Kallinowski F, Vaupel P, Neuringer LJ. Effects of hydralazine-induced vasodilation on the energy metabolism of murine tumors studied by in vivo ^{31}P-nuclear magnetic resonance spectroscopy. *J Natl Cancer Inst* **1988**;80:745-750
27. Constantinidis I, Bowser C, Wehrle JP, Glickson JD. The effects of hydralazine and flunarizine on the ^{31}P NMR spectrum of RIF-1 tumors in vivo. In: *Book of abstracts, Radiation Research Society.* Philadelphia, PA: Radiation Research Society, **1989**:100
28. Steen RG, Wilson DA, Bowser C, Rajan SS, Wehrle JP, Glickson JD. ^{31}P NMR spectroscopic and near-infrared spectrophotometric studies of effects of anesthetics on in vivo RIF-1 tumors: relationship to tumor radiosensitivity. *NMR Biomed* **1989**;2:87-92
29. Constantinidis I, Braunschweiger PG, Wehrle JP, et al. 31-P nuclear magnetic resonance studies of the effect of recombinant human Interleukin 1-alpha on the bioenergetics of RIF-1 tumors. *Cancer Res* **1989**;49: 6379-6382
30. Tozer GM, Bhujwalla ZM, Griffiths JR, Maxwell RJ. Phosphorus-31 magnetic resonance spectroscopy and blood perfusion in the RIF-1 tumor following X-irradiation. *Int J Radiat Oncol Biol Phys* **1989**;16:155-164
31. Rajan SS, Wehrle JP, Li S-J, Steen RG, Glickson JD. ^{31}P NMR spectroscopic study of bioenergetic changes in radiation-induced fibrosarcoma-1 after radiation therapy. *NMR Biomed* **1989**;2:165-171
32. Freyer JP, Fink N, Neeman M, Schor PL, Coulter JR, Sillerud LO. A system for viably maintaining a stirred suspension of multicellular spheroids during NMR spectroscopy. *NMR Biomed* **1990**;3:195-205
33. Freyer J, Schor PL, Jarrett KA, Neeman M, Sillerud LO. Cellular energetics measured by phosphorus NMR are not correlated with chronic nutrient deprivation in multicellular tumor spheroids. *Cancer Res* **1991** (in press)
34. Gadian DG. *Nuclear magnetic resonance and its applications to living systems.* New York: Oxford University Press, **1982**:29-36
35. Koutcher JA, Alfieri AA, Kornblith AB, et al. Changes in radiation sensitization induced by Fluosol-DA as measured by ^{31}P nuclear magnetic resonance spectroscopy. *Cancer Res* **1990**;50:7252-7256
36. Ng TC, Grundfest S, Vijayakumar S, et al. Therapeutic response of breast carcinoma monitored by ^{31}P MRS in situ. *Mag Reson Med* **1989**;10: 125-134
37. Gatenby RA, Kessler HB, Rosenblum JS, et al. Oxygen distribution in squamous cell carcinoma metastases and its relationship to outcome of radiation therapy. *Int J Radiat Oncol Biol Phys* **1988**;14:831-838
38. Sostman D, Dewhirst M, Charles C, et al. Prognostic evaluation and therapy monitoring in human soft tissue sarcomas with ^{31}P MRS. In: *Book of abstracts: Society of Magnetic Resonance in Medicine, 1990,* vol. 1. Berkeley, CA: Society of Magnetic Resonance in Medicine, **1990**:319
39. Rofstad EK, Fenton BM, Sutherland RM. Intracapillary HbO_2 saturations in murine tumors and human tumor xenografts measured by cryospectrophotometry: relationship to tumor volume, tumor pH, and fraction of radiobiologically hypoxic cells. *Br J Cancer* **1988**;57:494-502
40. Gerweck LE, Koutcher J, Salem J, Seneviratne T, Urano M. ^{31}P-spectroscopy and HPLC analyses of energy metabolites in two rodent tumor models with different hypoxic cell fractions. In: *Book of abstracts: Radiation Research Society.* Philadelphia, PA: Radiation Research Society, **1990**:161

Broncholithiasis: CT Features in 15 Patients

Dewey J. Conces, Jr.[1]
Robert D. Tarver
Vernon A. Vix

Broncholithiasis is a disorder characterized by peribronchial calcific nodal disease that either erodes into an adjacent bronchus or distorts the bronchi. The key radiologic finding is a calcified endobronchial or peribronchial lymph node. To determine the CT findings of broncholithiasis, we retrospectively reviewed the chest radiographs and CT scans of 15 patients with proved broncholithiasis. Ten patients had endobronchial nodes as proved by bronchoscopy, surgery, or lithoptysis. Broncholiths were identified on bronchoscopy in only five cases. Five patients had peribronchial nodes with associated bronchial distortion. Collimation of the CT scans varied; 1.0-cm-, 0.6-cm-, and 0.5-cm-thick sections were obtained. Three patients had both 1.0-cm- and 0.5-cm-thick sections. The calcified lymph node was identified on CT in all 15 patients. CT correctly localized six of 10 endobronchial nodes and four of five peribronchial nodes. Findings due to bronchial obstruction also were seen on CT; atelectasis ($n = 11$), infiltration ($n = 4$), bronchiectasis ($n = 4$), and air trapping ($n = 1$). An associated soft-tissue mass was not seen in any case. Difficulty in determining the relationship between lymph node and bronchus is due to volume averaging, which can be decreased by scanning thinner sections.

CT can suggest the diagnosis of broncholithiasis and is useful when bronchoscopy does not show a broncholith.

***AJR* 157:249-253, August 1991**

Broncholithiasis is an uncommon medical problem that often is a diagnostic challenge. Broncholithiasis traditionally is defined as a condition in which calcified material is present within the bronchus or in an adjacent communicating cavity [1]. More recently, the definition has been expanded to include those cases in which peribronchial calcific nodal disease distorts the tracheobronchial tree without erosion of the calcified lymph node into the bronchus [2].

Plain film radiography and tomography have been used to examine patients with suspected broncholithiasis [3, 4]. More recently, cases have been reported in which CT has been used [5-9]. With all radiologic studies, the goal is to identify a calcified lymph node located within or next to an involved bronchus.

The purpose of this study was to determine the CT findings in 15 patients with broncholithiasis and to assess the usefulness of CT in identifying endobronchial or peribronchial broncholiths.

Materials and Methods

We retrospectively evaluated the chest radiographs and chest CT scans of 15 patients with the diagnosis of broncholithiasis. The examinations were performed between 1982 and 1991 and include all known patients with broncholithiasis who underwent chest CT. Of the 15 patients, eight were men and seven were women. The age range was 24-76 years (mean, 48.5 years). All patients lived in a region where histoplasmosis is endemic.

The patients were divided into two groups on the basis of the location of the broncholith. The calcified lymph node was endobronchial in 10 patients [1]. The endobronchial location of the lymph node was confirmed during surgery in four patients, bronchoscopy in three patients,

Received January 25, 1991; accepted after revision March 27, 1991.

Presented at the annual meeting of the American Roentgen Ray Society, Boston, MA, May 1991.

[1] All authors: Department of Radiology, Indiana University Medical Center (X-64), 926 W. Michigan St., Indianapolis, IN 46202-5253. Address reprint requests to D. J. Conces, Jr.

0361-803X/91/1572-0249
© American Roentgen Ray Society

surgery and bronchoscopy in two patients, and by the expectoration of a calcified lymph node in one patient. In five patients, the calcified lymph node was peribronchial. In this group, a diagnosis of broncholithiasis was made if the patients had demonstrable peribronchial calcified lymph nodes on radiographs, evidence of peribronchial disease (bronchial distortion, compression, or stenosis) on bronchoscopy, and no other pulmonary disease to explain the changes [2]. Three patients had the peribronchial location of the lymph node confirmed surgically.

The most common symptom was a cough ($n = 13$). Other signs and symptoms included hemoptysis ($n = 6$), chest pain ($n = 3$), sputum production ($n = 3$), fever ($n = 2$), lithoptysis ($n = 2$), halitosis ($n = 1$), and wheezing ($n = 1$). One patient was asymptomatic. Four patients had had episodes of pneumonia. Two of these patients were examined for infiltrates that failed to clear after therapy for pneumonia.

All chest radiographs were obtained with a dedicated chest unit at a distance of 6 ft (1.83 m) and set at 140 kVp. The film-screen combination consisted of Cronex 10L film and Quanta Fast Detail screen (Du Pont, Wilmington, DE). CT was performed with several different CT scanners: Technicare 1440 or 2030 (GE Medical Systems, Milwaukee, WI), Picker 1200SX (Picker International, Highland Heights, OH), GE 9800 (GE Medical Systems, Milwaukee, WI), or Philips 310 (Philips Medical Systems North America, Shelton, CT). The scans consisted of contiguous 1.0-cm-thick sections in six patients, 0.5-cm-thick sections in four patients, 0.6-cm-thick sections in two patients, and both 1.0- and 0.5-cm-thick sections in three patients. Scanning time was 2 sec (4.6 sec with the Philips 310). Nine patients received a rapid IV infusion of either 150 ml of 60% diatrizoate meglumine or 200 ml of 43% iothalamate meglumine. Some patients received a 75-ml bolus of contrast material at the beginning of the infusion. None of the patients underwent oblique tomography.

The chest radiographs and CT scans were reviewed by two of the authors. The scans were analyzed for the presence and location of calcified lymph nodes, atelectasis, infiltrates, bronchiectasis, and soft-tissue masses. The radiologists were aware of the clinical diagnosis of broncholithiasis, but the bronchoscopic and surgical findings were not available.

Findings on the chest radiographs were abnormal in all patients. A calcified lymph node near a bronchus was seen in 11 patients (Fig. 1A). Atelectasis was identified in nine patients (Fig. 1A). The atelectasis was segmental in six cases and lobar in three. Parenchymal infiltrate was present in two cases. Calcified granulomas in the lung were seen in four patients.

Bronchoscopy was performed in 14 patients. CT was done before bronchoscopy in all cases. One patient had lithoptysis and did not undergo bronchoscopy. A follow-up chest radiograph showed that this patient, after several years of lithoptysis, had expectorated most of the calcified lymph node (Fig. 2). In the 14 patients examined, nine of whom had an endobronchial broncholith, a broncholith was identified in only five cases. In the remaining nine cases, bronchial distortion was found in seven and blood was found in three. In two cases, the blood precluded evaluation of the involved bronchus.

Nine patients underwent surgical resection of the involved lung. The lymph node was found to be endobronchial in six cases and peribronchial in three. One patient had partial bronchoscopic removal of an endobronchial node. Five patients were observed.

Results

Abnormalities were identified on CT scans in all patients. Calcified lymph nodes were identified in all 15 patients. In the 10 patients in whom the lymph nodes ultimately were proved to be endobronchial, six of the lymph nodes appeared to be endobronchial (Fig. 3) and four appeared to be peribronchial on CT. Of the five patients whose lymph nodes were peribronchial, one node appeared to be located within a bronchus (Fig. 4) and the remaining four appeared to be peribronchial. In two patients with endobronchial lymph nodes, the bronchus appeared to be occluded by material (Fig. 1B) that had the same density as soft tissue. The involved bronchi in these patients were found during bronchoscopy to be occluded by blood clot or edematous mucosa.

CT scans showed atelectasis in six patients with endobronchial lymph nodes (Fig. 1B) and in all five patients with peribronchial nodes (Fig. 4). Parenchymal infiltrate was seen in four patients with endobronchial nodes (Fig. 5). In three patients, the infiltrates were patchy, and in one patient, the involved lung was densely consolidated. Bronchiectasis was present distal to endobronchial lymph nodes in four patients (Figs. 1B and 3B). This was characterized by tubular dilatation of the bronchi, which in three cases was associated with atelectasis of the involved lung. Air trapping in the involved lung was seen in one patient with an endobronchial node.

Using CT, we determined that broncholithiasis involved the right lung in 13 patients and the left lung in two patients. The distribution in the right lung was the anterior segment upper

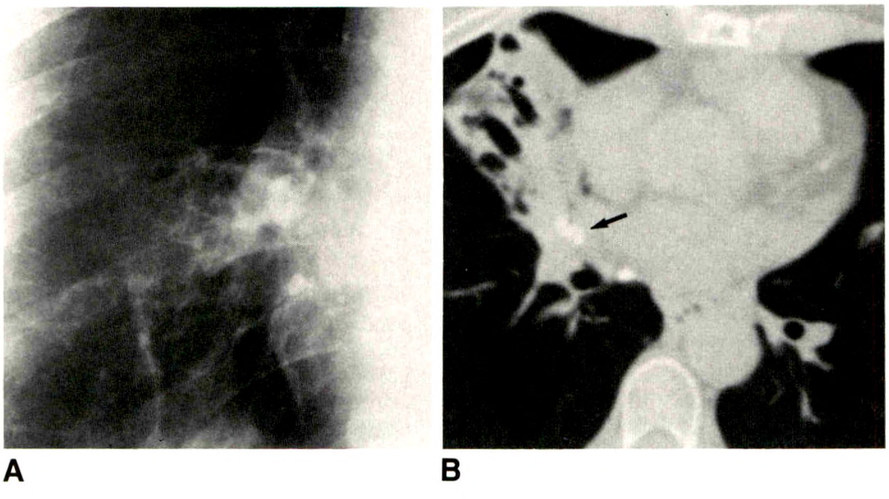

Fig. 1.—66-year-old asymptomatic woman with an endobronchial broncholith.

***A*, Posteroanterior chest radiograph shows atelectasis in right middle lobe and calcified lymph nodes near right-middle-lobar bronchus.**

***B*, CT scan through level of right-middle-lobar bronchus shows calcified lymph node (*arrow*) in expected location of right-middle-lobar bronchus and atelectasis and bronchiectasis distal to lymph node. Soft tissue within bronchus proximal to node represents blood clot and edematous mucosa seen during bronchoscopy. Lymph node was found during surgery to be endobronchial.**

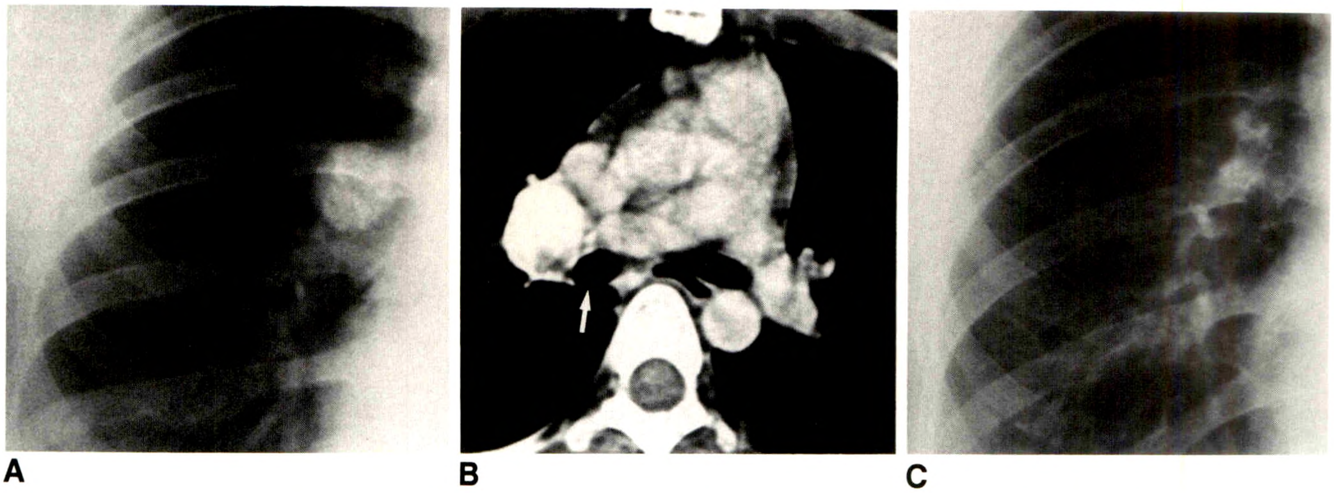

Fig. 2.—33-year-old woman with a chronic cough and lithoptysis.

A, Posteroanterior chest radiograph shows a large calcified lymph node in hilum of right lung.

B, CT scan obtained at same time as *A* shows a large calcified lymph node in right hilum that appears to be next to, but not within, bronchus intermedius (*arrow*).

C, Chest radiograph obtained after 2 years of lithoptysis (2 years after *A*) shows marked reduction in calcifications in right hilum of lung.

Fig. 3.—30-year-old woman with bronchiectasis due to chronic bronchial obstruction by an endobronchial broncholith.

A, CT scan at level of origin of right-middle-lobar bronchus shows proximal bronchus abuts an endobronchial broncholith (*arrow*).

B, CT scan at level immediately below *A* shows bronchus abutting distal side of broncholith (*arrow*). Bronchiectasis is present in lateral segment.

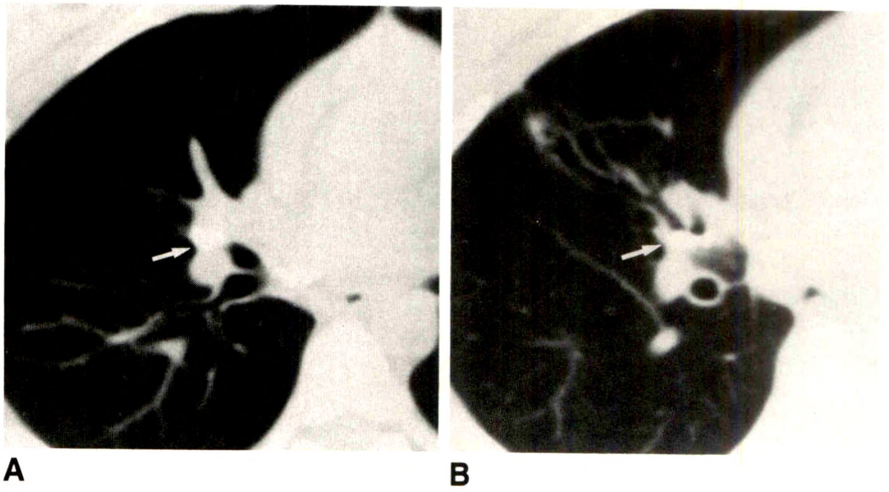

Fig. 4.—61-year-old man with a peribronchial broncholith that was incorrectly localized by CT as endobronchial. CT at level of anterior segment of right upper lobe shows calcified lymph node (*arrow*), apparently occluding bronchus, and associated distal atelectasis. During surgery, node was found to be peribronchial, and bronchial obstruction was due to postinflammatory bronchial distortion and stenosis.

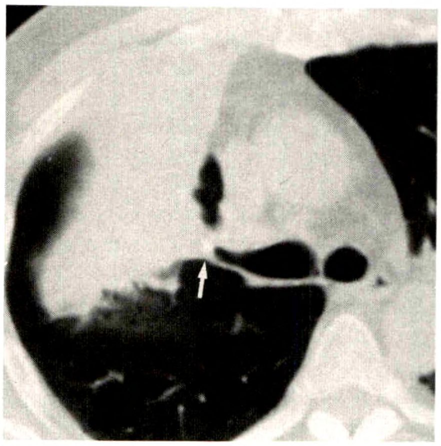

4

Fig. 5.—51-year-old woman who had persistent infiltrate in right upper lobe after therapy for pneumonia. CT scan shows endobronchial broncholith within anterior segment of right-upper-lobar bronchus and infiltrate within segment.

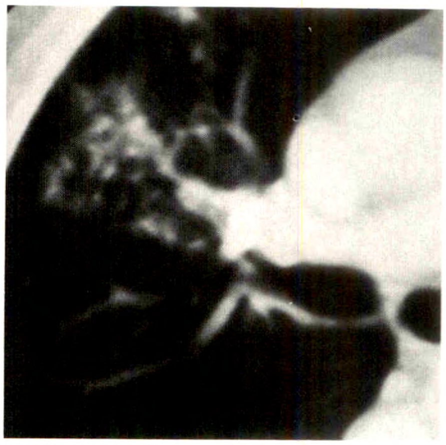

5

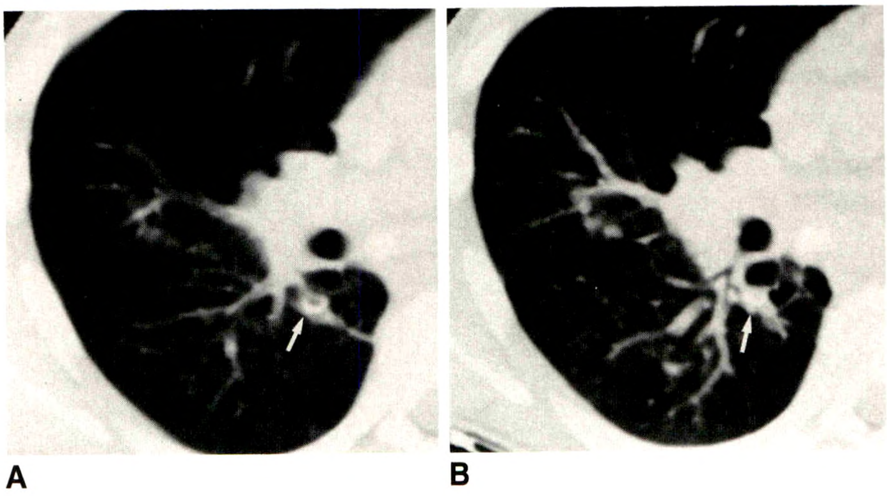

Fig. 6.—24-year-old man with hemoptysis.
_A_, CT scan (1.0-cm section) through superior segment of right lower lobe shows calcification (_arrow_) that does not appear to involve a bronchus.
_B_, CT scan of thinner section (0.5 cm) clearly shows broncholith (_arrow_) is in a subsegmental bronchus.

lobar bronchus in five cases, middle lobar bronchus in three cases, bronchus intermedius in two cases, and the superior segment lower lobar bronchus in three cases. In the left lung, the upper lobar bronchus and the lower lobar bronchus were involved in one case each.

In three patients, both 1.0- and 0.5-cm-thick sections were obtained. In two patients, both section thicknesses provided essentially equivalent information. In the other patient, the 0.5-cm-thick images provided much better definition of the relationship between the broncholith and the bronchus (Fig. 6). In this case, involvement of a subsegmental bronchus was depicted clearly on the thinner section but was not seen on the thicker sections.

Discussion

Most broncholiths arise from peribronchial lymph nodes that calcify after an inflammatory process. They may erode into an adjacent bronchus, and the associated inflammatory process may distort the bronchus. The CT findings were representative of this pathologic process. In all cases, CT showed a calcified lymph node. This lymph node was identified as endobronchial in only six of 10 cases in which it was located within the bronchus. In one case with a peribronchial node, CT showed that the node was endobronchial. These discrepancies are the result of volume averaging of the lymph node, bronchus, and surrounding tissues. In two cases of endobronchial lymph nodes, the bronchus appeared to be occluded by soft tissue, which represented edematous mucosa or blood. The difficulty CT had in determining the exact location of the lymph node is not of great practical significance because the key radiologic finding, a calcified lymph node in or adjacent to the involved bronchus, was shown in all cases.

Atelectasis, the most common parenchymal finding, is the product of bronchial occlusion by a broncholith or postinflammatory bronchial distortion. Infiltrates were present in four cases, appearing as either a patchy infiltrate or an area of consolidation. The infiltrates also are due to the occlusive effect of the broncholiths, which may result in postobstructive infection. Two of the patients were examined because of persistent infiltrates after therapy for pneumonia. Bronchiectasis, which was found in four patients, indicates that the bronchial obstruction may be chronic in some patients, resulting in repeated episodes of postobstructive infection. Of interest is that the bronchiectasis seen on CT was not identified on the plain radiographs. Air trapping is an unusual finding that reflects the obstructive nature of this disease.

No soft-tissue mass was associated with any of the broncholiths. This is in contrast to fibrosing mediastinitis, which as with broncholithiasis usually is associated with infection by *Histoplasma capsulatum* and may produce bronchial obstruction. In fibrosing mediastinitis, a soft-tissue mass is the main finding and usually is associated with calcification [10]. This difference reflects the much more localized disease that occurs in the development of a broncholith.

We did not specifically address the relative usefulness of thick vs thin sections. However, in one of the three cases in which both 1.0- and 0.5-cm-thick sections were used, the thinner sections provided superior definition of the broncholith in relation to the bronchus. This is because less volume averaging occurred with the thinner section. It seems reasonable that in cases in which broncholithiasis is suspected 0.5-cm-thick or thinner sections should be obtained through the area of interest. This would minimize the effect of volume averaging and allow better localization of the calcified lymph node. Although contrast material was administered in nine of the CT scans, it is not necessary for the evaluation of broncholithiasis.

Fiber-optic bronchoscopy is a relatively insensitive technique for the detection of broncholiths. In our series, only five (56%) of nine endobronchial broncholiths were identified with bronchoscopy. This is slightly better than other series, in which broncholiths were identified in 28–44% of patients examined [3, 11, 12]. The failure of bronchoscopy to identify some broncholiths is due either to the node being peribronchial or to bronchial distortion obscuring an endobronchial node. It is in these patients that CT is of value. The usefulness of CT for identifying the hidden broncholith provides information that is essential if broncholithiasis is to be diagnosed. An important role of bronchoscopy is to exclude an endobronchial neoplasm, which in rare cases may be calcified and simulate a broncholith [13].

The results of this study suggest that CT can provide useful information in the examination of patients with suspected broncholithiasis. A diagnosis of broncholithiasis is suggested strongly by the following CT findings: (1) a calcified lymph node that is either endobronchial or peribronchial; (2) the presence of changes due to bronchial obstruction: atelectasis, infiltrates, bronchiectasis, or air trapping; and (3) the absence of an associated soft-tissue mass. Bronchoscopy should be done then to exclude the presence of an endobronchial neoplasm and to look for either a broncholith or evidence of peribronchial disease (bronchial compression, stenosis, or distortion). If no other pulmonary disease is present to explain the findings, we think that the results of CT and bronchoscopy will be sufficient for a diagnosis of broncholithiasis.

REFERENCES

1. Schmidt HW, Claggett OT, McDonald JR. Broncholithiasis. *J Thorac Cardiovasc Surg* **1950**;19:226-245
2. Arrigoni MG, Bernatz PE, Donoghue FE. Broncholithiasis. *J Thorac Cardiovasc Surg* **1971**;62:231-237
3. Vix VA. Radiographic manifestations of broncholithiasis. *Radiology* **1978**;128:295-299
4. Freedman E, Billings JH. Active bronchopulmonary lithiasis. *Radiology* **1949**;53:203-214
5. Kowal LE, Goodman LR, Zarro VJ, Haskin ME. CT diagnosis of broncholithiasis. *J Comput Assist Tomogr* **1983**;7:321-323
6. Morris JF, Antonovic R, Galey WT, Khanijo V. Lithoptysis in a marathon runner. *Chest* **1989**;96:655-656
7. Hirshfield LS, Graver LM, Isenberg HD. Broncholithiasis due to *Histoplasma capsulatum* subsequently infected by actinomycetes. *Chest* **1989**;96:218-219
8. Shin MS, Ho KJ. Broncholithiasis: its detection by computed tomography in patients with recurrent hemoptysis of unknown etiology. *J Comput Tomogr* **1983**;7:189-193
9. Adler O, Peleg H. Computed tomography in the diagnosis of broncholithiasis. *Eur J Radiol* **1987**;7:211-212
10. Weinstein JB, Aronberg DJ, Sagel SS. CT of fibrosing mediastinitis: findings and their utility. *AJR* **1983**;141:247-251
11. Dixon GF, Donnerberg RL, Schonfeld SA, Whitcomb ME. Advances in the diagnosis and treatment of broncholithiasis. *Am Rev Respir Dis* **1984**;129:1028-1030
12. Trastek VF, Pairolero PC, Ceithami EL, Piehler JM, Payne WS, Bernatz PE. Surgical management of broncholithiasis. *J Thorac Cardiovasc Surg* **1985**;90:842-848
13. Shin MS, Berland LL, Myers JL, Clary G, Zorn GL. CT demonstration of an ossifying bronchial carcinoid simulating broncholithiasis. *AJR* **1989**;153:51-52

Book Review

The Lungs. Edited by B. Corrin. (Vol. 5 of Systemic Pathology, 3rd ed. General editor: W. St C. Symmers.) New York: Churchill Livingstone, 467 pp., 1990. $159

This book is a volume devoted to the pathology of lung diseases from a series of pathology texts on the major organ systems. Dr. Corrin, although listed as the editor, is the author or coauthor of most of the chapters in this book, ensuring some consistency of style and organization of content. Dr. Corrin is professor of thoracic pathology at the National Heart and Lung Institute (Brompton and London Chest Hospitals) in England.

The book is divided into 23 chapters. They discuss normal lung structure; perinatal and developmental lung disease; diffuse alveolar damage; viral, mycoplasmal, and rickettsial infections; acute and chronic bacterial infections and lung abscess; fungal and parasitic infections; atelectasis; diseases characterized by airflow limitation or restriction; occupational disease; metabolic disease; edema, infarction, and hypertension; vasculitis and granulomatosis; lymphoproliferative disease; inflammatory pseudotumors; lung cancer; other epithelial tumors; mixed tumors; connective tissue tumors; metastatic tumors; and pleural disease. References are not comprehensive but are adequate, with an average of about 50 per chapter. Topics are well illustrated, and illustrations are of high quality. Although most illustrations are of histologic studies, illustrations of gross pathologic changes and of whole lung sections are included in the descriptions of many entities; this is particularly important from a radiologic standpoint.

Discussions of individual diseases or entities do not simply cover pathologic and histologic findings. They also provide good reviews of what is known about the disease in question so far as its cause, clinical features, course, and differential diagnosis. Thus, although this is a text on pathology, it provides a rather well-balanced approach to understanding the basics of specific diseases. Pathologic features of the diseases discussed include gross morphology, localization of abnormalities relative to acini and pulmonary structures such as bronchioles and vessels (which might be useful in understanding high-resolution CT scans of the lung), and histology. Some discussion is included of the results of bronchoalveolar lavage and how it relates to histologic findings, although not in great detail.

The author is careful to use terminology that is commonly known in the United States, in addition to terms that are used more typically in the United Kingdom. For example, the terms "idiopathic pulmonary fibrosis" and "UIP" are given in addition to the British equivalent, "cryptogenic fibrosing alveolitis."

Although *The Lungs* appears to be a good textbook of lung pathology, from a radiologist's point of view, I can recommend it only to someone with a special interest in lung disease. Furthermore, discussions of similar completeness are included in the recently published third edition of *Diagnosis of Diseases of the Chest* by Fraser, Paré, Paré, Fraser, and Genereux (Saunders), which is probably available in most hospital and radiology libraries and stresses pathologic-radiologic correlations to a greater degree.

W. Richard Webb
University of California, San Francisco
San Francisco, CA 94143-0628

Noncardiogenic Pulmonary Edema Resulting from Intravascular Administration of Contrast Material

Gilles Bouachour,[1] Nicolas Varache,[1] Nathalie Szapiro,[1] Philippe L'Hoste,[2] Patrick Harry,[1] and Philippe Alquier[1]

Acute pulmonary edema after intravascular administration of contrast medium is an extremely rare complication [1]. This adverse reaction generally is ascribed to the effects of contrast-induced volume overload in patients with compromised cardiac status [2]. We report three cases of noncardiogenic pulmonary edema induced by contrast material, shown by Swan-Ganz pressure measurements, in which the edema may have been due to the toxic effect of the contrast material on the pulmonary capillary membrane.

Case Reports

Case 1

A 64-year-old man had angiography of the lower extremity for evaluation of an aortobifemoral prosthesis. His medical history included a left pneumonectomy and radiation therapy for epidermoid carcinoma of the lung and an aortobifemoral bypass performed 2 months earlier for aortic and femoral thrombosis. At that time, an arteriogram had shown no adverse effects after injection of contrast material. Within minutes of an IV bolus injection of 120 ml of sodium and meglumine ioxaglate (600 mOsm/kg, Hexabrix 320, Guerbet, Aulnay-sous-Bois, France), the patient complained of dyspnea, became cyanotic, and produced copious amounts of pink frothy sputum. Respiratory arrest developed. The patient was intubated immediately, ventilated mechanically, and transferred to the intensive care unit. At admission, his blood pressure was 105/70 mm Hg and his pulse rate was 72 beats per minute. Chest radiographs showed severe diffuse right-sided interstitial and alveolar pulmonary edema and a normal cardiac silhouette. The ECG showed sequela of inferior myocardial infarction with no acute changes when compared with a recent ECG. Serial measurements of cardiac enzyme levels remained within normal limits. Blood gas analysis on a fraction of inspired oxygen of 0.8 revealed an arterial oxygen tension of 61 mm Hg (8.1 kPa); calculated serum osmolality was 300 mOsm/kg H_2O (300 mmol/kg H_2O), and measured serum osmolality was 320 mOsm/kg H_2O (320 mmol/kg H_2O). A balloon-tipped, flow-directed thermodilution catheter revealed a right atrial pressure of 4 mm Hg, pulmonary artery pressure of 37/19 mm Hg, and pulmonary capillary wedge pressure of 8 mm Hg. Cardiac index was 1.35 $l/min/m^2$. The protein content of edematous fluid from the endotracheal tube was 46 g/l, whereas a simultaneous measurement of serum protein content was 65 g/l. After a fluid challenge of six units of 20% albumin and dobutamine infused at the rate of 10 $\mu g/kg/min$ during the next 48 hr, the patient's cardiopulmonary condition progressively improved. On the second day, results of fiber-optic bronchoscopic examination were normal. The bronchoalveolar lavage revealed no eosinophils or malignant cells, and the samples obtained by a protected specimen brush showed no significant bacterial growth. Levels of serum total hemolytic complement, C1 esterase inhibitor, and histamine 12 hr after admission were normal. The patient's pulmonary status gradually worsened in the ensuing weeks, complicated by a nosocomial pneumonia; he died on day 33. Autopsy showed nonspecific diffuse interstitial fibrosis of the lung.

Case 2

A 63-year-old man with a history of severe arterial hypertension controlled by nicardipine hydrochloride and betaxolol hydrochloride had diagnostic renal angiography. His medical history included uncomplicated myocardial infarction and percutaneous transluminal angioplasty 2 months earlier with no adverse effect after injection of contrast medium. IV bolus injection of 120 ml of sodium and meglumine ioxaglate was followed immediately by profound dyspnea, pink frothy sputum, cyanosis, and diaphoresis. The chest radiograph showed diffuse alveolar infiltrates. A presumptive diagnosis of cardi-

---

Received December 17, 1990; accepted after revision March 7, 1991.

[1] Intensive Care Unit (Service de Réanimation Médicale), Centre Hospitalier Régional et Universitaire, 49033 Angers Cedex, France. Address reprint requests to G. Bouachour.

[2] Department of Radiology, Centre Hospitalier Régional et Universitaire, 49033 Angers, France.

AJR 157:255-256, August 1991 0361-803X/91/1572-0255 © American Roentgen Ray Society

ogenic pulmonary edema was made, 80 mg of furosemide was infused IV, and oxygen (10 l/min) was administered via face mask. Despite this therapy and a diuresis of 750 ml during the next 2 hr, the patient's clinical status continued to deteriorate. The patient was intubated and ventilated mechanically. At that time, he produced copious amounts of pink frothy sputum. Blood pressure was 180/100 mm Hg, and pulse rate was 80 beats per minute. A myocardial infarction was excluded on the basis of ECG and serial measurements of cardiac enzyme levels. The arterial blood gases on a fraction of inspired oxygen of 0.8 showed an oxygen tension of 48 mm Hg (6.4 kPa). A pulmonary artery catheter showed that the right atrial pressure was 1 mm Hg, pulmonary artery pressure was 21/12 mm Hg, and pulmonary-capillary wedge pressure was 4 mm Hg. Cardiac index was 2.5 l/min/m^2. The protein content of edematous fluid from the endotracheal tube was 52 g/l, whereas a simultaneous measurement of serum protein content was 69 g/l. Calculated serum osmolality was 316 mOsm/kg H_2O (316 mmol/kg H_2O) and measured serum osmolality was 334 mOsm/kg H_2O (334 mmol/kg H_2O). Findings on a fiber-optic bronchoscopic examination were normal. Levels of serum total hemolytic complement, C3 and C4, C1 esterase inhibitor, and histamine 60 min after the beginning of the reaction were normal. During the next 3 days, the patient's pulmonary condition progressively improved, and the endotracheal tube was removed on the sixth day of hospitalization.

Case 3

A 61-year-old man had mesenteric arteriography for evaluation of chronic anemia. He had had a myocardial infarction and had undergone coronary arteriography without specific reaction 10 years before. Ten minutes after intraarterial injection of 60 ml of sodium and meglumine ioxaglate, the patient became tachypneic and peripherally cyanotic. He immediately was given 9 l of nasal oxygen, and 8 mg of betamethasone was administered IV. Blood pressure was 120/80 mm Hg, pulse rate was 110 beats per minute, and respiration rate was 26/min. ECG showed no acute changes, and serial measurements of cardiac enzyme levels remained within normal limits. A chest radiograph showed an interstitial and alveolar pattern of pulmonary edema. Blood gas analysis showed an arterial oxygen tension of 69 mm Hg (9.2 kPa). Calculated serum osmolality was 296 mOsm/kg H_2O (296 mmol/kg H_2O) and measured serum osmolality was 311 mOsm/kg H_2O (311 mmol/kg H_2O). A balloon-tipped thermodilution catheter revealed a right arterial pressure of 7 mm Hg, pulmonary artery pressure of 38/20 mm Hg, and pulmonary capillary wedge pressure of 14 mm Hg. Cardiac index was 3.75 l/min/m^2. Results of a fiber-optic bronchoscopic examination were normal. Levels of serum total hemolytic complement, C3 and C4, C1 esterase inhibitor, and histamine 20 min after the reaction started were in the normal range. Oxygen therapy via facial mask was continued for 2 days, with rapid resolution of symptoms.

Discussion

Both cardiogenic and noncardiogenic factors can cause contrast-induced pulmonary edema. Adverse reaction after administration of contrast material, similar to the adult respiratory distress syndrome, has been reported [3, 4]. Only five cases with a low pulmonary capillary wedge pressure or with a high protein concentration in pulmonary edematous fluid are well documented [5, 6]. Clinically, patients are usually young and have no history of cardiac or pulmonary disease.

The three patients described here did not have classic cardiogenic pulmonary edema. The peculiarity of these cases is that the cardiovascular history of our patients suggested a cardiac variety of pulmonary edema that was excluded by the results of right-sided cardiac catheterization. The pulmonary capillary wedge pressure never exceeded 15 mm Hg during the acute phase in the three cases, whereas a large volume of pulmonary edematous fluid issued spontaneously from the endotracheal tube in two cases. The edematous fluid protein: serum protein ratio was 0.7, indicating that the edema was caused by increased permeability of the alveolar capillary membrane.

About 12,000 patients received intravascular ioxaglate in our hospital during the 2 years in which these cases were observed. The contrast material used in the three patients was examined systematically, and no impurities or contamination was found. The pathogenesis of increased permeability of the alveolar capillary membrane caused by contrast material remains unclear. Two hypotheses are suggested in the literature: allergic or immunologic reaction and direct chemotoxic or osmotic effects on vascular endothelium. Our three patients had received contrast material previously without any adverse reaction. Most likely the pulmonary abnormality was mediated by nonimmunologic factors, as the levels of total serum hemolytic complement, C3, C4, C1 esterase inhibitor, and histamine were normal shortly after the onset of symptoms. It has been shown that contrast material can be directly toxic to pulmonary endothelial cells, with secondary capillary leakage. The rate and volume of injections and the osmolarity of the contrast material could account for such a mechanism, which may occur even with slightly hypertonic solutions like sodium and meglumine ioxaglate [7]. The role of dehydration before the procedures in increasing the osmolar effects of the injected solutions also should be considered [8]. Our three patients had a serum osmolality gap that can be attributed to the contrast material, and two were relativity dehydrated.

In conclusion, we speculate that contrast-induced pulmonary edema, possibly by direct toxic effects of the contrast material on the pulmonary capillary membrane, should be suspected even in patients with a history of a compromised cardiovascular system.

REFERENCES

1. Shehadi WH. Adverse reactions to intravascularly administered contrast media. *AJR* **1975**;124:145–152
2. Malins AF. Pulmonary oedema after radiological investigation of peripheral occlusive vascular disease: adverse reaction to contrast media. *Lancet* **1978**;1:413–415
3. Greganti MA, Flowers WM. Acute pulmonary edema after the intravenous administration of contrast media. *Radiology* **1979**;132:583–585
4. Boden WE. Anaphylactoid pulmonary edema ("shock lung") and hypotension after radiologic contrast media injection. *Chest* **1982**;81:759–761
5. Chamberlin WH, Stockman GD, Wray NP. Shock and non cardiogenic pulmonary edema following meglumine diatrizoate for intravenous pyelography. *Am J Med* **1979**;67:684–686
6. Delacour JL, Floriot C, Wagschal G, et al. Non-cardiac pulmonary edema following intravenous contrast injection. *Intensive Care Med* **1988**;15:49–50
7. Laerum F. Acute damage to human endothelial cells by brief exposure to contrast media in vitro. *Radiology* **1983**;147:681–684
8. Zack A, Mare K, Violante M. The aggravating effect of dehydration on pulmonary edema induced by ionic and non ionic contrast media. *Invest Radiol* **1985**;20:212–216

Lobular Carcinoma In Situ of the Breast: Clinical, Pathologic, and Mammographic Features

Bernard J. Beute[1]
Lester Kalisher[1]
Robert V. P. Hutter[2]

Lobular carcinoma in situ (LCIS) was diagnosed in 165 surgical specimens (119 patients) at our institution between 1974 and 1987. LCIS was seen more often in younger women (mean age, 49 years) than other breast carcinomas were (mean age, 58 years). Sampling of a single breast revealed multifocal disease in 70% (96/138). When both breasts were sampled, bilateral foci were found in 50% (41/82). Of 165 breasts with foci of LCIS, 37% (61/165) had simultaneously occurring invasive cancers in the same breast. Direct mammographic-pathologic correlation of foci of LCIS was possible in 73 breasts (67 patients). Microcalcifications were an indication for biopsy in 49% (20/41) of breasts with a mammographic abnormality, but were a nonspecific finding often found in tissues adjacent to foci of LCIS. The mammogram was normal in 44% (32/73) of breasts with foci of LCIS. The mammograms of patients with LCIS and those from a group of age-matched control subjects were compared by using a modified form of Wolfe's criteria and the percentage of fibroglandular elements. LCIS was seldom found in an N1 breast (1% vs 29%) or in a breast with less than 25% of its parenchymal area occupied by fibroglandular density (3% vs 33%). Compared with the control group, breasts with LCIS had more than 50% fibroglandular density (85% vs 45%) and a much higher frequency of the DY pattern (56% vs 36%). More fibroglandular density was seen in the LCIS group at all ages. Postmenopausally, the frequencies of the DY pattern and fibroglandular density greater than 50% in LCIS patients were nearly double those in the control group.

LCIS patients have disease of the entire breast parenchyma, characterized by multifocality and bilaterality of various forms of lobular disease. Their mammograms reveal a higher rate of the DY pattern and higher percentages of fibroglandular or parenchymal density than those of age-matched controls. In LCIS patients, persistence of the DY pattern or large amounts of fibroglandular density postmenopausally supports the concept that mammographically dense breasts are a marker for increased cancer risk in women 50 years old and older.

***AJR* 157:257-265, August 1991**

Lobular carcinoma in situ (LCIS) is an uncommon lesion arising in the lobule of the breast, often diagnosed as an incidental microscopic finding in tissue removed for a benign lesion. Only a handful of studies correlating the mammographic and pathologic features of this entity have appeared in the literature. In 1966, Snyder [1] described these features in 27 patients. In 1969, Hutter et al. [2] included an additional 34 patients in their series and provided follow-up on the original study group. Most recently, Pope et al. [3] described the mammographic features of this entity in a series of 26 patients.

In their landmark 1941 article, Foote and Stewart [4] described the pathologic features of a peculiar form of cancerous change arising from the lobules of the breast, which they termed *lobular carcinoma in situ*. In 1982, Hutter [5] reviewed his original report and summarized the combined clinical and pathologic experience with LCIS to that date. He stressed several pertinent clinical features of LCIS: (1) Multicentricity within the biopsied breast is as high as 90% in some series, with

Received February 15, 1990; accepted after revision January 23, 1991.

[1] Department of Radiology, St. Barnabas Medical Center, Old Short Hills Rd., Livingston, NJ 07039. Address reprint requests to B. J. Beute.

[2] Department of Pathology, St. Barnabas Medical Center, Livingston, NJ 07039.

0361-803X/91/1572-0257
© American Roentgen Ray Society

simultaneous bilateral foci in as many as 33–69% [6, 7]. (2) Both breasts are at almost equal risk for the subsequent development of infiltrating cancer once LCIS has been found in either breast [6, 8–10]. (3) Fifty percent of patients with proved microscopic foci of LCIS have "normal" mammograms, that is, no radiographic evidence of malignancy [2, 6]. (4) The probability of developing subsequent infiltrating cancer is seven to nine times greater in patients with untreated foci of LCIS than in women in the general population, and the risk of death from breast cancer is 11 times greater [10, 11]. (5) When there is progression to infiltrating lobular carcinoma, the survival rates are approximately the same as those for infiltrating ductal carcinoma [12].

Infiltrating ductal carcinoma is the most common invasive cancer that develops in patients with LCIS. Infiltrating lobular carcinoma, however, occurs much more frequently in patients with LCIS (35–50%) than in the general population of patients with breast cancer (5–10%) [13]. A synchronous association with invasive cancer of some type occurs in approximately 5% of patients with LCIS [14].

In a recent review article, Frykberg et al. [14] summarized the clinical, pathologic, and radiologic findings in LCIS. They noted that many authors consider LCIS a "marker lesion" for the future development of invasive cancer, with the entire breast parenchyma at risk. Others believe that individual foci of LCIS progress to invasive disease (the "transition" theory). Regardless of the means of progression from in situ to invasive disease, the advantages of early mammographic detection of LCIS are obvious. At the present time, preoperative detection of LCIS is not possible, since no specific mammographic features of this entity have been identified.

With hopes of being able to identify specific mammographic features or predictors of LCIS, we sought to analyze the clinical and pathologic data in the largest series of patients with LCIS to date, perform radiologic-pathologic correlation in breasts with foci of LCIS, and compare the mammographic findings in breasts with LCIS with those of age-matched controls.

Materials and Methods

Clinical and Pathologic Data Accumulation and Analysis

Computerized surveys of tumor registry data at our institution were analyzed for the years 1974–1987 for the diagnosis of LCIS in both breast biopsy and mastectomy specimens. The pathology results were reviewed for each case. The hospital record of each patient was reviewed for clinical history, demographic data, physical findings, and reason for breast biopsy.

In order to determine the mammographic presentation of pure LCIS, the final study group was selected on the basis of pathologic data. All patients with the pathologic diagnosis of LCIS were included to determine demographic data. Those cases in which the initial diagnosis of LCIS was associated with invasive carcinomas were excluded from the final study group.

Radiologic-Pathologic Correlation

Mammograms, xeromammograms, needle localizations, specimen radiographs, and original radiology reports were then correlated with the pathology data. In an attempt to identify the more common presentations of LCIS, each breast with at least one focus of LCIS was assigned to one of six categories based on its mammographic features: (1) microcalcifications alone; (2) microcalcifications with added or increased density; (3) mass alone, suggestive of malignancy; (4) mass alone, not suggestive of malignancy; (5) added density or asymmetry of parenchyma; and (6) no mammographic abnormality. When a discrete mammographic abnormality was present, that abnormal area was specifically identified and its presence confirmed by needle-directed biopsy and/or specimen radiography.

As has been done previously [1], the morphologic appearance of microcalcifications on the original mammograms or xeromammograms was described in cases of microcalcifications alone or microcalcifications with added or increased parenchymal density.

Comparison of LCIS Mammograms with Those of Age-Matched Control Subjects

In an attempt to identify similarities among parenchymal patterns in the LCIS group, the mammograms of the 67 LCIS patients were compared with those from a set of age-matched control subjects who underwent screening mammography. Parenchymal patterns were described by using Wolfe's criteria [15] and a separate classification scheme based on the percentage of the breast occupied by fibro-glandular density (0–25%, 26–50%, 51–75%, 76–100%). Since not all breasts could be easily assigned to one of the four original categories described by Wolfe, a modified form of these criteria was used in which parenchymal patterns were defined as: N1 = fatty replaced breast; P1 = mostly fatty with less than 25% prominent duct pattern; P2 = prominent duct pattern involving more than 25% of breast; DY = sheetlike areas of increased density; P2/DY = P2 pattern with large amounts of added density; and DY/N1 = large amounts of added density not occupying entire breast, no evidence of prominent ducts. By using these two separate classification schemes, we avoided subjective mammographic interpretation based on degrees of severity of fibrocystic changes.

Parenchymal patterns and percentages of fibroglandular density seen on LCIS mammograms were compared with those on control mammograms and correlated with pathology results. Although pathologic findings in LCIS breasts could be described in terms of severity, multifocality, and bilaterality, they could not be quantified by using the control group as a reference point, since random sampling of breast material from this group was not possible.

Results

Clinical and Pathologic Data Analysis

For the study period 1974–1987, the diagnosis of LCIS was made in a total of 165 breasts (119 patients) from biopsy or mastectomy specimens. LCIS alone (not associated with another malignancy) was the original diagnosis in 104 of the 165 breasts sampled. The average age at diagnosis was 49 years (range, 26–81 years).

When both breasts were sampled either by mirror-image biopsy or contralateral mastectomy in a patient with LCIS in one breast, the disease was found to be bilateral in 50% (41/82). When an entire breast was sampled for biopsy-proved LCIS, multifocal disease was found in 70% (96/138).

Of 165 breasts with foci of LCIS, 61 (37%) had invasive cancers at the time of diagnosis. These were most commonly infiltrating ductal carcinomas and next most commonly infiltrating lobular carcinomas.

Radiologic-Pathologic Correlation

A total of 104 breasts had foci of LCIS alone. Direct radiologic-pathologic correlation of foci of LCIS was possible in 73 of these breasts (67 patients). Each breast was assigned to one of six categories depending on its mammographic features. The majority of breasts with LCIS (56%) were found to exhibit one of the first five mammographic abnormalities used in this study (Table 1).

No specific mammographic features of LCIS could be identified. The presence of microcalcifications, either alone or associated with an area of added or increased density, was the most common indication for biopsy in those breasts with a mammographic abnormality (20/41 or 49%). No mammographic abnormalities were detected preoperatively in 44% of breasts (32/73) with single or multiple foci of LCIS.

In prior reports, the most common presenting problem in patients with LCIS was that of a mass in the breast [14]. In our series, 59% (19/32) of breasts with no mammographic abnormality had palpable masses (Table 2). Taken together, palpable abnormalities, mammographically detected masses, and areas of added density accounted for 68% (50/73) of all presenting symptoms.

Of those breasts not included in the final study group, those that contained areas of infiltrating ductal or intraductal carcinoma in addition to LCIS typically demonstrated coarse and irregular microcalcifications on mammography. When biopsies were done, LCIS was usually found in areas adjacent to the invasive cancer in a background of atypical lobular or ductal hyperplasia.

Radiologic-pathologic features are detailed below for each of the six categories of mammographic findings.

TABLE 1: Mammographic Indications for Biopsy in 67 Patients Found to Have Lobular Carcinoma In Situ

Mammogram	No. of Breasts (%)
Microcalcifications alone, no added density	10 (14)
Microcalcifications with added or increased density	10 (14)
Mass alone, suggestive of malignancy	6 (8)
Mass alone, not suggestive of malignancy	11 (15)
Added density or asymmetry of parenchyma	4 (5)
No radiologic findings	32 (44)
Total	73 (100)

TABLE 2: Indications for Biopsy in 32 Breasts Without Mammographic Abnormalities

Indication	No. of Breasts (%)
Palpable abnormalities	19 (59)
Reduction mammoplasty	6 (19)
Contralateral breast with proved lobular carcinoma in situ	5 (16)
Bloody nipple discharge	2 (6)
Total	32 (100)

Microcalcifications alone.—Ten breasts had solitary clusters of microcalcifications. Needle localization of the suspicious area was performed in eight cases. The number and distribution of microcalcifications varied (Table 3). Several breasts had tight clusters of punctate and irregular microcalcifications, whereas in others the microcalcifications were scattered throughout a larger area. Microscopically, these microcalcifications were most often seen in areas of sclerosing adenosis and/or apocrine metaplasia. Foci of LCIS were found in adjacent tissues, usually in areas of significant atypical lobular and ductal hyperplasia. Microcalcifications were rarely identified within the actual foci of LCIS.

Snyder [1] originally described the "stippled" type of microcalcifications thought to be typical of LCIS as "minute punctate or linear flecks, 3 or more in number, and arranged randomly in a group, sometimes fading in distinctness at the periphery." These types of clustered, punctate microcalcifications were identified on a single mammogram in this group (Fig. 1).

Microcalcifications with added or increased density.—Ten breasts had clusters of microcalcifications in an area of increased density or within a poorly defined mass. Preoperative mammograms were highly suggestive of malignancy. Needle localization of the suspicious area was performed in seven cases (Table 4).

The added density seen in these cases most commonly represented areas of fibrocystic mastopathy (Fig. 2). Foci of sclerosing adenosis and/or apocrine metaplasia were frequently seen, often in a background of atypical lobular and ductal hyperplasia. In one case, two smooth, benign-appearing microcalcifications were seen in an area of added density. Needle-directed biopsy revealed multifocal LCIS, sclerosing adenosis, and atypical ductal and lobular hyperplasia with microcalcifications adjacent to a small fibroadenoma. Five of the 10 breasts in this group demonstrated the punctate, clustered (stippled) microcalcifications thought at one time to be typical of LCIS [1].

Mass alone, suggestive of malignancy.—In three breasts, suspicious masses were characterized by smudged or incomplete borders on mammography or xeromammography. In one of these cases, LCIS was found in the wall of a benign cyst. Another mass with incomplete borders was found to represent multiple cysts with an adjacent single microscopic focus of LCIS.

Three other breasts had either spiculated or lobulated masses on preoperative mammography. One of these cases had a single area of microscopically invasive lobular carcinoma in a background of multifocal LCIS and atypical lobular hyperplasia. This case was included to demonstrate that florid lobular disease with minimal microscopic foci of invasion may present as a spiculated mass.

A second spiculated mass consisted of multifocal LCIS in a background of atypical lobular hyperplasia. There was no evidence of microscopic invasion in this case. A third patient had a lobulated mass in a background of severe fibrocystic changes that was found to represent multifocal LCIS within an area of microcysts and focal fibrocystic mastopathy.

Mass alone, not suggestive of malignancy.—Benign-appearing masses were seen on mammography in 11 breasts.

TABLE 3: Number, Concentration, and Morphology of Microcalcifications Seen on Preoperative Mammograms in Patients with Findings of Microcalcifications Alone

Specimen No.	Mammographic Findings				Pathologic Findings
	Arrangement of Calcifications	No. of Calcifications		Morphology	
		Per Cluster	Per cm^2		
1	Solitary cluster	10–12	<5	Rounded, various sizes	Two foci of LCIS, FCC, SA, ALH
2	Solitary cluster	8	>5	Short, linear	One focus of LCIS, FCC, AM, ALH, microscopic FA
3	Scattered in a quadrant	20–25	<5	Rounded, linear, small	One focus of LCIS, ALH, borderline ADH
4	Scattered in a quadrant	25–30	<5	Rounded and irregular, various sizes	Three foci of LCIS, marked FCC, AM, SA, fat necrosis
5	Solitary cluster	8–10	>5	Rounded and irregular, various sizes	One focus of LCIS, AM, SA, ALH, ADH
6	Multiple clusters	20–25	>5	Punctate, stippled	Three foci of LCIS, marked ALH, SA
7	Solitary cluster	10–12	>5	Short, linear, and rounded, various sizes	Multifocal LCIS, marked LA, FCC, AM
8	Scattered in a quadrant	30–40	<5	Short, linear, and rounded, various sizes	Multifocal LCIS, microcalcifications in foci of LCIS, ALH, ADH, FCC

Note.—Specimens were obtained with needle localization. LCIS = lobular carcinoma in situ; FCC = fibrocystic changes; SA = sclerosing adenosis; ALH = atypical lobular hyperplasia; AM = apocrine metaplasia; FA = fibroadenoma; ADH = atypical ductal hyperplasia; LA = lobular atypia.

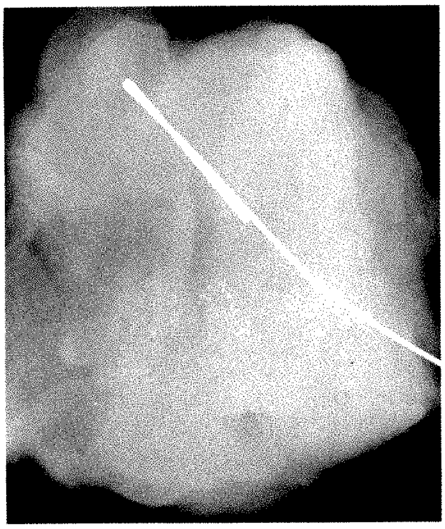

1

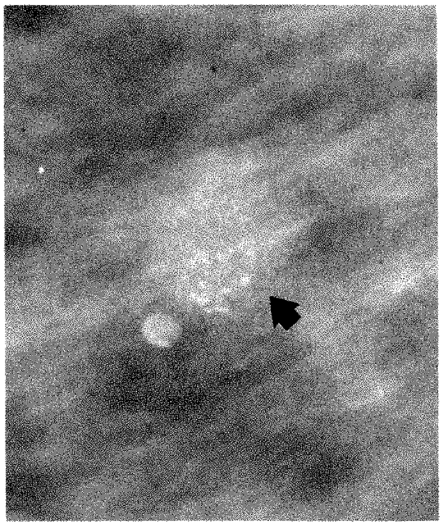

2

Fig. 1.—Microcalcifications alone (specimen 6 in Table 3). Cluster of microcalcifications suggestive of malignancy was found on a baseline mammogram of a 44-year-old woman. Needle localization was performed. Specimen radiograph shows area of stippled microcalcifications adjacent to wire. These types of microcalcifications were thought at one time to be typical for lobular carcinoma in situ (LCIS). Specimen contained foci of LCIS and sclerosing adenosis in a background of marked lobular atypia. Microcalcifications were found in areas of sclerosing adenosis and in adjacent normal lobules.

Fig. 2.—Microcalcifications with added or increased density (specimen 4 in Table 4). Magnified view of cluster of microcalcifications with area of added density (*arrow*) in inferomedial aspect of right breast of 57-year-old woman. Biopsy revealed a single microscopic focus of lobular carcinoma in situ (LCIS) in an area of fibrocystic mastopathy. Microcalcifications were present in fibrocystic areas and in adjacent normal lobules but not within focus of LCIS.

In five cases, biopsy revealed fibroadenomas either adjacent to or intimately associated with foci of LCIS. Of these five cases, two had foci of LCIS within fibroadenomas. In the third case, an atypical hyalinizing fibroadenoma containing stromal hypercellularity and ductal hyperplasia was found in an area of atypical lobular hyperplasia and LCIS. In the remaining two cases, multifocal LCIS was found adjacent to fibroadenomas in areas of atypical lobular hyperplasia.

In the other six cases, mammographically benign-appearing masses were seen preoperatively in breasts demonstrating

TABLE 4: Number, Concentration, and Morphology of Microcalcifications Seen on Preoperative Mammograms in Patients with Findings of Microcalcifications and Added or Increased Density

Specimen No.	Mammographic Findings				Pathologic Findings
	Arrangement of Calcifications	No. of Calcifications		Morphology	
		Per Cluster	Per cm^2		
1	Solitary cluster	12–20	>5	Punctate, stippled	Multifocal LCIS, significant ALH, SA, AM, FCC
2	Scattered clusters	8–10	>5	Punctate, short, linear	Multifocal LCIS, AM, pagetoid extension into terminal ducts
3	Scattered clusters	5–10	>5	Punctate, multiple, rounded	Multifocal LCIS, ALH, SA, AM
4	Focal cluster	6–10	>5	Rounded, short, linear	Single focus of LCIS, FCM, ADH, borderline LA
5	Solitary cluster	8–12	>5	Flocculent, cloudlike	Multifocal LCIS, SA, AM, ALH
6	Solitary cluster	2	<5	Smooth, rounded	Multifocal LCIS, FCC, pagetoid extension into terminal ducts
7	Solitary cluster	6–8	>5	Punctate, stippled	SA, FCC, microcalcifications adjacent to FA, ADH

Note.—Specimens were obtained with needle localization. LCIS = lobular carcinoma in situ; ALH = atypical lobular hyperplasia; SA = sclerosing adenosis; AM = apocrine metaplasia; FCC = fibrocystic changes; FCM = fibrocystic mastopathy; ADH = atypical ductal hyperplasia; LA = lobular atypia; FA = fibroadenoma.

moderate to severe fibrocystic changes. Foci of LCIS were found in areas of fibrocystic change with macrocyst and microcyst formation (Fig. 3).

One patient with bilateral, multifocal LCIS had multiple benign-appearing masses in one breast and a solitary benign-appearing mass in the other breast. The multiple masses were areas of macrocyst formation with associated foci of LCIS. The solitary mass in the contralateral breast represented the atypical hyalinizing fibroadenoma described above.

Added density or asymmetry of parenchyma.—Added density or areas suggestive of asymmetric parenchyma were seen on sequential mammograms in four breasts (Fig. 4). In two cases of malignant-appearing spiculated masses in one breast, areas of poorly defined density or asymmetric parenchyma were seen in the other breast. The first patient had invasive lobular carcinoma in a background of atypical lobular hyperplasia and multifocal LCIS manifesting as a spiculated mass in one breast. Biopsy of the other breast in an area of added density demonstrated multifocal LCIS without microscopic evidence of invasion.

The second patient had an infiltrating ductal carcinoma manifesting as a spiculated mass in one breast. Biopsy of the suggestive area of added density in the other breast revealed a single focus of LCIS in a background of atypical ductal hyperplasia.

One patient with invasive lobular carcinoma and multifocal LCIS in one breast and a mirror-image biopsy negative for malignancy in the contralateral breast opted for yearly mammographic follow-up of the unresected breast. On the first follow-up examination, a new area of added density was noted in the upper inner quadrant of her remaining breast. Biopsy of this area revealed multifocal LCIS.

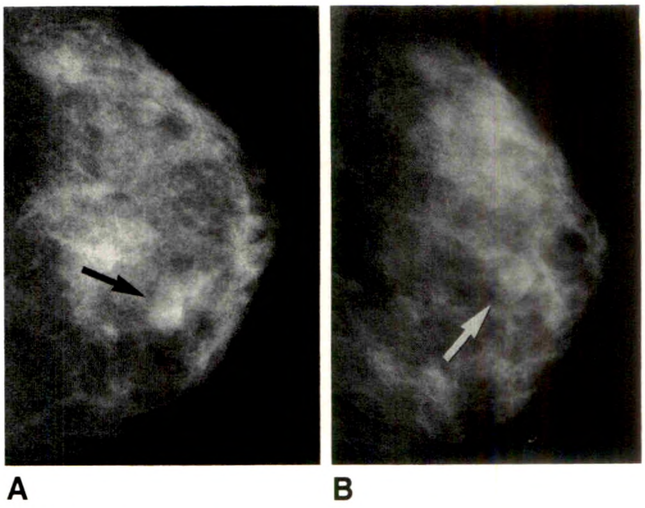

Fig. 3.—Mass alone, not suggestive of malignancy.
***A* and *B*, Craniocaudal (*A*) and mediolateral (*B*) views of left breast of asymptomatic 60-year-old woman show benign-appearing nodule (*arrows*), thought to represent a cyst or fibroadenoma. Biopsy revealed a single focus of lobular carcinoma in situ in area of fibrocystic mastopathy.**

No radiologic abnormalities.—Biopsies of 32 breasts with at least one focus of LCIS and no radiologic findings were done for various reasons (Table 2). The most common indication for biopsy in this group was the presence of a palpable abnormality in one breast or in both breasts in the same patient.

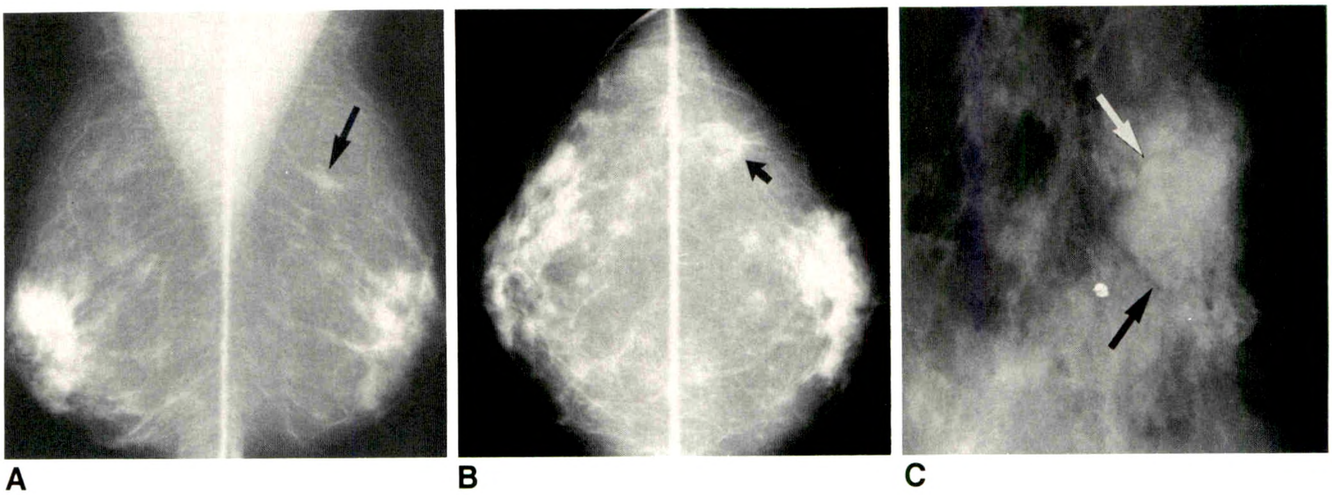

Fig. 4.—Added density or asymmetry of parenchyma.

A and *B*, Direct comparison of both breasts in mediolateral (*A*) and craniocaudal (*B*) projections shows area of asymmetric added density with adjacent benign-appearing calcification (*arrows*) in upper outer quadrant of left breast in this 56-year-old woman.

C, Magnified view of specimen radiograph. Added density (*arrows*) seen adjacent to benign-appearing calcification was area of atypical lobular and ductal hyperplasia with foci of lobular carcinoma in situ.

Fifteen patients with palpable abnormalities had markedly dense breasts on preoperative mammography. Three patients with bilateral palpable masses had bilateral multifocal LCIS.

Five patients with proved LCIS in one breast had mirror-image biopsies that were positive for malignancy in mammographically normal breasts. Two patients had bloody nipple discharge and normal mammograms. Biopsy specimens typically showed intraductal papillomas, duct ectasia, periductal mastitis, and foci of LCIS. Four patients with normal mammograms underwent reduction mammoplasty. Bilateral multifocal LCIS was found in two of these patients. The other two patients had unilateral multifocal LCIS, but both contralateral reduction mammoplasty specimens showed diffuse moderate to severe lobular atypia.

Comparison of LCIS Mammograms with Those of Age-Matched Control Subjects

The LCIS mammograms and those from a group of age-matched control subjects who underwent screening mammography were compared by using a modified form of Wolfe's parenchymal pattern classification (Fig. 5) and a separate classification scheme based on the percentage of the breast occupied by fibroglandular density (Fig. 6).

Breasts with LCIS tended to have greater than 50% fibroglandular density compared with the control group (85% vs 45%), with a higher prevalence of the DY pattern (56% vs 36%). Also, LCIS was rarely seen in an N1 breast (1% vs 29%) or in a breast with less than 25% fibroglandular density (3% vs 33%). There were, however, two exceptions to this trend. In one case, LCIS was found as an added parenchymal density in a fatty replaced breast (Wolfe's N1 pattern) in a patient with an obvious infiltrating ductal carcinoma in the contralateral breast. The other case had an added density with microcalcifications suggestive of an infiltrating ductal carcinoma in a mostly fatty-replaced breast with mildly prominent ducts (Wolfe's P1 pattern).

The percentage of breasts from each group with DY patterns (Fig. 7), with greater than 50% fibroglandular density (Fig. 8), and with less than 50% fibroglandular density (Fig. 9) were plotted against age. The breasts with LCIS tended to have higher percentages of fibroglandular density over the entire age range of the study. The frequency of the DY pattern in postmenopausal patients with LCIS was nearly double that of the control group (30% vs 16%). The frequency with which greater than 50% parenchymal density was present on mammograms after age 50 was also significantly higher in the patients with LCIS than in the control group. Conversely, fewer breasts with less than 50% fibroglandular density had LCIS compared with the control group.

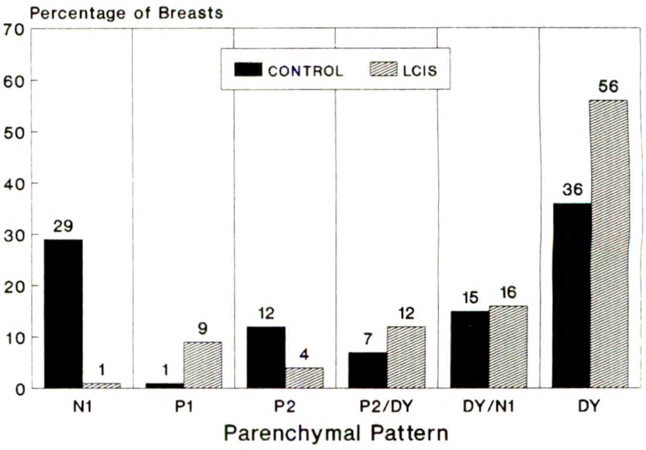

Fig. 5.—Percentages of breasts in lobular carcinoma in situ (LCIS) and control groups vs parenchymal patterns (n = 73 in each group). N1 = fatty replaced breast; P1 = mostly fatty with less than 25% prominent duct pattern; P2 = prominent duct pattern involving more than 25% of breast; P2/DY = P2 pattern with large amounts of added density; DY/N1 = large amounts of added density not occupying entire breast, with no evidence of prominent ducts; DY = sheetlike areas of increased density.

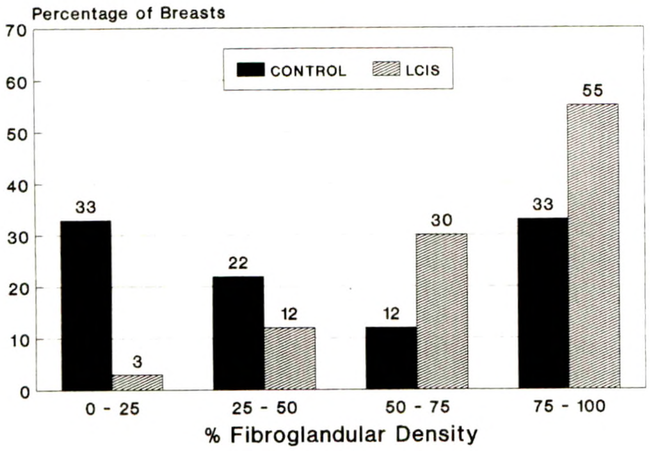

Fig. 6.—Percentages of breasts in lobular carcinoma in situ (LCIS) and control groups vs percent fibroglandular density ($n = 73$ in each group).

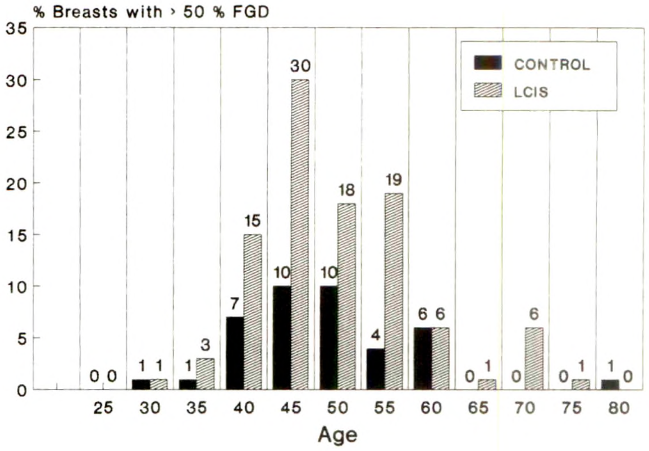

Fig. 8.—Percentages of breasts with greater than 50% fibroglandular density (FGD) vs age in lobular carcinoma in situ (LCIS) and control groups ($n = 73$ in each group).

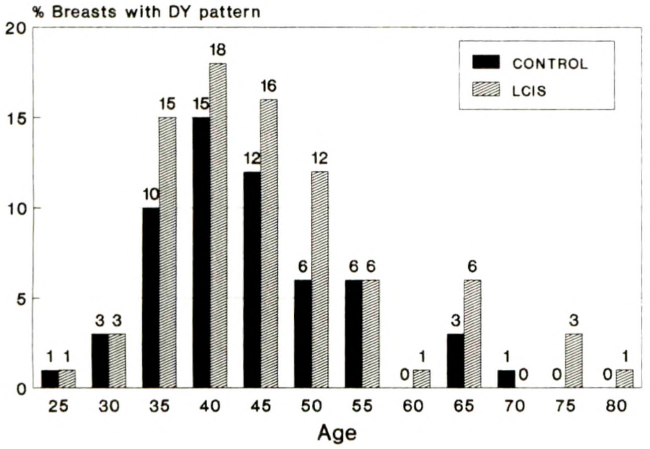

Fig. 7.—Percentages of breasts with any type of DY parenchymal pattern vs age in lobular carcinoma in situ (LCIS) and control groups ($n = 73$ in each group). DY parenchymal patterns include DY, sheetlike areas of increased density; P2/DY, P2 pattern with large amounts of added density; and DY/N1, large amounts of added density not occupying entire breast, with no evidence of prominent ducts.

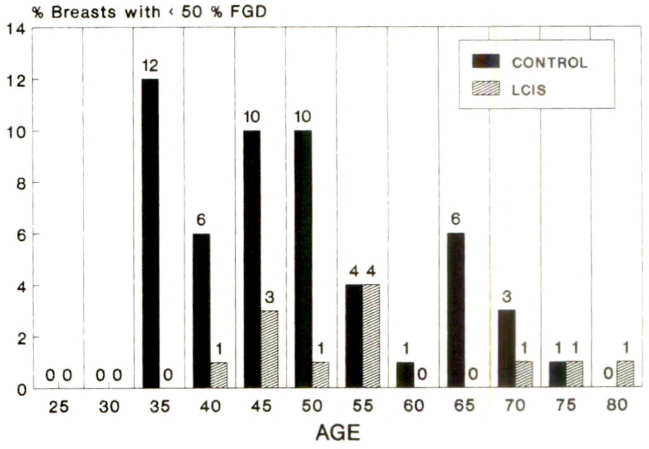

Fig. 9.—Percentages of breasts with less than 50% fibroglandular density (FGD) vs age in lobular carcinoma in situ (LCIS) and control groups ($n = 73$ in each group).

Discussion

One of our goals in undertaking this study was to add to the body of accumulated data on LCIS by describing the clinical, pathologic, and mammographic features of this entity in a series of patients diagnosed at our institution over a 13-year period. We had also hoped to be able to retrospectively identify specific mammographic features or predictors of LCIS that might lead to earlier diagnosis and treatment of this entity. Although we were unable to identify any diagnostic mammographic features of LCIS, analysis of the data reaffirmed previously reported clinical, pathologic, and mammographic features of this neoplasm.

Clinical and Pathologic Data

As in previous reports, LCIS was diagnosed more commonly in younger women (mean age, 49 years) than other breast carcinomas diagnosed at our institution during the same time period (mean age, 58 years). The rates of multifocality (70%) and bilaterality (50%) of disease were consistent with values reported previously in the literature [2, 7–9, 14, 16]. The association of LCIS with simultaneously occurring invasive cancers was also seen in our patients, although at a much higher rate (36%) than that typically quoted in the literature (approximately 5%) [14].

Radiologic-Pathologic Correlation

Radiologic-pathologic data underscore the important concept that LCIS is often present in the absence of mammographic findings. A substantial percentage (44%) of breasts in our series with unifocal or multifocal LCIS had no significant abnormalities on mammography.

Of those breasts with a mammographic abnormality, the majority presented with microcalcifications of various types.

The appearance of clustered, punctate, or stippled microcalcifications has been associated with LCIS in prior reports [1]. Others have found no distinctive morphologic features of the microcalcifications found in areas of LCIS [2, 3]. Radiologic-pathologic correlation failed to demonstrate any relationship between the punctate, clustered type of microcalcifications and foci of LCIS. As in previous studies, microcalcifications led to biopsy in the majority of cases in which LCIS was discovered, but they were not specifically diagnostic or pathognomonic. They are best described as cancer-associated microcalcifications, since they are typically found in tissue near a focus of LCIS and rarely within it [2].

When benign or suspicious clusters of microcalcifications (with or without added densities) were biopsied, LCIS was often found adjacent to areas of sclerosing adenosis or apocrine metaplasia. In fact, 12 of the 20 breasts with isolated LCIS that were biopsied for the presence of microcalcifications had foci of sclerosing adenosis or apocrine metaplasia or both in corresponding tissue specimens. The apparent association in our series between LCIS and sclerosing adenosis is a reflection of the lobular origin of these processes. The microcalcifications were merely present in tissue bearing a type of lobular abnormality (sclerosing adenosis), and when that tissue was sampled, another lobular process (LCIS) was discovered. As Egan [17] has stated, "Sclerosing adenosis has a lobular distribution, but so does lobular carcinoma in situ."

An additional observation was made from the data regarding the association of LCIS with fibroadenomas. It has been previously reported that the majority of carcinomas (60%) found within fibroadenomas are foci of LCIS [18]. In our series, five patients were found to have fibroadenomas with contiguous areas of LCIS; three patients had foci of LCIS extending into fibroadenomas; and two patients had subclinical (microscopic) fibroadenomas arising in areas of fibrocystic mastopathy, atypical lobular hyperplasia, and LCIS. Although our data seem to support the association of LCIS with fibroadenomas, we must emphasize the serendipitous nature of these findings. The discovery of LCIS within or adjacent to fibroadenomas in our series was in fact the result of the removal of a clinical lesion (fibroadenoma) in which incidental microscopic foci of LCIS were found. The association of LCIS with fibroadenomas most likely reflects the common lobular origin of these processes, similar to the association of LCIS with sclerosing adenosis. The true prevalence of carcinomas within fibroadenomas is so low as to be clinically irrelevant.

Comparison of LCIS Mammograms with Those of Age-Matched Control Subjects

For the entire age range of the study, there was a tendency for the DY pattern to occur more often in LCIS patients than in the control group (Fig. 7). This observation was described most recently by Pope et al. [3]. In their series of 26 patients with LCIS, 22 had either a DY or P2 parenchymal pattern. The remaining four breasts had a P1 pattern, and no N1 patterns were seen.

The relationship of in situ breast cancers to parenchymal patterns was addressed by Wolfe et al. [19] in their analysis of a series of 332 incident breast carcinomas. They found the rate of in situ forms of breast cancer (intraductal, LCIS, and combinations thereof) to be highest in patients with the DY pattern, with less frequent but identical rates in the P1 and P2 groups. In their series, as in ours, those patients with a DY pattern and noninvasive disease were diagnosed at a younger age than those with invasive disease.

Although the data in the literature are conflicting, it has been stated that the DY pattern is the least frequently observed mammographic pattern after 30 years of age, and is observed even less frequently after age 50 [20, 21). DeWaard et al. [22] noted a gradual decline in the DY and prominent duct patterns in the postmenopausal years in their series of 23,431 women, with an unexplained second peak occurring after age 60. In our study (Fig. 7), the percentage of breasts with the DY pattern in patients with LCIS older than 50 (30%) was nearly double that of the controls (16%).

Similar observations were made in analysis of the percentage of breasts with given amounts of fibroglandular density in the LCIS and control groups (Fig. 6). Percentage of fibroglandular density for both groups was also plotted against age (Figs. 8 and 9). Whereas 55% of mammograms of control subjects had less than 50% fibroglandular density, only 15% of mammograms of patients with LCIS had similar amounts. Indeed, the majority (85%) of patients with LCIS had greater than 50% fibroglandular density on mammograms, similar to the results obtained for the groups with DY parenchymal patterns (Fig. 5).

The parenchymal patterns and percentages of fibroglandular density seen on mammography were correlated with findings on pathologic examination of removed breast tissue. Breasts from the group with LCIS (particularly those with the DY pattern or with greater than 50% fibroglandular density) showed a propensity for bilaterality and multifocality of various forms of lobular disease. Sclerosing adenosis, fibroadenomatoid mastopathy, and the full spectrum of epithelial changes from lobular hyperplasia to LCIS were found repeatedly in pathologic specimens.

These findings lend further support to the thesis that patients with LCIS have a disease of the entire breast parenchyma, characterized in this study by higher percentages of fibroglandular density for age, a higher rate of the DY pattern compared with that of control subjects, and the almost invariable spectrum of multifocal lobular abnormalities seen in biopsy specimens.

The higher rate of the DY patterns and the higher percentages of fibroglandular density observed on mammograms of patients with LCIS are too nonspecific to be helpful in predicting whether or not a patient might have unrecognized foci of this disease, especially in the premenopausal age group. Another observation was made, however, regarding the relationship of parenchymal patterns and fibroglandular density with age. Unusual persistence of the DY pattern or large amounts of fibroglandular density in the postmenopausal (>age 50) patients with LCIS may be additional proof that mammographically dense breasts are a marker for increased cancer risk in women 50 years old and older [21], although the magnitude of that risk is probably small and may not be independent of other better-known markers of risk for breast cancer. Therefore, the only possible practical application of our data in detecting LCIS on preoperative mammograms is limited to the postmenopausal age group and is already a recognized marker for increased cancer risk in this population.

Despite the numerous technical advances in mammography since LCIS was first described by this method in 1966 [1], there appears to be little to offer in terms of mammographic analysis to aid in the preoperative detection of LCIS. It is interesting to note that, based on their experience over 40 years ago, Foote and Stewart [4] stated that a clinical diagnosis of LCIS could not be made. They openly discussed their inability to recognize LCIS reproducibly in gross specimens. If we consider the mammogram a reflection of gross breast pathology, it is not surprising that there are few, if any, reliable mammographic indicators of its presence.

ACKNOWLEDGMENTS

We thank Debra Correale and Martin Salowey of the medical photography section for assistance with this project.

REFERENCES

1. Snyder RE. Mammography and lobular carcinoma in-situ. *Surg Gynecol Obstet* **1966**;122:255-260
2. Hutter RVP, Snyder RE, Lucas CJ, Foote FW Jr, Farrow JH. Clinical and pathologic correlation with mammographic findings in lobular carcinoma in-situ. *Cancer* **1969**;23:826-839
3. Pope TL, Fechner RE, Wilhelm MC, Wanebo HJ, deParedes ES. Lobular carcinoma in situ of the breast: mammographic features. *Radiology* **1988**;168:63-66
4. Foote FW, Stewart FW. Lobular carcinoma in situ: a rare form of mammary cancer. *Am J Pathol* **1941**;17:491-495
5. Hutter RVP. Lobular carcinoma in situ. *CA* **1982**;32:232-237
6. Hutter RVP, Foote FW, Farrow JH. In situ lobular carcinoma of the female breast, 1939-1968. In: *Proceedings of the 13th annual clinical conference, breast cancer early and late.* Chicago: Yearbook Medical, **1970**:201-226
7. Powers RW, O'Brien PH, Kreutner A. Lobular carcinoma in situ. *J Surg Oncol* **1980**;13:269-273
8. Hutter RVP. The management of patients with lobular carcinoma in situ. *Cancer* **1984**;53:798-802
9. Hutter RVP, Foote FW. Lobular carcinoma in situ: long term follow-up. *Cancer* **1969**;24:1081-1085
10. Rosen PP, Lieberman PH, Braun DW, Kosloff C, Adair F. Lobular carcinoma in-situ of the breast: detailed analysis of 99 patients with average follow-up of 24 years. *Am J Surg Pathol* **1978**;2:225-251
11. Haagensen CD, Lane N, Lattes R, Bodian C. Lobular neoplasia (so-called lobular carcinoma in-situ) of the breast. *Cancer* **1978**;42:737-769
12. Howell A, Harris M. Infiltrating lobular carcinoma of the breast. *Br Med J* **1985**;291:1371-1372
13. Mendelson EB, Harris KM, Doshi N, Tobon H. Infiltrating lobular carcinoma: mammographic patterns with pathologic correlation. *AJR* **1989**;153: 265-271
14. Frykberg ER, Santiago F, Betsill WL, O'Brein PH. Lobular carcinoma in-situ of the breast. *Surg Gynecol Obstet* **1987**;164:285-301
15. Wolfe JN. Breast patterns as an index for risk of developing breast cancer. *AJR* **1976**;126:1130-1139
16. Benfield JR, Fingerhut AG, Warner NE. A multidiscipline view of lobular breast carcinoma. *Am Surg* **1972**;176:115-126
17. Egan RL. Breast calcifications. In: *Breast imaging: diagnosis and morphology of breast diseases.* Philadelphia: Saunders, **1988**:454-490
18. Pick PW, Iossifides IA. Occurrence of breast carcinoma within a fibroadenoma. *Arch Pathol Lab Med* **1984**;108:590-594
19. Wolfe JN, Albert S, Belle S, Salane M. Breast parenchymal patterns: analysis of 332 incident breast carcinomas. *AJR* **1982**;138:113-118
20. Wolfe JN. Breast parenchymal patterns and their changes with age. *Radiology* **1976**;121:545-552
21. Wolfe JN, Albert S, Belle S, Salane M. Breast parenchymal patterns and their relationship to risk for having or developing carcinoma. *Radiol Clin North Am* **1983**;21:127-135
22. DeWaard F, Rombach JJ, Collette HJA, Slotboom B. Breast cancer risk associated with reproductive factors and breast parenchymal patterns. *J Natl Cancer Inst* **1984**;72:1277-1282

Book Review

Clinical Radiology of the Breast. By Eric J. Roebuck. Oxford, England: Heinemann (distributed by Butterworths, Stoneham, MA), 273 pp., 1990. $75, softcover

This thin, softcover textbook from England intends to provide a general review of the clinical practice of mammography. The author emphasizes that it is not meant to compete with the excellent atlases that illustrate in detail the mammographic and sonographic findings of normal variants and pathologic processes. The emphasis is focused clearly on the major issues of screening and the management of the symptomatic patient.

The book has 12 chapters, 11 written by the author. The first chapter, on management of breast cancer, is written by his surgical colleague from the Nottingham breast team. In this first chapter, American readers will notice some differences in the approach to screening and management of breast cancer from what is generally accepted practice in the United States. For economic reasons, screening mammography is not offered to premenopausal women, and subcutaneous mastectomy still is advocated. The chapter has only a cursory discussion of radiation and medical adjunctive therapy. For a surgeon to state that the reasonable ratio of benign to malignant biopsy specimens from a mammography screening program should be 2:1 seems presumptuous when the positive predictive value for palpable masses in the largest surgical series published was 16%, or a ratio of 6:1.

A brief chapter on normal developments and their implications covers first embryology and then mammographic change from puberty through the adult state to involution. The next chapter covers normal variants in some detail, with an attempt to correlate the mammographic and histologic findings. The generic term aberration of normal development and involution (ANDI) is introduced here, and the chapter has a good description of the spectrum of mammographic findings, ranging from the normal variant to benign breast disease. A plea is made both here and in a later chapter on mammographic signs and the radiology report to standardize radiologic nomenclature on benign breast changes. The next chapter curiously is titled "Dangers of Mammography and Some Benefit" and concludes that a favorable benefit-to-risk ratio for mammography exists for women who are more than 30 years old. Chapter 5 addresses the basic principles of breast imaging, with strong emphasis on the technical aspects of film-screen mammography and only a cursory discussion of other techniques. This is supplemented by subsequent chapters on sonomammography and on positioning for radiographs, including needle localization of nonpalpable lesions.

Short shrift is given to mammographic signs. The book has 11 pages on calcifications and five pages on masses, with somewhat limited illustrations. A short section on quality assurance in reading and interpretation (terms that are defined carefully and are not used interchangeably in this text) complete this chapter.

Chapter 9 discusses risk factors, including histologic changes from cellular atypia to lobular carcinoma in situ, which are designated the biologic "border lands." The term "high chance area" is introduced, and the hypothesis is offered that this can be identified by using a combination of mammographic signs. A prospective trial is in progress, and if these nonmalignant changes can be shown to signify increased risk for the development of cancer, this will have a positive impact on the management of patients who have these changes. The chapter concludes with a discussion of several types of breast cancer and their mammographic appearance. The next two chapters cover the mammographic team and the workup of the symptomatic patient. The concluding chapter discusses in some detail screening philosophy and results and offers a series of rather complex algorithms arrived at by consensus of the radiologist, surgeon, and pathologist.

This easily read book provides a good review of the field, yet is concise and relatively complete. The organization is not always logical, and some redundancy occurs. The book lends itself better to reading in its entirety rather than as a reference work, particularly as the index is incomplete. When compared with *Breast Imaging*, by Daniel B. Kopans, a less expensive and more readily available textbook in the United States, it falls significantly short in several areas. The reproductions of the mammograms in the Roebuck text are definitely inferior, particularly when they are meant to demonstrate calcifications. The Kopans text is more comprehensive and much better organized, its references are more complete, the writing is more authoritative, and the index is much more useful. Therefore, I can recommend this book only to those readers who would like to broaden their professional horizon by being exposed to a somewhat different perspective on this timely subject.

Herbert F. Gramm
New England Deaconess Hospital
Harvard Medical School
Boston, MA 02215

Gadopentetate Dimeglumine-Enhanced Chemical-Shift MR Imaging of the Breast

Deborah Rubens[1]
Saara Totterman[1]
Anna K. Chacko[1,2]
Kamal Kothari[3]
Wende Logan-Young[4]
Jerzy Szumowski[1,5]
Jack H. Simon[1,6]
Elizabeth Zachariah[7]

Standard T1-weighted MR images enhanced with gadopentetate dimeglumine show relatively minimal enhancement of breast lesions due to the high background signal from fat in the breast. Strongly enhancing lesions may become isointense relative to the fat signal and become invisible or indistinct after contrast administration. Fat-suppressed chemical-shift imaging (CSI) combined with administration of gadopentetate dimeglumine improves lesion detection and characterization in other areas of the body where a strong lipid signal is present. We evaluated this technique in the breast. Twenty patients with mammographic lesions were studied with standard unenhanced T1- and T2-weighted images and enhanced T1-weighted images, as well as with CSI before and after administration of gadopentetate dimeglumine. The series were ranked independently for border and matrix characteristics. The border was assessed for a smooth, irregular, or spiculated margin. The matrix or internal substance was evaluated for visibility and type of enhancement, homogeneous or inhomogeneous. The enhanced CSI images were superior to all other images in the depiction of border and matrix characteristics. Of 20 patients, a corresponding mass was detected on MR in 14. In two of the 14 patients, the lesion was seen only on the enhanced CSI images. Chemical-shift artifacts on enhanced T1-weighted images obscured border detail in several cases.

Enhanced CSI improves visualization of breast lesions as compared with conventional MR imaging with or without enhancement. The enhanced CSI technique produces differential enhancement between glandular tissue and lesions while suppressing the signal from fat. This improves the visualization of border and matrix characteristics and depicts lesions that otherwise might be obscured.

***AJR* 157:267-270, August 1991**

Recent articles show significant enhancement of carcinomas of the breast after IV injection of gadopentetate dimeglumine [1, 2]. In one series, 20% of lesions were detected only because of the tumor enhancement [1]. On some enhanced breast images, the abnormal tissue became isointense relative to surrounding fat [1, 2]. This causes a problem because the borders of the lesion become indistinct and small or infiltrating lesions that blend in with the fat may go undetected. Breast lesions are unique in that they may be bordered by glandular tissue, fat, or a combination of the two. An optimal imaging technique must provide maximal contrast between the lesion, the fat, and the surrounding normal glandular tissue. Studies evaluating lipid suppression with chemical-shift (CSI) MR imaging have shown improvement at fat/soft-tissue interfaces in the orbit [3], pelvis [4], and musculoskeletal system [5]. The hybrid method of CSI increases the dynamic range of the gray scale, which accentuates water contrast differences [6]. The combination of CSI with paramagnetic contrast material enhancement [7] should improve lesion visibility in the breast, both by eliminating the strong background signal from the lipid and by expanding the effective gray scale of water.

Materials and Methods

MR images of the breast were obtained in 32 women in whom lesions had been detected on mammograms and/or in whom palpable abnormalities had been found. The MR images

Received September 24, 1990; accepted after revision February 15, 1991.

This work was supported by Berlex Laboratories, Wayne, NJ. Pulse sequence development was supported in part by a Seed Grant Award from the Radiological Society of North America to J. Szumowski.

[1] Department of Radiology, University of Rochester School of Medicine and Dentistry, 601 Elmwood Ave., Rochester, NY 14642. Address reprint requests to D. Rubens.

[2] Present address: Department of Radiology, Letterman Army Medical Center, Presidio of San Francisco, CA 94129-6700.

[3] Ridgewood Diagnostic Imaging, 3101 W. Ridge Rd., Rochester, NY 14626.

[4] Breast Clinic of Rochester, 1351 Mt. Hope Ave., Rochester, NY 14620.

[5] Present address: Department of Radiology, The Oregon Health Sciences University, 3181 S.W. Sam Jackson Park Rd., Portland, OR 97201.

[6] Present address: MRI, University of Colorado Health Sciences University, 4200 E. Ninth Ave., Denver, CO 80262.

[7] 492 Portlock Rd, Honolulu, HI 96825.

0361-803X/91/1572-0267
© American Roentgen Ray Society

of the first 20 patients with technically adequate scans were evaluated. Of these 20 patients, five had carcinoma, four had fibroadenomas, four had fibrocystic disease, four had cysts, two had sclerosing adenosis, and one was presumed to be without tumor after mammograms were unchanged after 18 months. Three of the 32 patients (two with carcinoma and one with a cyst) were excluded owing to inadequate CSI MR images.

MR imaging was performed with a 1.5-T magnet (Signa, General Electric Medical Systems, Milwaukee, WI). The patients were positioned prone, and a single breast was studied with a single-turn solenoid loop-gap resonator [8]. After an axial image was obtained to localize the lesion, a T1-weighted spin-echo (SE) series, 600/20 (TR/TE); a proton density-weighted series, 2000/20; a T2-weighted series, 2000/80; and a T1-weighted hybrid (CSI) series tuned for lipid suppression, 600/20, were performed [6]. All images were obtained in the sagittal plane in the same location of the breast and included the majority of the breast tissue, directed medially or laterally to include the region of the lesion detected on mammograms. The other imaging parameters included 5-mm slices with a 1.5-mm gap, two excitations, a 256 × 128 matrix, and a 14- to 18-cm field of view.

After these unenhanced images were made, gadopentetate dimeglumine (Magnevist, Berlex Labs., Wayne, NJ) was injected IV in 1–2 min at a dose of 0.1 mmol/kg. This was followed by immediate (0–15 min) and delayed (15–25 min) T1-weighted SE and CSI images with the slice and imaging parameters described above. According to protocol, the T1-weighted enhanced images were obtained before the enhanced CSI images for both the immediate and delayed images. To enable true evaluation of enhancement after contrast injection, we kept the transmit and receiver gains constant for each standard T1-weighted SE series. Different constant values were maintained for CSI series. Receiver gain in each unenhanced series was diminished to prevent saturation of the amplifiers from the increased signal intensity after contrast administration. Twelve slices were available on the CSI series, 16 slices on the T1-weighted SE series, and 20 slices on the T2-weighted SE series.

A total of eight image series were evaluated: T1-weighted, proton density-weighted (2000/20), T2-weighted (2000/80), and CSI unenhanced series; and immediate T1, delayed T1, immediate CSI, and delayed CSI enhanced series. The results of these series were ranked in ascending order; the best score was 8 and 1 was the worst. Rankings were given by consensus between two readers. Images were compared for the demonstration of the border characteristics of a lesion (smooth, irregular, or spiculated). The matrix or internal substance of the lesion was evaluated for visibility of heterogeneous enhancement, homogeneous enhancement, or lack of enhancement. Matrix ranking placed heterogeneity above homogeneity if the same lesion differed in the various series. If the pattern of lesion enhancement was the same, the series with the greatest enhancement scored highest. A tie between two series resulted in an averaging of the two rankings rather than arbitrarily ranking one above the other. For example, if two series tied for the best border discrimination, each would receive a score of 7.5. If a lesion was not visualized on an MR imaging series or a series was not performed, a score of 0 was assigned. After ranking, the results were tabulated by addition of the scores of each separate series.

Results

Although all lesions were visible on mammography, the abnormality was detected on MR images in only 14 of the 20 patients. Two of the 14 lesions were seen only with the enhanced CSI series. Both of these lesions were documented by histology as sclerosing adenosis. Of the six patients in whom no corresponding lesion was documented on MR imaging, five had microcalcifications on the mammogram with no associated mass. One of these patients had a 1- by 3- by 4-cm intraductal carcinoma. The remaining four had histologic evidence of benign lesions, including apocrine metaplasia, fibrosis, and fibrocystic disease. In the remaining patient in whom no lesion was identified on MR imaging, an asymmetric soft-tissue density was seen on a single mammogram view. This enhanced in a fashion similar to the remainder of the breast tissue on MR imaging and was thought to represent asymmetric glandular tissue. In six of the 20 patients, lesions were seen on MR imaging that were not seen on the mammogram. Three of these six lesions were cysts. The other three were solid tumors with smooth borders and showed uniformly increased signal intensity on T2-weighted images as well as on all enhanced CSI images. All three lesions measured less than 5 mm and were presumed to be incidental fibroadenomas.

The ranking of the border characteristics of the lesions on MR images was significant in that the immediately enhanced CSI images had a score of 118 out of the total maximum of 160 points. The sequence with the next highest score was the delayed enhanced CSI with a score of 91. The other series scored as follows: T2-weighted (2000/80) = 66, T1-weighted = 62.5, immediately enhanced T1-weighted = 62, delayed enhanced T1-weighted = 60.5, unenhanced T1-weighted CSI = 55, and proton density-weighted (2000–20) = 49. If the four patients with cysts as lesions were excluded, the maximum possible score was 128 points. The scores for immediately and delayed enhanced CSI images of solid lesions dropped to 106 and 81, respectively, but the T2-weighted score dropped to 34.

The matrix ranking, including all lesions, resulted in a score of 126 out of 160 possible points, for the immediately enhanced CSI series. The delayed enhanced CSI series scored 98.5, followed by T2-weighted at 77.5, delayed enhanced T1-weighted at 66, immediately enhanced T1-weighted at 61, unenhanced T1-weighted CSI at 60.5, proton density-weighted at 42.5, and T1-weighted at 33. Again, when cysts were excluded, the immediately and delayed enhanced CSI scores dropped to 105 and 78, respectively, and the T2-weighted series dropped to 49.

Discussion

Our results show that enhanced CSI imaging provided better delineation of the border characteristics of breast lesions than did standard SE sequences either with or without contrast material. In particular, the advantage of the enhanced CSI series over the unenhanced T1-weighted SE series was the improved contrast between the lesion and the normal breast tissue (Fig 1.). The expanded gray scale aids in delineation of small lesions surrounded either totally or in part by glandular tissue. For lesions adjacent to fat, the elimination of chemical-shift artifact improved the visibility of border irregularity (Fig 2.). By suppressing the signal from fat, enhanced CSI imaging also prevents an intensely enhancing lesion from becoming isointense relative to the surrounding lipid.

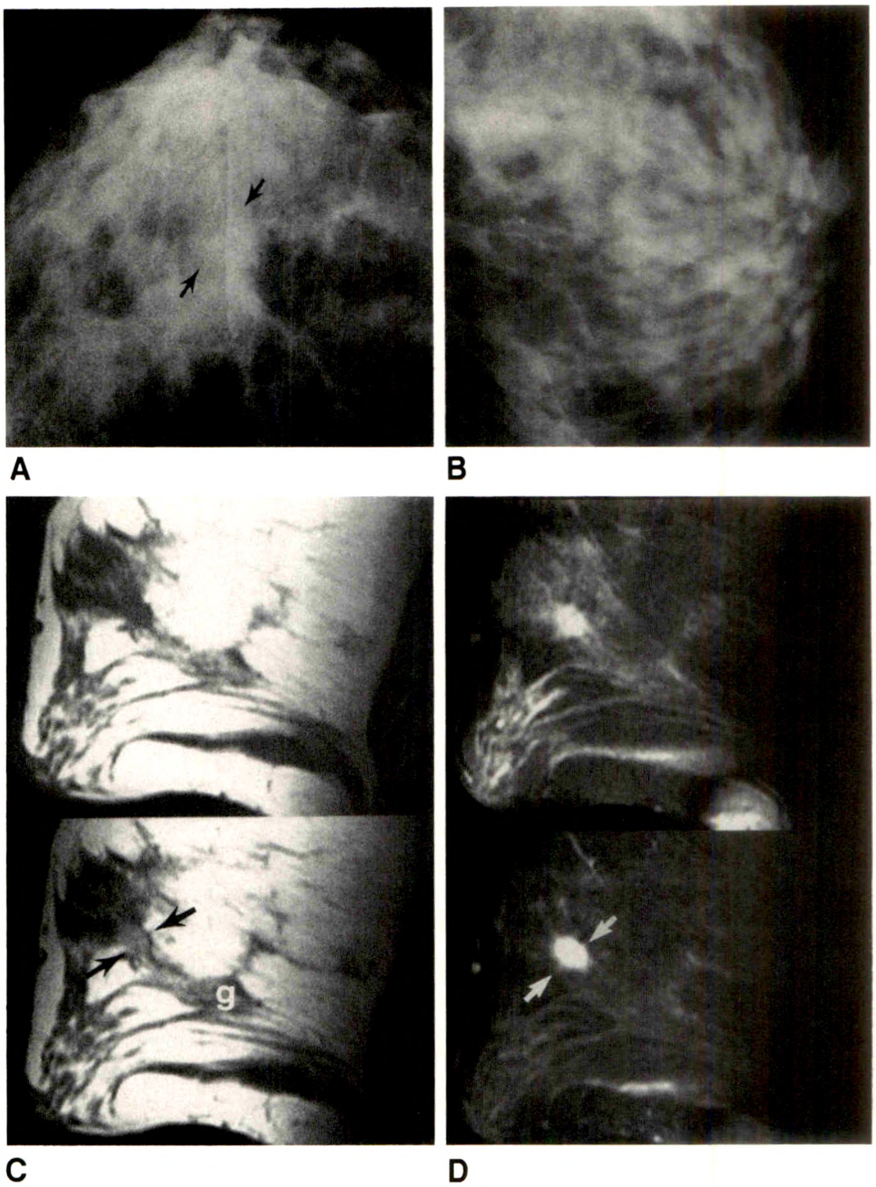

Fig. 1.—47-year-old woman with 5-mm infiltrating tubular carcinoma of the breast.

A, Craniocaudal mammogram of right breast suggests an 8-mm spiculated lesion (*arrows*) 3 cm posterior to nipple.

B, On lateral mammogram, lesion is difficult to distinguish from dense breast tissue.

C, T1-weighted SE MR images obtained before (*top*) and after (*bottom*) contrast administration show moderate enhancement of lesion (*arrows*) similar to that of adjacent glandular tissue (g). Note low signal intensity of posterior margin and smooth border characteristics anteriorly after contrast administration.

D, T1-weighted unenhanced chemical-shift imaging (CSI) (*top*) and enhanced CSI (*bottom*) series (600/20). Note marked enhancement of lesion after contrast administration as compared with adjacent glandular tissue. Border spicules (*arrows*) are visible on enhanced images because of elimination of chemical-shift artifact and improved contrast with respect to fat.

Matrix characteristics also were shown better on the enhanced CSI images because of the expanded gray scale of water that results from lipid suppression. In particular, peripheral enhancement with a lower-signal center was detected in carcinomas as compared with uniform enhancement in sclerosing adenosis and fibroadenomas. This has not been emphasized previously in the literature. A prospective evaluation with a larger number of patients will be necessary to evaluate the significance of this finding.

The next most valuable series to the enhanced CSI series for lesion diagnosis was the T2-weighted SE series. This was the most helpful sequence in evaluating cysts. If cysts are excluded, the value of the T2-weighted series becomes comparable to that of the T1-weighted SE series. The enhanced T1-weighted series, either immediate or delayed, was slightly worse at border delineation than the unenhanced T1-weighted SE series. This was due to pronounced postenhancement chemical-shift artifacts at the lesion margin, which interfered with border evaluation. The matrix was evaluated for degree and distribution of enhancement, and therefore was usually better seen on enhanced images. Considering the small number of patients in the series, and the relatively close ranking of the standard T1- and T2-weighted SE series, the only large difference in scores lies between the two enhanced CSI series and the remaining six series that were evaluated.

Previous studies [2, 7] have discussed the importance of signal intensity changes for differentiation of benign from malignant disease of the breast. We found it impossible to make identical slices with the various MR techniques because of involuntary patient motion. Because volume averaging would cause error in intensity measurements, we have not evaluated these series for absolute enhancement values of the lesions. The 5-mm slice thickness was sufficient, particularly in lesions 1 cm or larger, to allow preliminary matrix and border discrimination without significant error from volume averaging.

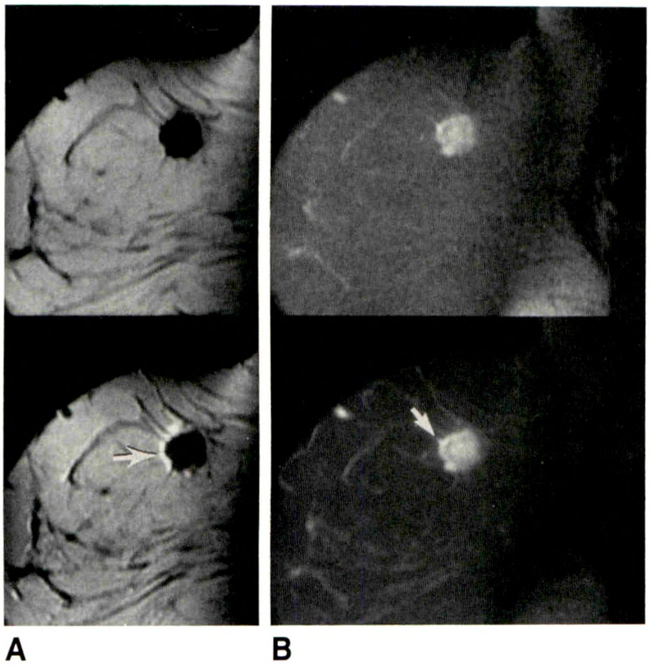

Fig. 2.—62-year-old woman with infiltrating intraductal breast carcinoma.

A, T1-weighted SE MR images of a 1.5- by 1.6-cm infiltrating carcinoma before (*top*) and after (*bottom*) contrast administration. Marked chemical-shift artifact (*arrow*) obscures border detail. Matrix appears fairly uniform and little enhancement is appreciated.

B, T1-weighted unenhanced chemical-shift imaging (CSI, *top*) and enhanced CSI (*bottom*) series (600/20). Chemical-shift artifact has been eliminated and a small spicule can be seen along anterior margin (*arrow*). Note heterogeneous matrix, which was not evident on standard SE series. Signal intensity of lesion has been held constant, while background intensity of enhanced CSI series has decreased, indicating lesion enhancement.

Six of 20 lesions seen on mammograms were not detected by MR imaging. The most significant lesion missed on the MR scans was the 1- by 3- by 4-cm intraductal carcinoma. Considering the 5-mm slice thickness used, the lesion should not have been missed because of its size. Perhaps the lack of invasiveness contributed to the problem in this carcinoma.

In conclusion, enhanced CSI imaging improves MR visualization of breast lesions as compared with conventional SE MR imaging with or without gadopentetate dimeglumine. This is accomplished by expansion of the gray scale, which yields differential visible enhancement between the glandular tissue of the breast and enhancing lesions. In addition, matrix characteristics of lesions can now be identified. The suppression of the signal from background fat eliminates chemical-shift artifacts and enables visualization of lesion detail in the border, which otherwise may be obscured. Our preliminary results suggest that enhanced CSI imaging should replace conventional T1-weighted enhanced imaging in the future. Further studies will be required to determine the usefulness of MR imaging in the characterization of lesions and to define its role as an adjunct to mammography and physical examination.

REFERENCES

1. Kaiser WA, Zeitler E. MR imaging of the breast: fast imaging sequences with and without Gd-DTPA. *Radiology* **1989**;170:681–686
2. Heywang SH, Wolf A, Pruss E, Hilbertz T, Eiermann W, Permanetter W. MR imaging of the breast with Gd-DTPA: use and limitations. *Radiology* **1989**;171:95–103
3. Simon JH, Szumowski J, Totterman S, et al. Fat suppression magnetic resonance imaging of the orbit. *AJNR* **1988**;9:961–968
4. Totterman S, Spataro R, Rubens D, et al. Fat suppression technique in the detection and staging of cervical, bladder and prostate carcinoma (abstr). *Radiology* **1987**;165(P):235
5. Totterman S, Weiss S, Szumowski J, et al. MR fat suppression technique in the evaluation of normal structures of the knee. *J Comput Assist Tomogr* **1989**;13(3):473–479
6. Szumowski J, Eisen JK, Vinitski S, Haake PW, Plewes DB. Hybrid methods of chemical shift imaging. *Magn Reson Med* **1989**;9:379–388
7. Simon JH, Szumowski J. Chemical shift imaging with paramagnetic contrast material enhancement for improved lesion depiction. *Radiology* **1989**;171:539–543
8. Hornak JP, Szumowski J, Rubens D, Janus J, Bryant RG. Breast MR imaging with loop-gap resonators. *Radiology* **1986**;161:832–834

Pictorial Essay

Lipid Cyst: Classic and Atypical Appearances

Kathryn Evers[1] and Rosalind H. Troupin

Lipid cysts, a specific type of fat necrosis, frequently have a pathognomonic appearance on radiographs. This consists of a lucent lesion surrounded by a smooth rim that may or may not be calcified. Occasionally, lipid cysts with unusual mammographic appearances are encountered. An appreciation of some of these appearances may prevent unnecessary biopsies.

Fat necrosis of the breast is a common benign condition that can cause a wide array of mammographic findings, including spiculated masses, calcifications of variable size and morphology, localized skin thickening, and lipid-filled cysts [1]. Although physical findings may be absent, fat necrosis

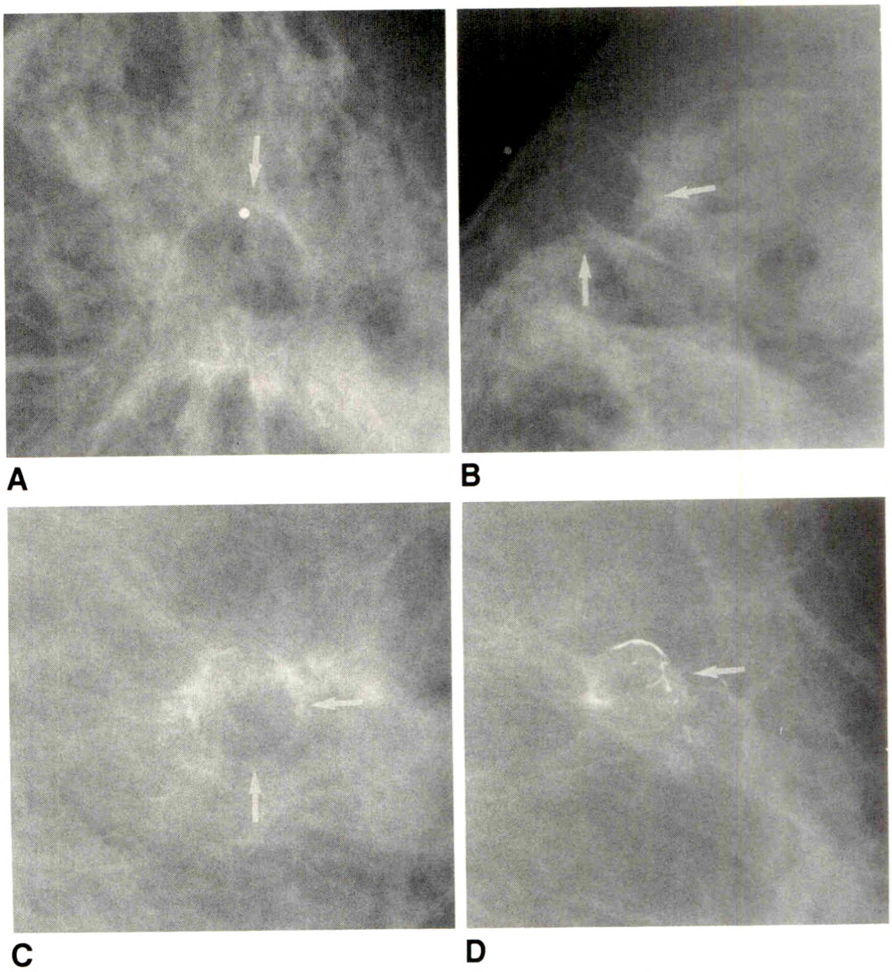

Fig. 1.—Typical lipid cysts in two patients.
A, Cephalocaudal view shows typical mammographic appearance of a lipid cyst (*arrow*): round, thin-walled, and radiolucent.
B, Mediolateral view shows superficial location of cyst (*arrows*) shown in *A*.
C, Mediolateral view in another patient shows a typical noncalcified lipid cyst (*arrows*) 6 months after lumpectomy and irradiation for an early carcinoma.
D, Mammogram of same patient in *C* obtained 2½ years later shows curvilinear calcifications of portions of cyst wall (*arrows*).

Received January 24, 1991; accepted after revision March 19, 1991.

[1] Both authors: Department of Radiology, Hospital of the University of Pennsylvania, 3400 Spruce St., Philadelphia, PA 19104. Address reprint requests to K. Evers.

AJR 157:271–273, August 1991 0361–803X/91/1572–0271 © American Roentgen Ray Society

can be manifested clinically as a hard mass with associated retraction and an alarming fixation to the overlying skin. The patient usually has a history of trauma or surgery. In our patient population, areas of fat necrosis most often are encountered in areas of previous surgery, particularly after reduction mammoplasty or lumpectomy with irradiation.

Pathologically, fat necrosis is a sterile, inflammatory process that varies in appearance depending on the stage of the lesion. Foreign-body giant cells, fat-filled macrophages, and interstitial infiltration by plasma cells are consistently present. Saponification of fat leads to the formation of vacuoles that then become surrounded by macrophages. Healing by fibrosis begins at the periphery and eventually may replace the entire area or leave a persistent cystic cavity.

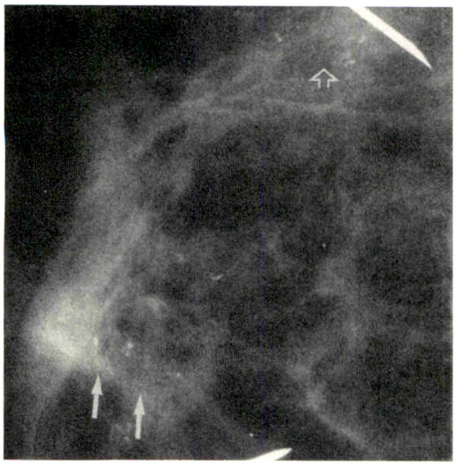

Fig. 2.—Atypical calcification. Coned-down view of subareolar region during needle localization shows noncurvilinear calcifications in area of a lipid cyst (*solid arrows*) after lumpectomy and irradiation in addition to a second area of calcification (*open arrow*). Biopsies of both areas showed fat necrosis.

A lipid cyst is the distinctive form of fat necrosis in which a macroscopic pool of oil develops, rimmed by a thin membrane. Such cysts have been aspirated and analyzed by Hoeffken and Lanyi [2], who have shown that the content consists almost entirely of pure neutral fat. These lesions most often have a pathognomonic mammographic appearance: a lucent center bordered by a smooth, thin, water-density rim (Figs. 1A and 1B). Although the rim may gradually calcify [3], the center of the lesion generally remains radiolucent (Figs. 1C and 1D). Under these circumstances, the mammogram is diagnostic, and no further evaluation is necessary.

Oil cysts with unusual mammographic appearances (Troupin RH, presented at the annual meeting of the American Roentgen Ray Society, May 1988) can be more troubling. Adjacent calcifying necrotic fat may form atypical calcifications (Fig. 2), including clustered linear or branching forms indistinguishable from a malignant lesion. At other times, the content of the cyst may lose its uniform radiolucency, thereby simulating a solid lesion, simple cyst, or abscess (Fig. 3). Fibrotic distortion of the rim may cause the edges of the cyst wall to become irregular. If this irregularity develops in conjunction with loss of the central radiolucency, the appearance basically becomes that of a spiculated nodule (Fig. 3C).

If the cyst contains a mixture of oil and serosanguineous fluid, the mixture can layer, as expected, on horizontal-beam lateral films (Fig. 4). In the case illustrated, a recommendation to follow up the patient rather than perform a biopsy was declined on the basis of highly suggestive clinical findings. Pathologic examination showed fat necrosis with no evidence of neoplasm.

In only one instance have we seen a spherical density within the lucent cyst, presumably some form of fibrin ball (Figs. 5A and 5B). Hoeffken and Lanyi [2] published one example of a nodule within a lipid cyst and stated that they would recommend biopsy in such a case if associated calcifications were present. We recommended follow-up for our

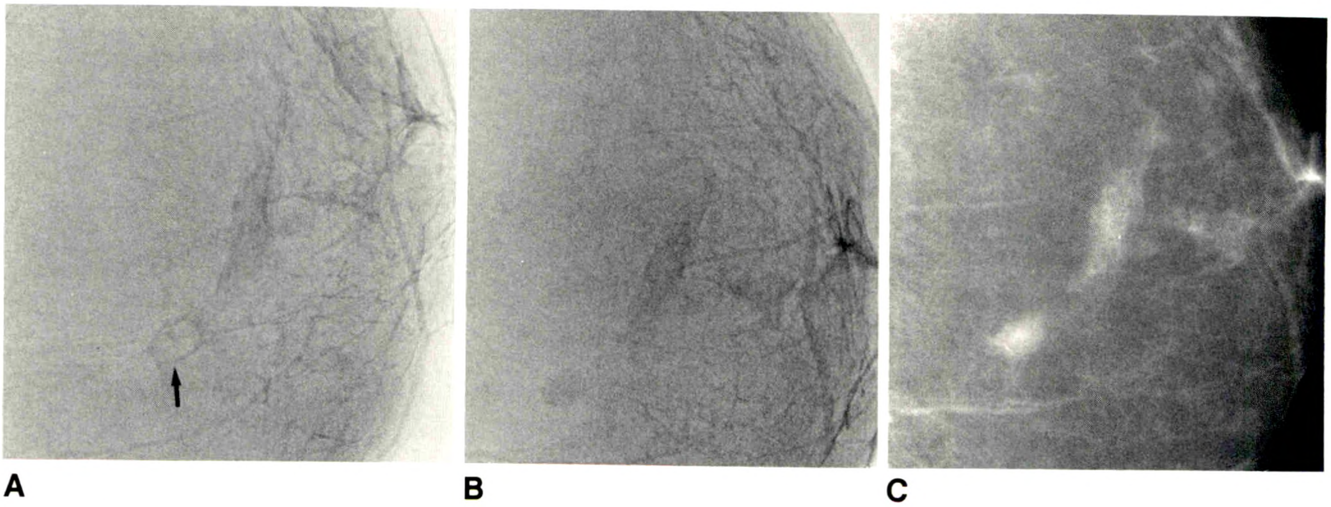

Fig. 3.—Opacifying lipid cyst.
A, Xeromammogram obtained 1 year after biopsy of a benign breast lesion shows a typical lucent lipid cyst (*arrow*) at end of biopsy scar.
B, Xeromammogram obtained 3 years after biopsy shows content of cyst is denser than in *A*.
C, Film-screen mammogram obtained 5 years after biopsy shows a spiculated nodule with a single coarse calcification at site of former lipid cyst.

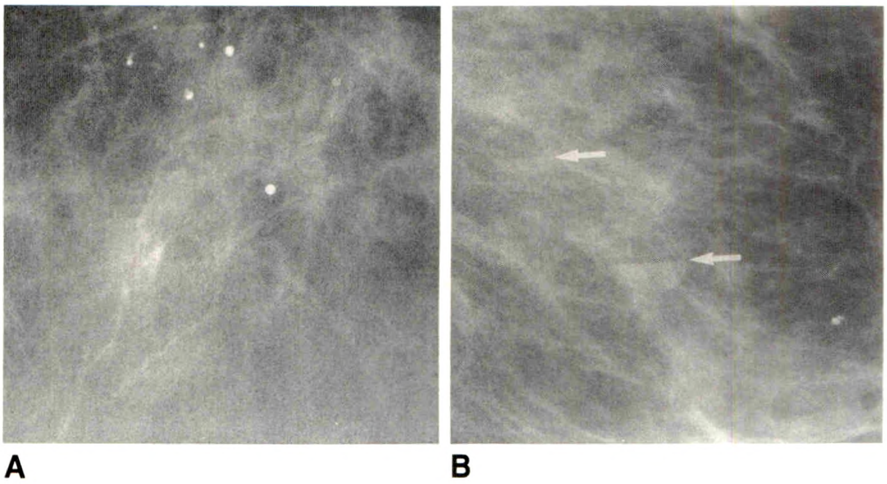

Fig. 4.—Fat-fluid levels. Patient noted a palpable mass approximately 1 year after trauma to chest wall.

***A*, Cephalocaudal view shows nonspecific heterogeneity with dense and lucent components.**

***B*, Mediolateral view (photographically coned down) with horizontal beam shows lipid cysts containing fat-fluid levels (*arrows*).**

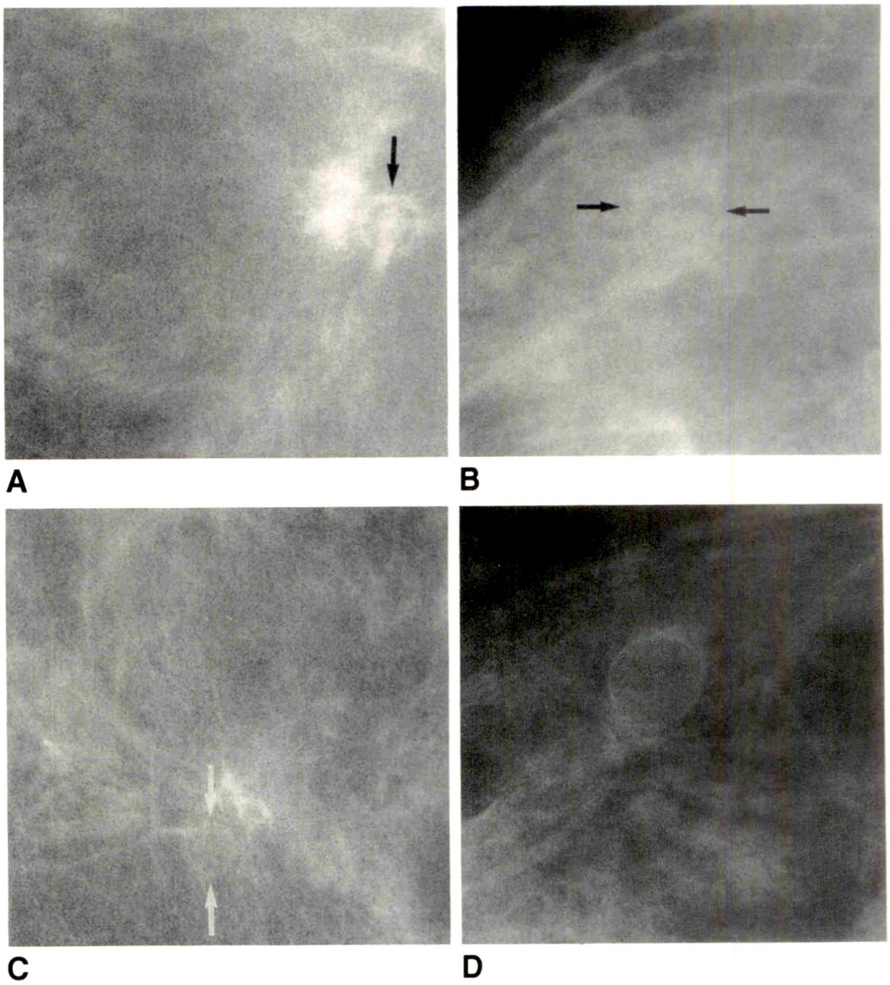

Fig. 5.—Lipid cyst with fibrin ball 1 year after biopsy of benign lesion.

***A*, Cephalocaudal view shows postoperative scar, rimmed lucency, and central density (*arrow*).**

***B*, Mediolateral view (photographically coned down) shows a spherical soft-tissue nodule within radiolucent cyst (*arrows*).**

***C*, Cephalocaudal view obtained 1 year later shows no nodule apparent within lipid cyst (*arrows*).**

***D*, Mediolateral view (photographically coned down) shows content of cyst is homogeneous and of medium density.**

patient, and subsequent films showed that the intracystic nodular component had resolved, leaving a homogeneous, ground-glass, medium-density center (Figs. 5C and 5D).

With increasing use of lumpectomy and irradiation as an alternative to mastectomy, fat necrosis in general and lipid cysts in particular will be encountered more frequently. Familiarity with unusual but acceptable variants may prevent some unnecessary biopsies.

REFERENCES

1. Bassett LW, Gold RH, Cove HC. Mammographic spectrum of traumatic fat necrosis: the fallibility of "pathognomonic" signs of carcinoma. *AJR* **1978**;130:112–122
2. Hoeffken W, Lanyi M. *Mammography*. Philadelphia: Saunders, **1977**: 244–245
3. Bassett LW, Gold RH, Mirra JM. Nonneoplastic breast calcifications in lipid cysts: development after excision and primary irradiation. *AJR* **1982**;138:335–338

Zum Grünen Glas

Philip C. Goodman[1] and Ronald L. Eisenberg[2]

Wilhelm Conrad Roentgen was born March 27, 1845, in a small wood-framed home in Lennep, a town in the Rhine Province of Germany. His parents and ancestors had for many generations been successful textile merchants, although some pursued other professions. When he was 3 years old, his family, perhaps prompted by political considerations, sold their home and moved to Apeldoorn, Holland. Here, at the appropriate age, Wilhelm began public school. The known records suggest that he was an ordinary student. Any inclination toward future brilliance in physics was well hidden and might have stayed that way. However, an uneventful educational experience was not to be Roentgen's fate. After a brief time at a private boarding school not far from his home, he surfaced at the Utrecht Technical School in 1862. One day he and his fellow students briefly found themselves alone in the classroom. In the instructor's absence, a classmate approached the fire screen and proceeded to draw on it a not too flattering caricature of the teacher. In his apparent desire to obtain a closer look, Roentgen approached the fire screen at the same time the teacher entered the room. Sensing the mirth among the students and noting Roentgen's proximity to the cause of the laughter, the instructor decided to make an example of young Wilhelm. He at first accused Roentgen of being the perpetrator of the prank. When finally convinced of Roentgen's innocence, he demanded that Wilhelm identify the real culprit. The stalwart Wilhelm was faithful to his classmate and would not divulge the name. In response to this defiance of authority, Roentgen was brought before a panel of school officials who decided that expulsion was appropriate punishment. The ramifications of this decision were far-reaching. By this time, Roentgen had decided to attend a university. Failure to graduate from high school would be a significant impediment to this goal. Family intercession failed to dissuade the panel from its course of action, and Roentgen was expelled. He now embarked on an independent course of study, hoping to someday obtain the equivalent of a high school diploma. Independent study suited him well, and his endeavors in classical Greek and Latin and in other subjects were enthusiastic and successful. For guidance, he had enlisted the aid of a man who not only served as his mentor but also would be one of his examiners. Unfortunately, just before Roentgen's high school equivalency examination, this instructor, a friend and supporter of Roentgen, became ill and was replaced by another man who had been on Roentgen's disciplinary panel. Whether this had a deleterious effect on Roentgen's performance or provided the means for sabotage of the examination, Roentgen's attempt to obtain a high school credential failed.

At this time, Roentgen's plans for higher education seemed bleak indeed. However, somewhat undaunted, he audited courses at the University of Utrecht, where he caught the attention of a young Swiss national named Thormann. Thormann's advice to Roentgen was to apply to the Polytechnical University of Zurich, where Roentgen was admitted in 1865. By this time, he had developed a discipline that he exhibited throughout his scientific career, and as a mature, somewhat older college student, he did considerably better at the University than he had at his elementary school. His courses led to a degree in mechanical engineering. After graduation in 1868, he met August Kundt, the head of the Department of Physics at the University of Zurich. Kundt offered, and Roentgen accepted, a position as a laboratory assistant. One year later, Roentgen received a Ph.D. in physics, having published his thesis on the properties of gases. His career was officially launched.

In Zurich, Roentgen lived in a modest upper-floor apartment on the busy Seilergraben (Fig. 1). It is easy to imagine his somewhat arduous daily walks up a hill to the University lecture halls and laboratories. However, it was in the opposite direction that he took some major steps toward another successful portion of his life: marriage. Walking approximately 5–10 min east, then south with an appropriate turn here and there, Roentgen frequently found himself at an ancient inn and restaurant named Zum Grünen Glas (Fig. 2). At the time, Zum Grünen Glas was already 500 years old and a popular gathering place for university students. Perhaps none was as faithful in attendance as Roentgen, whose many visits were inspired not only by the intelligent discussion conducted by the innkeeper but also by the presence of the innkeepers' daughter, Anna Bertha Ludwig. Anna and Wilhelm's relationship developed slowly, but eventually the two were wed in 1872. Roentgen often credited the loving affection of his wife for much of his success, and throughout their lives, Anna Bertha and Wilhelm Conrad were a devoted couple.

Zum Grünen Glas is still open for business. Its interior has seen many a university student, tourist, and notable, such as Roentgen and Richard Wagner. Over the years, it was surely a traditional Swiss inn and tavern. However, if you expect to visit it now for a stein of Swiss ale with fondue, choose another establishment. At least as of mid-1990, Zum Grünen Glas was a Chinese restaurant.

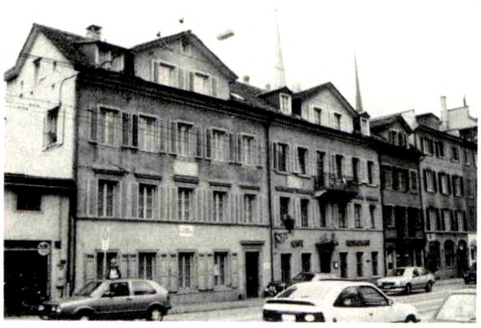

1

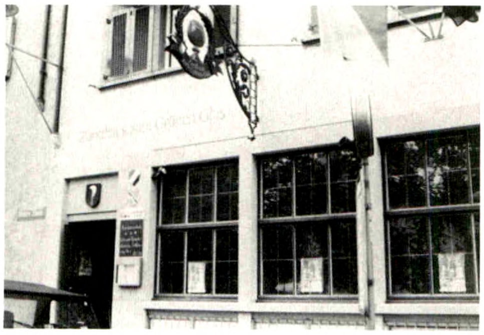

2

Fig. 1.—Building at Seilergraben 7 (*far left*) is where Roentgen lived while a student in Zurich (1866–1869). Note commemorative plaque high on front center of building.

Fig. 2.—Zum Grünen Glas is located on Untere Zäune not far from Roentgen's student dwelling. It was here that he met his future bride, Anna Bertha Ludwig.

Note. Facts about Roentgen's life are from Glasser O. *Dr. Wilhelm Conrad Roentgen,* 2nd ed. Springfield, IL: Thomas, **1958**.

[1] Department of Radiology, University of California Medical Center, San Francisco General Hospital, 1001 Potrero Ave., Rm. 1 × 57, San Francisco, CA 94110. Address reprint requests to P. C. Goodman.

[2] Department of Radiology, Louisiana State University, School of Medicine, Shreveport, LA 71130.

***AJR* 157:274, August 1991** 0361-803X/91/1572-0274 © American Roentgen Ray Society

Abdominal Desmoids: CT Findings in 25 Patients

David M. Einstein[1]
James R. Tagliabue
Robert K. Desai

Desmoids are histologically benign but locally aggressive fibrous tumors. Although overall they are rare lesions, they are a common manifestation of Gardner syndrome. We retrospectively reviewed clinical records and CT scans of 25 patients with abdominal desmoids. The number, location, and CT characteristics of the lesions were recorded for each patient. Tumors were solitary in 72% of patients and multiple in 28%. Fifty percent were located in the abdominal wall, 41% in the mesentery, and 9% in the retroperitoneum. More than two thirds of the lesions had well-defined borders, with the remainder displaying an infiltrative outer margin. The majority of tumors had attenuation values equal to (47%) or greater than (41%) the attenuation of muscle on contrast-enhanced CT scans. Complications attributable to the desmoid were commonly detectable on CT (hydronephrosis occurred in 36% and small-bowel obstruction in 20%).

Our results detail the spectrum of CT findings and complications caused by abdominal desmoids.

AJR **157:275–279, August 1991**

Desmoids are rare lesions with an estimated incidence of 3.7 new cases per million population per year [1]. They are currently included in the fibromatoses, a diverse group of conditions characterized by benign proliferation of fibrous tissue intermediate in biological behavior between benign fibrous lesions and fibrosarcomas [2]. Extraabdominal desmoids have a wide distribution; the shoulder girdle, trunk, and lower extremities are most commonly involved [3]. Abdominal desmoids, which may occur in the abdominal wall, mesentery, or retroperitoneum, have an increased incidence in Gardner syndrome.

As CT scanning is currently the most widely used technique in the initial diagnosis and monitoring of the response to therapy of these lesions, we retrospectively evaluated our experience with the CT appearance of abdominal desmoids.

Materials and Methods

Review of our institution's polyposis registry and general pathology records disclosed 25 patients in whom CT scanning was used for desmoid detection and/or follow-up between 1978 and 1990. Twenty-three (92%) of these patients had a diagnosis of Gardner syndrome, established by the clinical findings of colonic polyposis and the presence of characteristic extracolonic manifestations. The study group included 16 women (64%) and nine men (36%), ranging in age from 17 to 59 years, with 68% in the third and fourth decades. Pathologic proof was available in 80% of the patients, including the two patients without Gardner syndrome. The other 20% of cases were diagnosed on the basis of a typical presentation and CT appearance of an abdominal mass lesion in a patient with documented Gardner syndrome.

Because of the prolonged period of the study, CT scans were obtained with a variety of third- and fourth-generation CT scanners. Contiguous 10-mm slices were the routine, with all patients receiving oral and IV contrast material. A variety of different contrast materials and injection techniques were used, but as a rule, 100–150 ml of iodinated contrast material was

Received January 22, 1991; accepted after revision March 12, 1991.

[1] All authors: Department of Diagnostic Radiology (A21), Cleveland Clinic Foundation, 9500 Euclid Ave., Cleveland, OH 44195.

0361-803X/91/1572-0275
© American Roentgen Ray Society

given as either a bolus or bolus plus drip. Unenhanced scans were not obtained routinely.

Clinical records were reviewed to determine if any regional surgical procedure preceded the discovery of the desmoids. Fifteen (60%) of the 25 patients' desmoids occurred within 3 years of a regional surgical procedure, a total proctocolectomy and ileorectal anastomosis for Gardner syndrome in 14 patients and a cholecystectomy and inguinal hernia repair in one non–Gardner syndrome patient. However, six (24%) of the 25 patients, including five with Gardner syndrome, had desmoids either without any pertinent surgical history or at the time of their initial surgery for polyposis. In the final four patients (16%), all with Gardner syndrome, desmoids developed 4 years or more after a pertinent surgery. Complications of the lesion, including hydronephrosis and small-bowel obstruction, also were sought, whether detectable by CT, another imaging method, or clinical evaluation. At initial presentation, lesions on CT scans were evaluated for the following features: single or multiple; size and location; well-defined, infiltrative, or mixed appearance; and density greater than, equal to, or less than that of adjacent muscle. Sixteen (64%) of 25 patients had serial CT scanning.

Results

Thirty-four tumors were identified on initial CT scans in the 25 patients. Eighteen patients (72%) had a single desmoid, five (20%) had two lesions, and two (8%) had three concurrent lesions. No patient had more than three desmoids at one time; recurrent tumors were not tabulated as multiple lesions if they were present in the original tumor bed. Seventeen (50%) of the 34 tumors were located in the abdominal wall. Thirteen of these 17 involved the rectus muscles (Fig. 1), two were peristomal, one was in the suprapubic region, and another was located in the right flank at an adrenalectomy incision site. Fourteen (41%) of the 34 total lesions were located in the mesentery, and three (9%) were retroperitoneal.

On contrast-enhanced scans, four (12%) of 34 desmoids were lower in density than was adjacent muscle (Fig. 2), 16 (47%) were isodense (Fig. 3), and 14 (41%) were hyperdense (Fig. 4). As unenhanced scans were not routinely used, contrast-enhancing patterns could not be studied. A homogeneous appearance was seen in 71% of the lesions. In the remaining 29%, a variety of heterogeneous patterns was found, including a low-density center with a high-density rim (Fig. 1) and a whorled, striped appearance (Fig. 5).

The desmoids varied greatly in size as measured on the initial CT scan, ranging from 1 to 30 cm (mean, 8 cm) in greatest dimension; seven were larger than 10 cm when first seen. On the patients' initial CT scans, the larger lesions were obvious, but the smaller desmoids, particularly when located in the base of the mesentery, were subtle (Fig. 6) and required optimal bowel opacification for confident diagnosis (Fig. 7). Twenty-three (68%) of the 34 desmoids were shown as a well-defined spherical mass with grossly sharp contours. A mixed pattern of a solid central region with infiltrative margins was noted in seven (21%) of 34 lesions (Fig. 3), whereas a poorly defined infiltrative appearance without a solid central region was seen in four (12%) of 34 (Fig. 8). All but one (94%) of the 17 abdominal wall masses were well defined, with the remaining tumor appearing mixed. Conversely, of the 17 retroperitoneal/mesenteric tumors, seven (41%) were well defined, four (24%) were infiltrative, and six (35%) were mixed.

CT evidence of complications caused by the desmoids was common at some point during the disease. Hydronephrosis attributable to a desmoid was detected by CT in eight (32%) of the 25 patients. When small-bowel obstruction was suspected clinically or on the basis of plain film findings, the patients were managed either conservatively or with surgery, and CT scanning was not routinely performed at that time. Five (20%) of 25 patients had small-bowel obstruction proved

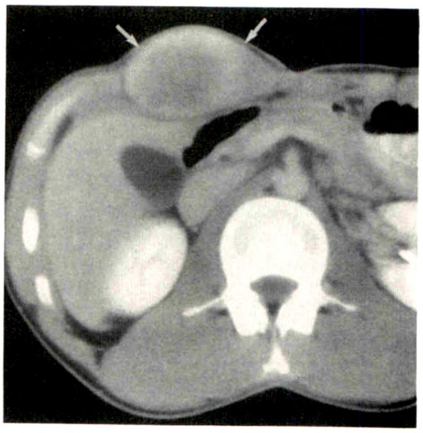

Fig. 1.—31-year-old man with Gardner syndrome 11 years after subtotal colectomy. CT scan shows a well-defined mass in right rectus abdominis muscle compatible with diagnosis of desmoid (*arrows*). Mass has a low-density center with a hyperdense rim. (Pathologically proved.)

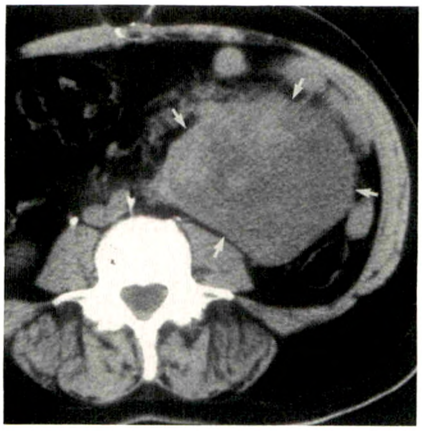

Fig. 2.—59-year-old man without evidence of Gardner syndrome. CT scan made 3 years after exploratory laparotomy and cholecystectomy shows a large mass arising from mesentery and occupying left side of abdomen (*arrows*). Mass is well defined along most of its borders but has an infiltrative medial margin. It is of mixed density, showing mostly decreased density, with high density along medial aspect of mass. (Pathologically proved.)

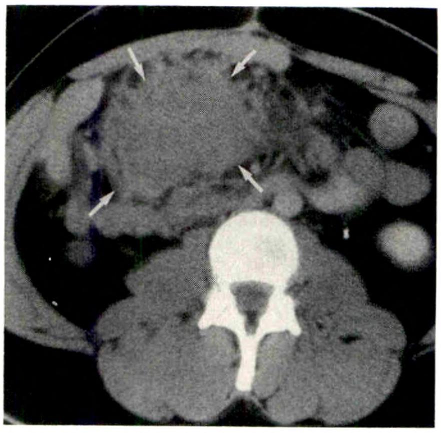

Fig. 3.—31-year-old man with Gardner syndrome and previous colectomy. CT scan obtained 2 years after surgery shows a solid mass with infiltrative borders involving mesentery (*arrows*). Density of mass is equal to that of muscle. (Pathologically proved.)

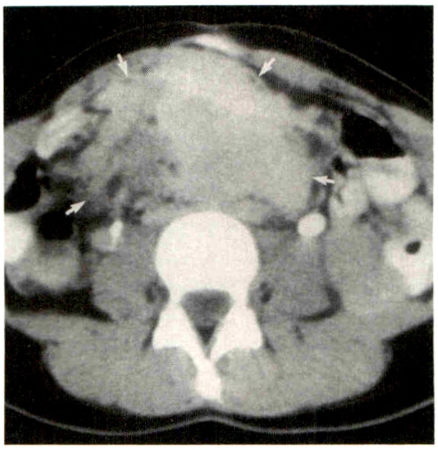

Fig. 4.—31-year-old woman with Gardner syndrome 3 years after colectomy. CT scan shows a large hyperdense desmoid involving mesentery (*arrows*). Mass is predominantly solid and has infiltrative borders. (Pathologically proved.)

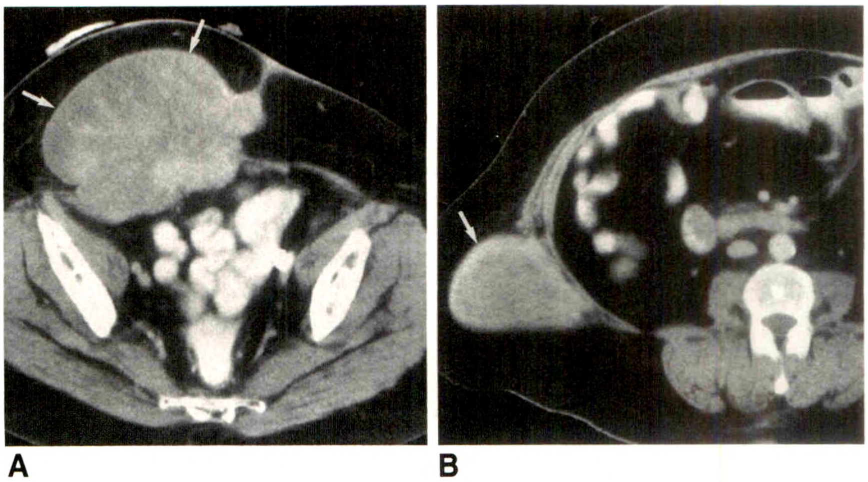

Fig. 5.—50-year-old woman with Gardner syndrome and history of a colectomy. First desmoid was found 6 years after surgery. (Pathologically proved.)

A, CT scan shows a desmoid that is heterogeneous with a whorled appearance (*arrows*).

B, CT scan shows a similar mass in right flank. Mass (*arrow*) arises from incision site from a right adrenalectomy performed 2 years earlier.

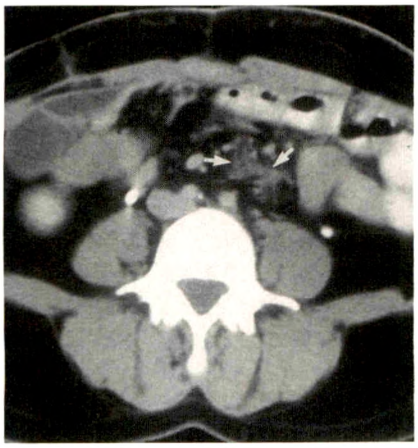

Fig. 6.—33-year-old woman with Gardner syndrome and colectomy 12 years before diagnosis of a desmoid. CT shows a subtle, small, infiltrating desmoid (*arrows*) in mesentery. (Pathologically proved.)

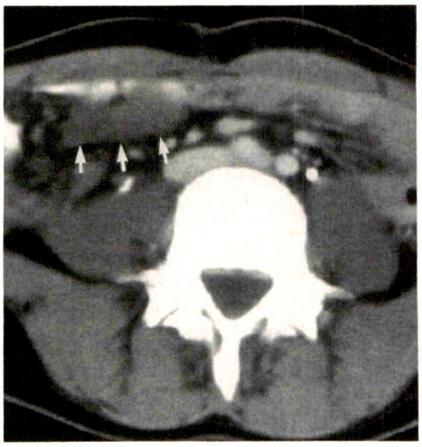

Fig. 7.—30-year-old woman with Gardner syndrome. Desmoid was found at initial presentation for colectomy. CT scan shows a small homogeneous desmoid (*arrows*) in mesentery next to contrast-filled bowel, demonstrating need for adequate bowel opacification in diagnosis of mesenteric desmoids. (Pathologically proved.)

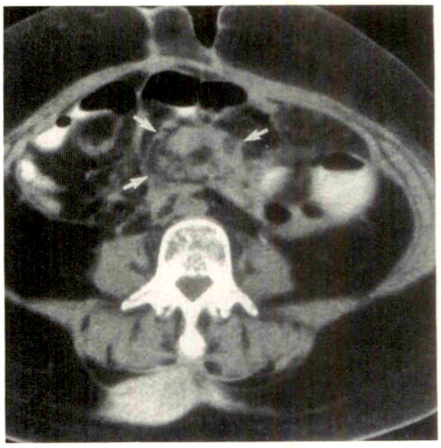

Fig. 8.—35-year-old woman with Gardner syndrome. Mesenteric desmoid was found during initial surgery. Follow-up CT scan through lower abdomen 3 years later shows an infiltrative soft-tissue desmoid (*arrows*) in mesentery. (Pathologically proved.)

at surgery to be directly related to the desmoid. Cases of bowel obstruction due to adhesions were not included in this tabulation.

Discussion

The fibromatoses are benign fibrous lesions that, although demonstrating a predilection for certain widely separated anatomic sites, share a characteristic histologic appearance and biological behavior. They arise from fascial and musculoaponeurotic structures and have a bandlike or tendonlike consistency, which led Mueller to coin the term *desmoid tumor* in 1838 [2]. Examples of superficial fibromatoses include Dupuytren contracture and Peyronie disease, whereas extraabdominal, abdominal wall, and intraabdominal desmoids are included in the deep fibromatoses [2].

Demographically, desmoids may occur in all age groups but are seen most commonly in the third and fourth decades; abdominal desmoids are rarely seen in patients less than 20 years old [3]. Females are affected more commonly than males are [1, 3]. Desmoids are locally aggressive tumors, with invasion of contiguous structures and a strong tendency toward recurrence, even after apparently complete surgical removal. Metastases, however, are not seen; so, despite their local aggressiveness, desmoids are classified as benign lesions [2, 3]. Most are painless except when they encroach on or obstruct bowel or the urinary tract. Multiple lesions are seen in 10% of cases [3].

Desmoids of the abdominal wall and mesentery may occur as isolated lesions or may be seen as a manifestation of Gardner syndrome. This subset of familial polyposis, first recognized in 1951 [4], has several characteristic extracolonic manifestations, including bony osteomas, sebaceous and epidermoid cysts, fibromas, and abdominal wall desmoids [5, 6]. It was recognized somewhat later that desmoids of the mesentery also were a component of Gardner syndrome [7]. The incidence of abdominal wall and mesenteric desmoids in patients with Gardner syndrome has varied between 4% and 29%. Although usually seen as a sequela of abdominal surgery, desmoids have appeared before familial polyposis has been diagnosed.

The optimal therapeutic regimen for desmoids has not been found. Postsurgical recurrence rates on the order of 77% for mesenteric lesions and 25% for abdominal wall lesions favor the use of nonsurgical therapy, such as nonsteroidal antiinflammatory drugs and antiestrogens. Surgery is reserved for those patients with bowel or urinary tract obstruction or intractable pain [8–10].

Abdominal desmoids have not been extensively reported in the imaging literature, due in part no doubt to their relative scarcity [11–15]. Early reports of mesenteric desmoids with small numbers of patients studied by CT scanning described well-defined, relatively homogeneous masses isodense with soft tissue, although some scans were obtained without IV contrast material [12, 14]. A second CT series dealing with abdominal wall desmoids describes them as well defined and of soft-tissue density, although no mention was made of whether IV contrast material was administered [13]. In the largest series before this one, CT scans of six patients with Gardner syndrome were evaluated. Mesenteric desmoids were present in five patients and abdominal wall desmoids in two patients. All but one of the lesions were well defined and homogeneous, and they appeared isodense or slightly hypodense with respect to muscle [11].

The population reported here represents the largest series of patients with this lesion studied with CT. The male-female ratio, interval between surgery and detection of desmoids, and incidence of multiple lesions are in keeping with reported demographic data. Our results again emphasize that desmoids may be discovered during the initial surgery for polyposis, and thus must be included along with adenopathy from colonic carcinoma in the differential diagnosis of an abdominal mass in the precolectomy patient with Gardner syndrome. The high incidence of hydronephrosis (32%) and bowel obstruction (20%) seen in our population should be kept in mind when the postcolectomy patient has acute abdominal pain.

By virtue of the large number of studies available for review, we were able to further refine the spectrum of CT findings in patients with abdominal desmoids. We detected a grossly infiltrative or mixed appearance in approximately one third of the desmoids, particularly in the mesentery. This appearance has not been previously described in the literature. These findings correspond to a study of nonabdominal desmoids [16], in which even more tumors (57%) with poorly defined borders were found. Analysis of our lesions shows that the majority were either isodense (47%) or hyperdense (41%) when compared with muscle on contrast-enhanced scans. The latter appearance also has not been stressed in discussions of abdominal desmoids, but the pattern was noted in Hudson's series of extraabdominal desmoids [16]. CT-pathologic correlations in a variety of fibrous lesions [17] and fibromatoses in general [18] have documented a high percentage of hyperdense lesions also. Although it was hypothesized that the high physical density of collagen and/or abundant capillary network might explain these appearances, histologic studies did not always confirm this. This hyperdense pattern seen with desmoids is, unfortunately, far from specific; it is seen also in vascular neoplastic and inflammatory masses, malignant neoplasms containing a desmoplastic component, acute hematomas, and calcium-containing masses [17]. In addition, the patterns seen in our study may reflect both tumor morphology and differences in contrast administration inherent in a prolonged retrospective study.

Because most of our patients had Gardner syndrome, the cause of the abdominal wall and mesenteric masses was seldom in doubt. Desmoid is the most common primary tumor of the mesentery, but in a review of 130 mesenteric desmoids by the Armed Forces Institute of Pathology, only 17 patients had Gardner syndrome, and more than 60% of the cases were initially misdiagnosed both clinically and pathologically [19]. Many other entities appear as solid mesenteric masses on CT scans, but associated clinical or radiologic findings may be helpful in reaching the proper diagnosis. Metastases are usually multiple, and additional CT findings or clinical history of a primary tumor may be present. Lymphomatous involvement of the mesentery is usually associated with splenomegaly and retroperitoneal lymphadenopathy. Mesenchymal tumors that have attained the large size often seen with desmoids have usually undergone necrotic or cystic change, a pattern only rarely seen in our series and then usually after prolonged medical therapy. Carcinoids should present with a characteristic clinical and biochemical syndrome, and in patients with a history of trauma or bleeding diathesis, mesenteric hematoma also must be included in the differential diagnosis [14]. When tissue diagnosis is required, the surgeon can easily perform a biopsy of palpable abdominal wall lesions, but CT-guided percutaneous biopsy of deeper lesions can provide the diagnosis while avoiding surgical intervention, which may induce further desmoid formation. We and other authors [11, 20] recommend serial CT scans as the optimal method of monitoring these patients for therapeutic response and development of complications, because it is more accurate than physical examination is in assessing tumor size.

REFERENCES

1. Reitamo JJ, Scheinin TM, Hayry P. The desmoid syndrome: new aspects in the cause, pathogenesis and treatment of the desmoid tumor. *Am J Surg* **1986**;151:230–237
2. Enzinger FM, Weiss SW. *Soft tissue tumors*. St. Louis: Mosby, **1983**:45–70
3. Kissane JM. *Anderson's pathology*, 9th ed. St. Louis: Mosby, **1990**:1844–1847
4. Gardner EJ. A genetic and clinical study of intestinal polyposis, a predis-

posing factor for carcinoma of the colon and rectum. *Am J Hum Genet* **1951**;3:167–176
5. Gardner EJ, Richards RC. Multiple cutaneous and subcutaneous lesions occurring simultaneously with hereditary polyposis and osteomatosis. *Am J Hum Genet* **1953**;5:139–147
6. Smith WG. Multiple polyposis, Gardner syndrome and desmoid tumors. *Dis Colon Rectum* **1958**;1:323-332
7. Simpson RD, Harrison EG Jr, Mayo CW. Mesenteric fibromatosis in familial polyposis: a variant of Gardner syndrome. *Cancer* **1964**;17:526–534
8. Easter DW, Halasz NA. Recent trends in the management of desmoid tumors: summary of 19 cases and review of the literature. *Ann Surg* **1989**;210:765–769
9. McKinnon JG, Neifeld JP, Kay S, Parker GA, Foster WC, Lawrence W Jr. Management of desmoid tumors. *Surg Gynecol Obstet* **1989**;169: 104–106
10. Eagel BA, Zentler-Munro P, Smith IE. Mesenteric desmoid tumours in Gardner syndrome: review of medical treatments. *Postgrad Med J* **1989**;65:497–501
11. Magid D, Fishman EK, Jones B, Hoover HC, Feinstein R, Siegelman SS. Desmoid tumors in Gardner syndrome: use of computed tomography. *AJR* **1984**;142:1141–1145
12. Baron RL, Lee JKT. Mesenteric desmoid tumors: sonographic and computed tomographic appearance. *Radiology* **1981**;140:777–779
13. Yeh HC, Rabinowitz JG, Rosenblum M. Complementary role of CT and ultrasonography in the diagnosis of desmoid tumor of abdominal wall. *Comput Radiol* **1982**;6:275–280
14. Forte MD, Brant WE. Spontaneous isolated mesenteric fibromatosis: report of a case. *Dis Colon Rectum* **1988**;32:315–317
15. Carr LY, Cohen BA, Goodman JD, Heimann TM, Mendelson DS. Gardner syndrome and mesenteric desmoids. *Am J Gastroenterol* **1985**;80: 310-312
16. Hudson TM, Vandergriend RA, Springfield DS, et al. Aggressive fibromatosis: evaluation by computed tomography and angiography. *Radiology* **1984**;150:495-501
17. Rubenstein WA, Gray G, Auh YH, et al. CT of fibrous tissues and tumors with sonographic correlation. *AJR* **1986**;147:1067–1074
18. Francis IR, Dorovini-Zis K, Glazer GM, Lloyd RV, Amendola MA, Martel W. The fibromatoses: CT-pathologic correlation. *AJR* **1986**;147:1063–1066
19. Burke AP, Sobin LH, Shekitka KM, Federspiel BH, Helwig EB. Intraabdominal fibromatosis: a pathologic analysis of 130 tumors with comparison of clinical subgroups. *Am J Surg Pathol* **1990**;14(4):335-341
20. Richards RC, Rogers SW, Gardner EJ. Spontaneous mesenteric fibromatosis in Gardner syndrome. *Cancer* **1981**;47:597-601

A Versatile Patriot

Stefan C. Schatzki[1]

Paul Revere's fame today is largely due to Longfellow's famous poem published in 1863. Despite Revere's many accomplishments, this versatile patriot was not mentioned in any dictionary of American biography before that date.

Paul Revere was born in Boston in 1735, the son of Apollos Rivoire, a French Huguenot who changed his name to Paul Revere. The younger Revere, working in his father's shop, became an accomplished silversmith at an early age. By 1764, he had become interested in copper engravings and produced a series of political caricatures attacking British rule over the colonies. Revere became a member of the Sons of Liberty and participated in the Boston Tea Party in December 1773.

As the leader of Boston craftsmen, Revere became friendly with such leaders of the American Revolution as Samuel Adams and John Hancock and served as a messenger between leaders in Boston and the other colonies. On April 19, 1775, Revere, together with William Dawes and Dr. Samuel Prescott, rode to Lexington and Concord to warn that the English were coming from Boston to attack the patriots. Revere and Dawes were captured after leaving Lexington, and only Prescott got through to Concord. Revere subsequently escaped and served as a lieutenant colonel during the Revolution.

Paul Revere maintained his interest in engraving and produced a number of important documents, including the first Massachusetts paper currency and treasury notes and the seal of the state of Massachusetts, which is still used today. His most famous engraving depicted the Boston Massacre of 1770.

In 1780, Dr. John Warren began to give a series of lectures on anatomy at the American Hospital in Boston. Revere produced the engraved certificate of attendance. Only two certificates have survived to today. The one shown here is dated 1785, after the establishment of Harvard Medical School. "American Hospital" has been scratched out, and "University at Cambridge" has been substituted. John Warren was one of the important forces that led to the establishment of Harvard Medical School in Cambridge in 1782, where he served as the first professor of anatomy and surgery. Warren was a member of a family that has played a pivotal role in the development of medicine in Boston and of Harvard Medical School from the days of the revolution until the present. The definitive history of medicine at Harvard lists 10 members of the Warren family who have been an important part of Harvard medicine. The early members of the family played prominent roles in Revolutionary and post-Revolutionary America and were the subjects of paintings by most of America's most prominent early painters, including Copley, Stuart, Thrumbull, West, and Peale. The death of Dr. Joseph Warren at Bunker Hill is the subject of a famous painting by John Thrumbull. The certificate shown here illustrates Revere's ability in engraving and contains the first American depiction of an anatomic dissection.

After the war, Revere returned to his career as a silversmith. Today, he is considered one of the most important early American silversmiths, and craftsmen continue to copy the graceful lines of his work. He also established an iron foundry to make cannons and church bells, many of which are still used throughout New England, and was responsible for all the brass and copper work on the frigate *Constitution*. In 1800, he built the first mill for rolling sheet copper in the United States, and this company continues to operate as the Revere Copper Company. He was a prosperous merchant at the time of his death in 1818.

Although Paul Revere's name is now chiefly associated with his famous midnight ride, he was an important and successful figure in the period that spans the years from before the American Revolution to the early 19th century. Patriot, silversmith, engraver, and industrialist, Revere was a most fascinating part of the early history of the United States.

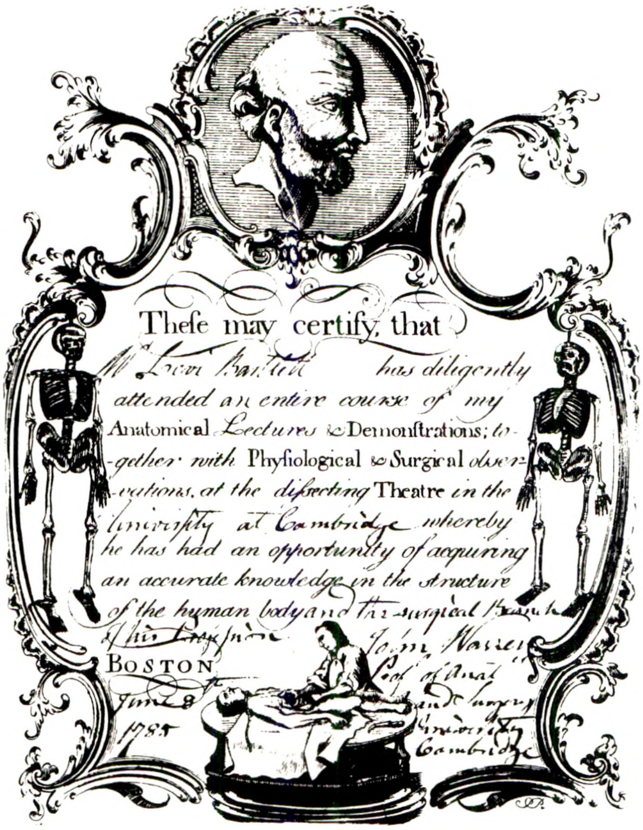

Theſe may certify, that
Mr Levi Bartlett has diligently
attended an entire course of my
Anatomical Lectures & Demonſtrations; to-
-gether with Phyſiological & Surgical obser-
-vations, at the diſsecting Theatre in the
Univerſity at Cambridge whereby
he has had an opportunity of acquiring
an accurate knowledge in the structure
of the human body and the surgical Branch
of this Profession
BOSTON
June 8
1785
John Warren
Prof of Anat
and Surgery
University
Cambridge

Paul Revere (1735–1828). *Certificate for Attendance at Anatomical Lectures, 1785*. Engraving, 7.5 × 6 in. (19 × 15.3 cm). Courtesy of American Antiquarian Society, Worcester, MA.

---

[1] Department of Radiology, Mount Auburn Hospital, 330 Mount Auburn St., Cambridge, MA 02238. Address reprint requests to S. C. Schatzki.

AJR 157:280, August 1991 0361–803X/91/1572–0280 © American Roentgen Ray Society

Bile Duct Diverticula and Webs:
Nonspecific Cholangiographic Features of Primary Sclerosing Cholangitis

David J. Gulliver[1]
Mark E. Baker[1]
William Putnam[2,3]
John Baillie[2]
Reed Rice[1]
Peter B. Cotton[2]

Biliary tree diverticula and webs are considered by several authors to be specific cholangiographic features of primary sclerosing cholangitis (PSC). Our experience suggested that these findings can be seen in patients without PSC. The purpose of this study was twofold: to establish whether diverticula and webs are indeed specific for PSC and to assess whether PSC can be accurately diagnosed without reference to diverticula or webs. We retrospectively reviewed 861 consecutive ERCP studies and found 32 cases of webs and/or diverticula. Using accepted cholangiographic, clinical, and histologic criteria, we diagnosed PSC in nine patients and excluded it in 21, with two instances of uncertain diagnoses. Webs and diverticula seen in PSC were cholangiographically indistinguishable from those in the group without PSC. All 21 patients without PSC had other biliary abnormalities, and were grouped by the predominant abnormality or finding believed to be associated with diverticulum or web formation: common duct stones or cholangitis ($n = 11$ patients), postoperative stricture ($n = 4$), bile duct stent and balloon dilatation ($n = 3$), malignant stricture ($n = 2$), and choledochoduodenostomy ($n = 1$). To assess cholangiographic diagnosis of PSC in these patients, a blinded reviewer studied the radiographs of the 30 patients with diverticula and/or webs who had confirmed diagnoses. By using established radiologic criteria alone (ignoring diverticula and webs), the correct diagnosis was made in 27, yielding a sensitivity of 89% and specificity of 91%.

We conclude that the presence of diverticula and/or webs on a cholangiogram is a nonspecific finding and may be due to inflammation or trauma to the bile duct wall. Further, PSC can be distinguished from other abnormalities on the basis of findings other than diverticula and webs.

***AJR* 157:281-285, August 1991**

Biliary tree diverticula and webs are well-recognized cholangiographic features of primary sclerosing cholangitis (PSC) and are considered to be specific for this disease [1-4]. We observed diverticula and webs on routine ERCP films in several patients who had no other radiologic or clinical evidence of PSC, but who did have calculi, biliary strictures, or internal biliary stents.

To investigate this further, we retrospectively reviewed our ERCP experience to determine the prevalence of diverticula and webs and their diagnostic significance in relation to PSC and other biliary diseases.

Materials and Methods

Eight hundred sixty-one consecutive ERCP studies performed in a 14-month period (November 1988 through December 1989) were retrospectively reviewed for the presence of biliary diverticula and webs. The clinical charts of those patients with diverticula and/or webs were then reviewed for possible causes of the bile duct changes, liver or common bile duct biopsy results, age and sex, surgical history, and alkaline phosphatase and bilirubin levels.

The cholangiograms were reviewed for sites of diverticula and webs (intra- vs extrahepatic), strictures, calculi, biliary dilatation, biliary stents, and balloon dilatation. Diverticula were

Received January 28, 1991; accepted after revision March 27, 1991.

[1] Department of Radiology, Box 3808, Duke University Medical Center, Durham, NC 27710. Address reprint requests to D. J. Gulliver.

[2] Department of Medicine, Division of Gastroenterology, Duke University Medical Center, Durham, NC 27710.

[3] Present address: 1560 N. 115th St., Suite 207, Seattle, WA 98133.

0361-803X/91/1572-0281
© American Roentgen Ray Society

defined as any saccular outpouching of the biliary tree (these outpouchings are difficult or impossible to categorize as the precise disease is not known). Webs were defined as any focal shelflike narrowing of the biliary tree, whether or not they completely encircled the duct.

Patients with diverticula or webs were categorized into one of three groups: PSC confirmed, PSC excluded, or indeterminate. The diagnosis of PSC was made on the basis of accepted criteria. These include clinical presentation: PSC may present with biliary obstruction (with or without secondary acute cholangitis); asymptomatic, raised enzyme levels on liver function tests (especially a prolonged increase in alkaline phosphatase); or cirrhosis and portal hypertension resulting from chronic biliary obstruction [4–8]; age and sex: PSC is most common in males in middle life [5, 6]; the presence of inflammatory bowel disease (seen in approximately 50–75% of PSC patients) [1, 6, 9]; liver or bile duct biopsy (diagnostic of PSC in approximately one third of PSC patients) [5, 6, 10]; typical cholangiographic findings: diffuse, multifocal, short anular strictures (sometimes causing a beaded appearance) frequently involving intrahepatic with or without extrahepatic bile ducts [1, 5, 6, 9, 11, 12], with dilatation often absent or mild despite tight strictures [9]; and, usually, absence of biliary calculi and prior biliary surgery (although previous cholecystectomy does not exclude the diagnosis) [4, 5]. None of these criteria alone was considered diagnostic of PSC, but features such as typical cholangiographic appearance, positive biopsy results, and the presence of inflammatory bowel disease were weighted more heavily than the patient's age or sex and general clinical presentation. Diverticula and webs were *not* used to diagnose or exclude PSC.

The radiographs and clinical records of those patients excluded from the PSC group were reviewed further to clarify possible causes of the ductal abnormalities. Associated biliary disease, surgical bypass, balloon dilatation, or stent placement was believed to have a role in the formation of diverticula and webs if their formation was observed over time (e.g., after balloon dilatation and endoscopic stent placement). Supportive evidence of a causal role was ascribed if diverticula and webs progressed over time or occurred in close proximity to the biliary abnormality (e.g., a common duct stone).

Finally, radiographs of all patients with diverticula and/or webs were randomized and reviewed in a blinded fashion by an experienced observer to determine if cholangiograms of patients with PSC could be distinguished from those without PSC, ignoring diverticula and webs. The observer was given the films and a form requesting a diagnosis (PSC or not PSC). In addition, the primary and secondary reasons for that diagnosis were chosen from the following list: multifocal strictures, single stricture, no stricture, stones, stent, biliary dilatation, no dilatation, and prior surgery. The results were used to determine the most useful cholangiographic criteria for diagnosing PSC in this group and were then statistically analyzed to assess the sensitivity and specificity of cholangiographic diagnosis of PSC without reference to diverticula and webs.

Results

Of 861 cholangiograms, there were 32 cases of biliary diverticula and/or webs. In some cases, both with PSC and not with PSC, differentiation of diverticula from webs was difficult because some diverticula in a nondistended duct took on the appearance of webs when further injection of contrast material produced more duct distension. Patients with these findings were classified as having both diverticula and webs.

Nine of the 32 patients had PSC. All nine had extrahepatic biliary diverticula (Fig. 1); one also had intrahepatic diverticula. Two had webs, both extrahepatic only. All nine patients had strictures, but the sites of strictures correlated poorly with the sites of webs and diverticula. All nine had diffuse strictures; in six these were intra- and extrahepatic and in three they were intrahepatic only.

Twenty-three additional patients (2.7% of all ERCP studies) had diverticula and/or webs without PSC. PSC was suspected in one patient, but the diagnosis was uncertain and this patient was excluded from the study. Another patient with probable PSC was subsequently also found to have disseminated abdominal malignancy, almost certainly a cho-

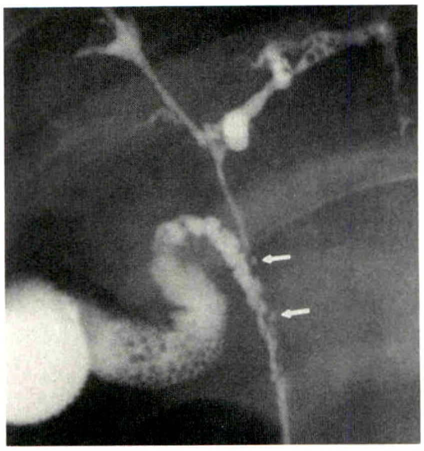

Fig. 1.—Biliary diverticula in a patient with primary sclerosing cholangitis. Cholangiogram shows multiple diverticula (*arrows*) in extrahepatic bile duct.

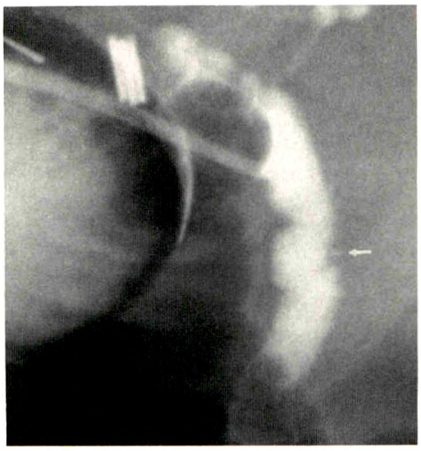

Fig. 2.—Biliary diverticulum in a patient without primary sclerosing cholangitis. Cholangiogram shows diverticulum (*arrow*) in distal common bile duct. This patient has had a choledochoduodenostomy, through which contrast material has been injected by using a balloon catheter.

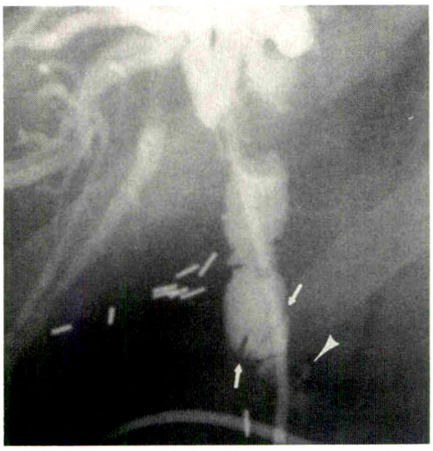

Fig. 3.—Biliary webs and diverticulum in a patient without primary sclerosing cholangitis. Cholangiogram shows multiple distal webs (*arrows*) in common bile duct and a single diverticulum (*arrowhead*) in a patient with a large calculus in common hepatic duct, 4 years after cholecystectomy. Contrast material was injected through a nasobiliary drain.

langiocarcinoma. This patient was also excluded from the study owing to the difficulty in determining which condition caused which radiologic features. In the remaining 21 patients, there were no clinical, histologic, or cholangiographic features to support a diagnosis of PSC.

Review of the cholangiographic and clinical features of the 21 patients without PSC who had diverticula and/or webs yielded the following predominant associated factors: common bile duct calculi with or without documented acute cholangitis ($n = 9$ patients), acute cholangitis without calculi ($n = 2$), postsurgical stricture ($n = 4$), balloon dilatation and bile duct stent ($n = 3$), malignant stricture ($n = 2$), and choledochoduodenostomy ($n = 1$).

Of the 21 non-PSC patients, 20 had diverticula (14 extrahepatic, one intrahepatic, five both) (Fig. 2) and 13 had webs (10 extrahepatic, one intrahepatic, two both) (Fig. 3). When present, most webs occurred in close proximity to diverticula. Of the 12 patients with diverticula and webs, both diverticula and webs were confined to extrahepatic ducts in nine, intrahepatic in one, and both intra- and extrahepatic in two. In patients with both diverticula and webs, these two structures tended to occur in close proximity to each other. The appearances of the individual webs and diverticula were indistinguishable from those seen in the PSC group. Common bile duct stones, when present, were always associated with extrahepatic diverticula (with or without extrahepatic webs), and did not occur in association with intrahepatic webs or diverticula.

Fourteen of the 21 non-PSC patients had elevated alkaline phosphatase and/or bilirubin levels, and 16 had a history of surgery (most commonly a cholecystectomy). Seventeen had biliary dilatation. All six patients with malignant or postsurgical strictures had biliary dilatation proximal to the strictures. Of the 11 patients with acute cholangitis or calculi, two had strictures and nine had biliary dilatation; six of these patients had both intra- and extrahepatic dilatation. Only one patient had multiple cholangiographic features mimicking PSC (multifocal intrahepatic strictures), but in this case, there was intra- and extrahepatic biliary dilatation, probable biliary calculi, a normal bilirubin level, history of cholangitis, and a previous choledochojejunostomy (Fig. 4).

Of the eight patients with internal biliary stents (all of whom had balloon dilatation at the time of stent placement), three had diverticula or webs before dilatation and stent placement, but they were more marked after these procedures. In an additional three patients, diverticula or webs were seen only after balloon dilatation and stent placement (Fig. 5). Reasons for stent placement in the six patients who had progression or formation of diverticula or webs associated with balloon dilatation and stents were diverse: cholangiocarcinoma, leukemic portal lymphadenopathy, choledochojejunostomy stricture, choledocholithiasis, cholangitis stricture, and biliary strictures after cholecystectomy and liver transplantation, respectively. It was not possible to determine whether the diverticula or webs in these patients were caused by balloon dilatation, stent placement, or both.

The blinded review of films by a single interpreter resulted in the correct diagnosis (PSC or not PSC) in 27 of the 30 cases. There were two false-positive and one false-negative diagnosis of PSC, yielding a sensitivity of 89 ± 10.5% and a specificity of 91 ± 6.4%. Of the eight cases correctly diagnosed radiologically as PSC, the presence of multifocal strictures was given as the most important reason for the diagnosis in all eight. Absence of dilatation was the most common secondary reason (six patients). Of the 19 cases correctly diagnosed as not PSC, the presence of a single stricture was the most important primary reason (10 patients), with lack of a stricture being the primary reason in four others. Biliary dilatation was easily the most common secondary reason (12 patients). The two false-positive cholangiographic diagnoses

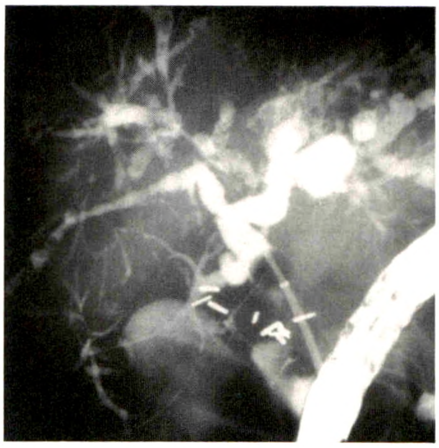

Fig. 4.—Cholangitis mimicking primary sclerosing cholangitis. ERCP shows multiple intrahepatic strictures and filling defects in intrahepatic duct. A cholecystectomy and choledochoduodenostomy had been performed 2 months before for multiple biliary tree calculi and episodes of acute cholangitis.

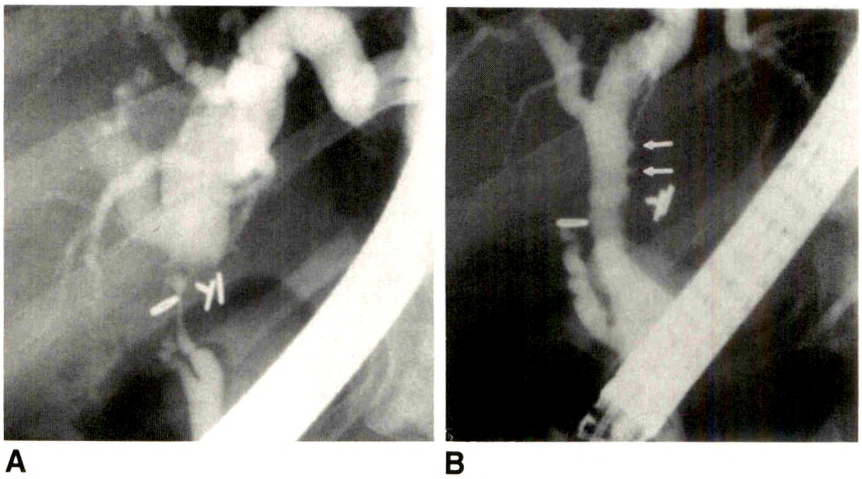

Fig. 5.—Formation of diverticula after endoscopic balloon dilatation and placement of biliary stent.

A, ERCP before balloon dilatation and stent placement for a benign postoperative common hepatic duct stricture that occurred after a cholecystectomy.

B, ERCP 3 months after balloon dilatation and stent insertion. Several diverticula (*arrows*) have appeared in common hepatic duct.

of PSC were in patients with acute cholangitis (with multifocal strictures) (Fig. 4) and postoperative stricture, respectively. In the single false-negative case, biliary dilatation was the reason given for (incorrectly) excluding PSC (Fig. 6).

Because not all patients had both diverticula and webs, our statistician argued that information arising from their differential appearance might have been used diagnostically by the blinded reviewer. To investigate this hypothesis, we estimated the conditional specificity and sensitivity in the diagnosis of PSC that would occur from the use of the presence or absence of diverticula or webs as diagnostic rules. These rules and their estimated conditional specificity and sensitivity are presented in Table 1. The observer was diagnostically superior to any of these rules, thus confirming the assumption that the diagnostic process used by the observer employed something other than just the differential appearance or the absence of diverticula and webs.

Discussion

Cholangiographic features of PSC [1, 6, 9, 13–17] include diffuse, short, anular biliary strictures involving intra- and extrahepatic ducts, sometimes producing a beaded appearance. Intrahepatic ducts may show decreased arborization or pruning, and nonfilling of hepatic segments due to stricturing. The union of right and left hepatic ducts is a common site of stricture formation [13]. Bile ducts may show mural irregularity, including diverticula and webs [18]. Strictures often alternate with areas of relative or actual dilatation, but dilatation is rarely marked. The presence of dilatation in a patient with PSC suggests cholangiocarcinoma [3, 9]. Cholangiographic differential diagnosis of PSC includes cholangiocarcinoma, cirrhosis, acute cholangitis, and advanced primary biliary cirrhosis [1, 4, 5, 9, 19].

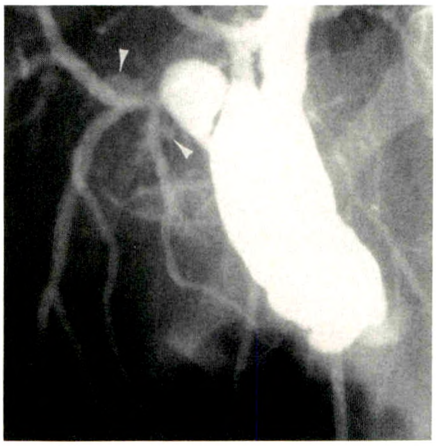

Fig. 6.—Biliary dilatation in primary sclerosing cholangitis (PSC). Dominant extrahepatic stricture with extrahepatic but not intrahepatic ductal dilatation. Cholangiogram shows several diverticula arising from intrahepatic bile ducts (*arrowheads*). A biliary stent is in place. This 20-year-old woman had choledochoduodenostomy for the above stricture, with no evidence of malignancy at surgery or on pathologic examination. Reevaluation 1 year later (including a second ERCP study) showed worsening of PSC but no evidence of malignancy.

TABLE 1: Specificity and Sensitivity of Cholangiographic Diagnosis of Primary Sclerosing Cholangitis When Based on the Presence or Absence of Webs and Diverticula

Cholangiographic Finding	% Specificity	% Sensitivity
Webs or diverticula absent	57	78
Webs absent or diverticula present	5	100
Webs present or diverticula absent	38	22
Webs or diverticula present	0	100

Biliary diverticula and webs, well-documented cholangiographic features of primary sclerosing cholangitis, have been thought by several authors to be specific for this disease [1–4]. Li-Yeng and Goldberg [9] have suggested that biliary diverticula may be seen in conditions other than PSC; they describe diverticula as a feature of PSC, but add that these findings had also been observed in acute ascending cholangitis and after intraductal infusion of cholic acid (however, no data were published). Diverticulumlike lesions in the biliary tree may also be seen in severe clonorchiasis [20]. A "corrugated" bile duct was also reported in an undiagnosed case in 1973 [21]. Webs have not been widely discussed in the literature, although Turner et al. [22] recently described transverse bands mimicking webs or strictures in dilated bile ducts and suggested that these bands may be due to mucosal redundancy. The results of our study confirm these suggestions that biliary diverticula and webs are seen in conditions other than PSC and are a nonspecific feature of several biliary abnormalities. Further, in our series, the majority of patients with cholangiographic diverticula and webs did not have PSC.

Another important finding of our study is that diverticula and webs did not occur in patients with otherwise normal cholangiograms. All of our patients without PSC had one or more of the following abnormalities or cholangiographic features: choledocholithiasis, cholangitis, biliary strictures (benign or malignant), biliary stents with balloon dilatation, and biliary diversion. We believe that the majority of these conditions are related to inflammation (usually associated with biliary stasis or infection), with balloon dilatation possibly being responsible in a smaller number of patients. Therefore, we propose inflammation as the primary causal factor in the formation of biliary diverticula and webs.

It was noted in several patients, both with and without PSC, that some biliary diverticula seen at ERCP could be "converted" into webs by further contrast injection and distension of the bile duct lumen. This suggests a close relationship between diverticula and webs, which probably represent different manifestations of the same abnormality. The cholangiographic appearance appears to be determined by the degree of ductal distension. Unfortunately, we could find no discussion of diverticula or webs in the pathology literature, and could not establish the morphologic feature that causes the radiologic findings. It is likely that there is some form of mucosal hypertrophy.

Our blinded review of the 30 cholangiograms with diverticula and/or webs shows that accurate radiographic diagnosis of PSC is possible when diverticula and webs are ignored.

The correct diagnosis was made by our blinded reviewer in 27 of 30 cases. The number of biliary strictures and the presence or absence of dilatation were the most important diagnostic criteria used by our reviewer when a correct diagnosis of PSC or non-PSC was made. Multifocal strictures and lack of biliary dilatation tended to confirm PSC, whereas a single stricture, lack of a stricture, and biliary dilatation tended to exclude PSC. Of the two false-positive results, one patient had a clear history of cholangitis with multifocal biliary strictures. The single false-negative result was in a patient who had marked biliary dilatation, an unusual feature in PSC.

The correct diagnosis should be possible in the great majority of patients with diverticula or webs, because most patients without PSC have other cholangiographic abnormalities that lead to exclusion of PSC (common duct stones, solitary strictures, stents, biliary diversion). The clinical setting is also important diagnostically. In our experience, the most difficult diagnostic problems were cholangitis causing multiple intrahepatic strictures mimicking PSC (Fig. 4) and PSC with biliary dilatation (Fig. 6).

Our findings indicate that diverticula and webs are a nonspecific cholangiographic feature, possibly related to inflammation or trauma to the bile duct wall. Diverticula and webs are not specific for PSC, and their diagnostic value is probably limited to being an indicator of biliary inflammation or trauma. However, in patients with diverticula and webs, PSC can be differentiated from other biliary abnormalities in most cases by using established radiologic criteria other than diverticula and webs.

REFERENCES

1. McCarty RC, LaRusso NF, Wiesner RH, Ludwig J. Primary sclerosing cholangitis: findings on cholangiography and pancreatography. *Radiology* **1983**;149:39-44
2. Wiesner RH, Ludwig J, LaRusso NF, MacCarty RL. Diagnosis and treatment of primary sclerosing cholangitis. *Semin Liver Dis* **1985**;5:241-253
3. Rohrmann CA, Ansel H, Freeny P, Silverstein F, et al. Cholangiographic abnormalities in patients with inflammatory bowel disease. *Radiology* **1978**;127:635-641
4. LaRusso NF, Weisner RH, Ludwig J, MacCarty RL. Primary sclerosing cholangitis. *N Engl J Med* **1984**;310:899-903
5. Sivak MV. Sclerosing cholangitis. *Scand J Gastroenterol* **1983**;88:18-23
6. Chapman RWG, Arborgh BAM, Rhodes JM, et al. Primary sclerosing cholangitis: a review of its clinical features, cholangiography and hepatic histology. *Gut* **1980**;21:870-877
7. Warren KW, Athanassiades S, Monge J. Primary sclerosing cholangitis: a study of 42 cases. *Am J Surg* **1966**;111:23-38
8. Porayko MK, Wiesner RM, LaRusso NF, et al. Patients with asymptomatic primary sclerosing cholangitis frequently have progressive disease. *Gastroenterology* **1990**;98:1594-1602
9. Li-Yeng C, Goldberg H. Sclerosing cholangitis: broad spectrum of radiographic features. *Gastrointest Radiol* **1984**;9:39-47
10. Craig JF, Liver. In: Kissane JM, ed. *Anderson's pathology*, 9th ed. St. Louis: Mosby, **1990**:1257
11. Wiesner RM, LaRusso NF. Clinicopathologic features of the syndrome of primary sclerosing cholangitis. *Gastroenterology* **1980**;79:200-206
12. Whelton MJ. Sclerosing cholangitis. In: Bouchier IAD, ed. *Clinics in gastroenterology*, vol. 2, No. 1. London: Saunders, **1973**:163-173
13. Cameron JL, Gayler BW, Sanfey M, et al. Sclerosing cholangitis: anatomical distribution of obstructive lesions. *Am Surg* **1984**;200:54-60
14. Doyle TC, Roberts-Thomson IC. Radiological features of sclerosing cholangitis. *Australas Radiol* **1983**;27:163-166
15. Albo R, Obata W. Radiologic diagnosis of primary sclerosing cholangitis. *Radiology* **1963**;81:123-125
16. Rogers JV, Copeland AJ, Schroder JS, Amerson JR. Sclerosing cholangitis: roentgenographic features. *South Med J* **1972**;65:587-594
17. Krieger J, Seaman WB, Porter MR. The roentgenologic appearance of sclerosing cholangitis. *Radiology* **1970**;95:369-375
18. Wells IP, Wheeles PG, Laws JW, Williams R. A new appearance of the common bile duct in sclerosing cholangitis. *Br J Radiol* **1980**;53:502-504
19. Abbruzzese AA. Retrograde cholangiography and sclerosing cholangitis. *Dig Dis Sci* **1974**;19:571-574
20. Choi TK, Wong KP, Wong J. Cholangiographic appearance of clonorchiasis. *Br J Radiol* **1984**;57:681-684
21. Dickson GH. A "corrugated" extrahepatic bile duct: a new cholangiographic picture. *Br J Surg* **1973**;60:161-162
22. Turner JA, Cho SR, Messmer JM. Pitfalls in cholangiographic interpretation. *RadioGraphics* **1987**;7:1067-1105

Book Review

Thyroid Disease. Endocrinology, Surgery, Nuclear Medicine, and Radiotherapy. Edited by Stephen A. Falk. New York: Raven, 670 pp., 1990. $125

This book has 40 chapters and 56 contributors and is edited by a thyroid surgeon. Although it attempts to integrate the perspectives of the many specialists who deal with thyroid disease—endocrinologists, surgeons, nuclear physicians, radiologists, radiotherapists, and oncologists—it appears to be weighted toward a surgical perspective.

The first chapters deal with anatomy, embryology, and thyroid hormone physiology and are well written and well illustrated. The chapter on the clinical approach to thyroid function tests is concise and contains up-to-date information. The chapter on dosimetry of radionuclides is overly comprehensive and could have been included in an abbreviated format as part of chapter 6. Chapter 6 deals with basic concepts in imaging with radiopharmaceuticals, but its scope of information is limited. Additional limitations of this chapter include overstressing the importance of flow studies during thyroid scintigraphy and the inclusion of multiple rectilinear images.

Chapter 7, which deals with diagnostic imaging of the thyroid, strays from the format used in the rest of the text by having an index of the 49 images included at the beginning of the chapter and by placing all its images at the end of the chapter. This significantly detracts from the integration of the visual and textual information. The chapter was written by two otolaryngologists and a nuclear medicine physician, who placed too much emphasis on the value of CT, MR, and angiography and too little on that of radionuclide scanning. The chapter on thyroid disease is not well organized; it is overly detailed and overly annotated with 929 references. Six well-written chapters on hyperthyroidism include discussions of systemic effects; differential diagnosis; and medical, surgical, and iodine-131 therapy. This includes two sections on Graves ophthalmopathy, including management and controversies. Additional chapters cover hypothyroidism, thyroiditis, thyroid nodules, and congenital thyroid disorders and are well written. Parts of chapter 25, on the etiopathogenesis of thyroid cancer, are interesting, but the chapter is twice as long as it should be. The four chapters on the surgical approach to different thyroid neoplasms are concise and well illustrated. The last six chapters of the text cover the surgical techniques of thyroidectomy and complications of thyroid surgery.

This book does have the expected problems of a text that has more than one author. Some redundancy occurs. As the editor notes, some of this redundancy is helpful because of different perspectives, but in some areas it is detrimental. The quality of the illustrations is variable. The CT scans and MR images and most of the radionuclide scans appear to be adequate, although some of the annotations are handwritten. The black-and-white photographs of surgical specimens are often suboptimal because of glare, and they would be more illustrative if they were accompanied by hand drawings.

Radiologists and nuclear physicians will not be persuaded to purchase this text on the basis of the imaging sections but rather will buy it for the interdisciplinary approach to the care and management of patients with thyroid disorders. This book will find its place in the libraries of physicians and institutions involved in the day-to-day care of thyroid patients, particularly thyroid patients who have surgical problems.

Gary G. Winzelberg
Shadyside Hospital
Pittsburgh, PA 15232

Biliary Lithotripsy: Correlation Between Gallbladder Contractility Before Treatment and the Success of Treatment

Jennifer J. Donald[1]
J. Stephen Fache
H. Joachim Burhenne

We perform biliary lithotripsy without adjuvant chemolitholytic agents, and therefore fragment clearance depends solely on the gallbladder's ability to evacuate its contents. We studied 205 patients to determine if gallbladder contractility before biliary lithotripsy is a predictor of treatment results and rate of fragment clearance. Percentage gallbladder contraction was calculated from the fractional difference in the sonographically measured gallbladder volumes before and after a fatty meal. Seventy-six patients (37%) were free of stones and fragments, and 129 patients (63%) had residual fragments at comparable follow-up intervals. Statistical analysis showed a significant difference in gallbladder contractility before biliary lithotripsy between the fragment-free group and the residual-fragment group ($p = .008$). Stone burden before treatment showed no significant difference between the groups ($p = .074$), but the number of stones was significantly less in the fragment-free group ($p = .022$). In the fragment-free group, a poor correlation ($r = .047$) was found between the percentage gallbladder contraction and the rate of fragment clearance.

These data indicate that contractility of the gallbladder before treatment correlates with overall success of biliary lithotripsy but is not a predictor of the speed of fragment clearance.

***AJR* 157:287–290, August 1991**

Biliary lithotripsy is a safe and well-established means of fragmenting gallbladder calculi, with reported efficacy rates of 80–99% in selected patients [1–3]. The factors that contribute to fragment clearance once the stones are disintegrated sufficiently to pass through the cystic duct are incompletely understood. The clinical success of biliary lithotripsy relies on the sonographic demonstration of a fragment-free gallbladder.

Unlike most other centers, we do not include oral chemolitholysis in our treatment protocol, and fragment clearance therefore depends solely on the gallbladder's ability to evacuate the fragments. To determine the influence of gallbladder contractility on the success or failure of biliary lithotripsy, we used follow-up sonographic examinations to determine fragment-clearance rates in 205 patients who had completed treatment. Gallbladder contractility was measured before biliary lithotripsy in all patients by using the sonographic method previously described [4].

Subjects and Methods

We used sonography to determine fragment-clearance rates in 205 patients (139 females, 66 males; mean age, 51 years; range, 14–84 years) who had undergone biliary lithotripsy for symptomatic cholecystolithiasis. Our selection criteria and treatment protocol were as previously described [5]. All patients were considered to have had successful fragmentation and completed biliary lithotripsy when sonographic examination showed that residual fragments were 3 mm or less in diameter.

Received January 22, 1991; accepted after revision March 7, 1991.

[1] All authors: Department of Radiology, University of British Columbia and Vancouver General Hospital, 855 W. 12th Ave., Vancouver, B.C., Canada V5Z 1M9. Address reprint requests to H. J. Burhenne.

0361-803X/91/1572-0287
© American Roentgen Ray Society

Before treatment, gallbladder volume was measured by using the ellipsoid method described by Dodds et al. [4]. Volumes were determined before and 45–60 min after the administration of a fatty meal containing cottonseed oil (Neo-Cholex; Horner, Montreal, Quebec). Percentage gallbladder contraction was calculated by dividing the difference between the preprandial and postprandial volumes by the initial preprandial volume and multiplying the result by 100. An index of pretreatment stone burden was devised; we assumed that if a patient had multiple calculi, the calculi made up one family of stones and the largest stone measured was representative of the size of other members of the family. The stone burden index was calculated by using the following equation: (maximum stone diameter in mm)^3 × number of stones.

During follow-up, treatment was considered successful only if sonography showed that the gallbladder was free of stones and fragments.

For statistical analysis, the patients were grouped according to their most recent sonographic findings either as being stone- and fragment-free or as having residual fragments. Follow-up periods available, measurements of gallbladder contractility before treatment, maximum stone size, number of stones, and stone burden index were evaluated by using the Mann-Whitney test. Results from patients who had only one stone before treatment were analyzed separately. In the successful group, the rate of fragment clearance was correlated with the percentage gallbladder contractility before treatment.

Results

To date, of the 205 patients studied, 76 (37%) are free of stones and fragments and 129 (63%) have residual fragments.

Values of percentage gallbladder contraction before biliary lithotripsy were between 20% and 94%, with an overall average of 62% for the study population. Values of percentage gallbladder contraction were between 20% and 94% (average, 66%) in fragment-free patients and 20% to 90% (average, 59%) in patients with residual fragments (Fig. 1). The fragment-free group had a significantly greater percentage gallbladder contraction than did the group with residual fragments ($p = .008$).

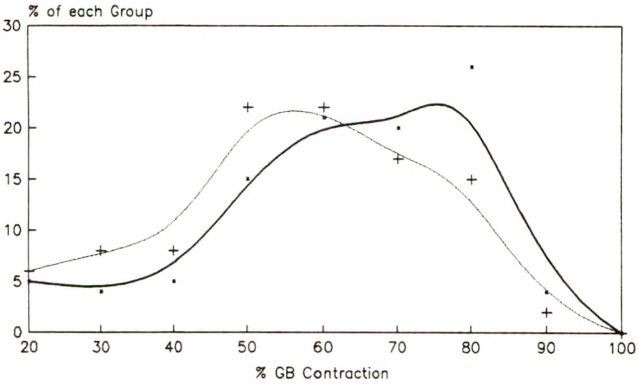

Fig. 1.—Distribution of measurements of gallbladder (GB) contractility before biliary lithotripsy. Fragment-free patients (*n* = 76, *thick line*) vs patients with residual fragments (*n* = 129, *thin line*).

TABLE 1: Details of the Stone Populations Before Treatment: Fragment-Free Group vs Residual-Fragment Group

	Stone and Fragment Free (*n* = 76)	Residual Fragments (*n* = 129)	*p* Value
Number of stones (average)	1–6 (1.53)	1–6 (1.98)	.022
Maximum size (mm) (average)	4–40 (14.9)	5–33 (16.2)	.100
Stone burden index (average)	64–69,120 (9535)	91–179,685 (11,792)	.074

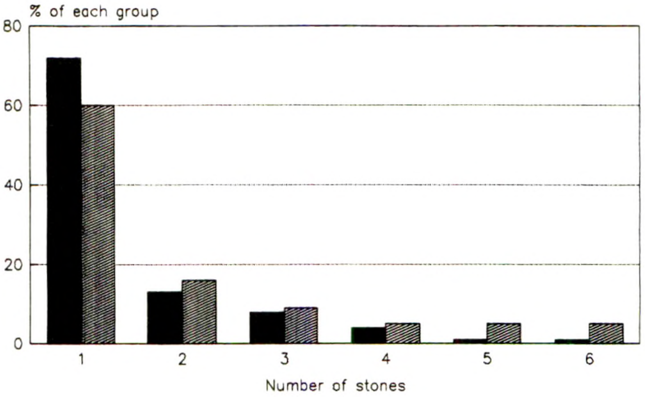

Fig. 2.—Distribution of number of stones before biliary lithotripsy. Fragment-free patients (*n* = 76, *solid bars*) vs patients with residual fragments (*n* = 129, *hatched bars*).

The number and maximum size of stones and the stone burden index before treatment are listed in Table 1. Initial stone burden index varied between 64 and 69,120 (average, 9535) in the fragment-free group and between 91 and 179,685 (average, 11,792) in the patients with residual fragments. No significant difference ($p = .074$) in the initial stone burden was found between the groups. A significant difference ($p = .022$) between the groups was found in the numbers of stones present before treatment (Fig. 2); a higher proportion of patients with only one stone were in the fragment-free group (72% vs 60%). Analysis of patients who had only one stone initially showed significantly greater gallbladder contractility before biliary lithotripsy in the fragment-free patients than in those with residual fragments ($p = .018$).

The follow-up interval from the last biliary lithotripsy in the fragment-free group varied from 0.7 to 110.0 weeks and in the residual-fragment group from 0.1 to 83.0 weeks. Statistical analysis showed no significant difference ($p = .418$) in the length of follow-up periods between the groups.

Within the fragment-free group, the interval from last biliary lithotripsy to a fragment-free gallbladder ranged from 0 to 83 weeks (average, 11 weeks). Percentage gallbladder contraction correlated poorly ($r = .047$) with the time interval from the last lithotripsy session to a stone-free gallbladder.

Discussion

The success of biliary lithotripsy without adjuvant oral chemolitholysis relies on adequate fragmentation of the gallbladder calculi and subsequent passage of the stone fragments from the gallbladder. In this situation, the fragments need to be as small as possible to enable unobstructed passage via the cystic duct. In order to achieve this, our treatment protocol, unlike others, allows up to 20,000 shocks to be administered to reduce the residual fragments to 3 mm or less in size. It is unclear why small stones are not all cleared from the gallbladder during their formation, yet we expect the majority of patients to clear all gallstone fragments after biliary lithotripsy. Spontaneous passage of implanted fragments up to a maximum diameter of 4 mm from the gallbladder of dogs has been shown to occur independently of fragment size, but this is of questionable clinical relevance as, unlike humans, dogs have no Heister valves [6]. In humans, the Munich group [7] found no relationship between the maximum size of the fragments and the occurrence of biliary pain, but a significant correlation between the size of the largest fragments and the time needed to complete clearance. Fragments up to 8 mm in size have been recovered from the feces of patients after biliary lithotripsy [8].

Gallbladder motility is impaired in most patients who have gallstones [9–14], but whether the increased gallbladder volume and decreased postprandial fractional emptying is a primary or a secondary abnormality remains to be determined [14]. Dissolution with bile acids is used routinely as adjuvant therapy in all other centers as part of their biliary lithotripsy protocol. Its role separate from the gallbladder's ability to expel the fragments therefore cannot be determined. Our overall results for biliary lithotripsy compare favorably with those from other groups, with complete clearance rates for single stones on the order of 70% at 12 months follow-up [15]. These findings therefore raise a question about the role of adjuvant chemolitholysis, particularly as it is expensive and both chenodeoxycholic acid and ursodeoxycholic acid therapy have been shown to affect gallbladder contractility adversely [16–18]. In view of the importance of gallbladder dynamics, it is of note that no long-term adverse effects on gallbladder motility have been shown after biliary lithotripsy, although the defect associated with gallstone disease does not appear to be abolished by removal of the stones [19, 20].

The percentage gallbladder contraction before biliary lithotripsy, was calculated from sonographic measurements of gallbladder volume made before and after a fatty meal stimulus. Sonography is a valid and accurate means of assessing gallbladder volume when compared with an in vitro model of known volume [4, 21] and simultaneous oral cholecystography [21]. The intraobserver and interobserver variation in measurement of gallbladder size is usually within 10% [4, 21]. Previously we have shown that a minimum value of 20% gallbladder contraction determined by sonography is as accurate as oral cholecystography in predicting cystic patency, and we regularly use this method to assess patients' eligibility for biliary lithotripsy (McGrath FP et al., presented at the Third International Interdisciplinary Symposium on Biliary Lithotripsy, September 1990). Our protocol excludes patients with values below 20%.

It seems reasonable that with improved gallbladder emptying, an associated increase in the success rate of biliary lithotripsy will occur. Our data support this hypothesis. However, it is not clear why the percentage gallbladder contraction correlates so poorly with the rate of fragment clearance. The apparently poor success rate of 37% in this series is misleading and is due to the limited follow-up (overall mean, 30.9 weeks) available in the majority of patients. The number of stones before treatment was significantly different between the groups, with a larger proportion of single stones occurring in the fragment-free patients. These findings agree with others, with the highest reported success rates occurring in patients with single stones up to 20 mm in diameter [3]. Gallbladder contractility remained significantly higher in the fragment-free patients even when we analyzed only the patients who initially had only one stone. Rather unexpectedly, we found that success did not depend on the original stone burden. This suggests that if fragmentation is adequate, successful treatment can be expected irrespective of the original stone burden.

The mechanism of fragment clearance most likely is multifactorial, including various aspects of gallbladder pathophysiology and dynamics. The need for adjuvant chemolitholysis is not proved, and our experience indicates that it is not a prerequisite for successful treatment. As fragmentation is usually not the limiting factor for the success of biliary lithotripsy, efforts should be taken to determine further possible factors that may influence the rate and success of fragment clearance, including medication to increase gallbladder contraction.

REFERENCES

1. Sackmann D, Delius M, Sauerbruch T, et al. Shock-wave lithotripsy of gallbladder stones: the first 175 patients. *N Engl J Med* **1988**;318:393–397
2. Rawat B, Fache JS, Malone DE, Burhenne HJ. Biliary lithotripsy without oral chemolitholysis: the Vancouver experience. In: Burhenne HJ, Paumgartner G, Ferrucci JT, eds. *Biliary lithotripsy II*. Chicago: Year Book Medical, **1990**:111–118
3. Barkun ANG, Ponchon T. Extracorporeal biliary lithotripsy: review of experimental studies and a clinical update. *Ann Intern Med* **1990**;112:126–137
4. Dodds WJ, Gron WJ, Darweesh RMA, Lawson TL, Kishk SMA, Kern MK. Sonographic measurement of gallbladder volume. *AJR* **1985**;145:1009–1011
5. Burhenne HJ, Becker CD, Malone DE, Rawat B, Fache JS. Biliary lithotripsy: early observations in 106 patients. *Radiology* **1989**;171:363–367
6. Delius M, Enders G, Brendel W. Passage of stone fragments from the gallbladders of dogs. *Surg Gynecol Obstet* **1988**;166:241–244
7. Sackmann M, Sauerbruch T, Holl J, Pauletzki J, Delius M, Paumgartner G. Fragment clearance after extracorporeal biliary lithotripsy. In: Burhenne HJ, Paumgartner G, Ferrucci JT, eds. *Biliary lithotripsy II*. Chicago: Year Book Medical, **1990**:73–78
8. Greiner L, Munks C, Heil W, Jakobeit C. Gallbladder stone fragments in feces after biliary extracorporeal shock wave lithotripsy. *Gastroenterology* **1990**;98:1620–1624
9. Shaffer EA, McOrmond P, Duggan H. Quantitative cholescintigraphy: assessment of gallbladder filling and emptying and duodenogastric reflux. *Gastroenterology* **1980**;79:899–906
10. Fischer RS, Stelzer F, Rock E, Malmud LS. Abnormal gallbladder emptying in patients with gallstones. *Dig Dis Sci* **1982**;27:1019–1024
11. Thompson JC, Fried GM, Ogden WD, et al. Correlation between release of cholecystokinin and contraction of the gallbladder in patients with gallstones. *Ann Surg* **1982**;195:670–675
12. Forgacs JC, Masey MN, Murphy GM, Dowling RH. Influence of gallstones and ursodeoxycholic acid therapy on gallbladder emptying. *Gastroenterology* **1984**;87:299–307

13. Pomeranz IS, Shaffer EA. Abnormal gallbladder emptying in a subgroup of patients with gallstones. *Gastroenterology* **1985**;88:787–791
14. Kishk SMA, Darweesh RMA, Dodds WJ, et al. Sonographic evaluation of resting gallbladder volume and postprandial emptying in patients with gallstones. *AJR* **1987**;148:875–879
15. Fache JS, Anderson FH, Forward AD, Burhenne HJ. Gallstone lithotripsy: the Vancouver experience. *Br Columbia Med J* **1990**;32:440–442
16. Howard P, Murphy GM, Dowling RH. Effects of chenodeoxy (CDCA) and ursocholic acids (UCA) on gallbladder (GB) emptying (abstr.) *Gut* **1985**;26:A1124
17. Sylwestrowicz TA, Shaffer EA. Gallbladder function during gallstone dissolution: effect of bile acid therapy in patients with gallstones. *Gastroenterology* **1988**;95:740–748
18. Shaffer EA. Influence of bile acid therapy on gallbladder function. In: Burhenne HJ, Paumgartner G, Ferrucci JT, eds. *Biliary lithotripsy II*. Chicago: Year Book Medical, **1990**:143–149
19. Spengler U, Sackmann M, Sauerbruch T, Holl J, Paumgartner G. Gallbladder motility before and after extracorporeal shock-wave lithotripsy. *Gastroenterology* **1989**;96:860–863
20. Rawat B, Fache JS, Burhenne HJ. Altered gallbladder contractility following extracorporeal shockwave cholecystolithotripsy. *AJR* **1991**;157: (in press)
21. Everson GT, Braverman DZ, Johnson MJ, Kern F Jr. A critical evaluation of real-time ultrasonography for the study of gallbladder volume and contraction. *Gastroenterology* **1980**;79:40–46

LIST OF BOOK AND VIDEOTAPE REVIEWS

254 **The Lungs, 3rd ed.** *Corrin B, ed.*
266 **Clinical Radiology of the Breast.** *Roebuck EJ*
286 **Thyroid Disease: Endocrinology, Surgery, Nuclear Medicine, and Radiotherapy.** *Falk SA, ed.*
310 **Therapeutic Endoscopy and Radiology of the Gut, 2nd ed.** *Bennett JR, Hunt RH, eds.*
330 **CT and MRI of the Genitourinary Tract.** *Goldman SM, Gatewood OMB, eds.*
340 **MRI of the Wrist and Hand.** *Reicher MA, Kellerhouse LE*
346 **The Radiologic Clinics of North America. Imaging of Joints.** *Kaye JJ, ed.*
352 **Radiology in the Management of Cancer.** *Johnson RJ, Eddleston B, Hunter RD, eds.*
380 **RSNA Today, Vol. 4, No. 4.** *Casarella WJ, moderator*
408 **Physics and Instrumentation of Diagnostic Medical Ultrasound.** *Fish P*

Technical Note

The Management of Occluded Metallic Self-Expandable Biliary Endoprostheses

James E. Jackson,[1] Mary E. Roddie,[1] Naren Chetty,[1] Irving S. Benjamin,[2,3] and Andreas Adam[1]

Self-expandable metallic endoprostheses are often inserted for the relief of bile duct obstruction due to inoperable malignant bile duct tumors [1-3]. Concern has arisen that these stents may be prone to early occlusion due to ingrowth of tumor through the side mesh [2] and that once occluded, further palliation might be difficult because the stents cannot be removed. In our experience, however, stent occlusion has only occurred with tumor overgrowth around the ends of the endoprosthesis and in these patients it has been easy to restore bile duct patency.

Materials and Methods

Since September 1988, 44 patients with malignant obstruction of the bile ducts have undergone 49 stent insertions that used a total of 79 Wallstent (Wallstent, Medinvent SA, Lausanne, Switzerland) endoprostheses. Five of these 44 patients have been lost to follow-up. Of the remaining 39 patients, 29 have died, with a mean stent patency (30 stent insertions) of 19 weeks. The 10 patients who are still alive have a mean stent patency (13 stent insertions) of 31 weeks. Four patients have returned on a total of five occasions with stent occlusion, and these patients form the basis of this article.

Between March 1989 and June 1990, four patients (three men and one woman), with ages ranging between 65 and 79 years, who had previously undergone insertion of a self-expandable metallic endoprosthesis were admitted on a total of five occasions with recurrent jaundice and pruritus. The tumors involving the bile ducts in these patients were hilar cholangiocarcinoma in two patients and metastases from rectal adenocarcinoma in the other two.

The original endoprostheses had been inserted 2, 13, 16, and 60 weeks before recurrence of jaundice and had been placed via a left hepatic duct approach in three patients and a right hepatic duct approach in one. Percutaneous transhepatic cholangiograhy (PTC) revealed the cause of the original stent dysfunction to be tumor overgrowth around the end of the endoprosthesis on three occasions and poor stent position on one occasion, in the patient who returned just 2 weeks after initial stent insertion. One patient returned 7 weeks after insertion of his second metallic endoprosthesis with recurrent jaundice. PTC again showed the cause to be tumor overgrowth around the top of the stent. The tumor growth around the ends of the endoprostheses was easily bypassed by using conventional catheter and wire techniques, and a further stent was introduced through the lumen of, and was placed overlapping with, the previously inserted endoprosthesis. On no occasion was there any difficulty in bypassing the occlusion or in catheterizing the stent. No complications occurred; in particular, no episodes of cholangitis or bleeding related to the procedures occurred. The new stent was a self-expandable metallic endoprosthesis on four occasions and a Miller plastic endoprosthesis (William Cook Europe, Bjaeverskov, Denmark) on one occasion.

All patients developed relief from jaundice and pruritus after the procedures. One patient has been lost to follow-up. One patient died 17 weeks after the insertion of the second stent. Two patients remain anicteric 18 and 24 weeks after their last stent insertion.

Discussion

Inoperable malignant tumors causing bile duct obstruction are often well palliated by the insertion of a biliary endoprosthesis, which can be introduced via a transhepatic or endoscopic route.

Plastic stents have been used for several years but, more recently, metallic self-expandable endoprostheses have been

---

Received December 12, 1990; accepted after revision February 26, 1991.

[1] Department of Diagnostic Radiology, Royal Postgraduate Medical School, Hammersmith Hospital, Du Cane Rd., London, W12 OHS, England.
[2] Department of Hepatobiliary Surgery, Royal Postgraduate Medical School, Hammersmith Hospital, Du Cane Rd., London, W12 OHS, England.
[3] Present address: Department of Surgery, King's College School of Medicine and Dentistry, Denmark Hill, London, SE5, England.

AJR 157:291-292, August 1991 0361-803X/91/1572-0291 © American Roentgen Ray Society

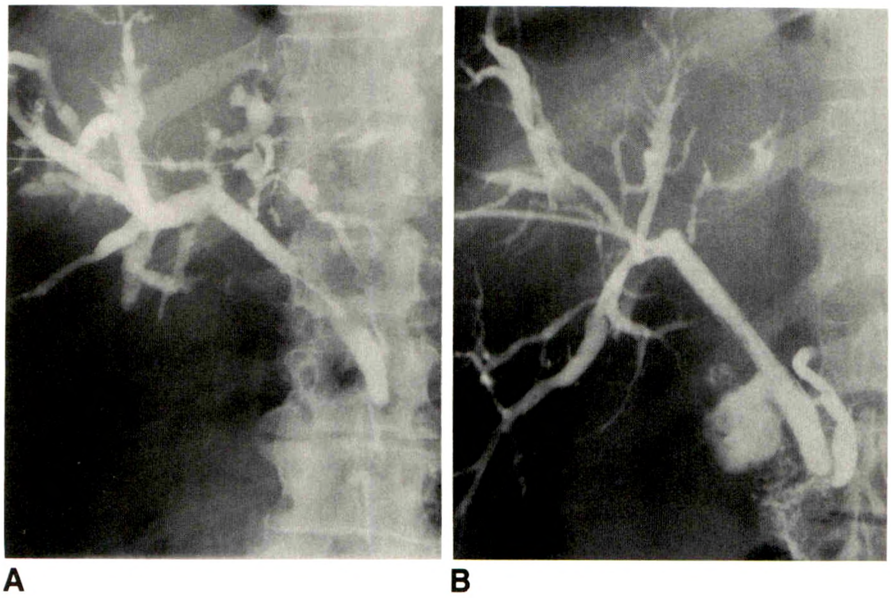

Fig. 1.—79-year-old woman with hilar cholangiocarcinoma.

***A*, A 5-cm-long, 10-mm-diameter, metallic endoprosthesis had been inserted 13 weeks previously. Percutaneous transhepatic cholangiogram shows dilated right hepatic ducts and atrophic, strictured left hepatic ducts. Metallic endoprosthesis extends from right hepatic duct into common bile duct and is patent. A tight stricture due to tumor overgrowth is present below stent.**

***B*, A 5-cm-long, 10-mm-diameter, metallic endoprosthesis has been inserted across stricture, overlapping original stent with its distal end just above papilla of Vater. Cholangiogram obtained 24 hr after insertion shows patency of two metallic endoprostheses with free flow of contrast medium into duodenum. The patient remained anicteric until she died of disseminated malignancy 17 weeks later.**

developed [1–3] and have several advantages. The small-caliber introducing catheters create a small transhepatic track and allow introduction in one session. Dilatation of a large track through the liver is unnecessary and the procedure is therefore safer, easier, and less uncomfortable for the patient [3]. When released, the stent expands to a maximum internal diameter of 10 mm, much larger than even the largest transhepatic or endoscopic plastic stent.

One of the reported disadvantages of self-expandable metallic endoprostheses in malignant bile duct obstruction is ingrowth of tumor through the mesh of the stent, which may result in early occlusion [2]. This has not been observed in our series of patients, in whom only four of 44 patients (49 stent insertions, 79 Wallstent endoprostheses) have returned with stent occlusion on a total of five occasions, and none has shown tumor ingrowth through the stent wall.

It is common to see the internal lumen of these self-expandable metallic endoprostheses narrowed soon after insertion; in fact, this is often seen during cholangiography done 24 hr after insertion of the stent, and it is therefore most probably due to the stent pressing into the tumor as has been seen on cholangioscopy (Dick R, personal communication). In our experience, this has never caused significant obstruction and has never progressed to occlusion. We have also found that the placement of the proximal end of the stent in a segmental duct does not occlude the segmental branches that the stent crosses. These continue to drain normally through the sides of the stent and are often seen to fill retrogradely during subsequent cholangiography. However, such a duct may occasionally require drainage at a later date because of occlusion by tumor. In such circumstances it may be possible to drain this duct through the side mesh of the endoprosthesis that is crossing its origin [4].

Long-standing patency of self-expandable metallic endoprostheses in malignant obstruction of the bile ducts at the liver hilum is more likely to be achieved by placing the stent across the stricture, with a large portion of the stent(s) both proximal and distal to the stricture in disease-free duct. This is particularly important in aggressive, more rapidly growing tumors such as metastases to hilar nodes.

Patients with obstructive jaundice due to inoperable tumors of the pancreatic head may also be palliated by the insertion of an endoscopic or percutaneous endoprosthesis. It is not uncommon, in this group of patients, to see not only occlusion of the lower common bile duct by the pancreatic head tumor, but also involvement of the ducts at the liver hilum by lymph node metastases. In view of this, it is our policy in those patients in whom endoscopic stent insertion is unsuccessful, to position a long metallic endoprosthesis percutaneously from the level of the papilla of Vater across the lower common bile duct stricture up to the bifurcation or into the right hepatic duct. This is in the hope of preventing, or at least postponing, occlusion of the biliary tree by hilar lymphadenopathy.

On the basis of our experience, we believe that metallic self-expandable biliary stents are easier to insert and are less likely to become occluded than are conventional endoprostheses. If occlusion occurs, it is easier to restore patency in patients with the metallic stents than it is in patients with plastic endoprostheses.

REFERENCES

1. Dick R, Gillams A, Dooley JS, Hobbs KEF. Stainless steel mesh stents for biliary strictures. *J Intervent Radiol* **1989**;4:95–98
2. Gillams A, Dick R, Dooley JS, Wallsten H, el-Din A. Self-expandable stainless steel braided endoprosthesis for biliary strictures. *Radiology* **1990**;174:137–140
3. Adam A, Yeung EYC, Chetty N, Roddie MR, Benjamin IS. Self-expandable stainless steel endoprostheses for the treatment of malignant bile duct obstruction. *AJR* (in press)
4. Boothroyd A, Williams SJ, Hatfield ARW, Mason R. Percutaneous insertion of a polyethylene biliary endoprosthesis through the side mesh of a self expanding metal stent. *J Intervent Radiol* **1990**;5:127–130

Diagnosis of Portal Vein Thrombosis: Value of Color Doppler Imaging

Franklin N. Tessler[1]
Brian J. Gehring[1]
Antoinette S. Gomes[1]
Rita R. Perrella[1]
Nagesh Ragavendra[1]
Ronald W. Busuttil[2]
Edward G. Grant[1]

This study was undertaken to determine the accuracy of color Doppler imaging in the diagnosis of portal vein thrombosis. Two hundred fifteen patients were studied with color Doppler imaging to determine patency of the main portal vein. Sonographic findings were confirmed in 75 patients, aged 19 to 66 years. Correlation with angiography was obtained in 13 patients, and surgical correlation was obtained in the remaining 62. Nine patients had portal vein thrombosis on the basis of these gold standards. Sonograms were classified as showing either patency or thrombosis, depending on the ability to show color flow within the main portal vein. Agreement between sonography and angiography or surgery was found in 69 patients (61 patent, eight thrombosed). One patient with a patent portal vein at sonography was found to have a thrombosed vessel at surgery, whereas five patients without portal venous flow at sonography had patent vessels at angiography (one patient) or surgery (four patients). Overall sensitivity and specificity for detection of portal vein thrombosis were 89% and 92%, with an accuracy of 92%, a false-negative rate of 0.11, a negative predictive value of 0.98, and a positive predictive value of 0.62. We postulate that the majority of errors in our study occurred in vessels that, although patent, had only sluggish flow, which could not be resolved because of technical limitations.

We conclude that color Doppler imaging is a valuable screening procedure for the assessment of portal vein patency. If the sonogram shows a patent portal vein, no further studies are required. However, a lack of demonstrable flow does not always indicate thrombosis, and other imaging studies should be performed for confirmation.

***AJR* 157:293–296, August 1991**

Portal vein thrombosis (PVT) can be diagnosed noninvasively by using either real-time or duplex Doppler sonography [1–9], CT [7], or MR [10]. Gray-scale sonography does not provide information about flow dynamics in the portal vein. Instead, the diagnosis of PVT is based on the demonstration of echogenic thrombus and other morphologic features [3]. Unfortunately, if the thrombus in hypoechoic, or if the lumen appears relatively echogenic despite vascular patency, portal venous thrombosis may be missed or falsely diagnosed [9]. Use of Doppler sonography, with its ability to detect and characterize blood flow, can improve diagnostic accuracy [5, 9]. However, duplex Doppler sonography only measures flow within a small volume at any given time; therefore, sampling from multiple sites is necessary to obtain a global impression of flow within the portal vein. Moreover, an apparently normal Doppler signal may be obtained from collateral vessels in patients who have occlusion of the portal vein [5].

By superimposing color-coded information on a gray-scale image, color Doppler imaging (CDI) provides a rapid, noninvasive means of mapping blood flow within a region of interest, thereby overcoming many of the limitations of gray-scale and duplex Doppler imaging [11]. CDI has been used to diagnose venous thrombosis in both the lower and upper extremities [12, 13]. In two recent studies, CDI was used for evaluation of the portal venous system; however independent confirmation

Received February 7, 1991; accepted after revision March 28, 1991.

[1] Department of Radiological Sciences, UCLA School of Medicine, CHS 77-132, 10833 Le Conte Ave., Los Angeles, CA 90024-6904. Address reprint requests to F. N. Tessler.

[2] Department of Surgery, UCLA School of Medicine, CHS BR-272, 10833 Le Conte Ave., Los Angeles, CA 90024-1721.

0361-803X/91/1572-0293
© American Roentgen Ray Society

of the sonographic findings was not performed [14, 15]. The purpose of our study was to determine if CDI could be used to diagnose PVT. The results of angiography and surgery were used as the gold standards.

Subjects and Methods

Between September 1988 and May 1990, CDI was used to evaluate the hepatic vasculature in 215 patients. Color flow imaging of the portal vein was performed by using commercially available equipment (Ultramark 9, Advanced Technology Laboratories, Bothell, WA) and 2.25- and 3.0-MHz phased-array transducers. Real-time sonography was used first to locate the portal vein at the level of the porta hepatis. The color flow system was then activated, the region of interest was placed over the portal vein, and the scanning parameters were adjusted until consistent, nonrandom color appeared within the vessel (Fig. 1).

Whenever flow could not be shown despite careful manipulation of CDI controls (Fig. 2), a duplex Doppler examination of the portal vein was performed also. If the portal vein could not be seen with real-time sonography, color and spectral Doppler imaging of the porta hepatis were performed to search for venous flow. CDI of the hepatic veins, the inferior vena cava, and the hepatic artery was performed also in selected cases, depending on the indication for the study. All the CDI studies were performed by experienced operators, without knowledge of angiographic findings.

Angiographic or surgical confirmation of portal vein patency or thrombosis was available in 75 of the 215 patients (34 men, 41 women; age range, 19 to 66 years, mean 45 years). These patients made up the final study group. Seventy sonograms were performed as part of a workup for hepatic transplantation, two because of transplant failure, one prior to portosystemic shunt surgery, and two after shunt procedures. Angiographic correlation was obtained in 13 patients. The portal venous system was evaluated angiographically with high-dose portal arteriography with selective celiac and/or splenic artery and superior mesenteric artery injections. Tolazoline 25 mg (Ciba-Geigy, Summit, NJ) was administered intraarterially for the superior mesenteric artery injections. Delayed films and film or digital subtraction techniques were used when needed to evaluate the portal venous system. The interval between CDI and angiography ranged from 0 to 334 days, with a median of 2 days. Surgical correlation was obtained in 62 patients. The interval between CDI and surgery ranged from 2 to 327 days, with a median of 90 days.

The sonograms and angiograms were classified as showing either patency or thrombosis of the main portal vein; no attempt was made to grade flow. Because our purpose was to determine the accuracy of CDI in detecting PVT, absence of color within the portal vein was our sole criterion for diagnosing PVT. Although cases were reviewed retrospectively, this classification was based entirely on the appearance of the portal vein at the time of the examination. Surgical correlation was obtained through a review of surgical reports and summary sheets, which clearly indicated the condition of the portal vein at surgery.

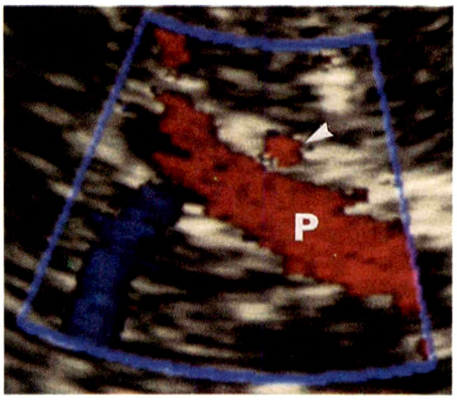

Fig. 1.—65-year-old woman with a patent portal vein, proved surgically. Oblique color Doppler sonogram of porta hepatis shows portal vein (P) filled with color. Because flow is directed toward transducer (into liver), it is depicted in red. Blue color indicates flow in a branch directed away from transducer. Hepatic artery (*arrowhead*) is seen in cross section, anterior to portal vein.

Results

In 13 patients in whom CDI was compared with angiography, the sensitivity for detection of PVT was 100%, with a specificity of 88% and a false-negative rate of zero. In the group of 62 patients with surgical correlation, sensitivity and specificity were 75% and 93%, respectively, with a false-negative rate of 0.25. In all, CDI agreed with the gold-standard examination in 69 patients (61 patent, eight thrombosed) and disagreed in six patients (five with a false-positive diagnosis of thrombosis and one with a false-negative diagnosis). Overall sensitivity was 89%, specificity was 92%, and the false-negative rate was 0.11. Accuracy for diagnosis of PVT in all 75 patients was 92%, with a negative predictive value of 0.98 and a positive predictive value of 0.62. In 12 patients in whom angiography was compared with surgery, sensitivity and specificity were 100% and 90%, with a false-negative rate of zero.

To assess the possible effect of an excessive delay between CDI and the gold-standard examination, we performed a separate analysis in a subset of 24 patients in whom 1 month or less elapsed between sonography and angiography or surgery. In this group, sensitivity for detection of PVT was 100%, specificity was 89%, and the false-negative rate was zero.

One patient in whom sonography showed a patent portal vein had a thrombosed vessel found during surgery; however, 9 months had elapsed between CDI and surgery. Another patient in whom the portal vein was patent on CDI and nonvisualized on angiography had a patent vessel at surgery.

Discussion

Several features of PVT on real-time sonography have been described, including echogenic thrombus, cavernous transformation of the portal vein, collateral formation, and venous enlargement [3]. However, Van Gansbeke et al. [3] were unable to show intraluminal thrombus in 33% of their patients with PVT. In another series comparing duplex Doppler sonography with angiography, Nelson et al. [5] had four patients with PVT; none of the four had intraluminal thrombus identified with real-time sonography, and the diameters of the portal vein were normal in all four. In our nine patients with proved PVT, portal vein echogenicity varied from hypoechoic with internal echoes to echogenic. Significantly, the portal vein could not be located by using real-time sonography in four patients in this group. However, the portal vein may not be visualized when gray-scale imaging is used, even in the absence of thrombosis [1].

Duplex Doppler sonography, with its ability to show flow, can provide direct evidence of portal vein patency [7]. However, Parvey et al. [16] characterized duplex Doppler sonography of the portal vein as "a prodigious technical undertaking" and speculated that CDI might be helpful. Although this might be overstating the difficulty somewhat, duplex Doppler sonography has a variety of pitfalls and technical limitations. In the study by Nelson et al. [5], seven of eight patients with what were described as "inadequate Doppler tracings" had patent vessels at angiography.

CDI combines gray-scale and spectral Doppler imaging and has been used to diagnose thrombosis in the extremities [12, 13], in portosystemic shunts [17], and in the hepatic veins [18]. In a recent study by Ralls [15], CDI was used to detect thrombosis of the main portal vein in 30 patients by using criteria similar to ours. Unfortunately, the findings were not validated independently by any correlative technique or by surgery.

For many patients in our series, considerable time elapsed between CDI and angiography or surgery. However, the results in our patients with a delay of 1 month or less were very similar to those in the overall group. This suggests that the results were not skewed because patients with long intervals between examinations were included. In cases in which both CDI and the gold-standard procedure showed patent vessels (61 of 75 patients), we felt that the interval was irrelevant. Similarly, we did not consider the interval relevant in five patients in whom the diagnosis of PVT based on the CDI findings was incorrect. Arteriography or surgery was performed after CDI, and it is unlikely that thrombosis completely resolved in these patients. The interval might have had an impact in cases in which CDI and the gold-standard procedure both showed PVT (eight patients). However, the mean interval between CDI and angiography was only 3.4 days in five patients with angiographic correlation. Of three patients with surgically proved thrombosis, two had an interval between examinations of only 21 days; 4 months elapsed between CDI and surgery in the remaining patient. We think that the probability that thrombosis developed after CDI in these patients is low.

An excessive interval may have contributed to a discrepancy between CDI and surgical findings in one patient who had a patent portal vein on CDI and a thrombosed vessel at surgery 9 months later. (This was the only false-negative result in our series. Had this patient been excluded, the overall sensitivity would have been 100%, with a false-negative rate of zero.) Apparent portal venous flow seen on CDI in this patient may have originated in a collateral vessel in the setting of cavernous transformation. Care must be taken not to mistake a tortuous hepatic artery (Fig. 3) for collateral vessels; the hepatic artery is characterized by a pulsatile spectral Doppler signal, in contrast to the relatively monophasic flow pattern seen in collateral veins.

Although we did not specifically attempt to determine the accuracy of angiography in the diagnosis of PVT, we were able to compare angiography and surgery in 12 patients. Angiography failed to visualize a portal vein in one patient in whom CDI and surgery both showed a patent vessel. Unfortunately, even the angiographic gold standard is not perfect.

Although CDI may obviate angiography, the techniques are not equivalent, despite the temptation to think of CDI as "sonographic angiography." Angiography directly demonstrates vascular patency by showing a lumen filled with contrast medium, whereas CDI can only imply patency by showing flow. Although vessels with flow on CDI can be considered patent, the converse is not always true.

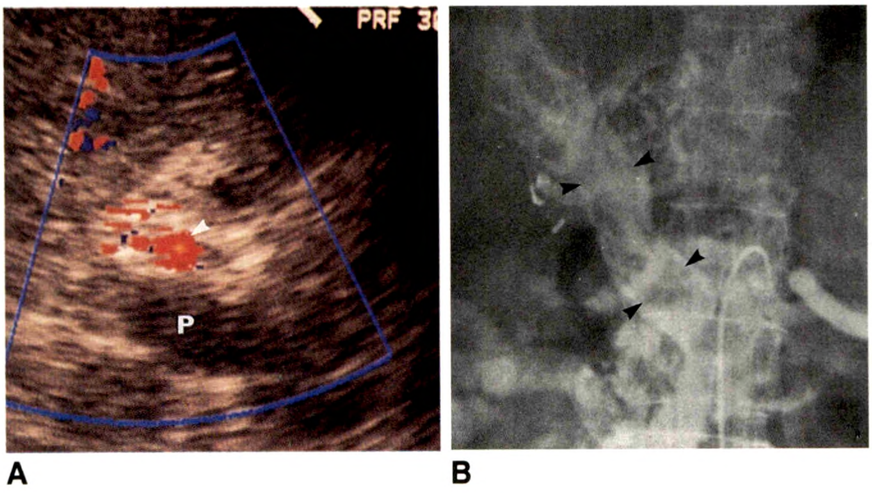

Fig. 2.—61-year-old woman with portal vein thrombosis proved angiographically.

A, Oblique color Doppler sonogram of porta hepatis. Lack of color indicates absence of flow in portal vein (P), implying thrombosis. Hepatic artery is seen anteriorly (*arrowhead*).

B, Venous phase angiogram shows thrombus (*arrowheads*) in portal vein.

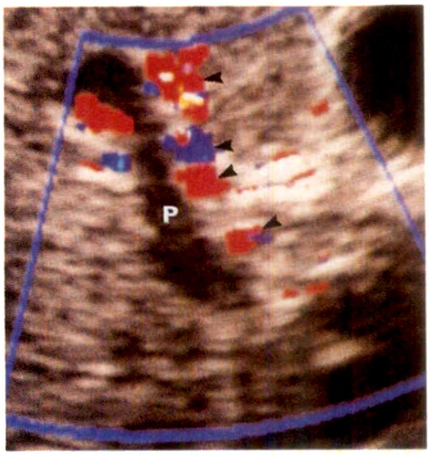

Fig. 3.—36-year-old man with false-positive diagnosis of portal vein thrombosis. Oblique color Doppler sonogram of porta hepatis. No color is seen in portal vein (P), implying thrombosis. Multiple, tortuous hepatic artery loops (*arrowheads*) are seen anteriorly. Main portal vein was found to be patent during surgery.

CDI has technical limitations and pitfalls that can lessen accuracy and lead to erroneous results [19]. In our study, five of six errors made using CDI were false-positives; that is, CDI failed to show flow in portal veins later shown to be patent. We were unable to rescan any of these patients, five of whom had surgery. Any of a number of technical factors (such as inappropriate color gain, output, sensitivity, and gray-scale vs color write priority settings) could have resulted in an artifactual lack of flow. However, in our patients without portal vein flow on CDI, we were always able to show concomitant flow in other vessels such as the inferior vena cava. It is therefore unlikely that significant missettings of the CDI scanning parameters went unnoticed.

Other technical factors could have led to a false-positive diagnosis of PVT in our series. CDI may be incapable of resolving slow flow in some instances [19], depending on the equipment used, the condition of the patient, and the experience of the operator. In CDI of the portal vein, the difficulty is compounded by the depth of the vessel and by the poor clinical status of many patients referred for examination. We postulate that the majority of errors in our series were related to vessels that, although patent, had only sluggish or absent flow. In his study, Ralls [15] diagnosed "static flow" in a portal vein branch that showed no flow on CDI but was opacified on contrast-enhanced CT.

We conclude that CDI, with its high negative predictive value, is a valuable screening procedure for detecting PVT—if the portal vein is shown to be patent, no further studies are required. In patients in whom CDI shows no flow in the portal vein, other imaging studies should be performed to confirm the diagnosis of PVT.

REFERENCES

1. Raby N, Karani J, Powell-Jackson P, Meire H, Williams R. Assessment of portal vein patency: comparison of arterial portography and ultrasound scanning. *Clin Radiol* **1988**;39:381-385
2. Freling NJM, Schuur KH, Haagsma EB, van der Meer J. Ultrasound as first imaging modality in superior mesenteric and portal vein thrombosis. *JCU* **1986**;14:554-557
3. Van Gansbeke D, Avni EF, Delcour C, Engelholm L, Struyven J. Sonographic features of portal vein thrombosis. *AJR* **1985**;144:749-752
4. Garra BS, Shawker TH, Doppman JL, Sindelar WF. Comparison of angiography and ultrasound in the evaluation of the portal venous system in pancreatic carcinoma. *JCU* **1987**;15:83-93
5. Nelson RC, Lovett KE, Chezmar JL, et al. Comparison of pulsed Doppler sonography and angiography in patients with portal hypertension. *AJR* **1987**;149:77-81
6. Koslin DB, Berland LL. Duplex Doppler examination of the liver and portal venous system. *JCU* **1987**;15:675-686
7. Miller VE, Berland LL. Pulsed Doppler duplex sonography and CT of portal vein thrombosis. *AJR* **1985**;145:73-76
8. Harkanyi Z, Temesi M, Varga G, Weszelits V. Duplex ultrasonography in portal vein thrombosis. *Surg Endosc* **1989**;3:79-82
9. Alpern MB, Rubin JM, Williams DM, Capek P. Porta hepatis: duplex Doppler US with angiographic correlation. *Radiology* **1987**;162:53-56
10. Bisset GSI, Strife JL, Balistreri WF. Evaluation of children for liver transplantation: value of MR imaging and sonography. *AJR* **1990**;155:351-356
11. Grant EG, Tessler FN, Perrella RR. Clinical Doppler imaging. *AJR* **1989**;152:707-717
12. Rose SC, Zweibel WJ, Nelson BD, et al. Symptomatic lower extremity deep venous thrombosis: accuracy, limitations, and role of color duplex flow imaging in diagnosis. *Radiology* **1990**;175:639-644
13. Grassi CJ, Polak JF. Axillary and subclavian venous thrombosis: follow-up evaluation with color Doppler flow US and venography. *Radiology* **1990**;175:651-654
14. Fraser-Hill MA, Atri M, Bret PM, Aldis AE, Illescas FF, Herschorn SD. Intrahepatic portal venous system: variations demonstrated with duplex and color Doppler US. *Radiology* **1990**;177:523-526
15. Ralls PW. Color Doppler sonography of the hepatic artery and portal venous system. *AJR* **1990**;155:517-525
16. Parvey HR, Eisenberg RL, Giyanani V, Krebs CA. Duplex sonography of the portal venous system: pitfalls and limitations. *AJR* **1989**;152:765-770
17. Grant EG, Tessler FN, Gomes AS, et al. Color Doppler imaging of portosystemic shunts. *AJR* **1989**;154:393-397
18. Grant EG, Perrella RR, Tessler FN, Lois J, Busuttil RW. Budd-Chiari syndrome: the results of duplex and color Doppler imaging. *AJR* **1989**;152:377-381
19. Mitchell DG. Color Doppler imaging: principles, limitations, and artifacts. *Radiology* **1990**;177:1-10

MR Imaging of the Portal Venous System: Value of Gradient-Echo Imaging as an Adjunct to Spin-Echo Imaging

Paul M. Silverman[1]
Richard H. Patt
Brian S. Garra
Steven C. Horii
Cirrelda Cooper
Wendolyn S. Hayes
Robert K. Zeman

We evaluated the use of gradient-echo (GRE) as an adjunct to spin-echo (SE) MR imaging of the portal venous system. GRE imaging was performed in 31 subjects, 15 normal volunteers and 16 patients with documented portal venous disease (15 cases) or suspected disease (one case). Eight of 16 patients had venous thrombosis, five had focal thrombus, and three had complete occlusion. Six patients had extrinsic venous compression by tumor. Of the two other patients, one had an arteriovenous fistula and the other a falsely positive angiogram, suggesting portal vein occlusion. In normal subjects, GRE scans had excellent visualization of the portal venous system with high intravascular signal compared with surrounding tissues. Nine (60%) of 15 normal subjects and three patients had an artifact consisting of a curvilinear area of decreased signal that could mimic clot. In three of five patients with focal thrombus, clot was identified on GRE but not on SE images. In all three patients with occlusion, SE and GRE images demonstrated similar findings. In five of the six patients with extrinsic venous compression by tumor, SE and GRE studies showed similar findings. Of the other two patients, an arteriovenous fistula was seen on GRE MR in one, and in the other, patency of the left portal vein was seen on SE and GRE images after angiography had suggested portal vein occlusion. Collateral vessels were seen in nine of 16 patients. In five of nine cases, GRE MR demonstrated more extensive collaterals than did SE MR.

In summary, GRE MR provides a useful adjunct to standard SE MR imaging. Benefits include high contrast between vascular structures and surrounding tissues, reduced motion artifact, and rapid scanning within a breath-hold.

***AJR* 157:297-302, August 1991**

Noninvasive imaging of the portal venous system (PVS) has been successfully accomplished with a variety of imaging techniques, including sonography, CT, and MR imaging [1-8]. Doppler sonography has proved to be highly accurate in determining the presence, direction, and velocity of portal blood flow, but is operator dependent [1, 9-11]. Although contrast-enhanced CT with dynamic scanning is sensitive in identifying thrombus in the main portal vein as well as large branch vessels, suboptimal opacification of portal vessels, occasionally may limit this examination.

Spin-echo (SE) MR provides anatomic information similar to that provided by CT without the necessity of using IV contrast material. However, motion and flow-related artifacts, including flow-related enhancement, may produce spurious signals in the portal vein that mimic thrombus [12-14]. Gradient-echo (GRE) pulse sequences have been used in the abdomen and peripheral extremities to image vascular structures [2, 15, 16]. The high-intensity signal produced by flowing blood clearly distinguishes the intraabdominal vasculature from surrounding stationary tissues. Additionally, the acquisition time is significantly reduced when using GRE imaging as compared with conventional SE imaging. This allows slice acquisition during a single breath-hold, minimizing motion-related artifact.

We have reviewed our experience with GRE imaging of the portal vein in 31 subjects, 15 normal volunteers and 16 patients with portal vein abnormalities. The

Received December 14, 1990; accepted after revision March 7, 1991.

[1] All authors: Department of Radiology, Georgetown University Hospital, 3800 Reservoir Rd., N.W., Washington, DC 20007. Address reprint requests to P. M. Silverman.

0361-803X/91/1572-0297
© American Roentgen Ray Society

purpose of the study was to evaluate GRE imaging as an adjunct to standard SE imaging of the PVS.

Subjects and Methods

Thirty-one subjects underwent MR imaging of the upper abdomen including the PVS. Fifteen were normal volunteers and 16 were patients in whom portal venous abnormalities were proved on CT (13 cases), Doppler sonography (eight cases), and angiography (four cases). Angiography was false-positive in one case. The 15 volunteers, 10 men and five women, were 15–55 years old. The 16 patients, 11 men and five women, were 43–77 years old (mean, 60 years). Eight of the sixteen patients had intrinsic thrombus in the PVS. Five patients had focal thrombus and three had complete portal vein occlusion. Two of these patients had cirrhosis. Six patients had extrinsic compression of the main or proximal right or left portal vein by tumor. Abnormalities included metastases (two patients), pancreatic neoplasm (two patients), lymphoma (one patient), and hepatoma (one patient). One patient had an arteriovenous fistula and the other a false-positive angiogram suggesting occlusion of the left portal vein.

All 31 subjects underwent GRE imaging of the portal vein performed at 1.5 T (Siemens, Magnetom, Erlangen, Germany). Fast imaging with steady-state free precession (FISP) was performed in all 31 cases. First-order (velocity) flow compensation was applied in the slice and frequency-encoding directions. FISP scan parameters included 50/14/45°/1 (TR/TE/flip angle/excitation), a 256 × 256 acquisition matrix, and a 5-mm slice thickness. Imaging time was 16 sec for each breath-hold image. Five of the patients who had difficulty holding their breath for this time had additional GRE imaging with fast-low-angle shot (FLASH) imaging, requiring only 9 sec per image. FLASH technical parameters included 30/10/30°/1, a 128 × 128 acquisition matrix, and a 5-mm slice thickness. Maximum-intensity-projection (MIP) angiographic MR images in the coronal plane were produced in eight patients to supplement standard GRE images. MIPs were calculated on a 256 × 256 grid from a stack of two-dimensional GRE slices. Images were viewed at rotational angles from −30° to +30° from the coronal plane at fixed 6° intervals. Reconstruction time was approximately 5 sec per view for a total time of approximately 1 min depending on the number of raw images used.

Standard SE imaging was performed by using 500/15/4 or 8, a 256 × 256 matrix, and a routine 10-mm thickness to provide enough coverage to include the entire liver. Six of the 15 volunteers and 15 of the 16 patients underwent SE imaging.

Thirteen of the 16 patients underwent CT of the upper abdomen with a GE 9800 scanner (General Electric, Milwaukee, WI) before MR imaging. In all cases, enhanced scans were obtained dynamically with a power injector, 1.0–1.2 ml/sec (Mark IV, Medrad, Pittsburgh, PA). Scans were obtained at 1-cm intervals as part of the standard examination of the upper abdomen. Eight of the patients also had sonographic evaluation, including color Doppler flow assessment (Ultramark 9, Advanced Technology Laboratories, Bothell, WA) and four patients had angiographic assessment of the liver and PVS.

GRE and SE scans in the volunteers were reviewed to assess the normal appearance of the main portal vein and its major radicles. GRE scans were also specifically assessed for any potential artifacts that might be confused with thrombus.

In the 16 patients with portal vein abnormality, GRE imaging was compared with SE imaging in 15 of 16 patients and with CT scans in 13 of 16 patients. Scans were compared to assess the presence and extent of intrinsic portal vein thrombosis, extrinsic vascular compression, and portal vein collaterals. Detailed statistical analysis was not feasible because of the small number of patients studied. In the five patients with thrombus, the CT criterion for thrombus was a focal area of decreased density in the PVS surrounded by contrast enhancement. In three patients, total occlusion was established by the inability to identify a patent main portal vein and numerous enhancing periportal collaterals. In the six patients with extrinsic portal venous compression, CT demonstrated porta hepatis adenopathy in four (two with pancreatic neoplasm, one with metastatic disease, and one with lymphoma) and intrahepatic metastases and primary hepatoma in the other two. In one patient, an arteriovenous fistula was confirmed by angiography; in the other, a false-positive angiogram suggested occlusion of the left portal vein. The false appearance of occlusion was related to a portion of the vessel being seen "end on" angiographically and confirmed to be patent by CT and Doppler sonography. In nine of the 16 patients, collateral vessels were seen on at least one imaging study (CT, sonography, or angiography). In patients with collaterals, the extent of collateralization, including periportal, mesenteric, perisplenic, retroperitoneal, and pericholecystic collaterals, was evaluated on SE MR, GRE MR, and CT. When Doppler sonography (eight patients) or angiography (four patients) was performed, the information from these studies agreed with CT findings. In all patients, MR, CT, and Doppler sonographic examinations were performed within 2 weeks of one another. All studies were reviewed by two observers, with consensus achieved in each case. Initial evaluation consisted of direct assessment of SE MR and GRE MR. Comparison with CT, Doppler sonography, and angiography was also performed when these examinations were available.

Results

GRE imaging was performed in all normal volunteers and showed high signal intensity in all the major intraabdominal vascular structures, including the PVS. In all cases, the main, left, and right portal veins were imaged successfully. In nine subjects, a linear or curvilinear area of decreased signal intensity was noted in the portal vein (Fig. 1). In four cases, it was isolated to the main portal vein, and in five cases it extended into the right or left branches of the main portal vein. Standard SE imaging, performed in six of nine volunteers, confirmed this as an artifact by demonstrating a normal PVS. Supplemental scanning in the coronal plane also confirmed the artifactual nature of this decreased signal.

Intrinsic PVS thrombus or occlusion was demonstrated in eight of 16 patients. When thrombus was seen on SE images, it appeared as an area of high signal intensity replacing the normal flow void in the portal vein; on GRE images, it was seen as an area of decreased signal intensity. On SE images, these areas of clot were separate from regions of artifact generated from pulsatile flow within adjacent vessels. In three of the five patients with focal thrombus, thrombus was demonstrated on GRE imaging but failed to be confidently identified on SE imaging (Figs. 2 and 3). In one case in which CT clearly demonstrated thrombus in the main portal vein and superior mesenteric vein, GRE and SE imaging were not conclusive. In the other case, thrombus was identified on both SE and GRE MR. In the three cases with complete occlusion of the portal vein, SE and GRE imaging showed similar findings, including failure to identify the main portal vein and numerous periportal collaterals (Fig. 4). Two of these patients had findings consistent with a diagnosis of cavernous transformation of the portal vein.

Six patients had extrinsic compression of the main or proximal right or left portal vein by tumor. In five of six patients with extrinsic portal vein compression, similar findings were demonstrated on SE and GRE imaging that correlated well with CT (Fig. 5). In one case, GRE imaging was unable to identify the extrinsic compression of the right portal vein seen on SE imaging. Although GRE and SE imaging both showed

Fig. 1.—Artifact on axial GRE MR image.

A, Axial GRE 50/14/45° MR image of normal volunteer shows curvilinear artifact in main and right portal veins (*arrowheads*).

B, Coronal GRE image does not substantiate any consistent defect in portal venous system. Subtle lucencies lack sharp margins and low signal intensity seen with thrombus.

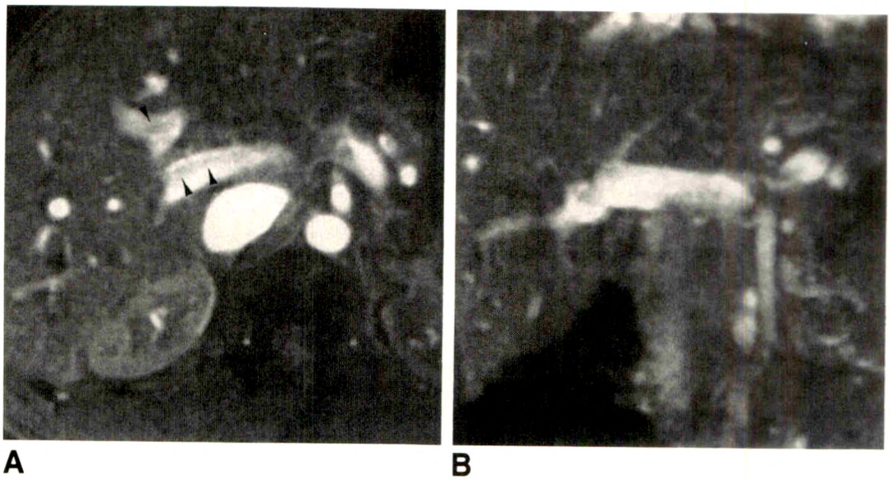

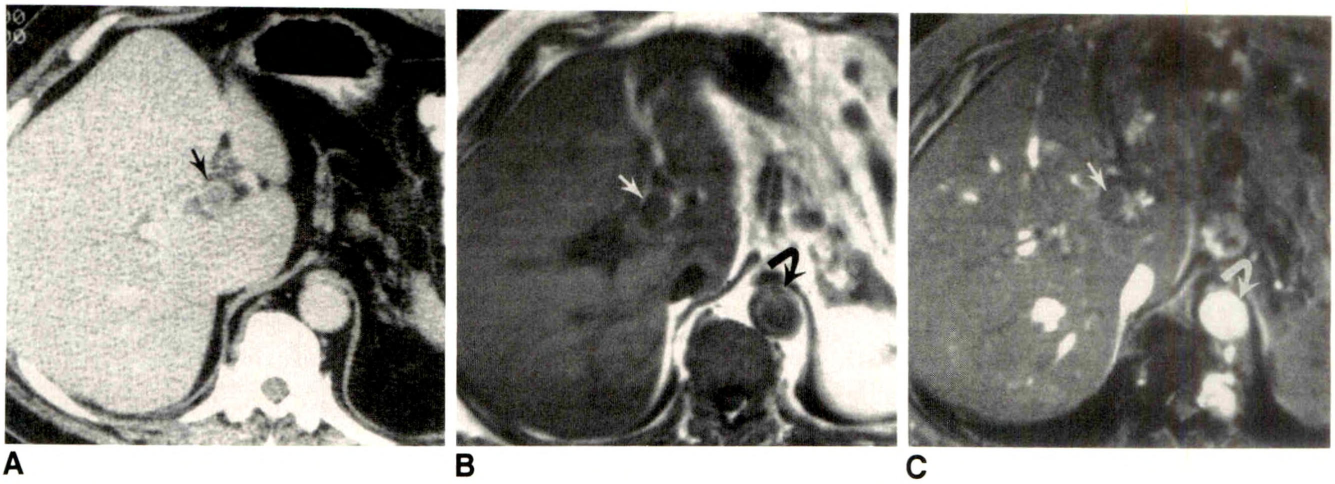

Fig. 2.—Portal vein thrombus equivocal on SE but diagnostic on GRE MR images.

A, CT scan at level of main portal vein (*arrow*) shows low attenuation in main portal vein consistent with thrombus.

B, SE 500/15 MR image shows spurious signal within aorta (*curved arrow*). Lack of clear flow void in aorta and main portal vein (*straight arrow*) does not allow confident diagnosis of portal vein thrombosis.

C, GRE 50/14/45° MR image. High signal in aorta (*curved arrow*) indicates flowing blood, and distinct lack of signal in main portal vein (*straight arrow*) is consistent with thrombosis. Dramatic contrast between flowing blood and clot allows a more confident diagnosis of portal vein thrombosis.

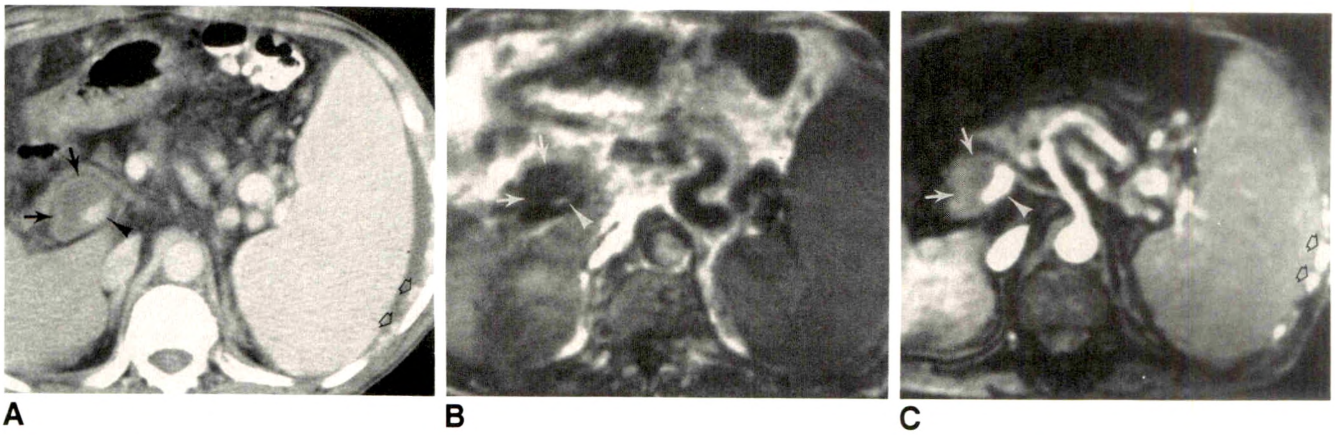

Fig. 3.—Portal vein thrombus identified on GRE but not SE MR images.

A, CT scan shows clot in portal vein (*solid arrows*) with patent lumen medially (*arrowhead*). Subtle evidence of perisplenic collaterals is seen (*open arrows*).

B, SE 500/15 MR image shows artifact. Clot could not be diagnosed confidently. Note high-signal artifact (*arrowhead*) in area with documented flow on CT and Doppler sonography and a relative signal void in area of documented clot (*arrows*). Perisplenic collaterals are not seen.

C, GRE 50/14/45° image shows findings similar to those on CT with clot peripherally (*solid arrows*) and a patent lumen medially (*arrowhead*). Perisplenic collaterals are best seen on GRE image (*open arrows*).

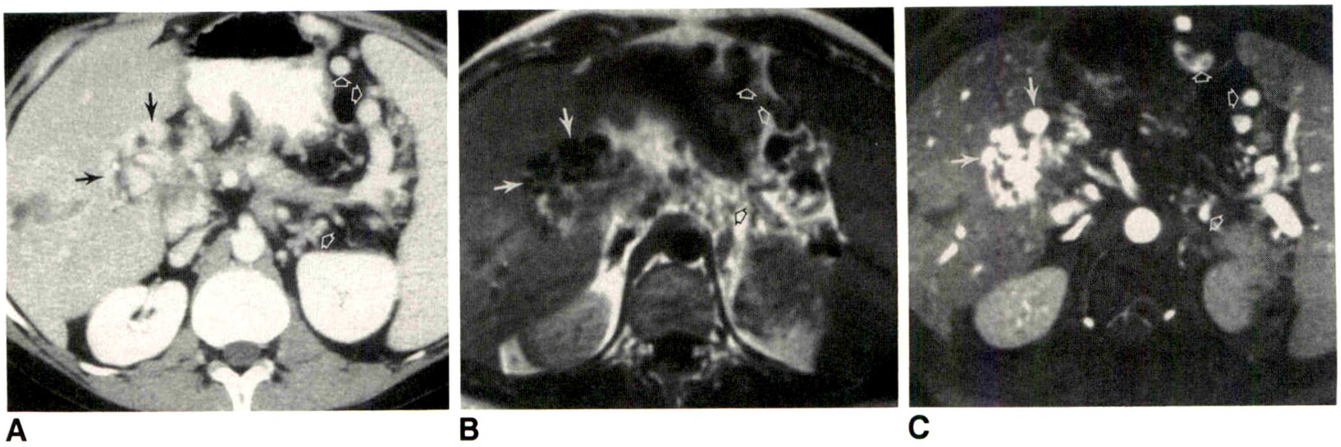

Fig. 4.—Occluded main portal vein and extensive collaterals seen on SE and GRE MR images.

A, CT scan shows extensive periportal collaterals (*solid arrows*) due to occlusion of main portal vein. Low-attenuation areas in liver represent metastatic disease. Retroperitoneal, mesenteric, and perisplenic collaterals are present (*open arrows*).

B and *C*, SE 500/15 (*B*) and GRE 50/14/45° (*C*) MR images show findings similar to those seen on CT, with numerous periportal collaterals (*solid arrows*). Additional collaterals appear as on CT (*open arrows*).

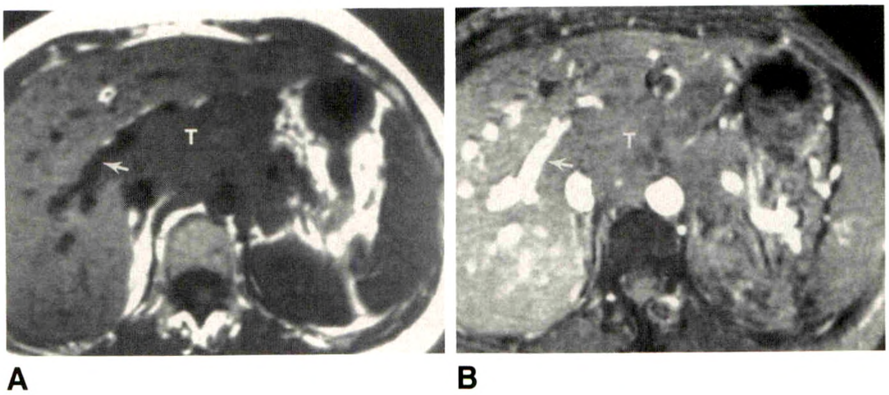

Fig. 5.—Extrinsic compression of portal vein by lymphoma. GRE compared with SE MR shows poorer contrast between tumor and liver.

A, SE 500/15 MR image shows lymphomatous tumor (T) to porta hepatis with compression of main portal vein (*arrow*). Tumor (T) is of low signal intensity.

B, GRE 50/14/45° image shows findings similar to those seen on SE MR, with very mild portal vein compression (*arrow*). However, contrast between tumor (T) and adjacent liver is not as good.

extrinsic portal vein compression in five of six patients, GRE displayed the tumor responsible for the venous compression less well than SE imaging did because of the poorer contrast between tumor and surrounding normal tissue on GRE images.

In one patient, an arteriovenous fistula seen on GRE imaging was confirmed angiographically. The patient in whom a false-positive angiogram suggested occlusion of the left portal vein was shown to have a patent vein on both SE and GRE MR.

In nine of the 16 patients, collateral vessels were shown by at least one imaging technique (CT, sonography, or angiography). In four cases, GRE and SE images were judged to be similar in showing these vessels. In five cases, GRE images better defined the presence of collaterals and showed more extensive collateralization than was appreciated on standard SE MR (Fig. 6). CT scans were obtained in six of nine patients. In those patients, CT and GRE showed collaterals to a similar extent in four patients, whereas in two cases GRE showed the collaterals better. MIP imaging did not provide information beyond that provided by GRE imaging, but coronal images did enhance the display of abnormalities, especially in patients with extensive collaterals.

Incidentally noted in three of 16 patients was focal signal within the main portal vein on standard SE imaging unrelated to areas of thrombus or vascular compression that potentially could have given the false impression of thrombus. In each case, the GRE study, CT, or color Doppler flow sonography was normal in this segment of portal vein. The linear or curvilinear low-intensity area encountered on GRE images in normal volunteers was seen similarly in the patient group but was readily recognized as artifactual by its typical appearance, correlation with other imaging studies, and experience gained in examining normal volunteers.

Discussion

The application of MR imaging in evaluating the abdominal vasculature provides a noninvasive imaging technique additional to CT and sonography. Standard assessment with SE imaging produces a typical signal void, "black-blood" phenomenon. The presence of high-intensity signal within the main portal vein is suggestive of thrombus, and the absence of a main portal vein and demonstration of tortuous collaterals is suggestive of complete portal vein thrombosis [17, 18]. The

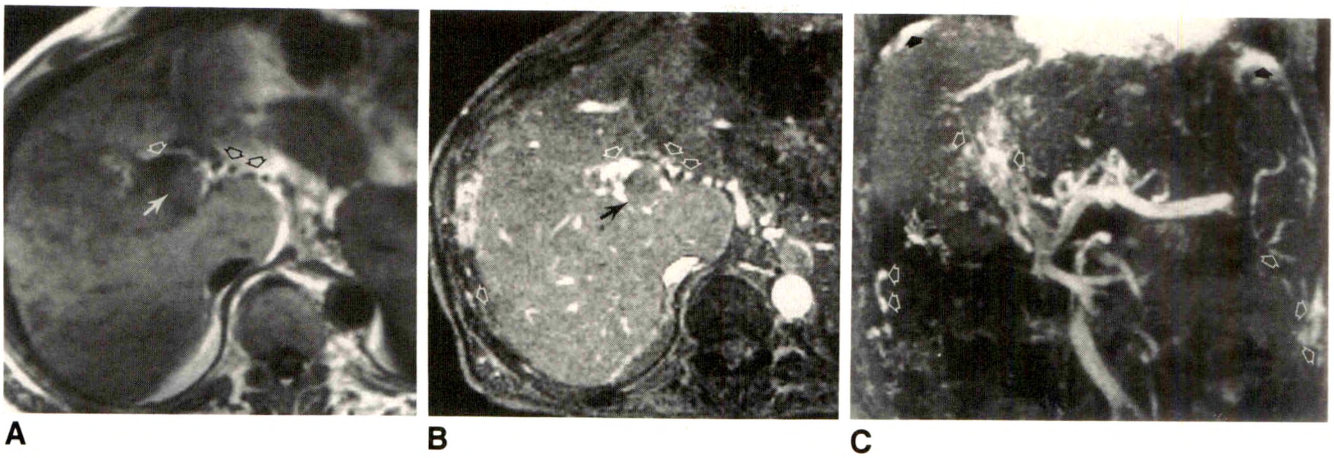

Fig. 6.—Improved depiction of collateral vessels with GRE MR images and maximum-intensity projection (MIP) angiographic images compared with SE MR images.

***A*, SE 500/15 MR image shows portal vein occlusion (*solid arrow*) and collaterals (*open arrows*) in periportal area. Low-intensity area around occluded portal vein mimics ascites but represents a confluence of distinct collaterals.**

***B*, GRE 50/14/45° image shows portal vein thrombosis (*solid arrow*) and more extensive collateralization (*open arrows*) than SE images does.**

***C*, MIP angiographic image, coronal plane, shows extensive collateralization (*arrows*).**

major pitfall in this type of imaging is caused by high signal from flow-related enhancement occurring within patent vasculature that mimics thrombus. Clot may rarely lack increased signal and therefore be undetected. Respiratory and motion artifacts may also superimpose high signal intensity artifacts onto vascular structures, making it difficult to assess their patency.

In one study, 14 patients with portal vein thrombosis were evaluated by CT, SE MR, and sonography [19]. Acute or subacute thrombi were hyperintense on both T1- and T2-weighted images. Chronic thrombi (greater than 5 weeks' duration) were hyperintense in eight of 11 cases on T2-weighted images. Although all patients had thrombosed portal vessels, MR more effectively showed the extent of thrombosis and periportal collateralization than did CT or sonography. Heavily T2-weighted, triple-echo imaging enhanced the ability to differentiate flow-related artifacts from thrombi by demonstrating a persistently high signal on late echoes in thrombosed vessels. These images, however, were significantly compromised by their poor signal-to-noise ratio.

In the present study, portal venous thrombosis was seen in eight patients. In three of five patients, GRE MR showed focal thrombus not appreciated on the SE MR image. In the three patients with portal vein occlusion and in five of six patients with extrinsic portal vein compression, SE and GRE images were comparable in showing the abnormality. However, in five of nine patients with collateral vessels caused by portal vein compromise, GRE imaging more completely demonstrated the extent of collateralization. A significant benefit of GRE imaging compared with SE imaging was the ability to image the porta hepatis rapidly and selectively with single-slice breath-hold images, as an adjunct to the much longer SE examination.

The recent development of practical techniques for MR angiography has allowed further clinical application in assessing the abdominal vasculature, especially the PVS [2, 15, 16]. The "bright-blood" images produced by GRE imaging create extremely high contrast between flowing blood and surrounding tissues. They are occasionally subject to prominent high-intensity artifacts from these vascular structures [20]. The sequential two-dimensional acquisition method is favored over three-dimensional techniques, which are particularly sensitive to motion, as they require minutes of acquisition rather than being accomplished within a single breath-hold. In standard SE imaging, spins must remain within the slice long enough to be exposed to both 90° and 180° RF pulses. With relatively rapid blood flow, washout effects dominate so that high-velocity moving spins flow out of the plane of section, yielding characteristic black-blood images. In contrast, GRE imaging does not require a 180° refocusing pulse, and echoes can be received sooner after each excitation. Blood entering a slice is more fully magnetized, with each slice acting as an entry slice with flow-related enhancement. Washout effects are minimized and flowing blood generates a stronger signal. When flow compensation techniques are applied, the phase shifts that would normally result in subsequent dephasing and signal loss are minimized. In most cases, correcting for first-order "velocity" phase shifts is adequate because additional compensatory gradients would prolong the TE and accentuate washout of high-intensity spins, diminishing the bright-blood effect [15].

The high-contrast signal produced by flowing blood makes GRE imaging well suited to construction of MIP images. These produce an angiographic effect that can enhance the display of vascular disease (Fig. 6). The MIP program used selects the maximum-intensity voxel in the projected ray, and therefore background signal is not additive as would occur with standard summation imaging [21]. Projectional images have the advantage of facilitating viewing by displaying, on a single image, the path of tortuous vessels that would otherwise need to be traced on numerous sequential images. In evaluating portal venous disease, MIPs can be a useful method of display without requiring invasive angiography. Some artifactual distortions characteristic of these images should be recognized [21]. A consistent distortion is an artifactual decrease in vessel width since the edges of vessels are less intense than their central areas. The decreased intensity of the peripheral portion of vessels is related in part to partial-volume effect and in part to different flow velocities in vessels. A periodic linear dark "striping" artifact may occur when vessels course obliquely between sections owing to the maximum signal intensity being shared between contiguous sections [21]. Thus, although these images provide a high-contrast angiographic display, these pitfalls require referral to the individual cross-sectional GRE slices for accurate interpretation.

Artifacts may significantly compromise the assessment of portal venous disease on MR. In three of our patients, artifactual signal in the PVS on SE imaging could have been mistaken for thrombus. In these cases, correlation with GRE imaging and with other imaging techniques allowed us to correctly attribute this to artifact. Presaturation pulses, not routinely available at the initiation of this study, can minimize or eliminate high-signal artifact in blood vessels when applied perpendicularly to the direction of flow. However, even when such pulses are applied, they are routinely used to eliminate flow in the aorta and inferior vena cava and diminish respiratory artifact. Presaturation pulses may also be useful in eliminating hepatic arterial flow. Selective presaturation of portal venous flow would require specific presaturation of blood flow perpendicular to the course of the portal vein. GRE vascular images are not as susceptible as SE images to respiratory motion or pulsatile vascular artifact mimicking clot. In the six cases of extrinsic compression of the PVS by tumor, GRE imaging techniques, although less degraded by motion artifact than SE imaging, provided poorer contrast between tumor and normal tissues. The appearance of tumor on GRE imaging is variable and complex depending on the specific parameters used, which affect the relative contribution of T1, T2, and T2* weighting. Increased sensitivity to magnetic susceptibility inherent in GRE imaging also compromises image quality, especially from artifacts related to bowel gas and clips. A linear to curvilinear artifact was encountered frequently on GRE imaging. The artifactual nature of this was usually recognizable from previous experience with normal volunteers and from correlation with other studies. A possible explanation of this effect is referred to as *flow separation.* Laminar streaming of flowing blood may occur on one side of a vessel, whereas flow on the opposing side may be relatively slower. The rapidly flowing blood is freely replaced with fresh unsaturated spins that appear bright, whereas the slowly flowing, more saturated blood appears darker. A less likely explanation would be flow-related displacement. When blood is flowing obliquely through the scanning plane it occupies one location initially when molecules are excited and a different position later when they are encoded for readout. Because GRE images are acquired rapidly, blood would not move a sufficient distance to make this a likely explanation. The limitations of GRE imaging, including poor contrast with surrounding tissues, difficulty in identifying vascular margins, and flow artifact, do not allow it at the present time to function as a gold standard for assessing portal venous thrombosis.

In summary, GRE imaging can be a useful adjunct to SE imaging of the portal venous system. The images provide high contrast between flowing blood, clot, and surrounding tissues. GRE imaging techniques allow marked flexibility in that they can be performed rapidly, as single breath-hold images that can be used in sick patients who might otherwise undergo nondiagnostic standard SE imaging. This imaging technique provides significant flexibility compared with standard SE MR because a few slices at a specific anatomic level can be performed to rapidly investigate potential disease. Because thrombus generally appears as an area of decreased signal rather than increased signal, as with standard SE imaging, these images are less subject to the common pitfall of high-intensity artifacts mimicking clot. Additionally, angiographic MIP images provide a unique display that may complement standard single-slice images in demonstrating vascular impression, encasement, and collateralization. However, GRE images provide limited anatomic resolution compared with SE imaging and suboptimal contrast between tumor and normal tissues, making them unsuitable as a replacement for SE imaging.

REFERENCES

1. Ralls PW. Color Doppler sonography of the hepatic artery and portal venous system. *AJR* **1990**;155:517–525
2. Edelman RR, Zhao B, Liu C, et al. MR angiography and dynamic flow evaluation of the portal venous system. *AJR* **1989**;153:755–760
3. Zeman RK, Paushter DM, Scheibler ML, Choyke PL, Clark LR, Jaffe MN. CT of the porta hepatis: normal and abnormal (abstr). *Radiology* **1985**;157(P):113
4. Alpern MB, Rubin JM, Williams DM, Capek P. Porta hepatis: duplex Doppler US with angiographic correlation. *Radiology* **1987**;162:53–56
5. Weinstein JB, Heiken JP, Lee JKT, et al. High resolution CT of the porta hepatis and hepatoduodenal ligament. *RadioGraphics* **1986**;6(1):55–74
6. Hricak H, Amparo E, Fisher MR, Crooks L, Higgins CB. Abdominal venous system: assessment using MR. *Radiology* **1985**;156:415–422
7. Williams DM, Cho KJ, Aisen AM, Eckhauser FE. Portal hypertension evaluated by MR imaging. *Radiology* **1985**;157:703–706
8. Ohtomo K, Itai Y, Furui S, Yoshikawa K, Yashiro N, Iio M. MR imaging of portal vein thrombus in hepatocellular carcinoma. *J Comput Assist Tomogr* **1985**;9(2):328–329
9. Walter JP, McGahan JP, Lantz BMT. Absolute flow measurements using pulsed Doppler US. *Radiology* **1986**;159:545–548
10. Miller VE, Berland LL. Pulsed Doppler duplex sonography and CT of portal vein thrombosis. *AJR* **1985**;145:73–76
11. Foley WD, Varma RR, Lawson TL, Berland LL, Smith DF, Thorsen K. Dynamic computed tomography and duplex ultrasonography: adjuncts to arterial portography. *J Comput Assist Tomogr* **1983**;7(1):77–82
12. Axel L. Blood flow effects in magnetic resonance imaging. *AJR* **1984**;143:1157–1166
13. Bradley WG, Waluch V. Blood flow: magnetic resonance imaging. *Radiology* **1985**;154:443–450
14. Bradley WG, Waluch V, Lai KS, Fernandez EJ, Spalter C. The appearance of rapidly flowing blood on magnetic resonance images. *AJR* **1984**;143:1167–1174
15. Edelman RR, Mattle HP, Atkinson DJ, Hoogewoud HM. MR angiography. *AJR* **1990**;154:937–946
16. Edelman RR, Wentz KU, Mattle H, et al. Projection arteriography and venography: initial clinical results with MR. *Radiology* **1989**;172:351–357
17. Ros PR, Viamonte M Jr, Soila K, Sheldon JJ, Tobias J, Cohen B. Demonstration of cavernomatous transformation of the portal vein by magnetic resonance imaging. *Gastrointest Radiol* **1986**;11(1):90–92
18. Silverman PM, Feuerstein I, Garra BS, Zeman BZ. STIR imaging as a complement to standard spin echo imaging in the evaluation of the porta hepatis/hepatoduodenal ligament. *Magn Reson Imaging* **1991**;9:73–77
19. Zirinsky K. Markisz JA, Rubenstein WA, et al. MR imaging of portal venous thrombosis: correlation with CT and sonography. *AJR* **1988**;150:283–288
20. Silverman PM, Patt RH, Baum PA, Teitelbaum GP. Ghost artifact on gradient-echo imaging: a potential pitfall in hepatic imaging. *AJR* **1990**;154:633–634
21. Anderson CM, Saloner D, Tsuruda JS, Shapeero LG, Lee RE. Artifacts in maximum-intensity-projection display of MR angiograms. *AJR* **1990**;154:623–629

Diagnosis and Staging of Hepatocellular Carcinoma:

Comparison of CT and Sonography in 36 Liver Transplantation Patients

William J. Miller[1]
Michael P. Federle
William L. Campbell

Radiologic studies are important in the detection of hepatocellular carcinoma and the selection of patients for partial liver resection, liver transplantation, or palliation. We retrospectively studied 36 patients with hepatocellular carcinoma who were examined with both CT and sonography before undergoing hepatic transplantation. Pathologic findings of the entire resected liver were correlated with results of imaging studies before transplantation. Parenchymal lesions were shown by sonography in 29 cases (81%) and by CT in 34 cases (94%). Although CT was more sensitive than sonography was, both CT and sonography frequently failed to depict reliably the size of tumor or the exact number of tumor nodules as determined pathologically. Pathologic findings showed vascular invasion in 19 cases (53%), whereas CT showed invasion in 11 cases (31%) and sonography showed it in only six (17%). Nodal metastasis to the porta hepatis was found in four patients; CT correctly showed two cases (three false-positive) and sonography correctly showed one case. Intrahepatic ductal dilatation was seen in eight patients on CT but was not identified on sonography.

We conclude that CT is more accurate for identifying and staging hepatocellular carcinoma, but both CT and sonography frequently fail to depict the extent (size and number of lesions) of disease, especially when underlying cirrhosis is present.

***AJR* 157:303-306, August 1991**

Surgery offers the only chance for cure of hepatocellular carcinoma, but only a small percentage of patients are acceptable candidates [1]. Even in patients who undergo partial hepatectomy, the 5-year survival rate is only 25% [2] because of a high prevalence of intrahepatic metastases (daughter nodules) that go undetected before or during surgery. Most cases of hepatocellular carcinoma in the United States are in patients with underlying cirrhosis (usually alcoholic) [3]; therefore, extensive liver resections such as trisegmentectomy are often not possible. For patients with tumor involving multiple lobes and/or with liver cirrhosis, orthotopic liver transplantation and orthotopic multivisceral organ transplantation have offered some hope for cure [4].

Patients being evaluated for liver transplantation routinely have multiple imaging studies, including CT and sonography, shortly before surgery. In a recent 4-year period, 36 patients with hepatocellular carcinoma had total hepatectomy and liver transplantation. This afforded us the unique opportunity to examine the entire liver in these patients and to correlate the pathologic findings with findings from imaging studies done before transplantation.

Materials and Methods

We retrospectively analyzed imaging studies in 36 patients with hepatocellular carcinoma who underwent total hepatectomy and liver transplantation at our center between March 1986 and April 1990. All patients had abdominal CT and sonography; studies were performed within 1 week of each other. Most imaging examinations were performed within 1 month of

Received February 6, 1991; accepted after revision March 27, 1991.

Presented at the 19th annual meeting of the Society of Gastrointestinal Radiologists, Big Island of Hawaii, January 1990.

[1] All authors: Department of Radiology, University of Pittsburgh School of Medicine, Presbyterian University Hospital, DeSoto at O'Hara Sts., Pittsburgh, PA 15213. Address reprint requests to M.P. Federle.

0361-803X/91/1572-0303

© American Roentgen Ray Society

transplantation, with a median of 22 days for CT and 23 days for sonography (range, 2–86 days).

The 36 patients included 24 males and 12 females between 10 and 69 years old (mean age, 49 years). There were 28 whites, three blacks, and five Asians. Because the patients were referred to our institution for transplantation, many had a known diagnosis of hepatocellular carcinoma and/or underlying liver disease (e.g., hepatitis, cirrhosis).

CT scans were done on GE 9800 scanners, except for two done on a GE 8800 model (General Electric Corporation, Milwaukee, WI). Scans consisted of contiguous 1.0-cm-thick sections from the dome of the diaphragm to the iliac crest or to the inferior margin of the liver. Thirty of the patients had scans obtained before and after rapid IV infusion of 150 ml of contrast material. Four patients had scans without IV contrast media only, and two patients had enhanced scans only. Contrast material was administered via power injector at 1.5 ml/sec with a 60-sec delay or by hand bolus injection if IV access was poor.

Sonography was performed on Acuson scanners (Acuson Corp., Mountain View, CA); both real-time and pulsed Doppler imaging were done in all patients by using 2.5- and 3.5-MHz transducers, depending on the patient's body habitus and the level of the structures of interest.

CT and sonographic studies were retrospectively reviewed and sonographic reports were reviewed, giving special attention to the number of lesions, size of lesions, and main vascular invasion. These results were compared with dictated pathology reports, in which the resected livers were described, and available gross photographs.

Pathology reports detailed the resected liver surface and the serially sectioned whole liver in either the coronal (old cases) or axial plane (newer cases). Specimen sections were 1.0-cm thick, and lesions (color, size, texture, etc.), vessels, and bile ducts were documented. Microscopic sections confirmed the gross findings and that all patients had hepatocellular carcinoma (not fibrolamellar hepatocellular carcinoma). In patients with multiple lesions, exact counts were not always done and the exact level of vascular invasion was often not stated clearly unless it was a main portal vein or a branch of a hepatic vein. Because the study was retrospective, false-negative and false-positive sonographic and CT findings (e.g., fat, fibrosis) could not be correlated with the pathologic findings accurately. Only tumors were documented during pathologic examination.

Results

We categorized patients by the number of lesions discovered on pathologic and imaging studies. A single lesion was found on pathologic study in 11 patients. Sonography correctly identified single lesions in seven patients, as did CT in seven patients. Two to four tumor nodules were found on pathologic study in 11 patients, but sonography and CT correctly categorized only one and four patients, respectively. Diffuse tumor or multiple daughter nodules were found pathologically in 16 of the resected livers. CT correctly categorized 11 of these patients, whereas eight patients were correctly categorized by sonography. Sonography failed to detect six hepatomas, whereas two tumors were missed by CT. The remaining cases that showed a lack of correlation between CT or sonography and pathology results were due to the imaging studies failing to categorize correctly by number of lesions (false-negative and false-positive).

We categorized the size of tumor nodules (using the diameter of the largest) into less than 5 cm, between 5 and 10 cm, and greater than 10 cm. Pathologic results showed 16 patients with nodules less than 5 cm in diameter. These cases were correctly identified in seven cases on sonography and 11 cases on CT. Six tumor nodules in this category were not shown at all by sonography, and two tumors were not shown by CT. In the other cases, tumor was seen, but the extent of the lesion was not correctly categorized. Lesions of 5- to 10-cm diameter were seen in four cases on pathologic results, in all four cases on CT, and in three cases on sonography. Sonography showed tumor in one patient but incorrectly categorized the size of the tumor. Lesions greater than 10 cm in diameter were seen in 16 patients on pathologic results, but the extent of tumor was correctly categorized by sonography in only 11 patients. CT did better, correctly sizing the tumor in all 16 patients. None of the large tumors went undetected by sonography or CT. In some cases, tumor size was overestimated (Fig. 1) and in others it was underestimated by CT. Sonography, when incorrect, was most likely to underestimate the size of the tumor (Fig. 2).

Vascular invasion was present on gross pathologic section in 19 cases, but the pathologist frequently did not detail the exact level of vascular invasion. Sonography showed six cases of major portal vein invasion by tumor; CT showed 11 cases of vascular invasion by tumor. It was difficult to distinguish vessel compression from invasion on both CT and sonography and both techniques routinely failed to identify tumor invasion of branch vessels.

Extrahepatic spread of tumor to lymph nodes in the porta hepatis was seen in only four cases in this select group of referral patients. Sonography showed one case of enlarged nodes. On CT, five cases were interpreted as having enlarged nodes, but only two of these cases had tumor confirmed by pathologic results. Intrahepatic biliary ductal dilatation caused by tumor obstruction was shown in seven patients by CT but was not identified on any of the sonographic studies or reports.

Ascites was shown in 20 of 36 patients by CT and sonography. Whether the ascites was due to end-stage liver disease or to the underlying malignant tumor was not determined by pathologic results. Tumor calcifications were shown in five patients by CT and in two patients by sonography.

Discussion

Tumor lesions in the liver that correlated with hepatocellular carcinoma were seen on CT in 34 (94%) of 36 patients and on sonography in 29 (81%) of 36 patients. Our tumor detection rate is similar to rates reported by others for CT [1, 5–8]. Our detection rate with sonography is similar to that for initial screening sonograms in patients with chronic liver disease. Slightly better detection rates of parenchymal abnormalities in hepatocellular carcinoma have been reported in sonography of cirrhotic patients with clinical suspicion of malignancy [9], known hepatocellular carcinoma [1], and second, more detailed sonographic examinations [6]. In these studies, the whole liver was not available for pathologic review, and biopsies, surgical exploration, direct follow-up, and partial liver resections were relied on to judge detection rate and accuracy.

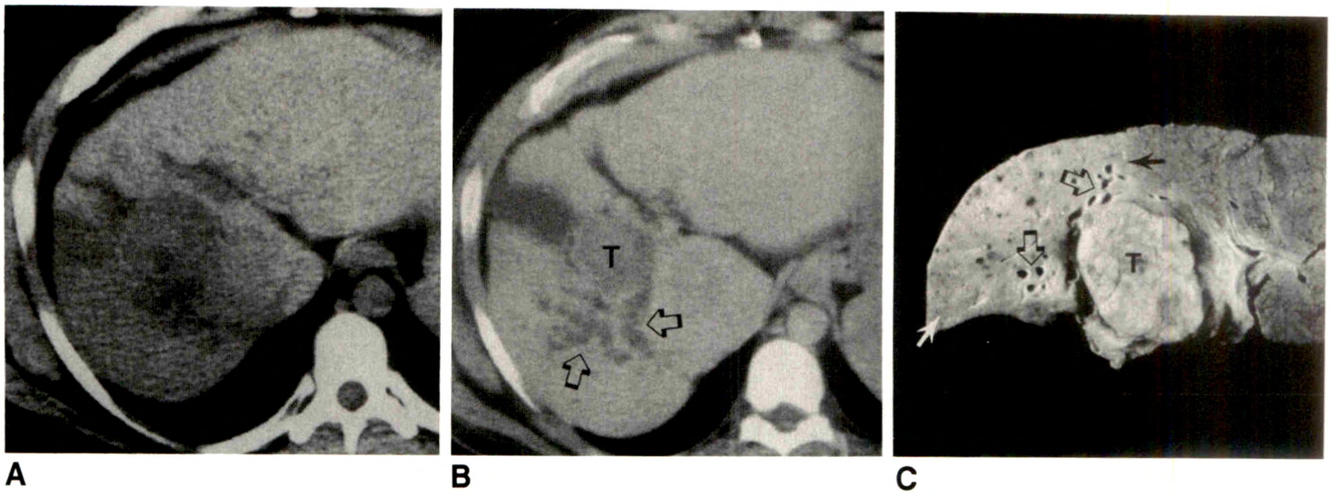

Fig. 1.—Overestimation of tumor extent by CT.

A, Unenhanced CT scan shows diffuse hypodensity throughout right and caudate lobes of liver.

B, Contrast-enhanced CT scan shows discrete tumor mass (T) and dilated bile ducts (*arrows*). Right and caudate lobes are nearly isodense in area of hepatocellular necrosis. Contrast bolus technique was suboptimal in this patient.

C, Coronal pathologic section shows discrete tumor mass (T). Pale area in right lobe (*solid arrows*) represents hepatocellular necrosis. Bile ducts (*open arrows*) are dilated.

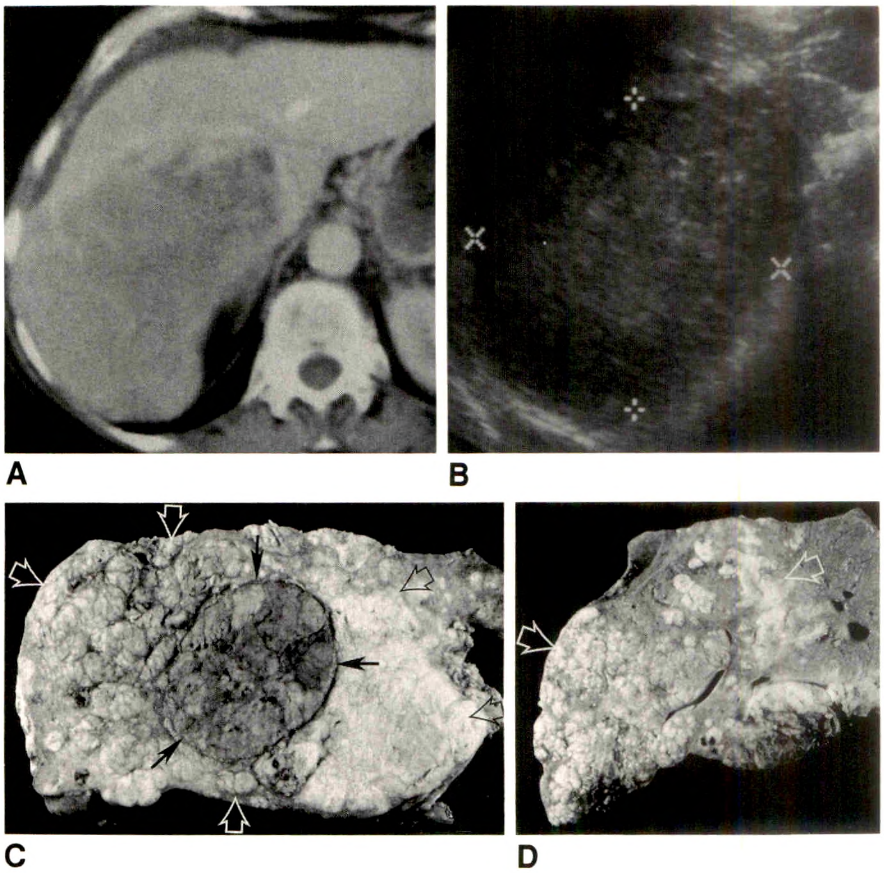

Fig. 2.—Discrepancy in size estimation by CT and sonography.

A, Contrast-enhanced CT scan accurately shows diffuse tumor in right lobe of liver.

B, Transverse sonogram underestimates tumor extent, showing only central spherical mass (*cursors*).

C and *D*, Coronal pathologic sections of liver specimen show large, discrete, spherical tumor mass (*solid arrows*), but also diffuse tumor throughout right lobe of liver (*open arrows*).

Number of Lesions

CT (34/36) was slightly better than sonography (29/36) for identifying hepatocellular carcinoma, but neither technique did well at categorizing the number of lesions. Sonography placed most of the patients into the single-lesion category (26/36), with only seven patients being correctly categorized. Cases of one main tumor nodule with a few small daughter nodules were the most frequently missed by both CT and sonography. When considering liver resection, detection of daughter nodules becomes extremely important. Other studies such as arterial portography CT [10-12], intraarterial iodized oil CT [10, 13, 14], or MR imaging [15, 16] may improve identification of additional lesions.

Size of Lesions

The size or extent of the main hepatocellular carcinoma lesion measured during pathologic study was compared with the measurement from the imaging studies. CT displayed tumor extent better than sonography did overall. Both CT and sonography frequently missed small tumor nodules and had difficulty in distinguishing tumor from other forms of hepatic disease, particularly in patients with underlying cirrhosis. CT had cases of both overestimation (false-positive) and underestimation (false-negative) of tumor size, whereas sonography was more likely to underestimate tumor size.

A great deal of effort has been directed toward improving CT detection of primary hepatic neoplasms. Reported techniques include dynamic incremental CT [11-13], single-level dynamic CT [13], CT arteriography [13, 17], arterial portography CT [10, 11, 13, 15, 16], and intraarterial iodized oil CT [10, 13, 14]. These studies used clinical follow-up, biopsy results, and resection (rather than the whole liver) as their gold standard for detection of tumor nodules. Heiken et al. [15] reported four patients with either hepatocellular carcinoma or metastatic disease who underwent hepatectomy and orthotopic liver transplantation. Their well-done prospective work showed arterial portography CT to be far superior to dynamic CT. Their dynamic, enhanced CT examination showed an accuracy of only 38%, with poor detection of lesions less than 2 cm in diameter. MR imaging has been shown to be more sensitive than dynamic, enhanced CT but not as sensitive as arterial portography CT [15, 16].

Limitations of our study include its retrospective nature and the lack of pathologic documentation of the exact number and size of tumor nodules in patients with diffuse disease, particularly early in the study. Nevertheless, we believe that CT shows tumor extent better than sonography does. On both CT and sonography, small tumor nodules were often missed and it was difficult to distinguish tumor from other forms of hepatic disease, particularly in patients with underlying cirrhosis. Most of the lesions that were missed were less than 2 cm in diameter.

CT may display vascular invasion better, although both CT and sonography are limited to assessing the main hepatic vessels. Causes for sonography failing to detect biliary dilatation were that the areas involved were focal, usually involved very large lesions, and were usually peripheral. Other causes could include operator error or failure to check hypoechoic branching structures with Doppler imaging.

Preoperative CT and sonography were performed mainly to screen for masses, vascular patency, and extrahepatic tumor spread. The number and size of lesions were of secondary concern. Had this been a primary goal, the results of sonography in particular would probably have been better. Similarly, our CT results definitely could have been improved by the more frequent use of optimal techniques for IV contrast administration. Because the study is retrospective, we do not know which patients received power-injected contrast material or had hand bolus injections because of poor IV access. Underlying cirrhosis of the liver is seen in 85% of the patients with hepatocellular carcinoma in the United States [3]. Cirrhosis with regenerating nodules, fibrosis, fat infiltration, and hepatocyte degeneration may make detection and determination of tumor extent difficult. The above pathologic changes also lead to false-positive imaging studies, especially on CT, and mask tumors in a heterogeneous liver on sonography and CT.

A prospective study including a larger number of patients is needed to compare imaging and pathologic results in hepatocellular carcinoma. We are currently undertaking this study to determine not only accuracy and sensitivity for tumor detection but also specificity for abnormalities that may mimic neoplasm.

ACKNOWLEDGMENT

We thank Frank Fusca for his helpful assistance with pathologic correlation.

REFERENCES

1. LaBerge JM, Laing FC, Federle MP, Jeffrey RB, Lim RC. Hepatocellular carcinoma: assessment of resectability by computed tomography and ultrasound. *Radiology* **1984**;152:485-490
2. Iwatsuki S, Starzl TE. Experience with resection of primary hepatic malignancy. *Surg Clin North Am* **1989**;69:315-322
3. Edmondson HA, Peters RL. Tumors of the liver: pathologic features. *Semin Roentgenol* **1983**;18:75-83
4. Adler M, Gavaler JS, Duquesnoy R, et al. Relationship between the diagnosis, preoperative evaluation, and prognosis after orthotopic liver transplantation. *Ann Surg* **1988**;208:196-202
5. Kunstlinger F, Federle MP, Moss AA, Marks W. Computed tomography of hepatocellular carcinoma. *AJR* **1980**;134:431-437
6. Kudo M, Hirasa M, Takakuwa H, et al. Small hepatocellular carcinomas in chronic liver disease: detection with SPECT. *Radiology* **1986**;159:697-703
7. Dunnick NR, Ihde DC, Doppman JL, Bates HR. Computed tomography in primary hepatocellular carcinoma. *J Comput Assist Tomogr* **1980**;4:59-62
8. Inamoto K, Tanaka S, Yamazaki H, Okamoto E. Computed tomography in the detection of small hepatocellular carcinoma. *Gastrointest Radiol* **1983**;8:321-326
9. Cottone M, Marceno MP, Maringhini A, et al. Ultrasound in the diagnosis of hepatocellular carcinoma associated with cirrhosis. *Radiology* **1983**;147:517-519
10. Merine D, Takayasu K, Wakao F. Detection of hepatocellular carcinoma: comparison of CT during arterial portography with CT after intraarterial injection of iodized oil. *Radiology* **1990**;175:707-710
11. Matsui O, Kadoya M, Suzuki M, et al. Work in progress: dynamic sequential computed tomography during arterial portography in the detection of hepatic neoplasms. *Radiology* **1983**;146:721-727
12. Hosoki T, Chatani M, Mori S. Dynamic computed tomography of hepatocellular carcinoma. *AJR* **1982**;139:1099-1106
13. Ohtomo K, Itai Y. Early diagnosis of hepatocellular carcinoma. In: Ferrucci JT, Mathieu DG, eds. *Advances in hepatobiliary radiology*. St. Louis: Mosby, **1990**:181-208
14. Yumoto Y, Jinno K, Tokuyama K, et al. Hepatocellular carcinoma detected by iodized oil. *Radiology* **1985**;143:19-24
15. Heiken JP, Weyman DJ, Lee JKT, et al. Detection of focal hepatic masses: prospective evaluation with CT, delayed CT, CT during arterial portography, and MR imaging. *Radiology* **1989**;171:47-51
16. Nelson RC, Chezmar JL, Sugarbaker PH, Bernardino ME. Hepatic tumors: comparison of CT during arterial portography, delayed CT, and MR imaging for preoperative evaluation. *Radiology* **1989**;172:27-34
17. Freeny PC, Marks WM. Computed tomographic arteriography of the liver. *Radiology* **1983**;148:193-197

Case Report

Acute Torsion of a Wandering Spleen: Diagnosis by CT and Duplex Doppler and Color Flow Sonography

Albert A. Nemcek, Jr.,[1] Frank H. Miller, and Steven W. Fitzgerald

The spleen is typically held in a relatively fixed position in the left upper quadrant by suspensory ligaments derived from the dorsal mesogastrium and by the pressure exerted by surrounding organs and musculature. The term *wandering spleen* is commonly applied to a splenic hypermobility that results from laxity or maldevelopment of its suspensory ligaments. Other acquired and congenital factors may accentuate this tendency. A wandering spleen is at risk for torsion of its vascular pedicle. We report a case of torsion of a wandering spleen in which the preoperative diagnosis was made based on serial CT scans and duplex Doppler and color flow sonography with confirmation by ^{99m}Tc-sulfur colloid scans. To our knowledge this is the first case in which duplex and color flow Doppler findings in this entity have been reported.

Case Report

A 42-year-old woman with suspected limb girdle muscular dystrophy had a 1-day history of intense, constant left lower quadrant pain and low-grade fever. Three years before admission, diverticulitis had developed that required resection of the descending colon and colostomy. Since surgery, she had had intermittent lower abdominal pain attributed to recurrent diverticulitis that was well documented with imaging studies, and had been treated presumptively with antibiotics.

Physical examination revealed a cachectic-appearing woman in mild distress. Her abdomen was mildly distended with hypoactive bowel sounds. She was tender to palpation in the left mid to upper abdomen, where a firm, large mass was felt. On questioning, the patient related that she had felt this mass shifting position intermittently in the past. She had diffuse muscular atrophy, most pronounced in the extremities and neck. Laboratory values included a hemoglobin level of 12.1 g/dl (which decreased over the next 3 days to 9.2 g/dl), a WBC count of 27,000/mm^3, and a normal platelet count.

A plain film of the abdomen showed a large pelvic soft-tissue mass. No splenic silhouette was identified in the left upper quadrant. Multiple CT scans obtained previously for other episodes of abdominal pain had demonstrated the spleen in a number of different positions (Figs. 1A–1C). Some of the CT examinations had been performed without enhancement because of a prior allergic reaction to contrast material. The ectopic location of splenic tissue suggested by the CT scans had been confirmed with ^{99m}Tc-sulfur colloid scanning.

An unenhanced CT scan was obtained on the present admission because of suspected diverticulitis (Fig. 1D). It showed an inhomogeneous spleen that had enlarged and changed position compared with the previous examinations. Evidence of acutely thrombosed splenic hilar vessels was noted also. Torsion and ischemia were strongly suspected. Color flow and duplex Doppler sonographic studies were performed with 3.5- and 7.0-MHz imaging transducers (Acuson, Mountain View, CA) (Fig. 1E). The spleen lay very close to the left anterior abdominopelvic wall and was easily visualized in its entirety. The splenic parenchyma was diffusely abnormal. Despite detection of flow in both small vessels of the abdominal wall immediately superficial to the spleen and abdominopelvic vessels deep to the spleen, thorough interrogation of the splenic substance with color flow and duplex Doppler sonography revealed no detectable flow. The findings were considered diagnostic of splenic infarction due to torsion. Doppler examination of the main splenic artery just distal to the celiac artery showed antegrade flow with low diastolic velocity and a high resistive index of 84%, while a characteristic low-impedance flow pattern was shown in the common hepatic artery. The main splenic vein behind the pancreas was patent and showed a normal hepatopetal direction of flow. A ^{99m}Tc-sulfur colloid scan was

---

Received January 22, 1991; accepted after revision March 12, 1991.

[1] All authors: Department of Diagnostic Radiology, Northwestern University Medical School and Northwestern Memorial Hospital, Olson Pavilion, 710 N. Fairbanks Ct., Chicago, IL 60611. Address reprint requests to A. A. Nemcek, Jr.

***AJR* 157:307–309, August 1991** 0361–803X/91/1572–0307 © American Roentgen Ray Society

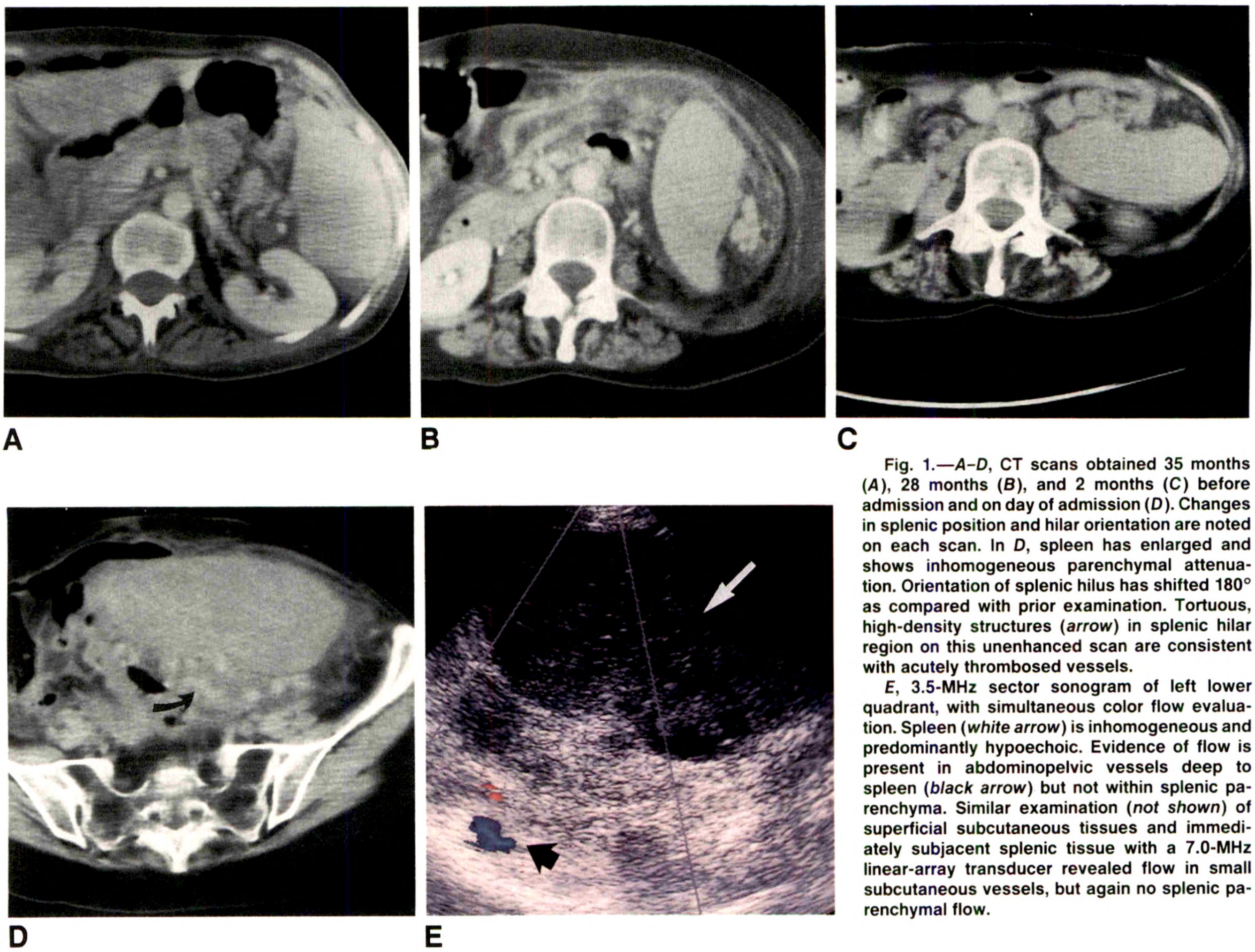

Fig. 1.—*A–D*, CT scans obtained 35 months (*A*), 28 months (*B*), and 2 months (*C*) before admission and on day of admission (*D*). Changes in splenic position and hilar orientation are noted on each scan. In *D*, spleen has enlarged and shows inhomogeneous parenchymal attenuation. Orientation of splenic hilus has shifted 180° as compared with prior examination. Tortuous, high-density structures (*arrow*) in splenic hilar region on this unenhanced scan are consistent with acutely thrombosed vessels.

E, 3.5-MHz sector sonogram of left lower quadrant, with simultaneous color flow evaluation. Spleen (*white arrow*) is inhomogeneous and predominantly hypoechoic. Evidence of flow is present in abdominopelvic vessels deep to spleen (*black arrow*) but not within splenic parenchyma. Similar examination (*not shown*) of superficial subcutaneous tissues and immediately subjacent splenic tissue with a 7.0-MHz linear-array transducer revealed flow in small subcutaneous vessels, but again no splenic parenchymal flow.

also obtained. It confirmed infarction by showing radionuclide accumulation in the liver but not the spleen.

Laparotomy revealed torsion of a freely mobile spleen attached only at its hilum by a long pedicle to other abdominal structures. The spleen had rotated about its axis several times and appeared congested. The distal pancreas and bowel were not incorporated into the torqued segment. Torsion of the splenic pedicle had resulted in splenic venous and arterial thrombosis. Surgical pathology revealed hemorrhagic infarction of a spleen weighing 989 g; a subcapsular hematoma also was noted. The clinical course after splenectomy was uneventful.

Discussion

Congenital maldevelopment of the suspensory ligaments of the spleen most likely precedes the majority of cases of wandering spleen [1, 2]. However, other congenital and acquired conditions may accentuate the tendency of the spleen to migrate about the abdomen and pelvis and to rotate around its vascular pedicle. In the present case, for example, increased abdominal wall laxity due to severe muscular atrophy and previous abdominal surgery most likely contributed to splenic torsion. The clinical presentation of wandering spleen ranges from the incidental finding of an abdominal mass in an asymptomatic patient to an acute abdominal crisis resulting from acute splenic torsion and infarction [3]. Intermittent and less severe abdominal pain may result from chronic mild or recurrent torsion; we speculate that in this case spontaneous torsion and detorsion of the splenic pedicle, rather than diverticulitis, may have been the cause of some of the other episodes of abdominal pain.

A number of reports and reviews have dealt with the various radiologic manifestations of wandering spleen [1, 4–8]. Recent reports of this entity have included findings on sonography or CT, reflecting increased use of these methods in the evaluation of patients with abdominal masses and pain. Findings noted on both imaging methods have included demonstration of an abdominal or pelvic soft-tissue mass and absence of the spleen in its typical location in the left upper quadrant [1, 4–8]. Previous radiographs may have demonstrated the spleen in a normal location. As in this case, serial studies may show a shifting position of the spleen and its hilum [8]. If infarction of the spleen occurs, part or all of the spleen will fail to enhance with IV contrast material on CT; on sonography the normal homogeneous, medium-level echogenicity of the spleen may be replaced by a heterogeneous appearance [8]. Complications associated with torsion, such as involvement of the pancreatic tail, have been diagnosed on both sonography and CT [5, 8].

The use of color flow and duplex Doppler sonography allows evaluation of organ blood flow. In the present case, no flow could be detected in the splenic parenchyma, consistent with infarction. The lack of any detectable flow in the splenic parenchyma could be blamed on lack of sufficient Doppler sensitivity to slow or low-amplitude flow, but this seems unlikely because of the very superficial location of the spleen in this patient and our ability to detect flow both immediately superficial and deep to the torqued organ. The finding of a high resistive index in the splenic artery deserves comment. Assessment of vascular impedance with a variety of calculations relating to Doppler spectra has received a great deal of attention in the assessment of normal physiology as well as abnormality in certain organs, such as the transplanted kidney. However, little has been published regarding assessment of normal and pathologic splenic arterial impedance. In one study, Nakamura et al. [9] investigated the pulsatility index in splenic, hepatic, and superior mesenteric arteries in fasting subjects and found a significantly lower pulsatility index (and thus lower vascular impedance) in the splenic artery as compared with the superior mesenteric artery. Whether the range of measurements of vascular impedance in the normal splenic artery will permit differentiation from certain pathologic states is an area we believe deserves further investigation; our own limited investigation since the appearance of this case has disclosed no instances in which a normal splenic artery has shown a resistive index of over 80%.

At first appraisal, the surgical finding of several rotations of the spleen about its axis and the finding of any flow in the main splenic artery and vein seem discrepant. We offer what we believe is a tenable explanation: Branches of the main splenic artery (short gastric and pancreatic arteries) may remain patent proximal to the site of torsion of the long splenic vascular pedicle characteristic of this disorder. This would allow some antegrade flow through the proximal splenic artery despite increased impedance caused by acute occlusion of the major portion of the splenic arterial bed. Similarly, the presence of a normal direction of blood flow in the main splenic vein most likely relates to continued patency of splenic vein tributaries that join the main spelnic vein beyond the point of torsion; such tributaries could include the inferior mesenteric vein or varices that have formed as a result of chronic venous congestion. We anticipate that the patterns of flow in these major vessels could change depending on the exact site of torsion.

We believe that the diagnosis of torsion in this case could have been made confidently if CT, sonography, or scintigraphy had been the first test. However, the preliminary diagnosis of wandering spleen had already been made. If this diagnosis is not suspected before signs and symptoms of torsion with infarction occur, we suspect that CT may most often suggest the specific diagnosis: sonography may be limited by bowel gas or body habitus in some patients, and nonvisualization of the spleen on scintigraphy is nonspecific and nonlocalizing. On the other hand, CT is relatively expensive compared with sonography, exposes the patient to ionizing radiation, and frequently subjects the patient to small but definable risks of contrast reaction. Sonography is used frequently as the initial imaging test in patients with abdominal pain; we believe that as long as visualization of a torqued spleen is not impaired, the combination of sonography with duplex Doppler and color flow evaluation should allow confident diagnosis of this condition. Confirmatory findings would include absence of the spleen in its normal location and demonstration of a mass elsewhere in the abdomen or pelvis; lack of demonstrable flow within the splenic parenchyma, both on the color flow survey and directed search with duplex Doppler; and possible alterations in main splenic arterial flow, specifically, elevation of the resistive index or other measures of vascular impedance.

In summary, we have reported a case of torsion of a wandering spleen for which there is correlative imaging by CT, sonography, and radionuclide scanning. To our knowledge, this is also the first reported case in which duplex Doppler and color flow sonography were used in the diagnostic evaluation because of their ability to noninvasively evaluate splenic parenchymal flow and flow in major splenic vessels.

REFERENCES

1. Dodds WJ, Taylor AJ, Erickson SJ, Stewart ET, Lawson TL. Radiologic imaging of splenic anomalies. *AJR* **1990**;155:805–810
2. Woodward DAK. Torsion of the spleen. *Am J Surg* **1967**;114:953–955
3. Abell I. Wandering spleen with torsion of the pedicle. *Ann Surg* **1933**;98:722–725
4. Dachman AH. Anomalies and congenital disorders. In: Friedman AC, ed. *Radiology of the liver, biliary tract, pancreas and spleen*. Baltimore: Williams & Wilkins, **1987**:917–930
5. Parker LA, Mittelstaedt CA, Mauro MA, Mandell VS, Jacques PF. Torsion of a wandering spleen: CT appearance. *J Comput Assist Tomogr* **1984**;8:1201–1204
6. Herman TE, Siegel MJ. CT of acute splenic torsion in children with wandering spleen. *AJR* **1991**;156:151–153
7. Kinori I, Rifkin MD. A truly wandering spleen. *J Ultrasound Med* **1988**;7:101–105
8. Sheflin JR, Lee CM, Kretchmar KA. Torsion of wandering spleen and distal pancreas. *AJR* **1984**;142:100–101
9. Nakamura T, Moriyasu F, Ban N, et al. Quantitative measurement of abdominal arterial flow using image-directed Doppler ultrasonography: superior mesenteric, splenic, and common hepatic arterial blood flow in normal adults. *JCU* **1989**;17:261–268

Book Review

Therapeutic Endoscopy and Radiology of the Gut, 2nd ed. Edited by John R. Bennett and Richard H. Hunt. Baltimore: Williams & Wilkins, 386 pp., 1990, $120

This volume includes contributions from a large number of gastroenterologists and leading interventional radiologists. It is an important reference and contains descriptions of the indications, complications, and technique of performing most of the nonoperative interventional procedures for treatment of gastrointestinal, biliary, and pancreatic diseases. The text is generally well written, is liberally referenced, and contains many useful illustrations.

Many chapters have special information that gives rapid and important insight into state-of-the-art gastrointestinal interventions. For example, a chapter dealing with management of esophageal strictures goes beyond initial information on etiology and clinical diagnosis to compare radiologic and endoscopic methods of diagnosis and to detail relevant aspects of endoscopic management. The types of endoscopes available, types of dilators in common use, and the relative value of each method are presented for comparison. Photographs of the dilators serve as a reference for rapid and easy identification. Whether to dilate with fluoroscopic guidance (not in the United Kingdom, but obligated by medicolegal implications in the United States), how to avoid complications, how much to dilate (and how often), and when to use guidewires are useful considerations. After even a brief review of this chapter, the reader will be able to amaze and astound gastroenterologic colleagues with knowledge of their procedures.

Similarly, a chapter dealing with endoscopic treatment of foreign bodies in the upper gastrointestinal tract provides a brief but thorough overview of endoscopic treatment and a description of the devices available for removing foreign material from the gastrointestinal tract. Rapid insight can be gained about types of foreign bodies requiring removal and optimal approaches. Also notable are contributions describing endoscopic approaches to gastrointestinal hemorrhage, such as obliteration of varices, endoscopic laser and diathermy control, and injection therapy. Chapters such as these provide extremely valuable first-line reference material for understanding the gastroenterologic approach to a variety of disorders for which radiologists are not primarily involved in therapy.

A series of chapters by gastroenterologists and radiologists compares treatment techniques of each discipline. Placement of intestinal tubes, gastrostomy, stenting of benign and malignant biliary strictures, removal of biliary stones, and treatment of hemorrhage are included. These offer the reader a comparison of the indications for each approach, provide technical information for performing the procedures, and indicate the expected outcome.

This text is highly recommended as an important resource for radiologists who treat and manage patients with a variety of gastrointestinal disorders. It will add important insight into the procedures performed primarily by gastroenterologists.

Charles A. Rohrmann, Jr.
University of Washington Hospital
Seattle, WA 98195

Gastric Carcinoma in Patients with Crohn Disease: Report of Four Cases

Seth N. Glick[1]

An association between Crohn disease and gastric carcinoma has not been described before. However, we report four patients with documented Crohn disease in whom gastric carcinoma developed later. In three of the four patients, onset of Crohn disease occurred after the age of 40. All of the patients had nonspecific constitutional symptoms and/or complaints referable to the upper gastrointestinal tract. No clinical evidence of active Crohn disease was present. In each patient, barium examination and CT showed either a mass (two cases) or other radiologic features of malignancy (two cases). Endoscopy with biopsy was performed in three patients and findings were misleading in two patients.

The possibility of an increased risk of malignancy in sites remote from inflamed bowel segments has been reported. The findings in this study suggest that patients with Crohn disease, particularly disease of late onset, may be predisposed to the development of gastric carcinoma.

AJR **157:311-314, August 1991**

The association between Crohn disease in the large and small intestine and the development of malignant tumors in these sites has been the subject of many reports [1-6]. Approximately 100 cases of colonic cancer and a similar number of small-bowel cancers associated with Crohn disease have been documented in the literature. Most of the information concerning the relationship between these entities is derived from case reports and small series. In addition, the possibility that patients with Crohn disease may be more susceptible to malignancy at sites remote (both gastrointestinal and extraintestinal) from the part of the intestine involved by the inflammatory process also has been considered. In the past year, gastric carcinoma was diagnosed at this institution in four patients with previously documented Crohn disease. Several unique clinical and radiologic features in these cases demonstrate the importance of radiology in clarifying the diagnostic problems in this setting and possibly in contributing to earlier diagnosis. The possible association between gastric carcinoma and Crohn disease also is discussed.

Subjects and Methods

Four patients with a known history of Crohn disease were referred between October 1989 and October 1990, for upper gastrointestinal barium examination for the investigation of a variety of upper abdominal and constitutional complaints. One patient had been treated with H_2-antagonists for 3 months. An upper gastrointestinal examination performed at another institution 1 year before had shown a duodenal ulcer. In three patients, the diagnosis of Crohn disease had been established on the basis of characteristic radiologic findings. The remaining patient had undergone ileal resection and total colectomy for intractable disease. A CT scan of the abdomen was obtained in all four patients. Three of the four patients underwent endoscopy and biopsy. In two of these three, the endoscopy was repeated. The gastric malignant neoplasm was resectable in all but one patient.

Received January 17, 1991; accepted after revision March 12, 1991.

[1] Department of Diagnostic Radiology, Hahnemann University Hospital, Broad and Vine Sts., Philadelphia, PA 19102. Address reprint requests to S. N. Glick.

0361-803X/91/1572-0311
© American Roentgen Ray Society

Results

There were two men and two women ranging in age from 29 to 68 (average, 54) years. The age at diagnosis of Crohn disease ranged from 15 to 60 (average, 45) years. Three of the four patients were more than 40 years old when Crohn disease was diagnosed and two of them were more than 60 years old. The interval between the diagnosis of Crohn disease and the diagnosis of gastric carcinoma ranged from 8 to 14 (average, 9.5) years; in three cases, it was exactly 8 years.

The distribution of Crohn disease was terminal ileum (two cases), colon (one case), and ileocolitis (one case). All four patients were asymptomatic with respect to the Crohn disease. One patient was being treated with sulfasalazine and another with steroids. Two were not taking medication but had received sulfasalazine in the past. One of these two also had been treated with steroids and the other with azathioprine.

Double-contrast upper gastrointestinal examinations showed abnormality in the gastric antrum in three patients and the gastric cardia in one patient. The antral abnormalities consisted of a large ulcer (Fig. 1A), concentric antral narrowing with thick nodular folds and multiple ulcers (Fig. 2A), and asymmetric antral narrowing with ulceration on the greater curvature (Fig. 3A). The fourth patient had mild narrowing of the distal esophagus and a mass in the gastric cardia (Fig. 4A). In all patients, the diagnosis of malignancy was suggested by the barium study. CT scans in these patients showed focal wall thickening (Fig. 1B), a gastric mass (Fig. 3B, 3C, 4B) and symmetric thickening of the antral wall (Fig. 2B). In the first three cases, the CT findings supported the diagnosis of a neoplasm, and in the last case they were inconclusive.

Endoscopy was performed in three patients. In one patient, the initial endoscopic diagnosis was gastric Crohn disease, whereas in another a firm region was found in the cardia but no definite mass was present. Biopsies in both patients did not show malignancy. A second endoscopic examination in both cases confirmed the diagnosis. During surgery, the tumor was found to have invaded the full thickness of the gastric wall and to have spread to perigastric lymph nodes in all four patients. One of the lesions was unresectable, and one patient also had liver metastases. Histologic evaluation revealed two of the neoplasms to be poorly differentiated carcinomas, another neoplasm was poorly differentiated signet cell, and the last neoplasm was moderately differentiated. None of the patients had evidence of Crohn disease in the resected specimen.

Discussion

The association between Crohn disease and malignancy is incompletely defined. Considerable evidence supports a direct pathogenetic relationship [1–7]. However, investigations attempting to document an increased risk of gastrointestinal cancer in patients with Crohn disease compared with the general population are less conclusive. These studies are limited by the small numbers of patients and the methods of selecting patients. Retrospective evaluations from tertiary referral centers have reported an increased risk that varies widely in magnitude for both colonic [1, 6, 8] and small-bowel cancer [4, 6]. Conversely, population studies have not shown an increased risk of gastrointestinal carcinoma or carcinoma at specific gastrointestinal sites in patients with Crohn disease [8, 9].

In view of the difficulties in documenting an increased risk of intestinal cancer in patients with Crohn disease in spite of pathologic and epidemiologic data supporting this association, it is understandable that a postulated association between gastric carcinoma and Crohn disease would be even more tenuous. The mechanism most widely accepted in Crohn-related intestinal cancer is long-standing inflammation. However, in our patients, this mechanism was absent. These patients may have a more generalized malignant diathesis. Immunologic compromise due to the underlying disease, the drugs used in its treatment, or both may play a role. Genetic predisposition to malignancy also could be a factor. Greenstein et al. [10] were unable to identify an overall increased risk of extraintestinal malignancy in patients with Crohn disease. However, there was a statistically significant increase

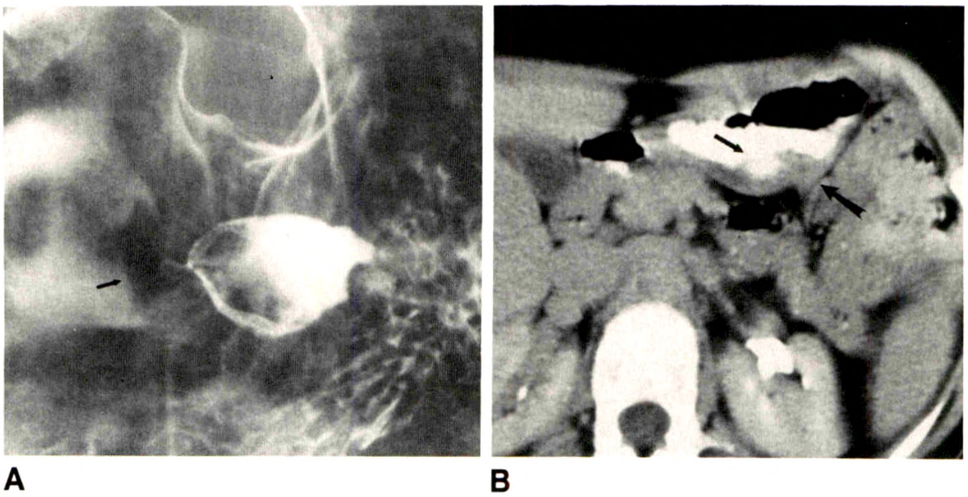

Fig. 1.—29-year-old woman with 2-month history of epigastric pain radiating to back.

A, Spot film from upper gastrointestinal study shows large irregular ulcer crater in proximal part of antrum. A faint defect in barium pool (*arrow*) surrounding ulcer suggests presence of malignant tumor.

B, CT scan from same patient shows gastric ulcer (*small arrow*) extending into focally and asymmetrically thickened gastric wall (*large arrow*).

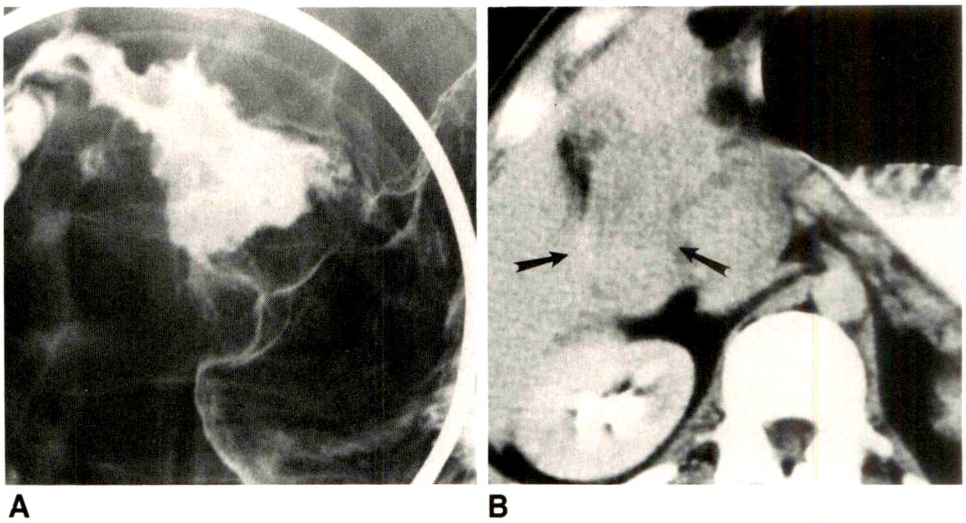

Fig. 2.—52-year-old man with increasing abdominal pain and weight loss for 10 months.

A, Spot film from upper gastrointestinal study shows concentric narrowing of antrum extending into duodenal bulb. Mucosa is ulcerated and contours are nodular. Proximal transition with normal wall is abrupt. These features suggest neoplasm rather than inflammation. Initial endoscopic impression was gastric Crohn disease.

B, CT scan shows uniform thickening of gastric antrum (*arrows*). Outer margins are indistinct, but no definite tumor mass is identified.

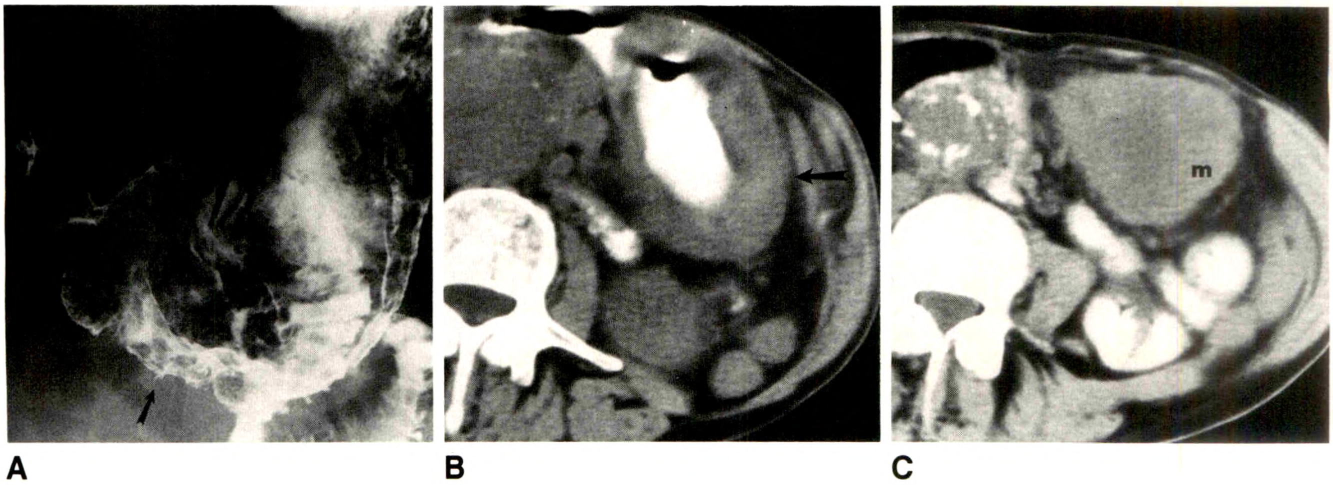

Fig. 3.—68-year-old woman with an 8-pound (3.6 kg) weight loss in 6 months and a palpable abdominal mass.

A, Spot film from upper gastrointestinal study shows large irregular mass (*arrow*) along greater curvature of antrum. Lumen is slightly compressed by extrinsic mass.

B, CT scan shows nonuniform mural thickening (*arrow*) at junction of body and antrum.

C, Lower section shows large heterogeneous soft-tissue mass (m), indicating presence of a neoplasm.

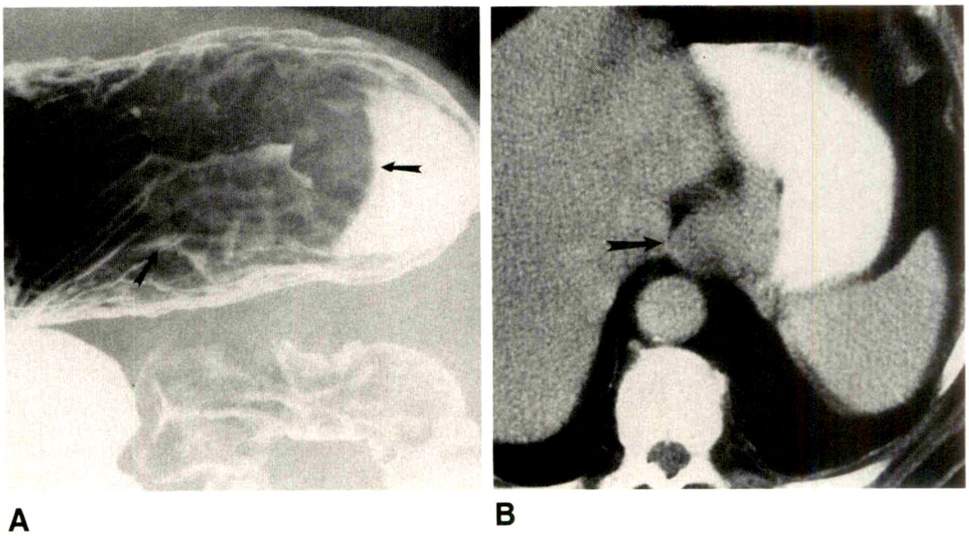

Fig. 4.—68-year-old man with a 3-month history of anorexia and dysphagia.

A, Lateral view of fundus shows a well-defined, smooth-surfaced mass (*arrows*) that surrounds and distorts cardiac orifice. Mucosa is preserved and intraluminal protrusion is minimal. Distal esophagus was slightly narrowed. Initial endoscopy and biopsy did not show tumor.

B, CT scan shows soft-tissue mass (*arrow*) arising from cardia and growing predominantly away from lumen.

in neoplasms of the reticuloendothelial system. Crohn disease in association with lymphoma has been described [11, 12]. In a population study [9] from Denmark, the prevalence of extraintestinal cancers was increased in women with Crohn disease. However, in a population study [13] from England, no increased risk for extraintestinal malignant tumors was seen in these patients.

Some evidence suggests that carcinoma of the gastrointestinal tract in Crohn disease may occur at sites remote from the inflammatory process [13]. Approximately one third of colonic carcinomas have arisen in segments uninvolved by Crohn disease [2]. Gyde et al. [13] found a statistically significant excess of tumors in the upper gastrointestinal tract. Eight of the nine lesions were at sites uninvolved by Crohn disease. Half of the gastrointestinal malignant neoplasms in this series were remote from the areas of inflammation. In another study [14], two (13%) of 15 gastrointestinal cancers of known origin were in the upper gastrointestinal tract and five (33%) of 15 were in uninvolved segments. A survey [15] of several institutions found 88 cases of gastrointestinal cancer with known site of origin. The malignant neoplasm was distant from the Crohn disease in seven patients (8%).

Specific information on gastric carcinoma and Crohn disease is limited. Anecdotal references without mention of clinical features have been noted [14, 15]. The only detailed analysis is the description by Gyde et al. [13] of four patients. Three were women. Three of the patients were more than 50 years old when Crohn disease was diagnosed. The duration of the Crohn disease ranged from 5 to 23 (average, 14) years. The age at diagnosis of carcinoma ranged from 56 to 75 (average, 66) years. In three patients, the Crohn disease was confined to the small bowel, and in one patient the distribution was ileocecal.

The number of patients with Crohn disease and gastric carcinoma may have been underestimated. In some cases, this association can go unrecognized, as the two entities are assumed to be unrelated. In other situations, the presence of Crohn disease in a patient with gastric carcinoma may be unsuspected. It is known that patients subsequently proved to have Crohn disease may have had vague symptoms for years. Alternatively, some patients initially have obstruction from a fibrotic stricture. In approximately 30% of patients with colonic carcinoma and Crohn disease, Crohn disease was not diagnosed until the patients were examined for symptoms related to the carcinoma [2]. Approximately 12% of the small-bowel neoplasms were identified either coincidently or within 1 year of diagnosis of regional enteritis [13].

It is interesting that three of the four patients described here and all of the patients reported by Gyde et al. [13] were more than 40 years old when Crohn disease was diagnosed. Patients with onset of Crohn disease after age 40 constitute less than 20% of the total population of patients with Crohn disease. No other consistent patterns relating to medications, disease distribution, or duration of disease were found.

Although a relationship between Crohn disease and gastric carcinoma is not established, these four cases demonstrate several important points. Patients with documented Crohn disease in whom symptoms referable to the upper gastrointestinal tract develop should undergo diagnostic examination. It should not be assumed that such symptoms are related to peptic disease, associated with drug therapy, or related to gastric Crohn disease. Radiologic evaluation with barium and CT scanning can be important in the diagnosis of gastric carcinoma because results of endoscopy and biopsy can be vague or misleading. Any gastric narrowing, ulceration, or fold thickening seen on upper gastrointestinal examination should be carefully assessed for features that suggest malignancy. Furthermore, as patients with Crohn disease often have an upper gastrointestinal examination done in conjunction with small-bowel evaluation during the course of the disease, increased scrutiny for subtle gastric mucosal abnormalities may be warranted. Although our four patients and those reported by Gyde et al. [13] had advanced disease, more aggressive treatment could result in earlier diagnosis. Increased awareness of this potential association should produce additional reports that may clarify this issue.

REFERENCES

1. Glotzer DJ. The risk of cancer in Crohn's disease. *Gastroenterology* **1985**;89:438–441
2. Hamilton SR. Colorectal carcinoma in patients with Crohn's disease. *Gastroenterology* **1985**;89:398–407
3. Collier PE, Turowski P, Diamond DL. Small intestinal adenocarcinoma complicating regional enteritis. *Cancer* **1985**;55:516–521
4. Senay E, Sachar DB, Keohane M, Greenstein AJ. Small bowel carcinoma in Crohn's disease: distinguishing features and risk factors. *Cancer* **1989**;63:360–363
5. Petras RE, Mir-Madjlessi SH, Farmer RG. Crohn's disease and intestinal carcinoma: a report of 11 cases with emphasis on associated epithelial dysplasia. *Gastroenterology* **1987**;93:1307–1314
6. Richards ME, Rickert RR, Nance FC. Crohn's disease-associated carcinoma: a poorly recognized complication of inflammatory bowel disease. *Ann Surg* **1989**;209:764–773
7. Savoca PE, Ballantyne GH, Cahow CE. Gastrointestinal malignancies in Crohn's disease. *Dis Colon Rectum* **1990**;33:7–11
8. Fireman Z, Grossman A, Lilos P, et al. Intestinal cancer in patients with Crohn's disease: a population study in central Israel. *Scand J. Gastroenterol* **1989**;24:346–350
9. Kvist N, Jacobsen O, Norgaard P, et al. Malignancy in Crohn's disease. *Scand J Gastroenterol* **1986**;21:82–86
10. Greenstein AJ, Gennuso R, Sachar DB, et al. Extraintestinal cancers in inflammatory bowel disease. *Cancer* **1985**;56:2914–2921
11. Glick SN, Teplick SK, Goodman LR, Clearfield HR, Shanser JD. Development of lymphoma in patients with Crohn disease. *Radiology* **1984**;153:337–339
12. Shepherd NA, Hall PA, Williams GT, et al. Primary malignant lymphoma of the large intestine complicating chronic inflammatory bowel disease. *Histopathology* **1989**;15:325–337
13. Gyde SN, Prior P, Macartney JC, Thompson H, Waterhouse JAH, Allan RN. Malignancy in Crohn's disease. *Gut* **1980**;21:1024–1029
14. Greenstein AJ, Sachar DB, Smith H, Janowitz HD, Aufses AH Jr. Patterns of neoplasia in Crohn's disease and ulcerative colitis. *Cancer* **1980**;46:403–407
15. Korelitz BI. Carcinoma of the intestinal tract in Crohn's disease: results of a survey conducted by the national foundation for ileitis and colitis. *Am J Gastroenterol* **1983**;78:44–46

Case Report

Diffuse Stenosis of the Ileum After Ureteroileal Interposition: Radiologic-Pathologic Correlation in Two Cases

Glenn A. Tung,[1] Nicholas Papanicolaou,[1] Lawrence R. Zukerberg,[2] and Isabel C. Yoder[1]

The small intestine has been effectively used for partial or complete replacement of a diseased ureter since 1906 [1, 2]. Indications include primary ureteral lesions, such as strictures and neoplasms; extrinsic processes involving the ureter, such as retroperitoneal neoplasms or fibrosis; and penetrating or surgical trauma. In recurrent nephrolithiasis, ileoureteral interposition is an attractive alternative because the large caliber of the intestine allows painless passage of stones.

When success is defined as a pain-free state and stable or improved renal function, a successful outcome for ureteroileal interposition can be expected in more than 80% of cases [2]. Focal strictures or dilatation with decompensation of the intestinal ureter have been reported [3, 4]. We present the imaging studies with pathologic correlation in two cases of ureterointestinal interposition complicated by narrowing of the entire intestinal segment, which occurred 3 months and $3\frac{1}{2}$ years after surgery.

Case Reports

Case 1

A 24-year-old man with cystinuria underwent right-sided ileoureteral interposition for a distal right-sided ureteral stricture resulting from recurrent nephrolithiasis that was refractory to dilatation. During surgery, it was noted that twisting the ileum on its mesentery to maintain orthoperistalsis generated a modest amount of venous congestion. A stentogram, obtained on the seventh day after surgery, revealed an edematous and largely effaced mucosal pattern of the ileal segment, although the caliber of the conduit was normal and pelvicaliceal dilatation had resolved (Fig. 1A). Peristalsis was sluggish.

Three months later, the patient had pain in the right flank. Excretory urography revealed right-sided urinary obstruction with poor visualization of the ureter. No vesicoureteral reflux was seen on voiding cystography. Antegrade pyelography and a ureteral perfusion study were performed to define the location and severity of obstruction [5]. The study revealed moderate pyelocaliectasis and marked narrowing of the lumen of the interposed segment of ileum (Fig. 1B). During ureteral perfusion, the differential pressure between the kidney and the bladder rose to 20 cm of water at a perfusion rate of 15 ml/min.

Surgery was performed to replace the stenotic ureteroileal segment. Pathologic examination revealed acute and chronic inflammation in the wall of the ileum, with marked fibrosis of the submucosa and muscularis propria and narrowing of the lumen. Widespread arterial and venous thrombosis of small and medium-sized vessels was noted, with prominent vascular recanalization suggestive of chronic ischemia (Fig. 1C).

Case 2

An 11-year-old boy had surgery at another hospital for a retroperitoneal mass. After resection of what proved to be a left-sided megaureter, the patient was transferred to our hospital, where a tapered ileal ureter was created on the left side. Mild caliectasis was noted on excretory urography done 6 months after surgery and was

---

Received January 28, 1991; accepted after revision March 20, 1991.

[1] Department of Radiology, Massachusetts General Hospital and Harvard Medical School, 32 Fruit St., Boston, MA 02114. Address reprint requests to N. Papanicolaou.

[2] Department of Pathology, Massachusetts General Hospital and Harvard Medical School, 32 Fruit St., Boston, MA 02114.

AJR 157:315-317, August 1991 0361-803X/91/1572-0315 © American Roentgen Ray Society

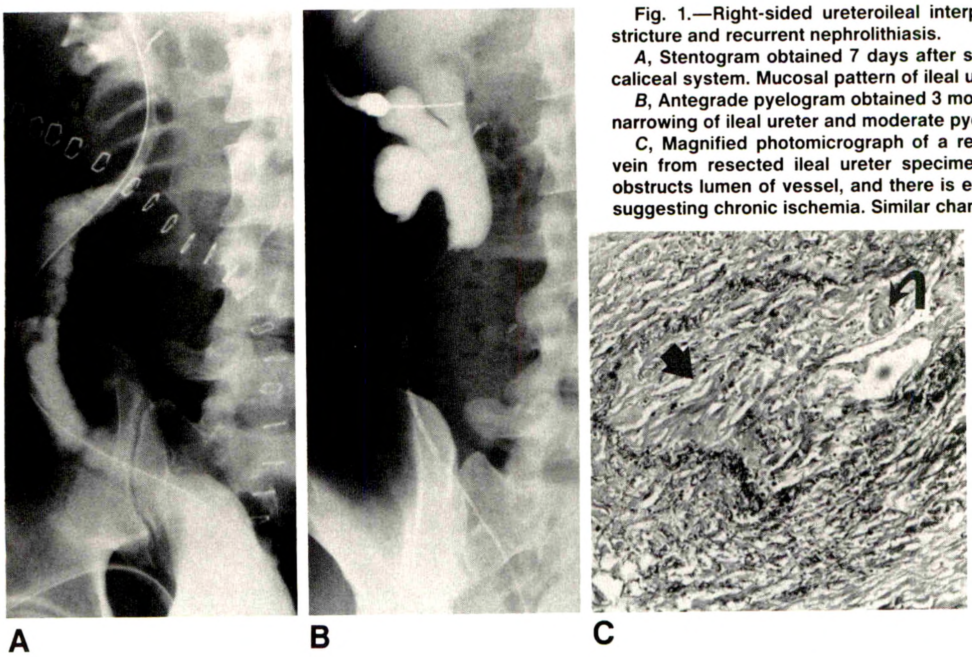

Fig. 1.—Right-sided ureteroileal interposition in a patient with distal ureteral stricture and recurrent nephrolithiasis.

A, Stentogram obtained 7 days after surgery shows a normal-appearing pyelocaliceal system. Mucosal pattern of ileal ureter is effaced.

B, Antegrade pyelogram obtained 3 months after surgery shows marked, diffuse narrowing of ileal ureter and moderate pyelocaliceal dilatation.

C, Magnified photomicrograph of a representative submucosal, medium-sized vein from resected ileal ureter specimen. Organized thrombus (*straight arrow*) obstructs lumen of vessel, and there is evidence of recanalization (*curved arrow*), suggesting chronic ischemia. Similar changes were noted in adjacent arteries.

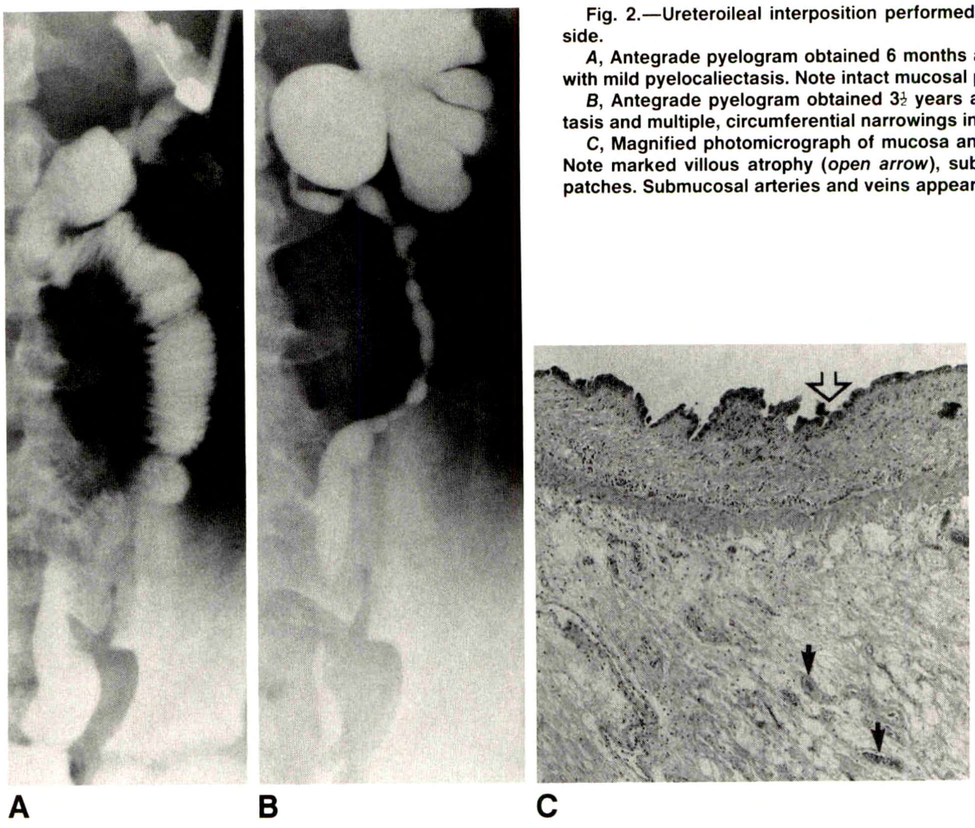

Fig. 2.—Ureteroileal interposition performed after resection of a megaureter on left side.

A, Antegrade pyelogram obtained 6 months after surgery shows a normal ileal ureter with mild pyelocaliectasis. Note intact mucosal pattern.

B, Antegrade pyelogram obtained 3½ years after surgery shows marked pyelocaliectasis and multiple, circumferential narrowings involving entire intestinal ureter.

C, Magnified photomicrograph of mucosa and submucosa from resected ileal ureter. Note marked villous atrophy (*open arrow*), submucosal edema, and absence of Peyer patches. Submucosal arteries and veins appear normal (*solid arrows*).

confirmed on an antegrade pyelogram (Fig. 2A). However, the ileal ureter appeared normal, peristalsis was active, and the perfusion study yielded normal pressures.

Three years later, the patient had intermittent pain in the left flank. Excretory urography showed delayed pyelogram effect and severe pyelocaliectasis. Antegrade pyelography showed serial stenoses involving the entire interposed ileal ureter, which had little peristaltic activity (Fig. 2B). A ureteral perfusion study revealed elevated differential pressures between the kidney and the bladder of 21 and 31 cm of water at perfusion rates of 10 and 15 ml/min, respectively.

During surgery, circumferential narrowings throughout the ileal segment were found with normal blood supply to the interposed bowel. Pathologic examination revealed villous atrophy and submucosal thickening by loose, edematous fibrovascular tissue, with compromise of the intestinal lumen. Submucosal lymphoid aggregates were absent, and chronic inflammation was minimal (Fig. 2C).

Discussion

When ureteroneocystostomy, autotransplantation, or transureteroureterostomy is not feasible for repair of a diseased ureter, partial or complete replacement of the ureter by intestine is an effective alternative. In a review of 89 patients' records after ileoureteral interposition, Boxer et al. [2] reported that 75% of patients had stable or improved renal function and 87% had no progression of renal collecting system dilatation after surgery. Fritzsche et al. [1] presented the radiologic changes of the kidneys in 39 patients followed up for up to 17 years after ureteroileal interposition. Pyelocaliceal dilatation decreased in 19 and was unchanged in 12 of 34 patients. Despite the frequent coexistence of ureteral reflux and bacteriuria, in no case was radiologically detectable renal parenchymal loss observed at follow-up [1]. However, neither series described changes in the appearance of the ureteral conduit itself.

Few complications have been reported after ureteroileal interposition. Tanagho [4] described five cases of dilatation of the interposed intestine, resulting in urinary stasis, infection, electrolyte imbalance, and renal parenchymal damage. He postulated that ileal segments, subjected to intermittent high bladder pressures within the closed-end urinary tract, are likely to decompensate. Hendren and McLorie [3] reported on five patients in whom solitary focal strictures developed in interposed bowel segments 2–19 years after surgery. Focal and diffuse strictures of ileal conduits have been reported in children and adults [6, 7]. The cause of strictures developing in segments of small bowel used as urinary diversion loops or ureters is not always clear. In some cases, the early onset of the pathologic process and the histologic findings support an ischemic insult. In other cases, onset is late or prolonged and the pathogenetic mechanism is one of inflammation and fibrosis of the mucosa and submucosa, mucosal atrophy, and hypertrophy of the muscular layer with normal-appearing blood vessels [6, 7]. Hendren and McLorie [3] ruled out ischemia as the cause of late focal strictures in intestinal ureters. Instead, they favored a hypothesis introduced by Tapper and Folkman [8], who described late strictures in canine intestinal segments exposed to urine. Microscopic examination of the specimens showed marked lymphoid depletion in submucosal sites and hypertrophy of adjacent mesenteric lymph nodes. A lymphotoxic effect of urine on mural lymphoid populations was postulated. Depletion of lymphoid cells together with reflux may predispose to recurrent inflammation, infection, and fibrosis.

As the radiologic changes in the appearance of an ileal ureter may be the deciding evidence that the surgical procedure has failed, the radiologist should be familiar with the features of normal ureteroileal interposition. In the early postoperative period, the normal ileal mucosal pattern is demonstrable and intestinal caliber is maintained. Often, the ileal segment may be tapered throughout its length or distally only, the latter to allow a nonrefluxing implantation. Early transient distortion of the intestinal conduit, due to edema of its mesentery from recent surgical manipulation, may occur. On the other hand, a featureless mucosal pattern with mural or mucosal changes suggestive of hemorrhage or edema soon after surgery is likely to be a harbinger of ischemia and eventual renal obstruction. Several years after surgery, some effacement of the mucosa due to columnar or urothelial metaplasia can be seen [3]; however, the intestinal origin of the replaced ureter should still be recognizable and its caliber should remain relatively unchanged.

The two cases reported here are unique in that the pathologic changes involved the entire interposed ileal segment. Both patients had urinary obstruction and similar radiologic appearance. They differ in the temporal evolution of the strictures and the histologic changes of the ileal ureters. The ischemic stricture in the first patient developed shortly after surgery. In the second patient, the stricture appeared late and the histologic findings were similar to those described in lymphoid-depleted ileal loops exposed to urine [8].

REFERENCES

1. Fritzsche P, Skinner D, Craven J, Cahill P, Goodwin W. Long-term radiographic changes of the kidney following the ileal ureter operation. *J Urol* **1975**;114:843–847
2. Boxer R, Fritzsche P, Skinner D, et al. Replacement of the ureter by small intestine: clinical application and results of the ileal ureter in 89 patients. *J Urol* **1979**;121:728–731
3. Hendren W, McLorie G. Late stricture of intestinal ureter. *J Urol* **1983**;129:584–590
4. Tanagho E. A case against the incorporation of bowel segments into the closed urinary system. *J Urol* **1975**;113:796–802
5. Pfister RC, Papanicolaou N, Yoder IC. Diagnostic morphologic and urodynamic antegrade pyelography. *Radiol Clin North Am* **1986**;24:561–571
6. Mitchell ME, Yoder IC, Pfister RC, Daly J, Althausen AF. Ileal loop stenosis: a late complication of urinary diversion. *J Urol* **1977**;118:957–961
7. Hardy BE, Lebowitz RL, Baez A, Colodny AH. Strictures of the ileal loop. *J Urol* **1977**;117:358–361
8. Tapper D, Folkman J. Lymphoid depletion in ileal loops: mechanism and clinical implications. *J Pediatr Surg* **1976**;11:871–880

Primary Esophageal Melanoma

James H. Brown[1] and Felix S. Chew

A 40-year-old woman had had dysphagia for 2 months. A lateral radiograph of the neck showed a mass in the upper esophagus (Fig. 1) that a subsequent barium esophagogram showed was an ulcerated intraluminal polypoid lesion. Chest CT showed involvement of the posterior esophageal wall; other mediastinal structures were uninvolved. The differential diagnosis included benign and malignant tumors, inflammatory polyp, and impacted food bolus. Esophagectomy was performed. The lesion was ulcerated and pigmented. Microscopy showed malignant melanocytes and deep invasion through the epithelium to the inner layer of the tunica muscularis. Melanocytic junctional activity and atypical melanocytic hyperplasia were present. The final pathologic diagnosis was primary malignant melanoma of the esophagus.

Primary malignant melanoma of the esophagus is rare, accounting for 0.1%–0.2% of esophageal malignancies and 0.5% of noncutaneous melanomas; melanoma metastatic to the esophagus may be even less common [1]. The lesion is thought to arise from benign melanocytes found in the normal esophageal epithelium. The tumors spread horizontally along the epithelium but also grow vertically to form polypoid masses that usually are covered by intact mucosa. Adjacent satellite nodules may exist. Symptoms of dysphagia are related to mass effect, at which time the lesions are clinically advanced. The biological behavior is aggressive, with hematogenous metastases to multiple organs and tissues and lymphatic metastases to the mediastinal and supraclavicular nodes. On barium esophagogram, the tumor usually appears as a polypoid intraluminal filling defect within a dilated esophageal segment [2]. The surface is usually smooth except for focal ulcerations. CT is unlikely to show the depth of invasion into the esophageal wall, but knowledge of the depth probably has no effect on outcome. Treatment is wide surgical resection, but the prognosis is dismal.

REFERENCES

1. Sabanathan S, Eng J, Pradam GN. Primary malignant melanoma of the esophagus. *Am J Gastroenterol* **1989**;84:1475–1481
2. Isaacs JL, Quirke P. Two cases of primary malignant melanoma of the oesophagus. *Clin Radiol* **1988**;39:455–457

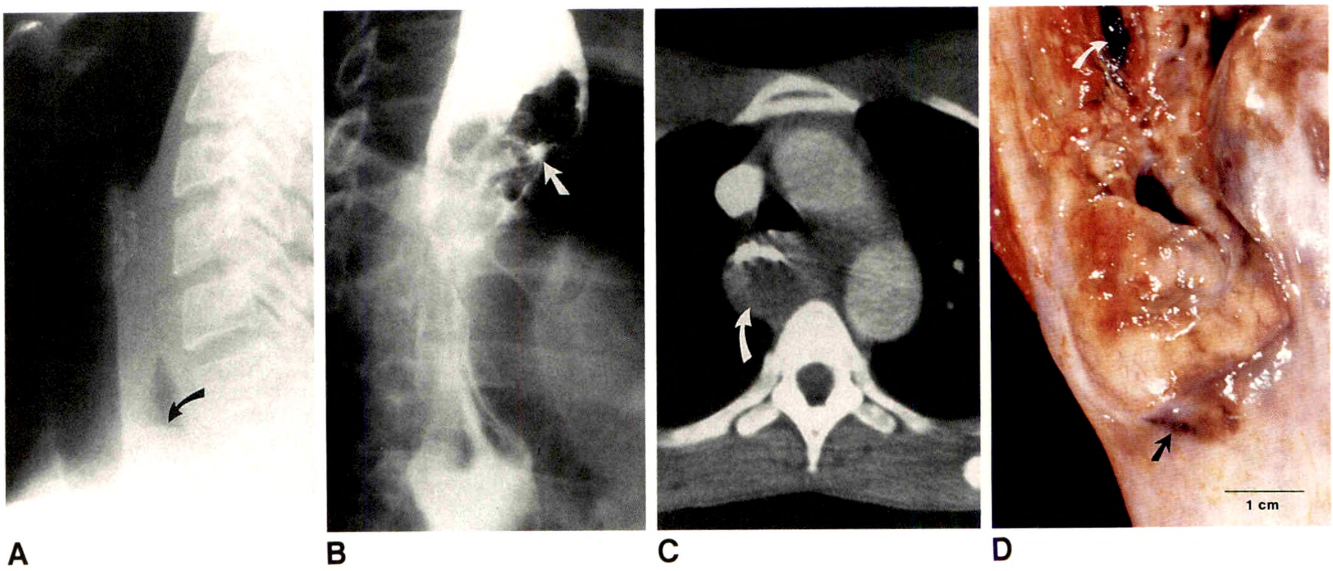

Fig. 1.—Primary esophageal melanoma.
A**, Lateral radiograph of neck shows top of soft-tissue mass in esophagus (*****arrow*****).**
B**, Barium esophagogram shows intraluminal polypoid lesion with deep ulceration (*****arrow*****).**
C**, Contrast-enhanced (oral and IV) CT scan at level of aortic arch shows mass (*****arrow*****) in posterior esophageal wall.**
D**, Esophagectomy specimen shows pigmented polypoid mass with three deep ulcers (one is indicated by *****white arrow*****). Superficial erosions cover mass, and an adjacent area of melanosis (*****black arrow*****) is present.**

From the weekly radiologic-pathologic correlation conferences conducted by Jack Wittenberg. Pathology editor: Andrew E. Rosenberg. Radiology editors: Felix S. Chew, Daniel P. Barboriak, William E. Palmer, and Daniel I. Rosenthal.

[1] Both authors: Department of Radiology, Massachusetts General Hospital and Harvard Medical School, 32 Fruit St., Boston, MA 02114. Address reprint requests to F. S. Chew.

***AJR* 157:318, August 1991** 0361–803X/91/1572–0318 © American Roentgen Ray Society

Giant Thoracic Osteophyte Causing Esophageal Food Impaction

Sharon Underberg-Davis[1] and Marc S. Levine

Dysphagia can occasionally be caused by giant vertebral osteophytes or exuberant bone formation associated with diffuse idiopathic skeletal hyperostosis (DISH). Almost all of the reported cases have resulted from large anterior osteophytes in the cervical spine that impinged on the hypopharynx or cervical esophagus [1-6]. Rarely, dysphagia can be caused by osteophytes in the thoracic spine [7]. It has been suggested that osteophytes are more likely to cause narrowing of the cervical esophagus because the esophagus is fixed in the neck at the level of the cricoid cartilage, whereas the thoracic esophagus is a relatively mobile structure that can be displaced anteriorly or laterally without being compressed [4, 5]. Nevertheless, we recently encountered a patient who had an esophageal food impaction above a giant thoracic osteophyte associated with DISH. To our knowledge, vertebral osteophytes have not been described previously as a cause of food impaction in the esophagus.

Case Report

A 76-year-old man came to the emergency department with acute onset of substernal dysphagia after ingesting a large piece of pork several hours earlier. His dysphagia was so severe that he was unable to swallow his saliva. The patient had experienced a similar episode 2 years earlier that had resolved spontaneously. Plain films of the neck and chest revealed no evidence of a radiopaque foreign body. However, there was exuberant osteophytosis in the cervical and thoracic spine (i.e., DISH) with a giant thoracic osteophyte seen extending anteriorly 2 cm from the intervertebral junction at the T9–T10 level (Fig. 1A). A single-contrast esophagogram revealed complete obstruction of the mid esophagus with barium outlining the superior border of a polypoid filling defect due to a meat bolus impacted in the esophagus above this giant osteophyte at the T9–T10 level (Fig. 1B). A small amount of aspirated barium was noted in the tracheobronchial tree. As the examination was being performed, the meat bolus dislodged spontaneously from the site of impaction and entered the stomach. The patient immediately experienced dramatic relief of symptoms. Reexamination of the esophagus revealed a smooth, extrinsic indentation on the right posterolateral wall of the esophagus caused by the osteophyte at the T9–T10 level (Fig. 1C). However, no evidence of intrinsic stricture formation was present in the esophagus, which otherwise appeared normal, except for disordered motility with poor primary peristalsis. The final diagnosis was a giant thoracic osteophyte causing an esophageal food impaction that resolved spontaneously during the barium study.

Discussion

Previous reports indicate that dysphagia can occasionally be caused by large anterior osteophytes in the cervical or thoracic spine [1-7]. However, most patients with cervical or thoracic osteophytes indenting the esophagus have no esophageal symptoms. As a result, osteophytes should be considered as the cause of dysphagia only when other pathologic lesions in the esophagus (e.g., tumors, webs, rings, and strictures) have been excluded. Our patient was unusual in that he had acute onset of dysphagia due to an esophageal food impaction that was apparently precipitated by a giant

---

Received January 24, 1991.; accepted after revision March 20, 1991.

[1] Both authors: Department of Radiology, Hospital of the University of Pennsylvania, 3400 Spruce St., Philadelphia, PA 19104. Address reprint requests to M. S. Levine.

AJR 157:319-320, August 1991 0361-803X/91/1572-0319 © American Roentgen Ray Society

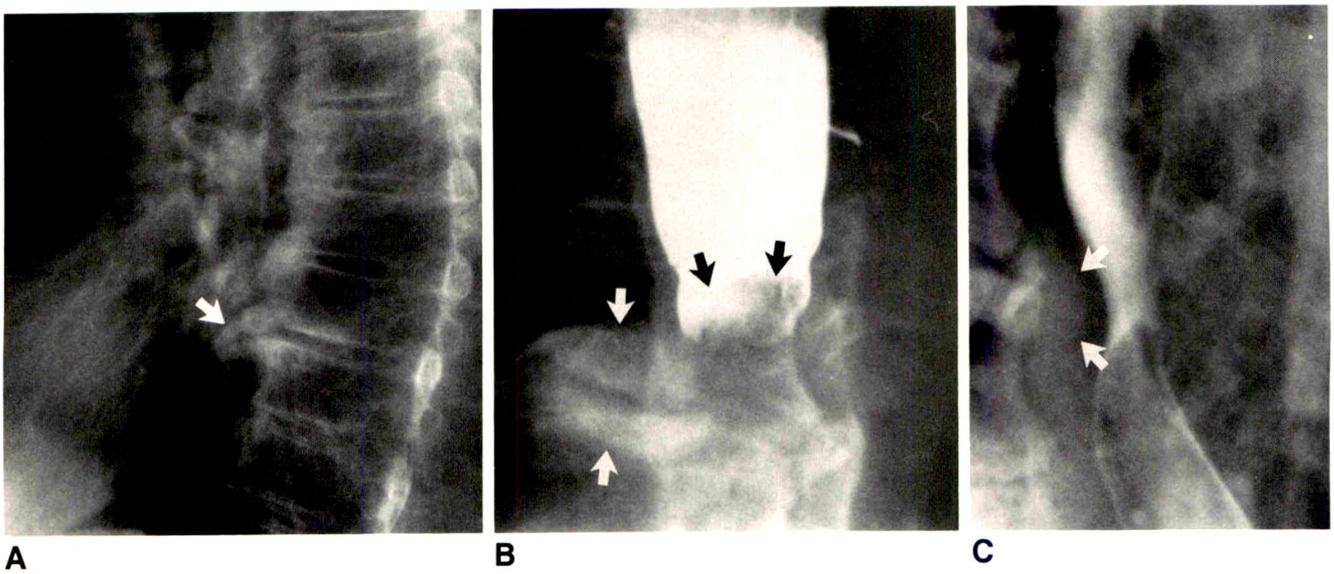

Fig. 1.—Giant thoracic osteophyte causing esophageal food impaction.

A, Close-up view from lateral chest radiograph shows bony changes of diffuse idiopathic skeletal hyperostosis in thoracic spine with giant anterior osteophyte (*arrow*) at T9–T10 level.

B, Initial esophagogram shows complete obstruction of mid esophagus with barium outlining proximal border of impacted meat bolus (*black arrows*) above osteophyte (*white arrows*), which is seen projecting to right of esophagus.

C, After spontaneous passage of meat bolus into stomach, second esophagogram in left posterior oblique projection shows smooth, extrinsic indentation on right posterolateral wall of esophagus caused by osteophyte (*arrows*), which is seen faintly in this projection. Note additional osteophytes proximally and distally.

thoracic osteophyte impinging on the esophagus (Fig. 1). We suspect that abnormal esophageal motility and the large size of the ingested meat bolus contributed to the impaction. Oral administration of a gas-forming agent or IV administration of glucagon can sometimes facilitate passage of the foreign body into the stomach [8]. In our patient, however, distension of the esophagus by the barium bolus caused the impacted meat to pass spontaneously from the esophagus.

Food impactions in the thoracic esophagus often result from a large bolus of unchewed meat lodging above an anatomic or pathologic area of narrowing, such as a lower esophageal ring or a benign or malignant stricture [8]. However, our experience indicates that giant thoracic osteophytes also should be recognized as a rare cause of dysphagia and esophageal food impaction. An osteophyte should be suspected as the cause of obstruction when an esophagogram reveals marked hypertrophic changes in the thoracic spine at this level. Nevertheless, a second esophagogram should be obtained after the impaction has been relieved in order to confirm that the osteophyte is impinging on the esophagus and to rule out underlying esophageal disease. In some cases, CT also may be helpful for documenting the presence of a bony mass that is encroaching on the esophagus and for excluding a neoplasm, vascular anomaly, or other extrinsic mass lesion in the posterior mediastinum [7]. When an esophageal food impaction is caused by a giant osteophyte, the patient should be advised to chew more carefully to avoid recurrent food impactions in the future. Rarely, surgical removal of the osteophyte may be required.

REFERENCES

1. Hilding DA, Tachdjian MO. Dysphagia and hypertrophic spurring of the cervical spine. *N Engl J Med* **1960**;263:11–14
2. Resnick D, Shaul SR, Robins JM. Diffuse idiopathic skeletal hyperostosis (DISH): Forestier's disease with extraspinal manifestations. *Radiology* **1975**;115:513–524
3. Gamache FW, Voorhies RM. Hypertrophic cervical osteophytes causing dysphagia. *J Neurosurg* **1980**;53:338–344
4. Lambert JR, Tepperman PS, Jiminez J, Newman A. Cervical spine disease and dysphagia. *Am J Gastroenterol* **1981**;76:35–40
5. Deutsch EC, Schild JA, Mafee MF. Dysphagia and Forestier's disease. *Arch Otolaryngol* **1985**;111:400–402
6. Davies RP, Sage MR, Brophy BP. Cervical osteophyte induced dysphagia. *Australas Radiol* **1989**;33:223–225
7. Willing S, Gammal TE. Thoracic osteophyte producing dysphagia in a case of diffuse idiopathic skeletal hypertrophy. *Am J Gastroenterol* **1983**;78:381–383
8. Levine MS. Trauma. In: Levine MS, ed. *Radiology of the esophagus*. Philadelphia: Saunders, **1989**:209–227

Review Article

Retroperitoneal Fibrosis

E. Stephen Amis, Jr.[1]

Retroperitoneal fibrosis is idiopathic in two thirds of cases and is found most commonly as an isolated fibrotic plaque centered over the lower lumbar spine and entrapping one or both ureters. It has been postulated that the fibrosis in the idiopathic cases results from a hypersensitivity reaction to antigens leaking into the retroperitoneum from atheromatous plaques in the aorta or common iliac arteries. In the remaining one third of cases, causes include ergot-derivative drugs, retroperitoneal hemorrhage or urine extravasation, and a desmoplastic response to a variety of tumors. In up to 15% of cases, associated fibrotic processes are found elsewhere in the body. Although the disease is imaged best with CT or MR, neither of these techniques can be used to differentiate benign from malignant plaques. Histologically, the disease is characterized in its early stages by inflammatory cells and edema in a loose collagen network. The mature plaque is composed of dense fibrous tissue with minimal cellular infiltration. This progression is important as it influences MR signal characteristics.

Retroperitoneal fibrosis (RPF) has been described in large part by anecdotal reports in the literature over the past 85 years. The noted French urologist Albarran [1] first advised ureterolysis (freeing of the ureter) in 1905 on the basis of three successes in patients whose ureters were encased in thick fibrous tissue. However, it was not until 1948 that John K. Ormond, a urologist at Henry Ford Hospital in Detroit, established as a recognized clinical entity the retroperitoneal fibrotic process that tends to entrap the ureters [2]. Since then, many names have been applied to this condition, including Ormond disease, nonspecific retroperitoneal inflammation, sclerosing retroperitonitis, retroperitoneal vasculitis with perivascular fibrosis, and periaortitis. Although we now know a great deal more about the clinical and imaging characteristics of RPF, its cause in most cases remains a puzzle. This review summarizes the current concepts about this fascinating disease.

Systemic Nature of Retroperitoneal Fibrosis

Although in most cases the fibrotic process is localized about the lower aorta and common iliac arteries in the retroperitoneal space, secondary manifestations of the disease are protean. Up to 15% of patients have additional fibrotic processes outside the retroperitoneum; occasionally several organ systems are involved simultaneously [3]. The most commonly recognized associated conditions are mediastinal fibrosis, Riedel fibrosing thyroiditis, sclerosing cholangitis, and fibrotic orbital pseudotumors [4]. These are thought to be major regional manifestations of a systemic sclerosing disease whose cause is poorly understood. Other associated fibrotic processes can occur in virtually every organ, from the frontal lobe of the brain to the parenchyma of the testes [5, 6]. Further, RPF occasionally may be associated with Weber-Christian disease (nonsuppurative panniculitis) and sclerosing mesenteritis [6].

In the abdomen, RPF may spread contiguously to involve multiple structures in both the retroperitoneum and the peritoneal cavity, or multiple unattached sites may be involved. Fibrous lesions in all of these locations have virtually the same histologic pattern, attesting to a similar origin.

Received January 24, 1991; accepted after revision March 20, 1991.

[1] Department of Radiology, Columbia-Presbyterian Medical Center, 622 W. 168th St., New York, NY 10032. Address reprint requests to E. S. Amis, Jr.

AJR 157:321-329, August 1991 0361-803X/91/1572-0321 © American Roentgen Ray Society

Etiology

About two thirds of all cases of RPF are considered idiopathic in that no specific cause can be proved [5–7]. These often are called Ormond disease. The remaining one third of cases usually can be traced to the use of various medications, to a retroperitoneal desmoplastic response to various malignancies, or to other inciting factors or conditions occurring in the retroperitoneum, such as infection or hemorrhage.

Several theories have been advanced about the cause of idiopathic RPF. Some reports have implicated a vasculitis because a prominent perivascular inflammation occurs in the early course of the disease [8]; others have postulated that RPF is a manifestation of a systemic collagen disease [9]. Yet another theory is that the fibrosis may be a local expression of an immunologically mediated systemic disease [10].

Idiopathic RPF usually occurs only in areas where the wall of an artery (usually the aorta) has severe atherosclerotic plaques and attenuation of the media. A commonly held theory on the origin of RPF is that fibrosis develops in response to leakage of an insoluble lipid (ceroid) from the atheroma into the periaortic tissue [3, 11]. Ceroid, often found in macrophages in the aortic adventitia or in adjacent nodes, is thought to induce an immune response that results in formation of the plaque. It has been suggested that all forms of fibrosis throughout the body are the result of hypersensitivity to such antigens in atheromatous plaques and therefore should be termed chronic periaortitis or periarteritis [11, 12]. However, this would not explain fibrosis occurring in children who have no atheromatous arterial disease. Although idiopathic RPF may be due to one or more of these causes, currently its true etiology remains unknown.

In those cases in which a cause of RPF can be deduced, the most well known is the use of methysergide, an ergot derivative that formerly was prescribed rather commonly for the treatment of migraine headache. This drug accounts for about 12% of all reported cases of RPF [5]. Usually, prolonged, uninterrupted use of methysergide is necessary for the development of RPF [13]. Other ergot derivatives reportedly associated with RPF include lysergic acid diethylamide and bromocriptine, a drug related to methysergide that is used in the treatment of parkinsonism [14]. Several other drugs may be causally related to RPF; these include beta blockers, methyldopa, hydralazine, and various analgesics and antibiotics [15, 16].

Specific infections such as tuberculosis, syphilis, actinomycosis, and various fungal infections have been reported as possible causes of RPF, as have nonspecific inflammatory processes such as diverticulitis and appendicitis [16]. Hemosiderin deposits in some fibrotic plaques indicate previous retroperitoneal hemorrhage as a factor in the development of RPF. Although such hemorrhage can be spontaneous or due to trauma, it also can occur after surgical procedures such as aortic bypass surgery and anterior spinal fusion, both of which have been complicated on rare occasions by subsequent RPF.

Malignancy accounts for approximately 8–10% of all cases of RPF [5]. In these cases, small metastatic foci in the retroperitoneum elicit a desmoplastic response, resulting in a fibrotic plaque that is grossly and clinically difficult to differentiate from RPF due to other causes, especially in patients with no known primary malignancy. Multiple malignancies have been reported as causing this fibrotic response, including carcinomas of the breast, lung, thyroid, gastrointestinal tract, and genitourinary organs, as well as lymphomas and some sarcomas [5, 6].

Another entity related to the cause of RPF is perianeurysmal fibrosis. Approximately 5–10% of all aortic or aortoiliac aneurysms form a perivascular rind that may surround the aneurysm only or may extend laterally far enough to envelop and obstruct the ureters [17]. These are sometimes referred to as inflammatory aneurysms [18]. Some authorities think that RPF and perianeurysmal fibrosis are separate diseases, but the clinical manifestations of the two can be similar, and the pathologic features are indistinguishable [19]. In the past, it was thought that perianeurysmal fibrosis might be the result of leakage from the aneurysm causing a fibrous reaction. However, hemosiderin has not been found in the fibrous tissue surrounding the aneurysm, making the theory of leakage of blood unlikely [20]. As with idiopathic RPF, it has been postulated that perianeurysmal fibrosis is an immune response to ceroid produced in an atheromatous plaque and that RPF and perianeurysmal fibrosis are probably the same disease [21].

Clinical Characteristics

RPF is rare, with a prevalence of about one per 200,000 population [22]. The average age at onset of signs and symptoms is approximately 50 years; in 70% of patients, the age at diagnosis is between 30 and 60 years [3]. In idiopathic RPF, males predominate over females by a factor of two to one; in RPF due to methysergide, this ratio is reversed [5]. However, in cases of RPF associated with malignancy, the sex distribution is equal. Although RPF is distinctly uncommon in childhood, it does occur in the preteen years and as early as the fetal period [23, 24].

Signs and symptoms may be related to entrapment and compression of the ureters, inferior vena cava, aorta and its branches, or gonadal vessels. The ureters are the most frequently compressed structures, probably because they offer less resistance than other vulnerable organs [25]. Ureteral obstruction, although often asymptomatic because of the insidious nature of the disease, may result in pain and tenderness in the flank or costovertebral angle, ureteral colic, oliguria or anuria, and eventual renal failure. Compression of the inferior vena cava, when severe enough, can cause edema of the lower extremities or scrotum or deep thrombophlebitis of the legs. Involvement of gonadal vessels and lymphatics can result in hydrocele and scrotal discomfort. As the condition progresses, the aorta and common iliac arteries eventually may be compressed, leading to claudication and gangrene of the lower extremities [26]. With extensive plaques, stenosis of the renal arteries may result in renovascular hypertension [27], and occlusion of the superior and inferior mesenteric arteries can lead to bowel ischemia [25].

Far less commonly, extensive fibrosis may result in biliary obstruction, portal hypertension, or blockage of the gastrointestinal tract [13, 19, 23, 25]. When mediastinal fibrosis occurs, common manifestations include the superior vena caval syndrome, constrictive pericarditis, and pulmonary hypertension [27].

Patients may also have nonspecific signs and symptoms, such as dull, noncolicky pain localized to the back or abdomen; fatigue; weight loss; and mild fever [5]. Laboratory findings are also nonspecific. The urine is typically sterile. Anemia is common, with the hematocrit frequently less than 33% (0.33) [3]. An elevated erythrocyte sedimentation rate is found in 94% of patients on the initial examination [6]. Some degree of renal compromise is found in up to 75% of patients with RPF [16].

Pathology

On gross examination, the fibrotic plaque has a woody consistency and is gray-white. The anterior margin of the lesion generally respects the posterior peritoneal boundary and is delineated clearly; the posterior margin is defined more poorly and cannot be separated easily from adjacent structures [28]. The plaque usually is centered over the anterior surfaces of the fourth and fifth lumbar vertebrae; surrounds the aorta, vena cava, and common iliac vessels; and usually does not extend laterally more than about 1 cm beyond the ureters [29] (Fig. 1).

In the formative stages of the disease, histologic examination of the plaque reveals an immature fibrotic process with many fibroblasts, inflammatory cells, and capillary proliferation in a loose network of collagen fibers [29] (Fig. 2A). This early process is typically paraaortic. In this stage, the tissue has a high fluid content because the new vessels have leaky interendothelial junctions, allowing the passage of proteins and RBCs into the extravascular space [30]. As the plaque matures, the collagen tends to become hyalinized, and cellular activity declines. The mature plaque is composed of dense hyalinized collagen containing few cellular elements [30] (Fig. 2B). This maturation appears to progress laterally from the midline. As the fibrosis envelops vascular structures and the ureters, a well-defined dissection plane usually remains, which allows these structures to be freed easily from the plaque.

When RPF is associated with metastatic neoplasm, it usually is impossible to distinguish grossly the resultant plaque from its benign counterpart [31]. Histologically, the pattern is similar to that of the early phase of idiopathic fibrosis, with the exception of having a few malignant cells scattered among the inflammatory cells in the collagen mesh [32] (Fig. 2C).

Imaging

The retroperitoneal space has been described as a "veritable jungle of strange things" [33] and a "hinterland of straggling mesenchyme, with vascular and nervous plexuses, weird embryonic rests and shadowy fascial boundaries" [34]. These descriptions were penned 25 years ago or more, and we now have a far better understanding of the anatomy of this region, gleaned from the results of cross-sectional imaging techniques such as CT and MR. However, at the time of its recognition as a clinical entity about four decades ago, RPF could be diagnosed only by showing the extrinsic compressive effect of the plaque on the ureters and great vessels. Therefore, because the most common consequence of the disease is ureteral compression, urography became the procedure of choice for diagnosing this condition. Not surprising, the term "squeezing disease" came to be used in describing RPF [35].

The scout film for the excretory urogram typically shows normal psoas outlines bilaterally because the fibrosis usually does not extend to the lateral borders of these muscles [29]. With a more extensive plaque, obliteration of the psoas outlines may be observed [36]. On the subsequent urographic study, the hallmark of RPF is a smooth extrinsic narrowing of one or both ureters in the region of the lower lumbar spine or upper sacrum, with proximal hydronephrosis of various degrees. Bilateral involvement occurs in two thirds of cases in adults and in about half in children [24]. Primary ureteral tumors, periureteral adenopathy, and postoperative or inflammatory strictures of the ureter can result in similar radiologic findings.

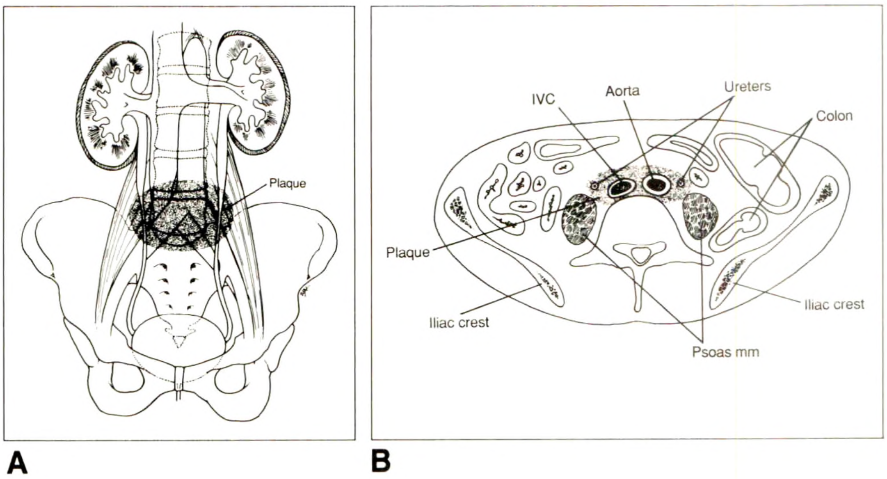

Fig. 1.—Diagrams of typical location and extent of retroperitoneal fibrosis.

***A*, Coronal view. Note that plaque usually does not extend to lateral borders of psoas muscles.**

***B*, Transverse view. Great vessels are enveloped by plaque but not elevated from spine. IVC = inferior vena cava, mm = muscles.**

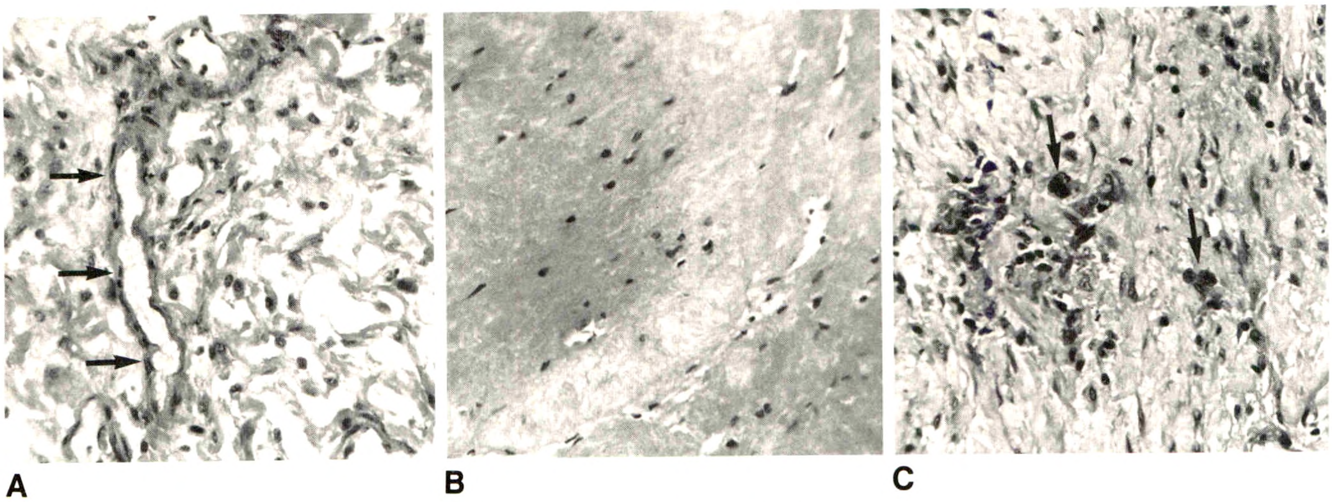

Fig. 2.—Histopathologic findings in retroperitoneal fibrosis. (Original magnification ×375)

A, Early stage of idiopathic plaque formation. Note hypercellularity, capillary proliferation (*arrows*), and edematous appearance.

B, Mature plaque. Note minimal cellularity in dense collagen.

C, Malignant retroperitoneal fibrosis associated with adenocarcinoma of stomach. Note paucity of malignant cells (*arrows*) and significant numbers of inflammatory cells in a somewhat edematous network of collagen.

(Courtesy of K. O'Toole, New York, NY.)

Early descriptions of the urographic findings also noted medial deviation of the involved ureters, which at the time was considered a pathognomonic sign of RPF [37]. However, two studies in the early 1970s found no significant difference in the position of normal ureters relative to the lumbar spine when compared with ureters trapped by RPF [38, 39]. Normal ureters overlapped or coursed medially to the lower lumbar or upper sacral pedicles in 18% of control subjects [39]. Further, hypertrophy of the psoas muscles can result in significant medial deviation of the ureters in muscular patients. It can be concluded, therefore, that in patients with RPF, the ureter, which is normally quite variable in its course, most likely is entrapped in its normal location by the expanding plaque rather than being pulled medially by the fibrotic process.

In the rare instances in which the fibrosis has extended into the true pelvis, circumferential compression of the bladder may result in a teardrop configuration, a pattern also seen with pelvic lipomatosis, pelvic hematoma, bilateral pelvic lymphadenopathy, and pelvic collateral vessels forming in response to occlusion of the inferior vena cava [40].

In some cases, excretory urography does not indicate the extrinsic nature of the ureteral obstruction. In these patients, retrograde or antegrade ureterography is necessary to define the obstruction adequately [41]. During retrograde studies, a 5- or 6-French catheter usually can be passed easily through the strictured area, suggesting that the cause of the obstruction is a loss of normal ureteral peristalsis due to entrapment of the ureter in the fibrotic plaque [6, 42]. Fluoroscopy confirms diminished ureteral peristalsis in such cases [6]. However, occasionally ureteral catheters will not pass through the tapered area, indicating that the cause of the obstruction is an extremely dense plaque mechanically compressing and possibly infiltrating the ureter [43].

Inferior vena cavography in patients with RPF typically shows a smooth, tapered narrowing of the inferior vena cava, also usually at the level of the lower lumbar spine or upper sacrum (Fig. 3); in some cases the vessel may be obstructed completely [44]. The length of constriction of the inferior vena cava was used as a measure of the extent of the plaque before the advent of cross-sectional imaging techniques. Aortography can show smooth or irregular narrowing of the distal aorta and common iliac arteries and, depending on the stage of development of the fibrotic process, may show hypervascular staining in the region of the plaque itself [45].

Lymphangiographic findings in RPF include dilatation and tortuosity of the lymph vessels, with delay in passage of contrast material through the periaortic nodes [46]. However, the lymphangiogram may be normal even when RPF is far advanced [47]. In the early stage of plaque development when active inflammation is present, ^{67}Ga-citrate scanning may show uptake of the radionuclide in the periaortic area [3, 11, 48].

Barium studies of bowel compressed by RPF show a smooth, extrinsic tapering of the lumen similar to that seen involving the ureter on urography. In such cases, the differential diagnosis is essentially the same as that given previously for ureteral narrowing. When the rectosigmoid is compressed, the appearance often is similar to that seen with pelvic lipomatosis or may resemble changes induced by radiation or even scirrhous carcinoma.

Sonography can suggest the presence of RPF. Characteristically, the fibrous plaque is seen as a smooth-bordered, relatively echo-free mass anterior to the lower lumbar spine or sacral promontory [49] (Fig. 4). This is true for both benign and malignant RPF as well as most cases of malignant lymphadenopathy. Perianeurysmal fibrosis is also essentially echo free and, depending on its extent, has an appearance similar to that of RPF [51]. Unfortunately, subtle or early changes of RPF can be missed on sonograms because of overlying gas- or fluid-filled bowel loops.

CT and MR are currently the most definitive techniques for diagnosing and determining the extent of RPF. The plaque typically begins below the aortic bifurcation at the level of the sacral promontory or the fourth or fifth lumbar vertebra and then spreads along the anterior surface of the spine cephalad toward the renal hila, where, on rare occasion, it may envelop the renal pelvis and even surround the kidney [15, 27, 52] (Fig. 5). As it progresses, it envelops the aorta and inferior vena cava and often entraps the ureters in its anterolateral margins as it extends laterally over the psoas muscles (see Fig. 4 [50]). If a significant length of ureter and the renal pelvis are involved, hydronephrosis may be minimal even when significant obstruction is present [42]. As previously noted, RPF also can spread inferiorly and involve the rectosigmoid, bladder, and other pelvic organs.

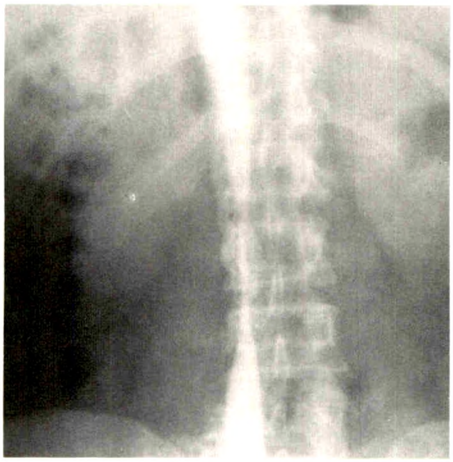

Fig. 3.—Compression of inferior vena cava by retroperitoneal fibrosis. Inferior venacavogram shows smooth, tapered narrowing of inferior vena cava at level of L3–L4 (area of plaque).

The appearance of the plaque on CT varies considerably: It can be midline or asymmetric, well circumscribed or poorly defined, and localized or extensive [53]. Rarely, the fibrotic process is seen on CT as only minimal soft-tissue stranding around the great vessels and ureters (Fig. 6). Thin sections may make it easier to visualize this tissue. The attenuation of the well-developed plaque is usually equivalent to that of the adjacent muscles [28]. After the administration of IV contrast material, the plaque enhances to various degrees, depending on the stage of development of the fibrous process; in other words, the immature plaque has greater vascularity and enhances to a greater degree [54]. Perianeurysmal fibrosis has a similar tendency to enhance and may be seen as a rind of tissue surrounding the dilated aorta (Fig. 7), or it may have a morphologic pattern similar to RPF with the exception that the encased aorta is aneurysmally dilated [55]. These similarities again support the unifying concept of a periaortitis as the common cause of RPF and perianeurysmal fibrosis.

CT generally cannot be used to differentiate among the various causes of RPF [56]. The major differential diagnosis is between the idiopathic variety of the disease and fibrosis associated with metastatic implants in the retroperitoneal tissue. Biopsy usually is required to establish the final diagnosis. However, it must be emphasized that in malignant RPF, the metastatic cells usually are dispersed so diffusely in the fibrotic plaque that multiple deep surgical biopsies are necessary to establish the diagnosis; CT-guided fine-needle aspiration or core biopsies, because of the small amount of tissue sampled, are considered far less effective [11, 56].

Occasionally, malignant adenopathy in the retroperitoneal area can become confluent, surround the great vessels, and resemble RPF [57]. This is especially true with lymphoma,

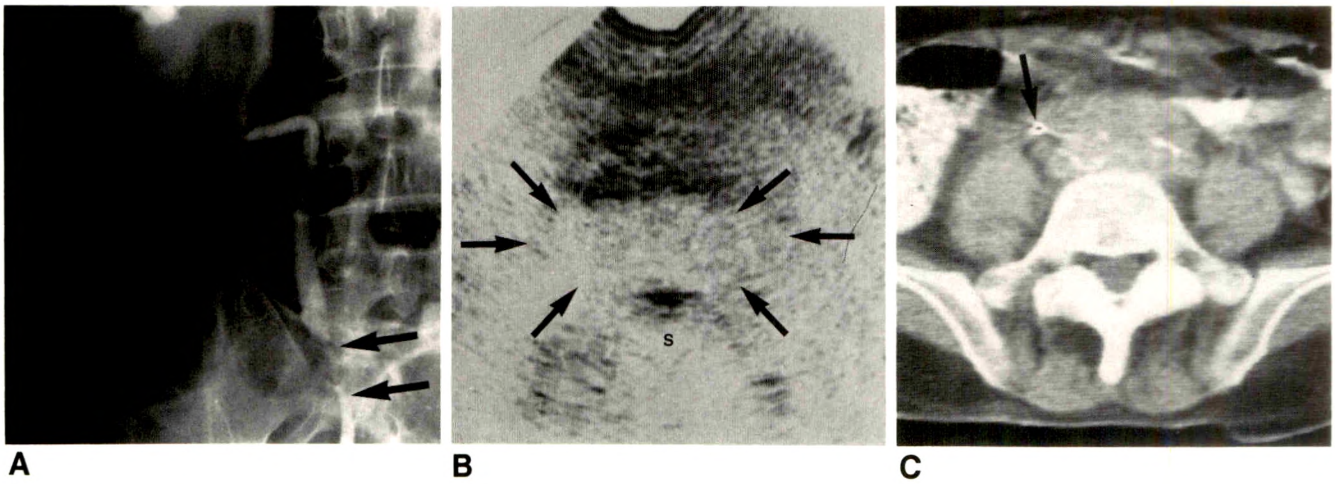

Fig. 4.—Common presentation of idiopathic retroperitoneal fibrosis.

A, Retrograde pyelogram shows extrinsic tapering of right ureter (*arrows*) at level of sacral promontory and mild proximal hydronephrosis.

B, Sonogram shows a hypoechoic, reasonably well-defined plaque in presacral area (*arrows*). S = sacrum.

C, CT scan at level of ureteral stricture after placement of right ureteral stent shows right ureter (*arrow*) entrapped in anterolateral margin of plaque. Common iliac arteries (defined by atherosclerotic calcification) are not elevated from sacrum.

(Reprinted with permission from Amis and Newhouse [50].)

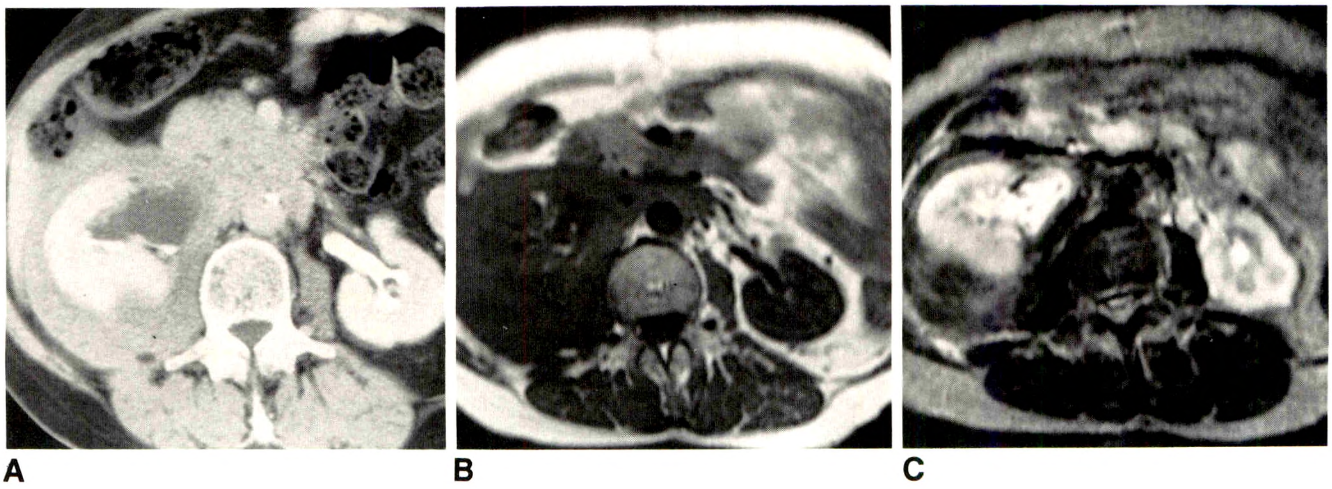

Fig. 5.—Extensive idiopathic retroperitoneal fibrosis surrounding right kidney.

A, CT scan shows retroperitoneal mass extending into right perirenal space and completely surrounding kidney.

B, T1-weighted transverse MR image shows tissue surrounding great vessels as well as right kidney. Tissue has a low signal intensity.

C, T2-weighted transverse MR image also shows tissue has low signal. Biopsy proved this was benign fibrosis.

(Courtesy of P. J. Kenney and J. Burns, Birmingham, AL.)

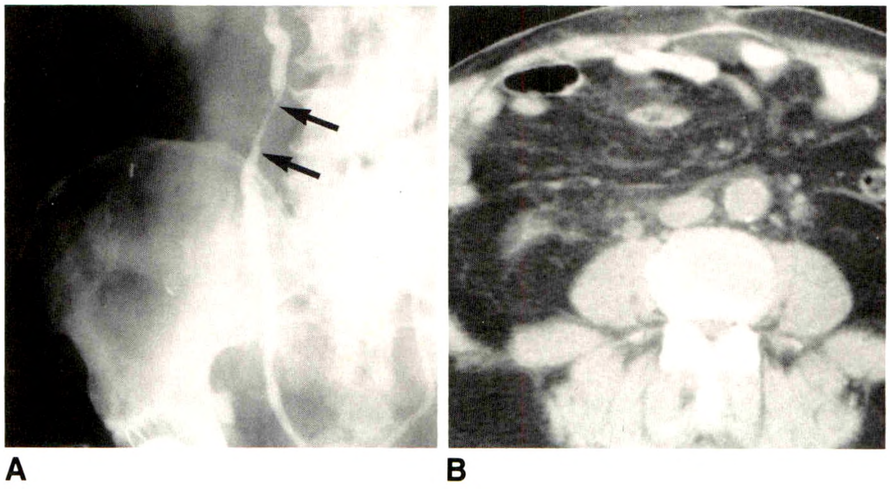

Fig. 6.—Idiopathic retroperitoneal fibrosis with minimal plaque seen on CT.

A, Retrograde study of right ureter shows tight extrinsic narrowing at level of L4 (*arrows*).

B, CT scan through area of ureteral narrowing shows only minimal soft-tissue strands around great vessels. No well-defined plaque is present. Lesion was surgically proved to be retroperitoneal fibrosis at time of ureterolysis.

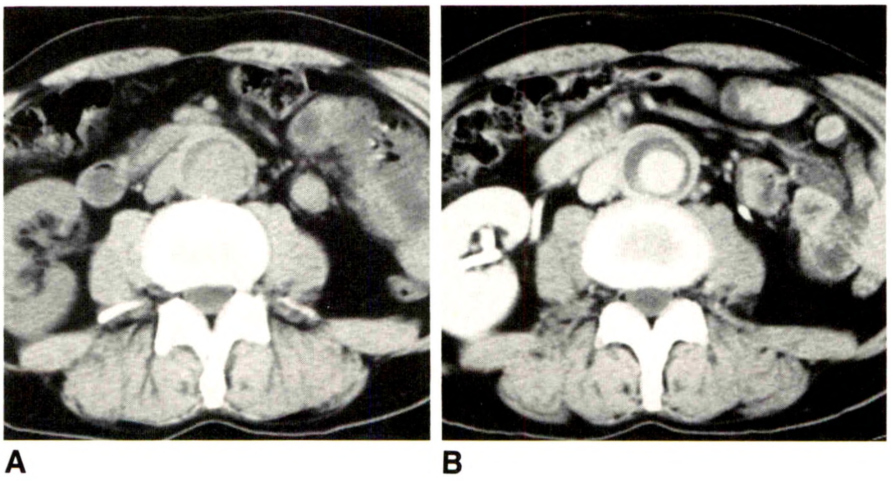

Fig. 7.—Perianeurysmal fibrosis.

A, Unenhanced CT scan shows small aneurysm of aorta with mural thrombus and thick periaortic rind.

B, CT scan after administration of IV contrast material shows enhancement of periaortic tissue. Although this tissue is beginning to involve inferior vena cava, it is far from ureters. However, more extensive fibrosis around aortic or aortoiliac aneurysms can extend laterally enough to entrap ureters.

and attenuation differences are not significant enough to help in the differential diagnosis [58]. These metastatic deposits also can take the form of solitary masses or infiltrating mantles of tissue that obliterate adjacent tissue planes [56]. Generally speaking, however, true metastatic disease to the retroperitoneum appears most commonly as lobular paraaortic and paracaval masses that are unmistakably enlarged nodes. Further, lymphoma and other malignant lymphadenopathies often elevate the aorta from the spine (Fig. 8), unlike benign RPF, which surrounds the aorta but usually does not cause significant anterior displacement [59]. However, this generalization does not always hold true; two cases have been reported recently of proved idiopathic RPF in which displacement of the aorta from the spine was caused by the presence of fibrous tissue posterior to the aorta [60].

Other entities in the differential diagnosis of RPF include amyloidosis, which can cause extensive retroperitoneal involvement [61], and retroperitoneal hematomas, though in the latter, particularly in acute collections, the attenuation value is usually higher than that found in RPF. If the fibrotic process has a tumefactive appearance, a primary mesenchymal retroperitoneal tumor also must be included in the differential diagnosis. When RPF is found in other than its typical retroperitoneal location, the differential diagnosis is expanded significantly. For example, fibrosis may occur in the pelvis in females and simulate cervical carcinoma [62]; may obliterate the peripancreatic fat planes and resemble pancreatic carcinoma [63]; and, when it occurs in the root of the mesentery, may be mistaken for an intraperitoneal tumor [64] (Fig. 9). Rarely, cystic areas occur, complicating even further the attempt to arrive at the correct diagnosis [65].

Like CT, MR easily can show the morphology of the fibrous plaque in RPF. The relationship of the mass to the great vessels can be determined by flow voids within these vascular structures. Further, the multiplanar imaging capability of MR is useful in defining all dimensions of the plaque.

On T1-weighted images, the plaque, whether benign or malignant, typically has low to medium signal intensity. A high signal intensity of the plaque on T2-weighted images may indicate malignant RPF [66, 67]. Another T2 imaging characteristic thought to be suggestive of malignant RPF is inhomogeneity of the plaque [67]. By contrast, the mature plaque typical of advanced benign RPF has a low signal intensity on T2- as well as on T1-weighted images (see Fig. 5). However, it has been recognized recently that benign RPF also can have a high signal intensity on T2-weighted images [30, 68] (Fig. 10). As discussed in the section on pathology, early idiopathic RPF is associated with inflammatory edema of the fibrous plaque; this is also true with most cases of malignant RPF. Therefore, it is not unreasonable to assume that the plaque in either benign or malignant RPF can have a high signal intensity on T2-weighted images because of its high free water content and hypercellularity [30]. A plaque showing low signal on both T1- and T2-weighted images is most likely benign RPF, because it would be unusual for the malignant variety to mature so completely. However, it is now clear that a high signal on T2-weighted images cannot be used to differentiate malignant from benign RPF, but rather reflects only the presence of inflammatory edema in the plaque.

It is not yet clear whether MR imaging can be used to distinguish between RPF and lymphoma. However, a recent report [69] suggests that the T1 values in RPF are lower than in lymphoma, at least at low field strengths.

Treatment

When RPF is caused by treatment with methysergide, cessation of drug therapy usually results in regression of the

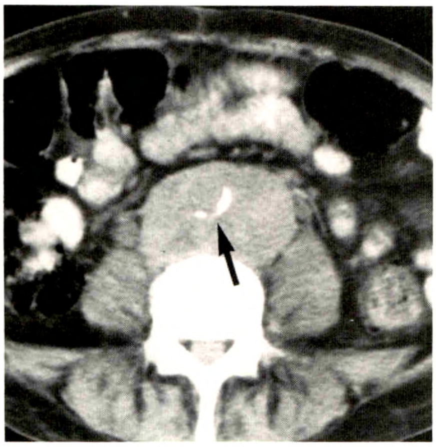

Fig. 8.—Metastatic neoplasm in retroperitoneum. CT scan in patient with prostatic carcinoma shows a thick plaque of tissue surrounding great vessels. Note that calcified aorta is elevated from vertebral body (*arrow*).

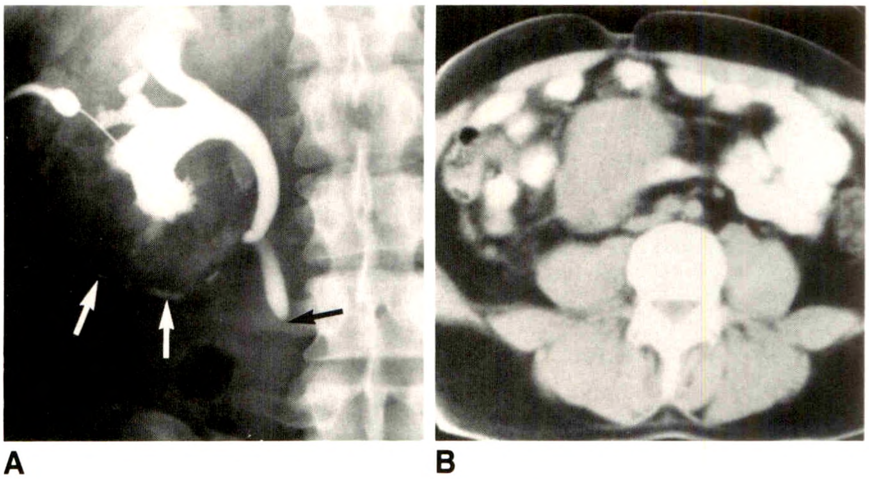

Fig. 9.—Unusual morphology of idiopathic retroperitoneal fibrosis.

A, Antegrade pyelogram shows extrinsic obstruction of right proximal ureter (*black arrow*). Minimal degree of dilatation of collecting system should not be taken to mean minimal obstruction, as collecting system is decompressing itself by pyelointerstitial extravasation of contrast material into subcapsular space (*white arrows*).

B, CT scan at level of ureteral obstruction shows a soft-tissue mass in root of mesentery. This was proved surgically to be an idiopathic fibrotic process with enough posterior extension to entrap right ureter. Great vessels are uninvolved.

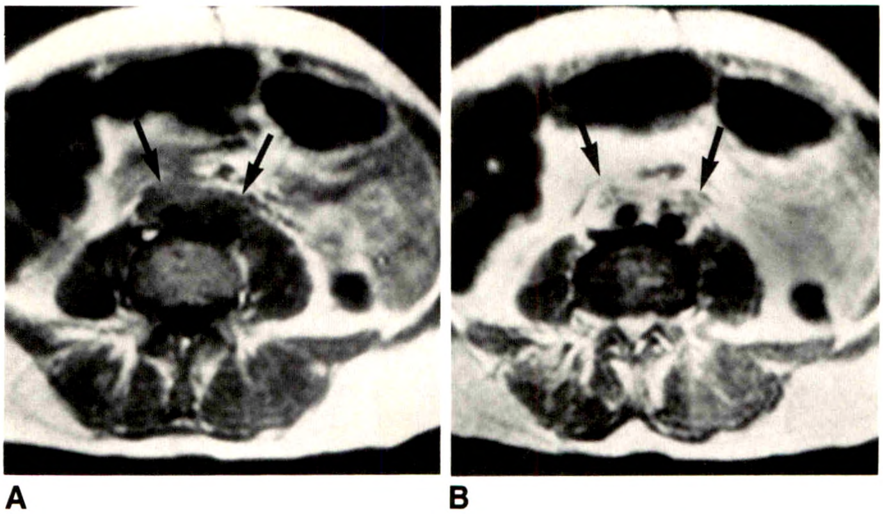

Fig. 10.—Idiopathic retroperitoneal fibrosis in early stages of plaque formation.

_A_, Transverse T1-weighted MR image shows medium-signal-intensity plaque (_arrows_) surrounding great vessels.

_B_, Transverse T2-weighted MR image at same level as _A_ shows plaque (_arrows_) is inhomogeneous and of high signal intensity, characteristics that previously were thought to indicate malignancy. These changes now are understood to reflect edema in plaque.

(Courtesy of J. H. Newhouse, New York, NY.)

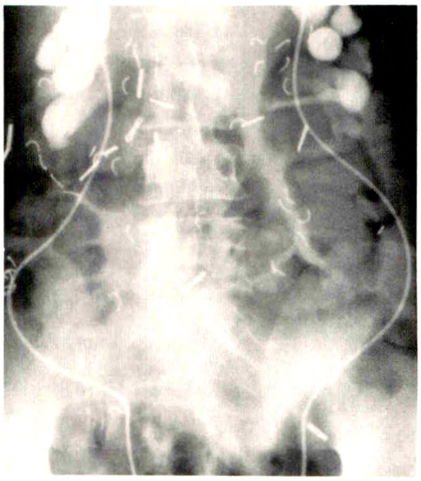

Fig. 11.—Bilateral ureterolysis (radiograph obtained immediately after surgery). Bilateral ureteral stents are in place; lateral bowing of midportion of ureters is typical of ureterolysis with intraperitonealization of ureters to remove them from region of plaque.

plaque and resolution of any ureteral obstruction the plaque may have caused [13]. Rarely, other nonmalignant forms of RPF resolve spontaneously without treatment [70].

Treatment of malignant RPF usually is related to the oncologic treatment of the primary tumor; the outcome for such patients is uniformly poor [3]. For idiopathic RPF, treatment is most commonly ureterolysis (freeing of the ureters from the encasing plaque), with or without concomitant corticosteroid therapy [71]. Aneurysmectomy usually is used in conjunction with ureterolysis for treatment of perianeurysmal fibrosis.

Most urologists are reluctant to use corticosteroids alone as the primary treatment for RPF because of the risk of mismanaging a potentially malignant process [72]. However, use of corticosteroids alone in patients with early idiopathic disease typically results in relief of ureteral obstruction within 7–10 days after the onset of therapy [72]. When RPF is resistant to corticosteroid therapy, or when ureteral obstruction recurs after withdrawal of corticosteroids, azathioprine is effective as an adjunctive medical treatment [73].

The use of indwelling ureteral stents is a useful alternative therapy for patients who have malignant RPF or who have benign disease and are poor surgical risks. Alternatively, percutaneous nephrostomy can be used to relieve renal obstruction. According to one report [74], percutaneous balloon dilatation of a midureteral obstruction associated with idiopathic RPF resulted in long-term relief of the occlusion. Generally, however, ureterolysis remains the mainstay in treatment of this disease. The ureter is dissected free from the plaque, and in order to prevent it from being caught again by the fibrotic process, it is displaced either laterally or intraperitoneally. An alternative procedure is to wrap the ureter with omentum to provide an effective barrier against reentrapment by the fibrosis [75]. Postoperative CT in cases in which an omental wrap has been used shows a low-attenuation halo surrounding the opacified ureter [75].

Patients who have had ureterolysis commonly have a lateral bowing of the midportion of the ureter(s) [50] (Fig. 11). Long-term follow-up with CT usually shows a progressive decrease in the size of the plaque, especially in patients treated with corticosteroids. However, the majority of patients will have a small residual mass that can persist for months to years [70].

In patients with idiopathic RPF, if the kidneys have not been badly compromised, and if ureterolysis has been performed adequately, the prognosis is generally excellent, with long-term success rates exceeding 90% [16].

REFERENCES

1. Albarran J. Retention renale per peri-ureterite: liberation externe de l'uretere. *Assoc Fr Urol* **1905**;9:511–517
2. Ormond JK. Bilateral ureteral obstruction due to envelopment and compression by an inflammatory retroperitoneal process. *J Urol* **1948**;59:1072–1079
3. Buff DD, Bogin MB, Faltz LL. Retroperitoneal fibrosis: a report of selected cases and a review of the literature. *N Y State J Med* **1989**;89:511–516
4. Stewart TW Jr, Friberg TR. Idiopathic retroperitoneal fibrosis with diffuse involvement: further evidence of systemic idiopathic fibrosis. *South Med J* **1984**;77:1185–1187
5. Koep L, Zuidema GD. The clinical significance of retroperitoneal fibrosis. *Surgery* **1977**;81:250–257
6. Lepor H, Walsh PC. Idiopathic retroperitoneal fibrosis. *J Urol* **1979**; 122:1–6
7. Gilkeson GS, Christensen CW, Rice JR. Retroperitoneal fibrosis: the forgotten connective tissue disease. *N C Med J* **1989**;50:192–194
8. Littlejohn GO, Keystone EC. The association of retroperitoneal fibrosis with systemic vasculitis and HLA-B27: a case report and review of the literature. *J Rheumatol* **1981**;8:665–669
9. Appel RA, Weiss RM. Retroperitoneal fibrosis and avascular necrosis of the femoral head. *JAMA* **1976**;236:2886
10. Zebetakis PM, Novich RK, Matarese RA, Michelis MF. Idiopathic retroperitoneal fibrosis: a systemic connective tissue disease? *J Urol* **1979**;122:100–102
11. Bullock N. Idiopathic retroperitoneal fibrosis (editorial). *BMJ* **1988**; 297:240–241
12. Mitchinson MJ. Chronic periaortitis and periarteritis. *Histopathology* **1984**;8:589–600
13. Stewart TW Jr. Idiopathic retroperitoneal fibrosis—past and present. *N Y State J Med* **1989**;89:503–504

14. Stecker JH Jr, Rawls HP, Devine CJ Jr, Devine PC. Retroperitoneal fibrosis and ergot derivatives. *J Urol* **1974**;112:30–32
15. Brooks MT, Magill HL, Hanna SL, et al. Pediatric case of the day: idiopathic retroperitoneal fibrosis. *RadioGraphics* **1990**;10:1096–1100
16. Srinivas V, Dow D. Retroperitoneal fibrosis. *Can J Surg* **1984**;27:111–113
17. Allibone GW, Saxton HM. The association of aorto-iliac aneurysms with ureteral obstruction. *Urol Radiol* **1980**;1:205–210
18. Lindell OI, Sariola HV, Lehtonen TA. The occurrence of vasculitis in perianeurysmal fibrosis. *J Urol* **1987**;138:727–729
19. Lorentzen JE, Sorensen IN, Brun B, Laursen K, Kristensen JK. Abdominal aortic aneurysm in combination with retroperitoneal fibrosis. *Acta Chir Scand* **1980**;502:94–97
20. Megibow AJ, Ambos MA, Bosniak MA. Computed tomographic diagnosis of ureteral obstruction secondary to aneurysmal disease. *Urol Radiol* **1980**;1:211–215
21. Mitchinson MJ. Retroperitoneal fibrosis revisited. *Arch Pathol Lab Med* **1986**;110:784–786
22. Debruyne FMJ, Bogman MJJT, Ypma AFGV. Retroperitoneal fibrosis in the scrotum. *Eur Urol* **1982**;8:45–48
23. Birnberg FA, Vinstein AL, Gorlick G, Lee FA, Hales MS. Retroperitoneal fibrosis in children. *Radiology* **1982**;145:59–61
24. Sherman C, Winchester P, Brill PW, Mininberg D. Childhood retroperitoneal fibrosis. *Pediatr Radiol* **1988**;18:245–247
25. Miles RM, Brock J, Martin C. Idiopathic retroperitoneal fibrosis: a sometime surgical problem. *Am Surg* **1984**;50:76–84
26. Mathew CV, Shanabo A, Zyka I, Eklof B. Retroperitoneal fibrosis with large-vessel obstruction: an uncommon vascular disorder. *Acta Chir Scand* **1985**;151:475–480
27. Morad N, Strongwater SL, Eypper S, Woda BA. Idiopathic retroperitoneal and mediastinal fibrosis mimicking connective tissue disease. *Am J Med* **1987**;82:363–366
28. Fagan CJ, Larrieu AJ, Ampara EG. Retroperitoneal fibrosis: ultrasound and CT features. *AJR* **1979**;133:239–243
29. Jones JH, Ross EJ, Matz LR, Edwards D, Davies DR. Retroperitoneal fibrosis. *Am J Med* **1970**;48:203–208
30. Lee JKT, Glazer HS. Controversy in the MR imaging appearance of fibrosis. *Radiology* **1990**;177:21–22
31. Usher SM, Brendler H, Ciavarra VA. Retroperitoneal fibrosis secondary to metastatic neoplasm. *Urology* **1977**;9:191–194
32. Thomas MH, Chisholm GD. Retroperitoneal fibrosis associated with malignant disease. *Br J Cancer* **1973**;28:453–458
33. Goodwin WE. Diagnostic problems in retroperitoneal disease. *Ann Intern Med* **1966**;65:160–184
34. Periureteric fibrosis (editorial). *Lancet* **1957**;2:780
35. Gelford GJ, Cromwell DK. Methysergide, retroperitoneal fibrosis and rectosigmoid stricture. *AJR* **1968**;104:566–570
36. Wagenknecht LV, Auvert J. Symptoms and diagnosis of retroperitoneal fibrosis: analysis of 31 cases. *Urol Int* **1971**;26:185–195
37. Utz DC, Henry JD. Retroperitoneal fibrosis. *Med Clin North Am* **1966**;50:1091–1099
38. Arger PH, Stolz JL, Miller WT. Retroperitoneal fibrosis: an analysis of the clinical spectrum and roentgenographic signs. *AJR* **1973**;119:812–821
39. Saldino RM, Palubinskas AJ. Medial placement of the ureter: a normal variant which may simulate retroperitoneal fibrosis. *J Urol* **1972**;107: 582–585
40. Shirley H, Gup AK, Spano J. Idiopathic pelvic fibrosis: report of a case with unusual histologic and radiographic features. *Ann Intern Med* **1967**;67:1248–1251
41. Minford JE, Davies P. The urographic appearances in acute and chronic retroperitoneal fibrosis. *Clin Radiol* **1984**;35:51–57
42. Lalli AF. Retroperitoneal fibrosis and inapparent obstructive uropathy. *Radiology* **1977**;122:339–342
43. Persky L, Huus JC. Atypical manifestations of retroperitoneal fibrosis. *J Urol* **1974**;111:340–344
44. Harris RD. The etiology of inferior vena caval obstruction and compression. *Crit Rev Diagn Imaging* **1976**;8:57–86
45. Kees CJ. Angiographic staining and hypervascularity in a case of fibrous retroperitonitis. *Radiology* **1974**;113:329–330
46. Webb AJ, Dawson-Edwards P. Non-malignant retroperitoneal fibrosis. *Br J Surg* **1967**;54:508–518
47. Halverstadt DB. Problems in the use of urography and lymphangiography in the diagnosis of idiopathic retroperitoneal fibrosis. *J Urol* **1968**;99: 423–426
48. Liebman R. Positive gallium scan in retroperitoneal fibrosis. *AJR* **1983**;141:949–950
49. Sanders RC, Duffy T, McLoughlin MG, Walsh PC. Sonography in the diagnosis of retroperitoneal fibrosis. *J Urol* **1977**;118:944–946
50. Amis ES, Jr, Newhouse JH. *Essentials of uroradiology.* Boston: Little, Brown, **1991**:77, 369
51. Henry LG, Doust B, Korns ME, Bernhard VM. Abdominal aortic aneurysm and retroperitoneal fibrosis: ultrasonographic diagnosis and treatment. *Arch Surg* **1978**;113:1456–1460
52. Yancey JM, Kaude JV. Diagnosis of perirenal fibrosis by MR imaging. *J Comput Assist Tomogr* **1988**;12:335–337
53. Dalla-Palma L, Rocca-Rossetti S, Pozzi-Mucelli RS, Rizzatto G. Computed tomography in the diagnosis of retroperitoneal fibrosis. *Urol Radiol* **1981**;3:77–83
54. Rubenstein WA, Gray G, Auh YH, et al. CT of fibrous tissues and tumors with sonographic correlation. *AJR* **1986**;147:1067–1074
55. Dixon AK, Mitchinson MJ, Sherwood T. Computed tomographic observations in periaortitis: a hypothesis. *Clin Radiol* **1984**;35:39–42
56. Megibow AJ, Mitnick JS, Bosniak MA. The contribution of computed tomography to the evaluation of the obstructed ureter. *Urol Radiol* **1982**;4:95–104
57. Chishom RA, Coltart RS, Cooper P, Dixon AK. Circumferential para-aortic masses: computed tomographic observations. *Clin Radiol* **1986**;37: 531–535
58. Sterzer SK, Herr HW, Mintz I. Idiopathic retroperitoneal fibrosis misinterpreted as lymphoma by computed tomography. *J Urol* **1979**;122:405–406
59. Degesys GE, Dunnick NR, Silverman PM, Cohan RH, Illescas FF, Castagno A. Retroperitoneal fibrosis: use of CT in distinguishing among possible causes. *AJR* **1986**;146:57–60
60. Brooks AP, Reznek RH, Webb JAW. Aortic displacement on computed tomography of idiopathic retroperitoneal fibrosis. *Clin Radiol* **1989**;40: 51–52
61. Glynn TP Jr, Kreipke DL, Irons JM. Amyloidosis: diffuse involvement of the retroperitoneum. *Radiology* **1989**;170:726
62. Bramm HG, Griffith RP, Griffith TH, Shasteen WJ. Retroperitoneal fibrosis simulating carcinoma of the cervix. *Obstet Gynecol* **1979**;53[suppl]: 77S–78S
63. Inaraja L, Franquet T, Caballero P, Encabo B, Humbert P. CT findings in circumscribed upper abdominal idiopathic retroperitoneal fibrosis: case report. *J Comput Assist Tomogr* **1986**;10:1063–1064
64. Brun B, Laursen K, Sorensen IN, Lorentzen JE, Kristensen JK. CT in retroperitoneal fibrosis. *AJR* **1981**;137:535–538
65. Feldberg MAM, van Waes FGM. Computed tomography of pseudocysts in retroperitoneal fibrosis. *J Comput Assist Tomogr* **1987**;11:485–487
66. Yuh WTC, Barloon TJ, Sickels WJ, Kramolowsky EV, Williams RD. Magnetic resonance imaging in the diagnosis and follow-up of idiopathic retroperitoneal fibrosis. *J Urol* **1989**;141:602–605
67. Arrive L, Hricak H, Tavares NJ, Miller TR. Malignant versus nonmalignant retroperitoneal fibrosis: differentiation with MR imaging. *Radiology* **1989**;172:139–143
68. Mulligan SA, Holley HC, Koehler RE, et al. CT and MR imaging in the evaluation of retroperitoneal fibrosis. *J Comput Assist Tomogr* **1989**;13:277–281
69. Brooks AP, Reznek RH, Webb JAW. Magnetic resonance imaging in idiopathic retroperitoneal fibrosis: measurement of T1 relaxation time. *Br J Radiol* **1990**;63:842–844
70. Brooks AP, Reznek RH, Webb JAW, Baker LRI. Computed tomography in the follow-up of retroperitoneal fibrosis. *Clin Radiol* **1987**;38:597–601
71. Abercombie GF, Vinnicombe J. Retroperitoneal fibrosis: practical problems in management. *J Urol* **1980**;52:443–445
72. Higgins PM, Bennett-Jones DN, Naish PF, Aber GM. Nonoperative management of retroperitoneal fibrosis. *Br J Surg* **1988**;75:573–577
73. McDougal WS, MacDonell RC Jr. Treatment of idiopathic retroperitoneal fibrosis by immunosuppression. *J Urol* **1991**;145:112–114
74. Downey DB, O'Connell D, Donohow J. Percutaneous balloon dilatation of a midureteric obstruction caused by retroperitoneal fibrosis. *Br J Urol* **1987**;60:84–85
75. Carini M, Selli C, Rizzo M, Durval A, Costantini A. Surgical treatment of retroperitoneal fibrosis with omentoplasty. *Surgery* **1982**;91:137–141

Book Review

CT and MRI of the Genitourinary Tract. Edited by Stanford M. Goldman and Olga M. B. Gatewood. (Vol. 13 in Contemporary Issues in Computed Tomography.) New York: Churchill Livingstone, 323 pp., 1990. $79.95

This is the 13th volume in a series called Contemporary Issues in Computed Tomography. The previous volume dealing with the urinary tract was volume 3, which Goldman and Gatewood also edited, and which was published in 1984. The current book brings us up-to-date on developments that occurred during the 6-year interval. The editors are to be congratulated. The contributors are superb, many of them internationally recognized experts in their fields, and even in the chapters with more than one author, at least one of the authors is of that stature. I have heard many of the authors represented here present this material before, at scientific meetings or postgraduate courses, but in every case, the information is still fresh and relevant, and each chapter contains many new pearls of wisdom.

In addition, the book is beautifully written. It reads like a novel; every sentence is packed with information. I can recall only one other medical book in my life that I read cover to cover in one sitting; this is the second. It is a beautiful book also, containing information found nowhere else. Though the number of illustrations has been kept relatively low, in order to keep the book small, each illustration functions beautifully, and all the chapters are well referenced.

In general, then, the volume is outstanding. This is not to say that it is without error. A number of the authors seem to have confused incidence and prevalence; others, in describing the performance characteristics most desirable for an examination in a given situation, could have benefited from the aid of a statistician or, better yet, a decision analyst.

Most chapters discuss technique, relevant anatomy, and clinical aspects, as well as imaging findings. Some chapters, however, written by clinicians, are entirely clinical. Chapter 1, by Richard Leder and Reed Dunnick, contains a superb description of CT and MR of the adrenal gland. Chapter 2, by Bernard Birnbaum and Morton Bosniak, is an outstanding and authoritative discussion of all the facets of CT and MR of renal cell carcinoma, and it reflects the authors' considerable experience with small renal cell carcinomas treated by partial nephrectomy. It also has a good discussion of hyperdense renal cysts and how to manage them. Chapter 3, by Byrn Williamson, is on benign renal neoplasms and contains a good discussion of oncocytomas. The discussion generally is balanced, particularly as regards the problem of metastases. The chapter also has a good discussion of adenomas.

The first author of chapter 4 is Goldman. This chapter is a classical discussion of inflammatory disease of the kidney. It reflects the view that Goldman has held for a number of years and is thought provoking, stimulating, and controversial. I agree with most of what is said. The chapter includes a good discussion of the merits of CT and sonography, a beautiful classification system, and a great many logical and precise statements. It also emphasizes when not to do studies, which is as important as knowing when to do them. Chapter 5, on metastatic disease to the urinary tract, is by John Volpe and Peter Choyke, and provides as interesting and informative a discussion of the pathogenesis of metastatic disease as I have seen. The authors emphasize that it is not necessary to do biopsies of kidney lesions that have the typical appearance of metastatic disease. Chapter 6, by Philip Kenney, is on obstruction of the upper urinary tract and contains a good description of the limited use of CT and the currently undefined use of MR.

Chapter 7, by Ray Stutzman, is on the clinical aspects of cancer of the prostate and is excellent. Chapter 8, by Andrew Yang and Shirley Yang, is on MR and CT of the prostate. Here I found myself in occasional disagreement. The authors state, for example, that preoperative CT for detection of enlarged lymph nodes in patients with cancer of the prostate is still the standard of care; this is certainly not true at Stanford or at the Palo Alto Veterans Affairs Medical Center, nor do we use routine preoperative MR for staging. The authors mention, but could not give in advance, the results of the cooperative study, which were about to be published in the *New England Journal of Medicine*, on MR staging. My own analyses of the results, which were published recently, however, do not support their enthusiasm.

Chapter 9, by Charles Brendler, is an excellent analysis of the epidemiology, biological behavior, histology, staging, grading, diagnosis, and treatment of cancer of the bladder. Brendler states, however, that IV pyelography is essential for evaluating bladder cancer, as it will detect 75% of bladder tumors more than 1 cm in diameter. In my opinion, however, a sensitivity of 75% is too low; any patient with hematuria, even if the excretory urogram is normal, needs to have cystoscopy.

Chapter 10, by Mario Amendola and Howard Pollack, is an outstanding overview of various bladder lesions in which CT and MR can be helpful. In the next chapter, Steven Brick et al. discuss the relatively rare urachal carcinoma; the discussion is excellent. Robert Mattrey then provides a superb discussion of MR of the testes, seminal vesicles, and urethra and predicts that MR will be the examination of choice for scrotal disease. This chapter contains an interesting description of undescended testis; Mattrey provides data suggesting that if MR is performed, surgical procedures may not be necessary in about 40% of patients (i.e., those with testicular atrophy). If this is true, it is indeed a reason for using MR. The final chapter, on the transplanted kidney, is by Judith Chezmar et al. This is followed by six case studies.

I have no doubt of this volume's value and importance. It is one that every radiologist should possess and not hesitate to refer to frequently.

Gerald W. Friedland
Department of Veterans Affairs Medical Center
Palo Alto, CA 94304

Color Doppler Sonography in the Evaluation of Erectile Dysfunction:

Patterns of Temporal Response to Papaverine

Steven W. Fitzgerald[1]
Scott J. Erickson[2]
W. Dennis Foley[2]
Elliot O. Lipchik[2]
Thomas L. Lawson[2]

Most studies of duplex Doppler sonography for the assessment of erectile dysfunction involve determination of peak systolic velocities 5 min after intracavernosal injection of papaverine. The purpose of this study was to determine the effect of the timing of Doppler measurements of flow after papaverine injection for establishing the presence of arterial and venous abnormalities. Color Doppler sonography was performed in 75 patients for evaluation of vasculogenic impotence. After intracavernosal injection of 60 mg of papaverine, measurements of peak systolic and end-diastolic velocities were obtained in each cavernosal artery at 5-min intervals for a total of 30 min. A peak systolic velocity of less than 25 cm/sec was used as the threshold for arterial insufficiency. An end-diastolic velocity of greater than 5 cm/sec was used to predict venous incompetence. Scanning was performed for direct assessment of dorsal venous flow. Thirty patients were subsequently evaluated by cavernosometry and cavernosography. In most patients (76%), maximum response to papaverine was achieved within the first 5 min. In eight patients, significant increases in systolic velocity were seen only after 5 min. In 10 patients, significant changes in end-diastolic velocity between 5 and 30 min resulted in diagnostic reclassification. Data acquisition for 30 min significantly improved the sensitivity (95%) and specificity (83%) for the prediction of venous incompetence in patients with correlative cavernosography. Transient, early dorsal vein flow was noted in normal subjects. Persistent dorsal vein flow had an 80% sensitivity and 100% specificity for venous incompetence.

Our results suggest that, when using color Doppler sonography, gathering data for 30 min may improve the prediction of vasculogenic impotence.

***AJR* 157:331-336, August 1991**

Duplex Doppler and color Doppler sonography have been shown to be useful in the evaluation of patients with erectile dysfunction. Specific diagnostic criteria have been reported for the assessment of arterial insufficiency [1-5] and venous incompetence [4, 5]. A study in normal volunteers has demonstrated that papaverine-induced erection is a complex multiphasic event that can be characterized by color Doppler sonography [6]. However, the time course of these events in normal subjects and in impotent men has not been well established. Most Doppler studies of erectile dysfunction are based on data acquisition from the cavernosal arteries within the first 3-5 min after papaverine injection [1-4]. Some authors emphasize the need for data acquisition in the first 5 min to avoid inaccuracies [1, 2, 7]. Although we believe that scanning should commence immediately after papaverine injection, we have noted that dynamic changes may occur in cavernosal artery flow and dorsal vein flow for up to 10-30 min after papaverine injection. These temporal changes may be useful in the evaluation of patients with erectile dysfunction.

The purpose of this study was to evaluate the temporal response to intracorporeal papaverine in men with suspected vasculogenic impotence and to assess the impact of the temporal response pattern on the diagnostic accuracy of color Doppler sonography.

Received September 21, 1990; accepted after revision March 20, 1991.

Presented at the annual meeting of the American Roentgen Ray Society, Washington, DC, May 1990.

[1] Department of Radiology, Northwestern Memorial Hospital, 710 N. Fairbanks Ave., Chicago, IL 60611. Address reprint requests to S. W. Fitzgerald.

[2] Department of Radiology, Medical College of Wisconsin, 8700 W. Wisconsin Ave., Milwaukee, WI 53226.

0361-803X/91/1572-0331
© American Roentgen Ray Society

Materials and Methods

Seventy-five men 29–74 years old referred consecutively from the urology clinic for the evaluation of suspected vasculogenic impotence were examined from November 1988 until January 1990. All examinations were performed with a 7.5-MHz transducer with a standoff wedge (QAD-1E, Quantum Medical Systems, Issaquah, WA). The transducer was placed over the dorsum of the penis with initial scanning performed in longitudinal and transverse planes before papaverine injection. A divided dose of 60 mg of papaverine hydrochloride was injected with a 25-gauge needle, with 30 mg injected into each corpus cavernosum near the penile base. Scanning was resumed approximately 2 min after papaverine injection, and each of the corpora was evaluated within each 5-min interval for a total of 30 min. Real-time color flow segments and angle-corrected spectral traces were recorded on digital videotape for review. Peak systolic and end-diastolic velocities were determined for both cavernosal arteries within each 5-min interval. All velocity measurements were obtained at the proximal penile shaft near the base. Doppler angles ranged from 45° to 65°. These velocities were recorded separately without averaging. Variations in flow velocity between the left and right cavernosal arteries of greater than 10 cm/sec were noted. The greater peak systolic velocity was used for classification. Velocities were corrected retrospectively from review of the digital videotape.

Scanning was routinely performed dorsally. In patients progressing to more complete erection, ventral scanning was occasionally necessary. Scanning of the midline dorsum of the penis was also performed during most of the 5-min intervals. Dorsal vein flow was sought by visual inspection and confirmed by spectral analysis. Care was taken to avoid compression of the relatively superficial dorsal veins during scanning.

Visual inspection of papaverine response and penile tumescence was recorded. After completion of the examination, patients were released after brief observation with instructions regarding possible complications. One patient returned with priapism requiring decompression. No other complications were observed.

Diagnostic criteria for determination of arterial and venous insufficiency were based on the published literature. A peak systolic velocity greater than 25 cm/sec was considered the threshold for a normal arterial supply [1, 4]. An end-diastolic velocity of 5 cm/sec or higher was used as an indicator of venous incompetence [4]. The presence of persistent dorsal vein flow was also used as an indicator of venous incompetence [2]. Dorsal vein flow that was detected beyond the initial 5 min and for at least 10 min was defined as persistent. For the purpose of this study, a delayed response was defined as any 5-cm/sec change in either peak systolic or end-diastolic velocity that occurred after the initial 5-min interval within the same cavernosal artery. The only exception to this definition was a decline in cavernosal artery velocities associated with loss of papaverine response and return to the flaccid state.

Patients were grouped by patterns of temporal response to papaverine injection as follows: no change in either peak systolic velocity or end-diastolic velocity occurring beyond 5 min or steady decline (group 1); delayed increase in peak systolic velocity to more than 25 cm/sec, stable end-diastolic velocity (group 2); stable or delayed increase in peak systolic velocity to greater than 25 cm/sec and delayed decrease in end-diastolic velocity (group 3); delayed increase in peak systolic velocity to greater than 25 cm/sec and delayed increase in the end-diastolic velocity to 5 cm/sec or higher (group 4); and stable or declining peak systolic velocity and delayed increase in end-diastolic velocity to 5 cm/sec or higher (group 5).

Correlative cavernosometry and cavernosography were subsequently performed in 30 patients. These studies were performed and interpreted according to techniques previously described [8, 9]. Cavernosometric criteria for venous incompetence include at least three of the following: a saline infusion rate of greater than 120 ml/min, maintenance infusion rate of greater than 60 ml/min, intracavernosal pressures less than 100 mm Hg, intracavernosal pressure drop of greater than 2 mm Hg/sec after termination of saline infusion, and contrast leakage into the venous system.

Results

Temporal Response by Group

Overall, 57 (76%) of our 75 patients had no significant change in either peak systolic or end-diastolic velocity beyond the first 5-min interval (group 1, Fig. 1). Of these patients, four met our criteria for normal arterial and venous integrity. Thirty-three men had peak systolic velocities less than 25 cm/sec and were thought to have arterial insufficiency. The remaining 20 had systolic velocities greater than 25 cm/sec but also had persistently elevated diastolic velocities consistent with venous incompetence.

Eight men (11%) had a significant rise in systolic velocity after the initial 5 min (group 2) that resulted in a change in their diagnostic classification (Fig. 2). Diastolic flow was stable in these patients. Two of the eight had normal diastolic velocities, whereas the other six had elevated diastolic flow.

Seven patients (9%) had significant changes in systolic and/or diastolic velocities (group 3) beyond 5 min and were reclassified as normal. Five of the seven in group 3 had a delayed rise in systolic velocity above 25 cm/sec that was associated with a dramatic drop in diastolic flow (Fig. 3). The other two patients had stable systolic velocities but also manifested diastolic flow loss and reversal.

Three patients (4%) had a delayed rise in systolic and diastolic velocities (group 4) that resulted in their reclassification as having venous incompetency (Fig. 4). None of the patients in our series had a significant rise in diastolic velocity with stable systolic velocities (group 5).

Peak Systolic Velocity

Although maximum peak systolic velocity was reached within the first 5 min in most of the 75 patients, 18 patients (groups 2–4) achieved maximum systolic velocity in the 6- to 25-min time range. Thirteen of these 18 patients had velocities exceeding 25 cm/sec only after 5 min. The range of systolic velocities was 6–72 cm/sec, and the mean time to maximum peak systolic velocity was 4.8 min. The temporal distribution of peak systolic velocities is shown in Figure 5.

Forty-two patients had a peak systolic velocity greater than 25 cm/sec. The remaining 33 did not exceed the threshold of 25 cm/sec. No significant variation in either systolic or diastolic velocity was noted in the latter group of patients. Thus, all of the patients meeting our criteria for arterial insufficiency were in group 1. Significant asymmetry of systolic velocities between the left and right cavernosal arteries was found in five of these patients; however, no temporal variation was seen in this group (group 1).

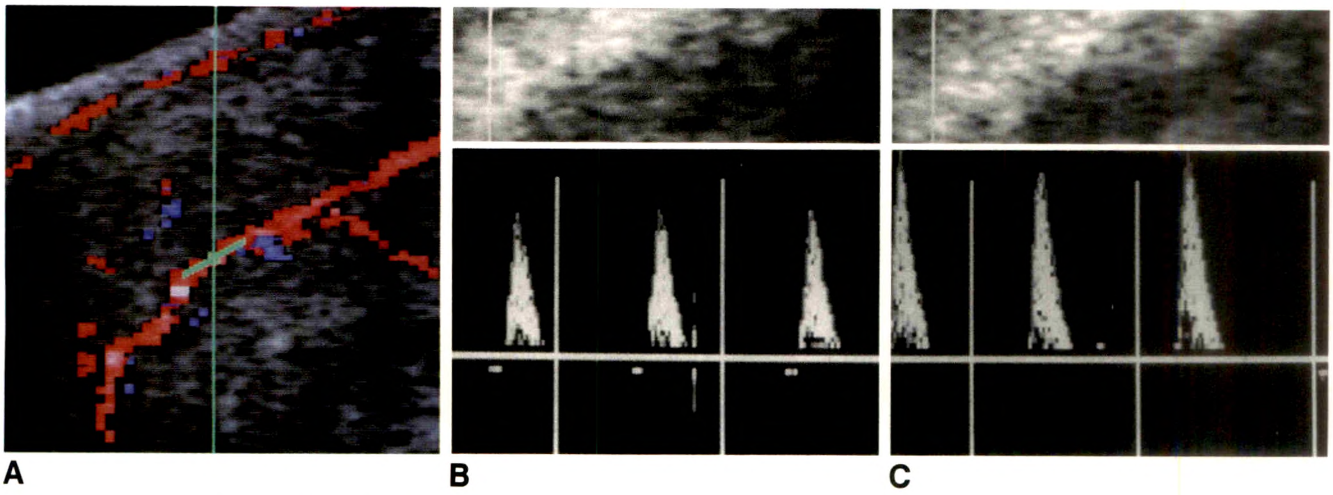

Fig. 1.—Group 1: maximum response within first 5 min.
A, Longitudinal color Doppler sonogram shows dorsal artery and cavernosal artery with angle-corrected cursor placement.
B, Spectral waveform 5 min after papaverine injection shows peak systolic velocity greater than 25 cm/sec and end-diastolic reversal.
C, Spectral waveform 10 min after papaverine injection, during rigid erection, shows slight decrease in peak systolic velocity. No further changes were seen at 15 min.

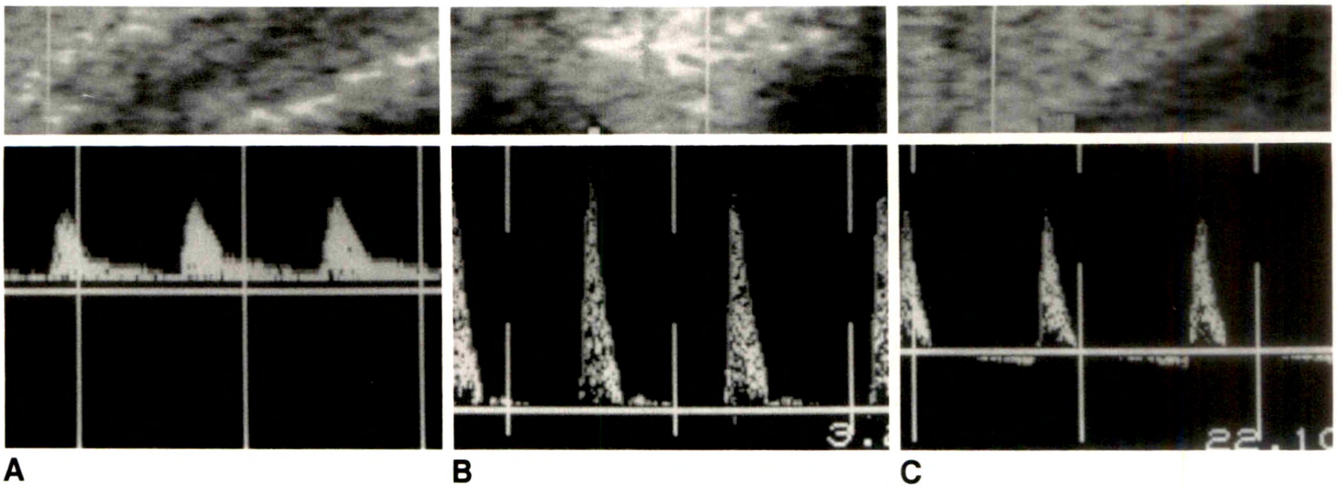

Fig. 2.—Group 2: delayed peak systolic velocity achieved after more than 5 min.
A, Spectral trace 4 min after papaverine injection shows peak systolic velocity less than 20 cm/sec with continuous diastolic flow; end-diastolic velocity is less than 5 cm/sec.
B, Spectral trace 10 min after papaverine injection shows peak systolic velocity now greater than 30 cm/sec and end-diastolic velocity equal to zero.
C, Spectral trace 15 min after papaverine injection shows peak systolic velocity stable at 30 cm/sec with end-diastolic flow reversal. Full erection is now present clinically.

Diastolic Flow

Diastolic flow in the cavernosal artery manifested a wide range of velocities, with end-diastolic velocities ranging from −7 to 31 cm/sec. In 10 (13%) of our 75 patients, significant changes in diastolic flow were seen after the initial 5 min. All seven of the patients in group 3 had a significant decline in diastolic velocity from greater than 5 cm/sec initially to diastolic flow loss or reversal. The three patients in group 4 had a delayed rise in end-diastolic velocity that exceeded the threshold of 5 cm/sec only after 5 min.

Dorsal Vein Flow

Overall, dorsal vein flow was identified in 44 (59%) of our 75 patients during some segment of the examination. Early, transient dorsal vein flow that was no longer seen during later intervals was seen in 12 patients. In none of these patients were diastolic velocities suggestive of venous leak. Interestingly, four of the patients were found to have retrograde dorsal vein flow during subsequent rigid tumescence. Reversal of dorsal vein flow was not identified in any other patients.

Persistent dorsal vein flow was identified throughout the

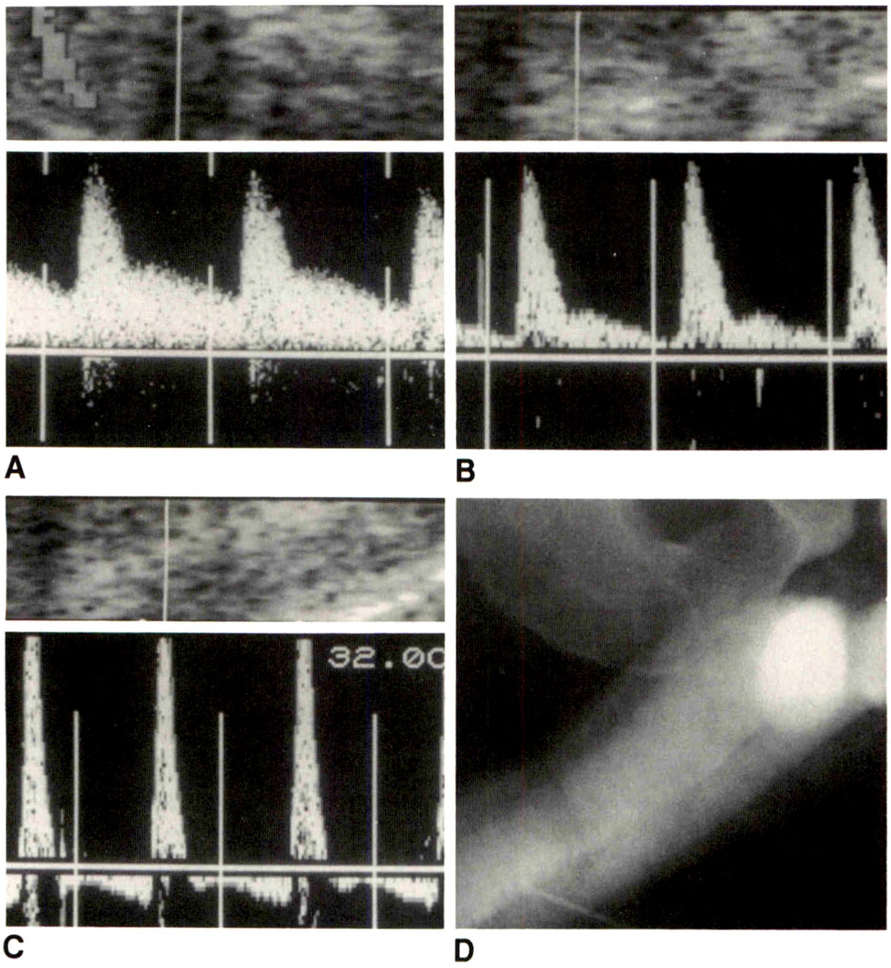

Fig. 3.—Group 3: delayed decline in end-diastolic velocity and diastolic flow after 5 min. This example shows potential for false-positive prediction of venous incompetence if early data only are acquired.

A, Spectral trace 4 min after papaverine injection shows normal peak systolic velocity and elevated end-diastolic velocity (15–20 cm/sec).

B, Spectral trace 10 min after papaverine injection shows waveform progression with decreasing diastolic flow; end-diastolic velocity now is less than threshold of 5 cm/sec.

C, Spectral trace 22 min after papaverine injection now shows diastolic flow reversal during full erection.

D, Spot film from pharmacocavernosogram shows no evidence of venous leak. Cavernosometry was also normal.

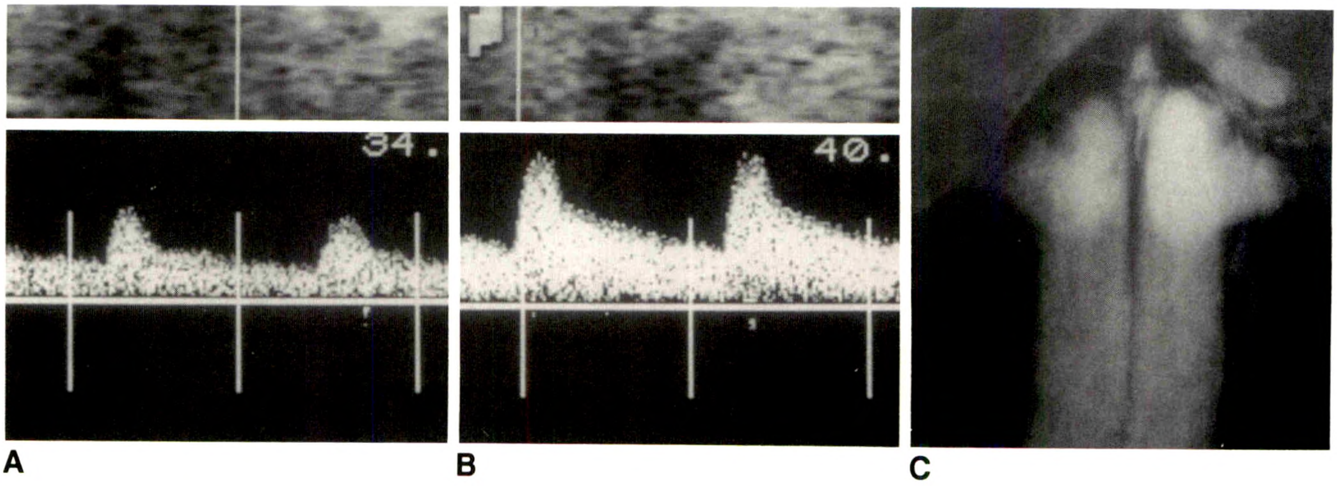

Fig. 4.—Group 4: delayed increase in peak systolic velocity accompanied by delayed increase in end-diastolic velocity. Representative example of potential false-negative diagnosis of venous incompetence if data acquisition is terminated before 10 min.

A, Spectral trace 4 min after papaverine injection shows peak systolic velocity less than 20 cm/sec and end-diastolic velocity 3–4 cm/sec.

B, Spectral trace 13 min after papaverine injection shows peak systolic velocity greater than 35 cm/sec and elevated end-diastolic velocity (12–14 cm/sec). These velocities were stable at 20 and 25 min.

C, Spot film from pharmacocavernosogram shows contrast leak into periprostatic plexus.

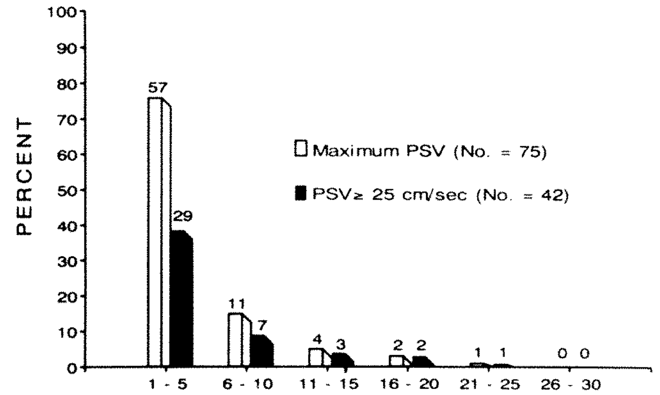

Fig. 5.—Temporal distribution of peak systolic velocity (PSV). ***White bars*** **indicate percentage of patients who achieved maximum peak systolic velocity during various time intervals.** ***Black bars*** **indicate only those patients who achieved a systolic velocity of greater than 25 cm/sec.**

study in 32 patients. All of these patients had elevated end-diastolic velocities consistent with venous incompetence.

Cavernosometry and Cavernosography

Thirty patients had correlative cavernosal studies. Six patients had normal pressure and contrast-enhanced studies. Two of these six were from group 1 and four were from group 3. The remaining 24 patients had abnormal pressure and abnormal contrast-enhanced studies consistent with venous incompetence. Of these patients, 17 were in group 1, five in group 2, and two in group 4.

If the diastolic velocity from only the first 5-min interval after papaverine injection was used to predict venous incompetence, an end-diastolic velocity of 5 cm/sec or higher had an 87% sensitivity and 50% specificity with an overall 80% accuracy. However, if diastolic data from the full 30-min study were used, sensitivity increased to 95%, specificity to 83%, and accuracy to 93%. This improvement occurred because patients in groups 3 and 4 were reclassified as a result of delayed changes in diastolic flow velocity.

The presence of persistent dorsal vein flow had an 80% sensitivity and 100% specificity for venous leak when compared with cavernosal studies. Persistent dorsal vein flow did not identify any additional venoincompetent patients who were not already identified by elevated diastolic flow velocity in the cavernosal artery.

Discussion

Papaverine hydrochloride works at the cavernosal level by producing smooth muscle relaxation at the level of the arterioles and sinusoids. This results in a loss of resistance to arterial inflow. The increased blood flow into the corpora cavernosa produces sinusoidal enlargement. Expansion of the sinusoids compresses the lacunar and emissary veins against the relatively rigid tunica albuginea and results in loss of venous egress from the corpora cavernosa producing erection [10–12]. The effectiveness of papaverine can be influenced by facilitating agents such as phentolamine and may be modified by the psychological state of the patient. In particular, anxiety may result in a diminished response to papaverine injection [13].

Intracavernosal injection of papaverine has been used clinically as a diagnostic and therapeutic technique in impotent men. It is interesting to note the timing of the tumescent response. Virag et al. [14] reported on the use of intracavernosal papaverine injection in 45 men. In 16 patients, including 10 patients with psychogenic impotence and six normally potent volunteers, the time to maximum response was 8–12 min. This was in contrast to a group of 29 patients with organic causes of impotence, in which the time to maximum response ranged from 10 to 20 min. Other authors have suggested that the normal response to intracavernosal papaverine injection may include a latency of 5–20 min [15]. This experience suggests that the Doppler evaluation of papaverine response may require extended observation times.

The use of intracavernosal papaverine injection and Doppler sonography for the investigation of erectile dysfunction was pioneered by Lue et al. [1]. In their initial article, measurements of peak systolic velocity were obtained 1, 3, and 5 min after papaverine injection. This decision was based on their experience with animal models in which there was a loss of systolic velocity during the rigid phase of erection. Subsequent work on the evaluation of arterial insufficiency has routinely used the acquisition of peak systolic velocities within the first 3–5 min after papaverine injection [2–4]. These studies report a high sensitivity (95–100%) for the use of peak systolic velocity measurements when compared with angiography for the documentation of arterial abnormalities. In addition, it has been suggested that delayed measurements will result in a decrease in diagnostic accuracy [2–4].

Our results in the extended evaluation of papaverine response in patients with suspected vasculogenic impotence confirm the need for early assessment of papaverine response for cavernosal artery flow. The majority of our patients did achieve their maximum peak systolic velocity within the first 2–5 min after papaverine injection. However, 24% of our patients subsequently reached their maximum peak systolic velocity 10–25 min after papaverine injection. In fact, 13 (31%) of 42 with maximum peak systolic velocities greater than 25 cm/sec went on to exceed the velocity threshold of 25 cm/sec only 6–25 min after papaverine injection. We believe that our data not only confirm the need for early initial assessment of cavernosal artery flow, but also argue for an extended study with repeated sampling of the cavernosal arteries for 20–30 min or until there is a plateau or decline in papaverine response.

Although the observation of temporal progression did allow for improvement in the theoretical predictive value of peak systolic velocity criteria for arterial incompetence, a much greater effect was observed in the accuracy of color Doppler sonography for the diagnosis of venous incompetence. After the injection of papaverine in many patients, the marked increase in arterial inflow results in a concomitant initial increase in diastolic flow, end-diastolic flow velocity, and dorsal venous flow. In patients with an intact venocclusive mechanism, diastolic flow reversal may ensue. However, these events may require 10–25 min. The use of diastolic velocities and dorsal vein flow from the initial 5–10 min of examination may yield an elevated false-positive rate. We believe this is supported by the comparison between the report of Quam et al. [4] and our series. When we evaluated our patients for end-diastolic velocities at 5 min, we found correlation with cavernosography to yield results similar to their published report. However, including diastolic velocities from the entire 30 min in our patients produced a significant increase in specificity by accurately characterizing those patients (group 3) with a delayed response and subsequent demonstration of an intact venous mechanism. The Mayo Clinic group has also made this observation, and they have subsequently revised their study protocol to include data acquisition at 5–20 min (King B, personal communication).

Delayed scanning also identified several patients who went on to exceed the diastolic threshold of 5 cm/sec at times beyond 5 min (group 4). These cases represented potential false-negative diagnoses for venous incompetence. Two of these three patients subsequently underwent cavernosography and were confirmed to have venous leakage. In these three patients, the rise in end-diastolic velocity was accompanied by a delayed rise in peak systolic velocity. In no patients in our study was a rise in end-diastolic velocity demonstrated without a concomitant rise in peak systolic velocity. This observation supports the decision to terminate scanning and data acquisition when peak systolic velocity remains stable at 20–30 min or begins to decline.

Experience with dorsal vein flow as a diagnostic indicator of venous incompetence is limited. Benson and Vickers [2] detected dorsal vein flow in four of 11 patients proved to have venous leak at cavernosography. They did not report the detection of dorsal vein flow in any patients with an intact venous mechanism. In our experience with color flow imaging, dorsal vein flow is readily detected if care is used to avoid compression of the dorsal veins with the transducer. Dorsal vein flow was identified in 59% of our patients. Early dorsal vein flow, which was associated with the continuous diastolic flow pattern, was seen in both normal and abnormal cases. In patients who progressed to diastolic flow reversal, a loss of dorsal vein flow occurred. We further observed an interesting phenomenon of dorsal vein flow reversal occurring in some patients who achieved rigid tumescence. The physiologic and diagnostic significance of this observation is uncertain. We believe early dorsal vein flow normally precedes the occlusion of the emissary veins as sinusoidal engorgement progresses, but should disappear as the venoocclusive mechanism is engaged. Persistence of dorsal vein flow had an 80% sensitivity and 100% specificity in patients with venous leak at cavernosography.

Although we believe our experience suggests that data acquisition should be extended to 30 min after papaverine injection, our study does have several limitations. Because arterial revascularization procedures are not currently performed at our institution, we do not routinely perform angiography and no angiographic correlation was available in this series of patients. The delayed response in our patients could be related to proximal arterial disease, which is not predicted by our systolic velocity threshold. Some workers [2, 4] have suggested a higher systolic velocity threshold might be more appropriate. Additionally, it may not be appropriate to use these early criteria for delayed scanning. The delayed response that we have observed may have some diagnostic significance with respect to vascular, psychogenic, or possibly neurogenic mechanisms. Further work in the assessment of patients' response to papaverine may help determine whether our patients represent a spectrum of the normal response or a subset of patients with dysfunction.

We believe that color Doppler sonography in association with intracavernosal papaverine plays an important role in the diagnostic workup of patients with erectile dysfunction. Color Doppler sonography is useful in the identification of both arterial and venous abnormalities in patients with suspected vasculogenic impotence. We suggest that sonographic data acquisition should begin immediately after papaverine injection, but should continue at regular intervals for 20–30 min after papaverine injection. This extended observation may improve diagnostic accuracy.

ACKNOWLEDGMENT

We thank Marilyn Bell for assistance in manuscript preparation.

REFERENCES

1. Lue TF, Hricak HH, Marich KW, Tanagho EA. Vasculogenic impotence evaluated by high-resolution ultrasonography and pulsed Doppler spectrum analysis. *Radiology* **1985**;155:777–781
2. Benson CB, Vickers MA. Sexual impotence caused by vascular disease: diagnosis with duplex sonography. *AJR* **1989**;153:1149–1153
3. Collins JP, Lewandowski BJ. Experience with intracorporeal injection of papaverine and duplex ultrasound scanning for assessment of arteriogenic impotence. *Br J Urol* **1987**;59:84–88
4. Quam JP, King BF, James EM, et al. Duplex and color Doppler sonographic evaluation of vasculogenic impotence. *AJR* **1989**;153:1141–1147
5. Shabsigh R, Fishman IJ, Quesada ET, Seale-Hawkins CK, Dunn JK. Evaluation of vasculogenic erectile impotence using penile duplex ultrasonography. *J Urol* **1989**;142:1469–1474
6. Schwartz AN, Wang KY, Mack LA, et al. Evaluation of normal erectile function with color flow Doppler sonography. *AJR* **1989**;153:1155–1160
7. Paushter DM. Role of duplex sonography in the evaluation of sexual impotence. *AJR* **1989**;153:1161–1163
8. Bookstein JJ, Valji K, Parsons LC, Kessler WO. Penile pharmacocavernosography and cavernosometry in the evaluation of impotence. *J Urol* **1987**;137:772–776
9. Delcour C, Struyven J. Techniques for performing cavernosometry and cavernosography. *Cardiovasc Intervent Radiol* **1988**;11:211–217
10. Lue TF, Tanagho EA. Physiology of erection and pharmacological management of impotence. *J Urol* **1987**;137:829–836
11. Aboseif SR, Lue TF. Hemodynamics of penile erection. *Urol Clin North Am* **1988**;15:1–7
12. Fournier GR, Juenemann KP, Lue TF, Tanagho EA. Mechanisms of venous occlusion during canine penile erection: an anatomic demonstration. *J Urol* **1987**; 137:163–167
13. Sidi AA. Vasoactive intracavernous pharmacotherapy. *Urol Clin North Am* **1988**;15:95–101
14. Virag R, Frydman D, Legman M, Virag H. Intracavernous injection of papaverine as a diagnostic and therapeutic method in erectile failure. *Angiology* **1984**;35:79–87
15. Sidi AAS, Cameron JS, Dykstra DD, Reinberg Y, Lange PH. Vasoactive intracavernous pharmacotherapy for the treatment of erectile impotence in men with spinal cord injury. *J Urol* **1987**;138:539–542

Abnormalities of the Seminal Tract Causing Infertility: Diagnosis with Endorectal Sonography

Patricia L. Abbitt[1]
Laurence Watson[2]
Stuart Howards[3]

Endorectal sonography, developed primarily for use in the diagnosis and staging of prostatic carcinoma, should be the first imaging technique used in the evaluation of an infertile man with low semen volume in whom either a hypoplastic or obstructed seminal tract is suspected. Endorectal sonography allows visualization of the seminal vesicles, which are otherwise difficult to examine. We used endorectal sonography to evaluate six young men, five of whom were being evaluated for azoospermia and infertility. One patient had no identifiable seminal vesicle on either side. Four patients had unilateral absence of the seminal vesicles. Of these four, three had a sonographically normal-appearing seminal vesicle on the contralateral side, and the fourth had an obstructed system contralaterally. The sixth patient had a hypoplastic system on the left and an obstructed system on the right.

The delineation of an obstructed or agenetic seminal vesicle and seminal tract on endorectal sonography allows decisions to be made regarding treatment and prognosis.

***AJR* 157:337-339, August 1991**

The seminal tract is difficult to evaluate clinically, and traditional enhanced studies such as vasography are invasive. Although endorectal sonography was developed primarily for the diagnosis and staging of prostatic carcinoma, it provides excellent visualization of the seminal vesicles [1, 2]. After retrograde ejaculation has been excluded as a cause of low ejaculate volume, endorectal sonography should be used in the infertile man in whom congenital absence or obstruction of the spermatic ductal system (vasa deferentia) and/or the seminal vesicles is suspected. We describe patients in whom endorectal sonography identified congenital abnormalities of the vas deferens or seminal vesicles.

Materials and Methods

Five men (24–34 years old) were being evaluated for infertility. A sixth patient, 36 years old, was studied after no left-sided vas deferens could be identified at the time of vasectomy.

All five infertile men had had multiple semen analyses showing very low volumes with either absent or very few sperm. Testicular biopsy, performed in two of the six patients, revealed normal spermatogenesis. Luteinizing hormone, follicle-stimulating hormone, and testosterone levels were tested and were normal in three patients. Seminal fluid fructose was tested and was present in three patients. Retrograde ejaculation was excluded by postejaculatory urinalysis in two patients.

Each of the five patients had physical examination of the genital region. No vas deferens could be palpated in one patient. There was some question as to whether or not the vas deferens was present in the remaining four patients. The seminal vesicles, which generally are not palpable, were not palpable in any of the patients.

All six patients were studied in the lithotomy position by using a Diasonics Urovue-200 unit (Clark Medical Technology, San Diego, CA) with a multiplanar 7.5-MHz transrectal probe.

Received September 21, 1990; accepted after revision March 25, 1991.

[1] Department of Radiology, University of Florida College of Medicine, Box J-374, JHMHC, Gainesville, FL 32610-0374. Address reprint requests to P. L. Abbitt.

[2] Department of Radiology, University of Virginia Health Sciences Center, Charlottesville, VA 22908.

[3] Department of Urology, University of Virginia Health Sciences Center, Charlottesville, VA 22908.

0361-803X/91/1572-0337
© American Roentgen Ray Society

Results

Figure 1 is a schematic drawing illustrating possible abnormalities of the seminal tract. The normal sonographic anatomy is shown in Figure 2.

One of our six patients had no identifiable seminal vesicle on either side. Four patients had unilateral absence of the seminal vesicle (Figs. 3 and 4). Of these, three had ipsilateral renal agenesis. Of the four patients with an absent seminal vesicle on one side, one had an obstructed seminal tract on the opposite side. The other three had a sonographically normal-appearing system on the opposite side. The sixth patient had a diminutive hypoplastic system on one side and an obstructed system on the other. Scrotal sonography, performed in all patients, demonstrated normal testes bilaterally.

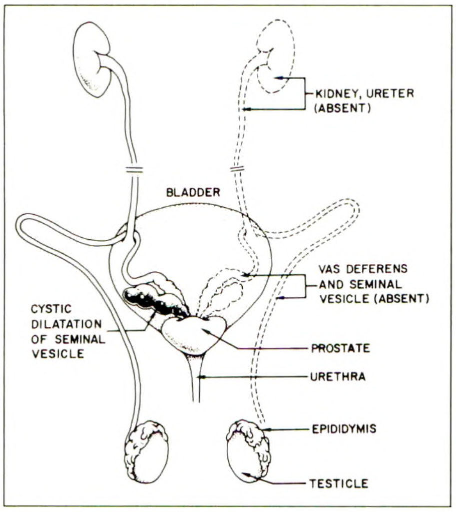
KIDNEY, URETER (ABSENT)
BLADDER
VAS DEFERENS AND SEMINAL VESICLE (ABSENT)
CYSTIC DILATATION OF SEMINAL VESICLE
PROSTATE
URETHRA
EPIDIDYMIS
TESTICLE

Fig. 1.—Schematic illustration shows abnormal lower genital conduit system for sperm transport and shared embryogenesis with upper genitourinary tract that may result in agenesis in both areas.

In four of the patients, no surgical remedy could be devised from the information obtained with endorectal sonography. One patient underwent surgical exploration, and the findings identified on endorectal sonography were confirmed. The sixth patient, the patient with no identifiable left-sided vas deferens at vasectomy, was confirmed by sonography to have unilateral absence of the seminal vesicle and vas deferens.

Discussion

Although congenital genitourinary malformations affect approximately 10–14% of the overall male population [3], congenital abnormalities of the seminal vesicles or lower genital ductal system may often be unsuspected until a boy reaches reproductive age. Men who have congenital abnormalities of the lower genitourinary tract are often asymptomatic. They may present in the reproductive years with vague symptoms of perineal discomfort, or may have palpable masses on rectal examination. Infertility is rarely the presenting problem. Delayed recognition of congenital lower genitourinary abnormalities may occur because of the relatively nonspecific symptoms and the difficulty and nonspecificity of the clinical examination of the seminal vesicles and vas deferens. Normal seminal vesicles are usually easily seen on endorectal sonography (Fig. 2). They can be evaluated for their presence, symmetry, and evidence of obstruction.

In infertile men with low semen volumes in whom retrograde ejaculation has been excluded, endorectal sonography may clarify anatomic abnormalities responsible for infertility. Endorectal sonography is easily performed and should be the initial imaging technique used if seminal vesicle disease is considered [2]. CT and MR imaging should be reserved for situations that require a larger field of view in the pelvis and lower abdomen, as may be true with more complex malformations [3–5].

The information provided by endorectal sonography can be used to determine if surgery is feasible and can determine the prognosis in patients with hypoplastic or agenetic ductal systems.

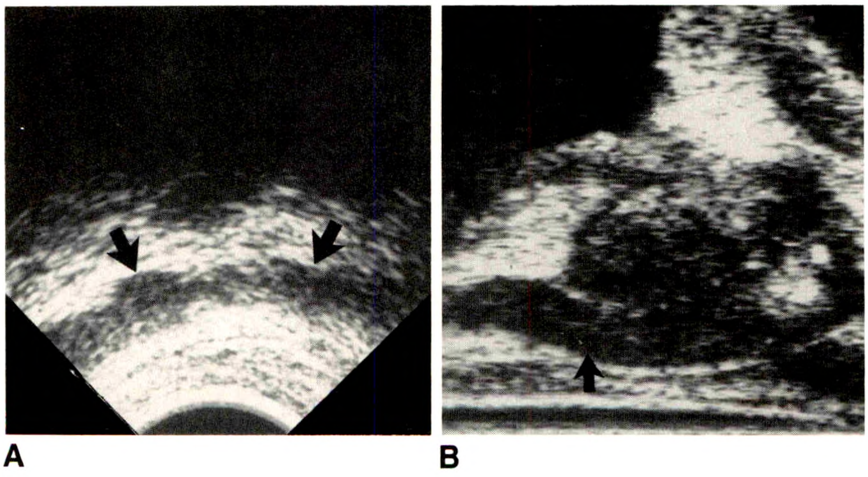

Fig. 2.—Normal patient.

***A*, Axial sonogram shows symmetry of seminal vesicles (*arrows*).**

***B*, Longitudinal sonogram shows normal relationship of seminal vesicle (*arrow*) to prostate.**

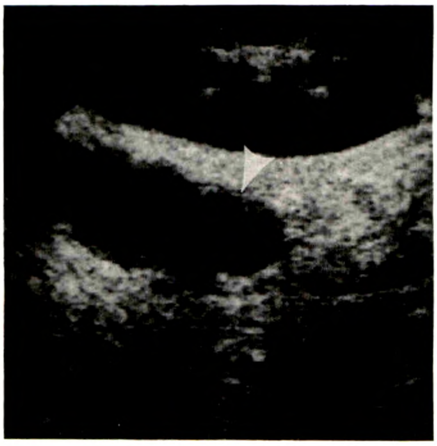

Fig. 3.—Sonogram of a 26-year-old infertile man shows cystic-appearing seminal vesicle (*arrowhead*) on right side. No seminal vesicle or kidney was identified on the left.

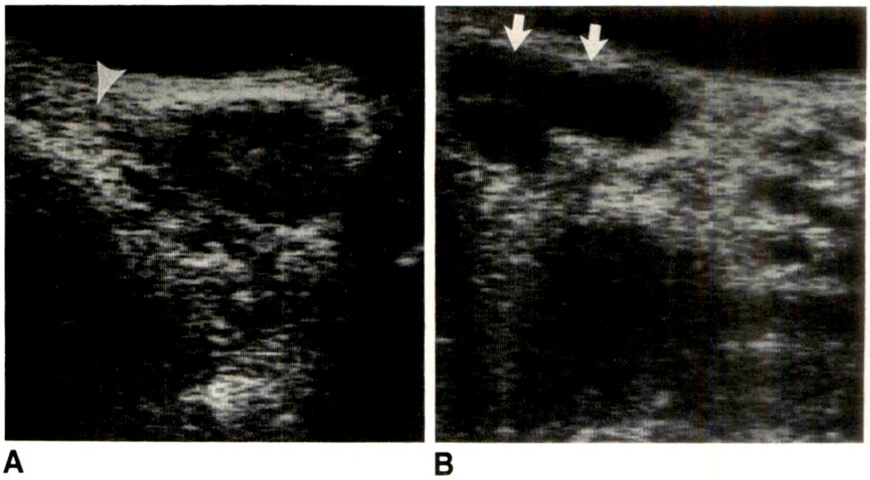

Fig. 4.—*A* and *B*, Sonograms of a 24-year-old infertile man show no seminal vesicle (*arrowhead*) on right side (*A*) and a short, cystic one (*arrows*) on left side (*B*).

REFERENCES

1. Rifkin MD, Dahnert W, Kutz AB. State-of-the-art: endorectal sonography of the prostate gland. *AJR* **1990**;154:691–700
2. Carter SSC, Shinohare K, Lipshultz L. Transrectal ultrasonography in disorders of the seminal vesicles and ejaculatory ducts. *Urol Clin North Am* **1989**;16:773–790
3. Malatinsky E, Labady F, Lepies P, Zajac R, Jancar M. Congenital anomalies of the seminal ducts. *Int Urol Nephrol* **1987**;19:189–194
4. Kenney PJ, Leeson MD. Congenital anomalies of seminal vesicles: spectrum of computed tomographic findings. *Radiology* **1983**;149:247–251
5. Kaneti J, Lissmer L, Smailowitz Z, Sober I. Agenesis of kidney associated with malformations of the seminal vesicle. Various clinical presentations. *Int Urol Nephrol* **1988**;20:29–33

Book Review

MRI of the Wrist and Hand. By Murray A. Reicher and Leland E. Kellerhouse. New York: Raven, 203 pp., 1990. $89

The applications of MR imaging with respect to the musculoskeletal system are increasing rapidly. One virtually untouched area is the wrist and hand. With improved technology, the small structures in the wrist and hand reliably can be discriminated from one another. However, no authoritative text has been published on the MR findings of normal and abnormal processes involving the hand and wrist. It is apparent from the wide array of cases presented that the authors have the experience necessary to write the first significant book on this subject. The authors state in the introduction that some readers will think this book is premature because most of the discussion is based on anecdotal experience (albeit extensive, with more than 1000 cases) and not scientific data. I would agree with this argument if the book simply showed a series of interesting cases. However, that is not the case.

What is presented is an excellent discussion of the normal anatomy and biomechanics of the wrist, of imaging techniques and protocols, and, most importantly, of the myriad of disease processes (many of which are poorly understood even by subspecialty radiologists) that affect this region. Detailed correlation of the pathophysiologic and MR findings of the various disease processes is the backbone of this book and provides the basis for the novice to venture into this challenging area of imaging.

The chapters that follow include discussion of carpal tunnel disease, flexor and extensor tendon disorders, carpal instability, and distal radioulnar joint, osteonecrosis, fractures, tumors, synovial processes, and early experience with pathologic changes of the finger. The discussions in each of these chapters are succinct, lucid, and instructive.

All of the major disease processes discussed are accompanied by high-quality illustrations, though I have to admit that it is difficult to visualize some of the findings even with arrows delineating the abnormality. The most likely explanation is my inexperience with hand and wrist MR, but I do wonder how many of the subtle ligamentous and tendinous changes were noted in retrospect or after clinical correlation. This does not detract from the excellence of this book in any way. It merely emphasizes the need for prospective studies now that the usefulness of MR imaging has been documented so well by the authors' experience.

No question exists that MR will become the imaging technique of choice for many of the pathologic conditions of the wrist and hand. For any radiologist (generalist or subspecialist) involved in the performance of wrist or hand MR, this book is mandatory reading. Because of the wealth of clinical information found in this work, I also recommend it as a reference text for radiologic and orthopedic departmental libraries.

David W. Nelson
Oregon Health Sciences University
Portland, OR 97201

John Caffey Award Paper

Avascular Necrosis: Early MR Imaging and Histologic Findings in a Canine Model

Alan S. Brody[1]
Munro Strong[2]
George Babikian[2]
Donald E. Sweet[3]
F. Glen Seidel[1,4]
Jerald P. Kuhn[1]

To examine the early MR and histologic changes of avascular necrosis, we surgically devascularized the distal femur of adult beagle dogs and performed short TR/short TE MR imaging and histologic examinations. MR showed increasing areas of low signal, and histologic examination showed changes of fat necrosis, inflammatory infiltrate, and fibrocytic and bony repair. These processes were divided into four stages. Stage 1 is seen in the first days after surgery and consists of homogeneous high signal on MR and only subtle histologic changes of early fat necrosis. Stage 2, seen by 7 days after surgery, shows linear low-signal areas within the high-signal marrow on MR and fat necrosis and an inflammatory infiltrate on histologic sections. Stage 3, seen by 16 days after surgery, shows patchy low signal occupying more of the marrow on MR with a fibrocytic infiltrate on histologic sections. Stage 4, seen by 23 days after surgery, shows a more homogeneous low and intermediate signal on MR and histologic findings of more organized fibrocytes and the onset of new bone formation.

Using this model, we have proved that MR imaging can show marrow changes as soon as 1 week after the onset of avascular necrosis. Whereas MR imaging showed a progression of increasing areas of low signal, the histologic findings seen during this time were diverse, including inflammatory infiltration (a previously unreported finding), fat necrosis, and fibrocytic and osseous repair.

***AJR* 157:341-345, August 1991**

Since 1983, reports have documented the ability of MR imaging to visualize avascular necrosis (AVN) [1]. More recent reports have shown MR to be the most sensitive means available for the detection of AVN [2-5]. This sensitivity is now well accepted. Several different patterns of MR imaging changes have been described, with all showing low signal in the subarticular marrow on short TR/short TE images [6].

A classic appearance, a ringlike low signal surrounding higher signal, is frequently seen in advanced AVN. However, studies have shown that bone with histologically proved AVN can appear normal on MR images [7]. No pattern of progression from normal bone marrow to the classic ringlike low density during a period after the onset of AVN has been documented. Other appearances, including a homogeneous intermediate gray appearance of the marrow in the femoral head, have been reported to occur in AVN [8]. This could represent either a second appearance of AVN or a stage in the development of MR imaging changes.

Although valuable information continues to be gained from clinical cases, these studies have limitations. First, in investigating MR imaging and AVN, histologic data are necessary to understand the physiologic changes that result in changes in MR imaging appearance. Although this has been done in some studies, histologic material has either been confined to the small samples provided by core biopsies or to very advanced cases [9, 10]. Second, in order to determine the onset and progression of MR changes, exact knowledge of the interval following the onset of AVN is also necessary. This usually is not possible in clinical cases. Third, as AVN

Received September 28, 1990; accepted after revision February 26, 1991.

Recipient of the John Caffey gold award at the annual meeting of the Society for Pediatric Radiologists, San Antonio, TX, 1989.

[1] Department of Radiology, Children's Hospital of Buffalo, 219 Bryant St., Buffalo, NY 14222.

[2] Department of Orthopaedic Surgery, Children's Hospital of Buffalo, Buffalo, NY 14222.

[3] Armed Forces Institute of Pathology, 6825 16th St., Washington, DC 20306-6000.

[4] Present address: Department of Radiology, Children's Mercy Hospital, 24th and Gillam Rd., Kansas City, MO 64108.

0361-803X/91/1572-0341
© American Roentgen Ray Society

can probably result from many different initial insults, clinical studies most likely reflect a heterogeneous population. In order to obtain histologic material at serial intervals after an identical insult, we used an animal model of AVN.

Using this model, we have been able to perform MR imaging on avascular bone during the first days and weeks of AVN. In addition, we have been able to show histologic changes that parallel the MR changes.

Materials and Methods

The distal femurs of adult beagle dogs were made surgically avascular by using the following technique. General anesthesia was induced with a 2.5% solution of Surital (thiamylal sodium, Park-Davis, Morris Plains, NJ) in isotonic sodium chloride. The dogs were then intubated and anesthesia maintained with Fluothane (halothane, Ayerst Laboratories, New York). A hind limb was disarticulated at the knee, and the lower limb was removed. Hemostasis was achieved by ligation of the larger vessels and electrocautery of smaller vessels. The distal femur was exposed by blunt dissection, and the distal 4 cm of the periosteum of the distal femur was removed by sharp dissection. Two and a half centimeters above the condyles, the medial and lateral cortex was drilled horizontally with a 4-mm bone drill. The marrow was removed at this level with a small spoon curette. The marrow proximal and distal to this level was not disturbed. The skin was then closed over the distal femur by using a fish-mouth closure. The dogs received 2 ml of Combiotic (procaine penicillin G and streptomycin sulfate, Pfizer Laboratories, New York) daily for 7 days postoperatively; postoperative care was otherwise routine.

Imaging sessions were performed postoperatively on the day of surgery and on postoperative days 3, 7, 10, 13, 17, 21, 23, 27, and 30. Plain radiographs and MR images were obtained at each session. One dog was used at each session; the series thus required 10 dogs. In vivo radiographs were taken on Quanta detail film (Dupont, Clifton, NJ). MR imaging was performed on a Diasonics MT/S 0.35-T system (Diasonics, South San Francisco) by using a temporomandibular joint small-field-of-view coil. T1-weighted sequences were used with 5-mm slices, 500/40 (TR/TE), and 2.5-mm slices, 500/50. Imaging was performed in the coronal, sagittal, and axial planes. The unamputated femur served as a control.

At the end of each session, the dog was sacrificed and the operated distal femur was removed and placed in formalin. Contact specimen radiographs were then obtained. The plane of histologic section was chosen to approximate the coronal MR plane. One unamputated femur was treated in the same manner as a control.

All plain films and MR images were examined by two radiologists. The histologic sections were examined by a pathologist without knowledge of the postsurgical interval. MR and pathologic interpretations were both performed on the entire distal femur, beginning 1 cm or more distal to the drilling site so that the area of focal posttraumatic repair at the drilling site was not included. The characteristics of the entire area examined were recorded for both the MR images and histologic sections. Specific point-to-point correlation was not attempted.

Results

The in vivo radiographs showed no changes throughout the study. The specimen radiographs showed periosteal new bone and new bone formation at the drilling site. A subtle loss of trabecular definition was noted in the subcondylar bone (Fig. 1).

Overall, MR showed a gradual increase in the amount of low signal seen within the normally high-signal marrow space. Some decrease in signal was seen by 3 days after surgery, with most areas of low signal well defined by 7 days after surgery. This low signal progressed from a linear heterogeneous pattern to a more homogeneous appearance. Histologic examination showed a progression of changes beginning with fat necrosis, followed by the appearance of an inflammatory infiltrate, and subsequently fibrocytes. Finally, by 23 days after surgery, new bone formation was seen.

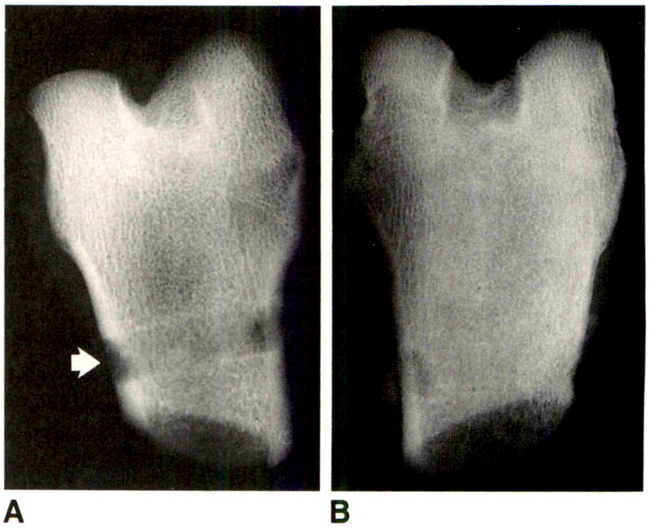

Fig. 1.—*A*, Specimen radiograph of distal femur of an adult beagle on day of surgery. Drilling site is visible in diaphysis (*arrow*).

***B*, Specimen radiograph of distal femur of an adult beagle 30 days after surgery. Note healing at drilling site. Trabecular pattern distally is less well defined than in *A*, and poorly defined areas of increased bone density are present.**

The MR and histologic appearances of the control specimen are shown in Figure 2. Stage 1 was defined as homogeneous high signal of the marrow on MR imaging. This normal MR appearance was seen postoperatively within 1 day of surgery (Fig. 3A); histologic examination of sections from the operated femur showed early fat necrosis and formation of microlipid lakes (Fig. 3B) because of disruption of the cell membrane of the lipocytes. The loss of the regular size of the lipocytes was the only histologic change of the stage 1 specimen when compared with normal controls.

Stage 2 was clearly seen by day 7, when irregular linear areas of low signal appeared within the high-signal marrow (Fig. 4A). The histologic sections showed fat necrosis and an inflammatory infiltrate (Fig. 4B) characterized by polymorphonuclear cells irregularly distributed throughout the marrow. These MR and histologic appearances persisted through day 13.

Stage 3 was seen by day 16, when the MR appearance had become more confluent and homogeneous, with a greater percentage of low-signal areas. Low- and high-signal areas occupied approximately equal portions of the marrow cavity (Fig. 5A). Histologic examination showed an unorganized fibrocytic infiltrate with residual inflammatory changes (Fig. 5B). This appearance persisted through day 21.

Stage 4 was seen by day 23, when the MR appearance became more homogeneous. The majority of the marrow was now intermediate or low in signal (Fig. 6A). Histologic exami-

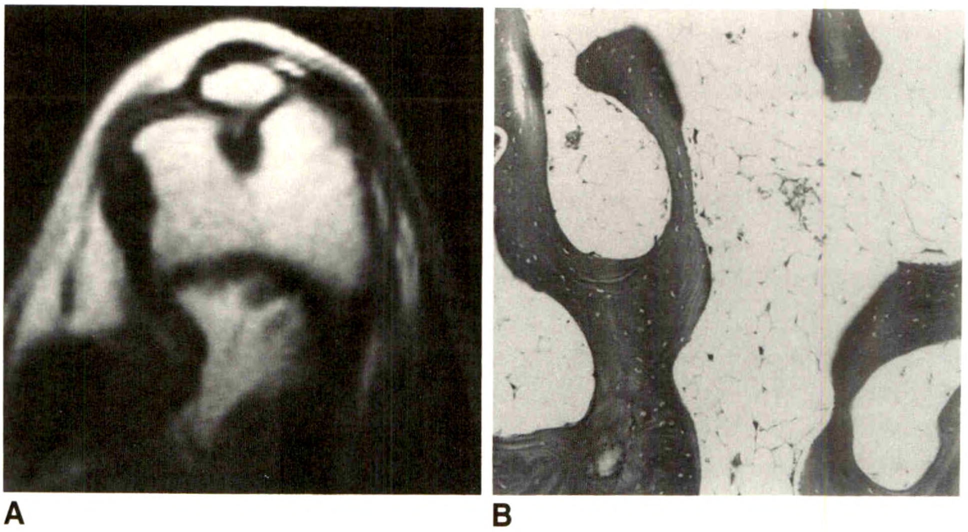

Fig. 2.—*A*, MR image (500/50, 2.5 mm thick) of control specimen from distal femur of adult beagle. Homogeneous high signal is seen in distal femoral marrow cavity.

B, Histologic section of control specimen from distal femur shows normal appearance of bone marrow. Note regular size of lipocytes. (H and E, original magnification ×25)

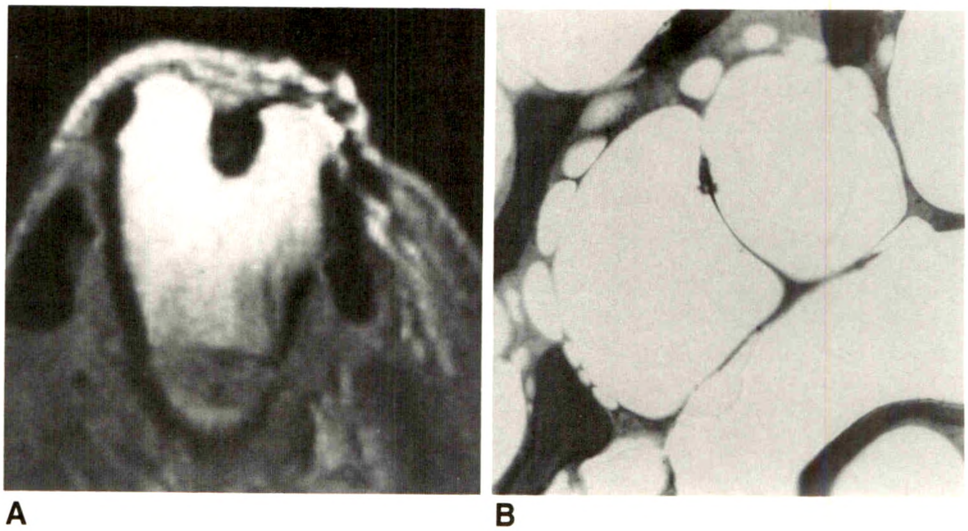

Fig. 3.—*A*, MR image (500/50, 2.5 mm thick) of distal femur of an adult beagle on day of surgery. Homogeneous high signal of marrow cavity is same as that seen in control specimen.

B, Representative histologic section of specimen shown in *A*. Lipid collections are heterogeneous in size, with most much larger than those in control specimen (see Fig. 2B), indicating loss of lipocyte integrity. These microlipid lakes indicate fat necrosis. (H and E, original magnification ×25)

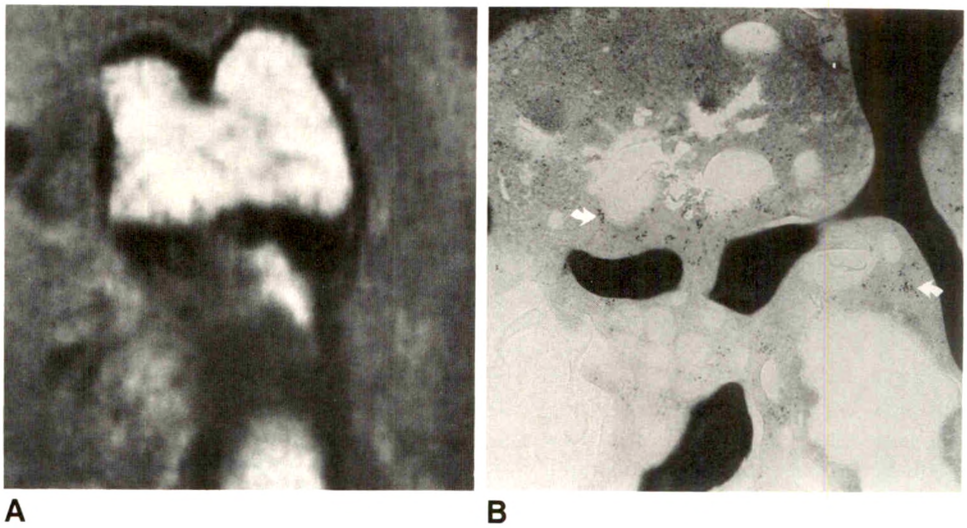

Fig. 4.—*A*, MR image (500/50, 2.5 mm thick) of distal femur of adult beagle 7 days after surgery shows linear areas of low signal within predominantly high-signal marrow.

B, Representative histologic section of specimen shown in *A*, with large irregular areas of amorphous debris. Some lipid persists, but no lipocyte cell membranes are seen. Polymorphonuclear cells are seen irregularly distributed throughout specimen (*arrows*). (H and E, original magnification ×25)

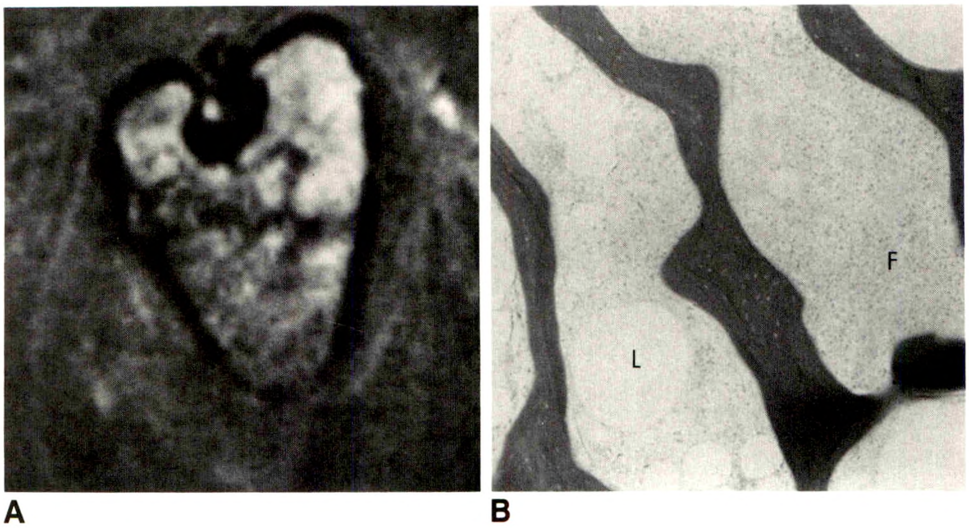

Fig. 5.—*A*, MR image (500/50, 2.5 mm thick) of distal femur of adult beagle 16 days after surgery. Low-signal areas are more confluent than on images obtained 7 days after surgery. Low signal has replaced much of originally high-signal marrow, and low and high signals occupy approximately equal portions of marrow cavity.

B, Histologic section from specimen shown in *A* shows replacement of amorphous debris by fibrocytes. Fibrocytes (F) with lipid lakes (L) were seen throughout specimen. (H and E, original magnification ×25)

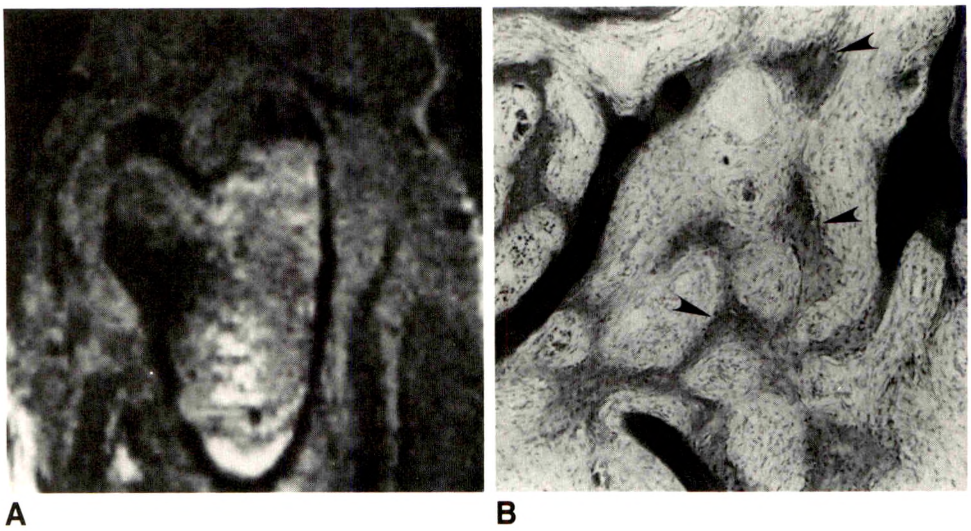

Fig. 6.—*A*, By 23 days after surgery, MR image (500/50, 2.5 mm thick) shows increased areas of low signal in marrow cavity of distal femur of adult beagle. Low signal is more confluent and occupies most of marrow cavity.

B, Histologic section from specimen shown in *A* shows evidence of continuing repair process. Fibrocytes now have a whirled, less randomly oriented appearance than was seen earlier (Fig. 5B), and new trabecular bone (*arrowheads*) is present. (H and E, original magnification ×25)

nation showed more organized fibrocytic repair with the onset of new bone formation (Fig. 6B). This appearance was seen through the end of the study period of 30 days.

Discussion

This study shows that MR changes can be seen as early as 1 week after acute interruption of the vascular supply. When these earliest MR changes occur, fat necrosis and an inflammatory infiltrate are seen histologically. This early inflammatory infiltrate has not been documented by other researchers, but the remaining findings of fat necrosis and fibroblastic repair correspond well to those of a recent clinical study [11]. It is possible that this type of acute inflammatory infiltration also occurs briefly in AVN of the femoral head in humans. The patient may be asymptomatic at this stage and therefore not undergo MR imaging or scintigraphy.

Bone marrow edema has been postulated to explain the MR appearance of many bone marrow changes including AVN [8, 12]; however, this edema has not been shown histologically. Our histologic study revealed only fat necrosis, cellular infiltrates, and new bone formation.

The lack of specificity of MR imaging makes it difficult to determine the physiologic mechanism underlying the MR changes without histologic correlation. The histologic data we obtained allowed us to describe the abnormality underlying the early MR imaging changes that occur within the avascular segment. It is important to define the early period of AVN because successful therapy, whether decompression or other, must begin at this time.

Our model did not develop a well-defined peripheral reactive zone. These findings therefore cannot be directly compared with the appearance seen in clinical studies of advanced AVN. Our findings are limited to the changes occurring within the avascular segment. Further studies are needed to correlate these findings with clinical studies of early AVN in order to evaluate their relevance to the clinical situation.

We were able to study the earliest changes of AVN, which appeared as early as 1 week after the onset of AVN. An inflammatory infiltrate, not previously described in AVN, was identified. Our model can be used to search for new MR imaging strategies that can identify early changes. The use of different pulse sequences, contrast agents, and MR spectroscopy needs to be investigated.

REFERENCES

1. Moon KL, Genant HK, Helms CA, Chafetz NI, Crooks LE, Kaufman L. Musculoskeletal applications of nuclear magnetic resonance. *Radiology* **1983**;147:161–171
2. Totty WG, Murphy WA, Ganz WI, Kumar B, Daum WJ, Siegel BA. Magnetic resonance imaging of the normal and ischemic femoral head. *AJR* **1984**;143:1273–1280
3. Bassett LW, Gold RH, Reicher M, Bennett LR, Tooke SM. Magnetic resonance imaging in the early diagnosis of ischemic necrosis of the femoral head. *Clin Orthop* **1987**;214:237–248
4. Mitchell MD, Kundel HL, Steinberg ME, Kressel HY, Alavi A, Axel L. Avascular necrosis of the hip: comparison of MR, CT, and scintigraphy. *AJR* **1986**;147:67–71
5. Coleman BG, Kressel HY, Dalinka MK, Scheibler ML, Burk DL, Cohen EK. Radiographically negative avascular necrosis: detection with MR imaging. *Radiology* **1988**;168:525–528
6. Gillespy T, Genant HK, Helms CA. Magnetic resonance imaging of osteonecrosis. *Radiol Clin North Am* **1986**;24:193–208
7. Genez BM, Wilson MR, Houk RW, et al. Early osteonecrosis of the femoral head: detection in high-risk patients with MR imaging. *Radiology* **1988**;168:521–524
8. Turner DA, Templeton AC, Selzer PM, Rosenberg AG, Petasnick JP. Femoral capital osteonecrosis: MR finding of diffuse marrow abnormalities without focal lesions. *Radiology* **1989**;171:135–140
9. Beltran J, Herman LJ, Burk JM, et al. Femoral head avascular necrosis: MR imaging with clinical-pathologic and radionuclide correlation. *Radiology* **1988**;66:215–220
10. Takatori Y, Kamogawa M, Kokubo T, et al. Magnetic resonance imaging and histopathology in femoral head necrosis. *Acta Orthop Scand* **1987**;58:499–503
11. Hauzeur JP, Pasteels JL, Schoutens A, et al. The diagnostic value of magnetic resonance imaging in non-traumatic osteonecrosis of the femoral head. *J Bone Joint Surg [Am]* **1989**;71:641–649
12. Pay NT, Singer WS, Bartal E. Hip pain in three children accompanied by transient abnormal findings on MR images. *Radiology* **1989**;171:147–149

American Roentgen Ray Society Residents' Award Papers, 1992

The ARRS announces competition for the 1992 President's Award and two Executive Council Awards for the best papers concerning the clinical application of the radiologic sciences.

Awards

The winner of the President's Award will receive a certificate and a $2000 prize. The winners of the two Executive Council Awards will each be given a certificate and a prize of $1000. The winners will be announced on March 16, 1992. Winning papers will be presented at the ARRS annual meeting at Marriott's Orlando World Center, Orlando, FL, May 10–15, 1992. Winning papers will be submitted for early publication in the *American Journal of Roentgenology*. All other papers will be returned to the authors.

Regulations

Eligibility is limited to residents or fellows in radiology who have not yet completed 4 years of approved training in a radiologic discipline. A letter from the resident's department chairman attesting to this status must accompany the manuscript. The resident must be the sole or senior author and be responsible for all or most of the project.

Submitted manuscripts must not exceed 5000 words and have no more than 10 illustrations. Four copies of the manuscript and illustrations are required. Submitted manuscripts should not contain previously presented or published material and should not be under consideration for publication elsewhere.

Deadline for submissions is February 14, 1992. Send papers to

Nancy O. Whitley, M.D.
Chairman, Committee on Education & Research
American Roentgen Ray Society
Department of Radiology
University of Maryland Medical Systems Hospital
22 S. Greene St.
Baltimore, MD 21201

Book Review

The Radiologic Clinics of North America. Imaging of Joints. Guest editor: Jeremy J. Kaye. Philadelphia: Saunders, September 1990;28(5):905–1138. $25; by subscription, 6 issues annually for $93

Musculoskeletal radiology has made great strides in the past 2 years with regard to imaging of the joints. The development of MR imaging and improvements in surface-coil technology have presented radiologists with an opportunity to show the internal anatomy of joints and joint disorders. The editor of this monograph, Jeremy J. Kaye, an eminent musculoskeletal radiologist, has enlisted a group of internationally known authors to produce this volume. The topics are timely and reflect the state-of-the-art imaging for each area described. The book is organized in a logical fashion, with individual chapters beginning with the wrist, the elbow, the shoulder, the hip, the knee, and the foot and ankle. Additional chapters cover the small joints (temporomandibular joint and facet joints) as well as the sacroiliac joints. A separate chapter on advanced imaging of the joints of infants and children is included because special consideration is required for the young patient. The volume concludes with a review of current concepts in the radiology of joint replacement surgery.

Overall, each chapter is well written and well illustrated. The quality of the illustrations, in keeping with the entire *Radiologic Clinics of North America* series, is excellent. Each chapter is also well referenced with up-to-date articles. With the exception of the chapters on the shoulder and the temporomandibular joint, each chapter emphasizes the value of plain films in the initial assessment of these joints. It is refreshing to find this emphasis in print in this age when it is so tempting to order a more sophisticated imaging study immediately.

Each chapter follows a format that begins with the technical aspects for each type of imaging procedure performed. The pertinent normal anatomy then is discussed. The remainder of the chapter is a brief, but cogent, discussion of the important pathologic entities that may be encountered in that joint.

This volume has few deficiencies. The chapters on the wrist and the ankle and foot have relatively few MR images. The authors have noted the value of these studies in evaluating the respective joints. Perhaps the lack of images reflects the authors' lack of access to MR units. These omissions, however, are minor and really do not detract from the overall value of this volume.

In summary, *Imaging of Joints* should be must reading for any radiologist who does many musculoskeletal studies. Once again, the publisher and editor should be commended for the excellent job in producing this volume.

Richard H. Daffner
The Medical College of Pennsylvania, Allegheny Campus
Pittsburgh, PA 15212

Preoperative Evaluation of Osteosarcoma: Value of Gadopentetate Dimeglumine–Enhanced MR Imaging

Leanne L. Seeger[1]
Bobbi E. Widoff[1]
Lawrence W. Bassett[1]
Gerald Rosen[2]
Jeffrey J. Eckardt[3]

Decisions regarding the surgical approach in osteosarcoma require accurate assessment of tumor extent. In order to determine whether enhancement with gadopentetate dimeglumine could add clinically significant information to that available with unenhanced MR imaging, 21 patients with osteosarcoma underwent preoperative MR imaging. T1- and T2-weighted spin-echo MR images obtained before and after administration of IV gadopentetate dimeglumine were evaluated to determine the conspicuity of marrow and soft-tissue extent of tumor, including tumor involvement of major neurovascular bundles and adjacent joints. MR results were correlated with tumor margins found at surgery. In some instances, use of gadopentetate dimeglumine obscured differentiation of tumor from normal marrow or tumor infiltration into perineurovascular fat, and tumor extension through pseudocapsule could not be differentiated from peritumoral edema after contrast administration. Contrast enhancement did assist in differentiation of intraarticular tumor from effusion; however, synovial invasion could be identified on unenhanced T1-weighted images by loss of synovial fat and cortical disruption.

These results indicate that gadopentetate dimeglumine does not assist in defining tumor margins of osteosarcoma.

***AJR* 157:347–351, August 1991**

Surgical intervention for osteosarcoma may consist of limb sparing procedures, amputation, or disarticulation. The choice of procedure requires that intramedullary and soft-tissue tumor margins be accurately defined, including tumor infiltration into vital neurovascular structures and joints. In order to determine if gadopentetate dimeglumine–enhanced MR images could assist in the preoperative evaluation of osteosarcoma, we performed pre- and postenhancement imaging preoperatively in 21 patients.

Subjects and Methods

The study included 21 patients with biopsy-proved primary intramedullary osteosarcoma. There were 11 males and 10 females 13–52 years old (mean age, 21 years). Eleven tumors originated in the distal femur, six in the proximal tibia, and two each in the proximal humerus and proximal femur. No patient had known metastatic disease when the MR images were made.

Four patients were imaged before initiation of preoperative chemotherapy, 13 were at the midpoint of therapy, and four had completed chemotherapy at the time of MR imaging. In all patients, chemotherapy consisted of a 12-week period of high-dose methotrexate, cisplatin, and Adriamycin [1].

MR images were acquired with a 0.3-T hybrid permanent resistive magnet. A surface coil was used for lesions of the knee and shoulder. The field of view varied from 14 to 25 cm, depending on the body part under investigation. Slice thickness and interslice gap were chosen to cover the entire tumor, with 13 images provided for each pulse sequence. Although multiplanar images were obtained in all patients, only axial images were evaluated for this study.

Received January 14, 1991; accepted after revision March 4, 1991.

Presented at the at the annual meeting of the American Roentgen Ray Society, Washington, DC, May 1990.

[1] Department of Radiological Sciences, University of California, School of Medicine, 10833 Le Conte Ave., Los Angeles, CA 90024-6952. Address reprint requests to L. L. Seeger.

[2] Department of Cedars Sinai Comprehensive Cancer Center, Cedars Sinai Medical Center, 8700 Beverly Blvd., Los Angeles, CA 90048.

[3] Department of Surgery, Division of Orthopaedic Surgery, University of California, Los Angeles, Los Angeles, CA 90048.

0361-803X/91/1572-0347
© American Roentgen Ray Society

In order to provide uniformity in image acquisition, a multiple echo, multiple repetition (MEMR) sequence was used both before and after enhancement [2]. T2-weighted images after contrast administration, however, were not used for analysis in the study. This is because gadopentetate dimeglumine–induced T2 shortening is not evident with the dose of contrast material and pulse sequences used for clinical MR scanning. The MEMR sequence allows simultaneous acquisition of spin-echo T1- and T2-weighted images. With a pulse sequence pair of 340/30 and 2200/85 (TR/TE), 13 images were available for each pulse sequence within a single scan acquisition. Two signal averages and 192 imaging levels gave an acquisition time of 17.5 min per scan set. One set was completed immediately before, and one within 20 min after IV administration of 0.1 mmol/kg of gadopentetate dimeglumine. No contrast reactions or complications occurred.

Scans were evaluated simultaneously by two experienced radiologists, and consensus was reached for all readings. Findings on MR images were compared with findings at surgery by evaluating the width of tumor-free margins. Pathologic results were not known at the time of image interpretation. Unenhanced and enhanced images were reviewed to determine intramedullary and soft-tissue tumor signal characteristics (and thus differentiation of tumor from normal surrounding tissue), the presence or absence of an intact tumor capsule or pseudocapsule, the relationship of tumor to major neurovascular structures, and evidence of synovial or intraarticular invasion by tumor.

For analysis of signal characteristics, intramedullary and soft-tissue tumors were independently classified as either homogeneous or inhomogeneous. The predominant signal intensity within the tumor was then determined to be either void, present but lower than that of normal muscle, equal to that of muscle, higher than that of muscle but lower than that of subcutaneous fat, equal to that of fat, or higher than that of subcutaneous fat.

A tumor capsule or pseudocapsule was considered present and intact when margins of the soft-tissue mass were sharply demarcated. If adjacent muscle showed poorly defined abnormal signal intensity with enhanced T1-weighted or unenhanced T2-weighted imaging, either peritumoral edema or tumor invasion was thought to be present within surrounding soft tissues.

Major neurovascular structures were evaluated as being either free of tumor, abutted by tumor, or encased by tumor. Joints were evaluated for a breech in the normal synovium as evidenced by loss of the normal high signal intensity of synovial fat. Joint distension was also noted and determined to represent either intraarticular tumor or fluid.

Results

Tumor Signal Characteristics

Intramedullary tumor.—On unenhanced T1-weighted images, the signal intensity of intramedullary tumor was equal to or less than that of muscle in all cases. This pattern was homogeneous in 16 cases and inhomogeneous in five. On T1-weighted images after administration of contrast material, intramedullary tumor enhanced in 11 cases (Fig. 1) and did not change in 10 cases. Four tumors that were homogeneous became inhomogeneous. The signal characteristics of intramedullary tumor on unenhanced T2-weighted images were more variable. Five tumors were of a signal intensity equal to or lower than that of muscle, 10 were higher than muscle and lower than fat, and six were equal to or higher than fat. Four tumors were homogeneous and 17 were inhomogeneous.

Soft-tissue tumor.—Five tumors were entirely intraosseous. Of the 16 with a soft-tissue mass, unenhanced T1-weighted images showed 15 with signal intensity equal to that of muscle and one with signal intensity higher than that of muscle but less than that of fat. Eleven of these were homogeneous and five were inhomogeneous. On T1-weighted images obtained after administration of contrast material, the signal intensity of 13 masses increased to become either higher than that of muscle and lower than that of fat (11 cases) or equal to that of fat (two). Three retained their unenhanced signal intensity. Only three tumors remained homogeneous. On unenhanced T2-weighted images, all soft-tissue masses but one showed signal intensity higher than that of muscle (13 equal to or higher than that of fat). Three were homogeneous and 13 were inhomogeneous. Five tumors showed uniform high signal intensity on unenhanced T2-weighted images and a rim of high signal intensity surrounding central intermediate signal intensity on unenhanced T1-weighted images, a pattern of tumor necrosis (Fig. 2).

Tumor Capsule/Pseudocapsule

In 15 of the 16 tumors with a soft-tissue mass, the soft-tissue component was sharply defined on both unenhanced

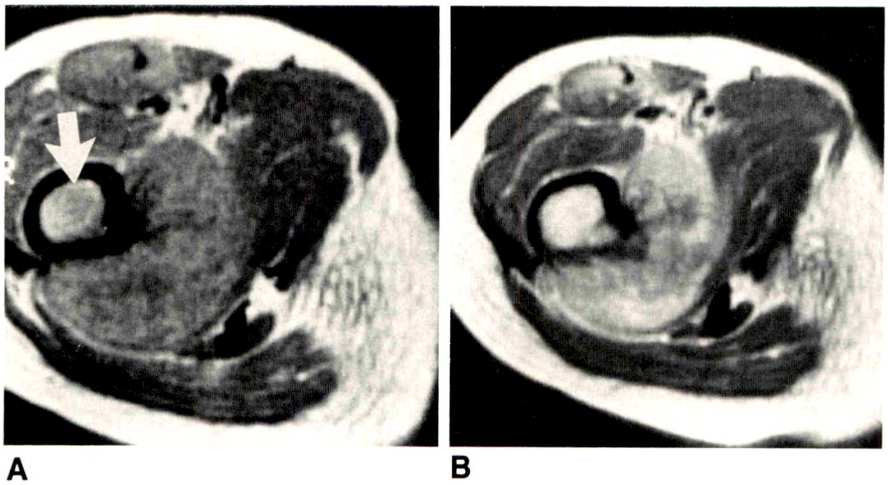

Fig. 1.—Intramedullary tumor enhancement.
A, **Unenhanced T1-weighted MR image of proximal thigh shows intramedullary tumor (*arrow*) of intermediate signal intensity in right femur. Marrow of left femur and subcutaneous fat were of normal high signal intensity.**
B, **Enhanced T1-weighted MR image shows signal intensity of intramedullary tumor in right femur to be equal to that of fat. Differentiation of intramedullary tumor from normal marrow is not possible.**

T2-weighted images and enhanced T1-weighted images, indicating the presence of a tumor capsule or pseudocapsule. In one patient, soft-tissue margins were poorly defined on both enhanced and unenhanced images. Unenhanced T2-weighted images in six of the 15 tumors with a capsule or pseudocapsule revealed poorly defined streaks of high signal intensity within adjacent muscle. In all six, there was gadopentetate dimeglumine enhancement in the same location (Fig. 3), and in four, this enhancement was greater than the enhancement of the predominant soft-tissue mass itself. Of these four, surgical margins revealed that this enhancement represented peritumoral edema in two cases and tumor infiltration in two cases.

Neurovascular Involvement

The major neurovascular structures were clearly free of tumor in 15 patients. Comparison of unenhanced T1- and T2-weighted images revealed tumor abutting the major bundles in five patients. On enhanced T1-weighted images, differentiation of tumor from normal fat surrounding the neurovascular bundle was less evident (Fig. 4). In one patient, a major

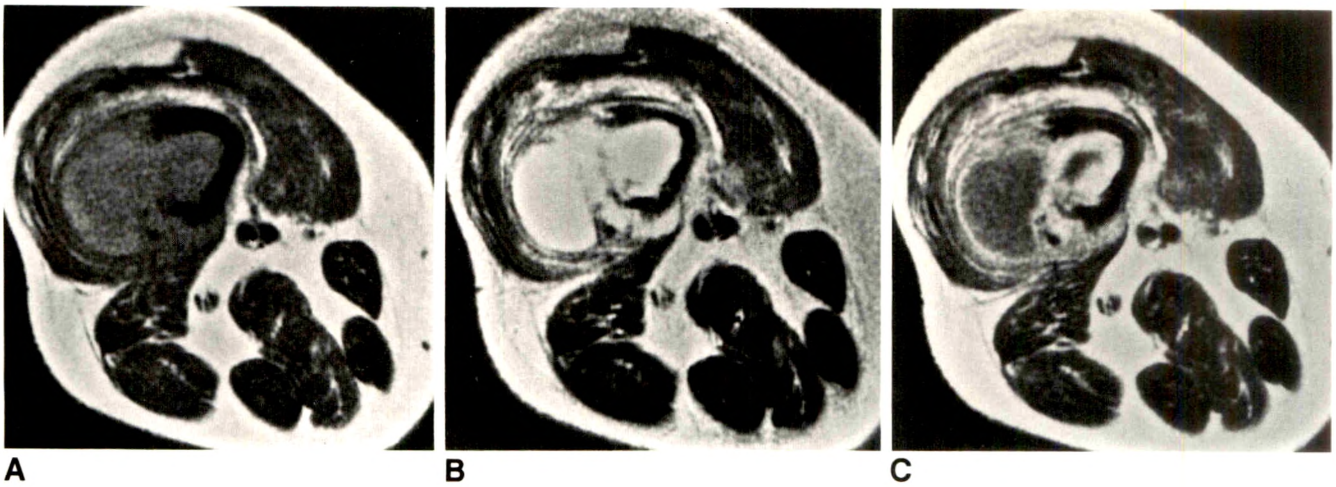

Fig. 2.—Tumor necrosis.

A, Unenhanced T1-weighted MR image of distal thigh shows marrow tumor and contiguous soft-tissue mass of homogeneous intermediate signal intensity.

B, Unenhanced T2-weighted MR image shows both intramedullary tumor and soft-tissue mass are of uniform high signal intensity.

C, Enhanced T1-weighted image shows persistent low signal intensity, indicating tumor necrosis. Had this represented tumor mineralization, it would not have had high signal intensity on T2-weighted image.

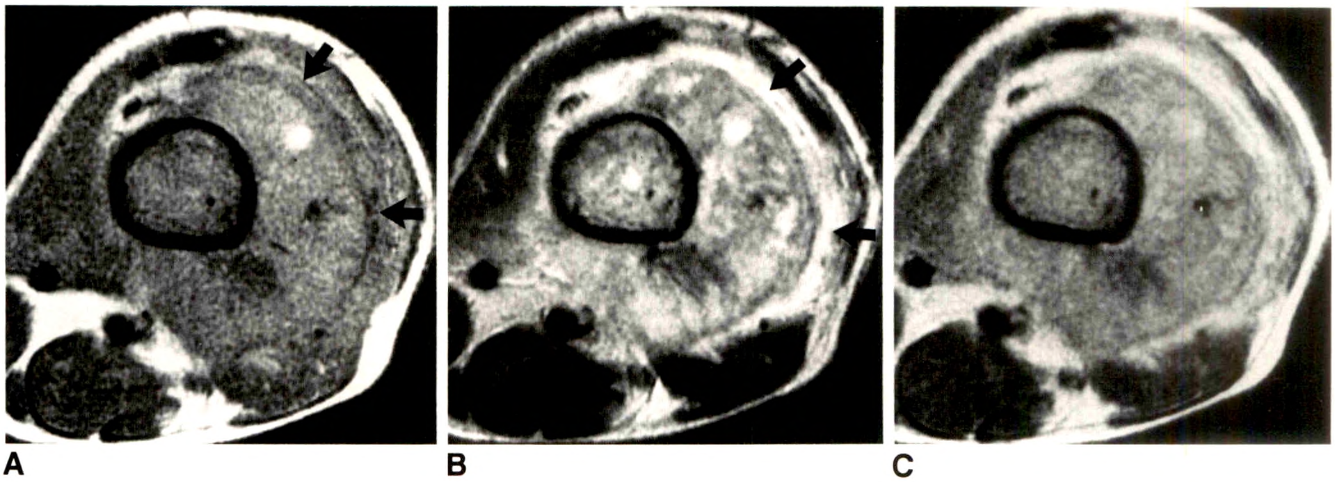

Fig. 3.—Tumor capsule.

A, Unenhanced T1-weighted MR image of distal thigh shows margin (*arrows*) of soft-tissue mass is well defined by pseudocapsule.

B, Unenhanced T2-weighted MR image shows low-signal-intensity pseudocapsule separating soft-tissue mass from surrounding muscles. High-signal-intensity peritumoral edema with poorly defined margins is seen laterally (*arrows*).

C, Enhanced T1-weighted MR image shows enhancement of both soft-tissue mass and peritumoral edema. In this patient, edema shows greater enhancement.

neurovascular bundle was obliterated by tumor. This was evident on all images.

Intraarticular Tumor

Adjacent joints were free of tumor in 16 patients. This was apparent on unenhanced T1-weighted images, and was evidenced as continuity of a thin band of normal synovial fat and lack of intraarticular mass. Unenhanced images in five patients revealed abnormal signal intensity interrupting synovium (synovial invasion) and joint distension. On T1-weighted images, intraarticular tumor was of intermediate signal intensity, while joint fluid was of very low signal intensity (Fig. 5). Intraarticular tumor became higher signal intensity on unenhanced T2-weighted and enhanced T1-weighted images. Joint fluid became very high signal intensity on T2-weighted images, but retained its low signal intensity on enhanced T1-weighted images. Normal synovium enhanced uniformly with gadopentetate dimeglumine.

Discussion

Preoperative imaging of osteosarcoma generally includes radiographs, scintigrams, and CT scans or MR images [3]. Cross-sectional imaging is used to determine marrow and soft-tissue extent of tumor, including the relationship of tumor to major neurovascular structures and adjacent joints. This information, together with clinical and histological studies, is essential for tumor staging and determining the most appropriate type of surgical treatment (limb-sparing procedure, amputation, or disarticulation).

On unenhanced T1-weighted MR images, determination of

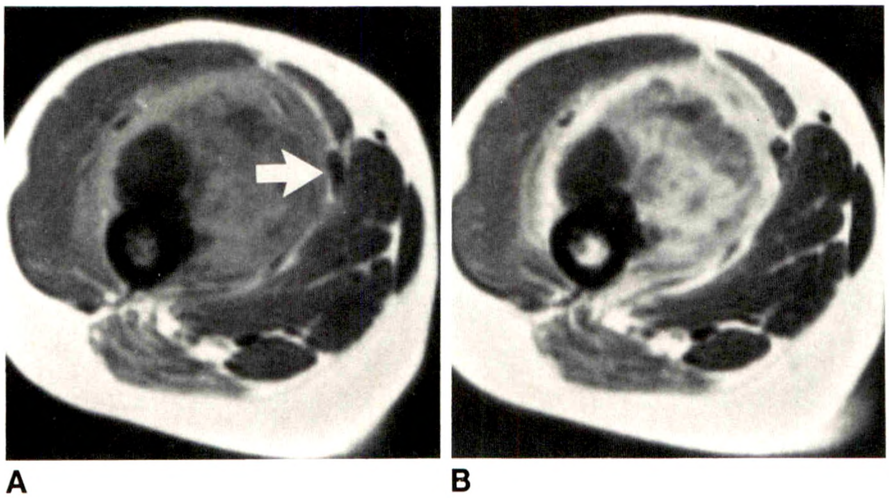

Fig. 4.—Neurovascular bundle.

A, Unenhanced T1-weighted MR image through proximal thigh shows soft-tissue mass abuts signal void of superficial femoral vessels. High-signal-intensity fat, however, separates tumor from vascular structures (*arrow*).

B, Enhanced T1-weighted image. Because both soft-tissue mass and peritumoral edema enhance, normal fat surrounding neurovascular structures is no longer evident.

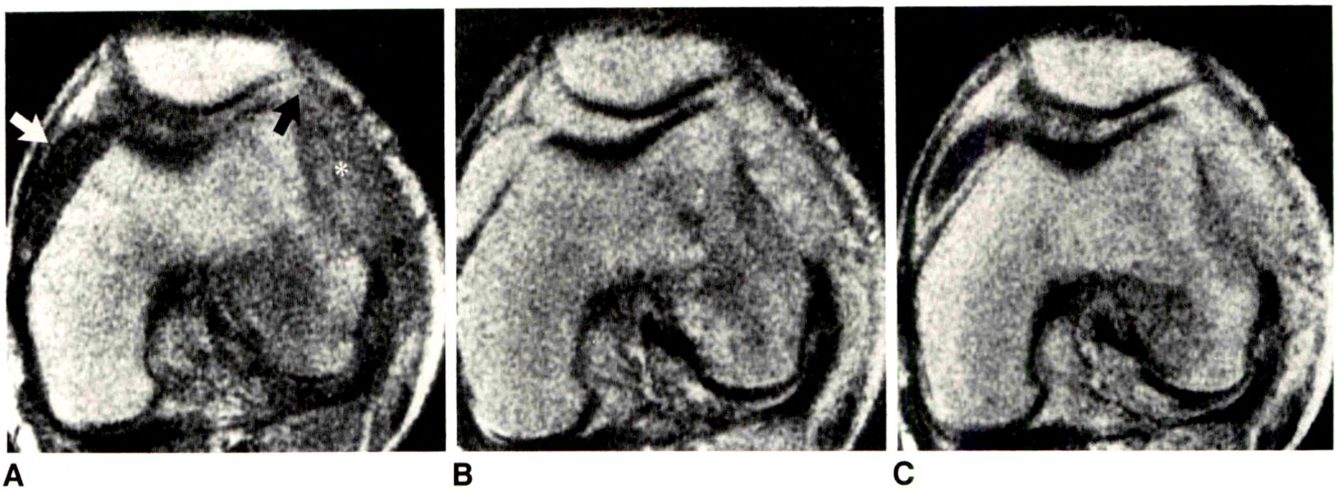

Fig. 5.—Normal synovial enhancement and joint invasion.

A, Unenhanced T1-weighted MR image through knee shows soft-tissue mass in region of lateral recess of knee joint (*asterisk*). Invasion of fat has occurred adjacent to patella (*black arrow*). Medially, very low signal joint fluid is present. An intact synovium is evident as a thin band of fat signal intensity (*white arrow*).

B, Unenhanced T2-weighted MR image shows tumor and fluid both have high signal intensity.

C, Enhanced T1-weighted MR image shows enhancement of both tumor in lateral recess and uninvolved synovium in medial recess. While lack of tumor invasion into medial recess is more striking on enhanced image, this information is available on unenhanced images.

intramedullary tumor extent is rendered possible by the inherent contrast differentiation between the high signal intensity of normal fatty marrow and the intermediate signal intensity of tumor. After administration of contrast material, intramedullary tumor enhanced in 11 of our patients, and the usual contrast differentiation between marrow and tumor was lost. This same phenomenon was observed by Stimac et al. [4] in the evaluation of spinal neoplasms.

The majority of intramedullary and soft-tissue tumors in our study increased in signal intensity after contrast administration. The clinical significance of this phenomenon, however, is questionable. Because contrast enhancement is an indication of vascularity, authors have attempted to characterize tumors according to their enhancement pattern. Stimac et al. [4] found that enhancement with gadopentetate dimeglumine could determine the vascular character of tumors of the spine, but determined that enhancement was not specific for tumor activity. Erlemann et al. [5] studied primary musculoskeletal tumors with dynamic gadopentetate dimeglumine–enhanced MR imaging with a 1.5-T magnet. They determined that dynamic imaging with gradient-echo techniques (flip angle of 90°) after contrast administration allowed differentiation of malignant vs benign lesions with an accuracy of 80% [5]. Others, however, have not been able to duplicate these findings using a 1.0-T magnet and a flip angle of 40° [6]. It was not noted in the study of Erlemann et al. whether differentiation between benign and malignant bone lesions was possible with plain radiography, a much less expensive and more readily available technique.

Sharp tumor margins, indicating the presence of a tumor capsule or pseudocapsule, were present in 15 patients. This was easily identified on both unenhanced T2-weighted and enhanced T1-weighted images. Of substantial clinical concern, however, was the peritumoral high signal intensity seen in adjacent soft tissues on the unenhanced T2-weighted and enhanced T1-weighted images of six patients. Pettersson et al. [7] studied five patients with soft-tissue tumors by using gadopentetate dimeglumine–enhanced MR and found that both richly vascularized tissues and edematous structures enhanced. Hanna et al. [8] found that viable tumor, granulation tissue after biopsy, and peritumoral edema enhanced with gadopentetate dimeglumine. We also found that this streaky pattern of high signal intensity could represent either edema or infiltration of tumor into adjacent tissues. In addition, peritumoral edema may enhance more dramatically than soft-tissue tumor. This is in contradistinction to the findings of Bloem et al. [9], who found that strong enhancement was a reliable indication of tumor.

Definition of the proximity of tumor to major neurovascular structures presents little problem with the combination of unenhanced T1-weighted and T2-weighted MR images. The high-signal-intensity fat surrounding large vessels and nerves is easily identified on T1-weighted images, and tumor increases in signal intensity on T2-weighted images. With gadopentetate dimeglumine, most soft-tissue tumors become high signal intensity, similar to fat. When tumor is very near the neurovascular bundle, demarcation between tumor and neurovascular bundle fat is either less evident or lost in T1-weighted images after contrast administration.

Normal synovial tissue can be identified on unenhanced images by the high signal intensity of synovial fat on T1-weighted images. Tumor that has invaded synovium, however, shows intermediate signal intensity on T1-weighted images and signal intensity equal to or higher than that of fat on T2-weighted images. Although distinction between joint effusion and intraarticular tumor is more obvious on enhanced T1-weighted images, the presence of tumor is nonetheless evident before contrast enhancement by identification of synovial infiltration and adjacent cortical disruption. In addition, joint fluid is of low signal intensity on the unenhanced T1-weighted images, and tumor is of intermediate signal intensity.

Our preliminary results suggest that enhancement with gadopentetate dimeglumine in preoperative MR imaging of osteosarcoma is not necessary. As compared with unenhanced T1-weighted images, differentiation of tumor from normal fat, including marrow, fat investing neurovascular structures, and fatty synovium is more difficult after injection of contrast material. Although circumstances may arise in which contrast enhancement may be useful, we believe that the routine use of gadopentetate dimeglumine adds unnecessary imaging time, cost, and remote but potential risk. Further investigation with large numbers of patients may provide clinically useful indications for gadopentetate dimeglumine in MR imaging of the musculoskeletal system.

REFERENCES

1. Rosen G. Spindle cell sarcoma, malignant fibrous histiocytoma, and fibrosarcoma. In: Schein P, ed. *Decision making in oncology*. Philadelphia: Decker, **1989**:164–169
2. Seeger LL, Sinha U, Sunha S, Bassett LW. Musculoskeletal MR imaging with a variable TE, variable TR sequence (abstr). *Radiology* **1988**;169(p):322
3. Seeger LL, Eckardt JJ, Bassett LW. Cross-sectional imaging in the evaluation of osteogenic sarcoma: MRI and CT. *Semin Roentgenol* **1989**;24:174–184
4. Stimac GK, Porter BA, Olson DO, Gerlach R, Genton M. Gadolinium-DTPA-enhanced MR imaging of spinal neoplasms: preliminary investigation and comparison with unenhanced spin-echo and STIR sequences. *AJR* **1988**;151:1185–1192
5. Erlemann R, Reiser MF, Peters PE, et al. Musculoskeletal neoplasms: static and dynamic Gd-DTPA–enhanced MR imaging. *Radiology* **1989**;171:767–773
6. Fletcher BD, Hanna SL. Musculoskeletal neoplasms: dynamic Gd-DTPA–enhanced MR imaging (letter). *Radiology* **1990**;177:287–288
7. Pettersson H, Eliasson J, Egund N, et al. Gadolinium-DTPA enhancement of soft tissue tumors in magnetic resonance imaging—preliminary clinical experience in five patients. *Skeletal Radiol* **1988**;17:319–323
8. Hanna LS, Magill HL, Parham DM, Bowman LC, Fletcher BD. Childhood chondrosarcoma: MR imaging with gadolinium-DTPA. *Magn Reson Imaging* **1990**;8:669–672
9. Bloem JL, Doornbos J, Taminiau AHM, Holscher HC. Gd-DTPA–enhanced MR imaging of bone tumors (abstr). *Radiology* **1988**;169:436

Book Review

Radiology in the Management of Cancer. Edited by R. J. Johnson, B. Eddleston, and R. D. Hunter. New York: Churchill Livingstone, 472 pp., 1990, $125

Twenty-five contributors have combined their considerable talents to produce this book, which aims to improve understanding of the role of radiology in the management of cancer. The main thrust of the book is related to the integration and limitations of available imaging techniques in staging cancer and in evaluating the therapeutic response or complications.

This book is well written and organized into 18 chapters. Chapter 1 is devoted to nuclear medicine imaging, and chapter 2 deals with MR imaging. Childhood malignancy is discussed specifically in chapter 3. Chapters 4 through 17 deal with tumors at specific sites, and the final chapter (chapter 18) discusses the use of radiology in planning radiotherapy.

The chapters are informative and, whenever relevant and possible, illustrated. However, I was somewhat disappointed by chapter 15, which deals virtually exclusively with CT rather than MR imaging for the evaluation of CNS tumors. Current developments in MR imaging usually far exceed the data available to even the most timely publication, and this may have been a problem with this book.

The references listed after each chapter are timely and adequate, and the index is properly arranged. The printing is excellent, and the 283 illustrations are sharp and of high quality.

I think that the authors have achieved their goal of making clinicians understand the particular relevance of all imaging techniques to the cancer patient's management so that patients can have the relevant tests and studies done as quickly and as efficiently as possible.

This book should appeal to all clinicians who treat cancer patients, although it is directed to radiologists and oncologists. The book is well worth its relatively high price, even though many of the concepts can be found elsewhere. This book should be included in radiology and oncology libraries.

E. Edmund Kim
University of Texas
M. D. Anderson Cancer Center
Houston, TX 77030

Soft-Tissue Sarcoma: MR Imaging vs Sonography for Detection of Local Recurrence After Surgery

Haesun Choi[1]
Datla G. K. Varma[1]
Bruno D. Fornage[1]
E. Edmund Kim[1]
Dennis A. Johnston[2]

To determine the value of MR and sonography in detecting local recurrences of soft-tissue sarcomas after surgery, 26 MR and sonographic studies performed in 21 patients were reviewed retrospectively. Recurrences were confirmed histologically in 12 (46%) of 26 studies. The MR images and sonograms were obtained within 1 month of each other. The findings were classified as recurrence, no recurrence, or indeterminate. Sonography was instrumental in guiding fine-needle aspiration biopsy of impalpable lesions. In two cases, the findings on sonography were indeterminate. In both of these cases, the sonograms had been obtained soon after surgery (at 2 and 4 months). The sensitivity and specificity in the detection of local recurrences were 83% and 93%, respectively, for MR and 100% and 79%, respectively, for sonography. These differences were not statistically significant.

We conclude that MR and sonography appear to be equally useful in the detection of local recurrences of soft-tissue sarcomas, sonography can be used for routine follow-up and in guiding needle biopsies, sonography may be more difficult to interpret than MR during the early postoperative period, and MR should be used if sonography is inconclusive.

***AJR* 157:353-358, August 1991**

Soft-tissue sarcomas account for 1% of malignant tumors; their most common location is in a lower extremity [1, 2]. These tumors are known to have a high tendency for local recurrence, depending on the tumor type, size, grade, and location. Although this tendency has been modified by improvements in radiation therapy and chemotherapy, the rate of local recurrence reportedly is as high as 90% after simple excision and approximately 30% after wide monobloc resection [1, 3]. The local recurrence rate is even higher after surgical resection of previously recurrent tumors [3].

Clinical detection of these recurrent tumors is difficult, especially when the tumor recurs in the scar or in deep tissue. MR imaging is well suited for examining the soft tissue of the extremities, where motion artifacts are avoided. Previous investigations have demonstrated that MR is superior to CT because of the higher contrast resolution and direct acquisition of three-dimensional images available with MR, although involvement of cortical bone is seen better on CT [4–10].

Sonography has recently become popular for evaluating soft-tissue masses, especially in children [11–13]. Sonography's usefulness has also been in detecting tumor recurrence [14]. Because sonography is easier to perform and provides easy guidance for biopsy, sonography might be advantageous in detecting locally recurrent tumors if it is as effective as MR.

The purpose of this study was to evaluate and compare MR and sonography for detecting local recurrence of tumor after surgery.

Received November 21, 1990; accepted after revision February 22, 1991.

[1] Department of Diagnostic Radiology, M. D. Anderson Cancer Center, University of Texas, 1515 Holcombe Blvd., Houston, TX 77030. Address reprint requests to H. Choi.

[2] Department of Biomathematics, M. D. Anderson Cancer Center, University of Texas, Houston, TX 77030.

0361-803X/91/1572-0353
© American Roentgen Ray Society

Materials and Methods

From 1987 through 1989, 38 sets of MR and sonographic examinations performed within 1 month of each other were selected randomly from the population of patients who had been treated surgically for soft-tissue sarcomas. If different sets of examinations were a part of follow-up in the same patient, only the first set was selected to review. Also, if a patient had more than one lesion (three cases) or more than one operation (two cases), the examinations for each surgical area were considered different studies.

Twenty-six sets of MR and sonographic examinations in 21 patients (seven men and 14 women) were available for review. The patients were 12–71 years old (mean, 28 years). MR and sonography were performed within 1 month of each other and between 1 and 32 months (mean, 12 months) after the last operation: seven within 6 months, including three 1-month postoperative examinations; six within 7–12 months; five within 13–18 months; three within 19–24 months; and five after 24 months.

All patients had soft-tissue sarcomas in the extremities: five malignant fibrous histiocytomas, five synovial sarcomas, three epithelioid sarcomas, two unclassified sarcomas, two fibrosarcomas, one pleomorphic sarcoma, one hemangiopericytoma, one liposarcoma, and one neuroepithelioma. All patients had had at least one surgical excision plus chemotherapy and/or radiation therapy before MR or sonography.

MR imaging was performed by using multislice spin-echo T1-weighted, 600/20 (TR/TE), and T2-weighted, 2000/30–80, sequences with a 1.5-T scanner (General Electric, Milwaukee, WI). Images were obtained in at least two planes: axial and either coronal or sagittal. Gadopentetate dimeglumine (Magnevist, Berlex Laboratories, Wayne, NJ) was used in a concentration of 0.1 mmol/kg of body weight in four patients. Gradient-echo sequences, 200/20/20° (TR/TE/flip angle), were used in two patients.

Sonography was performed in all patients by using real-time sonographic scanners with 7.5-MHz linear-array transducers. A 5-MHz transducer was used electively for evaluation of deep tissues in some cases. Examinations were performed with particular attention to scars and palpable nodules. When necessary, sonographically guided fine-needle aspiration was performed freehand.

The MR images and sonograms were reviewed independently by two experienced reviewers in each field without knowledge of the clinical or histologic outcomes and histologic diagnosis of the primary neoplasms. The two reviewers agreed with each other about most of the examinations; when there was disagreement, a consensus was reached.

The findings on MR and sonography were classified on the basis of visual analysis into three groups: recurrent/residual tumor, no recurrent/residual tumor, and indeterminate. On MR, a recurrence was suspected when there was a discrete nodule of low to medium signal intensity on T1-weighted images and increased signal intensity on T2-weighted images, with or without contour deformity in adjacent tissues (Fig. 1). Areas of low to medium signal intensity on both T1- and T2-weighted images without nodular configuration, whether or not theses areas were well defined, were considered postsurgical changes without tumor recurrence (Fig. 2). Fluid collections without solid nodules were included in postsurgical changes (Fig. 3). The possibility of tumor recurrence was excluded if no or minimal diffuse enhancement occurred after administration of gadopentetate dimeglumine (Fig. 2). Areas that could not be classified as either group and technically inadequate studies were considered indeterminate.

On sonograms, a lesion was considered a recurrent tumor when a discrete hypoechoic mass was present (Figs. 1 and 4). Areas of diffuse abnormal echogenicity without a discrete nodule (Fig. 3) were classified as no tumor recurrence. Sonographically indeterminate lesions were classified in the same way as with MR (Fig. 5). In two cases, the time elapsed since the previous surgery was provided; both of these cases were considered indeterminate.

Histologic confirmations were made by fine-needle aspiration and/or another operation in 18 areas that appeared suggestive of recurrent tumors with either MR or sonography. Twelve were confirmed as recurrent tumors. The remaining 14 cases were considered negative for recurrence, six proved by histologic results and eight by multiple follow-up examinations. Follow-up examinations were done for minimum of 8 months and up to 36 months (mean, 16 months). Only two cases had less than 1 year of follow-up.

For statistical analyses, indeterminate cases were included in the tumor recurrence group, as these would require close observation for a possible recurrent tumor in actual practice. The sensitivity and specificity of each technique were calculated with 95% confidence intervals [15, 16]. Results of MR and sonography were analyzed and compared with each other by using the chi-square and kappa statistic [17]. Overall comparative data were analyzed by using heterogeneity chi-square to see if the findings from two techniques were sufficiently similar that they could be pooled as if one technique [18].

Results

MR Imaging

Ten of 26 MR studies showed recurrent tumor, 15 did not, and one was indeterminate (only proton-density images were available to review). All of the 10 cases that showed tumor

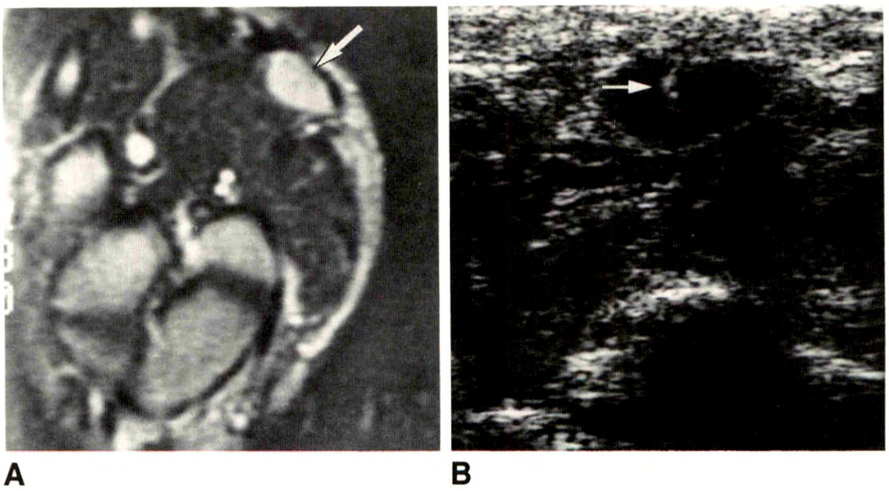

Fig. 1.—Recurrent synovial sarcoma at plantar surface of right foot.

A, **T2-weighted MR image obtained 10 months after surgery shows a nodule (*arrow*), approximately 1 cm in diameter, of high signal intensity.**

B, **Sonogram obtained 5 days later shows a discrete hypoechoic nodule at corresponding area. A needle (*arrow*) is seen within nodule during sonographically guided fine-needle aspiration.**

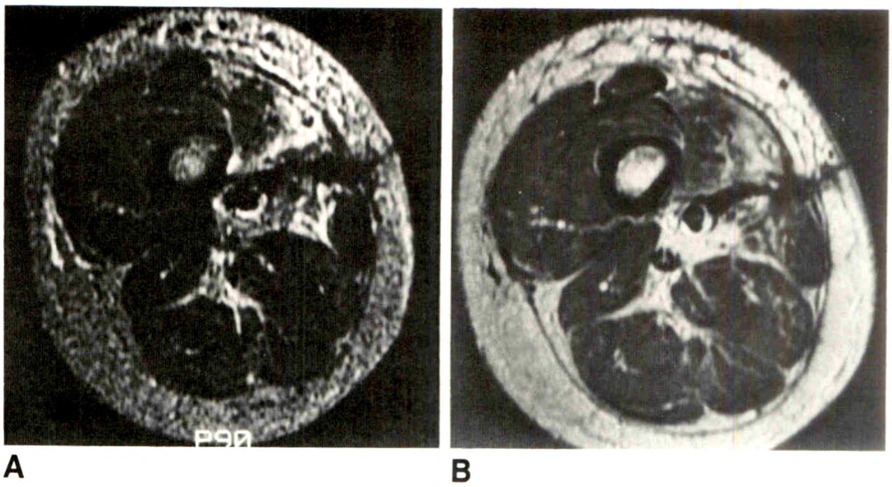

Fig. 2.—Hemangiopericytoma without recurrence. Tumor was resected 11 months earlier at medial aspect of right thigh.

***A* and *B*, T2-weighted MR image (*A*) and godopentetate dimeglumine-enhanced T1-weighted MR image (*B*) show postsurgical scar as an area of low signal intensity with no significant enhancement. No discrete mass is seen. Poorly defined area of high signal intensity (*A*) and minimal enhancement (*B*) were thought to be related to recent radiation therapy. Subcutaneous edema is present (*A*).**

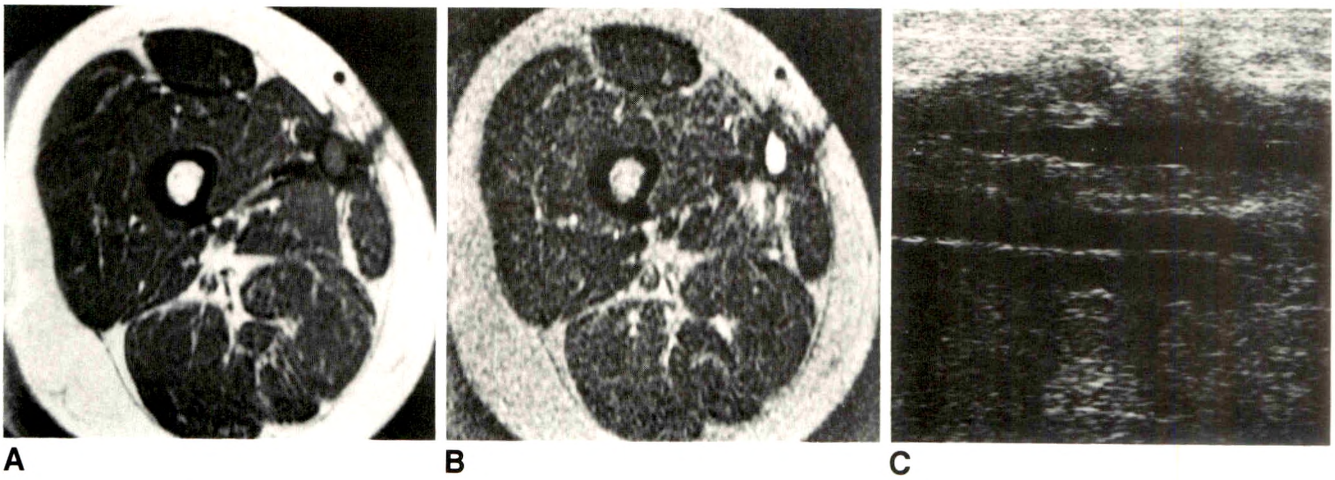

Fig. 3.—Hemangiopericytoma without recurrence. Tumor in right thigh was resected 4 months earlier.

***A–C*, T1-weighted (*A*) and T2-weighted (*B*) MR images show scar and fluid collection, corresponding to acute postsurgical change on sagittal sonogram (*C*). Note also poorly defined hypoechoic edema (*C*). Fluid collection and edema decreased progressively on multiple follow-up examinations.**

on MR were histologically confirmed as having recurrent tumors. Two of 15 cases that did not show tumor proved to have recurrent tumors: one synovial sarcoma (Fig. 4) proved by biopsy and one malignant fibrous histiocytoma (Fig. 5) proved by surgery. Two other patients who underwent subsequent surgeries had microscopic foci of tumor at the previous surgical margins. In another two, fluid collections were aspirated and showed no tumor cells. One had a second operation because of clinical suggestion of recurrence, but no tumor was found. The final eight areas that appeared abnormal after surgery remained unchanged or became smaller progressively on multiple follow-up examinations.

Considering the limitations in spatial resolution of MR, two microscopic tumors were considered true negative findings. Thus, only two results were false negative for tumor (Table 1). The sensitivity and specificity of MR were calculated to be 83% and 93%, respectively. Chi-square analysis ($\chi^2 = 15.4$, $p < .001$) indicates that the MR results are not random. The kappa statistic ($\kappa = .7665$) indicates a high degree of relationship between the MR and histologic findings.

Sonography

Thirteen of 26 sonographic studies showed recurrent tumors, 11 did not, and two were indeterminate. One of the indeterminate cases was proved to have macroscopic residual tumor after another operation (Fig. 5), and the other was considered to have no tumor recurrence on the basis of multiple follow-up examinations. Both of these studies were performed in the early postoperative period (2 and 4 months), and because of the recent surgeries, acute postoperative changes could not be differentiated with confidence. Eleven of 13 cases that showed tumor on sonograms proved to have recurrent tumors. One of the remaining two was found to have microscopic tumor after further surgery. The last one had no tumor cells on fine-needle aspiration, and the findings were stable on multiple follow-up examinations. One of 11 cases that did not show tumor was found to have microscopic tumor recurrence during further surgery. Another two had fluid collections. One underwent another operation because of a clinical suggestion of recurrence, but no tumor was found.

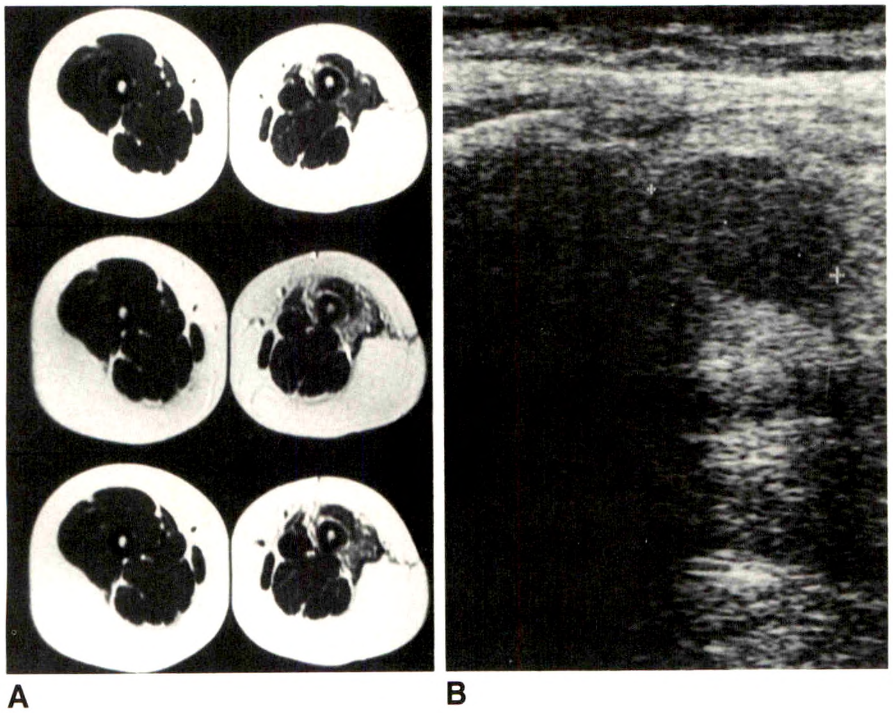

Fig. 4.—Recurrent synovial sarcoma in left thigh.

***A*, T1-weighted (*top*), T2-weighted (*middle*), and gadopentetate dimeglumine-enhanced T1-weighted (*bottom*) MR images obtained 29 months after surgery show scar and nonspecific changes with minimal diffuse enhancement after treatment. No discrete nodule is seen.**

***B*, Sonogram, however, shows a discrete hypoechoic nodule near femur.**

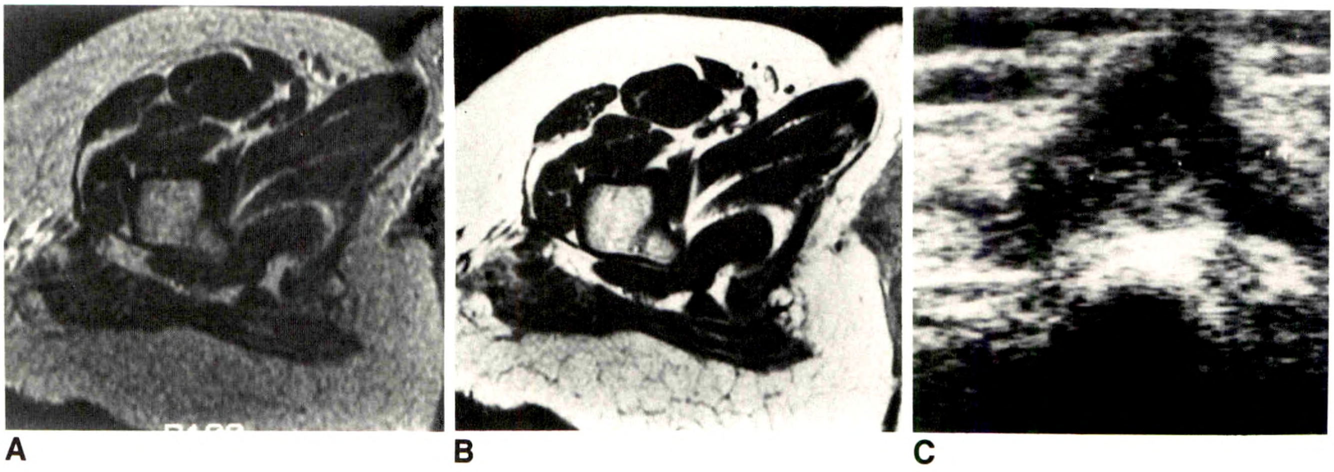

Fig. 5.— Recurrent malignant fibrous histiocytoma in right gluteal region.

***A* and *B*, T2-weighted (*A*) and gadopentetate dimeglumine-enhanced T1-weighted (*B*) MR images obtained 1 month after surgery show only nonspecific postsurgical edema and scar with no discrete mass.**

***C*, Sonogram shows a well-defined but not discrete hypoechoic area (3.2 × 2.0 cm) that was considered indeterminate. A 1.2 × 1.2 × 1.0 cm recurrent tumor was found embedded within scar (3 × 3 × 2 cm) after further surgery.**

TABLE 1: Histologic Correlation of MR and Sonographic Findings

Histologic Finding	MR		Sonography	
	Recurrence	No Recurrence	Recurrence	No Recurrence
Positive (*n* = 12)	10	2	12[a]	0
Negative (*n* = 14)	1[a]	13[b]	3[a, b]	11[b]

[a] Includes indeterminate cases.

[b] Includes microscopic tumors.

The final seven postsurgical abnormal-appearing areas remained unchanged or became progressively smaller and homogeneous on multiple follow-up examinations.

A discrete hypoechoic area confirmed to have microscopic tumor after further surgery was considered false positive for tumor. Including this case, two cases were false positive for tumor (Table 1). The sensitivity and specificity of sonography were calculated to be 100% and 79%, respectively. Chi-square analysis ($\chi^2 = 16.3$, $p < .001$) indicates that the sonographic results are not random. The kappa statistic ($\kappa = .7719$) indicates a high degree of relationship between the sonographic and histologic findings.

Comparison of MR and Sonography

The sensitivity of sonography was slightly higher than that of MR, and its specificity was slightly lower than that of MR. However, no significant statistical differences were found between MR and sonographic results by using heterogeneity chi-square (combined $\chi^2 = 31$, $p > .9$). Kappa statistics also did not show significant differences ($p > .3$), indicating that the rate of disagreement between MR and histology vs sonography and histology was not different.

Discussion

High signal intensity on T2-weighted images related to a long T2 relaxation time generally has been considered an indication of active tumor. However, the presence of relatively high signal intensity has not proved to be a reliable indicator for tumor recurrence after various therapies [5, 19–22]. In one report, only 70% of high-signal areas represented recurrent tumors [20]. Use of nodular configuration, in addition to abnormal signal intensity, as a diagnostic criterion seems to help increase the accuracy of MR, as seen in our study and in a recent prospective study by Reuther and Mutschler [4] on musculoskeletal neoplasms.

The criteria for tumor recurrence in the study of Reuther and Mutschler seem to be relatively specific compared with ours. They included nodules larger than 1 cm with short T2 relaxation times in the tumor recurrence group in addition to nodules of any size with long T2 relaxation times. This may be a helpful criterion if the histologic diagnosis of primary tumors is known, because some fibrous tumors do have short T2 relaxation times, depending on tissue components. However, both studies showed that a majority of these tumors still have long or relatively long T2 relaxation times and show high or increased signal intensity on T2-weighted images. As clinical histories were not available to our reviewers, which is often the case in actual practice, we simply followed our criteria, and no case was missed because such information was unavailable. In one false-negative case (Fig. 4), signal intensity was not the first issue, because no discrete nodule could be identified. Overall, the results of the two studies are identical (sensitivity: 83% in both studies; specificity: 93% in both studies), although the distribution of the primary tumors is somewhat different.

One of the two cases false negative for tumor on MR showed a discrete hypoechoic nodule (1.2 × 1.0 cm) on sonography that was confirmed to be a recurrent synovial sarcoma by sonographically guided fine-needle aspiration. Retrospectively, this small recurrent tumor might have been obscured by the area of diffuse nonspecific medium to high signal intensity on the T2-weighted images (Fig. 4). The second case false negative for recurrence on MR was considered indeterminate in the early postoperative period on the basis of sonographic criteria (Fig. 5). The actual tumor in this case was a 1.2- by 1.2- by 1.0-cm malignant fibrous histiocytoma surrounded by a 3- by 3- by 2-cm scar found during the subsequent surgery. Failure to detect malignant fibrous histiocytoma in this case cannot be explained by the smallness of the tumor and the routine 10-mm slice thickness alone. The various T2 relaxation times of such tumors, as described in previous reports [4, 10, 23, 24], might be responsible. Unfortunately, gadopentetate dimeglumine was not helpful in either case. An enhancement depends mainly on regional vascularity [25], the lesion would not be enhanced if the tumor were surrounded by avascular or hypovascular scar, as was seen in one of our cases.

Sonography has the advantage of allowing examination of superficial tissue easily and thoroughly in every plane without gaps. The single case in our study in which sonography was used to diagnose a recurrent tumor missed on MR does not allow the speculation that sonography is better than MR. However, this case illustrates the value of sonography in detecting small superficial lesions. Sonography would be particularly helpful in detecting recurrent tumors with short T2 relaxation times.

The one case still false positive for tumor on sonography 10 months after initial surgery, showed a fairly well-defined, elongated hypoechoic area (1.5 × 0.8 × 7.0 cm) (Fig. 6), but fine-needle aspiration failed to confirm tumor recurrence. We were not able to correlate sonography with MR in this case because only proton-density images were available to review. The lesion, however, was stable during the next 14 months on both sonography and MR. A rather elongated area, as

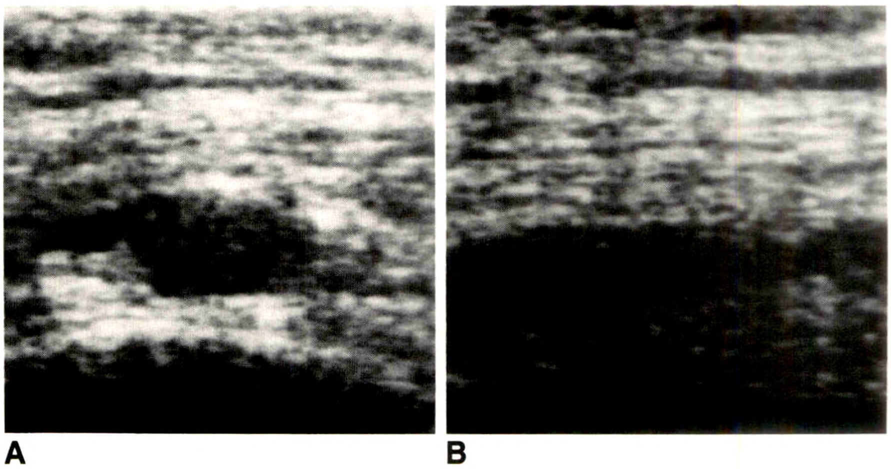

Fig. 6.—Malignant fibrous histiocytoma without recurrence. Tumor was resected 10 months earlier in right thigh.

***A* and *B*, Transverse (*A*) and sagittal (*B*) sonograms show a 7-cm-long discrete hypoechoic area. No tumor cells were found after fine-needle aspiration, and lesion was stable during next 14 months without further therapy. Appearance on transverse sonogram (*A*) mimics that of a recurrent tumor.**

seen in this case, seems to be a postsurgical change rather than tumor recurrence and probably represents scar, edema, or a fluid collection along the muscle plane or scar itself. This suggests that tumors may grow in multiple directions, especially when small, to produce a mass effect.

In the early postoperative period (approximately 3-6 months), inhomogeneous hypoechoic lesions on sonography could not be differentiated with certainty as recurrent tumors rather than hemorrhage, edema, new granulation tissue, or abscess. Although this uncertainty might have been partially due to the reviewers' inexperience with normal postoperative sonographic findings, the relative nonspecificity of sonography in general is well known. Serial follow-up examinations would be helpful to exclude or confirm a diagnosis of recurrent tumor. Meanwhile, MR was able to characterize recurrent tumors and early postoperative changes more easily and more accurately.

One of the well-known advantages of MR over other imaging techniques is its superior anatomic resolution. On sonography, exact locations of the lesions in relation to surrounding structures could not be delineated without the help of previous reports. This disadvantage of sonography could be eliminated if images were interpreted by an experienced operator at the site of examination.

We were not surprised that no microscopic residual or recurrent tumors were detected by either MR or sonography. This appears to be a limitation of currently available techniques.

Further prospective investigation is needed to determine the efficacy of these imaging techniques in evaluating possible tumor recurrence more accurately. In addition, further knowledge of the normal postoperative course on sonography might improve its accuracy. Although the gradient-echo MR technique did not add information to the routine spin-echo sequence in our cases, it provided much better contrast in a shorter acquisition time and has been suggested to improve the sensitivity of MR in detecting recurrent tumors [26]. In the same way, gadopentetate dimeglumine was not particularly helpful in detecting recurrent tumors in our two cases. However, it was useful for excluding recurrent tumors in two other cases in our study, in keeping with previous reports [27] (Kim EE et al., presented at the annual meeting of the Radiological Society of North America, November 1989). The values of the gradient-echo technique and gadopentetate dimeglumine require further investigation. Spectroscopic evaluation demonstrating biochemical changes may be helpful also.

In summary, the accuracies of MR and sonography in detecting locally recurrent tumors after surgery are comparable. Considering the fact that sonography is less costly and provides easy guidance for biopsy, it can be used for routine follow-up. An initial baseline study 4-6 weeks after surgery with both MR and sonography is recommended. When follow-up sonography is inconclusive, MR studies should be performed, possibly with gadopentetate dimeglumine, for further evaluation. MR also can be useful for a complete anatomic evaluation when sonographic studies indicate local tumor recurrence.

REFERENCES

1. Enterline HT. Histopathology of sarcomas. *Semin Oncol* **1981**;8(2):133-155
2. Carabell SC, Goodman RL. Radiation therapy for soft tissue sarcoma. *Semin Oncol* **1981**;8(2):201-205
3. Shiu MH, Hajdu SI. Management of soft tissue sarcoma of the extremity. *Semin Oncol* **1981**;8(2):172-179
4. Reuther G, Mutschler W. Detection of local recurrent disease in musculoskeletal tumors: magnetic resonance imaging versus computed tomography. *Skeletal Radiol* **1990**;19(2):85-90
5. De Lange EE, Fechner RE, Wanebo HJ. Suspected recurrent rectosigmoid carcinoma after abdominoperineal resection: MR imaging and histopathologic findings. *Radiology* **1989**;170:323-328
6. Gomberg JS, Friedman AC, Radecki PD, Grumbach K, Caroline DF. MR differentiation of recurrent colorectal carcinoma from postoperative fibrosis. *Gastrointest Radiol* **1986**;11:361-363
7. Glazer HS, Levitt RG, Lee JKT, et al. Differentiation of radiation fibrosis from recurrent pulmonary neoplasm by magnetic resonance imaging. *AJR* **1984**;143:729-730
8. Furst G, Pape H, Jurgens T, Kahn T, Modder U. Contrast media used in magnetic resonance tomography of soft tissue sarcomas. Follow-up examinations following multimodal therapy. *Radiologe* **1989**;29:336-342
9. Mahajan H, Kim EE, Wallace S, Abello R, Benjamin R, Evans HL. Magnetic resonance imaging of malignant fibrous histiocytoma. *Magn Reson Imaging* **1989**;7:283-288
10. Ebner F, Kressel HY, Mintz MC, et al. Tumor recurrence versus fibrosis in female pelvis: differentiation with MR imaging at 1.5 T. *Radiology* **1988**;166:333-340
11. Harcke HT, Grissom LE, Finkelstein MS. Evaluation of the musculoskeletal system with sonography. *AJR* **1988**;150:1253-1261
12. Glasier CM, Seibert JJ, Williamson SL, et al. High resolution ultrasound characterization of soft tissue masses in children. *Pediatr Radiol* **1987**;17:233-237
13. Yamaguchi M, Takeuchi S, Matsuo S. Ultrasonic evaluation of pediatric superficial masses. *JCU* **1987**;15(2):107-113
14. Fornage BD, Lorigan JG. Sonographic detection and fine-needle aspiration biopsy of non-palpable recurrent or metastatic melanoma in subcutaneous tissues. *J Ultrasound Med* **1989**;8:421-424
15. Feinstein AR. *Clinical biostatistics*. St. Louis: Mosby, **1977**:214-226
16. Steel RGD, Torrie JH. *Principles and procedures of statistics*. New York: McGraw-Hill, **1960**:458
17. Bishop YMM, Fienberg SE, Holland PW. *Discrete multivariate analysis: theory and practice*. Cambridge, MA: MIT Press, **1975**:385-397
18. Zar JH. *Biostatistical analysis*, 2nd ed. Englewood Cliffs, NJ: Prentice-Hall, **1984**:67-68
19. Sundaram M, McGuire MH, Herbold DR. Magnetic resonance of soft tissue masses: an evaluation of fifty-three histologically proven tumors. *Magn Reson Imaging* **1988**;6:237-248
20. Venel D, Lacombe MJ, Couanet D, Kalifa C, Spielmann M, Genin J. Musculoskeletal tumors: follow-up with MR imaging after treatment with surgery and radiation therapy. *Radiology* **1987**;164:243-245
21. Glazer HS, Lee JKT, Levitt RG, et al. Radiation fibrosis: differentiation from recurrent tumor by MR imaging. *Radiology* **1985**;156:721-726
22. Berquist TH. Magnetic resonance imaging of musculoskeletal neoplasms. *Clin Orthop* **1989**;244:101-118
23. Beltran J, Simon DC, Katz W, Weis LD. Increased MR signal intensity in skeletal muscle adjacent to malignant tumors: pathologic correlation and clinical relevance. *Radiology* **1987**;162:251-255
24. Sundaram M, McGuire MH, Schajewicz F. Soft-tissue masses: histologic basis for decreased signal (short T2) on T2-weighted MR images. *AJR* **1987**;148:1247-1250
25. Pettersson H, Eliasson J, Egund N, et al. Gadolinium-DTPA enhancement of soft tissue tumors in magnetic resonance imaging—preliminary clinical experience in five patients. *Skeletal Radiol* **1988**;17:319-323
26. Erlemann VR, Reiser M, Peters PE, Vassallo P, Harle A. Rational use of FLASH sequence in the staging of bone tumors and soft tissue tumors. *ROFO* **1988**;149:178-183
27. Erlemann R, Reiser MF, Peters PE, et al. Musculoskeletal neoplasms: static and dynamic Gd-DTPA-enhanced MR imaging. *Radiology* **1989**;171:767-773

Improved Imaging of Bone with Scan Equalization Radiography

J. C. Wandtke[1]
D. B. Plewes[1,2]

Use of scan equalization radiography (SER) for imaging bone in the head, face, neck, and shoulder was evaluated in a clinical comparison study with conventional radiographs of randomly selected patients. Two hundred nine pairs of normal and abnormal SER images and conventional radiographs were compared by four radiologists in a side-by-side viewing situation. The radiologists compared the visibility of specific anatomic features and rated the SER images as better than, equal to, or worse than the conventional radiographs. In the evaluation of the images of the cervical spine, the radiologists much preferred the SER images 63% of the time because of slight improvement in bone detail and marked improvement in detail of the soft tissues. In the evaluation of the images of the shoulder, the radiologists preferred the SER image 58% of the time and preferred the conventional radiograph only 5% of the time ($p < .05$). In the evaluation of the images of the skull, face, and mandible, the radiologists preferred the SER images 62% of the time and the conventional images 4% of the time ($p < .05$).

The superior image quality with the SER technique was recognized by all radiologists in the study and was the overwhelmingly preferred way of imaging the shoulder, neck, head, and face.

***AJR* 157:359-364, August 1991**

Conventional plain film radiography is often suboptimal when used to image portions of the body that exhibit large variations in tissue thickness. This results in areas of underexposure or overexposure on the radiograph. Nowhere is this problem more evident than in conventional chest and bone radiography. With bone radiography, the thickest part is optimally exposed but the thinner areas are overexposed. In response to these limitations of conventional radiography, scan equalization radiography (SER) was developed. SER generates a nonuniform field of radiation on the patient that is modulated in response to transmission variations of the particular positioning of the patient during film exposure [1-3].

The application of SER to chest radiography has been studied, and the results are a significant improvement in image quality [4, 5] and diagnostic accuracy [6, 7]. Similar studies with another equalization radiography unit (AMBER) have shown improvement in chest radiography [8]. The problem of large variations in transmission through different body tissues is a common problem associated with bone radiography also, especially radiography of the head, neck, shoulder, and spine. Most attempts to overcome these limitations have been studies of chest radiography with the use of specialized X-ray filters [9, 10]. Other approaches include the use of image processing of digitized radiographs [11, 12], photostimulable storage phosphor digital radiographic systems [13, 14], and direct digital scanning detector systems [15, 16].

Subjects and Methods

In this investigation, the application of SER to imaging of the cervical spine, head, face, mandible, and shoulder was studied. This was evaluated by a subjective assessment of

Received August 9, 1990; accepted after revision March 26, 1991.

This work was supported by grants from the National Cancer Institute (CA-27823) and the Eastman Kodak Co.

[1] Department of Diagnostic Radiology, University of Rochester Medical Center, 601 Elmwood Ave., Rochester, NY 14642. Address reprint requests to J.C. Wandtke.

[2] Present address: Department of Medical Biophysics, University of Toronto, 2075 Bayview Ave., North York, Ontario, Canada M4N 3M5.

0361-803X/91/1572-0359
© American Roentgen Ray Society

image quality by a panel of radiologists who reviewed matched conventional and SER images.

The details of the configuration and the operation of the SER system used in this study have been previously reported [1-3]. This SER system uses a 2.5- by 4.0-cm beam of radiation scanned in a series of 39 vertical lines. The X-ray output varies up to 2000 times during a 2-sec scan, and this is achieved by computer-controlled modulation of pulse width. The SER system was designed to be operated at 120 kVp for chest radiography, but was adjusted to provide artifact-free equalized images at 80–90 kVp with a maximum of 600 mA. The conventional radiographs were exposed with 75-kVp radiation by using a standard phototimed system. For the SER technique, the total scanning time ranged from 1.2 to 4.5 sec for posteroanterior, lateral, or oblique views depending on the thickness of the body part. Kodak T Mat-G film and Lanex regular screens were used for the conventional radiograph. This is the screen-film system most often used in our department. Because this prototype SER system is limited by tube output, a faster combination of Kodak T Mat-G film and Lanex fast screens was used for the SER images. The source-to-image distance for the SER images was fixed at 180 cm, but the conventional bone radiographs were obtained at 122 cm. The conventional radiographs were obtained with a wall-mounted Bucky grid assembly (grid ratio, 8:1). No grid was used for the SER images because scatter rejection was achieved by a 3.0-cm slit mounted in the aft collimator assembly.

All the comparison examinations were done in the upright position because this was a design limitation of the SER prototype. For the head and neck radiograph obtained with the SER system, the patient was positioned as close to the film cassette as possible, but, because of the size of the aft collimator assembly, it was not feasible to place the film cassette in direct contact with the exit side of the body part examined; however, only about 5% magnification resulted. During some examinations of the cervical spine and shoulder, there were slightly different degrees of magnification owing to slight differences in positioning of the patients. Positioning was as convenient with the SER system as with the conventional system. The comparison examinations were done in a different room 5–15 min after the initial examination. In about half of the cases, a different radiologic technologist positioned the patient for the SER examination. The conventional radiographs were obtained in the usual fashion with the usual film density and on-line monitoring of film quality by a radiologist. The SER system was set by using a phantom to provide an excellent image and was not readjusted during the study. Phantom studies have shown that for SER head and shoulder examinations, radiation exposure is less than for conventional studies. This is due to the elimination of overexposure around the thin edges of these anatomic structures and the film-screen used for SER, which is twice as fast.

Comparison SER and conventional radiographs were collected from 175 volunteers (38–76 years old) during a 3-month period after informed consent was obtained. Three or four volunteer patients were recruited on each of 3 days a week. Patients were recruited without bias as to type or severity of bone disease. Most of the patients asked to volunteer did participate. A variety of abnormal conditions were included as well as normal examinations. This resulted in 209 pairs of comparison radiographs of the neck (81), shoulder (65), and head (63). The comparison images were obtained within 15 min of each other.

The images were reviewed independently by four radiologists in viewing sessions that comprised approximately 50 comparison pairs each. Side-by-side comparison was used because the radiologist could not be blinded since it was obvious which radiograph was the conventional and which was the SER. A previous side-by-side and independent comparison study [4] showed no significant difference in the opinions of the radiologists about the relative quality of conventional and SER radiographs. Nonetheless, the radiologists in that study said that they preferred the side-by-side comparison. A side-by-side comparison permits easier selection of a preferred image when the differences are small.

The radiologists were asked to compare the visibility of all anatomic features and overall image quality and then indicate on a five-point scale whether the SER images were much better than (+2), slightly better than (+1), equal to (0), slightly worse than (−1), or much worse than (−2) the conventional images. The radiologists were provided with the patient's age and sex but not the patient's clinical history. There were no time constraints for viewing the radiographs. Before the study, the comparative features of the SER and conventional radiographs were illustrated in a 30-min training session with four demonstration cases. A brief technical explanation of the equalization technique was also given. The training sessions consisted of individual meetings with verbal instructions and the opportunity for discussion.

Results

The 175 patient examinations resulted in 209 pairs of comparison images on which each of four radiologists made 501 observations. A summary of the radiologists' opinions of the neck, shoulder, and head radiologic examinations is shown in Table 1. The radiologists had a marked preference for the SER images. The average improvement in score (on the scale of −2 to +2) of the 2004 SER images compared with conventional bone radiographs was +0.75. In 690 comparisons, no difference was seen. In 1233 comparisons, the SER image was better, whereas in 81 comparisons the conventional image was better. By chi-square analysis, SER was a significant ($p < .05$) improvement.

Cervical Spine

Cervical spine examinations of 47 patients resulted in 47 lateral, 20 oblique, and 14 anteroposterior comparison examinations. For each of these groups the radiologists were asked to comment on the clarity of the anatomy at the C1–C2 level, at the C3–C7 level, and of the soft tissues. Table 1 shows that for cervical spine examinations there was a preference for the SER images, with 209 (22%) regarded as much better, 395 (41%) as slightly better, and 333 (34%) as equivalent. Only 35 (3%) of the SER images were classified as inferior to the conventional images.

Comparison of an SER and conventional cervical spine examination is shown in Figure 1, where all four radiologists preferred SER. A markedly improved soft-tissue detail in the upper pharynx and larynx is usually seen. Most of the cases included in the study had normal soft tissue. The bones were frequently abnormal. The improved contrast in the bony structures and better visibility of C7 was due to the adjustments in exposure possible with SER.

Shoulders

For the 65 comparison shoulder examinations, the radiologists were asked to compare the visibility of all anatomic detail of the humerus, scapula, and clavicle. The SER images

TABLE 1: Ratings of Scan Equalization Radiography (SER) and Conventional Radiography by Four Radiologists

Region Imaged	Rating				
	+2	+1	0	−1	−2
Cervical spine					
Anteroposterior (*n* = 14)					
C1–C2	23	28	5	0	0
C3–C7	7	19	26	4	0
Soft tissues	19	33	4	0	0
Oblique (*n* = 20)					
C1–C2	17	37	25	1	0
C3–C7	0	20	51	9	0
Soft tissues	20	30	29	1	0
Lateral (*n* = 47)					
C1–C2	31	75	79	2	1
C3–C7	25	63	83	16	1
Soft tissues	67	90	31	0	0
Subtotal	209	395	333	33	2
Shoulder (*n* = 65)					
Humerus	20	107	117	16	0
Scapula	23	131	95	11	0
Clavicle	47	127	73	12	1
Subtotal	90	365	285	39	1
Head (*n* = 63)					
Skull (*n* = 11)	9	19	14	2	0
Face (*n* = 22)	24	42	20	2	0
Mandible (*n* = 30)	20	60	38	2	0
Subtotal	53	121	72	6	0
Total (*n* = 209)	352	881	690	78	3

Note.—A rating of +2 means SER is much better than conventional radiography, +1 means SER is slightly better than conventional, 0 means SER is equal to conventional, −1 means SER is slightly worse than conventional, and −2 means SER is much worse than conventional.

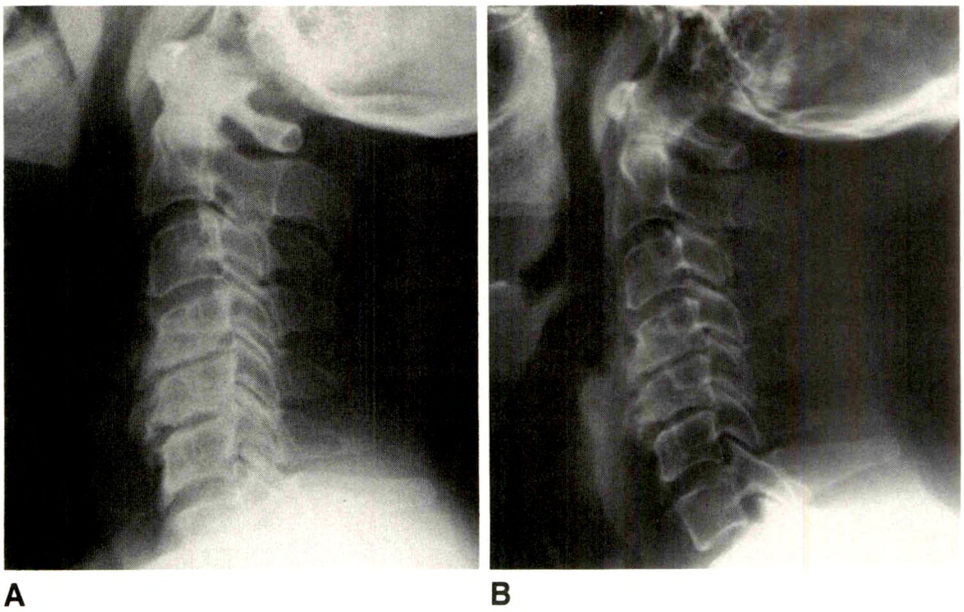

Fig. 1.—*A*, Conventional radiograph of cervical spine in a patient with severe degenerative arthritis.

***B*, Scan equalization radiograph shows better detail, especially of soft tissue, base of skull, and C7.**

were regarded as being either much better or slightly better than the conventional images 58% of the time. The SER images were equivalent 37% of the time, and 5% were found to be inferior. Examinations of the shoulder showed marked differences between the SER and conventional radiographs. With the SER technique, the soft tissues were seen uniformly. In many cases, the bony structures were seen optimally without the use of a bright light. An example in which all four radiologists thought the antomic detail was better with SER is shown in Figure 2.

Head

The 63 radiographic examinations of the head area included 11 radiographs of the skull, 22 of the face, and 30 of the mandible. The SER images were judged to be superior in 174 (69%) of the images, equivalent in 72 (29%), and inferior in six (2%) (Table 1).

Examinations of the head resulted in improved visibility of anatomic detail when examinations were performed not only of the skull but also of the face and mandible. The uniformity of exposure resulted in improved contrast and visibility, especially around the edges of the calvaria. The underexposure commonly seen in the thicker parts of the face and skull also was reduced. This is seen well in an example of the anteroposterior examination of the face (Fig. 3).

Table 2 is a summary of Table 1, grouped so that it is easier to compare the ratings of visibility in terms of percentages.

The preference of the individual radiologists for either the SER or conventional study is listed in Table 3; the categories of much better and slightly better and of much worse and slightly worse were grouped. Statistical analysis with the chi-square method showed a significant difference ($p < .05$) for all categories and radiologists except one.

Table 4 shows a summary of the data in Table 3, listing each radiologist's preferences for the images of the head, neck, and shoulder. The five categories were grouped into three because not all the radiologists found it easy to differ-

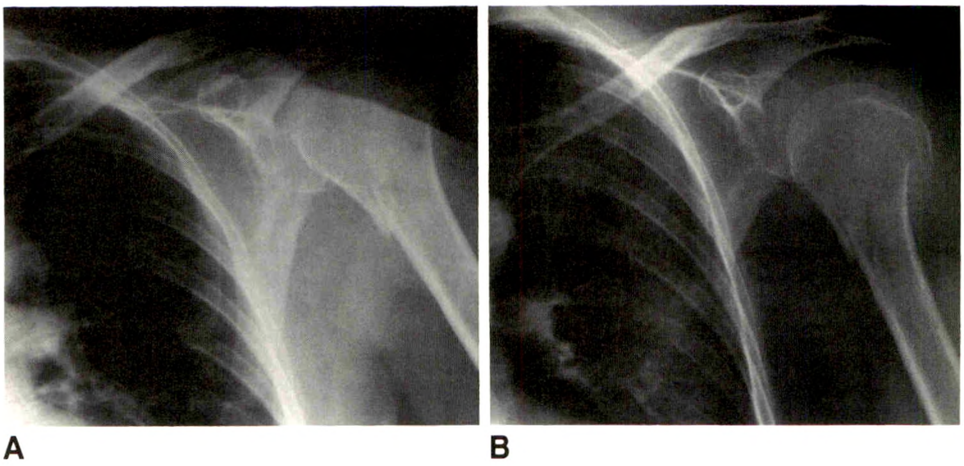

Fig. 2.—*A*, Conventional radiograph of shoulder in patient with fracture of humeral head shows overexposure of acromioclavicular joint.

B, Scan equalization radiograph shows better detail of soft tissue, acromioclavicular joint, and lateral part of humeral head.

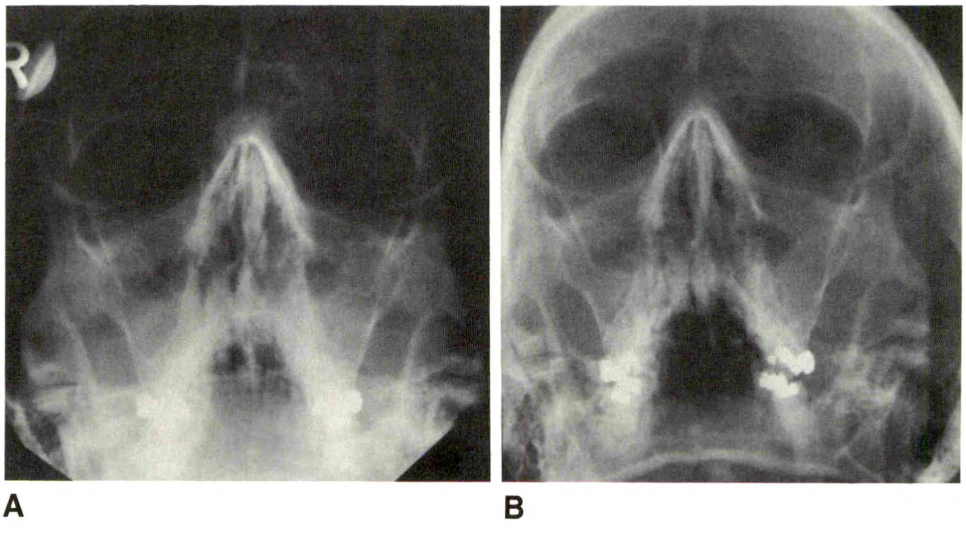

Fig. 3.—*A*, Conventional radiograph of face in patient with bilateral maxillary sinusitis.

B, Scan equalization radiograph shows more uniform exposure and improved contrast of all bony and soft-tissue structures.

entiate between slightly better and much better. Nonetheless, the difference between individual radiologists is still noticeable. The general trend was a preference for the SER images, ranging from 42% (radiologist 1) to 88% (radiologist 4) being judged as superior to the conventional images. Even though radiologists 1 and 4 had a different frequency of preference for the SER images, there was less of a difference in the opinion that the SER was rarely worse (2–11%) than the conventional image. There was a significant preference (chi square, $p < .05$) for SER by each individual radiologist when analyzed by body areas: cervical spine, shoulder, and head.

Diagnostic differences were noted in some comparison images, but the study did not include enough cases to observe statistical significance.

Discussion

The capability of SER to provide a more uniform exposure over the entire radiograph, regardless of variations in body tissue X-ray transmission, results in improved visibility of normal anatomic detail as judged by this subjective analysis by four radiologists. Despite the faster film-screen combination and higher-kilovoltage X-ray spectrum used for the SER images, the SER image quality was regarded as equivalent (34%) or superior (62%), with only a very few cases (4%) regarded as inferior. Most of the 4% of SER cases that were inferior were deemed so because of slight underexposure or differences in the positioning of the patients. Some of those SER examinations might have been repeated, but the protocol did not permit it. Some of the comparison conventional radiographic examinations were repeated. The frequency of repeat examinations was not recorded. We think that the primary value of the SER image is the consistency of image quality and exposure uniformity that is characteristic of all SER [4, 7]. Although anatomy that is overexposed on conventional radiographs can be visualized with a bright light, the consistency of exposure with SER precludes the need for bright lights and provides a significant increase in final image contrast owing to controlled film exposure at the peak film gradient.

TABLE 2: Ratings of Visibility of Anatomic Detail and Image Quality on Scan Equalization Radiography (SER) vs Conventional Radiography by Region

Region	Quality of SER Compared with Conventional Study (% of Images)		
	Better	Equal	Worse
Cervical spine	63	34	3
Shoulder	58	37	5
Skull	64	32	4
Face	74	24	2
Mandible	66	32	2
Average	62	34	4

The SER images were virtually free of artifacts. There were no scan lines or problems with overcompensation. The radia-

TABLE 3: Preference Ratings for Scan Equalization Radiographic (SER) Images by Individual Radiologists

Region/SER Rating	Radiologist No.			
	1	2	3	4
Skull				
Better	4	10	4	10
Equal	7	1	6	0
Worse	0	0	1[a]	1
Mandible				
Better	15	18	12	21
Equal	7	4	8	1
Worse	0	0	2	0
Facial bones				
Better	14	23	16	27
Equal	15	7	4	2
Worse	1	0	0	1
Humerus				
Better	14	39	26	48
Equal	51	26	25	15
Worse	0	0	14	2
Scapula				
Better	23	39	40	52
Equal	41	26	18	10
Worse	1	0	7	3
Clavicle/acromion				
Better	42	39	27	64
Equal	23	24	27	1
Worse	0	2	11	0
C1–C2				
Better	34	47	61	70
Equal	47	32	19	10
Worse	0	2	1	1
C3–C7				
Better	17	22	38	61
Equal	60	55	25	6
Worse	4	4	18	4
Soft tissue				
Better	48	56	74	78
Equal	33	25	6	3
Worse	0	0	1	0

Note.—Better = SER better than conventional radiography; equal = SER equal to conventional radiography; worse = SER worse than conventional radiography.

[a] Difference not statistically significant.

TABLE 4: Ratings of Visibility of Anatomic Detail and Image Quality by Individual Radiologists on Scan Equalization (SER) vs Conventional Radiographs

SER Rating	No. (%) of Images by Radiologist No.			
	1	2	3	4
Better than conventional radiography	211 (42)	291 (58)	298 (59)	441 (88)
Equal to conventional radiography	284 (57)	199 (40)	148 (30)	48 (10)
Worse than conventional radiography	6 (1)	8 (2)	55 (11)	12 (2)

tion dosage to the patient for each examination was approximately equal. Detailed radiation measurements were made of phantoms before the study. It was found with SER that the film and screen system, which was about twice as fast as the conventional one, required only slightly more radiation in the thicker areas and slightly less in the thin areas. Measurement of individual patient radiation exposure was not performed during the study because the unpublished phantom studies had provided sufficient information that the radiation exposure would be lower for head and shoulder examinations and would be similar for SER cervical spine examinations.

The amount of radiation to the patient may be slightly more or slightly less than in the conventional radiographic system. The important point is that, theoretically, with SER no radiation is wasted. Precisely the correct amount of radiation is always delivered because of the feedback system. There is never overexposure or underexposure. In our study, the SER system failed only a few times to provide optimal exposure. The limited radiation output in the experimental SER system could not provide sufficient output for the thickest body parts. Future SER systems should be designed to overcome this limitation.

This study was intended as an analysis of the quality of anatomic detail of head, neck, and shoulder examinations and does not address the question of the impact on overall diagnostic accuracy. It is difficult to determine why the radiologists preferred one image over another, but their opinions were consistent. In view of the definite improvement in overall image quality, we think that the potential for improved diagnostic accuracy will be similar to that observed in studies of chest radiography comparing SER with conventional imaging [7, 8].

It is anticipated that the fee charged for an SER examination will be similar to that of a conventional radiographic examination. It is hoped that the increase in cost of commercial equalization radiographic systems will be small. This SER prototype was designed to examine patients in the erect position, but patients also need to be examined while supine. Presumably, commercial systems will have this feature.

We anticipate that future clinical research with a careful, prospective study of hundreds of patients and normal subjects will compare equalization bone radiography with digital radiography and other new imaging methods. After further clinical testing, this theoretically ideal film radiography system may be the best alternative to expensive radiography.

REFERENCES

1. Plewes DB. A scanning system for chest radiography with regional exposure control: theoretical considerations. *Med Phys* **1984**;10:646–654
2. Plewes DB, Vogelstein EE. A scanning system for chest radiography with regional exposure control: practical implementation. *Med Phys* **1984**;10:654–663
3. Plewes DB. Scanning equalization radiography: a technical overview. In: Peppler WW, Alter AA, eds. *Proceedings of chest imaging conference 1987*. Madison, WI: Medical Physics Publishing, **1988**:30–41
4. Wandtke JC, Plewes DB, Vogelstein EE. Scanning equalization radiography of the chest: assessment of image quality. *AJR* **1985**;145:973–978
5. Wandtke JC, Plewes DB. Improved chest disease detection with scanning equalization radiography. *AJR* **1985**;145:979–983
6. Wandtke JC. Scanning equalization radiography: clinical results. In: Peppler WW, Alter AA, eds. *Proceedings of chest imaging conference 1987*. Madison, WI: Medical Physics Publishing, **1988**:42–48
7. Wandtke JC, Plewes DB. Comparison of scanning equalization and conventional chest radiography. *Radiology* **1989**;172:641–645
8. Vlasbloem H, Schultze Kool LJ. AMBER: a scanning multiple-beam equalization system for chest radiography. *Radiology* **1988**;169:29–34
9. Gray JE, Stears JG, Frank ED. Shaped lead-loaded acrylic filters for patient exposure reduction and imaging quality improvement. *Radiology* **1983**;146:825–828
10. Kelsey CA, Lane RG, Moseley RD, et al. Chest radiographs obtained with shaped filters: evaluation by observer performance tests. *Radiology* **1986**;159:653–655
11. Goodman LR, Foley WD, Wilson CR, et al. Digital and conventional chest images: observer performance with film digital radiography system. *Radiology* **1986**;158:27–33
12. Goodman LR, Foley WD, Wilson CR, Tikofsky RS, Hoffmann RG. Pneumothorax and other lung diseases: effect of altered resolution and edge enhancement on diagnosis with digitized radiographs. *Radiology* **1988**;167:83–88
13. Merritt CRB, Matthews CC, Scheinhorn D, Balter S. Digital imaging of the chest. *J Thorac Imaging* **1985**;1:1–13
14. Fuhrman CR, Gur D, Good B, Rockette H, Cooperstein LA, Feist JH. Storage phosphor radiographs vs conventional films: interpreters' perceptions of diagnostic quality. *AJR* **1988**;150:1011–1014
15. Fraser RG, Breatnach E, Barnes GT. Digital radiography of the chest: clinical experience with a prototype unit. *Radiology* **1983**;148:1–5
16. Sashin D, Sternglass EJ, Slasky BS, et al. Diode array digital radiography: initial clinical experience. *AJR* **1982**;139:1045–1050

Bacterial Osteomyelitis: Findings on Plain Radiography, CT, MR, and Scintigraphy

Richard H. Gold,[1] Randall A. Hawkins,[1] and Robert D. Katz[2]

Early detection of osteomyelitis is essential if appropriate therapy is to be started before bone devitalization. Although the ^{99m}Tc-methylene diphosphonate (MDP) bone scan may signify the possibility of osteomyelitis days or weeks before osseous changes are apparent on standard radiographs, the radiographic changes may provide important diagnostic clues. The ^{67}Ga-citrate scan augments the diagnostic value of the ^{99m}Tc-MDP scan, and the ^{111}In-labeled WBC scan is useful for detecting abscesses. CT aids in the detection of sequestra, and MR imaging is useful in defining the extent of the inflammatory process and in distinguishing osteomyelitis from cellulitis. In this article, we review and correlate the changes of bacterial osteomyelitis shown by these imaging methods.

Advances in imaging patients with bacterial osteomyelitis have improved the prognosis of the disease. In this article, we review and correlate the changes of bacterial osteomyelitis shown by various methods of imaging.

Plain Radiography

Because the clinical course of acute hematogenous osteomyelitis is rapid, early detection is essential if therapy is to be started before bone devitalization. Although changes on plain films occur relatively late in comparison with scintigraphic changes, plain radiography usually is the initial imaging examination and may provide important clues, such as the appearance of periosteal new bone (Fig. 1) and widening of the joint (Fig. 2). In infants, sonography is useful in confirming the presence of excess joint fluid, that, if drained early, obviates vascular tamponade and resultant osteonecrosis of the epiphysis. In childhood, the vascular metaphysis is the usual site of infection. After infancy, the physis prevents the spread of infection to the epiphysis (Fig. 3). Should the space-occupying exudate increase the intramedullary pressure and strip the periosteum, vascular thrombosis is followed by bone necrosis and formation of sequestra. Should an entire segment of bone become sequestrated, a thick sheath of periosteal new bone, or involucrum, may surround it. The infection

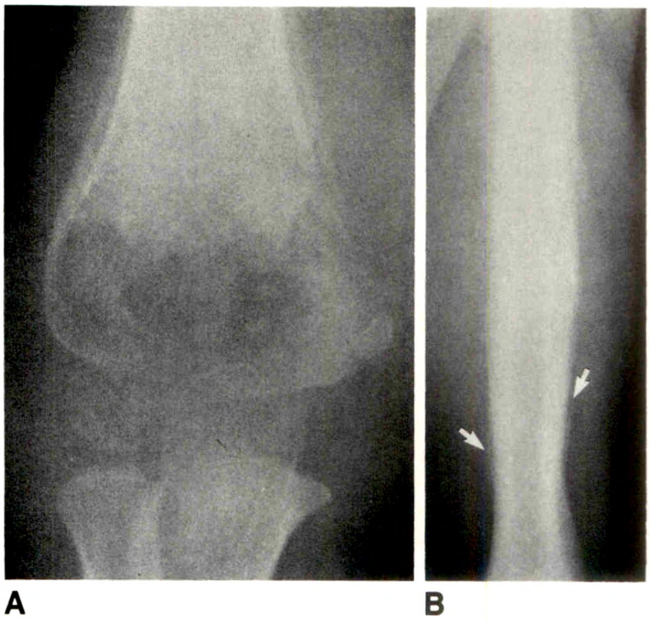

Fig. 1.—Anteroposterior radiographs show periosteal new bone: osteomyelitis vs malignancy.

***A*, Acute hematogenous staphylococcal osteomyelitis of humerus in a 7-year-old boy. Destructive changes are present in metaphysis. When activated by benign stimuli such as pus, blood, or edema, the inner layer of displaced periosteum produces uninterrupted new bone of uniform density.**

***B*, Ewing sarcoma of humerus in 18-year-old man. Periosteal new bone stimulated by underlying malignancy tends to be interrupted and not uniform, and may exhibit multiple delicate longitudinal layers or perpendicular spicules. The latter are reflected in fuzzy-appearing margins of mid shaft. Longitudinal layers ("onion skinning") terminate in Codman triangles (*arrows*), which commonly occur in association with Ewing sarcoma, but are uncommon with benign disease.**

Received January 15, 1991; accepted after revision March 11, 1991.

[1] Department of Radiological Sciences, University of California, School of Medicine, 10833 Le Conte Ave., Los Angeles, CA 90024. Address reprint requests to R. H. Gold.

[2] Department of Radiology, Beverly Hills Medical Center, 1177 S. Beverly Dr., Los Angeles, CA 90035.

***AJR* 157:365-370, August 1991** 0361-803X/91/1572-0365 © American Roentgen Ray Society

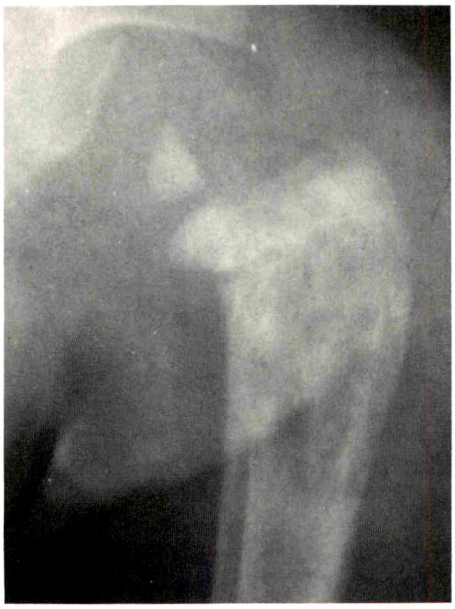

Fig. 2.—Anteroposterior radiograph of hematogenous osteomyelitis of humerus in a 10-month-old girl. In infants and children, osteomyelitis near end of a bone may cause joint to fill with a sympathetic effusion or exudate, leading to an increase in articular interspace. This phenomenon is uncommon in more constrained joints of adults. In infancy, transphyseal blood vessels may transmit infection from metaphysis to epiphysis, with secondary involvement of joint. A widened joint is obvious in this patient, as are destruction of humeral head and exuberant uniform periosteal new bone.

may perforate the involucrum in the form of a cloaca, leading to soft-tissue abscesses and sinus tracts. Because sequestra are foci for continued infection, their detection and excision are essential. Tomography or CT may be required to detect small sequestra. Ring sequestra may complicate pin-tract infections (Fig. 4) [1].

The onset of subacute hematogenous osteomyelitis (Brodie abscess) is insidious, and systemic manifestations are mild or absent (Fig. 5) [2]. Chronic osteomylitis results when there is continuation of the inflammatory process over many years, which leads to sclerosis and deformity.

Disorders associated with multifocal bacterial osteomyelitis include chronic granulomatous disease of childhood, immune deficiency disorders, sickle cell anemia and its variants (Fig. 6), IV drug abuse (Fig. 7), diabetes mellitus, and subacute bacterial endocarditis. Other predisposing factors are long-term indwelling urinary or vascular catheters and immunosuppressive therapy.

In contrast to nontuberculous osteomyelitis of the spine, tuberculous osteomyelitis has a more insidious onset and progression, and produces greater destruction and anterior wedging of the vertebral bodies. Tuberculous infection produces the larger soft-tissue ("cold") abscess (Fig. 8A). Tuberculosis of the spine may give rise to the aneurysmal syndrome (Fig. 8B) and calcific debris. Joint tuberculosis, unlike pyogenic infection, progresses very slowly, and is associated with the diagnostic triad of Phemister (Fig. 9). Tuberculosis in children tends toward multifocality and involvement of the short tubular bones (Fig. 10).

CT and MR Imaging

MR imaging is superior to CT for evaluating the extent of

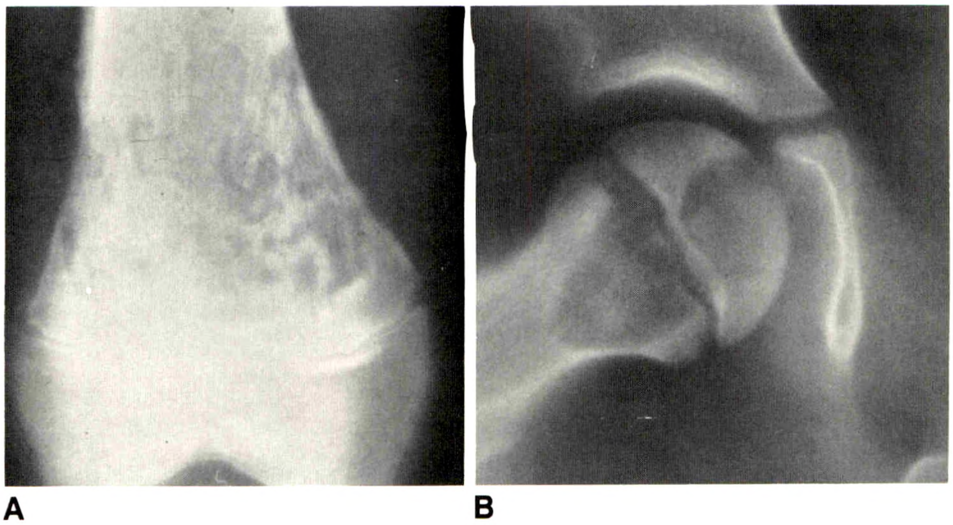

Fig. 3.—Tomograms show effect of physis as a barrier to spread of infection.

A, Staphylococcal osteomyelitis of femur in a 12-year-old girl. Serpentine foci of osteolysis in metaphysis and diaphysis represent abscess cavities. Disappearance of transphyseal blood vessels after infancy has allowed physis to prevent spread of infection to epiphysis.

B, Tuberculosis of the femur in a 7-year-old boy. As shown here, physis of older children is frequently breached by tuberculous infection. Alternatively, since metaphysis of hip joint is intracapsular, the infection might have spread to epiphysis by way of joint itself.

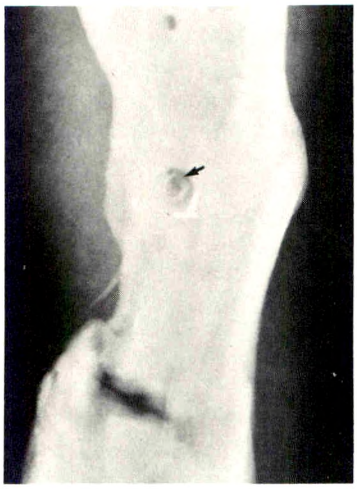

Fig. 4.—Radiograph shows ring sequestrum of pin-tract osteomyelitis complicating skeletal fixation of tibial fractures in a 25-year-old man. Diagnostic of a major pin-tract infection, necrotic ring of sclerotic bone (*arrow*) is separated from surrounding viable bone by exudate or granulation tissue. It is easily distinguished from clinically insignificant thermal osteonecrosis caused by high-speed drilling of a pinhole, which is characterized by a broad zone of sclerosis around the pin tract, but not by a separated ring; nor should it be confused with fluffy reparative bone in tract seen after pin removal.

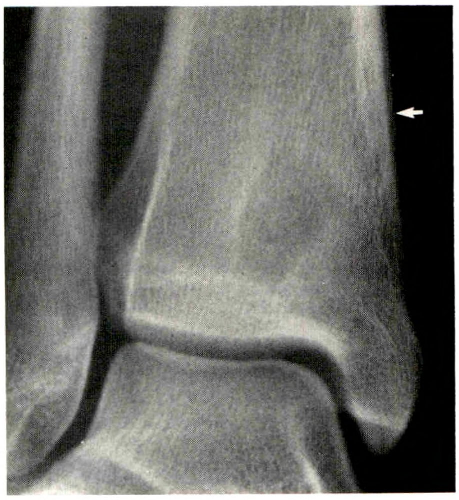

Fig. 5.—Brodie abscess in distal tibia of a 16-year-old girl. Oblique radiograph shows sharply marginated cavity. Sometimes cavity is surrounded by sclerosis. Soft-tissue swelling, while usually present, may be absent. Sequestra are uncommon and periosteal new bone inconspicuous (*arrow*). Abscess is characteristically found in lower tibial metaphysis in children and adolescents, and metaphysis or diaphysis of femur or tibia in adults. *Staphylococcus aureus* is the usual cause.

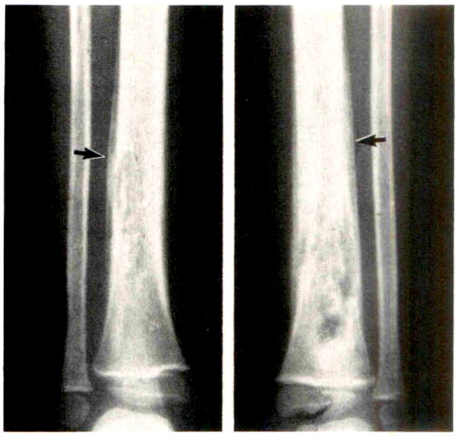

Fig. 6.—Anteroposterior radiograph shows changes of salmonellal osteomyelitis in tibias of a 3-year-old girl with sickle cell anemia. Susceptibility to hematogenous osteomyelitis is increased manyfold in patients with sickle cell anemia and related disorders. Approximately 50% of cases are caused by *Salmonella*. Osteomyelitis may occur within a region that has been previously devitalized by infarction. As in this case, multiple bones are frequently affected and lesions may be bilaterally symmetric. Thick and occasionally layered periosteal new bone (*arrows*) and longitudinal intracortical fissures may parallel extent of lesion. These findings, however, are not specific for osteomyelitis, and may accompany infarction alone.

infection. CT is superior to MR imaging for detection of sequestra (Fig. 11) and cloacae and can also depict intraosseous gas, an infrequent but reliable sign of osteomyelitis. However, in a collapsed vertebral body, a linear streak of gas merely signifies an intraosseous vacuum resulting from posttraumatic osteonecrosis (Kümmell disease). MR imaging aids in planning surgery by delineating sinus tracts and soft-tissue abscesses, by differentiating osteomyelitis from cellulitis, and by disclosing the extent of intramedullary involvement. MR is particularly helpful in the evaluation of the diabetic foot (Fig. 12) [3]. MR should be used only when it might provide information unavailable from less expensive imaging methods and when the results might affect management significantly. For evaluation of osteomyelitis, MR is as specific as or more specific and more sensitive than the three-phase ^{99m}Tc-methylene diphosphonate (MDP) bone scan (Fig. 13). The specificity of MR is increased by plain radiographic correlation and by obtaining both T1- and T2-weighted images. The edema and exudate of active infection have a low-intensity signal on T1-weighted images and a high-intensity signal on T2-weighted images.

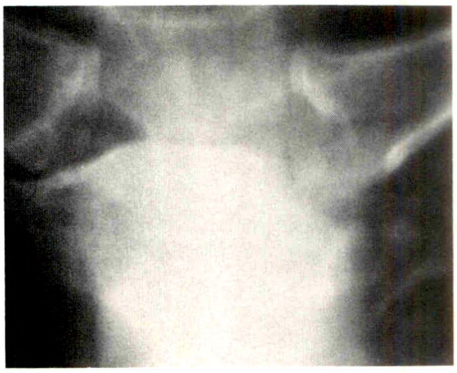

Fig. 7.—*Pseudomonas* infection of left sternoclavicular joint in a 30-year-old male heroin addict. Anteroposterior tomogram shows erosions and joint widening. An increased frequency of infection in IV drug abusers results from hematogenous spread from contaminated hypodermic needles. Spine, sacroiliac joint, sternoclavicular joint, and symphysis pubis, sites most commonly involved in order of decreasing prevalence, represent the four S's of osteomyelitis associated with IV drug abuse. In some series, Gram-negative organisms such as *Pseudomonas* and *Klebsiella* have predominated, while in others *Staphylococcus aureus* has been the organism most frequently cultured.

Scintigraphy

Radionuclide studies useful in examining patients with suspected osteomyelitis include the ^{99m}Tc-MDP scan, ^{111}In-labeled WBC scan, and ^{67}Ga-citrate scan [4]. The ^{99m}Tc-MDP bone scan may signify the possibility of osteomyelitis days or weeks before osseous changes are apparent on standard radiographs. ^{99m}Tc-MDP bone scans are sensitive indicators of altered osteoblastic activity, but local disturbances in vascular perfusion, clearance rate, permeability, and chemical binding also affect imaging. On standard ^{99m}Tc-MDP scans it sometimes may be difficult to differentiate soft-tissue uptake from bone uptake in patients with known cellulitis and possible underlying osteomyelitis. To address this problem, the three-phase ^{99m}Tc-MDP scan was developed, consisting of dynamic "flow" or "angiogram" images, blood-pool images, and 2- to 5-hr delayed images (Fig. 13). Cellulitis is characterized by an initially high soft-tissue uptake in the flow phase, and progressively lower uptake compared with bone uptake in later phases. In contradistinction, osteomyelitis gives rise to progressively increasing bone uptake over the course of the study. The combination of cellulitis and osteomyelitis produces increased bone and soft-tissue uptake in all three phases. The ^{99m}Tc-MDP scan is not specific for osteomyelitis, and in the appropriate clinical setting may suggest but cannot conclusively establish the diagnosis. A fourth phase (imaging 24 hr after infection) may be useful in patients with equivocal results at the end of three phases, as osteomyelitis usually

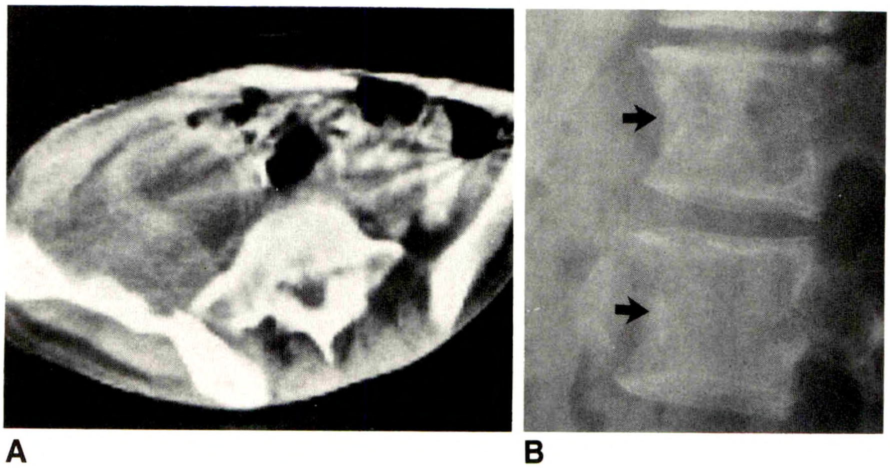

Fig. 8.—Tuberculosis of spine.

A, CT scan shows erosion of right ilium by a cold iliopsoas abscess that extended from spine to pelvis. Patient was a 23-year-old man with a 7-month history of pain and weakness of right lower limb.

B, Lateral radiograph of lumbar spine in a 45-year-old man shows aneurysmal syndrome due to tuberculosis. Although narrowing of intervertebral disk usually is earliest radiographic feature of both nontuberculous and tuberculous osteomyelitis, scalloping of anterior (and sometimes lateral) margin (*arrows*) of vertebral bodies (aneurysmal syndrome) is associated only with tuberculous infection. Aneurysmal syndrome is so-called because concavities simulate those caused by transmitted pulsations of an aortic aneurysm. Scalloped vertebrae lie within an abscess cavity.

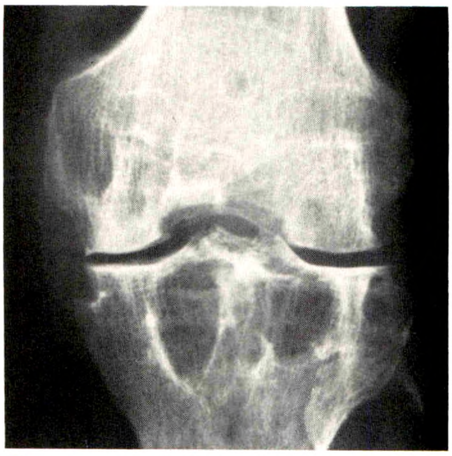

9

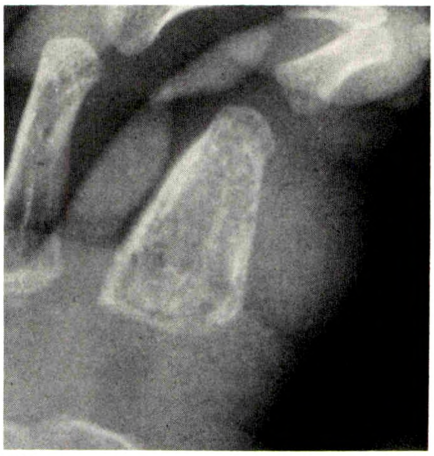

10

Fig. 9.—Anteroposterior radiograph of tuberculosis of the knee in a 46-year-old man. Tending to have a more insidious onset than nontuberculous septic arthritis, tuberculous arthritis is also associated with profound osteoporosis, marginal erosions, and long-standing preservation of contacting articular cartilage, the diagnostic triad of Phemister. Rarefactions in subchondral bone of tibia reflect undermining by tuberculous pannus.

Fig. 10.—Radiograph of tuberculous dactylitis in a 1-year-old boy. In children, tuberculosis has a tendency toward multifocality and involvement of short tubular bones. Lesion of tuberculous dactylitis, unlike tuberculosis of long bones, tends not to invade adjacent joints. In proximal phalanx of index finger, shown here, slow elaboration of periosteal new bone that accompanied gradual resorption of inner surface of cortex led to a typically expanded fusiform appearance called *spina ventosa* (literally, a wind-filled projection, such as a finger).

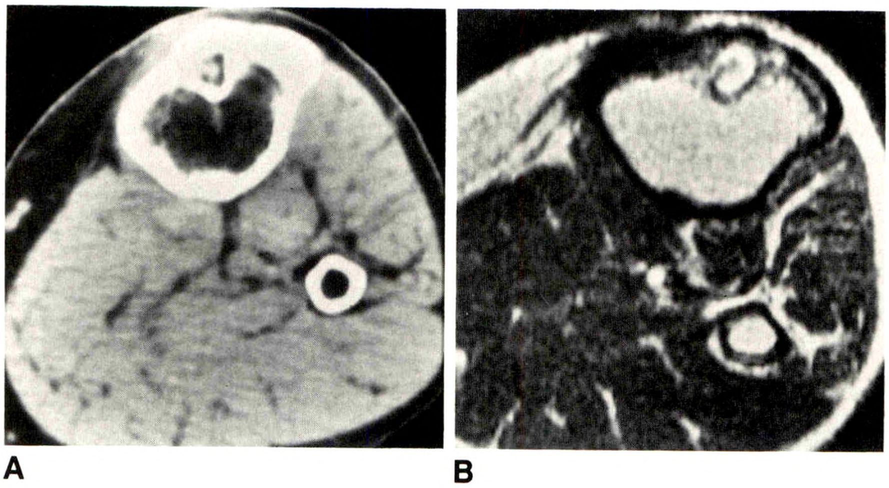

Fig. 11.—Chronic osteomyelitis with sequestrum of proximal tibia. Six years earlier, this 30-year-old man had a fracture of distal tibia that became infected after fixation with an intramedullary rod. Rod was subsequently removed. Current radiographs disclosed sclerotic reactive bone outlining track of former rod. Corresponding ^{99m}Tc-MDP bone scan revealed striking increase in activity in proximal tibia.

A, CT scan of proximal tibia shows rod track surrounded by a thick, sclerotic rim and containing a central sequestrum. Adjacent marrow appears normal.

B, Axial MR image (SE 1500/56) shows a bright, high-intensity abscess in rod track, with a central low-intensity sequestrum and a rim of low-intensity sclerotic bone. These findings, together with absence of high signal intensity in adjacent marrow and soft tissues, imply that active infection is present only in rod track.

provokes further increase in activity. Single-photon emission CT bone scans provide additional anatomic information.

Although the overall sensitivity of the ^{99m}Tc-MDP scan for active osteomyelitis is high (approximately 95%), false-negative diagnoses may occur, particularly in neonates. Both the ^{111}In-labeled WBC scan and the ^{67}Ga scan are useful adjuncts, and while usually no more sensitive than the combination of ^{99m}Tc-MDP bone scans and plain radiographs in detecting osteomyelitis, they are more specific (Figs. 14 and 15). The ^{111}In-WBC scan, although positive in some noninfected frac-

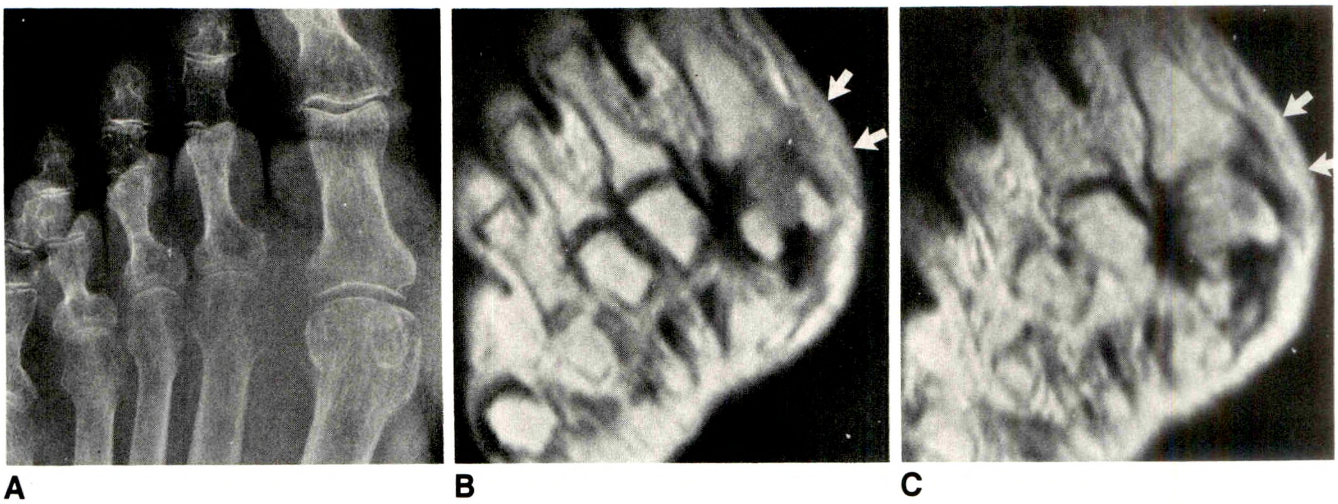

Fig. 12.—Differential diagnosis in this 84-year-old diabetic woman includes neuropathic osteoarthropathy, cellulitis, pyarthrosis, and osteomyelitis.

A, Anteroposterior radiograph of foot shows striking osteoporosis and possible erosion of medial margin of head of second metatarsal. Results of three-phase ^{99m}Tc-MDP bone scan were equivocal.

B and *C*, T1-weighted (SE 500/28, *B*) and T2-weighted (SE 1500/56, *C*) coronal MR images show normal signal intensity in bones and joints adjacent to clinically suspicious areas, thereby excluding osteomyelitis and pyarthrosis. Neuropathic osteoarthropathy is also unlikely in absence of joint effusions. Soft tissues medial to first metatarsophalangeal joint (*arrows*) have decreased signal intensity on T1-weighted image and increased intensity on T2-weighted image, consistent with cellulitis.

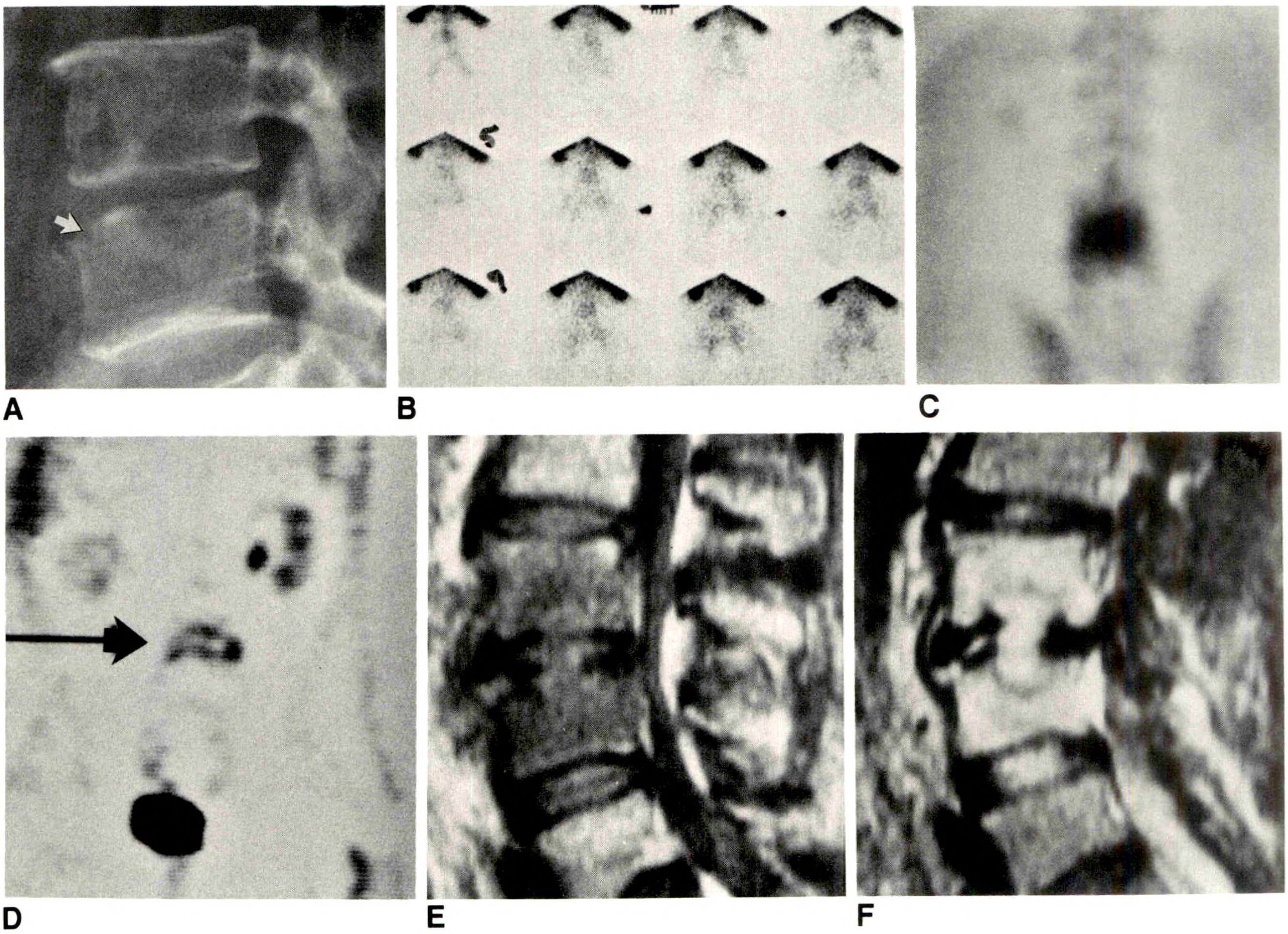

Fig. 13.—Acute hematogenous osteomyelitis of lumbar spine in a 59-year-old man, proved by biopsy. Comparison of imaging techniques.

A, Lateral radiograph shows narrowing of L3–L4 disk, osteolytic foci next to endplates, and erosion of superior endplate of L4 (*arrow*).

B and *C*, Three-phase ^{99m}Tc-MDP bone scan shows a corresponding gradual increase in activity in dynamic flow phase (*B*), which becomes even more intense on 5-hr postinjection image (*C*).

D, PET scan in coronal plane, performed as part of an investigational study approved by the Human Subjects Protection Committee, shows a corresponding mild increase in activity (*arrow*) due to a focus of leukocytes preferentially metabolizing glucose from IV-infused FDG.

E, T1-weighted sagittal MR image (SE 500/28) shows relatively high-intensity fatty marrow has been replaced by edema of intermediate intensity in bodies of L4 and L5, and adjacent endplates have undergone central destruction.

F, T2-weighted sagittal image (SE 2000/84) shows involved vertebrae have a high-intensity signal. An even more intense focus centered at intervertebral disk represents an abscess.

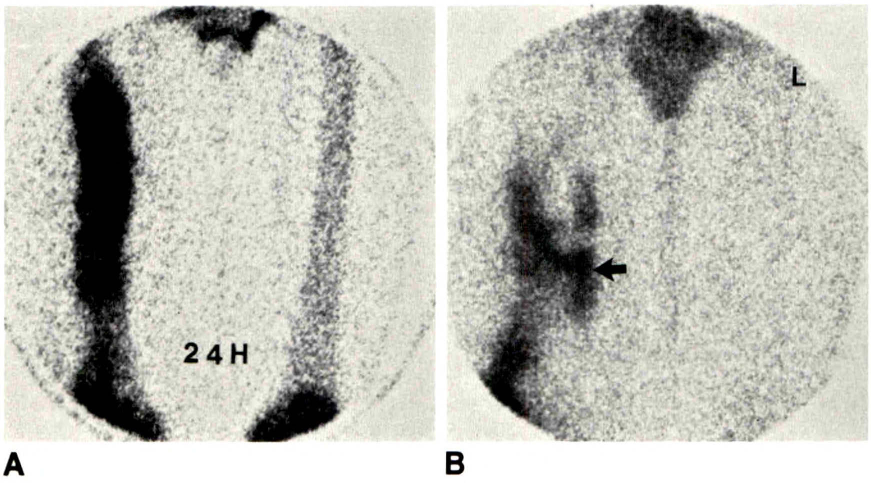

Fig. 14.—Usefulness of sequential ^{99m}Tc-MDP and ^{67}Ga scans in evaluating suspected chronic osteomyelitis. Eleven years earlier, a 34-year-old man had a fracture of the right femur that was stabilized with an intramedullary rod. One year later, fracture healed and rod was removed. Since then, he had had intermittent thigh discomfort that had increased during the past 6 months. New radiographs disclosed diffuse cortical thickening and mottled sclerosis of middle third of femur.

***A*, A ^{99m}Tc-MDP four-phase scan shows progressively increasing bone and soft-tissue activity throughout flow, blood-pool, and 4-hr phases, culminating in strikingly increased activity in femoral shaft on this 24-hr delayed image.**

***B*, Additional evidence of chronic osteomyelitis, as well as a soft-tissue abscess, is provided by a ^{67}Ga scan showing focus of intense activity extending from medial soft tissues (*arrow*) to femur.**

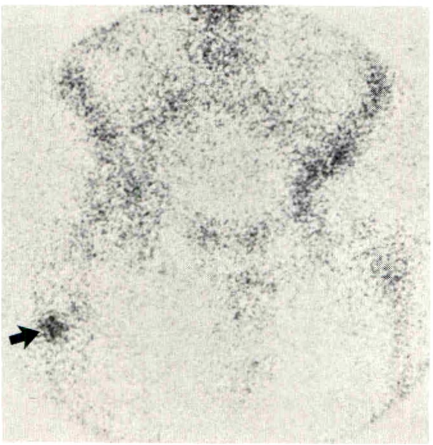

Fig. 15.—Abscess, complicating total hip arthroplasty, shown by ^{111}In-WBC scan. Fever and thigh pain developed 10 years after surgery in a 62-year-old man. Aspiration of joint yielded *Staphylococcus aureus*. ^{111}In-WBC scan shows an intense focus of activity (*arrow*) in abscess.

tures, still tends to be preferred over the ^{67}Ga scan because of its greater specificity for infection. The sensitivity of the ^{111}In-WBC scan is greater for acute than for chronic infection, whereas the ^{67}Ga scan is equally sensitive for both.

Positron emission tomography (PET) produces images of the skeletal system by using IV-infused fluorine-18, which, like ^{99m}Tc-MDP, is taken up by bone in proportion to osteoblastic activity and local vascular and physical factors. Although the PET bone scan is anatomically and quantitatively more precise than the MDP scan, it is not more specific for osteomyelitis. Because neoplasms tend to metabolize glucose to a greater extent than do inflammatory processes, the added use of 2-[^{18}F]-fluoro-2-deoxy-D-glucose (FDG) increases the specificity of PET. Osteomyelitis nevertheless may yield an abnormal finding on PET body scans (Fig. 13).

REFERENCES

1. Nguyen VD, London J, Cone RO III. Ring sequestrum: radiographic characteristics of skeletal fixation pin-tract osteomyelitis. *Radiology* **1986**;158:129–131
2. Miller WB Jr, Murphy WA, Gilula LA. Brodie abscess: reappraisal. *Radiology* **1979**;132:15–23
3. Yuh WTC, Carson JD, Baraniewski HM, et al. Osteomyelitis of the foot in diabetic patients: evaluation with plain film, ^{99m}Tc-MDP scintigraphy, and MR imaging. *AJR* **1989**;152:795–800
4. Gupta NC, Prezio JA. Radionuclide imaging in osteomyelitis. *Semin Nucl Med* **1988**;18:287–299

Synthetic vs Human Surfactants in the Treatment of Respiratory Distress Syndrome: Radiographic Findings

Deborah Levine[1]
David K. Edwards III[1,2]
T. Allen Merritt[2,3]

Exosurf, a synthetic surfactant, was instilled endotracheally in 49 neonates as treatment for respiratory distress syndrome. The radiologic courses of these neonates were compared with the courses of 18 neonates previously treated with human surfactant and of 18 untreated neonates. The radiologic severity of respiratory distress syndrome decreased significantly in neonates treated with Exosurf compared with that in untreated neonates. Radiologic improvement in those treated with Exosurf was slightly delayed when compared with the improvement of age-matched neonates treated with human surfactant. Otherwise no significant difference was noted between Exosurf and human surfactant in radiologic severity of respiratory distress syndrome or in the prevalence of pulmonary interstitial emphysema, pneumothorax, and bronchopulmonary dysplasia.

These findings support the thesis that artificial surfactant is an acceptable substitute for surfactants of biological origin, with possible benefits of safety and ease of use.

***AJR* 157:371-374, August 1991**

The endotracheal application of exogenous surfactants is variably effective in treating respiratory distress syndrome (RDS) in preterm neonates [1-4]. Exosurf Neonatal (Burroughs Wellcome, Research Triangle Park, NC) is a synthetic surfactant that has recently been approved by the United States Food and Drug Administration. Because it is a synthetic preparation, the difficulties in purifying and standardizing lipid mixtures extracted from biological materials are avoided. The potential risks of immunologic reactions and infectious agents that are possible with lung extracts and human and animal proteins are avoided also [5, 6].

The chest radiograph is useful and reliable in assessing the severity of RDS [7-9] and in evaluating the changes in RDS associated with treatment with human [10] and bovine [11-13] surfactants. We previously compared findings on chest radiographs of neonates with RDS who were treated with human surfactant with findings on radiographs of similar neonates treated with placebo [10]. We undertook the present study to evaluate the hypothesis that neonates treated with synthetic surfactant exhibit radiologic changes similar to those reported for neonates treated with human surfactant.

Materials and Methods

The patients treated with Exosurf were consecutive preterm neonates (gestational age, 25-36 weeks) born between October 6, 1989, and August 7, 1990, in whom RDS was diagnosed on the basis of clinical criteria (respiratory distress and respiratory failure requiring ventilatory assistance with an a/Ao_2 ratio < 0.22 2-24 hr after birth—the a/Ao_2 ratio is a unitless ratio defined as the arterial carbon dioxide partial pressure divided by the dry fraction of inspiratory oxygen minus the arterial carbon dioxide partial pressure: $Paco_2/[Fio_2\ (760 - 47) - Paco_2]$) and for whom parental informed consent was available. Of these 51 patients, the radiographs of one were lost, and one had no films exposed after surfactant administration; these two patients were excluded.

Received December 26, 1990; accepted after revision March 12, 1991.

---

[1] Department of Radiology (H-756), University of California, San Diego, Medical Center, 225 Dickinson St., San Diego, CA 92103. Address reprint requests to D. K. Edwards.

[2] Department of Pediatrics, University of California, San Diego, Medical Center, 225 Dickinson St., San Diego, CA 92103.

[3] Present address: University of California, Davis, Medical Center, 2516 Stockton Blvd., Sacramento, CA 95817.

0361-803X/91/1572-0371
© American Roentgen Ray Society

Exosurf Neonatal is a 13.5:1.5:1.0 mixture of dipalmitoyl-phosphatidylcholine, hexadecanol, and tyloxapol. For treatment, the surfactant was reconstituted with 8 ml of distilled water and administered endotracheally in a dose of 5 mg/kg body weight (54 mg/kg of dipalmitoyl-phosphatidylcholine). In order to promote uniform distribution, half the dose was given with the patient turned 45° to the left and half with the patient similarly turned to the right. A second dose was given 12 hr after the first dose.

The initial chest radiographs were a supine anteroposterior and horizontal-beam lateral view collimated from the chin to the umbilicus; subsequent films were anteroposterior only, collimated to the chest. Film was TML 1 (Kodak, Rochester, NY) with a Lanex fine screen (Kodak) with film factors that varied with the patient's size (approximately 2 mAs at 55 kVp). A 102-cm focus-film distance on a mobile machine (General Electric, Waukesha, WI) was used, with exposure timed to the end-inspiration phase of the ventilator or during quiet breathing for patients not receiving assisted ventilation. Films were exposed only as clinically indicated.

All chest radiographs for each patient were evaluated retrospectively by one of the authors and by a pediatric radiologist working concurrently without knowledge of the time of surfactant administration. Films were scored for the severity of RDS by using a previously described method [10] that assigns higher scores for more severe RDS (Table 1). Films were also examined for evidence of air leaks.

After the radiographs were evaluated, the times of surfactant administration were determined from the medical record. Films were divided into 0–5.9 hr, 6–11.9 hr, 12–23.9 hr, and 24–48 hr after-treatment groups, and radiologic severity scores were statistically analyzed by using films exposed during these periods after surfactant administration. If more than one film was taken during a given period, the average time and score were treated as a single datum.

Comparison was made with 18 neonates treated with human surfactant and with 18 neonates treated with randomized placebo (air) reported previously [10]. These neonates were generally similar to those treated with Exosurf, except for gestational age (<30 weeks), a more stringent clinical definition of RDS ($a/Ao_2 < 0.15$), and exclusion of neonates with suspected sepsis. Because the previous study included only neonates of less than 30 weeks' gestation, the Exosurf-treated neonates were considered both as a total group (49 neonates) and as a subgroup of less than 30 weeks' gestation (29 neonates).

The final radiographs of 11 Exosurf patients who were radiographed when 28 days old or older were examined for changes suggesting bronchopulmonary dysplasia [14], and these results were compared with the prevalence of bronchopulmonary dysplasia in the previous study.

Statistical methods included Student's t test and chi-square test.

Results

Exosurf-treated neonates were significantly older and larger than the neonates treated with human surfactant and the untreated neonates were [10]. The Exosurf-treated neonates of less than 30 weeks' gestation were not significantly different from these patients. Characteristics of the patients in these groups are shown in Table 2.

The scores of the severity of RDS on radiographs for these groups are presented in Figure 1; note that the time scale begins at birth, whereas the statistical analyses of severity scores were performed with respect to time since surfactant administration. At no time were the scores of the groups treated with Exosurf and human surfactant significantly different, and both showed significant improvement ($p < .025$) after surfactant treatment compared with untreated neonates. However, the neonates of less than 30 weeks' gestation treated with Exosurf took slightly longer to respond to surfactant than did the group treated with human surfactant. Compared with improvement in the untreated group, the improvement in Exosurf-treated neonates of less than 30 weeks' gestation did not become statistically significant until 6.0–11.9 hr after treatment ($p < .005$), whereas those treated with human surfactant showed significant improvement by 5.9 hr after treatment ($p < .025$).

Air leaks developed in nine (18%) of the Exosurf-treated neonates; all nine had pulmonary interstitial emphysema, and two had pneumothorax also. Of the 29 neonates of less than 30 weeks' gestation, air leaks developed in seven (24%), which was not significantly different by chi-square test from patients treated with human surfactant (11%) or untreated control subjects (44%).

Among all neonates radiographed by approximately 28 days after birth, changes suggesting bronchopulmonary dysplasia were seen in all groups (Table 2). These did not differ

TABLE 1: Radiographic Scoring System for the Severity of Respiratory Distress Syndrome

Score	Granularity	Air Bronchograms	Cardiac and Diaphragmatic Silhouettes	Aeration
1	Faint, requiring close observation to detect	None beyond center of chest	Sharp	Normal
2	Easily seen	Faint at the bases	Sharp	Normal
3	Prominent; light and dark areas of lung approximately equal	Obvious	Slightly fuzzy	Normal to slightly decreased
4	Marked; lungs substantially more light than dark	Marked	Indistinct	Decreased
5	Lungs essentially opaque	Sharp and distinct or absent	Indiscernible	Impossible to assess

Note.—Reproduced with permission from Edwards et al. [10].

TABLE 2: Characteristics of Exosurf Neonatal–Treated, Human Surfactant–Treated, and Untreated Neonates

	Exosurf-Treated		Human Surfactant-Treated (n = 18)	Untreated (n = 18)
	Total (n = 49)	<30 Weeks' Gestation (n = 29)		
Mean birth weight (g)	1481	1071	1029	1074
Mean gestational age (weeks)	29.7	27.7	27.7	28.5
Male/female ratio	27/22	17/12	9/9	10/8
Mean age at first treatment (hr)	7.7	6.0	6.1	—
Number died	9	8	0	4
Number with air leaks	9	7	2	8
Number radiographed ≥28 days after birth	11	11	12	12
Abnormalities suggesting BPD	9	9	6	9
Radiologically mild BPD	4	4	4	3
Radiologically moderate BPD	3	3	2	2
Radiologically severe BPD	2	2	0	4
Radiologically normal chest	2	2	6	2

Note.—BPD = bronchopulmonary dysplasia.

significantly between groups in either prevalence or radiologic severity. Bronchopulmonary dysplasia did not develop in any of the 20 Exosurf-treated neonates of more than 30 weeks' gestation.

Causes of death in the Exosurf-treated neonates were sepsis (three cases), disseminated intravascular coagulopathy (one), exsanguination after central venous catheter placement at the referring institution (one), respiratory failure (two), and intraventricular hemorrhage (two). None of these deaths were attributed to surfactant administration.

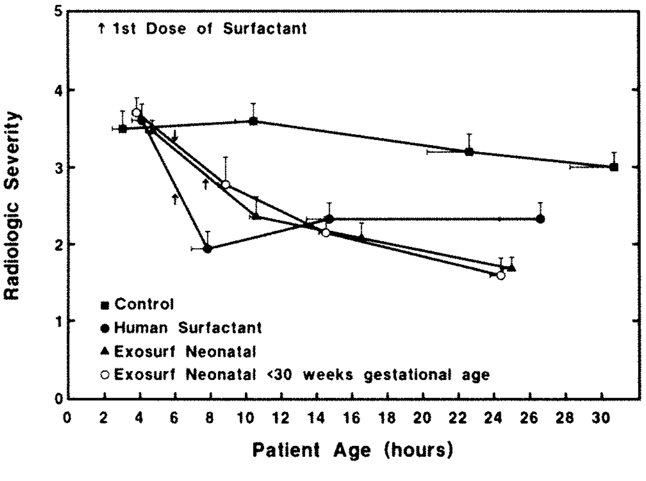

Fig. 1.—Scores of the radiologic severity of respiratory distress syndrome (RDS) in neonates treated with Exosurf Neonatal, human surfactant, and placebo. Higher scores reflect radiologically more severe RDS. Arrows indicate average times of surfactant administration. Bars indicate standard error of mean.

Discussion

Radiologic improvement of neonates with RDS after administration of human and bovine surfactant has been well documented in the literature [10–13]. Similar improvement occurs with Exosurf, which is a completely synthetic surfactant. The slight lag (approximately 6 hr) in response to Exosurf seen in neonates of less than 30 weeks' gestation is consistent with findings showing that Exosurf has physiochemical properties that approach but do not equal those of purified natural lung surfactant [6]. This lag time could be clinically important if pulmonary interstitial emphysema or other complications that would increase morbidity or mortality rates developed during this time.

The lack of difference in radiologic severity between the entire Exosurf-treated group and patients treated with human surfactant may be related to the fact that some of the more mature Exosurf-treated patients may have had relatively mild RDS; the criterion for Exosurf therapy ($a/A_{O_2} < 0.22$) was less stringent than the one for human surfactant therapy ($a/A_{O_2} < 0.15$). Neonates with relatively mature lungs would be expected to improve more rapidly than less mature neonates, regardless of treatment. This speculation is supported by the fact that bronchopulmonary dysplasia, which is generally considered to be a multifactorial complication of oxygen and ventilator therapy, did not develop in any of the more mature Exosurf-treated patients.

Number of deaths among the Exosurf-treated population (nine) were not significantly different from the number of deaths in the human surfactant–treated (zero) and untreated (four) populations, probably in part because of the small numbers of patients studied. A contributing reason may have been that the human surfactant study excluded neonates with signs of sepsis, whereas the Exosurf study did not; three of the Exosurf-treated neonates died of sepsis.

A major source of morbidity and mortality in neonates with RDS is intracranial hemorrhage. The prevalence of this disorder in our patients was not examined in this study because it appears well established in many trials that the administration of surfactant does not influence its prevalence [15].

In three patients treated with human surfactant, a transient interstitial lung disease developed [10]; this was not observed after administration of Exosurf, nor were findings suggestive of asymmetric surfactant deposition.

The validity of comparing Exosurf-treated patients with neonates treated 5 years earlier may be questioned. However, other than the composition of the exogenous surfactant, no major changes in the treatment of neonates with RDS have taken place in our nursery. Also, the pediatric principal investigator and the primary pediatric radiologist were the same in both studies.

Our results suggest that Exosurf, by radiologic criteria, is nearly as effective as human surfactant in ameliorating RDS. The availability, ease of preparation, and minimal expected harmful side effects from immunologic and infectious agents make Exosurf a potentially valuable therapeutic aid in the treatment of RDS.

REFERENCES

1. Enhoming GE, Shennan A. Possmayer F, Dunn M, Chen CP, Milligan J. Prevention of neonatal respiratory distress syndrome by tracheal instillation of surfactant: a randomized clinical trial. *Pediatrics* **1985**;76:145-153
2. Gitlin JD, Soll RF, Parad RB, et al. Randomized controlled trial of exogenous surfactant for the treatment of hyaline membrane disease. *Pediatrics* **1987**;79:31-37
3. Raju TNK, Vidyasagar D, Bhat R, et al. Double-blind controlled trial of single-dose treatment with bovine surfactant in severe hyaline membrane disease. *Lancet* **1987**;1:651-655
4. Smyth JA, Metcalfe IL, Duffty P, Possmayer F, Bryan MH, Enhorning G. Hyaline membrane disease treated with bovine surfactant. *Pediatrics* **1983**;71:913-917
5. Durand DJ, Clyman RI, Heymann MA, et al. Effects of a protein-free, synthetic surfactant on survival and pulmonary function in preterm lambs. *J Pediatr* **1985**;107:775-780
6. Tooley JA, Clements K, Muramatsu CL, Brown CL, Schlueter MA. Lung function in prematurely delivered rabbits treated with a synthetic surfactant. *Am Rev Respir Dis* **1987**;136:651-656
7. Kero PO, Makinen EO. Comparison between clinical and radiological classifications of infants with the respiratory distress syndrome. *Eur J Pediatr* **1979**;130:271-278
8. Tudor J, Young L, Wigglesworth JS, Stiner RE. The value of radiology in the idiopathic respiratory distress syndrome: a radiological and pathological correlation study. *Clin Radiol* **1976**;27:65-75
9. Weller MH. The roentgenographic course and complications of hyaline membrane disease. *Pediatr Clin North Am* **1973**;20:381-406
10. Edwards DK, Hilton SvW, Merritt TA, Hallman M, Mannino F, Boynton BR. Respiratory distress syndrome treated with human surfactant: radiographic findings. *Radiology* **1985**;157:329-334
11. Clarke EW, Siegle RL, Gong AK. Findings on chest radiographs after prophylactic pulmonary surfactant treatment of premature infants. *AJR* **1989**;153:799-802
12. Mortensson W, Noack G, Curstedt T, Herin P, Robertson B. Radiologic observations in severe neonatal respiratory distress syndrome treated with the isolated phospholipid fraction of natural surfactant. *Acta Radiol* **1987**;28:389-394
13. Wood BP, Sinkin RA, Kendig JW, Notter RH, Shapiro DL. Exogenous lung surfactant: effect on radiographic appearance in premature infants. *Radiology* **1987**;165:11-13
14. Edwards DK. Radiographic aspects of bronchopulmonary dysplasia. *J Pediatr* **1979**;95:823-829
15. Leviton A, VanMarter L, Kuban KCK. Commentary. Respiratory distress syndrome and intracranial hemorrhage: cause or association? Inferences from surfactant clinical trials. *Pediatrics* **1989**;84:915-922

Pictorial Essay

CT of the Pancreas in Children

Thomas E. Herman[1] and Marilyn J. Siegel

CT has become a frequently used imaging method for evaluating suspected pancreatic disease in children. Although the spectrum of CT findings in pancreatic disease is well documented in adults, there is a paucity of such information in children. Familiarity with CT patterns of pancreatic disease in childhood is important for diagnosis. In this essay, we illustrate the CT findings of pancreatic lesions in children.

Developmental Anomalies

Anomalies of pancreatic development include short pancreas, pancreas divisum, and anular pancreas. Congenitally short pancreas is believed to be due to agenesis of the dorsal pancreas. On CT, only the head of the pancreas is visible; the neck, body, and tail are absent. The pancreas that develops has a globular configuration (Fig. 1). In pancreas divisum, separate dorsal and ventral pancreatic moieties may be defined with thin-section CT. In anular pancreas, CT shows apparent thickening of the second portion of the duodenum caused by the surrounding pancreatic head (Fig. 2).

Hereditary Diseases

Cystic fibrosis is an autosomal-recessive condition, and 85% of patients have exocrine pancreatic insufficiency. On CT, the pancreas is usually small, with an attenuation value equal to that of fat, reflecting postobstructive necrosis, fibrosis, and fatty infiltration (Fig. 3). Fibrosis without fatty infiltration is less common. Other findings include single or multiple large cysts, referred to as pancreatic cystosis (Fig. 4); parenchymal calcifications (Fig. 5); and ductal dilatation [1].

Schwachman syndrome is an autosomal-recessive condition characterized by exocrine pancreatic insufficiency, neutropenia, bone marrow dysfunction, and metaphyseal chondroplasia. Affected patients have failure to thrive, diarrhea, and steatorrhea. The pancreas is replaced by fat (Fig. 6) and initially enlarged; later it tends to be normal in size or small.

Hereditary pancreatitis is an autosomal-dominant disease with a penetrance of 40–80%. This disorder is characterized by recurrent attacks of acute pancreatitis. The most striking CT manifestations are ductal dilatation, averaging 1.8 cm, and large, round calcifications located in the main pancreatic duct (Figs. 7 and 8). Pancreatic atrophy is usually present. Complications include pancreatitis, pseudocysts, and adenocarcinoma.

Von Hippel–Lindau disease is an autosomal-dominant disease characterized by retinal angiomatosis, cerebellar hemangioblastoma, and cysts in various organs. Pancreatic cysts are either simple cysts or mucinous cystadenomas. They tend to be multiple and involve the pancreatic body and tail (Fig. 9). Large cysts may lead to obstruction of the common bile duct. Rarely, calcifications occur.

Trauma

The spectrum of CT findings in pancreatic injuries includes pancreatitis, laceration, and transection [2]. The CT changes of pancreatitis include focal or diffuse gland enlargement, contour irregularity, and irregular areas of decreased density. Pancreatitis usually undergoes complete resolution, but pseudocysts are occasional complications.

Received December 28, 1990; accepted after revision March 19, 1991.

[1] Both authors: Mallinckrodt Institute of Radiology, Washington University School of Medicine, 510 S. Kingshighway Blvd., St. Louis, MO 63110. Address reprint requests to T. E. Herman.

AJR 157:375-379, August 1991 0361-803X/91/1572-0375 © American Roentgen Ray Society

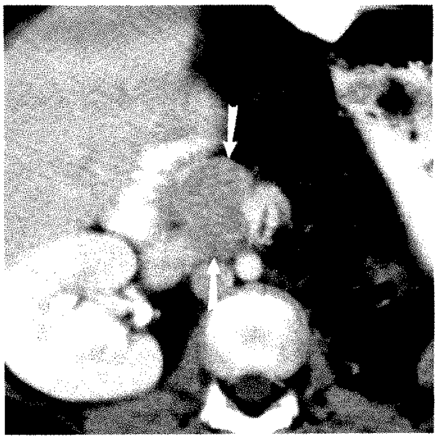

1

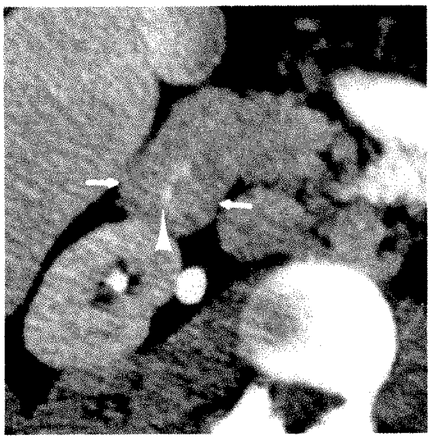

2

Fig. 1.—Congenital short pancreas. CT scan in a 10-year-old boy with polysplenia syndrome shows congenital absence of left kidney and a short rounded pancreas (*arrows*). No body or tail of pancreas is present.

Fig. 2.—Anular pancreas. CT scan at level of duodenum shows soft-tissue density, representing anular pancreas (*arrows*), surrounding contrast-filled duodenum (*arrowhead*).

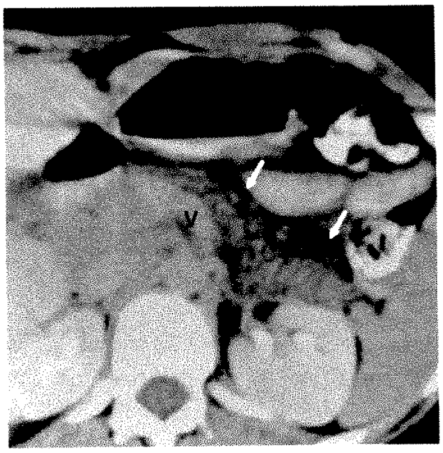

Fig. 3.—Cystic fibrosis in a 15-year-old girl. Enhanced CT scan at level of splenic vein. Pancreas anterior to splenic vein (v) has a mottled appearance with areas of low-density fat (*arrows*). This appearance is abnormal for patient's age.

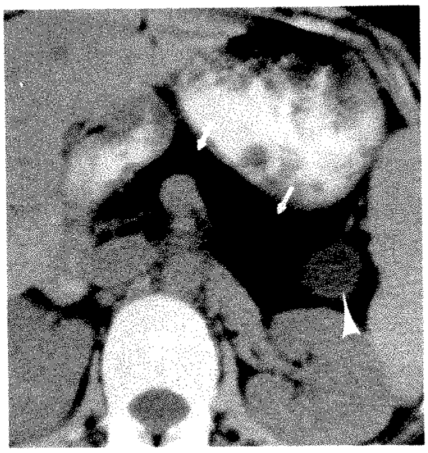

Fig. 4.—Cystic fibrosis with cystosis. Unenhanced CT scan in a 19-year-old patient with known cystic fibrosis shows diffuse fatty replacement of pancreas (*arrows*). A fluid-filled cyst is noted in pancreatic tail (*arrowhead*).

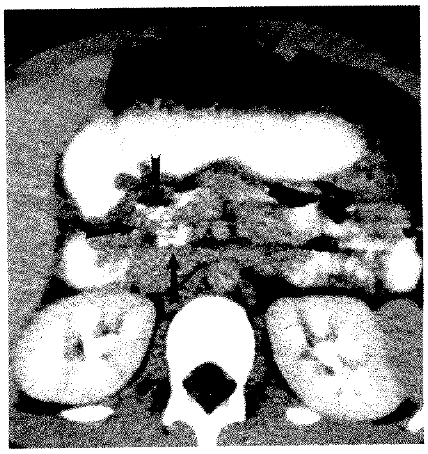

Fig. 5.—Cystic fibrosis with calcifications. CT scan in a 21-year-old man shows calcifications (*arrows*) within a small pancreatic head. Contrast material is dense in duodenum medially and stomach anteriorly.

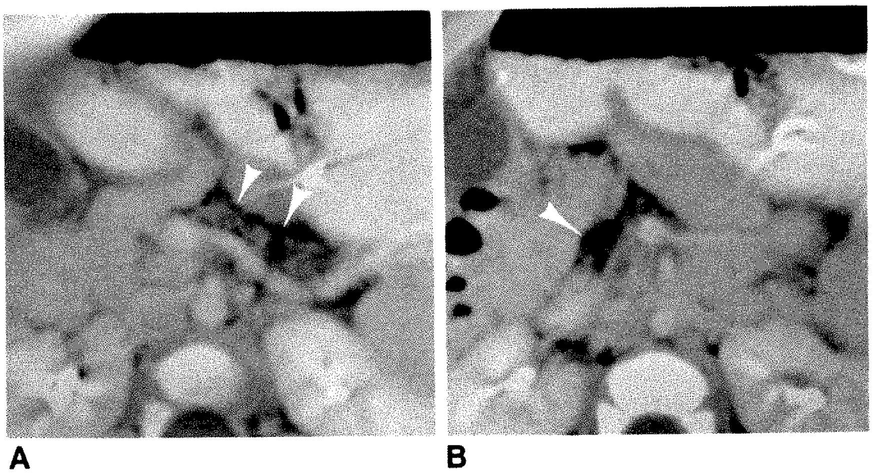

Fig. 6.—Schwachman syndrome in an 18-month-old boy with steatorrhea and failure to thrive.

A and *B*, CT scans at level of pancreatic body and head, respectively, show a low-density pancreas (*arrowheads*) with multiple areas of fat.

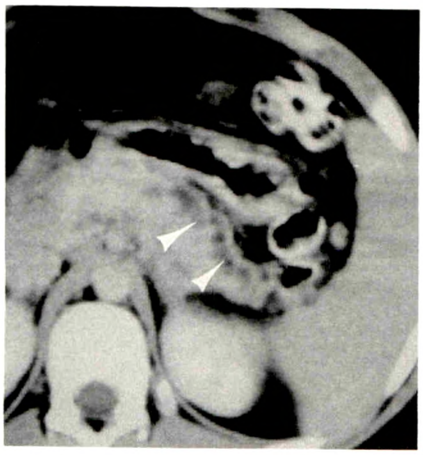

Fig. 7.—One of two siblings with hereditary pancreatitis. CT scan in an 8-year-old boy shows a tortuous, dilated main pancreatic duct (*arrowheads*).

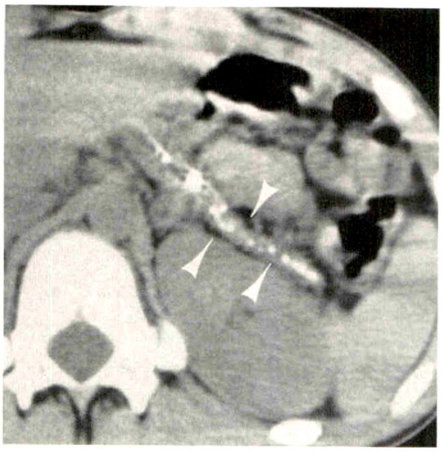

Fig. 8.—Hereditary pancreatitis. Unenhanced CT scan shows an atrophic gland and extensive calcifications (*arrowheads*).

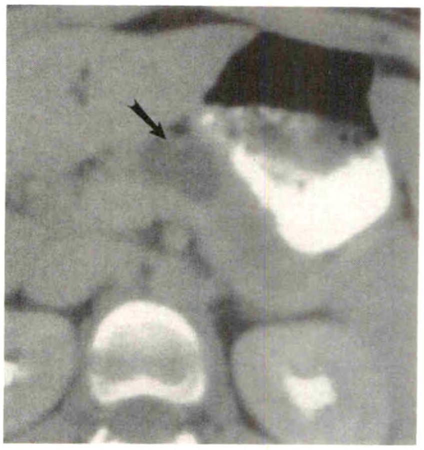

Fig. 9.—Von Hippel–Lindau syndrome in a 14-year-old boy. CT scan shows a well-defined cyst (*arrow*) within pancreatic body.

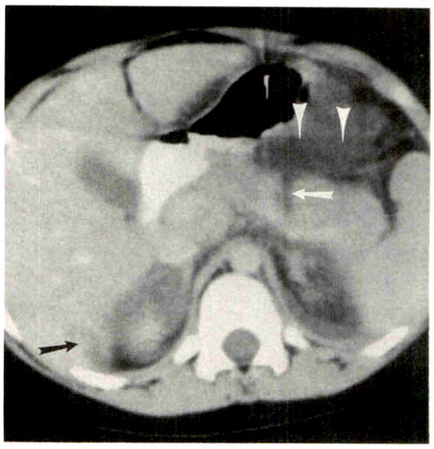

10

Fig. 10.—Pancreatic laceration. CT scan shows a laceration of pancreas just to left of midline (*white arrow*). Fluid is noted in peripancreatic soft tissues anteriorly (*arrowheads*). Also present was a small hepatic laceration (*black arrow*) and bilateral perinephric hematomas.

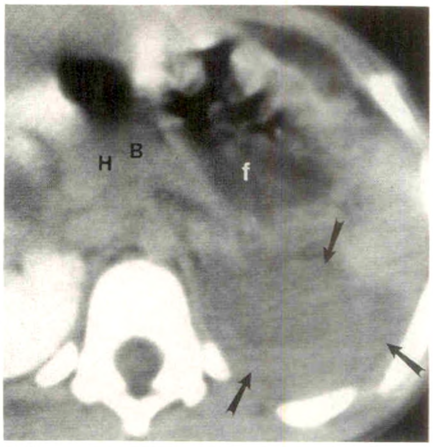

11

Fig. 11.—Pancreatic laceration. CT scan in a 3-year-old boy shows a normal pancreatic head (H) and body (B), but pancreatic tail is not seen on this or adjacent levels because it is avulsed and macerated. Note also nonfunctioning left kidney (*arrows*) and fluid (f) in lesser sac. Pancreatic fracture and avulsion of left renal pedicle were confirmed at surgery.

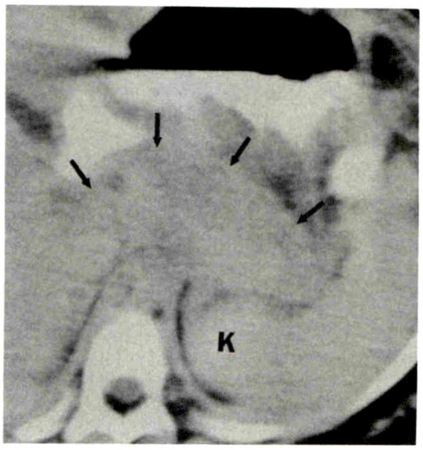

Fig. 12.—Acute pancreatitis. Enhanced CT scan shows a swollen pancreas (*arrows*) with blurred irregular outlines and fluid in immediate peripancreatic space. K = kidney.

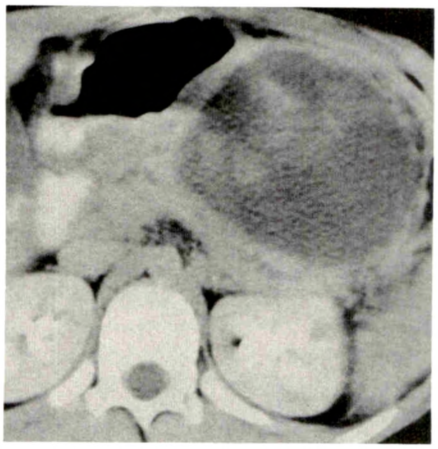

Fig. 13.—Pseudocyst. CT scan in an 11-year-old boy with acute pancreatitis shows large, well-defined fluid collection with heterogeneous contents in pancreatic tail. At surgery, pseudocyst contained hemorrhagic fluid.

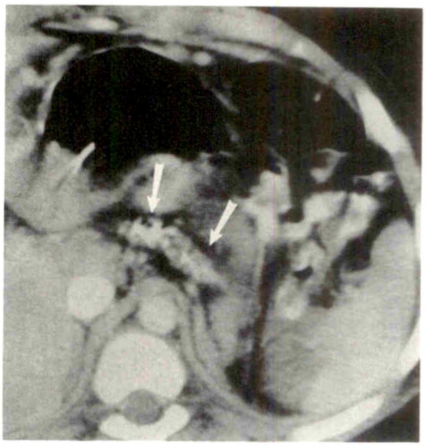

Fig. 14.—Chronic pancreatitis in an 8-year-old boy with hypercalcemia due to renal failure. CT scan shows atrophic calcified pancreas (*arrows*).

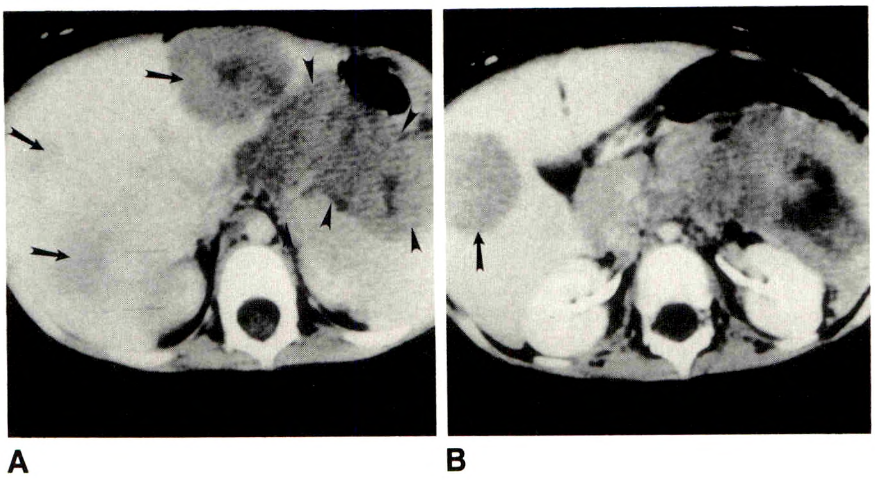

Fig. 15.—Pancreaticoblastoma in a 2-year-old girl.

A and *B*, Enhanced CT scans show a large necrotic mass with a low-density center in tail of pancreas (*arrowheads*). Hepatic metastases (*arrows*) are present. (Courtesy of C. Glasier, Little Rock, AR.)

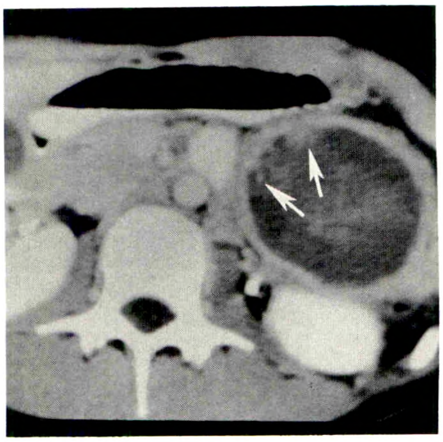

Fig. 16.—Papillary epithelial cystic tumor of pancreas in a 14-year-old girl. CT scan shows large, thick-walled, cystic mass with papillary excresences (*arrows*) in pancreatic tail. (Reprinted with permission from Osborn [5]).

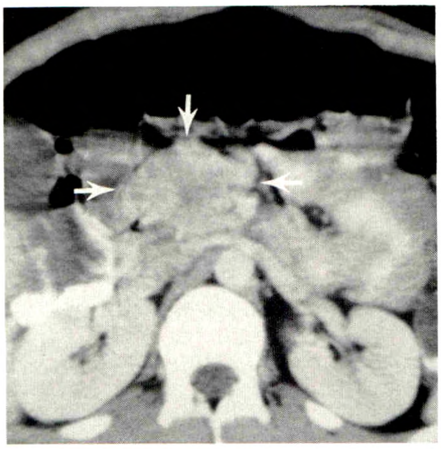

Fig. 17.—Vasoactive intestinal peptide-secreting tumor of pancreas. Enhanced CT scan shows a soft-tissue mass in pancreatic head (*arrows*) and several fluid-filled bowel loops. Vasoactive intestinal peptide-secreting tumor in pancreatic head was identified at surgery.

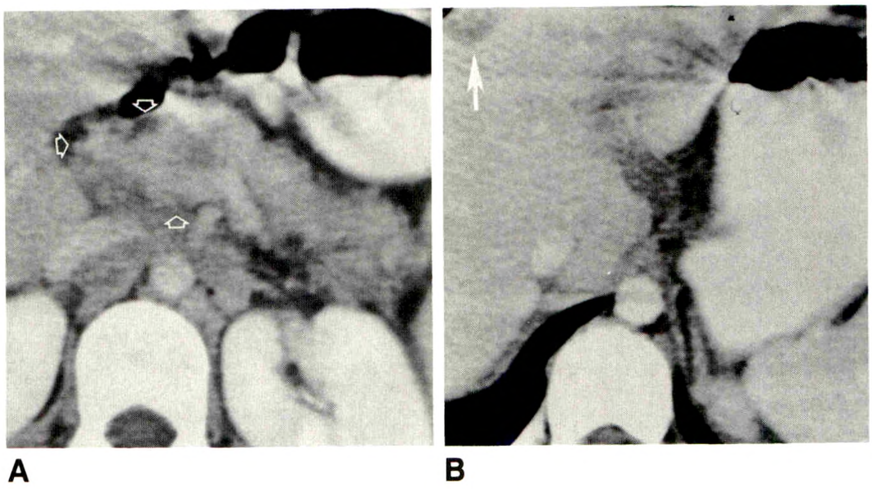

Fig. 18.—Inactive islet cell tumor in a 15-year-old girl with a clinical history of pancreatitis.

A, CT scan shows an irregular inhomogeneous pancreas with focal enlargement of pancreatic head (*arrows*). Also present is paraaortic and retrocaval adenopathy.

B, CT scan at a higher level shows a hepatic metastasis (*arrow*). Islet cell tumor in pancreatic head was found at surgery. Pancreatitis was due to obstruction of main pancreatic duct.

Pancreatic lacerations appear as irregular clefts of decreased attenuation in an anteroposterior plane. Complete transection is rare. Most pancreatic injuries occur at the junction of the tail and the body, just to the left of midline (Figs. 10 and 11). Occasionally, the fracture plane is difficult to recognize on CT because it is obscured by hemorrhage or artifacts from air or air and fluid within bowel. However, the presence of focal or generalized pancreatic enlargement and peripancreatic fluid collections and a failure to visualize a portion of the gland should suggest the diagnosis of pancreatic laceration.

Pancreatitis

Acute pancreatitis in childhood may be the result of drugs (steroids, L-asparaginase, acetaminophen, valproic acid, and sulfasalazine), viral infections (mumps, coxsackievirus), obstruction at the ampulla of Vater, ascariasis, hyperparathyroidism, hyperlipidemia, Schönlein-Henoch purpura, and cystic fibrosis as well as accidental and nonaccidental trauma. The CT findings are an enlarged edematous gland with poorly defined margins and inflammatory changes in peripancreatic fat and soft tissue (Fig. 12) [3]. Pseudocysts occur in up to 10% of cases of acute pancreatitis (Fig. 13).

Pseudocysts typically appear as round or oval fluid collections with thick, well-defined capsules. The contents of a pseudocyst are usually homogeneous and have an attenuation value close to that of water, but they may be heterogeneous or of increased density if infection or hemorrhage is present. Mature pseudocysts are relatively permanent in nature and change little in shape or location, in contrast to acute peripancreatic or pancreatic fluid collections, which are transient, poorly encapsulated, and variable in size and shape [3].

Chronic pancreatitis is rare in childhood and usually is the result of hereditary pancreatitis; other less frequent causes include steroid therapy, hyperparathyroidism, cystic fibrosis, and possibly pancreatic divisum. It has been suggested that in pancreatic divisum, the separate dorsal and distal pancreatic ducts are too small to transmit the volume of pancreatic secretions that must pass through them, producing a relative stenosis at the ampulla. The stasis of pancreatic juices predisposes to pancreatitis. CT manifestations include calcification, gland atrophy, and ductal dilatation (Fig. 14).

Pancreatic Tumors

Pancreatic tumors in childhood are usually of epithelial or islet cell origin and rarely of mesenchymal origin [4]. Pancreaticoblastoma is a rare epithelial tumor, occurring in children under 7 years of age. It tends to be encapsulated, large (average diameter of 10 cm), and located in the pancreatic head. On CT, the tumor usually appears as a focal mass of homogeneous soft-tissue density. Secondary signs include a dilated pancreatic duct, hepatic and lymph node metastases, and vascular encasement (Fig. 15).

Papillary cystic tumor is a lesion of young women (mean age, 26 years), with one third of cases occurring in adolescent girls. It has low potential for malignancy, is well encapsulated, and may be located in any part of the pancreas, but tends to occur most often within the tail. On CT, this neoplasm appears as a large (mean, 11.5 cm), well-defined, thick-walled cystic mass containing papillary projections and occasionally septa (Fig. 16). Its density ranges between 30 and 40 H.

Islet cell tumors are divided into those that are hormonally active and those that are inactive. The majority are functioning and include insulinomas, gastrinomas, vasoactive intestinal peptide–secreting tumors, glucagonomas, and somatostatinomas. These tumors are small, usually less than 2 cm in diameter (Fig. 17). The majority of functioning islet cell tumors are hyperdense relative to normal pancreas on contrast-enhanced CT performed with a bolus injection. CT may show metastatic lymphadenopathy and hepatic metastases even when the primary tumor is not detectable. Inactive islet cell tumors are usually large at the time of diagnosis, ranging from 3 to 20 cm in diameter. On CT, they appear as nonuniformly enhancing masses with hyperdense areas (Fig. 18). Approximately 20% contain calcifications.

REFERENCES

1. Daneman A, Gaskin K, Martin DJ, Cutz E. Pancreatic changes in cystic fibrosis: CT and sonographic appearances. *AJR* **1983**;141:653–655
2. Jeffrey RB, Federle MP, Crass RA. Computed tomography of pancreatic trauma. *Radiology* **1983**;147:491–494
3. Siegelman SS, Fishman EK. Computed tomography of pancreatitis. In: Siegelman SS, ed. *Computed tomography of the pancreas*. New York: Churchill Livingstone, **1983**:83–111
4. Grosfeld JL, Vane DW, Rescorla FJ, McGuire W, West KW. Pancreatic tumors in childhood. *J Pediatr Surg* **1990**;25:1057–1062
5. Osborn AG. *Radiographics* **1991**;11:154–155

Videotape Review

RSNA Today, Vol. 4, No. 4. Oak Brook, IL: The Radiological Society of North America, 1990. $55; by subscription, 6 issues annually at $185 for RSNA members and $225 for nonmembers (VHS videotape)

This educational tape is moderated by William J. Casarella. It consists of three sections of interest to both general radiologists and radiologists involved in subspecialties appropriate to the individual topics discussed.

The first section, "Cervical Spine Trauma," is presented by Thomas H. Berquist. A series of 2500 patients is reviewed, and details of the results are presented concerning the mechanisms of injury to the cervical spine, the radiologic evaluation of these types of cases, and the role of the radiologist in the workup and follow-up care of these patients. Using clearly understandable charts and case presentations, Dr. Berquist presents the complex topic of radiologic evaluation of the cervical spine in a logical sequence, beginning with a discussion of the various mechanisms of injury (e.g., flexion, extension, rotation), the various types of imaging necessary to arrive at the proper diagnosis (e.g., plain film radiography, tomography, CT, and MR), and the role the radiologist plays in this process. Of special interest to anyone responsible for interpretation of radiographs of trauma patients is a clear discussion of the three-column approach to the lateral film of the cervical spine and its relationship to instability and a discussion of the selection of the most advantageous filming technique in each individual case.

The second section, "US of the Neonatal Head," is presented by Thomas L. Slovis. The first part of the presentation deals with full-term infants. Various indications for the examination are discussed (e.g., congenital anomalies, tumors, syndromes), and several excellent examples are presented. Of more immediate everyday and historical significance, however, is the discussion of the premature infant, in whom there is such a remarkable prevalence of intracranial hemorrhage. Illustrative examples of the various types of intracranial hemorrhage are presented along with a discussion of the progression and neurodevelopmental outcome of these cases. Dr. Slovis also discusses the parameters for screening premature infants and the focal increased echogenic area, and he covers periventricular leukomalacia in some depth (e.g., risk factors, incidence, follow-up). Last, he presents applications of color flow Doppler imaging.

The third section, "Imaging Insights: Incomplete Pulmonary Fissures," is presented by Anthony V. Proto. These anatomic variants, which evidently occur in most patients, are explained clearly by using a combination of models, radiographs of autopsy specimens, and case presentations. This topic will be of great interest to any radiologist who interprets plain chest films. The patterns of the incomplete pulmonary fissures, their relationship to diagnostic pitfalls, and the effect on the representation of underlying disease as related to pleural fluid and collateral air flow are all presented in an interesting and easily understandable manner.

All three sections are of excellent quality, are informative, contain clearly illustrative high-quality films and charts, and are presented well.

Hano A. Siegel
Mercy Hospital
San Diego, CA 92103

Case Report

Esophageal Histoplasmosis in a Child with Immunodeficiency with Hyper-IgM

Raymond K. Tu,[1] Mary Ellen Peters,[1] Glenn R. Gourley,[2] and Richard Hong[3]

Infection with *Histoplasma capsulatum* is typically indolent and asymptomatic in healthy persons. However in immunocompromised patients, a progressive, serious disease involving the respiratory and gastrointestinal tracts can occur. Gastrointestinal infections of the stomach and the large and small intestines are well documented in these patients [1]. We describe a case of esophageal histoplasmosis in a child with the primary immunodeficiency disorder, immunodeficiency with hyper-IgM.

Case Report

A 3-year-old boy was well until age 2 years, when he had fever, nausea, vomiting, stomatitis of the gingiva, abdominal pain, fatigue, and irritability. Laboratory findings included cyclic neutropenia, eosinophilia, and anemia that required multiple transfusions. An immunodeficiency with normal to elevated IgM was diagnosed. Disseminated histoplasmosis was documented by bone marrow biopsy and was treated with amphotericin B, after which the symptoms improved and the bone marrow infection cleared.

Because of suspected esophagitis, an esophagogram was obtained, which showed poor motility with associated secondary and tertiary peristalsis. A large, 2.0-cm ulcer crater in the left anterolateral wall of the esophagus (Fig. 1) and persistent filling defects in the mid and lower esophagus were identified. Endoscopy revealed impressive pseudopolyps and ulceration. Multiple biopsy samples were obtained from the esophagus, stomach, and proximal duodenum. Culture of the esophageal biopsy grew *Histoplasma*, as did a simultaneous bone-marrow aspirate. Histologically, the esophageal biopsies showed chronic inflammation and ulceration, although the gastric and duodenal biopsy findings were normal.

Discussion

Infection by the common dimorphic soil fungus *Histoplasma capsulatum* is usually benign and asymptomatic, the yeast phase occurring in humans and animals. Rarely, serious or fatal extrapulmonary disease may develop, usually from other preexisting disease in an abnormal host with compromised immunity.

Clinical signs of disseminated histoplasmosis in Goodwin's series included a relentless fever (body temperature ranging from 101°F to 103°F) as the most common complaint. Other symptoms included malaise, cough, weight loss, and diarrhea [1]. The manifestations of intestinal infection are perforation, hemorrhage, and obstruction, usually affecting the ileum or colon [1–4].

The principal site of large- and small-bowel involvement in gastrointestinal histoplasmosis is the lymphoid tissue, with histiocyte proliferation and granuloma formation. Ulcerations develop as the inflammatory enlargement causes ischemia of the overlying mucosa. The radiographic patterns of large and

---

Received January 28, 1991; accepted after revision March 19, 1991.

[1] Department of Radiology, University of Wisconsin Hospital and Clinics, Clinical Science Center, 600 Highland Ave., E3/311, Madison, WI 53792. Address reprint requests to R. K. Tu.

[2] Division of Pediatric Gastroenterology, Department of Pediatrics, University of Wisconsin Hospital and Clinics, Clinical Science Center, 600 Highland Ave., Madison, WI 53792.

[3] Division of Pediatric Immunology, Department of Pediatrics, University of Wisconsin Hospital and Clinics, Clinical Science Center, 600 Highland Ave., Madison, WI 53792.

AJR 157:381–382, August 1991 0361-803X/91/1572-0381 © American Roentgen Ray Society

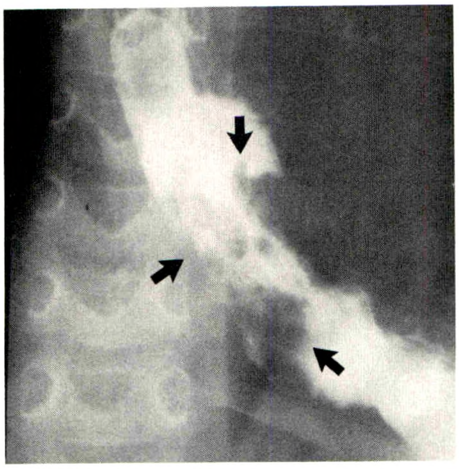

Fig. 1.—Esophagogram shows smooth, large polyploid protrusions into lumen of esophagus (*arrows*).

small intestinal *Histoplasma* infection include thickened folds and mucosal edema, ulcerations, and constricting lesions [5].

Digestive tract histoplasmosis is rare; however, in the immunocompromised patient, disseminated disease involving the stomach and the large and small intestines is well described. In primary immunodeficiencies, generalized histoplasmosis is not a common pathogen [6]. This may be due to a regional distribution of the organism and the role of neutrophils in fungal disease control.

Disseminated histoplasmosis is well documented in persons infected with human immunodeficiency virus (HIV). Sites of involvement have included the colon and rectum [7]. Presently, there are no specific culture-proved cases of esophageal *Histoplasma* infections in HIV patients.

In most cases of primary immunodeficiency, number and function of neutrophils are normal. Immunodeficiency with hyper-IgM is characteristically associated with cyclic neutropenia. During the periods of neutropenia, ulcers in the mouth are very common. Conceivably, similar lesions occurring in other portions of the gastrointestinal tract would predispose such patients to gastrointestinal infection with histoplasmosis. The patient was a resident of Kentucky, an area endemic for histoplasmosis.

This unique case documents esophageal infection by this parasite. In patients with prolonged fever and poor health, early recognition, diagnosis, and treatment are essential to prevent possible complications of perforation, obstruction, and hemorrhage. Such insults to the hollow viscus complicate the course of an already immunocompromised patient. The prevalence of the various complications in esophageal infection by *Histoplasma* is not known; we believe this is the first case report. The most severe complication of ulcer formation is lack of recognition. Untreated cases are usually fatal.

ACKNOWLEDGMENT

We are indebted to Robert B. Broughton, University of Kentucky Medical Center, Lexington, KY, for referral of this patient and provision of expert care during follow-up.

REFERENCES

1. Goodwin RA, Shapiro JL, Thurman GH, et al. Disseminated histoplasmosis: clinical and pathologic correlations. *Medicine* **1980**;59:1–33
2. Brett MT, Kwan KTC, Bending MR. Caecal perforation in renal transplant patient with disseminated histoplasmosis. *J Clin Pathol* **1988**;41:992–995
3. Adekunle OO, Sudhakaran P, Timeyin ED. African histoplasmosis of the jejunum: report of a case. *J Trop Med Hyg* **1978**;81:88–90
4. Mohanty SK, Reddy P, Polk JW. *Mo Med* **1970**;67:100–103
5. Lee RK, Lin FL. Gastrointestinal histoplasmosis, roentgenographic, clinical and pathological correlation. *Am J Gastroenterol* **1975**;63:255–265
6. Ochs HD, Wedgewood RD. Disorders of the B cell system. In: Stiehm ER, ed. *Immunologic disorders in infants and children*, 3rd ed. Philadelphia: Saunders **1989**:226–257
7. Graybill JR. Histoplasmosis and AIDS. *J Infect Dis* **1988**;158:623–626

Case Report

Renal Tubular Dysgenesis

Atchawee Luisiri,[1] Luis Salinas-Madrigal,[2] Akihiko Noguchi,[3] E. Richard Graviss,[1] and Michael J. Silberstein[1]

We report a case of a patient with renal tubular dysgenesis associated with Potter syndrome, oligohydramnios, and abnormal findings on renal sonography. This condition has recently been documented in the pathology and genetics literature.

A 1.4-kg, female neonate of 32 weeks' gestation was born to a 20-year-old prima gravida mother. The patient was delivered by emergent cesarean section because of transverse lie and poor biophysical profile. At delivery, Apgar scores were 1 and 6 at 1 and 5 min, respectively, and the infant was stained with meconium. She was intubated because of poor oxygenation and transferred to our hospital for treatment of prematurity and respiratory distress.

Physical examination revealed tachycardia, tachypnea, and hypotension. Her features were dysmorphic with posteriorly rotated and low-set ears, flattened nose with broad nasal bridge, and deeply set eyes. The anterior fontanelle was wide. The heart, lungs, abdomen, and genitalia were unremarkable. The hands had bilateral simian creases and clinodactyly, and she had rocker-bottom feet. Muscle tone was generally poor.

The chest radiograph revealed a bell-shaped thorax, bilateral medial pneumothoraces, pneumomediastinum, and diffuse pulmonary opacifications. The patient was slightly anemic, and analysis of the blood gases showed hypoxia and acidosis. The blood urea nitrogen level was normal, but the serum creatinine level was increased to 115 μmol/l (normal, 35.3–61.9 μmol/l). The clinical diagnoses were severe respiratory distress syndrome, Potter syndrome with multiple congenital malformations, and possible sepsis. Despite aggressive mechanical ventilation, it was difficult to maintain a good P_{O_2}. A renal sonogram, requested because of postnatal anuria, showed normal position and size (4 × 2 × 2 cm) without hydronephrosis or macroscopic cysts. Corticomedullary differentiation was indistinct, with cortical echogenicity equal to that of the liver. The findings suggested renal dysplasia without macroscopic cysts (Figs. 1A–1C). Findings on cranial sonography were normal. Severe bradycardia developed and the infant died 17 hr after birth.

Autopsy revealed Potter syndrome and hypoplastic lungs with reduced bronchial generations. Histologically, the lungs showed hyaline membrane disease and occasional interstitial and intraalveolar hemorrhage. The kidneys were normal in size, shape, and combined weight (15.2 g—normal combined weight is 14.5 ± 4.8 g). The external surface was smooth with no fetal lobation. The cortical surface was wide and extended to the medulla. No cysts were evident. The pelvicaliceal systems and the bladder were unremarkable. The renal arteries were patent. Microscopically, the glomeruli were normal but increased in number. The cortical tubules were lined with poorly differentiated cuboidal epithelial cells (Fig. 1D), all of which stained with epithelial membrane antigen. The medullary pyramids were small, with increased interstitial connective tissue in the medulla. The chromosome study revealed a normal female karyotype.

Discussion

Renal tubular dysgenesis is a newly reported entity [1–3]. It is thought to be inherited as an autosomal recessive trait

---

Received December 10, 1990; accepted after revision March 19, 1991.

[1] Department of Diagnostic Imaging, Cardinal Glennon Children's Hospital, 1465 S. Grand Blvd., St. Louis, MO 63104. Address reprint requests to A. Luisiri.

[2] Department of Pathology, Cardinal Glennon Children's Hospital, 1465 S. Grand Blvd., St. Louis, MO 63104.

[3] Department of Neonatology, Cardinal Glennon Children's Hospital, 1465 S. Grand Blvd., St. Louis, MO 63104.

***AJR* 157:383–384, August 1991** 0361–803X/91/1572–0383 © American Roentgen Ray Society

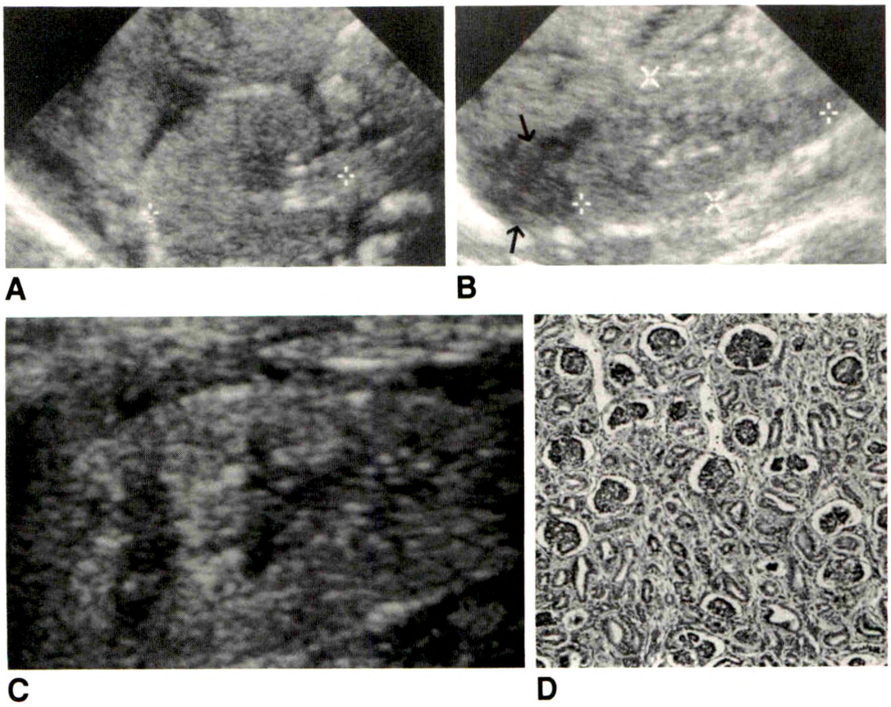

Fig. 1.—*A* and *B*, Transverse and longitudinal sonograms of right kidney. Note poor corticomedullary differentiation, giving appearance of homogeneity of renal parenchyma and a thickened cortex. No cysts are evident. Size of kidney is normal. Arrows mark normal adrenal gland.

C, Close-up longitudinal sonogram of left kidney shows same findings.

D, Histologic section of renal cortex. Note crowding of glomeruli (increased glomerulogenesis), immature tubules, and absent medullary rays. (H and E, original magnification ×150)

[3]. Although the condition is associated with oligohydramnios in later pregnancy, sonography before 22 weeks' gestation may show an adequate amount of amniotic fluid. Potter syndrome is present. Flexion or extension deformity of the joints, rocker-bottom feet, and simian creases of the hand are reported. CNS and cardiac anomalies are occasionally present. Respiratory failure due to pulmonary hypoplasia is frequently the cause of death. Renal size is normal, or occasionally enlarged, but never small. The external renal surface is normal. The lobar structure is usually preserved. The corticomedullary margin is well demarcated, but the corticomedullary rays are usually indistinct. The glomeruli are normal, but increased in number [1].

The most striking abnormality is the presence of immature and poorly differentiated tubules in the cortex, with absence of proximal tubules. The medulla shows an increase in interstitial tissue. The pathogenesis is unknown. The decrease in amniotic fluid is presumably related to renal tubular dysgenesis, but the mechanism is far from clear.

The renal sonographic findings in our patient correspond to the pathologic abnormalities. Both showed normal renal size, no macroscopic renal cysts, and abnormal parenchyma. The corticomedullary demarcation, which is usually seen from 27 weeks' gestation [4], was not appreciated sonographically. The lack of corticomedullary differentiation gives the appearance of thick cortex, corresponding to the crowded glomeruli, very immature tubules, and small medullary pyramids found histologically. The echogenicity of the cortex can be increased, as reported by Swinford et al. [3], or equal to that of the liver, as in our patient.

Other conditions that show poor corticomedullary differentiation are recessive-type polycystic kidneys [5], acute corticomedullary necrosis, renal vein thrombosis [6], and renal dysplasia [7]. Although the clinical presentation and the findings on physical examination in patients with these diagnoses may overlap with those in our patient, the renal sonographic findings will differ. Occasionally, renal dysplasia may be difficult to distinguish from renal tubular dysgenesis.

It is important for a radiologist or a sonographer to be aware of this relatively new entity. The diagnosis of renal tubular dysgenesis can be suggested by the prenatal or postnatal renal sonogram, as described earlier. Upon diagnosis, the parents need to be alerted to the grave prognosis and the risk of recurrence in future offspring.

REFERENCES

1. Voland JR, Hawkins EP, Wells TR, Saunders B, Jones M, Benirschke K. Congenital hypernephronic nephromegaly with tubular dysgenesis: a distinctive inherited renal anomaly. *Pediatr Pathol* **1985**;4:231–245
2. Schwartz BR, Lage JM, Pober BR, Driscoll SG. Isolated congenital renal tubular immaturity in siblings. *Hum Pathol* **1986**;17:1259–1263
3. Swinford AE, Bernstein J, Toriello HV, Higgins JV. Renal tubular dysgenesis: delayed onset of oligohydramnios. *Am J Med Genet* **1989**;32:127–132
4. Jeanty P, Dramaix-Wilmet M, Elkhazen N, Hubinont C, Regemorter N. Measurement of fetal kidney growth on ultrasound. *Radiology* **1982**;144:159–162
5. Melson GL, Shackelford GD, Cole BR, McClennan BL. The spectrum of sonographic findings in infantile polycystic kidney disease with urographic and clinical correlation. *JCU* **1985**;13:113–119
6. Rosenberg ER, Trought WS, Kirks DR, Summer TE, Grossman H. Ultrasonic diagnosis of renal vein thrombosis in neonates. *AJR* **1980**;134:35–38
7. Sanders RC, Nussbaum AR, Solez K. Renal dysplasia: sonographic findings. *Radiology* **1988**;167:623–626

MR Imaging of the Brain in Patients with Migraine Headaches

Robin E. Osborn[1,2]
Daniel C. Alder
Craig S. Mitchell

Forty-one patients with migraine headaches were referred for MR imaging of the brain. Intermediate and T2-weighted images were obtained to determine the frequency of areas of high intensity within the white matter. The average age of these patients was 29.8 years; only five were over 40 years old. Each patient was evaluated in the axial plane with long TR/short and long TE images. Twenty-three patients also had T1-weighted short TR/short TE MR scans; enhancement with gadopentetate dimeglumine was used in three patients. Intracranial abnormalities were seen in only six patients: foci or white matter high intensity on intermediate and T2-weighted images in five and a venous angioma in one. Prior studies have indicated that parenchymal brain abnormalities may be found in up to 46% of patients with migraines. The current study demonstrated parenchymal brain lesions in only 12%.

This study suggests that the frequency of foci of high intensity seen on long TR sequences in the migraine patient is much lower than previously reported, especially in patients under 40 years old (5.5% in our series).

***AJNR* 12:521–524, May/June 1991; *AJR* 157:385–388, August 1991**

Until the advent and widespread use of MR imaging for the evaluation of the brain in patients with migraine headaches, CT was the primary method of radiologic screening. The CT results were usually normal, although atrophy, ischemic changes, and cerebral edema have been reported [1–3].

Only a few reports on the MR evaluation of patients with migraine headaches have appeared in the literature [4–6]. The prevalence of MR abnormalities in these patients has been considered to be relatively high. Previous authors found high-signal white matter foci on long TR images in migraineurs 17–46% of the time [4–6]. Since this has not been our experience, a prospective study was performed to determine the prevalence of such white matter abnormalities.

Subjects and Methods

Forty-one patients who had been clinically diagnosed as having migraine headaches were evaluated prospectively with MR. These patients represented 41 consecutive referrals for brain MR from the neurology clinic at the Naval Hospital, San Diego, CA. Entry into the study was based on the clinical diagnosis of migraine, regardless of the patient's age and duration and severity of symptoms. Each patient was followed in the neurology clinic for 3–18 months. The criteria for diagnosis were based on a pattern of pulsatile recurrent headaches dating from childhood or adolescence, the presence of a positive family history, and other clinical factors including scintillating scotoma, aura, subjective neurologic findings, headache that was sickening or disabling, and usually a normal neurologic examination.

The current study group comprised 24 men and 17 women. Thirty-one patients had common migraine, four had classical migraine, four had complicated migraine, and one each had basilar artery and orbital migraines. All of the MR scans were interpreted by a neuroradiologist. The average age of the patients was 29.8 years (range, 18–66 years). Only five patients were over 40 years old. Review of patients' records indicated that five patients

Received August 24, 1990; revision requested November 17, 1990; revision received December 10, 1990; accepted January 1, 1991.

The views expressed in this article are those of the authors and do not reflect the official policy or position of the Department of the Navy, the Department of Defense, nor the U.S. Government.

This work was supported by The Chief, Navy Bureau of Medicine and Surgery, Washington, DC, Clinical Investigation Program, study #90-16-2749-00.

[1] All authors: Departments of Radiology and Clinical Investigation, Naval Hospital, San Diego, CA 92134-5000.

[2] Present address: Department of Radiology, Children's Memorial Hospital, 2300 Children's Plaza, Chicago, IL 60614. Address reprint requests to R. E. Osborn.

0361-803X/91/1572-0385
© American Roentgen Ray Society

smoked cigarettes, one was hypertensive, one had unilateral sensorineural hearing loss, one had somatic hemiatrophy, three had remote head injuries, one took birth control pills, one was pregnant, and one had had renal lithiasis 12 years earlier. Of the patients with additional medical problems, only the patient with previous renal lithiasis had white matter lesions.

The MR studies were performed with four scanners: a 1.5-T Siemens (Iselin, NJ) Magnetom SP unit (19 patients), a 0.35-T Diasonics (Milpitas, CA) unit (14 patients), a 1.0-T Siemens Magnetom unit (three patients), and a 1.5-T General Electric (Milwaukee, WI) Signa unit (five patients). All of the scans included long TR/short and long TEs, 2500–3000/25–30, 80–90 (TR/TE), axial images. Short TR/short TE sagittal, coronal, or axial images were obtained in 23 patients. Three patients received IV gadopentetate dimeglumine. Matrix size was 128 × 256 for the General Electric scanner and 256 × 256 for the others. The field of view was 23 or 24 cm. Slice thicknesses were 5 or 6 mm.

Results

Foci of high signal intensity involving the white matter were detected on long TR scans in five of the 41 patients. Three (two women and one man) of the five patients were over 40 years old (43, 50, and 66 years old); the other two were 30- and 36-year-old men. Of the 36 migraineurs in whom foci of high intensity were not seen, only two were over 40 years old (41- and 44-year-old men). The other 34 patients were 18–37 years old and included 15 women and 19 men.

Three of the five abnormal MR scans with abnormal white matter lesions had only one or two foci of abnormality (Fig. 1). The remaining two abnormal scans each had multiple bilateral white matter lesions (Fig. 2). No cortical lesions were seen in any of the patients. A left frontal lobe venous angioma was seen in one patient; mild to moderate degrees of chronic sinus changes manifested by mucosal thickening and retention cysts were seen in 15 patients. None of the findings in these 16 patients were clinically considered to be related to a migraine symptomatology.

Four patients had neurologic findings and thus were classified as having complicated migraines. In only one of these patients was the MR scan abnormal. Three of the five MR scans positive for white matter lesions were obtained in three of the five patients over the age of 40 (Table 1). Enhancement with gadopentetate dimeglumine resulted in no additional findings.

Discussion

Approximately 20% of all headaches are of the migraine type and this was the first specific type of headache to be classified [7]. Migraine headaches are associated with an initial vasoconstriction of the cerebral vasculature, which may be associated with relative cerebral ischemia. This may partially explain or suggest a theory for the aura, the clinical findings associated with classical migraine and the possible ischemic genesis for the white matter lesions seen with MR. Later cerebral vasodilatation results in the pulsatile headache. Numerous vasoactive substances have been implicated and investigated as possible contributors to the development of migraine headaches [7–9].

The origin of migraine headache remains incompletely understood, as is the cause of the white matter lesions identified with MR in some of the patients so affected [7]. We found only three MR studies in the literature that specifically addressed migraine headaches [4–6]. These authors described the findings in 24, 18, and nine patients; white matter abnormalities were found in 46%, 33%, and 17% of cases, respectively, for a combined average of 33% (17/51). Kaplan et al. [6] presented nine patients with a mean age of 39.8 years; the three patients with abnormal MR scans were aged

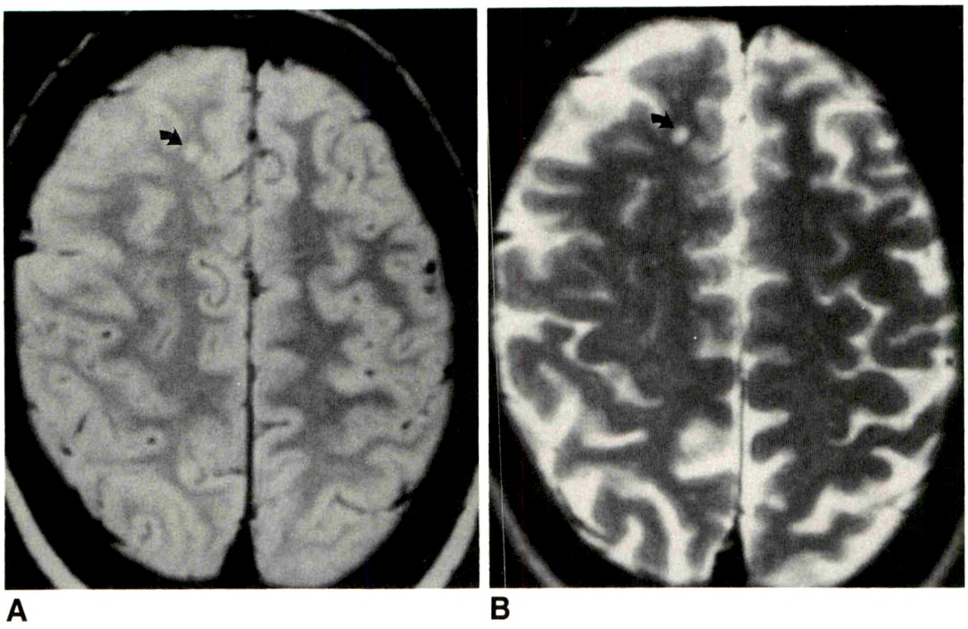

Fig. 1.—43-year-old woman with basilar artery migraine.

A and *B*, Focal high-intensity subcortical white matter lesion involving right frontal lobe (*arrows*) seen on axial long TR/short TE (2800/25) scan (*A*) is also present on long TR/long TE (2800/90) scan (*B*). Additional lesions were present on other sections.

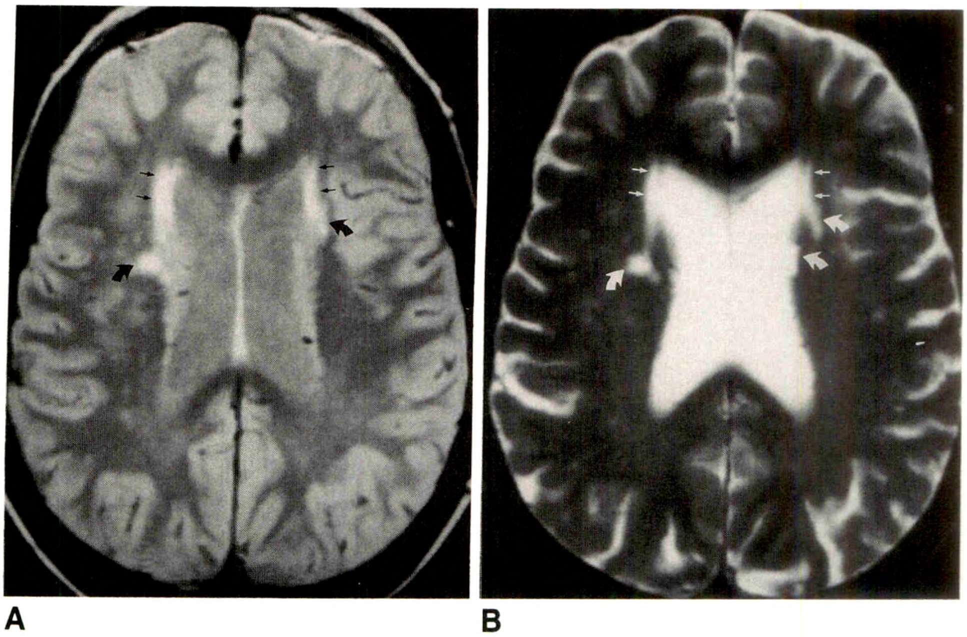

Fig. 2.—66-year-old woman with common migraine.

A and *B*, Multiple bilateral periventricular foci of high intensity seen within white matter (*curved arrows*) on long TR/short TE scan (*A*) are also delineated on long TR/long TE scan (*B*). These scans also show "normal" periventricular halo (*straight arrows*).

24, 49, and 56. The average age of the 18 patients in the report by Jacome and Leborgne [5] was 30 years, which was similar to that in our patient group. The ages of their patients with abnormal MR scans were 34, 37, and 38. Soges et al. [4] reported the largest series to date of migraine patients studied with MR. The average age of their patients was 36.8 years. The average age of the 11 patients with an abnormal MR result was 36.4 years, whereas the average age of the 13 patients with normal MR scans was 33.8 years. Six of the 11 abnormal and four of the 13 normal patients were over 40 years old. In our study, the average age of the five patients with abnormal MR scans was 45 years (range, 30–66), whereas the average age of the 36 subjects with normal scan results was about 28 years (range, 18–44). Current and previous studies demonstrate that the older patients with migraines tend to be those most often shown to have foci of high signal intensity of the white matter on intermediate and T2-weighted images. Still, it was interesting to note that even when considering the patients of Soges et al. [4] who were under the age of 40 years, 27% were found to have white matter abnormalities. This is approximately five times more than the 5.5% found in the 36 patients in our study under 40 years of age.

TABLE 1: Summary of Findings in Migraine Patients with Foci of High Intensity on MR

Age (yr)	Sex	MR Findings	Diagnosis
43	F	Multiple 2- to 4-mm, round, bilateral, subcortical white matter lesions	Basilar artery migraine
50	M	Single 2-mm, right-sided, periventricular white matter lesion	Complicated migraine
36	M	One 3-mm oval, left frontal, subcortical white matter lesion; one 5-mm, oval, insular, subcortical white matter lesion	Common migraine
66	F	Multiple bilateral, subcortical, periventricular, 2- to 8-mm round and oval white matter lesions	Common migraine
30	M	Single 4-mm, oval, periventricular, left frontal white matter lesion	Common migraine

Although precise data do not appear to be available, normal young persons have a low rate of white matter lesions whereas elderly people have a higher rate of such lesions (30–80%) with increasing age [10–14]. The presence of white matter, high-intensity foci on long TR scans is typically nonspecific and may represent or appear similar to a variety of pathologic conditions including atrophic perivascular demyelination, vascular malformations, white matter infarction, or multiple sclerosis [4, 11]. More white matter lesions are detected on MR in older patients with migraine headaches than in their younger counterparts. Five of the 17 patients with abnormal MR scans described in this and other articles [4–6] were over the age of 50 years and six of the 17 were between the ages of 40 and 49 years. Our data also showed that MR findings tended not to be abnormal in young migraineurs.

There is a variety of possible explanations for the increased frequency of abnormal white matter foci found in migraineurs over the age of 40 years. Advancing age is a consideration, especially in combination with a long duration of migraine headaches or severe or complicated migrainous events. Whether or not there is an increased prevalence of such high-intensity white matter foci in young normal vs young migraine patients (5.5% in this study) is not known and would require specific study.

In conclusion, foci of high intensity involving the white matter on intermediate and long TR MR images appear to be found less commonly in all migraineurs than previously thought, and their prevalence in younger patients is lower still. However, a relatively increased prevalence of white matter lesions in older migraineurs has yet to be proved. We suggest that these lesions may be due in part to the intolerance of an aging brain to the stresses of migrainous events long in duration or of a severe nature.

REFERENCES

1. Du Boulay GH, Ruiz JS, Rose FC, Stevens JM, Zilkha KJ. CT changes associated with migraine. *AJNR* **1983**;4:472–473
2. Cuetter AC, Aita JF. CT scanning in classic migraine. *Headache* **1983**;23:195
3. Mathew NT, Meyer JS, Welch KMA, Neblett CR. Abnormal CT scans in migraine. *Headache* **1977**;16:272–279
4. Soges LJ, Cacayorin ED, Petro GR, Ramachandran TS. Migraine: evaluation by MR. *AJNR* **1988**;9:425–429
5. Jacome DE, Leborgne JL. MRI studies in basilar artery migraine. *Headache* **1990**;30:88–90
6. Kaplan RD, Solomon GD, Diamond S, Freitag FG. The role of MRI in the evaluation of a migraine population. Preliminary data. *Headache* **1987**;27:315–318
7. Raskin NH. Migraine: clinical aspects and pathogenesis. In: Raskin NH, ed. *Headache*, 2nd ed. New York: Churchill Livingstone, **1988**:35–133
8. Posner JB. Headache and other pain. In: Wyngaarten JB, Smith LH, eds. *Cecil textbook of medicine.* Philadelphia: Saunders, **1988**:2129–2136
9. Johnson CE, Zimmerman RD. Imaging decisions in the evaluation of headache. *Magn Reson Imaging Decisions* **1989**;3:2–16
10. Brant-Zawadzki M, Fein G, Van Dyke C, Kiernan R, Davenport L, de Groot J. MR imaging of the aging brain: patchy white matter lesions and dementia. *AJNR* **1985**;6:675–682
11. Kirkpatrick JB, Hayman LA. White-matter lesions in MR imaging of clinically healthy brains of elderly subjects: possible pathologic basis. *Radiology* **1987**;162:509–511
12. Drayer BP. Imaging of the aging brain: Part I. Normal findings. *Radiology* **1988**;166:785–796
13. Braffman BH, Zimmerman RA, Trojanowski JQ, Gonatas NK, Hickey WF, Schlaepfer WW. Brain MR: Pathologic correlation with gross and histopathology. 2. Hyperintense white-matter foci in the elderly. *AJNR* **1988**;9:629–636
14. Hendrie HC, Farlow MR, Austrom MG, Edwards MK, Williams MA. Foci of increased T2 signal intensity on brain MR of healthy elderly subjects. *AJNR* **1989**;10:703–707

High-Intensity Signals Within the Posterior Pituitary Fossa: A Study with Fat-Suppression MR Techniques

Leighton P. Mark[1]
Victor M. Haughton
Lloyd E. Hendrix
David L. Daniels
Alan L. Williams
Leo F. Czervionke
Russell J. Asleson

Five different theories have been proposed to explain the high-intensity signals within the posterior pituitary fossa seen on MR: (1) a paramagnetic effect of phospholipids in the posterior lobe, (2) lipid in pituicytes in the posterior lobe of the pituitary, (3) neurosecretory granules in the posterior lobe, (4) fat within the sella but outside the pituitary gland, and (5) fat in bone marrow in the dorsum sellae. Previous reports have contained conflicting evidence on which of these structures is the cause of the high-intensity signals within the posterior sella. The purpose of this study was to examine the high-intensity signals of the normal posterior sella with fat-suppression MR techniques to reevaluate the contribution of fat to those signals. The sellae of 19 normal volunteers and two cadavers were imaged with MR with a commercially available unit and a research fat- water-suppression technique. High-intensity signals in the posterior sella were observed in all 21 subjects on conventional T1-weighted MR images. In two volunteers, the high-intensity signals in the posterior sella were suppressed with fat-suppression techniques; in 17 subjects the signals were suppressed with water-suppression techniques. In two volunteers the results were indeterminate. The high-intensity signals in the posterior sella do not behave like lipid in the majority of cases.

Our study supports the conclusion that high-intensity signals in the posterior sella may have more than one source. It appears that most of these sources do not suppress with fat-suppression techniques.

***AJNR* 12:529–532, May/June 1991; *AJR* 157:389–392, August 1991**

The high-intensity signals that have been observed near the posterior pituitary fossa on T1-weighted MR images have received different interpretations. On the basis of anatomic, clinical, and experimental observations, there are five hypothetical sources for these signals: a paramagnetic effect of phospholipids in the posterior lobe [1], fat in the sella outside the gland [2], a short T1 substance in neurosecretory granules in the posterior lobe [3–6], lipid in pituicytes in the posterior lobe [7, 8] (Sze G et al., presented at the annual meeting of the American Society of Neuroradiology, May 1987), and lipid in the dorsum sellae and posterior clinoid bone marrow adjacent to the sella. The purpose of this study was to examine the high-intensity signals of the normal posterior sella with thin MR sections and fat-suppression techniques to evaluate the contribution of fat to those signals.

Subjects and Methods

Twenty-one subjects, including 19 normal volunteers and two cadavers, were studied with a 1.5-T General Electric Signa imager. In each case sagittal spin-echo images, 600–800/20–25 (TR/TE), were obtained with a 256 × 256 matrix, 16- to 24-cm field of view, two averages, and 3-mm slice thickness. Sagittal images of each subject were also obtained with two fat- and water-suppression imaging techniques: (1) a commercially available version of the Dixon method (PREFCMEMP, General Electric) [9–11] and (2) a research technique (hybrid 1331 chopper) [12]. In the former, a frequency-selective pulse is used to suppress the water- or

Received August 22, 1989; revision requested October 16, 1989; final revision received December 11, 1990; accepted December 12, 1990.

Presented at the annual meeting of the American Society of Neuroradiology, Orlando, FL, March 1989.

[1] All authors: Department of Radiology, Medical College of Wisconsin, Froedtert Memorial Lutheran Hospital, 9200 W. Wisconsin Ave., Milwaukee, WI 53226. Address reprint requests to L. P. Mark.

0361-803X/91/1572-0389
© American Roentgen Ray Society

fat-proton signal. In the latter, temporally asymmetric imaging is used to distinguish signals from fat and water protons. In some cases, a 1.5-mm slice thickness was used in place of or in addition to a 3.0-mm thickness. The MR images without fat suppression were compared with fat- and water-suppression images of the same subject. All images were evaluated by two interpreters. Classification of each case as suppressing with fat suppression or with water suppression was made by a consensus of the two interpreters. If the interpreters did not agree, or if they were unsure as to how to classify the case, it was called indeterminate.

Results

Technically adequate fat- and water-suppression images were obtained in 19 of the 21 subjects; technically satisfactory fat-suppression images without technically satisfactory water-suppression images were obtained in two (Table 1). Results with the hybrid 1331 chopper and PREFCMEMP techniques were identical.

Of the 21 studies, 17 (including the two cadavers) showed suppression with water suppression (Fig. 1), two showed suppression with fat suppression (Figs. 2 and 3), and two were judged indeterminate because both interpreters believed the suppression was incomplete with both water- and fat-suppression techniques. With the exception of these two cases, suppression with water- and fat-suppression techniques were mutually exclusive.

TABLE 1: Results of Fat- and Water-Suppression Studies in 21 Cases of High-Intensity Signal in the Posterior Sella

No. of Cases	Technique	
	Fat Suppression	Water Suppression
16	No suppression	Suppression
1	No suppression	Not available
1	Suppression	No suppression
1	Suppression	Not available
2	Indeterminate	Indeterminate

Discussion

Results of fat and water suppression were not identical in all subjects in this study. In 79% of cases the high-intensity signals in the posterior sella were suppressed with water-suppression techniques but not with fat-suppression techniques. Fat-suppression images were not available for one subject. In these cases, therefore, the high-intensity signals in the posterior sella are likely the result of a short T1 substance that is within the posterior lobe [1], not of fat in pituicytes in the posterior inferior sella, or in bone marrow. In 10% of the subjects studied, the high-intensity signals showed suppression with fat-suppression but not with water-suppression techniques. Water-suppression images were not available in one case. In these cases the high-intensity signals may originate from fat and not a short T1 substance. In 10% of cases, in which neither fat nor water suppression eliminated the high signal intensity in the sella, both a lipid and a paramagnetic (i.e., phospholipid) source might have been present.

The technical limitations of the study do not discount the observation. The signal intensities were studied qualitatively and not quantitatively. Because of the small number of subjects of the study group, the relative proportions of fat- or water-suppressing signals can only be estimated. Although magnetic susceptibility artifacts seen in the suppression techniques may to some degree obscure high-intensity signals in the region of the posterior pituitary fossa, the artifacts observed were not judged to be sufficiently conspicuous to do so completely. Our study supports the conclusions that the source of the high-intensity signals in the pituitary fossa is not the same in all cases and that the source does not behave like fat in the majority of cases.

In previous investigations, a single explanation was as-

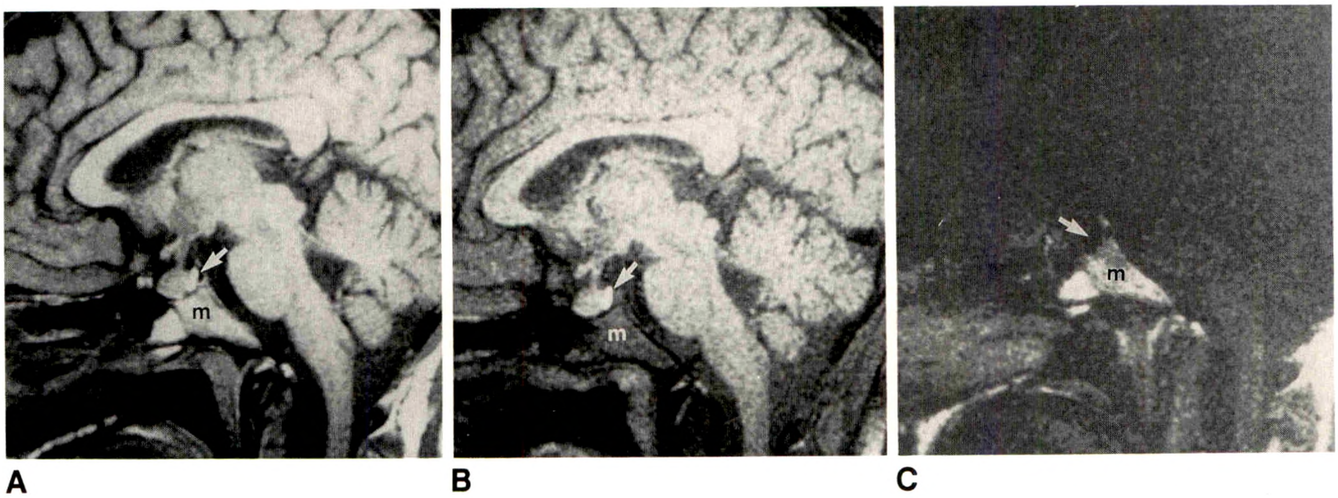

Fig. 1.—Suppression of high-intensity signals in posterior pituitary fossa with water-suppression techniques.

A, **Sagittal T1-weighted spin-echo MR image shows high-intensity signals from posterior pituitary fossa (*arrow*) and sphenoid marrow elements (m).**

B, **Sagittal fat-suppression MR image (hybrid 1331 chopper technique) shows suppression of high-intensity signals from sphenoid marrow elements (m) but no suppression of high-intensity signals from posterior pituitary fossa (*arrow*).**

C, **Sagittal water-suppression MR image (hybrid 1331 chopper technique) shows suppression of high-intensity signal (*arrow*) in posterior pituitary fossa. Signals from brain are suppressed also; high-intensity signals from sphenoid marrow elements (m) are not.**

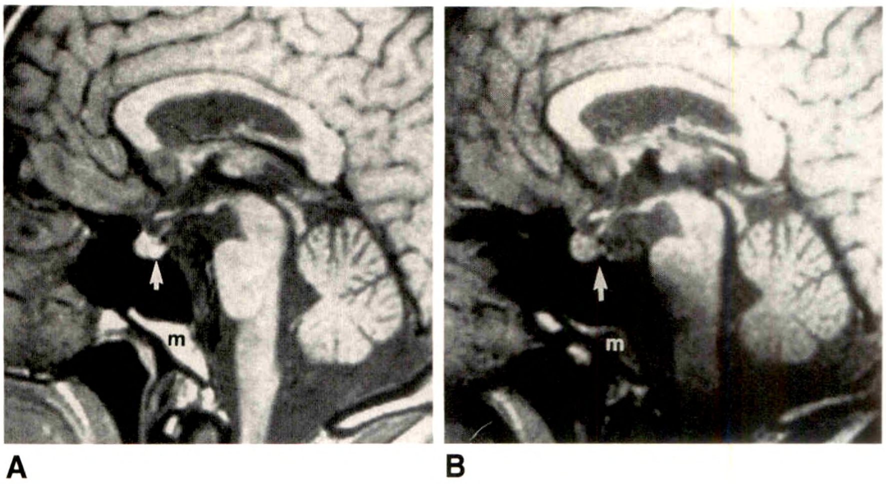

Fig. 2.—Suppression of high-intensity signals in pituitary fossa with fat-suppression techniques.

***A,* Sagittal T1-weighted spin-echo MR image shows high-intensity signals in posterior pituitary fossa (*arrow*) and sphenoid marrow elements (m).**

***B,* Sagittal fat-suppression MR image (hybrid 1331 chopper technique) shows suppression of high-intensity signals in posterior pituitary fossa (*arrow*) and sphenoid marrow (m). Partial obscuring of posterior sella signals by susceptibility artifact is shown also. Water-suppression image was not obtained in this case.**

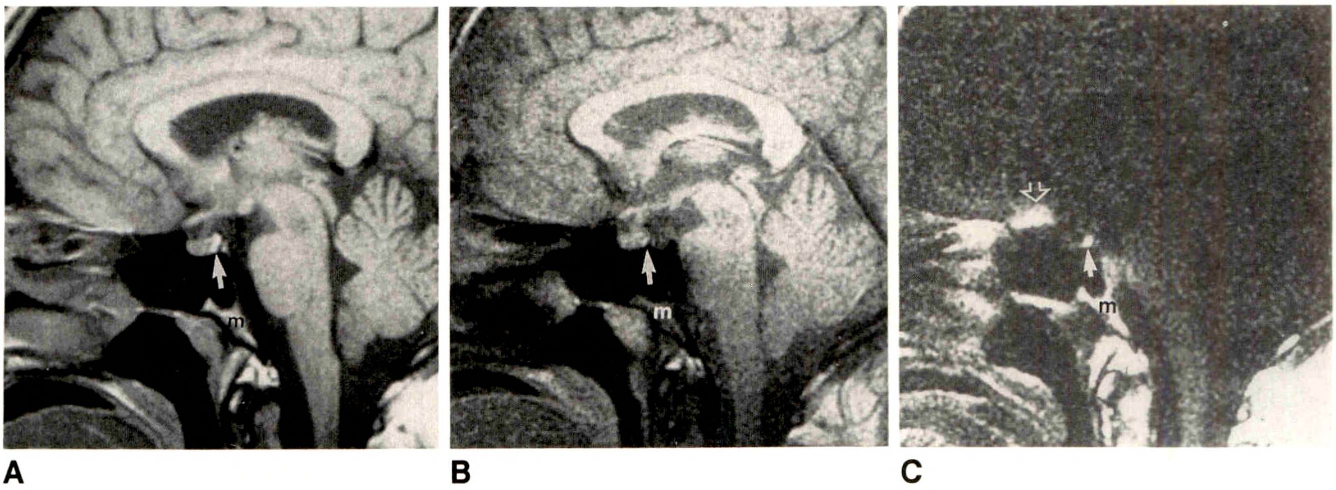

Fig. 3.—Second case illustrating suppression of high-intensity signals in pituitary fossa with fat-suppression techniques.

***A–C,* Sagittal T1-weighted spin-echo MR image (*A*), PREFCMEMP fat-suppression MR image (*B*), and water-suppression MR image (*C*). High-intensity signals in posterior pituitary (*solid arrows*) and sphenoid (m) are labeled. Air in sphenoidal sinus causes artifacts (*open arrows*) and distortion of high-intensity signals in water-suppression study.**

sumed for the high-intensity signal in the posterior sella. In one study, high-intensity signals were present in the posterior sella in most of the subjects, and a small crescent-shaped area of extraglandular fat was observed in the posterior sella in anatomic images, especially in paramidline sections. Therefore, the high-intensity signal from the pituitary fossa was assumed to correlate with the extraglandular fat [2]. The study suggested that at least in some cases, a region of high-intensity signal in the posterior pituitary fossa may represent fat inside the sella but outside the gland. Others have documented the presence of a fat pad in the sella (Blatter D et al., presented at the annual meeting of the American Society of Neuroradiology, March 1989).

A possible association between the high-intensity signals in the posterior sella and neurosecretory granules in the pituitary posterior lobe was reported by Fujisawa et al. [3–5] on the basis of observations in normal volunteers [3], patients with diabetes insipidus [4], and patients with idiopathic pituitary dwarfism and pituitary stalk transection [5]. Fujisawa et al. [6] also performed experimental studies in rabbits that supported the concept of neurosecretory granules with high-intensity signals [6]. Nishimura et al. [14] concluded that the source of the high-intensity signal was not fat because they observed no chemical-shift effect associated with the region of high-intensity signal.

Two investigators who recognized that pituicytes contained lipid bodies suggested that the high-intensity signals in the posterior sella were from lipid in the pituitary posterior lobe [7, 8]. Colombo et al. [7] reviewed the MR images of 200 patients and attributed the high-intensity signals in the posterior sella to the posterior lobe because of the size and position of the hyperintense signal and the changes in the appearance of this signal in various pathologic states. On the basis of MR images in animals and corresponding histologic and electron microscopic studies of the pituitary gland before and after pharmacologic stimulation, Kucharczyk et al. [8] suggested that the pituitary hyperintensity represented intracellular lipid in pituicytes. Others have found an inconsistency between chemical-shift imaging and the theory that the high-intensity signals originate from intracellular lipid [13] (Blatter et al., ASNR, March 1989). Kucharczyk et al. [1] performed experimental studies on the MR characteristics of phospholipid vesicles. Their observations supported the concept that a phospholipid is a relaxation enhancer of water protons that creates MR characteristics approximating the appearance of the high-intensity signals in the posterior sella.

The majority of our cases showed high-intensity signals in the posterior sella that suppressed with water-suppression techniques but not with fat-suppression techniques. These observations are consistent with those by Kucharczyk et al. [1], Blatter et al. (ASNR, March 1989), and Kim et al. (Kim BJ et al., ASNR, March 1989). The two cases that showed signal suppression with fat-suppression techniques suggest the presence of a lipid source instead of or in addition to a relaxation-enhancing substance in the posterior lobe. No chemical-shift effect [12] was observed to support the suggestion. Nonetheless, the possibility that fat or other substances such as cholesterol, complex proteins, triglycerides, and fatty acids [1] occasionally may be present as a confounding factor in the analysis of the sella should be considered.

Our study supports the conclusion that there may be more than one source of the high-intensity signals in the posterior sella. Sources that do not suppress with fat-suppression techniques appear to account for the majority of cases, as suggested by Kucharczyk et al. [1], Blatter et al. (ASNR, March 1989), and Kim et al. (ASNR, March 1989). Sources that suppress with fat-suppression techniques account for the minority of cases. In these cases, artifact, a fat pad in the sella, or lipid in pituicytes or, less likely, bone marrow may provide the explanation. The two sources may not be mutually exclusive. In future investigations of the sella, more than one source for high-intensity signals may need to be considered.

REFERENCES

1. Kucharczyk W, Lenkinski RE, Kucharczyk J, et al. The effect of phospholipid vesicles on the NMR relaxation of water: an explanation for the MR appearance of the neurohypophysis? *AJNR* **1990**;11:693–700
2. Mark L, Pech P, Daniels D, Charles C, Williams A, Haughton V. The pituitary fossa: a correlative anatomic and MR study. *Radiology* **1984**;153:453–457
3. Fujisawa I, Asato R, Nishimura K, et al. Anterior and posterior lobes of the pituitary gland: assessment by 1.5 T MR imaging. *J Comput Assist Tomogr* **1987**;11:214–220
4. Fujisawa I, Nishimura K, Asato R, et al. Posterior lobe of the pituitary in diabetes insipidus: MR findings. *J Comput Assist Tomogr* **1987**;11:221–225
5. Fujisawa I, Kikuchi K, Nishimura K, et al. Transection of the pituitary stalk: development of ectopic posterior lobe assessed with MR imaging. *Radiology* **1987**;165:487–489
6. Fujisawa I, Asato R, Kawata M, et al. Hyperintense signal of the posterior pituitary on T1-weighted images: an experimental study. *J Comput Assist Tomogr* **1989**;13:371–377
7. Colombo N, Berry I, Kucharczyk J, et al. Posterior pituitary gland: appearance on MR images in normal and pathologic states. *Radiology* **1987**;165:481–485
8. Kucharczyk J, Kucharczyk W, Berry I, et al. Histochemical characterization and functional significance of the hyperintense signal on MR images of the posterior pituitary. *AJNR* **1988**;9:1079–1083
9. Keller P, Hunter W Jr, Schmalbrock P. Multisection fat-water imaging with chemical shift selective presaturation. *Radiology* **1987**;164:539–541
10. Dixon W. Simple proton spectroscopic imaging. *Radiology* **1984**;153:189–194
11. Brateman L. Chemical shift imaging: a review. *AJR* **1986**;146:971–980
12. Szumowski J, Plewes D. Separation of lipid and water MR imaging signals by chopper averaging on the time domain. *Radiology* **1987**;165:247–250
13. Nishimura K, Fujisawa I, Togashi K, et al. Posterior lobe of the pituitary: identification by lack of chemical shift artifact in MR imaging. *J Comput Assist Tomogr* **1986**;10:899–902

The Role of Contrast-Enhanced MR Imaging in the Diagnosis of Neurocysticercosis

Kee Hyun Chang[1]
Jeong Hun Lee
Moon Hee Han
Man Chung Han

Pre- and postcontrast MR images of 17 patients with the diagnosis of neurocysticercosis were reviewed to evaluate the role of gadopentetate dimeglumine in MR imaging of this disease. The MR images, which were obtained on either a 0.5-T or 2.0-T superconducting system, revealed a total of 92 cysticerci in 17 patients. On contrast-enhanced T1-weighted images, 23 parenchymal cysticerci showed contrast enhancement. Ring-shaped enhancement was seen in only 6% (3/54) of cysticerci with intensity paralleling the CSF, while it was noted in 67% (16/24) of the cysticerci with intensity higher than CSF. Nodular enhancement was seen in granulomatous lesions with surrounding edema (29%, 4/14). Of 18 cysticerci with surrounding edema, 17 showed contrast enhancement. Basal meningeal enhancement, indicating meningitis, was observed in three patients.

The results indicate that contrast enhancement usually occurs in patients in whom precontrast MR findings have shown active inflammatory reaction in the degenerating stage of the worm. Thus, postcontrast imaging is useful in a limited number of patients with neurocysticercosis; it should be used selectively in those whose clinical or precontrast MR studies show meningitis, granulomatous lesions, or cysts with surrounding edema.

***AJNR* 12:509–512, May/June 1991; *AJR* 157:393–396, August 1991**

MR imaging proved to be a useful imaging method in diagnosing neurocysticercosis and appears to be superior to CT in almost all patients with neurocysticercosis except those with only small calcification [1–9]. Although gadopentetate dimeglumine has increasingly been used in patients with CNS abnormalities [10], it remains undetermined whether the patient suspected of having neurocysticercosis should have contrast-enhanced MR imaging. The purpose of this study is to evaluate the role of gadopentetate dimeglumine in the MR evaluation of neurocysticercosis.

Subjects and Methods

Seventeen patients (14 men and three women) with neurocysticercosis who ranged in age from 29 to 67 years old (mean, 47.7 years) were studied with MR imaging before and after enhancement with gadopentetate dimeglumine, and the images were evaluated retrospectively. The diagnosis of neurocysticercosis was made on the basis of the combined results of the imaging findings and positive serologic test, enzyme-linked immunosorbent assay (ELISA) for cysticercus-specific immunoglobulin G (IgG) antibody in both serum and CSF. In eight patients diagnosis was confirmed surgically. In nonsurgically confirmed cases, MR findings of multiple round cysts, each containing a tiny eccentric nodule, representing the scolex of the worm, were considered as definite confirmation of neurocysticercosis, regardless of ELISA test. Such findings are virtually pathognomonic of neurocysticercosis, particularly in an endemic area such as Korea. When the scolex was not visible within the cysts, only the cases with both positive ELISA results in CSF and MR findings of multiple cysts were regarded as neurocysticercosis. The patients with MR findings of only nodular lesion(s) were not included here, regardless of ELISA results.

The MR images were obtained on a 0.5-T superconducting unit (Supertec-5000, GoldStar, Seoul) in seven patients and a 2.0-T superconducting unit (Spectro-20000, GoldStar, Seoul)

Received August 13, 1990; revision requested September 17, 1990; revision received November 5, 1990; accepted November 6, 1990.

[1] All authors: Department of Diagnostic Radiology, Seoul National University Hospital, 28 Yongondong Chongno-gu, Seoul 110-744, Korea. Address reprint requests to K. H. Chang.

0361-803X/91/1572-0393
© American Roentgen Ray Society

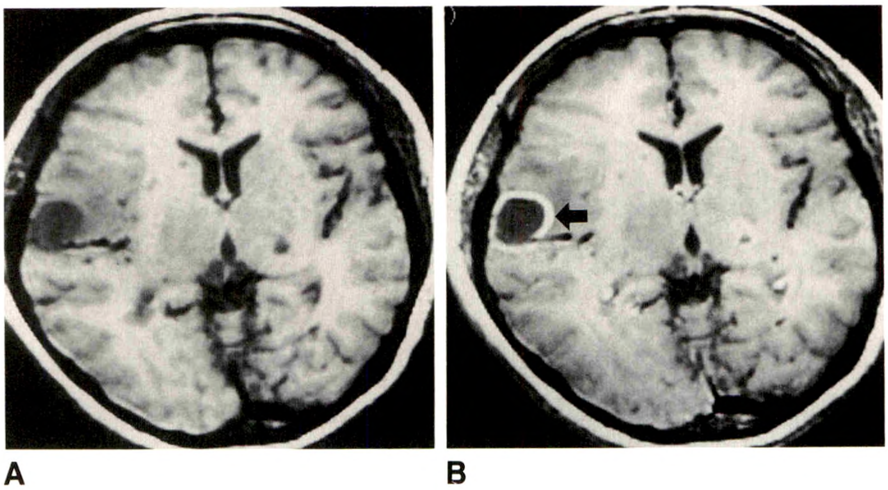

Fig. 1.—Cysticercosis in various stages.

***A*, Precontrast axial SE 500/30 MR image shows a cyst of low (but higher than CSF) intensity in right parietal lobe with surrounding edema of low intensity. Multiple small nodular lesions of iso- or low intensity are also seen in left frontal lobe, left thalamus, and right basal ganglia.**

***B*, Contrast-enhanced axial SE 500/30 MR image shows thick, ring-shaped enhancement of cysticercus in right parietal lobe (*arrow*). There is also faint nodular enhancement in left thalamic lesion.**

in 10 patients, with multiecho, multislice, spin-echo (SE) pulse sequences. Before contrast administration, T1-weighted (500/30, TR/TE) sagittal images and proton-density-weighted (2000–3000/30) and T2-weighted (2000–3000/80–100) axial images were obtained. After IV injection of gadopentetate dimeglumine (0.07–0.1 mmol/kg body weight), T1-weighted axial and sagittal, and sometimes coronal, images were obtained. The slice thickness/gap was 5 mm/2 mm for the 2.0-T unit and 7 mm/2 mm for the 0.5-T unit. In one case of spinal cord cysticercosis, slice thickness/gap was 3 mm/1 mm in the sagittal plane and 5 mm/2 mm in the axial plane. The acquisition matrix was 256 × 256, with spatial resolution of 1 mm × 1 mm. The number of excitations ranged from 4 to 6 for T1-weighted images and 1 to 2 for T2-weighted images.

The MR images were reviewed with attention to the location of cysticerci, pericysticercal edema, signal intensity of the cyst contents, presence and pattern of contrast enhancement, and their relationships, by two neuroradiologists and a senior radiology resident experienced with high-field MR imaging and the use of contrast material, together with all clinical information and results of ELISA.

Results

Ninety-two cysticerci were observed in 17 patients; 82 cysticerci were in the parenchyma, seven on the leptomeninges, two within the fourth ventricle, and one within the cervical spinal cord. Among the 92 cysticerci, contrast enhancement was shown in 23 parenchymal cysticerci in 10 patients: ring-shaped enhancement (Figs. 1–3) was seen in 19, and nodular enhancement (Fig. 4) in four. Of 54 cysticerci with signal intensity identical to that of CSF on all pulse sequences, only three revealed thin ring-shaped contrast enhancement. Sixteen of 24 cysticerci with signal intensity higher than that of CSF on T1- and proton-density-weighted images showed thin or thick ring-shaped enhancement (Figs. 1 and 3). The remaining 14 lesions had a nodular appearance on precontrast MR without cystic content; they measured 10 mm or less in diameter. Ten of the lesions appeared hypointense or isointense relative to brain parenchyma on precontrast T1- and T2-weighted images, and the other four appeared slightly hypointense on the T1-weighted images, and markedly hypointense on proton-density- and T2-weighted images. Of the former group (10 lesions), four with surrounding edema of variable degrees showed nodular or microring enhancement (Figs. 1 and 4), while none of the latter group (four lesions) demonstrated the contrast enhancement that proved to be calcifications on precontrast CT scans.

Seventeen of 18 lesions with surrounding edema of variable degrees were included in the 23 lesions with contrast enhancement. Only one of the 18 lesions with surrounding edema revealed no contrast enhancement. Twelve of 13 cysticerci with both surrounding edema and signal intensity higher than that of CSF on T1- and proton-density-weighted images enhanced; only four of 60 cysticerci both without surrounding edema and with signal isointense with CSF enhanced. The relationship between the focal contrast enhancement, the surrounding edema, and the appearance of the cysticerci is summarized in Table 1.

Three cases demonstrated meningeal enhancement. One case with multiple leptomeningeal cysticerci in the right sylvian

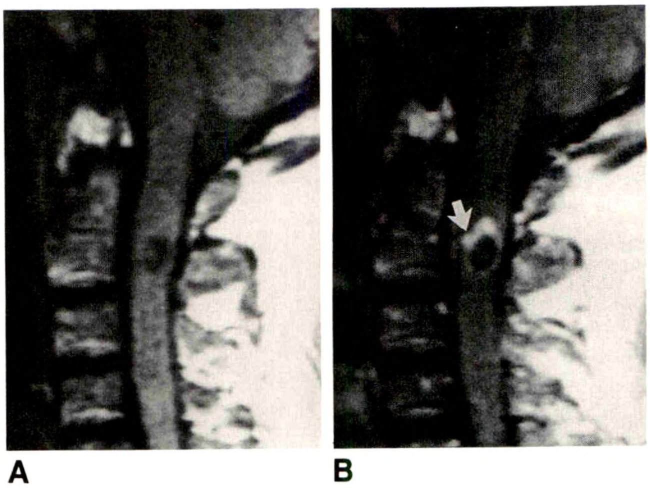

Fig. 2.—Cysticercosis of the spinal cord.

***A*, Precontrast sagittal SE 500/30 MR image shows cyst of low signal intensity with eccentric dotlike structure, suggesting a scolex in spinal cord at level of C2–C3.**

***B*, Contrast-enhanced sagittal SE 500/30 MR image shows "signet ring-shaped" enhancement (*arrow*).**

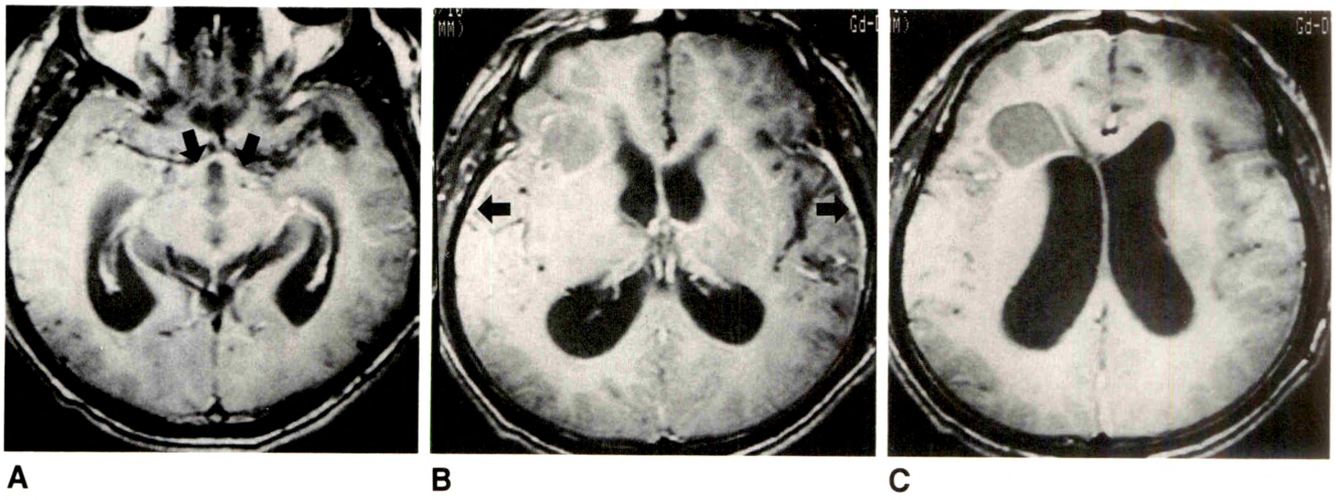

Fig. 3.—Cysticercal meningitis.
A–C, Contrast-enhanced SE 500/30 MR images show meningeal enhancement at suprasellar cistern and bilateral temporal convexities (*arrows*) in association with a cysticercus with ring enhancement in right frontal lobe.

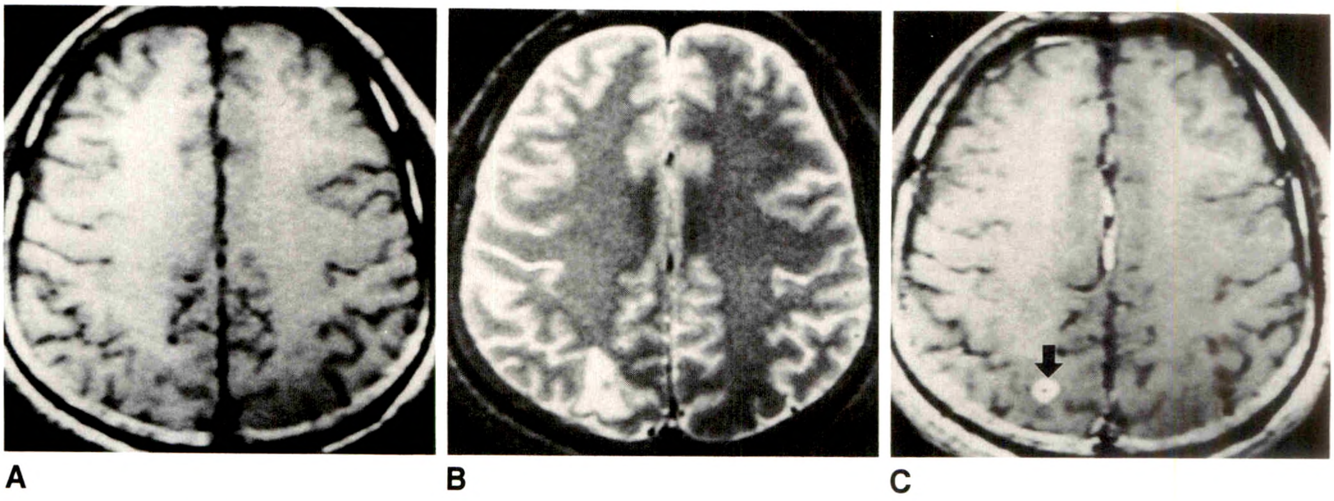

Fig. 4.—Cysticercosis in granulomatous nodular stage.
A, Precontrast SE 500/30 MR image shows small cysticercus of slight hypointensity or isointensity relative to brain parenchyma in right parietal lobe.
B, Precontrast SE 3000/80 MR image shows surrounding edema of high signal intensity with a small central nodule of slightly low intensity.
C, Contrast-enhanced SE 500/30 MR image shows nodular or microring-shaped enhancement of nodule (*arrow*).

cistern showed linear meningeal enhancement in the right sylvian cistern. The second case revealed a solitary parenchymal cysticercus with ring enhancement in the right frontal lobe associated with meningeal enhancement along the suprasellar cistern and bilateral temporal convexities (Fig. 3). The remaining case, with cysticerci in the left frontal lobe and the fourth ventricle, demonstrated meningeal enhancement along the right sylvian cistern and left side of the tentorium in association with multiple subacute enhancing infarcts in both temporal lobes, the right thalamus, and pons.

Discussion

MR findings of neurocysticercosis are variable, depending on the stage in evolution of the infection [1, 2, 6, 7, 11, 12]. In the vesicular stage, the larva is seen as a small marginal nodule projecting into a cyst containing clear fluid. A thin capsule surrounds the cyst at this stage. The inflammatory reaction is well localized to the adjacent brain tissue and there may be only a small ring of edema and glial proliferation. In this stage, the cysticercus appears as a round cyst with a mural nodule (scolex) without enhancement or edema on MR and CT. The cystic fluid appears isointense with CSF on all MR pulse sequences [1, 2, 11]. In the present study, only 6% (3/54) of the cysticerci in the vesicular stage revealed contrast enhancement.

In the next stage (colloidal vesicular stage), the larvae begin to degenerate. The cyst fluid becomes turbid, and the capsule thickens. As the cysticerci degenerate, an acute encephalitic stage may ensue from humoral and tissue response to cysticerci, causing surrounding edema and enhancement on MR

TABLE 1: Relationship Between Contrast Enhancement, Edema Surrounding Lesions, and Appearance of Cysticerci

	Postcontrast Enhancement on MR		
	Positive	Negative	Total
Lesions with surrounding edema on precontrast MR			
Positive	17	1	18
Negative	6	68	74
Total	23	69	92
Appearance of cysticerci on precontrast MR			
Cystic type			
Fluid isointense with CSF[a]	3	51	54
Fluid hyperintense relative to CSF[b]	16	8	24
Nodular type			
Isointense with brain parenchyma[c]	4	6	10
Hypointense relative to brain parenchyma[d]	0	4	4
Total	23	69	92

[a] Isointense with CSF on all pulse sequences.

[b] Hyperintense relative to CSF on T1- and proton-density-weighted images.

[c] This group includes all the nodules of slight hypointensity or isointensity on all pulse sequences.

[d] This group includes all the nodules of slight hypointensity on T1-weighted images, and marked hypointensity on proton-density- and T2-weighted images.

and CT [1, 2, 11]. The enhancement is a result of an inflammatory reaction caused by degenerating larvae, which are known to release metabolic products that break down the blood-brain barrier [2, 6, 12]. The turbid cyst fluid is responsible for the signal intensity higher than that of CSF on T1- and proton-density-weighted images. On T2-weighted images, the cyst fluid and surrounding edema appear as high intensity, while the cyst wall and central scolex appear as low intensity [11]. In our series, 67% (16/24) of the cysticerci in this stage showed ring-shaped enhancement.

By the third (granular nodular) stage, the cyst has undergone retraction, its contents begin to mineralize, and its capsule is quite thick and collagenous. There is a steady decline and involution to granulomatous lesions, some of which may appear as enhancing nodules or microring-like lesions with or without surrounding edema [11, 12]. In our series, 10 cysticerci with isointense nodular patterns corresponded to this stage, and 40% (4/10) of them showed nodular or microring enhancement, suggesting granuloma.

By the final (nodular calcified) stage, the lesion is shrunken and completely mineralized. The granulomatous lesions are replaced by gliosis and, eventually, by calcified nodules [1, 2, 11, 12]. In the present series, four calcified nodules with hypointensity belonged to this stage; none of them showed contrast enhancement.

The results indicate that the contrast enhancement around the cysticerci seems to occur when there are both surrounding edema and signal intensity of the cyst contents higher than CSF on T1- and proton-density-weighted images. Such enhancement probably reflects degeneration of the worms and inflammatory reaction of the adjacent brain tissue. The degree of contrast enhancement on MR imaging may indicate the degree of focal parenchymal inflammatory reaction around the cysts, although contrast enhancement did not play a critical role in the actual diagnosis of neurocysticercosis in the vast majority of the patients. Without contrast enhancement, it may be difficult to identify the cysticerci, especially, when they are smaller than 1 cm and isointense with brain parenchyma [9]. In these cases, contrast-enhanced MR imaging appears to be indispensable for the detection of the cysticerci. In cysticercal meningitis, as seen in three patients with meningeal enhancement in the present series, it is impossible to identify the meningeal inflammation by precontrast MR imaging alone.

In conclusion, since precontrast MR imaging provides enough information to make a diagnosis of neurocysticercosis in the vast majority of patients, and contrast enhancement seems to be useful in a limited number of neurocysticercosis cases, it is suggested that contrast imaging be used selectively in patients whose clinical or precontrast MR studies show meningitis, granulomatous lesions, or cysts with surrounding edema.

REFERENCES

1. Zee CS, Segall HD, Boswell W, Ahmadi J, Nelson M, Colletti P. MR imaging of neurocysticercosis. *J Comput Assist Tomogr* **1988**;12:927–934
2. Suss RA, Maravilla KR, Thompson J. MR imaging of intracranial cysticercosis: comparison with CT and anatomopathologic features. *AJNR* **1986**;7:235–242
3. Chang KH, Kim WS, Cho SY, Han MC, Kim CW. Comparative evaluation of brain CT and ELISA in the diagnosis of neurocysticercosis. *AJNR* **1988**;9:125–130
4. Chang KH, Choe YH, Han MC, Kim CW. Magnetic resonance imaging of intracranial cysticercosis: comparison with computed tomography. *Korean J Radiol* **1987**;23:524–531
5. Rhee RS, Kumasaki DY, Sarwar M, Rodriguez J, Naseem M. MR imaging of intraventricular cysticercosis. *J Comput Assist Tomogr* **1987**;11:598–601
6. Handler LC, Mervis B. Infections and infestations: cerebral cysticercosis with reference to the natural history of parenchymal lesions. *AJNR* **1983**;4:709–712
7. Rodriguez-Carbajal J, Salgado P, Gutierrez-Alvarado R, Escobar-Izquierdo A, Aruffo C, Palacios E. The acute encephalitic phase of neurocysticercosis: computed tomographic manifestations. *AJNR* **1983**;4:51–55
8. Zee CS, Segall HD, Miller C, et al. Unusual neuroradiological features of intracranial cysticercosis. *Radiology* **1980**;137:397–407
9. Suh DC, Chang KH, Han MH, Lee SR, Han MC, Kim CW. Unusual MR manifestations of neurocysticercosis. *Neuroradiology* **1989**;31:396–402
10. Hesselink JR, Healy ME, Press GA, Brahme FJ. Benefits of Gd-DTPA for MR imaging or intracranial abnormalities. *J Comput Assist Tomogr* **1988**;12:266–274
11. Lotz J, Hewlett R, Alheit B, Bowen R. Neurocysticercosis: correlative pathomorphology and MR imaging. *Neuroradiology* **1988**;30:25–41
12. Kramer LD, Locke GE, Byrd SE, Daryabagi J. Cerebral cysticercosis: documentation of natural history with CT. *Radiology* **1989**;171:459–462

Imaging of the Basal Cerebral Arteries and Measurement of Blood Velocity in Adults by Using Transcranial Real-Time Color Flow Doppler Sonography

Takashi Tsuchiya[1]
Masahiro Yasaka
Takenori Yamaguchi
Kazumi Kimura
Tsuyoshi Omae

We report an attempt to obtain images of the basal cerebral arteries and to measure the quantitative flow velocity in these arteries from outside the skull via the color Doppler imaging method. In 25 healthy volunteers, 22–41 years old, the transducer was positioned just superior to the zygomatic arch and anterior to the external ear canal. The absolute flow velocity was calculated by dividing the measured velocity by the cosine of the incident angle. The middle cerebral artery was readily identified in all subjects, but the anterior cerebral artery was seen in only 7/50, and the posterior cerebral artery in 27/50. The corrected mean velocity of the horizontal middle cerebral artery was 86 ± 17 cm/sec at an average incident angle of 49°. However, it was difficult to calculate the absolute flow velocity in the anterior and posterior cerebral arteries because the length of those arteries delineated was too short to read the incident angle. The reproducibility of the mean blood velocity in the middle cerebral artery was tested by two examiners on two different occasions, and showed a linear regression with a correlation coefficient of 0.93 ($p < .001$) when the correction with the incident angle was made.

Transcranial real-time color-flow Doppler imaging permits more accurate noninvasive quantification of cerebral hemodynamic consequences than previous methods do.

***AJNR* 12:497–502, May/June 1991; *AJR* 157:397–402, August 1991**

In 1982, Aaslid et al. [1] demonstrated that signals could be obtained from the basal cerebral arteries with a 2-MHz probe directed intracranially from the temporal bone just above the zygomatic arch. Assessment of blood velocity in the basal cerebral arteries provides valuable information with regard to the functional capacity of the circle of Willis. Transcranial Doppler techniques have recently been used to evaluate vasospasm following subarachnoid hemorrhage, intracranial arterial stenosis, and arteriovenous malformation [2–5]. In addition, the patterns of collateral circulation in patients with extracranial carotid artery disease may be determined with this technique [6]. However, for measuring blood velocity, Doppler imaging presents several problems. Precise placement of the sample volume as well as angle correction is not possible by means of the transcranial Doppler technique.

Recently, in neonates and infants, the effectiveness of color Doppler imaging has been shown for visualizing intracranial vessels through the anterior fontanel, which serves as an acoustic window [7, 8]. But, in adults, imaging of the intracranial vessels from outside the skull has not been documented previously. In this study we chose a color Doppler technique (transcranial real-time color flow Doppler sonography) to visualize the intracranial vessels. The objectives were to investigate the possibility of obtaining images of the basal cerebral arteries with a noninvasive method and to measure more accurate flow velocity following angle correction than previously reported.

Materials and Methods

Subjects consisted of 25 healthy individuals, 11 men and 14 women, 21 to 41 years old (mean age, 28 years). Examinations were performed with a real-time B-mode and color

Received June 25, 1990; revision requested September 10, 1990; revision received October 17, 1990; accepted November 7, 1990.

[1] All authors: Cerebrovascular Division, Department of Medicine, National Cardiovascular Center, 5-7-1 Fujishirodai, Suita City, Osaka 565, Japan. Address reprint requests to T. Tsuchiya.

0361-803X/91/1572-0397
© American Roentgen Ray Society

Doppler duplex scanner (SSH 160A; Toshiba, Inc., Tokyo). The transducer was operated at 2.5 MHz for both B-mode imaging and Doppler functions. This system permits rapid visualization of arterial flow patterns by superimposing a real-time color image showing regions of blood flow on a two-dimensional B-mode tissue image. This combination is made possible by high-speed, electric array processing of ultrasound signals. Flow toward the transducer was displayed in red, flow away from the transducer in blue.

The B-mode and Doppler information within the scan fields was updated six times per second for the approximately 40° field of view. The pulse repetition frequency was mainly 3.0 KHz, and low-pass filter was 300 Hz. Proper adjustment of velocity scale to match the flow velocity of the vessels was one of the important factors for obtaining a good image. A change in the velocity scales directly reflected a change in the pulse repetition frequency or the sampling rate. Doppler color gain was first turned down completely and then increased very gradually until the static background noise barely appeared.

The subjects were examined first in the left lateral decubitus position and then in the right lateral decubitus position. The transducer was placed just superior to the zygomatic arch and anterior to the external ear canal (Fig. 1). Particular care was taken to obtain a long axis view of the desired vessel, especially of the horizontal portion of the middle cerebral artery (MCA), by means of tilting, rotating, or shifting the transducer.

For the purpose of identifying the color-flow images obtained by this system, we compared those images with the basal cerebral arteries displayed as flow-void in MR imaging in two of the subjects.

A range-gate pulsed Doppler sample volume, 5 mm in size, was used to measure both the blood flow velocity within the vessel and the angle of incidence (θ) to the vessel of interest.

The reproducibility of the MCA flow velocity was investigated in all subjects. Measurements of the MCA blood velocity were repeated within a 7-day period by two examiners. The data of each examiner were not shown to the other until the second measurement had been made.

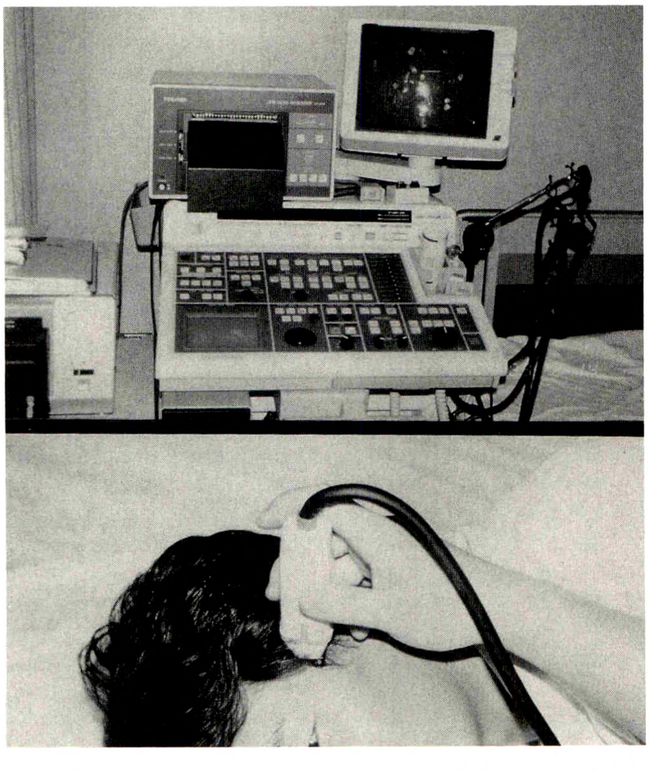

Fig. 1.—Photograph of the equipment used and the location of the ultrasonic window.

For the statistical evaluation, mean velocity was calculated from the time-averaged peak Doppler shift over one cardiac cycle. Then, the absolute velocity was calculated by dividing the measured velocity by the cosine θ. The correlations of the values measured by the two examiners were assessed by linear regression analysis.

Results

All MCAs were readily identified in all subjects, but the anterior cerebral artery (ACA) was visualized only in 7/50, and the posterior cerebral artery (PCA) in 27/50. The horizontal portion of the MCA was imaged as a slightly curved red column anterior to the small wing of the sphenoidal bone (Figs. 2 and 3). The ACA was imaged as a blue line above the sella turcica (Fig. 4), the PCA as a red line posterior to the image of the MCA. The color Doppler images of the basal cerebral arteries delineated by transcranial real-time color-flow Doppler sonography corresponded well with those displayed as flow void by MR imaging in their course and location (Fig. 2).

The measured mean velocity of the horizontal portion of the MCA in the whole series was 55 ± 16 cm/sec (mean ± standard deviation) at an average angle to the Doppler beam of 49°. The angle of incidence to the horizontal portion of the MCA varied considerably among the cases, ranging from 9° to 73°. The absolute mean velocity by angle correction was 87 ± 16 cm/sec in the horizontal portion of the MCA. However, it was difficult to calculate the absolute velocity in the ACA and PCA, because the length of the images of those arteries was too short to read the correct angle between the pulsed Doppler beam and the flow direction.

In the reproducibility study of measuring the flow velocity in the MCA, the depth of sample volume determined by the two examiners was 53.9 ± 4.3 mm and 55.5 ± 3.6 mm, respectively. The correlation between the values measured by the examiners was relatively poor, with a correlation coefficient of 0.40 ($p < .005$; Fig. 5, left). The incident angle to the horizontal MCA measured by the examiners was 49.1° ± 12.3° (range, 9° to 73° degrees) and 41.8° ± 17.7° (range, 4° to 74°), respectively. The coefficient of correlation $r = .38$ ($p < .005$) again indicated poor correlation of both measurements (Fig. 5, right).

The mean blood velocity of the horizontal MCA measured by the examiners was 55 ± 16 cm/sec and 60 ± 16 cm/sec, respectively (Fig. 6, left). When the individual flow velocity was corrected with incident angle, however, it became 87 ± 16 cm/sec and 86 ± 13 cm/sec, respectively, showing nearly the same values (Fig. 6, right). The correlation coefficient between the values of mean flow velocity obtained by both examiners markedly improved from 0.65 ($p < .001$) to 0.93 ($p < .001$), when correction was made by the incident angle (Fig. 6).

Representative color-flow images and Doppler recordings of one case obtained by the two examiners are shown in Figure 7. The depth of the sampling volumes was different

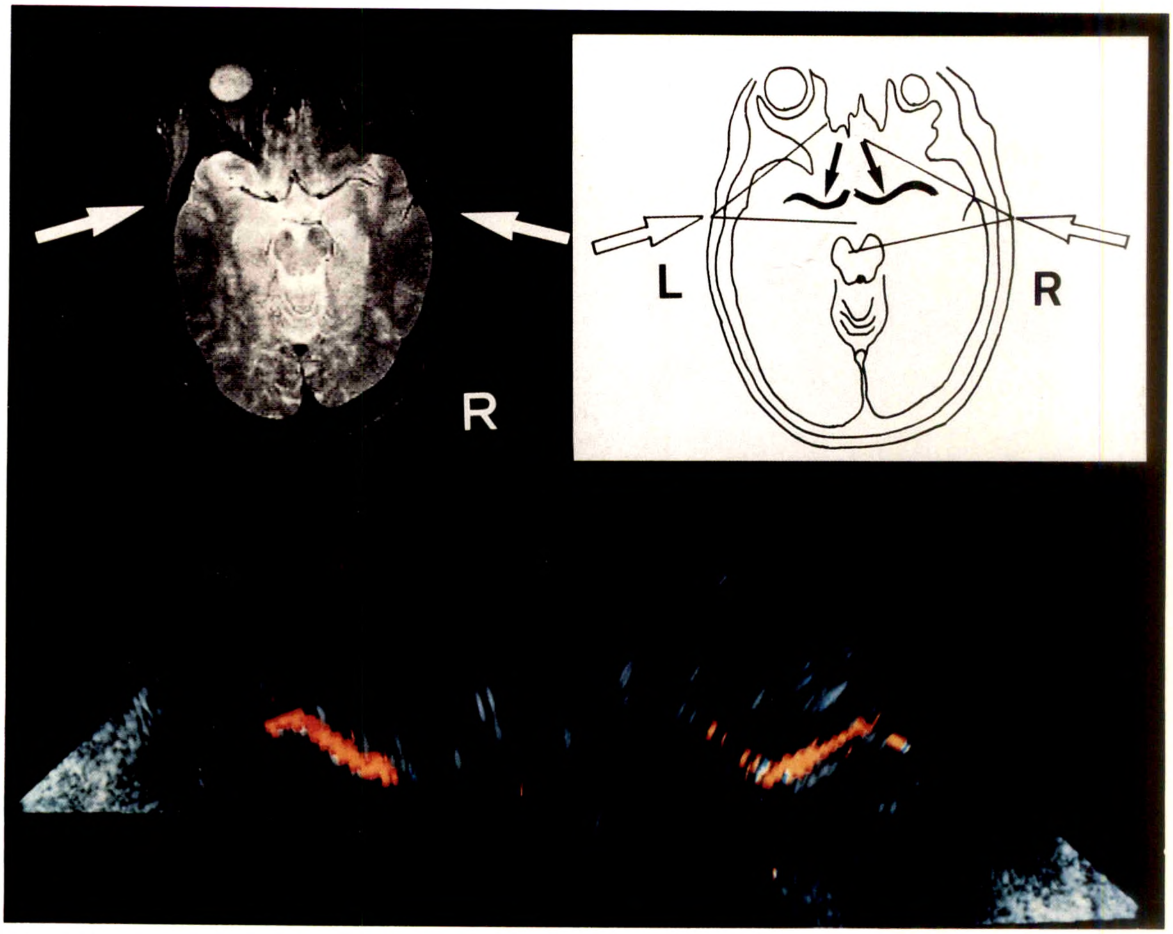

Fig. 2.—*Upper image*, T2-weighted (2000/23) MR image and corresponding graphic representation. Horizontal portion of middle cerebral artery (MCA) is displayed with intraluminal flow void (*closed arrows*). *Open arrows* indicate location of ultrasonic window used.

Lower image, Transcranial real-time color-flow Doppler sonogram of MCA in same subject. Horizontal portion of MCA is clearly imaged as red column. Course and location of horizontal MCA coincides closely with that shown by MR.

for each examiner. The mean velocities measured by the examiners were 58 cm/sec and 93 cm/sec, respectively, which were considerably different. When correction according to incident angle was made, the flow velocities approximated more closely, with respective values of 91 cm/sec and 93 cm/sec.

Discussion

Transcranial Doppler recordings of flow velocity by Aaslid et al. [1] in 1982 have been reported to be useful for evaluation of intracranial hemodynamic alterations from outside the skull [2, 3]. However, two important features of this method should be borne in mind. First, in their previous reports the insonation angle was ignored, because the angle of incidence to the MCA and ACA from the temporal window was assumed to be close to zero on the basis of the anatomic structure of the cerebral arteries. The error in the velocity measured by transcranial Doppler recordings would be less than 15%, if assuming the angle of incidence ranges from 0° to 30°. Second, the location of the sample volume used in transcranial Doppler recordings is uncertain because of a blind technique. Therefore, the source of the information of artery identification depends on the spatial relation of the signal to other intracranial signals, the direction of flow, and the response of the signal to compression test [9].

In general, accurate measurement of flow velocity by the Doppler principle requires the identification of the location of sample volume and the estimation of both the angle of incidence and the Doppler shift. The Doppler methods are capable of good absolute accuracy with systemic errors of 6% or less when suitably designed equipment is used in appropriate situations [10].

The Doppler shift is given by the following equation:

$$\delta f = 2(v \cos \theta) f_0 / C$$

where δf = Doppler shift, v = magnitude of the scatterer's velocity, θ = angle between ultrasonic beam and direction of motion, f_0 = frequency of ultrasound transmitted, and C = speed of propagation of ultrasound in blood.

Since f_0 and C are generally known, measurement of the Doppler shift allows calculation of the product ($v \cos \theta$). Any error in estimating the angle could directly affect the meas-

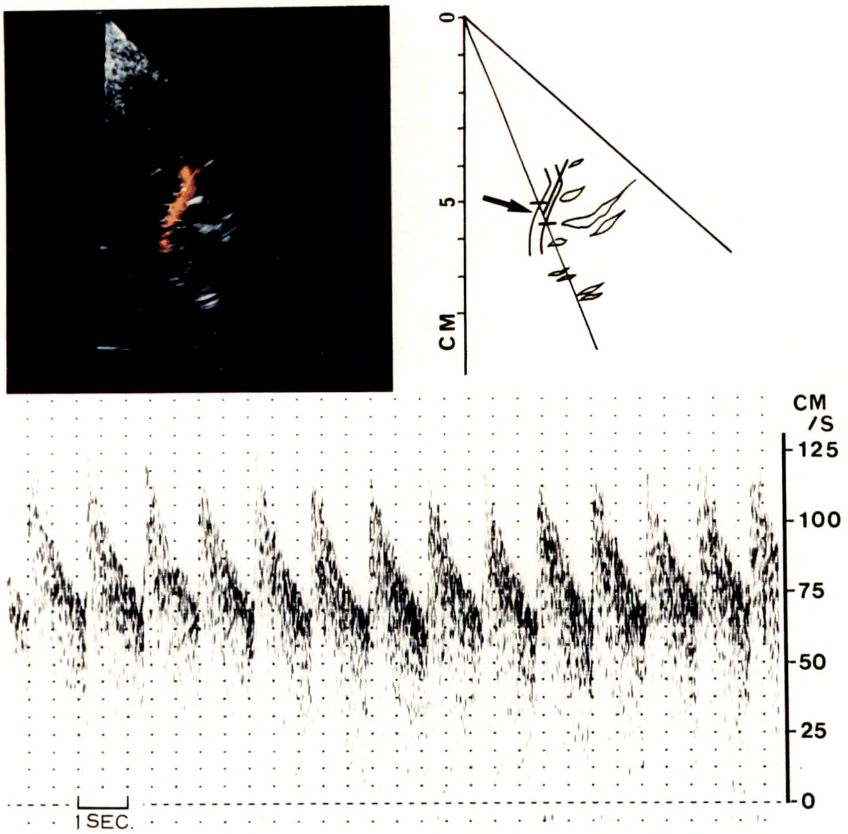

Fig. 3.—Color-flow Doppler imaging and Doppler spectrum of horizontal portion of middle cerebral artery (MCA). Length of horizontal portion of MCA is long enough to obtain accurate reading of incident angle. *Arrow* indicates location of sample volume.

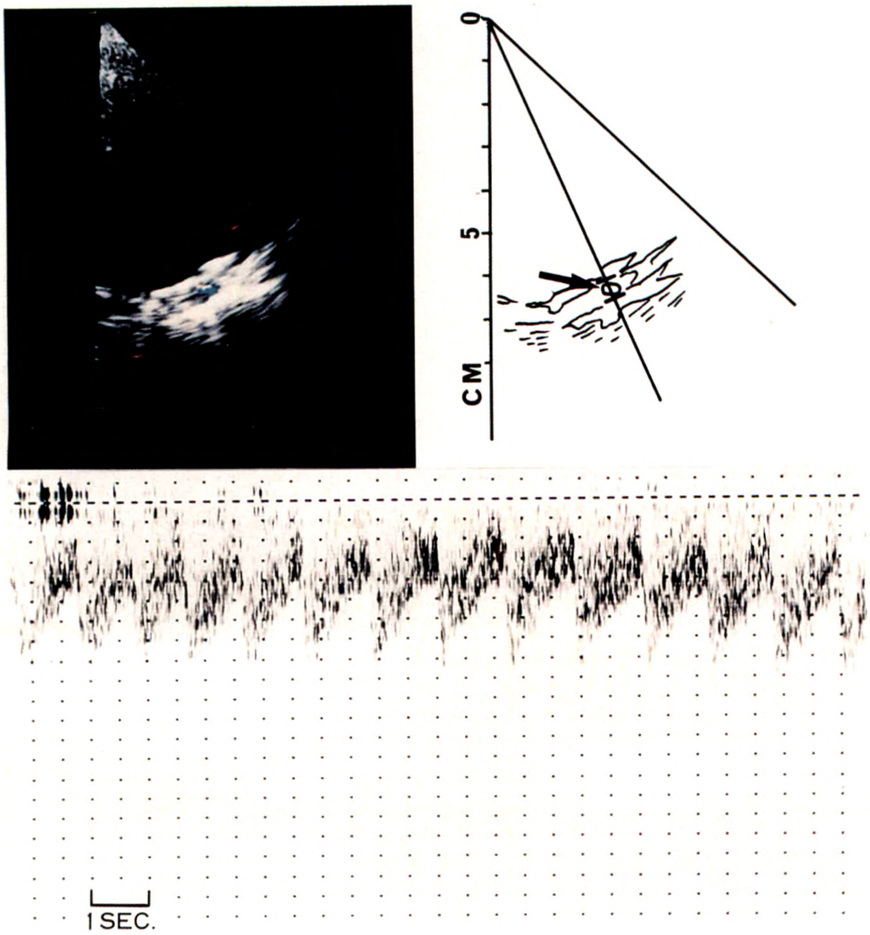

Fig. 4.—Color-flow Doppler imaging and Doppler spectrum of anterior cerebral artery (ACA). Length of ACA on color-flow Doppler image is too short to read the correct angle between pulsed Doppler beam and flow direction. *Arrow* indicates location of sample volume.

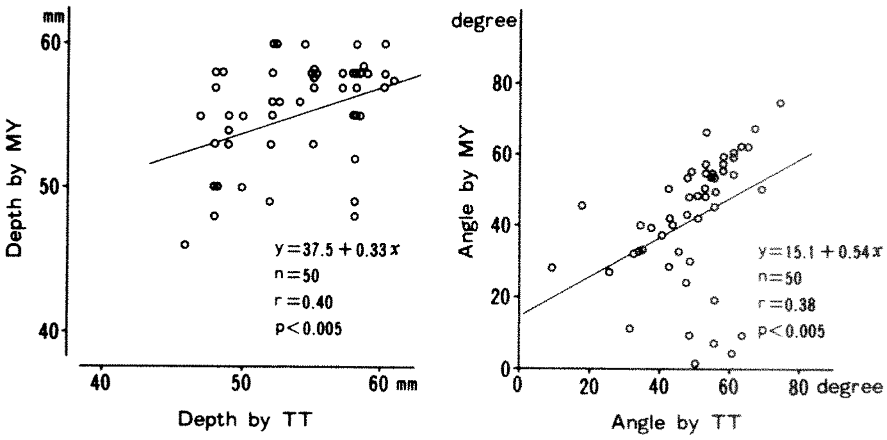

Fig. 5.—Graphs indicate reproducibility of sample volume depth (*left*) and of incident angle (*right*). Correlation between two examiners (TT, MY) was relatively poor.

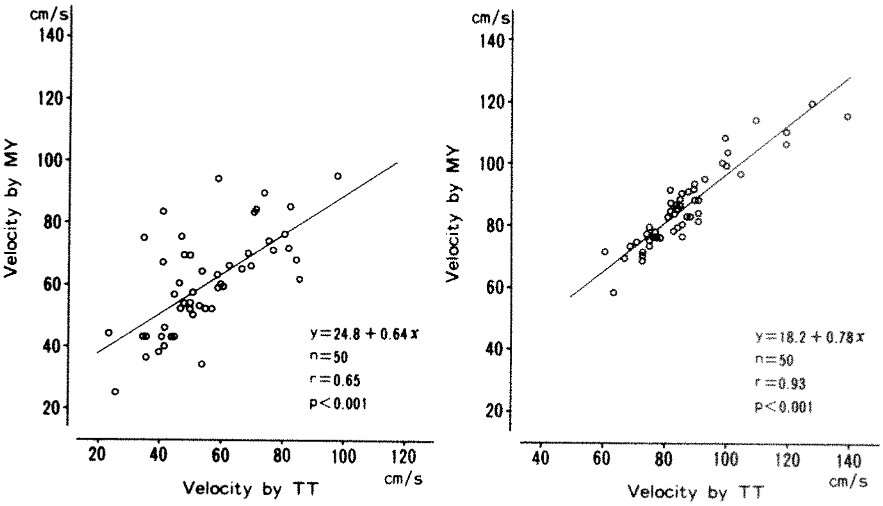

Fig. 6.—Graphs show reproducibility of measured velocity (*left*) and of corrected velocity (*right*). The values of two examiners (TT, MY) were derived by linear regression analysis.

urement of blood velocity. Moreover, when the angle θ is large, cos θ varies greatly with θ. If, for example, the angle of incidence (θ) is assumed to be 0 but is in fact 20°, the flow velocity will be underestimated by 6%. However, if the actual angle of insonation is 60°, blood velocity would be underestimated by 50%.

We succeeded in imaging the basal cerebral arteries and measuring their absolute flow velocities from outside the skull, using a real-time color-flow Doppler imaging system, which is commercially available mainly for cardiac use (SSH 160A). This instrument, which can display the bloodstream in colors superimposed on a real-time B-mode image, makes it possible to measure the angle of incidence to the vessel of interest and to identify the location of the sample volume.

In all the previous reports it was assumed that for the horizontal portion of the MCA, the angle of insonation was probably small, so that measured values corresponded well to true velocity. However, our results demonstrated that the average value of the angle between the horizontal MCA and ultrasonic beam was 49°, which was much larger than that previously assumed by Aaslid et al. [1, 11]. Moreover, the measured values of the incident angle varied from subject to subject and from side to side.

Reproducibilities for the positioning of depth of sample volume and for the incident angle between the pulsed Doppler beam and blood flow column by the two examiners were relatively poor before correction by incident angle. These results are considered to be based on the difference in positionings of the echo window and sample volume by the examiners.

The location of the ultrasonic window is one of the very important factors that decides the incident angle to the vessels of interest. According to Aaslid et al. [9], it is useful to discriminate between three different locations of the temporal window: the anterior, middle, and posterior temporal window. The anterior temporal window, which is located posterior to the frontal process of the zygomatic arch, allows the angle of insonation of almost 0° to the MCA. On the other hand, the posterior temporal window, which is located just anterior to the ear, is more suitable for insonation in elderly patients than the anterior temporal window is. From the posterior window, a somewhat more obtuse angle to the MCA might be expected. In this study, the anterior temporal window showed a poor signal-to-noise ratio in almost all subjects, and it was used in only rare cases. We used the posterior and middle temporal windows in the majority of cases in this study, at

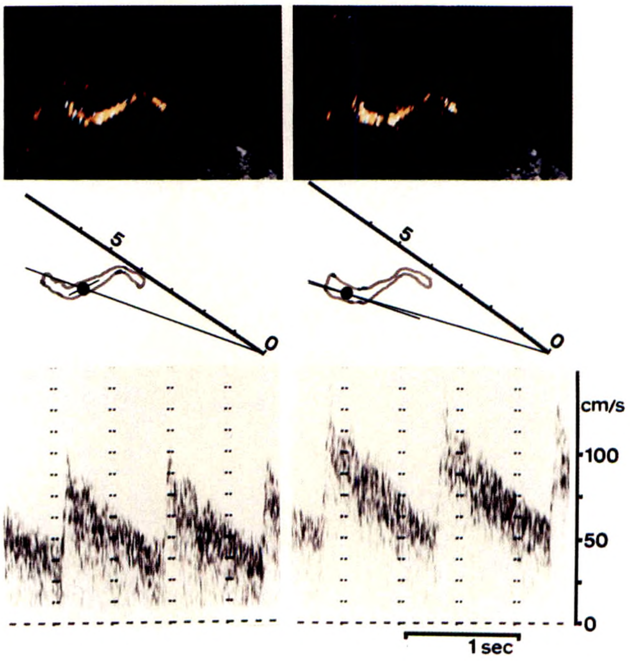

Fig. 7.—Color-flow images and spectral displays of Doppler signal from right middle cerebral artery (MCA) measured by the two examiners. *Left*, measurement by TT; *Right*, measurement by MY.

***Upper images*, Color-flow images of right MCA.**

***Middle images*, Locations of sample volume (*closed circles*) and direction of pulse Doppler beam and blood column at each location of sample volume.**

***Lower images*, Spectral display of Doppler signal at each sample volume position.**

the point where the best signal-to-noise ratio was obtained. This may have resulted in a much larger angle of incidence to the MCA (49° in a mean value) than that previously assumed.

Moreover, the angle of incidence was not always constant even if the insonation was made from the same window. This inconstancy was derived partly from individual variation of the course of the horizontal portion of the MCA and partly from the difference in positioning of the sample volume from examiner to examiner. The course of the basal cerebral arteries showed considerable variation, although the horizontal portion of the MCA was shown as a slightly curved image in most cases. Different values of the measured velocity were obtained by positioning the sample volume in the proximal or distal portion of the horizontal MCA, if not corrected by the angle of insonation.

The mean value of the MCA flow velocity in normal subjects younger than 40 years old has been reported to be 58.4 ± 8.4 cm/sec by Hennerici et al. [12]. This value corresponded well with the value of 55 ± 16 cm/sec obtained by this method before angle correction in similar subjects. When angle correction was made, however, the mean velocity of the horizontal MCA in our subjects proved to be 87 ± 16 cm/sec, higher than those in previous reports. This study demonstrated that the absolute value of the MCA flow velocity was much higher than that previously assumed.

Transcranial real-time color-flow Doppler sonography has proved to be a useful, noninvasive technique for providing an accurate estimation of cerebral hemodynamics, especially for the assessment of blood flow in the MCA. But this method does have some problems; for example, it did not produce images of the ACA and PCA that were as good as those of the MCA. Moreover, in a color Doppler imaging system, the color flow information depends on the amplitudes of the components reflected from the red blood cell; that is, on the size of the bloodstream in cross section. Thus, if the target vessels are very small in cross section, it is difficult for Doppler imaging to display the bloodstream of those arteries in colors with a good signal-to-noise ratio. As for the ACA and PCA, their anatomic course might play an important role in this result. For the purpose of obtaining better signal-to-noise imaging, further technical modification of the transcranial real-time color-flow Doppler technique is required.

REFERENCES

1. Aaslid R, Markwalder TM, Nornes H. Noninvasive transcranial Doppler ultrasound recording of flow velocity in basal cerebral arteries. *J Neurosurg* **1982**;57:769–774
2. Lindegaard KF, Bakke SJ, Grolimund P, Aaslid R, Huber P, Nornes H. Assessment of intracranial hemodynamics in carotid artery disease by transcranial Doppler ultrasound. *J Neurosurg* **1985**;63:890–898
3. Aaslid R, Huber P, Nornes H. Evaluation of cerebrovascular spasm with transcranial Doppler ultrasound. *J Neurosurg* **1984**;60:37–41
4. Wechsler LR, Ropper AH, Kistler JP. Transcranial Doppler in cerebrovascular disease. *Stroke* **1986**;17:905–912
5. Grolimund P, Seiler RW, Aaslid R, Huber P, Zurbruegg H. Evaluation of cerebrovascular disease by combined extracranial and transcranial Doppler sonography: experience in 1039 patients. *Stroke* **1987**;18:1018–1024
6. Schneider PA, Rossman ME, Bernstein EF, Torem S, Ringelstein EB, Otis SM. Effect of internal carotid artery occlusion on intracranial hemodynamics: transcranial Doppler evaluation and clinical correlation. *Stroke* **1988**;19:589–593
7. Wong WS, Truruda JS, Liberman RL, Chirino A, Vogt JF, Gangitano E. Color Doppler imaging of intracranial vessels in the neonate. *AJNR* **1989**;10:425–430
8. Deeg KH. Color flow imaging of the great intracranial arteries in infants. *Neuroradiology* **1989**;31:40–43
9. Aaslid R. Transcranial Doppler examination techniques. In Aaslid R, ed. *Transcranial Doppler sonography*. New York: Springer-Verlag, **1986**:39–59
10. Gill RW. Measurement of blood flow by ultrasound: accuracy and sources of error. *Ultrasound Med Biol* **1985**;11:625–641
11. Aaslid R, Lindegaard KF, Sorteberg W, Nornes H. Cerebral autoregulation dynamics in humans. *Stroke* **1989**;20:45–52
12. Hennerici M, Rautenberg W, Sitzer G, Schwartz A. Transcranial Doppler ultrasound for the assessment of intracranial arterial flow velocity. Part 1: Examination technique and normal values. *Surg Neurol* **1987**;27:439–448

Carotid Duplex Sonography:

Bisferious Pulse Contour in Patients with Aortic Valvular Disease

Cindy E. Kallman[1,2]
Barbara B. Gosink[1]
Douglas J. Gardner[1,3]

Characteristic systolic and diastolic pulse contours occur in the carotid Doppler waveforms of patients with aortic valvular disease that have not previously been described in publications concerning carotid duplex sonography. The purpose of this study was to evaluate the presence and characterize the nature of these carotid duplex waveform abnormalities in patients with known aortic valve disease and to correlate these changes with the severity of valve dysfunction. The study group consisted of 26 patients with aortic regurgitation or combined aortic regurgitation and aortic stenosis. Duplex studies were retrospectively reviewed by two radiologists for the presence of two systolic peaks, and for the presence of diastolic reversal of flow direction. This pattern of two systolic peaks, characteristic of aortic regurgitation, is called bisferious from the Latin "twice beating." Aortic regurgitation was graded by echocardiography as mild, moderate, or severe by the cardiologists reviewing the examination. A group of 20 age-matched patients without aortic valvular disease were similarly assessed. The bisferious pattern was demonstrated in 13 (50%) of 26 patients. Five (19%) of 26 patients had significant reversal of diastolic flow. Four patients were studied both before and after aortic valve replacement. Three had bisferious wave contours preoperatively; two of these also had diastolic reversal of flow. The fourth patient had retrograde flow in diastole without systolic contour abnormality. Postoperatively, all carotid waveforms were normal. None of the duplex waveforms in the control group demonstrated characteristic systolic or diastolic abnormalities.

The bisferious waveform and retrograde diastolic flow are Doppler patterns associated with aortic valvular disease. These patterns are reversible after aortic valve replacement. While echocardiography remains the study of choice in the evaluation of suspected valvular dysfunction, up to one third of patients with aortic regurgitation may not have a detectable murmur. Therefore, identifying these patterns on carotid duplex examinations may provide clinically useful information and serve as a clue to previously unsuspected cardiovascular disease.

AJR **157:403–407, August 1991**

The bisferious arterial pattern of aortic regurgitation has been described in pressure tracings of the carotid artery, the ascending aorta, and the aortic arch. Reversal of diastolic flow direction has also been documented by echocardiography and aortography in the aortic arch and left ventricle in patients with aortic regurgitation [1–4]. Flow patterns in the cardiac chambers have been studied with MR imaging in patients with aortic regurgitation [5–10]. Retrograde diastolic flow in carotid arteries has been identified in the duplex examinations of infants with patent ductus arteriosus [11, 12]. The presence of a bisferious pulse contour or retrograde diastolic flow has never been reported in the carotid duplex waveforms of patients with aortic valve disease.

This study was designed to investigate the presence and characterize the nature of systolic and diastolic pulse waveform abnormalities in a group of patients with known aortic valve disease, and to correlate these abnormalities with the severity of valve regurgitation.

Received December 21, 1990; accepted after revision February 22, 1991.

Presented at the annual meeting of the American Institute of Ultrasound in Medicine, New Orleans, LA, March 1990.

[1] Department of Diagnostic Radiology, Veterans Affairs Medical Center, San Diego, and University of California, San Diego Medical Center, 225 Dickinson St., San Diego, CA 92103-1990.

[2] Present address: Department of Radiological Sciences, University of California, Los Angeles, 10833 Le Conte Ave., Los Angeles, CA 90024-1721. Address reprint requests to C. E. Kallman.

[3] Present address: 700 Tecumseh Rd. E., Suite 1, Windsor, Ontario N8X 413, Canada.

0361–803X/91/1572–0403
© American Roentgen Ray Society

Materials and Methods

We retrospectively reviewed all cases of aortic regurgitation and combined aortic regurgitation and stenosis as determined by echocardiography from the records of the Veterans Affairs Medical Center in San Diego between January 1989 and April 1990. We then selected only patients who had duplex carotid sonograms and echocardiography within a 2-week period for inclusion in our study. The study group consisted of 26 patients, 25 men and one woman, 33–90 years old (mean, 60 years). Indications for examination varied. The majority were seen for preoperative evaluation before coronary artery bypass graft or valve replacement. Six patients had undergone aortic valve replacement with porcine valves 5–13 years before. Retrospective evaluation of carotid duplex sonograms was also performed in 20 age-matched patients with a variety of cardiovascular diseases but with no evidence of aortic valve disease.

All carotid studies were performed on an Acuson 128 (Mountain View, CA) sonographic unit with either a 5.0- or 7.5-MHz transducer. Images were obtained of the common, internal, and external carotid arteries. Doppler waveforms and velocity measurements were obtained at three levels in the common and internal carotid arteries and at one site in the external carotid artery. The Doppler angle of incidence was assigned parallel to the direction of blood flow in the segment of vessels being insonated, and was always less than 70°. Echocardiograms were obtained with an Irex Meridian (Ramsey, NJ) sonographic unit with a 3.5-MHz imaging/2-MHz Doppler transducer. Patients were imaged from the parasternal and apical windows in the 90° left lateral decubitus position. Pulsed Doppler mapping of the width of the aortic regurgitant jet and depth of jet penetration into the left ventricle was performed in the parasternal short- and long-axis projections. Regurgitation was graded as mild (diastolic flow at or just below aortic valve), moderate (jet as far as the anterior mitral leaflet), or severe (jet beyond mitral leaflet into left ventricular apex).

All carotid sonograms were reviewed, and a consensus was reached by two experienced radiologists. The nature and severity of the valvular disease was not known to the reviewers. A team of cardiologists interpreted the echocardiograms, and their final consensus report served as the basis for case selection.

The following criteria were used in the determination of the bisferious waveform: (1) two distinct systolic peaks separated from a well-defined dicrotic notch that served to distinguish systolic from diastolic portions of the waveform; (2) height of the second systolic peak equal to or greater than the first; (3) presence of this pattern in at least two beats of the cardiac cycle; and (4) presence of this pattern in at least one vessel (common carotid artery, internal carotid artery, or external carotid artery) bilaterally (Fig. 1). Retrograde diastolic flow was considered present if the duplex tracing was below the zero baseline for more than 50% of the duration of diastole.

Fig. 1.—Bisferious waveform with two systolic peaks.

***A*, Diagram shows two systolic peaks (P1, P2) separated by midsystolic retraction (SR). DN = dicrotic notch; S1 = first heart sound, due to atrioventricular valves closing and pulmonic and aortic valves opening; S2 = second heart sound, due to aortic and pulmonic valves closing.**

***B*, Duplex tracing of external carotid artery in 50-year-old man with moderate aortic regurgitation.**

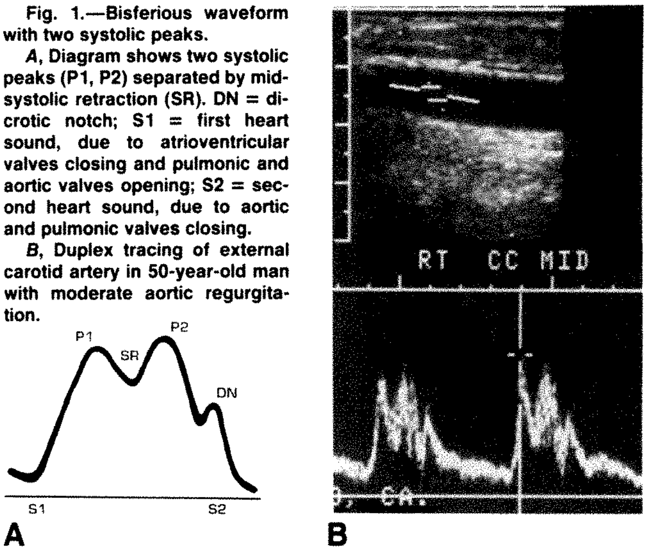

Results

A total of 13 (50%) of 26 patients with aortic regurgitation had bisferious waveforms that met our criteria. Eight (47%) of 17 of the patients with mild regurgitation and five (56%) of nine with moderate aortic regurgitation had bisferious waveforms. Five patients had retrograde diastolic flow. Three of these five had bisferious patterns in addition to reversal of diastolic flow (one with mild aortic regurgitation and moderate stenosis, one with mild regurgitation and severe stenosis, and one with moderate regurgitation and moderate stenosis). Two had diastolic flow reversal without bisferious patterns. Both of these patients had moderate aortic regurgitation without aortic stenosis. A total of 15 patients (57%) had abnormal waveforms (bisferious pattern, diastolic reversal, or both).

Four patients in our study group subsequently had aortic valve replacement. All had abnormal waveforms preoperatively (two bisferious with diastolic reversal, one bisferious with no diastolic reversal, and one diastolic reversal with no systolic abnormality). All had normal waveforms postoperatively (Fig. 2).

The carotid pattern of one patient with moderate aortic regurgitation did have two distinct peaks, but a clearly defined dicrotic notch could not be identified; therefore, this case was classified as indeterminate (Fig. 3).

A pattern characteristic of a dicrotic pulse with two peaks was identified in the duplex tracing of one patient with moderate aortic regurgitation and severe aortic stenosis. This pattern with one systolic peak and one diastolic peak is associated with low stroke volume and low cardiac output [13–15]. This patient had a severe dilated cardiomyopathy with markedly depressed left ventricular function (ejection fraction = 37%).

Four patients in our study had hemodynamically significant carotid stenoses. None of these four had reversal of flow in diastole. Two of these patients had no bisferious pattern (one with >90% stenosis of the external carotid artery, one with 50–75% stenosis of the internal carotid artery). One patient had an indeterminate waveform (no dicrotic notch, 50–75% stenosis of the internal carotid artery). One patient with a unilateral 50% stenosis of the internal carotid artery and moderate aortic regurgitation had bisferious waveforms in all three vessels bilaterally, including the stenotic vessel.

Discussion

Our study demonstrates that bisferious pulse and diastolic reversal may be demonstrated in the carotid duplex study of patients with aortic regurgitation. Our observations have been based on the analysis of waveforms in patients with aortic

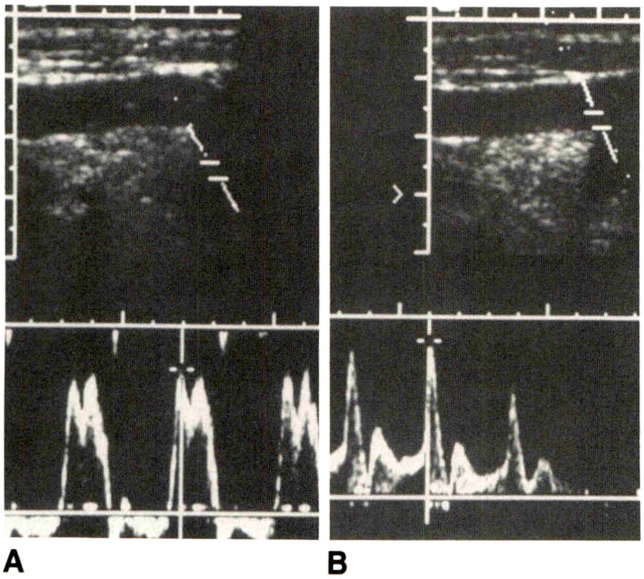

Fig. 2.—Changes in carotid waveform after aortic valvular replacement in a 59-year-old man with severe aortic stenosis and moderate aortic regurgitation.

***A*, Initial duplex sonogram shows both a bisferious pattern and retrograde flow throughout diastole.**

***B*, Duplex sonogram obtained 8 days after aortic valvular replacement shows normal carotid waveforms with a single systolic peak and antegrade diastolic flow.**

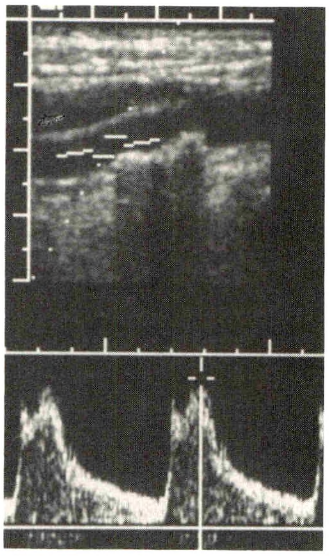

Fig. 3.—Duplex tracing from a 78-year-old man with moderate aortic regurgitation has two distinct peaks but no well-defined dicrotic notch. This case was characterized as indeterminate.

regurgitation documented by echocardiography. Although echocardiography remains the diagnostic examination of choice in the evaluation of suspected valvular heart disease, studies have shown that up to one third of patients with aortic regurgitation may not have an audible murmur and therefore escape detection by physical examination alone. Low cardiac output may mask significant regurgitation [16, 17]. Mild regurgitation may be undetected clinically in 20–25% of patients with bioprosthetic valves [18]. Because many patients with suspected carotid disease are often referred for echocardiographic evaluation as well as evaluation by duplex sonography, recognition of these characteristically abnormal pulse contours may provide potentially useful information regarding central hemodynamics and provide a clue to previously unsuspected aortic valvular disease.

Aortic regurgitation is characterized by reflux of a significant volume of blood from the aorta into the left ventricle during diastole. This results in a widened pulse pressure (systolic pressure − diastolic pressure) and increased stroke volume. Left ventricular dilatation and wall thickening occurs. If untreated, deterioration of left ventricular function and congestive heart failure ensue. Clinical findings include a blowing diastolic murmur (due to the regurgitant jet) and harsh systolic ejection murmur (turbulent systolic ejection of increased stroke volume).

The carotid pulse contour, as delineated on pressure tracings, has four distinct phases: upstroke, peak, dicrotic notch, and diastolic wave (Fig. 4). The normal upstroke, or rate of rise of the pulse, may be increased in hypertrophic cardiomyopathy; proximal to a coarctation; in patent ductus arteriosus; in large arteriovenous fistulas; in hyperkinetic states such as thyrotoxicosis, pregnancy, fever, and anemia; or by aortic regurgitation as a result of increased stroke volume and increased aortic runoff. A slow upstroke is associated with left ventricular outflow obstruction or severe heart failure [15].

The normal peak has early and late systolic components, representing an early percussion wave followed by a reflected, or tidal, wave. In youth the first component is dominant. With age, the second component increases in height, giving a more sustained peak. In addition, systemic hypertension and atherosclerosis may produce a sustained peak [15, 19]. The normal dicrotic notch occurs at the completion of closure of the aortic valve and signifies the onset of diastole.

The bisferious pulse consists of two distinct systolic peaks, separated by a midsystolic retraction. The bisferious pulse is characteristic of three clinical entities: aortic regurgitation,

Fig. 4.—Diagram and duplex tracing of normal carotid waveform.

***A*, Diagram shows dicrotic notch (DN), first heart sound (S1), and second heart sound (S2).**

***B*, Duplex tracing from normal 45-year-old man.**

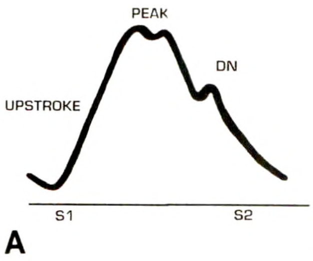

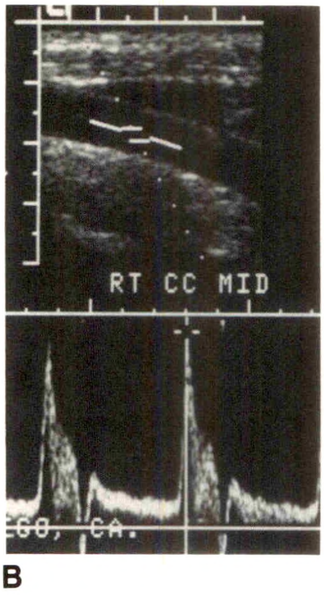

combined aortic stenosis and regurgitation, and severe obstructive hypertrophic cardiomyopathy [2, 15, 20]. The first reference to the bisferious pulse contour was published in Latin by Galen in 1532. He described a pulse with two separate impulses with a *quies media ictus*—a central pause in the stroke. Many theories exist as to the exact mechanism of the bifid systolic peak in aortic regurgitation. Some authors describe a high initial percussion wave caused by the increased ventricular stroke volume, which falls off rapidly as a result of increased runoff followed by a normal reflected tidal wave. Others favor the concept that the rapid ejection of the increased ventricular volume that exists in aortic regurgitation produces a suction, or Venturi, effect within the aorta, accounting for the midsystolic retraction [20, 21].

In our review, the bisferious pulse contour was most often identified in the tracings of the external and common carotid arteries. This may be a function of the higher-resistance circulation in these vessels compared with that in the internal carotid artery (13 bisferious: nine in all three vessels, four in common carotid and external carotid arteries). In no patient was the pattern seen in the internal carotid artery alone.

Although four patients in our study had hemodynamically significant carotid stenosis, in only one was a bisferious waveform demonstrated. Because of these small numbers, however, no conclusions can be drawn about the effect of carotid artery stenosis on the bisferious pattern.

The difficulty in differentiating between the dicrotic and bisferious patterns without ECG correlation for the timing of systole and diastole represents a limitation of our analysis. Our study was retrospective; ECG gating is not routinely used for carotid arterial evaluations in our institution. Therefore, for the purpose of our review, a pulse was considered bisferious only if two distinct systolic peaks could be separated from a well-defined dicrotic notch, which reliably indicates the closure of the aortic valve and denotes the onset of diastole. In only one of our 14 patients was a well-defined dicrotic notch not present. This case was characterized as indeterminate.

Flow reversal throughout diastole was present in four patients. Although identification of a small postsystolic reversal is a normal finding, reverse flow that persists through diastole is abnormal and has been described in the carotid arterial pressure tracings of patients with aortic regurgitation. The same pulse contour has been described in the carotid duplex tracings of infants with patent ductus arteriosus [11, 12]. Diastolic flow reversal in the heart and aorta has also been noted with pulsed Doppler, arteriography, and MR imaging in patients with aortic regurgitation [4–7, 9, 22].

It is interesting that even mild grades of regurgitation produced pulse changes of bisferious and diastolic reversal in the carotid arteries, which are remote from the aortic valve. Our findings correlate with previous reports from pulsed Doppler studies, which noted that the diastolic abnormalities persisted at a greater distance from the aortic valve in combined aortic stenosis and regurgitation than for the same degree of regurgitation alone. The explanation for this finding is unclear [2]. In our study, both patients with mild aortic regurgitation and diastolic reversal had coexistent moderate or severe stenosis.

Conversely, the absence of a bisferious pattern or diastolic reversal of flow does not imply that the valvular defect is small. Approximately 30% of patients with severe regurgitation may not have the characteristic abnormal pulse contours [23]. In addition, the amount and duration of diastolic flow reversal is known to vary with cardiac output and heart rate [4, 21, 23]. While these factors may play a role, no attempt was made in this study to correlate abnormal patterns with left ventricular function or heart rate.

In our patients, the size of the second systolic peak was quite variable. Our criteria required that both peaks be equal in height or the second peak be higher than the first. Adherence to these criteria excluded the possibility that the systolic pulse abnormality represented some form of sustained systolic peak, may occur in increasing age, atherosclerosis, or systemic hypertension.

The bisferious waveform and retrograde diastolic flow are Doppler patterns associated with aortic valvular disease. Recognition of these characteristically abnormal patterns may provide potentially useful clinical information and provide a clue to previously unsuspected aortic valvular disease.

REFERENCES

1. Benchimol A, Desser KB, Gartlin JL. Bidirectional blood flow velocity in the cardiac chambers and great vessels studied with the Doppler ultrasonic flowmeter. *Am J Med* **1972**;52:467–473
2. Veyrat C, Cholot N, Abitol G, Kalmanson D. Non-invasive diagnosis and assessment of aortic valve disease and evaluation of aortic prosthesis function using echo pulsed Doppler velocimetry. *Br Heart J* **1980**;43: 393–413
3. Stein PD, Sabbah HN. Turbulent blood flow in the ascending aorta of humans with normal and diseased aortic valves. *Circ Res* **1976**;39:58–65
4. Takenaka K, Dabestani A, Gardin JM, et al. A simple Doppler echocardiographic method for estimating severity of aortic regurgitation. *Am J Cardiol* **1986**;57:1340–1343
5. Higgins CB, Holt W, Pflugfelder P, Sechtem U. Functional evaluation of the heart with magnetic resonance imaging. *Magn Reson Med* **1988**;6: 121–139
6. Utz JA, Herfkens RJ, Heinsimer JA, Shimakawa A, Glover G, Pelc N. Valvular regurgitation: dynamic MR imaging. *Radiology* **1988**;168:91–94
7. Pflugfelder PW, Landzberg JS, Cassidy MM, et al. Comparison of cine MR imaging with Doppler echocardiography for the evaluation of aortic regurgitation. *AJR* **1989**;152:729–735
8. Mirowitz SA, Lee JK, Gutierrez FR, Brown JJ, Eilenberg SS. Normal signal-void patterns in cardiac cine MR images. *Radiology* **1990**;176:49–55
9. Mitchel L, Jenkins JP, Watson Y, Rowlands DJ, Isherwood I. Diagnosis and assessment of mitral and aortic valve disease by cine-flow magnetic resonance imaging. *Magn Reson Med* **1989**;12:181–197
10. Klipstein RH, Firmin DN, Underwood SR, O'Rees RS, Longmore DB. Blood flow patterns in the human aorta studied by magnetic resonance. *Br Heart J* **1987**;58:316–323
11. Kupferschmid C, Lang D, Pohlandt P. Sensitivity, specificity and predictive value of clinical findings, M-mode echocardiography and continuous-wave Doppler sonography in the diagnosis of symptomatic patent ductus arteriosus in preterm infants. *Eur J Pediatr* **1988**;147:279–282
12. Bomelburg T, Jorch G. Abnormal blood flow patterns in renal arteries of small preterm infants with patent ductus arteriosus detected by Doppler ultrasonography. *Eur J Pediatr* **1989**;148:660–664
13. Ewy GA, Rios JC, Marcus FI. The dicrotic arterial pulse. *Circulation* **1969**;39:655–661
14. Orchard RC, Craige E. Dicrotic pulse after open heart surgery. *Circulation* **1980**;62:1107–1113

15. Ewy GA, Groves BM. *Venous and arterial pulsations*. New York: Medcom, **1973**
16. Aronow WS, Kronzon I. Correlation of prevalence and severity of aortic regurgitation detected by pulsed Doppler echocardiography with the murmur of aortic regurgitation in elderly patients in a long-term health care facility. *Am J Cardiol* **1989**;63:128–129
17. Rahko PS. Prevalence of regurgitant murmurs in patients with valvular regurgitation detected by Doppler echocardiography. *Ann Intern Med* **1989**;111:466–472
18. Schapira JN. *Two-dimensional echocardiography and cardiac Doppler*, 2nd ed. Baltimore: Williams & Wilkins, **1990**
19. Freis ED, Heath WC, Luchsinger PC, et al. Changes in the carotid pulse which occur with age and hypertension. *Am Heart J* **1956**;71:757–765
20. Fleming P. The mechanism of the pulsus bisferiens. *Br Heart J* **1957**;19:519–524
21. Tavel ME. *Clinical phonocardiography and external pulse recording*, 4th ed. Chicago: Year Book Medical, **1985**:53–63, 204–218
22. Sectem U, Pflugfelder PW, Cassidy MM, et al. Mitral or aortic regurgitation: quantification of regurgitant volumes with cine MR imaging. *Radiology* **1988**;167:425–430
23. Benchimol A. *Non-invasive diagnostic techniques in cardiology*, 2nd ed. Baltimore: Williams & Wilkins, **1981**:157–197

Come to the
American Roentgen
Ray Society
92nd
ANNUAL MEETING
Orlando, FL
Marriott's Orlando World Center
May 10–15, 1992

Scientific Program (200 papers)
Instructional Courses (60 hours)
Categorical Course on Neuroradiology
The Caldwell Lecture
Award Papers
Scientific Exhibits
Social, Golf, and Tennis Programs
Guest Programs

Book Review

Physics and Instrumentation of Diagnostic Medical Ultrasound. By Peter Fish. New York: Wiley, 250 pp., 1990. $34.50

This excellent text was written primarily for radiologists and residents, but most technologists will have no trouble with the material, and graduate students in medical physics will find it a good introduction to ultrasound theory and practice. The material on physics is accurate, and nonessential formulas have been omitted. All the concepts are illustrated with line drawings that do a good job of explaining complex subjects. The major thrust of the text is to explain how sonographic instruments work, and in this it succeeds admirably. Rearrangement of the conventional order of ultrasound texts is quite successful. For example, spatial peak, temporal average (SPTA) intensity is defined in chapter 2, when energy, power, and intensity are defined, rather than at the end of the text in the chapter on bioeffects. Frequency spectra also are defined in chapter 2, rather than in the chapter on Doppler imaging, so that the term can be used naturally when transducer performance is discussed.

Although this text is written more simply than *Ultrasound Physics and Instrumentation* by Hykes, Hedrick, and Starchman, it covers a great deal more material and will be more useful to radiologists and ultrasound technologists. Peter Fish also wrote a chapter on Doppler imaging in *Physical Principles of Medical Ultrasonics*, edited by C. R. Hill, but that chapter was addressed to engineers and ultrasound physicists. It scarcely overlaps with the two chapters on Doppler imaging in this text, which emphasize how Doppler instruments work and what they can be used to measure clinically. Although the first chapter on Doppler imaging is rather conventional and implies a red-blue artery-vein assignment in the section on color flow imaging, chapter 12, on Doppler measurements, is unique in its coverage of all the indexes, ratios, and analysis techniques currently provided by duplex Doppler instruments. In addition, this chapter warns of inaccuracies caused by transducer frequency spectrum, sample volume placement, angle correction, wall filters, and other complexities not always discussed in other texts.

Although chapters on A- and B-mode scanning precede a chapter on real-time scanning, and the reader may be tempted to skip them because they are outmoded and of historical interest only, they are necessary introductions to the chapter on real-time scanning. This last chapter introduces phasing by first discussing annular arrays rather than linear arrays, the more conventional introduction to this subject. However, elevation (or slice thickness) focus is barely mentioned here, but is described extensively in the chapter on artifacts. Electronic focusing covers apodization, aperature control, curved linear arrays, and transmit-and-receive focusing.

The last four chapters are rather special because they cover digital techniques (such as pre- and postprocessing, interpolation), image artifacts, quality control phantoms, and bioeffects. The chapter on bioeffects covers heating, mode conversion, streaming, stable and transient cavitation, and nonlinear effects of ultrasound. A short section on experiments on bioeffects is followed by a review of measurements of radiation force balance and intensity. The chapter ends with safety recommendations and the ranges of intensity and pressure in commercially available instruments (Table 16.2). This chapter can stand alone and could be distributed to physicians in fields associated with ultrasound to inform them of the concern, experimentation, and problems associated with bioeffects dosimetry.

Nine useful appendixes end this text. In addition to explanations of how cathode ray tubes and filters work, numerical examples of ultrasound formulas are placed in the appendixes rather than interrupting the text. The index is complete, so that this book can be used as a reference as well as a teaching text.

Carolyn Kimme-Smith
University of California, Los Angeles
Los Angeles, CA 90024

Perspective

Radiologic Physics Instruction for Diagnostic Radiologists: A Survey of Residency Programs

Committee on Training of Radiologists,[1] American Association of Physicists in Medicine

A survey concerning physics instruction in radiology residency training programs was conducted by the Committee on Training of Radiologists of the American Association of Physicists in Medicine (AAPM). A previous survey of radiologists' overall impression of the quality and inclusiveness of their physics instruction during their residencies was conducted by this committee [1]. The present survey was thought to be necessary to compare residents' impressions of their physics instruction with the curricula of existing programs. Toward that end, a list of 250 radiology training programs was obtained from the American College of Radiology. The survey was mailed to the programs with a cover letter requesting that the survey be forwarded to the person who is in charge of physics instruction. Ninety-nine programs responded.

The survey consisted of 20 questions covering the areas of general program information (e.g., demographics, program specialties), curriculum, background of instructors, and use of instructional materials. Respondents were invited to submit written comments and suggestions also.

Results

The full text of the survey and tabulation of responses is available from the American Association of Physicists in Medicine (AAPM) Committee on Training of Radiologists. The results are summarized here.

Program Information

Fifty-three percent of the programs were university based, 44% hospital based, and 3% clinic based. The mean number of residents in each year of residency was four, with a staff consisting of 17 radiologists, three physicists, and three "other" scientists/professional staff. Seventy-three percent listed their physics instruction program specialty as diagnostic, with only 5% specializing in nuclear medicine. The remaining 22% listed both.

Curriculum Information

An average of 41 classroom (didactic) hours were reported. The typical program consisted of 1–2 meetings per week for 1.3 hr (usually 12:00 noon or 4:00 p.m. on a Monday) with 82% requiring mandatory attendance during the first postgraduate year, 70% for the second year, 65% for the third year, and 27% for the fourth year. Classroom hours dropped to a mean of 18 during the fifth postgraduate year. Mean number of laboratory hours varied more than didactic hours during training, with a high of 12 hr in nuclear medicine physics and 6 hr in diagnostic radiologic physics both occurring in the second postgraduate year. Homework problems were assigned in 45% and regular tests were given in 48% of the responding programs. Residents' overall performance in the course was graded in 27% of the programs.

Received November 26, 1990; accepted after revision March 4, 1991.

[1] The members of the committee are Wei-Kom Chu, Karen P. Doppke, Lance V. Hefner, Pavel V. Houdek, David S. Marsden (chair), Richard L. Morin, William Pavlicek, E. Russell Ritenour, Alan H. Schoenfeld, Raymond K. Wu, F. Marc Edwards (consultant), and Lincoln B. Hubbard (ex-officio). Address reprint requests to Executive Officer, American Association of Physicists in Medicine, 335 E. 45th St., New York, NY 10017.

AJR 157:409–410, August 1991 0361–803X/91/1572–0409 © American Roentgen Ray Society

A special physics review course was given in-house before the American Board of Radiology examinations in 66% of the programs. Lasting 1.5 hr, 1 day per week, the typical review course began June–August and ended August–September. Residents in 94% of the programs attended off-site review courses.

Physics Course Instructors

The primary physics instructor was certified in either diagnostic or radiologic physics by the American Board of Radiology. The mean number of physics instructors included two Ph.D. physicists, one M.S. physicist, one radiologic technologist, and two M.D.s with 8–15 years experience for each instructor. The relative extent of involvement of each category of instructor was not surveyed.

Instructional Materials

Handouts were the most frequently used materials (72%) with specific mention of the Radiological Physics Examination (RAPHEX), produced by the Radiological and Medical Physics Society of New York, in 68% of the responses. High on the list of materials that were never used were live video (92% never used it), audiovisual series (Society of Nuclear Medicine, 76% never used it; Radiological Society of North America, 59% never used it), and videotape (47% never used it).

Comments and Suggestions of Respondents

Respondents were invited to submit written statements as suggestions for improvements of physics instruction or under the heading General Comments. A total of 48 statements were received, the full text of which is available from the AAPM Committee on Training of Radiologists. Most of the suggestions for improvement concerned the need for regular attendance (seven responses); the need to teach basic principles that directly affect image quality, such as spending less time on radiobiology (six responses); and the need for high quality, standardized teaching materials (nine responses). These suggestions reflect the perceptions of the person in charge of physics instruction, who is usually a physicist.

Conclusions

As with any survey, the results are a reflection of the responding population and not necessarily of the parent population of residency programs, although the 40% response rate and the breakdown of the respondents' programs into university-, hospital-, and clinic-based programs suggests an appropriate representation. Also, the committee has no way of knowing whether the survey response represents a thorough evaluation of details of the program or a momentary estimate from the respondent. For example, the year-by-year breakdown of classroom hours during residency may not have been accurate horizontally (i.e., as a breakdown of hours spent for each postgraduate year), but the committee feels that the vertical breakdown of hours spent in different subject areas is a reasonable representation of the distribution of lecture hours in the program. For example, computer science was reported to occupy 4% of the time devoted to classroom hours.

This survey is not intended to serve as an evaluation of the performance of training programs. Rather, it provides some objective information concerning existing programs that can be compared with statements of need that have been made [1].

Results of the previous survey [1] of radiologists who had recently completed their residencies indicated the perception of a need for more practical instruction, particularly in the areas of dosimetry of patients and evaluation of equipment. Although these categories were not specified in the present survey, the comments from physics program directors seem to echo those of the radiologists.

Radiologists in the previous survey also expressed a great deal of interest in increasing the amount of time devoted to "teaching with images" or at least correlating physics principles with images. The fact that audiovisual materials were not generally used by the programs surveyed may indicate a need for further development in this area or at least more promotion of existing materials. The radiologists' survey also indicated a need for more coverage of computers. The current survey indicates that the subject of computers currently takes up approximately 4% of didactic hours. Although percentage of class time is not an indication of the quality of instruction, it is interesting to note that neither computers nor display stations were mentioned as teaching materials although they may have figured into the 4–6 hr of laboratories/demonstrations. Evaluation of the efficacy of various teaching materials was not within the scope of this survey. A common theme in the surveys of radiologists and residency programs was a desire for more standardized teaching materials. Again, this may indicate a need for development of materials that should be met by various organizations, or it may indicate a need for more promotion of existing materials such as *The Physics of Diagnostic Radiology: Syllabus and Study Guide*, produced jointly by the American College of Radiology (ACR) Physics Commission and the American Association of Physicists in Medicine, and the ACR Physics Film Teaching Files. In any case, the results of this survey indicate that physics instruction encompasses a significant time commitment during radiology residency programs. The level of satisfaction of both instructors and residents varies widely, but a number of avenues for improvement are recognized by both groups. It is hoped that the results of this survey, when correlated with the perceptions of radiologists about their training collected in the previous survey, may provide useful, conjectural information to training programs.

ACKNOWLEDGMENT

The committee thanks the American College of Radiology for providing the mailing list used in this study.

REFERENCE

1. Committee on Training of Radiologists, American Association of Physicists in Medicine. Radiologic physics instruction for diagnostic radiologists: results of an opinion survey (perspective). *AJR* **1989**;152:393–397

Letters

Diaphragmatic Rupture Due to Blunt Trauma: Sensitivity of Plain Chest Radiographs

The article by Gelman et al. [1] describes various important findings seen with diaphragmatic rupture. Although informative, it uses the term "elevation of hemidiaphragm" as one of the findings associated with diaphragmatic rupture. Of course it is not the diaphragm but the lung base that is elevated (the diaphragm has been ruptured). This term is commonly misused in radiology practice. For example, often when someone is referring to the possibility of subpulmonic pleural effusions, elevated hemidiaphragm is used; again, of course, it is not the diaphragm that is elevated but the lung base. On chest radiographs, the location of the diaphragm can only be inferred on the basis of air in adjacent lung. If the lung base is elevated, an elevated diaphragm is only one of numerous possible causes, including diaphragmatic rupture and hernia, subpulmonic pleural effusion, subdiaphragmatic process, and even diaphragmatic mass. Communication is one of the greatest responsibilities of radiologists, and using terminology that is as anatomically correct as possible indicates radiologists' thorough understanding of the films they are interpreting and improves credibility of radiologists to other physicians. When a lung base is elevated, it should be described as such, and a differential diagnosis that can include elevated diaphragm should be given.

Myron D. Kirshenbaum
Illinois Masonic Medical Center
Chicago, IL 60657

REFERENCE

1. Gelman R, Mirvis SE, Gens D. Diaphragmatic rupture due to blunt trauma: sensitivity of plain chest radiographs. *AJR* **1991**;156:51–57

Reply

We appreciate the comments of Dr. Kirshenbaum on our article [1]. Of course, he is correct when he reminds us that it is actually the lung base that is elevated when the diaphragm is ruptured. The elevation of the lung base is the result of herniation of abdominal viscera through the diaphragmatic defect. This causes the "pseudodiaphragm effect" [2] on plain radiographs, where elevation of the apparent hemidiaphragm is visualized. The term "elevated lung base" is technically correct, but we prefer to use the term elevated apparent hemidiaphragm for routine reporting, as we find that our physicians understand this term and its implications.

Russel Gelman
Stuart E. Mirvis
David Gens
University of Maryland Medical System
Baltimore, Maryland 21201

REFERENCES

1. Gelman R, Mirvis SE, Gens D. Diaphragmatic rupture due to blunt trauma: sensitivity of plain chest radiographs. *AJR* **1991**;156:51–57
2. Fataar S, Schulman A. Diagnosis of diaphragmatic tears. *Br J Radiol* **1979**;52:375–381

Bottle Cap Ingestion

I wish to amplify the observation of Brandser and Smith [1] that the childproof caps on medicine bottles can become esophageal foreign bodies. A 62-year-old man had the habit of placing all his pills on a bottle cap and then using the cap to throw the pills to the back of his throat for ingestion. He had done this many times. On the day of admission, he inadvertently lost hold of the cap and swallowed it along with his pills. This caused a sticking sensation in the throat and some difficulty in swallowing. A lateral soft-tissue view of the neck

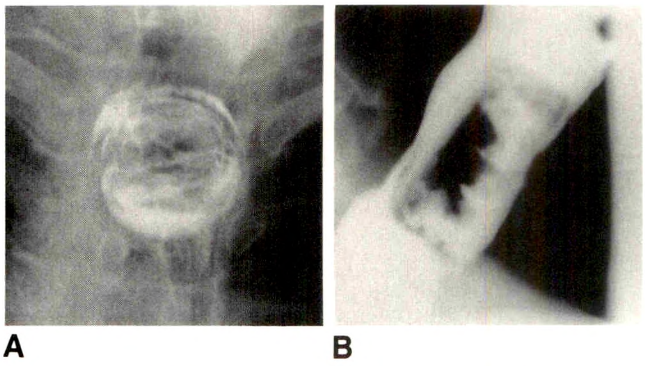

Fig. 1.—*A* and *B*, Frontal (*A*) and lateral (*B*) spot films from a barium swallow show pill-bottle cap lodged in lower hypopharynx.

and a subsequent barium swallow (Fig. 1) confirmed the presence of the pill cap in his hypopharynx. The cap was removed via endoscopy, and the patient was discharged the next day. In this particular case, the patient had ingested the entire cap, which did not have an inner plastic liner.

This case illustrates once again the risk involved if someone uses a pill cap or similar small object to help him or her swallow several pills at one time. An inner plastic liner may dislodge from the main part of the cap as discussed in the previous report [1], or the patient may swallow the entire cap as illustrated by this case. Patients should be encouraged to swallow their pills one at a time. If they feel the need to ingest several pills all at once, they should be advised to use something safe, such as a teaspoon or a tablespoon.

Tim B. Hunter
Arizona Health Sciences Center
Tucson, AZ 85724

REFERENCE

1. Brandser E, Smith C. Childproof cap on medicine bottles as risk for esophageal foreign body (letter). *AJR* **1991**;156:201

Reply

The habit of using bottle caps for pill ingestion may be quite widespread. This practice can have potentially dangerous consequences, as illustrated by our case and the case of Dr. Hunter.

Again, we think that the practice of using medicine bottle caps for the ingestion of medication should be discouraged.

Eric Brandser
Claire Smith
Rush-Presbyterian-St. Luke's Medical Center
Chicago, IL 60612

Gallbladder Function in Patients with Spinal Cord Injury

In "Gallbladder Contractility in Patients with Spinal Cord Injuries: A Sonographic Investigation" [1], which appeared in the March 1990, issue of *AJR*, Nino-Murcia et al. conclude that gallbladder contractility in patients with spinal cord injuries is normal and unchanged from that observed in an able-bodied control population. We think that the conclusions of Nino-Murcia et al. are tenuous and are not supported by the data presented in the paper. Their conclusions are inconsistent with our current understanding of the impact of spinal cord injury (SCI) on the upper gastrointestinal tract [2] and contradict the findings of research that has shown significant impairment of gallbladder function in patients with cervical SCI (Milne et al., paper presented at the annual meeting of the Society of Nuclear Medicine, June 1987; Chassin-Kaplan et al., paper presented at the annual meeting of the American Spinal Injury Association, May 1988).

We think that the results and conclusions of Nino-Murcia et al. are questionable for the following reasons: (1) It is grossly misleading to lump together and homogenize the data obtained from quadriplegic and paraplegic subjects. Paraplegic patients with low injuries (T11 and below) who are likely to have normal gallbladder function and gastric emptying made up 25% of the paraplegic population and 15% of the total SCI study group. Small but significant differences between quadriplegic patients and able-bodied controls or paraplegic subjects could thus easily be obfuscated, resulting in the acceptance of a false null hypothesis and the commission of a type II error. (2) Studying a single SCI population composed of both patients with new injuries and patients with chronic injuries of more than 1 year duration as Nino-Murcia et al. did can be both incorrect and misleading. (3) The completeness of the SCI in any subject is never given. A simple grading system is not applied, and the number of subjects with incomplete SCI, and thus with potentially normal or only minimally impaired gallbladder function, is not recorded. Data from these patients would, of course, only serve to "normalize" the SCI group and obscure any true differences. Again, a type II error would have been committed. (4) Serial sonography has not been unequivocally established as the most accurate and reproducible method of assessing gallbladder emptying or contractility. Changes in estimates of gallbladder volumes based on sonographic findings do not reflect gallbladder volumes as accurately as does cholescintigraphy, nor does sonography at 10-min intervals for only 60 min adequately show closely spaced or delayed changes in motility or emptying. (5) Using the ellipsoid method, an assumption-rich, geometric computation, to calculate gallbladder volumes has not been validated in patients with SCI and thus may be misleading. (6) The text is inconsistent in accounting for the total number of paraplegic patients with injury below T10. Two such paraplegics are inexplicably lost from the study between the first paragraph of page 522, line 8, and the fourth line of the third paragraph of the Discussion section (page 522). Although the total number of SCI patients remains at 26, only two patients are now reported as having injuries below T10, and a 50% decrease in the number of the paraplegic patients apparently has taken place. On which sample population of paraplegics were the authors' calculations and conclusions based?

In summary, we remain unconvinced that gallbladder contractility is normal in SCI patients and solicit comments from Nino-Murcia et al. and, if possible, from the reviewers on our interpretation or understanding of this study.

Jack L. Segal
Norah Milne
University of California, Irvine
Irvine, CA 92717
Veterans Affairs Medical Center
Long Beach, CA 90822

REFERENCES

1. Nino-Murcia M, Burton D, Chang P, Stone J, Perkash I. Gallbladder contractility in patients with spinal cord injuries: a sonographic investigation. *AJR* **1990**;154:521-524
2. Segal JL, Milne N, Brunnemann SR, Lyons KP. Metoclopramide-induced normalization of impaired gastric emptying in spinal cord injury. *Gastroenterology* **1987**;82(11):1143-1148

Reply

We would like to respond to the questions Drs. Segal and Milne have raised, in the order in which they were raised. (1) We reanalyzed our data excluding the four low lesions. The mean gallbladder resting volume of patients with spinal cord injury (SCI) was 20 ml (SE = 2.3), which was significantly different from the mean resting volume of the normal control group ($p = .01$). The mean gallbladder residual volume of SCI patients was 10 ml (SE = 1.0); this was not significantly different from that of the normal control group ($p = .61$). The mean emptying time of the gallbladder in SCI patients was 43 min (SE = 3.3); this was not a significant difference from the normal control group ($p = .31$). Thus, SCI patients do not show significant differences in gallbladder contractility from a normal population. The observed difference in the ejection fraction reflects the lower resting gallbladder volume in SCI patients [1]. Great care was taken to minimize a type II error. The experimental design using matched controls, and the number of patients studied was specifically selected to achieve 95% power (beta error = 0.05) for a 5% one-tailed test, with a critical effect size of 0.4. Such a critical effect size roughly corresponds to a minimal difference of about 3 ml in gallbladder volume and 10 min in emptying time, numbers that are well within 1 SD of the measured normal mean values. (2) Damage to the autonomic nervous system becomes stable within 6 months of the injury. Thus, using patients whose injuries occurred 6 months or more before the study is scientifically correct. (3) All SCI patients had complete lesions. (4) The key parameter with respect to our measuring system is its reproducibility, not its absolute accuracy, as our experimental design included a matched control group. Only the "relative" observed differences in measured changes in volume are important; actual absolutely accurate determinations of volume are unimportant. The published literature [2, 3] supports this view of the reproducible standard in using sonography to measure gallbladder volumes. (5) We have no reason to suspect that using sonography to measure gallbladder volume would be any different in SCI patients than in the normal population or in any other patient. (6) Drs. Segal and Milne did detect a typographic error: The number of patients with lesions below T10 was four, not two.

For these reasons, we stand by our conclusions as stated in the original article [1].

Matilde Nino-Murcia
Inder Perkash
Stanford University Medical School
Stanford, CA 94305
Veterans Affairs Medical Center
Palo Alto, CA 94304
Paul J. Chang
University of Iowa Hospital and Clinics
Iowa City, IA 52242
and colleagues

REFERENCES

1. Nino-Murcia M, Burton D, Chang P, Stone J, Perkash I. Gallbladder contractility in patients with spinal cord injuries: a sonographic investigation. *AJR* **1990**;154:521–524
2. Dodds WJ, Grosh WJ, Darweesh RA, Lawson TL, Kishk SA, Kern MK. Sonographic measurement of gallbladder volume. *AJR* **1985**;145:1009–1011
3. Everson GT, Braverman DZ, Johnson ML, Kern F Jr. A critical evaluation of real-time ultrasonography for the study of gallbladder volume and contraction. *Gastroenterology* **1980**;83:773–776

Primary Liver Lymphoma: A Diagnostic Dilemma

Only 53 cases of primary lymphoma of the liver have been reported [1]. These lesions usually are misinterpreted as hepatocellular carcinoma, hepatoblastoma, or metastasis. Primary lymphoma of the liver is not suspected until it is proved by biopsy. In our experience, primary lymphoma of the liver should be suspected when a patient has increased serum levels of liver enzymes, normal serum levels of alpha-fetoprotein and carcinoembryonic antigen, and CT findings of one or two nonenhancing hypodense lesions in the liver. We describe a case that illustrates this point.

A 53-year-old man had had nausea, vomiting, right-sided abdominal pain, and hepatomegaly for 1 month. Serum levels of liver enzymes were elevated: aspartate aminotransferase (SGOT), 124 IU/l; alanine aminotransferase (SGPT), 79 IU/l; and alkaline phosphatase, 270 King-Armstrong units/dl (1917 U/l). Serum levels of alpha-fetoprotein and carcinoembryonic antigen were normal. CT showed two well-defined, hypodense, nonenhancing lesions in the liver (Fig. 1). Needle biopsy showed diffuse non-Hodgkin lymphoma of the poorly differentiated lymphocytic type. The patient had a good response to combination chemotherapy.

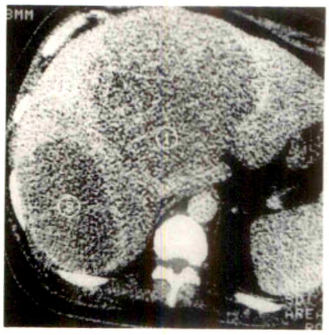
Fig. 1.—CT scan with contrast material shows two large, well-defined, hypodense, nonenhancing hepatic lesions.

The differential diagnosis of lesions with this appearance on CT includes hepatocellular carcinoma, hepatoblastoma, and metastasis from an unknown primary tumor [2]. Neither CT nor MR imaging has been helpful in differentiating, with certainty, these conditions from primary lymphoma of the liver [3]. Moreover, the results of pathologic examination of biopsy specimens of primary or large cell lymphomas can be misinterpreted. Occasionally, frozen sections have artifacts that distort large cell lymphoma so that it assumes a carcinomatous appearance [2]. As in our case, most cases of primary lymphoma of the liver have discrete masses without significant variation in attenuation values or other intrinsic characteristics [4]. The detection of such lesions on CT scans in the clinical setting described here suggests the diagnosis of primary lymphoma of the liver.

C. Mohan
S. S. Alurkar
O. P. Sharma
S. H. Advani
Tata Memorial Hospital
Bombay 400 012, India

REFERENCES

1. Kayano H, Katoyama I. Primary hepatic lymphoma presenting as intravascular lymphomatosis. *Arch Pathol Lab Med* **1990;**114:580–584
2. Osborne BM, Butler JJ, Guarda LA. Primary liver lymphoma: report of ten cases and review of literature. *Cancer* **1985;**56:2902–2910
3. Boechat MI, Kangarloo H, Ortega J, et al. Primary liver tumors in children: comparison of CT and MR imaging. *Radiology* **1988;**169:727–732
4. Zornoza J, Ginaldi S. Computed tomography in hepatic lymphoma. *Radiology* **1981;**138:405–410

Doppler Sonography in Osler-Weber-Rendu Disease

Osler-Weber-Rendu disease, or hereditary hemorrhagic telangiectasia, is a vascular disease with autosomal dominant transmission. Hepatic involvement is characterized by telangiectases. We report the duplex Doppler findings in the liver in a case with extensive telangiectases.

A 46-year-old woman was admitted because of cardiac failure. Physical and radiologic examinations showed pulmonary arteriovenous fistulas and multiple gastrointestinal telangiectases. The diagnosis was Osler-Weber-Rendu disease. Results of liver function tests were as follows: alkaline phosphatase, three times higher than the normal upper limit; γ-glutamyltransferase, eight times higher than the normal upper limit; and alanine and aspartate aminotransferases, three times higher than the normal upper limits. Abdominal sonography showed a dilated hepatic artery (12 mm in diameter) with numerous tortuous intrahepatic branches and dilated hepatic veins. The portal vein was normal. Duplex sonography showed a high velocity

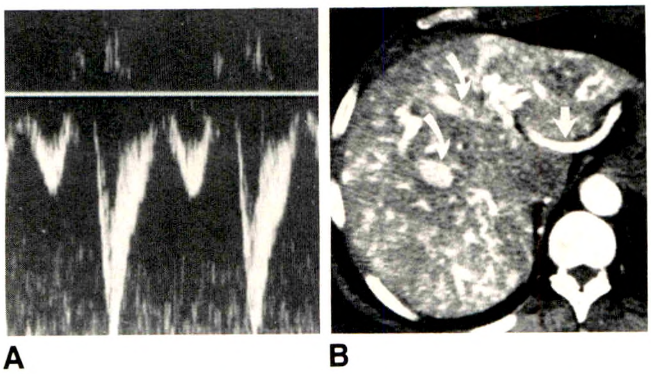

Fig. 1.—Osler-Weber-Rendu disease.
A, Doppler waveform of hepatic vein shows high-velocity signal.
B, CT scan with contrast medium shows dilated left hepatic artery (*straight arrow*) with dilated intrahepatic arteries and early enhancement of hepatic veins (*curved arrows*).

signal in the hepatic artery. Portal flow was normal. The hepatic veins had an "arterialized" pattern, with abnormal peaks indicating the communication between the hepatic arteries and the hepatic veins (Fig. 1A). CT and hepatic angiography confirmed the hepatic arterialization and the arteriovenous fistulas by showing simultaneous enhancement of the arteries and the hepatic veins (Fig. 1B).

Osler-Weber-Rendu disease is a vascular disease with multiple manifestations. The most frequent localizations are the skin and mucosa, but all organ systems may be involved. The liver involved more often than was suspected originally [1]. The vascular abnormalities include telangiectases and arteriovenous fistulas, sometimes associated with fibrosis and cirrhosis [1–3]. Sonographic findings in the liver consist of dilated common hepatic artery, multiple ectatic vascular structures with pulsations, and dilated hepatic veins [4]. Although these sonographic findings suggest vascular disease, duplex Doppler imaging can be used to confirm the diagnosis. Duplex Doppler sonography shows high velocity signal in the hepatic artery, with increased arterial hepatic output; arterial signal in the intrahepatic vascular structures; and abnormal high velocity signal in the hepatic veins. This last finding mimics an arterial flow and confirms the arteriohepatic communications. We did not use color Doppler imaging in this case, but it can be helpful by showing high color signal in the extrahepatic and intrahepatic arteries and large hyperkinetic hepatic veins.

In conclusion, conventional and Doppler sonography can be used to diagnose hepatic involvement in Osler-Weber-Rendu disease. Sonography shows large and numerous arteries and dilated hepatic veins. Doppler sonography gives information on increased arterial flow, arterial signal in the intrahepatic vascular structures, and abnormal high velocity signal in the hepatic veins. Angiography is not necessary if no treatment is indicated.

Valérie Vilgrain
Yves Menu
Henri Nahum
Hôpital Beaujon
92118 Clichy Cedex, France

REFERENCES

1. Martini GA. The liver in hereditary haemorrhagic teleangiectasia: an inborn error of vascular structure with multiple manifestations: a reappraisal. *Gut* **1978**;19:531–537
2. Nikolopoulos N, Xynos E, Vassilakis JS. Familial occurrence of hyperdynamic circulation status due to intrahepatic fistulae in hereditary hemorrhagic telangiectasia. *Hepatogastroenterology* **1988**;35:167–168
3. Bourgeois N, Delcour C, Deviere J, François A, Lambert M, Cremer M. Osler-Weber-Rendu disease associated with hepatic involvement and high output heart failure. *J Clin Gastroenterol* **1990**;12:236–237
4. Cloogman HM, DiCapo RD. Hereditary hemorrhagic telangiectasia: sonographic findings in the liver. *Radiology* **1984**;150:521–522

Bilateral Urinomas in an Adult

Urinomas associated with renal trauma, iatrogenic injury, ureteric obstruction by calculus, neoplasms, renal transplants, and obstruction of the bladder outlet caused by posterior urethral valves are well known [1]. However, to our knowledge, bilateral urinomas in an adult and their association with urethral injury that occurred during parturition have not been reported previously.

A large abdominal mass was noted in a 35-year-old woman 2.5 months after parturition. The mass apparently had originated 1 week after parturition. CT scans showed bilateral uniformly hypodense (10 H) encapsulated masses in the perirenal regions (Fig. 1). No enhancement of the masses was seen with contrast material. Both kidneys showed normal excretion. On sonograms, the mass on the left was anechoic; the mass on the right contained multiple linear echoes and had a thick, smooth capsule.

Sonography and CT have often been used to diagnose urinoma when pseudonephromegaly has suggested tumor invasion. Other entities that must be considered in the diagnosis of perirenal urinomas include tumors, hematomas, and abscesses, CT is the most useful imaging procedure, particularly if dynamic-phase scans and reconstructions in the sagittal and coronal planes are used. Attenuation values of urinomas are normally −10 H to 30 H [2], and the attenuation usually is homogeneous as compared with that of abscesses and hematomas, which is heterogeneous. CT also gives specific information about the precise extent and location of the fluid collection and its relationship to the kidneys, ureters, and fascial planes and compartments [1]. The indirect evidence of round cell infiltration in necrotic fat and adjacent renal fascia that form the perirenal fibrous sac, in response to the accumulated urine, is shown better on sonograms [3].

K. K. Sen
Meenakshi Thakur
O. P. Sharma
Tata Memorial Hospital and Cancer Research Centre
Bombay 400 012, India

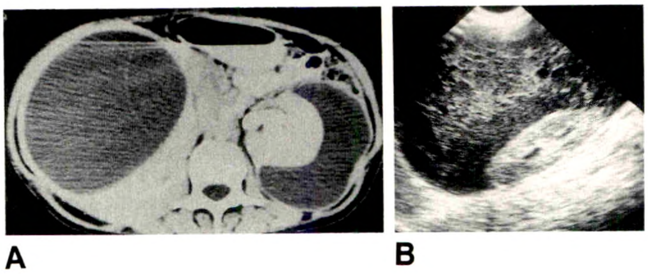

Fig. 1.—Bilateral urinomas.
A, Contrast-enhanced CT scan shows bilateral hypodense encapsulated perirenal masses. Mass on right extends from inferior surface of right lobe of liver to right iliac fossa, displacing renal parenchyma inferomedially. Smaller mass on left displaces left kidney cephalad and anteromedially. Capsule of mass on right is slightly thicker than that of mass on left and is smooth and shows noticeable enhancement. Ureters are displaced medially and bowel loops anteriorly.
B, Sonogram shows possible secondary infection on left side.

REFERENCES

1. Land EK, Glorioso L III. Management of urinomas by percutaneous drainage procedures. *Radiol Clin North Am* **1986**;24:551–559
2. Healy ME, Teng SS, Moss AA. Uriniferous pseudocyst: computed tomographic findings. *Radiology* **1984**;153:757–762
3. Feinstein KA, Fernbach SK. Septated urinomas in the neonate. *AJR* **1987**;149:997–1000

Fallopian Tube Nomenclature

I commend Dr. Thurmond both on her review article [1] on selective salpingography and fallopian tube recanalization and on her original contributions to these techniques. I would make one semantic observation.

Throughout her article, and in most recent communications on this subject, there is a confusing, and I think incorrect, use of the terms *proximal* and *distal* as they refer to the fallopian tubes. Almost all authors define proximal as the uterine or cornual end of the tube and distal as the ampullary, fimbriated, or ovarian end. This is the operator's perception during catheterization and injection of contrast medium. However, even the term retrograde catheterization, used by some authors, but not Thurmond, implies that the uterine end of the fallopian tube is the distal end.

Standard medical convention defines proximal and distal vessels or ducts not by their proximity to the midline or the cannulating instrument, but relative to in vivo physiologic flow. Hence, the proximal inferior vena cava is more caudal. A similar problem in nomenclature arose with the introduction of ERCP (endoscopic retrograde cholangiopancreatography), and, after initial confusion, radiologists agree that the proximal pancreatic duct is located in the tail of the pancreas (where it should be, and always has been). Physiologic flow in the fallopian tube is toward the uterus, and unless we take a male chauvinistic view regarding sperm movement, the distal end of the tube is toward the uterus.

Ferris M. Hall
Beth Israel Hospital
Harvard Medical School
Boston, MA 02215

REFERENCE

1. Thurmond AS. Selective salpingography and fallopian tube recanalization. *AJR* **1991**;156:33–38

Reply

I thank Dr. Hall for taking the feminist point of view. I hope he finds it equally refreshing that in this instance I take the male chauvinist point of view.

Amy S. Thurmond
Oregon Health Sciences University
Portland, OR 97201

MR Imaging of Growth Recovery Lines in Fossil Vertebrae

Previous attempts at MR imaging of fossilized bone failed because the volume of protons was too small to produce signals strong enough for image acquisition and processing. By hydrating the specimen, we have used MR imaging successfully to study fossil vertebrae.

Vertebrae from a prehistoric dolphin from the Miocene Epoch (approximately 12 million years old) from the National Museum of Natural History (Vertebrate Paleontology) Washington, DC, were studied. The fossils were hydrated by placing them in a plastic cylinder containing 500 ml of water. A 1.0-T (Siemens Magnetom) magnet was used with the specimen in a Helmholtz surface coil. Spin-echo, proton-density, and T2-weighted sequences (TE 30, 90; TR 2.0; slice thickness 4.0 mm; 2 acquisitions; 256 × 256 matrix) were obtained in axial and coronal planes. MR images provided sufficient anatomic detail to allow diagnosis of transverse lines and bands within the bones (Fig. 1).

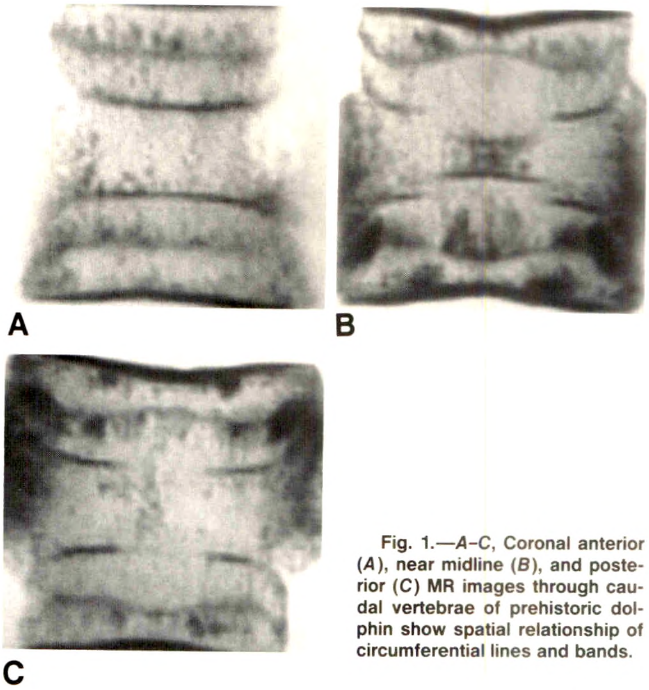

Fig. 1.—*A–C*, Coronal anterior (*A*), near midline (*B*), and posterior (*C*) MR images through caudal vertebrae of prehistoric dolphin show spatial relationship of circumferential lines and bands.

Growth recovery lines, frequently referred to as transverse lines, growth arrest lines, stress lines, or lines of Park or Harris, have been studied extensively in the human appendicular skeleton [1]. These lines cross bone horizontally at right angles to the longitudinal trabeculae and represent a markedly thickened interconnected network of trabecular bone. The lines and bands result from resumption of growth after an episode of growth cessation. Transverse lines in the vertebral column have been studied less well but have been described as mimicking osteopetrosis, with a “vertebra within a vertebra” appearance [2]. Although the lines may be normal, poor nutritional status during youth and a large variety of other causes have been described: infection; metabolic, neoplastic, and vitamin deficiency states; and poisoning, by either heavy metals or vitamins.

False bands and lines of variable thickness representing pseudopathologic changes also have been described [3]. Fine silt may filter into the spongiosa of bone, producing opaque lines, particularly if the deposited sediment contains silicon compounds. However, these dense compounds are deposited in an irregular pattern and therefore lack uniformity in thickness and are not circumferential. Because the deposition of artifacts is governed by gravity, the widest of these dense lines is found in the most dependent portion of fossilized bone. The results suggest that growth recovery bands and lines were present in mammals during prehistoric times. If hydration of fossils is feasible, MR imaging appears to be useful for detecting skeletal abnormalities.

Jeno I. Sebes
James W. Langston
Morris L. Gavant

University of Tennessee, Memphis
Memphis, TN 38163
Bruce Rothschild
Northeast Ohio University
Youngstown, OH 44512

REFERENCES

1. Park EA. The imprinting of nutritional disturbances on the growing bone. *Pediatrics* **1964**;33:815–862
2. Stammel CA. Multiple striae parallel to epiphyses and ring shadows around bone growth centers. *AJR* **1941**;46:497–505
3. Decker FH, Bohrod MG. Medullary artifacts in prehistoric bones. *AJR* **1939**;42:374–375

MR of Intraspinal Synovial Cyst: Rim Enhancement with Gadopentetate Dimeglumine

Silbergleit et al. [1] recently described uniform rim enhancement of a synovial cyst on MR after administration of gadopentetate dimeglumine. Pathologically, the cyst wall was composed of fibrous connective tissue with numerous vascular foci within it. The peripheral enhancement was thought to be caused by the chronic inflammatory changes around the synovial cyst. We describe a similar case with pathologic confirmation. We think that the cyst wall functions much like scar tissue. Gadolinium diffuses rapidly across the rich vascular network into the extracellular space through discontinuous epithelial membranes, which results in early rim enhancement [2].

Our patient, a 50-year-old woman with a history of progressive lower back pain had had new right-sided radicular symptoms for 3 months. The symptoms were confirmed on physical examination. Surface-coil MR was performed on a Siemens Magnetom SP 1.5-T unit. Routine double-echo (700/15, 2400/45, 2400/90) sagittal and short TR/TE (600/15) axial images without and with gadopentetate dimeglumine showed a well-defined cystic structure intimately related to a degenerative L4–L5 facet joint on the right side. The cyst was slightly hyperintense relative to CSF on T1- and T2-weighted images and had a hypointense rim that enhanced diffusely after administration of contrast medium. A correct preoperative diagnosis of a nonhemorrhagic synovial cyst was made. After total excision of the synovial cyst, the patient reported complete resolution of her symptoms.

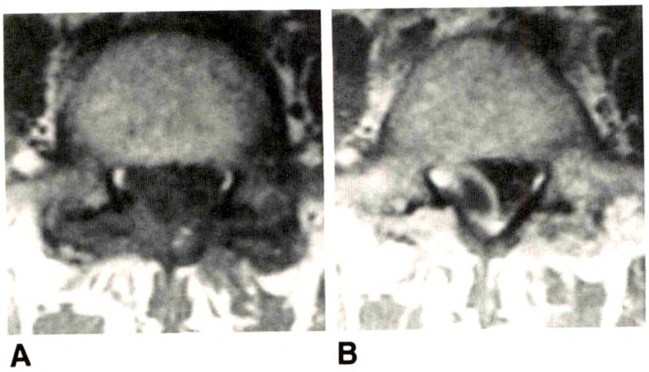

Fig. 1.—Intraspinal synovial cyst.
***A*, Axial T1-weighted MR image at L4–L5 level shows a heterogeneous dorsolateral mass on right intimately related to ligamentum flavum and facet joint. Signal intensity of central area of mass is lower than that of peripheral aspects.**
***B*, Gadolinium-enhanced axial T1-weighted MR image at same level as *A* shows diffuse rim enhancement of synovial cyst.**

Synovial cysts are rare causes of intraspinal extradural masses. Most commonly, they arise from degenerative apophyseal joints, in particular at the L4–L5 level, and are associated with radicular symptoms [3, 4]. Such cysts are more prevalent in females and after the age of 50 years [1, 3]. Synovial cysts contain watery or mucinous fluid [4]. Nonhemorrhagic synovial cysts may be isointense or hyperintense relative to CSF on spin-pulse sequences [4]. Some authors have attributed the hypointense rim to calcification or hemosiderin, but more likely it is related to the cyst membrane and surrounding inflammatory tissue [3, 4].

Differential diagnosis for a cystic dorsal extradural intraspinal mass includes extruded disk fragments, cystic neurofibromas, arachnoid cysts, and perineural cysts [4]. Rim enhancement with gadopentetate dimeglumine of recurrent disk herniation ("wrapped disc") has been shown to be caused by peridiskal fibrosis [2].

The noninvasiveness, multiplanar capabilities, and inherent contrast characteristics of MR imaging and the additional information provided by the use of contrast medium make MR an optimal imaging technique for evaluating spinal lesions.

Karl S. Chiang
Ya-Yen Lee
Michel E. Mawad
Baylor College of Medicine
Houston, TX 77030

REFERENCES

1. Silbergleit R, Gebarski SS, Brunberg JA, McGillicudy J, Blaivas M. Lumbar synovial cysts: correlation of myelographic, CT, MR, and pathological findings. *AJNR* **1990**;11:777–779
2. Price AC, Runge VM. MRI efficacy in spine expands with Gd-DTPA. *Diagn Imaging* **1989**;11(11):172–177
3. Liu SS, Williams KD, Drayer BP, Spetzler RF, Sonntag VKH. Synovial cysts of the lumbosacral spine: diagnosis by MR imaging. *AJR* **1990**;154:163–166
4. Jackson DE, Atlas SW, Mani JR, Norman D. Intraspinal synovial cysts: MR imaging. *Radiology* **1989**;170:527–530

High CT Attenuation Values in Paranasal Aspergillosis

A 14-year-old boy complained that his nose was blocked on the left side. He had a history of aspergillosis of the right paranasal sinuses and had had surgery for this about 8 months earlier. CT showed a soft-tissue mass in the left nasal cavity extending into the left maxillary antrum, ethmoid air cells complex, and frontal and sphenoid sinuses (Fig. 1). These mass lesions were patchy, with a zone of lower attenuation in the periphery. Mucoperiosteal thickening was present in some places. No bony destruction was seen. The attenuation values of these masses on unenhanced CT scans were

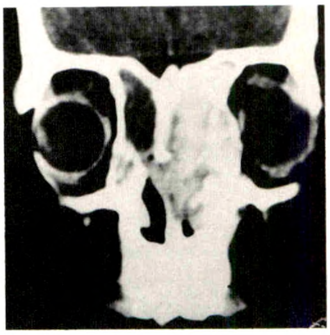

Fig. 1.—Coronal unenhanced CT scan of paranasal sinuses shows a heterogeneous soft-tissue mass with areas of high attenuation (about 90 H) in left nasal cavity and maxillary antrum. Peripheral rim of low attenuation represents thick mucoperiosteum.

90–100 H. No significant enhancement was seen after administration of contrast material. The diagnosis of recurrence of aspergillosis was confirmed histologically after surgery.

Limited studies have been done on the CT features of paranasal aspergillosis. Centeno et al. [1] have described various CT features of fungal sinus disease, but the high attenuation values seen in our case have not been mentioned before. This finding probably is due to the presence of calcium salts in the *Aspergillus* mycelia, which was reported by Stammberger et al. [2].

The high attenuation value is an important feature that can be used to differentiate a fungal mass from neoplasm. No neoplasms have such high attenuation values on unenhanced CT scans. Tumors of bone and cartilage can have a high attenuation value, but their appearance is different.

Kamlesh C. Khandelwal
Rajul J. Udani
Nikhil H. Merchant
Omprakash Sharma
Tata Memorial Hospital
Bombay 400 012, India

REFERENCES

1. Centeno RS, Benston JR, Macuso AA. CT scanning in rhinocerebral mucoromycosis and aspergillosis. *Radiology* **1981**;140:383–389
2. Stammberger H, Jakse R, Beaufort F. Aspergillosis of the paranasal sinuses: X-ray diagnosis, histopathology and clinical aspect. *Ann Otol Rhinol Laryngol* **1984**;93:251–256

Guard for Prevention of Finger-Stick Injuries Caused by Stylets

Because needle-stick injuries are potentially life-threatening events [1], I wish to describe a device that can be used to prevent needle-stick injuries that occur during replacement of the stylet in stylet needles.

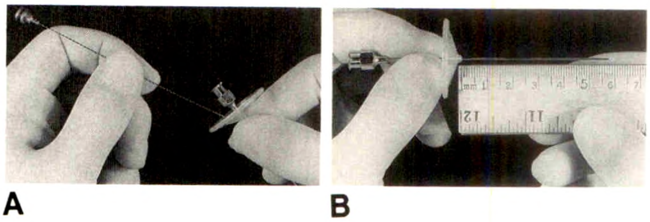

Fig. 1.—Guard for prevention of finger-stick injuries.
***A,* Guard protects finger from puncture when stylet is replaced.**
***B,* Device can be positioned at predetermined depth on needle for accurate placement of needle into a particular body space.**

The device is made of sterilizable, puncture-proof plastic. It is cone shaped, about 3 cm in diameter, and made so that it can be positioned at the hub end of the needle. The user's fingers are placed beneath the device and are protected from inadvertent needle-stick injuries during replacement of the stylet into the needle (Fig. 1A). The device can be positioned at a desired depth on the needle to ensure accurate placement of the needle into a body space (Fig. 1B). After use, the needle and the guard are discarded. Commercial availability in the fall is anticipated.

Andrew M. Singer
Beth Israel Hospital
Harvard Medical School
Boston, MA 02215

REFERENCE

1. Jagger J, Hunt EH, Brand-Elnaggar J, Pearson RD. Rates of needle-stick injury caused by various devices in a university hospital. *N Engl J Med* **1988**;319:284–288

Letters are published at the discretion of the Editor and are subject to editing.

Letters to the Editor must not be more than two *double-spaced*, typewritten pages. One or two figures may be included. Abbreviations should not be used. See Author Guidelines, page A5.

Material being submitted or published elsewhere should not be duplicated in letters, and authors of letters must disclose financial associations or other possible conflicts of interest.

Letters concerning a paper published in the *AJR* will be sent to the authors of the paper for a reply to be published in the same issue. Opinions expressed in the Letters to the Editor do not necessarily reflect the opinions of the Editor.

Forthcoming Articles

1991 ARRS PRESIDENTIAL ADDRESS

Reflections on radiology as a career. *Kirkpatrick JA Jr*

REVIEW ARTICLE

Imaging of vascular complications associated with renal transplants. *Dodd GD III, Tublin ME, Shah A, Zajko AB*

CARDIOPULMONARY RADIOLOGY

Diffuse pulmonary alveolar hemorrhage after bone marrow transplantation: radiologic findings in 39 patients. *Witte RJ, Gurney JW, Robbins RA, et al.*

Motion artifact simulating aortic dissection on CT. *Burns MA, Molina PL, Gutierrez FR, Sagel SS*

Commentary. Current status of mediastinal sonography in the posttreatment evaluation of patients with lymphoma. *Marglin SI, Laing FC, Castellino RA*

Case report. Torsion of the upper lobe of the lung after surgery: findings on pulmonary angiography. *Munk PL, Vellet AD, Zwirewich C*

BREAST RADIOLOGY

The American College of Radiology Mammography Accreditation Program. *McLelland R, Hendrick RE, Zinninger MD, Wilcox PA*

Self-referred mammography patients: analysis of patient characteristics. *Reynolds HE, Jackson VP*

GASTROINTESTINAL RADIOLOGY

Altered gallbladder contractility after extracorporeal shock-wave cholecystolithotripsy. *Rawat B, Fache JS, Burhenne HJ*

Case report. Placement of a metallic biliary endoprosthesis via cholecystostomy. *Dawson SL, Girard MJ, Saini S, Mueller PR*

Perspective. Primary sclerosing cholangitis: a modified classification of the cholangiographic findings. *Majoie CBLM, Reeders JWAJ, Sanders JB, Huibregtse K, Jansen PLM*

Case report. MR demonstration of edema adjacent to a liver metastasis: pathologic correlation. *Lee MJ, Saini S, Compton CC, Malt RA*

Pictorial essay. Endorectal sonography in the evaluation of rectal and perirectal diseases. *St Ville EW, Jafri SZH, Madrazo BL, Mezwa DG, Bree RL, Rosenberg BF*

GENITOURINARY RADIOLOGY

Transurethral balloon dilatation of the urethra: effectiveness in highly selected patients with prostatism. *Wasserman NF, Reddy PK, Zhang G, Kapoor DA, Berg P*

Case report. Iliac artery stenosis causing renal transplant–mediated hypertension: angiographic diagnosis and treatment. *Weigele JB*

Case report. Bilateral testicular infarction caused by epididymitis. *Eisner DJ, Goldman SM, Petronis J, Millmond SH*

Technical note. Insertion of the Simon nitinol caval filter: value of the antecubital vein approach. *Kim D, Schlam BW, Porter DH, Simon M*

MUSCULOSKELETAL RADIOLOGY

Cervical paraspinal calcification in collagen vascular diseases. *Schweitzer ME, Cervilla V, Manaster BJ, et al.*

Diagnosis of osteomyelitis of the foot in diabetic patients: value of ^{111}indium-leukocyte scintigraphy. *Larcos G, Brown ML, Sutton RT*

Osteoarthritis of the knee: comparison of radiography, CT, and MR imaging to assess extent and severity. *Chan WP, Lang P, Stevens MP, et al.*

Photostimulable phosphor digital radiography of the extremities: diagnostic accuracy compared with conventional radiography. *Wilson AJ, Mann FA, Murphy WA Jr, Monsees BS, Linn MR*

PEDIATRIC RADIOLOGY

Diagnosis of acute pyelonephritis in children: comparison of sonography and ^{99m}Tc-DMSA scintigraphy. *Björgvinsson E, Majd M, Eggli KD*

Normal length of fetal kidneys: sonographic study in 397 obstetric patients. *Cohen HL, Cooper J, Eisenberg P, et al.*

Benign hemorrhagic adrenal cortical macrocysts in the Beckwith-Wiedemann syndrome. *McCauley RGK, Beckwith JB, Elias ER, Faerber EN, Prewitt LH Jr, Berdon WE*

Parotid enlargement in HIV-positive children: imaging findings. *Soberman N, Leonidas JC, Berdon WE, et al.*

Case report. Goitrous cretinism presenting as newborn stridor: CT evaluation. *Optican RJ, White KS, Effmann EL*

Arteriopathy and coarctation of the abdominal aorta in children with mucopolysaccharidosis: imaging findings. *Taylor DB, Blaser SI, Burrows PE, Stringer DA, Clarke JTR, Thorner P*

Pictorial essay. Biological classification of soft-tissue vascular anomalies: MR correlation. *Meyer JS, Hoffer FA, Barnes PD, Mulliken JB*

NEURORADIOLOGY

MR imaging of cerebral ischemia: findings in the first 24 hours. *Yuh WTC, Crain MR, Loes DJ, Greene GM, Ryals TJ, Sato Y*

Cerebral ischemia: evaluation with contrast-enhanced MR imaging. *Crain MR, Yuh WTC, Greene GM, et al.*

Diagnosis of acute cerebral infarction: comparison of CT and MR imaging. *Bryan RN, Levy LM, Whitlow WD, Killian JM, Preziosi TJ, Rosario JA*

MR imaging of primary trochlear nerve neoplasms. *Gentry LR, Mehta RC, Appen RE, Weinstein JM*

PERSPECTIVES

Analysis of economics and use of MR imaging units in the United States in 1990. *Evens RG, Evens RG Jr*

The total volume and cost of radiologic services in the United States in 1990. *Sunshine JH, Mabry MR, Bansal S*

Editorial. Is plagiarism ever insignificant? *Berk RN*

MEETING NEWS

Meeting news. Fourteenth annual course: Society of Computed Body Tomography, April 1991. *Whalen E*

ARRS 1991 ANNUAL MEETING

Summary of scientific program

Gold medal recipients. *Kirkpatrick JA*

Secretary's report. *Ferrucci JT*

Administrative report. *Fullagar PR*

Award-winning exhibits

New members

Review of Current Literature

Initials and addresses of corresponding authors are provided in parentheses for each article so that the reader can obtain reprints directly. Abstracts are printed verbatim from each journal.

The New England Journal of Medicine

Pulmonary aspergillosis in the acquired immunodeficiency syndrome. Denning DW, Follansbee SE, Scolaro M, Norris S, Edelstein H, Stevens DA (DAS, Santa Clara Valley Medical Center, 751 S. Bascom Ave., San Jose, CA 95128). *N Engl J Med* 324(10):654–662, March 1991

Background and Methods. Symptomatic pulmonary aspergillosis has rarely been reported in patients with the acquired immunodeficiency syndrome (AIDS). We describe the predisposing factors, the clinical and radiologic features, and the therapeutic outcomes in 13 patients with pulmonary aspergillosis, all of whom had human immunodeficiency virus (HIV) infection and 12 of whom had AIDS.

Results. Pulmonary aspergillosis was detected a median of 25 months after the diagnosis of AIDS, usually following corticosteroid use, neutropenia, pneumonia due to other pathogens, marijuana smoking, or the use of broad-spectrum antibiotics. Two major patterns of disease were observed: invasive aspergillosis (in 10 patients) and obstructing bronchial aspergillosis (in 3). Cough and fever, the most common symptoms, tended to be insidious in onset in patients with invasive disease (median duration, 1.3 months before diagnosis). Breathlessness, cough, and chest pain predominated in the three patients with obstructing bronchial aspergillosis, who coughed up fungal casts. Radiologic patterns included upper-lobe cavitary disease (sometimes mistaken for tuberculosis), nodules, pleural-based lesions, and diffuse infiltrates, usually of the lower lobe. Transbronchial biopsies were usually negative, but positive cultures were obtained from bronchoalveolar-lavage fluid or percutaneous aspirates. Dissemination to other organs occurred in at least two patients, and direct invasion of extrapulmonary sites was seen in two others. The results of treatment with amphotericin B, itraconazole, or both were variable. Ten of the patients died a median of 3 months after the diagnosis (range, 0 to 12 months).

Conclusions. Pulmonary aspergillosis is a possible late complication of AIDS; if diagnosed early, it may be treated successfully.

Effective surgical adjuvant therapy for high-risk rectal carcinoma. Krook JE, Moertel CG, Gunderson LL, et al. (CGM, Mayo Clinic, Rochester, MN 55905). *N Engl J Med* 324(11):709–715, March 1991

Background. Radiation therapy as an adjunct to surgery for rectal cancer has been shown to reduce local recurrence but has not improved survival. In a previous study, combined radiation and chemotherapy improved survival significantly as compared with surgery alone, but not as compared with adjuvant radiation, which many regard as standard therapy. We designed a combination regimen to optimize the contribution of chemotherapy, decrease recurrence, and improve survival as compared with adjuvant radiation alone.

Methods. Two hundred four patients with rectal carcinoma that was either deeply invasive or metastatic to regional lymph nodes were randomly assigned to postoperative radiation alone (4500 to 5040 cGy) or to radiation plus fluorouracil, which was both preceded and followed by a cycle of systemic therapy with fluorouracil plus semustine (methyl-CCNU).

Results. After a median follow-up of more than seven years, the combined therapy had reduced the recurrence of rectal cancer by 34 percent ($P = 0.0016$; 95 percent confidence interval, 12 to 50 percent). Initial local recurrence was reduced by 46 percent ($P = 0.036$; 95 percent confidence interval, 2 to 70 percent), and distant metastasis by 37 percent ($P = 0.011$; 95 percent confidence interval, 9 to 57 percent). In addition, combined therapy reduced the rate of cancer-related deaths by 36 percent ($P = 0.0071$; 95 percent confidence interval, 14 to 53 percent) and the overall death rate by 29 percent ($P = 0.025$; 95 percent confidence interval, 7 to 45 percent). Its acute toxic effects included nausea, vomiting, diarrhea, leukopenia, and thrombocytopenia. These effects were seldom severe. Severe, delayed treatment-related reactions, usually small-bowel obstruction requiring surgery, occurred in 6.7 percent of all patients receiving radiation, and the frequencies of these complications were comparable in both treatment groups.

Conclusions. The combination of postoperative local therapy with radiation plus fluorouracil and systemic therapy with a fluorouracil-based regimen significantly and substantively improves the results of therapy for rectal carcinoma with a poor prognosis, as compared with postoperative radiation alone.

A comparison of surfactant as immediate prophylaxis and as rescue therapy in newborns of less than 30 weeks' gestation. Kendig JW, Notter RH, Cox C, et al. (JWK, University of Rochester Medical Center, Dept. of Pediatrics, Box 651, 601 Elmwood Ave., Rochester, NY 14642). *N Engl J Med* 324(13):865–871, March 1991

Background. Exogenous pulmonary surfactants are administered into the trachea either to prevent respiratory distress syndrome in premature infants or to treat it. In a randomized, multicenter trial, we compared the results of surfactant therapy initiated as prophylaxis with the results of rescue therapy with surfactant.

Methods. Before birth, 479 infants with an estimated gestational age of less than 30 weeks were randomly assigned to receive surfactant as prophylaxis ($n = 235$) or rescue therapy ($n = 244$). The infants in the prophylaxis group received a 90-mg intratracheal dose of an exogenous calf-lung surfactant extract at the time of delivery, whereas the infants in the rescue-therapy group received 90 mg of the surfactant several hours after delivery if the fractional inspiratory oxygen concentration was at least 0.40 or if the mean airway pressure was at least 0.686 kPa (7 cm of water), or both. Infants in both groups received additional doses of surfactant at intervals of 12 to 24 hours if these criteria were met.

Results. The proportion of infants surviving until discharge to their homes was significantly higher in the prophylaxis group than in the rescue-therapy group (88 vs. 80 percent, P = 0.028). This difference was due primarily to the longer survival of very premature infants (≤26 weeks' gestation) in the prophylaxis group than in the rescue-therapy group (75 vs. 54 percent, P = 0.006). According to proportional-hazards regression analysis, the distribution of survival times was better for all infants in the prophylaxis group (P = 0.007) and for the subgroup of infants in the prophylaxis group who were delivered at 26 weeks' gestation or earlier (P = 0.0048). Infants in the prophylaxis group who were delivered at 26 weeks' gestation or earlier had a lower incidence of pneumothorax than similar infants in the rescue-therapy group (7 vs. 18 percent, P = 0.03).

Conclusions. We found a significant advantage to the administration of the initial dose of surfactant as prophylaxis rather than as rescue therapy in very premature infants.

Cancer

Percutaneous fine-needle aspiration cytologic study of main pancreatic duct stenosis under pancreatographic guidance. Gagnon P, Boustiere C, Ponchon T, Valette PJ, Genin G, Labadie M (PG, CHUL, Service de Gastroentérolgie, 2705, blv. Laurier, Ste-Foy, Québec, Canada G1V-4G2). *Cancer* 67:2395–2400, 1991

When pancreatography shows a stenosis of the main pancreatic duct in patients with normal or inconclusive ultrasound and computed tomography, the exact nature of such stenosis is sometimes difficult to precise before surgical exploration. In such cases, the authors systematically performed a percutaneous fine-needle aspiration cytologic study of the stenosis under pancreatographic guidance. Fifteen patients were referred because of suspected pancreatic malignancy. The tumor markers, carcinoembryonic antigen (CEA) and CA 19-9 were normal in 11 patients and elevated in one patient, whereas only CA 19-9 was elevated in three others. In 14 cases, both the ultrasound and computed tomography did not show any obvious pancreatic mass. The pancreatography was done through endoscopic retrograde cholangiopancreatography (ERCP) (12 patients) or percutaneously in case of failure at ERCP[3] and showed a main pancreatic duct stenosis that underwent aspiration by percutaneous fine needle precisely positioned using biplane fluoroscopy. The aspirated material was then smeared on glass slides, air-dried, and stained by Giemsa. In nine of the 15 patients, cytologic study revealed adenocarcinoma. This was confirmed by surgery in five and by progressive deterioration followed by death in four. In six patients, cytologic study gave a nonmalignant result. Chronic pancreatitis was found in five of them, confirmed at surgery in three and based on uneventful follow-up of at least 12 months in two others. In one case, a pancreatic adenocarcinoma not detected by cytologic study was found at surgery. Thus, the sensitivity and specificity of this diagnostic approach were 90% and 100%, respectively. No serious complication was noticed. The authors conclude that when ultrasound and computed tomography are inconclusive, percutaneous fine-needle aspiration cytologic study of main pancreatic duct stenosis under pancreatographic guidance is a safe, simple, and helpful procedure in the investigation of patients with suspected pancreatic malignancy.

Reprinted by permission from the American Cancer Society.

A prospective study of magnetic resonance imaging in lymphoma staging. Skillings JR, Bramwell V, Nicholson RL, Prato FS, Wells G (JRS, London Regional Cancer Centre, 790 Commissioners Rd. E., London, Ontario, Canada N6A 4L6). *Cancer* 67:1838–1843, 1991

In this prospective study, magnetic resonance imaging (MRI) was compared with computed tomography (CT) in patients with non-Hodgkin's lymphoma (NHDL), and with CT and laparotomy in patients with Hodgkin's disease (HD). Among 31 patients with NHDL, there was agreement between MRI and CT findings in 21 patients; MRI findings were positive and CT findings were negative in 8 patients; and MRI findings were negative and CT findings were positive in 2 patients. The false-negative findings of MRI included a laparotomy-proven mesenteric mass and a 6.6-cm lesion in the spleen, both shown by CT. In 13 evaluable patients with HD, there was agreement between MRI and laparotomy findings in 8 patients; MRI findings were positive and laparotomy findings were negative in 4 patients; and MRI findings were negative and laparotomy findings were positive in 1 patient. CT findings agreed with laparotomy findings in nine patients; CT findings were positive and laparotomy findings were negative in one patient; and CT findings were negative and laparotomy findings were positive in three patients. This suggested that MRI, although more sensitive than CT, was less specific with more false-positive findings. The spin-lattice relaxation time (T1) for the spleen was generally higher in patients with HD who had pathologically confirmed splenic involvement, and tended to increase with increasing spleen weight. This study was performed on a prototype 0.15 Tesla (Technicare Inc., Solon, OH) resistive unit at at time when methods and reporting for MRI were still being developed. Although MRI appears to have fewer false-negative findings than CT in evaluating the abdomen of lymphoma patients, the lack of a gastrointestinal contrast agent and specificity of T1 elevations in the spleen would not suggest that MRI could replace CT or laparotomy as a staging technique.

Reprinted by permission from the American Cancer Society.

Second cancers following non-Hodgkin's lymphoma. Travis LB, Curtis RE, Boice JD Jr, Hankey BF, Fraumeni JF Jr (LBT, Executive Plaza North, Ste. 408, National Cancer Institute, Bethesda, MD 20892). *Cancer* 67:2002–2009, 1991

The risk of second malignancies following non-Hodgkin's lymphoma (NHL) was estimated in 29,153 patients diagnosed with NHL between 1973 and 1987 in one of nine areas participating in the National Cancer Institute's Surveillance, Epidemiology, and End Results Program. Compared with the general population, NHL patients were at a significantly increased risk of developing second cancers (observed/expected [O/E] = 1.18; O = 1231). The O/E ratio increased significantly with time to reach 1.77 in 10-year survivors. Significant excesses were noted for acute nonlymphocytic leukemia (O/E = 2.88), cancers of the bladder (O/E = 1.30), kidney (O/E = 1.47), and lung (O/E = 1.57), malignant melanoma (O/E = 2.44), and Hodgkin's disease (O/E = 4.16). Chemotherapy appeared related to subsequent acute nonlymphocytic leukemia (ANLL) and bladder cancer. Radiation therapy was associated with ANLL and possibly cancers of the lung, bladder, and bone. Malignant melanoma was not clearly related to initial NHL treatment.

Reprinted by permission from the American Cancer Society.

Cost-effectiveness analysis of mass screening for breast cancer in Japan. Okubo I, Glick H, Frumkin H, Eisenberg JM (JME, Dept. of Medicine, 3400 Spruce St., Philadelphia, PA 19104). *Cancer* 67:2021–2029, 1991

The official Japanese recommendation for breast cancer screening is physical examination by a physician, in contrast to US recommendations of mammography. In this analysis of breast cancer screening, the authors used Japanese data in a cost-effectiveness model to compare the following five strategies: (1) no screening (N); (2) physical examination alone (PE); (3) mammography (MG); (4) PE followed by MG if PE findings were abnormal (PE → MG); and (5) PE combined with MG for all screened women (PE + MG). None of these programs would save medical expenditures. The total discounted net costs per patient (in US dollars) were as follows: N, $54; PE, $412; MG, $517; PE → MG, $340; and PE + MG, $731. The number of years of life saved per cohort of 100,000 asymptomatic Japanese women would range from 708 (PE → MG) to 3724 (PE + MG). The additional costs of each strategy (compared with N) per additional year of life would be $49,700 for PE, $40,400 for PE → MG, $14,300 for MG, and

$18,200 for PE + MG. The least costly screening option (PE ⟶ MG) does not have the lowest cost per additional year of life saved (MG does). MG would be preferable to the current Japanese recommendation of PE alone.

Reprinted by permission from the American Cancer Society.

Chest

High-resolution ultrafast chest CT in the clinical management of febrile bone marrow transplant patients with normal or nonspecific chest roentgenograms. Barloon TJ, Galvin JR, Mori M, Stanford W, Gingrich RD (TJB, Dept. of Radiology, University of Iowa Hospital, Iowa City, IA 52242). *Chest* 99:928–933, April 1991

Plain chest roentgenograms may be normal or show nonspecific abnormalities during the frequent febrile episodes that occur in patients after bone marrow transplantation. In this group, ultrafast 10-mm and 3-mm high-resolution CT scans were prospectively performed in 33 patients to determine if useful information was provided that either changed the patient's clinical management or added confidence to the clinical diagnosis. The 36 symptomatic episodes that occurred in 33 patients included fever in 20 episodes and fever combined with cough, dyspnea, chest pain, or rales in 16. Fourteen chest roentgenograms were interpreted as normal, and 22 were interpreted as demonstrating nonspecific changes; however, none of the roentgenograms was considered helpful in that they did not provide sufficient information for further management. In 2 of 14 episodes in patients with normal chest roentgenograms and in 9 of 22 episodes in patients with nonspecific chest roentgenograms, CT scanning resulted in a change in clinical management that included performing bronchoscopy, increasing or changing antibiotic coverage, starting white blood cell transfusions, requesting surgical biopsy, or a combination of these. In 1 of 14 episodes in patients with normal chest roentgenograms and in 8 of 22 episodes in patients with nonspecific roentgenograms, CT added confidence to the diagnosis. In the remaining 16 episodes, CT scans provided no additional information. We conclude that in many instances, noncontrast ultrafast chest CT scans can provide information that may either change a patient's clinical management or more clearly establish the extent of pulmonary disease.

Gastroenterology

Cancer surveillance in ulcerative colitis. Nugent FW, Haggitt RC, Gilpin PA (FWN, Dept. of Gastroenterology, Lahey Clinic Medical Center, Burlington, MA). *Gastroenterology* 100:1241–1248, 1991

During a 13-year period, 213 patients with ulcerative colitis who had no clinical or endoscopic evidence of colonic carcinoma were enrolled in a biopsy surveillance program for dysplasia and carcinoma. The aims of the study were to determine whether such a program could decrease the cancer risk in this group of patients, to determine whether patients with a low risk of carcinoma could be identified, thus enabling them to retain their colon, and to accomplish these goals with a reasonable expenditure of resources. Eighteen patients had dysplasia detected in the initial biopsy specimens; 15 of these patients underwent colectomy, and 7 had unsuspected carcinoma (1 Dukes' stage A, 2 stage B, and 4 stage C). Eleven patients had dysplasia detected during follow-up; 7 of these patients had colectomy, and only 1 patient had carcinoma (Dukes' B). Dysplasia developed in 5 of 20 patients with indefinite changes on initial biopsy samples; 3 of these patients underwent colectomy, and 1 patient had carcinoma (Dukes' B). There was no difference in the prevalence of dysplasia between patients with left-sided disease and patients with extensive disease. With the exception of 2 patients with inadequate surveillance, there has been no clinical evidence of carcinoma in any of the 148 patients whose biopsy results remained negative throughout the study; carcinoma has not developed in any of 175 patients without dysplasia on initial biopsy sample. All 4 patients who died of carcinoma had high-grade dysplasia in their initial colonoscopic biopsy samples. It is concluded that a biopsy surveillance program can be an effective aid in helping control the risk of carcinoma in patients with long-standing ulcerative colitis, that the short-term risk of carcinoma for patients with negative biopsy results is low and colectomy for risk of carcinoma can be deferred in this group, and that patients with extensive and left-sided disease share the same risk of the development of dysplasia.

Reprinted with permission by the American Gastroenterological Association.

Prevalence of primary sclerosing cholangitis in patients with ulcerative colitis. Olsson R, Danielsson Å, Järnerot G, et al. (RO, Medical Clinics at Sahlgrenska Sjukhuset, Götebord, Sweden). *Gastroenterology* 100:1319–1323, 1991

All patients ≥16 years old with a diagnosis of ulcerative colitis were identified in five well-defined catchment areas, representing 12.7% of the Swedish population. Exactly 1500 patients were retrieved, giving a point prevalence of $170/10^5$ inhabitants. It was possible to obtain liver function test results <2 years old in 94% of the patients and to obtain endoscopic retrograde cholangiographic results in 65 of the 72 patients with abnormal serum alkaline phosphatase values. Primary sclerosing cholangitis was diagnosed in 55 of the patients (3.7%). The prevalence of the disease was 5.5% in patients with substantial colitis and 0.5% in patients with distal colitis. There was a marked male predominance in cholangitis patients compared with colitis patients without cholangitis. Ninety-five percent of the patients with cholangitis had substantial colitis, which was more than the 62% of patients without cholangitis who had colitis. Female patients with colangitis were older than male patients at the time of diagnosis of both cholangitis and colitis, which contrasted to the equal age at diagnosis of colitis in male and female patients without cholangitis.

Reprinted with permission by the American Gastroenterological Association.

Endoscopic transpapillary therapy for disrupted pancreatic duct and peripancreatic fluid collections. Kozarek RA, Ball TJ, Patterson DJ, Freeny PC, Ryan JA, Traverso LW (RAK, Section of Therapeutic Endoscopy, Virginia Mason Medical Center, Seattle, WA). *Gastroenterology* 100:1362–1370, 1991

Eighteen patients with active pancreatic ductal disruptions, including 14 with definable fluid collections, were treated with transpapillary pancreatic duct drains or stents. Twelve of these patients had undergone a previous percutaneous or surgical pancreatic drainage procedure or both, and 8 had long-term drainage tubes in chronic fistulous tracts. Transpapillary catheters could be placed across the ductal disruption or directly into the fluid collection in each case, and 16 of 18 patients had resolution of the disrupted pancreatic duct. Twelve of 14 fluid collections resolved. Complications were limited to mild exacerbation of pancreatitis symptoms in 2 patients and 2 patients who developed subsequent stent occlusion leading to recurrent pancreatitis (1 patient) or recurrent duct blowout with pseudocyst (1 patient). Nine patients had variably significant ductal changes attributable to pancreatic duct stents. At a median follow-up of 16 months, 7 patients ultimately required surgery for ongoing pancreatic pain or residual/recurrent fluid collection. The transpapillary treatment of ongoing pancreatic ductal disruption with or without fluid collection has the potential to obviate surgery in some patients, change an urgent surgical procedure into an elective one, or even assist the surgeon in the performance of intraoperative pancreatography. Further study of this technique appears warranted and must be placed into the perspective of current therapies.

Reprinted with permission by the American Gastroenterological Association.

Digestive Diseases and Sciences

Pathogenetic role of *Helicobacter pylori* in duodenal ulcer disease: multivariate analysis of factors affecting relapse. Hui WM, Ho J, Lam SK (HWM, Dept. of Medicine, University of Hong Kong, Queen Mary Hospital, Pokfulam Rd., Hong Kong). *Dig Dis Sci* 36(4):424–430, April 1991

The pathogenesis of duodenal ulcer disease is multifactorial and the contribution of *Helicobacter pylori* in relation to the other factors to the release of duodenal ulcer is unknown. To investigate this, we studied 147 patients with endoscopically proven healed ulcers. These patients were randomized to receive either placebo, misoprostol 200 μg or misoprostol 300 μg four times daily, and clinical, personal, physiological and endoscopic characteristics were obtained prospectively. Endoscopy was performed at the active phase of the ulcer and when the ulcer healed. Biopsies were taken from the antrum to assess histologically for: (1) the activity of gastritis as assessed by the degree of polymorph infiltration, (2) the degree of chronic inflammation by the degree of chronic inflammatory cells infiltration and degree of mucosal degeneration, and (3) bacteriologically for the presence of *H. pylori.* The severity of the gastritis and the bacterial density were graded independently by two pathologists. The patients were assessed at two-month intervals for 12 months or until the ulcer relapsed. The results demonstrated that the relapse rates of duodenal ulcer were similar in the three treatment groups. The relapse rate was higher in the group with higher density of the bacteria ($P < 0.05$). The degree of gastritis did not affect the relapse rate of duodenal ulcer in either the placebo or misoprostol group or in all patients combined. Stepwise logistic regression analysis identified that increased duodenal inflammation, male sex, early-onset disease, and *H. pylori* adversely affected relapse of the ulcer. We conclude that multiple factors affect the relapse of duodenal ulcer and *H. pylori* is one of them.

Gastrointestinal Endoscopy

Total colonoscopy: is it always possible? Waye JD, Bashkoff E (JDW, 650 Park Ave., New York, NY). *Gastrointest Endosc* 37(2):152–154, 1991

One-thousand three hundred fifty-one consecutive colonoscopies were performed in an office setting without fluoroscopy. Three different models of colonoscopes were utilized; all were manufactured by the Olympus Corporation of America, and included a videoendoscope, a CF-20L immersible OES-type instrument, and an older fiberoptic colonoscope, CFLB-3W. In all colonoscopies, the cecum was reached in 95.9%, even when an obstructing lesion or stenosis was present. Total intubation was performed in 97% of cases with the videoendoscope, 95.5% with the CF-20L, and 95.7% with the CFLB-3W. In a subgroup of 865 colonoscopies, total colonoscopy was performed in 98% of cases when obstructing lesions (carcinoma or stricture) were excluded from analysis. In this subgroup, total colonoscopy could not be performed in 16 patients because of colonic fixation, tortuosity, or for unknown anatomical reasons. Forty-five percent of this subgroup was female, but of the 16 patients in whom total colonoscopy was not possible, 15 were women, 5 of whom had a previous hysterectomy.

We conclude that in the absence of any obstruction lesion, an expert can perform complete colonoscopy in 98% of examinations, and in 95% of all patients presenting for colonoscopy. Total colonoscopy may be more difficult in women than men, but a previous hysterectomy does not seem to adversely affect the ability to perform colonoscopy. The type of instrument used for colonoscopy does not impact on the ability to visualize the entire colon.

Prospective blinded trial of colonoscopic miss-rate of large colorectal polyps. Hixson LJ, Fennerty MB, Sampliner RE, Garewal HS (MBF, Dept. of Medicine, Section of Gastroenterology, University Medical Center, 1501 N. Campbell, Rm. 6406, Tucson, AZ 85724). *Gastrointest Endosc* 37(2):125–127, 1991

We prospectively studied the colonoscopic miss-rate of large colorectal polyps in a blinded trial featuring tandem colonoscopy. Sixty-three lesions $\geq$1 cm in size were discovered and none were missed. Confidence intervals of 95% are a miss-rate of 0 to 4.6%. We conclude that <5% of large colorectal polyps are missed during the index colonoscopic examination in a well-prepared colon.

Mucinous pancreatic tumors: ERCP findings. Nickl NJ, Lawson JM, Cotton PB (NJN, Division of Digestive Diseases and Nutrition, MN 654, Albert B. Chandler Medical Center, University of Kentucky, Lexington, KY 40536-0084). *Gastrointest Endosc* 37(2):133–138, 1991

Mucin-producing tumors of the pancreas are rare and difficult to diagnose neoplasms. To further characterize the nature of these lesions, four such cases are described here in which the diagnosis was suspected at endoscopic retrograde cholangiopancreatography by the presence of ampullary or intraductal mucus. In one patient, pancreatoscopy directly visualized the tumor. Ultrasound and computed tomography failed to suggest the presence of a neoplasm in the majority of these cases, but endoscopic ultrasound was performed in one and correctly identified the multi-cystic tumor. A high incidence of acute pancreatitis was seen in these cases and was felt to be secondary to intermittent ductal obstruction by mucus. The characteristic appearance of intra-ductal mucus provides an important clue to the presence of this type of pancreatic neoplasia.

The Journal of Bone and Joint Surgery

Radiographic assessment of instability of the knee due to rupture of the anterior cruciate ligament: a quadriceps-contraction technique. Franklin JL, Rosenberg TD, Paulos LE, France EP (JLF, Ballard Orthopedic and Fracture Clinic, 1801 N.W. Market St., #403, Seattle, WA 98107). *J Bone Joint Surg [Am]* 73-A(3):365, March 1991

We compared the results of a radiographic technique for the measurement of instability of the knee with those obtained with a KT-1000 arthrometer. The study was conducted on both knees of sixty patients who had a ruptured anterior-cruciate ligament in one knee, as well as in ten control subjects. The radiographic technique included the examination of a true lateral radiograph, made while the knee was in full extension and the quadriceps was maximally contracted, with a 66.7-newton downward force produced by a 6.8-kilogram weight suspended from the ankle. As demonstrated by both techniques, the maximum difference between the displacements of the right and left knees in the control subjects was 2.5 millimeters and the mean difference between the displacements in the two knees in the patients was 7.5 millimeters.

In fourteen of the sixty knees in which the ligament was ruptured, the injury was acute. The forward translation of the medial side in these fourteen knees was compared with that in the forty-six knees in which the injury was chronic. The mean difference in the displacement of the medial side in the right and left knees was 3.5 millimeters in the fourteen patients who had an acute injury and 5.0 millimeters in the forty-six patients who had a chronic injury. Thirteen of the sixty patients had disruption of the posteromedial corner of the injured knee, and the translation of the medial side in these knees was significantly increased compared with that in the intact knees of the same patients.

The radiographic technique was as accurate as the KT-1000 arthrometer in the diagnosis of unilateral rupture of the anterior cruciate ligament. The quadriceps contraction radiographic technique is an accurate and simple method for diagnosis.

Bone scans in the diagnosis of bone crisis in patients who have Gaucher disease. Katz K, Mechlis-Frish S, Cohen IJ, Horev G, Zaizov R, Lubin E (KK, Dept. of Orthopedic Surgery, Beilinson Medical Center, Petah Tiqva 49100, Israel). *J Bone Joint Surg [Am]* 73-A(4):513-517, April 1991

Of thirty-four occurrences of bone pain in seventeen children and young adults who had type-I Gaucher disease, twenty-five were finally diagnosed as bone crises. On the basis of a bone scan with technetium-99m methylene diphosphonate, a correct diagnosis of bone crisis was made for twenty-three occurrences, with a sensitivity of 0.92.

At the onset of a crisis, the bone scan typically showed decreased uptake of radionuclide at the involved area. After six weeks, a repeat bone scan of the long bones showed a ring of increased uptake surrounding an area of decreased uptake. At six months, the appearance of the bones on the radionuclide scan was normal.

Clinical Orthopaedics and Related Research

Magnetic resonance imaging in acetabular residual dysplasia. Bos CFA, Bloem JL, Verbout AJ (CFAB, Dept. of Orthopedic Surgery, University Hospital Leiden, Rijnsburgerweg 10, 2333 AA Leiden, the Netherlands). *Clin Orthop* 265:207–217, April 1991

Eighteen hips in 15 children showed persistent roentgenographic evidence of congenital acetabular residual dysplasia at four- to eight-year follow-up evaluations. The mean follow-up period was 5.8 years. These hips were subsequently evaluated by magnetic resonance (MR) imaging. MR imaging studies revealed thick unossified chondroepiphyseal cartilage of the acetabular roof adjoining the ilium in all hips. The cartilage in these hips counterbalanced the steep acetabular slope seen on roentgenograms. Initially these hips were regarded as candidates for an acetabular reconstruction, but 11 hips displayed sufficient cartilaginous acetabular coverage on MR images. MR imaging promotes more accurate selection of patients for acetabular reconstruction and aids in the choice of the most appropriate type of acetabular reconstruction.

The Journal of Urology

Correlation of testicular color Doppler ultrasonography, physical examination and venography in the detection of left varicoceles in men with infertility. Petros JA, Andriole GL, Middleton WD, Picus DA (GLA, Division of Urologic Surgery, 4960 Audubon Ave., St. Louis, MO 63110). *J Urol* 145:785–788, April 1991

High resolution color Doppler ultrasound is a noninvasive means of simultaneously imaging and evaluating the blood flow to the testes. To define the ability of color Doppler ultrasound to detect clinically evident as well as subclinical varicoceles men referred to our urology division with oligospermia and infertility underwent spermatic vein venography of the left testis if there was physical examination and/or color Doppler ultrasound evidence of a varicocele. The detection of valvular incompetence on venography was considered diagnostic for a varicocele. Of 17 study patients physical examination detected 10 of 14 venographically evident varicoceles (71%), whereas color Doppler ultrasound detected 13 of 14 (93%). Of 5 patients with a normal physical examination but with color Doppler ultrasound evidence of a varicocele 4 had a confirmatory venogram, and 1 of 2 patients with a varicocele on physical examination and a normal Doppler ultrasound had a positive venogram. These data suggest that color Doppler ultrasound of the testis may more appropriately direct further invasive testing and therapy of infertile men than physical examination alone.

Journal of Thoracic Imaging

A prospective evaluation of plain radiographic signs of chronic obstructive pulmonary disease. Woodring JH, Phillips BA, West JW, Ulmer J, Cooper JK (JHW, Dept. of Diagnostic Radiology, University of Kentucky Medical Center, 800 Rose St., Lexington, KY 40536-0084). *J Thorac Imaging* 6(2):14–21, 1991

Plain film signs of COPD, spirometric evidence of airflow obstruction, and smoking history were correlated in a group of 182 men aged 32 to 85 years (average, 57.5 years) who presented for evaluation of possible pulmonary disability. There were 148 current or past smokers (range, 0.66 to 150 pack-years; average, 31.89 pack-years) and 34 lifetime nonsmokers. A single observer, who had no knowledge of the other parameters, prospectively evaluated posteroanterior chest radiographs for 11 signs of COPD. Airflow obstruction was defined as a reduction in $\text{FEV}_1/\text{FVC}\%$ below the 95% confidence limit of normal. Obstruction was classified on the basis of the reduction in FEV_1 as mild ($\text{FEV}_1 > 2.5$ L), moderate ($\text{FEV}_1 > 1.0$ L and < 2.5 L), or severe ($\text{FEV}_1 < 1.0$ L). Spirometric evidence of airflow obstruction was present in 67 patients; obstruction was mild in 26, moderate in 36, and severe in 5. We found a statistically significant association between smoking and airflow obstruction on spirometry ($P < 0.001$) and an equally significant association between smoking and radiographic signs of COPD on plain chest films ($P < 0.001$). Both airflow obstruction and radiologic signs of COPD were generally absent in lifetime nonsmokers. The plain film signs of COPD were only of moderate value in predicting spirometric evidence of airflow obstruction in smokers; spirometric evidence is not the gold standard for the presence of COPD, however, and the strong association between smoking and these radiologic signs may indicate that in smokers the presence of plain film signs of COPD reflects morphologic abnormality in the lungs indicative of disease. The chest radiograph therefore may routinely detect the presence of early disease, before the development of spirometric abnormality in many cases, and should have a prominent role in the clinical assessment of COPD.

Journal of Ultrasound in Medicine

Single umbilical artery: prenatal detection of concurrent anomalies. Nyberg DA, Mahony BS, Luthy D, Neisner D, Kapur R (DAN, Seattle Ultrasound Associates, 1229 Madison St., Ste. 1150, Seattle, WA 98104). *J Ultrasound Med* 10:247–253, May 1991

Prenatal sonographic findings were reviewed in 30 fetuses with a single umbilical artery (SUA) to determine the reliability of ultrasound for detecting concurrent anomalies. Additional anomalies were identified in 15 fetuses, including 3 fetuses with minor anomalies and 12 fetuses with major or multiple concurrent anomalies. Minor anomalies observed in 3 fetuses included 1 case each of pelvic kidney, unilateral absent kidney, and mild cerebral ventricular dilatation. Major abnormalities detected in 12 fetuses involved a variety of organ systems and included cardiac defects, holoprosencephaly, skeletal dysplasia, hydrocephalus, omphalocele, hydrothorax, enlarged cistema magna, and diaphragmatic hernia. Clinical and pathologic correlation showed that all fetuses were correctly categorized regarding the presence of other anomalies; none of the 15 fetuses in whom an SUA was considered an isolated finding had a significant anomaly at birth. Chromosome abnormalities were found in 6 of 12 fetuses with major abnormalities but in none of the 18 remaining fetuses. We conclude that prenatal ultrasound can reliably identify major concurrent anomalies in fetuses with SUA. In the absence of additional anomalies, prenatal detection of SUA should not alter obstetric management.

Reprinted with permission by the American Institute of Ultrasound in Medicine.

Radiology Outreach Foundation

The Radiology Outreach Foundation (ROF) is a nonprofit corporation whose goal is to help disadvantaged countries improve their health care by providing radiology equipment, books, consultation, education, and training to their practitioners. This assistance is on an application basis that is independent of political, ethnic, or religious orientation of the grantee. It depends on the need of the people and the ability of the ROF to meet that need. The ROF is approved by the U.S. Internal Revenue Service as a tax-exempt organization. It is endorsed by the following radiologic societies:

American Association of Women Radiologists
American College of Radiology
American Roentgen Ray Society
Association of University Radiologists
Radiological Society of North America
Society of Chairmen of Academic Radiology Departments
Society for Pediatric Radiology
European Society of Pediatric Radiology

All donations to the ROF are tax deductible. Persons who would like to contribute financially to the ROF, would be interested in being a visiting professor, would like to send books or journals to any of the institutions supported by the ROF, or would like further information about the ROF should write to

Charles A. Gooding, M.D.
President
Radiology Outreach Foundation
3415 Sacramento St.
San Francisco, CA 94118 USA

News

Practicum in Breast Imaging

The Breast Imaging Division, Dept. of Radiology, The Johns Hopkins Medical Institutions, is offering a practicum, by appointment only, for radiologists who wish to develop an understanding of the full spectrum of currently used techniques of breast imaging, including preoperative needle localization and fine-needle aspiration. The registrant will accompany a preceptor on a one-to-one basis through the daily activities of the Breast Imaging Center. These will include observation of a quality control program, observation of proper positioning of patients, evaluation of routine mammograms, workup of patients who have abnormal mammograms, and sonographic examination of the breast. Access to the center's extensive teaching file will be provided. Category 1 credit: 40 hr. Fee: $650. Information: Program Coordinator, The Johns Hopkins Medical Institutions, Office of Continuing Education, Turner Bldg., 720 Rutland Ave., Baltimore, MD 21205; (301) 955-2959.

Update on Diagnostic Imaging

Stanford University Medical Center is sponsoring Diagnostic Imaging Update: MRI, CT, US, Interventional, July 29–Aug. 2, at the Westin Bayshore Hotel, Vancouver, B.C. Program director: R. Brooke Jeffrey. Category 1 credit: 18 hr. Fee: physicians, $530; Stanford Radiology alumni, $490; residents, fellows, and technologists, $340. Information: Dawne Ryals, Ryals and Associates, P. O. Box 1925, Roswell, GA 30077-1925; telephone: (404) 641-9773; fax: (404) 552-9859.

Breast Imaging in the 90's

The Depts. of Radiology and Continuing Medical Education, Loyola University of Chicago, is sponsoring Breast Imaging in the 90's, Aug. 10–11, at the Oak Brook Hills Hotel & Conference Center, Oak Brook, IL. The course, which is designed for radiologists in clinical practice, will discuss the principles and latest advances in the detection and diagnosis of breast cancer. The impact of new biopsy techniques and breast cytology also will be considered. The format includes lectures and work stations that will provide hands-on experience and the opportunity for self-assessment. Category 1 credit: 16 hr. Fee: physicians, $240; residents, $175. Information: Loyola University Stritch School of Medicine, Division of Continuing Medical Education, 2160 S. First Ave., Maywood, IL 60153; (708) 216-3236.

Midwest Interventional Radiology Seminar

The Midwest Institute for Interventional Therapy, St. Francis Medical Center, and the University of Illinois College of Medicine at Peoria will present Midwest Interventional Radiology Seminar, Aug. 16–18, at the Continental Regency Hotel, Peoria, IL. The course will provide information about state-of-the-art nonsurgical alternatives for management of disorders of the vascular, urologic, biliary, neurologic, and other systems. Category 1 credit: 20 hr. Fee: physicians, $425; residents, fellows, and technologists, $225. Information: Rose Holcomb, University of Illinois College of Medicine at Peoria, Box 1649, Peoria, IL 61656; (309) 671-8475.

Abdominal Imaging Review Course

The Armed Forces Institute of Pathology (AFIP) will offer the 1st annual AFIP Abdominal Imaging Review Course, Sept. 7–8, at the Hyatt Regency Bethesda, Bethesda, MD. Lectures will present the radiologic features of diseases that affect the liver, biliary tract, spleen, ovaries, and peritoneum. Radiologic-pathologic correlation will be emphasized. Course directors: James L. Buck and Pablo R. Ros. Guest faculty: A. H. Dachman, M. Federle, W. S. Hayes, G. L. Miller III, and R. K. Zeman. Information: Ms. Wendy S. Baker, Course Coordinator, Armed Forces Institute of Pathology, Washington, DC 20306-6000; (202) 576-2162 or 576-2973.

Course on Color Doppler Imaging

The University of California, Los Angeles, will present its 3rd annual course on color Doppler imaging, Sept. 20–21, at the Beverly Hilton Hotel, Beverly Hills, CA. Category 1 credit: 11 hr. Information: Mary Grooms, UCLA Ultrasound Section, 10833 Le Conte Ave., Los Angeles, CA 90024; (213) 825-8813.

Applied Imaging: A Practical Course

The University of Alabama at Birmingham is sponsoring Applied Imaging: A Practical Course, Sept. 22–25, at the Ritz-Carlton Resort Hotel, Naples, FL. Program director: Lincoln Berland. Category 1 credit: 15.5 hr (pending). Fee: physicians, $425; residents, fellows, technologists, and sonographers, $300. Information: Dawne Ryals, Ryals and Associates, P. O. Box 1925, Roswell, GA 30077-1925; telephone: (404) 641-9773; fax: (404) 552-9859.

Dublin 91: Joint Annual Scientific Meeting

The Royal College of radiologists of Great Britain and the Faculty of Radiologists of the Royal College of Surgeons in Ireland will hold a joint annual scientific meeting Sept. 25–28 in Dublin. The meeting will include refresher courses on a range of topics in clinical radiology, lectures, and papers. Symposia will be presented on the diagnosis and treatment of primary bone tumors, the next decade against cancer in Europe, malignant lymphoma, and the individualization of radiation therapy. Fee: clinical radiology program: entire program, £245; day registration, £90; clinical oncology program: entire program, £200; day registration, £90. Information: The Conference Office, The Royal College of Radiologists, 38 Portland Pl., London, England W1N 3DG; telephone: 071 636 4432; fax: 071 323 3100.

Current Concepts of Magnetic Resonance Imaging/Physics

Stanford University Medical Center is sponsoring Current Concepts of Magnetic Resonance/Physics, Oct. 3–6, at the Silverado Hotel, Napa Valley, CA. Program director: Gary Glover. Category 1 credit: 19 hr. Fee: physicians, $530; residents, fellows, and technologists, $340. Information: Dawne Ryals, Ryals and Associates, P. O. Box 1925, Roswell, GA 30077-1925; telephone: (404) 641-9773; fax: (404) 552-9859.

MR Update: NR and Musculoskeletal

The University of Alabama at Birmingham will sponsor MR Update: NR and Musculoskeletal, Oct. 7–12, at the Westin Resort Hotel, Hilton Head, SC. Program director: Taher El Gammal. Category 1 credit: 25 hr. Fee: physicians, $595; residents, fellows, and technologists, $395. Information: Dawne Ryals, Ryals and Associates, P. O. Box 1925, Roswell, GA 30077-1925; telephone: (404) 641-9773; fax: (404) 552-9859.

Nuclear Cardiology Symposium and Workshops

The Cardiovascular Disease Center, University of Wisconsin Medical School, Sinai-Samaritan Medical Center, Mount Sinai Campus, and Continuing Medical Education, University of Wisconsin, will present Nuclear Cardiology Symposium and Workshops, Oct. 9–11, at the Marc Plaza Hotel, Milwaukee, WI. Category 1 credit will be awarded. Information: Sarah Aslakson, Continuing Medical Education, 2715 Marshall Ct., Madison, WI 53705; (608) 263-2956.

Ultrasound: 1991

The University of California, Davis School of Medicine, will present Ultrasound: 1991, Oct. 12–13, at the Red Lion Inn, Sacramento, CA. The course is designed to provide a rapid update on the techniques and applications of ultrasound for obstetrics and gynecology. Category 1 credit: 11 hr. Fee (approximate): physicians, $195; others, $165. Information: Office of Continuing Medical Education, University of California, Davis School of Medicine, 2701 Stockton Blvd., Sacramento, CA 95817; telephone: (916) 734-5390; fax: (916) 736-0188.

Chest Imaging

The Dept. of Radiology, Brigham and Women's Hospital, and the Dept. of Continuing Education, Harvard Medical School, will present Chest Imaging, Oct. 15–18, at the Ritz-Carlton Hotel, Boston. Program director: Robert D. Pugatch. Category 1 credit: 22 hr. Fee: physicians, $550; residents, fellows, and technologists, $375. Information: Harvard Med-CME, P. O. Box 825, Boston, MA 02117: (617) 432-1525.

Mammography Update 1991

The Dept. of Radiology and Continuing Medical Education, University of Wisconsin School of Medicine, and the University of Wisconsin-Extension are sponsoring Mammography Update 1991, Oct. 17–18, at the Edgewater Hotel, Madison, WI. Category 1 credit will be awarded. Information: Sarah Aslakson, Continuing Medical Education, 2715 Marshall Ct., Madison, WI 53705; (608) 263-2856.

Michigan Fall Radiology Conference

William Beaumont Hospital, Royal Oak, MI, will present Michigan Fall Radiology Conference Oct. 18–19. The conference is intended to be both a refresher course and an update on the practical aspects of diagnostic radiology, including modern imaging techniques. Lecturers will discuss subjects related to problems in daily practice. Guest faculty: J. T. Ferrucci, R. L. Lebowitz, R. D. McLeary, and S. E. Mirvis. Category 1 credit: 14 hr. Fee: physicians, $175; residents, $75. Information: Miss Mary Anne Smith, William Beaumont Hospital, 3601 W. Thirteen Mile Rd., Royal Oak, MI 48073; (313) 551-6199.

Magnetic Resonance Imaging and CT Update

The Dept. of Radiology, Brigham and Women's Hospital, and the Dept. of Continuing Education, Harvard Medical School, will present Magnetic Resonance Imaging and CT Update, Oct. 28–Nov. 1, at the Hyatt Regency Hotel, Cambridge, MA. Program directors: Steven E. Seltzer, Ferenc Jolesz, and Amir Zamani. Category 1 credit: 33 hr. Fee: physicians, $600; residents, fellows, and technologists, $350. Information: Harvard Med-CME, P. O. Box 825, Boston, MA 02117; (617) 432-1525.

Advanced Seminars in Diagnostic Imaging

The University of California, San Diego, is sponsoring Advanced Seminars in Diagnostic Imaging, Nov. 15–17, at the Ritz-Carlton Resort Hotel, Laguna Niguel, CA. Program director: David S. Feigin. Category 1 credit is pending. Fee: physicians, $400; residents, fellows, and technologists, $275. Information: Dawne Ryals, Ryals and Associates, P. O. Box 1925, Roswell, GA 30077-1925; telephone: (404) 641-9773; fax: (404) 552-9859.

European Symposium on Uroradiology

The 3rd European Symposium on Uroradiology will be held Aug. 24–27, 1992, at Herlev Hospital, University of Copenhagen, Herlev, Denmark. Some of the featured topics will be renal calculi, including extracorporeal shock-wave lithotripsy and intervention; pediatric uroradiology; renovascular hypertension; glomerular filtration rate; MR imaging in uroradiology; cancer of the lower urinary tract; radiology of the female genitals; and scrotal imaging. The official language of the conference will be English. The deadline for abstracts is March 1, 1992. Information: Henrik S. Thomsen, M.D., Dept. of Diagnostic Radiology 54E2, Herlev Hospital, Herlev Ringvej 75, DK-2730 Herlev, Denmark; telephone: + 45 44 53 53 00, ext. 278; fax: + 45 44 53 53 32.

National Council on Radiation Protection and Measurements Elections

The National Council on Radiation Protection and Measurements has announced the results of the regular membership elections that took place at its 1991 annual meeting. Newly elected members are A. Bertrand Brill, Gail de Planque, John B. Little, and Lester J. Peters. Seymour Abrahamson, John D. Boice, Jr., Robert L. Brent, Antone L. Brooks, Jacob I. Fabrikant, William R. Hendee, A. Everette James, Jr., Bernd Kahn, Dade W. Moeller, and William L. Templeton were reelected. Edward L. Alpen, Randall S. Caswell, Gerald D. Dodd, Warren K. Sinclair, George L. Voelz, and George M. Wilkening were elected honorary members of the council.

The American Board of Radiology Examinations

Written examinations for the American Board of Radiology (ABR) are scheduled for Oct. 3-4, 1991; Oct. 1-2, 1992; and Oct. 14-15, 1993. Oral examinations will be held at the Executive West Hotel in Louisville, KY, June 1-5, 1992, and May 31-June 4, 1993. The ABR will accept applications for admission to the examinations after July 1, but not later than Sept. 30, in the year *preceding* the year in which the examination is to be taken. For application forms and further information: Office of the Secretary, The American Board of Radiology, 300 Park, Ste. 440, Birmingham, MI 48009.

Meeting and Course Review

For the reader's convenience, a summary of upcoming meetings and courses is provided. Detailed listings are given in the *AJR* issue given in parentheses.

Visiting Fellowships in Interventional Radiology, times arranged, Baltimore (Oct 1990)
Swallowing Center Preceptorship, times arranged, Baltimore (Jan)
Imaging Fellowship, times arranged, Miami Beach, FL (Jan)
Preceptorships in Ultrasound at Johns Hopkins, time arranged, Baltimore (June)
Abdominal Ultrasound, July 29–Aug. 1, Philadelphia (June)
Contemporary Diagnostic Imaging, July 29–Aug. 2, Aspen, CO (April)
Pittsburgh Breast Imaging Seminar, Aug. 1-4, Pittsburgh (May)
Prostate Ultrasound, Aug. 2, Philadelphia (June)
Napa Valley Imaging Update, Aug. 4-8, Napa, CA (June)
MR Imaging Fellowships at LAC/USC Imaging Science Center, Aug. 5-9, Sept. 16-20, Oct. 7-11, and Nov. 4-8, Los Angeles (Feb)
Body Imaging, Aug. 5-9, Santa Fe, NM (April)
Summer Imaging and Interventional Techniques IX, Aug. 5-9, Amelia Island, FL (July)
Symposium on Diagnostic Imaging, Aug. 12-15, Newport, RI (June)
Imaging of the Head, Spine, and Musculoskeletal System, Aug. 12-16, Whistler, B.C. (April)
Radiology for Clinicians, Aug. 12-16, Coronado (San Diego), CA (April)
Society of Computed Body Tomography Summer Practicum, Aug. 18-22, Keystone, CO (April)
Registry Preparation Courses for Sonographers: Abdominal Ultrasound, Aug. 22-23, Washington, DC; **OB/GYN Ultrasound Review**, Aug. 24, Washington, DC, and Sept. 22, Los Angeles; **Ultrasound and Doppler Physics**, Aug. 25-26, Washington, DC; Sept. 7-8, Chicago; Sept. 20-21, Los Angeles; and Oct. 5-6, Dallas; and **Vascular Technology**, Aug. 27-28, Washington, DC (July)
Diagnostic Imaging Update, Aug. 26-30, Vancouver, B.C. (April)
Radiation, Physics, and Biology, Aug. 26-30, New York City (May)
World Congress in Ultrasound, Sept. 1-6, Copenhagen (Sept 1990)
Physics of Diagnostic Radiology, Nuclear Medicine, and Radiation Biology, Sept. 5-8, Sacramento, CA (July)
Pacific Northwest Diagnostic Ultrasound Symposium, Sept. 6-8, Seattle (June)
International Workshop on Hypertrophic Osteoarthropathy, Sept. 8-11, Dubrovnik, Yugoslavia (Jan)
European Society of Gastrointestinal Radiologists Annual Meeting, Sept. 8-11, Oxford, England (March)
Sonography Update Conference and Exhibit, Sept. 11-13, Coronado (San Diego), CA (May)
Mallinckrodt Institute's 60th Anniversary Celebration, Sept. 12-14, St. Louis (May)
Transrectal Ultrasound in the Diagnosis and Management of Prostate Cancer, Sept. 13-14, Chicago (May)
Diagnostic Ultrasound in Gynecology and Obstetrics and Abdomen, Sept. 13-15, Baltimore (June)
Sonography Registry Review, Sept. 14-15, Coronado (San Diego), CA (May)
European Congress of Radiology 1991, Sept. 15-20, Vienna, Austria (Oct 1990)
Mammographic Interpretation: A Practical Approach, Sept. 23-26 and Oct. 28-31, Boston (March)
Applied Ultrasound: Accent on Doppler, Sept. 23-26, Laguna Niguel, CA (May)
Diagnosis of Musculoskeletal Disorders, Sept. 25-28, Coronado (San Diego), CA (May)
Diagnostic Uses of Radiolabeled Monoclonal Antibodies, Sept. 26-27, Washington, DC (June)
International Imaging Course, Sept. 30–Oct. 5, Hong Kong (July)
Magnetic Resonance Imaging 1991: Back to the Future, Oct. 2-5, Cincinnati (July)
Annual International Body Imaging Congress, Oct. 5-12, Maui, HI (June)
Breast Cancer Diagnosis: State-of-the-Art, Oct. 7-8, New York City (July)
Practical Training in Interventional Radiology, Oct. 7-11 and Nov. 4-8, Lund, Sweden (July)
MRI: Clinical State of the Art 1991, Oct. 9-12, New York City (July)
Western Neuroradiological Society Annual Meeting, Oct. 17-20, Laguna Niguel, CA (June)
Progress in Magnetic Resonance Imaging, Oct. 24-25, Cologne, Germany (June)
Neuroradiologic and Musculoskeletal Seminars, Oct. 24-27, Orlando, FL (June)
Advanced Imaging of the Musculoskeletal System, Oct. 26-27, Coronado (San Diego), CA (June)
San Diego Postgraduate Radiology Course, Oct. 28–Nov. 1, Coronado (San Diego), CA (June)
Interventional Radiology Course, Nov. 1-3, Coronado (San Diego), CA (July)
Seminar on Bone and Joint Diseases, Nov. 15-17, Scottsdale, AZ (July)
Diagnosis and Treatment of Bone and Soft-Tissue Tumors, Nov. 21-23, Sacramento, CA (May)
Asian Oceanian Congress of Radiology, Dec. 14-18, New Delhi (July)
International Symposium on Recent Advances in Diagnostic Imaging and Radiation Oncology, March 24-27, 1992, Kathmandu, Nepal (June)

AJR carries announcements of courses, symposia, and meetings of interest to its readers if received a minimum of 5 months before the event. There is no charge; receipt of items by the *AJR* Editorial Office is not acknowledged. Submit items for publication typed double-spaced. Provide title, date, location, brief description, sponsor, course directors, fees, category I credit, and address and telephone number for additional information. Faculty from the host institution will not be listed. Guest faculty names will appear **only** if initials are provided. Mail news items to *AJR* Editorial Office, 2223 Avenida de la Playa, Suite 103, La Jolla, CA 92037-3218.

American Roentgen Ray Society 92nd Annual Meeting
May 10–15, 1992, Orlando, FL
Marriott's Orlando World Center

Registration and Hotel Reservations

Forms for advance registration and hotel reservations will be in the February and March 1992 issues of the *AJR*.

Scientific Program

Abstracts of papers to be considered for the program must be submitted by November 1, 1991. Forms on which to submit abstracts are in this issue of the *AJR*. The ARRS Program Committee will select papers and notify authors in early January. The *AJR* has first rights to all papers accepted for presentation at the ARRS meeting. Mail original and five copies to

A. Everette James, Jr., M.D.
c/o Paul R. Fullagar
American Roentgen Ray Society
1891 Preston White Dr.
Reston, VA 22091

Scientific Exhibits

Proposals for scientific exhibits must reach the Chairman of Exhibits by November 1, 1991. Forms, which may be photocopied, are in this issue of the *AJR*. Send completed form to

N. Reed Dunnick, M.D.
c/o Paul Fullagar
American Roentgen Ray Society
1891 Preston White Drive
Reston, VA 22091
Telephone (703) 648-8992

Refresher Course Program

A summary of the refresher courses will appear in the *AJR* in February along with advance registration forms. Early registration is an advantage in ensuring preferred courses in this popular program.

Local Program

A program of sightseeing, shopping, and entertainment will be developed by the Local Arrangements Chairman. Information and advance registration forms will be in the February issue of the *AJR*.

Residents' Award Papers

The society offers several cash awards for the best scientific papers prepared by residents in radiology. The President's Award has a $2000 prize. There are two Executive Council awards of $1000 each. All are presented at the annual meeting. Papers should be submitted by February 15, 1992, for consideration in this competition. Send entries to

Nancy O. Whitley, M.D.
Dept. of Radiology
University of Maryland Medical Systems Hospital
22 S. Greene St.
Baltimore, MD 21201

Deadlines

Abstracts of papers: November 1, 1991
Scientific exhibit proposals: November 1, 1991
Residents' Award papers: February 14, 1992

Call for Papers

American Roentgen Ray Society 1992 Annual Meeting: May 10–15, 1992, Orlando, FL

ADDRESS OF PRESENTING AUTHOR

Department

Institution

Street

City, State Zip

Phone: ____________

Type title, authors, and abstract in the space provided below. (Instructions are on reverse side of this page. Abstract should not exceed 300 words.)

Select one category: ______Angio/Interventional ______Breast ______Chest ______CT ______Gastrointestinal Tract ______Genitourinary Tract ______MR ______Neuroradiology ______Skeletal ______Sonography ______Pediatric

Projection Requirements: ______35 mm, single or double (circle one) ______16 mm silent film ______½''VHS ______¾''

Has this been presented elsewhere? ______yes ______no. If yes, please describe on reverse side of this page.

Instructions for Scientific Abstracts

1. Type the information single-spaced. Underline the name of the presenting author. Append as a last line of the abstract any research grant support, if applicable (e.g., Supported by USPHS Grant HE-80144). If the abstract is accepted, it will not be proofread; it will appear exactly as typed. Use the following format:

   MR IMAGING OF THE SPINE AND NECK
   F. S. Lau, M.D., A. N. Kirk, M.D., and R. A. Beck, Ph.D.
   University of California, Bakersfield, Bakersfield, CA 92338

2. Abstracts should include four paragraphs devoted sequentially to the following topics: (1) object or purpose of the study, (2) materials, methods, and procedures, (3) results, (4) significance of the results and conclusions. The text should not exceed 300 words. Specific data are essential. The abstract should be a succinct summary of work done rather than a promissory note.
3. The Program Committee will grade each abstract and determine acceptance. Further information will be forwarded to those whose abstracts are accepted for presentation.

Deadline for submission of abstract is November 1, 1991. Mail abstract and four copies to

A. Everette James, Jr., M.D.
c/o Paul R. Fullagar
American Roentgen Ray Society
1891 Preston White Dr.
Reston, VA 22091

Telephone: (703) 648-8992

Call for Scientific Exhibits

American Roentgen Ray Society
1992 Annual Meeting:
May 10–15, 1992, Orlando, FL

FOR COMMITTEE USE ONLY

Date Received______	Application No. ______
Subject______	Score______
Rejected______	Accepted______
Assigned______	Space No. ______

Principal Exhibitor's Mailing Address

Name________________ Institution________________

Department____________ Street Address____________ City______

State________ Zip Code________ Telephone: office (   ) ______ home (   ) ______

Names of Exhibitors (List principal exhibitor first and telephone number of each person.)

Last	First	Middle	Telephone	Degree (one only)	Member ARRS?

Title of Exhibit________________________

Type abstract single-spaced in the space provided below. (See instructions on the reverse side of this page.)

Instructions for Abstract

The abstract should be a brief paragraph that states the purpose, principal information, and conclusions of the exhibit. Promissory statements are not acceptable. Type single-spaced in the space provided on the reverse side. Brevity is desirable but not at the expense of specific information. **The abstract will appear in the program book as submitted.** Please use typewriter and complete the application form on both sides. List space requirements.

What Type of Exhibit Is Proposed? (Check one and fill in all appropriate blanks.)

______**Free-standing.** This is a self-contained display created in total by the exhibitor. It may be a fold-open unit, a unit shipped in cases and assembled on site, or a tabletop unit. Linear feet required ______.

______**Poster Board (backboard panels).** Backboard panels are 4 × 8 ft. (1.2 × 2.5 m). Number of panels required ______. If two panels are needed, there will be a ¼-in. frame separating the panels, thus requiring a separation in the presentation.

______**Viewbox.** Mounted materials (radiographs and other transparencies) for display on the society's illuminators. Each illuminator is 39.5 × 59.5 in. (100 × 151 cm). Number of illuminators required ______. Materials should not be glass mounted.

Please Indicate Most Appropriate Category.

______Bone ______Cardiovascular ______Chest ______Gastrointestinal ______Genitourinary ______Breast ______Medical physics
______Neuroradiology ______Nuclear medicine ______Pediatric ______Radiation oncology ______Sonography

Exhibits will be chosen on the basis of the quality of the abstract and space available. Poster board and computer-based exhibits are encouraged, as they do not require a viewbox.

Signature of Principal Exhibitor____

Exhibitors will receive instructions for exhibit preparation.

Applications must be received no later than November 1, 1991. Mail original and five copes to

N. Reed Dunnick, M.D.
c/o Paul R. Fullagar
American Roentgen Ray Society
1891 Preston White Dr.
Reston, VA 22091

Telephone: (703) 648-8992

American Roentgen Ray Society:

Officers, Committees, and Membership Information

Officers

President: John A. Kirkpatrick, Jr.
President-elect: A. Everette James, Jr.
1st Vice-president: Andrew K. Poznanski
2nd Vice-president: George R. Leopold
Secretary: Joseph T. Ferrucci, Jr.
Treasurer: Beverly P. Wood

Executive Council: R. N. Berk, M. P. Capp, W. J. Casarella, N. R. Dunnick, R. G. Evens, J. T. Ferrucci, Jr., A. E. James, Jr., J. A. Kirkpatrick, Jr., A. M. Landry, Jr., G. R. Leopold, J. E. Madewell, T. C. McLoud, A. A. Moss, A. K. Poznanski, R. J. Stanley, J. H. Thrall, K. H. Vydareny, N. O. Whitley, B. P. Wood, R. J. Alfidi, chairman

Committees

Editorial Policy: R. N. Berk, E. Buonocore, Melvin M. Figley, M. S. Huckman, C. R. B. Merritt, A. G. Osborn, K. Valji, C. A. Rohrmann, Jr., W. J. Casarella, chairman

Education and Research: R. R. Hattery, C. B. Higgins, B. J. Hillman, R. J. Stanley, W. M. Thompson, N. O. Whitley, chairman

Finance and Budget: R. K. Gedgaudas-McClees, A. A. Moss, J. R. Thornbury, K. H. Vydareny, J. H. Thrall, chairman

Nominating: R. G. Evens, P. J. Fritzsche, A. A. Moss, chairman

Publications: E. Buonocore, C. R. B. Merritt, A. G. Osborn, C. A. Rohrmann, Jr., W. J. Casarella, chairman

Membership: J. E. Madewell, T. C. McLoud, A. A. Moss, K. H. Vydareny, chairman

Representatives to Other Organizations

American Board of Radiology: W. J. Casarella, J. A. Kirkpatrick, Jr., L. F. Rogers

American College of Radiology: R. A. Gagliardi, J. E. Madewell, B. L. McClennan, R. J. Stanley

American Medical Association: S. F. Ochsner, delegate; K. L. Krabbenhoft, alternate; K. L. Kidd, CPT Advisory Committee

American National Standards Institute: M. E. Haskin

National Council on Radiation Protection and Measurements: F. D. Miraldi, E. L. Saenger

Armed Forces Institute of Pathology: J. E. Madewell

Meeting Arrangements

Annual Meetings: May 10–15, 1992, Marriott's World Center, Orlando, FL; April 25–30, 1993, Marriott San Francisco, San Francisco, CA

Annual Meeting Committee: J. K. Crowe, N. R. Dunnick, R. R. Lukin, N. H. Messinger, R. J. Stanley, R. D. Steele, Jr., A. M. Landry, Jr., chairman

Instructional Courses: Bruce L. McClennan, associate chairman; R. J. Stanley, chairman

Scientific Program: P. H. Arger, T. B. Hunter, D. Kushner, T. C. McLoud, L. B. Talner, J. H. Thrall, A. E. James, Jr. chairman

Scientific Exhibits: J. R. Haaga, D. S. Hartman, R. G. Ramsey, N. R. Dunnick, chairman

ARRS Membership

An application form is printed in this issue of the Journal. For consideration at the 1992 ARRS meeting, send completed forms before February 1, 1992, to American Roentgen Ray Society, 1891 Preston White Dr., Reston, VA 22091. Active members are graduates of an approved medical or osteopathic school or hold an advanced degree in an allied science. They must practice radiology or work in an associated science in the United States or Canada and be certified by the American Board of Radiology, American Osteopathic Board of Radiology, or Royal College of Physicians of Canada or otherwise adequately document training and credentials. Corresponding members are foreign radiologists or scientists who are active in radiology or an allied science. Members-in-training are residents or fellows in radiology or postgraduate students in an allied science. Additional application forms can be obtained from the ARRS offices in Reston, VA.

Business Office

Paul Fullagar, Executive Director, American Roentgen Ray Society, 1891 Preston White Dr., Reston, VA 22091; (703) 648-8992.

Information and Application for Membership in the American Roentgen Ray Society

General Information

The American Roentgen Ray Society, founded in 1900, has been a forum for progress in radiology since shortly after the discovery of X-rays. From its beginning and continuing to today, the ARRS has been guided by dedication to the goal of the advancement of medicine through the science of radiology and its allied sciences.

The goal of the ARRS is maintained through an annual scientific and educational meeting, and through publication of the *American Journal of Roentgenology*.

The annual meeting consists of instructional courses, scientific sessions, a symposium, scientific exhibits, and commercial exhibits. A special categorical course is also offered. Category I CME credits are available on an hour-for-hour basis.

The monthly *American Journal of Roentgenology* is a highly respected peer review journal with a worldwide subscription base. For over 75 years the *AJR* has been accepted as one of the best specialty journals available in the world, and this reputation grows each month.

A recently developed quarterly ARRS newsletter keeps members informed of events and general Society news.

Application Instructions

Candidates for Active Membership

1. An Active member must be a graduate of an approved medical school or hold an advanced degree in one of the physical, chemical or biological sciences and be certified by the American Board of Radiology, the American Osteopathic Board of Radiology, the Royal College of Physicians of Canada, or document training and credentials that are adequate to qualify for membership. Active members shall actively practice radiology or one of its branches in the United States or Canada. Such members are eligible to participate in all activities of the Society, including membership on committees, and have full voting privileges.
2. Application must be on an official form, signed by the applicant and at least two members of the American Roentgen Ray Society, active or emeritus, in good standing, who endorse the applicant.
3. Application fee is $50 (payable when billed for dues).
4. Annual dues are $150, payable on January 1 of each year following the initial year. First year dues will be invoiced following candidate election at the annual meeting. Of this amount, $50 is for a 1-year subscription to the *American Journal of Roentgenology*, beginning with the July issue following election to membership.
5. Application must be received by February 1 for action during the current year's meeting.

Candidates for In-Training Membership

1. In-training members must be serving in a radiology residency program approved by the Radiology Residency Review Committee, the American Osteopathic Board of Radiology, or the Royal College of Physicians of Canada, or in an approved post-residency fellowship, or be a postgraduate student in an allied science. Training status must be verified by the program director. In-training members have special consideration in fees and subscription rates to the Society journal. Such members cannot hold Society offices or vote.
2. Application must be on an official form and signed by the applicant and by the applicant's training or residency program director.
3. In-training status is limited to a maximum of five years starting with the entrance date into the radiology residency. In the last year, each in-training member will receive an application for active membership from the Society. Those who do not apply for transfer to active membership shall be dropped from membership at the end of the fifth year, but can later apply as a new member through the process outlined for active status.
4. There is no application fee. Annual dues are $25. Membership includes a subscription to the *American Journal of Roentgenology* and admission to the annual meeting without payment of the registration fee.
5. Membership applications will be acted on when received.

Corresponding Membership

A corresponding member must meet the qualifications of active membership, but reside and practice in a foreign country. Corresponding members shall pay dues and fees, but shall not have the privileges of voting nor of holding elective office.

All Applicants

1. **Do not remit application fee or dues until requested.**
2. **Send completed forms to: American Roentgen Ray Society**

1891 Preston White Drive
Reston, Virginia 22091

For ARRS
Office Use

Date Rec'd ____________

I.D.# ____________

AMERICAN ROENTGEN RAY SOCIETY
APPLICATION FOR MEMBERSHIP

Date: ____________________

Category of Membership: (Check One)
☐ Active
☐ Corresponding
☐ In-Training

Name (Please Print) ______________________________ Degree(s) ____________
First Initial Last

Mailing Address ______________________________ Date of Birth ____________
Street/Box

______________________________ Telephone (   ) ____________
City/State/Country Zip Code

A. Education: (List name of institution, years attended, and degree and type received.)

Undergraduate: ______________________________

____

Graduate (Medical School, Graduate School, etc.):

____

____

Postgraduate (Internship, Residency, Fellowship, etc.):

____

____

____

B. Licensure:

Licensed to practice ____________ in ____________ since ____________
(Type) (State, Province, etc.)

C. Appointments/Memberships: (In-Training applicants: skip to Section F on reverse.)

Present Appointments: Academic ______________________________

____

Hospitals ______________________________

____

Memberships in Scientific Societies: ______________________________

____

Offices or Committee Assignments: ______________________________

____

Government Service (Military or Civilian) ______________________________
(Position) (Years)

Credentials: (To be completed by Active and Corresponding applicants only.)

I hereby certify that I was issued a certificate of qualification in ____________________
(Specialty)

in ____________ by the ____________________________
(Year) (Name of Qualifying Board)

Other Credentials: ____________________________

Signature: ____________________________

. References: (To be completed by Active and Corresponding applicants only.)

We, active or emeritus members in good standing of the American Roentgen Ray Society, and acquainted with the applicant, do recommend him/her for membership in the Society. (Two references are required.)

Name (Please Print) 1. ____________________ 2. ____________________

Address ____________________ ____________________

____________________ ____________________

Signatures: ____________________ ____________________

IN-TRAINING APPLICANTS MUST COMPLETE THIS SECTION

Credentials:

I certify that I am serving as a Resident/Fellow in ____________________
(Specialty)

at ____________________. Date program began (begins): ____________;
(Name of Institution)

date program to end: ____________. I understand that in-training membership is limited to a maximum of 5 years.

Applicant Signature: ____________________________

Verification: (Program Director or Department Chairman *only*)

I certify that the applicant is in training at the institution named and qualifies for enrollment as a member-in-training of the American Roentgen Ray Society.

Name (Please Print) ____________________

Address: ____________________

____

Signature ____________________

Send completed form to: **American Roentgen Ray Society**
1891 Preston White Drive

Classified Advertisements

Positions Available

THE DEPT. OF DIAGNOSTIC RADIOLOGY, OREGON HEALTH SCIENCES UNIVERSITY, PORTLAND, OR, invites applications for a board-certified musculoskeletal radiologist. Rank will be commensurate with experience and qualifications. Please send CV and references to William Weidner, M.D., Chairman, Diagnostic Radiology, UHN 72, Oregon Health Sciences University, Portland, OR 97201-3098. OHSU is an affirmative action, equal opportunity employer. 8–9a

BC RADIOLOGIST position available to join group of 3 radiologists in a large, multispecialty health-care facility in Seattle. Strong interest and experience in ultrasound, including OB, desired. Strong mammography experience a plus. Diverse patient population includes a mix of managed care and fee-for-service. Outpatient radiology only, limited call, competitive salary, and excellent benefits. Contact Mary Anderson, Pacific Medical Center, 1200 12th Ave. S., Seattle, WA 98144; (206) 326-4100. 8–9ap

CHIEF OF ABDOMINAL IMAGING—The Dept. of Radiology, University of Maryland School of Medicine at Baltimore is seeking a chief for the abdominal imaging section. This encompasses abdominal and gastrointestinal CT and MRI, including CT-guided interventional procedures. The dept. is affiliated with the soon-to-be-completed digital radiology dept. in the VA hospital. It is situated in the midst of the new downtown redevelopment area of Baltimore, which offers exciting opportunities for relocation. Candidates should be board-certified, have specialist training, and be interested in teaching and research. Income and academic rank are dependent on qualifications and experience. Please forward CV to Gerald S. Johnston, M.D., Dept. of Radiology, University of Maryland Medical System, 22 S. Greene St., Baltimore, MD 21201. Affirmative acting, equal opportunity employer and applications from members of minority groups are encouraged. 8ap

CHAIR, DEPT. OF RADIOLOGY—West Virginia University School of Medicine invites applicants for chair of the Dept. of Radiology. This endowed position, vacant due to the retirement of the chairman, requires the leadership of a nationally recognized radiology educator with strong clinical, teaching, and research credentials to administer the clinical and academic programs of the dept. The dept. enjoys superb facilities and state-of-the-art diagnostic equipment in a beautiful, new teaching hospital on the campus of the health sciences center of the parent university. The application deadline is Aug. 19, 1991. Interested candidates should forward CV and the names of 3 references to William A. Neal, M.D., Radiology Search Committee Chairman, Dept. of Pediatrics, WVU School of Medicine, Morgantown, WV 26506. An equal opportunity/affirmative action employer. 9a

DIAGNOSTIC RADIOLOGIST, HOUSTON—Immediate opening for 2 BC/BE radiologists to join 5 BC radiologists associated with a large, internal medicine clinic near the Texas Medical Center. Primarily outpatient practice with regular hours. Also cover adjacent general, medical-surgical hospital. On-site ultrasound, CT, MRI, and nuclear medicine. Experience in angio and interventional is desired. Please send CV to Robert B. Hall, Administrator, Diagnostic Clinic of Houston, 6448 Fannin, Houston, TX 77030; (713) 797-9191. 8–10a

PART-TIME, BOARD-CERTIFIED RADIOLOGIST needed in private Boston office. Competitive salary, benefits included. Immediate opening. Send CV to E. Wilson, 38 Winfield St., Norwood, MA 02062. 8ap

DIAGNOSTIC IMAGING AND NEURORADIOLOGY, TWO POSITIONS—The 11-member imaging section of Guthrie Clinic–Robert Packer Hospital desires associates with fellowship training and/or expertise in the above areas. The Guthrie Clinic provides tertiary care in the southern tier of New York and the northern tier of Pennsylvania in the beautiful, endless mountains. Outstanding practice opportunities in an environment free of urban hassle. Please send letter of inquiry with CV or call Thomas F. Bednarek, M.D., Chairman, Dept. of Radiology, Guthrie Healthcare System, Sayre, PA 18840; (717) 882-4025. 8–10a

ANGIO/INTERVENTIONAL RADIOLOGIST, LANCASTER, PA—Position available immediately for well-trained, enthusiastic, BC/BE angiographer to join diversified group of 19. Stimulating practice includes 550-bed hospital with trauma accreditation, full-service imaging center, 2 MRI facilities, and radiation therapy. The angiography division has 5 technologists working 2 state-of-the-art angio suites. Last yr over 2000 total exams were performed (nearly 300 were interventional procedures including atherectomies). Excellent working relationship with surgical and medical staff. Lancaster is a pleasant, small city, rich in historical tradition, located in a growing county with many cultural and recreational amenities. Beautiful surrounding farms and countryside are in close proximity, yet Philadelphia and Baltimore/Washington are within easy reach. Contact Robert Gress, M.D., Lancaster Radiology Associates, Ltd., Box 3555, Lancaster, PA 17603; (717) 299-4173. 8–9ap

PRACTICE OPPORTUNITY FOR 5 RADIOLOGISTS at a 1000-bed, major teaching hospital located within the New York City metropolitan area. There is an affiliated, off-site imaging center opening Jan. 1, 1992. Neuroradiologist: New York state medical license, board certification, fellowship training, MRI, CT, angiography, and myelography experience necessary. Diagnostic radiologist with MRI experience: New York state medical license, board certification, fellowship training in neuro MRI, body MRI, orthopedic MRI, CT, and ultrasound necessary. In addition to a fellowship, previous experience in an imaging center is a plus. Diagnostic radiologist with imaging background: New York state medical license, board certification, fellowship training, MRI, CT, and ultrasound experience necessary. Experience in CT and ultrasound-guided procedures a plus. Diagnostic radiologist with mammography experience: New York state medical license, board certification/eligibility, with specific experience, expertise, and training in mammography and breast localization procedures. General diagnostic radiologist: New York state medical license, board certification/eligibility with experience in all conventional and routine diagnostic radiology modalities. Our dept. performs 150,000 procedures/yr, including ultrasound, CT, angiography, interventional radiology, mammography and breast localizations, neuroradiology, and all basic and routine radiographic studies. Staffing in our dept. consists of 13 full-time staff radiologists, including 2 in the subdivision of nuclear medicine and 1 in the subdivision of radiation therapy. Attractive salaries are being offered, which will be commensurate with the level of experience. An extensive comprehensive benefits package, including vacation and conference time, is being offered. The imaging center opening in Jan. 1992 will include MRI, CT, ultrasound, mammography, and R&F. Please respond in confidence with CV, which should include potential date of availability, to Director of Radiology, The Brookdale Hospital Medical Center, Linden Blvd., at Brookdale Plaza, Brooklyn, NY 11212-3198. 8ap

NEURORADIOLOGIST—The Dept. of Radiology at the University of Arkansas for Medical Sciences is seeking a neuroradiologist at the assistant or associate professor rank. Neuroradiology coverage is for 3 hospitals with state-of-the-art equipment including 2 1.5-T MRI units, 5 CT scanners, and 4 angiographic suites. Facility for neurointerventional work is available. Dedicated animal laboratory with advanced NMR spectroscopy units available for research. Candidate must be board-certified and preferably a senior member in ASNR. University of Arkansas for Medical Sciences is an equal opportunity employer. Address inquiries and a current CV to Edgardo Angtuaco, M.D., Chief, Neuroradiology, Dept. of Radiology, University of Arkansas for Medical Sciences, 4301 W. Markham St., Slot 596, Little Rock, AR 72205; (501) 686-6032, (501) 686-6900 (fax). 8–10a

DIAGNOSTIC RADIOLOGIST WITH SPECIAL COMPETENCY IN NUCLEAR MEDICINE, LANCASTER, PA—Position available immediately for well-trained, enthusiastic, BC/BE diagnostic radiologist with nuclear medicine interest and expertise to join diversified group of 19. Busy practice includes 550-bed hospital with trauma accreditation, full-service imaging center, 2 MRI facilities, and radiation therapy. Nuclear medicine section has 9 technologists who performed 9500 exams last yr using 6 cameras including 1 SPECT unit. Additional SPECT unit to be added within 6 mo to supplement busy nuclear cardiology program. Lancaster is a pleasant, small city, rich in historical tradition, located in a growing county with many cultural and recreational amenities. Beautiful surrounding farms and countryside are in close proximity, yet Philadelphia and Baltimore/Washington are within easy reach. Contact Robert Basarab, M.D., Lancaster Radiology Associates, Ltd., Box 3555, Lancaster, PA 17603; (717) 299-4173. 8–9ap

BC/BE DIAGNOSTIC RADIOLOGIST, PHOENIX, AZ—Immediate openings available for nonpartnership positions with 23-member group in Phoenix, AZ. Practice is well-diversified with office and hospital facilities. Flexible scheduling. General diagnostic skills with experience in CT/ultrasound and mammography preferred. Area offers superior lifestyle and recreational attractions. Please send letter and CV to Chief of Radiology, 5322 W. Northern Ave., Glendale, AZ 85301. 8ap

HEAD OF MAMMOGRAPHY SECTION—The Dept. of Radiology of the Ochsner Clinic is seeking a radiologist to head a rapidly growing Section of Mammography. Currently over 15,000 mammograms and 500 localization procedures are performed annually. Equipment includes 4 ACR-accredited mammographic units and stereotactic localization equipment. The individual who joins us in the next few months will have the opportunity to participate in the planning of a major expansion of the facilities of the mammography section scheduled to be completed in mid-1992, providing capability for approximately 30,000 procedures annually. The mammography section provides imaging services for a multidisciplinary breast center with a high degree of clinical and research interaction with surgical, medical, and pathology services. The radiology dept. is active in teaching and clinical research with a staff of 22 residents and fellows. Candidates for this position should have fellowship training or a strong background in mammography and be interested in teaching and clinical research as well as patient care. Compensation and benefits are highly competitive. For additional information, contact Christopher R.B. Merritt, M.D., Chairman, Dept. of Radiology, Ochsner Clinic, 1514 Jefferson Highway, New Orleans, LA 70121; (504) 838-3495. 8–9a

ULTRASOUND STAFF POSITION—The Dept. of Radiology of the Ochsner Clinic is seeking an additional radiologist to meet growing clinical needs in the Section of Ultrasonography. The ultrasound section of the dept. currently performs over 12,000 procedures/yr, including a full range of abdominal, OB/GYN, vascular, operative, interventional, and pediatric studies. State-of-the-art imaging, duplex color Doppler, and intraoperative equipment is available. The individual who joins us in the next few months will have the opportunity to participate in the planning of a major expansion of the facilities of the ultrasound section scheduled to be completed in mid-1992. The dept. is active in teaching and clinical research, with a staff of 22 residents and fellows. Candidates for this position should have fellowship training or a strong background in ultrasonography and be interested in teaching and clinical research as well as patient care. Compensation and benefits are highly competitive. For additional information, contact Christopher R. B. Merritt, M.D., Chairman, Dept. of Radiology, Ochsner Clinic, 1514 Jefferson Highway, New Orleans, LA 70121; (504) 838-3495. 8–9a

NEURORADIOLOGIST—Senior ASNR member needed for excellent hospital and imaging center position in Tucson, AZ. Early partnership opportunity. Send CV to Arizona State Radiology, 7250 E. Ventana Canyon Dr., Tucson, AZ 85715. 8–7ap

HARTFORD, CT—Position available immediately for board-certified radiologist to join an established group of 8. Practice includes hospital and 4 private offices, all fully equipped, including CT. Mammography experience is helpful. CT and MRI experience is essential. Competitive starting salary and benefits. Please enclose CV with initial correspondence to Jeffrey Blau, M.D., 40 Hart St., New Britain, CT 06052; (203) 229-2059. 8–9a

THE DEPT. OF RADIOLOGY AT THE UNIVERSITY OF SOUTH FLORIDA, COLLEGE OF MEDICINE is currently seeking a non-tenure track assistant professor. The candidate should have an M.D. degree and be board-certified in diagnostic radiology. The salary range is negotiable for a 12-mo period. This is a nontenure grant position. Applications or nominations for the position should be addressed to Robert Halpert, M.D., Dept. of Radiology, H. Lee Moffitt Cancer Center, 12902 Magnolia Dr., Tampa, FL 33612. The University of South Florida is an affirmative action/equal opportunity institution. 8ap

VASCULAR/INTERVENTIONAL RADIOLOGIST, LONG ISLAND, NY—Board-certified radiologist with fellowship training or equivalent experience in vascular/interventional radiology needed to join a 5-member group starting July 1992. Angio suite currently being upgraded to latest state-of-the-art equipment. Must be willing to do most aspects of diagnostic radiology. This well-established practice includes a 325-bed community hospital, a private diagnostic radiology office, and a 1-yr-old MRI facility. Generous salary leading to full partnership. Contact Ira Langer, M.D., 250 Hospital Rd., Patchogue, NY 11722; (516) 475-1030. 8–11ap

PRIVATE PRACTICE IN MIDTOWN MANHATTAN seeks a board-certified diagnostic radiologist with experience and interest in mammography and ultrasound. Send CV to Julie S. Mitnick, M.D., and Bala Subramanyam, M.D., Murray Hill Radiology, 30 E. 40th St., Ste. 1100, New York, NY 10016. 8ap

IMMEDIATE OPENING FOR BE/BC RADIOLOGIST in a regional hospital with a patient base of 25,000 located in a scenic western Wyoming community. Great outdoor recreation area. Competitive reimbursement. Ultrasound/CT/general radiology. Interested persons contact Paul Sonntag, M.D., P. O. Box 629, Ogden, UT 84402; (801) 625-2092. 8–1ap

ALASKA AREA NATIVE HEALTH SERVICE—Public-service-oriented radiologists needed for cross-cultural health care in Anchorage and Sitka, AK. Salary $85–$95K+, excellent benefits. Medical school loan repayment up to $25K/yr additional. Contact Ken Bartline, RN. (907) 257-1457, collect. Indian Health Service. An equal opportunity employer. 8–1a

TWO RADIOLOGISTS, KANSAS CITY—There is an opening for 2 radiologists, 1 immediately and 1 in July 1992, to join an expanding 4-person group in a 300-bed hospital and a future large, outpatient center. We are looking for a radiologist to head special procedures and the interventional section. The other person could be a general radiologist or have any other subspecialty training. Competitive salary. All benefits lead to early full partnership. Reply to George F. Drasin, M.D., 4949 Rockhill Rd., Kansas City, MO 64110. 8–10ap

FACULTY POSITION IN ABDOMINAL IMAGING Dartmouth-Hitchcock Medical Center is seeking a faculty member at the associate professor level with experience and interest in abdominal imaging radiology. Clinical responsibility will be in an entirely new 400-bed, clinical facility opening in Oct. 1991 with state-of-the-art instrumentation. Position will involve responsibility for residency training in GI/GU area. Proven record of academic performance including research and teaching with an interest in providing academic guidance for energetic staff of younger radiologists necessary. Interested candidates write with CV to Peter K. Spiegel, M.D., Chairman, Dept. of Diagnostic Radiology, Dartmouth-Hitchcock Medical Center, Hanover, NH 03756. AA/EOE. 8xap

THE DEPT. OF RADIOLOGY AT BROOKE ARMY MEDICAL CENTER, SAN ANTONIO, TX, is recruiting academic radiologists for several divisions of the dept., including ultrasound, chest, skeletal, neuroradiology, general diagnostic, interventional radiology, and mammography. Our dept. offers a fully accredited residency program with 24 residents and 16 attending full-time staff. Numerous consultants from across the country lecture on a continuing and regular basis. The hospital is a modern, tertiary-care center serving Texas, Oklahoma, and Louisiana. A strong residency program, interesting patient population, excellent equipment, teleradiology and digital radiology implementations underway, coupled with a south Texas lifestyle are positive aspects of the practice. Academic credentials and/or experience are necessary. Recently graduated fellows are encouraged to apply. Board certification is mandatory. Candidates should be particularly interested in patient care, teaching, and research. Salary and benefits are competitive and generous. Brooke is an EO/EEO employer. Please contact Dr. Billy E. Cunningham, COL, MC, Assistant Chief, Dept. of Radiology, Brooke Army Medical Center, Fort Sam Houston, TX 78234-6200; (512) 221-8418/8218. 8a

THE DEPT. OF RADIOLOGY AT WALTER REED ARMY MEDICAL CENTER is recruiting academic radiologists. We need board-certified radiologists to work in this famous and modern health-care center. Our dept. has a residency program consisting of 24 residents and several fellows. Subspecialists are needed in ultrasound, chest, mammography, genitourinary, gastrointestinal, pediatric, CT, MRI, and interventional radiology, as well as general radiology. Excellent opportunity to live in the nation's capital and also become an integral part of a large teaching program. Salaries are competitive and generous. Highly motivated applicants should contact Col. Mark F. Hansen, Radiology Consultant to the Army Surgeon General, Dept. of Radiology, TAMC, HI 96859-5000; (808) 433-6393. 8a

THE RADIOLOGY DEPT. AT DWIGHT DAVID EISENHOWER ARMY MEDICAL CENTER is recruiting academic radiologists. The dept. provides a full range of services including angiography, ultrasound, CT (with a new GE 9800 Advantage system), and MRI (with a new 1.5-T GE Signa system). Development is underway for the installation of a digital teleradiology link to area medical facilities. The dept. is also beginning a radiology residency program in affiliation with the program at the Medical College of Georgia in Augusta. With this growth, the dept. has generated a need for several academic diagnostic radiologists. Board-certified diagnostic radiologists with academic credentials and/or experience are urged to apply. Fellowship training is desired, especially in interventional radiology and/or angiography, however candidates at all levels will be considered. Candidates should be particularly interested in patient care, teaching, and research. The medical center is located on Fort Gordon, GA, adjacent to Augusta and is the tertiary-care hospital supporting 9 Army community hospitals of the southeastern region and Puerto Rico. The hospital supports fully accredited residency programs in family practice, general surgery, medicine, orthopedics, pathology, and psychiatry. Salary and benefits are competitive and generous. The medical center is an EO/EEO employer. Please contact Dr. Thomas M. Ralston, LtC., Chief, Radiology Dept., Eisenhower Army Medical Center, Fort Gordon, GA; (404) 791-6245. 8a

CHAIRMAN, DEPT. OF DIAGNOSTIC RADIOLOGY, ALBERT EINSTEIN MEDICAL CENTER Albert Einstein Medical Center is a tertiary-care, 600-bed hospital with major affiliations with Temple University School of Medicine. We are now seeking a full-time chairman for the Dept. of Diagnostic Radiology, which includes an independent, fully accredited residency program. The dept. has active divisions of general radiology, ultrasound, body imaging, mammography, cardiac radiology, nuclear medicine, advanced muscular skeletal imaging, MRI, and special procedures. It is equipped with state-of-the-art equipment and has an active research program consisting of dedicated M.D.'s and Ph.D. scientists who provide special expertise in radiation biology. The professional staff consists of full-time, board-certified, diagnostic radiologists who hold faculty positions at Temple University School of Medicine. Currently the dept. provides over 180,000 diagnostic and nuclear exams/yr and provides ancillary services at 2 other satellite locations. The successful candidate must possess strong academic credentials and demonstrate capabilities in patient care, education, research, and administration. He/she would be expected to qualify for an appointment as a free professor and a senior associate chairman of the Dept. of Radiology at Temple University School of Medicine. Please submit CV to I. Daskal, M.D., Ph.D., Chairman, Dept. of Pathology and Laboratory Medicine, and Chairman, Dept. of Radiology Search Committee, Albert Einstein Medical Center, 5501 Old York Rd., Philadelphia, PA 19141-3098. Equal opportunity employer. 8a

PEDIATRIC RADIOLOGIST—The Mallinckrodt Institute of Radiology has an opening for a pediatric radiologist. Faculty rank of instructor, assistant, or associate professor will be based on experience. Work site is St. Louis Children's Hospital in a well-equipped pediatric section performing approximately 58,000 studies/yr. Duties include ultrasound, body CT, and general pediatric radiology. MR to be installed on-site within the yr. Interested persons should contact William H. McAlister, M.D., Mallinckrodt Institute of Radiology, 510 S. Kingshighway Blvd., St. Louis, MO 63110. 8–9a

MRI RADIOLOGIST/MEDICAL DIRECTOR—The Western New York MRI Center, a consortium of 7 large hospitals in Buffalo, NY, is seeking a board-eligible/certified radiologist with fellowship training in MRI. The Center is affiliated with a university residency program. Responsibilities include supervision of a Siemens SP63 1.5-T freestanding imaging center, clinical body and neuro MRI interpretation, and teaching. Please send letter of inquiry and CV to David W. Shoemaker, M.D., Western New York MRI Center, 222 Genesee St., Buffalo, NY 14203. 8ap

MUSCULOSKELETAL RADIOLOGIST, UNIVERSITY OF ARKANSAS FOR MEDICAL SCIENCES, LITTLE ROCK—Join a busy group serving 2 hospitals covering CT, MRI, arthrography, and occasional biopsies, with additional coverage in mammography and some general radiology. Excellent rapport with orthopedic dept. Little Rock gives many large city amenities without the crowded, hectic lifestyle. Send CV to Richard L. FitzRandolph, M.D., or Ernest J. Ferris, M.D., University of Arkansas for Medical Sciences, 4301 W. Markham, Slot #556, Little Rock, AR 72205. 8a

CHIEF, AMBULATORY CARE CLINIC, UNIVERSITY OF ARKANSAS FOR MEDICAL SCIENCES—We are seeking a person with excellent general radiology experience with special interest and competence in bone radiology and mammography to oversee a busy outpatient clinic immediately attached to the hospital and the Arkansas Cancer Research Center. Excellent lifestyle opportunities afforded by both large-city amenities and multiple outstanding outdoor recreational opportunities. Send CV to Richard L. FitzRandolph, M.D., or Ernest J. Ferris, M.D., University of Arkansas for Medical Sciences, 4301 W. Markham, Slot #556, Little Rock, AR 72205. 8a

CLINICAL DIRECTOR, MRI—MetroHealth Medical Center, a 1,000-bed teaching hospital affiliated with Case Western Reserve University (CWRU), is seeking a clinical director for its MRI section. MHMC is a Level I trauma center providing tertiary care in the Cleveland metropolitan area. The director of MRI will head a major research and clinical service. Responsibilities include overseeing daily operations, research leadership in investigative MR, and development of collaborative ventures with the physics research group and other members of the Dept. of Radiology, hospital, and university. The position provides an excellent opportunity for research and resident education as well as professional development. The Dept. of Radiology is an active, academic dept. with state-of-the-art equipment in angiography, CT, ultrasound, and nuclear medicine and has an approved residency program. The MR section includes a 1.5-T imager (2nd system will be installed by Fall 1991), independent development workstation, 3-D engine (Voxel-Flinger), RF lab, and Starden Titan minicomputer. The research group includes 4 Ph.D. scientists and 4 graduate students. Candidates will be board-certified, have demonstrated experience in MRI research, have dedicated MR training, and be eligible for Ohio medical licensure. The ideal candidate will currently possess an assistant professor or higher rank with administrative experience preferred. MetroHealth Medical Center offers attractive compensation and benefits. The selected candidate will be recommended for a faculty appointment at CWRU School of Medicine commensurate with his/her experience. Interested candidates should forward CV and other pertinent information to Errol M. Bellon, M.D., Director, Dept. of Radiology, MetroHealth Medical Center, 3395 Scranton Rd., Cleveland, OH 44109; fax (216) 459-4072. MetroHealth Medical Center and Case Western Reserve University are equal opportunity employers. 8–10a

FACULTY RADIOLOGIST, BODY MRI DIVISION, THOMAS JEFFERSON UNIVERSITY HOSPITAL—The Dept. of Radiology at Thomas Jefferson University Hospital has an opening for a radiologist in an active, body MRI section that encompasses a clinical mix of approximately 50% musculoskeletal and 50% chest/abdomen/pelvis cases. Equipment includes 4 1.5-T GE Signa systems with state-of-the-art and advanced prototype hardware and software. A full-yr body MRI fellowship and/or 1 yr of academic MRI experience is preferred. Clinical cross coverage in ultrasound and/or general radiology also can be incorporated depending on the interests and qualifications of the candidate. Dedicated, nonclinical research time is provided, and the dept. has excellent research facilities and support, including 2 MRI physicists, a radiology animal facility, radiology research funding, and a team of research assistants. Excellent faculty incomes and benefits are offered within a financially secure dept. and university hospital. This is a unique opportunity for an academically oriented MRI radiologist to join a dynamic and rapidly growing dept. Interested candidates should contact Donald G. Mitchell, M.D., Director of MRI, Dept. of Radiology, 1032 Main Bldg., Thomas Jefferson University Hospital, Philadelphia, PA 19107; (215) 955-4809. Jefferson is an equal opportunity/affirmative action employer. 8xa

THE DEPT. OF RADIOLOGY, VIRGINIA COMMONWEALTH UNIVERSITY/MEDICAL COLLEGE OF VIRGINIA, AND THE MCGUIRE VA MEDICAL CENTER, RICHMOND, VA, seek faculty for positions in diagnostic radiology (chest, GI, mammography, CT/ultrasound/MR, musculoskeletal, pediatrics, ER, angio/interventional, and neuroradiology), nuclear medicine, and radiologic physics. MCV is a 1058-bed facility (205 for children) and a Level I trauma center. The McGuire VAMC is an 800-bed facility (pediatrics excluded). ABR certification of eligibility required. Individual should have experience working in a culturally diverse environment. Academic rank and salary commensurate with experience. For position description or to submit CV write or phone A. V. Proto, M.D., Dept. of Radiology, MCV Box 470, Richmond, VA 23298-0470; (804) 786-7212. VCU/MCV is an equal opportunity/affirmative action employer. Women and minorities are encouraged to apply. 8–9ap

CHAIRMAN, DEPT. OF RADIOLOGY—The University of Texas Medical School at Houston is seeking a chairman of the Dept. of Radiology to provide leadership of the programs at the medical school and its affiliated institutions, Hermann Hospital and Lyndon B. Johnson General Hospital. Significant experience and accomplishments in academic radiology and documented evidence of administrative and managerial skills are required. Dedication to the pursuit of excellence in research, teaching, and clinical service in an academic environment is essential. Applicant must be certified by the American Board of Radiology or its equivalent. Applications will be accepted until a suitable candidate is selected. Interested applicants should submit a CV to Dr. L. Maximilian Buja, Chairman, Search Committee for Radiology Chair, Dept. of Pathology and Laboratory Medicine, The University of Texas Medical School at Houston, 6431 Fannin, MSB2.136, Houston, TX 77030; (713) 792-5210. The University of Texas is an equal opportunity employer. Women and minorities are encouraged to apply. 8a

INTERVENTIONAL/NEURORADIOLOGIST needed for large, private-practice group. Salary leading to partnership. Respond to Marc A. Hertz, M.D., Northern Metropolitan Radiology Associates, P.C., 3630 Hill Blvd., Jefferson Valley, NY 10535; (914) 245-8935. 8ap

DIAGNOSTIC RADIOLOGIST, WASHINGTON—The Moses Lake Clinic is seeking a well-trained diagnostic radiologist to join a group of progressive multispecialty physicians. This is an opportunity to work in a beautiful facility that offers mammography, fluoroscopy, ultrasound, diagnostic radiology, and CT. Competitive compensation, excellent benefit package, located in central Washington. Contact Terry W. Coplin, Administrator, 840 Hill Ave., Moses Lake, WA 98837; (509) 765-0216. 8–10a

DIAGNOSTIC RADIOLOGIST, NEW MILFORD, CT—A third radiologist is sought for a busy, private practice located in 1 of the most beautiful areas of Connecticut. We provide the full range of diagnostic services for a modern, well-equipped, community hospital. Choice environment; excellent compensation. Send inquiries and CV to Jules White, M.D., New Milford Hospital, 21 Elm St., New Milford, CT 06776; (203) 355-2611, ext. 235. 8–11ap

DIAGNOSTIC RADIOLOGIST needed to join an expanding, multimodality breast center located in east Tennessee, near the foothills of the Smoky Mountains. Please send CV to Kamilia Gitschlag, M.D., Bluepointe Pl., 6307 Lonas Dr., Knoxville, TN 37909. 8–9ap

THE DEPT. OF RADIOLOGY OF THE CHILDREN'S MEMORIAL HOSPITAL CHICAGO, is seeking a pediatric radiologist. Children's Memorial Hospital is a 265-bed facility, well-equipped with state-of-the-art MR, CT, ultrasound, and nuclear medicine equipment. Currently there are 11 attending radiologists in the dept. Applicants must be certified by the American Board of Radiology and have completed a fellowship in pediatric radiology. Duties include clinical services, teaching, and research. Children's Memorial is affiliated with Northwestern University Medical School. This is a full-time position starting as soon as possible. Please send CV to Andrew K. Poznanski, M.D., Radiologist-in-Chief, Children's Memorial Hospital, 2300 Children's Plaza, Chicago, IL 60614. For inquiries, please call (312) 880-3520. Children's Memorial Hospital and Northwestern University are affirmative action/equal opportunity employers. Hiring is contingent on medical licensure in Illinois. 8–9a

ANGIOGRAPHY/INTERVENTIONAL RADIOLOGIST needed to join the staff at William Beaumont Hospital, a modern, major, tertiary-care, teaching medical center in southeastern Michigan with residency and fellowship programs in diagnostic radiology. The dept. is expanding its state-of-the-art facilities to accommodate increasing demands on patient care. Fellowship in angiography/interventional radiology is required. Past experience in academic institutions is desirable. Area offers 1 of the best educational and recreational facilities. Excellent compensation. Write to Jalil Farah, M.D., Chairman, Diagnostic Radiology, William Beaumont Hospital, 3601 W. 13 Mile Rd., Royal Oak, MI 48073. 6–8ap

COME TO CALIFORNIA WITH A LICENSE FROM ANY STATE—Loma Linda VA Hospital has a vacancy for a board-certified radiologist. A current license from any state is acceptable. Loma Linda is located 70 mi. east of Los Angeles near beaches, mountain ski resorts, and southland theme parks. This is a 500-bed, full-service hospital with a comprehensive diagnostic facility including ultrasound, CT, and MRI integrated with the Loma Linda University Medical Center residency training program. Opportunities exist to pursue clinical or academic interests. For additional information, contact Peter Dure-Smith, M.D., Chief, Radiology (114), Jerry L. Pettis Memorial Veterans Hospital, 11201 Benton St., Loma Linda, CA 92357; (714) 422-3069, fax (714) 422-4106. Equal opportunity employer. 3–8ap

TRAUMA RADIOLOGIST—The State University of New York Health Science Center at Brooklyn seeks to add a board-certified/eligible radiologist to join the Division of Traumatology at Kings County Hospital Center, a 1300-bed tertiary facility and Level I Trauma Center with an international reputation in trauma services. The radiologist is an integral member of the trauma service of the Dept. of Surgery. Opportunities to join ongoing clinical investigations of the use of radiography, CT, angiography/interventional radiology, and ultrasound in the trauma patient are available. Academic rank and salary are commensurate with experience. CV should be addressed to Salvatore J. A. Sclafani, M.D., Dept. of Radiology, Kings County Hospital Center, 451 Clarkson Ave., Brooklyn, NY 11203. An EO/AA employer. 7–9ap

IMMEDIATE OPENING IN PALM SPRINGS, CA Radiologist with MRI expertise/specialization needed to join 10-person group in community hospital/office practice. Contact Marvin J. Friedenberg, M.D., Dept. of Radiology, Desert Hospital, 1150 N. Indian, Palm Springs, CA 92262. 8xa

IMMEDIATE OPENING IN PALM SPRINGS, CA Radiologist with mammography expertise/specialization needed to join 10-person group in community hospital/office practice. Contact Marvin J. Friedenberg, M.D., Dept. of Radiology, Desert Hospital, 1150 N. Indian, Palm Springs, CA 92262. 8xa

RADIOLOGIST/ANGIOGRAPHER—There is an opportunity to join a progressive group of 11 board-certified radiologists practicing at the Lehigh Valley Hospital Center, a 500-bed, university-affiliated hospital. The position requires angiographic/interventional skills and an interest in general radiology including CT and ultrasound. The radiology dept. has state-of-the-art equipment including 2 angiographic suites, 3 CT scanners, color flow Doppler, and MRI. The hospital is an acute-care facility and a state-designated Level 1 Trauma Center, located 1 hr from Philadelphia and 1½ hr from New York. The radiology dept. offers a postresidency fellowship program that includes training in angiography. The position offers a competitive salary and benefit package that leads to full partnership. For further information, contact Robert Kricun, M.D., Dept. of Radiology, Lehigh Valley Hospital Center, P.O. Box 689, Allentown, PA 18105; (215) 776-8088. 6–8ap

SUPERB PARTNERSHIP POSITION IN LAS VEGAS, NV—Rapidly expanding, 7-member group practice covering 2 full-service imaging centers and a small hospital has an immediate opening. We are looking for an additional board-certified radiologist with an uncommon dedication to excellence in patient care. Our outpatient facilities include 2 MR, 2 CT, angio with a 4-bed recovery area, 5 ultrasound, 5 mammography, 2 SPECT, plus R & F. This is an excellent opportunity for a partnership position with a well-respected group in a growing community. Please send CV to Dr. Mark Winkler, SDMI, 2950 S. Maryland Pkwy., Las Vegas, NV 89109. 5–10a

PHYSICIAN/RADIOLOGIST—Full-time opening for board-certified radiologist in a desirable southern New Jersey shore location. This is an active, challenging, expanding hospital- and office-based practice. Must have training in CT, ultrasound, and MRI. Send CV to RABC, P.O. Box 729, Mt. Holly, NJ 08060. 6–8ap

DIAGNOSTIC RADIOLOGIST—Position for a board-certified radiologist to provide sole coverage for a 27-bed hospital in a southeast Idaho community of 20,000. Immediate potential for a $220,000 practice while still having time to enjoy geographical amenities. Contract available. Please call or write Randall G. Holom, 1224 8th St., Rupert, ID 83350; (208) 436-0481. 6–8a

DIAGNOSTIC RADIOLOGIST, LONG ISLAND, NY—Board-certified radiologist with expertise in MRI needed to join a 5-member group starting in July 1991. Fellowship training in MRI or neuroradiology is desirable. Must be willing to do most aspects of diagnostic radiology. This well-established practice includes a 325-bed community hospital, a private diagnostic radiology office, and a 1-yr-old MRI facility with a high-field-strength magnet. Generous salary leading to full partnership. Contact Ira Langer, M.D., 250 Hospital Rd., Patchogue, NY 11772; (516) 475-1030. 7–8ap

DIAGNOSTIC RADIOLOGIST, FLORIDA—Staff radiologist is being sought by the University of Florida Health Science Center/Jacksonville for a full-time faculty position. Special interest, expertise, or fellowship training in CT, ultrasound, MR, interventional, or nuclear radiology is preferable. Salary and fringe benefits are excellent. An academic appointment will be at the instructor/assistant professor/associate professor/professor academic rank depending on training, background, and experience. Application recruiting deadline is Sept. 1, 1991. Send CV and references to Chairman, Search Committee, Dept. of Radiology, University Medical Center, 655 W. Eighth St., Jacksonville, FL 32209. AA/EOE. 7–8a

RADIOLOGIST—BC/BE radiologist needed to join 2-person practice covering 2 hospitals in the central mountains of Colorado. Ample free time and excellent outdoor recreational opportunities. Contact E. J. Loeffel, M.D., P.O. Box 415, Buena Vista, CO 81211; (719) 539-3782. 7–9ap

THE DEPT. OF RADIOLOGY AT THE UNIVERSITY OF MASSACHUSETTS MEDICAL CENTER in Worcester is seeking a BC/BE radiologist with a major interest in abdominal radiology with fellowship experience desirable. A strong interest in teaching and collaborative clinical research is desired. Rank and salary are commensurate with experience. The medical center is a 370-bed university hospital and medical school located approximately 40 mi. west of Boston. The dept. consists of 22 staff, 13 residents, and 2–4 fellows and does approximately 130,000 exams/yr. The dept. is well-equipped with 2 GE 9800 HiLite CT scanners, 2 GE 1.5-T MRI scanners in a standalone facility, a 2.0-T small-bore unit for animal research, several state-of-the-art ultrasound scanners, color Doppler, transrectal ultrasound, etc. The hospital is a major trauma center and is serviced by 2 Life Flight helicopters. For further information, contact Edward H. Smith, M.D., Professor and Chair, Dept. of Radiology, University of Massachusetts Medical Center, 55 Lake Ave. N., Worcester, MA 01655; (508) 856-3252. UMMC is an equal opportunity/affirmative action employer. 8xa

THE DIVISION OF NUCLEAR MEDICINE, Oregon Health Sciences University, Portland, OR, invites applications for a faculty position available immediately either part-time in nuclear medicine or full-time divided between nuclear medicine and another division of diagnostic radiology. Board certification in nuclear medicine is required. Send CV and references to William Weidner, M.D., Chairman, Diagnostic Radiology, UHN 72, Oregon Health Sciences University, Portland, OR 97201-3098. OHSU is an affirmative action, equal opportunity employer. 7–8a

DIAGNOSTIC RADIOLOGIST—BC/BE radiologist wanted to join expanding practice of 12 radiologists in northeastern Pennsylvania. Practice includes 3 hospitals (720 beds) and free-standing MRI. Candidate must have experience in angiography and interventional radiology, and be willing to cover other areas of diagnostic imaging. Contact Paul M. Leiman, M.D., Dept. of Radiology, Moses Taylor Hospital, 700 Quincy Ave., Scranton, PA 18501; (717) 963-2601. 8–9ap

IMMEDIATE OPENING FOR A BC/BE DIAGNOSTIC RADIOLOGIST—Join 1 other as a full-time partner under fee-for-service billing. Ideal family community located in western Pennsylvania, approximately 60 mi. north of Pittsburgh. This is an acute-care hospital with 180 beds doing approximately 30,000–35,000 exams/yr. Need experience in general radiology, some angiography and interventional procedures, ultrasound, CT, MRI (mobile), and mammography services. Applicant should respond as soon as possible with letter of interest and current CV to Wan Jo Kim, M.D., Director of Radiology, St. Francis Hospital of New Castle, 1000 S. Mercer St., New Castle, PA 16101; (412) 656-6011/6116 (before 5 p.m.), (412) 656-0752 (after 5 p.m.). 7–9ap

CARDIOVASCULAR AND INTERVENTIONAL RADIOLOGIST—The State University of New York Health Science Center at Brooklyn seeks a board-certified/eligible radiologist with fellowship training in interventional radiology for a faculty position. The institution is a 1700-bed facility, including the Kings County and the State University hospitals. The medical center performs approximately 2000 diagnostic and interventional procedures, including angioplasty, embolization, caval filters, gastrointestinal, genitourinary, and pulmonary interventions. When ongoing renovations are complete, there will be 5 new vascular digital rooms. Research time and facilities are available. Rank and salary are commensurate with qualifications. CV should be addressed to Salvatore J. A. Sclafani, M.D., Kings County Hospital Center, Dept. of Radiology, 451 Clarkson Ave., Brooklyn, NY 11203; (718) 245-4447. An EO/AA employer. 7–9ap

NORTHERN CALIFORNIA—The Permanente Medical Group, Inc., is seeking a BC radiologist with multimodality interests and fellowship training in MR to join a 12-person group serving a 337-bed, acute-care hospital and 2 outpatient clinics. Teaching opportunities are available with residents of subspecialty services on rotation from Stanford University Hospital as well as our own medical residents. We have sited a GE 1.5-T MRI system. Competitive salary and excellent benefits. Send CV to Bruce Baker, M.D., Chief, Dept. of Radiology, Kaiser Permanente Medical Center, 900 Kiely Blvd., Santa Clara, CA 95051; (408) 236-4444. EOE. 7–8a

FAIRBANKS, AK—Four diagnostic radiologists seek fifth partner for diversified practice including general radiology, ultrasound, nuclear medicine, MRI (GE 1.5-T), and CT (GE 9800). Hospital and office practice. Desirable life-style advantages in a university town. Unlimited access to the outdoors. Excellent salary, benefits, retirement, and vacation. One yr to full partnership. Contact Douglas Hutchinson, M.D., 1919 Lathrop #5, Fairbanks, AK 99701; (907) 452-5092. 8–10ap

LARGE, GROWING RADIOLOGY PRACTICE IN CENTRAL NEW JERSEY and adjacent Pennsylvania region seeks diagnostic radiologist with expertise in 1 or more of the following: CT/ultrasound, angio/interventional, or nuclear medicine. Send resume to E. Tarasov, M.D., 838 W. State St., Trenton, NJ 08618. 7–9a

INDIANAPOLIS, IN—Practice opportunity for a radiologist to serve as medical director of a new, freestanding, privately owned, imaging center with CT and high-field MR. Facility will be managed by and affiliated with the Center for Diagnostic Imaging in Minneapolis, MN. MR experience mandatory. Subspecialty experience in MR desirable. Board certification and ability to obtain licensure in Indiana required. Please send inquiries with CV to Cooper R. Gundry, M.D., Center for Diagnostic Imaging, 5775 Wayzata Blvd., Ste. 190, Minneapolis, MN 55416. All inquiries entirely confidential. No telephone calls please. 7–9ap

SOUTHERN OREGON—Opportuniy for BC/BE, general diagnostic radiologist to join group of 5 board-certified radiologists. Experience in all modalities desired. Practice includes 2 hospitals and own private office. Competitive starting salary with early full partnership. Excellent lifestyle with many outdoor activities from Pacific Coast to Oregon Cascades. Send CV to Larry Strickland, Administrator, Roseburg Radiologists, P.C., P. O. Box 1547, Roseburg, OR 97478. 8–1ap

SAN FRANCISCO BAY AREA, DIAGNOSTIC RADIOLOGY—Full-time position available as of July 1992 for BC/BE radiologist to join established group based in growing SF Bay area communities. Competence in all modalities including MRI and angiography required; fellowship training desirable. Contact J. Fish, M.D., c/o Walnut Creek Radiology, 1844 San Miguel Dr., #302, Walnut Creek, CA 94596; (415) 947-0560. 8–10xa

ISRAEL, DIAGNOSTIC RADIOLOGY. Opportunities for 3–4 week or longer working vacations in a number of Israeli medical centers, on a volunteer basis. Positions varied, arrangements flexible. For information contact: Jonathan H. Fish, M.D., 1844 San Miguel Dr., #302, Walnut Creek, CA 94596; (415) 947-0560. 8–10xa

THE DEPT. OF RADIOLOGY AT TRIPLER ARMY MEDICAL CENTER, HONOLULU, HI, is recruiting academic radiologists for several divisions of the dept. including ultrasound, chest radiology, skeletal, neuroradiology, general diagnostic radiology, MRI, interventional radiology, and mammography. Our dept. offers a fully accredited residency program with 21 residents and 16 attending full-time staff. Numerous consultants from across the country lecture on a continuing and regular basis. The hospital is a modern, tertiary-care center serving Hawaii and the entire Pacific Basin. A strong residency program, diverse and interesting patient population, excellent equipment, and tropical lifestyle are positive aspects of the practice. Academic credentials and/or experience are necessary. Recently graduated fellows are encouraged to apply. Board certification is mandatory. Candidates should be particularly interested in patient care, teaching, and research. Salary and benefits are competitive and generous. Tripler is an EO/EEO employer. Please contact Dr. Mark F. Hansen, Col., MC, Chief, Dept. of Radiology, TAMC, HI 96859-5000; (808) 433-6393. 7–6a

PEDIATRIC RADIOLOGIST—The Division of Pediatric Radiology, Oregon Health Sciences University, Portland, OR, invites applications for a faculty position available on or about July 1, 1991. Completion of approved fellowship in pediatric radiology and ABR certification required. Send CV to William Weidner, M.D., Diagnostic Radiology, UHN-72, Oregon Health Sciences University, Portland, OR 97201-3098; (503) 494-4498. Equal opportunity, affirmative action employer. 7–9a

MRI/ABDOMINAL IMAGING NEW YORK/NEW JERSEY METROPOLITAN AREA—Board-certified/eligible radiologist needed for a position beginning July 1, 1991. Must have fellowship training in MRI and training in CT, ultrasound, and GI studies. Private practice with 400-bed hospital and outpatient imaging center located in northern New Jersey, near New York City. Send inquiries to James A. Heimann, M.D., Dept. of Radiology, Clara Maass Medical Center, 1 Franklin Ave., Belleville, NJ 07109. 7–12ap

NORTHERN CALIFORNIA, IMMEDIATE OPENING—Large, diagnostic group seeks BC/BE radiologist to join diversified practice (4 hospitals and 7 offices) on full partnership basis. All modalities available. Send CV or call Andrew Koo, M.D., P.O. Box 9525, San Jose, CA 95157; (408) 244-2100. 7–9ap

CHEST RADIOLOGIST, CLEVELAND CLINIC FOUNDATION—The Cleveland Clinic Foundation has an opening for a staff position in the Section of Thoracic Imaging. The foundation is a 1000-bed hospital with a large outpatient population and an international referral base. Successful applicants will be involved in all diagnostic modalities, including CT, MRI, and interventional procedures. A strong interest in teaching, research, and patient care is required. Applicants should be board-certified, fellowship-trained, or have equivalent experience. Excellent salary and benefit package. Send CV to Moulay A. Meziane, M.D., Head, Section of Thoracic Imaging, Cleveland Clinic Foundation, One Clinic Center Dr., Cleveland, OH 44195-5021. The Cleveland Clinic Foundation is an equal opportunity employer. 5–10ap

DIAGNOSTIC RADIOLOGIST, EL PASO, TX—BE/BC radiologist with special competence in body imaging sought to join busy hospital radiology practice at a community medical center with a total of 330 beds. Modern imaging dept. with 1.5-T GE MR, CT, nuclear medicine with SPECT, ultrasound, angiography with DSA, mammography, and diagnostic radiography. Excellent salary, vacation, and benefits leading to early partnership. Send inquiries with CV to Roy K. Poth, M.D., 1625 Medical Center Dr., El Paso, TX 79902. 5–8ap

LOCUMS NATIONWIDE—BC or BE diagnostic radiologists needed for nationwide locums. Opportunities range from 1 wk to several mo. Exceptional compensation and all travel expenses. Call Professional Temporary Services, Inc., 790 Cardinal Rd., P.O. Box 2702, New Bern, NC 28561; (800) 872-4534. 5–8a

THE UNIVERSITY OF MASSACHUSETTS MEDICAL CENTER, a tertiary-care hospital situated 40 mi. from Boston, is seeking a third pediatric radiologist. The pediatric dept. services central and eastern Massachusetts as well as southern New Hampshire and northern Connecticut. All medical and surgical pediatric subspecialties are represented and a broad range of pediatric pathology is encountered. Pediatric radiologists have the primary responsibility in ultrasound, CT, MRI, and interventional procedures in general radiologic exams. Competitive salaries and generous benefits are provided. For further information, contact Paul K. Kleinman, M.D., Dept. of Radiology, University of Massachusetts Medical Center, 55 Lake Ave., N., Worcester, MA 01655; (508) 856-3124, fax (508) 856-4669. 8xa

PRACTICE OPPORTUNITY IN FAST-GROWING LAS VEGAS, NV—Expanding, 6-member radiology group is seeking 2 additional BE/BC radiologists for July 1991 and Jan. 1992. We currently serve 2 hospitals with an outpatient imaging center to open in Jan. 1992. Outstanding salary and benefits package leading to full partnership in 2 yr. Send CV or contact Marc Pomerantz, M.D., Head of Search Committee, 1925 Spode Ave., Henderson, NV 89014; (702) 388-4640. 5–9ap

DIAGNOSTIC RADIOLOGIST, IMMEDIATE OPENING—Ten-person radiology group seeks a diagnostic radiologist with fellowship training, including body MRI/body imaging, to join a busy, hospital-based practice located in rapidly growing north Dallas. GE 1.5-T magnet, Toshiba midfield magnet, 2 GE 9800 scanners, Acuson 128 with color flow Doppler, and new special procedures suite with DSA. Please send CV to Box K54, *AJR* (see address this section). 8xa

SAN ANTONIO, TX—Group covering multiple hospitals and clinics seeks radiologists with imaging and angiography skills. Send CV to Search Committee, M & S X-Ray Associates, P.O. Box 15920, San Antonio, TX 78212-9510. 3–8ap

THE DEPT. OF RADIOLOGY AT THE UNIVERSITY OF MASSACHUSETTS MEDICAL CENTER in Worcester is seeking a BC/BE general radiologist with a major interest in chest and musculoskeletal radiology. A strong interest in teaching and collaborative clinical research is desired. Rank and salary are commensurate with experience. The medical center is a 370-bed university hospital and medical school located approximately 40 mi. west of Boston. The dept. consists of 22 staff, 13 residents, and 2–4 fellows and does approximately 130,000 exams/yr. The dept. is well-equipped with 2 GE 9800 Quick CT scanners as well as 2 GE 1.5-T MRI scanners in a stand-alone facility and a 2.0-T small-bore unit for animal research. The hospital is a major trauma center and is serviced by 2 Life Flight helicopters. For further information, contact Edward H. Smith, M.D., Professor and Chair, Dept. of Radiology, University of Massachusetts Medical Center, 55 Lake Ave., N., Worcester, MA 01655; (508) 856-3252. UMMC is an equal opportunity/affirmative action employer. 8xa

OREGON—Opportunity for BC/BE radiologist to join 7 BC radiologists in growing practice in the Portland metropolitan area. Training/expertise in all aspects of radiology including MRI is required. The practice includes 2 suburban hospitals, an outpatient clinic, and a new multimodality outpatient imaging clinic. Competitive compensation with generous fringe package and partnership in 2 yr. Send letter and CV to Jon C. Sewell, M.D., P.O. Box 227, Oregon City, OR 97045; (503) 655-1439. 7–8ap

LOCUM TENENS—Earn top pay. Don't work for an agency. Work for yourself. For details, send name and address to Dr. Monroe, 7035 Hwy. 6 South, Ste. R 175, Houston, TX 77083; (713) 341-9703. 7–8ap

OPENING FOR BE/BC DIAGNOSTIC RADIOLOGIST to join a 6-person group in Missoula, a university city of 45,000 located in mountainous western Montana. Looking for a general radiologist with proficiency in MRI, ultrasound, CT, angiography, etc. Administrative skills preferable. Our group of 6 full-time radiologists covers both of Missoula's hospitals (210 and 130 beds). Progressive medical environment with 200 physicians. One yr to full partner income and 2 yr to partnership. Competitive salary. Abundant nearby recreational opportunities include skiing, fishing, backpacking, and hunting. Send CV to Missoula Radiology, Inc., P.O. Box 2039, Missoula, MT 59806. 7–11ap

UTMB, GALVESTON, TX—The Dept. of Radiology of the University of Texas Medical Branch in Galveston has openings for persons trained and experienced in ultrasonography and mammography. The opportunity for academic advancement is great and benefits are generous. Salaries are competitive and living conditions are desirable. Interested persons should contact Melvyn H. Schreiber, M.D., Chairman, Dept. of Radiology, UTMB, Galveston, TX 77550; (409) 761-1823. UTMB is an equal opportunity M/F/H/V affirmative action employer. UTMB hires only individuals authorized to work in the United States. 4–9a

DALLAS, TX—A 12-member, subspecialty group seeks a board-certified, general radiologist for an immediate opening. Fellowship training preferred, but will consider qualified individual with special expertise. CT/ultrasound, MRI, nuclear medicine, or angiography background particularly helpful. All imaging modalities available (state-of-the-art CT, angio, ultrasound, R & F, SPECT nuclear medicine, and MRI center). Salary and bonuses are excellent. Health and malpractice paid. No buy-in to partnership. Send CV to H. Stuart Peake, M.D., P.O. Box 814129, *Dallas*, TX 75381; (214) 888-7055. 4–9ap

BC/BE RADIOLOGIST—Group practice in New Orleans, LA, has a great opportunity leading to partnership. Looking for a radiologist with imaging background or interest in special procedures. Imaging center with 1.5-T GE Advantage System. Excellent hospitals and working conditions. Send CV to B.B.N. & H., 440 General Meyer Ave., Ste. 211, New Orleans, LA 70131; (504) 368-5074. 7–10ap

DIAGNOSTIC RADIOLOGIST with skills in CT, MR, interventional, ultrasound, and nuclear medicine needed to join group of 8 board-certified radiologists. Growing practice in eastern Washington at a 228-bed hospital, a new multimodality imaging center, and 2 private offices. Potential for long-term practice is excellent. Top-notch school system, including 3 first-rate universities. Excellent hunting, fishing, boating, and skiing. Contact L. E. Crecelius, M.D., N. 5901 Lidgerwood, Ste. 18B, Spokane, WA 99207; (509) 482-2385. 5–10ap

CROSS-SECTIONAL IMAGING/MRI/CT/ULTRASOUND—Diagnostic Radiology, Oregon Health Sciences University, Portland, OR, is recruiting a board-certified radiologist for its Body Imaging Section. Academic rank and salary depend on candidate's experience and achievements. Send CV and reference letters to William Weidner, M.D., Chairman, Diagnostic Radiology, UHN 72, Oregon Health Sciences University, Portland, OR 97201-3098. OHSU is an equal opportunity, affirmative action employer. 7–8a

BOSTON, IMMEDIATE OPENING—Radiologist wanted to join busy, well-established, private-practice group with 4 outpatient facilities. Expertise in ultrasound and mammography. No evening or weekend call. Excellent life-style, partnership opportunity. Send letter and CV to Box E49, *AJR* (see address this section). 6–11ap

SEATTLE COLLEAGUE WANTED—Growing radiology group seeks new member. Full-service radiology dept. (50,000 procedures/yr) offers diagnostic, nuclear medicine, ultrasound (including vascular-Doppler), interventional, CT, and MRI. Outpatient imaging dept. (building permits pending) scheduled to open late 1991 that will include high-field GE Signa MR with MRA. Extremely favorable track for partnership. For further information regarding this opening, please contact Mr. Richard G. Wedig, Highline Community Hospital, 16251 Sylvester Rd., S.W., Seattle, WA 98166; (206) 248-4561. 7–8ap

IMMEDIATE OPENING FOR BC/BE GENERAL RADIOLOGIST with experience in interventional and vascular radiology. Join a group of 4 radiologists in a 160-bed hospital located in Allentown, PA, about 60 mi. northwest of Philadelphia. The daily practice includes all aspects of general radiology, CT, ultrasound, and nuclear medicine. Please call or send CV to Asad Shohadai, M.D., Allentown Osteopathic Medical Center, 1736 Hamilton St., Allentown, PA 18104; (215) 770-8700. 8xa

DIAGNOSTIC RADIOLOGIST needed in Conway Hospital, a community hospital located 10 mi. west of the resort/seaside community of Myrtle Beach, SC. The dept. performs 44,000 exams/yr including CT, MRI, nuclear medicine, ultrasound, mammography, and special procedures. All exams are done on state-of-the-art equipment. Our 3-person group offers a very strong financial package with all benefits including 17-wk vacation. Lovely, rapidly growing resort area includes 60 mi. of sandy beaches, 70 golf courses, and beautiful seaside homes. Contact Gary Rike, M.D., P.O. Box 917, Conway, SC 29526; (803) 347-7277. 6–8ap

Positions Desired

MUSCULOSKELETAL RADIOLOGIST, fellowship-trained at a major university program with over 10 yr experience in all imaging techniques, including CT and MR, seeks a full-time position in an academic or private musculoskeletal radiology practice. Currently an active clinical faculty member at 2 university programs and chief of a bone section in a radiology residency program at a large teaching/county facility (1 of the hospitals covered by our large, private-practice group). Current duties include a significant amount of general radiology. Priorities include high-quality practice of radiology, state-of-the-art equipment, and congenial working environment. Western U.S. preferred, but not mandatory. Enthusiastic, healthy, ABR-certified, mid-40s, and looking for a change. Excellent references. Reply to Box N42, *AJR* (see address this section). 7–9bp

Fellowships and Residencies

FELLOWSHIP IN BODY CT—The Dept. of Radiology at the University of Minnesota has 1- to 2-yr postresidency fellowship training positions in body CT available at the rank of instructor (temporary, annual renewable) beginning July 1, 1992, and July 1, 1993. Minimum requirements include successful completion of an accredited radiology residency and board certification in radiology by beginning date of fellowship appointment. In addition to clinical practice and training, responsibilities will include graduate and undergraduate medical instruction in abdominal, thoracic, and musculoskeletal CT imaging as well as assisting with related departmental research projects. Percutaneous biopsy and drainage techniques using CT guidance will be emphasized. Salary is negotiable and competitive and dependent on past scholarly productivity and post-M.D. experience. Applicants must be licensed or able to obtain license to practice medicine in the state of Minnesota before appointment date. Applications for these positions will be accepted through Sept. 30, 1991, and Dec. 31, 1991, respectively. Send letters to James Walsh, M.D., Dept. of Radiology, Box 292 UMHC, University of Minnesota, 420 Delaware St., S.E., Minneapolis, MN 55455. The University of Minnesota is an equal opportunity educator and employer. 8c

FELLOWSHIP IN CARDIOVASCULAR/INTERVENTIONAL RADIOLOGY—The Dept. of Radiology at the University of Minnesota has 1- to 2-yr postresidency fellowship training positions in cardiovascular/interventional radiology available at the rank of instructor (temporary, annual renewable) beginning July 1, 1992, and July 1, 1993. Minimum requirements include successful completion of an accredited radiology residency and board certification in radiology by beginning date of fellowship appointment. In addition to clinical practice and training, responsibilities will include graduate and undergraduate medical instruction in cardiovascular/interventional radiology as well as assisting with related departmental research projects. Salary is negotiable and competitive and dependent on past scholarly productivity and post-M.D. experience. Applicants must be licensed or able to obtain license to practice medicine in the state of Minnesota before appointment date. Applications for these positions will be accepted through Sept. 30, 1991, and Dec. 31, 1991, respectively. Send letters to Kurt Amplatz, M.D., Dept. of Radiology, Box 292 UMHC, University of Minnesota, 420 Delaware St., S.E., Minneapolis, MN 55455. The University of Minnesota is an equal opportunity educator and employer. 8c

FELLOWSHIP IN MUSCULOSKELETAL RADIOLOGY—The Dept. of Radiology at the University of Minnesota has 1- to 2-yr postresidency fellowship training positions in musculoskeletal radiology available at the rank of instructor (temporary, annual renewable) beginning July 1, 1992, and July 1, 1993. Minimum requirements include successful completion of an accredited radiology residency and board certification in radiology by beginning date of fellowship appointment. In addition to clinical practice and training, responsibilities will include graduate and undergraduate medical instruction in musculoskeletal radiology as well as assisting with related departmental research projects. This fellowship will encompass all aspects of musculoskeletal radiology, including CT, arthrography, and MR. Salary is negotiable and competitive and dependent on past scholarly productivity and post-M.D. experience. Applicants must be licensed or able to obtain license to practice medicine in the state of Minnesota before appointment date. Applications for these positions will be accepted through Sept. 30, 1991, and Dec. 31, 1991, respectively. Send letters to Harry Griffiths, M.D., Dept. of Radiology, Box 292 UMHC, University of Minnesota, 420 Delaware St., S.E., Minneapolis, MN 55455. The University of Minnesota is an equal opportunity educator and employer. 8c

FELLOWSHIP IN NEURORADIOLOGY—The Dept. of Radiology at the University of Minnesota has 4 1- to 2-yr postresidency fellowship training positions in neuroradiology available at the rank of instructor (temporary, annual renewable) beginning July 1, 1992, and July 1, 1993. Minimum requirements include successful completion of an accredited radiology residency and board certification in radiology by beginning date of fellowship appointment. In addition to clinical practice and training, responsibilities will include graduate and undergraduate medical instruction in neuroradiology as well as assisting with related departmental research projects. Salary is negotiable and competitive and dependent on past scholarly productivity and post-M.D. experience. Applicants must be licensed or able to obtain license to practice medicine in the state of Minnesota before appointment date. Applications for these positions will be accepted through Sept. 30, 1991, and Dec. 31, 1991, respectively. Send letters to Richard Latchaw, M.D., Dept. of Radiology, Box 292 UMHC, University of Minnesota, 420 Delaware St., S.E., Minneapolis, MN 55455. The University of Minnesota is an equal opportunity educator and employer. 8c

FELLOWSHIP IN NUCLEAR MEDICINE—The Dept. of Radiology at the University of Minnesota has 1- to 2-yr postresidency fellowship training positions in nuclear medicine available at the rank of instructor (temporary, annual renewable) beginning July 1, 1992, and July 1, 1993. Minimum requirements include successful completion of an accredited radiology residency and board certification in radiology by beginning date of fellowship appointment. In addition to clinical practice and training, responsibilities will include graduate and undergraduate medical instruction in nuclear medicine as well as assisting with related departmental research projects. Salary is negotiable and competitive and dependent on past scholarly productivity and post-M.D. experience. Applicants must be licensed or able to obtain license to practice medicine in the state of Minnesota before appointment date. Applications for these positions will be accepted through Sept. 30, 1991, and Dec. 31, 1991, respectively. Send letters to Robert Boudreau, M.D., Dept. of Radiology, Box 292 UMHC, University of Minnesota, 420 Delaware St., S.E., Minneapolis, MN 55455. The University of Minnesota is an equal opportunity educator and employer. 8c

FELLOWSHIP IN PEDIATRIC RADIOLOGY—The Dept. of Radiology at the University of Minnesota Hospital and Minneapolis Children's Medical Center has 1- to 2-yr postresidency fellowship training positions in pediatric radiology available at the rank of instructor (temporary, annual renewable) beginning July 1, 1992, and July 1, 1993. Minimum requirements include successful completion of an accredited radiology residency and board certification in radiology by beginning date of fellowship appointment. In addition to clinical practice and training, responsibilities will include graduate and undergraduate medical instruction in pediatric radiology as well as assisting with related departmental research projects. Seven experienced pediatric radiologists will be actively involved in the training process. The clinical experience will be equally distributed between the Minneapolis Children's Medical Center and the University Hospital. Salary is negotiable and competitive and dependent on past scholarly productivity and post-M.D. experience. Applicants must be licensed or able to obtain license to practice medicine in the state of Minnesota before appointment date. Applications for these positions will be accepted through Sept. 30, 1991, and Dec. 31, 1991, respectively. Send letters to Deborah Day, M.D., Dept. of Radiology, Box 292 UMHC, University of Minnesota, 420 Delaware St., S.E., Minneapolis, MN 55455. The University of Minnesota is an equal opportunity educator and employer. 8c

FELLOWSHIP IN ULTRASOUND—The Dept. of Radiology at the University of Minnesota has 2 1- to 2-yr postresidency fellowship training positions in ultrasound available at the rank of instructor (temporary, annual renewable) beginning July 1, 1992, and July 1, 1993. Minimum requirements include successful completion of an accredited radiology residency and board certification in radiology by beginning date of fellowship appointment. In addition to clinical practice and training, responsibilities will include graduate and undergraduate medical instruction in ultrasound as well as assisting with related departmental research projects. The clinical practice will provide experience in general abdominal, obstetrical, gynecologic, and vascular ultrasound using conventional, as well as color Doppler, intracavitary, and intravascular technology. It will also provide experience with interventional procedures under sonographic guidance. Salary is negotiable and competitive and dependent on past scholarly productivity and post-M.D. experience. Applicants must be licensed or able to obtain license to practice medicine in the state of Minnesota before appointment date. Applications for these positions will be accepted through Sept. 30, 1991, and Dec. 31, 1991, respectively. Send letters to Janis Letourneau, M.D., Dept. of Radiology, Box 292 UMHC, University of Minnesota, 420 Delaware St., S.E., Minneapolis, MN 55455. The University of Minnesota is an equal opportunity educator and employer. 8c

MAMMOGRAPHY FELLOWSHIP—Mallinckrodt Institute of Radiology, Washington University Medical Center in St. Louis, MO, has an opening for a 1-yr fellowship in breast imaging starting July 1, 1992. The section performs more than 21,000 mammograms/yr with an active screening program that includes mobile mammography. Adjunctive procedures such as breast needle localization, stereotactic fine-needle aspiration biopsy, galactography, and breast ultrasound are performed in the breast center. For further information, contact Drs. Judy Destouet or Barbara Monsees, Mallinckrodt Institute of Radiology, Washington University Medical Center, 510 S. Kingshighway Blvd., St. Louis, MO 63110; (314) 362-2911. 8–10c

FELLOWSHIP IN ABDOMINAL IMAGING—The Dept. of Radiology at the University of Minnesota has 1- to 2-yr postresidency fellowship training positions in abdominal imaging, including body MRI, body CT, and ultrasound, available at the rank of instructor (temporary, annual renewable) beginning July 1, 1992, and July 1, 1993. Minimum requirements include successful completion of an accredited radiology residency and board certification in radiology by beginning date of fellowship appointment. The fellowship will consist of body MRI, CT, and ultrasound rotations. Fellows will perform biopsy and drainage procedures using CT and ultrasound guidance. State-of-the-art equipment is available in all these imaging areas. In addition to clinical practice and training, responsibilities will include graduate and undergraduate medical instruction in abdominal, thoracic, and musculoskeletal CT imaging and assisting with related departmental research projects. Salary is negotiable and competitive and dependent on past scholarly productivity and post-M.D. experience. Applicants must be licensed or able to obtain license to practice medicine in the state of Minnesota before appointment date. Applications for these positions will be accepted through Sept. 30, 1991, and Dec. 31, 1991, respectively. Send letters to Stephen Trenkner, M.D., Dept. of Radiology, Box 292 UMHC, University of Minnesota, 420 Delaware St., S.E., Minneapolis, MN 55455. The University of Minnesota is an equal opportunity educator and employer. 8c

FELLOWSHIP IN MRI—The Dept. of Radiology at the University of Minnesota has 4 1- to 2-yr postresidency fellowship training positions in MRI available at the rank of instructor (temporary, annual renewable) beginning July 1, 1992, and July 1, 1993. Minimum requirements include successful completion of an accredited radiology residency and board certification in radiology by beginning date of fellowship appointment. In addition to clinical practice and training, responsibilities will include graduate and undergraduate medical instruction in MRI as well as assisting with related departmental research projects. We have 2 clinical MR scanners (a 1.0-T unit and a 1.5-T unit) and apart from experience with MR scanning of the brain and spine, a large amount of experience with musculoskeletal and body MR will be possible. In addition to the clinical MR scanners, a whole-body 4-T scanner (1 of 4 presently in operation worldwide) and a small-bore animal system are available for research. Clinical and basic science research projects are available and encouraged. Salary is negotiable and competitive and dependent on past scholarly productivity and post-M.D. experience. Applicants must be licensed or able to obtain license to practice medicine in the state of Minnesota before appointment date. Applications for these positions will be accepted through Sept. 30, 1991, and Dec. 31, 1991, respectively. Send letters to Arthur E. Stillman, M.D., Ph.D., Dept. of Radiology, Box 292 UMHC, University of Minnesota, 420 Delaware St., S.E., Minneapolis, MN 55455. The University of Minnesota is an equal opportunity educator and employer. 8c

FELLOWSHIP IN BODY CT/MRI AND ULTRASOUND—The Dept. of Radiology of Loyola University Medical Center has 2 1-yr fellowship positions available July 1, 1992. The dept. performs more than 180,000 exams/yr. Fellowship training in all aspects of ultrasound is available. All imaging equipment is state-of-the-art and includes 4 GE 9800 CT scanners, 4 Acuson units, and 2 GE 1.5-T magnets. Candidates must be board-certified/eligible in diagnostic radiology and have an Illinois medical license. For further information, contact Mary Olson, M.D., Dept. of Radiology, Loyola University Medical Center, 2160 S. First Ave., Maywood, IL 60153. 8–11cp

FELLOWSHIP POSITIONS AVAILABLE 1992—One-yr fellowships in cross-sectional imaging (includes CT/ultrasound/MRI), angiography/interventional radiology, and MRI at MetroHealth Medical Center, Cleveland, OH, are available starting July 1992. Ideal candidates will have completed an approved diagnostic radiology residency program and have an interest in research as he/she will be responsible for a specific research project during the fellowship. The Dept. of Radiology is an active, academic dept. with state-of-the-art equipment in angiography, CT, ultrasound, and MRI and an approved residency program. MetroHealth Medical Center is a 1000-bed teaching hospital affiliated with Case Western Reserve University and offers attractive compensation and benefits. Interested candidates should forward CV, a letter outlining expectations in the fellowship, and other pertinent information to Errol M. Bellon, M.D., Director, Dept. of Radiology, MetroHealth Medical Center, 3395 Scranton Rd., Cleveland, OH 44109; fax (216) 459-4072. MetroHealth Medical Center and Case Western Reserve University are equal opportunity employers. 8–10c

BREAST IMAGING FELLOWSHIP—The Susan G. Komen Breast Center in Peoria, IL, affiliated with St. Francis Medical Center, is offering a 1-yr fellowship in breast imaging beginning immediately. St. Francis Medical Center is a 750-bed, general hospital affiliated with the University of Illinois College of Medicine. The center is staffed with 2 radiologists devoted full time to breast imaging. Approximately 20,000 breast imaging studies are performed/yr. This 1-yr fellowship will provide exceptional experience in all aspects of breast imaging, including film/screen mammography and breast ultrasound. The fellow will also acquire skills in interventional procedures including ductography, preoperative localizations, cyst aspirations, and stereotactic needle biopsies (FNA and core biopsies). A 6-wk combined surgery and pathology rotation is provided to acquaint the fellow with surgical concerns in biopsies and mastectomies and to acquire a basic understanding of breast pathology. Opportunity exists and the fellow will be encouraged to participate in research projects relating to breast imaging. Send inquiries with CV to G. W. Eklund, M.D., Medical Director, Susan G. Komen Breast Center, 4911 Executive Dr., Ste. 300, Peoria, IL 61614. 8–10cp

MRI FELLOWSHIP AVAILABLE 1992—One-yr fellowships in MRI at MetroHealth Medical Center, Cleveland, OH, are available starting July 1992. Ideal candidates will have completed an approved diagnostic radiology residency program and have an interest in research as he/she will be responsible for a specific research project during the fellowship. The Dept. of Radiology is an active, academic dept. with state-of-the-art equipment in angiography, CT, ultrasound, and nuclear medicine and an approved residency program. The MR section includes a 1.5-T imager (2nd system will be installed in Fall 1991), independent development workstation, 3-D engine (Voxel-Flinger), RF lab, and Starden Titan minicomputer. The research group includes 4 Ph.D. scientists and 4 graduate students. MetroHealth Medical Center is a 1000-bed teaching hospital affiliated with Case Western Reserve University and provides tertiary care in the Cleveland metropolitan area. Interested candidates should forward CV, a letter outlining expectations in the fellowship, and other pertinent information to Errol M. Bellon, M.D., Director, Dept. of Radiology, MetroHealth Medical Center, 3395 Scranton Rd., Cleveland, OH 44109; fax (216) 459-4072. MetroHealth Medical Center and Case Western Reserve University are equal opportunity employers. 8–10c

FELLOWSHIP IN VASCULAR/INTERVENTIONAL RADIOLOGY—The University of Arizona in Tucson has a 1-yr fellowship opening in vascular/interventional radiology beginning July 1, 1992. The full spectrum of vascular and interventional procedures are performed by the section. Tucson is a desirable part of the country, where our competitive salary and reasonable cost of living assure an enjoyable stay as well as an academically productive experience. An informational videotape is available if desired. Applicants must be board-eligible and must submit a recent CV and 3 letters of recommendation including 1 from the program chairman. For further information, please contact Linda Fowler; (602) 694-7136. 8–10cp

RADIOLOGY RESIDENCY POSITION, JULY 1991—Unexpected immediate opening for an R3- or R4-radiology resident commencing July 1991 at Sacred Heart Medical Center (SHMC) in Spokane, WA. SHMC is a large, 650-bed tertiary-care hospital with a state-of-the-art radiology dept. The 11-member faculty are all fellowship trained. Residency program currently includes 2 residents/yr. Please direct all inquiries to Royce L. Zobell, M.D., Program Director, Dept. of Radiology, Sacred Heart Medical Center, W. 101 8th Ave., TAF-C9, Spokane, WA 99220; (509) 455-3020. 8c

FELLOWSHIP IN BODY MRI, THOMAS JEFFERSON UNIVERSITY HOSPITAL—The Dept. of Radiology at Thomas Jefferson University Hospital has an unexpected opening for a 1-yr MRI fellow beginning July 1, 1992. This is an active body MRI section that encompasses a clinical mix of approximately 50% musculoskeletal and 50% chest/abdomen/pelvis cases. Equipment includes 4 1.5-T GE Signa systems with state-of-the-art and advanced prototype hardware and software. Ample opportunity for research is provided. The dept. has excellent research facilities and support, including 2 MRI physicists, a radiology animal facility, radiology research funding, and a team of research assistants. Interested candidates should contact Donald G. Mitchell, M.D., Director of MRI, Dept. of Radiology, 1032 Main Bldg., Thomas Jefferson University Hospital, Philadelphia, PA 19107; (215) 955-4809. Jefferson is an equal opportunity/affirmative action employer. 8–1c

MUSCULOSKELETAL RADIOLOGY FELLOWSHIP—Applications are now being accepted for a musculoskeletal fellow position for 1992 at the Cleveland Clinic Foundation (CCF). CCF is a 1000-bed, tertiary-care, teaching medical center with a large radiology residency program. Local, national, and international patients provide an interesting and varied mix of bone pathology. Training includes all aspects of musculoskeletal radiology including MR, CT, arthrography, biopsy, bone densitometry, and a large plain film experience. Fellowship includes patient care, teaching, and research. There is a close working relationship with the orthopedic, rheumatology, and endocrinology depts. There are presently 4 musculoskeletal staff in the section. For further information, please contact Bradford J. Richmond, M.D., Head, Section of Musculoskeletal Radiology, Desk A-21, 9500 Euclid Ave., Cleveland, OH 44195; (216) 444-3931. 5–10c

CARDIOVASCULAR-INTERVENTIONAL RADIOLOGY FELLOWSHIP—Unexpected opening available July 1, 1991, for a 1-yr fellowship program at a 750-bed teaching hospital. Extensive clinical experience involving all aspects of cardiovascular imaging, interventional vascular and nonvascular procedures, and availability for clinical or animal research. Send CV and inquiries to Oscar H. Gutierrez, M.D., Dept. of Radiology, Box 648, University of Rochester, Rochester, NY 14642-8648. An equal opportunity employer (M/F). 5–8c

FELLOWSHIPS IN PEDIATRIC RADIOLOGY AND PEDIATRIC NEURORADIOLOGY—The Dept. of Radiology, Children's Hospital Medical Center, Cincinnati, OH, offers 1- or 2-yr fellowships in pediatric radiology beginning July 1, 1993. A 1-yr pediatric neuroradiology fellowship program is also offered and may be taken separately or combined with 1 yr of adult neuroradiology fellowship at the University of Cincinnati Medical Center. Children's Hospital Medical Center (CHMC) is a 355-bed institution. The dept. performs over 105,000 radiologic exams annually in the largest children's hospital and ambulatory practice in the U.S. The dept. has 14 full-time faculty pediatric radiologists, 6 fellows, and many resident trainees. Five pediatric radiology and 1 pediatric neuroradiology fellowship positions are available annually. Training includes all aspects of pediatric imaging: neonatal radiology, neuroimaging, musculoskeletal radiology, cardiovascular and thoracic imaging, abdominal imaging, oncologic imaging, ultrasonography, nuclear medicine, CT, MRI, and vascular/interventional procedures. The dept. has an active clinical service with state-of-the-art equipment as follows: digital fluoroscopy; Acuson, AI, and ATL ultrasound units with Doppler and color flow Doppler capabilities; planar SPECT gamma cameras; GE 9800 Quick CT scanner; 1.5-T GE MRI with spectroscopy; and cardiac catheterization/angiographic suite with digital vascular imaging. The fellowship provides a broad clinical experience in pediatric radiology as well as numerous opportunities to participate in both clinical and basic research. Candidates must be board-certified or board-qualified in diagnostic radiology and must be able to obtain an Ohio medical license. Salary and fringe benefits are highly competitive. Applications are due before Jan. 1992, with interviews scheduled during the fall and winter of 1991–1992. There are numerous career opportunities in pediatric radiology in academic and private practice settings. To receive more information about the fellowships at CHMC or careers in pediatric radiology, please contact Donald R. Kirks, M.D., Director, Dept. of Radiology, Children's Hospital Medical Center, Cincinnati, OH 45229-2899; (513) 559-8058. Children's Hospital Medical Center and the University of Cincinnati College of Medicine are affirmative action/equal opportunity employers. 5–4cp

FELLOWSHIP POSITIONS—The Dept. of Radiology and Radiological Sciences of Vanderbilt University School of Medicine is offering fellowship positions for 1992–1993 in angiography, musculoskeletal radiology, neuroradiology (2), and pediatrics. Research opportunities are available and encouraged. Candidates must be board-certified or qualified in diagnostic radiology and able to obtain a Tennessee medical license. Address inquiries and CV to Martin P. Sandler, M.D., Director, Fellowship Programs, Dept. of Radiology and Radiological Sciences, Vanderbilt University, Nashville, TN 37232-2675. An equal opportunity/affirmative action employer. 7–9cp

FELLOWSHIP IN CROSS-SECTIONAL IMAGING The Dept. of Radiology, Dartmouth-Hitchcock Medical Center, has an opening for July 1992 for a 1-yr fellowship in MRI/CT/ultrasound. Training includes experience in all aspects of MRI, including neuro and body, CT, and ultrasound, including obstetric and vascular imaging. Imaging-guided biopsies and drainage procedures will be an integral part of the program. The Medical Center has a completely new 420-bed, tertiary-care hospital with state-of-the-art imaging equipment opening in the fall of 1991. Protected research time will be available for the fellow. There is ample opportunity for clinical radiologic research as well as technology assessment and outcome analysis in collaboration with Dartmouth Medical School Center for Evaluative Sciences. For further information, contact Robert D. Harris, M.D., Dept. of Radiology, Dartmouth-Hitchcock Medical Center, Hanover, NH 03756; (603) 646-5686. 8xc

CARDIOVASCULAR AND INTERVENTIONAL RADIOLOGY—The Harvard Medical School and Brigham and Women's Hospital, Dept. of Radiology, is offering a 2-yr fellowship starting July 1, 1992, in cardiovascular and interventional radiology including peripheral and coronary angiography, cardiac catheterization, digital vascular imaging, all types of interventional procedures, noninvasive vascular techniques, and cardiovascular MRI. Research time available for participation in original or ongoing clinical and/or laboratory projects. Please send CV to B. Leonard Holman, M.D., Chairman, Dept. of Radiology, Brigham and Women's Hospital, 75 Francis St., Boston, MA 02115. Brigham and Women's Hospital/Harvard Medical School is an affirmative action/equal opportunity educator and employer. 3–8c

FELLOWSHIPS AT THOMAS JEFFERSON UNIVERSITY HOSPITAL—The Dept. of Radiology at Thomas Jefferson University Hospital in Philadelphia offers the following fellowship programs each yr. Ultrasound/CT/MRI — Jefferson's ultrasound division is 1 of the largest in the world and performs all currently available exams including obstetric, vascular, lithotripsy, invasive, and endoluminal. We also operate 4 GE 1.5-T MRI units and 3 CT scanners. Contact Barry Goldberg, M.D., regarding this program. Cardiovascular/interventional — this division is housed in a new suite containing Philips angio units with DSA and performs the full range of vascular and nonvascular interventional procedures. Contact Geoffrey Gardiner, Jr., M.D. Neuro/ENT radiology — very active clinical services supply a wealth of material to this division, which is housed in a neurosciences imaging center containing all imaging modalities. Contact Carlos Gonzalez, M.D. Breast Imaging — Jefferson's new breast imaging center performs approximately 85 studies/day including ultrasound and needle localizations. Contact Stephen Feig, M.D. Chest — includes biopsies and CT. Contact Robert Steiner, M.D. MRI — a dedicated body MRI program including excellent research opportunities in addition to a large clinical case load. Contact Matthew Rifkin, M.D. Ultrasound — a dedicated ultrasound program. Contact Barry Goldberg, M.D. Musculoskeletal — includes MRI of the musculoskeletal system. Contact David Karasick, M.D. All program directors listed above can be contacted at the Dept. of Radiology, Thomas Jefferson University Hospital, Philadelphia, PA 19107. Jefferson is an equal opportunity/affirmative action employer. 8xc

IMAGING FELLOWSHIP—A 1-yr fellowship in ultrasound, MRI, and body CT is available July 1, 1992–June 30, 1993, at a 576-bed teaching hospital. The Dept. of Radiology performs more than 140,000 exams with state-of-the-art equipment. The ultrasound section is responsible for all aspects of sonography including OB-GYN, pediatric, abdominal, and small parts. Extensive training in color flow imaging, duplex Doppler, transvaginal, transrectal techniques, and sonographically guided procedures. Two GE MRI scanners and 2 GE 9800 Quick CT units provide high-volume caseloads in these areas. Opportunities are available for participation in imaging research. For further information, please contact Marcela Bohm-Velez, M.D., Imaging Fellowship Director, West Penn Hospital, 4800 Friendship Ave., Pittsburgh, PA 15224. 5–10c

Tutorials/Courses

MUSCULOSKELETAL MRI, 1ST L.A. FALL CONFERENCE, SEPT. 14–15, 1991—Loews Santa Monica Beach Hotel, Medical Seminars International, Inc., 18981 Ventura Blvd., #303, Tarzana, CA 91356; (818) 774-9077, fax (818) 774-0244. 8–9d

MAUI, HAWAII 1991—16th Annual Body Imaging Congress, October 5–12, 1991. CME I, Grand Hyatt Wailea. Medical Seminars International, Inc., 18981 Ventura Blvd., Ste. 303, Tarzana, CA 91356; (818) 774-9077, fax (818) 774-0244. 6–9d

AJR Classified Advertisements Information

Box Responses and Address for Ad Placement

Write Box ______, *AJR,* 2223 Avenida de la Playa, Suite 103, La Jolla, CA 92037-3218; Telephone: (619) 459-2229; FAX: (619) 459-8814.

How to Place an Ad

AJR accepts classified advertising for Positions Available, Positions Desired, Fellowships and Residencies, and Tutorials/Courses. Ads are accepted by mail or FAX.

Rates: $6.00/line with a $30 minimum charge. Box service is $10 additional for each month the ad appears. There are discounts for multiple insertions: 10% for 2–3 insertions; 20% for 4 or more. To estimate lines, count all words and divide by 7.

Billing: Ads *must* be prepaid, or advertisers will be billed after the ad appears *providing* a purchase order number is submitted with the advertising copy. Terms are net 30 days.

Deadlines: 6 weeks prior to issue date. For specific deadlines, telephone the *AJR* editorial office.

Estimating Ad Charges

Line charge: divide total words by 7 and multiply by $6.00 . . . . . $ ______

Multiple insertions? If so, multiply by number . . . . × ______

Subtotal . . . . $ ______

Discount applies to two or more insertions. Subtract 10% if ad appears 2–3 months; 20% if 4 months or more . . . . . . − ______

Subtotal . . . . $ ______

Box response requested? If so, multiply number of months by $10.00 . . . . + ______

Approximate advertising charge . . . . $ ______

The Osler Institute
Radiology Review Course
September 26-October 1, 1991 – Chicago
May 25-30, 1992 – Louisville

OBJECTIVES

- Improve basic knowledge and clinical skills in radiology
- Assist residents and fellows to study efficiently
- Prepare recent graduates to meet their next milestones
- Provide practicing radiologists with a review and update

METHODS

- HOME STUDY MATERIALS consisting of written questions with assignments and answers with explanations
- SEMINAR with projection slides and syllabus
- PRACTICE EXERCISES with oral and written parts

*"The faculty was outstanding. The most pleasant thing was learning a tremendous amount, not only from world-famous authorities but from people who are relatively unknown as well."**

Radiologic Physics
Radiation and Radiology
X-rays and Imaging
Fluoroscopy
Tomography
Computed Tomography
Ultrasonography
MRI
Quality Assurance

Chest
Infiltrates and Cavities
Nodules and Masses
Mediastinum

Cardiovascular
Heart and Aorta
Coronary Arteries
Peripheral Arteries
Echocardiography

Nuclear Radiology
Decay and Detectors
Statistics & Instruments
Radiopharmaceuticals
Quality Control
Endocrine Scans and Rx
GI, GU, Bone, and Brain
Liver, Spleen, and Lung
Ga, In, and Heart

Gastrointestinal
Esophagus and Stomach
Small Bowel and Colon
Liver and Gallbladder
Pancreas and Spleen

Genitourinary
Kidney and Ureter
Bladder and Pelvis
Abdominal Ultrasound
Pelvic Ultrasound

Bone and Joints
Tumors and Trauma
Metabolic and Endocrine
Infection
Dysplasia
Articular Disorders

Mammography

Neuroradiology
Skull and Contents
Spine, Disc and Cord
Temporal and Facial Bones
Sinuses, Larynx and Neck

Pediatric
Pediatric Chest
Cardiovascular System
Gastrointestinal Tract
Genitourinary Tract
Bones and Joints
Central Nervous System

FACULTY

Behrooz Azar-Kia, M.D.
Loyola Univ. of Chicago

Michael Blend, Ph.D., D.O.
Univ. of Illinois at Chicago

Richard Cooper, M.D.
Loyola Univ. of Chicago

Harry Griffiths, M.D.
University of Minnesota

Fernando Gutierrez, M.D.
Washington University

Donald Jacobson, M.S.
Med. College of Wisconsin

Stephen Karesh, Ph.D.
Loyola Univ. of Chicago

Gary Loy, M.D.
University of Chicago

Mahmood Mafee, M.D.
Univ. of Illinois at Chicago

Geno Sebes, M.D.
University of Tennessee

Robert Seevers, Ph.D.
Michael Reese, Chicago

Marilyn Siegel, M.D.
Washington University

Andrew Taylor, M.D.
Med. College of Wisconsin

Aruna Vade, M.D.
Loyola Univ. of Chicago

William Wehunt, M.D.
George Washington Univ.

Limited Enrollment: RADIOLOGY REVIEW REGISTRATION

Name______________________________

Address______________________________

City/State/Zip______________________________

Phone______________________________

Mail today to:

1094 Dawn Lane, Dept. 108
P.O. Box 2218
Terre Haute, IN 47802

For: ☐ Sept. 26-Oct. 1, 1991 – Chicago
☐ May 25-30, 1992 – Louisville
☐ Check enclosed for $_______
☐ Please send **FREE SAMPLE**

*"Accommodations were comfortable...."**

COURSES AND LOCATION: These courses are designed, scheduled and located to serve the needs of radiology residents and recent graduates. Home study questions are sent upon registration. The courses include both lectures and question sessions — faculty and students both questioning and answering in practice for what will follow. Fall courses are more written-oriented, and spring courses are more clinical. Your best value is to repeat the seminar for half price. The September course will be at the Hilton Inn, Lisle, Illinois. Our group room rates will be $85 single and $110 double.

*"...and those little extras...."**

LOWEST AIR FARES: Please call toll-free 1-800-548-8185 for special group fares.

*"...the most education for the money."**

FEES AND COURSE HOURS:

Physician or Resident:	**Phy.**	**Res.**	**hrs.**
• Sept. 26: Radiology Physics	$135	$ 90	10
• Sept. 27-Oct. 1: Clin. Rad.	$660	$440	50
• Sept. 26-Oct. 1: Full Course	$750	$500	60
Repeating within 2 years:	$375	$375	60
• Mock oral exams:	$ 70	$ 70	1/2
• Private mock orals:	$100	$100	1/2

- **Add 10% within 10 days of the course.**
- Attendees not in course hotel add $20/day.
- $50.00 will reserve your position.
- Most home study material will be mailed after half of the registration fee is received.

*"...home study material was extremely helpful."**

REFUNDS: Subject to a $50 fee, refunds will be made up until the seminar begins.

- Cancellation after mailing home study material requires retention of half the fee.

INFORMATION:

Joseph H. Selliken, Jr., M.D.
The Osler Institute
1094 Dawn Lane, P.O. Box 2218
Terre Haute, IN 47802
(800) 356-7537 or **(812) 299-5658**

* *Comments by past Osler participants*

54th Annual Course

RADIOLOGY/91
Cardiovascular and
Interventional Radiology

October 14-18, 1991
Minneapolis, Minnesota

Presented by
Department of Radiology
University of Minnesota

PROGRAM

Radiology/91 will be a comprehensive course emphasizing both conventional diagnostic techniques and advanced imaging modalities. New features of this year's course include workshops on Monday and Thursday and live cases on Tuesday afternoon.

GUEST SPEAKERS

Gary J. Becker (Miami); Claire E. Bender (Rochester); Joseph J. Bookstein (San Diego); Flavio Castaneda (Peoria, Illinois); Andrew H. Cragg (Iowa City); Richard Ehman (Rochester); Grant Hieshima (San Francisco); John Huston (Rochester); Andrew J. Leroy (Rochester); Peter Mueller (Boston); Steve H. Parker (Englewood, Colorado); Donald Schwarten (Indianapolis); Arina van Breda (Alexandria, Virginia); Eric van Sonnenberg (San Diego); Robert K. Zeman (Washington, DC).

FEES: $550
$300 (Resident/Fellow, Military, VA)

ACCREDITATION: 27.75 hours Category 1, AMA

DIRECT INQUIRIES TO: RADIOLOGY/91, Continuing Medical Education, University of Minnesota, Radisson Hotel Metrodome, 615 Washington Avenue S.E., Suite 107, Minneapolis, Minnesota 55414; telephone 612-626-7600. Equal Educational Opportunity.

UPDATE IN FILM SCREEN MAMMOGRAPHY

The University of Virginia will offer its sixth annual postgraduate course, Update in Film Screen Mammography, September 4-6, 1991 at the Jefferson Sheraton Hotel, Richmond, Virginia.

The fee is $424.00 for MD's and $300.00 for Techs and carries 20 hours of AMA credit (Category 1).

Course director: Ellen S. deParedes, MD

For further information write to:

R.L. Boswell
Program Coordinator
Department of Radiology, Box 170
University of Virginia
Health Sciences Center
Charlottesville, VA 22908
Phone: (804) 924-9387

RADIOLOGIST

The University of California, San Francisco and its affiliate, VA Medical Center, Fresno, seek a full-time radiologist. Responsibilities will include teaching and supervising residents in general radiology, as well as subspecialty such as MRI, CT, or interventional radiology.

Qualifications include board certification in radiology and interest, skill, and background in clinical instruction and interest in research. Though candidates at all levels will be considered, the position is ideal for a recent graduate starting an academic career.

The central California location offers pleasant living conditions for family life with affordable housing, good schools, and ready access to both coastal and mountain recreational areas.

Address inquiries and send c.v. to:

Malcolm F. Anderson, M.D.
Chief, Department of Radiology
2615 E. Clinton Ave. (114)
Fresno, CA 93703
209-228-5328

UCSF is an AA/EOE, M/F/H/V.

NEURORADIOLOGIST

Temple University Hospital and School of Medicine is searching for a third Neuroradiologist at the rank of Assistant Professor. The candidate should have fellowship training in Neuroradiology, be board-certified, qualify for senior membership in the Society of Neuroradiology, and have experience in invasive neuroradiology procedures. Candidate should have skills in resident and medical student teaching as well as in patient care. A candidate with a research background is preferable.

The Department is currently adding two new CT scanners and a state of the art 1.5 tesla MRI unit. An excellent angiographic facility is also available.

Candidates should contact **Francis J. Shea, M.D., Professor & Acting Chairperson, Department of Diagnostic Imaging, TEMPLE UNIVERSITY SCHOOL OF MEDICINE, Broad & Ontario Streets, Philadelphia, PA 19140.**

Temple University is an Affirmative Action, Equal Opportunity Educator and Employer.

UNIVERSITY

Choose
TEMPLE

Volume 157 **American Journal of Roentgenology** **August 1991**

REVIEW ARTICLES

223 **The biliary tract: imaging for the 1990s.** *Burrell MI, Zeman RK, Simeone JF, et al.*

235 **Laparoscopic cholecystectomy: evolution, early results, and impact on nonsurgical gallstone therapies.** *Brandon JC, Velez MA, Teplick SK, et al.*

241 **Commentary. A surgeon's perspective on laparoscopic cholecystectomy.** *Easter DW*

243 **Characterization of tumor hypoxia by ^{31}P MR spectroscopy.** *Steen RG*

PULMONARY RADIOLOGY

249 **Broncholithiasis: CT features in 15 patients.** *Conces DJ Jr, Tarver RD, Vix VA*

255 **Case report. Noncardiogenic pulmonary edema resulting from intravascular administration of contrast material.** *Bouachour G, Varache N, Szapiro N, L'Hoste P, Harry P, Alquier P*

BREAST RADIOLOGY

257 **Lobular carcinoma in situ of the breast: clinical, pathologic, and mammographic features.** *Beute BJ, Kalisher L, Hutter RVP*

267 **Gadopentetate dimeglumine–enhanced chemical-shift MR imaging of the breast.** *Rubens D, Totterman S, Chacko AK, et al.*

271 **Pictorial essay. Lipid cyst: classic and atypical appearances.** *Evers K, Troupin RH*

GASTROINTESTINAL RADIOLOGY

275 **Abdominal desmoids: CT findings in 25 patients.** *Einstein DM, Tagliabue JR, Desai RK*

281 **Bile duct diverticula and webs: nonspecific cholangiographic features of primary sclerosing cholangitis.** *Gulliver DJ, Baker ME, Putnam W, Baillie J, Rice R, Cotton PB*

287 **Biliary lithotripsy: correlation between gallbladder contractility before treatment and the success of treatment.** *Donald JJ, Fache JS, Burhenne HJ*

291 **Technical note. The management of occluded metallic self-expandable biliary endoprostheses.** *Jackson JE, Roddie ME, Chetty N, Benjamin IS, Adam A*

293 **Diagnosis of portal vein thrombosis: value of color Doppler imaging.** *Tessler FN, Gehring BJ, Gomes AS, et al.*

297 **MR imaging of the portal venous system: value of gradient-echo imaging as an adjunct to spin-echo imaging.** *Silverman PM, Patt RH, Garra BS, et al.*

303 **Diagnosis and staging of hepatocellular carcinoma: comparison of CT and sonography in 36 liver transplantation patients.** *Miller WJ, Federle MP, Campbell WL*

307 **Case report. Acute torsion of a wandering spleen: diagnosis by CT and duplex Doppler and color flow sonography.** *Nemcek AA Jr, Miller FH, Fitzgerald SW*

311 **Gastric carcinoma in patients with Crohn disease: report of four cases.** *Glick SN*

315 **Case report. Diffuse stenosis of the ileum after ureteroileal interposition: radiologic-pathologic correlation in two cases.** *Tung GA, Papanicolaou N, Zukerberg LR, Yoder IC*

319 **Case report. Giant thoracic osteophyte causing esophageal food impaction.** *Underberg-Davis S, Levine MS*

GENITOURINARY RADIOLOGY

321 **Review article. Retroperitoneal fibrosis.** *Amis ES Jr*

331 **Color Doppler sonography in the evaluation of erectile dysfunction: patterns of temporal response to papaverine.** *Fitzgerald SW, Erickson SJ, Foley WD, Lipchik EO, Lawson TL*

337 **Abnormalities of the seminal tract causing infertility: diagnosis with endorectal sonography.** *Abbitt PL, Watson L, Howards S*

MUSCULOSKELETAL RADIOLOGY

341 **John Caffey Award Paper. Avascular necrosis: early MR imaging and histologic findings in a canine model.** *Brody AS, Strong M, Babikian G, Sweet DE, Seidel FG, Kuhn JP*

347 **Preoperative evaluation of osteosarcoma: value of gadopentetate dimeglumine-enhanced MR imaging.** *Seeger LL, Widoff BE, Bassett LW, Rosen G, Eckardt JJ*

353 **Soft-tissue sarcoma: MR imaging vs sonography for detection of local recurrence after surgery.** *Choi H, Varma DGK, Fornage BD, Kim EE, Johnston DA*

359 **Improved imaging of bone with scan equalization radiography.** *Wandtke JC, Plewes DB*

365 **Pictorial essay. Bacterial osteomyelitis: findings on plain radiography, CT, MR, and scintigraphy.** *Gold RH, Hawkins RA, Katz RD*

PEDIATRIC RADIOLOGY

371 **Synthetic vs human surfactants in the treatment of respiratory distress syndrome: radiographic findings.** *Levine D, Edwards DK III, Merritt TA*

375 **Pictorial essay. CT of the pancreas in children.** *Herman TE, Siegel MJ*

381 **Case report. Esophageal histoplasmosis in a child with immunodeficiency with hyper-IgM.** *Tu RK, Peters ME, Gourley GR, Hong R*

383 **Case report. Renal tubular dysgenesis.** *Luisiri A, Salinas-Madrigal L, Noguchi A, Graviss ER, Silberstein MJ*

NEURORADIOLOGY

385 **MR imaging of the brain in patients with migraine headaches.** *Osborn RE, Alder DC, Mitchell CS*

389 **High-intensity signals within the posterior pituitary fossa: a study with fat-suppression MR techniques.** *Mark LP, Haughton VM, Hendrix LE, et al.*

393 **The role of contrast-enhanced MR imaging in the diagnosis of neurocysticercosis.** *Chang KH, Lee JH, Han MH, Han MC*

397 **Imaging of the basal cerebral arteries and measurement of blood velocity in adults by using transcranial real-time color flow Doppler sonography.** *Tsuchiya T, Yasaka M, Yamaguchi T, Kimura K, Omae T*

403 **Carotid duplex sonography: bisferious pulse contour in patients with aortic valvular disease.** *Kallman CE, Gosink BB, Gardner DJ*

RADIOLOGIC RESIDENCY TRAINING

409 **Perspective. Radiologic physics instruction for diagnostic radiologists: a survey of residency programs.** *Committee on Training of Radiologists, American Association of Physicists in Medicine*

OTHER CONTENT

234 **Figley Fellowship announcement**
274 **History page**
280 **Medicine in American art**
290 **List of book and videotape reviews**
318 **Radiologic-pathologic conference**
345 **ARRS 1992 resident award papers information**
411 **Letters**
418 **Forthcoming articles**
419 **Review of current literature**
425 **News**
428 **ARRS 1992 meeting announcement, calls for papers and exhibits**
433 **American Roentgen Ray Society information**
434 **ARRS membership information and application**
437 **Classified advertisements**
A6 ***AJR* business and subscriber information**
A17 **Guidelines for authors**

1992 ARRS Meeting: May 10–15, Orlando, FL